ASTES

Advances in Science, Technology & Engineering Systems Journal

VOLUME 4-ISSUE 4|JUL-AUG 2019

www.astesj.com
ISSN: 2415-6698

Editorial

Advances in Science, Technology and Engineering Systems Journal (ASTESJ) is an online-only journal dedicated to publishing significant advances covering all aspects of technology relevant to the physical science and engineering communities. The journal regularly publishes articles covering specific topics of interest.

Current Issue features key papers related to multidisciplinary domains involving complex system stemming from numerous disciplines; this is exactly how this journal differs from other interdisciplinary and multidisciplinary engineering journals. This issue contains 68 accepted papers in Computer Science domain.

Editor-in-chief
Prof. Passerini Kazmersk

ADVANCES IN SCIENCE, TECHNOLOGY AND ENGINEERING SYSTEMS JOURNAL

Volume 4 Issue 4 **July-August 2019**

CONTENTS

ASTES

Advances in Science, Technology and Engineering Systems Journal
Vol. 4, No. 4, 1-11 (2019)
www.astesj.com

ASTES Journal
ISSN: 2415-6698

Development of Tactile Display and an Efficient Approach to Enhance Perceptual Analysis in Rehabilitation

Vaibhav B. Vaijapurkar *, Yerram Ravinder

Department of Electronics and Telecommunication Engineering, Pune Institute of Computer Technology, Pune, 411043, India

ARTICLEINFO

Article history:
Received: 03 March, 2019
Accepted: 15 June, 2019
Online: 07 July, 2019

Keywords:
Tactile display
Solenoid actuator
Braille display
Discrimination index
Psychological experiments
Tactile evaluation

ABSTRACT

Tactile displays are widely used in the rehabilitation and education of blind persons, as it is one of the media of communication amongst them. Tactile display performance is measured in terms of accuracy in presenting pattern, accuracy in identification, recognition and reading time of presented pattern. However, it has had meager attention from researchers. This paper presents a novel 3 x 2 solenoid actuators pin array tactile display and evaluates its effectiveness in presenting alphabets to blind and normal subjects as well as compute facilitation and discrimination value. The proposed actuator requires 75 % of the current and 90 % of the power in comparison with presently available actuators. This is achieved due to the incorporation of conical spring. Two psychological experiments were conducted to evaluate system performance, also to measure perception (reading) and key pressing sense (writing) accuracy for the first time. The low-cost developed system achieved an average reading time of about 15.7 s, recognition time of 39 s and prediction accuracy to be 93 % using a confusion matrix. The developed prototype model has resulted in 94% facilitation value and 11 % discrimination index during psychological experiments for intended users.

1 Introduction

Tactile devices have proved their value in educating blind persons. In the human sensory system, skin plays a significant role in touch and feel. A visually disabled person uses predominantly uses touch and feel as a medium to communicate. The tactile display is developed using a different kind of actuator such as a piezoelectric, solenoid, electromagnetic, Shape memory alloy (SMA) wires and spring, soft gel, etc. The various performance parameters of tactile devices are reading speed, recognition rate, and perception accuracy. Miniaturization of such devices obviously has challenges and limitations in fabricating and assembling. A diverse range of technology is used to develop tactile displays.

A sixty-four elements tactile display using shape memory alloy (SMA) wires and 8 tactel modules was developed reported by [1]. A piezoelectric bimorph was used to form 6 and 8 dot Braille cells. Touching force varying between 0.03 to 0.39 N was reported by [2]. A portable eBook reader for the blind with 10 Braille cells using a piezoelectric ultrasonic actuator was presented in [3]. Thermal bimorph microactuator was developed by [4] and was analyzed for changing mechanical dimensions rather than changing the input voltage to reduce power consumption. A vibrotactile display using a pen-like haptic interface to represent textures on it was also developed. Different textures were represented and 80.83 % accuracy was reported by [5]. Xiaosong Wu et al. have devised a portable pneumatically actuated refreshable Braille cell. A 2 X 3 micro-bubble actuator by UV lithography process formed to achieve 0.56 mm displacement [6].

A compact planar distributed tactile display was developed by Ki-Uk Kyung. Also, observed the effect of frequency on texture judgment through the developed display. The correct answer reported is dependent on the stimulus 90-90 % times. Small-scale shapes, patterns, and gratings have conveyed good tactile information to subjects; the correctness achieved is 90 %. Stimuli with higher frequencies have shown the worst discrimination of patterns as reported in [7]. Makoto Takamiya et al. proposed a low power and flexible

*Corresponding Author: Vaibhav B. Vaijapurkar, Department of Electronics and Telecommunication Engineering, Pune Institute of Computer Technology, Pune, 411043, India, vaibhav.vaijapurkar@gmail.com

https://dx.doi.org/10.25046/aj040401

Braille sheet with a plastic actuator. It uses back-gated OFETs SRAM technology to enhance speed [8]. The speed of Braille sheet display was improved to 1580 times that of the speed without SRAM. H. R. Choi et al. used the tactile display as a Braille display. The frequency by which the dots activate is 15-60 Hz [9]. Achieved average recognition rate for HRR is 60 % while for NRR, it is 40 %. T. Matsunaga et al. fabricated and developed 2-D and 3-D tactile pin display to represent the character and graphics information dynamically using an SMA micro-coil actuator [10]. Christopher R. Wagner et al. used RC servomotors to develop a tactile shape display. The 6 x 6 pin array tactile display was developed with 1 mm pin diameter; The result showed that displacement is limited by the slew rate [11]. Masashi Konyo et al. artificially created a soft gel tactile feel display. The most sensitive frequency was found to be 180 Hz close to physiology [12]. Also, signals with varying shapes such as sinusoidal, triangular, rectangular and sawtooth waves confirmed that rectangular is the most significant signal and the sinusoidal wave is the next most significant. The stimuli of a compound signal had shown a significant tactile feel.

Pruittikorn Smithmaitrie designed and analyzed a piezoelectric Braille display. The touching force of the reader while sensing a Braille character on the tactile display was measured by [13]. Ramiro Velaquez et al. created a tactile binary information display using an SMA actuator. The designed actuator was excited by a 200-500 mA current to achieve a displacement of 3 mm [14]. Michael J.Mosley et al. proposed the dynamics of an SMA wire bundle actuator through design [15]. Jun Su Lee and Stepan Lucyszyn have developed a refreshable Braille cell using micromachining. They developed electrothermally controlled actuators forming a 3 x 2 Braille cell consuming an average power of 0.30W and an actuation time 50 s [16].T. Nobels et.al. had designed high power density electromagnetic actuators for a portable Braille display. It used small linear electromagnetic actuators mounted on a computer mouse displaying 3 characters one at a time [17]. Sarah F. and Paul B proposed a four-level fingertip search display for the blind using 64 solenoids. Overall power consumption was 30 W. It was difficult to control the displacement of each actuator uniformly with the suggested method [18]. K. Deng and E. T. Enikov used electromagnetic localization and actuation to present an on shape display. A prototype module of 4 x 4 was developed to experiment with the perception of curvature shapes. The size of the actuator was analyzed to determine its minimal diameter. It had an outer diameter of 1.5 mm, which is suitable for right perception [19].

Different 84 devices were compared with their functionality and readiness levels by [20]. It was observed that only 19 % of total the developed systems were commercialized and others were available in prototype forms. Also, many of them were not evaluated to test performance parameters of a developed unit. In recent years, a portable device with a tactile keyboard and the refreshable display is patented by [21] consist of a touch-sensitive surface, Braille tactile display, and processing unit. The developed unit uses a touch-sensitive screen used to form a tactile pattern on the Braille display. A single piezoelectric Braille cell display is proposed and patented by [22] uses MOSFET drives to magnetize each piezo-actuator to form an expected pattern.

Granit and Eduardo investigated text recognition using six channel vibrotactile wearable display. They experimented skin sensation for the letter, word, and short sentences. The reported recognition accuracy is 82 % and interaction duration 38 seconds. It is observed that repetition in such experiments improves accuracy reported in [23]. Daniele and Claudio designed refreshable Braille display recently [24]. It includes four Braille cells actuated by a solenoid and external magnetic field. It was operated on the 9V battery to achieve 1mm displacement. Zhiyun Lu had developed a bistable electroactive polymer one cell tactile display. This display is capable of representing Braille letters using air pressure [25]. The author reported 100 mmHg air pressures to raise dot to achieve 0.7mm height. It uses 90 V supply to raise each dot.

Although great efforts have been put into developing such devices throughout the globe; there are some issues that need to be resolved for it to be converted into a product. The accuracy in reading Braille is reported to be 80% [5] and 90 % [7], while recognition rate is about 60 %[9]. As mentioned in[26]; reading/ perception accuracy, recognition rate, and reading speed are the performance parameters for tactile displays. The above review reveals that although different types of tactile displays have been developed, to the best of our knowledge, meager attention has been paid towards performance parameters. Evaluation of developed tactile displays needs to be given more attention for finding accuracy, recognition rate, reading speed.

A survey was conducted in a blind school to understand the usage of electronic gadgets in teaching. It showed that the computer is one of the most commonly used tools but it has a dependency on the school laboratory hence, it is required to have a handheld device to read and write Braille letters. This display caters to the needs of disabled such as training, rehabilitation, and education through play and entertainment. Few more problems raised by participants were, dots remain unraised after frequent use of Braille on paper, that creates difficulty in reading. It is difficult to carry such a document or book because of its weight and size. The device should be easily portable during their primary education.

This paper presents; a low-cost design and implementation of a novel tactile display and its parametric performance evaluation. The designed display is capable of displaying alphabets and numbers in bilingual; effectively experimented during the evaluation of it. The proposed display is the least power consuming prototype as compared with literature. The tapered spring used to actuate is one of its kind and novel, none of the authors reported such spring for actuation over a

linear spring. Also, it has achieved maximum displacement in the least time compared with a similar type of actuators mentioned in the literature. The developed unit advances in identification accuracy and reading rate. It addresses the key pressing sense of subjects with very high accuracy; which is tested first time in existing work. To support the results; 25 blind and 25 normal subjects are evaluated to test the effectiveness and confirmed use of the display for education. Facilitation and discrimination analysis of experiment finding is done and it confirms desired values. Solenoid actuators are robust, high speed and fast response actuators as compared to the other actuators. It is a tool for educating and training visually impaired persons in their primary stage with or without the help of a trainer. Such systems are also useful in rehabilitation of motor system disorders in humans [27].

Section I presents a detailed study of the available literature to understand the current scenario in the space of the proposed work. Section II presents the development of a six solenoid actuators tactile display and discusses; improvement in solenoid operation with modified spring design. The discussion covers the organization of six solenoids to make a 3 x 2 Braille cell. Section III covers the evaluation of the developed tactile display with psychological experiments aimed at understanding the performance parameter. A statistical tool called confusion matrix technique was used to find percentile accuracy in prediction and mis-prediction. Item analysis was used to assess the discrimination index and facilitation value of the developed technique. Performance of device along with the results of the experiments is discussed in section III.

2 Design and development of tactile display

The micro solenoid actuator available in the market works on 12 V and requires 0.5 A current to actuate to have a displacement of 4 mm. The power consumed by one such actuator is 6 W, which is higher compared to piezoelectric or electromagnetic actuators. Tactile display requires six such actuators to form a Braille cell, consuming the power of 36 W. First challenge in the development was to reduce this power consumption. Following steps were taken to develop a more efficient tactile actuator.

1. Design of a solenoid actuator
2. Testing of a single actuator
3. Performance test of the designed actuator
4. Control system design

2.1 Design of a solenoid actuator

Solenoid actuator has four major components as a metal rod, compression spring, coil, and housing. New actuator design includes the design of a rod which will move vertically after excitation and represents a Braille dot, a compression spring which will move a rod back to its original position after excitation is removed, a coil which will generate an electromagnetic field to hold the rod at the un-raised position once excited. It was required to reduce current consumed by an actuator and hence compression spring design was important. This spring helps actuator to come back to the normal position when the actuator was not actuated. The stainless steel metal rod that moves vertically has a diameter of 2.9 mm and length of 4.2 mm. The conical spring was designed using music wire. The use of linear spring [1, 5, 9, 10, 18, 24] is limiting the performance of the actuator hence, the conical spring instead of linear is proposed to use the first time to improve its performance. The proposed spring provides a constant spring rate and improves displacement; which is verified through experimentation. The wire of a diameter 0.15 mm available in music wire type was selected to generate a stroke of 4 mm. The free length of the spring was 9 mm with 7 active coils. The housing was designed using iron material press fit assembly. Two sides are kept open for natural cooling. This spring is capable of generating a deflection force of 1 N showed in Table 1.

Table 1: Proposed conical spring parameters.

Parameter(symbol)	Value	Unit
Wire diameter(d)	0.15	mm
Small OD(SOD)	5.8	mm
Large OD(LOD)	7	mm
Number of active coils (N_a)	7	–
The free length(l_f)	9	mm
Density of material(ρ)	8000	Kg/m^3
Spring constant(k)	94.8	N/mm
Pitch of leads (P_s)	2	mm
Shear stress(τ)	2.16	MPa
Deflection force(F)	1	N

2.2 Testing of a single actuator

A single solenoid actuator was evaluated to test performance parameters, such as displacement, the current required for actuating to achieve desired displacement, the time required to actuate, etc. The experiment carried out to test this included a DC power supply which can supply 5 V and 500 mA current. The electrical parameters are listed in Table 3. It has shown that total power consumed by one existing actuator is 2.5 W and the proposed actuator is 0.6 w. The power consumption is very low as compared with displays developed by [14, 18, 24] for a similar purpose. However total displacement achieved was 4 mm, which is higher than reported by [1, 11, 14, 18]. A transistorized driver was designed to drive a solenoid by providing logical input at the base terminal of a transistor as shown in Figure 1a. As soon as a logical input was available from the control unit to the base terminal of a transistor; solenoid actuated. Table 2 shows that 4 mm

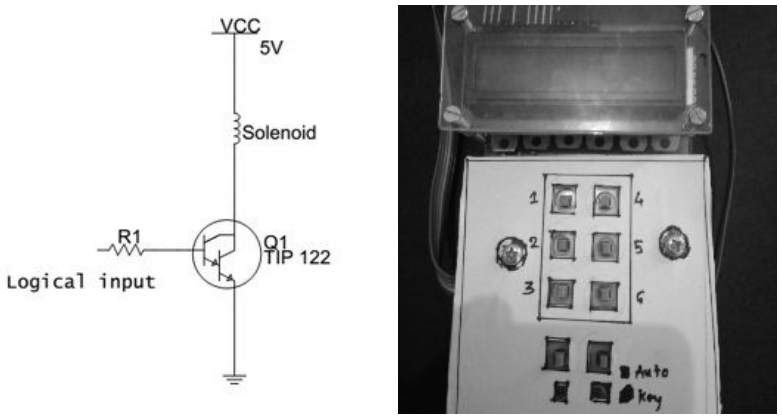

(a) Solenoid actuator driver circuit. (b) Control unit front panel.

Figure 1: showing driver circuit and control unit.

displacement is achieved by an existing actuator in 11.8 s with an applied direct current of 0.5 A. While the proposed actuator only takes 0.12 A and 10 s for similar displacement.

Table 2: Comparison of existing and proposed actuator performance parameter value

	Existing actuator		Proposed actuator	
Displacment (mm)	I (mA)	Time (s)	I (mA)	Time (s)
0	100	2.3	0	0
1	200	3.7	25	4
1.5	250	4.3	45	5
2	300	7.3	55	6.3
2.5	350	8.2	75	7.4
3	400	10.2	90	8.5
3.5	450	11	105	9.6
4	500	11.8	120	10

2.3 Performance test of an actuator array

A 3 x 2 matrix was created using six solenoids close to each other in such a way that they will not affect the operation of neighbor pins. Two acrylic sheets of 3 mm thickness were used to host 6 solenoids as shown in Figure 2b. Each actuator is operated on 5 Vdc and 0.12 A current. According to the excitation signal, maximum displacement achieved is 4 mm as shown in Figure 2c. Figure 2a. shows a solenoid an unexcited state. Figure 2c shows a side view of the closely placed actuator. Figure 2d is the top view of the tactile display showing the pin placing. Each pin was tested for its operation and combined six pins as well. This ensured the equal height of all pins when raised to avoid any misunderstanding because of adjacent pins. Also, the refresh rate is defined as actuation and de-actuation of pins; which is observed approximately 0.5 s. However, during experimentation height (displacement) of the pin 2 mm was sufficient to interpret raised or un-raised pin from the reference surface. This reduced further power consumption of Braille cell to 1.6 W. It was one of the achievements of the proposed display.

The newly designed actuator has resulted in a reduced current requirement to actuate to have 4 mm of displacement. It has also reduced the power consumption by each actuator. There is 75 % reduction in the current required for actuation, which was achieved by increasing coil resistance by 4 times and 90 % reduction in total power consumption by the tactile display as mentioned in Table 3.

Table 3: Comparison between old and newly designed actuator parameters.

Parameter	Existing actuator	Proposed actuator
Max current requirement(A)	0.5	0.120
Operating DC voltage(V)	5	5
Max displacement (mm)	4	4
Length of the rod(mm)	3.2	4.2
Coil resistance (ohm)	10	42
Power consumption by single actuator(W)	2.5	0.6
Power consumption by six actuator(W)	15	3.6

2.4 Control system design

The developed circuit board uses an Arduino Mega board as a control unit to sequentially control solenoid actuator to represent the desired alphabet as shown in Figure 3. The microcontroller was able to generate bilingual, that is English and Hindi alphabets and numbers. However, presently the evaluation is done for English alphabets only. The control unit has 6 keys used to write Braille letters on a tactile display as shown in Figure 1b. Two keys are provided to select the mode of operation, one for auto training or reading mode and the other for manual mode or writing mode. This module is accompanied by an LCD display for a normal trainer to check the key combinations pressed and the tactile pattern expected on the tac-

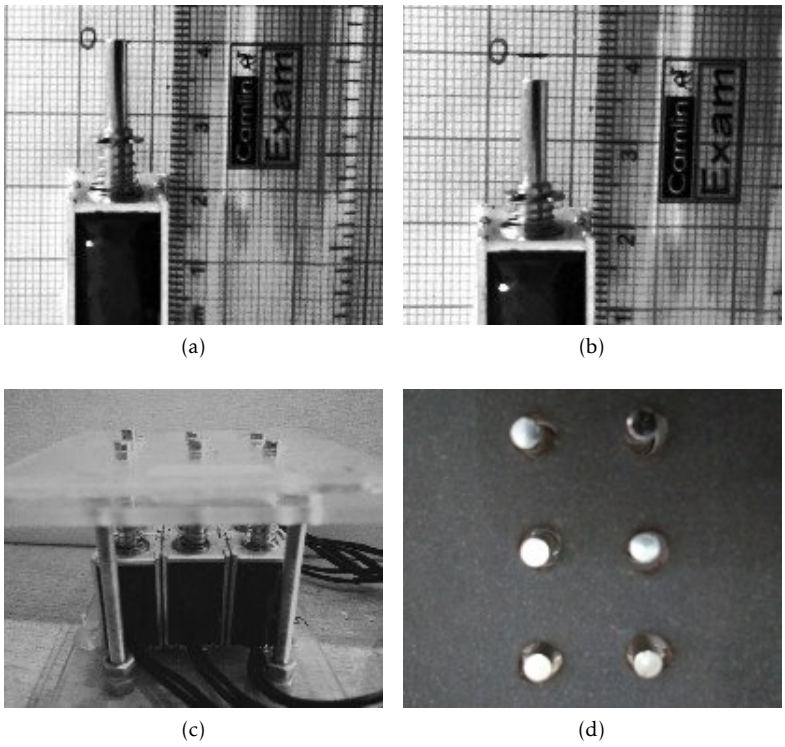

(a) (b) (c) (d)

Figure 2: a) Actuator initial position, b) Actuator showing 4 mm displacement, c) Side view of developed six actuator cell showing compactness, d) Top view of six pin array to show pin to pin distance

tile display accordingly. A 3 x 2 matrix was created using six solenoids close to each other in such a way that they will not affect the operation of neighbor pins. The intention to use this arrangement is that even in the absence of an instructor; students can operate it in auto mode or learn Braille writing using keypress mode. The research work aims to test Braille reading by touching to pins of actuator and writing by key pressing electronically.

3 Evaluation of tactile display

A psychological experiment was carried out to understand the limitations of perception, accuracy, etc. The developed display was evaluated in the school Blind school for girls, Pune. Total 50 subjects, 25 blinds and 25 normal were selected for both experiments [26, 30]. Currently, restricted alphabets are successfully read and written by subjects. The delay of 1 s is set after every alphabet. This delay time was calculated through experimentation with the subjects during trials. The following two experiments were conducted.

- Tactile perception (Reading)
- Key Pressing sense (Writing)

3.1 Experiment for tactile perception (reading)

In Braille letters, the representations of letters such as e and i, d, h and j, s and t only differ by one dot. Thus, there is a possibility of misperception into the account with the developed display; alphabets were selected taking this in to account. The six dots formed by each actuator make up a display and raised or un-raised dots are felt by subjects by touching each pin. The raised height of each dot and the spacing between the dots play significant roles in the discrimination [30]. Intentionally selected 10 English alphabets were represented for subjects to touch and feel. Each subject was given the training to use the developed display for 5 minutes. They were instructed to use the index finger for touch and feel. Participating subjects were asked to read as rapidly as they could. Few samples manually highlighted for clarity as shown in Figure 3. English alphabets a, l, s, v, e, t, z, b, g, y were randomly presented. The time required to follow the alphabets with touch and reproduce them mentally and vocally is called reading time. For this experiment; time taken by each subject to read all ten alphabets by touch was considered as reading time. The time required to identify a letter as known before and realize the validity is called recognition time. For this experiment; time taken by all subjects to identify one alphabet was considered as recognition time.

The experiment aimed to measure the reading time and recognition time of the user. Reading time varies with user experience in reading Braille or the frequency of use of the tactile display. Minimum time for reading was observed to be 12 s by blind subjects and 11 s by normal subjects, while the maximum time was noted to be 22 s by blind and 20 s the normal as shown in Table 4.In an alphabet reading experiment, the time required to identify an alphabet is measured in seconds irrespective of the accuracy. Expected average

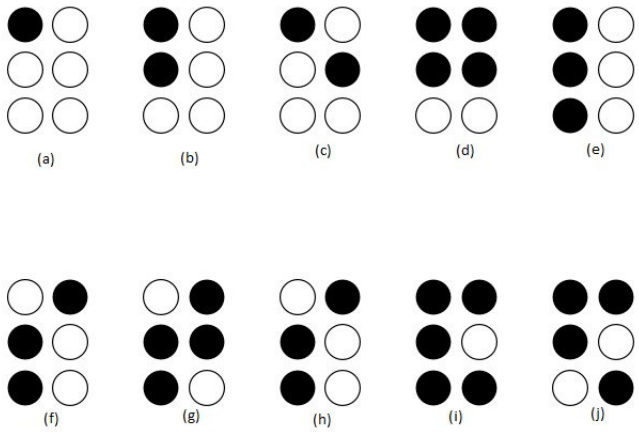

Figure 3: Manually highlighted (for clarity) alphabets presented on the developed display (a) a, (b) b, (c) e, (d)g, (e) l, (f) s,(g) t, (h) v, (i) y, (j)z

time to read 10 alphabets was assumed to be 10 s. In the identification table; alphabets identified correctly were marked with 1 and incorrectly identified with 0. The matrix was maintained as 10 alphabets in rows and 25 subjects in columns. During the recognition experiment; the average time expected was 1.5 s which was more than that of reading time. The column wise sum indicated reading time for all 10 alphabets of each subject and row wise sum indicated recognition time of each alphabet for all 25 subjects. Each subject had one attempt for each experiment.

Table 4: Reading and recognition time for blind and normal subjects.

	Reading time (s)		Recognition time(s)	
Subjects	Min	Max	Min	Max
Blind	12	22	28	54
Normal	11	20	28	57

As shown in Figure 4a English alphabet a, b, g were identified by all the subjects from each type. Alphabet t has shown a less amount of correct identification compared to other letters. Figure 4a shows the accuracy of alphabet identification in percentage. It shows that the letter a, b, g has shown 100 % accuracy in identification by 50 subjects; while the letter t was only identified 80 % accuracy. As shown in Figure 4c the average reading time of 50 subjects was found to be 15.7 s using the developed tactile display. It is also required to test both types of subjects on the identification of each letter. Letter t was identified by 19 blind persons and 21 normal persons out of 25 each. The reason for this was that blind persons missed dot number four.

Recognition time may vary with language.Figure 4d shows recognition time for blind and normal subjects. The average recognition time required by 50 subjects was observed to be 39 s. The total test time for the blind subject was 798 s for blind subjects and 764 s for normal subjects. During this experiment, it was observed that the minimum letter identification accuracy achieved was 80 % and the maximum was 100 %. Blind subject no. 19 recorded the minimum time to all alphabets (12 s) while subject no. 2 recorded the highest time of 22 s for the same. Normal subject no. 25 recorded the minimum time to read all alphabets (11 s), while subject no.2 recorded the highest time of 20 s for the same. As shown in Figure 4d the recognition time for each alphabet by both types subjects was very small. The reason for this was observed to be the distance between adjacent pins.

3.2 Experiment to test key pressing sense (writing)

Key pressing sense testing is one of the major requirements to replace the existing Braille writing system. 3 x 2 keys were arranged in such a way that the key position representing Braille dots as usually they work with nails to form a dot. All of the participants involved have shown quite an interest as they were trying to relate this to their Braille writing technique. They pointed out that; their usual way of writing Braille letters is similar to the experimental process introduced here. However, reading is by reversing the page, which while reverses dot positions. the developed unit serves this aspect. When a particular key or combination of keys is pressed the respective Braille letter will be formed on the tactile display. The subjects are trained to press keys in a particular order to form the same Braille alphabet on a tactile display. The subjects had to touch the display and identify so that the representation is successful. This experiment was carried out immediately after Braille reading. Each subject used a test unit for 5 minutes to understand the keys. They were instructed to generate the same letters that they read in the previous experiment. The distance between the adjacent keys was 150 mm which is greater than the minimum discrimination distance required to sense pressed or un-pressed keys [30].

On the other hand, an invalid key combination in the set of alphabets is not displayed in a tactile form and a warning is generated on the LCD display for a normal trainer with a beep sound. Figure 4b shows the response of subjects to the key pressing experiments. Total of 500 responses was recorded with 50 subjects and 10 alphabets. Assuming that each subject would

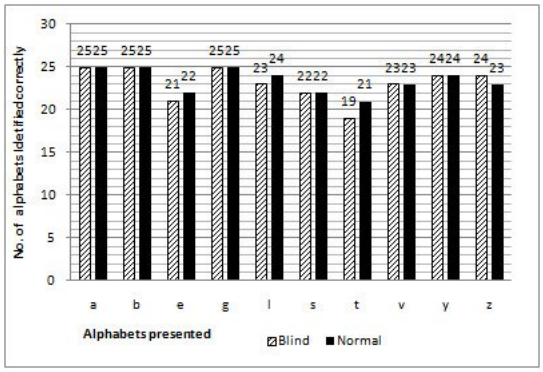

(a)

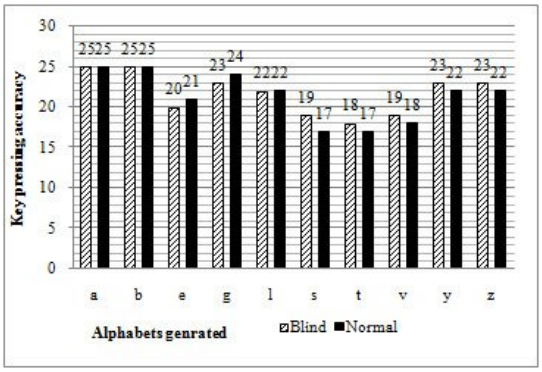

(b)

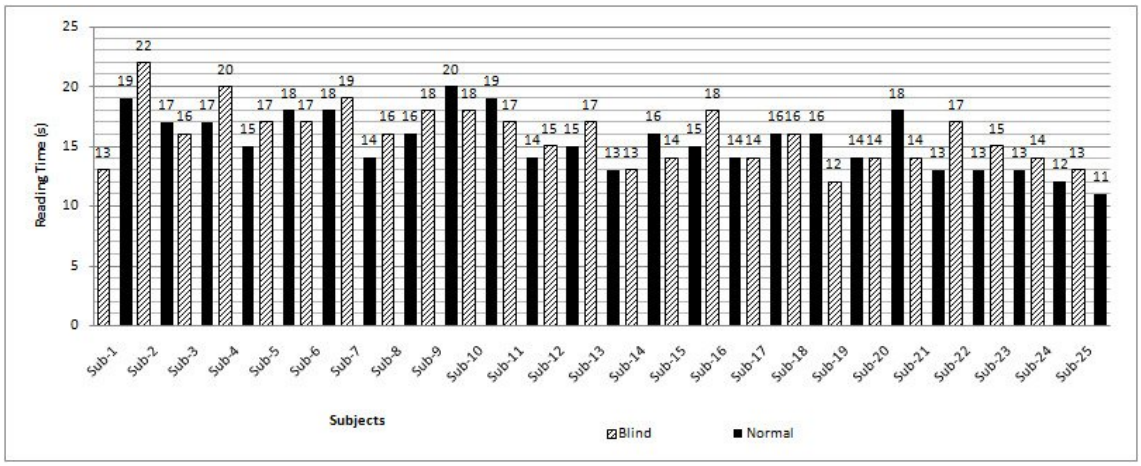

(c)

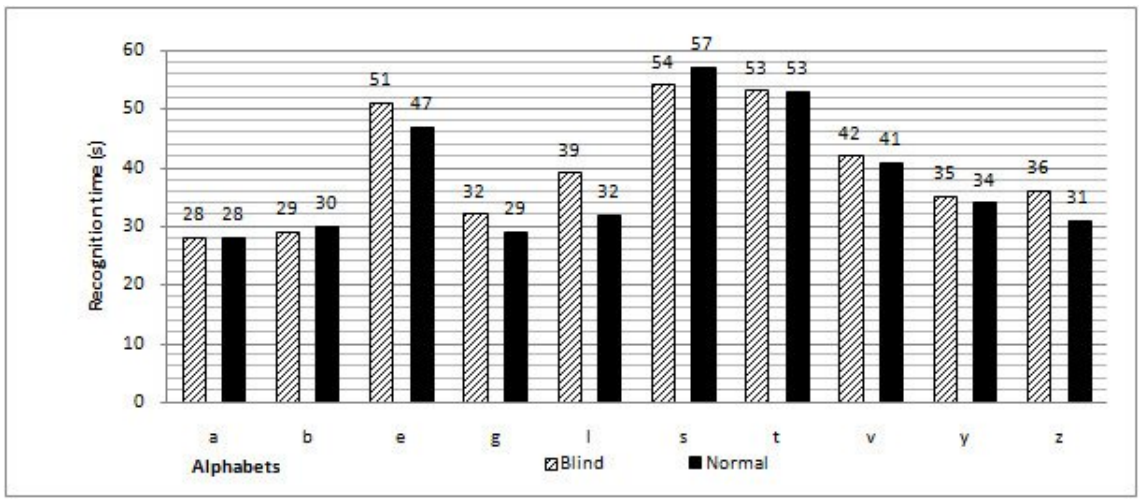

(d)

Figure 4: a) Number of alphabets identified correctly by each subject, b)Key pressing accuracy by both type of subjects,c) Reading time of each subject, d) Recognition time of each alphabet

take approximately 1.5 s to form an alphabet on the display. The time estimated to conduct the test was 900 s. Time taken for completion of the entire test was 750 s. It was seen that on an average 86 % of subjects pressed the correct keys to represent the target alphabet. In case of the letters a and b, both types of subjects showed 100% success. In case of the letter s blind participants showed 76 % success, while normal showed 68 %. The reason may be because of dot number five being mispressed by several subjects. In the case of the letter g, normal subjects showed 96 % accuracy while the blind showed only 92 %. The overall impression from this experiment was that the subjects a good sense of key pressing and that in the absence of trainer; they can use the developed system to learn alphabets through touch and feel. This experiment was validated through a tool known as a confusion matrix. Item analysis was also conducted to understand the degree of ease of perception using the developed model.

4 Result and discussion

In the identification test, a correctly identified letter was marked as 1 and others as 0. The values obtained through identification for blind subjects and normal subjects have a very small difference, indicating that participants have a similar experienced in terms of touch and feel. An average of 23 subjects from each group identified alphabets with 93% accuracy. Alphabets a, b, g were correctly identified by all of the participants, while alphabet t was identified by the least number of participants. An average of 9 alphabets are identified by 13 blind and 14 normal subjects. The average time taken to read 10 alphabets was 16 s for blind subjects and 15 s for normal subjects. The reading rate was found to be 10 char/16 s. Overall reading accuracy was 93.9 % for blind subjects and 94.74 % for normal subjects it is listed in Table 5. The reading rate was recorded as 1 char/1.6 s for blind subjects and 1 char/1.5 s for normal subjects. Although the reading rate was higher than the target rate, the reason for that was found to be the excessive closeness of tactile pins. The error rates recorded were 6.1 % for blind subjects and 5.26 % for normal subjects.

The recognition time taken was 798 s for all of the blind subjects combined and 764 s for all of the normal subjects combined. The average time taken to recognize 10 alphabets using developed tactile display was 40 s for 25 blind subjects 38 s for 25 normal subjects. For both types of subjects, the minimum recorded time to recognize 1 alphabet was 28 s and the minimum 10 alphabets with the developed display was 12 s. The overall impression of the experiment was that there is very little difference in the recognition rate and reading rate. It indicates that some subjects may learn at a slower pace than the others and that some alphabets have fast perception while others require more time. In the experiment, an average reading or recognition time for 10 alphabets or 25 subjects was noted to be 1.6 s.

Some subjects faced trouble in forming letters t and s by pressing keys due to the difference of one dot in the representations. They were unable to differentiate between keys and hence, pressed them an incorrect manner. Interaction with the subjects revealed that key pressing and then immediately reading may have led to some amount of confusion. There were two letters and b which were most correctly represented because they are consecutive and they involves less number of key pressing combinations. It was also observed that the distance between the keys during pressing and then the distance between the tactile pins significant affect accuracy. On an average, 8 alphabets were correctly presented by both types of participants. The accuracy calculated for key pressing sense was 86.6 % for blind subjects and 85.2% normal subjects. The accuracy target was set to 90%. A major observation was that the distance between push buttons (keys)reduced accuracy. Subjects were allowed only one attempt to form the desired alphabet. Recognition accuracy rates reported by previous developers for tactile displays varies from 60% to 90%; 60% by [9], 80.83% by [5],85% by[28], and 90% by [7]. The proposed work has achieved a rate of 95.7%. To confirm achieved results two statistical techniques were used to analyze the data collected from these experiments.

- Confusion matrix technique
- Item analysis

4.1 Confusion matrix

Confusion matrix technique was applied to the collected data. Table 6 shows the presented patterns in rows and the answers given by subjects in the columns. Diagonal values are the responses of the subjects. The matrix shows that a, b, g was presented to 50 subjects and all of them recognized them correctly. Alphabet e was presented to 50 participants out of which 43 identified it as l and 7 unexpectedly identified a letter; that was not listed in the test set. Alphabet l was presented to 50 participants and 3 out of them identified it as v. Similarly, alphabet s was presented to all participants and 6 out of them identified it as t. Alphabet t was presented to all participants and 10 out of them identified it as s. Alphabet v was presented to all participants; 4 out of them identified it as l. Alphabet y is presented to all participants; 2 out of them identified it as z. Alphabet z is presented to all participants 3 out of them identified it as y.

The total 500 response were recorded as shown in Table 6. It shows the accuracy of 93 %. Misprediction is measured. The calculations show that mis-prediction was 7%. This may be because the distance between pins is not as per suggestions were given by psychological experiments in [30]. The accuracy was high even though it was not par with Braille standards. This was because most of the subjects had been reading and writing Braille for more than 5 years [7]. The time required needs to be reduced further aligning the design with international Braille standards.

Table 5: Comparison of performance parameters for blind and normal subjects.

Parameter	Blind	normal
Identification accuracy(%)	94	95
Reading rate (char per second)	1/1.6	1/1.5
Average reading Time(s)	16	15
Average recognition Time(s)	40	38
Key Pressing Accuracy (%)	86.6	85.2

Table 6: Confusion matrix: letters presented in rows and prediction in columns.

	Answers received											
		a	b	e	g	l	s	t	v	y	z	Total
	a	50	0[a]	0	0	0	0	0	0	0	0	50
Presented	b	0	50	0	0	0	0	0	0	0	0	50
	e	0	0	43	0	0	0	0	0	0	0	43
	g	0	0	0	50	0	0	0	0	0	0	50
	l	0	0	0	0	47	0	0	3	0	0	50
	s	0	0	0	0	0	44	6	0	0	0	50
	t	0	0	0	0	0	10	40	0	0	0	50
	v	0	0	0	0	4	0	0	46	0	0	50
	y	0	0	0	0	0	0	0	0	48	2	50
	z	0	0	0	0	0	0	0	0	3	47	50
	Total	50	50	43	50	51	54	46	49	51	49	493

4.2 Facilitation and descrimination analysis

Item analysis is a statistical method of judging the quality of an individual's discrimination power. It also yields the relationship of each item with the other items. Kelly T. L. proposed the technique to evaluate the facilitation value and discrimination index for a given data set [31]. The facilitation value (F_V) is a measure of ease of perception? In this experiment, it indicates how easy it is to rightly identify a presented letter on a tactile display. A discrimination index (D_I) indicates how well differentiating among different values? In our case, it is a measure of how well it discriminates amongst letters and dot positions.

$$F_V = \frac{(R_U + R_L)}{(2 \times n \times max\ marks)} \quad (1)$$

$$D_I = \frac{(R_U - R_L)}{(n \times max\ marks)} \quad (2)$$

The given data set was arranged in descending order of marks obtained in the perception test. To calculate F_V and D_I the number of right and wrong answers are taken into account. According to [31] 27% of the subjects are selected for the upper right (R_U) answers segment and lower right (R_L) answers segment of the group of subjects. There were 50 participants in total. Hence, 14 subjects were each from the top and the bottom of the list in descending order of total marks respectively called R_U and R_L. In the test, each correct answer gave one mark, with 10 letters presented, the maximum possible score was 10. The sum of R_U marks is 140 and the sum of R_L marks 114 as reported in Table 7.

Table 7: Mark obtained during identification test ordered from high to low.

Upper right answer		Lower right answer	
Subject no.	Marks	Subject no.	Marks
5	10	33	9
7	10	34	9
8	10	36	9
11	10	38	9
13	10	43	9
17	10	48	9
18	10	2	8
19	10	6	8
20	10	14	8
21	10	44	8
22	10	46	8
23	10	10	7
24	10	12	7
26	10	27	6
Total	140	Total	114

Facilitation value is calculated as per Eq.1, and discrimination index is calculated as per Eq.2, where n indicates the number of participants.

Table 8: Comparison with previously developed systems (NR:represents not reported).

Parameter (unit)	[5]	[29]	[28]	[18]	proposed work
Display Size(mm)	$12 \times 12 \times 12$	6.4×8.7	$15 \times 15 \times 15$	40×40	$15 \times 30 \times 30$
Cell size	3×3	8×1	3×2	NR[a]	3×2
Stroke or displacement (mm)	1	1	NR	NR	4
Type of actuator	Piezo	Piezo	SMA wire	Solenoid	Solenoid
Force (N)	0.2	NR	NR	NR	1
Operating Frequency (Hz)	0-5	200	100	NR	0.2 to 5
Weight(gm)	2.5	NR	NR	NR	150
Reading Accuracy (%)	80.83	90.0	85	NR	94
Duration of trial (s)	5.5	300-600	10	NR	750
Presented alphabet\numbers	0 to 9 Numbers	NR	10 Alphabets	NR	10 Alphabets
Power per cell(W)	NR	NR	0.08	2	1.6

$F_V = 0.94$ (Ideal value =1 and desired value is between 0.2 and 0.85[31]) and $D_I = 0.11$ (Ideal value=0 and desired value is between 0.3 and 0.65). Thus, F_V quite high and discrimination index is well within desired range.

5 Summary

A detailed comparative for parametric analysis is carried out for the proposed work in this paper and displays implemented by [5], [18], [28], [29] in terms of dimensions, mechanical considerations, and performance parameters and reported in Table 8. It shows that displacement is highest in comparison with literature and power consumption is least. These displays were designed in a similar line. It was found that the proposed display is efficient in presenting alphabets, and has shown the best discrimination in identifying characters within a small duration. The system is capable of facilitating the need for intended users. The duration of the trial was long because it was the first tactile experience for the users. It was learnt that training is required for the first use. To overcome this issue the proposed prototype was evaluated and experimented to assess every minute parameter.

6 Conclusion

In this paper, a prototype module for the novel 3 x 2 tactile display using 6 solenoid actuators was designed, implemented and evaluated. The extensive psychological experiments carried out show that the accuracy is 93 % for the selected random alphabets. The reading time is 10 char per 16 seconds, and the recognition time is 31 s. The average reading time is about 15.7 s the average recognition time achieved is 39.3 seconds. Facilitation value of the developed display is 94%, which is close to the desired value. The discrimination index is low, suggesting that the developed display has good discrimination amongst various characters identification tactile systems. The cost of the developed system is approximately $22.Obtained results confirmed the superior performance of proposed display as compared to existing displays.

Conflict of Interest The authors declare no conflict of interest.

Acknowledgement(s) This work was supported by the Board of Colleges and University Development (BCUD, Savitribai Phule Pune University (SPPU), Pune, India (Proposal number 15ENG001916). Special thanks to Management and principal of The Poona School and home for blind girls, Kothrude, Pune, and Maharashtra for conducting the test in the school.

References

[1] Taylor PM., Moser A., Creed A., "A sixty-four element tactile display using shape memory alloy wires" Elsevier Displays., 18(3,163–168, 1998.doi.org/10.1016/S0141-9382(98)00017-1

[2] Pruittikorn smithmaitrie, Jinda Kanjantoe, Pichaya Tandayya, "Touching force response of piezoelectric Braille cell" Disability and Rehabilitation: Assistive technology, 6,360365,2008. doi.org/10.1080/17483100802281442

[3] Velazquez Ramiro, Hermes Hernandez, Enrique Preza, "A portable eBook reader for the blind" 32nd Annual International Conference of IEEE Engineering in Medicine and Biology Society (EMBS), Buenos Aires, Argentina, Sep 2010. DOI: 10.1109/IEMBS.2010.5626218

[4] Ang Beng Seng, Zuraini Dahari, Othman Sidek, "Design and analysis of thermal microactuator". European Journal of Scientific Research., 35(2), 281–292, 2009.

[5] Kyung Ki-Uk, Jun-Young Lee, Junseok Park "Design and applications of a pen-like haptic interface with texture and vibrotactile display" Frontiers in the Convergence of Bioscience and Information Technologies, FBIT 2007(IEEE), Jeju Island, Korea, 2007. DOI: 10.1109/FBIT.2007.92

[6] Wu X., Zhu H., Kim S H. Mark A., "A portable pneumatically-actuated refreshable braille cell". IEEE Conference on Solid-State Sensors, Actuators, and Microsystems (TRANSDUCERS 2007), Lyon, France, Jun 2007. DOI: 10.1109/SENSOR.2007.4300407

[7] Kyung Ki-Uk, Minseung Ahn, Dong-soo Kwon,Shrinivasan M. A., "A compact planar distributed tactile display and effects of frequency on texture judgment" Advanced Robotics,20(5),563–580, 2006. doi.org/10.1163/156855306776985540

[8] Takamiya Makoto, Tsuyoshi Sekitani, Yusaku Kato, Hiroshi Kawaguchi, Takao Someya, Takayasu Sakurai. "Low power and flexible braille sheet display with organic FET's and plastic actuators", International Conference On IC Design and Technology (ICICDT'06) IEEE, Padova, Italy, May2006. DOI: 10.1109/ICICDT.2006.220831

[9] Choi H R, Lee S W, lung K M, Koo I C,Lee S I,Choi H G,,Jeon J W,Nam J D, "Tactile display as a braille display for the visually disabled" Proceedings IEEE/RSJ International conference on Intelligent Robots and Systems (IROS 2004),Sendal, Japan,nSep 2004. DOI: 10.1109/IROS.2004.1389689

[10] Matsunaga T, Totsu K, Esashi M, Haga Y., "2-D and 3-D tactile pin display using SMA micro-coil actuator and magnetic latch", The 13th International Conference on Solid-State Sensors, Actuators, and Microsystems, Digest of Technical Papers (TRANSDUCERS'05 IEEE),Seoul, South Korea, June 2005. DOI: 10.1109/SENSOR.2005.1496422

[11] Wagner Christopher R, Susan J Lederman, Robert D Howe, "A tactile shape display using RC servo motors", IEEE Proceedings of 10th Symposium on Haptic Interfaces for Virtual Environment and Teleoperator Systems,(HAPTICS, 2002), Orlando, FL, USA, March 2002. DOI: 10.1109/HAPTIC.2002.998981

[12] Konyo Masashi, Satoshi Tadokoro, Toshi Takamori, "Artificial tactile feel display using soft gel actuators", Proceedings of IEEE international conference on Robotics and Automation, (ICRA'00), San Francisco, CA, Apr 2000. DOI: 10.1109/ROBOT.2000.845250

[13] Smithmaitrie Pruittikorn, Jinda Kanantoe P., "Analysis and design of Piezoelectric Braille display", Rehabilitation Engineering, InTech, 2009. Available from: https://www.intechopen.com

[14] Velazquez R, Pissaloux E, Szewczyk,Hafez M., "Miniature shape memory alloy actuator for tactile binary information display", Proceedings of IEEE International Conference on Robotics and Automation,ICRA 2005, Barcelona, Spain, Apr 2005, DOI: 10.1109/ROBOT.2005.1570302.

[15] Mosley M, Constantinos Mavroidis, Charles Pfeiffer, "Design and dynamics of a shape memory alloy wire bundle actuator",Proceedings of the ANS, 8th Topical Meeting on Robotics and Remote Systems,Mar 1999. DOI:10.1.1.41.4629

[16] Lee Jun Su, Stepan Lucyszyn, "A micromachined refreshable Braille cell", Journal of Microelectromechanical Systems, 14(4),673–682, 2005. DOI: 10.1109/JMEMS.2005.845415

[17] Nobels Tiene, Frank Allemeersch, Kay Hameyer, "Design of a high power density electromagnetic actuator for a portable Braille display", Proceedings of 10th international power electronics & motion control conference, EPE-PEMC, 2002.

[18] Sarah F Frisken Gibson, Paul Bach Y Rita, Willis J TOMPKINS,John G Webster, "A 64-solenoid, four-level fingertip search display for the blind", IEEE Transactions on Biomedical Engineering (BME), 34(12),963–965, 1987. DOI: 10.1109/TBME.1987.325937

[19] Deng Kai, Eniko T Enikov, P Marek, "A shape display method based on electromagnetic localization and actuation,PIERS Online,26(2),157–160, 2010.

[20] Francesca Sorgini, Renato Calio, Maria Chiara Carrozza,Calogero Maria Oddo, "Haptic-assitive technologies for audition and vision sensory disabilities",Haptic-assitive technologies for audition and vision sensory disabilities, Disability and rehabilitation: Assistive technology; 2017. DOI: 10.1080/17483107.2017.1385100.

[21] Dominic R Labbe, Guy Santerre, Sabastien McKenzie Faucher et a.l . US patent no.9,965,974 B2.Drummonville(Quebec), CA, 2018.

[22] Shyam Shah.(2018).US patent no. US2018/0033336A1, Ahemadabad, India.

[23] Luzhnica G, Veas E., "Investigating Interactions for Text Recognition Using a Vibrotactile Wearable Display",In 23rd International Conference on Intelligent User Interfaces ACM,453-465,Tokyo, Japan, 2018. DOI:10.1145/3172944.3172951

[24] Leonardis D, Loconsole C.,"Braille cursor: An innovative and affordable refreshable braille display designed for inclusion", In 10th International Conference on Applied Human Factors and Ergonomics Springer, 302-311,Washington DC, USA, Jul 2019. DOI:10.1007/978-3-319-94622-129.

[25] Lu Zhiyun, "Fabricating One Cell of Refreshable Braille Display Using New Bistable Electroactive polymers. MS Theses University of california; 2017; Los Angeles.

[26] V B Vaijapurkar, Y Ravinder, "A survey on recent trends and technologies in tactile interfaces with sensing perspective",Proceedings of annual IEEE India Conference (INDICON 2015),New Delhi, India, Dec 2015. DOI: 10.1109/INDICON.2015.7443158

[27] Sara Demain, Cheryl D Metcalf, Geoff Merrett V, Deyi Zheng, Sarah Cunningham, "A narrative review on haptic devices: relating the physiology and psychophysical properties of the hand to devices for rehabilitation in central nervous system disorders", Disability and Rehabilitation: Assistive Technology, 8(3),181–189, 2013.Doi/abs/10.3109/17483107

[28] Feng Zhao, Changan Jiang, Hideyuki Sawada, "A novel Braille display using the vibration of SMA wires and the valuation of Braille presentations", Journal of Biomechanical Science and Engineering Japan,7(4),416–432, 2012. https://doi.org/10.1299/jbse.7.416

[29] Joseph Luk, Jerome Pasquero, Shanon little,MacLean Karon, Lvesque Vincent,Hayward Vincent, "A role for haptics in mobile interaction: initial design using a handheld tactile display prototype", Proceedings of CHI 2006 conference on Human Factors in computing systems ACM,22-27, Montreal, Canada,2006 Apr. DOI:1124772.1124800

[30] Kenneth O Johnson, John R Phillips, "Tactile spatial resolution-I, two-point discrimination, gap detection, grating resolution, and letter recognition",Journal of Neurophysiology, 46(6),1177–1192, 1981. DOI:abs/10.1152/jn.1981.46.6.1177

[31] Kelly T L., "The selection of upper and lower groups for the validation of test terms", Journal of Educational psychology, 46(6),1981. Doi=10.1037%2Fh0057123

ASTES

Advances in Science, Technology and Engineering Systems Journal Vol. 4, No. 4, 12-20 (2019)

www.astesj.com

ASTESJ

ISSN: 2415-6698

Permutation Methods for Chow Test Analysis an Alternative for Detecting Structural Break in Linear Models

Aronu, Charles Okechukwu[1,*], Nworuh, Godwin Emeka[2]

[1]*Chukwuemeka Odumegwu Ojukwu University (COOU), Department of Statistics, Uli, Campus, 431124, Nigeria*

[2]*Federal University of Technology Owerri (FUTO), Department of Statistics,460114, Nigeria*

ARTICLE INFO

Article history:
Received:22 February, 2019
Accepted:19 June, 2019
Online: 09 July, 2019

Keywords:
Chow Test
Economic Growth
Structural Break
Permutation Method

ABSTRACT

This study examined the performance of two proposed permutation methods for Chow test analysis and the Milek permutation method for testing structural break in linear models. The proposed permutation methods are: (1) permute object of dependent variable and (2) permute object of the predicted dependent variable. Simulation from gamma distribution and standard normal distribution were used to evaluate the performance of the methods. Also, secondary data were used to illustrate a real-life application of the methods. The findings of the study showed that method 1(permute object of dependent variable) and Method2 (permute object of the predicted dependent variable) performed better than the traditional Chow test analysis while the Chow test analysis was found to perform better than the Milek permutation for structural break. The methods were used to test whether the introduction of Nigeria Electricity Regulatory Commission (NERC) in the year 2005 has significant impact on economic growth in Nigeria. The result revealed that all the methods were able to detect presence of structural break at break point 2005. Also, the methods were used to test for structural break at January, 2015 for monthly reported cases of appendicitis in Nigeria. Result revealed that all the methods were able to detect presence of structural break at break point January, 2015.

1. Introduction

Detection of structural changes in economics has often pose a long standing problem in econometrics [1]. However, most existing tests are designed for structural breaks. Some researchers argued that it's un-likely that a structural break could be immediate and might seem more reasonable to allow a structural change to take a period of time to take effect. Hence, the technological progress, preference change, and policy switch are some leading driving forces of structural changes that usually exhibit evolutionary changes in the long term.

Structural break examines a shift in the parameters of the model of interest. However, when the conditional relationship between the dependent and explanatory variables contains a structural break, estimates of model coefficients will be inaccurate across different regimes [2]. As such, estimations that do not account for structural breaks will be biased and inconsistent.

According to [3], one of the traditional methods of detecting structural break is the Chow test analysis. The Chow test as a method of detecting structural break has the ability of testing for equality of sets of coefficients in two regression models. In this situation, part of the maintained hypothesis of the test is that the error variances will be the same for the two regressions. If this is not the situation, then the Chow test may be misleading and this can result to a situation where by the true size of the test (under the null hypothesis) may not be equal to the prescribed alpha-level. Due to problem like this, the present study will be proposing permutation methods for Chow test analysis for detecting structural break in a linear model.

The permutation test evaluates the probability of getting a value equal to or more extreme than an observed value of a test statistic under a specified null hypothesis. This is achieved by recalculating the test statistic after random shuffling of the data labels. Such tests are computationally intensive and the use of these tests never receive much attention in the natural and behavioral sciences until the emergence of widely accessible fast

*Charles Aronu, Email: amaro4baya@yahoo.com

computer. The basic idea behind permutation methods is to generate a reference distribution by recalculating a statistic for many permutations of the data.

Permutation methods have been found very useful because of their flexibility, distribution-free nature and intuitive formulation, which makes it easy to communicate the general principles of such test procedures to users.

One advantage of the permutation tests over their parametric counterparts is their solid foundations. This is because the validity of the parametric tests relies on random sampling while the permutation tests have their justification on the idea of random allocation of experimental units, with no reference to any underlying population[4, 5].

For researchers in the area of econometrics and users of the traditional Chow test, the most convincing reason to choose the proposed permutation methods for Chow test in determining structural break in linear models is because of the exactness of the p-value obtained using the permutation methods for Chow test instead of the approximated/asymptotic significant value which is often obtained in other methods. Hence, the permutation method yields a more accurate prediction of how random a given result can be [6-7].

The objectives of this study is to compare the performance of the proposed permutation methods for Chow test analysis against the traditional Chow test and the Milek permutation method for detecting structural break for the Gamma and Standard Normal distribution.

2. Literature Review

In [8], permutation test was defined as a type of non-parametric randomization test in which the null distribution of a test statistic is estimated by randomly permuting the class labels of the observations.

According to [9], permutation tests for linear model have applications in behavioral studies especially in situations where traditional parametric assumptions about the error term in a linear model are not tenable. In such situations, an improved validity of type I error rates can be achieved with properly constructed permutation tests. More importantly, increased statistical power, improved robustness to effects of outliers, and detection of alternative distributional differences can be achieved by coupling permutation inference with alternative linear model estimators.

In [10], authors explored the framework of permutation-based p-values for assessing the performance of classifiers. Their study examined two simple permutation tests, the first test which assess whether the classifier has found a real class structure in the data where the corresponding null distribution is estimated by permuting the observations in the data and the second test which examines whether the classifier is exploiting the dependency between the features in classification. They observed that the tests can serve to identify descriptive features which can serve as valuable information in improving the classifier performance. The findings of their study revealed that studying the classifier performance through permutation tests is effective. In particular, the restricted permutation test clearly reveals whether the classifier exploits the interdependency between the features in the data.

According [11], permutation test require very few assumptions about the data and can be applied to a wider variety of situations than the parametric counterpart. However, only few of the most common parametric assumptions need to hold for non-parametric test to be valid. The assumptions that are avoided include, the need for normality for the error terms, the need of homoscedasticity and the need for random sampling. With a very basic knowledge of sample properties or of the study design, errors can be treated as exchangeable and/or independent and symmetric and inferences that are not possible with parametric methods can become feasible.

According to [12], permutation tests for structural change from the framework of [13] cannot only be derived for the simple location model but for both the nonparametric and parametric (model-based) permutation tests. Literally, they found that exchangeability of the errors might be a too strong assumption in time series applications where the dependence structure of the observations cannot be fully captured within the model. Although there are time series applications where the errors are not correlated, this assumption impedes the application of permutation methods to many other models of interest.

In [14], author assessed the performance of his permutation for structural break alongside the Chow test, the Nyblom-Hansen test and CUSUM which were all used to detect structural changes in time series. The proposed Milek permutation method was used to detect a trend especially in process control and detection of changes in the average value. The result of the study showed that the proposed method was effective especially in the case of small structural changes.

3. Material and Methods

3.1. *Method of Data Collection*

The source of data used for this study were simulation from the Gamma distribution and the Standard Normal distribution for sample size 15, 20, 25, 30, 40, 50, 60, 70, 80, 90 and 100. Secondary data collected from the National Bureau of Statistics and Central Bank of Nigeria (CBN) statistical bulletin on Real GDP and Electricity net generation in Nigeria was used to illustrate the methods. Also, secondary data on monthly reported cases of appendicitis were collected from the records of patients at Federal Hospital Kaura-Namoda, Zamfara State, Nigeria.

3.2. *Chow Test*

The Chow test is often used to determine whether there exist different subgroups in a population of interest. The single/full model of a Chow test is written as:

$$Y_t = X_t \beta + \varepsilon_t \quad (1)$$

where,

Y_t : is nx1 random vector called the response

β : is (k+1) x 1 vector of unknown parameters .

X_t : is n x (k+1) matrix of scalars

Recall that to estimate the regression parameters β properly using the least-squares estimation, the assumption that n > p holds and X is of full rank. Here n is the number of observation while p is the number of regression coefficients.

The null hypothesis, tested by Chow, states that two disjoint models with the sum of squares residual is:

$$Y_{1t} = X_{1t}\,\beta_1 + \varepsilon_{1t} \tag{2}$$

$$Y_{2t} = X_{2t}\,\beta_2 + \varepsilon_{2t} \tag{3}$$

where,

Y_{1t} and Y_{2t} : represents the random variable called the response or dependent variable for the first group and second group respectively.

β_1 and β_2 : represents constants or parameters whose exact value are not known and thus must be estimated from the experimental data for the first group and second group respectively.

X_{1t} and X_{2t} : represents the mathematical variable called regressor or covariate or predictor independent non-random variable whose value are controlled or at least accurately observed by the experimenter for the first group and second group respectively.

This suggest that model (2) applies before the break at time t, while model (3) applies after the structural break.

The Chow test asserts that $\beta_1 = \beta_{1t}$ and $\beta_2 = \beta_{2t}$ with the assumption that the model errors ε_t are independent and identically distributed from a normal distribution with unknown variance [15]. The Chow test basically tests whether the single regression line or the two separate regression lines fit the data best.

Taking advantage of the various F-test [16, 17], to test for presence of structural break in a given set of data, a special and useful application of the F test procedure is found in the Chow test statistic. We must understand that a structural break is when the coefficients of the model change with respect to a time parameter for the Chow test.

Suppose we consider a simple case of (1), that is a simple linear model with one independent variable;

$$Y_t = \beta_0 + \beta_1 x_t + \varepsilon_t \tag{4}$$

Y_t : is the response variable

β_0 : is the intercept and β_1 the slope

x_t : represents the independent variable

The corresponding two disjoint models as required by the Chow test are given as:

$$Y_{1t_b} = \beta_{01} + \beta_{11} x_{1t_b} + \varepsilon_{1t_b} \tag{5}$$

$$Y_{2t_a} = \beta_{02} + \beta_{12} x_{2t_a} + \varepsilon_{2t_a} \tag{6}$$

where,

t_a: represents the time at break point and $t_b = t_a - 1$, Y_{1t_b} and Y_{2t_a} : represents the dependent variables for the two disjoint models ($Y_{1t_b}, Y_{2t_a} \in Y_t$), β_{01} and β_{02} : represents the intercepts for the two disjoint models ($\beta_{01}, \beta_{02} \in \beta_0$), β_{11} and β_{12} : represents the slopes for the two disjoint models ($\beta_{11}, \beta_{12} \in \beta_1$), ε_{1t_b} and ε_{2t_a} : represents the random error for the two disjoint models ($\varepsilon_{1t_b}, \varepsilon_{2t_a} \in \varepsilon_t$), and x_{1t_b} and x_{2t_a} : represents the independent variables for the two disjoint models ($x_{1ta}, x_{2tb} \in x_t$).

Recall that the residual sum of squares for the full model can be denoted as RSS_T,

$$RSS_T = \sum_{t=1}^{T} \left(y_t - \hat{y}_t\right)^2 \tag{7}$$

The residual sum of squares for the two disjoint models are

$$RSS_1 = \sum_{t=1}^{t_b} \left(y_t - \hat{y}_t\right)^2 \tag{8}$$

$$RSS_2 = \sum_{t_a=1}^{T} \left(y_t - \hat{y}_t\right)^2 \tag{9}$$

Hence, the corresponding F-test is written as

$$F = \frac{\left(\sum_{t=1}^{T}\left(y_t - \hat{y}_t\right)^2 - \left(\sum_{t=1}^{t_b}\left(y_t - \hat{y}_t\right)^2 + \sum_{t_a=1}^{T}\left(y_t - \hat{y}_t\right)^2\right)\right) \Big/ k}{\left(\sum_{t=1}^{t_b}\left(y_t - \hat{y}_t\right)^2 + \sum_{t_a=1}^{T}\left(y_t - \hat{y}_t\right)^2\right) \Big/ (n_1 + n_2 - 2k)} \tag{10}$$

Thus, the general Chow test statistics in matrix form is given as

$$F = \frac{\left((Y_t'Y_t - Y_t'X_t(X_t'X_t)^{-1}X_t'Y_t - ((Y_{1t}'Y_{1t_b} - Y_{1t_b}'X_{1t_b}(X_{1t_b}'X_{1t_b})^{-1}X_{1t_b}'Y_{1t_b}) + (Y_{2t_a}'Y_{2t_a} - Y_{2t_a}'X_{2t_a}(X_{2t_a}'X_{2t_a})^{-1}X_{2t_a}'Y_{2t_a}))\right) \Big/ k}{\left((Y_{1t}'Y_{1t_b} - Y_{1t_b}'X_{1t_b}(X_{1t_b}'X_{1t_b})^{-1}X_{1t_b}'Y_{1t_b}) + (Y_{2t_a}'Y_{2t_a} - Y_{2t_a}'X_{2t_a}(X_{2t_a}'X_{2t_a})^{-1}X_{2t_a}'Y_{2t_a})\right) \Big/ (n_1 + n_2 - 2k)} \tag{11}$$

Substituting,

$$RSS_T = Y_t'Y_t - Y_t'X_t(X_t'X_t)^{-1}X_t'Y_t$$

$$RSS_1 = Y_{1t_b}'Y_{1t_b} - Y_{1t_b}'X_{1t_b}(X_{1t_b}'X_{1t_b})^{-1}X_{1t_b}'Y_{1t_b}$$

$$RSS_2 = Y'_{2t_a} Y_{2t_a} - Y'_{2t_a} X_{2t_a} (X'_{2t_a} X_{2t_a})^{-1} X'_{2t_a} Y_{2t_a}$$

Then, (10) will become

$$F = \frac{(RSS_T - (RSS_1 + RSS_2))/k}{(RSS_1 + RSS_2)/(n_1 + n_2 - 2k)} \approx F(k, n_1 + n_2 - 2k) \qquad (12)$$

where,

RSS_T: represents the residual sum of squares for the full model

RSS_1: represents the residual sum of squares for the first sub sample or first reduced model

RSS_2: represents the residual of the second sub sample or second reduced model,

k: is the number of parameters,

n_1 and n_2: represents the length of the two subsamples.

3.3. *Procedure for Running the Chow Test*

The stages of running the chow test analysis are as follows:

1. Firstly, run the regression using all the data, before and after the structural break. Collect the sum of squares residual for error RSS_T.
2. Run two separate regression on the data before and after the structural break, collecting the RSS in both cases, giving RSS_1 and RSS_2.
3. Using the three values, calculate the test statistic using (12)
4. Find the critical values in the F-test tables, which has F(k, $n_1 + n_2$ -2k) degrees of freedom, where k is the number of regressors
5. Take decision and conclude appropriately. The null hypothesis state that there is no structural break against the alternative hypothesis which state that there exist structural break.

Decision Rule

H_0 will be rejected at the significance level α if

$$F \geq F(k, n_1 + n_2 - 2k)$$

The other criterion equivalent to the decision rule above is to compare the p-value for F-statistics with α and reject H_0 if

$$\Pr(F) \leq \alpha$$

where P(F) is the asymptotic p-value and note that the rejection of $H_0 : \beta_1 = 0$ would mean that β_1 is likely to be different from 0.

A parametric test of significance of the Chow test can be carried out using an F-statistic under the assumption of normality. If this condition is not met, a permutation method becomes an alternative to perform the test. Under normality, one expects a permutation test to produce approximately the same results as the parametric F-test. So, the parametric F-test will be used as a reference to assess some important properties of the various permutation methods proposed in this study.

3.4. *The Proposed Permutation Methods for Chow Test*

The proposed permutation methods considered in this study include:

1. Permute object of dependent variable Y_t
2. Permute object of predicted dependent variable $\hat{Y}_t$

3.4. 1. Method 1: Permute object of dependent variable Y_t

This method considers a situation where we permute the dependent variable Y_t in (4). For the permutation of Y_t we shall substitute $Y_t^* = Y_t$ to obtain (10) for the simple linear model situation while other variables remain unchanged (Y_t^* represents the permutated dependent variable of the full model) . The F-test statistic for the permutation of the object of dependent variable for the simple linear model is given as

$$F^* = \frac{\left(\sum_{t=1}^{T} \left(y_t^* - \hat{y}_t\right)^2 - \left(\sum_{t=1}^{t_b} \left(y_t - \hat{y}_t\right)^2 + \sum_{t_a=1}^{T} \left(y_t - \hat{y}_t\right)^2 \right) \right) \Big/ k}{\left(\sum_{t=1}^{t_b} \left(y_t - \hat{y}_t\right)^2 + \sum_{t_a=1}^{T} \left(y_t - \hat{y}_t\right)^2 \right) \Big/ (n_1 + n_2 - 2k)} \qquad (13)$$

where,

y_t^* represents the permuted variable while other variables remain the same.

The matrix equivalence of (13) is given by (14)

$$F^* = \frac{\left((Y_t^{*\prime} Y_t^* - Y_t^{*\prime} X_t (X_t' X_t)^{-1} X_t' Y_t^* - ((Y'_{1t_b} Y_{1t_b} - Y'_{1t_b} X_{1t_b} (X'_{1t_b} X_{1t_b})^{-1} X'_{1t_b} Y_{1t_b}) + (Y'_{2t_a} Y_{2t_a} - Y'_{2t_a} X_{2t_a} (X'_{2t_a} X_{2t_a})^{-1} X'_{2t_a} Y_{2t_a})) \right) \Big/ k}{\left((Y'_{1t_a} Y_{1t_a} - Y'_{1t_a} X_{1t_a} (X'_{1t_a} X_{1t_a})^{-1} X'_{1t_a} Y_{1t_a}) + (Y'_{2t_b} Y_{2t_b} - Y'_{2t_b} X_{2t_b} (X'_{2t_b} X_{2t_b})^{-1} X'_{2t_b} Y_{2t_b}) \right) \Big/ (n_1 + n_2 - 2k)} \qquad (14)$$

Substituting,

$$RSS_{YT}^* = Y_t^{*\prime} Y_t^* - Y_t^{*\prime} X_t \left(X_t' X_t\right)^{-1} X_t' Y_t^*$$

$$RSS_1 = Y'_{1t_b} Y_{1t_b} - Y'_{1t_b} X_{1t_b} \left(X'_{1t_b} X_{1t_b}\right)^{-1} X'_{1t_b} Y_{1t_b}$$

$$RSS_2 = Y'_{1t_a} Y_{1t_a} - Y'_{1t_a} X_{1t_a} \left(X'_{1t_a} X_{1t_a}\right)^{-1} X'_{1t_a} Y_{1t_a}$$

Then, (14) can be simplified as

$$F^{*}=\frac{(RSS^{*}_{YT}-(RSS_{1}+RSS_{2}))/k}{(RSS_{1}+RSS_{2})/(n_{1}+n_{2}-2k)}\approx F(k,n_{1}+n_{2}-2k) \qquad (15)$$

where,

RSS^{*}_{YT} : represents the permuted residual sum of squares for the full model

RSS_{1} : represents the residual of the first sub sample or first reduced model

RSS_{2} : represents the residual of the second sub sample or second reduced model,

k: is the number of parameters,

n_1 and n_2 : represents the length of the two subsamples

t_a: represents the time at break point and $t_b = t_a - 1$

The procedure for running the permute the raw data of the dependent variable for the full model Y_t is stated as follows:

1. Compute the sum of squares residual for the single model and the sub sample as RSS_T, RSS_1 and RSS_2. Calculate the reference value of the F-statistic, F using (12).
2. Permute variable Y_t at random to obtain Y_t^{*}
3. Compute the sum of squares residual for the single model using Y_t^{*} and the sub samples to obtain RSS^{*}_{YT} , RSS_1 and RSS_2 as calculated in step 1, compute using (15).
4. Repeat step 2 and 3 large number F^{*} of times to obtain the distribution of F^{*} under permutation. Add the reference value F to the distribution.
5. For a one – tailed test involving the upper tail, calculate the probability as the proportion of values F^{*} greater than or equal to F. In the lower tail, the probability is the proportion of values F^{*} smaller than or equal to F.

3.4. 2 Method 2: Permute object of the predicted dependent variable $\hat{Y}_t$

This method considers permuting the predicted dependent variable of the full model. In this method, the object of the predicted variable will be permuted and used to obtain the corresponding residual sum of squares. We shall express this method using the simple linear model before generalizing using the matrix form. The F-test statistic for the permutation of the object of predicted dependent variable for the simple linear model is given as

$$F^{*}=\frac{\left(\sum_{t=1}^{T}\left(y_t-\hat{y}_t^{*}\right)^2-\left(\sum_{t=1}^{t_b}\left(y_t-\hat{y}_t\right)^2+\sum_{t_a=1}^{T}\left(y_t-\hat{y}_t\right)^2\right)\right)\Big/k}{\left(\sum_{t=1}^{t_b}\left(y_t-\hat{y}_t\right)^2+\sum_{t_a=1}^{T}\left(y_t-\hat{y}_t\right)^2\right)\Big/(n_1+n_2-2k)} \qquad (16)$$

where,

$\hat{y}_t^{*}$: represents the permuted predicted variable while other variables remain the same.

The matrix equivalence of (16) is given by (17)

$$F^{*}=\frac{\left((Y_t'Y_t-(Y'X_t(X_t'X_t)^{-1}X_t'Y_t)^{*}-((Y'_{1t_b}Y_{1t_b}-Y'_{1t_b}X_{1t_b}(X'_{1t_b}X_{1t_b})^{-1}X'_{1t_b}Y_{1t_b})\right.\right.}{\left.\left.+(Y'_{2t_a}Y_{2t_a}-Y'_{2t_a}X_{2t_a}(X'_{2t_a}X_{2t_a})^{-1}X'_{2t_a}Y_{2t_a}))\right)\Big/k}$$
$$\frac{\left((Y'_{1t_b}Y_{1t_b}-Y'_{1t_b}X_{1t_b}(X'_{1t_b}X_{1t_b})^{-1}X'_{1t_b}Y_{1t_b})+\right.}{\left.(Y'_{2t_a}Y_{2t_a}-Y'_{2t_a}X_{2t_a}(X'_{2t_a}X_{2t_a})^{-1}X'_{2t_a}Y_{2t_a}))\right)\Big/(n_1+n_2-2k)} \qquad (17)$$

Substituting,

$$RSS^{*}_{\hat{Y}T}=Y_t'Y_t-\left(Y'X_t(X_t'X_t)^{-1}X_t'Y_t\right)^{*}$$

$$RSS_1=Y'_{1t_b}Y_{1t_b}-Y'_{1t_b}X_{1t_b}\left(X'_{1t_b}X_{1t_b}\right)^{-1}X'_{1t_b}Y_{1t_b}$$

$$RSS_2=Y'_{1t_a}Y_{1t_a}-Y'_{1t_a}X_{1t_a}\left(X'_{1t_a}X_{1t_a}\right)^{-1}X'_{1t_a}Y_{1t_a}$$

Then, (17) can be simplified as

$$F^{*}=\frac{(RSS^{*}_{\hat{Y}T}-(RSS_1+RSS_2))/k}{(RSS_1+RSS_2)/(n_1+n_2-2k)}\approx F(k,n_1+n_2-2k) \qquad (18)$$

where,

$RSS^{*}_{\hat{Y}T}$: represents the permuted predicted residual sum of squares for the full model

RSS_1 : represents the residual of the first sub sample or first reduced model

RSS_2 represents the residual sum of squares for the second sub sample or second reduced model,

k: is the number of parameters,

n_1 and n_2: represents the length of the two subsamples

t_a: represents the time at break point and $t_b = t_a - 1$

The procedure for running the permute the predicted dependent variable for the full model $\hat{Y}_t$ is stated as follows:

1. Compute the sum of squares residual for the single model and the sub sample as RSS_T, RSS_1 and RSS_2.. Calculate the reference value of the F-statistic, F using (12).
2. Permute variable $\hat{Y}_t$ at random to obtain $\hat{Y}_t^{*}$

3. Compute the sum of squares residual for the single model using $\hat{Y}_t^*$ and the sub samples to obtain $RSS^*_{\hat{Y}T}$, RSS_1 and RSS_2 as calculated in step 1, compute F^* using (18).
4. Repeat step 2 and 3 large number of times to obtain the distribution of F^* under permutation. Add the reference value F to the distribution.
5. For a one – tailed test involving the upper tail, calculate the probability as the proportion of values F^* greater than or equal to F. In the lower tail, the probability is the proportion of values F^* smaller than or equal to F.

3.5. *Milek (2015) Permutation Method for Structural Break*

In [14], the author proposed a permutation method for structural break as

$$T = \left|b_2 - b_1\right| + \left|\frac{a_2}{a_1}\right| \tag{19}$$

where,

$$a_1 = \frac{\sum_{t=1}^{k}(t-\bar{t}_{1t})(y_t-\bar{y}_{1t})}{\sum_{t=1}^{k}(t-\bar{t}_{1t})^2}, \quad a_2 = \frac{\sum_{t=k+1}^{n}(t-\bar{t}_{2t})(y_t-\bar{y}_{2t})}{\sum_{t=k+1}^{k}(t-\bar{t}_{2t})^2},$$

$$b_1 = \bar{y}_{1t} - a_1\bar{t}_{1t}, \; b_2 = \bar{y}_{2t} - a_2\bar{t}_{2t}, \; \bar{y}_{1t} = \frac{\sum_{t=1}^{k} y_t}{k}, \; \bar{y}_{2t} = \frac{\sum_{t=k+1}^{n} y_t}{n-k},$$

$$\bar{t}_{1t} = \frac{\sum_{t=1}^{k} t}{k}, \text{ and } \bar{t}_{2t} = \frac{\sum_{t=k+1}^{n} t}{n-k}$$

The testing procedure for the permutation test to detect a structural change at time t = k is as follows as described by [14] , was presented as:

1. Establishment of the level of significance α
2. Calculate the T_0 value of statistic T based on simulated data.
3. Executing the time series permutations of N times, then calculating the value of the test statistics.
4. On the basis of the empirical distribution of the test statistics T, the asymptotic significance level (ASL) value is calculated. If ASL < α, then the hypothesis H0 is rejected, otherwise there is no basis to reject H_0. As the number of repetitions of permutations assumed N = 1000.

3.6. *Power performance of the Methods*

To determine the power of the methods in this study, data were simulated from the gamma distribution and the standard normal distribution. The null hypothesis was stated as:

H_0: There is no presence of structural break in the model or $\beta_1 = \beta_{1t}$

The power of the methods were examined using the following criteria:

1. The size of the samples n={15, 20, 25, 30, 40, 50, 60, 70, 80, 90, 100}
2. The break points were varied randomly to avoid bias
3. The significant level (α) was set at 95%
4. The permutation was set at 10, 000 permutations

The power was reported as the rate (fraction) of rejection of the null hypothesis after 200 simulations.

$$\text{Power (P)} = \frac{\text{number of rejection of } H_0(\alpha)}{\text{number of simulation (nsim)}} \tag{20}$$

The value of power is expected to fall between zero and one ($0 \le P \le 1$), and the decision rule is: the more closely the value of the power is to one, the better the method [18]. Hence, the method with its power more closely to 1 becomes the best method for detecting structural break.

Also, the average power of the methods were calculated as:

$$\text{Average Power} = \frac{\text{Sum of Power (P)}}{\text{number of sample size points}} = \frac{\sum_{i=1}^{S} P_i}{S} \tag{21}$$

where the number of sample size points, S= 1, 2, ..., 11

Also, simple bar chart was used to express the visualization of the average power of the methods, where the method with the highest bar is considered the best method. Thereby, the height of the bar determines the magnitude or performance of the methods.

3.7. *Data Presentation*

Table 1: Summary of Annual Real Gross Domestic Product and Electricity Net Generation from 1989-2015

Year	RGDP("B" N)	ENG ("B" kwh)	Year	RGDP ("B" N)	ENG ("B" kwh)
1989	236.7	12.251	2003	477.5	19.352
1990	267.5	12.029	2004	527.6	23.171
1991	265.4	13.613	2005	561.9	22.524
1992	271.4	14.247	2006	595.8	22.109
1993	274.8	13.913	2007	634.3	21.922
1994	275.5	14.877	2008	672.2	22.680
1995	281.4	13.889	2009	716.9	22.879
1996	293.7	14.367	2010	775.3	23.143
1997	302	14.697	2011	884	27.522
1998	310.9	14.732	2012	888.9	29.240
1999	312.2	15.432	2013	950.1	29.538
2000	329.2	14.131	2014	955.2	29.697
2001	357	14.837	2015	536.68	34.65
2002	433.2	19.953			

Source: Central Bank of Nigeria Statistical Bulletin and National Bureau of Statistics Annual Abstract of Statistics for various years

Key: RGDP = Real Gross Domestic Product in billions of Naira and ENG=Electricity Net Generation in billion Kilo Watt per hour

Table 2: Number of Monthly Reported Appendicitis cases for the period of 2011 to 2017

MONTHS	YEARS						
	2011	2012	2013	2014	2015	2016	2017
January	7	8	4	8	5	4	2
February	4	6	5	6	4	3	3
March	7	8	3	4	3	2	1
April	9	4	6	5	2	4	2
May	5	9	4	4	4	5	1
June	3	7	5	2	5	0	1
July	9	9	1	7	5	3	1
August	6	9	4	5	3	5	3
September	7	7	5	5	0	3	2
October	6	5	6	4	5	1	3
November	9	8	7	7	4	2	2
December	6	4	6	3	6	3	1
Total	78	84	56	60	46	35	22

Source: Federal Hospital Kaura-Namoda, Zamfara State, Nigeria, 2018

4. Data Analysis and Result

In this section, the result of simulation was obtained for the various methods discussed in the previous section. Also, result of the real life application of the methods were equally presented in this section. The data analysis was done using computer program written in R.

4.1. Result of Data Analysis for Gamma Distribution

This section presents the power of the various methods using data generated from the gamma distribution at α=0.05.

Table 3: Performance of the methods for Gamma Distribution

Sample Size / Methods	Chow	Method1	Method2	Milek (2015)
15	0.42	0.8	0.56	0.04
20	0.44	0.84	0.56	0.04
25	0.68	0.9	0.58	0.04
30	0.7	0.9	0.66	0.06
40	0.82	0.94	0.72	0.06
50	0.84	0.96	0.82	0.06
60	0.84	0.96	0.86	0.06
70	0.9	0.96	0.88	0.08
80	0.9	0.96	0.88	0.08
90	0.94	0.96	0.88	0.08
100	0.94	0.97	0.9	0.14
Average Power	0.77	0.92	0.75	0.07
Rank	2	1	3	4

4.2. Result of Data Analysis for Standard Normal Distribution

This section presents the power of the various methods using data generated from the standard normal distribution at α=0.05.

Table 4: Performance of the methods for Standard Normal Distribution

Sample Size / Methods	Chow	Method1	Method2	Milek (2015)
15	0.56	0.92	0.52	0.2
20	0.56	0.92	0.52	0.2
25	0.58	0.92	0.54	0.2
30	0.58	0.92	0.54	0.2
40	0.6	0.94	0.56	0.2
50	0.6	0.94	0.56	0.2
60	0.58	0.94	0.86	0.28
70	0.7	0.95	0.86	0.6
80	0.7	0.96	0.88	0.8
90	0.73	0.98	0.88	0.8
100	0.74	0.98	0.88	0.8
Average Power	0.63	0.94	0.69	0.41
Rank	3	1	2	4

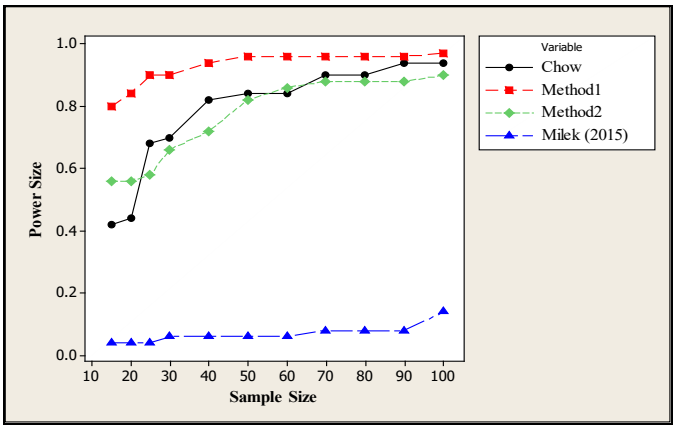

Figure 1: Performance of the methods for the Gamma Distribution

Table 5: Performance of the methods across the Distributions

Methods	Gamma Distribution	Standard Normal Distribution	Average Power for all distribution	Rank
Chow	0.77	0.63	0.70	3
Method1	0.92	0.94	0.93	1
Method2	0.75	0.69	0.72	2
Milek (2015)	0.07	0.41	0.24	4

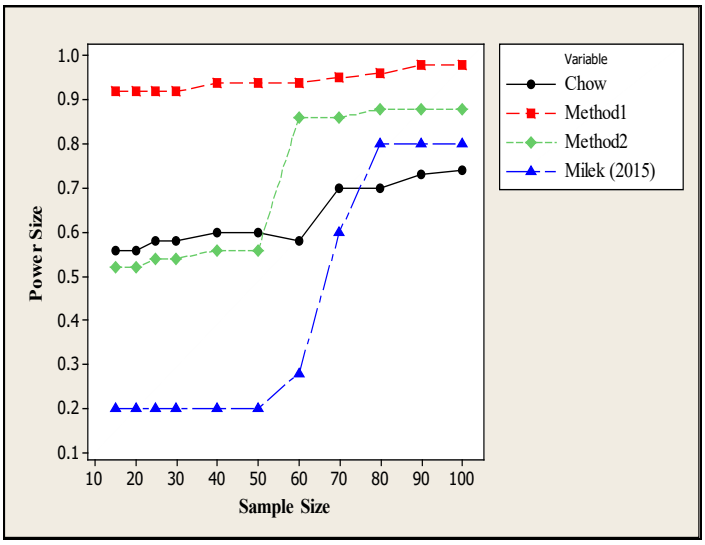

Figure 2: Performance of the methods for the Standard Normal Distribution

4.3. Discussion of Result

The result of the analysis presented in table 3 using data for the gamma distribution showed that Method1 performed best in terms of rejecting the null hypothesis when it is true at 95% Confidence level while the least performing method was the Milek, since their corresponding performance/rank were obtained as Method1 = 1, Chow= 2, Method2=3 and Milek (2015) =4. The findings was presented in figure 1 and it was revealed that the performance of the methods increases as the sample size increases.

Similarly, it was found from the result presented in table 4 for the standard normal distribution that Method1 performed best in terms of rejecting the null hypothesis when it is true at 95% Confidence level while the least performing method was the Milek, since their corresponding performance/rank were obtained as Method1 = 1, Method2 = 2, Chow=3 and Milek = 4. The findings was presented in figure 2 and it was revealed that the performance of the methods increases as the sample size increases.

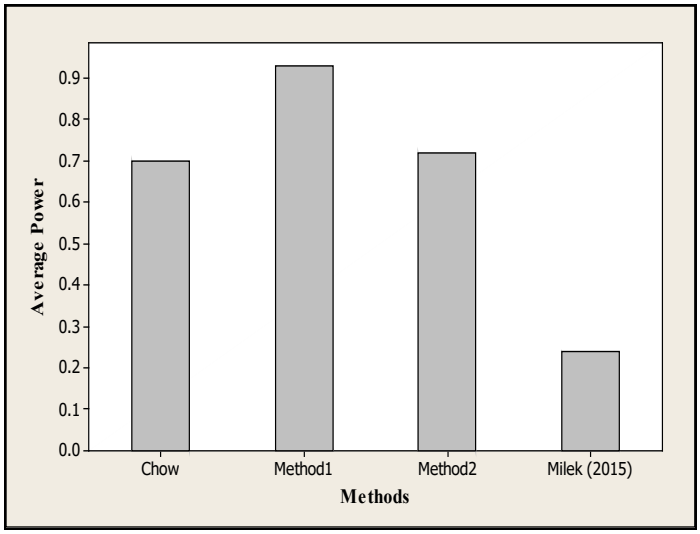

Figure 3: Performance of the methods across the Gamma and Standard Normal Distribution

Also, Method1 was found to perform better than the other methods across the distributions (see table 5). The performance of the methods were in the following order of magnitude Method1=1, Method 2=2, Chow=3 and Milek = 4.

4.4. Real Life Application of the Methods

Example 1: Real Life Application of the Methods for Small Sample Situation

Secondary data collected from the National Bureau of Statistics and Central Bank of Nigeria (CBN) statistical bulletin on Real GDP and Electricity net generation in Nigeria from 1989–2015 was used to illustrate the methods (see Table 1). This example was considered as small sample case since the data points/number of observation were 27. The methods were used to test whether the introduction of Nigeria Electricity Regulatory Commission (NERC) in the year 2005 has significant impact on economic growth in Nigeria. This implies testing for structural break at year 2005. The method 1, 2 and Milek (2015) permutation methods were performed for 10, 000 permutation. The result obtained was summarized in table 6.

Table 6: Performance of the Methods for example 1

Methods	Chow	Method1 (Ref= 849.087)	Method2 (Ref= 849.087)	Milek (2015) (Ref= 409.81)
P-value	0.000	0.005	0.005	0.005

The result of the example 1, real life application presented in table 6 found a Chow test value of 849.087 which was used as the reference value for the proposed permutation methods for Chow test. The result revealed p-values of 0.005, 0.005, and 0.005 for Method 1, Method 2 and Milek respectively. This result implies that all the methods were able to detect the presence of structural break at break point 2005.

Example 2: Real Life Application of the Methods for Large Sample Situation

This example employed secondary data collected from the records of patients at Federal Hospital Kaura-Namoda, Zamfara State. The data comprises of monthly reported cases of appendicitis from 2011 to 2017. This example was considered as large sample case since the data points/number of observation were above 30. The methods were used to test whether there exist structural break at point 49. This implies testing for structural break at January, 2015 when the President Buhari administration started (t_a=49). The method 1, 2 and Milek permutation methods were performed for 10, 000 permutation. The result obtained was summarized in table 7.

Table 7: Performance of the Methods for example 2

Methods	Chow	Method1 (Ref= 526.79)	Method2 (Ref= 526.79)	Milek (2015) (Ref= 486.94)
P-value	0.000	0.0049	0.0196	0.0194

The result of the example 2, real life application presented in table 7 found a Chow test value of 526.79 which was used as the reference value for the proposed permutation methods for Chow test analysis. The result revealed p-values of 0.0049, 0.196, and

0.0194 for Method 1, Method 2 and Milek respectively. This result implies that all the methods were able to detect the presence of structural break at break point 49.

5. Conclusion

This study proposed two new permutation methods for Chow test analysis. The study compared the performance of the proposed permutation methods against the traditional Chow test method and the Milek permutation for structural break using the gamma distribution and the standard normal distribution. Method1 was found to perform better than Method2 followed by the traditional Chow test analysis for both the gamma and standard normal distribution. While the Chow test analysis was found to perform better than the Milek permutation for structural break.

The result of the example 1, revealed that all the methods were able to detect presence of structural break at break point 2005. Hence, we conclude that the introduction of NERC in 2005 has significant effect on economic growth in Nigeria with regards to electricity net generation. Similarly, the result of the example 2, revealed that all the methods were able to detect presence of structural break at break point 2015. This indicate that the emergence of the president Buhari administration has significant impact on the number of reported cases of appendicitis at Federal Hospital Kaura-Namoda, Zamfara State, Nigeria.

In view of the outcome of the study, it is recommended Method1 (permute the dependent variable of the full model) be used for detecting structural break in linear models until future studies proves it otherwise.

Conflict of Interest

The authors declare no conflict of interest in this study.

Acknowledgment

We appreciate review comments and inputs from Prof. O. I. Chiaghanam, Prof. S. I. Iwueze, Prof. C. F. R. Odumodu, Dr. Osuji, G. A., Dr. Umedum, C. U. and Dr. G. U. Ebuh in making this work a success.

References

[1] B. Chen, Hong, Y. "Testing For Smooth Structural Changes In Time Series Models Via Nonparametric Regression" *Econometrica*, 80(3), 1157–1183, 2012. https://www.jstor.org/stable/41493847. DOI:10.3982/ECTA7990

[2] J. Wongsosaputro, L. L. Pauwels, and F. Chan "Testing for structural breaks in discrete choice models" 19th International Congress on Modelling and Simulation, Perth, Australia, 12–16 December 2011.

[3] P. Schmidt and R. Sickles "Some Further Evidence on the Use of the Chow Test under Heteroskedasticity" *Econometrica*, 45(5), 1293-1298, 1977. DOI: 10.2307/1914076

[4] E. S. Edgington "Randomization Test". Marcel Dekker, New York. DOI: https://doi.org/10.1007/978-3-642-04898-2_56

[5] B. F. J. Manly "Randomization, Bootstrap and Monte Carlo Methods in Biology, 3rd edition" Chapman and Hall, London, 2007.

[6] D. A. Jackson and K. M. Somers "Are probability estimates from the permutation model of mantel's test stable?" Canadian Journal of Zoology, 67(3): 766–769, 1989.

[7] C. O. Aronu, G. U. Ebuh "Application of mantels permutation technique on asphalt production in Nigeria. International Journal of Statistics and Applications", 3(3): 81–85, 2013.

[8] B. Phipson, G. K. Smyth "Permutation p-values should never be zero: calculating exact p-values when permutations are randomly drawn" Statistical Applications in Genetics and Molecular Biology, 9(1), Article 39, 1-12, 2010.

[9] B. S. Cade "Linear Models: Permutation Methods". Encyclopedia of Statistics in Behavioral Science, 2: 1049-1054, 2005.

[10] M. Ojala, G. C. Garriga "Permutation Tests for Studying Classifier Performance". Journal of Machine Learning Research, 11: 1833-1863, 2010.

[11] A. M. Winkler, G. R. Ridgway, M. A. Webster, S. M. Smith, T. E. Nichols "Permutation Inference for the general Linear Model" Neuroimage, 92, 381-397, 2014.

[12] Z. Achim, T. Hothorn "A Toolbox of Permutation Tests for Structural Change" Springer-Verlag Statistical Papers, 54(4), 931–954, 2013. https://link.springer.com. doi:10.1007/s00362-013-0503-4

[13] H. Strasser, C. Weber "On the Asymptotic Theory of Permutation Statistics". Mathematical Methods of Statistics, 8, 220–250, 1999.

[14] M. Miłek "Detecting structural changes in the time series in the use of simulation methods" The 9th Professor Aleksander Zelias International Conference on Modelling and Forecasting of Socio-Economic Phenomena, Cracow University of Economics and the Committee on Statistics and Econometrics of the Polish Academy of Sciences, Zakopane, Poland. Pp:145-153, 2015.

[15] G. C. Chow "Tests of Equality between Sets of Coefficients in Two Linear Regressions" *Econometrica*, 28.3: 591–605, 1960.

[16] A. M. Mood "Introduction to the theory of statistics" New York, NY: McGraw Hill, 1950.

[17] T. E. Davis "The consumption function as a tool for prediction", *Review of Economics and Statistics*, 6(34), 270-277, 1952.

[18] P. Legendre "Comparison of Permutation Methods for the Partial Correlation and Partial Mantel Tests. J. Statist. Comput. Simulation, (67), 37 – 73, 2000.

ASTES

Advances in Science, Technology and Engineering Systems Journal Vol. 4, No. 4, 21-28 (2019)

www.astesj.com

Special Issue on Advancement in Engineering and Computer Science

ASTESJ

ISSN: 2415-6698

Emulation of Bio-Inspired Networks

Zdenek Kolka[*,1], Viera Biolkova[1], Dalibor Biolek[1,2], Zdenek Biolek[1,2]

[1]*Brno University of Technology, 616 00 Brno, Czech Republic*

[2]*University of Defence, 662 10 Brno, Czech Republic*

ARTICLE INFO

Article history:
Received:17 May, 2019
Accepted:10 June, 2019
Online: 09 July, 2019

Keywords:
Continuous-Time System
Discrete-Time System
Emulation
Neuron Modeling

ABSTRACT

The paper deals with hardware emulation of bio-inspired devices and nonlinear dynamic processes of complex nature by means of mixed-mode analog-digital emulators. The discretized state model of the emulated system serves for real-time calculation of dependent quantities. In contrast to input-output emulation known in control systems, the proposed approach emulates the ports of an electrical multiport network. The paper discusses the stability of the emulation process and the possibility of partitioning the system into two parts, one being emulated digitally and the other via an analog circuitry. The procedure is illustrated on the example of emulating the Fitzhugh-Nagumo model of neuron and the model of amoeba adaptation. The paper is an extension of our paper presented at the NGCAS 2018 conference in Valletta, Malta. The extended version deals newly with the choice of the integration method and provides a deeper stability analysis and more examples of emulation of biological models.

1. Introduction

Emulation consists in replacing a part of the electrical system with another system that has similar characteristics but is more convenient to implement. This technique has become popular in the field of electronic circuits with the (re)introduction of mem elements [1, 2]. For example, the memristors and other promising nanodevices for digital computational systems, massively parallel analog computations or elegant modeling of the neuron cells, are still in the experimental phase and are not available as off-the-shelf components. Emulation allows performing circuit experiments with equivalents of these novel elements and is also useful for demonstration and educational purposes [3].

The first emulators were proposed as analog circuits. Single-purpose emulators such as [4–6] are simple and elegant, but their disadvantage is the inability to change easily their characteristics. Emulators of memristive, memcapacitive and meminductive devices based on mutators provide large universality because they transform a nonlinear resistor, which can be easily modified, to the respective constitution relation of the mem element [7–8].

Another problem is the emulation of blocks with floating ports, which is difficult for purely analog emulators. Several two-terminal floating emulators were proposed [5, 9, 10]. However, all the emulators are based on grounded devices and are "floating" only in the case of neglecting parasitic parameters. In [11], a genuinely floating memcapacitor was proposed on the principle of switched capacitors. The first implementation of a floating resistive port using a mixed-mode system was proposed in [12] with the use of a digital potentiometer, whose resistance was controlled by a microcontroller by means of pre-programmed algorithms.

On the other hand, there are dynamic systems that cannot be emulated via the above single-purpose emulators. For example, the well-known Hodgkin-Huxley model of the cell membranes in a neuron is represented by a set of nonlinear differential equations [13]. The equivalent electrical model is a two-terminal device, consisting of a linear capacitor, two nonlinear memristive devices, and biasing sources [14]. Usually, these models contain large-value inductors and capacitors, which are not useful for practical laboratory experiments.

The demand for emulating general dynamic systems resulted in developing mixed-mode analog-digital emulators [15, 16]. They consist of a central digital unit, which controls one or more floating analog ports of three possible types: controlled voltage source, controlled current source, and digital potentiometer [17]. The independent port currents and voltages are digitally processed

[*]Corresponding Author: Zdenek Kolka, Brno University of Technology, Email: kolka@feec.vutbr.cz

according to the mathematical model of the emulated device, and the computed dependent quantities are used for controlling the analog ports. A great advantage of such an approach is the ability to change easily the emulated system by means of changing the software and the possibility of designing truly floating ports with the use of digital isolators without compromising the precision.

The paper summarizes our experience of the emulation of two complex nonlinear dynamic systems via the mixed-mode approach [15]. The problem of discretization analog system and its (in)stability, which occurs when connecting a digital emulator to an analog circuitry, is analyzed. The paper is an extension of our paper [1] presented at the NGCAS 2018 conference in Valletta, Malta. The extended version deals newly with the choice of the integration method and provides a deeper stability analysis and more examples of emulation of biological models.

2. Emulation Principle

2.1. Basic Setup

In general, the emulator represents a mixed-mode analog-digital system with m floating electrical ports. For the purpose of emulation, let us constrain ourselves to such systems where each port has an independent input quantity (voltage or current) and the other quantity (current or voltage) is computed as a response.

Thus, the emulator consists of a digital core, implemented in a microcontroller (MCU) or FPGA, and ports in the form of controlled current or voltage sources, Figure 1. Using A/D converters with a supporting circuitry, the core measures independent quantities, computes the response, and sets the dependent quantities using D/A converters, followed by reconstruction filters and corresponding controlled sources.

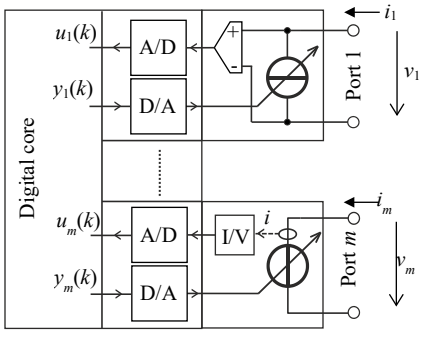

Figure 1: Multiport emulator shown with controlled current source at Port 1 and controlled voltage source at Port m.

The emulated system is generally a nonlinear discrete-time system of the n-th order with m inputs and m outputs, whose mathematical representation can be written as

$$\mathbf{x}(k+1) = \mathbf{f}(\mathbf{x}(k), \mathbf{u}(k)), \quad (1)$$

$$\mathbf{y}(k) = \mathbf{g}(\mathbf{x}(k), \mathbf{u}(k)), \quad (2)$$

where $\mathbf{x}(k) \in \mathrm{R}^n$ is the state vector, $\mathbf{u}(k) \in \mathrm{R}^m$ are the samples of independent (input) quantities, and $\mathbf{y}(k) \in \mathrm{R}^m$ are the dependent (output) quantities. The continuous functions $\mathbf{f}:(\mathrm{R}^n,\mathrm{R}^m) \to \mathrm{R}^n$ and $\mathbf{g}:(\mathrm{R}^n,\mathrm{R}^m) \to \mathrm{R}^m$ are generally nonlinear.

Figure 2 shows the time characteristics of a discrete-time system (1), (2) implemented in a real logical device and connected to a continuous-time circuit. The inputs $\mathbf{u}(k)$ are sampled with a period T and the outputs $\mathbf{y}(k)$ are available after the computation and transfer delay $t_c < T$. The analog circuit the emulator is connected to, which formally includes the anti-aliasing and reconstruction filters, responds to the new outputs $\mathbf{y}(k)$, and the response is sampled as the next input $\mathbf{u}(k+1)$.

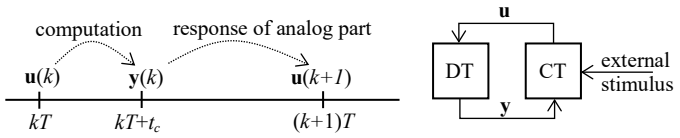

Figure 2: Timing of the emulation process (DT – discrete-time emulator, CT – continuous-time analog circuit).

2.2. Stability of Emulation

As shown in Figure 2, connecting the emulator to an application circuit creates a feedback system, which combines discrete-time and continuous-time parts. Let us consider the one-port case ($m = 1$). The stability of some fixed point of the system (1), (2) can be examined by linearizing the state description

$$\mathbf{x}(k+1) = \mathbf{A}\mathbf{x}(k) + \mathbf{B}u(k), \quad (3)$$

$$y(k) = \mathbf{C}\mathbf{x}(k) + Du(k), \quad (4)$$

where $\mathbf{A} \in \mathrm{R}^{n\times n}$, $\mathbf{B} \in \mathrm{R}^{n\times 1}$, $\mathbf{C} \in \mathrm{R}^{1\times n}$, and $D \in \mathrm{R}$ are real matrices.

Equations (3), (4) represent a single-input single-output linear system, which can be characterized by the z-domain input-output transfer function [18]

$$H(z) = \frac{Y(z)}{U(z)} = \mathbf{C}\frac{\mathrm{adj}[z\mathbf{I} - \mathbf{A}]}{\det[z\mathbf{I} - \mathbf{A}]}\mathbf{B} + D, \quad (5)$$

where "adj" denotes the adjoint matrix, $\mathbf{I}$ is the unity matrix, and $U(z)$ and $Y(z)$ are the z-transforms of the sequences $u(k)$ and $y(k)$.

The D/A converter generates a continuous-time signal $y(k) \to y(t)$, which stimulates the analog circuit, and the circuit response is sampled by the D/A converter as $u(t) \to u(k)$. The continuous-time circuit, which also includes the anti-aliasing and reconstruction filters, can be linearized around an operating point, which corresponds to the fixed point of the discrete system. The input-output small-signal transfer function will be

$$G_C(s) = \frac{U(s)}{Y(s)}, \quad (6)$$

where $U(s)$ and $Y(s)$ are the Laplace transforms of the continuous-time signals $u(t)$ and $y(t)$.

Considering the signal conversion $y(k) \to y(t) \to G_c \to u(t) \to u(k)$, the properties of the analog circuit can also be characterized in the discrete domain by means of the pulse transfer function [18]. For the zero-order hold (ZOH) D/A converter the transfer function will be

$$G(z)=\frac{U(z)}{Y(z)}=Z\left\{\frac{1-e^{-Ts}}{s}G_C(s)e^{-t_c s}\right\}, \qquad (7)$$

where $Z\{\bullet\}$ denotes the z-transform of the sampled impulse response of the continuous-time transfer function, $(1\text{-}e^{-Ts})/s$ is the transfer function of ZOH, and $e^{-t_c s}$ represents the processing delay t_c, which was formally added to the response of the analog circuitry. Note that (7) neglects the quantization introduced by real D/A and A/D converters.

Then the characteristic closed-loop equation will be

$$H(z)G(z)=1. \qquad (8)$$

The roots of (8) determine the stability of the emulation process.

The existence of two types of port (controlled current or voltage source, see Figure 1) is also dictated by the requirement of emulation stability. Let us consider a simple emulation of the resistor R_E by a controlled current source. Then the independent quantity will be the voltage ($u := v$) and the dependent quantity will be the current ($y := i$). The emulator transfer function (5) will be simply

$$H(z)=\frac{Y(z)}{U(z)}=\frac{I(z)}{V(z)}=\frac{1}{R_E}, \qquad (9)$$

i.e. $i(k) = v(k)/R_E$.

Let the emulator port be loaded with a physical resistor R. Considering a first-order reconstruction filter, but no anti-aliasing filter and no processing delay the small-signal transfer function (6) will be

$$G_C(s)=-R\frac{1}{1+s\tau_r}, \qquad (10)$$

where τ_r is the time constant of the reconstruction filter. The positive current i flows into the positive terminal of the emulator port, i.e. (10) has the negative sign.

The pulse transfer function (7) will be

$$G(z)=Z\left\{-\frac{1-e^{-Ts}}{s}\frac{R}{1+s\tau_r}\right\}=R\frac{1-c}{z-c}, \qquad (11)$$

where $c = exp(-T/\tau_r)$.

Substituting (9) and (11) into the characteristic equation (8) leads to

$$-\frac{R}{R_E}\frac{1-c}{z-c}=1. \qquad (12)$$

Considering the stability condition $|z| < 1$ for the root of (12) and with respect to the typical choice $\tau_r \approx T$, which gives $0 < c < 1$, we obtain the condition

$$R < R_E\frac{1+c}{1-c} \qquad (13)$$

for stable operation of the emulating process. Thus, if the Thévenin-equivalent resistance of the analog circuitry connected to the emulator port is higher than the limit (13), the system will oscillate, although the emulated device is a positive-value resistor. A more detailed analysis for other types of devices can be found in [19].

The example underlines the necessity for an emulation-stability analysis. A circuit that would be perfectly stable if realized from physical components may become unstable if some parts are emulated by a discrete-time system.

3. Demonstrations

3.1. Emulator Hardware

The emulator used for demonstrations is a two-port modification [17] of our emulator [15]. The system consists of the main board STM NUCLEO-F722ZE with a 32-bit MCU ARM Cortex-M7 with a single-precision floating-point unit connected to PC via USB. An add-on card implements two isolated ports, each with 16-bit A/D and D/A converters. The ports are fully floating, which is achieved by the use of integrated DC-DC converters and digital SPI isolators for converter control. The total parasitic capacitance of the floating part to the ground is about 11 pF.

A pluggable controlled voltage or current source can be connected to the ports as shown in Figure 3. The operating area of the four-quadrant voltage and current modules is ±3 V and ±3 mA. The emulator can easily achieve a sampling rate of 100 kHz. Depending on the software, it can emulate one or two independent floating devices or a general two-port network.

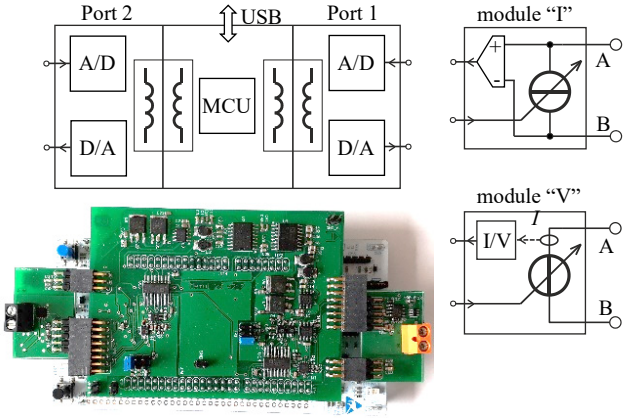

Figure 3: Emulator with pluggable IO modules.

3.2. FitzHugh-Nagumo Model

The FitzHugh-Nagumo (FHN) model of neuronal excitability [20] is a simplification of the well-known Hodgkin-Huxley model [13]. The model represents the prototype of an excitable system. When the input quantity exceeds some certain threshold, the system will generate a pulse. The two-dimensional FHN model is given in its normalized form as

$$\frac{d\upsilon}{d\tau} = \upsilon - \frac{\upsilon^3}{3} - w + j\,, \tag{14}$$

$$\frac{dw}{d\tau} = \frac{1}{\sigma}\left(\upsilon + a - bw\right), \tag{15}$$

where υ represents the normalized membrane potential, w is an auxiliary variable, j is a stimulus current, and τ is the model time. The model dynamics is determined by a set of three parameters with the usual values $a = 0.7$, $b = 0.8$, and $\sigma = 12.5$ [21].

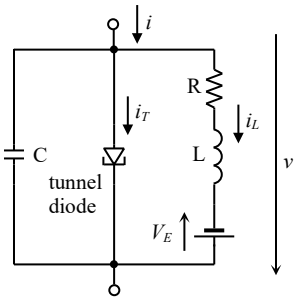

Figure 4: Equivalent circuit to (14) and (15) proposed by Nagumo [20].

The system (14), (15) can be represented by an equivalent electrical circuit shown in Figure 4 with a nonlinearity similar to that of the tunnel diode, which was proposed by Nagumo [20]. Let us consider the following mapping of FHN model quantities to the physical circuit in Figure 4:

$$v = \kappa_v\,\upsilon\,,\ i = \kappa_i\,j\,,\ i_L = \kappa_w\,w\,,\ t = \kappa_t\,\tau\,. \tag{16}$$

The transformation coefficients were chosen such that the variable υ will represent voltage in volts ($\kappa_v = 1$ V), j and w will be currents in milliamps ($\kappa_i = \kappa_w = 1$ mA), and one unit of model time τ will correspond to one millisecond of the physical time ($\kappa_t = 1$ ms), i.e. the dynamics will be speeded up a thousand times to get a convenient duration of generated pulses.

Considering (16), the parameters of the circuit elements will be

$$C = \frac{\kappa_t\,\kappa_i}{\kappa_v},\ R = \frac{b\,\kappa_v}{\kappa_w},\ L = \frac{\kappa_t\,\kappa_v\,\sigma}{\kappa_w},\ V_E = a\,\kappa_v\,. \tag{17}$$

For the chosen transformation coefficients we have $C = 1$ µF, $L = 12.5$ H, $R = 800$ Ω, and $V_E = 0.7$ V. The i-v characteristic $i_T(v)$ of the "tunnel diode" will be

$$i_T(v) = \kappa_i\left(\frac{(v/\kappa_v)^3}{3} - v/\kappa_v\right), \tag{18}$$

which corresponds to the first two terms of RHS of (9).

1) Direct Digital Emulation

Equations (14), (15) represent a dynamical system with the input current j and output potential υ. In accordance with the electrical model in Figure 4 the system can be emulated by a controlled voltage source. The output voltage $\upsilon(k)$ will be computed from the samples $j(k)$ of the measured current.

The real-time operation of the emulator requires the use of explicit integration methods with low numerical complexity [22]. Let us consider an ordinary differential equation of the n-th order in the form

$$\frac{d\mathbf{x}}{dt} = \mathbf{f}(\mathbf{x}, u)\,, \tag{19}$$

where $\mathbf{x} \in \mathrm{R}^n$ and u is a scalar input. Then the explicit multistep linear integration scheme can be formulated as

$$\mathbf{x}(k+1) = \mathbf{x}(k) + h\sum_{i=0}^{r-1}\gamma_i\,\mathbf{f}(\mathbf{x}(k-i), u(k-1))\,, \tag{20}$$

where r is the order of the method, h is the integration step, and γ_i are coefficients. For $r = 1$ we get the classical forward Euler method with $\gamma_1 = 1$, and for $r = 2$ the Adams-Bashforth method of the 2nd order (AB2) with $\gamma = \{3/2, -1/2\}$ [22].

The practical implementation of the multistep scheme (20) has a relative low numerical complexity as it requires just storing r-1 past values $\mathbf{f}(k\text{-}i) := \mathbf{f}(\mathbf{x}(k\text{-}i), u(k\text{-}i))$.

The computation of each step starts with the evaluation of RHS of (14), (15) for current values of the quantities

$$\mathbf{f}(k) = \begin{array}{|c|}\hline \upsilon(k) - \upsilon(k)^3/3 - w(k) + j(k) \\ \hline \left(\upsilon(k) + a - b\,w(k)\right)/\sigma \\ \hline \end{array}\,. \tag{21}$$

In the case of the Euler method the next step is

$$\begin{array}{|c|}\hline \upsilon(k+1) \\ \hline w(k+1) \\ \hline \end{array} = \begin{array}{|c|}\hline \upsilon(k) \\ \hline w(k) \\ \hline \end{array} + h\,\mathbf{f}(k) \tag{22}$$

and for AB2 we have

$$\begin{array}{|c|}\hline \upsilon(k+1) \\ \hline w(k+1) \\ \hline \end{array} = \begin{array}{|c|}\hline \upsilon(k) \\ \hline w(k) \\ \hline \end{array} + \frac{h}{2}\left[3\mathbf{f}(k) - \mathbf{f}(k-1)\right], \tag{23}$$

where $h = T/\kappa_t$. The coefficient $\kappa_t = 1$ ms scales the time axis so that the time unit in the original system (14), (15) corresponds to one millisecond in (22) and (23).

The emulator was configured as a current-controlled voltage source using the module "V", where the output quantity is the transformed state variable $v(k) = \upsilon(k)\ \kappa_v$ and the control quantity is $j(k) = i(k)/\kappa_i$. The sampling rate was set to 100 kHz.

Figure 5 shows the results of an experiment where the digital FHN model was "excited" by short pulses with an amplitude of 3 V, a width of 8 ms, and a period of 100 ms applied through a 10 kΩ resistor R_d. It can be seen that each pulse triggers a characteristic excursion, after which the system relaxes back to the equilibrium state.

The discretization and emulation of the continuous-time system bring two problems with the stability: the stability of the

integration method itself and the stability of the feedback emulation process as introduced in Section 2.2.

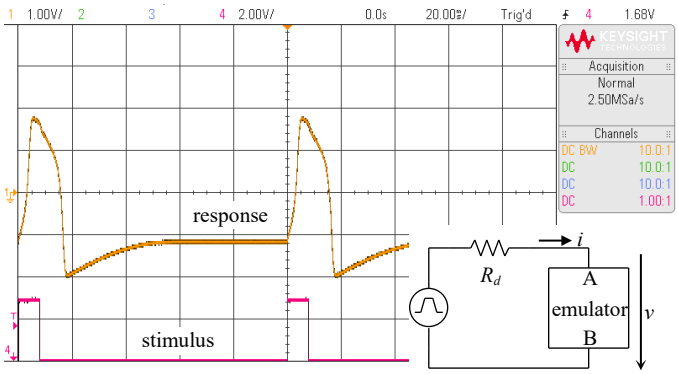

Figure 5: Response (channel 1 - orange) to excitation pulses (channel 4 - red).

In particular, it is known for explicit methods that an inappropriate choice of the integration step can lead to instability and an excessive truncation error [22]. Figure 6 shows a qualitative study comparing the performance of the methods (22) and (23) for the same setup as in Figure 5. For the 10 μs sampling period used, the results are indistinguishable from the nominal solution within the uncertainty introduced by the quantization by A/D and D/A converters. When the sampling period was increased to 500 μs, the waveform computed by AB2 showed numerical oscillations. Therefore, the first-order method was preferred in the experiments.

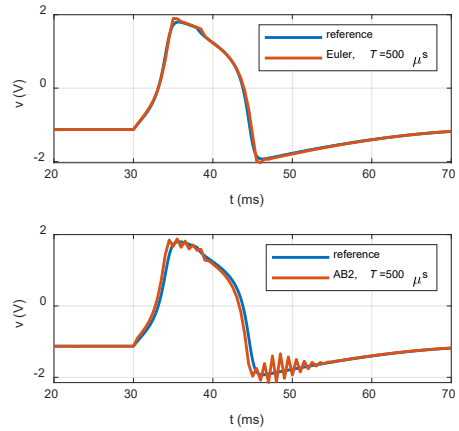

Figure 6: Comparison of forward Euler and 2nd–order Adams-Bashforth methods for large integration steps.

The stability of emulation as introduced in Section 2.2 can be qualitatively assessed based on the equilibrium stability analysis for $v = 0$, which corresponds to the OFF period of the signal source. The equilibrium of the FHN model can be obtained via solving the system (14), (15) for $d\upsilon/d\tau = 0$ and $dw/d\tau = 0$, and also by considering the relation $v = -R_d\, i$ determined by the driving circuit in Figure 5 during the OFF periods. After the transformation (16) the relation becomes $\upsilon\, \kappa_v = -R_d\, j\, \kappa_i$ and we obtain the system

$$0 = \tilde{\upsilon} - \frac{\tilde{\upsilon}^3}{3} - \tilde{w} - \frac{\tilde{\upsilon}\,\kappa_v}{R_d\,\kappa_i}, \tag{24}$$

$$0 = \tilde{\upsilon} + a - b\,\tilde{w}, \tag{25}$$

whose solution is

$$\tilde{\upsilon} = -1.129,\ \tilde{w} = -0.536\,. \tag{26}$$

Let us start with the forward Euler method. The equilibrium corresponds to a fixed point of the discretized system (22), because $\mathbf{f}_k = \mathbf{0}$ and thus $\upsilon(k+1) = \upsilon(k)$, $w(k+1) = w(k)$. The structure of the system (22) corresponds to (1), (2) and its linearization at the fixed point ($\tilde{\upsilon}$, $\tilde{w}$) leads to the following matrices (3) and (4):

$$\mathbf{A} = \begin{bmatrix} 1+h(1-\tilde{\upsilon}^2) & -h \\ h/\sigma & 1-hb/\sigma \end{bmatrix},\ \mathbf{B} = \begin{bmatrix} h \\ 0 \end{bmatrix},$$

$$\mathbf{C} = \begin{bmatrix} 1 & 0 \end{bmatrix},\ D = 0\,. \tag{27}$$

Using (5), the emulator transfer function is

$$H(z) = \frac{V(z)}{I(z)} = \frac{\kappa_v}{\kappa_i}\,\frac{zh\sigma - h(\sigma - bh)}{z^2\sigma + z[h\sigma(\tilde{\upsilon}^2 - 1) - 2\sigma + bh] + (bh - \sigma)[h(\tilde{\upsilon}^2 - 1) - 1] + h^2}\,. \tag{28}$$

The simulator uses a 1st-order reconstruction filter with the time constant τ_r and no anti-aliasing filter. The Laplace-domain transfer function between the output of the D/A converter and the input of the A/D converter corresponding to the application schematics in Figure 5 will be

$$G_C(s) = \frac{I(s)}{V(s)} = -\frac{1}{R_d}\,\frac{1}{1 + s\,\tau_r}, \tag{29}$$

where the negative sign stems from the chosen orientation of v and i.

Using the standard s- and z-transforms, the pulse transfer function can be easily obtained as [23]

$$G(z) = Z\left\{\frac{1 - e^{-Ts}}{s}\,G_C(s)\,e^{-t_c s}\right\} = -\frac{1}{R_d}\,\frac{(1 - cd)z^{-1} + c(d-1)z^{-2}}{1 - c\,z^{-1}}, \tag{30}$$

where $c = exp(-T/\tau_r)$ and $d = exp(t_c/\tau_r)$.

The time constant of the reconstruction filter was $\tau_r = T = 10$ μs, which smoothed reasonably its staircase output, and the processing delay was $t_c = 3$ μs. Then the roots of the characteristic equation (8) are as follows:

$$\lambda_{1,2} = 0.9978 \pm j\ 0.002289,\ \lambda_3 = 0.3692,\ \lambda_4 = -3.4988 \times 10^{-4},$$

which indicates a stable operation. It can be shown that the doublet $\lambda_{1,2}$ corresponds to the poles of (28) because the FHN model is driven by a high-resistance source, which behaves like a stimulation by a current source (see Figure 5). The doublet is close to the unity circle, reflecting the fact that the sampling rate is orders of magnitudes faster than the modeled dynamics, i.e. the update in each step is relatively low ($v(k+1) \approx v(k)$). The roots λ_3 and λ_4 are predominantly influenced by the chosen time constant of the

reconstruction filter and MCU processing delay, and represent fast-decaying artifacts of the emulation process.

To compute the z-domain transfer function (5) for higher-order integration methods, the difference equation (20) should be transformed to an equation of the 1st order.

In the case of the Adams-Bashforth method of the 2nd order the scheme (23) can be transformed to

$$\begin{bmatrix} v(k+1) \\ w(k+1) \end{bmatrix} = \begin{bmatrix} v(k) \\ w(k) \end{bmatrix} + \frac{h}{2}\left(3\mathbf{f}(k) - \tilde{\mathbf{f}}(k)\right), \tag{31}$$

$$\tilde{\mathbf{f}}(k+1) = \mathbf{f}(k), \tag{32}$$

where $\tilde{\mathbf{f}}(k)$ is the vector of RHS of (14) and (15) delayed by one period. Then the linearization of (31) and (32) leads to

$$\mathbf{A} = \begin{bmatrix} 1+\frac{3h}{2}(1-v^2) & -\frac{3h}{2} & -\frac{h}{2} & 0 \\ \frac{3h}{2\sigma} & 1-\frac{3hb}{2\sigma} & 0 & -\frac{h}{2} \\ 1-v^2 & -1 & 0 & 0 \\ 1/\sigma & -b/\sigma & 0 & 0 \end{bmatrix}, \quad \mathbf{B} = \begin{bmatrix} 3h/2 \\ 0 \\ 1 \\ 0 \end{bmatrix},$$

$$\mathbf{C} = \begin{bmatrix} 1 & 0 & 0 & 0 \end{bmatrix}, \; D = 0\,. \tag{33}$$

Repeating the same procedure as for the Euler method, we obtain the roots:

$\lambda_{1,2} = 0.9978 \pm j\,0.003594$,

$\lambda_3 = 0.3681$, $\lambda_4 = -0.0136$, $\lambda_5 = 0.0130$, $\lambda_4 = -3.0454 \times 10^{-4}$.

The doublet characterizes the emulated system dynamics and the other roots represent the artifacts of the discretization. Also in this case, the emulation is stable.

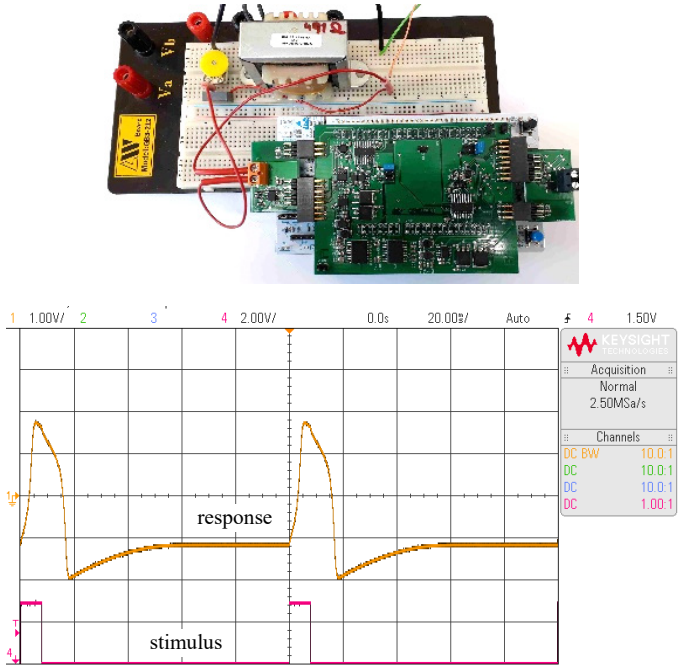

Figure 7: Hybrid circuit setup and response (orange) to excitation pulses (red).

2) Hybrid Circuit

In the hybrid approach the emulator is used to implement some parts of the model, while the rest of the model can be realized using standard electronic components as in Figure 4. In the case of the FHN equivalent circuit the emulator implements just the "tunnel diode". The cubic nonlinearity (18) was emulated as a voltage-controlled current source using the module "I".

Figure 7 shows the experiment setup on a breadboard and the response of the model for the same conditions as in Figure 5. The parameter L was changed to 16.2 H in this experiment to match the inductance of the available off-the-shelf choke.

Figure 8 compares the measured pulses with a PSpice simulation, the latter being regarded as a reference solution. All three waveforms overlap.

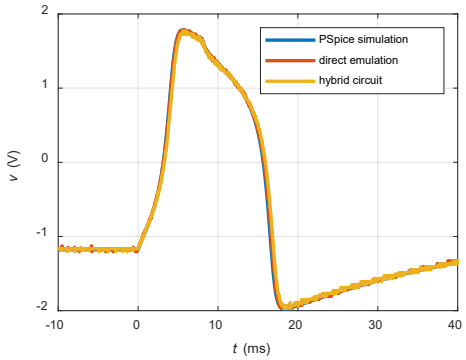

Figure 8: Comparison of the measured and simulated responses for L = 16.2 H (all waveforms overlap).

3.3. Model of Amoeba Adaptation

The amoeba can adapt to periodic environmental changes. An electrical model of the process was presented in [24], see Figure 9. The environmental conditions (temperature and humidity) are represented by a single quantity – the voltage $v(t)$, which is applied to the circuit. The response is the change in amoeba movement velocity represented by the voltage $v_c(t)$.

The memristor in Figure 9 is a voltage-controlled memristor with a threshold whose memristance R_M is governed by the following state equation [24]

$$\frac{dR_M}{dt} = f_A(v_M)\, f_W(R_M, v_M)\,, \tag{34}$$

where v_M is the voltage across memristor ($v_M = v_C$ here). The memristor activation function

$$f_A(v_M) = \frac{\beta - \alpha}{2}\left(|v_M + V_T| - |v_M - V_T|\right) - \beta v_M \tag{35}$$

is shown in Figure 9(b). The parameter α is the slope of the inner segment and β is the slope of outer segments.

The window function

$$f_W(R_M, v_M) = \theta(v_M)\theta(R_M - R_1) + \theta(-v_M)\theta(R_2 - R_M) \tag{36}$$

confines the memristance between the boundary values R_1 and R_2, and θ is the Heaviside step function.

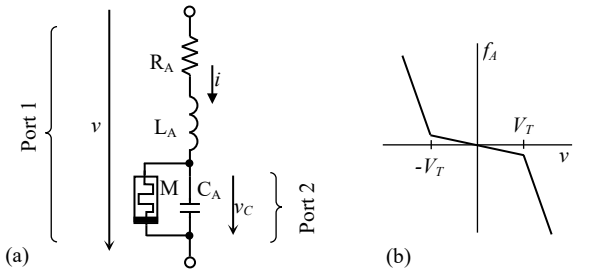

Figure 9: (a) Equivalent electrical model of amoeba's adaptation; (b) Activation function of memristor.

The model leads to a system of the 3rd order [25]

$$\frac{di}{dt} = \frac{1}{\kappa_t L_A}\left(-R_A i + v - v_c\right), \tag{37}$$

$$\frac{dv_c}{dt} = \frac{1}{\kappa_t C_A}\left(-\frac{v_c}{R_M} + i\right), \tag{38}$$

$$\frac{dR_M}{dt} = \frac{1}{\kappa_t} f_A(v_c) f_W(R_M, v_c), \tag{39}$$

where the parameters were identified as [24]: $R_A = 0.1\ \Omega$, $L_A = 2$ H, $C_A = 1$ F, $R_1 = 3\ \Omega$, $R_2 = 20\ \Omega$, $\alpha = 0.1\ \Omega$/Vs, $\beta = 100\ \Omega$/Vs, $V_T = 2.5$ V. The amoeba adaptation occurs on the time scale of ≈100 s, which is rather slow for laboratory experiments even with a digital memory oscilloscope. Therefore the time-axis scaling $\kappa_t = 10^{-3}$ was added to the equations. Now, one second of the model time corresponds to one millisecond of the real time.

The emulator was configured as a two-port network. The excitation voltage $v(t)$ is applied to Port 1 with the "I" module (controlled current source). Although the current i(t) is just an internal variable of the system (37)-(39), it can be generated at Port 1 to emulate fully the circuit from Figure 9(a). One ampere in the model corresponds to one milliampere in the emulated circuit. The model response based on $v_c(t)$ is generated at Port 2 with the "V" module. Alternatively, the output can be set as the memristance R_M to monitor the internal state of the model.

Equations (37)-(39) were discretized using the forward Euler method, similar to (22). The window function f_W was realized in the algorithm as a correction of the state variable R_M after each integration step. Whenever $R_M > R_2$, it is set back to R_2 and vice versa for the lower limit R_1.

The excitation voltage $v(t)$ represents environmental conditions of the amoeba. Favorable conditions correspond to a positive voltage and unfavorable conditions to a negative voltage. Long-term exposure to favorable conditions ($v > 0$) leads to $dR_M/dt < 0$ and after a sufficiently long interval the memristance R_M will be at its lower limit, i.e. $R_M = R_1$.

It has been observed that periodic intervals of unfavorable conditions make the amoeba adapt so that the organism can anticipate the intervals and decrease its velocity. The process can be demonstrated on an experiment from [24]. The "training" voltage waveform consists of three negative cosine pulses

$$v(t) = V_F + V_P \sum_{i=1}^{3} \left\{ \cos\left[\frac{2\pi(t - t_i)}{W_p}\right] - 1 \right\} \frac{w(t)}{2}, \tag{40}$$

where $w(t) = \theta(t - t_i)\theta(t_i + W_p - t)$ is a window function for masking the individual periods of the cosine function. The parameters used were $V_F = 0.1$ V, $V_p = 2$ V, and $W_p = 5$ ms. With respect to the time-axis scaling, the times of pulse starts for the irregular sequence were $t_i^{(irregular)} = \{10\text{ ms}, 19\text{ ms}, 34.5\text{ ms}\}$ and for the regular sequence $t_i^{(regular)} = \{10\text{ ms}, 19\text{ ms}, 28\text{ ms}\}$. The excitation signal was generated using the arbitrary waveform generator Keysight 33521B.

The output voltage on Port 2 was generated as [24]

$$v_{out}(t) = \min(v_C(t), V_F). \tag{41}$$

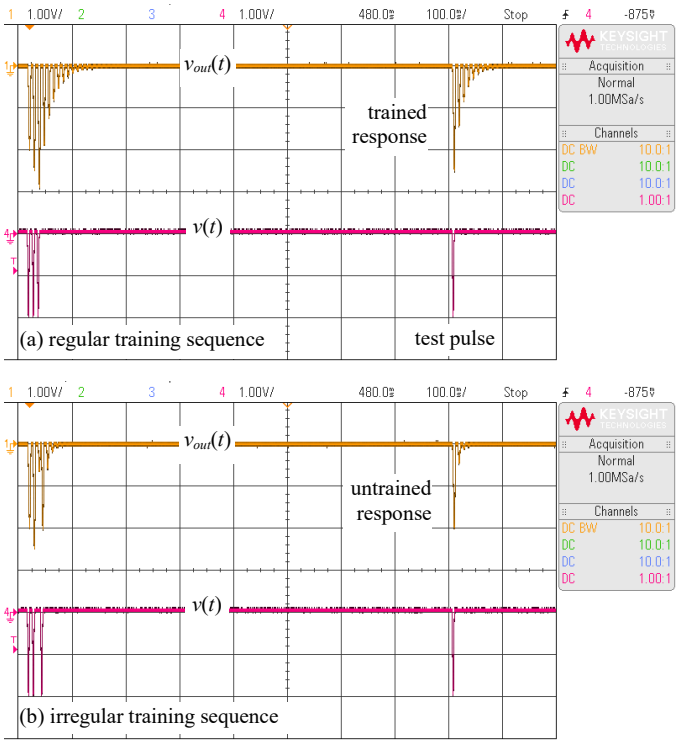

Figure 10: Excitation voltage (channel 4 – red) and amoeba response (channel 1 – orange) for (a) regular and (b) irregular training sequence.

Figure 10 shows the excitation voltage $v(t)$ and the response $v_{out}(t)$ generated by the emulator. The amoeba adaptation is represented in the model by the change of memristance R_M. The application of the irregular sequence of training pulses after a long period of favorable conditions (V_F) does not change the memristance significantly. On the other hand, the regular training sequence makes R_M increase to R_2 and the amoeba becomes "adapted". Both states can be tested by a single pulse at 800 ms after the training sequence start. The adapted response consists of several pulses of motion slowdown where the organism anticipates other unfavorable intervals. The response of the untrained organism is visibly smaller. Both results are in agreement with computer simulations in [24].

4. Conclusions

The results presented in the paper can be summarized as follows:

(1) Emulation provides the possibility of substituting an *m*-port network with a mixed-mode analog-digital system. The network modeled via multi-dimensional differential equations, which link terminal voltages and currents and internal state variables, can be emulated via digitally controlled current or voltage sources. The sources are controlled based on the port voltages or currents and the state variables via discrete-time equations of motion of the system being emulated.

(2) In some cases, it can be useful to emulate digitally only some key parts of the circuit, while the rest can be made up of (preferably passive) analog components.

(3) The combination of continuous-time and discrete-time blocks can bring stability problems, even in very simple circuits. The paper presents a methodology that can be used to assess the emulated system stability.

(4) Stability problems can be alleviated by an appropriate selection of the type of controlled source (voltage or current) which is used to realize each port. Details are given in our previous work [17].

(5) The paper presents a mixed-mode emulator with pluggable IO ports that has proven itself to emulate unconventional circuit elements (memristors, memcapacitors, meminductors, etc.) and also bio-inspired circuits. Especially in the case of models of biological systems it can avoid using bulky inductors and capacitors, which are common there.

Conflict of Interest

The authors declare no conflict of interest.

Acknowledgment

This work was supported by the Czech Science Foundation under grant No. 18-21608S. The research was also supported by the Project of Specific Research, K217 Department, UD Brno.

References

[1] Z. Kolka, V. Biolkova, D. Biolek, Z. Biolek, "Hardware Implementation of Bio-Inspired Models" in 2018 New Generation of CAS (NGCAS), Valletta, Malta, 102-105, 2018. https://doi.org/10.1109/NGCAS.2018.8572072

[2] D. Biolek, Memristor emulators. In Memristive networks. Springer book, New York, 2014.

[3] Y. V. Pershin, M. Di Ventra, "Teaching memory circuit elements via experiment-based learning" IEEE Circuits and Systems Magazine, **12**(1), 64—74, 2012. https://doi.org/10.1109/MCAS.2011.2181096

[4] Q. Zhaoa, C. Wangb, X. Zhangc, "A universal emulator for memristor, memcapacitor, and meminductor and its chaotic circuit" Chaos **29**, 013141, 2019. https://doi.org/10.1063/1.5081076

[5] D.S.Yu, H.Chen, H.H.C.Iu, "Design of a practical memcapacitor emulator without grounded restriction" IEEE Trans Circuits Syst II, **60**(6), 207–211, 2013. https://doi.org/10.1109/TCSII.2013.2240879

[6] M.Pd.Sah, R.K.Budhathoki, C.Yang, H.Kim, "Charge Controlled meminductor Emulator" J. of Semiconductor Technology and Science, **14**(6), 750–754, 2014. https://dx.doi.org/10.5573/JSTS.2014.14.6.750

[7] D. Biolek, V. Biolková, "Mutator for transforming memristor into memcapacitor" Electronics Letters, **46**(21), 1428—1429, 2010. https://doi.org/10.1049/el.2010.2309

[8] D.Yu, Y.Liang, H.H.C.Iu, L.O.Chua, "A universal mutator for transformations among memristor, memcapacitor, and meminductor" IEEE Trans. on Circ Syst Express Briefs, **61**(10), 758–762, 2014. https://doi.org/10.1109/TCSII.2014.2345305

[9] Y. V. Pershin, M. Di Ventra, "Emulation of floating memcapacitors and meminductors using current conveyors" Electronics Letters, **47**(4), 243—244, 2011. https://doi.org/10.1049/el.2010.7328

[10] M. Kumngern, "A floating memristor emulator circuit using operational transconductance amplifiers" in 2015 IEEE International Conference on Electron Devices and Solid-State Circuits (EDSSC), Singapore, 679–682, 2015. https://doi.org/10.1109/EDSSC.2015.7285207

[11] D. Biolek, V. Biolkova, Z. Kolka, J. Dobes, "Analog Emulator of Genuinely Floating Memcapacitor with Piecewise-Linear Constitutive Relation" Circuits Syst. Signal Process, 35(1), 43-62, 2016. https://doi.org/10.1007/s00034-015-0067-8

[12] Y. V. Pershin, M. Di Ventra, "Practical approach to programmable analog circuits with memristors" IEEE Trans. Circ. Syst. I, 57(8), 1857–1864, 2010. https://doi.org/10.1109/TCSI.2009.2038539

[13] A. L. Hodgkin, A. F. Huxley, "A Quantitative Description of Membrane Current and its Application to Conduction and Excitation in Nerve" J. Physiol., **117**(4), 500—544, 1952. https://doi.org/10.1113/jphysiol.1952.sp004764

[14] L. Chua, V. Sbitnev, H. Kim, "Hodgkin-Huxley Axon is Made of Memristors" Int. J. of Bifurcation and Chaos, **22**(3), 1230011-1-48, 2012. https://doi.org/10.1142/S021812741230011X

[15] D. Biolek, Z. Kolka, J. Vávra, S. Doan, "Universal Emulator of Memristive and Other Two-Terminal Devices" International J. of Unconventional Computing, **12**(4), 281—302, 2016.

[16] K. Ochs, E. Solan, S. Dirkmann, T. Mussenbrock, "Wave digital emulation of a double barrier memristive device" in Proceedings of 59th International Midwest Symposium on Circuits and Systems (MWSCAS), Abu Dhabi, 1-4, 2016. https://doi.org/10.1109/MWSCAS.2016.7869946

[17] J. Vavra, Z. Kolka, D. Biolek, "Two-Port Hybrid Emulator of Analog Devices and its Application in Emulation of Memistor" Journal of Advanced Manufacturing Technology (in print).

[18] W.Y. Yang, Signals and Systems with MATLAB. Springer-Verlag Berlin Heidelberg, 2009.

[19] Z. Kolka, V. Biolkova, D. Biolek, "Stability of Digitally Emulated Mem-Elements" in 2015 International Conference on Computing, Communication and Security (ICCCS), Pointe aux Piments, Mauritius, 415—419, 2015. https://doi.org/10.1109/CCCS.2015.7374184

[20] J. Nagumo, S. Arimoto, S. Yoshizawa, "An Active Pulse Transmission Line Simulating Nerve Axon" Proceedings of the IRE, **50**(10), 2061—2070, 1962. https://doi.org/10.1109/JRPROC.1962.288235

[21] A. Fuchs, Nonlinear Dynamics in Complex Systems: Theory and Applications for the Life-, Neuro- and Natural Sciences. Springer-Verlag Berlin Heidelberg, 2012.

[22] J. C. Butcher, Numerical Methods for Ordinary Differential Equations, 3rd edition. John Wiley & Sons, Chichester, UK, 2016.

[23] D. Zwillinger, CRC Standard Mathematical Tables and Formulae, 32nd Edition, CRC Press, Boca Raton, 2011.

[24] Y.V. Pershin, S. La Fontaine, M. Di Ventra, "Memristive model of amoeba learning" Physical Review E, **80**(2), 021926-1-6, 2010. https://doi.org/10.1103/PhysRevE.80.021926

[25] F. Caravelli, J. Carbajal, "Memristors for the Curious Outsiders" Technologies, **6**(4), 118, 2018. https://doi.org/10.3390/technologies6040118

ASTES

Advances in Science, Technology and Engineering Systems Journal
Vol. 4, No. 4, 29-41 (2019)
www.astesj.com

ASTES Journal
ISSN: 2415-6698

Career Recommendation System for Scientific Students Based on Ontologies

Alimam Mohammed Abdellah*, Alimam Mohammed Karim, Seghuiouer Hamid

Abdelmalek Essaâdi University, Avenue Khenifra, Tétouan 93000, Morocco

ARTICLEINFO

Article history:
Received: 18 March, 2019
Accepted: 05 July, 2019
Online: 11 July, 2019

Keywords:
Guidance
Grades
Ontologies
Science Process Skills
Education

ABSTRACT

Students are usually unaware of their own skills. They choose to follow the trend, rather than the proper pathway. Which negatively affects the professional sector, and the development of the country. Orienting students, and guiding them would offer considerable benefits. Building the appropriate student's profiles is the golden key for an accurate orientation. To do so, relying on the simple use of the grade point average (GPA) will not be sufficient, and mislead the guidance. Instead, studying their personality and skills has to be done, in order to provide them with their reel orientation. The presented solution aims to orient students to the most suitable career, based on a mathematical model, valid for all education systems, and takes into account the trades trends and students capabilities.

1 Introduction

This paper is an extension of work originally presented in conference Computing Conference, London, UK 2017 [1].

Education has an important function in the economic development. Its anticipation and success are among the factors that explain the essential differences in standards of living between different countries. Recently Romer, Lucas, Mankiw have shown that education is the engine of economic growth [2]: In [3], the author shows that education is the basic need of every individual. Nowadays, anyone is concerned about selecting the right institution, that suits better his choices and interests. In making these decisions, individuals must consult a large number of physical records and institutional perspectives. To make the right decision becomes a hard mission for them [3].

Although career choice is fundamental to the future of the individual, the assignment is done in an unqualified, unreliable way. On the other hand, the use of new technologies has become a necessity nowadays in all areas. The benefits they can bring are unmistakable. This has led scientists and researchers to find the most optimal way to use, implement, and benefit as best as possible. According to [4] several economic and socio-educational problems can be solved by introducing genuine career guidance in the education system.

By providing guidance to students, their academic and professional success is greatly enhanced by helping them discover their interests, values, and skills [5].

Without the latest user information, user profiling would be more difficult. In fact, data is available across multiple platforms, where users interact with different web content: social activities, online learning platforms, and more. Proper use of this data will significantly help to build a profile of these users in any system. [6], [7]. In this context, building profiles based on ontology for career recommendation is proposed in this paper.

This paper consists of five sections: First, it starts with a description of the Moroccan education system (MES). After that, it introduces the classification of students based on a combination of grades and skills. Then, it focuses on the prerequisites needed to integrate the desired field or pathway. It continues by describing our solution for career recommendation. Finally, it'll conduct an experiment on different students, and evaluate the effectiveness of the proposed solution as shown in figure 1 and 2.

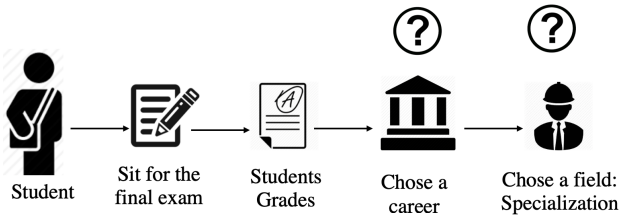

Figure 1: Problematic of career guidance

*Corresponding Author: Alimam Med Abdellah, Morocco, Tangier, ma.alimam@gmail.com

2 State of the Art

2.1 General Context

In [8], the author defined 'Career guidance and orientation' as: a procedure that helps the individual to make himself known and understand with himself, and the world of work, with the specific purpose of making professional, instructive life choices.

Services that intend to set any person at any phase of his life, in order to make educational, training or occupational choices or manage his career' is another definition made by [9].

Though, in the MES, students select a pathway, without consideration of their personal skills and capabilities. The main cause is the strong dependence between the assignment and the cumulative grade point average (GPA): The higher your GPA, the more likely you are to integrate your desired filed, even if you do not have the required skills. Which penalizes the education system, as well as the students, causing them to miss their careers. In [10], the author emphasizes that, reflection and personalization can be directly related to student profiles to resolve this issue.

The objective of this work is to offer a guidance system to scientific students, at any stage. In [11], a model for guiding the 9th Grade students in an e-learning context was presented. Still, this solution couldn't work on the higher level studies: the 9th Grade students study roughly the same materials as in the first year of high school. But it's not the general situation: students will study subjects totally different from what they have in their current year. Which prevents us from comparing these subjects.

In [12], Amines proposed a solution for affecting the 9th's grades, of the MES (Described in detail in Chap 2.2) student to their adapted pathway.

However, this model couldn't be applied in a higher scale. It wouldn't work on the students of preparatory classes for the integration of engineering school (PCGE), because it wouldn't be possible to compare their actual subjects with the ones that that'll encounter in the engineering schools.

Then, in [1], the author came up with a solution by developing an automated system that realizes the affectation of the PCGE students t to their adapted engineering specializations, by converting the extracted to the same type.

After that, in [13], a general model for career recommendation was established, enabling the guidance of scientific students, at any stage on their life.

In this paper, students profiles will be built by the aid of ontologies, allowing more performance and accuracy for the proposed solution, of career recommendation.

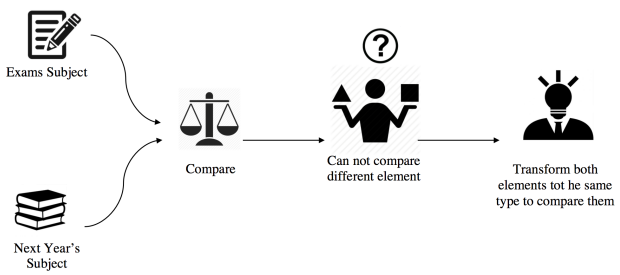

Figure 2: Problematic of guidance process

2.2 The Moroccan Education System: A general description

In the MES, there is:

1. Elementary education, or primary school: 6 years
2. Middle school (MS): 3 years. All the students study the same subjects untill the 9th grade.
3. High school:3 years. At this point, the student will have to choose a field from the 15^{th} offered by the MES. 5 from the are scientific. In the 2^{nd} year, the student sits for a primary exam. In the 3^{rd} and final year, he will have to sit for the final exam as shown in figure 3.

In the MES, the grades are scaled from 0 as a minimum, to 20 as a maximum.

2.3 Process of Career Guidance

From figure 4, it can be shown that the MES consists of 4th principals stages.

In the 1^{st} and 2^{nd} one, guidance is not required: there are only common studies.

In the 3^{rd} stage (high school), the student will have to select one from the 15^{th} fields offered by the MES: Career recommendation is mandatory at this stage. To do so, the solution proposed in [1] will be used, based on RAISEC . This model is based on comparing the students' grades of their actual year, with those of the next year, calculated according to subjects' coefficient of each field.

In the 4^{th} stage, using the same solution for higher education is not possible, due to the great difference between the subjects of the university and those of the high school.

As a solution, the skills model can be used: the subjects will be converted into a standard type, of the same range. Thus, comparing these subjects one with another can be easily done, without any confusion.

In this paper, the science process skill (SPS) model is chosen, because it suits the most the goal of this work: SPS is developed on the basis of scientific research and is in association with cognitive and investigative skills [14], and this work aims to study scientific students.

2.4 Student Profile

According to [3] [15], Profiling can be defined as the 'process of Extracting, Integrating and Identifying the keyword-based information, in order to produce a structured Profile, and visualize the knowledge outside of these results. It's a major concept for retrieving the user pertinent information and solving difficult problems of a recommender system, such as items classification according to an individual's interest. [3].

The process of profiling a web user, consist of the act of getting values of different properties, that forms the user's model [16]. It can be either behavior based or knowledge based (already known/factual) [16].

Social profiling [17] techniques will be used also for user profiling: This process can be simplified by implicit usage of user's data, while their registration via Facebook [17]. We

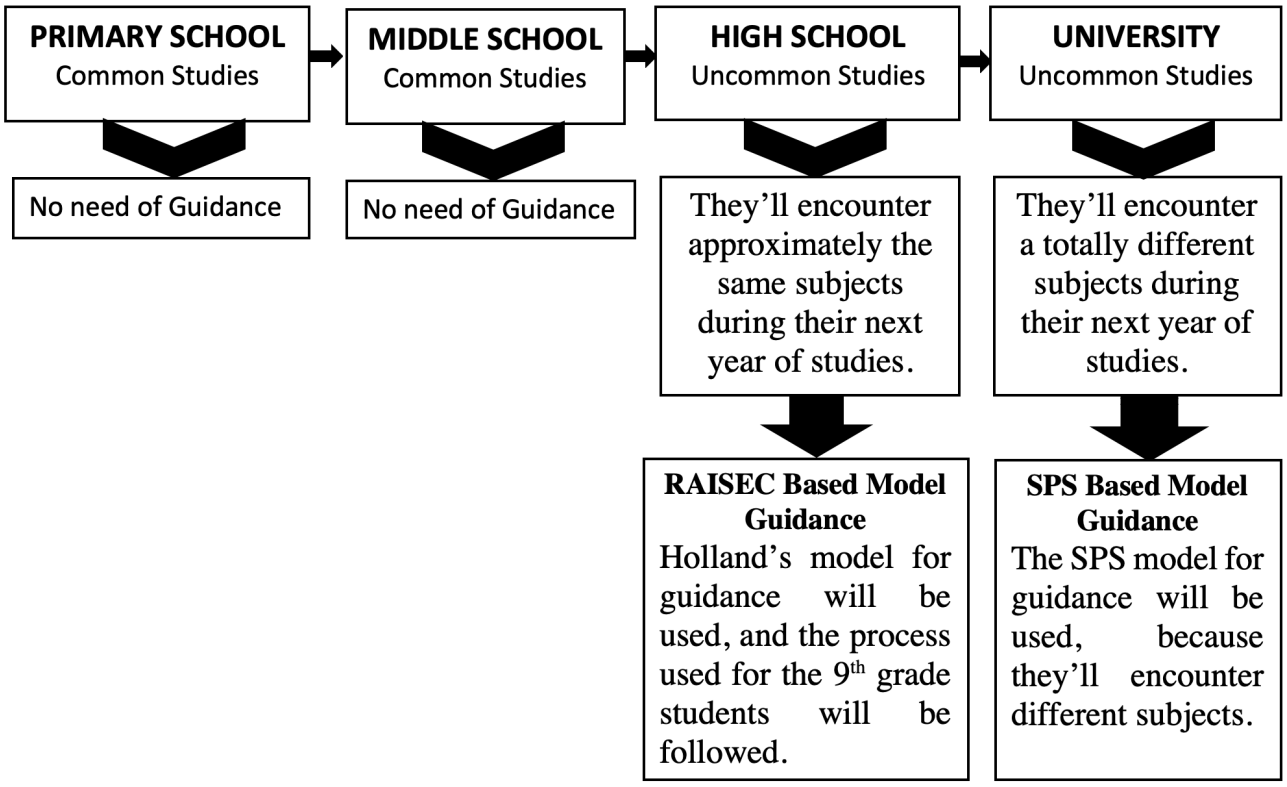

Figure 3: Description of the Process of Career Guidance

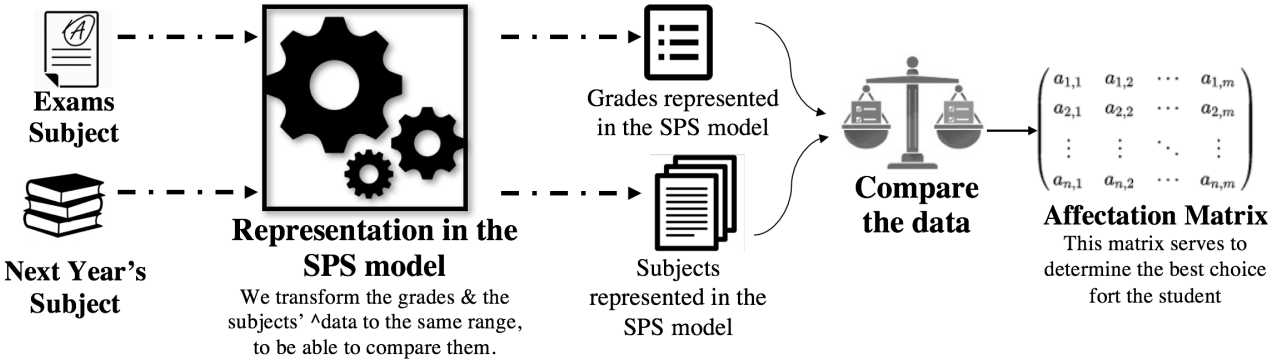

Figure 4: Guidance Process Model

do use this last to extract variable user's attributes from the user's Facebook accounts [15].

2.5 Student Ontology

Collect the student's modeling data is time-consuming process, that demands the development of complex data structures to represent student's personal information, knowledge and behavior in the learning domain [18].

Recently, student modeling researchers have begun to adopt technologies, applications, and standards from the Semantic Web to solve the problems mentioned above [18]. Chen & Mizoguchi were the first to introduce using ontologies for modeling learners[19]. Kay also asserts about using this technology, for reusable and scrutable student models[20].

2.6 Ontology Use

After collecting the student's data, converting it into a format compatible with knowledge representation and reasoning systems to operate as the input for the adaptive systems should be processed. Faced with these requirements, student modeling data is stored in general in proprietary and hard-to-access formats, which won't motivate reusing it, or its distribution.[18].

Choosing RDF and RDFS as a solution for developing the student ontology would be a good approach. However, it would be better to use Web Ontology Language, in order to beneficiate from its wide functionalities, actualities, tools support, and being an official W3C recommendation [18].

This work presents a different method of student model representation. It demonstrates a way of its achievement using the semantic web technologies.

TO build an efficient student model based on web ontologies: OIL, DAML+OIL, RDF/RDFS, OWL, languages is not evident .

The ontology language chosen is OWL DL [21], for being an official W3C recommendation in addition to its functions, tool support, and more especially the Protege 3.0 development tool. In addition, (OWL) have the benefits of

formal semantics, easy reuse, easy portability, and automatic serialization into a format compatible with popular logical inference engines [18].

2.7 Guidance Skill Model

The concept lies on supposing that a subject consists of a set of skills, assigned with different weights, enabling the comparison of the student's grades of the actual year, with next year subjects, even if they belong to dissimilar ranges, without any confusion. This work is based on the SPS, for the reason that it corresponds well to the needs if this research, and suits its goal: SPS was developed on the basis of scientific research, and this research targets scientific students. With this approach, the grades can be described as a set of SPS weighted vectors, and detect the student's reel skills.

An SPS test was developed for measuring the students' skills, with the same approach that the author did in [22]: The Test of Science Process Skill (TSPS) consisted of multiple choice items. According to [23], SPS can be classified into two categories:

- BSPS: Basic science process skills.
- ISPS: Integrated science process skills.

This work is limited to 10 skills, considered pertinent by the developing team members. These skills are enough to describe any subject. For that matter, the subjects will be described as a set of skills, with different weight. The weight will vary from 0 as a minimum, to 10 as a maximum.

The skills selected are:

1. 1^{st} skill: Observing, as (s1),
2. 2^{nd} skill: questioning (s2),
3. 3^{rd} skill: hypothesizing (s3),
4. 4^{th} skill: predicting (s4),
5. 5^{th} skill: measuring (s5),
6. 6^{th} skill: using numbers (s6),
7. 7^{th} skill: experimenting (s7),
8. 8^{th} skill: interpreting (s8),
9. 9^{th} skill: communicating (s9),
10. 10^{th} skill: memorizing (s10).

To compare two different subjects, you can compare only their skills weights.

3 System Architecture and Design

3.1 General Architecture

We'll use the general architecture developed by Amine [12], for career guidance. (fig Process Architecture). It consists of four main modules:

- Assignment module: which relies on algorithm, assigning each student to an appropriate category, according to the RAISEC / SPS test results, as well as his or her academic background.
- Ontology module: Store all the student's data. This module demonstrates the way in which the content of information is structured.
- Recommendation module: Exploit the assignment results, and usage history, to give directions to the Adaptation module
- Adaptation module: Adjust the contents, for student individual needs.

Initially, a student profile will be created by filling a form. By entering the student's 'national code' (NC), the system will connect to the student personal information and academic background. If an educational system is not yet structured, the student will have to directly supply this static information. After being registered, the elementary school students answer to a questioner based on Holland's model, and the university ones answer to SPS based test. This will determine his personal and professional tendencies and his reel capabilities. After that, these answers will be exploited, with the help of his educational background, to determine his profile. RCS usage is necessary to do it. The profile will be modeled by ontologies. We can also determine his interaction preferences, content preferences and motivations (dynamic information),by means of the browsing history, and its interaction or behavior. The results will be stored in the system, so that they can be available at any time for the adaptation module as shown in figure 5.

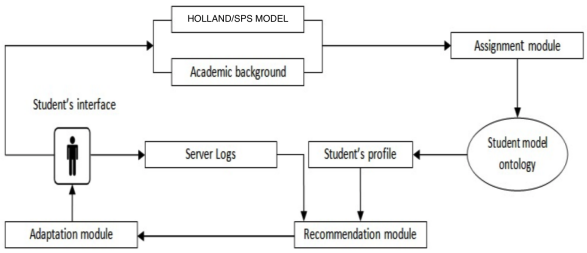

Figure 5: General Architecture

Ontology-based on the semantic web can be used to model and structure the educational domain, to be shared by a student's group. It is an explicit specification of conceptualization or a model [24].

In this paper, ontologies will be used to identify pedagogical concepts and semantic links, for representing the existing. So, students can get educational resources, and interest dynamically, and adapt it to their interests.

Figure 6, represents a part of the ontology diagram, composed of 4 main higher levels:

- Student's Level: Student's background, his actual level and results based on the proposed solution.
- Student's Profile: Student's classification based on RAISEC/SPS model, and his actual career pathway assignment.

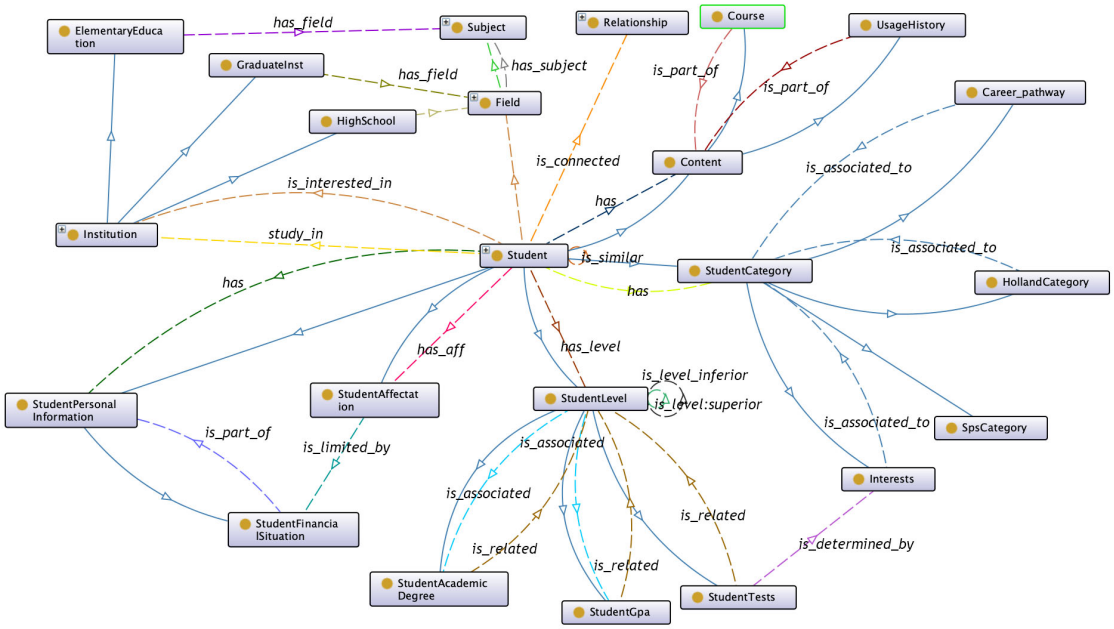

Figure 6: Part of the Student Ontology diagram

- Student's Personal Information: presents static/permanent students' information.
- Content: Information related to the pedagogical content of the students' interface.

The purpose of this career recommendation ontology is to take advantage of student orientation in order to personalize their web content and define similarities of profiles.

The figure 7 shows a partial part of the ontology's object properties.

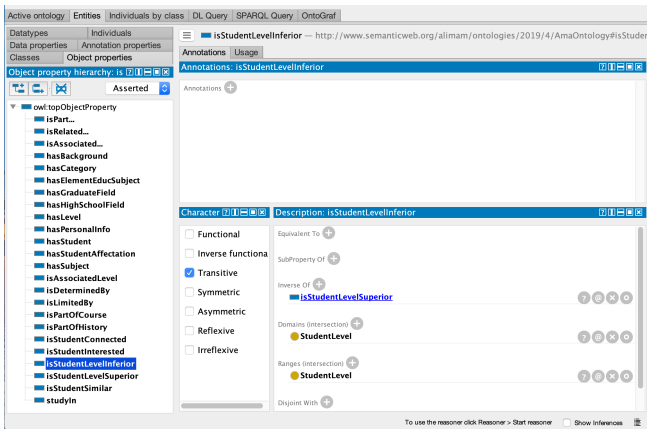

Figure 7: Part of the ontology object properties

3.2 Notations

This work, uses the same nomenclatures used in [1]:

n : Total students number.
Std_i : student's number i.
m : Total number of skills.
S_k: skill number k.
p : Actual year Total subjects number.
Sub_j: subject number j.
q : Total School's field subjects number.
t : Total School's field number.
g_{ij} : The grade of the student' i on the subject j.

3.3 Representation of a Subject on the Skill Mode

Using SPS is essential for learning with understanding [25]. For that matter, this paper propose a model for representing a subject on the Skill Mode. Comparing 2 subjects of different types, implies that they can be represented in the same format. For that reason, the author in [1] proposed the theory of Skill mode:

Given a subject j, j can be described as a vector Sub_j composed of a set of skills, with different weight ω_{jk}:

$$Sub_j = \left(\omega_{j1}, \quad \omega_{j2}, \quad \ldots \quad \omega_{jm}\right) \tag{1}$$

Where m is the total skills' number

For instance, the Mathematics can be described as follow:

$$Math\left(2 \quad 8 \quad 9 \quad 8 \quad 2 \quad 6 \quad 2 \quad 9 \quad 3 \quad 4\right)$$

meaning that the Observing Skill S_1 has a weight of 2, the Questioning Skill S_2 has 8, ..., and the Memorizing Skill S_{10} has 4 as a weight. These weights can be assigned according to the institution requirements, and the tutors' vision. Which means that they can vary from a school to another one.

After building all the subjects vectors of total number q, the matrix of the skill mode composed of these subjects is defined as follow:

$$M_{Subj} = \begin{array}{c} \\ \mathbf{S}ubj_1 \\ Subj_2 \\ \vdots \\ Subj_q \end{array} \begin{array}{c} \begin{array}{cccc} S_1 & S_2 & \cdots & S_m \end{array} \\ \begin{pmatrix} \omega_{11} & \omega_{12} & \cdots & \omega_{1m} \\ \omega_{21} & \omega_{22} & \cdots & \omega_{2m} \\ \vdots & \vdots & \ddots & \vdots \\ \omega_{q1} & \omega_{qe} & \vdots & \omega_{qm} \end{pmatrix} \end{array} \quad (2)$$

3.4 Representing a student's grades on the Skill Mode

The first step is to transform the grades of the students, like what was done previously for the subjects, to a standard form. The skill mode representation is the solution that'll allow as the manipulation, usage, and comparison of the grades with high flexibility.

Let $G_{Student_i} = \begin{pmatrix} g_{i1}, & g_{i2}, & \dots & g_{ip} \end{pmatrix}$ be the student grades,

And let M_{Subj} with weights ω_{jk} the skill mode matrix, of the student's grades. The weights ω_{jk} refers to the weight of the skill k, and for the subject i.

With the same process done to the subjects, the student can be represented by a vector composed of his subjects' grades, converted to skill mode: $G^*_{Student_i} \begin{pmatrix} g^*_{i1}, & g^*_{i2}, & \dots & g^*_{im} \end{pmatrix}$ where:

$$g^*_{ik} = \frac{\sum_{l=1}^{m} (g_{il} * \omega_{l,k})}{\sum_{l=1}^{m} \omega_{l,k}} \quad (3)$$

3.5 Calculus of the student's Reel Grades

The singular use of GPA, without taking into consideration the real abilities of the learner, will lead to an erroneous orientation [23]. Using an SPS test is crucial for understanding and validating one's real abilities, allowing a more realistic representation of one's profile.

In this paper, in addition to the usage of the SPS test, the profiling vector will be added to the vector the results in order to have more accuracy in the results.

Let $C_i = \begin{pmatrix} c_{i1}, & c_{i2}, & \dots & c_{im} \end{pmatrix}$ be the vector representing the coefficients of the students' skills, resulted from his SPS test.

The vector $P_i = \begin{pmatrix} p_{i1}, & p_{i2}, & \dots & p_{im} \end{pmatrix}$ is representing the coefficients of the students' skills, calculated based on his profiling data.

The student's reel grades are defined as follow:

$R_i \begin{pmatrix} r_{i1}, & r_{i2}, & \dots & r_{im} \end{pmatrix}$, where :

$$r_{il} = g^*_{il} \cdot max_{(}c_{il}, p_{il}) \quad (4)$$

The vector R_i represents the reel student profile and capacities, that will be used later on for calculating his affectation.

Given F_f a field of a certain school, this field consists of a set of subjects S_j. The vector $SF_f \begin{pmatrix} S_1, S_2 \dots, S_n \end{pmatrix}$ represents the representation on the skill mode of F_f, that referes to the field f

We can define the School Fields Matrix as:

$$SF = \begin{pmatrix} S_{1,1} & S_{1,2} & \cdots & S_{1,m} \\ S_{2,1} & S_{2,2} & \cdots & S_{2,m} \\ \vdots & \vdots & \ddots & \vdots \\ S_{t,1} & S_{t,2} & \cdots & S_{t,m} \end{pmatrix} \quad (5)$$

Where t is the fields' total number.

From: R_i, the reel grade vector of the student i, and, SF, the representation of the fields on the skill mode, The affectation vector can be inferred, and calculated as follow: $A_i = \begin{pmatrix} a_{i1}, & a_{i2}, & \dots & a_{it} \end{pmatrix}$ on the basis of his grades of each field, where:

$$a_{if} = \frac{\sum_{l=1}^{m} (r_{il} * S_{f,l})}{\sum_{l=1}^{m} S_{f,l}} \quad (6)$$

From 6, it can inferred that the affectation is proportionally relative to a_{if}: The greater is a_{if}, the better it would be the student's grade on the field F_f, leading to a more preferable affectation. Finally, the student α best choice would be the field χ, calculated as follow:

$$a_{i\chi} = \max_{1 \le l \le t} a_{il} \quad (7)$$

F_χ would be the student best-fitted choice.

4 Experiments and Results

In this chapter, experimentation of the model presented will be realized. To do this, a sample of 50 baccalaureate students who passed the final high school exam chose to study them. It will be calculated their assignments, and an analysis of the results will be established thereafter. The scientific fields that have been chosen for this experiment are:

- Mathematics Sciences (SMA).
- Life and Earth Sciences (SVT).
- Physics and Chemistry (PC).
- Mechanical Technics Science (STM).
- Electrical Technics Science (STE).

10 students from each field were chosen to form the test sample.

Two among the main institutions of the city of Tangier, were chosen, namely:

- The faculty of Science of Tangier (FST).
- Office of Vocational Training and Promotion of Labor (OFPPT)

The fields available at the fst are:

- Mathematics, Computer science, Physics and chemistry (MIPC).
- Biology, Chemistry and Geology (BCG).
- Electric and Mechanics (GE Gm).

For the Ofppt, it has 4 fields or specializations. The duration of studies is 2 years, with a total of 4 semesters.

The fields taught at the Ofppt are:

- Computer developing Technics (TDI).
- Computer Networks Technic (TRI).
- Multimedia Development Technics (TDM).
- Infographics (Inf).

At first, student grades will be extracted from their final exams.

These notes will then be studied for a career recommendation purpose.

The tables 1 to 5 show students' grades in their last year of high school.

Table 1: Mathematics Science student grades

Mathematics sciences								
Subj	Ar	Fr	HG	Math	PC	SVT	Philo	Eng
Student/Coef	2	4	2	9	7	3	2	2
Student 10	8	19	14	17	18	15	6	9
Student 11	15	18	17	15	16	9	15	19
Student 12	16	14	15	18	19	17	14	15
Student 13	15	12	16	20	19	13	10	10
Student 14	11	16	10	17	14	10	8	13
Student 15	14	8	12	11	17	9	15	9
Student 16	7	12	14	9	15	17	9	15
Student 17	13	16	13	12	13	19	12	14
Student 18	12	14	14	10	16	13	14	12
Student 19	10	12	12	16	8	15	10	10

Table 2: SVT Students Grades

SVT								
Subj	Ar	Fr	HG	Math	PC	SVT	Philo	Eng
Student/Coef	2	4	2	7	5	7	2	2
Student 20	13	14	19	20	14	17	14	12
Student 21	15	8	18	20	19	17	12	10
Student 22	16	6	11	14	18	10	13	14
Student 23	18	14	12	19	13	10	7	10
Student 24	19	14	13	13	13	12	9	10
Student 25	13	12	12	14	17	15	9	12
Student 26	12	8	9	11	17	14	13	13
Student 27	18	8	12	14	15	14	6	14
Student 28	15	8	6	12	15	15	12	15
Student 29	11	5	14	16	18	8	12	8

Table 3: PC Students Grades

Physics Chemistry							
Subj	Ar	Fr	Math	PC	SVT	Philo	Eng
Student/Coef	2	4	7	7	5	2	2
Student 30	20	13	17	17	15	12	14
Student 31	18	15	13	14	17	12	17
Student 32	13	10	18	13	12	11	6
Student 33	11	14	16	11	15	11	16
Student 34	12	11	14	14	17	5	9
Student 35	16	12	15	16	9	6	12
Student 36	18	13	10	13	11	6	13
Student 37	16	14	17	13	9	10	11
Student 38	14	13	13	14	12	10	9
Student 39	18	6	15	17	12	10	10

Table 4: MTS Students Grades

Sc tech Mecanic							
Subj	Ar	Fr	Math	PC	SI	Philo	Eng
Student/Coef	2	4	6	6	8	2	2
Student 40	13	13	11	20	12	6	9
Student 41	14	12	14	16	12	13	13
Student 42	15	13	13	13	15	14	11
Student 43	10	12	14	15	12	12	14
Student 44	14	12	12	15	13	12	14
Student 45	9	13	13	16	11	10	11
Student 46	19	13	9	13	11	14	10
Student 47	12	13	5	13	12	10	4
Student 48	17	13	10	14	9	6	9
Student 49	11	11	11	13	12	19	7

Table 5: ETS Students Grades

Sc tech Mecanic							
Subj	Ar	Fr	Math	PC	SI	Philo	Eng
Student/Coef	2	4	6	6	8	2	2
Student 50	14	14	14	15	11	10	16
Student 51	19	12	12	16	15	8	11
Student 52	15	15	16	16	11	13	11
Student 53	11	3	12	18	15	12	13
Student 54	10	7	11	17	14	12	11
Student 55	10	16	13	11	13	13	15
Student 56	9	7	13	16	14	16	9
Student 57	10	10	10	13	17	14	9
Student 58	14	10	11	14	13	12	12
Student 59	11	14	12	15	12	10	12

Each line of these tables represents the vectors of the students' grades $G10$, $G11$, ...and $G59$ respectively of $Student10$, $Student11$,...$Student59$.

4.1 Matrix Subjects of final year High School

Let M_{BAC} be the Matrix of the final year of high school exam Subjects. After assigning the skills weights of each subject by the members of the research team, M_{BAC} can be written as bellow:

$$M_{BAC} = \begin{array}{c} \\ Ar \\ Fr \\ M \\ PC \\ SV \\ SI \\ Ph \\ En \end{array} \begin{array}{c} \begin{array}{cccccccccc} S1 & S2 & S3 & S4 & S5 & S6 & S7 & S8 & S9 & S10 \end{array} \\ \begin{pmatrix} 3 & 1 & 1 & 1 & 1 & 1 & 1 & 1 & 10 & 9 \\ 3 & 1 & 1 & 1 & 1 & 1 & 1 & 1 & 10 & 9 \\ 2 & 8 & 9 & 8 & 2 & 6 & 2 & 9 & 3 & 4 \\ 7 & 4 & 7 & 5 & 7 & 4 & 7 & 7 & 2 & 6 \\ 7 & 5 & 7 & 7 & 6 & 2 & 6 & 7 & 3 & 7 \\ 7 & 4 & 7 & 5 & 7 & 4 & 7 & 7 & 2 & 6 \\ 5 & 7 & 7 & 5 & 1 & 1 & 3 & 7 & 7 & 7 \\ 3 & 1 & 1 & 1 & 1 & 1 & 1 & 1 & 10 & 9 \end{pmatrix} \end{array}$$

4.2 Representation of the student Grades on the skill mode

The first step is to calculate $G10$, $G11$, ...$G59$, that represents the student's grade on the skill mode, using (3), and calculate G^*10, G^*11, ...G^*59,

For G^*10, (3) will be used in order to calculate $G^*_{10}(2)$, $G^*_{10}(3)$, ...till $G^*_{10}(10)$.

For example:

$$G^*_{10}(1) = \frac{8*2*3+19*4*3+14*2*1+17*9*2+18*7*7+15*3*7+6*2*5+9*2*3}{3+3+1+2+7+7+5+3}$$
$$G^*_{10}(1) = 62.$$

With the same way, $G^*_{10}(2)$, $G^*_{10}(3)$, ...and $G^*_{10}(10) = 49,3$. will be calculated, in order to get G^*_{10} at the end:

$$G^*_{10}\ (\ 62{,}0 \quad 74{,}4 \quad 78{,}2 \quad 75{,}3 \quad 80{,}4 \quad 97{,}8 \quad 74{,}2 \quad 76{,}5 \quad 43{,}1 \quad 49{,}3\ )$$

In the same way, the other grades vectors represented in the skill mode of the students will be calculated. For calculation details and results, please refer to the appendix.

4.3 Calculus of the students' Reel Grades

The real grades of the students will be calculated from:

- Grades vectors represented in the skill mode G^*10, $G^*11, \ldots G^*59$.
- The skill coefficients of the students $C10$, $C11$,... and $C59$.

The Grades vectors represented in the skill mode were calculated in the previous chapter. For students' skill coefficients, they are described in detail in the appendix 'Calculus of the student Reel Grades'. (4) can be used then in order to calculate the reel grades. For example, to calculate R_{G10}, the student 10 real grade:

C_{10}(0,70 0,90 0,80 0,50 0,60 0,60 0,60 0,90 0,70 0,50)

Then:

G^*_{10}	(62,0	74,4	78,2	75,3	80,4	97,8	74,2	76,5	43,1	49,3)
*										
$max_{c,p(10)}$	(0,70	0,90	0,80	0,50	0,60	0,60	0,60	0,90	0,70	0,60)
------	----	----	----	----	----	----	----	----	----	----
$=R_{G10}$	(43,4	66,9	62,5	37,6	48,2	58,7	44,5	68,9	30,2	29,6)

The same calculus will be to all the other students. For the full results and calculus, please refer to the appendix, subsection 'Calculus of the student Reel Grades'.

4.4 Calculus of the School fields Matrix

The following abbreviations will be used for the Faculty of science of Tangier:

- F_{MP} : Mathematics, Physics, Chemistry & Computer science
- F_{GEM},Electrical and mechanical.
- and F_{BCG} Biology Geology & Chemistry field.

For the offpt, the following abbreviations will be used :

- F_{TDI} Computer software technics.
- F_{TRI} Network Technics.
- F_{TDM} multimedia developing technics.
- F_{Inf} Infographics.

The matrix FieldR_G will be deduct from the calculation of all the skill vectors, for all the modules and fields:

	S1	$S2$	$S3$	$S4$	$S5$	$S6$	$S7$	$S8$	$S9$	$S10$
F_{MP}	5	6	9	8	3	7	6	6	3	4
F_{GEM}	6	6	9	6	7	7	7	6	5	5
F_{BCG}	8	8	7	6	3	4	7	8	2	6
F_{TDI}	1	7	7	9	3	7	4	9	5	4
F_{TRI}	9	7	9	1	4	5	4	4	5	6
F_{TDM}	9	6	5	3	8	5	7	5	3	4
F_{Inf}	7	1	1	5	5	2	6	1	4	3

4.5 Calculus of the Affectation Vector

Using (7), the affectation of $Student10$ can be calculated as follow:

$$a_{10fst} = \max_{1 \le j \le f} a_{\alpha j} = 55,1 = a_1$$

which means that $F_{fst} = 1$, corresponding to F_1. The $Student10$ should be affected to the MP.
In the same way, the assignment of the other students will be calculated.

The following tables, show the results of the affectation, for each student.

The results are grouped by students' high school fields. The grades can be easily compared, with the affectation of each field, for each institutions.

The tables 6 to 10 show the results of the differents fields.

Table 6: Mathematics Science Affectation

	GPA	FST				Ofppt		
		F_{TDI}	F_{TRI}	F_{TDM}	F_{Inf}	F_{MIP}	F_{GEM}	F_{BCG}
Std11	14.4	52.0	50.5	50.2	45.5	55.1	51.7	51.6
Std12	14.5	43.2	46.2	45.8	30.7	47.7	48.9	42.6
Std13	15.8	57.7	56.5	55.2	47.3	60.0	56.3	57.6
Std14	15.2	47.8	53.8	49.6	47.2	55.3	50.5	52.0
Std15	13.0	41.2	41.0	38.7	36.5	46.1	41.1	39.0
Std16	11.4	41.3	41.2	41.2	36.5	43.0	42.3	41.9
Std17	11.4	33.4	36.2	36.4	23.1	33.9	37.8	35.0
Std18	12.8	37.1	41.1	40.8	35.0	41.1	43.1	37.9
Std19	12.2	41.6	40.4	40.7	33.7	44.7	42.5	40.1
Std20	11.4	38.2	36.9	37.0	32.9	41.7	39.5	35.8

Table 7: SVT Affectation

	GPA	FST				Ofppt		
		F_{TDI}	F_{TRI}	F_{TDM}	F_{Inf}	F_{MIP}	F_{GEM}	F_{BCG}
Std21	16.2	49.6	50.4	48.5	43.8	52.9	50.6	47.8
Std22	16.0	52.5	50.6	51.0	45.3	55.2	54.8	51.5
Std23	12.6	36.1	37.8	36.3	28.3	42.8	39.6	35.4
Std24	13.6	41.9	41.1	40.3	33.3	44.3	42.0	42.7
Std25	12.8	41.7	37.9	39.6	28.1	42.8	42.5	38.3
Std26	14.0	45.5	46.8	47.4	45.7	49.2	50.6	45.9
Std27	12.5	35.9	38.6	39.0	29.9	36.1	39.9	37.8
Std28	13.1	41.2	40.4	40.0	39.9	43.8	43.3	38.9
Std29	12.5	38.2	38.5	38.6	39.5	43.1	41.0	38.3
Std30	11.9	41.0	41.1	41.1	32.9	45.6	45.1	38.6

Table 8: PC Students Grades

	GPA	FST				Ofppt		
		F_{TDI}	F_{TRI}	F_{TDM}	F_{Inf}	F_{MIP}	F_{GEM}	F_{BCG}
Std31	15.3	36.8	44.2	41.7	39.9	40.2	40.6	44.0
Std32	14.7	44.3	43.7	43.9	44.0	46.7	44.9	45.2
Std33	13.0	38.5	39.9	40.5	37.6	41.4	42.9	39.1
Std34	13.3	34.0	36.3	35.2	31.3	36.8	36.5	33.9
Std35	13.2	36.0	37.7	38.3	31.9	38.1	39.8	36.5
Std36	13.2	34.5	35.3	35.1	31.6	37.3	36.9	33.0
Std37	12.0	30.8	33.5	32.8	33.6	34.1	33.8	33.4
Std38	13.0	40.1	39.5	39.3	37.4	43.3	42.3	37.1
Std39	12.6	35.0	34.9	36.7	30.9	36.9	39.0	34.0
Std40	13.0	37.5	39.9	42.8	32.9	39.6	46.0	38.6

Table 9: MTS Students Grades

	GPA	FST				Ofppt		
		F_{TDI}	F_{TRI}	F_{TDM}	F_{Inf}	F_{MIP}	F_{GEM}	F_{BCG}
Std41	13.2	36.2	36.2	36.7	26.3	37.1	38.7	34.9
Std42	13.3	32.9	33.3	32.0	41.9	34.7	33.1	32.3
Std43	13.5	33.7	32.1	32.9	24.6	33.1	33.5	33.4
Std44	13.1	30.3	30.7	28.0	33.4	32.5	27.9	29.0
Std45	12.8	29.4	29.7	30.1	38.0	30.4	30.0	31.2
Std46	12.3	29.0	27.7	26.8	29.4	25.9	25.0	29.2
Std47	11.9	29.2	25.5	27.2	34.7	29.6	29.4	24.0
Std48	10.9	23.0	21.5	23.6	23.9	22.0	23.2	22.7
Std49	11.5	27.7	27.0	25.9	28.8	27.2	25.7	27.2
Std50	12.0	26.0	27.0	28.3	19.7	26.7	29.3	27.3

Table 10: ETS Students Grades

	GPA	FST				Ofppt		
		F_{TDI}	F_{TRI}	F_{TDM}	F_{Inf}	F_{MIP}	F_{GEM}	F_{BCG}
Std51	13.6	30.5	27.9	28.0	33.3	29.9	28.1	29.7
Std52	13.8	36.7	34.6	34.1	33.7	37.1	35.1	33.9
Std53	13.6	34.7	33.5	31.9	48.1	36.5	32.2	33.2
Std54	13.2	32.8	36.2	35.5	35.6	33.4	35.4	36.9
Std55	12.9	36.6	36.6	35.1	34.1	38.4	35.3	38.1
Std56	13.0	33.2	35.0	35.3	31.7	35.7	36.0	34.9
Std57	12.8	31.7	33.8	36.1	32.7	32.5	37.9	33.4
Std58	12.9	28.9	30.2	30.2	31.6	30.6	31.3	30.0
Std59	12.3	28.8	27.0	27.3	20.8	26.9	27.3	29.1
Std60	12.8	31.9	32.1	33.3	29.2	31.8	33.8	33.2

From the tables 6 to 10, the table 11 can be established, where the affectation summary of the students is illustrated. The table shows their affectation for both institution, the FST and OFPPT. In each institution, the affectation for each student will be calculated. Then, compare their real choice, with their best suitable field, that is expressed in the relevance column: A 'True' mention for an accurate choice, and 'False' in the other case.

5 Analysis

In this section, an analyze the results will be done.

According to these calculations, the percentage of relevant choices made by the student can be inferred. In global, more than 50% of the students made a wrong choice, which means that 1 out of 2 students will follow a wrong pathway, leading him to failure. We can notice also, that all the students with a high GPA, chose the FST rather than the Ofppt. In this institution, many students tend to select the MIP field, just because it's the tendency, while they would perform better in other fields. It is the case for the student 12, 31 and others. We can conclude that students chose a given field, only if their GPA allows it. Figure 8 compares the affectation with the real choices for the FST.

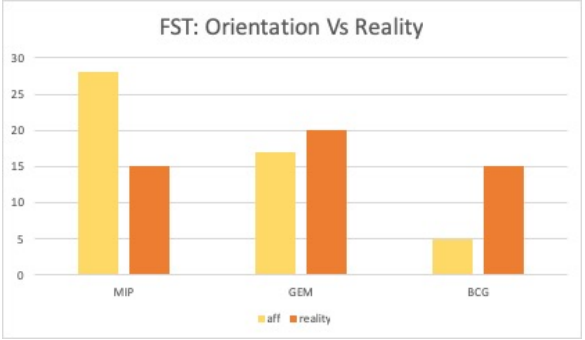

Figure 8: FST: Orientation Vs Reality

Table 11: Students affectation summary

	Affectation Ofppt		Affectation FST		Relevance	
	$affo_{fppt}$	F_{Ofppt}	$affo_{FST}$	F_{FST}	Reel choice	T/F
Std11	52.0	F_{TDI}	55.1	F_{MIP}	F_{MIP}	T
Std12	46.2	F_{TRI}	48.9	F_{GEM}	F_{MIP}	F
Std13	57.7	F_{TDI}	60.0	F_{MIP}	F_{MIP}	T
Std14	53.8	F_{TRI}	55.3	F_{MIP}	F_{MIP}	T
Std15	41.2	F_{TDI}	46.1	F_{MIP}	F_{GEM}	F
Std16	41.3	F_{TDI}	43.0	F_{MIP}	F_{Inf}	F
Std17	36.4	F_{TDM}	37.8	F_{GEM}	F_{TDM}	F
Std18	41.1	F_{TRI}	43.1	F_{GEM}	F_{TDI}	F
Std19	41.6	F_{TDI}	44.7	F_{MIP}	F_{TDM}	F
Std20	38.2	F_{TDI}	41.7	F_{MIP}	F_{Inf}	F
Std21	50.4	F_{TRI}	52.9	F_{MIP}	F_{MIP}	T
Std22	52.5	F_{TDI}	55.2	F_{MIP}	F_{MIP}	T
Std23	37.8	F_{TRI}	42.8	F_{MIP}	F_{TRI}	F
Std24	41.9	F_{TDI}	44.3	F_{MIP}	F_{BCG}	F
Std25	41.7	F_{TDI}	42.8	F_{MIP}	F_{TDI}	F
Std26	47.4	F_{TDM}	50.6	F_{GEM}	F_{BCG}	F
Std27	39.0	F_{TDM}	39.9	F_{GEM}	F_{TDM}	F
Std28	41.2	F_{TDI}	43.8	F_{MIP}	F_{BCG}	F
Std29	39.5	F_{Inf}	43.1	F_{MIP}	F_{TRI}	F
Std30	41.1	F_{TDM}	45.6	F_{MIP}	F_{TDM}	F
Std31	44.2	F_{TRI}	44.0	F_{BCG}	F_{MIP}	F
Std32	44.3	F_{TDI}	46.7	F_{MIP}	F_{MIP}	T
Std33	40.5	F_{TDM}	42.9	F_{GEM}	F_{GEM}	T
Std34	36.3	F_{TRI}	36.8	F_{MIP}	F_{BCG}	F
Std35	38.3	F_{TDM}	39.8	F_{GEM}	F_{GEM}	T
Std36	35.3	F_{TRI}	37.3	F_{MIP}	F_{GEM}	F
Std37	33.6	F_{Inf}	34.1	F_{MIP}	F_{Inf}	F
Std38	40.1	F_{TDI}	43.3	F_{MIP}	F_{GEM}	F
Std39	36.7	F_{TDM}	39.0	F_{GEM}	F_{TDM}	F
Std40	42.8	F_{TDM}	46.0	F_{GEM}	F_{GEM}	T
Std41	36.7	F_{TDM}	38.7	F_{GEM}	F_{GEM}	T
Std42	41.9	F_{Inf}	34.7	F_{MIP}	F_{BCG}	F
Std43	33.7	F_{TDI}	33.5	F_{GEM}	F_{GEM}	T
Std44	33.4	F_{Inf}	32.5	F_{MIP}	F_{GEM}	F
Std45	38.0	F_{Inf}	31.2	F_{BCG}	F_{TDI}	F
Std46	29.4	F_{Inf}	29.2	F_{BCG}	F_{Inf}	F
Std47	34.7	F_{Inf}	29.6	F_{MIP}	F_{Inf}	F
Std48	23.9	F_{Inf}	23.2	F_{GEM}	F_{Inf}	F
Std49	28.8	F_{Inf}	27.2	F_{MIP}	F_{Inf}	F
Std50	28.3	F_{TDM}	29.3	F_{GEM}	F_{TDM}	F
Std51	33.3	F_{Inf}	29.9	F_{MIP}	F_{GEM}	F
Std52	36.7	F_{TDI}	37.1	F_{MIP}	F_{GEM}	F
Std53	48.1	F_{Inf}	36.5	F_{MIP}	F_{GEM}	F
Std54	36.2	F_{TRI}	36.9	F_{BCG}	F_{GEM}	F
Std55	36.6	F_{TRI}	38.4	F_{MIP}	F_{TRI}	F
Std56	35.3	F_{TDM}	36.0	F_{GEM}	F_{GEM}	T
Std57	36.1	F_{TDM}	37.9	F_{GEM}	F_{TRI}	F
Std58	31.6	F_{Inf}	31.3	F_{GEM}	F_{TDI}	F
Std59	28.8	F_{TDI}	29.1	F_{BCG}	F_{TRI}	F
Std60	33.3	F_{TDM}	33.8	F_{GEM}	F_{TDI}	F

We expected that more than 25 students will choose the MIP, 5 the BCG, and 17 the GEM.

But in the reality, 15 preferred to attend the MIP, 15 the BCG, and 20 the GEM.

It's due to the quota imposed by the institution. The students can not make a choice above the threshold. They're aware of their acceptance probabilities, and not applying for a field where they have better chances in order not to miss their opportunities.

Figure 9 compares the affectation with the reel choices for the Ofppt.

The table 12 illustrates the final choice made by the students, and compare it to the affectation for each institution.

c refers to choice and *R* to relevance.

Table 12: Final affectation summary

	Affectation Ofp			Affectation Fst			Global aff		
	a_{Ofp}	C	R	a_{Fst}	C	R	Inst	F	R
St11	F_{TDI}	F_{Inf}	F	F_{MIP}	F_{MIP}	T	Fst	F_{MIP}	T
St12	F_{TRI}	F_{TDI}	F	F_{GEM}	F_{MIP}	F	Fst	F_{MIP}	F
St13	F_{TDI}	F_{TDM}	F	F_{MIP}	F_{MIP}	T	Fst	F_{MIP}	T
St14	F_{TRI}	F_{Inf}	F	F_{MIP}	F_{MIP}	T	Fst	F_{MIP}	T
St15	F_{TDI}	F_{TRI}	F	F_{MIP}	F_{GEM}	F	Fst	F_{GEM}	F
St16	F_{TDI}	F_{Inf}	F	F_{MIP}	F_{GEM}	F	Ofp	F_{Inf}	F
St17	F_{TDM}	F_{TDM}	T	F_{GEM}	F_{GEM}	T	Ofp	F_{TDM}	T
St18	F_{TRI}	F_{TDI}	F	F_{GEM}	F_{MIP}	F	Ofp	F_{TDI}	F
St19	F_{TDI}	F_{TDM}	F	F_{MIP}	F_{BCG}	F	Ofp	F_{TDM}	F
St20	F_{TDI}	F_{Inf}	F	F_{MIP}	F_{MIP}	T	Ofp	F_{Inf}	F
St21	F_{TRI}	F_{TDM}	F	F_{MIP}	F_{MIP}	T	Fst	F_{MIP}	T
St22	F_{TDI}	F_{TDI}	T	F_{MIP}	F_{MIP}	T	Fst	F_{MIP}	T
St23	F_{TRI}	F_{TRI}	T	F_{MIP}	F_{GEM}	F	Ofp	F_{TRI}	T
St24	F_{TDI}	F_{TDI}	T	F_{MIP}	F_{BCG}	F	Fst	F_{BCG}	F
St25	F_{TDI}	F_{TDI}	T	F_{MIP}	F_{GEM}	F	Ofp	F_{TDI}	T
St26	F_{TDM}	F_{TDM}	T	F_{GEM}	F_{BCG}	F	Fst	F_{BCG}	F
St27	F_{TDM}	F_{TDM}	T	F_{GEM}	F_{MIP}	F	Ofp	F_{TDM}	T
St28	F_{TDI}	F_{TRI}	F	F_{MIP}	F_{BCG}	F	Fst	F_{BCG}	F
St29	F_{Inf}	F_{TRI}	F	F_{MIP}	F_{GEM}	F	Ofp	F_{TRI}	F
St30	F_{TDM}	F_{TDM}	T	F_{MIP}	F_{BCG}	F	Ofp	F_{TDM}	T
St31	F_{TRI}	F_{TRI}	T	F_{BCG}	F_{MIP}	F	Fst	F_{MIP}	F
St32	F_{TDI}	F_{TDI}	T	F_{MIP}	F_{MIP}	T	Fst	F_{MIP}	T
St33	F_{TDM}	F_{TDM}	T	F_{GEM}	F_{GEM}	T	Fst	F_{GEM}	T
St34	F_{TRI}	F_{TRI}	T	F_{MIP}	F_{BCG}	F	Fst	F_{BCG}	F
St35	F_{TDM}	F_{TRI}	F	F_{GEM}	F_{GEM}	T	Fst	F_{GEM}	T
St36	F_{TRI}	F_{TDM}	F	F_{MIP}	F_{GEM}	F	Fst	F_{GEM}	F
St37	F_{Inf}	F_{Inf}	T	F_{MIP}	F_{MIP}	T	Ofp	F_{Inf}	T
St38	F_{TDI}	F_{TDM}	F	F_{MIP}	F_{GEM}	F	Fst	F_{GEM}	F
St39	F_{TDM}	F_{TDM}	T	F_{GEM}	F_{BCG}	F	Ofp	F_{TDM}	T
St40	F_{TDM}	F_{TDI}	F	F_{GEM}	F_{GEM}	T	Fst	F_{GEM}	T
St41	F_{TDM}	F_{TDM}	T	F_{GEM}	F_{GEM}	T	Fst	F_{GEM}	T
St42	F_{Inf}	F_{TDI}	F	F_{MIP}	F_{BCG}	F	Fst	F_{BCG}	F
St43	F_{TDI}	F_{TDM}	F	F_{GEM}	F_{GEM}	T	Fst	F_{GEM}	T
St44	F_{Inf}	F_{Inf}	T	F_{MIP}	F_{GEM}	F	Fst	F_{GEM}	F
St45	F_{Inf}	F_{TDI}	F	F_{BCG}	F_{BCG}	T	Ofp	F_{TDI}	F
St46	F_{Inf}	F_{Inf}	T	F_{BCG}	F_{BCG}	T	Ofp	F_{Inf}	T
St47	F_{Inf}	F_{Inf}	T	F_{MIP}	F_{BCG}	F	Ofp	F_{Inf}	T
St48	F_{Inf}	F_{Inf}	T	F_{GEM}	F_{BCG}	F	Ofp	F_{Inf}	T
St49	F_{Inf}	F_{Inf}	T	F_{MIP}	F_{MIP}	T	Ofp	F_{Inf}	T
St50	F_{TDM}	F_{TDM}	T	F_{GEM}	F_{GEM}	T	Ofp	F_{TDM}	T
St51	F_{Inf}	F_{TRI}	F	F_{MIP}	F_{GEM}	F	Fst	F_{GEM}	F
St52	F_{TDI}	F_{TDI}	T	F_{MIP}	F_{GEM}	F	Fst	F_{GEM}	F
St53	F_{Inf}	F_{TDM}	F	F_{MIP}	F_{GEM}	F	Fst	F_{GEM}	F
St54	F_{TRI}	F_{TDM}	F	F_{BCG}	F_{GEM}	F	Fst	F_{GEM}	F
St55	F_{TRI}	F_{TRI}	T	F_{MIP}	F_{MIP}	T	Ofp	F_{TRI}	T
St56	F_{TDM}	F_{TDM}	T	F_{GEM}	F_{GEM}	T	Fst	F_{GEM}	T
St57	F_{TDM}	F_{TRI}	F	F_{GEM}	F_{MIP}	F	Ofp	F_{TRI}	F
St58	F_{Inf}	F_{TDI}	F	F_{GEM}	F_{BCG}	F	Ofp	F_{TDI}	F
St59	F_{TDI}	F_{TRI}	F	F_{BCG}	F_{BCG}	T	Ofp	F_{TRI}	F
St60	F_{TDM}	F_{TDI}	F	F_{GEM}	F_{BCG}	F	Ofp	F_{TDI}	F

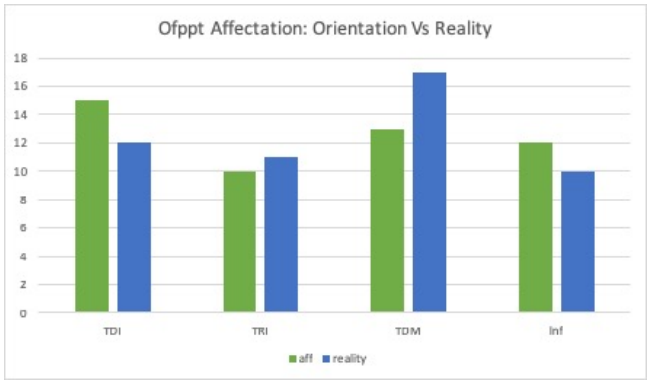

Figure 9: Ofppt Affectation: Orientation Vs Reality

We expected that 12 will choose the TDI, 10 the TRI , 13 the TDM , and 12 the Inf. But in the reality, preferred the 12 TDI, 11 the TRI , 17 the TDM , and 10 the Inf. The difference is not as great as for the FST, except for the TDM field. But in general, the students tend to choose.

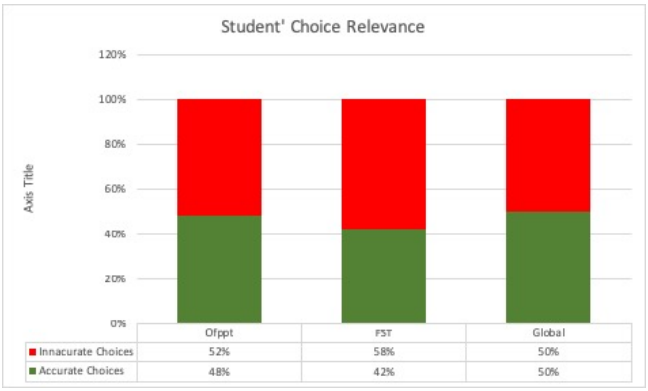

Figure 10: Student' Choice Relevance

From 12, the graph 10 can be generated, that describes the relevance for each institution, and the, a general affectation accuracy statistics.

6 Conclusion

In this work, an orientation model for science students towards their most suitable career was presented, tested and analyzed. The results of this research show that the current system of orientation penalizes students, who are forced to choose courses that are not dedicated to them, and make erroneous choices. The proposed solution would provide better guidance, to promote a better future for students, and at home.

The developed model has been submitted to the School, working in collaboration with the research team, for the purpose of using the first version of the solution. This model can be easily adapted to any education system, and be customized according to each organization needs.

We intend in the future works to integrate methodologies from Artificial Intelligence (AI) based on mathematical theories to add more significance and improvements to the actual model.

References

[1] Alimam Mohammed Abdellah, SEGHIOUER Hamid, Alimam Mohammed Amine, Cherkaoui. Automated System For Matching PCGE Students To Their Appropriate Engineering School Pathway . In :Computing Conference 2017, 18-20 July 2017 London, UK.

[2] Robert Lucas, Econometrica,61, Making a Miracle 1993

[3] Sumitkumar Kanojea, Debajyoti Mukhopadhyaya, Sheetal Girase, User Profiling for University Recommender System using Automatic Information Retrieval, Procedia Computer Science 78 (2016) 5 ' 12

[4] Antonia Martinez-Pellicera , Antonio Llamas-Botiab, Ma Belen Garcia-Palma. Career guidance in universities as a tool for the improvement of employability. The case of the University of Murcia. Procedia - Social and Behavioral Sciences 139 (2014) 56 64.

[5] Martinez R., Danalache P., Socio-professional insertion: the analysis of transition towards active life and adult life in the context of the European Union. Sociologie Romaneasca, Vol. VI, no. 2/2008, pp. 61-75

[6] Fawcett, Tom, and Foster J. Provost. "Combining Data Mining and Machine Learning for Effective User Profiling." In KDD, pp. 8-13, Portland, Oregon, USA 1996.

[7] McGarry, Ken, Andrew Martin, and Dale Addison. "Data Mining and User Profiling for an E-Commerce System." In Classification and Clustering for Knowledge Discovery, pp. 175-189. Springer Berlin Heidelberg, 2005.

[8] , B. A. Khivsara, Kale Ruchira, Naval Mayuri, Shinde Rashmi, Sonwane Ratna, IJETT, 1, Career Guidance System,4, 2017

[9] A. G. Watts, Career guidance and orientation, Chapter 7, p 241

[10] Chatchai Kruea-Ina, Nantarat Kruea-In, Witat Fakcharoenphol. A Study of Thai In-Service and Pre-Service Science Teachers Understanding of Science Process Skills. Procedia - Social and Behavioral Sciences 197 (2015) 993 997

[11] Martina Hodosyova, Jana Utlaa, MonikaVanyova, Petra Vnukova, Viera Lapitkova. The Development of Science Process Skills in Physics Education. Procedia - Social and Behavioral Sciences 186 (2015) 982 989.

[12] Alimam Mohammed Amine, SEGHIOUER Hamid, et ELYUSUFI, Yasyn. Building profiles based on ontology for career recommendation in E-learning context. In : Multimedia Computing and Systems (ICMCS), 2014 International Conference on. IEEE, 2014. p. 558-562.

[13] Alimam Mohammed Abdellah, SEGHIOUER Hamid, Alimam Mohammed Amine, Cherkaoui. Automated system for guiding scientific students to their most appropriate career. In :EDUCON Conference 2017, 25-28 July 2017 Athens, Greece.

[14] B. Jean Luc. "Methods of personality assessment". Topos Dunod, 2008.

[15] Burke, R. 2000. Knowledge-based Recommender Systems. In: A. Kent (Ed.) Encyclopaedia of Library and Information Systems, Vol. 69, Supplement 32.

[16] Sumitkumar Kanoje, Sheetal Girase, Debajyoti Mukhopadhyay, 'User Profiling for Recommender System,' 4th Post Graduate Conference for Information Technology (iPGCon-2015), Amrutvahini College of Engineering, Sangamner, 24-25 March 2015.

[17] Li, Rui, Shengjie Wang, et.al. "Towards social user profiling: unified and discriminative influence model for inferring home locations." In Proceedings of the 18th ACM SIGKDD international conference on Knowledge discovery and data mining, pp. 1023-1031. ACM, Beijing, China, 2012

[18] Desislava Paneva Ontology based student modelling Conference: Chiron Open Workshop 'Ubiquitous Learning Challenges: Design, Experiments and Context Aware Ubiquitous Learning'

[19] Chen, W., Mizoguchi, R. (1999) Communication Content Ontology for Learner Model Agent in Multi-Agent Architecture, In Proceedings of AIED99 Workshop on Ontologies for Intelligent Educational Systems

[20] Kay, J. (1999) Ontologies for reusable and scrutable student model, In Proceedings of AIED99 Workshop on Ontologies for Intelligent Educational Systems

[21] OWL Web Ontology Language Overview. W3C Recommendation 10 February 2004, Available Online: http://www.w3.org/TR/owl-features/

[22] Hidi, S. Interest and its contribution as a mental resource for learning. Review of Educational Research, 60(4), 549-571. (1990)

[23] National Science Foundation, Shaping the Future: New Expectations for Undergraduate Education in Science, Mathematics, Engineering and Technology, (Report NSF 96-139) National Science Foundation, Washington, DC, 1996.

[24] A. Altun "Ontologies for Personalization: A new challenge for instructional designers", Procedia - Social and Behavioral Sciences 64, 691 - 698, Elseiver, 2012.

[25] Abbas H. El-Zein, Chris Hedemann. Beyond problem solving: Engineering and the public good in the 21st century. Journal of Cleaner Production 137 (2016) 692-700.

[26] LTSC Learner Model Working Group of the IEEE (2000) IEEE p1484.2/d7, 2000-11-28 Draft Standard for Learning Technology - Public and Private Information (PAPI) for Learners (PAPI Learner),

[27] Claudia C, Anis oara Paveleab, Oana Ghimbulut, A Need Assessment on Students Career Guidance. BProcedia - Social and Behavioral Sciences 180 2015 1022 1029

[28] Rajaraman, Anand, and Jeffrey David Ullman. 'Mining of massive datasets'. Cambridge University Press, 2011.

[29] Smythe, C., Tansey, F., Robson R. (2001) IMS Learner Information Package Information Model Specification,

[30] Makinde. Fundamentals of guidance and counselling. Macmillan Publisher, 1993.

[31] WYNNE HARLEN (1999) Purposes and Procedures for Assessing Science Process Skills, Assessment in Education: Principles, Policy & Practice, 6:1, 129-144.

A Annexure

A.1 Representation of the student Grades on the skill mode

The representation of the vectors for SM:

G^*_{10} (62,0 74,4 78,2 75,3 80,4 97,8 74,2 76,5 43,1 49,3)
G^*_{11} (59,6 70,5 72,5 69,2 71,0 89,2 67,3 71,3 49,5 52,3)
G^*_{12} (68,9 82,9 86,5 83,1 86,9 104,8 81,5 84,5 48,3 54,6)
G^*_{13} (64,2 83,4 86,4 83,0 83,8 108,2 78,0 84,8 43,8 50,6)
G^*_{14} (52,8 68,3 69,9 67,8 66,0 89,3 61,5 68,3 41,1 44,3)
G^*_{15} (52,5 58,8 62,6 57,9 66,3 73,9 63,0 61,1 34,3 40,0)
G^*_{16} (53,2 54,2 58,7 55,9 67,1 67,4 62,6 57,3 35,7 41,6)
G^*_{17} (56,5 62,6 65,3 64,0 68,2 76,1 64,1 63,8 42,8 46,8)
G^*_{18} (55,4 58,2 62,1 58,4 67,9 72,1 64,3 60,7 39,5 44,4)
G^*_{19} (44,6 63,4 62,8 63,7 54,1 77,1 51,0 61,9 36,1 38,7)

The representation of the vectors forFor SVT:

G^*_{20} (67,7 80,1 82,4 85,2 82,8 89,4 77,6 80,7 47,1 54,5)
G^*_{21} (69,8 81,6 85,5 86,9 89,8 94,1 84,0 83,6 42,5 52,5)
G^*_{22} (55,0 61,5 64,7 63,9 68,9 72,7 65,5 63,2 36,0 42,5)
G^*_{23} (53,8 65,6 67,0 68,4 65,9 79,1 61,4 65,6 41,3 45,4)
G^*_{24} (54,3 58,0 60,6 62,1 65,4 66,8 61,1 59,2 40,2 44,9)
G^*_{25} (63,1 66,0 70,4 71,6 79,5 76,5 74,1 68,5 39,9 47,9)
G^*_{26} (58,7 59,2 63,6 63,8 73,2 66,8 69,2 61,7 35,3 43,0)
G^*_{27} (58,0 61,8 65,6 67,3 73,4 72,6 67,9 64,0 37,9 45,0)
G^*_{28} (58,4 59,1 63,1 64,2 71,8 66,4 67,6 60,8 36,2 43,0)
G^*_{29} (50,4 62,4 64,9 64,0 65,7 75,0 62,3 63,9 31,2 38,5)

The representation of the vectors for PC:

G^*_{30} (65,4 68,9 73,5 72,0 82,1 86,3 77,4 70,6 42,1 48,4)
G^*_{31} (63,4 62,7 67,0 66,7 76,6 75,5 72,2 64,1 43,2 48,2)
G^*_{32} (52,3 62,8 65,5 64,7 66,6 77,5 62,9 63,0 32,2 37,7)
G^*_{33} (54,6 60,2 62,8 63,1 66,0 72,6 62,2 60,3 38,0 41,9)
G^*_{34} (58,1 60,0 65,0 64,7 75,7 75,1 70,3 62,4 33,3 40,8)
G^*_{35} (52,7 57,2 61,0 59,0 67,6 76,1 63,2 58,8 35,3 40,0)
G^*_{36} (49,8 47,6 51,5 50,5 61,2 60,9 57,3 49,4 34,9 38,6)
G^*_{37} (51,6 59,9 62,2 61,0 63,7 76,3 60,2 59,9 36,9 40,3)
G^*_{38} (53,3 55,7 59,5 58,2 66,6 69,4 62,9 57,1 34,3 39,3)
G^*_{39} (57,0 61,8 66,4 64,4 74,4 78,6 70,1 63,9 32,8 40,0)

The representation of the vectors for STM:

G^*_{40} (50,8 58,8 64,3 61,1 56,2 64,3 55,4 63,8 45,9 52,1)
G^*_{41} (52,6 59,5 63,8 61,5 58,5 63,1 57,6 64,4 48,2 54,9)
G^*_{42} (58,2 57,2 63,3 60,0 66,8 63,8 65,2 63,8 48,1 56,6)
G^*_{43} (52,6 58,6 63,2 60,6 58,8 61,7 58,1 64,0 46,9 54,4)
G^*_{44} (53,6 57,8 62,7 59,8 59,7 62,1 59,0 62,8 46,3 53,1)
G^*_{45} (47,6 54,9 58,9 56,8 53,0 58,5 52,1 59,5 44,1 50,2)
G^*_{46} (50,1 51,0 55,1 53,1 55,5 57,0 54,0 54,9 44,9 49,5)
G^*_{47} (46,0 45,0 50,5 47,6 53,3 54,0 51,4 49,4 35,9 41,2)
G^*_{48} (42,9 46,6 50,5 48,3 45,3 50,1 44,8 50,5 42,8 46,5)
G^*_{49} (51,3 53,9 58,2 56,7 61,6 61,4 58,9 58,8 41,4 48,7)

The representation of the vectors for STE:

G^*_{50} (52,7 57,5 61,7 59,1 55,9 59,1 55,9 62,5 51,2 57,0)
G^*_{51} (56,5 58,5 65,0 61,1 63,0 64,4 62,2 64,9 48,4 56,1)
G^*_{52} (52,8 59,7 63,6 62,0 58,4 63,5 57,0 65,0 52,7 59,0)
G^*_{53} (55,1 62,9 69,4 65,4 66,2 68,6 65,3 69,3 38,4 49,4)
G^*_{54} (52,4 59,6 65,3 62,0 61,8 65,4 60,6 65,2 39,9 48,9)
G^*_{55} (55,1 54,8 59,7 56,8 60,3 58,0 59,8 60,4 49,3 56,1)
G^*_{56} (54,7 60,3 66,1 63,2 66,6 67,4 64,5 66,5 40,1 50,3)
G^*_{57} (59,4 57,4 65,1 60,7 70,9 66,0 69,2 64,8 41,4 52,1)
G^*_{58} (51,5 54,1 59,4 56,3 58,4 59,0 57,5 59,4 42,4 49,7)
G^*_{59} (49,9 54,2 58,8 56,2 55,2 58,1 54,5 59,1 45,3 51,5)

A.2 Calculus of the student Reel Grades

The vectors $C10$, $C11$,... and $C59$ represents respectively the coefficients of the students Skills, calculated on the basis of their SPS test:

The SPS coefficients for SM:

C_{10}(0,70 0,90 0,80 0,50 0,60 0,60 0,60 0,90 0,70 0,50)
C_{11}(0,90 0,90 0,80 0,20 0,70 0,80 0,30 0,50 0,40 0,20)
C_{12}(0,70 0,90 1,00 0,60 0,60 0,50 0,60 0,70 0,70 0,30)
C_{13}(0,90 0,90 0,90 0,10 0,50 0,50 0,20 0,80 0,60 0,70)
C_{14}(0,70 0,80 0,80 0,30 0,40 0,70 0,30 0,70 0,60 0,50)
C_{15}(0,80 0,90 0,70 0,60 0,50 0,60 0,40 0,80 0,70 0,60)
C_{16}(0,90 0,90 0,80 0,50 0,60 0,40 0,30 0,50 0,50 0,20)
C_{17}(0,90 0,80 0,70 0,30 0,70 0,70 0,30 0,60 0,60 0,50)
C_{18}(0,50 0,80 0,80 0,50 0,60 0,80 0,80 0,70 0,70 0,40)
C_{19}(0,60 0,70 0,70 0,40 0,80 0,70 0,40 0,80 0,70 0,50)

The SPS coefficients for SVT:

C_{20}(0,80 0,90 0,70 0,50 0,50 0,80 0,30 0,60 0,60 0,30)
C_{21}(0,80 0,50 0,90 0,70 0,60 0,50 0,30 0,80 0,70 0,30)
C_{22}(0,70 0,80 0,80 0,20 0,50 0,90 0,20 0,60 0,40 0,30)
C_{23}(0,90 0,90 0,80 0,50 0,40 0,60 0,50 0,80 0,20 0,40)
C_{24}(0,50 0,80 0,80 0,60 0,70 0,70 0,60 0,90 0,60 0,10)
C_{25}(0,90 0,80 0,70 0,40 0,70 0,80 0,30 0,60 0,40 0,60)
C_{26}(0,90 0,80 0,70 0,60 0,40 0,60 0,50 0,40 0,70 0,40)
C_{27}(0,80 0,60 0,80 0,70 0,60 0,70 0,30 0,70 0,60 0,40)
C_{28}(0,60 0,60 0,60 0,20 0,50 0,80 0,50 0,80 0,70 0,60)
C_{29}(0,80 0,70 0,90 0,30 0,80 0,80 0,30 0,70 0,70 0,40)

The SPS coefficients for PC:

C_{30}(0,90 0,80 0,80 0,20 0,30 0,40 0,50 0,50 0,40 0,70)
C_{31}(0,60 0,80 0,80 0,30 0,50 0,50 0,60 0,80 0,60 0,70)
C_{32}(0,90 0,80 0,70 0,60 0,60 0,80 0,40 0,30 0,20 0,70)
C_{33}(0,80 0,70 0,50 0,30 0,50 0,50 0,10 0,60 0,80 0,30)
C_{34}(0,80 0,70 0,50 0,30 0,50 0,70 0,30 0,60 0,80 0,30)
C_{35}(0,60 0,70 0,70 0,40 0,40 0,70 0,50 0,50 0,80 0,40)
C_{36}(0,80 0,60 0,80 0,40 0,20 0,60 0,60 0,60 0,60 0,70)
C_{37}(0,80 0,70 0,70 0,40 0,70 0,80 0,30 0,60 0,70 0,60)
C_{38}(0,70 0,60 0,50 0,40 0,70 0,60 0,30 0,90 0,80 0,20)
C_{39}(0,90 0,70 0,60 0,50 0,90 0,60 0,40 0,50 0,50 0,50)

The SPS coefficients for STM:

C_{40}(0,90 0,70 0,40 0,60 0,50 0,70 0,40 0,60 0,60 0,20)
C_{41}(0,70 0,50 0,50 0,60 0,20 0,70 0,10 0,30 0,60 0,60)
C_{42}(0,50 0,60 0,70 0,60 0,50 0,40 0,60 0,60 0,50 0,10)
C_{43}(0,50 0,70 0,60 0,40 0,20 0,80 0,40 0,30 0,50 0,30)
C_{44}(0,50 0,50 0,50 0,40 0,60 0,40 0,30 0,50 0,30 0,70)
C_{45}(0,40 0,90 0,50 0,70 0,40 0,20 0,30 0,50 0,50 0,50)
C_{46}(0,30 0,50 0,30 0,50 0,70 0,80 0,40 0,30 0,50 0,60)
C_{47}(0,30 0,70 0,20 0,40 0,40 0,30 0,60 0,50 0,40 0,50)
C_{48}(0,60 0,60 0,50 0,60 0,40 0,30 0,20 0,70 0,70 0,50)
C_{49}(0,70 0,70 0,40 0,30 0,40 0,50 0,60 0,40 0,30 0,20)

The SPS coefficients for STE:

C_{50}(0,50 0,60 0,30 0,60 0,30 0,50 0,20 0,70 0,40 0,50)
C_{51}(0,40 0,50 0,70 0,40 0,60 0,30 0,40 0,70 0,80 0,30)
C_{52}(0,10 0,50 0,60 0,60 0,50 0,70 0,50 0,40 0,40 0,80)
C_{53}(0,80 0,70 0,80 0,60 0,50 0,40 0,50 0,20 0,20 0,60)
C_{54}(0,70 0,70 0,70 0,50 0,40 0,50 0,40 0,50 0,40 0,40)
C_{55}(0,60 0,50 0,50 0,30 0,40 0,60 0,80 0,60 0,60 0,40)
C_{56}(0,80 0,70 0,50 0,60 0,60 0,70 0,40 0,20 0,10 0,40)
C_{57}(0,70 0,30 0,10 0,40 0,30 0,50 0,30 0,60 0,60 0,50)
C_{58}(0,70 0,60 0,30 0,70 0,20 0,30 0,40 0,50 0,50 0,20)
C_{59}(0,70 0,50 0,60 0,40 0,70 0,40 0,70 0,60 0,60 0,40)

The real grades for SM:

R_{G10}(43,4 66,9 62,5 37,6 48,2 58,7 44,5 68,9 30,2 29,6)
R_{G11}(53,6 63,5 58,0 27,7 49,7 71,3 33,6 35,6 24,7 10,5)
R_{G12}(48,2 74,6 86,5 49,9 52,1 52,4 48,9 67,6 33,8 27,3)
R_{G13}(57,8 75,0 77,8 8,3 50,3 54,1 15,6 67,8 26,3 35,4)
R_{G14}(37,0 54,7 55,9 27,2 33,0 62,5 18,4 47,8 24,7 22,1)
R_{G15}(42,0 52,9 50,1 34,7 39,8 44,3 37,8 48,9 24,0 24,0)
R_{G16}(47,8 48,8 52,8 33,6 46,9 27,0 25,0 28,7 17,8 8,3)
R_{G17}(50,9 50,1 45,7 19,5 54,5 53,0 19,2 38,3 25,7 23,4)
R_{G18}(27,7 46,6 55,9 29,2 40,7 57,7 51,4 42,4 27,7 17,8)
R_{G19}(30,7 44,4 44,0 25,5 43,3 53,9 25,5 49,5 25,3 19,4)

The real grades for SVT:

R_{G20}(57,6 72,1 57,5 42,6 41,4 71,5 23,3 48,4 33,0 27,2)
R_{G21}(55,8 40,8 76,9 60,9 53,9 47,1 42,0 66,9 29,7 26,3)
R_{G22}(38,5 49,2 51,7 12,8 34,5 65,5 19,6 44,2 14,4 12,7)
R_{G23}(48,4 59,0 53,6 41,0 26,4 47,4 30,7 52,5 12,4 18,2)
R_{G24}(32,6 46,4 48,5 43,4 45,8 46,8 36,7 53,3 24,1 9,0)
R_{G25}(56,6 53,0 53,5 43,0 55,7 61,2 29,6 48,0 16,0 33,6)
R_{G26}(52,8 47,4 44,5 38,3 36,6 40,1 41,5 24,7 24,7 17,2)
R_{G27}(46,4 37,1 52,5 47,1 44,0 50,5 20,4 44,7 26,5 27,0)
R_{G28}(35,0 35,5 44,2 19,3 43,1 53,1 33,8 54,7 25,3 30,1)
R_{G29}(40,3 43,6 58,4 32,0 52,6 60,3 24,9 44,7 21,9 15,4)

The real grades for PC:

R_{G30}(58,8 55,1 58,8 14,4 32,8 34,5 38,7 35,3 25,3 33,9)
R_{G31}(38,0 50,4 53,8 33,3 45,9 45,3 43,3 57,7 25,9 33,7)
R_{G32}(47,0 50,2 45,9 38,8 40,0 62,3 37,8 25,2 9,7 26,4)
R_{G33}(43,7 48,2 37,7 18,9 39,6 43,6 12,4 42,2 30,4 21,0)
R_{G34}(46,6 48,0 32,5 25,9 37,9 52,6 35,1 37,4 26,6 20,4)
R_{G35}(31,6 40,0 42,7 23,6 40,5 53,3 31,6 29,4 28,3 20,0)
R_{G36}(39,8 28,6 41,2 20,2 24,6 42,6 40,1 29,7 20,9 27,0)
R_{G37}(41,3 47,9 43,5 36,6 44,6 61,0 18,1 42,0 25,9 24,2)
R_{G38}(37,3 39,0 29,8 23,3 53,3 41,6 25,2 51,4 27,4 19,7)
R_{G39}(51,3 43,3 39,9 32,2 66,9 47,1 35,1 38,4 16,4 20,0)

The real grades for STM:

R_{G40}(45,7 41,2 38,6 36,6 33,7 45,0 33,3 38,3 32,1 10,4)
R_{G41}(42,1 29,8 31,9 36,9 23,4 44,2 17,3 32,2 28,9 38,4)
R_{G42}(29,1 40,0 44,2 36,0 33,4 25,5 39,1 38,4 24,1 11,3)
R_{G43}(26,3 41,0 37,9 24,2 11,8 49,7 23,3 19,5 28,2 27,2)
R_{G44}(26,8 29,2 31,4 23,9 35,8 24,8 29,5 37,7 18,5 37,2)
R_{G45}(28,5 49,5 29,4 39,8 21,2 11,7 15,6 29,7 22,1 25,1)
R_{G46}(15,0 25,5 16,5 37,2 38,9 51,3 21,6 22,0 22,5 29,7)
R_{G47}(13,8 35,3 10,1 19,0 32,0 27,0 30,8 24,7 14,4 20,6)
R_{G48}(30,0 28,0 30,3 29,0 22,6 15,0 13,5 40,4 34,2 23,3)
R_{G49}(35,9 37,7 23,3 22,7 24,6 37,2 35,3 23,5 12,4 9,7)

The real grades for STE:

R_{G50}(31,6 34,5 18,5 35,5 16,8 29,5 22,6 43,7 25,6 28,8)
R_{G51}(28,2 35,1 45,5 36,7 37,8 32,2 24,9 45,4 38,8 22,5)
R_{G52}(21,1 29,9 44,5 37,2 29,2 44,4 28,5 26,0 26,4 47,2)
R_{G53}(44,1 44,0 55,5 39,3 33,1 29,4 39,4 13,9 7,7 29,7)
R_{G54}(36,6 47,7 52,3 31,0 24,7 32,7 30,3 45,7 19,9 24,5)
R_{G55}(33,1 32,9 41,8 17,0 36,2 40,6 47,8 36,4 29,6 22,4)
R_{G56}(43,8 42,2 33,0 37,9 46,6 47,0 38,7 13,3 4,0 25,1)
R_{G57}(41,5 28,7 26,1 24,3 28,4 33,0 20,8 38,9 24,9 26,1)
R_{G58}(36,0 32,5 29,7 39,4 11,7 17,7 34,5 35,6 25,4 9,9)
R_{G59}(35,0 32,4 35,3 28,1 38,7 23,3 38,1 41,4 27,2 20,6)

Advances in Science, Technology and Engineering Systems Journal Vol. 4, No. 4, 42-46 (2019)

www.astesj.com

Special Issue on Recent Advances in Engineering Systems

ASTESJ

ISSN: 2415-6698

Comparison of Electrogastrograms in Seated and Supine Positions Using Wayland Algorithm

Yasuyuki Matsuura[1,*], Hiroki Takada[2]

[1]Department of Cross Cultural Studies, Gifu City Women's College, 501-0192, Japan

[2]Department of Human & Artificial Intelligence Systems, Graduate School of Engineering, University of Fukui, 910-8507, Japan

ARTICLE INFO

Article history:
Received:18 December, 2018
Accepted:26 June, 2019
Online: 11 July, 2019

Keywords:
Electrogastrogram
Gastrointestinal motility
Postural Change
Wayland algorithm

ABSTRACT

In previous study, it is difficult to estimate the biological states such as postural ones and aetas in accordance with the previous analysis of electrogastrograms (EGGs), basically the frequency resolution of healthy individuals. In addition, few studies have compared gastric myoelectrical activity in supine and sitting posture. The aim of this study is to evaluate the severity of 3D sickness in daily life. The authors herein conduct nonlinear analysis of EGGs of the healthy young and give the feasibility to discriminate the postural differences. It is suggested that the EGGs acquired in the seated position have increased wavelength irregularity and attractor complexity than those acquired in the supine position.

1. Introduction

There are a myriad of activities in our sitting posture, including paper work, light work and others, and fatigue accumulates if this position is maintained for long periods. People usually sleep and respite in a supine position. Likewise, sick people and those affected by 3D sickness take a break in the supine posture. Moreover, humans hardly get motion sickness while maintaining a supine position [1]. In contrast, a seated position can lead to experience both motion sickness, especially in moving ships, cars, and trains, and visually induced motion sickness (VIMS) that occurs while viewing stereoscopic movies. Still, few studies have made a comparison between gastrointestinal motilities in supine and those in seated posture to evaluate the severity of the VIMS.

One of the most relevant theories for VIMS is the sensory conflict theory [2-4]. According to this theory, sensory mismatch between visual and vestibular signals would be induced in virtual space compared to the real world [5]. Moreover, close anatomical and electrophysiological relationships between the autonomic and vestibular nervous systems have been reported [6]. It has been known that there is interaction between vestibular and autonomic nervous systems in the physiological fields; the motion sickness might affect both systems because dizziness and hidropoiesis are induced by the reaction of the autonomic nervous system due to the excessive stimulus for the vestibular system. For instance, it has been reported that the level of histamine increased in the hypothalamus and brainstem in rats due to the rotation stimuli, which is possibly associated with vomiting during the motion sickness [7]. In addition, motion sickness seems to be induced by the contradiction among visual, vestibular, auditory, and proprioceptive inputs. These sensory informations can be compared with the previous experiences. The sensory informations are expected from the previous ones, however, they might be deviating from the previous experiences. According to the sensory conflict theory, the motion sickness would be occurred by this kind of the divergence.

Physiological and psychological measurements are used to evaluate the influence of VIMS on the body. The latter method to evaluate VIMS is the simulator sickness questionnaire [8]. On the other hand, physiological evaluation of VIMS has been conducted using parameters such as the high- and low- frequency components of electrogastrography, skin resistance, blood pressure, heart rate volubility, sweat rate, number of blinks, and respiratory rate [9–11].

A unique rhythm is associated with each variation of a physiological phenomenon. These include short repeated cycles, such as pulses, which are repeated in units of seconds, and long cycles, such as seasonal variations, which repeat in units of years. For instance, we can observe the circadian-dependent variability in the human blood pressure [12]. This is known as intra-day blood pressure fluctuation and can have an intra-day variation pattern characterized by high blood pressure in the daytime and decreased blood pressure at night [13]. Autonomous nerve activity

*Yasuyuki Matsuura, 7-1 Hitoichiba Kitamachi Gifu 501-0192 Japan, +81-58-296-3131 & matsuura@gifu-cwc.ac.jp

https://dx.doi.org/10.25046/aj040405

considerably affects this variability. Blood pressure increases or decreases depending on the variations in circulating blood volume and postural blood pressure reflex activity due to variations in posture. Heartrate and blood pressure intra-day variations are known to act as an evaluation index for autonomic nervous function. Additionally, the head-up tilt test is known as an autonomic nervous functional test associated with passive postural change [14]. Heart rate in healthy individuals increases, and the R -R interval estimated from the Electrocardiogram (ECG) decreases when using a tilt-table to switch from a supine to standing position [14]. Also, the same effects are reportedly observed when switching from a supine to seated position [15]. In these cases, the blood is accumulated in the lower extremities, however, vasoconstriction is automatically conducted to prevent from the hypostasis. The arterial baroreceptor is known as an sensory organ to detect the variations in blood pressure owing to the postural changes and other activities. This bio-signal reaches the brain stem vasomotor center (BSVC) through afferent pathways in the medium of vagus or glossopharyngeal nerve. The BSVC is activated with decline in the activity of the afferent pathways when the blood pressure decreases, and an effect is observed in excitability toward the sympathetic nerve; Noradrenaline is secreted from vascular wall sympathetic nerve endings, and adrenaline is, therefore, secreted from the adrenal medulla. Hence, the blood pressure can be maintained. As venous return decreases, the vagus nerve activity in the afferent pathway decreases through the low-pressure receptors in pulmonary veins and the atrium. As this information is received by the brain stem and reaches the hypothalamus, arginine vasopressin is secreted from the posterior pituitary, and an increased effect occurs in vasoconstriction and circulating plasma volume. Although cardiocirculatory research after postural changes is readily available, studies regarding the impact of posture changes on electrogastrograms are limited.

Percutaneous electrogastrography allows to noninvasively examine gastric myoelectrical activity. Human gastric myoelectrical activity cannot be measured by any other conventional method such as computed tomography, gastro-fiberscopes or magnetic resonance imaging. An electrogastrogram (EGG) is usually evaluated using Fourier analysis, running spectral analysis, and other spectrum analysis. However, the information retrieved by this analysis is limited, and EGGs are not as usual as electrocardiograms, electroencephalograms, and other biosignal measurements, thus compromising their development.

In 1921, Walter Alvarez [16] recorded the first human EGG. EGGs are recorded by placing Ag-AgCl electrodes on the surface of the epigastrium. EGG records the electrical signals which travel through the stomach muscles and control the muscle contractions. Human gastric slow wave or pacesetter potential activity generated by the interstitial cells of Cajal (ICCs) occurs at a frequency of 3 cycles per minute [17] [18], as shown in Figure 1. The ICCs are known as pacemaker cells that spontaneously depolarize and repolarize. The ICCs set the myoelectrical rhythmicity of the stomach and other areas of gastrointestinal tract. Recorded EGG signals that have noise with higher frequencies > 0.15 Hz must be filtered out [19]. These filters such as a low-pass filter, a band-pass filter eliminate most respiratory and cardiac rhythms in electromyogram.

Many previous studies on electrogastrography have been conducted but have been mostly related to the clinical field [20]. For instance, hormone, drugs, and motion sickness effects on EGG have been evaluated. Likewise, EGG has been used to study the

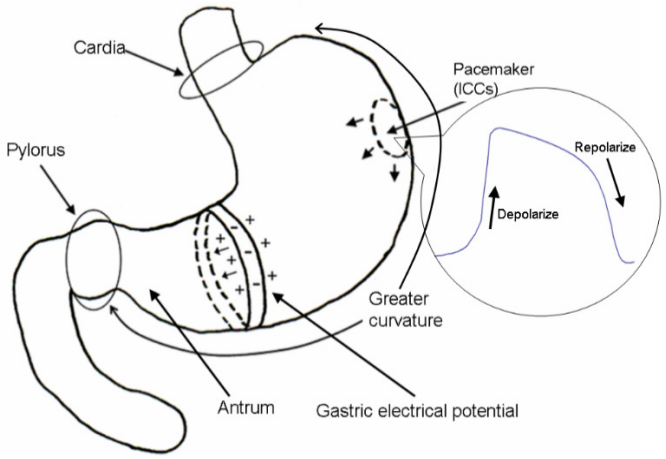

Figure 1: Traveling slow waves. The ICCs set the myoelectrical rhythmicity of the stomach and other areas of gastrointestinal tract.

effects of warm compresses on both gastrointestinal activity [21] and the epigastric region for relieving constipation [22], and to characterize the intestinal activity in patients with chronic constipation [23]. However, studies on clinical applications mainly consider patients, and hence scarce research is available on the EGG dynamics of healthy subjects.

More specifically, few studies have been focused on gastrointestinal motility in seated and supine positions to evaluate the severity of motion sickness. As it has been reported that three-dimensional motion sickness is strongly elicited when viewing stereoscopic movies for prolonged periods, it is important to assess the safety while viewing such movies. Therefore, in this study the authors compared EGGs in seated and supine positions using the Wayland algorithm to evaluate motion sickness induced by stereoscopic movies.

2. Material and Method

The participants were 5 healthy females aged 19 to 24 years. The Ethical Committee of Graduate School of Natural Sciences, Nagoya City University approved the experiment. Prior to the experiment, each participant signed their informed consents.

The design of experiment is Figure 2. This experiments was conducted, considering the order effect in the protocol. In Addition, postural change on experiment B is passive position change to remove the effect of muscle sympathetic nerve activity.

The experimental room and chair condition is Table 1. The experimental condition is Table 2. Participants finished their meals 120 mins beforehand. Therefore, the experiments were not affected by the presence of food.

Electrodes of EGG pasted on abdominal surface using 2 disposable Ag-AgCl electrodes as shown in Figure 3. Their abdominal surface of the pasting points was cleaned out with cotton moistened with ethanol and the skin abrasion (SkinPure, Nihon Kohden, Japan).

Using A/D converter, the analog signals of their EGGs were A/D-converted to digital signals at 1 kHz. A low-pass filter of 0.15 Hz eliminated the activity in respiratory, cardiac rhythms, electromyogram, and the noise of electronic devices. In addition, resampling was performed every 1 Hz to remove the noise in the abovementioned measurement.

Experiment A (Seated)

Seated Posture (Rest) 30 min	Seated Posture 90 min

t_0

Experiment B (Supine)

Seated Posture (Rest) 30 min	Supine Posture 90 min

t_0

Figure 2: Experiments A and B

Table 1: Experimental room and chair condition

Items	Conditions
Room Condition	Without windows
Sound-insulated	40dB
Room temperature	20–24°C
Air current	below 0.1 m/s
Chair size (Seating surface)	55cm (width) × 55cm (Length)
Chair size (Seating back)	55cm (width) × 58cm (Length)
Chair angle between the seating surface and the back	100 degrees

Table 2 Experimental condition and machines

Items	Condition/Machine
Measurement Start time	14:00 - 15:00
EGGs Sampling Rate	1KHz
Bio-amplifier	MT11; NEC Medical, Japan
Recorder	PC216Ax; Sony Precision Technology, Japan
A/D converter	AD16-16U (PCI) EH; CONTEC, Japan
Electrodes	Vitrode Bs, Nihon Kohden, Japan

Every 300-second, we analyzed time series data of the EGG for a 1024-second time window to divide the data (Figure 4). In this study, the authors calculated the translation error (E_{trans}) using Wayland algorithm from EGG time series data in 1 to 10 dimensional phase space [24-26].

3. Results

EGGs in seated (experiment A) and supine (experiment B) positions of healthy women over 5 min after 70 min from the beginning of measurements are shown in Figures 5(a) and (b), respectively. The EGG in seated position (Figure 5(a)) shows a large amplitude and unstable fluctuations. In contrast, the EGG in supine position (Figure 5(b)) shows a regular pattern. Figures 6(a) and (b) show the two-dimensional attractors ($\tau = 3$) generated from the EGGs in seated (Figure 5(a)) and supine (Figure 5(b)) positions, respectively.

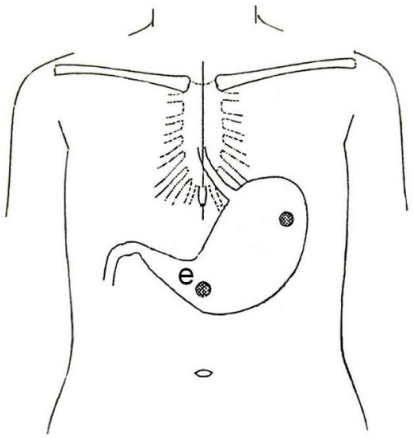

Figure 3: Electrodes position pasted on the surfece of body.

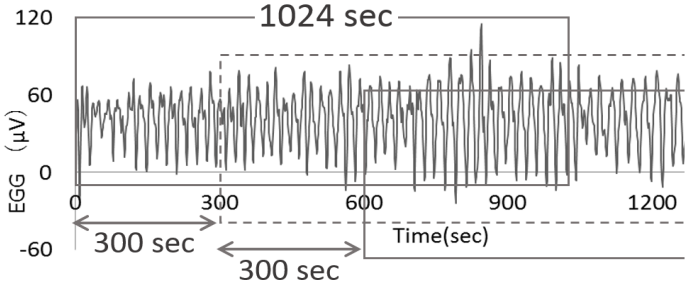

Figure 4: Moving segment of EGG-data.

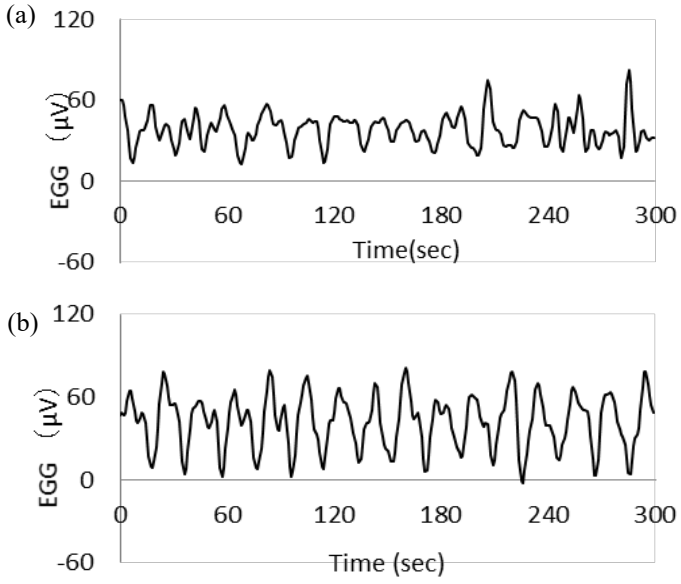

Figure 5: Typical examples of EGG in (a) experiment A and in (b) experiment B.

The EGG translation errors over a ten-dimensional embedding space in the seated position (excluding control) ranged from 0.27 to 0.58, with average of 0.46 and standard deviation of 0.07. The similar EGG translation errors in the supine position ranged from 0.23 to 0.52, with average of 0.40 and standard deviation of 0.08. The authors compared the translation errors estimated from the EGGs of experiment A with those of experiment B. Variations of z-scores of translation error (average ± standard error) were

estimated from the EGGs of the individuals in the ten-dimensional embedding space (Figure 7). The *z*-scores in the seated position (excluding control) ranged from –2.48 to 2.45, with average of 0.07 and standard error of 0.42, and those in the supine position ranged from –1.63 to 3.18, with average of 0.04 and standard error of 0.42.

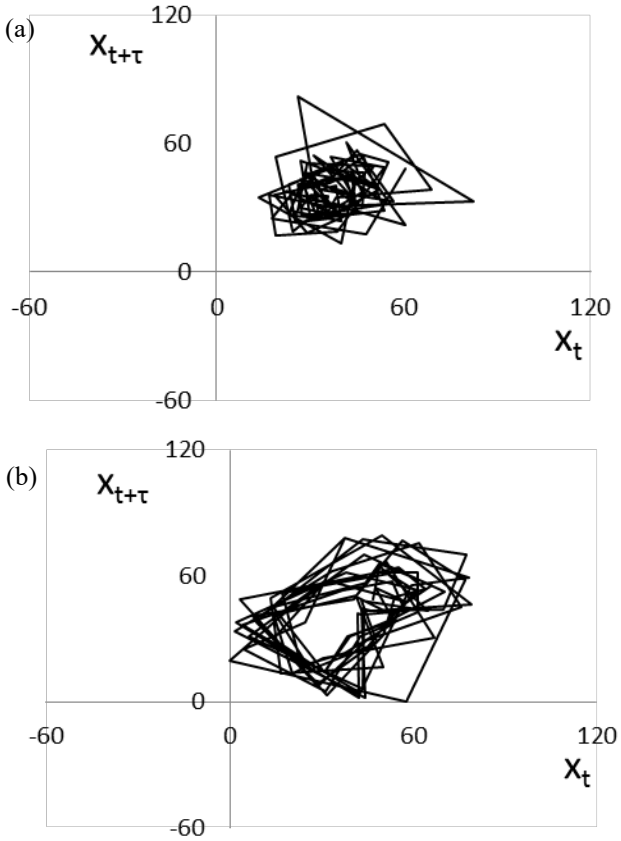

Figure 6: Attractors of EGG in (a) experiment A (Figure 5(a)) and in (b) experiment B (Figure 5(b)).

Then, the values of the translation errors estimated from the EGGs of experiments A and B were compared using the Wilcoxon signed-rank test. Significant differences were observed 50 and 55 min after the end of the resting period with $p < 0.05$. The authors confirmed that translation errors in the ten-dimensional embedding space are sufficiently stable compared to those in embedding spaces with lower dimension. Figure 8 shows variations of the difference between the translation error estimated from the EGG at time t and that at onset time t_0, except for the resting period in the ten-dimensional embedding space. The variations were calculated as *DTE* in the seated position (excluding control) ranged from –0.19 to 0.13, with average of –0.001 and standard error of 0.035, and that in the supine position ranged from –0.13 to 0.086, with average of –0.011 and standard error of 0.021.

4. Discussion

To estimate the EGG dynamics, the authors analyzed EGG signals using the Wayland algorithm. The regularity and periodicity of the EGGs was considered the cause of the abovementioned results. As shown in Figures 7 and 8, significant differences in translation errors estimated from EGGs in seated and supine positions were determined after 50 and 55 min from the resting period.

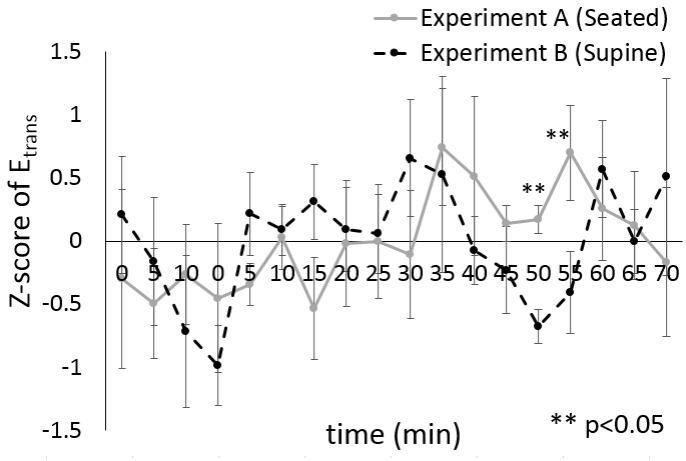

Figure 7: Z-scores of translation error (average ± standard error).

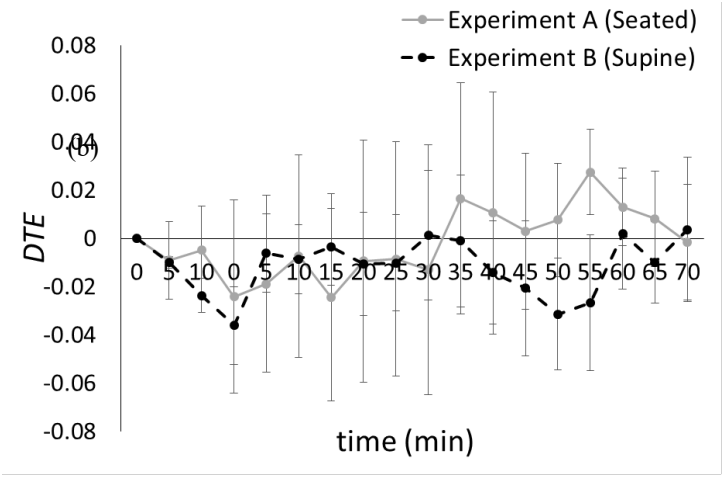

Figure 8: Difference translation errors (average ± standard error).

$$DTE(t) = E_{trans}(t) - E_{trans}(t_0).$$

Some studies have reported about the effect of postural change on the cardiocirculatory system after subjects changes from a supine to seated/standing postures, however, few does not have studied the effect of postural change on the autonomic nervous system, especially on the EGGs recorded over a prolonged period. Measuring bowel sounds, Kobayashi et al. tried to investigate the effect of the postural changes on the intestinal peristalsis [27]. Healthy middle-aged women voluntary participated in this study. Their bowel sounds were recorded during the right lateral recumbent following the supine for an hour. The results showed that intestinal peristalsis was significantly rose 30-75 min after the postural change whereas these results are questionable owing to the considerable differences prevalent among the participants [27]. In the other previous work, it has been reported that intestinal peristalsis would be temporarily suppressed if the intra-abdominal organ were affected by sudden postural changes [28]. Recording the bowel sounds 30 min after the postural change to the supine is appropriate for stationary measurements [29]. These results suggest that the stomach or intestines become active by means of parasympathetic nerve activity acceleration after a determined amount of time has passed since resuming supine position.

In general, EGGs are recorded in either a seated or supine position [30], and motion sickness is more often induced in the seated than in the supine position. In addition, the effect of postural

change on the autonomic nervous system, especially in the digestive system, has been investigated in some studies, although with focus on the cardiovascular system [31][32]. In this study, the authors conducted a basic experiment to investigate the effect of postural change on the autonomic nervous system with focus on the digestive system.

5. Conclusions

Motion sickness and diseases are usually settled in a seated position. In fact, humans can hardly get motion sickness in a supine position. This study aimed to compare EGGs acquired in seated and supine positions using the Wayland algorithm to evaluate motion sickness induced by stereoscopic movies. The authors verified that the supine position retrieves more stable EGG signals in the supine than in the seated position, thus confirming the benefits of the supine position to relieve motion sickness. There are various cycles that occur in biorhythms, and many of the variations are affected by regional differentiation of the sympathetic system. Biorhythms are also impacted by variations in posture as well as the physical condition of a person and their lifestyle. Integrative and multifaceted evaluation of impact from biorhythm and posture variations is therefore useful for evaluating autonomic nervous function and estimating biological condition. The lack of research on gastric motility and intestinal peristalsis due to variation in posture warrants an ongoing necessity for accumulation of foundational research. In upcoming studies, the authors will measure heart rate, blood pressure and multichannel EGG signals in seated and supine positions.

Conflict of Interest

The authors declare no conflict of interest.

Acknowledgment

This study was supported in part by the Kayamori Foundation of Informational Science Advancement, the Japan Society for the Promotion of Science, and Grant-in-Aid for Scientific Research (C) (Grant numbers 17K00715 and 18K11417).

References

[1] G.W. Manning, G.W. Stewart, “Effect of body position on incidence of motion sickness,” J Appl Physiol. 1(9), 619-628, 1949.
[2] J.T. Reason, J.J. Brand, Motion Sickness, 3rd ed, San Diego: Academic Press Inc, 1975.
[3] J. A. Irwin, "The pathology of sea-sickness," The Lancet. 118(3039), 907-909, 1878.
[4] B. Keshavarz, H. Hecht, B. D. Lawson., "Visually induced motion sickness: Causes, characteristics, and countermeasures," in Handbook of Virtual Environments, 2nd Edition, K. S. Hale, K. M. Stanney, Ed, FL, CRC Press, 2015, 647-698.
[5] N.H. Barmack, “Central Vestibular System: Vestibular nuclei and posterior cerebellum,” Brain Res Bull 60(5-6), 511-541, 2003.
[6] C.D. Balaban, J.D. Porter, “Neuroanatomical substrates for vestibuloautonomic interactions,” J Vestib Res. 8, 7-16, 1998.
[7] N. Takeda, M. Morita, T. Kubo, A. Yamatodani, T. Watanabe, H. Wada, T. Matsunaga, “Histaminergic mechanism of motion sickness neurochemical and neuropharmacological studies in rats,” Acta Otolaryngol. 101(5-6), 416-421, 1986.
[8] R.S. Kennedy, N.E. Lane, K.S. Berbaum, M.G. Lilienthal, “Simulator Sickness Questionnaire: An Enhanced Method for Quantifying Simulator Sickness,” Int J Aviat Psychol. 3(3), 203-220, 1993.
[9] S.R. Holmes, M.J. Griffin, “Correlation Between Heart Rate and the Severity of Motion Sickness Caused by Optokinetic Stimulation,” J Psychophysiol, 15, 35-42, 2001.
[10] N. Himi, T. Koga, E. Nakamura, M. Kobashi, M. Yamane, K. Tsujioka, “Differences in autonomic responses between subjects with and without nausea while watching an irregularly oscillating video,” Auton Neurosci. 116(1-2), 46-53, 2004.
[11] Y. Yokota, M. Aoki, K. Mizuta, Y. Ito, N. Isu, “Motion sickness susceptibility associated with visually induced postural instability and cardiac autonomic responses in healthy subjects,” Acta Otolaryngol. 125(3), 280-285, 2005.
[12] R.C. Hermida, D.E. Ayala, J.R. Fernandex, L.M. Ruilope, J.E. Lopez, “Modeling the circadian variability of ambulatorily monitored blood pressure by multiple-component analysis”, Chronol Int., 19, 461-481, 2002.
[13] A.M. Birkenhanger, A.H. van den Meiracker, “Causes and consequences of a non-dipping blood pressure profile”, Netherland J Med., 65, 127-131, 2007.
[14] S. Iwase, T. Mano, M. Saito, “Effects of graded head-up tilting on muscle sympathetic activities in man”, Physiologist, 20, S62-S63, 1987.
[15] H. Noro, I. Watanabe, N. Yabunaka, Y. Ohtsuka, Y. Agishi, “Quantitative Evaluation of Changes in pulse Rate and Blood Pressure by the Supine - to - Sitting active Postural Change Test”, The Autonomic nervous system 32(2), 111-118, 1995.
[16] W.C. Alvarez, “The electrogastrogram and what it shows,” JAMA. 78(15), 1116-1118, 1922.
[17] D. Couturier, C. Roze, J. Paolaggi, C. Debray, “Electrical activity of the normal human stomach: A comparative study of recordings obtained from the serosal and mucosal sides,” Dig. Dis. Sci. 17(11) 969-976, 1972.
[18] E.J. Van Der Schee, A.J.P.M. Smout and J.L. Grashuis, “Application of running spectrum analysis to electrogastrographic signals recorded from dog and man,” in Motility of the digestive tract, M. Wienbeck, Ed, New York: Raven Press, 1982, 241-250.
[19] J.Z. Chen, R.W. McCallum, Electrogastrography: Principles and Applications, New York: Raven Press, 1994.
[20] M. Nagai, M. Wada, Y. Kobayashi, S. Togawa, “Effects of lumbar skin warming on gastric motility and blood pressure in humans,” Jpn. J. of Physiol. 53(1), 45-51, 2003.
[21] N. Kawachi, S. Iwase, H. Takada, D. Michigami, Y. Watanabe, N. Mae, “Effect of wet hot packs applied to the epigastrium on electrogastrogram in constipated young women,” Autonomic Nervous System 39(5), 433-437, 2002.
[22] Y. Matsuura, S. Iwase, H. Takada, Y. Watanabe, E. Miyashita, “Effect of three days of consecutive hot wet pack application to the epigastrium on electrogastrography in constipated young women,” Autonomic Nervous System. 40(4), 406-411, 2003.
[23] S.R. Cajal, Histologie du systeme nerveux de l'homme et des vertebras, Vol. 2. Paris :Maloine, 1909, p. 942. (in French); S.R. Cajal, N. Swanson, L.W. Swanson, Histology of the nervous system of man and vertebrates, New York: Oxford University Press, 1995. (reprinted in English)
[24] R. Wayland, “Recognizing Determinism in a Time Series,” Phys. Rev. Lett. 70-5, 580-582, 1993.
[25] H. Takada, T. Morimoto, H. Tsunashima, T. Yamazaki, H. Hoshina, M. Miyao, “Applications of Double-Wayland Algorithm to Detect Anomalous Signals,” Forma, 21(2), 159–167, 2006.
[26] Y. Matsuura, H. Takada, K. Yokoyama, K. Shimada, “Proposal for a New Diagram to Evaluate the Form of the Attractor Reconstructed from Electrogastrography”, Forma, 23, 25-30, 2008.
[27] T. Kobayashi, T. Yazaki, Y. Hujihara, H. Ozawa, J. Nakahashi, “Analysis of Change in Bowel Sound and Movement by the Posture Change: Using an Actigraph Micromini Type Sound Sensor”, Bulletin of Faculty of Nursing, Yamanashi Prefectural University 13, 37-46, 2011.
[28] K. Fukai, N. Sakamoto, N. Tanaka, “Effect of Oral Water Intake, Exercise and Hot Compresses on Bowel Sounds in Healthy Women”, Kawasaki medical welfare journal 6(1), 99-106, 1996.
[29] N. Sakamoto, K. Fukai, N. Tanaka, “The Relationship Between Bowel Sounds and Constipation Assessment in Healthy Women”, Kawasaki medical welfare journal 6(2), 341-346, 1996.
[30] K. L. Koch, R. M. Stern, Handbook of Electrogastrography, New York: Oxford University Press, 2004.
[31] K. Nishijo, “The Relation between the Penpheral Clrculatory Behaviour and the Changes of the Body Posrtron”, Bulletin of defectology, 2, 33-45, 1978.
[32] S. Mukai, J. Hayano, “Heart rate and blood pressure variabilities during graded head-up tilt”, J. Appl. Physiol., 78(1), 212-216, 1995.

ASTES

Advances in Science, Technology and Engineering Systems Journal Vol. 4, No. 4, 47-50 (2019)

www.astesj.com

Special Issue on Advancement in Engineering and Computer Science

ASTESJ

ISSN: 2415-6698

The Study of PSi & PSo Algorithm for Reducing Power of the Mobile Communication Network

Jongsin Kim[*,1], Yonggil Choi[2], Younghoon Oh[2]

[1]*Department of IT Policy and Management, Soongsil University, 06978, South Korea*

[2]*SK Telecom, Western Infra Engineering Team, 62355, South Korea*

ARTICLE INFO

Article history:
Received: 09 April 2019
Accepted: 26 June, 2019
Online: 11 July, 2019

Keywords:
Power Saving
Energy Saving
4G/5G
LTE
Algorithm

ABSTRACT

Recently, the trend of mobile communication network in Korea has been dramatically increasing the number of operating equipment for managing the explosion of wireless data traffic in 4G LTE network. This phenomenon has caused an increase in the operating cost to the mobile telecommunication service provider. Especially, the study about the reduction of the operating cost through the reduction of the power consumption in the power consumption area and the efficient operation method are under study. Through these studies, we consider the method to maintain the best service quality of mobile communication subscriber while minimizing the power consumption of LTE equipment, find out PSi & PSo algorithm that can realize this and verify it in commercial network. Applying this algorithm to a commercial network will save both power consumption and service experience of mobile subscribers to the best level, and it will be more effective in the 5G era that has already begun.

1. Introduction

This paper is an extension of work originally presented in *2018 International Conference on Information and Communication Technology Convergence (ICTC)* [1].

The world has already begun to enter the 5G world, and the first 5G signal in Korea has started to be transmitted. There are also many killer services available to satisfy customers' needs. This means that a lot of people are using smartphones and are getting into daily life. In the past, the use patterns of voice-based usage changed with data, and the network that accommodates customers changed quickly. As the LTE network matured, the frequency bandwidth and the number of equipment services are continuously increasing to accommodate the increasing subscriber traffic [2].

This provides a pleasant environment for various services and accommodates a growing number of subscribers, but the cost of operating of equipment has increased. SK Telecom's electricity costs account for about 30% of the total cost of operating a network, exceeding 30% in 2017, which is still rising. In 2019, electricity costs are expected to account for 35% of total operating costs.

This increase in network operating costs is bringing considerable stress to mobile telecom operators, and it is also evolving to a level that significantly affects corporate EBITDA [3]. As a result, each company has a great interest in reducing the cost of network operation, especially in the field of electric power. In previous mobile communication areas, there has been much interest in battery efficiency aspects such as SoC (System on Chip) upgrade [4] and C-DRX(Connected Mode Discontinuous Reception) [5]. Recently, attention has been focused on the reduction of power consumption of network equipment itself.

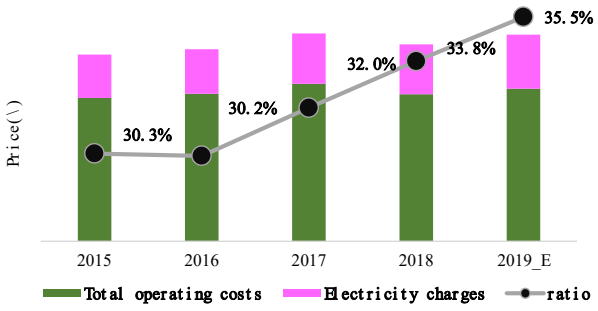

Figure 1: Electricity charges and ratio in operating costs

We used the power saving function of SK Telecom's NOKIA equipment to investigate how to reduce the power consumption of the network equipment itself. Through the derivation of optimal values of PSi and PSo, which are control variables for triggering

*Jongsin Kim, +8210-3768-6309, Email: kjs3838@sk.com

power saving to be explained later in detail, Consumption is decreasing. The optimal PSi and PSo values mean the point where the quality of the mobile communication subscriber can be maximized while minimizing the power consumption.

In this paper, we propose an operation algorithm that can reduce the power consumption of wireless network service equipment while providing optimal service without inconvenience to mobile communication subscribers. In this process, SK Telecom's commercial network is divided into several cases, and results are derived. The power saving function of the wireless network service equipment and the algorithms discussed in this study are used to reduce the actual power consumption.

2. Basic direction of power saving of LTE wireless network

Table 1: Number of subscribers per 10Mbps

Freq. Combination	Number of eligible subscribers
800M	7.5
800M+1.8G	22.5
800M+1.8G+2.1G	30.0
800M+1.8G+2.1G+2.6G	52.5

Table 1 shows the number of subscribers per frequency configuration operated by SK Telecom. As shown in the table, the number of subscribers that can be accommodated for each frequency combination is linear. (However, in LTE network, the service required for voice, messaging, video, and FTP is different according to service type, but it is calculated based on 10Mbps speed for convenience.) In order to service many subscribers, more frequency and bandwidth are needed. On the contrary, it is not necessary to provide the frequency and bandwidth of mobile communication subscribers in every place. This is because the number of subscribers and traffic vary with time. In other words, the frequency and bandwidth need to be tailored to the region's maximum traffic, but not all-time full-band service. Taking operational efficiency in accordance with the traffic volume and characteristics of subscribers is a basic direction for power saving in LTE networks.

In order to reduce power consumption in LTE mobile communication, there is a method to utilize a SON (Self Organizing Network) [6] implemented by a mobile communication provider. As mentioned above, this study utilized the power saving function provided by NOKIA equipment.(Other vendors, however, offer similar functionality.) The basic concept of power saving is that when the same area is served by several frequencies, the subscriber traffic of the service area is judged as a combined load, and when this value is low, the power consumption is reduced by turning off the output of some frequencies.

As can be seen in Figure 2, when several frequencies are serviced in the same area, the number of subscribers and traffic varies with time, and thus the number of frequencies required varies. Typically, however, mobile operators have been providing full-band services in their area, which means that unnecessary power consumption is still happening. One thing to notice is that traffic loads do not change over time in all locations. It should be noted that the traffic varies according to the characteristics of the area and the subscriber, and thus the service quality of the mobile communication subscriber may be changed by such a change. In addition, it is necessary to avoid the factor that hinders the service quality of the mobile communication subscriber in this process.

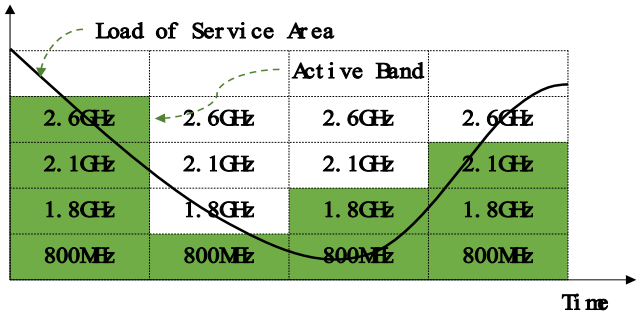

3. PSi & PSo Algorithm

It is an ideal point of execution of power saving to minimize power consumption without affecting service quality of mobile subscriber. If you do not mind this ideal goal and run power saving, it is very likely that you will be shifting to negative side. When the service quality of the mobile communication subscriber is considered, the power saving level is lowered. On the contrary, if the power saving level is increased, the service quality of the subscriber is lowered. This means that when running power saving, you should not have to break down either your service quality or your power consumption. In this study, we have developed an algorithm that derives the optimal value between service level and power saving through three step approach.

① Power saving operation control variable regulation

② Subscriber service impact index calculation

③ PSi & PSo algorithm exploration

In order to find a clear power saving algorithm, we first define the control variables that can control the operation and clarify the input variables that the operator can set and control the algorithm. Then, in the step of measuring the change of the result, it is necessary to find an index capable of quantitatively judging the influence of the service of the mobile communication subscriber. After excavation, the amount of change must be analyzed through tracking and observation. After the analysis, we set the design direction of the algorithm by considering the determinants of the service impact. Finally, it is necessary to find a point that can maximize the power saving level while ensuring service quality for mobile phone subscribers. The PSi & PSo algorithm established and stipulated these step - by - step core requirements and repeated the process of setting and analyzing each variable and outcome indicator.

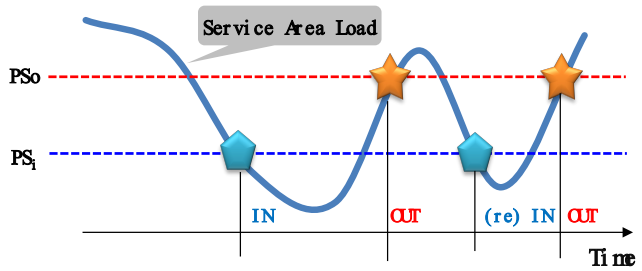

Figure 3: Power saving operation control variable

3.1. Control variables related to power saving operation

First, in order to control the power saving operation, PSi, which is the power saving operation start step and PSo, which is the step of canceling the power saving operation, are defined based on the total load value of the service area.

As shown in Figure 3, the load on the service area changes over time. There is no difference in the fact that there is a difference in the number of times the load increases and decreases in each service area, but changes with time. When the load of the service area falls below a certain level in consideration of this variability, the power saving mode is entered (IN), and the value of this moment is defined as PSi. Conversely, when the load of the service area rises to a certain level or more, power saving mode is released (OUT), and the value of this moment is defined as PSo. When the power saving mode is entered (IN), the equipment of the specific frequency is turned off, and the remaining frequencies that are not off are able to handle the traffic of the subscriber, and power consumption is reduced from this moment. When the subscriber and traffic increase and the load is increased at the moment, it is necessary to turn on the frequency that was turned off to secure the proper capacity. Is turned on. From this moment on, power consumption is not reduced. Two variables, PSi and PSo, allow specific frequencies to be turned on or off to accommodate changing traffic in the service area. However, frequent entry (IN) and release (OUT) to the power saving mode may occur depending on changing traffic and load, which negatively affects the service quality of the mobile communication subscriber. In this paper, we try to find a way to maximize the reduction of power consumption through power saving operation and to minimize the influence of service quality of subscribers in the process.

3.2. Definition of subscriber service impact indicators

Although there are various indicators for calculating the service quality in the mobile communication network, it is necessary to adopt the connection rate (%) and the truncation rate (%) that can comprehensively judge the quality of voice and data service. A new index CEI (Customer Experience Index) is calculated by multiplying two indicators and calculated by the following formula.

$$\text{Call Connection Rate}(\%) = \frac{Number\ of\ Connection\ Successful}{Number\ of\ Connection\ Attempt} \times 100 \quad (1)$$

$$\text{Call Drop Rate}(\%) = \frac{Number\ of\ Call\ Drop}{Number\ of\ Connection\ Successful} \times 100 \quad (2)$$

$$CEI(\%) = Call\ Connection\ Rate \times (100 - Call\ Drop\ Rate) \quad (3)$$

Equation 1: Estimation of the calculated index

Let's look at Equation 1. As shown (1), it is possible to determine the success rate when the mobile communication terminal attempts to connect to the wireless network for the first time, and the truncation rate can be determined based on the connection rate of the mobile communication subscriber. It is possible to judge the situation in which the connection is released irrespective of the will of the user. (1) and (2), the environment of the service to be connected to the first wireless network, and the maintenance level of the connected state after the connection, and calculates the instant when the mobile communication subscriber attempts to connect to the network through the CEI of (3). It can be used as an indicator to represent the quality from the moment to the end.

3.3. PSi & PSo algorithm

PSi and PSo, which are the control variables of power saving, are classified into three phases (high, mid, and lower) and the conditions for each stage are defined as follows.

Table 2: Understanding of PS control variable condition

Division	Step	Condition
PSi (Entry Variable)	High	Difficult to Entry
	Mid	Normal to Entry
	Low	Easy to Entry
PSo (Release Variable)	High	Easy to Release
	Mid	Normal to Release
	Low	Difficult to Release

Combining the three stages of PSi and the three stages of PSo, it can be combined the following nine cases. PSi & PSo value means integrated load of one site.

Table 3: Test Case by PS Control

Division	PSo(High): 30	PSo(Mid): 40	PSo(Low) : 50
PSi(High): 20	Case1	Case2	Case3
PSi(Mid): 30	Case4	Case5	Case6
PSi(Low): 40	Case7	Case8	Case9

Each case was tested in the commercial network of Namwon and Jangsu in Korea, which provides CA service of SK Telecom. The results of changing the PSi and PSo are summarized by the above CEI and the time when the equipment is off and not operated, and the cumulative calculated power saving value is added. Also, the values of PSi & PSo set in each case are arbitrarily set, and they are set to a wide range in order to derive the optimal value.

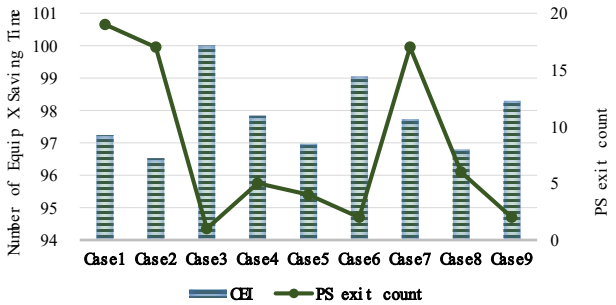

Figure 4 : Power saving exits and CEI by case

As shown in Figure 4, it can be seen that the CEI value varies depending on the case under test. And it can be clearly seen that it is inversely proportional to the number of times the power saving

mode is abandoned. In other words, the more frequent the entry and exit into the power saving mode, the more negative the service quality of the subscribers. Conversely, the lower the number of exits (the longer stay in power saving Mode), the less negative impact on the service quality of the subscriber can be interpreted. Case # 3, 6, and 9 had the fewest number of exits, and the service quality of the subscriber was maximized. As a result, it can be seen that adjusting the PSo to make it difficult to exit in power saving mode and reducing the number of exits has contributed to the optimum result preserving the CEI value.

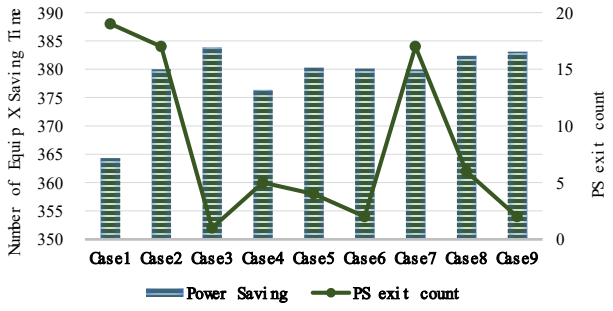

Figure 5 : Power saving level according to the number of power saving mode exits per case

The power saving level can be interpreted as PSi, which determines the entry, rather than the PSo condition, which interferes with the mobile communication subscriber experience when interpreting Figure 4 and Figure 5. In Case # 1, 2, and 3, which are difficult to enter, the power saving level is low and the condition of entry is high in Case # 7, 8, and 9.

3.4. Expanded application of PSi & PSo algorithm

The optimal values of PSi and PSo were selected as 20 and 50 respectively in SK Telecom. NOKIA developed a function to monitor the power consumed by mobile communication service equipment in real time. As a result of using this function, it is possible to save 0.12kW when 1 hour off of 2.6G equipment. We extended it to the commercial network in 2019 and saved about $ 93,000 over five months. Also, it is confirmed that CEI, which is an indicator of service quality, is maintained within the normal range.

As mentioned above, the lower the number of exits to the power saving mode, the lower the service quality of the subscriber can be prevented. As a result of applying power saving to 2.6G equipment in Jeju region of Korea, we found a device with maximum mode change count of 66 times. The site has a lot of tourists, and the traffic load is very volatile. There are two options for these areas. In order to maintain the service quality of the subscriber, it is necessary to abandon the power saving or set the PSi value low to make it difficult to enter the power saving mode (IN), thereby performing the power saving only for the necessary time. The author chose to give up power saving in the area. It is also important to reduce electricity consumption by reducing electricity consumption. However, it is because the company regards the service quality of its subscribers as more important. If one day the company's policy changes and minimizes operating costs become more important, it can turn into a situation where power savings can be applied to these areas and the service quality degradation of subscribers can be tolerated to some extent.

SK Telecom will continue the power saving in order to reduce the electricity cost to operate the network. However, it considers the quality preservation of service subscribers as the top priority and repeats the process of continuously checking the PSi & PSo algorithm and deriving the optimum value will be.

4. Conclusion

The PSi and PSo algorithms for the power saving method that maximize the reduction of power consumption while maintaining the service quality of the mobile communication subscriber are discussed. In order to derive the results, we have divided into 9 cases and the optimal value of PSi and PSo in the area managed by the author can be derived as PSi = 20 & PSo = 50. This number will vary depending on the traffic conditions in each region served. We concluded that we can adjust the power saving mode deviation to minimize PSo and access the ideal result of power saving execution if the PSi-controlled entry operation is easily set up. Although this study investigated algorithms for power saving, we did not discuss the various ISSUEs that can occur when applying this algorithm to commercial networks and the values that should be prioritized by each company's policy. This is because it depends on the value and philosophy of the mobile service provider and operator adopting this algorithm. However, the load fluctuation differs according to the service area and the load level that can be tolerated during the power saving execution may be different between the mobile communication company executing the same and the organization within it. Thus, the task of identifying the optimal value for the demand level is left as an additional research area. In addition, this approach has a weak point that it can partially obstruct the service quality of the mobile communication subscriber during the process, but it has a strong point that it is possible to draw conclusions that can be immediately expanded through direct execution in the commercial network.

Based on the results of this study, the operators who are interested in the reduction of the electricity cost among the network operation cost will be able to execute immediately because they have obtained the initial value and the method that maximizes the power consumption reduction while minimizing the quality deterioration of the subscriber.

References

[1] Kim, Jongsin, Yonggil Choi, and Younghoon Oh. "The Study of PSi & PSo Algorithm for Reducing Power of the Mobile Communication Network." 2018 International Conference on Information and Communication Technology Convergence (ICTC). IEEE, 2018.

[2] 3GPP TR 36.822, LTE Radio Access Network (RAN)enhancements for diverse data applications (Release 11)

[3] Korea Communication Commission, Jung Woo-su, Kim Seung-gun. A study on "Research on the ripple effects of telecom operators' investment activities". Research on broadcasting communication policy, A Reserch report.

[4] Hyun suk-bong, Kang sung-won, Um nak-woong. Low Power SoC Technology Wireless Terminals. Electronics and telecommunications trends, Vol.23 No.6

[5] Kim tae-yong, Cho gyu-seong, Jo sung-ho. A Study on CDRX operation of eNB for battery saving in LTE smartphone. The Journal of Korean Institute of Communications and Information Sciences.

[6] Aderemi A. AtayeroOluwadamilola I. AduAdeyemi A. Alatishe, “Self Organizing Networks for 3GPP LTE”

ASTES

Advances in Science, Technology and Engineering Systems Journal Vol. 4, No. 4, 51-57 (2019)

www.astesj.com

Special Issue on Advancement in Engineering and Computer Science

ASTESJ

ISSN: 2415-6698

Frequency-Tunable Narrow-Band Ladder-Shape Microstrip Patch Antenna for TV Applications

Maria Moussa*, Mervat Madi, Karim Kabalan

Electrical and Computer Engineering Department, American University of Beirut, 1107 2020, Lebanon

ARTICLE INFO

Article history:
Received:11 April 2019
Accepted:26 June, 2019
Online: 11 July, 2019:

Keywords:
Digital TV
UHF
Ladder shape
Frequency tuning
Varactors

ABSTRACT

In this paper, a frequency-tunable antenna is proposed based on a previous antenna which has a ladder shape and a size of 120 x 50 mm^2. It is fed using a coaxial cable and it is operational at 700 MHz which is in the UHF band with a bandwidth of 30 MHz. Varactors, having a very low resistance value and a wide range of capacitance values, are implemented on the surface of the antenna which achieves tunability in the DTV applications band used for mobile handheld devices. By using such varactors, the electromagnetic characteristics of this antenna could be changed by changing its electrical length. Multiple cases are studied; either adding a varactor on each step of the ladder antenna or adding only one varactor in a certain well justified position. The operating frequency is swept in different ranges where all of the obtained frequencies could be used for digital TV broadcasting on mobile devices.

1. Introduction

Digital TV broadcasting is now the median of exchanging information and that is thanks to the progress in digital TV technology in the form of wireless devices as well as the ways of sending and receiving signals. The new mobile devices have an attractive feature which is to allow users to watch TV on their own handheld devices; however, this feature presents some challenges in the field of designing antennas for this purpose. The antenna has to have a small size to fit in the devices and a high performance to satisfy interested users.

This paper is an extension of the work originally presented in the conference paper entitled "Ladder Shape Microstrip Patch Antenna", [1]. It is known that the operational frequency and the size of the antenna are inversely proportional. Since our targeted frequency is in the UHF band, it is then obvious that the size of the antenna operating in the high MHz range will increase. One advantage in the design process is that the designer is capable of slightly sacrificing the efficiency of the antenna because digital TV is a receive-only system in which lower total efficiency is acceptable as stated in [2].

Other than the fact that the antenna has to have a small size, it has to have good impedance matching conditions also. This is where the designer is required to add a matching circuit in the purpose of achieving the best possible power transfer between the amplifier and the antenna, which leads to the optimal antenna efficiency. Also, the designer has to take into account the fact that all the used components in the matching circuit add some losses to the design, which affects the whole performance of the system.

In the literature, there exists many papers that present designs of digital TV broadcasting antennas for mobile handheld devices. Some of these antennas are the grating monopole antenna, [3], having dimensions of 240 x 35 mm^2 and operating between 458 MHz and 960 MHz, the asymmetric fork shaped monopole antenna, [4], having dimensions of 245 x 35 mm^2 and operating between 451 MHz and 912 MHz, the coplanar waveguide-fed dipole antenna, [5], having dimensions of 241 x 58.5 mm^2 and operating between 430 MHz and 1180 MHz and the monopole slot antenna, [6], of dimensions 128 x 51 mm^2 and operating at 600 MHz. In [7], two small microstrip antennas and one planar inverted F antenna are proposed. These antennas are used in the TV band for transmission of cognitive radios. The three of them operate between 700 MHz and 900 MHz. Some new references could be found in the literature such as [8] in which the authors designed and fabricated a flexible printed active antenna having a meander line shape for the DTV reception. It has a size of 180 x 50 mm^2 and a wide operational band ranging from 510 MHz to 790 MHz due to the usage of coplanar waveguide feeding technique. This antenna has an omnidirectional radiation pattern and a maximum gain of about 18 dB. A compact 46 x 46 mm^2 antenna is designed in [9] covering a wide band from 490 MHz to 720 MHz. The bandwidth enhancement is achieved by changing the size of the ground plane of the antenna and the size reduction

* Maria Moussa, Email: mnm33@mail.aub.edu

is achieved by incorporating the meander line shape in the radiating patch.

In [1], the goal was to design a small antenna for digital TV after modifying the antenna proposed in [10], which is also a ladder shaped antenna but operational at 90 GHz. Considerable modifications were done on the latter one to function in the MHz frequencies despite the fact that wireless devices impose some size constraints on the antenna. The resulting patch antenna has the shape of a ladder and a size of 120 x 50 mm^2 which overrides some of the antennas presented in the literature. Many of the ladder dimensions were studied in [1] to try to improve the matching conditions. The software used for the design and simulation of the antenna is HFSS. It is then fabricated and tested. The simulated and measured results showed good agreement. It has a narrow operational bandwidth of 30 MHz only ranging from 685 MHz to 715 MHz, which do not cover the whole UHF band channels. The solution proposed for that issue is to add surface mounted varactors to the ladder patch antenna to be able to tune the operational bandwidth. A DC bias voltage should be applied to the varactors to change their capacitance values and hence achieve frequency tunability to different UHF channels.

In the upcoming wireless communication systems, reconfigurable antennas are used widely for many reasons. A re-configurable antenna could have the ability of changing many of its characteristics. Frequency, radiation pattern, bandwidth and polarization could be altered to adapt to the environment, [11], using a reconfigurable antenna. Besides their re-configurable capability, re-configurable antennas contain many other features such as reduced cost, size miniaturization and multipurpose functions and they use microstrip antennas as a platform. In addition, recent systems must be able to receive signals over a wide range of frequencies so they require, as stated in [12], either wide-band or tunable narrow-band antennas. The requirement of receiver filters is relaxed because tunable narrow-band antennas, in contrary to broadband antennas, provide frequency selectivity. Tunable antennas, [13], are of interest for wireless communication systems because they could substitute multiple antennas operating at different frequencies, which will reduce the implementation size and its cost as well as the complexity of the system. Another advantage presented by such antennas is the ability to reject the interference from services coexisting in the spectrum. Slot antennas are one of the common types of antennas used in frequency tuning because varactors or switches could be used easily to change their resonant frequency. The frequency tuning is achieved by varying the effective length of the slots using varactor diodes embedded across the slots. Therefore, a tunable antenna could be obtained by loading the patch antennas with varactor diodes, [14], thus having a change in the resonant frequency of the patch.

The authors of [15] present a slot antenna that uses switches to change its electrical length and obtain an effective wide bandwidth. A small patch antenna that could be tuned to different frequencies, ranging from 800MHz to 900 MHz, is designed in [16], this antenna uses variable capacitors and transistors. A radio baseband processor sends commands to a digital control unit implemented in the antenna to control it. In [17], two lumped variable capacitors, also known as varactors, are placed in properly chosen positions on a slot antenna. The antenna is changed to a dual-band antenna having two operational frequencies that could be controlled individually.

In this paper, the varactors are placed according to three different scenarios. The first thing done is to plot the current magnitude on the surface of the antenna in [1] and indicate the points where it is the highest and the lowest. The first scenario is designed by placing a varactor component where the current gets cancelled out, which is in the middle of each ladder step. The two other scenarios are designed by choosing two different points where the current is circulating with high magnitude. These two points appeared to be on the side strip connecting the ladder elements at the same side of the feeding point, one between the third and the fourth element and the other one is between the fourth and the fifth ladder element. Two designs were tested for the second and third scenarios; first, the copper strip facing the varactor had to be removed to avoid short-circuiting the inductors and drive the current to pass through the varactor. The second design was done by removing all strips similar to the one facing the varactor from the ladder patch. All the proposed designs were fabricated and tested and good agreement was obtained between the simulated and the measured reflection coefficients.

2. Original Ladder Antenna: Design and Fabrication

The antenna in [1] is designed with a size of 120 x 50 mm^2 on an FR4 epoxy substrate with a dielectric constant of 4.4 and a thickness of 1.6 mm. All the dimensions of the antenna are shown in Figure 1(a).

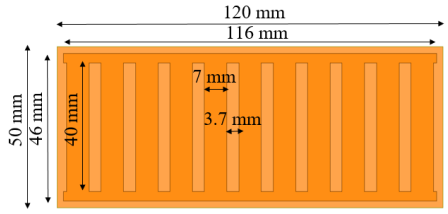

(a) Dimensions.

(b) Prototype.

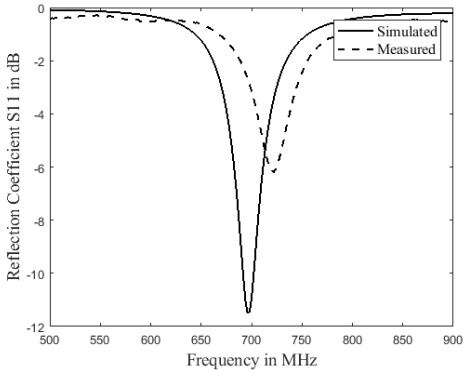

(c) Simulated and measured S_{11}.

Figure 1: Original ladder shape antenna.

The substrate has a rectangular shape of length 120 mm and a width of 50 mm. The patch has also a rectangular shape of length 116 mm and a width of 46 mm which means that it is smaller than the substrate by 2 mm from each side. The ladder is composed of eleven copper rectangular steps of length 40 mm and of width 7 mm with a spacing of 3.7 mm between each two steps. Finally, the width of each of the two side strips connecting the eleven steps is 3 mm. As already said, the antenna is fed using a coaxial cable and the position of the feeding point was chosen to be in the middle of one of the side strips connecting the ladder elements. A parametric study was done before making the best choice of the feeding position to get the best possible performance of the antenna. The fact that this antenna occupy the entire space of the PCB does not affect the addition of other antennas necessary for the functionality of the device because most of the antennas designed now are very small strip antennas and could use different PCBs.

After the fabrication of the antenna as shown in Figure 1(b), measurements were done on its reflection coefficient. Both the simulated and the measured S_{11} are shown in Figure 1(c). There is a good agreement between the simulated and the measured results. The value of -6 dB is the threshold of acceptable S_{11} values for TV antennas therefore the antenna is found to be operational at 700 MHz with a bandwidth of 30 MHz.

The reflection coefficient of the antenna shows that it has a narrow band covering only one TV channel. However, to be able to cover a wider bandwidth in the UHF band, many solutions could be proposed one of which is the use of surface mounted varactors and changing their capacitance values which allows the tuning of the operational frequency of the antenna to different UHF channels.

3. Optimization Approaches

To improve matching conditions at 700 MHz, four approaches were tested in [1]. The first approach, Figure 2(a), was to decrease the number of ladder steps to six. The second, Figure 2(b), was to use the design obtained after applying the first approach and increase the width of the steps to 10 mm which is an increase of 43% of their original width. The third approach, Figure 2(c), was to reuse the original design and subtract eleven slots of size 5 x 2 mm^2 from both, upper and lower, side strips connecting the steps making them look like film strips. The final approach tested, Figure 2(d), was to decrease the number of slots subtracted to six and check their influence on the reflection coefficient. The four approaches mentioned are combined with Figure 2(e) that shows the reflection coefficients of the antennas obtained after applying these approaches as well as that of the original antenna simulated using Ansoft HFSS.

No major improvement is shown in the reflection coefficient of the antenna. Instead, resonant frequency is shifted away from 700 MHz in the four cases. Therefore, since the chosen frequency is 700 MHz and also thanks to the simplicity of the design and its easy fabrication, the antenna of the original design is the one chosen to be fabricated and measured. The network analyzer used to do the measurements is the "FieldFox RF Analyzer N9914A" from the Keysight Company. A small acceptable difference between the simulated and the measured S_{11} could be noticed and it is caused by some fabrication losses therefore, the ladder antenna fabricated is a good candidate to be used for TV applications.

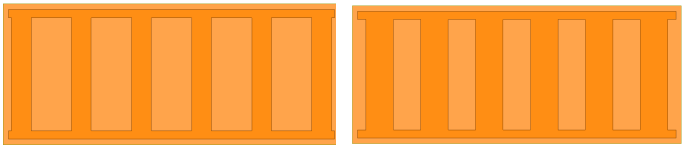

(a) Approach 1. (b) Approach 2.

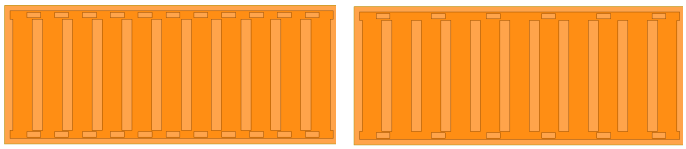

(c) Approach 3. (d) Approach 4.

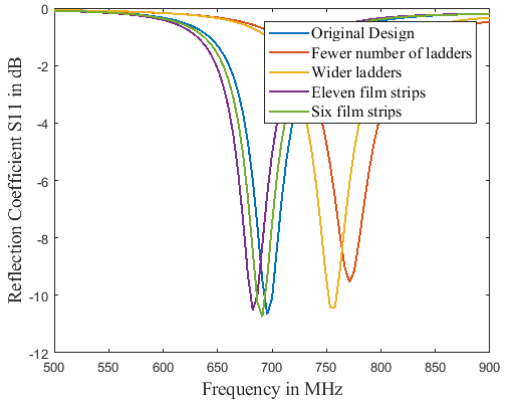

(e) Simulated S_{11} of the above approaches.

Figure 2: Investigated optimization approaches.

4. Frequency Tunable Ladder Antenna Scenarios: Designs and Fabrication

The addition of varactor diodes along the current path leads to changing the electrical length of the patch and hence the operating frequency. It all depends on the capacitance value of the varactor; for some capacitances the electrical length increase and the resonant frequency decrease and for some other cases, the inverse occurs.

To plainly explain the effect of the capacitance on the transmission line length, it is necessary to introduce the Smith Chart. The Smith Chart is a way of graphically determining transmission line parameters rather than mathematically. Consider a transmission line, it has an impedance which is usually a complex number expressed by (1) where R is the resistance and X is the reactance and can be plotted on the smith chart using the resistance and the reactance circles. A complete circle on the Smith Chart represents a half wavelength transmission line. One of the important applications of a Smith Chart is the length calculation of a short-circuited piece of transmission line to provide a required capacitive or inductive reactance. The addition of a series RC circuit will change the impedance of the transmission line by adding R to its real part and X_c, calculated using (2), to its imaginary part.

$$Z = R + jX \quad (1)$$

$$X_c = \frac{1}{2\pi f C} \quad (2)$$

f is the frequency in Hertz and C is the capacitance in Farads. Any change in the position of the transmission line impedance point on the Smith Chart, caused by adding matching circuits such as a series RC circuit, will lead to a change in the electrical length of the transmission line as well as its impedance which modifies its matching conditions. The electrical length will either increase or decrease, therefore the operational frequency which is directly related to it, will also change. The distance traveled by a current signal along a transmission line is expressed in relation to its source frequency. The wavelength calculated by (3), where c is the speed of light, is this distance considered for a given frequency.

$$\lambda = \frac{c}{f} \quad (3)$$

In the two suggested scenarios, the varactors are connected serially across a slot subtracted from the radiating patch, which means between two halves of the patch as in [18] and [19]. According to [20], the tunability of the antenna is therefore achieved by cutting small slots from the copper lines and inserting varactors in their place.

The diode model used here is a serial connection between a capacitor and a resistor as shown in Figure 3. The resistor has a very small value of 0.01 Ω. The capacitance of the varactor that is used, 1SV325, is varied between 7 pF and 80 pF when a reverse voltage between 0V and 6V is applied.

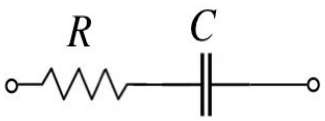

Figure 3: Used configuration of the varactor model depending on resistance R and capacitance C implemented in series.

In what follows, the simulated reflection coefficients are presented for some capacitance values ranging between 7 pF and 80 pF. The measured reflection coefficients are captured while varying the DC bias voltage. It is varied between 0V and 6V for the case of only one varactor added to the surface of the ladder patch antenna represented by scenarios 2 and 3 in the following figures. However, the voltage could be varied in a greater range for the antenna of scenario 1 that has a varactor added to each of its ladder steps because the varactors are in a parallel connection to each other so the voltage would be divided across all the varactors.

Figure 4(a) represents the first antenna scenario where eleven varactors are added each in the middle of one of the steps, with the simulated S_{11} in Figure 4(b) and the measured S_{11} in Figure 4(c).

In the second antenna scenario, the varactor is added between the third and the fourth ladder step. Figure 5(a) represents the first design of the second scenario with only one copper strip removed. The simulated S_{11} is represented in Figure 5(b) and the measured S_{11} in Figure 5(c).

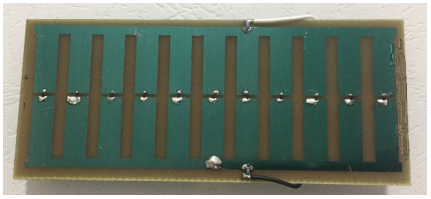

(a) One Varactor in the middle of each ladder step.

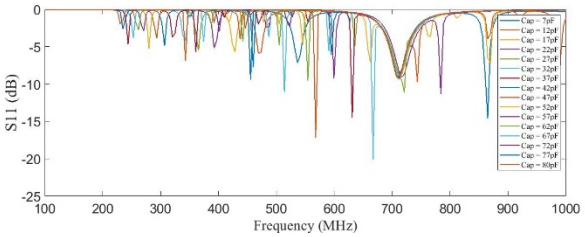

(b) Simulated Reflection Coefficient.

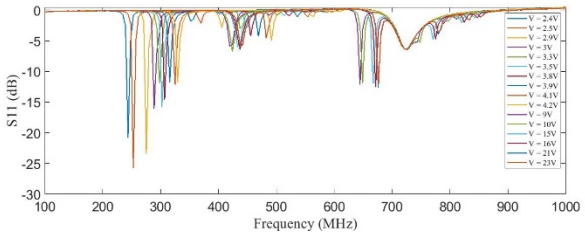

(c) Measured Reflection Coefficient.

Figure 4: Scenario 1.

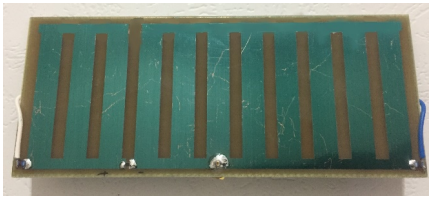

(a) One Varactor between the third and the fourth step with one facing copper slot removed.

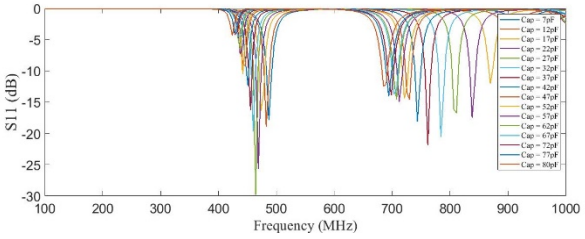

(b) Simulated Reflection Coefficient.

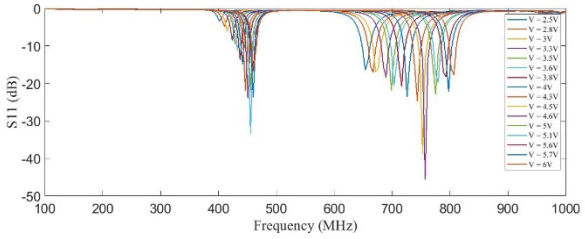

(c) Measured Reflection Coefficient.

Figure 5: Scenario 2 - Design 1.

Figure 6(a) represents the second design of the second scenario with all copper strips removed. Its simulated S_{11} is represented in Figure 6(b) and the measured S_{11} in Figure 6(c).

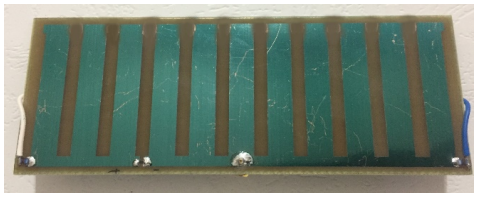

(a) One Varactor between the third and the fourth step with all copper slots removed.

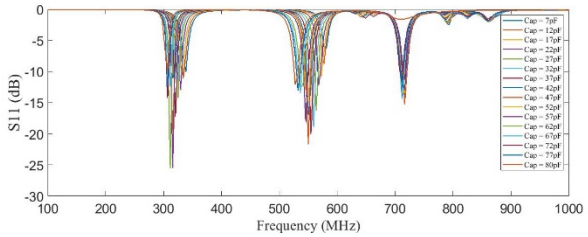

(b) Simulated Reflection Coefficient.

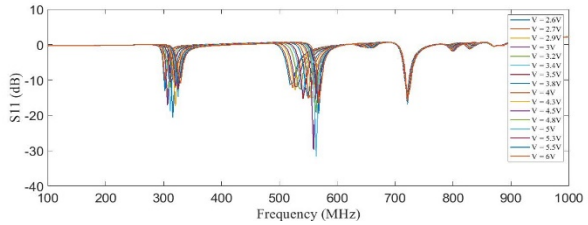

(c) Measured Reflection Coefficient.

Figure 6: Scenario 2 - Design 2.

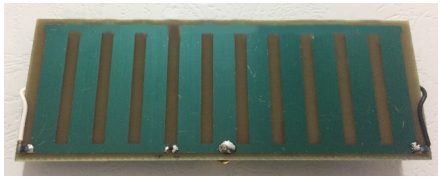

(a) One Varactor between the fourth and the fifth step with one facing copper slot removed.

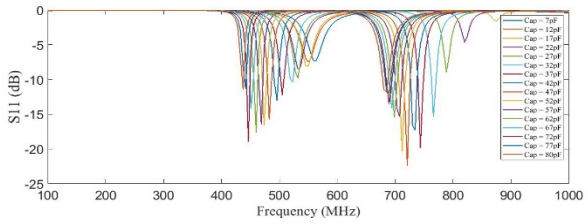

(b) Simulated Reflection Coefficient.

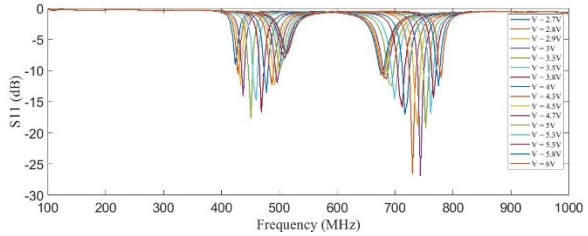

(c) Measured Reflection Coefficient.

Figure 7: Scenario 3 - Design 1.

In the third antenna scenario, the varactor is added between the fourth and the fifth ladder step. Figure 7(a) represents the first design of the last scenario where only one copper strip is removed. The simulated S_{11} is represented in Figure 7(b) and the measured S_{11} in Figure 7(c).

Figure 8(a) represents the second design of the last scenario with all copper strips removed. Its simulated S_{11} is represented in Figure 8(b) and the measured S_{11} in Figure 8(c).

In the figures showing the simulated and the measured reflection coefficients for all the antennas deigned, a slight difference could be noticed. This difference is due to the fabrications inaccuracies as well as the losses that could be encountered in the measurement process. However, it is well shown that all the tunable frequencies fall in the same frequency ranges when comparing simulated and measured results for each design.

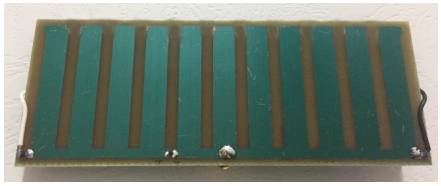

(a) One Varactor between the fourth and the fifth step with all copper slots removed.

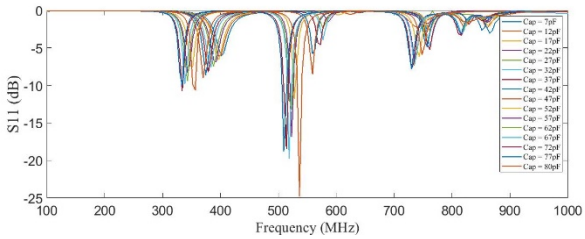

(b) Simulated Reflection Coefficient.

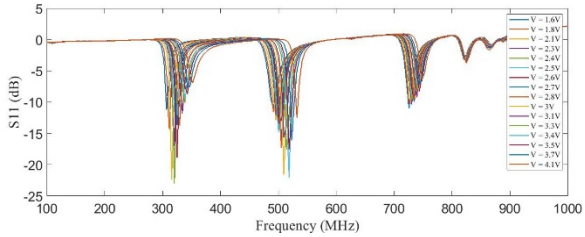

(c) Measured Reflection Coefficient.

Figure 8: Scenario 3 - Design 2.

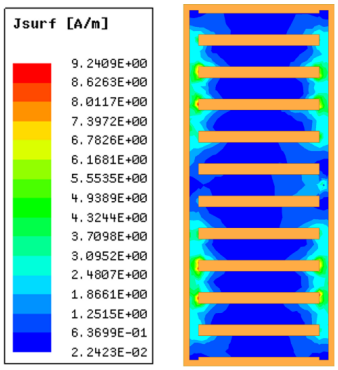

Figure 9: Current distribution for antenna [1].

5. Current Distribution

Figure 9 shows the current distribution on the surface of the ladder patch antenna in [1] at the resonant frequency 700 MHz. It is shown that the current magnitude is not equal in all of the points on the patch; the current on the ladder steps is lower than the one circulating on the side strips connecting them. This is obvious since the current is being canceled out in the middle of the steps because of the fact that it is traveling in opposite directions.

Figure 10 represents the current distribution on the surface of the ladder patch for the five tunable designs discussed above at 700 MHz frequency.

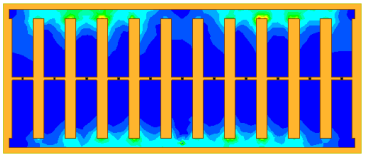

(a) Scenario 1.

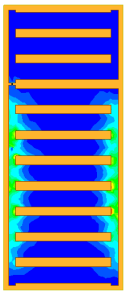

(b) Scenario 2 - Design 1.

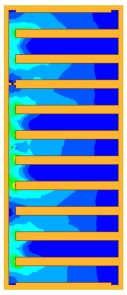

(c) Scenario 2 - Design 2.

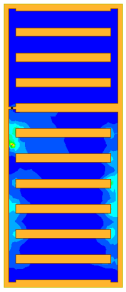

(d) Scenario 3 - Design 1

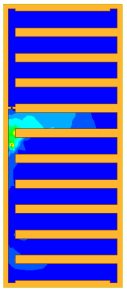

(e) Scenario 3 - Design 2

Figure 10: Current distribution for the tunable antennas.

6. Radiation Characteristics

Figure 11(a) shows antenna [1] positioned in the xyz-plane. The three-dimensional radiation pattern of the antenna is shown in Figure 11(b). The main lobe of the antenna is directed in the plane formed by theta equals 90° and phi equals 45°.

Figure 12(a) represents the first antenna design of the second scenario which is having the varactor placed after the third step and removing the copper strip facing it. Two plots of the radiation pattern are presented in Figures 12(b) and 12(c) for resonating frequencies 840 MHz and 870 MHz respectively. Both plots show that the main lobe changed its direction when compared to that of antenna [1].

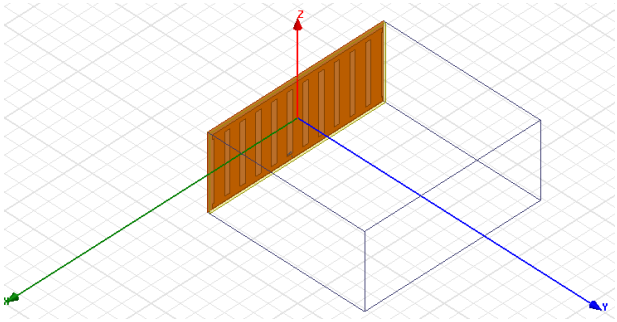

(a) Antenna [1] in the xyz plane.

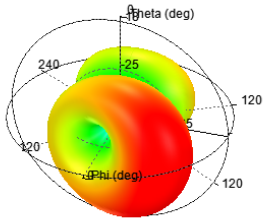

(b) 3D Radiation pattern.

Figure 11: Antenna [1] - Radiation Characteristics.

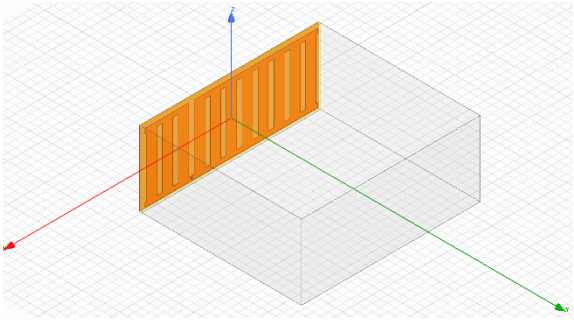

(a) Antenna of scenario 2 - Design 1.

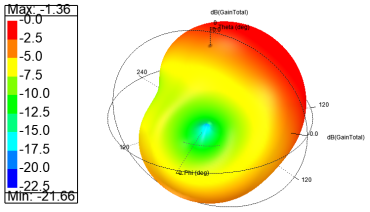

(b) 3D Radiation pattern at 840 MHz.

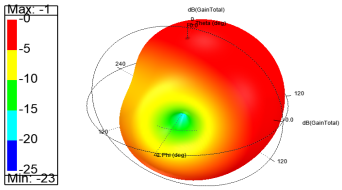

(c) 3D Radiation pattern at 870 MHz.

Figure 12: Antenna of scenario 2 - Design 1 - Radiation Characteristics.

It is shown that the gain of this antenna is negative; that is due to its small size compared to what it should have been for operational frequencies in the UHF band. For 700 MHz frequency, the wavelength is around 400 mm however the length of this antenna is 120 mm, which means that the current is circulating on a path that is much smaller than what it should be. However, as

already stated in the introduction, this antenna is considered as a receive-only system in which efficiency could be sacrificed more than in a transmit-system.

7. Conclusion

The antennas presented in this paper are an extension of the ladder-shape microstrip patch antenna design presented in the conference paper [1]. When comparing the antenna presented in [1] to other antennas in the literature designed for the same purpose, it shows good improvement in terms of the compactness of its size. It has a length of 120 mm whereas other antennas are of length 240 mm, [3], and 245 mm, [4]. Even though its size suits most of the mobile phones used in the market, this antenna has one drawback which is its narrow operational bandwidth of 30 MHz.

The proposed solution in this paper is to transform this antenna into a frequency tunable antenna by adding varactors onto its surface. A slight change in the geometrical shape of the antenna will create new current paths and new radiation edges which will introduce multiple shifts in the resonant frequency. According to [21], the position of the varactors obviously affect the current flow path, so to tune the obtained resonant frequency, changing these positions is a must.

The varactors are placed in certain positions that achieve frequency tuning while keeping sufficient matching conditions with minimal perturbation. The antennas presented in this paper resonated on new sets of frequencies falling between 200 MHz and 1 GHz, which allows them to be used for Digital TV broadcasting applications on mobile handheld devices.

These antennas have a negative gain because of their small size according to their frequency of operation however, many techniques could be used to improve the antenna gain such as changing the substrate and using a different material having lower losses such as air, adding parasitic patches or meandering edges, cutting parts of the ground plane, etc…

Acknowledgment

The authors would like to acknowledge the support of Mr. Issam Darwish and Mr. Mohammad Darwish for supporting this work.

References

[1] M. Moussa, M. Madi and K. Kabalan, "Ladder Shape Microstrip Patch Antenna," in *International Conference on High Peformance Computing and Simulation*, Orleans, France, July 2018.

[2] P. Vainikainen, J. Holopainen and M. Kyro, "Antennas for Digital Television Receivers in Mobile Terminals," *Proceedings of the IEEE,* vol. 100, no. 7, pp. 2341-2348, July 2012.

[3] C.-Y. Huang, B.-M. Jeng and J.-S. Kuo, "Grating Monopole Antenna for DVB-T Applications," *IEEE Transactions on Antennas and Propagation,* vol. 56, no. 6, pp. 1775-1776, June 2008.

[4] C.-Y. Huang, B.-M. Jeng and C.-F. Yang, "Wideband monopole antenna for DVB-T applications," *Electronics Letters,* vol. 44, no. 25, pp. 1448-1450, December 2008.

[5] O. T.-C. Chen and C.-Y. Tsai, "CPW-Fed Wideband Printed Dipole Antenna for Digital TV Applications," *IEEE Transactions on Antennas and Propagation,* vol. 59, no. 12, pp. 4826-4830, December 2011.

[6] C.-Y. Tsai and O. T.-C. Chen, "Compact Broadband Monopole Slot Antenna for Digital TV Applications," in *IEEE Asia-Pacific Conference on Antennas and Propagation*, Singapore, October 2012.

[7] M. Y. Abou Shahine, M. Husseini, A. H. Ramadan, K. Kabalan and Y. Nasser, "Antenna Designs for Cognitive Radio Applications in the TV Band," *International Journal of Scientific & Engineering Research,* vol. 6, no. 2, pp. 975-980, February 2015.

[8] T. Pratumsiri and P. Janpugdee, "Flexible Printed Active Antenna for Digital Television Reception," in *Progress in Electromagnetics Research Symposium (PIERS-Toyama)*, Toyama, Japan, August 2018.

[9] S. Bhole, A. Rathod, S. Doddipalli, S. Kannaiyan and A. Kothari, "A Compact Planar Antenna with Meander Lines for TV White Space Applications," in *IEEE International Students Conference on Electrical, Electronics and Computer Science*, Bhopal, India, November 2018.

[10] R. K. Venkata, D. Mrthy and I. a. N. M. N. Govardhani, "Multi-Band Ladder-Shape Micro-Strip Patch Antenna," *International Journal of Scientific & Engineering Research,* vol. 3, no. 3, pp. 1-6, March 2012.

[11] G. Singh and m. Kumar, "Design of Frequency Reconfigurable Microstrip Patch Antenna," in *6th International Conference on Industrial and Information Systems*, Kandy, Sri Lanka, 2011.

[12] M. S. Nishamol, C. K. Aanandan, P. Mohanan and K. Vasudevan, "Dual Frequency Reconfigurable Microstrip Antenna Using Varactor Diodes," in *XXXth URSI General Assembly and Scientific Symposium*, Istanbul, Turkey, August 2011.

[13] A. Khidre, F. Yang and A. Elsherbeni, "A Patch Antenna with a Varactor-Loaded Slot for Reconfigurable Dual-Band Operation," *IEEE Transactions on Antennas and Propagation,* vol. 63, no. 2, pp. 755-760, February 2015.

[14] B. Babakhani and K. S. Sharma, "Investigations on Frequency Agile Microstrip Patch Antenna Loaded with Varactor Diode," in *IEEE Antennas and Propagation Society International Symposium (APSURSI)*, Orlando, FL, USA, July 2013.

[15] D. Peroulis, K. Sarabandi and L. Katehi, "Design of Reconfigurable Slot Antennas," *IEEE Transactions on Antennas and Propagation,* vol. 53, no. 2, pp. 645-654, February 2005.

[16] J. T. Aberle, S.-H. Oh, D. T. Auckland and S. D. Rogers, "Reconfigurable Antennas for Wireless Devices," *IEEE Antennas and Propagation Magazine,* vol. 45, no. 6, pp. 148-154, December 2003.

[17] N. Behdad and K. Sarabandi, "Dual-Band Reconfigurable Antenna with a Very Wide Tunability Range," *IEEE Transactions on Antennas and Propagation,* vol. 2006, no. 2, pp. 409-416, February 2006.

[18] N. Fayyaz, S. Safavi-Naeini, E. Shin and N. Hodjat, "A Novel electronically Tunable Rectangular Patch Antenna with One Octave Bandwidth," in *IEEE Canadian Conference on Electrical and Computer Engineering*, Waterloo, Ontario, Canada, May 1998.

[19] S. V. Hum and H. Y. Xiong, "Analysis and Design of a Differentially-Fed Frequency Agile Microstrip Patch Antenna," *IEEE Transactions on Antennas and Propagation,* vol. 58, no. 10, pp. 3122-3130, October 2010.

[20] J. Costantine, C. Christodoulo and S. E. Barbin, "A New Reconfigurable Multi Band Patch Antenna," in *SBMO/IEEE MTT-S International Microwave and Optoelectronics Conference*, Brazil, October 2007.

[21] M. A. Madi, M. Husseini, A. Ramadan, K. Y. Kabalan and A. El-Hajj, "A Reconfigurable Cedar-Shaped Microstrip Antenna for Wireless Applications," *Progress in Electromagnetics Research,* vol. 25, pp. 209-221, 2012.

ASTES

Advances in Science, Technology and Engineering Systems Journal Vol. 4, No. 4, 58-64 (2019)

www.astesj.com

Special Issue on Advancement in Engineering and Computer Science

ASTESJ

ISSN: 2415-6698

Performance Analysis of Thyristors Switched Capacitors used for Reactive Power Compensation of Induction Motor

Dmitry Ivanovich Panfilov[*,1], Ahmed Elsayed ELGebaly[2], Michael Georgievich Astashev [3], Alexander Nikolaevich Rozhkov [1]

[1]*Department of industrial electronics, Moscow power engineering institute, Moscow, 111250, Russia*

[2]*Electrical power and machines department Faculty of engineering, Tanta university, Tanta, 31527, Egypt*

[3]*A G. M. Krzhizhanovsky power engineering institute (JSC ENIN), Moscow, 119991, Russia*

ARTICLE INFO

Article history:
Received:29 April 2019
Accepted:26 June, 2019
Online: 11 July, 2019

Keywords:
Reactive power compensation
Thyristors switched capacitors
Induction motor starting

ABSTRACT

This paper analyzes the process of reactive power compensation using thyristors switched capacitors TSC topology based on multiterminal switch during the starting of induction motor. The paper explains the control principle of this TSC topology which depends on the multiterminal switch. To actively track the required reactive power for the dynamic load and to perfectly transit from it from one level to other, proper control system is established. MATLAB/SIMULINK is used to develop a simulation model to prove the dynamic performance of the proposed TSC during the compensation of reactive power required for induction motor during starting.

1. Introduction

This paper is an extension of work originally presented in 2018 X International Conference on Electrical Power Drive Systems (ICEPDS) under title (Performance Assessment of Thyristors Switched Capacitors during Reactive Power Compensation of Dynamic Load) [1]. It is well known that; the induction motors are the most broadly utilized motors in the world due to their high rigidness [2]. The powers of the used induction motors vary from the fraction of kilowatt up to several megawatt [3]. The induction motors require reactive power during their operation either they are supplied from conventional AC source or through drive system [4]. But, the connection of reactive power compensators with the induction motors improves the power system quality where they are supplied [5]. The compensation of the reactive power may be achieved by the connection of fixed capacitor on the terminals of the induction motor. But, this method doesn't adapt the requirements of the motor for the various operation modes. The application of dynamically changed reactive power supply improves the power factor for wider operation range particularly during the starting of the motors [6]. The induction motors speed may be changed using dynamically changed reactive power source [7].

Several references [8,9] study the usage of conventional static VAR compensators needed by the induction. The production of harmonics is an essential demerit of the conventional SVCs. Therefore, they require the application of filters [10,11]. The switched-based SVC present a vital solution to remove the harmonics during the control of the reactive power. But, it should be considered that, the switched SVCs have discrete performance during the control of reactive power; consequently, they require different control and design methodology to obtain the smoothest characteristic [12].

This research analyzes the process of reactive power compensation for the starting of induction motor depending on switched SVC. The thyristor switched capacitors TSC which has 25 discrete steps of operation is the type of SVC applied in this study. The design of such TSC topology requires special design to dynamically change the developed capacitive reactive power. The control methodology applied for the TSC topology is established to regulate the proper amount of reactive power during the starting of the induction motor. The detailed induction motor model is illustrated to study the effect of the SVC on its operation. By using MATLAB/SIMULINK package, Simulation model of the whole system is established to demonstrate the TSC performance during the compensation of reactive power.

[*]Department of industrial electronics, Moscow power engineering institute Moscow, Russia, +79859699550, Dmitry.panfilov@inbox.ru

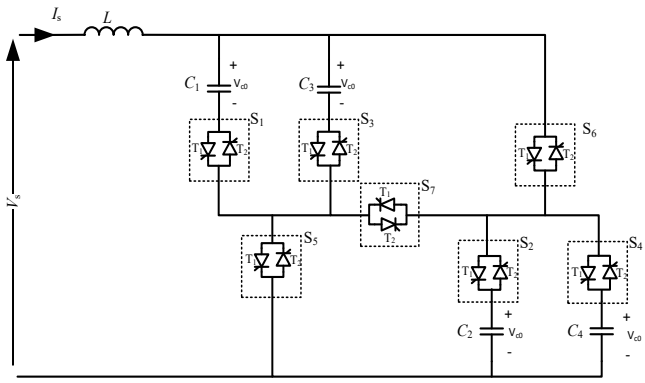

Figure 1: TSC produces 25 discrete levels of capacitive reactive power

2. Principle of operation of multiterminal switch TSC

Figure 1 illustrates the proposed TSC scheme which can produce 25 level of operation by providing 25 different equivalent capacitances [13]. In compared with binary TSC and for the same number of capacitors, the developed scheme produces more steps of operation where the binary TSC only produces 16 steps [14]. Therefore, the developed TSC provides more flexible operation to produce capacitive reactive power while there is no need for application of thyristor-controlled reactor TCR for reactive power regulation. The proposed TSC topology produces zero harmonics during its operation.

Table 1 demonstrates the several equivalent capacitances produced by the proposed TSC. The connected reactor L in the topology is important related to the reduction of current rate of change [15] and related to the restoring of the stored energy on capacitors back to the source [13].

The proposed TSC parameters is obtained depending on an optimization technique which assures the most smooth variation of the distinct characteristic [16,17]. The developed capacitive reactive power has discrete characteristic as shown in Figure 2. The function of control system of this topology is the determination the required reactive power in another words the required susceptance. Therefore, the control system should regulate the operation state of each switch of the seven switches to produce specific capacitance as in Table 1. The TSC reactive power control system needed by induction motor at starting will be explained in section 4.

As shown in Table 1, some of the equivalent capacitance include series connection of certain capacitors. The series connection of capacitors during generation of certain levels of reactive power leads in appearance of permanent different DC voltages on capacitors after termination of the reactive power level generation. To change the equivalent capacitance to another level, the capacitors which were connected in series on previous stage should be discharged. The discharging process should be completed in very short time to make the system response faster. The discharging of capacitors achieved by regenerative method by recovery the capacitors stored energy to the power supply. The

recovery process can be accomplished by connection of reactor L shown in the scheme Figure 1.

Table 1: The equivalent capacitance obtained by the proposed TSC with four capacitors and seven switches

No.	Equivalent capacitance	Switches state						
		S_1	S_2	S_3	S_4	S_5	S_6	S_7
1	0	OFF	OFF	OFF	OFF	OFF	OFF	OFF
2	C_1+C_2	ON	ON	OFF	OFF	OFF	OFF	ON
3	C_2+C_3	OFF	ON	ON	OFF	OFF	OFF	ON
4	$(C_1//C_3) + C_2$	ON	ON	ON	OFF	OFF	OFF	ON
5	C_2	OFF	ON	OFF	OFF	OFF	ON	OFF
6	C_1+C_4	ON	OFF	OFF	ON	OFF	OFF	ON
7	$(C_2//C_4) + C_1$	ON	ON	OFF	ON	OFF	OFF	ON
8	C_3+C_4	OFF	OFF	ON	ON	OFF	OFF	ON
9	$(C_2//C_4) + C_3$	OFF	ON	ON	ON	OFF	OFF	ON
10	C_1	ON	OFF	OFF	OFF	ON	OFF	OFF
11	$(C_1//C_3) + C_4$	ON	OFF	ON	ON	OFF	OFF	ON
12	$(C_1//C_3)+ (C_2//C_4)$	ON	ON	ON	ON	OFF	OFF	ON
13	$C_1//C_2$	ON	ON	OFF	OFF	ON	ON	OFF
14	C_3	OFF	OFF	ON	OFF	ON	OFF	OFF
15	C_4	OFF	OFF	OFF	ON	OFF	ON	OFF
16	$C_2//C_3$	OFF	ON	ON	OFF	ON	ON	OFF
17	$C_2//C_4$	OFF	ON	OFF	ON	OFF	ON	OFF
18	$C_1//C_3$	ON	OFF	ON	OFF	ON	OFF	OFF
19	$C_1//C_4$	ON	OFF	OFF	ON	ON	ON	OFF
20	$C_1//C_2//C_3$	ON	ON	ON	OFF	ON	ON	OFF
21	$C_1//C_4//C_2$	ON	ON	OFF	ON	ON	ON	OFF
22	$C_3//C_4$	OFF	OFF	ON	ON	ON	ON	OFF
23	$C_3//C_4//C_2$	OFF	ON	ON	ON	ON	ON	OFF
24	$C_1//C_4//C_3$	ON	OFF	ON	ON	ON	OFF	OFF
25	$C_1//C_2//C_3//C_4$	ON	ON	ON	ON	ON	ON	OFF

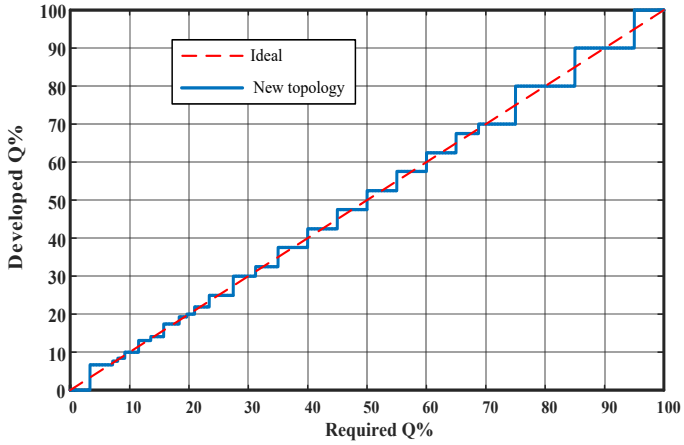

Figure 2: The characteristic of the proposed TSC

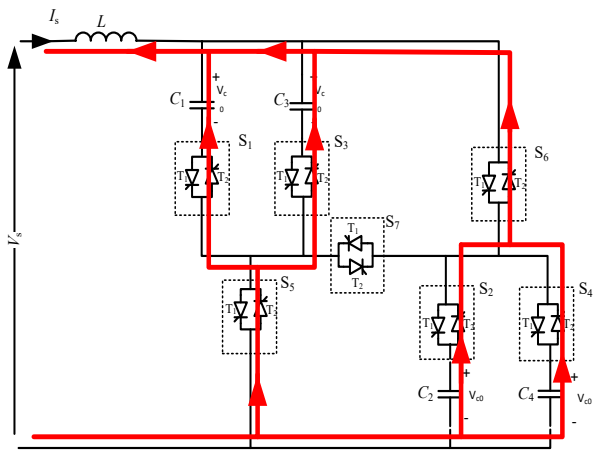

Figure 3: Discharging path for positively charged capacitors of TSC

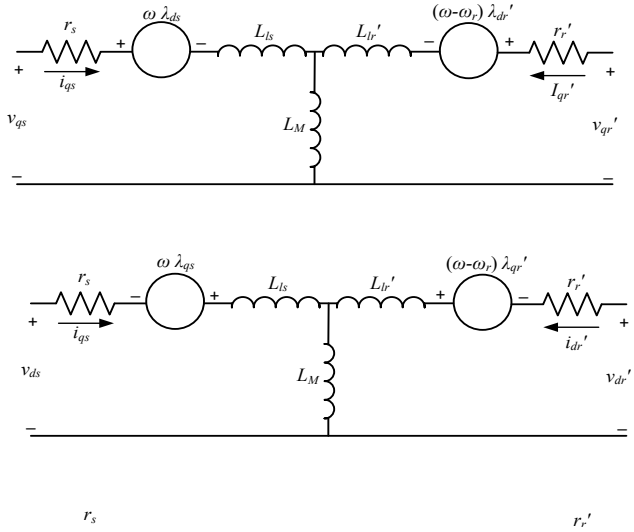

To discharge all capacitors, the time presents a critical factor, So, in this study, the TSC system is designed to discharge the capacitors in very short less than quarter of the voltage period. The added reactor and any combination of capacitors is considered resonance circuit. By the help of this resonance circuit, the stored energy on capacitors can be recovered to the power source. Figure 3 illustrates the discharging path for the charged capacitors. The regeneration can be completed within time less than the one quarter of the entire period [14]. The semiconductor switches in this scheme has a vital rating related to the maximum amplitude of current during discharging. The inductance value and firing angle to start the process affect the performance of discharging process. The resonance frequencies ω_k relates between the inductance L and the total capacitance C_{eq} by the following relation:

$$\omega_k = \frac{1}{\sqrt{L\,C_{eq}}} \tag{6}$$

The frequency ω_k determines the time of the discharging time which should be fewer than one-quarter of the fundamental period. So, the relation between ω_b and ω_k is as the following, while $k > 4$:

$$k = \frac{\omega_k}{\omega_b} \tag{7}$$

Therefore, the inductance is obtained consistent with the subsequent relation:

$$L = \frac{1}{\left(k\,\omega_0\right)^2 C_{eq}} \tag{8}$$

In this study, k is set at 24. The total required capacitance is determined consistent with the reactive power requirement of the induction motor as will be explained in section 5.

3. The Detailed Dynamic Model of the Induction Motor

The three-phase induction motor consists of six windings; three windings are in the stator and three are in the rotor. The equations of the stator voltage are as the following:

$$\begin{bmatrix} v_{as} \\ v_{bs} \\ v_{cs} \end{bmatrix} = \begin{bmatrix} R_s & 0 & 0 \\ 0 & R_s & 0 \\ 0 & 0 & R_s \end{bmatrix} \begin{bmatrix} i_{as} \\ i_{bs} \\ i_{cs} \end{bmatrix} + \frac{d}{dt} \begin{bmatrix} \lambda_{as} \\ \lambda_{bs} \\ \lambda_{cs} \end{bmatrix} \tag{1}$$

where, v_{as} , v_{bs} and v_{cs} are the voltages on the stator windings, R_s is stator resistance and λ_{as}, λ_{bs} and λ_{cs} are the linkage fluxes of the three windings. The flux linkage can be described as the following

$$\begin{bmatrix} \lambda_s^{abc} \\ \lambda_r^{abc} \end{bmatrix} = \begin{bmatrix} L_{ss}^{abc} & L_{sr}^{abc} \\ L_{rs}^{abc} & L_{rr}^{abc} \end{bmatrix} \begin{bmatrix} i_s^{abc} \\ i_r^{abc} \end{bmatrix} \tag{2}$$

where subscript 'r' specifies rotor and 's' specifies stator. Moreover, L_{ss}^{abc} and L_{rr}^{abc} are stator and rotor inductance matrixes. As well known, both of L_{sr}^{abc} and L_{rs}^{abc} are stator and rotor mutual inductance matrixes which have time variant parameters. To solve the dynamic equation (1), some difficulties should be faced. So, the using of transformation theory through Klark matrix (equation (3)) presents a solution to solve the dynamic model.

$$\left[T_{qd0}(\theta)\right] = \frac{2}{3} \begin{bmatrix} \cos\theta & \cos\left(\theta - \frac{2\pi}{3}\right) & \cos\left(\theta + \frac{2\pi}{3}\right) \\ \sin\theta & \sin\left(\theta - \frac{2\pi}{3}\right) & \sin\left(\theta + \frac{2\pi}{3}\right) \\ 0.5 & 0.5 & 0.5 \end{bmatrix} \tag{3}$$

The voltage equations after transformation are presented as in the following equation.

$$\left[V_{sqd0}\right] = R_s\left[i_{qd0}\right] + p\left[\lambda_s^{qd0}\right] + \omega\begin{bmatrix}0 & 1 & 0\\ -1 & 0 & 0\\ 0 & 0 & 0\end{bmatrix}\left[\lambda_s^{qd0}\right] \quad (4)$$

where λ_s^{qd0} is the stator windings flux linkage, i^{qd0} the arbitrary reference frame currents and ω is the rotational speed reference frame. The arbitrary reference frame equivalent circuits for symmetrical three-phase induction motor are illustrates in Figure 4.

It is common to present the parameters of machines and power system in ohms, per-unit or percent of base impedance, so, it will be more suitable to express both of flux linkage and voltage equations in terms of reactances instead of inductances as in the following equations [1, 2, 3].

$$v_{qs} = r_s i_{qs} + \frac{\omega}{\omega_b}\psi_{ds} + \frac{p}{\omega_b}\psi_{qs} \quad (5)$$

$$v_{ds} = r_s i_{ds} - \frac{\omega}{\omega_b}\psi_{qs} + \frac{p}{\omega_b}\psi_{ds} \quad (6)$$

$$v_{0s} = r_s i_{0s} + \frac{p}{\omega_b}\psi_{0s} \quad (7)$$

$$v'_{qr} = r'_r i'_{qr} + \left(\frac{\omega - \omega_r}{\omega_b}\right)\psi'_{dr} + \frac{p}{\omega_b}\psi'_{qr} \quad (8)$$

$$v'_{dr} = r'_r i'_{dr} - \left(\frac{\omega - \omega_r}{\omega_b}\right)\psi'_{qr} + \frac{p}{\omega_b}\psi'_{dr} \quad (9)$$

$$v'_{0r} = r'_r i'_{0r} + \frac{p}{\omega_b}\psi'_{0r} \quad (10)$$

$$\psi_{qs} = X_{ls} i_{qs} + X_M\left(i_{qs} + i'_{qr}\right) \quad (11)$$

$$\psi_{qs} = X_{ls} i_{ds} + X_M\left(i_{ds} + i'_{dr}\right) \quad (12)$$

$$\psi_{0s} = X_{ls} i_{0s} \quad (13)$$

$$\psi'_{qr} = X'_{lr} i'_{qr} + X_M\left(i_{qs} + i'_{qr}\right) \quad (14)$$

$$\psi'_{dr} = X'_{lr} i'_{dr} + X_M\left(i_{ds} + i'_{dr}\right) \quad (15)$$

$$\psi'_{0r} = X'_{lr} i'_{0r} \quad (16)$$

$$T_e = \left(\frac{3}{2}\right)\left(\frac{P}{2}\right)\left(\frac{1}{\omega_b}\right)\left(\psi'_{qr} i'_{dr} - \psi'_{dr} i'_{qr}\right) = T_l + Jp\omega_r \quad (17)$$

where ω_b is the base electrical angular velocity used to calculate the reactances. The flux linkages λ in equation 4 are converted to ψ flux linkages per second. ω_r is the rotational speed of rotor. X_l is leakage reactance and X_M is the mutual reactance. T_e and T_l are electromagnetic and load torque respectively. J is the inertia for motor and load. By using the previous dynamic equations, the motor can be analyzed using any simulation package such as MATLAB/SIMULINK used in this paper. All variable states of the induction motor can be determined by this model specially the variables estimate the required reactive power.

4. Control System of Reactive Power for the Operation of Induction Motor

Figure 5 shows the block diagram of the control system for the proposed TSC to regulate the reactive power of the motor. The voltages and currents of the motor terminal are measured to get the feedback signals. Therefore, the amount of capacitive reactive power is determined. The corresponding amount of susceptance B can be estimated from both of terminal voltage and reactive power. Consequently, the required susceptance presents the input of TSC lookup table characteristic in Table 1 and Figure 2. One step of the 25 steps is the lookup table output. The changing of the developed

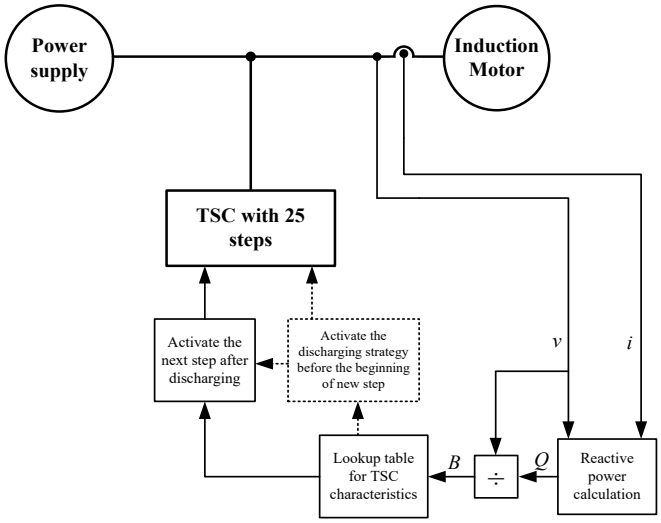

Figure 5: The block diagram for the TSC control system for reactive power compensation

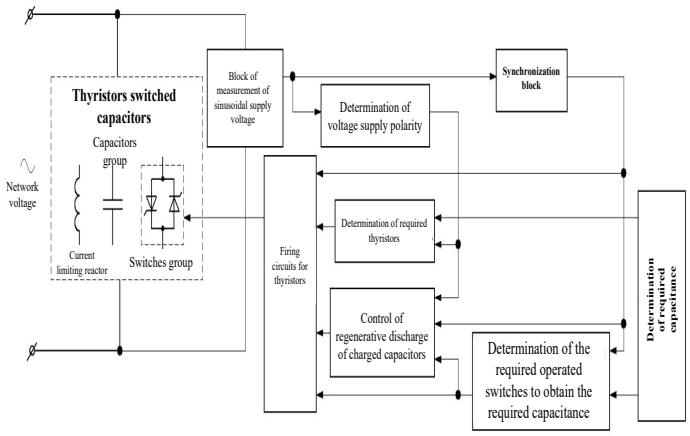

Figure 6: Block diagram of new topology of TSC control system

steps from look up table activates the capacitors discharging process once before the implementation of the following step [13]. Figure 6 illustrates the proposed TSC control system for both implementation of any susceptance and the activation of the discharging process [14].

When the discharging process is activated, the produced capacitive reactive power equals zero. If the next step is activated after the discharging process, the SVC continues the production of reactive power. The control proposed algorithm depends on the tracking of the required reactive power for the motor to produce it by the TSC. The transfer function describes the performance of the TSC can be described as:

$$\frac{B_{TSC}}{B_{ref}} = \frac{e^{-sT_d}}{1 + s\,T_b} \tag{18}$$

where B_{TSC} is the produced susceptance, B_{ref} is the reference susceptance, T_d is the dead-time and T_b is the delay-time [18].

5. Simulation Results of the compensated motor by TSC

In this study, the reactive power compensated induction motor by the proposed TSC is simulated depending on MATLAB/SIMULINK package. The reactive power compensation is imitated throughout the induction motor starting to illustrate the performance of effective control system proposed to regulate the reactive power. Figure illustrates the parallel connection of the TSC in parallel with the motor. The line-to-line voltage of power supply equals 400 V. The induction motor has the following ratings: nominal power of 37.3 kVA, 400 V line-to-line voltage, 50 Hz, 4-poles. The motor has the following parameters: r_s = 0.087 Ω, X_{ls} = 0.302 Ω, r_r' = 0.228 Ω, X_{lr}' = 0.302 Ω, X_m = 13.08 Ω and inertia constant J = 8 kg.m2.

The ratings of the connected TSC are as the following: rated line voltage of 400 V and rated power of 243 kVAR capacitive. Although the power rating of the TSC is much higher than the rating of the motor itself, the TSC reactive power is enough to compensate the reactive power required by the motor during starting. At free running, the TSC can compensate the reactive power of several connected motors because the required reactive power by the motor is reduced by the speed increment.

If the induction motor starts running, the TSC starts to compensate the reactive power compensation with the full rating then the compensated reactive power is gradually decreased. The TSC control system adjusts the reactive power by producing the maximum reactive power presented by level number 25 (Figure 2 and Table 1) at zero speed. At no-load, the required reactive power by the motor is reduced to lower level presented by level number 2. The motor with and without TSC is simulated to illustrate the TSC influence on the motor performance. The motor needs around 12 seconds to reach its full speed; consequently, the emulation period is 15 seconds which are sufficient to study the influence of the reactive power compensation on the motor performance. Figure 7 shows the supply reactive power in two cases; compensated and uncompensated motor. The using of TSC enables to reduce the total apparent power produced by the power source. Figure 8 shows the produced capacitive reactive power if the motor is compensated. Figure 9 illustrates the step of operation required to produce the corresponding reactive power. Several benefits are achieved by the reactive power compensation. The first advantage is shown in Figure 10; the compensation causes the reduction of the line current of the power source. The second benefit is the enhancement of the motor terminal voltage as illustrated in Figure 11. Therefore, the enhancement of voltage causes the increasing of motor acceleration as illustrated in Figure 12. Due to the reduction of the supply current, the internal losses of the motor are reduced where the internal winging resistance equals r = 0.5 Ω as in Figure 13. The changing of the compensation level leads to the appearance of spikes in the system response. The transition needs one full period to discharge the installed capacitors as explained in section 2.

The power factor of the system is improved due to compensation. This is due to the reduction of the phase shift between the voltage and current as illustrated in Figure 14

As explained earlier, the transition between two steps of reactive power requires the discharging process to be activated. To discuss this interval, the instantaneous waveforms of currents and voltages are illustrated. Throughout the changing of the developed steps from 25 to 24, Figure 15(a) shows the waveform of supply voltage and its produced current. As shown in the figure, the phase shift between current and voltage is around zero. In steady state, the waveform of the supply current is pure sin wave except some distortion during the transition period. The time span of the distorted current equals about one period. As shown in Figure 15(b), the phase shift between the TSC current and the supply terminal voltage is 90° lead. During the transient period, the TSC supplies zero current except spike current owing to the process of capacitors discharging. Furthermore, Figure15(c) illustrates that the voltage and the motor current are not in phase; therefore, the power factor below unity. Nevertheless, the usage of TSC enhances the power factor to unity by reducing the phase-shift between the voltage and current.

6. Conclusion

TSC has been developed as a reactive power supply to produce the required reactive power for the induction motor during starting period. The circuit topology of the proposed TSC is introduced to control the reactive power with 25 discrete steps. The principle of operation and characteristic of the proposed TSC scheme is analyzed to produce compensation system suitable for dynamically changed load. The induction motor and TSC dynamics have been introduced to analyze the dynamic performance of the whole system. The control system block diagram is constructed to track the needed reactive power for the motor. The concept of regeneration of capacitive unit energy has been explained to assure the dynamic reactive power production for the TSC. The design parameters of the TSC have been determined to produce the required reactive power and to carry out the discharging process effectively. using MATLAB/SIMULINK package, simulation and model have been developed for the whole system contains induction motor, the TSC and its control system. The simulation results demonstrate the efficiency of the proposed TSC topology during the reactive power compensation needed by the induction motor through the dynamic performance. The control system efficiently controls the TSC response to actively produce the proper reactive power.

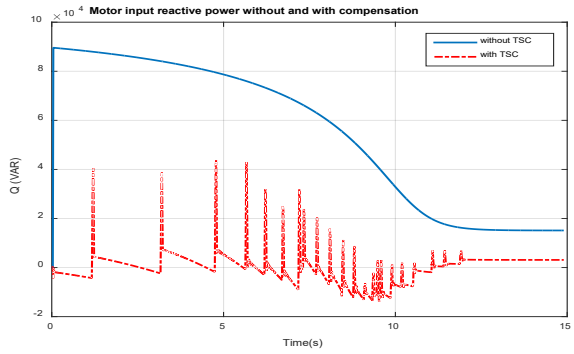

Figure 7: The supply reactive power produced for the motor in the compensated and uncompensated cases

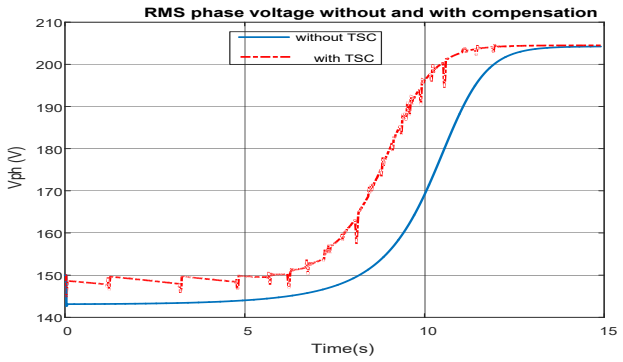

Figure 11: The IM motor terminal phase voltage throughout starting period

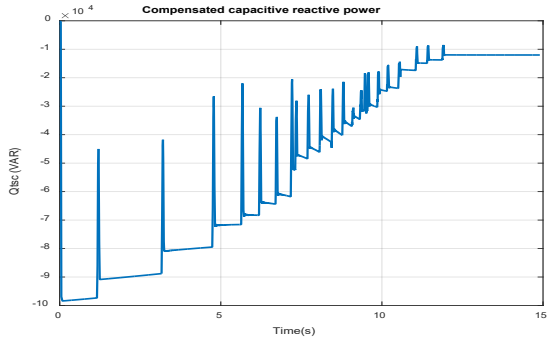

Figure 8: TSC produced capacitive reactive power

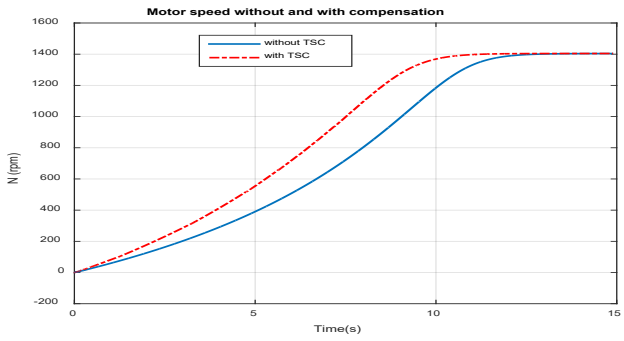

Figure 12: The speed of the IM during starting period

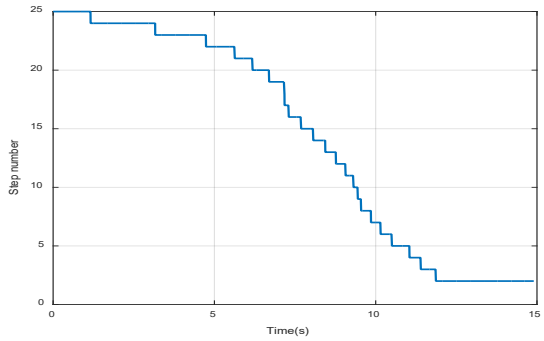

Figure 9: TSC step number to regulate the produced reactive power.

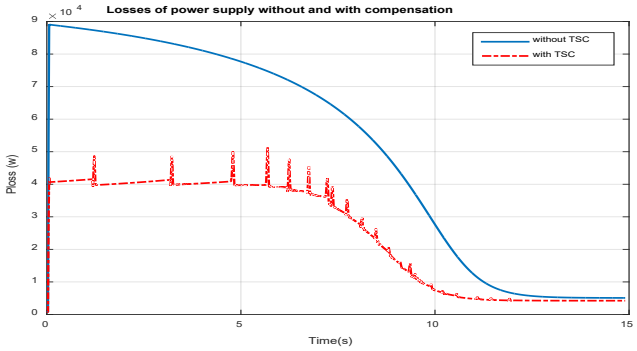

Figure 13: The internal supply losses during starting

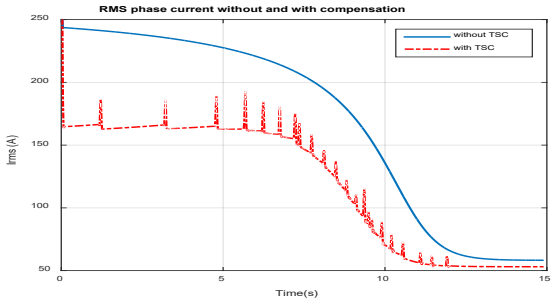

Figure 10: The power supply phase current throughout the motor starting

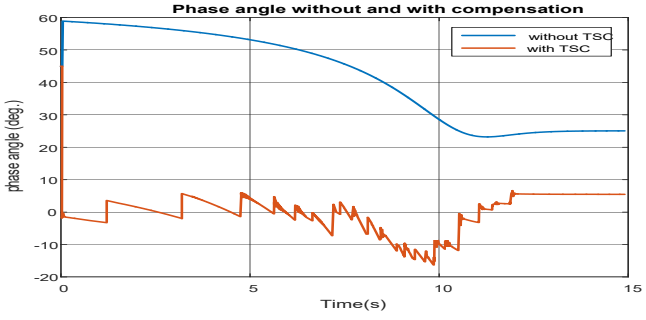

Figure 14. Phase shift between phase voltage and current

Acknowledgment

The study is achieved at Stock Company G. M. Krzhizhanovsky Power Engineering Institute in the framework of the project " Development of a controlled source of reactive power with the absence of the higher-order harmonics currents during the regulation of the electrical energy and with the

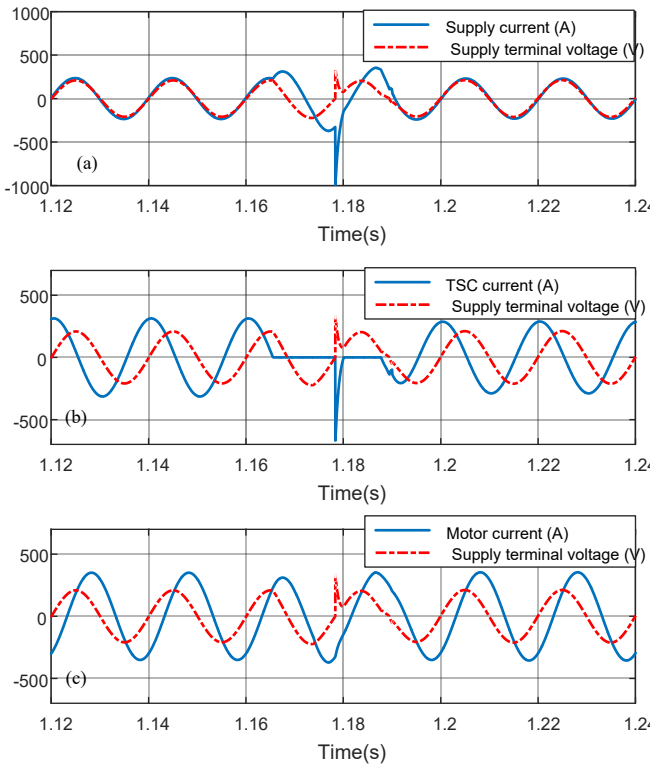

Figure 15. Waveforms of the source terminal phase voltage and current, motor current and TSC current throughout the transition between two levels between 25 and 24 steps

improved technical and economic indicators on the basis of the domestic component base of power electronics for automatic control of the voltage and the power flows in the electric power distribution networks of 6-110 kV (RFMEFI57917X0140)" with the financial support of the Ministry of Education and Science of the Russian Federation.

References

[1] D. I. Panfilov, A. E. ElGebaly, M. G. Astashev and Alexander N. Rozhkov. "Performance Assessment of Thyristors Switched Capacitors during Reactive Power Compensation of Dynamic Load." 2018 10th International Conference on Electrical Power Drive Systems, ICEPDS, Novocherkassk, Russia, 2018. https://doi.org/10.1109/ICEPDS.2018.8571426

[2] Krause, Paul C., Oleg Wasynczuk, and Scott D. Sudhoff. Analysis of Electric Machinery and Drive Systems. IEEE, 2002.

[3] Bird, J. in Electrical and Electronic Principles and Technology 467–485 (Routledge, 2018). doi:10.4324/9781315561875-26.

[4] Nigim, K. in Handbook of Automotive Power Electronics and Motor Drives 387–404 (CRC Press, 2017). doi:10.1201/9781420028157

[5] El-Saady, Gaber, Ali M. Yousef, and Farag K. Abo-Elyousr. "Fuzzy FACTS Voltage Regulator for Isolated Wind Energy Conversion Systems under Different Wind Speed and Loading Conditions." 2016 Saudi Arabia Smart Grid Conference, SASG 2016. doi: 10.1109/SASG.2016.7849677

[6] Omran, A. S., Abbasy, N. H. & Hamdy, R. A. Enhanced performance of substation dynamics during large induction motor starting using SVC. Alexandria Engineering Journal 57, 4059–4070 (2018)

[7] K. Smitanjali et.al "Design of Digital-Static VAR Compensator for Induction Motor" Imperial Journal of Interdisciplinary Research (IJIR), Vol-3, Issue-5, 2017

[8] A. Abd Elraouf et.al, "Ant lion-Based Optimization of Facts Devices' Controllers to Enhance Three Phase Induction Motor Dynamic Performance" European Journal of Research № 4 (4), 2017

[9] A. E. ElGebaly, A. El-Wahab Hassan, M. K. El-Nemr, "Reactive Power Compensation by Multilevel Inverter STATCOM for Railways Power Grid." in Proceedings of the 2019 IEEE Conference of Russian Young Researchers in Electrical and Electronic Engineering, ElConRus, Moscow, Russia, 28-31 January 2019. doi: 10.1109/EIConRus.2019.8657058

[10] D. I. Panfilov, A. E. ElGebaly, "Modified Thyristor Controlled Reactors for Static VAR Compensators" 2016 IEEE 6th International Conference on Power and Energy (PECON 2016), Melaka, Malaysia, November 2016.

[11] D. I. Panfilov, A. E. Elgebaly and M. G. Astashev, "Design and Assessment of Static VAR Compensator on Railways Power Grid Operation under Normal and Contingencies Conditions", 16th EEEIC conference, Florence, Italy, 7-10 June 2016

[12] D. I. Panfilov, A. E. ElGebaly and M. G. Astashev, "Design and evaluation of control system for static VAR compensators with thyristors switched reactors" IEEE 58th International Scientific Conference on Power and Electrical Engineering of Riga Technical University (RTUCON), Riga, Latvia, 12-13 October 2017

[13] D. I. Panfilov, A. E. ElGebaly, M. G. Astashev and A. Rozhkov "New Approach for Thyristors Switched Capacitors Design for Static VAR Compensator Systems" 19th International Conference of Young Specialists on Micro/Nanotechnologies and Electron Devices June 29 - July 3, 2018

[14] Panfilov, D. I., ElGebaly, A., Rozhkov, A. N. & Astashev, M. "Control Strategy of Thyristors Switched SVCs with High Power Quality". Transactions on Environment and Electrical Engineering 3, 15 (2018)

[15] Panfilov, D. I., Elgebaly, A. E., Astashev, M. G. & Rozhkov, A. N. "Control System Operation in Thyristors Switched SVCs with Improved Quality of Reactive Power". in Proceedings - 2018 IEEE International Conference on Environment and Electrical Engineering and 2018 IEEE Industrial and Commercial Power Systems Europe, EEEIC/I and CPS Europe 2018 (Institute of Electrical and Electronics Engineers Inc., 2018). doi:10.1109/EEEIC.2018.8493791

[16] D. I. Panfilov, A. E. ElGebaly and M. G. Astashev, "Design and Optimization of New Thyristors Controlled Reactors with Zero Harmonic Content", 18th International Conference of Young Specialists on Micro/Nanotechnologies and Electron Devices June 29 - July 3, 2017

[17] A. E. Elgebaly, D. I. Panfilov and M. G. Astashev "Comparative Evaluation of Binary and Conventional Static VAR Compensators" Mechanics, Materials Science & Engineering journal (mmse), vol. 17, 2018

[18] Panfilov, D. I., Elgebaly, A. E. & Astashev, M. G. Implementation of thyristors controlled reactors for reactive power control with zero harmonics content. in 17th IEEE International Conference on Smart Technologies, EUROCON 2017 - Conference Proceedings 353–358. doi:10.1109/EUROCON.2017.8011134

ASTES

Advances in Science, Technology and Engineering Systems Journal Vol. 4, No. 4, 65-72 (2019)

www.astesj.com

Special Issue on Multidisciplinary Sciences and Engineering

ASTESJ

ISSN: 2415-6698

All-Pass RC-Filters Architecture with Independent Adjustment of the Main Parameters Based on Differential Difference Amplifiers

Darya Denisenko[1,2,*], Nikolay Prokopenko[1,3], Nikolay Butyrlagin[1]

[1]*Information systems and radio engineering, Don State Technical University, DSTU, Rostov-on-Don, 344000, Russia*

[2]*Systems of automation control, Southern Federal University, SFedU, Taganrog, 347928, Russia*

[3]*Institute for Design Problems in Microelectronics of Russian Academy of Sciences, IPPM RAS, Zelenograd, 124681, Russia*

ARTICLE INFO

Article history:
Received:28 May, 2019
Accepted:04 July, 2019
Online: 11 July, 2019

Keywords:
All-Pass ARCF
Low-Pass Filter
High-Pass Filter
Band-Pass Filter
Rejection Filter
Differential Difference Amplifier
Pole Q-Factor
Pole Frequency
ARCF Transfer Ratio
Filter Parameters Trimming

ABSTRACT

We have suggested an architecture of the second-order all-pass active RC-filter (ARCF), based on three differential difference amplifiers (DDA's), which provides full set of amplitude-frequency responses (AFR's) (low pass filter (LPF), high pass filter (HPF), band pass filter (BPF), rejection filter (RF)). We have given the basic equations, which allow ARCF's. The results of computer simulation of the LPF, HPF, BPF and RF's are discussed. In case of small volume production it is possible to produce the given ARCF in a form of specialized structural arrays, in which LPF, HPF, BPF and RF characteristics are realized by using one of the seven inputs, to which the processed signal is supplied, and four outputs, from which the said signal is outputted. The ARCF is noted, because its transfer ratio and pole frequency are not changed, when the pole Q-factor is adjusted.

1. Introduction

All-pass active RC-filters (ARCF), which provide amplitude-frequency responses (AFR) of low-pass filter (LPF), high-pass filter (HPF), band-pass filter (BPF), rejection filter (RF) [1-16] at different outputs, are attractive for production in a form of special structural crystals [17,18] in conditions of small volume specific type of electronic equipment. At the same time, the application of promising electronic component base in ARCF, for example, differential difference amplifiers (DDAs) [19-33], which provides new properties of frequency selection devices of this class, is of considerable interest.

The present article's purpose and novelty are analysis of all-pass ARCF's new structure's properties [34]. The filter is provided with independent adjustment of base parameters (for example, with digital potentiometers or passive elements' digital switching. A full set of LPF, HPF, BPF, RF's characteristics are implemented by switching seven inputs, on which the signal is supplied, and four outputs, form which the said signal is outputted.

2. ARC-Filter Base Architecture's Properties

There is a circuit of the suggested all-pass ARC-filter (LPF, HPF, BPF, RF) on Fig. 1 [34]. It provides an independent adjustment of pole Q-factor, when pole frequency and transfer ratio, which depend on other elements' parameters, are constant. The independent adjustment is achieved by controlling resistors' resistance. It significantly simplifies a process of frequency selection devices' trimming and adjustment, based on the suggested ARCF circuit. The buffer amplifier (BuffAmp) in scheme Fig. 1 is implemented on a base of traditional operational amplifiers (OpAmps) or DDA, it provides a wide range of R3, R4 resistors' resistance change.

All types active RC-filters' (LPF, HPF, BPF, RF) generalized transfer function is written as (the filters are implemented on the circuit, given on Fig. 1):

*Corresponding Author: Nikolay Butyrlagin, Don State Technical University, Russia | Email: butyrlagin@gmail.com

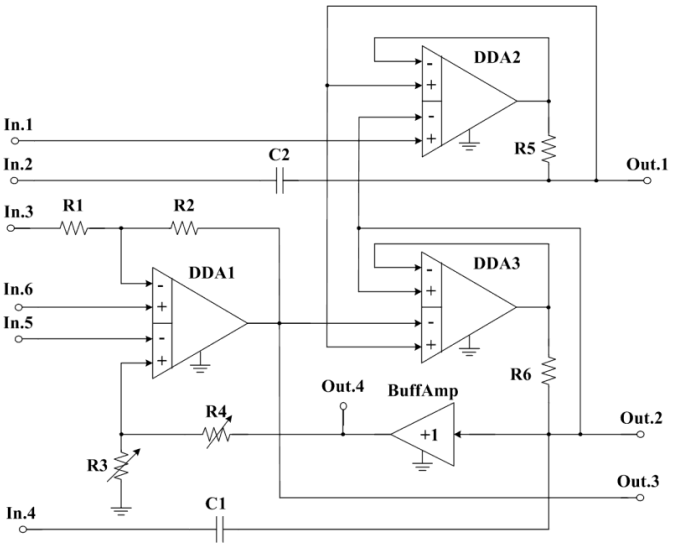

Figure 1: Suggested ARC-Filter's Circuit

$$F(p)=\frac{a_2p^2+a_1p+a_0}{b_2p^2+b_1p+b_0}, \quad (1)$$

where a_i, b_j are equation (1) numerator's and denominator's coefficients, which depend on components' parameters and inputs and outputs in circuit on Fig. 2.

A set of transfer function's numerator coefficients a_i defines a type of ARC-filter (LPF, HPF, BPF, RF).

There are transfer functions' (1) numerator coefficients ai, which are realized in particular ARCF of the Fig. 1 connection circuits, given in Table 1.

The sensitivity functions of the basic parameters of ARCF (Fig. 1) easily correspond to formulas (1) and Table 1.

In the proposed ARCF schemes, typical schemes are applicable, including digital potentiometers or digital switching passive elements, which are described in detail in [35, 36].

The implemented filters' (LPF, HPF, BPF, RF) transfer functions' (1) denominator coefficients b_j relate to elements of the circuit on Fig. 1 by the following equations:

$$b_0=\frac{1}{\tau_1\tau_2}, \quad b_1=\frac{KK_4}{\tau_1}1, \quad b_2=1, \quad . \quad (2)$$

Here the following notation are used in formulas (1), (2):

$$K=\frac{R_3}{R_3+R_4}, \quad K_1=\frac{R_2}{R_1}, \quad K_2=K_3=K_4=1+\frac{R_2}{R_1}, \quad (3)$$
$$\tau_1=R_6C_1, \quad \tau_2=R_5C_2,$$

where R_{ij} are resistance of ij-resistor, C_1, C_2 are capacitance of capacitors C1 and C2.

The active RC-filters, shown in Table 1 and defined as $LPF^{(+)}$, $HPF^{(+)}$, $BPF^{(+)}$, $RF^{(+)}$, have the pole Q-factor, transfer ratio's and pole frequency's independent adjustment properties. Here the pole Q-factor adjustment does not change the filter's transfer ratio and its pole frequency. These filters have the greatest practical interest.

The active RC-filters, defined in Table 1 as LPF, HPF, BPF, RF, do not have the Q-factor, transfer ratio's and pole frequency's independent adjustment properties. Here the transfer ratio and pole frequency coefficients may change, when the pole Q-factor is changed.

The active RC-filters, defined in Table 1 as $LPF^{(-)}$, $HPF^{(-)}$, $BPF^{(-)}$, $RF^{(-)}$, have an amplitude-frequency response slope, which corresponds the first-order transfer function. It limits application scope for these circuit solutions.

There are variants of ARCF Fig. 1 inputs and outputs application on Fig. 2-Fig. 6, they provide AFR different modifications' implementation. In this case, connecting a signal source, for example, to the first input (In.1) assumes that unused inputs are connected to a common bus.

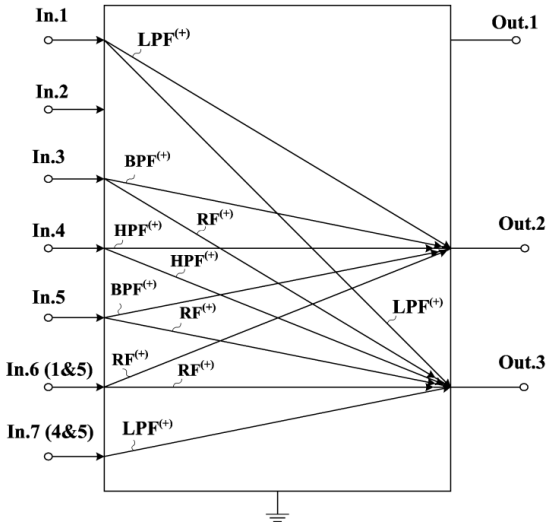

Figure 2: ARCF (Fig. 1) Inputs and Outputs Application Variants, which Provide $BPF^{(+)}$, $RF^{(+)}$, $LPF^{(+)}$,$HPF^{(+)}$ Implementation with Pole Q-Factor Independent Adjustment

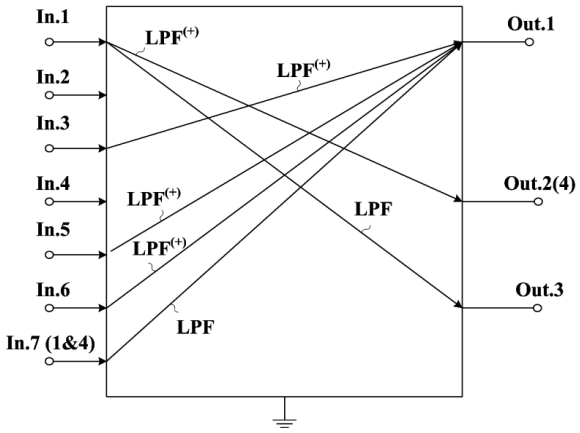

Figure 3: ARCF (Fig. 1) Inputs and Outputs Application, which Provide Low-Pass Filters $LPF^{(+)}$ and LPF Implementation

Table 1: ARC-Filters' Transfer Functions' (1) Numerator Coefficients a_i, Implemented on Base of Circuit, Given on Fig. 1

OUTPUTS / INPUTS	Out.1	Out.2(4)	Out.3
In.1 AFR curves Fig. 7b	HPF$^{(-)}$&BPF$^{(-)}$ $a_2 = \frac{KK_4}{\tau_1\tau_2}$ $a_1 = \frac{1}{\tau_2}$ $a_0 = 0$	LPF$^{(+)}$ $a_2 = a_1 = 0$ $a_0 = \frac{1}{\tau_1\tau_2}$	LPF $a_2 = a_1 = 0$ $a_0 = \frac{KK_4}{\tau_1\tau_2}$
In.2 AFR curves Fig. 8b	HPF$^{(-)}$&BPF$^{(-)}$ $a_2 = 1$ $a_1 = \frac{KK_4}{\tau_1}$ $a_0 = 0$	BPF $a_2 = a_0 = 0$ $a_1 = \frac{1}{\tau_1}$	BPF$^{(+)}$ $a_2 = a_0 = 0$ $a_1 = \frac{KK_4}{\tau_1}$
In.3 AFR curves Fig. 9b	LPF$^{(+)}$ $a_2 = a_1 = 0$ $a_0 = -\frac{K_1}{\tau_1\tau_2}$	BPF $a_2 = a_0 = 0$ $a_1 = \frac{K_1}{\tau_1}$	RF$^{(+)}$ $a_2 = -K_1$ $a_1 = 0$ $a_0 = -\frac{K_1}{\tau_1\tau_2}$
In.4 AFR curves Fig. 10b	BPF $a_2 = a_0 = 0$ $a_1 = -\frac{1}{\tau_2}$	HPF$^{(+)}$ $a_2 = 1$ $a_1 = a_0 = 0$	HPF $a_2 = KK_4$ $a_1 = a_0 = 0$
In.5 AFR curves Fig. 11b	LPF$^{(+)}$ $a_2 = a_1 = 0$ $a_0 = -\frac{K_3}{\tau_1\tau_2}$	BPF $a_2 = a_0 = 0$ $a_1 = \frac{K_3}{\tau_1}$	RF$^{(+)}$ $a_2 = -K_3$ $a_1 = 0$ $a_0 = -\frac{K_3}{\tau_1\tau_2}$
In.6 AFR curves Fig. 12b	LPF$^{(+)}$ $a_2 = a_1 = 0$ $a_0 = \frac{K_2}{\tau_1\tau_2}$	BPF $a_2 = a_0 = 0$ $a_1 = -\frac{K_2}{\tau_1}$	RF$^{(+)}$ $a_2 = K_2$ $a_1 = 0$ $a_0 = \frac{K_2}{\tau_1\tau_2}$
In.1&4 AFR curves Fig. 13b	LPF $a_2 = a_1 = 0$ $a_0 = \frac{KK_4}{\tau_1\tau_2}$	RF$^{(+)}$ $a_2 = 1$ $a_1 = 0$ $a_0 = \frac{1}{\tau_1\tau_2}$	RF $a_2 = KK_4$ $a_1 = 0$ $a_0 = \frac{KK_4}{\tau_1\tau_2}$

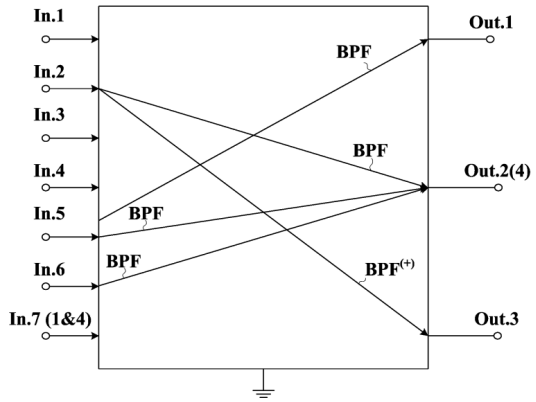

Figure 4: ARCF (Fig. 1) Inputs and Outputs Application, which Provide Band-Pass Filters $BPF^{(+)}$ and BPF Implementation

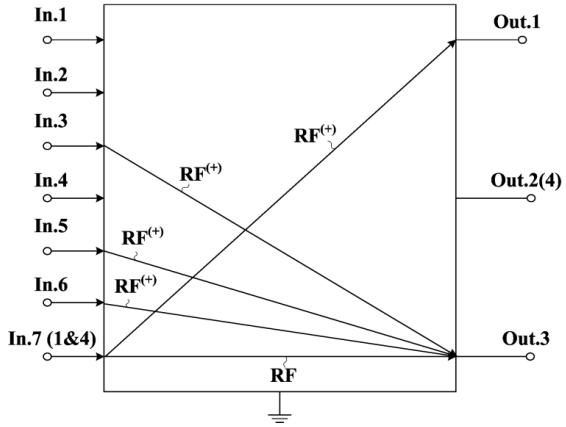

Figure 5: ARCF (Fig. 1) Inputs and Outputs Application, which Provide Rejection Filters $RF^{(+)}$ and RF Implementation

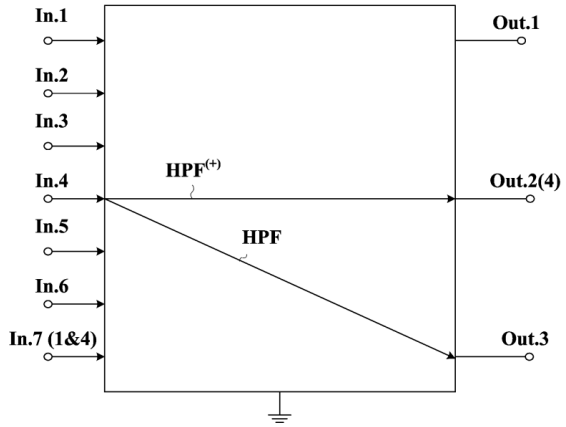

Figure 6: ARCF (Fig. 1) Inputs and Outputs Application, which Provide High-Pass Filters $HPF^{(+)}$ and HPF Implementation

The computer simulation of the ARCF Fig. 1 different modifications, which correspond Fig. 2-Fig. 6, was made in MicroCap on AD830 DDA. It has confirmed the above properties of the suggested ARCF's circuit solution.

3. Low-Pass Filter $LPF^{(+)}$

ARCF's inputs (Fig. 1) are connected according to the circuit, given on Fig. 7a, it provides amplitude-frequency responses of $HPF^{(-)}$&$BPF^{(-)}$, $LPF^{(+)}$, LPF on outputs Out.1, Out.2(4), Out.3.

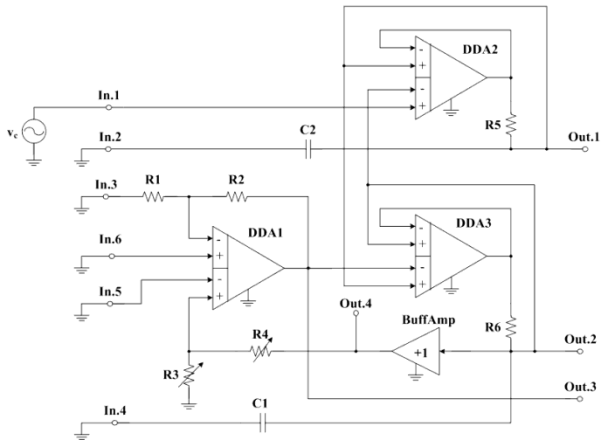

(a)

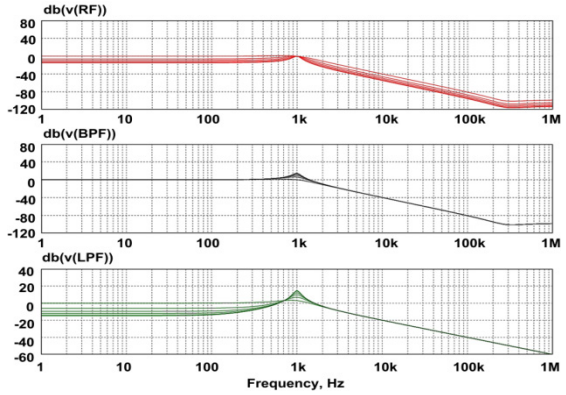

(b)

Figure 7: Special ARC-Filter's Switching Circuit (a) and its AFRs (b)

Analysis of the AFR's curves (Fig. 7b) has shown, that transfer ratio and pole frequency are not changed in $LPF^{(+)}$, implemented for output Out.2(4), when the pole Q-factor is adjusted (by changing R3 and R4 resistors resistance). At the same time, the pole frequency in this circuit can be tuned using resistors R5 and R6.

4. Band-Pass Filter $BPF^{(+)}$

ARCF's inputs (Fig. 1) are connected according to the circuit, given on Fig. 8a, it provides amplitude-frequency responses of $HPF^{(-)}$&$BPF^{(-)}$, BPF, $BPF^{(+)}$ on outputs Out.1, Out.2(4), Out.3.

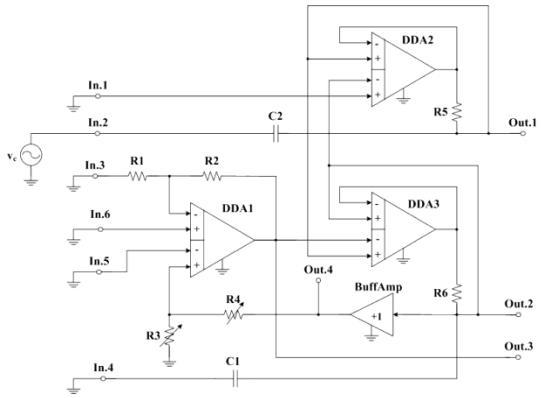

(a)

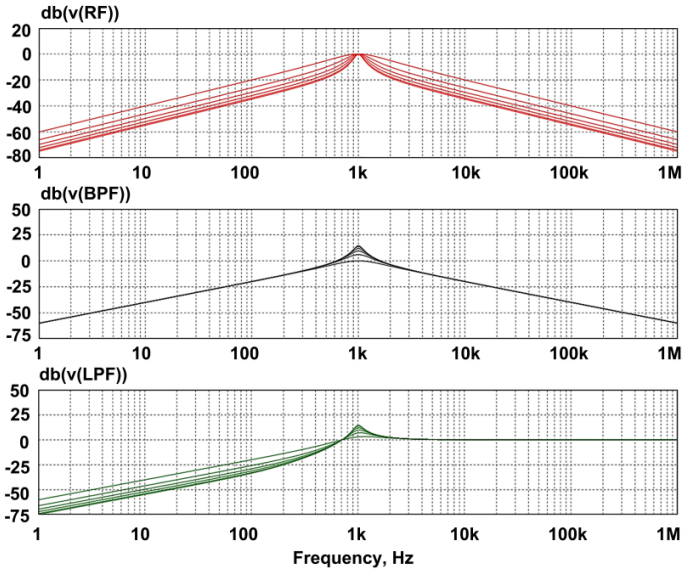

(b)

Figure 8: Special ARC-Filter's Switching Circuit (a) and its Amplitude-Frequency Responses (b)

Based on the BPF(+)'s AFRs curves (Fig. 8b) for output Out.3, can be concluded, that transfer ratio and pole frequency are not changed, when the pole Q-factor is adjusted (by changing R3 and R4 resistors' resistance). In this case, the pole frequency in this circuit can be tuned with resistors R5 and R6, and the transfer ratio change with resistors R1 and R2.

5. Rejection Filter RF(+) and Low-Pass Filter LPF (+)

ARCF's inputs (Fig. 1) are connected according to the circuit, given on Fig. 9a, it provides amplitude-frequency responses of LPF(+), BPF, RF(+) on outputs Out.1, Out.2(4) and Out.3.

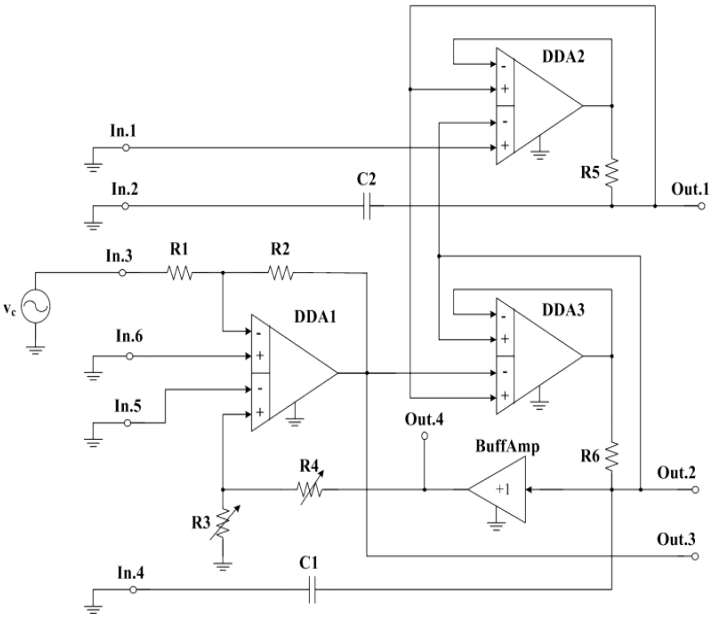

(a)

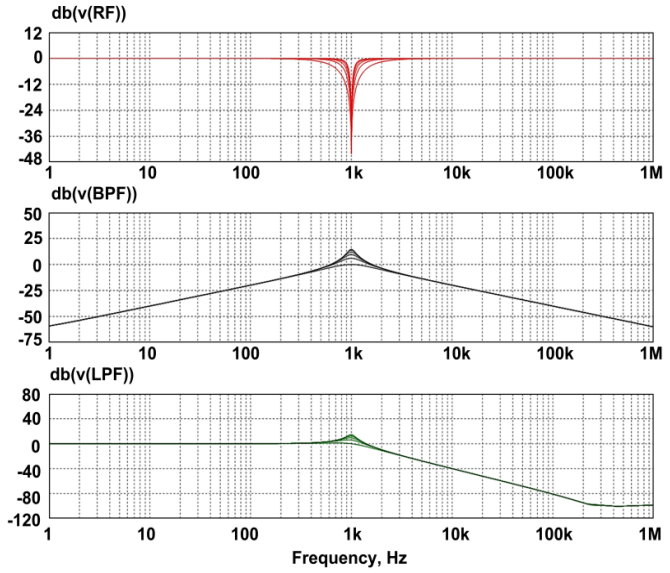

(b)

Figure 9: Special ARC-Filter's Switching Circuit (a) and its Amplitude-Frequency Responses (b)

So the ARC's curves (Fig. 9b) show, that transfer ratio and pole frequency are not changed in the implemented LPF(+) and RF(+) for outputs Out.1 and Out.3, when the pole Q-factor is adjusted by changing R3 and R4 resistors' resistance. The pole frequency in this circuit can be tuned with resistors R5 and R6, and the transfer ratio with resistors R1 and R2.

6. High-Pass Filter HPF(+)

ARCF's inputs (Fig. 1) are connected according to the circuit, given on Fig. 9a, it provides amplitude-frequency responses of BPF, HPF(+) and HPF on outputs Out.1, Out.2(4), Out.3.

It should be noted that when the pole Q-factor is adjusted, the transfer ratio and pole frequency of HPF(+) for output Out.2(4) are not changed, which follows from AFR on Fig. 10b. At the same time, the pole frequency in this circuit can be tuned using resistors R5 and R6.

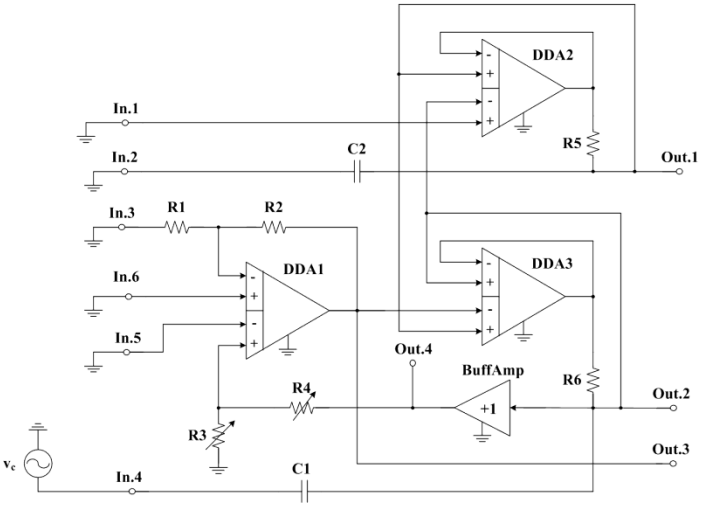

(a)

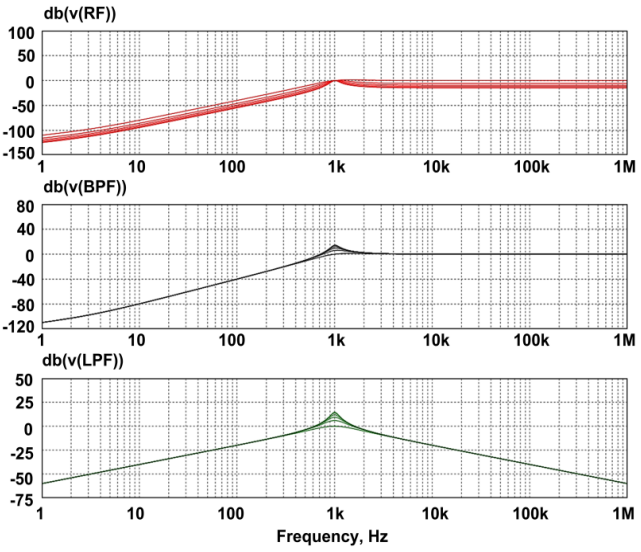

(b)

Figure 10: Special ARC-Filter's Switching Circuit (a) and Amplitude-Frequency Responses (b)

7. Low Pass Filter LPF(+) and Rejection Filter RF(+), Inverting Input Signal

ARCF's inputs (Fig. 1) are connected according to the circuit, given on Fig. 11a, it provides amplitude-frequency responses of LPF(+), BPF, RF(+). on outputs Out.1, Out.2(4), Out.3.

The given AFRs' curves' (Fig. 11b) analysis has shown, that the transfer ratio and pole frequency in LBF(+) and RF(+) for outputs Out.1 and Out.3 are not changed, when the pole Q-factor is adjusted by changing R3 and R4 resistors' resistance. At the same time, the pole frequency in this circuit can be tuned with resistors R5 and R6, and the transfer ratio with resistors R1 and R2.

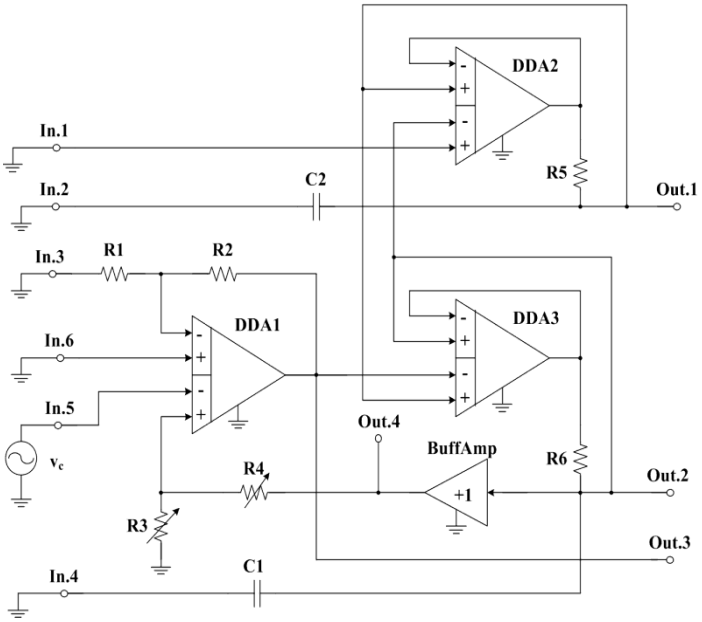

(a)

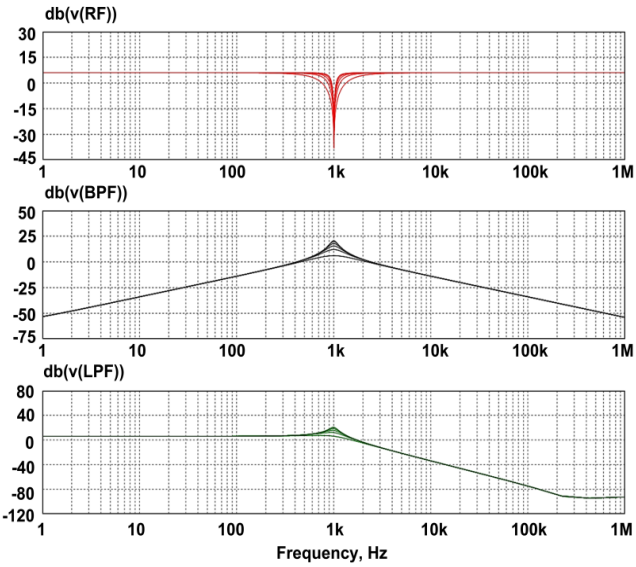

(b)

Figure 11: Special ARC-Filter's Switching Circuit (a) and its Amplitude-Frequency Responses (b)

8. Low Pass Filter LPF (+) and Rejection Filters (+), Non-inverting Input Signal

ARCF's inputs (Fig. 1) are connected according to the circuit, given on Fig. 12a, it provides amplitude-frequency responses of LPF(+), BPF, RF(+) on outputs Out.1, Out.2(4) and Out.3.

When the pole Q-factor is adjusted (by changing R3 and R4 resistors resistance), the transfer ratio and pole frequency of LPF(+) and RF(+) (for outputs Out.1 and Out.3 correspondently) are not changed. At the same time, the pole frequency in this circuit can be adjusted using resistors R5 and R6, and the transfer ratio using resistors R1 and R2.

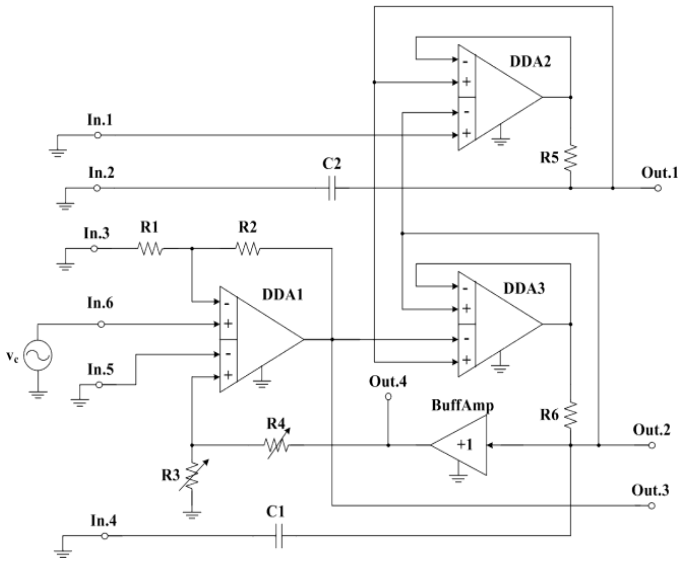

(a)

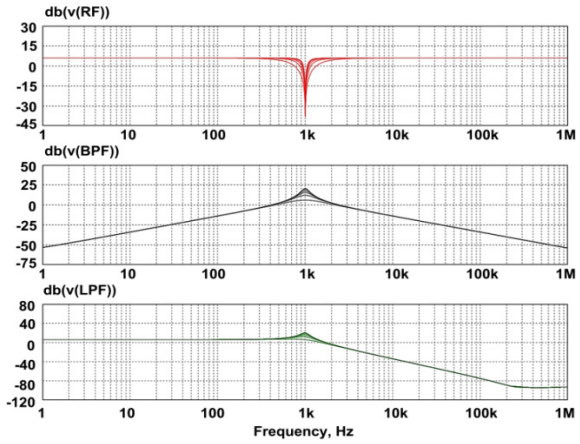

(b)

Figure 12: Special ARC-Filter's Switching Circuit (a) and its AFRs (b)

9. Rejection Filter RF(+)

ARCF's inputs (Fig. 1) are connected according to Fig. 13a, it provides amplitude-frequency responses of LPF, RF(+), RF on outputs Out.1, Out.2(4), Out.3.

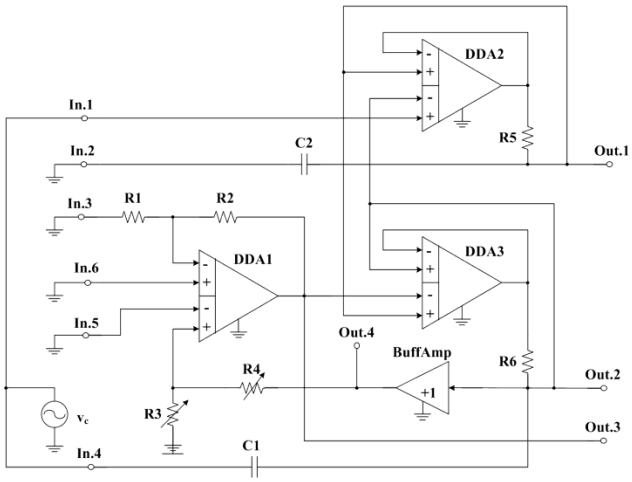

(a)

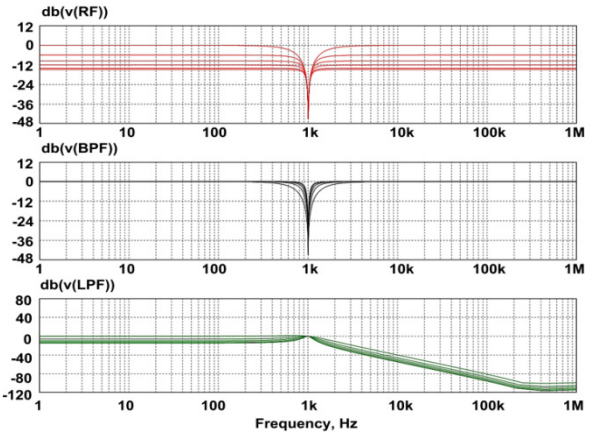

(b)

Figure 13: Special ARC-Filter's Switching Circuit (a) and its Amplitude-Frequency Responses (b)

From the analysis of the AFRs' curves (Fig. 13b), it may be concluded, that the transfer ratio and pole frequency are not changed in the RF(+), implemented for output Out.2(4), when the pole Q-factor is adjusted (by changing R3 and R4 resistors resistance). At the same time, the pole frequency in this circuit can be tuned using resistors R5 and R6.

10. Conclusion

We have developed a structure of all-pass ARCF with pole Q-factor, transfer ratio and pole frequency independent adjustment for the whole spectrum of amplitude-frequency responses of the second-order filter (LPF, HPF, BPF, RF) implemented. This is a significant advantage of the considered circuit design solutions in comparison with the known ARCF of this class. We recommend using the suggested ARCF as a specialized chip of a structural array because of its universality. It is possible to implement a wide range of frequency selection devices in the said ARCF, because the signal source is connected to one of seven inputs and four outputs.

Conflict of Interest

The authors declare that there is no conflict of interests regarding publication of this paper.

Acknowledgments

The research is carried out at the expense of the Russian Science Foundation Grant (Project No. 18-79-10109).

References

[1] W. Chiu and J. Horng, "High-Input and Low-Output Impedance Voltage-Mode Universal Biquadratic Filter Using DDCCs," in IEEE Transactions on Circuits and Systems II: Express Briefs, vol. 54, no. 8, pp. 649-652, Aug. 2007. DOI: 10.1109/TCSII.2007.899460

[2] Miao Huijing, Liu Xiaoyan, Tan Boxue, Shen Jin and Wang Yajing, "A universal active filter design method," 2010 International Conference on Information, Networking and Automation (ICINA), Kunming, 2010, pp. V1-18-V1-22. DOI: 10.1109/ICINA.2010.5636442

[3] C. Chang, "Universal active current filter with single input and three outputs using CCIIs," in Electronics Letters, vol. 29, no. 22, pp. 1932-1933, 28 Oct. 1993. DOI: 10.1049/el:19931286

[4] Xifeng Zhou, Shanshan Li and Jiake Wang, "An electronically tunable active-C current-mode universal filter employing CCCII and OTA," 2011 IEEE International Conference on Computer Science and Automation Engineering, Shanghai, 2011, pp. 647-651. DOI: 10.1109/CSAE.2011.5952930

[5] F. Khateb, S. B. A. Dabbous, M. Kumngern and T. Kulej, "Novel current controlled differential-input buffered output active element and its application in all-pass filter," 2015 38th International Conference on Telecommunications and Signal Processing (TSP), Prague, 2015, pp. 335-338. DOI: 10.1109/TSP.2015.7296279

[6] P. Ahmadi, B. Maundy, A. S. Elwakil, L. Belostotski and A. Madanayake, "A New Second-Order All-Pass Filter in 130-nm CMOS," in IEEE Transactions on Circuits and Systems II: Express Briefs, vol. 63, no. 3, pp. 249-253, March 2016. DOI: 10.1109/TCSII.2015.2482578

[7] B. Metin, N. Herencsar, J. Koton and E. Arslan, "All-pass filter application using electronically tunable DDCC," 2014 24th International Conference Radioelektronika, Bratislava, 2014, pp. 1-4. DOI: 10.1109/Radioelek.2014.6828413

[8] L. Mohammadi and K. Koh, "Integrated C-band (4–8 GHz) frequency-tunable & bandwidth-tunable active band-stop filter in 0.13-µm SiGe BiCMOS," 2015 IEEE MTT-S International Microwave Symposium, Phoenix, AZ, 2015, pp. 1-4. DOI: 10.1109/MWSYM.2015.7167026

[9] T. S. Arora, M. Gupta and S. Gupta, "Current mode universal filter employing operational transconductance amplifier and third generation current conveyor," 2016 IEEE 1st International Conference on Power Electronics, Intelligent Control and Energy Systems (ICPEICES), Delhi, 2016, pp. 1-4. DOI: 10.1109/ICPEICES.2016.7853305

[10] S. Gautam, P. Yunqing, M. Kashif, Y. R. Kafle, Z. Z. Hua and L. Bo, "Study on software phase locked loop for single phase active power filter," Fifth

International Conference on Advances in Recent Technologies in Communication and Computing (ARTCom 2013), Bangalore, 2013, pp. 319-327. doi: 10.1049/cp.2013.2191

[11] N. Herencsar, J. Jerabek, J. Koton, K. Vrba, S. Minaei and İ. C. Göknar, "Pole frequency and pass-band gain tunable novel fully-differential current-mode all-pass filter," 2015 IEEE International Symposium on Circuits and Systems (ISCAS), Lisbon, 2015, pp. 2668-2671. DOI: 10.1109/ISCAS.2015.7169235

[12] N. Herencsar, J. Koton, K. Vrba and O. Cicekoglu, "Low-voltage fully cascadable resistorless transadmittance-mode all-pass filter," 2014 IEEE 57th International Midwest Symposium on Circuits and Systems (MWSCAS), College Station, TX, 2014, pp. 185-188. DOI: 10.1109/MWSCAS.2014.6908383

[13] A. Upadhyay and K. Pal, "A DVCC based voltage mode all pass filter using operational amplifier pole," 2014 International Conference on Power, Control and Embedded Systems (ICPCES), Allahabad, 2014, pp. 1-4. DOI: 10.1109/ICPCES.2014.7062817

[14] N. Wattikornsirikul and M. Kumngern, "Three-input one-output voltage-mode universal filter using simple OTAs," 2014 Twelfth International Conference on ICT and Knowledge Engineering, Bangkok, 2014, pp. 28-31. DOI: 10.1109/ICTKE.2014.7001530

[15] R. Sotner, J. Jerabek, J. Petrzela, K. Vrba and T. Dostal, "Design of fully adjustable solution of band-reject/all-pass filter transfer function using signal flow graph approach," 2014 24th International Conference Radioelektronika, Bratislava, 2014, pp. 1-4. DOI: 10.1109/Radioelek.2014.6828418

[16] I. Mondal and N. Krishnapura, "A 2-GHz Bandwidth, 0.25–1.7 ns True-Time-Delay Element Using a Variable-Order All-Pass Filter Architecture in 0.13 μ m CMOS," in IEEE Journal of Solid-State Circuits, vol. 52, no. 8, pp. 2180-2193, Aug. 2017. doi: 10.1109/JSSC.2017.2693229.

[17] J. Teifel, R. S. Flores, S. Pearson, C. Begay, K. K. Ma and J. Palmer, "ViArray standard platforms: Rad-hard structured ASICs for digital and mixed-signal applications," 2012 IEEE Aerospace Conference, Big Sky, MT, 2012, pp. 1-9. DOI: 10.1109/AERO.2012.6187235.

[18] "Analogue arrays from Sweden, " SLA description, Dec. 1999, pp. 1-4.

[19] V. Stornelli, L. Pantoli, G. Leuzzi, G. Ferri, "Fully differential DDA-based fifth and seventh order Bessel low pass filters and buffers for DCR radio systems, " Analog Integr Circ Sig Process 2013;75(2):305–10. https://doi.org/10.1007/s10470-013-0051-9.

[20] F. Khateb, T. Kulej, M. Kumngern and C. Psychalinos, "A compact power-efficient 0.5 V fully differential difference amplifier, " AEU - International Journal of Electronics and Communications, 105, 71–77. DOI:10.1016/j.aeue.2019.04.007

[21] F. Khateb, M. Kumngern, T. Kulej and V. Kledrowetz, "Low-voltage fully differential difference transconductance amplifier," in IET Circuits, Devices & Systems, vol. 12, no. 1, pp. 73-81, 1 2018. DOI: 10.1049/iet-cds.2017.0057

[22] H. Alzaher and M. Ismail, "A CMOS fully balanced differential difference amplifier and its applications," in IEEE Transactions on Circuits and Systems II: Analog and Digital Signal Processing, vol. 48, no. 6, pp. 614-620, June 2001. DOI: 10.1109/82.943332.

[23] M. Kumngern, F. Khateb, "0.8-V Floating-Gate Differential Difference Current Feedback Operational Amplifier, "2014 11th International Conference on Electrical Engineering/Electronics, Computer, Telecommunications and Information Technology (ECTI-CON), 14-17 May 2014, pp. 1-5. DOI: 10.1109/ECTICon.2014.6839780

[24] M. Kumngern, K. Klangthan, "0.5-V Fourth-Order Low-Pass Filter, " 2017 2nd International Conference on Automation, Cognitive Science, Optics, Micro Electro-Mechanical System, and Information Technology (ICACOMIT), Oct. 23, 2017, Jakarta, Indonesia, pp. 119-122. DOI: 10.1109/ICACOMIT.2017.8253398

[25] J. Wang, Zh. Zhu, S. Liu, R. Ding, "A low-noise programmable gain amplifier with fully balanced differential difference amplifier and class-AB output stage, " J. Microelectronics, 2017, no. 64, pp. 86–91.

[26] S.G. Krutchinsky, N.N. Prokopenko, E.A. Zhebrun, N.V. Butyrlagin. The Peculiarities of the Structural Optimization of the Energy-Efficient Precision ARC-Filters on the Base of Classical and Differential Difference Operational Amplifiers // IEEE East-West Design & Test Symposium (EWDTS'2015), 26 – 29 Sep. 2015. - Batumi, Georgia. DOI: 10.1109/EWDTS.2015.7493136

[27] N. N. Prokopenko, N. V. Butyrlagin, S. G. Krutchinsky, E. A. Zhebrun and A. E. Titov, "The Advanced Circuitry of the Precision Super Capacitances Based on the Classical and Differential Difference Operational Amplifiers," 2015 IEEE 18th International Symposium on Design and Diagnostics of Electronic Circuits & Systems, Belgrade, 2015, pp. 111-114. DOI: 10.1109/DDECS.2015.46

[28] D. Jana and A. K. Mal, "Design of low noise amplifier for sensor applications," 2017 Devices for Integrated Circuit (DevIC), Kalyani, 2017, pp. 451-455.doi: 10.1109/DEVIC.2017.8073990

[29] Q. Hu, L. Yang and F. Huang, "A 100–170MHz fully-differential Sallen-Key 6th-order low-pass filter for wideband wireless communication," 2016 International Conference on Integrated Circuits and Microsystems (ICICM), Chengdu, 2016, pp. 324-328. DOI: 10.1109/ICAM.2016.7813617

[30] J. S. Mincey, C. Briseno-Vidrios, J. Silva-Martinez and C. T. Rodenbeck, "Low-Power Gm-C Filter Employing Current-Reuse Differential Difference Amplifiers," in IEEE Transactions on Circuits and Systems II: Express Briefs, vol. 64, no. 6, pp. 635-639, June 2017. DOI: 10.1109/TCSII.2016.2599027

[31] N. Van Helleputte, R. F. Yazicioglu, "Instrumentation amplifier and signal amplification method, " U.S. Patent 9 294 048, Mar. 22, 2016.

[32] J. Koton, N. Herencsar, J. W. Horng, "Differential second-order voltage-mode all-pass filter using current conveyors, " Elektronika ir Elektrotechnika, 2016, vol. 22, no. 5, pp. 52-57. DOI: 10.5755/j01.eie.22.5.16344

[33] A. Yesil, F. Kacar, "Band-pass filter with high quality factor based on current differencing transconductance amplifier and current amplifier, " AEU-International Journal of Electronics and Communications, 2017, vol. 75, pp. 63-69. DOI: 10.1016/j.aeue.2017.03.007

[34] D. Yu. Denisenko, N. N. Prokopenko, "All-pass Active RC Filter Based on Differential Difference Amplifiers, " Patent Appl. RU 2019107341, March 15, 2019. (In Russian).

[35] D. Y. Denisenko, Y. I. Ivanov, N. N. Prokopenko and N. A. Dmitrienko, "Digital potentiometers in the tasks of settings precision analog RC-filters taking into account the tolerances for passive components," 2017 18th International Conference of Young Specialists on Micro/Nanotechnologies and Electron Devices (EDM), Erlagol, 2017, pp. 205-210. https://doi: 10.1109/EDM.2017.7981741

[36] Digital Potentiometers (DigiPOT). URL: https://www.analog.com/en/products/digital-to-analog-converters/digital-potentiometers.html

ASTES

Advances in Science, Technology and Engineering Systems Journal
Vol. 4, No. 4, 73-93 (2019)
www.astesj.com
Special Issue on Advancement in Engineering and Computer Science

ASTES Journal
ISSN: 2415-6698

Intelligent Foundations for Knowledge Based Systems

Mukundan Kandadai Agaram*

Delta Dental of Michigan, 4100 Okemos Road, Okemos, MI 48864, U.S.A,

ARTICLEINFO

Article history:
Received: 18 April, 2019
Accepted: 23 June, 2019
Online: 15 July, 2019

Keywords:
Knowledge Based Systems
Rule Based Information Systems
Intelligent Discovery
Data Visualization
Enterprise Decision Management
Master Data Management
Software Architecture
Enterprise Architecture
Domain Driven Design
Healthcare Adjudication

ABSTRACT

Knowledge Based Systems play a very important role, within Healthcare, with a primary goal of supporting a high quality service at an optimal cost. A widely accepted knowledge acquisition technique is through the use of Business Rules in a natural language like format. As clinical terminology is centric to HealthCare, a large percentage of these rules use industry standard codes to describe clinical concerns. Usually there is a large number of codes to denote the various clinical processes and procedures within Healthcare. These can translate to a combinatorially explosive number of Business Rules within the HealthCare IT system. It is common practice to leverage a Rule Engine to execute these rules and produce decisions within the system. A Rule Engine accepts a collection of rules called a ruleset. Within Healthcare Insurance, these rules and rulesets embody regulatory, policy and contractual concerns. To effectively manage this huge body of rules and rulesets, it is typical for Knowledge Based Systems to reuse rules across rulesets. Further, the knowledge required to author these rules and constructing comprehensive rulesets is specialized and requires deep expertise within the domain. Further, this also requires an expertise with authoring unambiguous business rules and operating the Rule Management Systems or Knowledge Based Systems. There is a need for the continuous Governance of these rule based knowledge assets for the organization. Typically knowledge experts in this field have a decade or more of experience. An emergent challenge or trend witnessed within the industry is that the experienced knowledge workers are retiring and their positions are being replaced by people not as experienced. This paper proposes techniques to build a layer of intelligent capabilities that can transform the methods for the automation, creation and maintenance of knowledge artifacts, that can aid and support the inexperienced knowledge workers with the effective management and administration of these assets within a Healthcare system.

1 Introduction

Healthcare domains are characterized by a rich knowledge accumulated through a combination of science, technology, experience, innovation within the industry and standardization through regulatory entities. Given the high cost of administration of health care, it is common practice to be reliant on a strong infrastructure of insurance to fund the high costs of administering healthcare. Further, there is a strong demand and pressure for absorbing scientific and technological advances within the field into operational practice within a short period of time. There is a high risk of adverse practice effects, fueling the necessity for standardization of practice, within the industry. This paper is an extension of the paper titled *Intelligent discovery features for EDM and MDM Systems* originally presented at 2018 IEEE 22nd International Enterprise Distributed Object Computing Workshop (EDOCW) [1]. This paper further extends the concepts beyond the discovery features described in the original paper. It further formalizes these concepts into a set of foundational patterns, called *intelligent foundations*, with a view to providing automation towards hard to scale and hard to automate human labor intensive processes around business rule mining and knowledge manage-

*Mukundan Kandadai Agaram, Delta Dental of Michigan, 4100 Okemos Road, Okemos, MI 48864, U.S.A, Phone: +1 (517) 381-4736, Email: magaram@deltadentalmi.com

ment. This paper further lays down a formalized foundation of ingredients to construct recipes for building intelligent virtual knowledge working software agents to aid a new breed of digitally savvy, but functionally inexperienced workforce.

1.1 Healthcare in the United States

In the US, healthcare can be broadly categorized into the *Provider* i.e. the clinical entity viz., hospitals, doctor's offices, clinics etc. that provides the clinical services and the *Payor* i.e. the funding entity a.k.a insurance companies that pays for these services. The cost of healthcare is expensive and exorbitant to the general population. In addition it is highly susceptible to litigation, which further acutely drives up the cost. Healthcare insurance infrastructure is predominantly operated by the private sector, through a combination of "for profit" and "not for profit" entities. Stereotypically, healthcare insurance within the US is offered as a benefit, to employees of companies. The employers purchase health insurance for their employees through customized benefit plans, from healthcare payor companies. The health insurance costs are more affordable when bought in bulk for larger groups of people and is often referred to as the "group discount". This is due to the fact that the risk of "adverse selection" is significantly lowered. The cost of insurance is high for the average citizen seeking to buy it [2], [3], [4], [5]. Recent reforms in healthcare have attempted to introduce competitive pricing through the notion of healthcare exchanges at competitive rates. The general gist of this is to be able to provide insurance for healthcare to citizens, who otherwise cannot participate in employer health benefit plans either due to lack of employment or lack of availability of the benefit from the employer. In the US, there is a specialization of insurance products for *Medical* healthcare, *Dental* healthcare and *Vision* healthcare.

1.2 Background

The work presented in this paper and the original foundational paper is part of an evolving case study in the practical application of data science, analytics and visualization techniques that can automate the process of knowledge analysis and mining at a Dental Insurance company. Delta Dental of Michigan, Indiana and Ohio is the leading provider of dental benefits, serving the mid-western part of the US, with a subscriber base of nearly 15 million members throughout the states of Michigan, Indiana, Ohio and it's growing base of other affiliated states in other parts of the US. The company has witnessed a strong growth over the last decade of it's 60+ years of history. A key factor for this growth is it's highly automated insurance and benefits administration software platform, that achieves an industry enviable 95% auto adjudication rate (the percentage of claims that are entirely processed by the software platform with no human intervention). The cornerstone of the software platform is a sophisticated rule management system called BRIDE, which enable the domain *knowledge workers* or Subject Matter Experts (SMEs), to author, test and manage the operational rules, using highly configurable *Domain Specific Languages* and a semantically rich *Business Vocabulary* [6]. The BRIDE platform is an innovative homegrown product which is the result of original collaborative work by the author and other fellow contributors, which is elaborated in a published conference paper [7]. The knowledge externalized into BRIDE as operational *Business Rules*, can be translated and deployed to any forward chaining production rule engine format [8].

1.3 Motivation

The process of deciding to pay a claim a.k.a *adjudication* in the healthcare claims arena, requires a deep understanding of healthcare clinical knowledge. Within the dental healthcare space, it is not uncommon to manually adjudicate complex and costly dental procedures, by dental experts who have had prior hands on experience with the clinical aspect of the science. Further a second dimension of expertise is to understand, the payor's business policy as it pertains to the interpretation of allowances and coverages. As a consequence, a typical knowledge worker has decades of experience within the industry and/or company. However, these experts are now reaching retirement age and will be transitioning their responsibilities to younger and lesser experience functional specialists. This provides strong motivation to build *"intelligent capabilities"* into the platform, that can automate laborious manual processes and to provide a decision support system for generating or recommending rules to the knowledge workers as they author these rules. This will be elaborated further in subsequent sections.

1.4 Organization

This paper is organized as follows. In 2, we will explore the characteristics of knowledge sources, their nature and consequences, within the context of healthcare claims processing and adjudication. We will cast a wider net to describe how the patterns presented by these problems can be applied to other functional verticals with similar characteristics. This will then provide a segue to 3, where the subject of *intelligent capabilities* will be explored with a viewpoint of automating manually intensive tasks and to provide seamless decision support to the act of *rule/knowledge mining*. In 4, we will explore the subject of building intelligent foundations and capabilities with the backdrop of the BRIDE [7] case study, that can support a growing and diverse eco-system of artificial intelligence. In 5 we will discuss inherent challenges in addressing the intelligent automation of knowledge/rule mining. This will naturally set the stage for discussion of future research/work, in 6. We will finally provide a meaningful conclusion for the work in 7.

2 Knowledge Characteristics

Knowledge/Rule Mining through traditional means can be a manually intensive process. Traditional Rule-based Information Systems, rely on the ability of human experts, to author high quality, non-ambiguous system enforceable rules. Further, knowledge rich areas such as clinical domains, yield a high number of such rules. These rules exhibit symptoms of combinatorial explosion, when certain influencing parameters change. These parameters are commonly influenced by external forces, such as customer needs, advances in science, market trends, regulatory mandates , adherence to standards etc. Second, the complexity of the rules can be high. In certain cases automation of the business logic, through procedural programming techniques can yield, very large (in the order of 10K lines of code), extremely complex programs [9]. The maintenance cost of such programs increase dramatically over time. In the face of such complexity, a system of externalized rules provides significant cost savings and improved agility to change. However, the system of rules that are mined out from large legacy procedural language programs is iterative in nature and is best achieved in a phased manner.

The original paper [1], outlines the complexities of the problem, especially around the mining, discovery and management of business domain knowledge as externalized business rules, into six different categories viz., *Volume and Growth Complexity*, *Organizational and Reuse Complexity*, *Rule Logic Complexity*, *Domain and Subject Matter Complexity*, *Healthcare Complexity*, *Healthcare Consolidation Complexity*. In this section we will contrast these with other intrinsic characteristics surrounding *Knowledge* and their relevance within surrounding eco-systems.

Healthcare systems operate around a hub of knowledge. This hub is surrounded by a triad of pillars, *People*, *Process* and *Technology*, which is depicted in 1. The *People* realm represents the Clinical knowledge workers, Business User Community, Claims/Insurance Practitioners etc., and their collective knowhow. The *Process* realm represents the organization's conscious act of documenting the knowhow with a view to standardizing, documenting and repeating them in a predictable fashion. The *Technology* realm reflects the collective collage of automation software, which in the case of the Healthcare Payor business, could be the Claims Processing System, Benefits Administration System, Accounting System etc. The company's knowledge assets live in the hub of these three pillars. We will now proceed to examine the characteristics of knowledge which intersects with each of these pillars. We will further examine the influences of introducing *intelligent foundations* to *Knowledge Management* and how it helps to preserve the most valuable assets of the organization i.e *knowledge*.

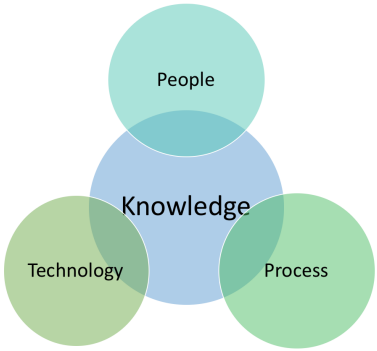

Figure 1: Knowledge Hub

2.1 Documented Knowledge

Documented Knowledge as the name suggests, represents all documented artifacts describing business processes, policies, contracts etc. Documented knowledge, exists in a variety of formats for different audiences. Healthcare is a highly regulated domain and is subject to a variety of audits. Non-compliance with regulation and audit findings present dire consequences, in the shape of costly penalties and potential litigation. Hence, it is crucial to maintain detailed documentation of processes, contracts and such. The basis of *Documented Knowledge* is depicted in 2.

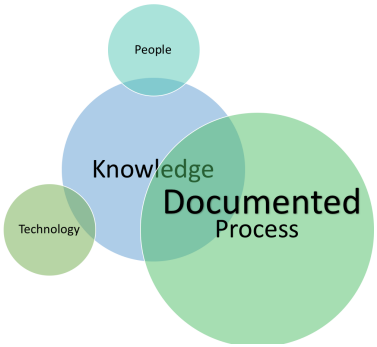

Figure 2: Documented Knowledge

Documented Knowledge, has the following consequences.

1. Footprint of *Documented Knowledge* can be huge and verbose. As it grows over time, the maintenance and upkeep of it becomes increasingly labor intensive and costly. As a result it is necessary to have quick and correlated discovery available to navigate the knowledge bases.

2. *Documented Knowledge* through traditional means is not *interactive* and *adaptable* to different audiences and contexts. Unlike *tribal* knowledge where knowledge workers can decide to provide a detailed explanation or high level overview depending on the appropriate audience and context, documented knowledge needs to be captured at varying levels of abstraction.

3. The knowledge can become outdated quickly, i.e. the knowledge bases if not updated periodically

can lose its accuracy, and hence its efficacy and value. To derive continual value from this source of knowledge, proper controls need to be put in place to effect the timely update of these knowledge resources.

4. Being textual and descriptive, semantics can get distorted. To mitigate this, the documented knowledge bases need to be reviewed and updated periodically by knowledge workers.

But if done right, this is an important source of knowledge and as such an asset to the enterprise. We will further explore how building a foundation of intelligent capabilities within the Knowledge Based Systems will capture the documented knowledge at the source of knowledge, through explicit means i.e. where the users can document aspects of pertinent contextual knowledge and implicit means where the underlying system learns, predicts and creates knowledge content.

2.2 Tribal Knowledge

Tribal knowledge is any undocumented information that is not commonly known by others within a company. It can also be thought of as the collective wisdom of the organization. It is the sum of all the knowledge and capabilities of all the people [10]. In a highly specialized functional domain such as healthcare, detailed nuances of claims adjudication procedures, interpretation of high level organizational policy or adaptation of external regulatory stances or standards can reside in this domain. Typical knowledge workers, with decades of experience in the field and more importantly experience administering the knowledge, within the domain within the same company are a very rich source of such knowledge. The origins of *Tribal Knowledge* in the *People* domain is depicted in 3.

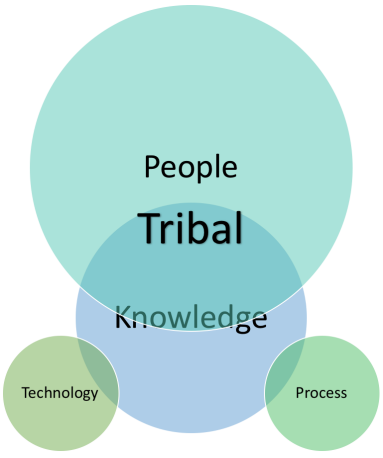

Figure 3: Tribal Knowledge

This form of knowledge has the following consequences.

1. There is a high risk of erosion, as the people holding them leave the organization through attrition or retirement. This presents a strong motivation to build intelligent systemic capabilities that can tap into this rich source of tacit knowledge and be able to capture and leverage where possible, within the organization.

2. Traditional methods for capturing or documenting the knowledge i.e. transforming it into *Documented Knowledge*, in entirety is challenging at the least.

3. Tribal Knowledge can be clouded by subjective influences.

4. Some aspects of tribal knowledge pertains to the expertise or experience of the knowledge workers and their innate ability to leverage different sources of knowledge. This can be very contextual and situational by nature and unless well integrated into the knowledge management platform can become very hard to assimilate and correlate contextually. Hence, there is a very strong need to not only capture knowledge, but to artfully disseminate, correlate and index it for easy and fuzzy discovery.

The industry at large has been undergoing a significant generational workforce transition [11], which puts a heavy burden on the organization to effectively transition the tacit tribal knowledge held by the seasoned "baby boomer" generation, to a younger inexperienced generation. Special attention needs to be paid towards building a foundation of *Artificial Intelligence*, that can aid in the seamless capture from the older generation while effecting a smooth transition with interactive decision support capabilities back to the newer generation joining the workforce. On the other side of the coin, there is a strong need to attract and retain digitally-savvy, millennial and post-millennial generations of workers [13], while training them to be future knowledge workers.

2.3 Knowledge Systemization

We will now examine the concept of *systemization* of knowledge. This is the act of capturing the knowledge into a software system with a view of automating it. This can be achieved with one of two approaches.

1. In this approach, the knowledge is programmed and automated into software applications that capture the essence of the knowledge. We will call this the *Black Box* approach, for the obvious reason that the knowledge is now buried deep within the implementation of a software system, as depicted in 4.

   This approach while being non-transparent to the non-programming business user community, at least does captures the knowledge within the bounds of a software. In theory this knowledge could be mined out (albeit painfully) and documented. However, there are some drawbacks.

(a) The organization might not own the software system, which implements the business logic. In this scenario the organization has limited control on the mining effort at a later stage and has to entirely depend on the owning vendor of the software to mine out their business logic as metadata.

(b) The software system is programmed in a legacy technology, with limited technical resources who understand the technology. This presents the same consequences challenges of erosion as posed by *Tribal Knowledge*, described earlier in 2.2

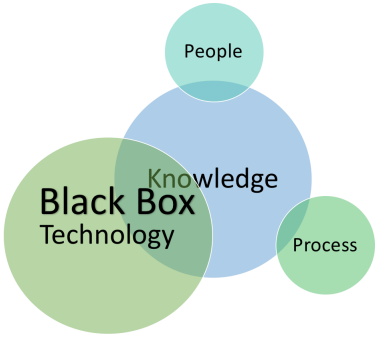

Figure 4: Blackbox Knowledge

2. This approach can be described as the act of formally capturing the knowledge in a *Knowledge Management System*. The most tangible forms of knowledge are *business rules* and *business policies* as these tend to be precise statements describing aspects of the business. Within the healthcare payor space, these are typically captured as operational rules that can be automated. Such knowledge is *externalized* into a Rule Management System a.k.a Decision Management System as operational rules intended for consumption by a software system for automation, but more importantly externalized to be human readable and comprehendible by non-programming savvy users. We will call this the *White Box* approach, as this knowledge is *externalized* and is now transparently available to be understood and manipulated by the organization. The knowledge is externalized and managed under *Knowledge Management*, as shown in 5.

   Externalization of the knowledge, presents the following benefits.

   (a) Externalization as described above, makes the organization more *agile*, as they now have the ability to change the operational business rules without making systemic changes which require a software release cycle. Further these changes can be directly controlled by the end business users, rather than the Information Technology community within the organization.

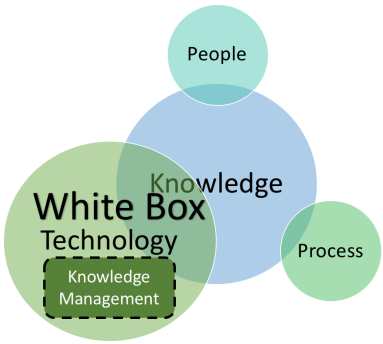

Figure 5: Whitebox Knowledge

3. Externalization of knowledge makes the organization's operation more transparent, but more importantly explainable as opposed to the *Black Box Approach*.

   However, these are some consequences of knowledge externalization that need to be considered.

   (a) The number of externalized operational rules and policies could be large. Further, these rules are combined into large rulesets can present a combinatorially explosive [7], difficult to manage scenario over time. It takes highly experienced rule authors and knowledge workers well versed in the science and the organization's business operations, to effectively manage this, over time. This exposes the organization to the risk of knowledge erosion.

   (b) While the externalized knowledge is more transparent and explainable, to be able to comprehend far reaching cause and effect, the underlying system needs rich traceability capabilities [12], to provide detailed comprehensive explanations to the business users. This provides the deep motivation for *Intelligent Foundations* and providing an intelligent way to manage knowledge and sets up the business case for a *Virtual Knowledge Worker*, that is capable of answering deep *knowledge* questions, something that can aid and support the new younger generation of *digitally savvy* knowledge workers.

2.4 Intelligent Foundations

As discussed in 2.2, transition of the labor force [11], and catering to a diverse workforce with different knowledge assimilation requirements [13], presents a big challenge. This bolsters the case to build sophisticated and *intelligent capabilities* to address these needs. The intelligent capabilities will be elaborated further in 3. In this section, we will introduce the concept of *intelligent foundations*. Building such a foundation can then enable *intelligent capabilities*, that can rapidly train a new generation of young workforce, on the deep knowledge expertise. This is depicted in 6. The idea is as *Tribal Knowledge* erodes in an organization, the

new business users can learn rapidly, thereby restoring the tribal knowledge held by the people who leave the organization.

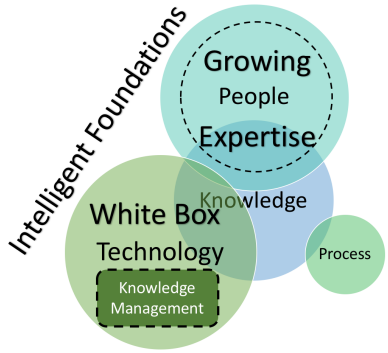

Figure 6: Intelligent Foundations

These *Intelligent Foundations*, can also be articulated as *capability* statements. We define a capability as a simple statement that describes an *ability* or feature of the system. Here are the ten foundational capabilities, at a high level, that enable building more specific intelligent capabilities around knowledge analysis, management and intelligent automation. These will be discussed in more depth in 4, against the backdrop of a case study, within BRIDE [7].

1. *Discovery:* Ability to fuzzily discover diverse artifacts
2. *Tagging:* Ability to *tag* or decorate knowledge artifacts with manual and generated metadata.
3. *Visualization:* Ability to graphically visualize *affinity* between artifacts
4. *Classification:* Ability to classify artifacts based on characteristics
5. *Correlation:* Ability to build correlation between different artifacts
6. *Event Processing:* Ability to generate, process and react to system and user events, within the platform.
7. *Recommending:* Ability to recommend action to take based on correlation between artifacts
8. *Language Processing:* Ability to absorb, disseminate and score keywords from textual content/documentation at detailed inflection points
9. *Generation:* Ability to generate new content
10. *Learning:* Ability to learn from data patterns and from human feedback

2.5 Knowledge Governance

Healthcare as discussed earlier is a highly regulated, knowledge rich domain. There is a strong need to formalize, document and more importantly *govern* the knowledge, which refers to choosing structures and mechanisms that can influence the processes of sharing and creating knowledge [14], surrounding the detailed aspects of administration, business rules, business policy and processing. Within healthcare the business rules around administration are driven by different motivations, varying from regulatory, industry standardization, organization policy to client contractual customizations. Understanding and cataloging the various business rules and associated knowledge artifacts, contributes to better organizational management of the same. This consequently enhances the documented process knowledge surrounding them. By building intelligent capabilities around integrating and automating aspects of *Knowledge Governance* into the Knowledge Management System, aids in better administration of the governance process. Further it centralizes and promotes the use of the externalized knowledge across all three pillars i.e. *People*, *Process and Technology*, in a seamless fashion. This is shown in 7 .

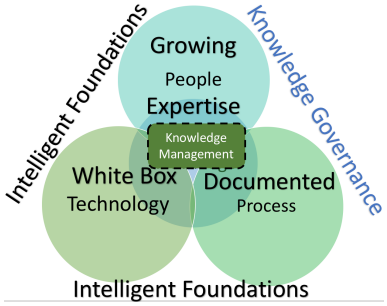

Figure 7: Intelligent Foundations with Governance

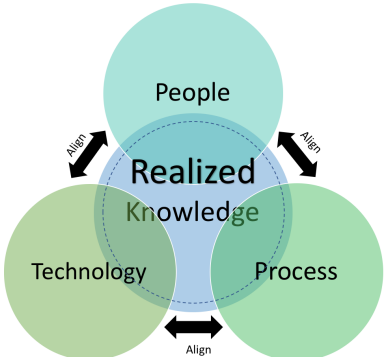

Figure 8: Realized Knowledge

A big goal is to better *align* knowledge sources across the three pillars of knowledge and unify them as a net sum of *Realized Knowledge*, as shown in 8. The introduction of *Intelligent Foundations*, coupled with *Knowledge Governance* strives to achieve that [15].

3 Intelligent Capabilities

In this section we will describe a subset of *Intelligent Capabilities* that are built on top of the set of ten foundational intelligent capabilities i.e. *intelligent foundations*

described in 2.4. These *Intelligent Capabilities* cover the vast gamut of functions needed to effectively manage a complex, vast, functionally diverse and growing footprint of externalized knowledge, as seen in healthcare. A logical viewpoint of this framework is shown in 9.

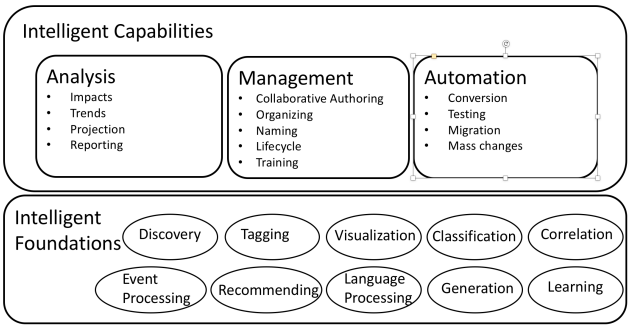

Figure 9: Intelligent Knowledge Management Framework

The capabilities are broken up into these broad categories viz., *Analysis*, *Management* and *Automation*. We will elaborate each of these broad categories of capabilities.

3.1 Analysis

Analysis covers the most important and far reaching capability across the organization. Practically every *business user* would need access to some or all aspects of this capability to perform their job effectively. As mentioned earlier, authoring operational *business rules* is a central part of knowledge externalization. With healthcare, some of the most complex rules are around *clinical terminology*.

To illustrate this further, we will contrast this with a Dental Insurance use case. With dental health insurance, clinical rules are specified using ADA (American Dental Association) mandated CDT (Current Dental Terminology) Procedure Codes. The knowledge workers are making changes to these rules as contractual benefits with customers change, or when the ADA releases a new version of the CDT, each year. Each Dental Procedure has a nomenclature that describes the procedure using key clinical terminology. When a certain aspect of dental clinical science changes, the ADA makes appropriate changes to the CDT to -

1. Introduce new Procedure Codes to reflect new clinical procedural advances
2. Retire obsolete Procedure Codes

In the United States, all healthcare business participants are mandated to be HIPAA (Health Insurance Portability and Accountability Act) compliant. In Dental Insurance, among other things, this means that Dental Providers (Dentists, Dental Offices) and Payors (Dental Insurance companies) are CDT compliant. This translates to the Dental Insurance adjusting thousands of dental clinical rules to reject or adjudicate claims based on the correct/appropriate dental procedure code being submitted.

These are some of the more fine-grained use cases within the *Analysis* capability.

1. *Impact Analysis:* Sometimes there are business rule changes across segments or the whole book of business, to specific areas of treatment, caused by a variety of reasons. These reasons, for example can be one of the following:
   (a) Periodic ADA CDT version changes that are introduced on a yearly basis.
   (b) Changes to a large client's contractual benefits on renewal, on a periodic basis.
   (c) Introduction of a new line of business or product.
   (d) Regulatory mandates.
   (e) Corporate directional changes.

   There is a strong need, for an ability to analyze and make micro-level operational rule changes based on macro-level shifts in function. To be able to do this the system needs the ability to correlate and analyze impacts across varying granulation of knowledge assets.
2. *Trend Analysis:* Trend Analysis can offer up useful insights to the organization and is intrinsic to the collective knowledge it holds. Here are some examples of trend analysis.
   (a) *Reuse Trending:* As mentioned in 2, certain knowledge rich domains, can have combinatorially explosive rules under certain conditions. Therefore there is a need to provide appropriate tools for managing the analysis of trends to minimize the explosion of such rules through intelligent optimization and reuse.
   (b) *Metric Trending:* The collection of accurate metrics leads to better knowledge governance and quality of rules/knowledge that yield better business decisions. For example, within the dental claims adjudication arena, we would like to analyze the most popular rules and be able to see seasonal or long term trends in their usage. Another useful analysis is to study the trending of the auto adjudication metric, which is the percentage of adjudicated claims that do not require any form of manual expert intervention, as this directly ties to the cost of administration.
   (c) *Volatility Trending:* It is important to understand how frequently a knowledge artifact or rule changes. These can lead to deeper questions that would help analyze - are there seasonal influences to the change ? Are these changes reflective of changes to the book of business ? Can we use this as a future predictor of like phenomena?

(d) *Variance Trending:* When looking at a collective body of knowledge artifacts for example, an entire set of rules, there is typically a variant component and an invariant component. This form of trending is again useful as a future predictor to study correlational causal effects with underlying books of business. For example the variance trending for Government Contracts can differ from Contracts, underwritten for small commercial clients, or clients within a certain vertical industry like car manufacturers or the demographic makeup of a certain group of underwritten people within a group.

(e) *Complexity Trending:* Are knowledge artifacts (i.e. rules, rulesets, policy, key terms etc.) within a certain sub-domain of the business growing in complexity ? This form of trend analysis helps identify and proactively address the management of such artifacts.

(f) *Obsolescence Trending:* It is not uncommon to *retire* knowledge artifacts i.e. business rules or policies, over time and this form of trending can be an indicator in correlating the obsolescence of knowledge with evolving the book of business. In a certain sense this is similar to the volatility trending, discussed above, however obsolescence of knowledge can provide certain key insights and indicators around directional change for the organization, especially around obsolete business models or outdated processes, which are valuable.

3. *Projection Analysis:* Projection Analysis is the ability to analyze existing knowledge artifacts, to generate or "project" inductively, through inferred heuristics, gained from historical correlation of associated historical contextual changes to the corresponding changes of knowledge artifacts. This technique of analysis provides an approach for both the system and humans within the knowledge economy to project or generate knowledge artifacts based on the correlated data. This correlated data can further be used to generate features, to develop future state capabilities such as machine learning based on the generation and validation of projections based on correlation between characteristics of knowledge artifacts and high-level characteristics.

4. *Reporting Analysis Results:* With *Intelligent Capabilities*, built on AI foundations of fuzzy discovery, classification and correlation, business users can now be empowered to gather insights with deep drill down capabilities. It is important however to be able to package the results of ad-hoc analysis sessions into interactive reporting that can be exported and shared to a broader audience or community within the organization. It is also important to be able to provide interactive *data visualization* features, packaged into this capability. By combining multiple *Intelligent Foundation* concepts, new users can be onboarded and trained on complex interrelated concepts in a more effective, timely and continual manner.

3.2 Management

Traditionally, management of knowledge assets within an organization requires deeply experienced multifaceted knowledge workers, well versed in the domain terminology and the functional vertical. In addition, the knowledge workers tasked with authoring externalized business rules, need to possess traits that can translate complex functional subject matter into clearly articulated, unambiguous business rules and policies. Lastly, they need to be adept at navigating a complex knowledge management system, replete with a rich interconnected set of business vocabularies and complex features for other life cycle functions of knowledge management. The *Intelligent Capabilities* around management can be broken up into these following broad areas:

1. *Collaborative Knowledge Authoring:* This capability is at the heart of any Knowledge Management System, and to a large extent determines the success and efficacy of such a system. With traditional means i.e. with no *intelligent foundational* capabilities, a big part of the success and efficacy of the external knowledge hinges on the skills of the knowledge workers to deliver the quality. By building this capability on an intelligent foundation, new possibilities abound. For example here are a few plausible use cases, that leverage intelligent management capabilities. With a *collaborative* approach, the system collaborates seamlessly, with the users and facilitates collaboration amongst participating knowledge workers

   (a) *The authoring tool provides a guided wizard like experience for complex rules.* For example, for new business rule authors who are not familiar with the intricacies of the detailed business vocabulary of a complex domain, the act of authoring a complex business rule that achieves a granular operational business decision can be a daunting task. In such scenarios, a high level, questionnaire driven wizard can step the business rule author through the act of authoring.

   (b) *The authoring tool provides impromptu training sequences for guided authoring.*An extension of 1a, described above could show a step by step progression of an authored business rule to the new business rule author. This will help train that business rule author to learn the intricacies of the business domain vocabulary and it's associated key terms. Further, such sessions could be

recorded for future playback as interactive help topics.

(c) *The authoring tool provides help based on correlation with keywords used in key business vocabulary.* This feature is another interactive training feature for the authoring tool to train new users. Further, while this use case is centric to the day to day management of knowledge, it can be used as a key analysis feature, that can help the business rule authors to do integrated impact and correlation analysis as they author business rules, policies and other knowledge artifacts.

(d) *The authoring tool disseminates complex authored rules to catalog and correlate keywords to contextual help topics.* As new knowledge assets i.e. Business Rules, Policies etc., are created inside the Knowledge Management System, new business terms and language could be introduced. A consequence of this is that only small segments of the business community are aware of the semantics and impact of the newly introduced terminology. This bolsters the case for cataloging and correlating this information at the point of entry, into the management system. This could make the system smarter through the continual layering of correlational metadata.

(e) *The authoring tool provides a means for a community of knowledge workers, to collaboratively author related knowledge artifacts, concurrently by providing push notifications of changes and preventing conflicting or inconsistent changes to occur.* This capability leverages the intelligent foundations in 6, (the seminal book [16] provides a sound introduction to the science of events). Using this, the platform is capable of sending push notifications of user edit events, to different users, analyzing sequences of events, to make inferential decisions about dynamically constraining certain situational edit operations for certain knowledge assets, by certain participating knowledge workers.

2. *Knowledge Organization:* To manage the combinatorially explosive growth of knowledge assets, there is a compelling need for a sophisticated organization method that promotes the optimal reuse of knowledge assets. To be able to effectively reuse common knowledge assets like business rules, the first barrier to overcome is the ability to discover (rather fuzzily) that such a business rule or a *similar* business rule does exist. In the absence of this, a lot of duplicate or near duplicate knowledge assets are created. Organization of knowledge is key to enabling knowledge recall, management, mining and last but not the least Governance. We will now consider the organization of knowledge from the following vantage points.

(a) *Structure and Granulation:* Here we need to consider how the knowledge is structured and abstracted. Typically the knowledge artifacts can be structured in a hierarchical fashion, from most granular to least granular (i.e. high-level to low-level). Further each level of granulation can have several viewpoints. For example in dental insurance, the highest level of knowledge can be emblematically represented in a client/customer contract, which in turn, can be represented as a ensemble of *business policy* statements, which are high level statements of business purpose, that are driven through a combination of regulatory, contractual and administrative concerns.

These business policies are implemented through sets of operational *business rule* statements, that enforce the intent of the policy, within the Claims Administration platform. The breakdown of artifacts from a high-level perspective to a low-level perspective has to be well thought through and it is desirable to follow some form of a structured dissemination, based on some pre-established categorization. For example, the clinical adjudication policies are administered through a set of well established *treatment categories* within BRIDE [7]. This helps in managing combinatorial explosion of rule artifacts through a controlled reuse of pre-existing configurations of sets of rules. In the absence of such a categorized structure, there would be significant redundancy and duplication in structure as each hierarchical structure would end up duplicating, sub-structural elements of it's hierarchy. However, in spite of this form of structured organization duplication and redundancy can be introduced due to the lack of *discovery*, as discussed in 2.4.

Lastly, to achieve these hierarchical structures of granulated knowledge artifacts with reuse, the underlying domain structures share a many to many correlation amongst each other, which are elaborated in more length in [7].

(b) *Ownership* This is an important aspect of *Knowledge Governance*, that can influence the level of reusability discussed in 2a. With a growing consciousness and need for privacy, customers and clients are increasingly unwilling to share common data. Within, the consolidating healthcare payor space, this presents some interesting consequences.

Within the dental insurance space, the collective knowledge i.e. policies and rules

gained to preempt Fraud, Waste and Abuse, can be a shared asset, as these knowledge assets are gained through collective experiences. But to effectively leverage the shared operational knowledge, the historical claims *data*, across customer boundaries are needed to effectively adjudicate them. But privacy considerations and constraints can explicitly govern and prevent us from leveraging cross-customer data and knowledge, across boundaries, thereby limiting the potential to act on opportunities, that can minimize claims utilization.

Another consequence of ownership is that there are strict rules, that can be driven by a contractual agreements that dictate, who *owns* the knowledge and who has the rights to view, use or change them, under specific conditions. This poses interesting challenges to sharing and pooling of knowledge assets

(c) *Correlation and Connectivity* To effectively organize knowledge, we need the ability to *correlate* and *connect*, pieces of knowledge assets. This introduces the important notion of *traceability* [12], which provides the users the ability to perform key activities such as root cause analysis, answer audit questions and explain processing and/or adjudication reasoning to customers and other stakeholders. Correlation can be achieved through the following three means or mechanisms.

i. *Structural* This is the strongest and most basic form of correlation and connectivity that can be built to correlate different knowledge assets, explicitly correlated through well defined data and object models relationships. Within the BRIDE eco-system [7], different knowledge assets such as Rule Stores, Rule Packages, Rule Packets, Rules etc. are correlated in this fashion, which lends to easy organization.

ii. *Manual or Explicit* This form of correlation is weaker, but equally important. This allows the business users to explicitly tag or store metadata about various knowledge assets. These can be used to connect and organize knowledge assets based on the explicitly defined metadata.

iii. *Derivative or Implicit* This form of correlation builds on the above two forms of correlation. Here, we leverage smart algorithms to derive, infer, classify, tag, index, store, visualize and report additional correlations.

3. *Knowledge Artifact Naming:* As mentioned earlier, the detailed or granular knowledge assets i.e. operational business rules and policies can grow combinatorially. The business users usually would like to introduce some mnemonic naming conventions to better organize and catalog the knowledge base. Hence, introducing capabilities to automate naming of newly introduced knowledge assets that adhere to user introduced naming conventions make sense. Further smart automated algorithms that manage the naming and cataloging of the knowledge assets especially when knowledge assets split, morph or converge, make the continued governance of such assets, over time, error and conflict free. Here are some of the explicit advantages or automation opportunities that can be realized by automated enforced mnemonic naming conventions.

(a) Infer stereotypical characteristics of knowledge assets based on the mnemonic name

(b) Projection and generation of *new* knowledge content based on mnemonic name of close affinity.

(c) Proactive discovery of semantically like knowledge assets based on mnemonic name similarities

4. *Knowledge Lifecycle Management:* From a systemic standpoint knowledge assets need to honor constraints placed by systems. In addition, knowledge externalization and development processes need to synthesize knowledge asset development and lifecycle with systemic software development, especially for emergent areas of knowledge externalization and management. In doing so, at a very high level, knowledge assets goes through the following main lifecycle phases:

(a) *Creation:* This is where the knowledge asset is generated.

(b) *Change:* This is when the semantics or content of the asset morphs.

(c) *Culmination:* This is where the knowledge asset loses relevance and is retired or terminated.

Within an environment, certain knowledge assets, such as business rules and rulesets have their own miniature lifecycle, before they are utilized by the automated system. For example BRIDE [7], has the following lifecycle

(a) *Author:* The business rule is authored or edited within the BRIDE Guided Editor.

(b) *Translate:* The authored business rule is translated to a format that can be interpreted by an *Rule Engine* [8]. This action is implicit for the standard use cases within BRIDE i.e. the Business User does not need to explicitly translate the rule, but it is tied into the Authoring phase of the lifecycle.

(c) *Deploy to Sandbox* The overarching *Rule Package*, that contains the *Rule Packet*, that contains the *Rule*, is deployed to a safe sandbox, where the business users can test the rules.

(d) *Deploy to System* The overarching *Rule Package* is deployed to the System, where the operational business processes can consume the decisions, made by these rules.

It is a common practice for knowledge based systems in organizations to have different environments. Broadly the environments can be categorized into:

(a) *Production:* This is where the knowledge is applied to day to day operational business processes. New business rules and policies for established areas i.e. business decisioning services can still be developed here by the business users without any software or systemic development impacts. The BRIDE system supports this type of configuration, wherein the Business Rule authors enjoy such autonomy, wherein they can fully develop, test and deploy new operational knowledge assets *Rule Packages* [7], to the running production Claim Administration Platform.

(b) *Non-Production:* This is where the organization develops, tests and validates the effects of newly introduced knowledge on the overall system. For emergent areas of knowledge externalization, the process entails the development of a standardized set of *Business Vocabulary* [6], that are mapped to an underlying implementation model, that integrates well with the other systemic components. Non-production environments can vary in number and purpose depending upon the organization's software and automation capability development processes. For example, here is a list of plausible non-production environments:

i. *Production Dry-run and Training Environment:* Intended for the Business Users to run live simulations, where they can do large scale application of knowledge without impacting live production business processes.

ii. *User Acceptance Testing Environment:* Intended for Business Users to run full scale end to end software release testing regiments, applying emergent areas of knowledge externalization and applying existing large knowledge bases with large scale impact changes.

iii. *Integration Testing Environment* Intended for component level integration testing of new and existing knowledge bases with systemic components.

iv. *Development Environment* Intended for the development of business vocabulary and unit testing it's effects in a limited sense.

Finally, as knowledge assets take birth in different environments i.e. *Production* or *Non-Production*, there is a strong need to be able to migrate these assets from one environment to another in a safe and secure manner, without loss of integrity and fidelity. The BRIDE system [7], supports these capabilities in full, which enable the business knowledge workers to autonomously migrate and administer these knowledge assets.

5. *Knowledge Training:* It is crucial to have succession planning amongst knowledge workers, to avoid large scale dissipation of knowledge. With this capability the Knowledge Management System, uses intelligent foundations 1, 2, 4, 5, 8 and 10 described in 2.4 to absorb knowledge topics about the use and context of knowledge assets, to fuzzily discover, classify, correlate, disseminate and analyze language, learn and recommend actions to the knowledge worker in a proactive fashion.

3.3 Automation

As the externalized knowledge bases, grow, evolve and diversify within the organization, there is a strong need to *automate*, aspects of analysis, management and lifecycle management. We will now explore the intelligent capabilities needed to support this.

There are several tasks in the lifecycle that the knowledge workers have to do to externalize and create knowledge assets and related collateral. The biggest task is the process of authoring business rules and policies. Business Rules in particular are more challenging, for the following reasons:

1. The business logic captured by a single business rule could be complex and if not authored properly will not enforce the policies accurately or worse, introduce errors in claims processing and adjudication. Another consequence is they could introduce unforeseen loopholes that can be exploited by Fraud, Waste and Abuse scenarios.

2. There could be a high number of business rules due to combinatorially explosive sets of conditions. The knowledge workers have to expend significant analysis effort to analyze if there are gaps or conflicts in the logic and implementation. As a consequence, there could be a lot of duplicate, equivalent or subsumed business rules that get created over time, by knowledge workers, as there were no sophisticated discovery mechanisms present to discover them.

3. The business rules need to be carefully assembled into sets of rules, to form executable rulesets.

Many of the rules in a ruleset can have overlapping conditions and prioritization of rules within a ruleset matter. Between business rules in a ruleset there could be partial or complete overlaps of logic called subsumption. The knowledge workers need to make sure that these are minimized and restricted, only allowing some legitimate partial overlaps.An error in configuration of these rulesets causes errors in processing. The BRIDE system [7], provides a sophisticated system of configurations such as *Rule Packages* and *Rule Packets*. The Rule Packages are deployed as executable rulesets, that can be executed by a Rule Engine [8].

Here are some of the more fine-grained use cases within the *Automation* capability.

1. *Automating Conversion:* Consolidation and Digital Transformation are driving organizations to consolidate and transform their business operations. Within the healthcare payor space, healthcare insurance companies are seeking to move their operations to either:

   (a) Homegrown healthcare administration platforms of healthcare insurance companies.

   (b) Commercially available healthcare administration platforms.

   The process of mining, converting and automating the knowledge i.e. Business Rules and Policies, of an insurance company on to a new benefits administration platform, is a risky, time-consuming and expensive process. There is a high risk of failure for the business and if not implemented accurately, there are hidden and ongoing costs introduced due to sub-optimal claims utilization, which can run the company out of business. Traditional methods for mining the knowledge from legacy systems [9] are manual, subjective and error-prone. The conversion process is dependent on multiple documented knowledge sources and is heavily reliant on knowledge workers who have had prior experience with the systemized knowledge, within the legacy platform. The challenges posed by traditional manual methods are:

   (a) It is dependent on knowledge workers intimately familiar with knowledge sources in the legacy platform.

   (b) It is ad-hoc and situational to the conversion project or customer.

   (c) It is time-consuming, typically a couple of years or more.

   (d) It is labor intensive, i.e. needs focused effort from a dedicated team of skilled knowledge workers.

   (e) It is not scalable to handle conversions of large magnitude or multiple parallel conversion efforts.

Partially automated approaches to *mining* information from legacy platforms entail, writing customized conversion programs/scripts that perform extraction and transformation of the knowledge to a mapping schema or file. The knowledge workers can then, manually analyze the data in the mapping data source and manually author the knowledge assets, into the target platform. Unfortunately, this again poses the same challenges except for challenge 1a, which is automated through the conversion program.

This is where more comprehensive and intelligent automation capabilities help solve the problem. As a case-study, using intelligent automation capabilities, the conversion effort was dramatically reduced from two or more years to under six months. The case study leveraged building automation capabilities that relied on an ensemble of *intelligent foundations* viz., 1, 2, 3, 8, 5 and 9, from 2.4.

Figure 10, depicts the steps to automate the mining and conversion of knowledge.

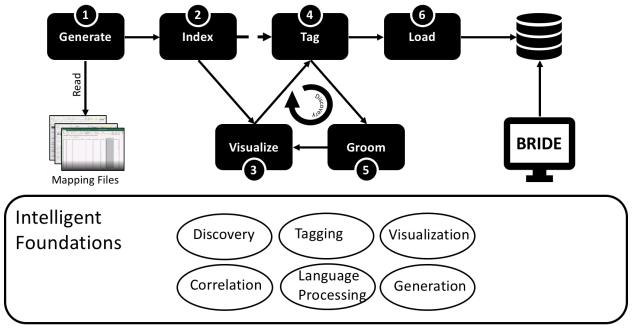

Figure 10: Automated Conversion Process

The conversion automation process is described through a sequence of six steps described below:

(a) *Generate:* This is the first step, that analyzes the conversion data in the Mapping File and generates business rules, organizing them into rulesets, which for BRIDE [7] entail, organizing them into *Rule Packages* made up of reusable *Rule Packets*, containing the *generated* business rules. The generation algorithm follows the structural organizational rules mandated by BRIDE to stereotype the packets and rules with the appropriate *Treatment Category*. The generated artifacts are assigned a generated systemic naming convention in this step. The complex normalized data in the mapping files are put through a sequence of file transformations.

(b) *Index:* The intermediate data that is generated by the above step is then loaded in an ElasticSearch database, which is a search engine based on the Lucene library, to enable

them for easy and fuzzy discovery. This enables the intelligent foundation of *Discovery*, for the steps detailed below.

(c) *Visualize:* Once loaded, custom data drilldown visualization programs aid the knowledge workers to analyze and proof the generated knowledge assets. In this step we use intelligent foundations of Visualization, Discovery and Correlation..

(d) *Tag:* In this step, specialized algorithms analyze the generated business rules and elicit important parametric data to tag the knowledge asset. The two fundamental intelligent foundations used here are Tagging and Language Processing.

(e) *Groom:* This is the phase of feedback for the algorithm to learn from knowledge workers, more specialized scenarios, to enable more accurate auto generation of knowledge assets. In addition, this is a process that is well integrated into the overall conversion capability to allow the knowledge workers to work collaboratively with the automated conversion process.

(f) *Load:* This is the phase, where the generated rules are loaded into the BRIDE knowledge platform, into the *authored representation* [8]. Techniques such as rule parametrization (i.e. the variant information from rules are externalized as rule parameters) and mnemonic rule template selection are used to select the appropriate rule template and the parameters are substituted using macro substitution. Alternatively, more sophisticated intelligent builder approaches can be employed, wherein the authored representation for the rule can be generated based on structure of the generated rule, which can be gleaned by a command pattern generated during the *Generate* phase. Finally, the knowledge workers can resume normal knowledge management activity with the generated rules within BRIDE.

Figure 11, depicts the anatomy of an index for a Rule. This is created during the *Index* process, from the outputs generated from the *Generate* step. In addition to the generated rule, the additional metadata generated during the *Tag* phase sets the stage for the subsequent grooming and accurate and automated loading into BRIDE knowledge base.

Figure 12 depicts the anatomy of an index for a Rule Packet. The basic structural data for the Rule Packet is created during the the *Generate* phase. The intelligent conversion algorithm blends in manually authored rules by knowledge workers with the generated rules, to construct a fully functional subset of rules that constitute a Rule Packet for a given Treatment Category. Further during the *Tag* phase, there is an abstraction phase of the algorithm that filters only relevant or important tags from rules that are emblematic of characterization for the Rule Packet. Lastly, the algorithm generates a descriptive name for the Rule Packet that facilitates easy discovery for knowledge workers for higher level activities such as contract implementations.

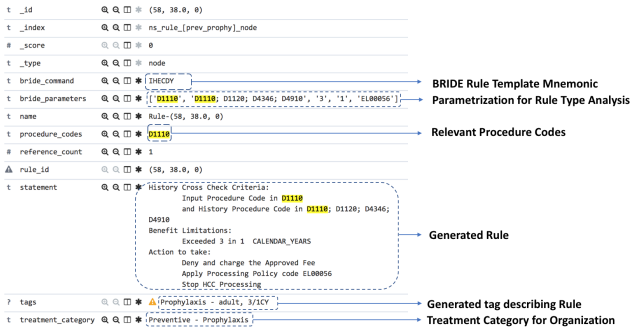

Figure 11: Anatomy of a Rule Index

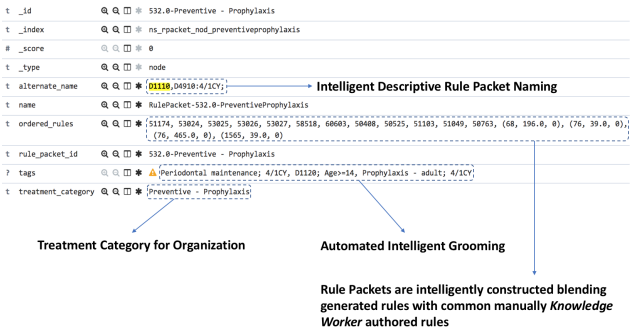

Figure 12: Anatomy of a Rule Packet Index

2. *Automating Testing* With rapid growth of knowledge assets within the platform, especially in the form of operational business rules, there is a compelling necessity for having an intelligent automation technique that can analyze rules within a ruleset and generate appropriate test scenarios. For example within the BRIDE [7] framework, there are over 17,000 test cases in just one area of adjudication rules. These are test cases that have been created by knowledge workers during their testing phase of knowledge management. A significant chunk of these test cases were generated from live claim processing data scenarios. However, with a strong and steady growth of operational business rules, more sophisticated techniques are needed to conquer the scale problem. Here are some use cases that explain this capability further:

(a) An automated test scenario creation algorithm intelligently interprets semantic tags about the rule parameters collectively con-

tained within a ruleset to generate test data and scenarios.

(b) As new rules are authored and included into a ruleset, an algorithm amends or augments test scenarios to test out new semantic consequences of the change.

(c) As knowledge workers decide to edit rules, an algorithm that can analyze the impacts from a test scenario perspective interactively communicates consequences of the change to the knowledge worker. This is a capability that can grow in the degree of sophistication.

3. *Automating Migration:* As we discussed in 4, it is typical for knowledge workers to manage knowledge assets across multiple *production* and *non-production* environments. Within BRIDE, select knowledge workers can elevate their role to an administrator, to perform critical administrative functions of knowledge asset management. *Migration* of knowledge assets across environments is one such function, that needs to be done with care.

   Here are a few challenges with administering this function, where the administrator is performing these tasks manually.

   (a) The number of physical environments can grow within an organization, over time. With consolidation the number of knowledge tenants in a multi-tenant environment, further impact the number of environments to manage.

   (b) The number of knowledge assets to migrate across environments grow. This puts an increased burden on the knowledge administrator to keep knowledge assets consistent across environments.

   (c) Not all environments, especially not all tenants may share the same assets i.e. business rules, policies, business vocabulary, test scenarios etc.. This introduces increased complexity for the migration path of these assets.

   (d) Maintenance in target environments can impede or impact the migration of knowledge artifacts. This problem is very similar to supply chain inventory and inventory movement, within Supply Chain Management.

   (e) Associated management functions such as deployment need to occur in target environments, post migration. This puts an extra burden on the administrator to ensure that these activities occur in a timely fashion.

   Strong intelligent foundations can help with the automation of pieces of this important function. Here are a few of the scenarios, that can help intelligently automate this function and reduce the dependency and burden on the knowledge worker.

   (a) Tag and inventory knowledge assets with migration specific metadata that is human and more importantly system consumable. This can enable intelligent algorithms to proactively audit, report and govern knowledge assets, migrating to target environments. Here intelligent foundation 2 is primarily leveraged.

   (b) Restrict the migration of knowledge artifacts to target environments that are undergoing maintenance or is being reserved for some focused activity. This prevents undesirable collisions and interference with activities in the target environment. Here the intelligent foundation 6 is leveraged.

   (c) Automatically include related artifacts impacted by the inclusion of a knowledge asset within a migration manifest. Knowledge Assets are intricately related, sometimes explicitly and structurally, but other times through correlation as explained in 2a. Hence movement of such knowledge assets should do the necessary impact analysis to ensure consistency and integrity of the knowledge assets. Here intelligent foundation 5 is primarily used. In addition, intelligent foundation 7 can be leveraged when the inclusion needs to be reported or recommended to the knowledge worker performing the administrative role.

   (d) The *Automated Migration Assistant* participates as a *virtual knowledge worker* in the target environment, as described in 1e. Here the intelligent foundation 6 is leveraged.

4. *Automating Mass Changes:* Sometimes it is necessary to make large scale or *mass* changes to knowledge assets. For instance, a large number of business rules need to be changed because a key business policy changed or the semantics of a key business term changed.

   Through traditional methods, this would mean knowledge workers need to track down every single relevant knowledge asset that are impacted by the change and modify them to reflect the macro-change. A classic example of this are new yearly versions of the *Common Dental Terminology*, released by the *American Dental Association*.

   Here by leveraging all the 10 intelligent foundations, intelligent capabilities that automate making mass changes can significantly reduce human labor, erroneous edits and significantly reduce cost.

4 BRIDE Case Study

4.1 Background

Delta Dental of Michigan, Indiana and Ohio is the leading provider of dental benefits within the midwestern part of United States. The company has been in business for over 60 years and has witnessed a dramatic growth within the last decade. The reason for this dramatic growth is a highly automated and sophisticated benefits administration software platform, powered by BRIDE [7], a powerful homegrown, elegant Enterprise Decision Management System. BRIDE houses the company's growing pool of complex, externalized operational business rules which allows the company to automate the vast majority of it's claims adjudication process allowing it to scale it's business footprint to unprecedented levels, while keeping operation costs at an optimal level. The current metric for measuring this automation level is called *"Drop to pay"* or *"Auto Adjudication Rate"*, which is currently hovering at around 96%, which is an industry leading score.

To keep up with the fast growth, it was necessary for the BRIDE platform, at inception to introduce industry leading capabilities for surfacing full life cycle rule management functions, such as authoring, testing, deployment, migration, such that non-technical knowledge workers and subject matter experts could entirely manage these with little to no involvement form the IT Department. Over the last decade the BRIDE platform has kept up with innovation, by expanding the capabilities and staying a step ahead of the business needs.

The BRIDE ecosystem organizes its knowledge artifacts in a structured, highly reusable and componentized fashion. A logical view of the domain model for BRIDE at a high level is depicted in refbrideDomainModelFig.

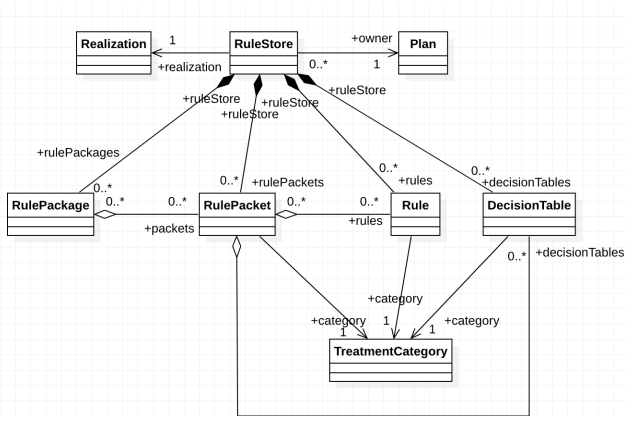

Figure 13: Highlevel BRIDE Domain Model

The core BRIDE constructs [7] are:

1. *Plan:* Represents a Dental Insurance Owner, that owns the rule artifacts.

2. *Rule Store:* A repository for storing rule artifacts, each rule store holds the reusable rule artifacts that can be reused within it, in a structured and constrained manner.

3. *Realization:* Represents an area of business functionality that require specialized terminology to externalize and articulate operational business rules using a structured vocabulary. There are over 30 areas of business functionality for the dental insurance domain so far, ranging from several detailed aspects of claims administration to billing, rating and actuarial applications. This is a growing body of knowledge as opportunities for automation and externalization are identified.

4. *Rule Package:* Represents an *executable* set of rules, that can be executed in a forward chaining, fact inferential rules engine [8]

5. *Treatment Category:* A mechanism to categorize finely granular rule artifacts. Within the clinical domains, the treatment category construct allows the business to categorize specialized clinical rules to literal clinical treatment categories as recommended by clinical standard bodies such as American Dental Association. For non-clinical domains, the treatment category construct is repurposed to category sub functional constituent components of processing.

6. *Rule Packet:* Represents a subset of rules for a given treatment category. Each Rule Packet is stereotyped for a treatment category and should only contain Rules of that same treatment category.

7. *Rule:* Represents a reusable authored production rule (i.e. a rule containing conditions followed by actions) authored in a "Domain Specific Language" using an english-like vocabulary. It is also the most

The next wave of innovation within the BRIDE platform introduces the application of *Artificial Intelligence* techniques to effectively address a new, growing breed of current and anticipated challenges. The work done on developing some of these capabilities has gone towards shaping and developing the concepts discussed in this paper.

The approach to building this new wave of innovation, has been to implement a strong foundational architecture i.e. *"Intelligent Foundations"*. We will discuss these foundational capabilities, their motivation, the architectural choices and application, subsequent sections.

4.2 Discovery

"Ability to fuzzily discover diverse artifacts" As the number of rule artifacts have grown over time, in spite of the ability to reuse rules a lot of unneeded redundancy and duplication have proliferated causing the knowledge base of operational rules and rulesets to

bloat. A major reason for this has been attributed to *discoverability*.

Within the original architecture, the BRIDE system provided SQL based searches against a relational database backdrop of the BRIDE schema. With this, the knowledge workers could search for specific rules with key terms and vocabularies and see their association with rule packets and rule packages. This was a bottom up search. They could also search for Rule Packages with specific Rule Packets in their configuration. With this they could search for full or partial rule package configurations, generate a report and then drill down. In spite of these rich search capabilities, discovery was not sufficient to prevent the proliferation of redundant rule assets overtime. Here are the main reasons why this alone is not sufficient:

1. *Layered Reuse Complexity:* BRIDE uses a layered reuse paradigm for constructing Rule Packages that eventually translate to executable rulesets. While this approach in and off itself is a sound from a component reuse vantage point, the major complexity is the inability of the traditional search functions to get a comprehensive and 360°view of the Rule Package.

2. *Naming Complexity:* With the componentized approach promoted by BRIDE, the knowledge workers set about building reusable Rule Packets, which in essence were combinations of rules, within treatment categories. In the interest of providing meaningful names that described Rule Packets, the knowledge workers resorted to lengthy descriptive names that sought to summarize the semantics of emblematic rules contained within the Rule Packet. However, this approach is highly manual, lacks predictable standardization and is not sufficient to describe huge and complex Rule Packets.

3. *Variational Complexity:* The characteristics of specific clinical domains require blending of specific clinical terminology that by the very nature can lead to a combinatorial explosion of sorts. With the nuances and subtleties in books of business and the semantic authoring flavors introduced by different knowledge workers there were subtle variations of sequences of rules, individual rules that were introduced over time. Some of these were made deliberately to support the variational needs of the requirements. Yet, others were made unknowingly introducing inconsistencies in approach. These were challenging to discover.

ElasticSearch, is a search engine built on the Lucene library. Nowadays, it is a common trend with modern IT architectures to leverage this tool to enable and enhance fuzzy discoverability. Data can be loaded or *indexed* into ElasticSearch as JSON (JavaScript Object Notation) documents. Subsequently this data can be discovered through a textual search of terms or fields contained in the JSON documents loaded and the tool will return all documents that match or nearly match textual patterns searched.

With complex natural language rules, this enables easy discoverability of these assets in a fuzzy fashion, that traditional relational queries do not allow. But this alone is not sufficient as the knowledge workers not only need to discover individual rules based on key business terms and vocabularies, but they also need to be able to discover the connections between rule artifacts, their levels of similarity and the characteristics of their similarities. With that there are five intelligent foundations that need to be applied in conjunction to fully realize the benefits of *discovery*. How these intelligent foundations collaborate is shown in 14. To understand these relationships:

1. *Language Processing* is used to disseminate the textual data in policies and rules, filtering key business terms and builds important metadata for *Correlation*.

2. *Classification* runs advanced algorithms, leveraging data created by *Correlation* to build more detailed correlation data.

3. *Tagging* is the default mechanism for storing metadata generated during *Correlation* and *Classification*

4. *Classification* and *Correlation* builds the foundation for *Discovery*.

5. *Visualization* helps makes sense out of *Discovery*, especially when there is a large amount of interdependent, connected data.

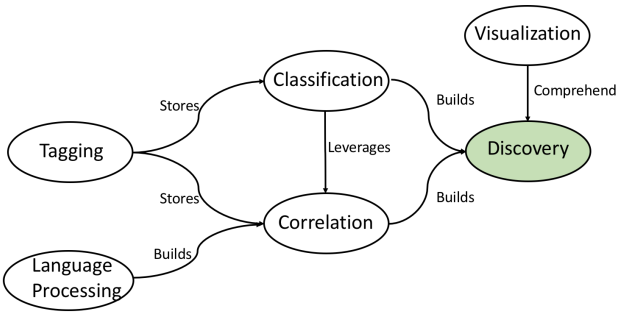

Figure 14: Collaborative Foundations for Discovery

4.3 Tagging

"Ability to tag or decorate knowledge artifacts with manual and generated metadata."

The basic implementational notion of a tag is to assign a key and description tuple to an artifact of interest. However sometimes, there can be more than one tag to decorate the artifact with. Therefore, it makes sense to introduce these key concepts:

1. *Tag Aggregation (Tagregation):* A Tag Aggregation is a composite structure of sub aggregations and Tags.

2. *Tag:* A Tag is simple key and description.

3. *Taggable Artifact (ITagArtifact)* A Taggable Artifact is any entity that needs tagging metadata.

The logical domain models for the basic tag constructs and taggable artifact constructs are shown in 15 and 16. The actual implementation of tags with the artifacts is more relevant when indexed into ElasticSearch for discoverability. A JSON representation of a Rule with a sample of extracted tags, used for discovery, is shown in 17. In this example, the tags for dental procedure codes used in the rule are, extracted to the tag "procedureCodes". Similarly, other useful correlational metadata could be extracted.

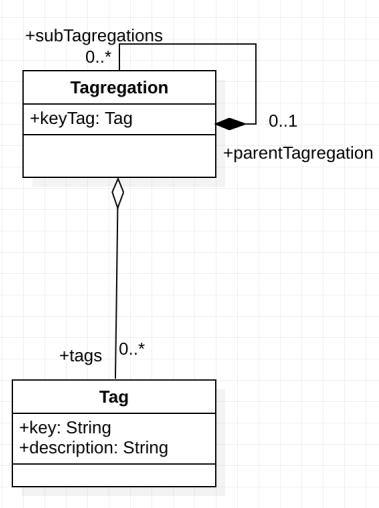

Figure 15: Tagging Domain

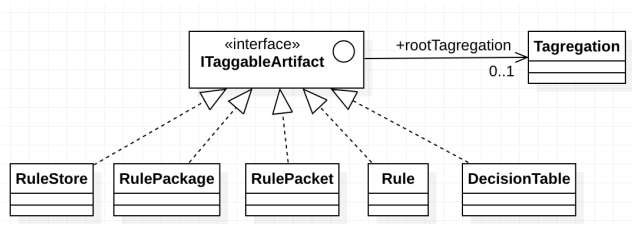

Figure 16: Taggable Artifact Domain

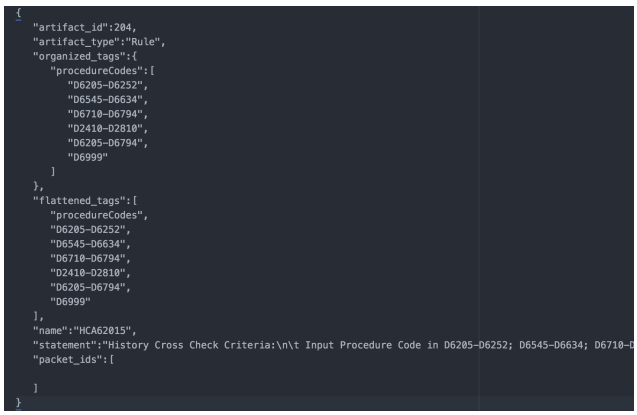

Figure 17: JSON of a Tagged Artifact

4.4 Visualization

"Ability to graphically visualize affinity between artifacts"

To enhance the discoverability of the knowledge assets data visualization is an effective method of analysis. Here a few different visualization techniques have been leveraged, with the correlation and classification data collected through tagging. Knowledge assets as a graph visualization with color coded edges to depict the different types of classifications, is depicted in 18. This is an effective way to discover common trends and patterns. The original workshop paper [1], outlined six different affinity classification measures, which are shown in this visual with different colors. This kind of visual is very useful for identifying common clusters of affinitive rules within an area and the nature of their affinity. There has been significant research and work on the efficacy of applying topological data analysis techniques, to use cases within healthcare [17]

Figure 18: Color Coded Clustered Affinity Visualization

An edge configuration for the same visual is shown in 19. This shows the nodes on the circumference and different colored edges criss-cross connecting the different nodes which represent the rule artifacts. The advantage of this visual is that useful, metadata can be shown on the edges, on hover that aid immensely during knowledge analysis.

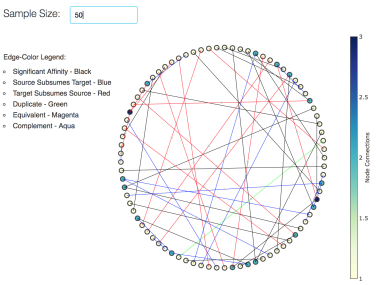

Figure 19: Color Coded Edge Affinity Visualization

A common themed rule asset, is picked out from a crowd of assets, in 20. This form of visualization is useful in identifying an emblematic asset for a certain area.

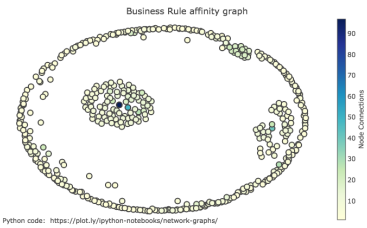

Figure 20: Clustering to identify baseline rule

A term cloud visualization is shown in 21. This is a very useful visualization for performing impact analysis based on key term correlation. In conjunction with correlation of key terms across rule and knowledge assets, it is possible to do end to end impact analysis.

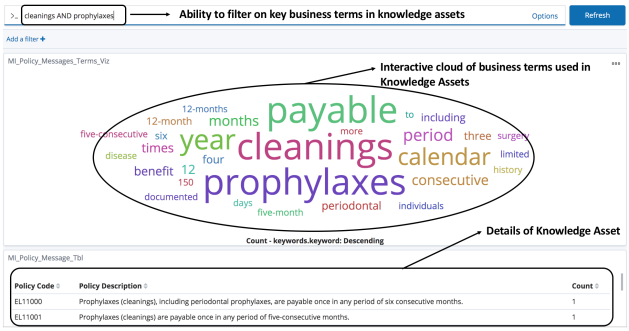

Figure 21: Interactive Term Cloud Visualization

A few observations when building data visualizations are:

1. It is useful to provide a way to filter based on category. This helps with narrowing sample sets and separation of concerns.

2. It is useful to provide a way to configure the size of a sample set. With certain types of analysis the knowledge workers are seeking understand common trends, to make informed decisions about management and governance.

3. It is useful to provide a mechanism for searching or filtering for combinations of terms. This aids in narrowing down the analysis. The visualization in 21, provides this mechanism.

4. It is useful to provide a detailed drill down capability on visualizations where possible. This allows the knowledge worker to identify the concrete knowledge assets with a single visual.

4.5 Classification

"Ability to classify artifacts based on characteristics"

Several sophisticated algorithms were developed to study the affinities between business rules and to classify them. Techniques to classify rule and knowledge assets ranged from naive simple bag-of-words to more sophisticated variations that combined bag-of-words with correlation to relevant master data assets. In the original workshop paper six different classifications were developed, comparing business rules, which were:

1. *Duplicate:* When two rules were exact duplicates with different names. These were top candidates for elimination and consolidation.

2. *Equivalent:* When two rules were semantically the same but had conditions that were in a different order. The classification algorithm here was shallow and only checked for conditions or actions in a different order. Deeper semantic analysis of rules will be able to identify equivalent rules beyond these narrow confines, creating the opportunity for better cleanup of these redundant rules.

3. *Complement:* These were specific to this area of rules where clinical procedures were complemented across the input and history procedures, to provide a complete adjudication coverage. Often times, claims are submitted out of order and these kind of rules analyze logical completeness. The scope for these can be expanded to cover other clinical criteria such as teeth, tooth surfaces etc. in the future. Further this pattern can be applied to other functional verticals to analyze logical completeness.

4. *Subsumption:* Here there were captured as two classifications i.e. Source subsumes Target and Target subsumes Source. Here again deeper semantic analysis can analyze more subtle aspects of subsumption, like analyzing inclusive procedure patterns etc. In the absence of these deeper analysis capabilities, come subsumptions could miss this classification.

5. *Significant Affinity:* Here the algorithm used a threshold of score similarity to identify rules that were closely affinitive with each other. However this was pretty effective and did capture rules that were significantly affinitive with each other.

4.6 Correlation

"Ability to build correlation between different artifacts"

This has been a centric intelligent foundation, for connecting different concepts together, to perform associative analysis and impact analysis. The implementation of correlation relied on algorithms, that analyzed, indexed and decorated knowledge assets with metadata in the form of tags and/or first class correlative attributes, in specific cases. Within the BRIDE case study we implemented correlation for three forms of correlation and connectivity as explained in 2c. Here are a few architectural aspects to consider, while integrating this intelligent foundation within the Knowledge based system.

1. Correlative algorithms need to run close to point of knowledge. There is an inherent risk of running correlation algorithms in a batch fashion

as morphing data conditions could either miss certain temporal correlation or miss transient changes that can be critical information to capture.

2. The initial correlations should be captured at well designed intermediate sink points and should be verbose enough to not miss seemingly inconsequential details, that might add value at a later point. Intermediate logging could be an option for such an architectural implementation. Generating and storing changes as events is another option.

3. The correlation algorithms should be designed in an idempotent fashion where possible, especially with the dimension of temporality. There are use cases that might require the regeneration and storage of correlation, especially during software upgrades and patching.

4. Even though, for the most part correlation of knowledge assets do not include PHI (Personal Health Information) or PII (Personal Identification Information), there are some corner cases where indirect correlation of operational data that have such concerns might crop up. One example of this is the reverse engineering capability of BRIDE for test cases from live data. In such cases de-identification and regular purge of such correlation need to occur to address security concerns.

4.7 Event Processing

"Ability to generate, process and react to system and user events, within the platform"

This intelligent foundation forms the basis of a very important infrastructural capability. As stated earlier, it can be leveraged for Collaborative Authoring. But it can also be leveraged for Correlation and Connectivity. Within the BRIDE case study, this is currently on the roadmap but has not yet been implemented. However, a lot of work is projected on the roadmap to innovate this intelligent foundation, especially for capturing fine grained operational execution metrics to aid correlation, for machine learning and machine training purposes.

4.8 Recommending

"Ability to recommend action to take based on correlation between artifacts"

Within the BRIDE case study this was implemented as an explorative proof of concept, wherein the system could recommend close rules based on the current authored content. While this could be foreseen as a useful feature in and off itself, this is barely scratching the surface. The BRIDE case study, hopes to leverage this intelligent foundation for deeper more sophisticated scenarios, which can be the subject of another paper.

4.9 Language Processing

" Ability to absorb, disseminate and score keywords fro textual content/documentation at detailed inflection points"

Within the BRIDE Case Study, this intelligent foundation has been used to disseminate policy descriptions, and procedure code descriptions, to correlate business rules and other artifacts such as Rule Packages, Rule Packets, Rules, Benefit Plans etc, with key term correlation. The Language Processing capabilities with Python and NLTK give a good starting point to filter out key business terminology, which can then be used to correlate. Again there is not more to report here from a case study perspective as we are in very early stages of fully realizing and leveraging this intelligent foundation.

4.10 Generation

"Ability to generate new content" Within the BRIDE Case Study, this intelligent foundation was used to automate conversion as discussed in 1. However, this is just one use case or application of this intelligent foundation. However, there are some other scenarios where Generation can help.

1. Perform mass changes to rules. As mentioned earlier the ADA, publishes a new version of the CDT every year. With the ability to generate new or change existing content, based on high level heuristics, it will be possible to automate the mass changes to Rules.

2. Generate new rule templates based on mnemonic naming patterns that are generated based on high level heuristics. Within the BRIDE Case Study, this was exercised in a limited purview, as new rules had to be generated based on the conversion data.

3. Automatically generate test cases based on rule content. Based on semantic analysis of knowledge and rule artifacts, intelligent generators can automate the act of building test cases on the fly and saving them for regression purposes.

4.11 Learning

"Ability to learn from data patterns and from human feedback"

This has not yet been implemented within BRIDE, but it is there in the roadmap. This is an area of future work and builds on the other intelligent foundations.

5 Automation challenges for Knowledge-intensive systems

In this section we will consider some of the challenges around automation, for knowledge intensive systems. In 3.3, automating the task of authoring was identified as a the biggest opportunity for automation. Within

the BRIDE case study, automating conversion was one of the biggest opportunities. Automating the process of knowledge acquisition, reduced the time effort from 2 years to a few months. However, there are some inherent challenges with automation of the rule mining and authoring process. They are:

1. *Standardization :* For an automated rule conversion process to work repeatedly, the data for that area of functionality needs to be standardized into a well thought out canonical format.

2. *Specificity:* It is not uncommon for the quality of knowledge mined out from legacy blackbox systems to contain a lot of noise and inconsistencies that are specific to the legacy system. Further the nature of the inconsistencies can vary across different target systems and conversion initiatives. The automation processes while being streamlined should allow for custom transformation rules that can be externalized and customized for each conversion effort.

3. *Semantics:* The interpretation of standard benefit clauses implemented in rules in the legacy source system could have different semantics and might need specialized handling or transformation into the target system's knowledge base.

4. *Inconsistencies:* Sometimes there are misinterpretations of documented high level policies and contracts in the source legacy system, that are being converted. Technically one point of view amongst knowledge workers is to rectify these during the conversion process. Yet, this can have dire behavioral regressions on the target system, post-conversion. These kind of situations, need to identified during the automated conversions, traced back to the source and have a good explanation facility. Whether this method *can* be formalized consistently to bolster the efficacy of such automation efforts, remains a tantalizing proposition.

5. *Universal applicability:* For the BRIDE case study, the automated mining and generation process is fairly well established for a specific area of adjudication rules, that had the most number of rules and artifacts, that could not have been authored manually. But, whether this automated process can be streamlined and applied universally to other areas of rule mining is the subject of future work. This could be an area of research in the future.

6 Future Work

The paradigm of *intelligent foundations* to knowledge based systems holds great promise and potential. Especially within healthcare these techniques are making some significant differences. However there are areas that need further research and elaboration. Current state of the art AI techniques involve an ensemble of methods. Intelligent Foundations, strives to formalize and document a set of reusable patterns, language and processes to effectively apply them on a large and universally diverse setting. This paper was born out of a case study to address seemingly unsolvable and hard to automate and humanly unscalable problems. Here are some high level areas for future work.

1. *Universal application of techniques:* One area of future work is to continue the rigorous formalization of the techniques described here for universal application to other diverse verticals.

2. *Identifying more intelligent foundations:* While this paper attempted to do a reasonable job in identifying key intelligent foundational capabilities and building a framework for intelligent knowledge base systems, there is a significant opportunity for more research and elaboration, to further refine and enhance this concept and framework. Future work should continue to investigate other intelligent foundations that can introduce other intelligent capabilities that make the reality of a *virtual knowledge worker* real.

3. *Exploration of intelligent capabilities:* While this paper, outlined a few of the capabilities that can be built atop these intelligent foundations, there are more to be discovered and documented. This will motivate AI researchers to apply techniques to effectively solve the one real problem i.e. make healthcare cost effective to the general populace.

4. *Automation of conversion and generation of knowledge content:* Lastly, this is a major challenge as current methods are fairly ad-hoc, human and expert intensive. While prevalent data science methods and machine learning techniques seek to solve *"well defined"* problems, the challenge of replacing or augmenting the loss of a human subject matter expert by *emergent* system capabilities is an alien concept. The automation of conversion, rule mining and generation holds great promise and should open up rich areas of research.

7 Conclusion

As stated earlier, this paper came out of a case study, but introduces concepts that hold great potential. The work motivating this paper is a project to modernize and improve the *state of the art* of the BRIDE platform. The case study for automation and generation of rules and knowledge artifacts into the BRIDE platform has been instrumental in practically implementing and proving out a majority of the *intelligent foundations* discussed in this paper. The primary goal has been to, introduce elements of Artificial Intelligence at a grass root level that can provide an ambitious shift in capabilities. *Intelligent Foundations for Knowledge*

Based Systems, provide a perfect foil for solving the giant problem of generational shift, which seems to be driving Digital Transformation.

Conflict of Interest The author declares no conflict of interest.

Acknowledgment The author would like to acknowledge the executive leadership at Delta Dental for sponsoring and fueling the innovation, and for their continual commitment and support for the BRIDE platform, which remains a source of inspiration and innovation to the organization.

References

[1] M. K. Agaram, "Intelligent Discovery Features for EDM and MDM Systems," 2018 IEEE 22nd International Enterprise Distributed Object Computing Workshop (EDOCW), Stockholm, 2018, pp. 135-144. doi: 10.1109/EDOCW.2018.00028

[2] A. Finkelstein, et. al. "Moral Hazard in Health Insurance", Columbia University Press, 2015.

[3] D.M.Cutler, R.J.Zeckhauser "Adverse Selection in HealthCare", 1997

[4] D.M.Cutler, S.J.Reber "Paying For Health Insurance: The Trade-off Between Competition And Adverse Selection"

[5] T. Hall, "'Monte Carlo Estimation of the Impact of Adverse Selection on Multiple Option Dental Plans", 2010.

[6] M. K. Agaram and C. Liu, "Vocabulary Model Requirements for Production Rule Systems," 2012 IEEE 16th International Enterprise Distributed Object Computing Conference Workshops, Beijing, 2012, pp. 132-139. doi: 10.1109/EDOCW.2012.26

[7] M. K. Agaram and B. Laird, "A Componentized Architecture for Externalized Business Rules," 2010 14th IEEE International Enterprise Distributed Object Computing Conference, Vitoria, 2010, pp. 175-183. doi: 10.1109/EDOC.2010.26

[8] M. K. Agaram and C. Liu, "An Engine-Independent Framework for Business Rules Development," 2011 IEEE 15th International Enterprise Distributed Object Computing Conference, Helsinki, 2011, pp. 75-84. doi: 10.1109/EDOC.2011.20

[9] M. K. Agaram "The Phased Approach to Mining Business Rules" Business Rules Journal Vol. 8, No. 5, (May 2007)" URL: http://www.brcommunity.com/a2007/b344.html

[10] L.F.Bertain, G.Sibbald "The Tribal Knowledge Paradigm", 2012

[11] Adam Starks PhD (2013) The Forthcoming Generational Workforce Transition and Rethinking Organizational Knowledge Transfer, Journal of Intergenerational Relationships, 11:3, 223-237, DOI: 10.1080/15350770.2013.810494

[12] M.K.Agaram "Traceability Aspects for Business Rules Management" Business Rules Journal Vol. 9, No. 1, (Jan. 2008)" URL: http://www.brcommunity.com/a2008/b384.html

[13] Cahill, Terrence F., EdD, FACHE; Sedrak, Mona, PhD, PA Leading a Multigenerational Workforce: Strategies for Attracting and Retaining Millennials, Frontiers of Health Services Management: October 2012 - Volume 29 - Issue 1 - p 315

[14] Foss et. al. "Knowledge Governance Processes and Perspectives", Oxford University Press, 2009.

[15] Attila Bruni, Silvia Gherardi, Laura Lucia Parolin Knowing in a System of Fragmented Knowledge, Mind, Culture, and Activity, 14:1-2, 83-102, 2007

[16] D.C.Luckham "The Power of Events: An Introduction to Complex Event Processing in Distributed Enterprise Systems", Addison-Wesley Longman Publishing Co., 2001

[17] F.X.Campion, G. Carlsson "Machine Intelligence for Healthcare", 2017

ASTES

Advances in Science, Technology and Engineering Systems Journal
Vol. 4, No. 4, 94-105 (2019)
www.astesj.com
Special Issue on Advancement in Engineering and Computer Science

ASTES Journal
ISSN: 2415-6698

An Extension of Throughput Drop Estimation Model for Three-Link Concurrent Communications under Partially Overlapping Channels and Channel Bonding in IEEE 802.11n WLAN

Kwenga Ismael Munene[1], Nobuo Funabiki[*,1], Md. Manowarul Islam[1], Minoru Kuribayashi[1], Md. Selim Al Mamun[2], Wen-Chung Kao[3]

[1]*Department of Electrical and Communication Engineering, Okayama University, Okayama, Japan.*

[2]*Department of Computer Science and Engineering, Jatiya Kabi Kazi Nazrul Islam University, Bangladesh.*

[3]*Department of Electrical Engineering, National Taiwan Normal University, Taipei, Taiwan.*

ARTICLEINFO

Article history:
Received: 22 April, 2019
Accepted: 07 June, 2019
Online: 15 July, 2019

Keywords:
WLAN
Access point
IEEE 802.11n
Partially overlapping channel
Throughput estimation model
Three links

ABSTRACT

The IEEE 802.11n wireless local-area network (WLAN) has been extensively deployed around the world due to the flexibility, lower cost, and the high-speed data transmission capability at 2.4 GHz ISM band. However, in the WLAN deployment, one key challenge is to optimize the channel assignment of access-points (APs) under the small number of partially overlapping channels (POCs) to reduce radio interference, particularly for the channel bonding. In POCs, the frequency spectrums of adjacent channels are partially overlapped with one another, which will result to low throughput for concurrently communicating links using them. The accurate throughput estimation of a link is critical in the optimal WLAN deployment. Previously, we studied the throughput drop estimation model using the receiving signal strength (RSS) from the interfered link for two concurrently communicating links under POCs. In this paper, based on measurement results, we have extended this model for three concurrently communicating links. The accuracy of this model extension is verified by comparing the estimated results with the measured ones.

1 Introduction

Nowadays, the *IEEE 802.11 wireless local-area network (WLAN)* has been used across various sectors around the world, due to the unlicensed frequency bands in wireless medium and availability of low-cost devices [1]–[3]. It is suggested that WLAN has become a crucial business and the common asset [4]. For the access to the Internet using WLAN, a host is connected to an *access point (AP)* wirelessly, where the AP is connected to the Internet with wires. Therefore, a host can move randomly in the network area with the current association. As the data transmission speed increases due to technological advancements, WLAN has proved popular even for static settings of personal computers in offices and homes [5].

The IEEE 802.11 WLAN can function in two unlicensed frequency bands [6, 7]. One is the 2.4 GHz *Industrial, Scientific, and Medical (ISM)* band, and the other is the 5 GHz *Unlicensed National Information Infrastructure (U-NII)* band.

For either band, the IEEE 802.11 standards define the small number of channels for use. Each channel has 22 MHz width, conventionally called a 20 MHz channel. The frequency gap between two adjacent channels is merely *5MHz*. Thus, the spectrums of adjacent channels are partially overlapped with one another, called the *partially overlapping channels (POCs)*. Figure 1 shows the 2.4 GHz spectrum with 40 MHz channels to illustrate the POCs in IEEE 802.11n.

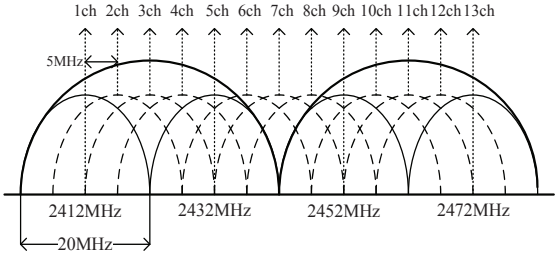

Figure 1: 40MHz channels at 2.4 GHz band.

While the IEEE 802.11 WLANs referred to in this paper use the unlicensed frequency bands, *the Industrial, Sci-*

*Corresponding Author: Nobuo Funabiki, Dep. of Elect. and Comm. Eng., Okayama Univ., Okayama, Japan, Email: funabiki@okayama-u.ac.jp

entific, and Medical (ISM) 2.4 GHz band and *the Unlicensed National Information Infrastructure (U-NII) 5 GHz band*, the 802.11y is licensed to use [8]. The unlicensed IEEE 802.11ad, which represents modifications of IEEE 802.11 physical layer (PHY) and medium access control layer (MAC) [9], provides the very high speed, which is equivalent to the fiber optic. However, its short range limitation coupled with the expensive hardware makes the global adoption of IEEE 802.11ad to be low [10].

Similarly, the IEEE 802.11af is advantageous due to its long-range transmission and low power consumption. However, it requires expensive band-specific hardware, which is not readily available in the global market where it is primarily used in US and Canada. In addition, since it utilizes the frequencies for unused TV channels, they may not be available everywhere [11].

The proposed model in this paper targets WLANs on the IEEE 802.11n unlicensed frequency band. Since this protocol has been widely adopted, the related devices are much easily and cheaply available, compared to those of emerging standards of the IEEE 802.11ad and IEEE 802.11af.

At the 2.4 GHz band, 13, 20MHz POCs are possible, which indicates that the number of *orthogonal channels (OCs)* is four at most. Since orthogonal channels do not overlap with one another, APs assigned OCs are not interfered for the medium access, if any pair of nearby APs do not operate on the same OC.

Currently, the *IEEE 802.11n* is most used in WLAN due to the high-speed data transmission capability at the 2.4 GHz band using the *channel bonding* that combines two neighboring 20 MHz channels together to form one 40 MHz channel as shown in Figure 1, [12]–[14]. Then, the number of OCs is reduced to at most two, and the channel assignment using OCs to the APs without interference cannot be avoided. [15] has shown that channel bonding improves performance, although it may increase frequency competition with adjacent LANs.

To overcome this limitation of the OC assignment in WLAN, it has been reported that the POCs will be beneficial to enhance the performance by fully utilizing the available spectrum [16, 17]. Then, the *throughput estimation model* under POCs is essential to identify the proper POC assignment to the APs while evaluating the performance accurately. Specifically, in a dense WLAN, the model must consider the *throughput drop* caused by the interference that each AP suffers from the neighboring APs on the adjacent POCs.

Previously, we have studied the *throughput estimation model* for a single communicating link, which consists of the *log-distance path loss model* and the *sigmoid function* [18]. Then, we move to estimate the *throughput drop* caused by the interference for two concurrently communicating links under POCs [19]. It is examined according to the *receiving signal strength (RSS)* from the interfering link and the *channel distance (chD)* between the two links.

The proper use of POCs should be considered for the full utilization of the limited frequencies, since there are limited orthogonal channels available in the IEEE 802.11n protocol with the channel bonding. Besides, the estimated throughput should be directly used as the metric for selecting POCs by estimating the network performance, since the interference does not exhibit the exact performance of the network, which has been observed in this paper.

Our model considers the channel bonding and POCs, to directly estimate the throughput from the channel distance and the RSS of the interfering AP. From the estimated throughput, the POC assignment can be optimized under the channel bonding.

Besides, in our previous studies [20, 21], we considered the indoor network environment inside a building for the target field, since WLANs are usually deployed there. A lot of environmental factors, such as wall attenuations and multipath effects, can affect the throughput performance. To accurately estimate the throughput, we have developed the throughput estimation model that consider the environmental factors.

In this research work, we extend the *throughput drop estimation model* for three concurrently communicating links under POCs. Firstly, we conduct extensive measurements of *receiving signal strength (RSS)* and throughputs under three links. Then, we extend the model based on the measurement results.

To confirm the effectiveness of our proposal, we compare the estimated throughputs by the model with the measured ones, and through simulations. It has been demonstrated that the proposal can estimate the throughput for three interfered links under POCs with the considerably high degree of accuracy.

The rest of this paper is organized as follows: Section 2 describes related works. Section 3 discusses the implementations of the auto-channel selection in vendor AP devices and the significance of the throughput estimation model. Section 4 reviews our previous studies. Section 5 presents experiments with three concurrently communicating links under POCs. Section 6 proposes the model extension for them. Section 7 evaluates the proposal with experiments and simulations. Section 8 introduces the application to the channel assignment. Section 9 concludes this paper with future directions.

2 Related Works

In this section, we discuss specific works related to our proposal. A significant amount of research works have addressed the problem of interferences in WLAN to improve the throughput performance by applying partially overlapping channels.

In [22], Mishra et al. revealed that the orthogonal channel assignment to APs in WLAN is inefficient in a network field, if a substantial number of access points are deployed there. In such a case, the number of APs in the network field is higher compared to that of orthogonal channels, hence any AP could exist in the interference ranges of other APs as indicated in [23].

In [24], Mishra et al. also noted that partially overlapping channels have previously been avoided due to their interferences. However, through their model and measurements, it is demonstrated that the careful use of some POCs does not only improve the spectrum utilization but also the throughput performance.

In [25], Feng et al. proposed POCs as a means of reducing interference from the traditional use of OCs. Through

testbed experiments, they reported that POCs offers better flexibility in wireless frequency allocation, and can increase overall network performance. Similarly, in [26], Zhang et al. proposed the use of POCs for interference management which outperforms the OCs.

In [27], Zhao et al. observed that with increased frequency reuse which has been reported in POCs, the network capacity can be scaled up through activating more APs in the network field as the expected distance from the users to their connected APs becomes smaller. However, it is reported that since POCs are partially overlapped with each other, one AP may suffer interference from multiple other APs. They conclude by proposing a need to have a maximum and a minimum bound for the number of APs based on the size of the network field and the number of POCs available.

In [28], Mukherjee et al. explored the AP selection, channel assignment, and the host association. They reported that the three aspects are critical in maximizing the throughput in WLAN, where the appropriate combination of both non-overlapping channels and POCs can further improve the overall throughput of the network.

In [29], Tewari et al. emphasized that multiple overlapping transmissions cause low network performance due to high interference from the limited non-overlapping channels. They have proposed a combined power control and POC assignment, where the former reduces the AP's transmission and the interference range while the latter improves spatial reuse.

In [30], Zhao et al. demonstrated that the effect of interference on the network performance depends on the channel separation and the degree of frequency overlap among the interfered APs. In particular, it is noted that two interferes cause higher performance deterioration than a single interfere, but less than twice the interference caused by a single interfere or the summation of interference from the two interferes.

Furthermore, in [31], Su et al. measured the interference among the APs when POCs are used from the perspective of the physical characteristics of the communication. They reported a clear distinction between in-range and hidden terminal interferences with POCs, where the latter has worse throughput performance due to high packet loss.

In [28], POC interference is evaluated by considering the interference factor defined in [32]. Where more than one APs interferes, [27] [28] and [29] considers summation of interfering signal powers at the target node. However, since the MAC protocol lowers the data transmission rate of the target AP depending on the level of interference with individual interfere, calculating the summation may fail to identify a real value of interference.

At present, there is no research work that has proposed the throughput drop estimation model for multiple interfering APs under POCs that considers the channel distance and the interfering RSS.

3 Auto-channel Selection Implementations and Model Significance

In this section, we survey implementations of the auto-channel selection in vendor AP devices, and discuss the significance of the throughput estimation model under it.

The auto-channel selection is the dynamic adjustment mechanism of the assigned channel to the AP, in order to avoid radio interferences from other WiFi devices. Each AP vendor has its own implementation approach.

In [33], Cisco describes their implementation of the auto-channel selection, where the AP operating in the 2.4 GHz band with 11 POCs can be set only to one of the three orthogonal channels of 1, 6, and 11 under the non-bonded channels with the *(20 MHz)* width. It means that up to three APs can be assigned the channels. The assignment for other POCs must be done manually.

However, when the channel bonding with the *(40 MHz)* width is applied, which is commonly used in IEEE 802.11n WLANs to improve the throughput performance, the AP can have only one choice of channel 3, since all the other channels are partially overlapping with it. It means that the auto-channel selection cannot work for the channel bonding.

On the other hand, our proposal can assign any POC to the AP with the channel bonding by considering the throughput drop from the other up to two interfered links.

Besides, from our experimental observations, the orthogonal channels can interfere with each other when the APs are closely located together, which would further affect the auto-channel selection in the Cisco Meraki APs.

Furthermore, Cisco's approach scans for a possible channel change after every 15 minutes, in addition to the three necessary situations: 1) a new AP joins the network, 2) the network administrator manually runs the auto-channel), and 3) the currently assigned channel fails to work. This would lead to the performance overhead, since the services of an AP must be stopped when channel change is applied. To avoid the frequent service stops, our approach changes channels of APs when an AP joins or leaves the network.

In [34], Fujitsu reports the auto-channel selection such that the total interference is minimized, where the details of the implementation are not given. However, the interference index is not a good metric to evaluate the throughput performance, because the interference and the throughput performance are not proportional as our paper reported. Instead, the throughput drop of each link from the other interfered links should be evaluated to more accurately estimate the network performance under a lot of interfered links.

In [35], Buffalo implements the auto-channel selection that tries to find the non-interfered channel for a new AP. By scanning all the channels, it selects a non-interfered channel if it exists. However, they also reported that the channel selection performs poorly, if no non-interfered channels exist. In real network environments, as demonstrated in our paper, several APs coexist together where any channel is interfered by an existing AP. On the other hand, our proposal is applicable in such real cases.

Similarly, in [36], Vodafone limits the auto-channel selection only to the non-interfered channels or the least interfered channel. In [37], Google WiFi works on the similar principle by selecting an orthogonal channel.

It should be pointed out that the proposed throughput estimation model can be incorporated into an auto-channel selection mechanism to improve the resulting performance of WLAN. Our model considers the channel bonding, POCs, and the direct throughput estimation. Therefore, we believe

that this model can improve the auto-channel selection. In future works, we will compare the performance by our model with existing auto-channel selections.

4 Review of Throughput Estimation Model

In this section, we review our previous works.

4.1 Motivation of Empirical Model

In [5], Reis et al. indicates that most of physical protocol explorations with respect to interference may adopt simple abstract models with multiple assumptions, including that the signal propagation obeys a simple function of the distance, the radio coverage area forms a circle, and the interference range is twice of the transmission range. Unfortunately, experimental data using a real WLAN have shown that all of these models appear to be largely inaccurate [38, 39].

In contrast to a physical model, an empirical model is based on observations on actual network environments. Thus, the empirical model for interference in WLAN is expected to be more descriptive and accurate compared to a physical model. Therefore, we have developed the empirical throughput drop estimation model for multiple-link concurrent communications based on experimental results.

4.2 Definitions of Three Distances

The *channel distance*, the *physical distance*, and the *link distance* are defined to illustrate the throughput estimation model under partially overlapping channels.

4.2.1 Channel Distance

The *channel distance* (*chD*) of the two links is defined as the least channel difference between the channels of these links. For instance, if the two links are activated with the same channel, then *chD* is 0, and they will be entirely overlapped. When one link is assigned *channel 3* and another link is *channel 5*, *chD* is 2, in this case, these channels are overlapped by 50% for 20MHz, and by 75% for 40MHz. The largest *chD* is 12 for 20MHz and 8 for 40MHz, in which any frequency overlapping does not exist theoretically.

4.2.2 Physical Distance

The *physical distance* (*phD*) is defined as the Euclidean distance between the two links. As it represents the separation distance among the interfering links, the farther the two links are placed, that is, the higher the physical distance is, the interference will become lesser. By increasing the physical distance between the links, the signal interference between them fades due to the path loss and the absorption by obstacles on the path.

4.2.3 Link Distance

The Euclidean distance between the sender and the receiver of the link is defined as the *link distance*. The longer link distance generally reduces RSS at the receiver and degrades the throughput.

4.3 Throughput Estimation Model

Generally, the throughput of a link will be affected by a variety of factors like the modulation and coding scheme (MCS), the transmission power, the transmission distance, and the channel interference [13, 40], which have made it hard for the theoretical calculation of the throughput. In [18], we proposed the throughput estimation model for the single link communication based on empirical results. This model first estimates the *receiving signal strength (RSS)* at the host using the *log-distance path loss model* [41]. Next, it estimates the throughput from the RSS using the *sigmoid function*.

4.3.1 Received Signal Strength Estimation

Firstly, the Euclidean distance *d (m)* between each link (AP/host pair) is calculated by:

$$d = \sqrt{(AP_x - H_x)^2 + (AP_y - H_y)^2} \tag{1}$$

Here, AP_x, AP_y and H_x, H_y denotes the x and y coordinates for the AP and the host respectively.

Then, *RSS* at the host from the AP is estimated by:

$$P_d = P_1 - 10\alpha \log_{10} d - \sum_k n_k W_k \tag{2}$$

Here, P_d denotes *RSS* (dBm) at the host, P_1 does *RSS* at the $1m$ distance from the AP where no obstacle exists, α does the path loss exponent, *d (m)* does the Euclidean distance calculated between the AP and the host, n_k does the number of *type_k* obstacles found on the path between the AP and the host, and W_k represents the signal attenuation factor (dB) for *type_k* obstacle.

4.3.2 Throughput Estimation

From P_d, the throughput is estimated by;

$$tp_{ij} = \frac{a}{1 + e^{-(\frac{(120+P_d)-b}{c})}} \tag{3}$$

where tp_{ij} denotes the estimated throughput ($Mbps$) and, a, b, and c are constant coefficients.

4.4 Throughput Drop Estimation Model for Two-Link Concurrent Communications

In [19], we proposed the *throughput drop estimation model* to consider the frequency interference between concurrently communicating adjacent two links using interfering channels. The *throughput drop* of the target link can be estimated by the receiving signal strength at the receiver, called the *interfering RSS*, (RSS^i), from the interfered link, and the channel distance *chD* between the two links:

$$tpD(RSS^i, chD) = p(chD) \times \ln(q(chD) + RSS^i) + r(chD). \tag{4}$$

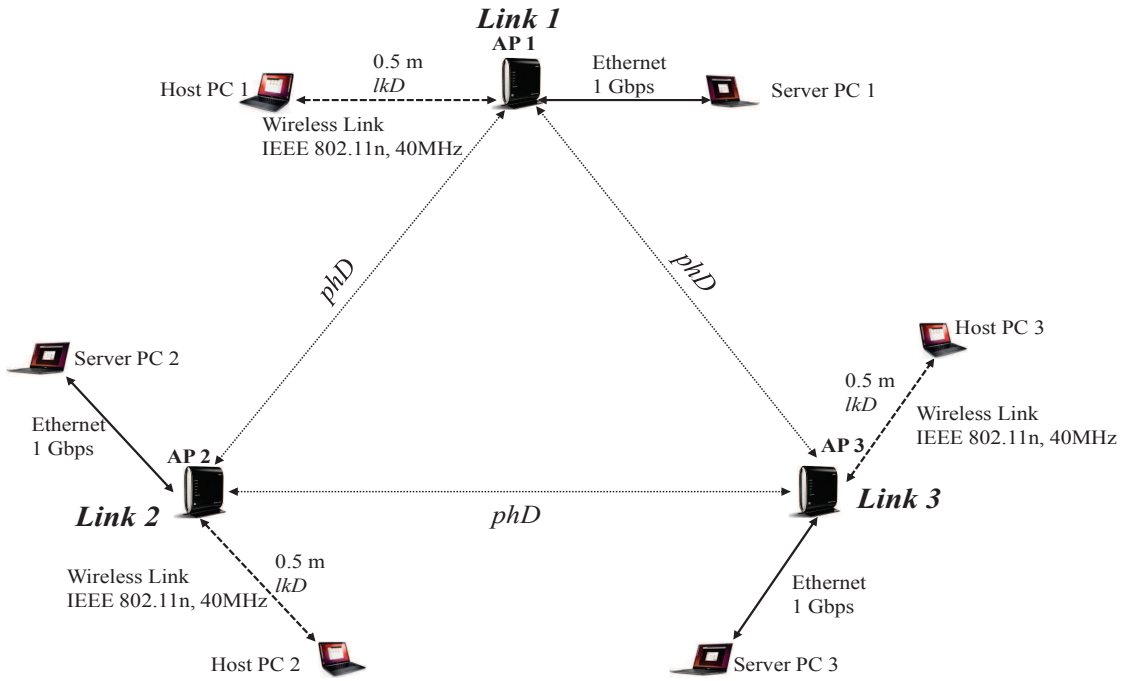

Figure 2: Measurement setup.

where $tpD(RSS^i, chD)$ represents the estimated throughput drop ($Mbps$), and $p(chD)$, $q(chD)$, and $r(chD)$ represent constants determined by the channel distance (chD).

The values of the three constants p, q, and r in the model were obtained from the throughput drop measurement results for every channel distance. Table 1 shows them.

Table 1: Constants for each channel distance.

channel distance	p	q	r
0	27	88.17	-20
1	27	87.36	-20
2	27	89.00	-22
3	25	94.50	-22
4	33	92.00	-56
5	34	92.00	-57
6	45	91.00	-98
7	45	88.00	-100
8	40	75.50	-80

Then, the throughput estimation model under POCs for two interfered links is modified by:

$$tp^i_{ij} = tp_{ij} - tpD(RSS^i_j, chD^i_j) \quad (5)$$

where tp^i_{ij} represents the throughput of the target link from node i to node j under the interference from the interfered link, tp_{ij} does the throughput of this link estimated by the original model, RSS^i_j does RSS from the interfered link at node j, and chD^i_j does the channel distance between the two links.

5 Experiments in Three-Link Concurrent Communications

In this section, we present the experiment results to examine the extension of the throughput drop estimation model for three concurrently communicating links.

5.1 Experiment Setup

Table 2 indicates the necessary devices and software used in the experiments. It is noticed that if different devices are used, the parameter values of the model will vary accordingly.

Table 2: Measurement devices and software.

Access Point (*all links*)	
maker/ type	NEC WG2600HP
protocol	IEEE 802.11n
operating band	2.4 GHz
frequency width	40 MHz
host PC (*all links*)	
maker/ type	Toshiba dynabook R731/B
operating system	Ubuntu 14.04 LTS
processor	Intel Core i5-2520M 2.54 Ghz
network adapter	Intel HM65 Express chipset
server PC ($link_1$)	
maker/ type	Toshiba dynabook R731/B
processor	Intel Core i5-2520M 2.54 Ghz
operating system	Ubuntu 14.04 LTS
network adapter	Intel HM65 Express chipset
server PC ($link_2$, $link_3$)	
maker/ type	Fujitsu lifebook S761/C
processor	Intel Core i5-2520M 2.5GHz
operating system	Ubuntu 14.04 LTS
network adapter	Mobile Intel QM67 Express

Figure 2 shows the topology of three links ($link_1$, $link_2$ and $link_3$) in experiments. The server PC connects to the AP through the Gigabit Ethernet, and the host PC is connected to the AP by the 11n wireless link. The host is 0.5m from its connected AP, and each AP is 5m from the other AP. The maximum transmission power is selected for any AP with the equal antenna gain [16]. The *minimax AP setup optimization approach* in [18] is applied to maximize the throughput for each link. The *iperf 2.05* [42] is used to generate the TCP traffic between the server and the host.

5.2 Experiment Fields

The experiments were carried out in indoor fields on the 2nd floor of *Graduate School of Natural Science and Technology Building* and the 3rd floor of *Engineering Building #2* in Okayama University. Each field consists of several rooms, walls, and floors, which can affect the throughput through the multi-path effect. RSS^i and the throughputs are measured while increasing the physical distance, *phD*, between the two APs and their channel distance, *chD*. By using *Homedale* [43], the frequencies of the links under measurements and the external interfering links are recorded. Figure 3 shows the site while Figure 4 reveals the frequency utilization for measurements, where several channels are highly utilized by non-target APs.

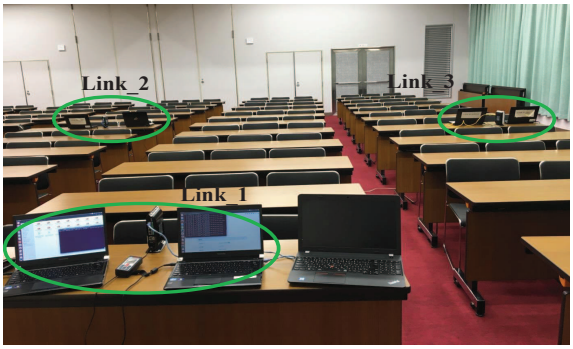

Figure 3: Experiment in Graduate School Building.

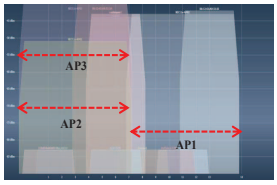

(a) AP1= ch11, AP2 = ch3, AP3 = ch3

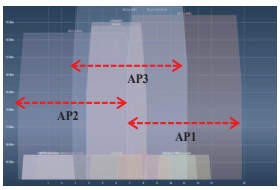

(b) AP1= ch11, AP2 = ch3, AP3 = ch7

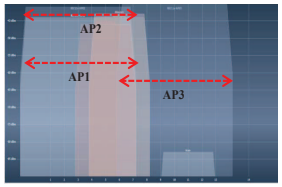

(c) AP1= ch3, AP2 = ch3, AP3 = ch8

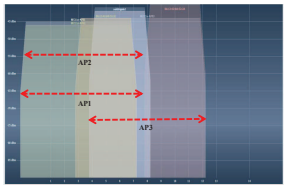

(d) AP1= ch3, AP2 = ch3, AP3 = ch10

Figure 4: Frequency utilization in experiments.

5.3 Experimental Results

For AP_1 (and AP_2 for three links), the bonded channel 3 is always assigned. For AP_2 (AP_3 for three links), the assigned channel is changed from 3 to 11 one by one, so that the channel distance *chD* increases from 0 to 8. The throughput was measured at the same time for all the links. The experiments were conducted on weekends and at night on weekdays to reduce the interference from other Wi-Fi devices.

Figures 5 and 6 show measured individual and average throughput under concurrently communicating two links and three links, respectively. The individual throughput fluctuates, because the contention among the links is not well resolved by the current *carrier sense mechanism* [44], which may cause the unfair channel occupation among them. Thus, in this paper, we use the average throughput among them for the single link throughput.

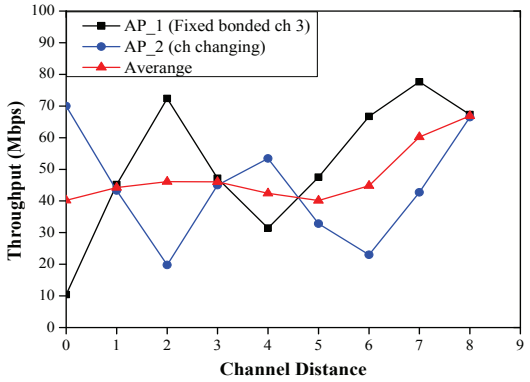

Figure 5: Throughput results for two links.

Figure 6 demonstrates that when the three APs are assigned the same channel, one AP takes the entire medium, which makes the others have the lower throughput. As *chD* increases, the throughput of AP_3 will enhance gradually, due to the reduced channel interference.

In this experimental setup, the measured maximum throughput of one link is about 140$Mbps$ under no interference. Then, it drops significantly to about 40$Mbps$ under two links, when the channel distance is smaller than seven. Furthermore, it drops to about 20$Mbps$ under three links.

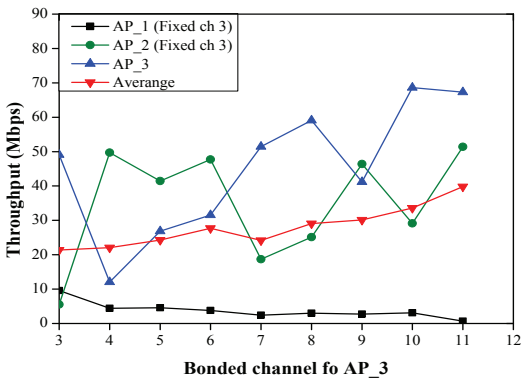

Figure 6: Throughput results for three links.

5.4 Observations from Experiment Results

According to the evaluation, it is observed that for the target link, the interference from the first interfering link causes the larger throughput drop (from 140$Mbps$ to 40$Mbps$), and the interference from the second causes the smaller drop (from 40$Mbps$ to 20$Mbps$). That is to say, when the target link is interfered by the first link, the rate adaptation mechanism lowers the transmission rate by adopting the robust MCS. Then, the second interfering link further lowers the rate by adopting the more robust MCS [30][31]. Here, the rate can be lowered exponentially in MCS.

6 Model Extension for Three-Link Concurrent Communications

In this section, we present the extension of the throughput drop estimation model for three concurrently communicating links based on experimental results.

6.1 Idea of Throughput Drop Estimation under Three Links

As observed before, the throughput drop from multiple interfering links can be estimated one by one through calculating each drop using the model in Section 4.4 in descending order of the interference. That is, the drop from the link with the largest interference is first estimated, assuming the original maximum throughput. Then, the drop from the link with the second largest interference will be estimated, assuming the maximum throughput has been reduced by the first drop.

6.2 Throughput Drop Estimation Procedure

The throughput of the target link $link_{ij}$ under three-link concurrent communications is evaluated by the following procedure:

1. Estimate the throughput of each of the three concurrently communicating links using the original model in Section 4.3.
2. Estimate the throughput drop tpD from each of the two interfering links using Eq. (4) in Section 4.4.
3. Sort them in the descending order: let tpD^{1st} and tpD^{2nd}.
4. For the largest interfering link, adjust tpD^{1st} by the maximum speed of the AP of the target link, because different APs have different throughput performances:

$$tpD^{1st}_{adj} = tpD^{1st} \times \frac{tpM^{AP}}{140} \quad (6)$$

where tpD^{1st}_{adj} represents the adjusted throughput drop by the largest interfering link, and tpM^{AP} does the maximum throughput for the AP of the target link.

Then, the throughput tp^{1st}_{ij} of the target link after considering the drop by the first link interference is estimated by:

$$tp^{1st}_{ij} = tp_{ij} - tpD^{1st}_{adj} \quad (7)$$

5. For the second largest interfering link, adjust the tpD^{2nd} by;

$$tpD^{2nd}_{adj} = tpD^{2nd} \times \frac{tpM^{AP} - tpD^{1st}_{adj}}{140} \quad (8)$$

Then, the throughput tp^{2nd}_{ij} of the target link after considering the drop by the second link interference can be estimated by;

$$tp^{2nd}_{ij} = tp^{1st}_{ij} - tpD^{2nd}_{adj} \quad (9)$$

In [31], Su et al. observed that the throughput drop by the accumulated interference from two interfering links is greater than that from a single interferer, but less than the sum of the drops from the individual interference. The second interfering link will cause a smaller drop than the first one. This observation also supports our throughput drop estimation model for concurrently communicating three links.

7 Evaluations of Model Extension

In this section, we evaluate the throughput drop estimation model for three concurrently communicating links under POCs and the channel bonding through experiments and simulations.

7.1 Experiment Results in One Room

First, the devices and one-room field in Sections 5.1 and 5.2 are used in experiments.

7.1.1 Channel Assignments

In experiments, the bonded channel 3 is always assigned to AP_1. Then, the either channel of 3, 7, and 11 is assigned to AP_2. To AP_3, the assigned channel is moved from 3 to 11 one by one so that the channel distance is changed. The throughputs are measured at the same time for all the links.

7.1.2 Throughput Results

Figures 7, 8, and 9 show the measured average throughput among the three APs when the channel 3, 7, and 11 is assigned AP_2, respectively.

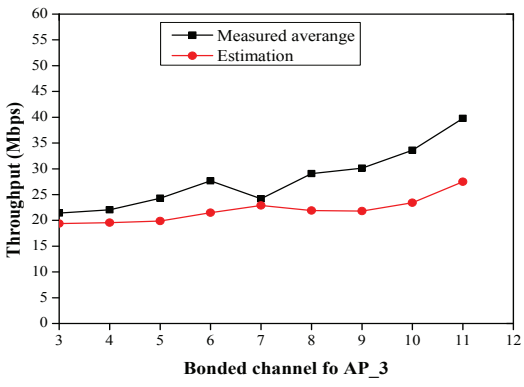

Figure 7: Throughput results in one room for AP_1:ch3, AP_2:ch3.

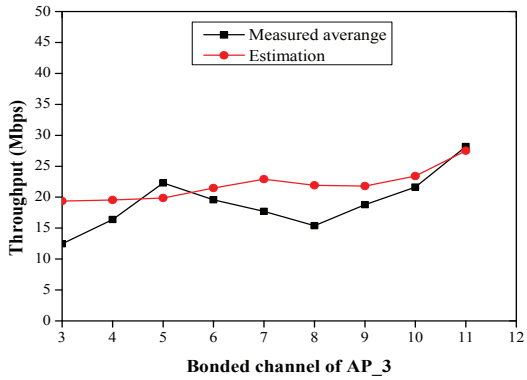

Figure 8: Throughput results in one room for AP_1:ch3, AP_2:ch7.

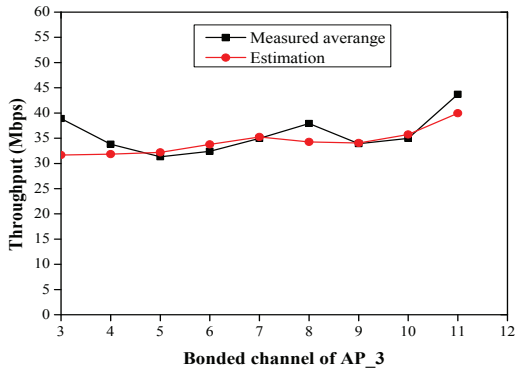

Figure 9: Throughput results in one room for AP_1:ch3, AP_2:ch11.

When the three results are compared, Figure 8 indicates the lowest throughput among them, because AP_2 is interfered with both AP_1 and AP_3. Figure 9 presents the highest throughput in general, because AP_1 and AP_2 are not interfered. On the other hand, Figure 7 shows that as the channel distance increases, the throughput will raise as the reduction of the interference between (AP_1 and AP_2) with AP_3.

Then, the estimated throughput is calculated by the proposed throughput drop estimation model, and is compared with the measured throughput. Figures 7- 9 demonstrate that these throughput are similar in any case. Thus, the accuracy of the proposed model for three concurrently communicating links is confirmed.

7.2 Experiment Results in Three Rooms

Next, the experiments are conducted using three rooms on the 3rd floor of *Engineering Building #2* to examine the accuracy of the model.

7.2.1 Experiment Field

The physical distance between the APs is changed by locating each AP in a different room from the previous experiments, as revealed in Figure 10. By locating each AP in a separate room, the overall interference between them is reduced. The link distance between the AP and its associated host is set 0.5m or 4m. The channel assignments in Section 7.1.1 are adopted.

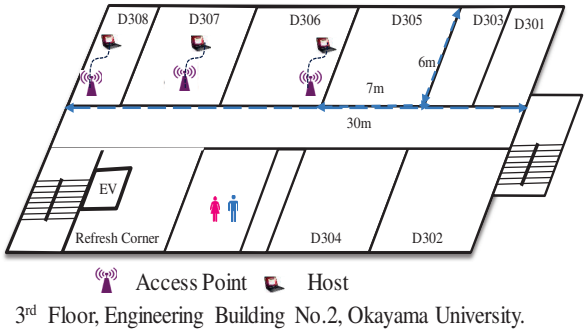

Figure 10: Three room topology.

7.2.2 Throughput Results with 0.5m Link Distance

Figures 11 - 13 show the measured and the estimated throughput results when the link distance is 0.5m. These throughput turns out to be similar at any channel distance, which confirms the accuracy of the proposed model. At the same time, they are higher than the ones in Figures 7- 9, since they are less interfered here.

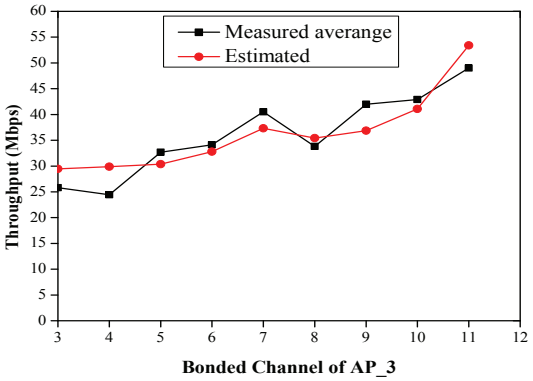

Figure 11: Throughput results in three rooms with 0.5m link distance for AP_1:ch3, AP_2:ch3.

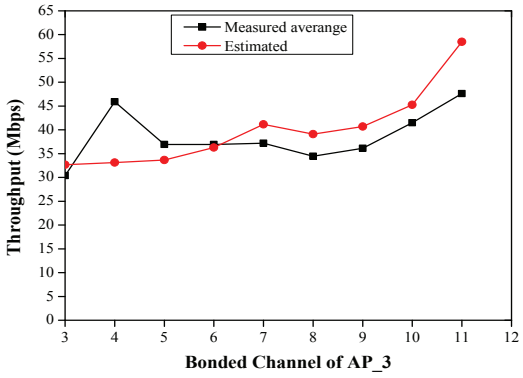

Figure 12: Throughput results in three rooms with 0.5m link distance for AP_1:ch3, AP_2:ch7.

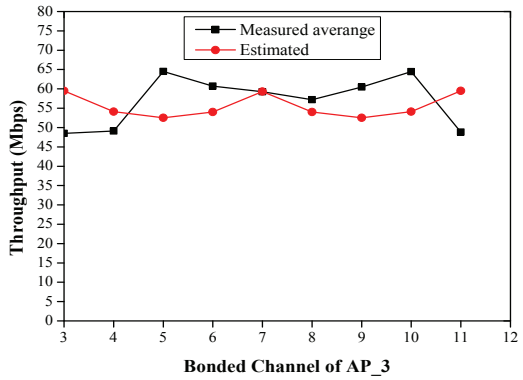

Figure 13: Throughput results in three rooms with 0.5m link distance for AP_1:ch3, AP_2:ch11.

7.2.3 Throughput Results with 4m Link Distance

Figures 14- 16 show the measured and the estimated results when the link distance is 4m. In Figures 15 and 16, they are similar at any channel distance. Thus, the accuracy of the model is verified in the larger link distance as well. However, in Figure 14, the measured throughput is lower than the estimated one at each channel distance. This is because the interference from non-target APs in the field is stronger around the channel 3, as shown in Figure 4. It is a must to conduct experiments in environments with less interference, which will be included in future works.

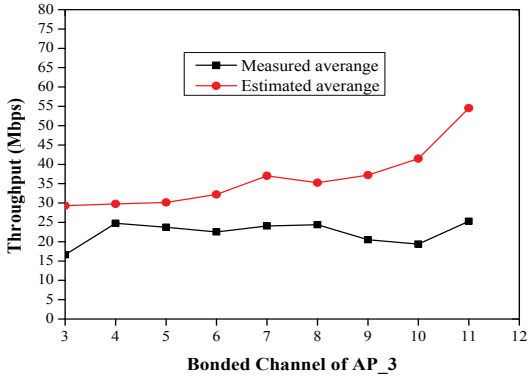

Figure 14: Throughput results in three rooms with 4m link distance for AP_1:ch3, AP_2:ch3.

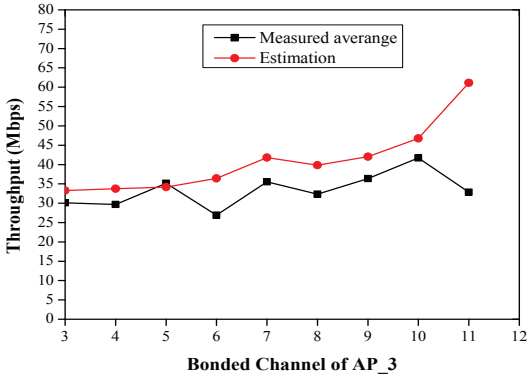

Figure 15: Throughput results in three rooms with 4m link distance for AP_1:ch3, AP_2:ch7.

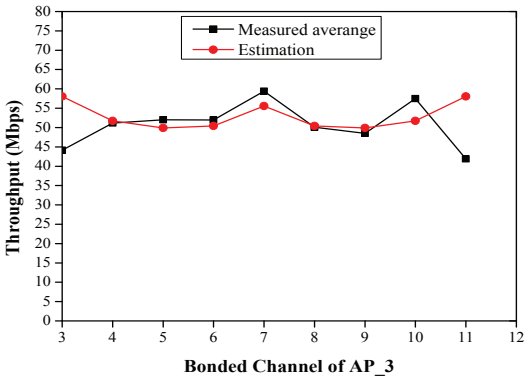

Figure 16: Throughput results in three rooms with 4m link distance for AP_1:ch3, AP_2:ch11.

8 Application to Channel Assignment

In this section, we discuss the application of the proposed throughput drop estimation model to the POC assignment to the APs.

8.1 Modification of Channel Assignment Phase

The channel assignment phase of the *active AP configuration algorithm* in [45] is modified to assign POC using the proposed model. Specifically, the formulations for this phase are revised from the previous one in [45] as follows:

8.1.1 Modification of Input

The number of partially overlapping channels is adopted in place of the number of orthogonal channels for C.

8.1.2 Modification of Output

The partially overlapping channel assigned to every active AP is adopted rather than the orthogonal channel assigned to every active AP.

8.1.3 Modification of Objective

The total interfered communication time E_3 is modified to consider partially overlapping channels by:

$$E_3 = \sum_{i=1}^{N} [IT_i^i] \tag{10}$$

where IT_i^i denotes the interfered communication time under partially overlapping channels for AP_i.

Under POCs, the link speed drop by the interfered links needs to be examined in the throughput estimation model. Therefore, IT_i^i can be simply given by:

$$IT_i^i = \sum_{j \in AH_i} \frac{1}{tp_{ij}^{2nd}} \tag{11}$$

where AH_i denotes the set of hosts associated with AP_i.

Our current throughput estimation model for partially overlapping channels only examines the interference between three links. In this paper, we assume that the target link is interfered by the two strongest interfering links, while the other interfering links may have negligible effects. This can be supported by the results in Section 5.4, where the highest interfering link causes the large drop and the second link causes the far small drop.

8.2 Evaluations by Simulations

First, we evaluate the performance of the POC assignment via simulations.

8.2.1 Simulation Platform

The *WIMNET simulator* [46] is adopted for simulations. Table 3 sums up the parameters for simulations [45].

Table 3: Simulation Parameters in WIMNET Simulator.

parameter	**value**
packet size	2360 bytes
max. transmission rate	150 Mbit/s
propagation model	log-distance path loss model
rate adaptation model	sigmoid function
carrier sense threshold	−85 dBm
transmission power	19 dBm
collision threshold	10
RTS/CTS	yes

8.2.2 Results for Random Topology

To evaluate the performance in various network environments for WLAN, first, the *random topology* is considered. As shown in Figure 17, in this topology we consider a network field of size $800m \times 200m$, where two rooms are located, each of length $400m$. Eight APs and 25 hosts are allocated randomly.

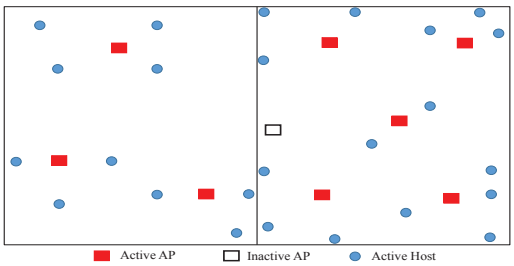

Figure 17: Random topology for channel assignment.

.

Then, the minimum host throughput and the overall throughput are compared between the POC assignment and the conventional OC assignment through simulations. Two channels (3, 11) are used for the OC assignment all the time. On the other hand, three channels (3, 7, 11), six channels (3, 5, 7, 8, 9, 11), and nine channels (3, 4, 5, 6, 7, 8, 9, 10, 11) are used for the POC assignment. Table 4 shows the results.

Table 4: Throughput results for *random topology*.

channel assignment	OC	POC		
# of channels	2	3	6	9
min. host throu. (Mbps)	7.12	9.16	8.42	8.63
overall throu. (Mbps)	174.56	196.74	197.04	198.46

8.2.3 Results for Regular Topology

Next, the *regular topology* in the third floor of Engineering Building #2 at Okayama University is considered. The room size is either $7m \times 6m$ or $3.5m \times 6m$. Eight APs and 55 hosts are regularly allocated, as signified in Figure 18.

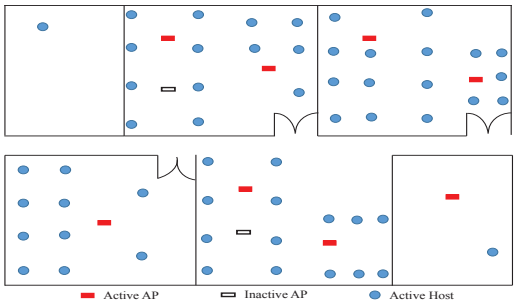

Figure 18: Regular topology.

The same two, three, six, and nine channels as for *random topology* are considered. Table 5 shows the minimum host throughput and the overall throughput for them.

It is noted that in both topologies, as the number of POCs is increased, the overall throughput will enhance by reducing the interference while maintaining the minimum host throughput.

Table 5: Throughput results for *regular topology*.

channel assignment	OC	POC		
# of channels	2	3	6	9
min. host throu. (Mbps)	2.68	3.11	3.06	3.15
overall throu. (Mbps)	147.76	170.88	168.76	173.49

8.2.4 Results for Regular Topology with Large APs

Finally, in Figure 19 we evaluate the model by simulations in a new instance by increasing the number of APs from 8 to 10 in the regular topology. The number of hosts remains as 55.

The evaluation in a real environment using the testbed is more important to confirm the effectiveness of the model. Thus, it will be in our future studies.

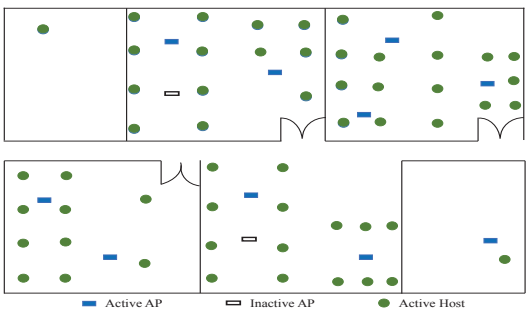

Figure 19: Regular topology for 10 APs.

Table 6 shows the results. As the number of APs increases, the total performance also increases, because more hosts can be located nearer to the APs, which increase the throughputs of them.

Table 6: Throughput results for *regular topology on 10 APs*.

channel assignment	OC	POC		
# of channels	2	3	6	9
min. host throu. (Mbps)	3.97	4.66	4.49	4.55
overall throu. (Mbps)	218.24	250.72	247.29	251.24

8.3 Evaluations by Experiments

Lastly, the throughput of the POC assignment is evaluated through experiments using the *two-rooms topology* in Figure 20. Two channels 3 and 11 are used for the OC assignment, and three channels 3, 7, and 11 are for the POC.

Table 7 shows the simulation and measurement results. This table indicates the following: 1) the POC assignment improves the overall throughput, and 2) the estimated throughput is well coincident with the measured one. The accuracy of the throughput estimation model and the effectiveness of the POC assignment are confirmed.

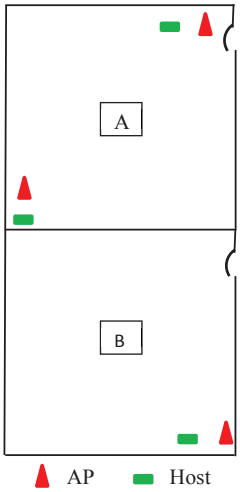

(a) Two-rooms topology

Figure 20: Two-rooms topology.

Table 7: Throughput results for *Two-room topology*.

channel assignment	OC	POC
# of channels	2	3
measurement (Mbps)	146.36	158.2
simulation (Mbps)	143.5	157.31

9 Conclusion

In this paper, we presented the *throughput drop estimation model* extension for concurrently communicating three IEEE 802.11n links under *partially overlapping channels (POCs)* and the *channel bonding*. Also, we proposed the model application to the POC assignment to the access-points in WLAN. Through extensive experiments and simulations, we confirmed the accuracy of the model and the effectiveness of the POC assignment. In future, we will upgrade this model for four or more interfering links. Then, we will evaluate it in a variety of network scenarios, such as for dense WiFi environments.

Acknowledgments

This work is partially supported by JSPS KAKENHI (16K00127).

References

[1] M. Balazinska, and P. Castro, "Characterizing mobility and network usage in a corporate wireless local-area network," in Proc. Int. Conf. Mob. Syst., pp, 303 - 316, 2003.

[2] M. Elkhodr, S. Shahrestani, and H. Cheung, "Emerging wireless technologies in the Internet of things: A comparative study," Int. J. Wirel. Mob. Netw. (IJWMN) vol. 8, no. 5, pp 67-82, Oct. 2016.

[3] A. B. Makhlouf and M. Hamdi, "Design and experimentation of rate adaptation for IEEE 802.11n WLANs," IEEE Trans. Wirel. Comm., vol. 12, no. 2, pp. 908916, Aug. 2011.

[4] S. Murthy, A. Goswami, and A. Sen, "Interference-aware multicasting in wireless mesh networks," in Proc. Networking, pp. 299-310, 2007.

[5] C. Reis, R. Mahajan, M. Rodrig, D. Wetherall, and J. Zahorjan, "Measurement-based models of delivery and interference in static wireless networks," in Proc. Conf. Appl., Tech., Arch. Proto. Comput. Comm., pp. 51-62, 2006.

[6] Supplement to IEEE standard for information technology telecommunications and information exchange between systems - local and metropolitan area networks - specific requirements. Part 11: wireless LAN medium access control (MAC) and physical layer (PHY) specifications: high-speed physical layer in the 5 GHz band, IEEE STD 802.11a-1999, 1999.

[7] IEEE Std 802.11-2012, IEEE standard for information technology-telecommunications and information exchange between systems - local and metropolitan area network - specific requirements - Part 11: wireless LAN medium access control (MAC) and physical layer (PHY) specifications, IEEE STD 802.11-2007, pp. 1184, 2007.

[8] IEEE Standards Association, `https://standards.ieee.org/standard/802_11y-2008.html`, Accessed 28 May, 2019.

[9] IEEE Standards Association, `https://standards.ieee.org/standard/802_11ad-2012.html`, Accessed 29 May, 2019.

[10] T. Nitsche, C. Cordeiro, A. B. Flores, E. W. Knightly, E. Perahia, and J. C. Widmer, "IEEE 802.11ad: Directional 60 GHz Communication for Multi-Gigabit-per-Second Wi-Fi," IEEE Comm. Magazine, vol. 52, no. 12, pp 132-141, Dec. 2014.

[11] S. Banerji, "Upcoming Standards in Wireless Local Area Networks," Wirel. Mob. Tech., vol. 1, no. 1, pp 6-11, 2013.

[12] "IEEE 802.11n - standard for wireless LAN medium access control (MAC) and physical layer (PHY): enhancements for high throughput," IEEE, Oct. 2009.

[13] T. D. Chiueh, P. Y. Tsai, and I. W. Lai, "Baseband receiver design for wireless MIMO-OFDM communications," 2nd ed., Wiley-IEEE Press, 2012.

[14] L. Deeky, E. Garcia-Villegas, E. Belding, S. J. Lee, and K. Almeroth, "Intelligent channel bonding in 802.11n WLANs," IEEE Trans. Mob. Comput., vol. 13, no. 6, pp. 1242-1255, 2014.

[15] B. Boris, C. Alessandro, Z. Alessandro, B. Jaume, "On the interactions between multiple overlapping WLANs using channel bonding," IEEE Trans. Vehi. Tech., vol. 65, no. 2, Feb. 2015.

[16] S. Bokhari and V. Zaruba, "i-POCA: interference-aware partially overlapping channel assignment in 802.11-based meshes," in Proc. IEEE WoWMoM, 2013.

[17] K. Zhou1, X. Jia, Y. Chang, and X. Tang, "Partially overlapping channel assignment for WLANs using SINR interference model," IInt. J. Comm. Syst, vol. 27, no. 11, pp. 3082-3095, March 2014.

[18] K. S. Lwin, N. Funabiki, C. Taniguchi, K. K. Zaw, M. S. A. Mamun, M. Kuribayashi, and W.-C. Kao, "A minimax approach for access point setup optimization in IEEE 802.11n wireless networks," Int. J. Netw. Comput., vol. 7, no. 2, pp. 187-207, July 2017.

[19] I. M. Kwenga, N. Funabiki, M. Kuribayashi, R. W. Sudibyo, and W.-C. Kao "A throughput estimation model under two-link concurrent communications with partially overlapping channels and its application to channel assignment in IEEE 802.11n WLAN", Int. J. Space-Base. Situ. Comput., vol. 8, no. 3, pp. 123-137, 2018.

[20] M. E. Islam, N. Funabiki, and T. Nakanishi, "An access-point aggregation approach for energy-saving wireless local area networks", IEICE Trans. Commun., vol. E96-B, no.12, pp. 2986-2997, Dec. 2013.

[21] M. E. Islam, N. Funabiki, and T. Nakanishi, "Extensions of access-point aggregation algorithm for large-scale wireless local area networks", Int. J. Netw. Comput., vol.5, no.1, pp. 200-222, Jan. 2015.

[22] A. Mishra, E. Rozner, S. Banerjee, and W. Arbaugh, "Exploiting partially overlapping channels in wireless networks: turning a peril into an advantage," in Proc. ACM Conf. Inter. Meas., pp. 311-316, 2005.

[23] M. Elwekeil, M. Alghoniemy, M. El-Khamy, H. Furukawa, and O. Muta, "Optimal channel assignment for IEEE 802.11 multi-cell WLANs," in Proc. Signal Proc. Conf., pp. 694-698, 2012.

[24] A. Mishra, V. Shrivastava, S. Banerjee, and W. Arbaugh, "Partially overlapped channels not considered harmful", in Proc. Joint Int. Conf. Meas. Model. Comp. Sys., pp. 63-74, 2006.

[25] Z. Feng and Y. Yang, "How much improvement can we get from partially overlapped channels?," in Proc. IEEE WCNC, pp. 2957-2962, April 2008.

[26] Z. Zhang, L. Song, Z. Han, and W. Saad, "Coalitional games with overlapping coalitions for interference management in small cell networks", IEEE Trans. Wireless Comm., vol. 13, no. 5, pp. 2659-2669, May, 2014.

[27] W. Zhao, H. Nishiyama, Z. Fadlullah, N. Kato, and K. Hamaguchi, "DAPA: capacity optimization in wireless networks through a combined design of density of access points and partially overlapped channel allocation", IEEE Trans. Vehi. Tech., vol. 65, no. 5, pp. 3715-3722, May 2016.

[28] S. Mukherjee and S. C. Ghosh, "Throughput improvement using partially overlapping channels in WLAN with heterogeneous clients", Wired/Wireless Inter. Comm., pp. 335-347, 2016.

[29] B. P. Tewari, and S. C. Ghosh, "Combined power control and partially overlapping channel assignment for interference mitigation in dense WLAN", in Proc. IEEE Int. Conf. Adv. Info. Netw. Appli., pp. 646-653, March 2017.

[30] G. Zhao, Q. Wang, C. Xu, and S. Yu, "Analyzing and modelling the interference impact on energy efficiency of WLANs", in Proc. IEEE Int. Conf. Comm., May 2018.

[31] Y. Su, Y. Wang, Y. Zhang, Y. Liu, and J. Yuan, "Partially overlapped channel interference measurement implementation and analysis", in Proc. IEEE Conf. Comp. Comm. Work., pp. 760-765, April 2016.

[32] H. A. Mohammad, H. Xiaoyan, A. Farhana, "Multiple radio channel assignment utilizing partially overlapped channels", in Proc. IEEE GLOBECOM conf., pp. 4737-4743, 2009.

[33] Cisco Meraki, https://documentation.meraki.com/MR/Radio_Settings/Auto_Channel, Accessed 30 May, 2019.

[34] Fujitsu corporation https://www.fujitsu.com/global/about/resources/news/press-releases2015/0909-01.html, Accessed 30 May 2019.

[35] Buffalo corporation, http://buffalo.jp/download/manual/html/air1200/router/whrg300n/chapter118.html, Accessed 30 May 2019.

[36] Vodafone corporation, http://www.vodafone.co.uk/cs/groups/public/documents/contentdocuments/vfcon090503.pdf, Accessed 30 May 2019.

[37] Google WiFi, https://support.google.com/wifi/thread/412017?hl=en Accessed 30 May 2019.

[38] C. Newport, D. Kotz, Y. Yuan, R. S. Gray, J. Liu, and C. Elliott, "Experimental evaluation of wireless simulation assumption," J. Simu., vol. 83, no. 9, pp. 643-661, Sept. 2007.

[39] J. Padhye, S. Agarwal, V. N. Padmanabhan, L. Qiu, A. Rao, and B. Zill, "Estimation of link-interference in static multi-hop wireless networks," in Proc. ACM IMC, pp. 28, Oct. 2005.

[40] M. S. A. Mamun, N. Funabiki, M. E. Islam, M. Kuribayashi and I-W. Lai, "An active access-point configuration algorithm for elastic wireless local-area network system using heterogeneous devices," Int. J. Netw. Comput., vol. 6, no. 2, pp. 395-419, 2016.

[41] D. B. Faria, "Modeling signal attenuation in IEEE 802.11 wireless LANs," Tech. Report, TRKP06-0118, Stanford Univ., July 2005.

[42] iPerf - TCP, UDP and SCTP network bandwidth measurement tool, https://iperf.fr/, Accessed 29 Dec. 2017.

[43] Homedale: Wi-Fi / WLAN Monitor (2017, Dec.), http://www.the-sz.com/products/homedale/.

[44] L. B. Jiang and S. C. Liew, Improving throughput and fairness by reducing exposed and hidden nodes in 802.11 networks, IEEE Trans. Mob. Comput., vol. 7, no. 1, pp. 34-49, Jan. 2008.

[45] M. S. A. Mamun, N. Funabiki, K. S. Lwin, M. E. Islam, and W.-C. Kao, "A channel assignment extension of active access-point configuration algorithm for elastic WLAN system and its implementation using Raspberry Pi," Int. J. Netw. Comput., vol. 7, no. 2, pp. 248-270, July 2017.

[46] N. Funabiki, ed., "Wireless mesh networks," InTech-Open Access Pub., Jan. 2011. http://www.intechopen.com/books/wireless-mesh-networks, Accessed 20 Jan., 2017.

ASTES

Advances in Science, Technology and Engineering Systems Journal Vol. 4, No. 4, 106-114 (2019)

www.astesj.com

ASTESJ

ISSN: 2415-6698

Exploring of The Employee Information Management System using HOT-Fit and UTAUT2 Model

Angelina Pramana Thenata, Suyoto*, Albertus Joko Santoso

Universitas Atma Jaya Yogyakarta, Yogyakarta, 55281, Indonesia

ARTICLE INFO

Article history:
Received:03 May, 2019
Accepted:04 July, 2019
Online: 13 July, 2019

Keywords:
HOT-Fit
UTAUT2
Information System
GeSCA

ABSTRACT

Information Systems are a combination of information technology and activities of people who use these technologies to support operations, management, data, and technology. Based on Indonesian Minister of Home Affairs Decree No. 17 of 2000, the Regional Office of the Ministry of Law and Human Rights of West Sulawesi implements the Employee Management Information System (SIMPEG) which functions to process data, information and employee management. Acceptance of information system users determines whether the information system is successful or failed. Thus, this study proposes an integrated model between HOT-Fit and UTAUT2 models to identify behaviours and factors that influence system user acceptance. The online survey was conducted among SIMPEG users as many as 311 respondents consisting of 69.1% men and 30.9% women with an age group dominated by 26-35 years as many as 44.1% to test hypotheses based on an integrated model using GeSCA. The results of the study prove (1) human factors with the moderation of gender and organisation have a significant influence on behavioural intention; (2) behavioural intention has a significant influence on user satisfaction; (3) human, technology and organisational factors have a relationship of compatibility with each other. Besides, the results showed that the integrated model between HOT-Fit and UTAUT2 had GFI (0.995) and SRMR (0.079) which indicated an acceptable model fit. The results of the study support the importance of human and organizational involvement to achieve success acceptance of technology adoption in the government.

1. Introduction

Current technological advances have been widely used in various environments, especially the government in Indonesia. One of the technologies utilised is the Employee Management Information System that has been set in the Decree of the Minister of Home Affairs No. 17 of 2000. Article 1 in the Decree states that the Employee Management Information System, hereinafter abbreviated as SIMPEG, is an integrated totality consisting of processing devices including collectors, procedures, processing employee and software; storage devices include data centres and data banks as well as communication devices that are interrelated, interdependent and mutually determine in order to provide information in the field of employee [1].

Therefore, the Regional Office of the Ministry of Law and Human Rights (Kanwil Kemenkumham) of West Sulawesi applies SIMPEG which is used to process data, information, and management as well as employee administration so that it can support employee performance and can simplify the staff administration process [2].

SIMPEG has been developed web-based with fast installation and implementation, and structurally SIMPEG was developed with a modular method so that it can be adapted to user needs in a short time. The implementation of SIMPEG is the realisation of a management information system that integrates into a computer network that is capable of producing quality information to support employee management decision-making in the agency environment. However, to achieve a system that can contribute to organisational performance, employees must be able to use the system effectively and correctly [3], so that the successes and failures of the systems used to depend heavily on user acceptance of the system [4]. The adoption of new systems is the lack of training using Information Communication Technology (ICT), the quality of the technology itself, and organisational support [5]. Therefore, this study aims to identify behaviour and factors that

* Suyoto, Universitas Atma Jaya Yogyakarta, Yogyakarta, Indonesia.
Email: suyoto@uajy.ac.id

influence user acceptance of employee management information systems by using an integrated model between HOT-Fit and UTAUT2 models.

The integration of the two models is the HOT-Fit Model from Yusof et al. (2006) [6], and the UTAUT2 model from V.Venkatesh et al. (2012) [7] were conducted to check the use of SIMPEG. The proposed integrated model contributes to the literature review because there is no recent research on the integration of HOT-Fit and UTAUT2 in one model to identify behaviour and factors that influence the acceptance of employee management information systems from a human, technology and organisation perspective. Furthermore, this study analyses the data using the GeSCA, which is a model of the structural equation model (SEM) [8].

2. Literature Review

Evaluation of information systems is crucial to find out whether information systems fail or succeed. Evaluation of this system has been carried out in various fields, such as health by Jiunn-Woei Lian, David C. Yen, Yen-Ting Wang (2013) investigated important aspects that had an influence in making decisions to adopt cloud computing in the Taiwan hospital industry using the TOE (Technology-Organization-Environment) framework and combined with HOT-fit model (Human-Organization-Technology fit) [9]. Furthermore, Noor Azizah K. S. Mohamadali and Jonathan M. Garibaldi (2010) proposed an integrated evaluation model namely UTAUT, DeLone and McLean, TTF to evaluate user responses to software technology in the health sector [10]. Then, Lourent Monalizabeth E., Ahmad Holil NA, Anisah Herdiyanti (2015) who conducted research to evaluate the EMR system used in hospitals using the HOT-Fit model and this study is useful to help understand aspects interrelated aspects between humans, organisations, and technology [11]. In the field of finance, Abdullah M. Baabdullah, Ali Abdallah Alalwan, Nripendra P. Rana, Hatice Kizgin, Pushp Patil (2019) conducted research to combine UTAUT2 and D & M to understand what aspects can influence mobile banking, and how to use the system can contribute both to customer satisfaction and loyalty [12].

Based on previous research, the HOT-Fit model is useful for identifying interrelated aspects between humans, environment, organisation, and technology. UTAUT2 is useful for identifying only responses from users regarding the use of information systems. The UTAUT2 model can also be integrated with other evaluation models to find out the correlation between responses from users and other aspects related to system user acceptance. The integration model will produce a more effective evaluation of information systems so that this study proposes an integrated model between HOT-Fit and UTAUT2 models that are tailored to the case of information system evaluation to be studied to identify behaviours and factors that affect user acceptance of the Employee Management system Information System (SIMPEG).

3. Proposed Integrated Model and Hypothesis Development

Mohamadali and Garibaldi's research (2010) proposed an integrated evaluation model by combining three IS evaluation models, namely DeLone and McLean (D & M) models, UTAUT models and TTF models. The D & M model that has been developed into a HOT-Fit Model uses the term intention to use or use while the UTAUT2 model uses the term behavioural intention or use. The term is almost the same in describing the dimensions of dependent factors, namely the intention to use a system. However, each model has different independent factors, such as the HOT-Fit Model has human factors, technology organizations affect the use of the system, and the UTAUT2 Model has seven main factors in the form of human factors namely performance expectancy, effort expectancy, social influences, hedonic motivations, price value, and habits affect the behaviour of system usage.

Conformity between human, technological, and organisational factors influences IS successes and failures [4]. However, the UTAUT2 model only examines the relationship of the influence of human factors on system use and has not examined the relationship between technological and organisational factors on system usage. Whereas HOT-Fit has examined the relationship of human, technological, and organisational factors in the use of the system, but this model has not elaborated further the effect of the relationship of the human factor dimension to IS use.

Based on the strengths and weaknesses of the HOT-Fit and UTAUT2 models, independent factors in the two models are combined to produce integrated models that provide a better representation of the determinants of IS use. The integrated model between HOT-Fit and UTAUT2 with modifications that are adjusted to government characteristics can be seen in Figure 1.

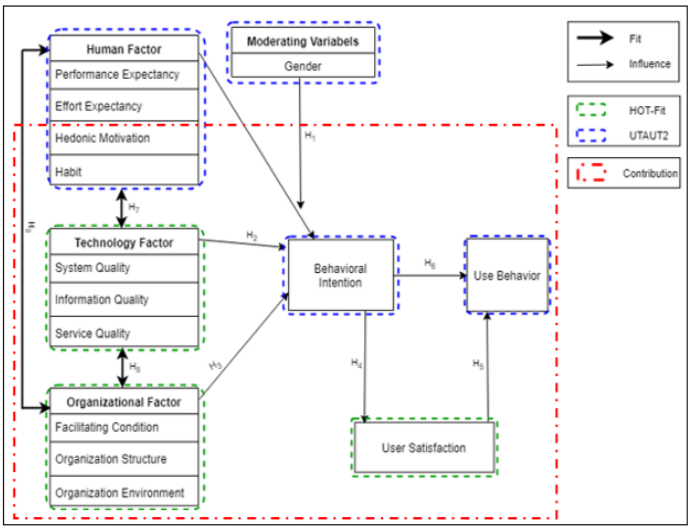

Figure 1. Proposed Integrated Model

3.1. Human

Human is an important factor in the development and application of IS. This study has human factors consisting of several variables explored in Table 2. Social influence variables and price value are not included in human factors because they are adjusted to the characteristics of the government scope that implements all employees must use SIMPEG without any costs to be spent by employees in using the system.

For the effects of gender, previous research shows that gender differences in completing tasks affect performance expectations [15]. Also, efforts were found to be more prominent in women

than men [16] whereas previous studies have found that men are more schematic in processing information and relevant details tend to be ignored, while women tend to be piecemeal and detail in processing information so that it will weaken the effects of habits on intention or behaviour [17].

Table 2. Definition of Variable Human Factors

Variables Human Factor	
Performance Expectancy (PE)	The extent to which people believe using SIMPEG will provide increased performance in their work [13].
Effort Expectancy (EE)	The level of ease experienced by users when using SIMPEG [13].
Hedonic Motivation (HM)	The extent to which people get pleasure from using technology [14].
Habit (HT)	The extent to which the tendency to conduct causal behaviour is a recurring action in using SIMPEG [14].

Furthermore, it is found that consumer technological innovation is related to gender differences [18]. Using new technology at an early stage, men tend to trace innovation and novelty [19]. In turn, this tendency will increase hedonic motivation in the initial decisions on the use of technology in men. Thus, this study proposes:

H_1. Human factors influence the behavioural intention to use the system with gender moderation

3.2. Technology

An information system is one technology that can simplify the process of human work. A good information system is assessed in terms of the quality of information, systems, and services that this research explored in Table 3 [20].

Table 3. Definition of Variable Technology Factors

Variable Technology Factors	
System Quality (SQ)	Measuring SIMPEG quality related interfaces, response time, system integration, and system security.
Information Quality (IQ)	The quality of SIMPEG information is measured by the accuracy, relevance, completeness, and accuracy of the information produced.
Service Quality (SQ)	Refer to SIMPEG manager support in providing assistance services and speed in responding to complaints/problems that occur.

Technology has a close relationship with humans because humans as users are in direct contact with the system. Several factors that influence decision making using a new system are benefits, namely that users are confident that their performance will improve with this system. Thus, this study proposes:

H_2. Technology factor influences the behavioural intention to use the system
H_7. There is a relationship of fit between human and technology factors

3.3. Organisational

Organisations are a group of people formally along with inseparable sources to achieve management goals and need to pay attention to their policies. This study has organisational factors consisting of several variables explored in Table 4.

Table 4. Definition of Variable Organizational Factors

Variable Organizational Factors	
Facilitating Condition (FC)	The extent to which people believe that resources, facilities and infrastructure, training, and assistance facilities are available to support users in using SIMPEG [21].
Organisation Structure (OS)	The extent to which people believe that the organisation has carried out a strategy and plan for SIMPEG implementation [22].
Organisation Environment (OE)	The extent to which people believe that organisations have provided full support for SIMPEG implementation [22].

Organisational and human factors have an important role in developing and implementing SI. Besides, harmony between humans and organisations is needed to ensure the success of SI implementation by harmonising user needs, management, and work routines as the introduction of systems in complex ways affecting different dimensions of fit [23]. Furthermore, organisational suitability (goals, structures, and processes) and technology are important starting points in the implementation of SI because it is one of the strategies that can affect organisational performance [24]. Based on this, this study proposes:

H_3. Organisational factors influence the behavioural intention to use the system
H_8. There is a relationship of fit between technology and organisational factors
H_9. There is a relationship of fit between organisational and human factors

3.4. User Satisfaction, Behavioral Intention, and Use Behavior

User Satisfaction (US), namely, feedback and response from users who have used the system [6]. The attitude of users towards information systems is a subjective criterion of how users like the system used. According to DeLone and McLean (2003), user satisfaction can be seen from the whole system of information presented [20]. In general, user satisfaction as a result of a comparison between expectations or needs of information systems with received system performance and benefits in the system input-output process that can affect user behaviour. Also, behavioural intention affects the use of using SIMPEG. Thus, this study proposes:

H_4. Behavioural factor intention influences user satisfaction
H_5. User satisfaction influences use behaviour
H_6. Behavioural intention influences use behaviour

4. Methodology

This research collects data using online surveys because it is by the conditions of the Indonesian people who mostly have internet access. Easy validation facilities provided online surveys to ensure respondents resolved all questions without error [25]. The collected data is validated and used for data analysis, with a 100% response rate. The sample of this study was 311 respondents who were employees of the Kemenkumham Region of West Sulawesi and were randomly selected. There are two parts to this questionnaire. The first part consists of questions related to information on respondents' characteristics, which can be seen in Table 5. Furthermore, the second part consists of 28 questions representing measurement items in an integrated model between the UTAUT2 and HOT-Fit models (see Appendix A) using a 4 Likert scale.

Table 5. Characteristics of Respondents

Characteristics		Frequency	Percent(%)
Gender	Men	215	69.1
	Women	96	30.9
Age	18 – 25	82	26.4
	26 – 35	137	44.1
	36 - 45	43	13.8
	Above 45	49	15.8

Table 5 shows the respondents collected in this study consisted of 69.1% men and 30.9% of women with age 18-25 (26.4%), 26-35 (44.1%), 36 - 45 (13.8%) and over 45 years old around 15.8%. Furthermore, the data obtained will be analyzed using the Structure Equation Model (SEM) model in the form of a Generalized Structured Component Analysis (GeSCA). GeSCA was chosen because it can analyse the combined approach of factor analysis, structural models and path analysis together and can do three activities at once, namely testing reliability, testing between variables and testing the model used [16].

5. Result and Discussion

Two stages of SEM were applied in this study, namely the measurement model to measure the level of fit of the model adequately and to test the reliability and validity of latent constructs through confirmatory factor analysis. Then the structural model is tested to verify the integrated model related to the hypothesis in this study.

5.1. Measurement Model

5.1.1. Overall Goodness of Fit

The overall size of the fit model is carried out before the structural model stage, including FIT, AFIT, GFI, SRM, and NPAR [8].

- FIT indicates the total variance that can be explained from all variables for model specifications. The FIT value ranges from 0 to 1. The FIT value recommended is ≥ 0.5. The higher the FIT value indicates, the greater the variance of the variable can be explained from the model specifications.
- Adjusted FIT (AFIT) is similar to FIT but takes into account the complexity of the model. The more AFIT values close to FIT values can be said to support the conclusion of FIT. The AFIT value can be calculated based on the FIT value using the following formula.
- The goodness of FIT Indices (GFI) and Standardized Root Mean Square Residual (SRMR) are fit criteria that indicate the difference between sample covariances and covariances generated from the estimated GeSCA parameters. The GFI value approaches 1, and the SRMR value close to 0 can be considered an indication of compatibility. The recommended GFI value for fit model size is> 0.90, and the recommended SRMR value for fit model size is ≤ 0.80.
- The number of Free Parameters (NPAR) is the sum of free parameter estimates, weights, loading and path coefficients.

The overall results of the measurement of the integrated model used in this study can be seen in Table 6. The FIT value is obtained at 0.609 or 60.9%, which indicates that the model can explain the total variance of all the variables in this study. Besides, the AFIT value is obtained at 0.609, which indicates that the AFIT value is close to the FIT value; it can be said to support the conclusion of the FIT. From the results of FIT and AFIT, it can be concluded that performance expectancy, effort expectancy, hedonic motivation, habit, system quality, information quality, service quality, organisation structure, organisation environment, behavioural intention, user authentication, and user behaviour can determine research models. Then the GFI value of 0.995 indicates that the model is feasible because it approaches the value 1. The SRMR value of 0.066 approaches the value of 0, indicating a good fit. The NPAR value shows the estimated number of free parameters of 60. The result means that the proposed integrated model is compatible with this study.

Table 6. Measurement Model

Model Fit	
FIT	0.609
AFIT	0.607
GFI	0.995
SRMR	0.066
NPAR	60

5.1.2. Test Validity and Reliability

Before going further in the analysis of structural models, it is necessary to test the reliability of construction and validity. Table 7 describes the value of loading factors, average variance extracted (AVE) and composite reliability (CR). Convergent validity recommendation value is >0.7 [26]. Therefore, UB1 was dropped. Besides the value of the loading factor of other construct items is more than 0.7, it can be said that all indicators in the model have met the convergent recommendation for validity> 0.7. Likewise, the AVE value of all arranged variables is between 0.605 - 0.937 so that it can be said that the AVE values of all the variables in the model meet good discriminant validity which is >0.50 and show that more than 50% of the variance of the indicators can be explained [27]. The CR was considered in this study. Latent variables can be said to be reliable if they have a value of CR> 0.70 [27]. All latent variables have a CR value above 0.70. Based on the results of the analysis obtained it can be

concluded that all variables are valid and reliable because they have met the requirements of a good model.

Table 7. Loading Factor, AVE, CR

Factor	Item	Loading Factor	AVE	CR
Human	PE1	0.807	0.628	0.931
	PE2	0.753		
	EE1	0.804		
	EE2	0.798		
	HM1	0.796		
	HM2	0.846		
	HT1	0.779		
	HT2	0.757		
Technology	SQ1	0.795	0.605	0.902
	SQ2	0.766		
	IQ1	0.809		
	IQ2	0.796		
	SEQ1	0.761		
	SEQ2	0.735		
Organizational	FC1	0.774	0.605	0.902
	FC2	0.767		
	OS1	0.723		
	OS2	0.823		
	OE1	0.781		
	OE2	0.797		
Behavioral Intention	BI1	0.820	0.804	0.925
	BI2	0.925		
	BI3	0.941		
User Satisfaction	US1	0.969	0.937	0.967
	US2	0.967		
Use Behavior	UB1	-0.874	Dropped	
	UB2	0.792	0.692	0.817
	UB3	0.868		

Table 8. Overview of Structural Models

Path	Estimate	CR
Human → Behavioral Intention	0.796	32.64*
Technology → Behavioral Intention	0.094	0.94
Organizational → Behavioral Intention	0.460	5.67*
Behavioral Intention → User Satisfaction	0.604	13.3*
User Satisfaction → Use Behavior	-0.128	2.09*
Behavioral Intention → Use Behavior	-0.319	4.14*

Table 9. Analysis of the impact of moderating variable gender

Path	Gender			
	Men		Women	
	Estimate	CR	Estimate	CR
Human → Behavioral Intention	0.633	14.24*	0.676	12.95*

5.2. *Structural Model and Testing Hypothesis*

The structural model analysis was conducted to determine the effect between variables hypothesised by this study. Also, testing using GeSCA can show hypotheses that are accepted or rejected. The hypothesis is accepted if it has a positive relationship that can be seen from the estimated and significant values which can be seen from the value of CR> 1.96 marked by a sign (*) [28]. The analysis of the moderating variable is done using a multigroup approach at GeSCA. The results of the analysis of structural models can be seen in Table 8 and an analysis of the impact of the moderating variables in this study is described in Table 9.

Table 8 shows the results of the structural model test. Organizational factors (Estimate = 0.460, CR = 5.67*) are known to have a positive and significant effect on behavioral intention while technological factors (Estimate = 0.094, CR = 0.94) have a positive effect on behavioral intention but are not significant. Then, it is known that behavioural intention has a positive and significant effect on user satisfaction (Estimate = 0.604, CR = 13.3*). However, behavioral intention (Estimate = -0.319, CR = 4.14 *) and user satisfaction (Estimate = -0.128, CR = 2.09*) does not have a significant effect on use behavior.Also, Table 9 shows an analysis of human factors with moderating gender variables. The results of the analysis show that human factors with gender men and women moderation have a positive and significant effect on behavioural intention. Furthermore, a correlation test is carried out to determine whether there is a relationship between human, technological and organisational compatibility can be seen in Table 10.

Table 10. Relationship of Human, Technology, and Organization Factors

Relationship		Correlation Value of Latent Variables
Human	Technology	0.796
Technology	Organisational	0.758
Organisational	Human	0.736

Table 11. Summary of the Hypothesis

Hypothesis		Remarks
H_1.	Human factors influence the behavioural intention to use the system with gender moderation	Yes
H_2.	Technological factors influence the behavioural intention to use the system	No
H_3.	Organisational factors influence the behavioural intention to use the system	Yes
H_4.	Behavioural factor intention influences user satisfaction	Yes
H_5.	User satisfaction influences use behaviour	No
H_6.	Behavioural intention influences use behaviour	No
H_7.	There is a relationship of fit between human and technology factors	Yes
H_8.	There is a relationship of fit between technology and organisational factors	Yes
H_9.	There is a relationship of fit between organisational and human factors	Yes

Table 10 shows the test results with the fit between human, technology and organisation factors that have a correlation value>

0.05, so the hypothesis is accepted [29]. Human factors with technology (0.782), factor technology with the organisation (0.758) and factors with human organisations (0.736) are known to have conformity relationships. These results indicate that there are nine hypotheses in this study consisting of 6 accepted hypotheses and 3 rejected hypotheses which can be seen in Table 11 and the overall summary of the results of the research model can be seen in Figure 2.

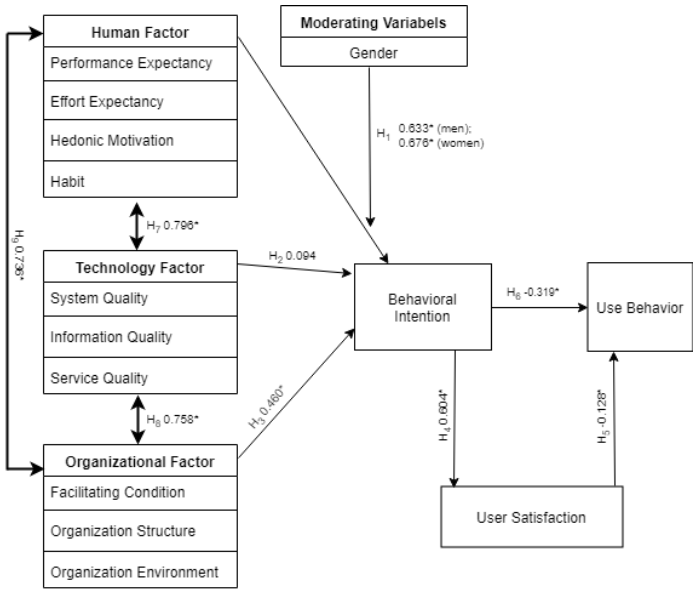

Figure 2. Summary of the results of the research model

According to the results of the analysis, human factors have a positive and significant effect on the behavioural intention with gender moderation (H_1). In the female sex, the effect is stronger in influencing behaviour intentions using SIMPEG than men. The results of this study support previous research, which states that gender differences are associated with difficulties in allocating attention to information at work so that it will affect intention or behaviour using the system [7,30].

Technological factors were found to have a positive effect on behavioural intention (H_2) but were not significant. The quality of the system, information, and services of a good system will have a strong influence on the intention to use the system [31]. However, in this case when the employee as a user accesses SIMPEG it is found that the quality of information produced is less accurate and relevant to the information needed by employees and the quality of service is not quick to deal with problems related to errors in the field that weaken the technological relationship with intention to use.

Organisational factors have a positive and significant effect on behavioural intention (H_3). This result is by previous studies conducted by Frendy and Holzmann [32,33]. Organizationally, the West Sulawesi Regional Office of Kemenkumham has provided support and implemented appropriate strategies based on the organisational environment to influence behavioural intentions using SIMPEG.

Behavioral intention has a positive and significant effect on user satisfaction (H_4). Yusof et al. said user satisfaction is an overall assessment of user experience in using information systems and their potential impact [6]. Increasing user satisfaction requires an effort to increase the intention to use SIMPEG. Increasing the intention to use SIMPEG can be done by increasing proven human, technological and organisational factors (H_1-H_3) having a positive effect on behavioural intentions using SIMPEG.

User satisfaction and behavioural intention to use the system have a negative and insignificant relationship to system usage behaviour (H_5-H_6). User satisfaction and interest in using information systems refer to the results of system performance received and benefits in the process of input-output systems that affect individual decisions to use or not use the system in completing a series of tasks. While in this case it was found that the system was less accurate and relevant to the information needed by employees and was not quick to deal with problems related to errors giving a negative relationship to the behaviour of using the system.

Furthermore, the results of the analysis of the correlation value in the 7th hypothesis correlate> 0.05 so that it can be said that human factors have a relationship of conformity with technology. The result can be explained from humans as users who come in direct contact with the system have several things that influence the decision making to use the system, namely users believe that their performance will increase with the use of systems and systems easy to use with the complete user guide. Also, users with certain information technology (IT) skills are not sufficient requirements for system use or acceptance, but their skills in using IT must be by the requirements of the system itself. The result shows the need for 'conformity' between humans and technology. The system failure can occur due to several causes, namely system failure, technical failure including hardware, software and communication errors. Also, usability failure is at the technical level when the system does not match the tasks needed in the organisation; failure as desired when the situation is technically correct and according to specific needs but the system is unsuccessful because the user does not approve it or rejected by them. Finally, it will result in a system rejecting behaviour if it is 'fit' between users or humans and low technology [34].

Meanwhile, this study also found that technological factors have a relationship with an organisation (H_8). These results support previous studies by Yusof and Mohamadali [22,23]. Yusof stated that the lack of compatibility between the main organisational elements contributed to a large number of system failures that needed support from the organisation. One form of this suitability, namely strategy, planning and support from the organisation in implementing SIMPEG can be a budget for facilities and infrastructure. The selection of SI needs to support the strategy and goals of the organisation. Each system needs to be aligned with organisational settings. The system shows the need for 'fit' between technology and organisation. Also, evaluation of information systems not only discusses how well the system works but also needs to discuss how well a system works in certain settings with certain users and further what functions the system itself and why the system works like that [35]. The clearly shows the need to evaluate technology together with organisations, as well as humans who use the system, namely conformity with the factors that influence acceptance. One thing

that can be done to improve the performance and productivity of employees is to increase voting, information technology infrastructure that supports the implementation of the SIMPEG.

Then, the results of the analysis in this study found that human factors have a relationship of conformity with the organisation (H_9). Organisations are a group of people formally along with inseparable sources to achieve management goals and need to pay attention to policy. One form of this suitability is, for example, if certain individuals or users do not have the skills to use the system, organisational management is responsible for providing the necessary training [22,36]. To achieve a management information system (MIS), that is successful and has a positive impact on the organisation, and the information system must first have an impact on the individual. The MIS will ultimately affect users to accept technology so that it can improve the performance and productivity of employees.

6. Conclusion and Future Research

This study used 311 respondents with men (69.1%) and women (30.9%) to test the factors that influence SIMPEG user acceptance and identify user behaviour. To achieve this goal, the researchers propose an integrated model based on HOT-Fit and UTAUT2 that has a Goodness of Fit Index (GFI) of 0.995 and a Standardized Root Mean Square Residual (SRMR) of 0.079 indicating the model is compatible with this study. Based on the results of the analysis and discussion concluded from the nine hypotheses proposed, there are six hypotheses accepted, and three hypotheses rejected, among others:

- Human factors with the moderation of gender, technology, and organisation have a positive and significant effect on behavioural intention. While technology has a positive effect on behavioural intention but is not significant.
- The behavioural intention has a significant effect on user satisfaction.
- Behavioural intention and user satisfaction do not have a significant effect on user behaviour. It can occur because the system is less accurate and relevant to the information needed by employees and is not quick to deal with problems related to errors that weaken the relationship to behaviour to use the system.
- Humans and technology are compatible, technology and organisations, as well as organisations and humans in the adoption of information systems.

Future research will expand research into other fields (for example education, health, and media) which include human factor variables with age and experience moderation, and other variables such as social influence and price value. Finally, the new integration between the HOT-Fit and UTAUT2 models is a contribution to the current information system literature and provides an understanding of the importance of technology and the involvement of humans and organisations to achieve successful acceptance of the technology itself.

References

[1] Menteri Dalam Negeri Republik Indonesia, "Keputusan Menteri Dalam Negeri Nomor: 17 Tahun 2000" Indonesia, 2000.

[2] Kementerian Hukum dan Hak Asasi Manusia, "Peraturan Menteri Hukum dan Hak Asasi Manusia Republik Indonesia Nomor 10 Tahun 2016" Indonesia, 2016.

[3] Suryanto, T. L. M., Setyohadi, D. B., & Faroqi, A, "Analysis of the effect of information system quality to intention to reuse of employee management information system (Simpeg) based on information systems success model", MATEC Web of Conferences, EDP Sciences, 58, 2016.

[4] Laudon KC, Laudon JP, "Management Information Systems: Organization and Technology in The Networked Enterprise" 6th ed., USA: Prentice-Hall, 2000.

[5] Setyohadi, D. B., & Purnawati, N. W, "An investigation of external factors for technological acceptance model of nurses in Indonesia", IOP Conference Series: Materials Science and Engineering 403(1), IOP Publishing, 2018.

[6] Yusof MM, Paul RJ, Stergioulas LK, "Towards a Framework for Health Information Systems Evaluation" Proceedings of the 39th Hawaii International Conference on System Sciences, 1–10, 2006.

[7] Venkatesh V, Morris MG, Davis GB, Davis FD, "Consumer Acceptance and Use of Information Technology: Extending the Unified Theoryof Acceptance and Use of Technology" Management Information Systems Research Center, 27(3), 425–78, 2012.

[8] Hwang H, Takane Y, "Generalized Structured Component Analysis, Psychometrika" 81–99, 2004.

[9] Lian J, Yen DC, Wang Y, "An exploratory study to understand the critical factors affecting the decision to adopt cloud computing in Taiwan hospital" International Journal of Information Management 34(1), 28–36, 2014, Available from: http://dx.doi.org/10.1016/j.ijinfomgt.2013.09.004

[10] Mohamadali NAKS, Garibaldi JM, "A Novel Evaluation Model of User Acceptance of Software Technology in Healthcare Sector" Journal of Management Information Systems, 392–7, 2010.

[11] Erlirianto LM, Holil A, Ali N, Herdiyanti A, "The Implementation of the Human , Organization , and Technology – Fit (HOT – Fit) Framework to evaluate the Electronic Medical Record (EMR) System in a Hospital" Procedia - Procedia Computer Science, 72, 580–7, 2015, Available from: http://dx.doi.org/10.1016/j.procs.2015.12.166

[12] Baabdullah AM, Abdallah A, Rana NP, Kizgin H, "Consumer use of mobile banking (M-Banking) in Saudi Arabia: Towards an integrated model" International Journal of Information Management, 44, 38–52, 2019" Available from: https://doi.org/10.1016/j.ijinfomgt.2018.09.002

[13] E. Yumami, D. Setyohadi, Suyoto, "Factors Influencing the Adoption of E-Tilang Empirical Evidence from the UTAUT Model" Journal on Computing, 3(1), 23-32, 2018.

[14] Abdallah A, Dwivedi YK, Rana NP, Algharabat R, "Examining factors influencing Jordanian customers' intentions and adoption of internet banking: Extending UTAUT2 with risk" Journal of Retailing and Consumer Services, 40, 125–38, 2018, Available from: http://dx.doi.org/10.1016/j.jretconser.2017.08.026

[15] Venkatesh V, Morris MG, Davis GB, Davis FD, "User Acceptance of Information Technology: Toward a Unified View" Management Information Systems Research Center, 27(3), 425–78, 2003.

[16] Venkatesh V, Morris MG, Ackerman PL, "A Longitudinal Field Investigation of Gender Differences in Individual Technology Adoption Decision-Making Processes, Organizational Behavior and Human Decision Processes" 83(1), 33–60, 2000.

[17] Meyers-Levy J, Maheswaran D, "Exploring Dif- ferences in Males' and Females' Processing Strategy" Journal of Consumer Research, 18(1), 63–70, 1991.

[18] Lee H, Cho HJ, Xu W, Fairhurst "A, The Influence of Consumer Traits and Demographics on Intention to Use Retail Self-Service Checkouts" Marketing Intelligence & Planning, 28(1), 46–58, 2010.

[19] Chau PY., Hui KL, "Identifying Early Adopters of New IT Products: A Case of Windows 95" Information & Management, 33(5), 225–30, 1998.

[20] Delone WH, Mclean ER, "The DeLone and McLean Model of Information Systems Success: A Ten-Year Update" Journal of Management Information Systems, 37–41, 2014.

[21] Ukut IT, Krairit D, "Justifying students' performance: A comparative study of both ICT students' and instructors' perspective" Interactive Technology and Smart Education, 16(1), 18–35, 2019.

[22] Yusof MM, Kuldis J, A. Papazafeiropoulou, Stergioulas LK, "An Evaluation Framework for Health Information Systems: Human, Organization, and Technology-Fit Factors (HOT Fit)" International Journal of Medical Informatics, 77, 386–98, 2008.

[23] Mohamadali NAKS, Garibaldi JM, "Understanding and Addressing The "Fit" Between User, Technology and Organization Evaluating User Acceptance Of Healthcare Technology" International Conference on Health Informatics, 119–24, 2012.

[24] Alharbi F, Atkins A, Stanier C, "Understanding the determinants of Cloud Computing adoption in Saudi healthcare organisations" Complex & Intelligent Systems, 2(3), 155–71, 2016.

[25] Creswell J, "Research Design: Qualitative, Quantitative, and Mixed Method Approach" 4th ed., California: Sage, 2014.

[26] Fornell C, Larcker DF, "Evaluating Structural Equation Models with Unobservable Variables and Measurement Error" Journal of Marketing Research, 18(1), 39–50, 1981.

[27] Garson GD, "Testing Statistical Assumptions" Asheboro: Statistical Associates Publishing, 2012.

[28] Henseler J, "On the Strength of-Fit Statistic of Generalized Structured Component Analysis" 2011.

[29] Hwang H, Moon-Ho RH, Lee J, "Generalized Structured Component Analysis with Latent Interactions" Psychometrika, 75(2), 228–42, 2010.

[30] de Vaus D, "Analyzing Social Science Data" London: Thousand Oaks; 2002.

[31] Lynott PP, McCandless NJ, "The Impact of Age vs. Life Experiences on the Gender Role Attitudes of Women in Different Cohorts" Journal of Women and Aging, 12(2) 5–21, 2000.

[32] Liu G, Huang S, Zhu X, "User acceptance of Internet banking in an uncertain and risky environment" Internasional Conference on Risk Management & Engineering Management, 381–6, 2008.

[33] Rumambi FR, Santoso AJ, Setyohadi DB, "Identification of Factors Influencing the Success of Hospital Information System (SIRS) by Hot-Fit Model 2006: A Case Study of RSUD Dr Samratulangi Tondano, Minahasa Regency, North Sulawesi, 2017" International Conference on Soft Computing, Intelligent System and Information Technology (ICSIIT), 202–7, 2017, Available from: http://ieeexplore.ieee.org/document/8262568/

[34] Holzmann P, Schwarz EJ, Audretsch DB, "Understanding the determinants of novel technology adoption among teachers: the case of 3D printing" The Journal of Technology Transfer, 2018, Available from: https://doi.org/10.1007/s10961-018-9693-1

[35] Tsiknakis M, Kouroubali A, "Organizational factors affecting successful adoption of innovative ehealth services: A case study employing the FITT framework" International Journal of Medical Informatics, 1–13, 2008.

[36] Kaplan B, Shaw N, "Future Directions in Evaluation Research: People, Organizational and Social Issues" Methods Inf Med, 43, 215–231, 2004.

[37] Hsiao J, Chen R, "Critical factors influencing physicians ' intention to use computerized clinical practice guidelines: an integrative model of activity theory and the technology acceptance model" BMC Medical Informatics and Decision Making, 1–15, 2016, Available from: http://dx.doi.org/10.1186/s12911-016-0241-3

Appendix A. Questionnaire

Factor	Items	Question	Sources
Human	PE1	I feel New SIMPEG is easy to use	Venkatesh et al. (2012)
	PE2	Using SIMPEG New can help me get things done quickly	
	EE1	I easily learn how to use SIMPEG New	
	EE2	It's easy to master how to use SIMPEG New	
	HM1	I feel that using SIMPEG New is fun	
	HM2	I enjoy using SIMPEG New	
	HT1	The use of New SIMPEG has become a habit for me	
	HT2	I have to use SIMPEG New	
Technology	SQ1	The New SIMPEG process does not require a long time	Yusof et al. (2006)
	SQ2	SIMPEG New has high security regarding data integration	
	IQ1	The application of the New SIMPEG reduces the errors in the staff data management process	
	IQ2	The application of SIMPEG New creates accurate information and staffing	
	SEQ1	There is a guide to using SIMPEG New	
	SEQ2	I get help quickly when an error occurs	
Organisational	FC1	Regional Office of Kemenkumham West Sulawesi has the tools needed to use SIMPEG New	
	FC2	SIMPEG New is compatible with the technology that I use	
	OS1	The application of New SIMPEG is the Kemenkumham strategy for	

Factor	Items	Question	Sources
		performance improvement	
	OS2	The implementation of New SIMPEG has been well planned by the Ministry of Law and Human Rights	
	OE1	SIMPEG New has adequate financial support in providing the hardware needed from the Ministry of Law and Human Rights	
	OE2	All agencies of the West Sulawesi Kemenkumham Regional Office support and assist in the implementation of New SIMPEG	
Behavioural Intention	BI1	I intend to use New SIMPEG in the future	Venkatesh et al. (2012)
	BI2	I will always try to use SIMPEG New in my daily work life	
	BI3	I plan to use SIMPEG New often	
User Satisfaction	US1	SIMPEG New simplifies the staff administration process	Yusof et al. (2006)
	US2	SIMPEG New accelerates the staff administration process	
Use Behavior	UB1	Every working day I regularly use SIMPEG New	Venkatesh et al. (2012)
	UB2	I rarely use New SIMPEG in a week	
	UB3	I rarely use New SIMPEG in a month	

ASTES

Advances in Science, Technology and Engineering Systems Journal Vol. 4, No. 4, 115-120 (2019)

www.astesj.com

ASTESJ

ISSN: 2415-6698

Application of Feature Extraction for Breast Cancer using One Order Statistic, GLCM, GLRLM, and GLDM

Dian Candra Rini Novitasari[*,1], Ahmad Lubab[1], Asri Sawiji[2], Ahmad Hanif Asyhar[1]

[1]*UIN Sunan Ampel Surabaya, Mathematics Department, Indonesia*

[2]*UIN Sunan Ampel Surabaya, Marine Science Department, Indonesia*

ARTICLE INFO

Article history:
Received:20 May, 2019
Accepted:24 June, 2019
Online: 13 July, 2019

Keywords:
Breast Cancer
Feature Extraction
GLCM
GLRLM
GLDM

ABSTRACT

The increasing number of breast cancer in recent years has attracted numerous researchers' attention. Several techniques of Computer Aided Diagnosis System have been proposed as alternative solutions to diagnose breast cancer. The flaw of simply using the naked eye to see the differences between normal and with cancer mammogram images makes the texture analysis play an important role in classifying breast cancer. In this study, the results of the classification were compared using various methods of texture analysis in extracting a feature of the mammogram image. Some texture analysis methods, including first order, which consist of GLCM, GLRLM, and GLDM, have successfully extracted features based on their characteristics. The statistical features of these methods are used as input for the ECOC SVM classification, which three kernel comparisons; linear, RBF, and polynomial, build the classification. The results show that the best kernel is polynomial kernels with statistical features built by GLRLM with 93.9757% accuracy value.

1. Introduction

Breast cancer is one of the most common cancers for women around the world. Early diagnosis and treatment are very important in reducing the mortality rate. The advances of screening and treatment toward cancer have a contribution to increasing the survival rates since 1989. There are around 3.1 million breast cancer sufferers in the United States (U.S.). The possibility of women dying because of breast cancer is about 1 in 37, or 2.7 percent [1]. Some factors associated with breast cancer are obesity, the age of the first giving birth, breastfeeding history, and age of menarche [2]. The symptoms identification and routine screening can give early detection toward cancer to prevent the occurrence of acute breast cancer. A mammogram is one of the X-ray imaging test technique to screen and diagnose the initial cancer sufferers. The Mammogram produces an image that helps to detect lumps or abnormalities. The mammographic image sometimes shows abnormal areas that are not cancer, which may cause unnecessary stress and intervention. Ultrasound scanning can help to distinguish a solid mass or a fluid-filled cyst. In addition, research as an effort to prevent breast cancer has been conducted by using BIRADS 2,3 and four which stages of cancer that can be prevented and the fourth stage is called "No lesions" where veins and networks are detected by high pass Gaussian filters. The diagnosis accuracy for breast cancer patients is very critical because it can affect the patient's mentality. Similarly, Yuhana [3] has found that the analysis of K-Nearest Neighbor algorithm method showed to screen breast cancer has an accurate prediction from 39 cases.

Considers computer-aided diagnosis is a medically necessary adjunct to mammography. Computer Aided Diagnosis System (CADS) plays an important role in the medical field, specifically in performing medical image processing [4]. CADS has several benefits, such as an alternative diagnosis that can save costs, time, reduce the possibility of diagnostic errors, and help medical workers to diagnose disease objectively [5]. In CADS, medical images are classified using various stages; those are preprocessing, feature extraction, and classification [5–8]. Afterward, the medical image should be improved by using the various method. As a result, the medical image quality can meet the required standard. In short, the medical image is a raw source where further treatment should be processed to meet the contrast, size, and uniformity of image lighting [4,6].

Medical images that have adequate quality are overviewed by using texture analysis to obtain the characteristic texture parameters of the image [4]. Texture analysis of medical images

[*]Corresponding Author: Dian Candra Rini Novitasari, UIN Sunan Ampel Surabaya, Indonesia, +62 8113456646, Diancrini@uinsby.ac.id

represents a feature extraction form that facilitates the correct classification of images based on their characteristics. However, texture analysis with different methods will produce different groups classification as well, even it uses the same medical image. Therefore, feature extraction is needed to match data and analysis. There are four feature extraction methods based on the statistical order. They are: first statistic (first-order extraction) [1], second statistics (Gray Level Co-occurrence Matrix) [5,6], run-length high order statistics (Gray Level Run Length Matrix) [9–11] and, other order statistics (Gray level Difference Method) [12]. Thus, the purpose of this study is to determine the appropriate feature extraction method in a disease diagnosis system. As a result, the best feature extraction method will contain the characteristics of the image texture and classify the medical image correctly into the group.

In recent years, there has been an increasing interest in the development of CADS techniques, and an increase in breast cancer cases have attracted the attention of many researchers. Saban Ozturk and Bayram Akdemir implemented feature extraction methods of GLCM, LBP, LBGLCM, GLRLM, and SFTA in the classification of histopathological images [10–13]. Various feature extraction methods are used as training and testing in classifying histopathological images to obtain the most applicable method and suit the characteristics of existing data [10]. Similarly, Aswini K Mohanty et al. have classified benign mass and malignant mass using a combination of GLCM and GLRLM methods on mammogram images. The results showed a combination of the two methods with a fairly good accuracy value, 94.9% [10]. Moreover, Naga Padmaja and Shudir implemented GLCM, GLRLM, and hybrid metaheuristic - GLRLM method in classifying breast cancer. The results, after conducting various types of testing methods, showed that Hybrid GLRLM provided better accuracy than other methods [11]. For this reason, this research implements feature extraction methods using statistical order to assist the diagnosis process of breast cancer cases. Afterward, The result of the statistical order will be used as an input in the classification stage.

In addition, various studies have also used various methods in the classification of mammogram images, for example, the Backpropagation method [14,15], Support Vector Machine [5,16,17], Fuzzy Neural Network [18], and Adaptive Neuro-Fuzzy Inference System (ANFIS) [18–23], etc. Some of these methods are subcategories of artificial neural network methods that have been widely implemented for various types of diseases by previous researchers [20]. However, in this study, the researcher used the SVM method to classify mammogram images. The SVM method provides a high degree of accuracy in classifying both linear and nonlinear case. A research finding by [24], also points towards how the SVM maximizes the hyperplane boundary as a benchmark for classifying. In addition, SVM can handle well nonlinear separate data case through the SVM kernel [24]. Moreover, SVM provides excellent classification results, especially in complex cases, with moderately short training times. *Computer-aided diagnosis system*

2. Literature Review

2.1. Support Vector Machine

The multiclass SVM method has three approaches; one-against-all (OAA), one-against-one (OAO), and error computing output code (ECOC) approach [24]. This study used the ECOC approach since the way how these approach works are to add redundant data into messages which are sent in the form of a codeword. Thus, the message recipient can detect errors in the messages and recover the original message if there are several small errors [13,14]. Furthermore, the ECOC SVM approach is very suitable for several noise data that has become a common problem of breast cancer classification Kernel SVM

2.2. Kernel SVM

The method applied in SVM to solve nonlinear cases is kernel [5]. The kernel maps data to a higher dimensional space using the mapping function $\theta(x)$, by multiplying the mapping function $\theta(x)$, each multiplication $x_i.x_j$ will be calculated by using $K(x_i, x_j)$ where x_i' 'will be mapped to space with higher dimensions as follows:

$$\left(\theta(x_i).\theta(x_j)\right) = K(x_i, x_j) \quad (1)$$

SVM has some basic kernels; linear, Gaussian (RBF), quadratic, and polynomial kernels [5,24,25]. Each kernel is used in the training and testing stages to get the best classification results based on the distribution of the data. This study will a comparison of three kernels compared three kernels; linear, Gaussian (RBF), and polynomial.

2.3. Texture Analysis

Texture analysis used in the mammogram image is in the form of statistical matrix order distribution based on pixel intensity. It consists of several orders; first-order statistics, second-order statistics (GLCM), high-order run-length statistics (GLRLM), and GLDM

The first-order statistic is a first-order extraction method based on the histogram image characteristics which represents an opportunity for the appearance of the gray degree value of pixels in an image based on its surrounding pixels. There are several parameters in first-order statistics, those are mean, standard deviation (variance), smoothness, a third moment, uniformity, skewness, kurtosis, and Entropy [4].

The second-order statistic is an extraction method that counts the relationship between two pixels (surrounding pixels) in the image. For analysis needs, second-order texture analysis requires the help of matrix co-occurrence for gray images, usually called GLCM [9,10]. Second-order texture analysis is better at representing image textures in measured parameters, such as contrast, correlation, homogeneity, entropy, and energy [14,18].

From these various statistical orders, GLRLM has a higher statistical feature than the others [5,6,14]. GLRLM is a high-order statistical feature that applies a run-length matrix. The run length shows the number of pixels (distance) covered from Pixel of Interest (PoI) to pixels with the same intensity value (in the horizontal and vertical direction) [26].

1. GLDM [12]

First-order statistics, GLCM, GLRLM, and GLDM, have several statistical features. In this study, the statistical features used are mean, standard deviation, contrast, correlation, energy, homogeneity, SRE, LRE, GLN, RLN, RP, LGRE, and HGRE [6]. The definitions of these features are as follows:

2. Mean

mean is the size of the dispersion of an image that can be calculated by equation (2) [4]:

$$\mu = \sum_{i=1}^{L}\sum_{j=1}^{L} i\big(Y(i,j)\big) \quad (2)$$

1) Standard Deviation
Standard deviation is a variety of histograms of an image that can be calculated by equation (3) [4]:
:

$$\sigma = \sqrt{\sum_{i=1}^{L}\sum_{j=1}^{L} Y(i,j)(i-\mu_i)^2} \quad (3)$$

2) Contrast
Contrast is the size of diversity or gray intensity variation of an image [27]. Equation (4) is the equation of contrast.

$$Contrast = \sum_{i}^{L}\sum_{j}^{L}|i-j|^2 Y(i,j) \quad (4)$$

3) Correlation
Correlation is a measure of the linear shape of gray image degree. Equation (5) is an equation of correlation [9].

$$Correlation = \sum_{i=1}^{L}\sum_{j=1}^{L}\frac{(i-\mu_i)(j-\mu_i)Y(i,j)}{\sigma_i\sigma_j} \quad (5)$$

With the mean and standard deviation, it can be found from equations (6) to (9)

$$\mu_i = \sum_{i=1}^{L}\sum_{j=1}^{L} i\big(Y(i,j)\big) \quad (6)$$

$$\mu_j = \sum_{i=1}^{L}\sum_{j=1}^{L} j\big(Y(i,j)\big) \quad (7)$$

$$\sigma_i = \sqrt{\sum_{i=1}^{L}\sum_{j=1}^{L} Y(i,j)(i-\mu_i)^2} \quad (8)$$

$$\sigma_j = \sqrt{\sum_{i=1}^{L}\sum_{j=1}^{L} Y(i,j)\big(j-\mu_j\big)^2} \quad (9)$$

4) Energy
Energy shows the measure of the concentration of pixel pairs in the intensity of the congruent matrix at several coordinates [27]. Equation (10) is the equation of energy

$$Energy = \sum_{i=1}^{L}\sum_{j=1}^{L} Y(i,j)^2 \quad (10)$$

5) Homogeneity
Homogeneity shows an image with a degree of gray similarity [4]. Equation (11) is the equation of homogeneity

$$Homogeneity = \sum_{i=1}^{L}\sum_{j=1}^{L}\frac{Y(i,j)^2}{1+(i-j)^2} \quad (11)$$

6) $SRE, LRE, GLN, RLN, RP, LGRE$, and $HGRE$
Equation (12) to (19) is a statistical feature equation for GLRLM [5,6,19].

$$SRE = \frac{1}{N_r}\sum_{i=1}^{G}\sum_{j=1}^{R}\frac{Y(i,j)}{j^2} \quad (12)$$

$$LRE = \frac{1}{N_r}\sum_{i=1}^{G}\sum_{j=1}^{R} j^2 Y(i,j) \quad (13)$$

(2.2)

$$GLN = \frac{1}{N_r}\sum_{i=1}^{G}\Big(\sum_{j=1}^{R} Y(i,j)\Big)^2 \quad (14)$$

$$RLN = \frac{1}{N_r}\sum_{i=1}^{R}\Big(\sum_{j=1}^{G} Y(i,j)\Big)^2 \quad (15)$$

$$RP = \frac{N_r}{\sum_{i=1}^{G}\sum_{j=1}^{R} j\,Y(i,j)} \quad (16)$$

(2.3)

$$LGRE = \sum_{i=1}^{G}\sum_{j=1}^{R}\frac{Y(i,j)}{i^2} \quad (17)$$

$$HGRE = \sum_{i=1}^{G}\sum_{j=1}^{R} i^2 Y(i,j) \quad (18)$$

Explanation:

(2.4)

i = line
j = column
$Y(i,j)$ = Probability of the congruent matrix that appears on the mammogram image
Nr = number of all elements in the run length matrix

2.4. Breast Cancer

Cancer is a body cell that experiences mutations (changes) and grows in a way that is uncontrolled by dividing itself faster than normal cells. Cancer cells do not die after they are old enough, rather, they grow increasingly and are invasive that press the normal cells in the body and even die [12]. Early diagnosis is important to find out the breasts are either normal or abnormal. One of the initial tests is mammography. Mammography test is cancer examination tests, especially breast cancer, which can see cancer mass and the abnormalities symptom in the breast to decide the early treatment. Test results from mammography produced two diagnoses of tumors, namely benign tumors and malignant tumors (cancer) [20]. Therefore, mammographic images are classified into three classifications; normal, benign tumors and malignant tumors. Figure 1 is a picture of three classes of mammographic images. In addition to the mammogram image with three classes classification, it is important to detect the abnormalities, in the breast through the presence of mass or micro-classification [9,11]. Figure 1 is mammographic imagery for normal, benign and malignant breast tumor. Figure 2 mass and micro-classification.

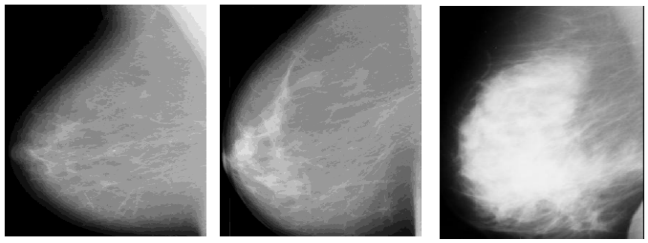

Figure 1: Mammographic imagery for normal breast (left), benign breast tumor (middle), malignant breast tumor (right)

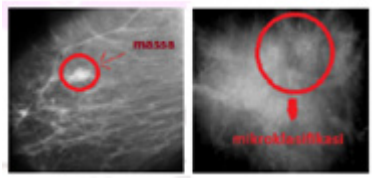

Figure 2: Mass (left), Micro classification (right)

3. Research Method

Research on Application of Feature Extraction for Breast Cancer using One Order Statistical, GLCM, GLRLM, and GLDM is a type of descriptive quantitative research which can be included as applied research considering its functional aspects. The results of the diagnosis of the comparison of four feature extraction methods aim to find an appropriate method for alternative breast cancer diagnoses. The data used in this study is a mammogram image obtained from mammographic images analysis society (MIAS) [28]. Then, the focus of this study is to compare several feature extraction methods that best match the data to obtain closely perfect values of the classification results. The existing mammogram data are uniformly sized through ROI and processed using Contrast-limited adaptive histogram equalization (CLAHE) to improve image quality. The next step is to get statistical features as input for SVM classification by comparing four feature extraction methods. Furthermore, the ECOC SVM classifies mammogram data into three classes; normal, benign, or malignant. Figure 3 is a flowchart from the classification of mammogram images.

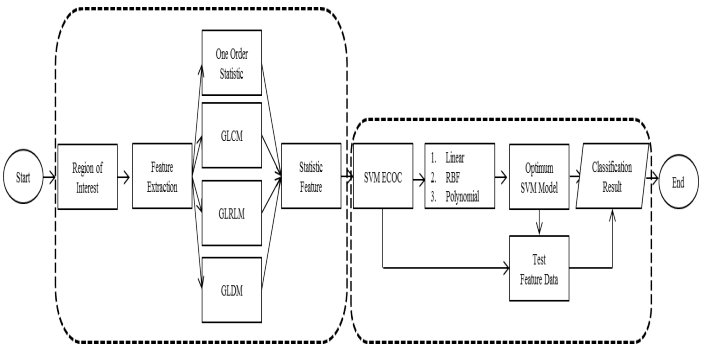

Figure 3: Flowchart

The steps of breast cancer diagnosis include preparing datasets, pre-processing, feature extraction, and classification.

1. Breast image data is a mammogram (gray scale) image from several data samples. There are 191 data for training and 83 data for testing which are stored in one file with .jpg format.
2. The next stage is pre-processing all data by manually cutting the image (ROI) to reduce the size of the image that can speed up the next process.
3. The images that have the same size are repaired using CLAHE to improve the image quality. As a result, the contrast of the mammogram image will be in the same feature to ease the next process.
4. The next step is to extract features in the image that has been improved using four feature extraction methods. The method includes first order statistics, GLCM, GLRLM, and GLDM.
5. The four texture analysis methods showed several statistical features in the form of mean, standard deviation, energy, contrast, correlation, homogeneity, SRE, LRE, GLN, RLN, RP, LGRE, and HGRE.
6. The overall statistical features from texture analysis were used as input for ECOC's SVM classification.
7. After building the ECOC SVM model, then the model was tested to obtain the results of classification, accuracy, sensitivity, and specificity of each classification.
8. Eventually, the conclusion was made based on the accuracy obtained from the Order-1-SVM ECOC, ECOC GLCM-SVM, ECOC GLRLM-SVM, and ECOC GLDM-SVM classification,

The best method will classify data into three classes of cancer; normal, benign or malignant.

4. Result

This study uses gray scale images (mammogram) from mammographic images analysis society (MIAS) [28]. In this study, the number of data is 191 as training and 83 as testing, which then is stored in one file with .jpg format. In total, the data used in both training and testing were 113 normal breast data, 115 benign breast data, and 46 malignant breast data. The image processing in this study was conducted through three stages; first, image quality improvement, feature extraction stage, and a classification stage. The stage of image quality improvement used ROI, CLAHE, and gray scale. In ROI, mammogram image was cropped manually to focus on the target feature and make image size the same, 480 x 480 pixels. The following Figure 4 is the result of preprocessing mammogram images.

The next step was a comparison of order-1 texture analysis, GLCM, GLRLM, and GLDM on mammogram images to find statistical features of the mean, standard deviation, energy, contrast, correlation, homogeneity, SRE, LRE, GLN, RLN, RP, LGRE, and HGRE. Extraction of these features was calculated using 2.2 Equation to 2.18 Equation, which was used as an input feature matrix for the ECOC SVM classification. The orientation of order-1, GLCM, GLRLM, and GLDM orientation uses the orientation direction $0^0, 45^0, 90^0$ and 135^0 with distance $s = 1$ pixel. Afterward, ECOC SVM model was built from the compiling results of encoding to form a binary SVM model. The model was in form of cancer breast types combination; {normal} with {benign, malignant}, then {normal, benign} with {malignant} and {normal, malignant} with {benign}. Then, the Hamming distance for each distribution of data was calculated to match the closest class. There were three kernel tests used in ECOC SVM; linear, RBF, and polynomial kernels. After obtaining the optimal ECOC SVM model, measurements were

made using the confusion matrix as a measure of the work of the classification system made. The confusion matrix compared the accuracy values of each feature extraction result. The results of the four confusion matrix feature extraction methods are presented in Table 1.

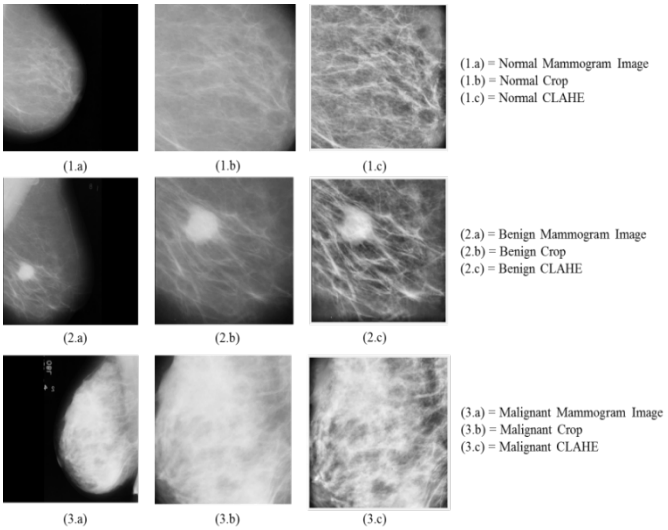

Figure 4. Pre Processing Mammogram image

Table 1. Results from Classification of Mammogram Images

		First Order	GLCM	GLRLM	GLDM
Accuracy	Linear	92.77108	78.31325	93.9757	62.6506
	RBF	91.56627	86.74699	78.31325	65.06024
	Polynomial	90.36145	83.13253	93.9757	65.06024
Precision	Linear	91.74	78.45	92.03	72.14
	RBF	90.86	83.86	77.58	68.96
	Polynomial	90.02	79.89	91.82	66.19
Sensitivity	Linear	93.85	62.74	94.70	48.28
	RBF	92.74	80.67	77.23	50.51
	Polynomial	91.62	82.43	94.96	50.77

Table 1 shows that the best kernel to build ECOC SVM model for breast cancer classification is the polynomial kernel because the polynomial kernel with GLRLM and GLDM input in texture analysis has overtaken the linear and RBF kernels. In addition, compared with the first-order method, the polynomial kernel has a slight difference accuracy, 2.40963. However, the best feature extraction method was built by GLRLM texture analysis with accuracy value 93.9757% in the SVM ECOC linear kernel, 78.31325% in the ECB SVM RBF kernel and 93.9757% in the polynomial SVM ECOC Conflict of Interest kernel. In addition, this is due to the polynomial kernel in the GLRLM method having a precision of 91.82% and a sensitivity of 94.96%. This means that normal data is classified as normal, data on cancer classified as cancer, tumor data classified by tumor using the GLRLM method with a polynomial kernel.

5. Conclusion

In this study, the diagnosis results of four comparisons method in feature extraction influence the following steps of taking the appropriate method for breast cancer alternative diagnoses. Based on the training and testing, the result shows that the best kernel to build ECM SVM model for breast cancer classification is the polynomial kernel and the best feature extraction method is built by GLRLM texture analysis with an accuracy value 93.9757% in the SVM ECOC linear kernel as well as in SVM ECOC polynomial kernel.

Acknowledgment

Our gratitude goes to the Indonesian Ministry of Religious Affairs for giving a research grant in 2018.

References

[1] C. Nordqvist, What You Need to Know About Breast Cancer, 2018.
[2] N.S. Mulyani, "Kanker Payudara dan PMS pada Kehamilan," Jakarta: Nuha Medika, **8**(2), 1–3, 2013, doi:10.1117/12.474399.
[3] A. Yuhana, Implementasi Metode K-Nearest Neighbor dan Artificial Neural Network untuk Memperkirakan Ketepatan Hasil Diagnosis Pasien Kanker Payudara, 2018.
[4] U. Ahmad, "Pengolahan Citra Digital dan Teknik Pemrogramannya," Yogyakarta: Graha Ilmu, 2005.
[5] M.S. Kavitha, S.-Y. An, C.-H. An, K.-H. Huh, W.-J. Yi, M.-S. Heo, S.-S. Lee, S.-C. Choi, "Texture Analysis of Mandibular Cortical Bone on Digital Dental Panoramic Radiographs for The Diagnosis of Osteoporosis in Korean Women," Oral Surgery, Oral Medicine, Oral Pathology and Oral Radiology, **119**(3), 346–356, 2015.
[6] R.C. Gonzalez, R.E. Woods, Digital Image Processing, 2002.
[7] R. Manavalan, K. Thangavel, "Evaluation of Textural Feature Extraction from GRLM for Prostate Cancer Trus medical Images," International Journal of Advances in Engineering & Technology, **2**(1), 401, 2012.
[8] W.N.H.W. Kairuddin, W.M.H.W. Mahmud, "Texture Feature Analysis for Different Resolution Level of Kidney Ultrasound Images," in IOP Conference Series: Materials Science and Engineering, IOP Publishing: 12136, 2017.
[9] A.K. Mohanty, S. Beberta, S.K. Lenka, "Classifying Benign and Malignant Mass using GLCM and GLRLM Based Texture Features from Mammogram," International Journal of Engineering Research and Applications, **1**(3), 687–693, 2011.
[10] S. Öztürk, B. Akdemir, "Application of Feature extraction and Classification Methods for Histopathological Image using GLCM, LBP, LBGLCM, GLRLM and SFTA," Proc. Comput. Sci, **132**, 40–46, 2018.
[11] N. Padmaja, T. Sudhir and D. E. S. Reddy, "A Hybrid Content Based Image Retrieval for Classification of Mammograms," in International Journal of Engineering Research & Technology (IJERT), 1122–1125, 2014.
[12] R. Llobet, R. Paredes, J.C. Pérez-Cortés, "Comparison of Feature Extraction Methods for Breast Cancer Detection," in Iberian Conference on Pattern Recognition and Image Analysis, Springer: 495–502, 2005.
[13] T.K. Hazra, S. Dutta, "A New Approach to Identify the Fracture Zone and Detection of Bone Diseases of X-Ray Image," International Journal of Science and Research (IJSR), **5**(9), 2016.
[14] I.M.D.U. Putra, G.K. Gandhiadi, L.P.I. Harini, "Implementasi Backpropagation Neural Network Dalam Prakiraan Cuaca di Daerah Bali Selatan," E-Jurnal Matematika, **5**(4), 126–132, 2016.
[15] D.C. Rini, "Klasifikasi Sinyal EEG Menggunakan Metode Fuzzy C-Means Clustering (FCM) Dan Adaptive Neighborhood Modified Backpropagation (ANMBP)," Jurnal Matematika" MANTIK", **1**(1), 31–36, 2015.
[16] V.M. Zobin, "Development of the 10 – 11 July 2015 two-stage sequence of multiple emplacements of pyroclastic density currents at Volcán de Colima , México : Insight from associated seismic signals," Journal of Volcanology

and Geothermal Research, **351**(July 2015), 29–40, 2018, doi:10.1016/j.jvolgeores.2017.12.012.

[17] A.Z. Foeady, D.C.R. Novitasari, A.H. Asyhar, M. Firmansjah, "Automated Diagnosis System of Diabetic Retinopathy Using GLCM Method and SVM Classifier," in 2018 5th International Conference on Electrical Engineering, Computer Science and Informatics (EECSI), 154–160, 2018, doi:10.1109/EECSI.2018.8752726.

[18] M. Feylizadeh, A. Hendalianpour, M. Bagherpour, "A Fuzzy Neural Network to Estimate at Completion Costs of Construction Projects," International Journal of Industrial Engineering Computations, **3**(3), 477–484, 2012.

[19] H. Sahraie, A. Ghaffari, M. Amidpour, "Adaptive Neuro-Fuzzy Inference System (ANFIS) Approach to Evaluate The Debutanizer Top Product," Int. J. Eng, **6**(02), 8269, 2014.

[20] D.A. Adyanti, A.H. Asyhar, D.C.R. Novitasari, A. Lubab, M. Hafiyusholeh, "Forecasts Marine Weather on Java Sea Using Hybrid Methods: TS-ANFIS," in International Conference on Electrical Engineering, Computer Science and Informatics (EECSI), 2017, doi:10.11591/eecsi.4.1114.

[21] D.C. Rini, A.Z. Arifin, A. Fanani, G.B.D. Prasanda, W.N.P. Sunaryo, "Penerapan Fuzzy Inference System Dalam Pengoptimalan Suhu Ruangan Pada Double Air Conditioner (Ac) Secara Otomatis," MathVisioN, **1**(1), 11–16, 2019.

[22] D.C. Rini, A.H. Asyhar, M. Hafiyusholeh, G. Purnamasari, Y. Monita, "Analisis Sinyal Ekg Aritmia untuk Deteksi Risiko Jantung Koroner Menggunakan Adaptive Neuro Fuzzy Inference (Anfis)," MathVisioN, **1**(1), 7–10, 2019.

[23] S. Suwanto, M.H. Bisri, D.C.R. Novitasari, A.H. Asyhar, "Classification of EEG Signals using Fast Fourier Transform (FFT) and Adaptive Neuro Fuzzy Inference System (ANFIS)," Jurnal Matematika" MANTIK", **5**(1), 35–44, 2019.

[24] F.F. Ting, Y.J. Tan, K.S. Sim, "Convolutional neural network improvement for breast cancer classification," Expert Systems with Applications, **120**, 103–115, 2019.

[25] R. Diani, "Analisis Pengaruh Kernel Support Vector Machine (SVM) pada Klasifikasi Data Microarray untuk Deteksi Kanker," Indonesian Journal on Computing (Indo-JC), **2**(1), 109, 2017, doi:10.21108/indojc.2017.2.1.169.

[26] S. Azhari, Y. Diputra, E. Juliastuti, A.Z. Arifin, "Analisis Citra Radiografi Panoramik pada Tulang Mandibula untuk Deteksi Dini Osteoporosis dengan Metode Gray Level Cooccurence Matrix (GLCM)," MKB J, **46**, 207, 2014.

[27] D.C.R. Novitasari, "Klasifikasi Alzheimer dan Non Alzheimer Menggunakan Fuzzy C-Mean, Gray Level Co-Occurence Matrix dan Support Vector Machine," Jurnal Matematika" MANTIK", **4**(2), 83–89, 2018.

[28] J. Suckling, J. Parker, D. Dance, S. Astley, I. Hutt, C. Boggis, I. Ricketts, E. Stamatakis, N. Cerneaz, S. Kok, "Mammographic Image Analysis Society (MIAS) Database v1. 21," 2015.

ASTES

Advances in Science, Technology and Engineering Systems Journal Vol. 4, No. 4, 121-127 (2019)

www.astesj.com

Special Issue on Advancement in Engineering and Computer Science

ASTESJ

ISSN: 2415-6698

Aggrandized Random Forest to Detect the Credit Card Frauds

Jisha. Mulanjur Vadakara*, Dhanasekaran Vimal Kumar

Department of Computer Science, Nehru Arts and Science College, Coimbatore, 641105, Tamilnadu, India

ARTICLE INFO

Article history:
Received: 05 April, 2019
Accepted: 29 June, 2019
Online: 17 July, 2019

Keywords:
Aggrandized random forest
Bagging
Boosting
Credit card
Rose
Random forest
Smote

ABSTRACT

From the collection of supervised machine learning technique, an ensemble procedure is used in Random Forest. In the arena of Data mining, there is an excellent claim for machine learning techniques. Random Forest has tremendous latent of becoming a widespread technique for forthcoming classifiers as its performance has been found analogous with ensemble techniques bagging and boosting. In the present work we have proposed an algorithm, Aggrandized Random Forest to detect fraud from credit card transactions/ATM transactions with high accuracy considering both balanced and imbalanced dataset, comparatively to the defined classification algorithm Random Forest in Data mining.

1. Introduction

The statistical analysis, machine learning, artificial intelligence, database techniques and pattern recognition concepts have magnified the origin of Data mining. Traditional techniques may be inapt due to enormity of data, high dimensionality of data, heterogeneous and dispersed nature of data. In this era, data mining is prevalent in the field of commerce, trade, science, architecture, education and medication fair to remark a few. The area of data mining applications we come across are the mining of genome sequencing, market exchange, clinical experiments and in the transactions of credit card. With the immense of devices gifted of accumulating data, Big data is now used more widely with the collection of data attractively and cheaply.

Frauds existing in tax return, claims of insurances, usage of cell phones, credit card transactions etc. represent substantial problems for corporate and the government but spotting and foiling fraud is not so modest task. Frauds are claimed to be an adaptive crime, so it desires distinct means of intellectual data mining algorithms which are coming raised in the field of investigation to sense and prevent fraud. These are methods that exist in the areas of machine learning, statistical analysis and knowledge discovery databases. These methods in different zones of fraud crimes do offer appropriate and fruitful solutions.

There are mainly two procedures used for fraud detection statistical performances and artificial intelligence. Fraud supervision is a knowledge-intensive activity. The main AI

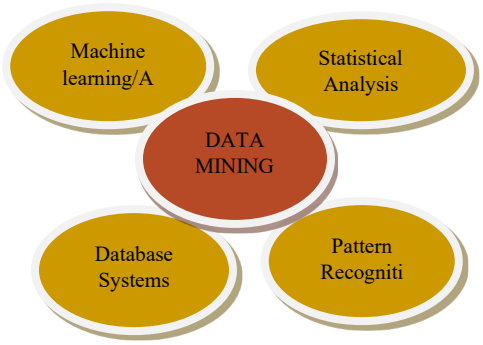

Figure 1. Applications of Data Mining.

Techniques used in the analysis of detecting fraud management include:

- Data mining is the process where facts are classified, clustered and segmented and connotations and

*Jisha.M. V, Nehru Arts and Science College, Thirumalayampalayam, Tamilnadu -641105. Contact No-9745222933 & jisharudhra@gmail.com

instructions in the agreed data are mechanically found that may indicate stimulating patterns, together with those correlated to fraud.

- Expert systems will help to scramble know-how to perceive scam in the way of rules.
- Pattern recognition sense estimated patterns, classes or clusters of mistrustful deeds either routinely or to match assumed inputs.
- Machine learning methods to mechanically find features of frauds.
- Neural networks learn doubtful patterns from samples and used advanced to detect them.

Other techniques such as Bayesian networks, Link analysis, Decision trees and sequence matching are also used for fraud detection.

In field of data mining and knowledge discovery, to handle the problems it is mainly classified into two types supervised learning and un-supervised learning respectively. Supervised learning is further sub-classified depending on the properties of the response variable into classification and regression methods. If the response variable is categorical and discrete, it is classification problems. Otherwise, if the response variable is continuous, it is regression problems. There are different Classification methods for detecting fraud from large data transactions. Selecting Random Forest, Support Vector Machine, Logistic regression and K-Nearest Neighbors [1], our previous work of comparative analysis of these algorithms detected Random Forest to be the best having high accuracy to detect fraud from credit card transactions/ATM card transactions [1].

In this paper, we have given an introduction to Random Forest in section II, description of smote sampling model in section III, about ROSE function in section IV, Theoretical description in section V, proposed algorithm in section VI, followed by Conclusion and References.

2. Introduction to Random Forest

Random Forest can be used to resolve regression as well as classification problems. The dependent attribute or variable is continuous in regression and in classification problems it is categorical. Random Forest is a very influential ensembling machine learning algorithm in which decision tree works as the base classifiers, forming multiple decision trees and then merging the output generated by each of them. Decision tree is a classification model in which it classifies each node with maximum information gain. This search is continued until all the nodes are beat or there is no more information to gain. Decision trees are very modest and informal to know models; however, their predictive power is less, thus called as weak learners [1].

Random Forest works as an ensemble of random trees. It syndicates the yield of multiple random trees and then to originate up with its own output. Random Forest as similar to Decision Tress [1] but will not select all the data points and variables in each of the trees. It arbitrarily assembles data points and variables in each of the tree that it produces and then it is united to arrive at the output at the end. It takes away the prejudice that was encountered in a decision tree model. Also, it improves the predictive power significantly [2].

Random forest stays a tree-based algorithm which take in building several trees (decision trees), were the manipulator generates the number of trees. The elective of all created trees fixes final classifying outcome.

3. Smote Sampling Method

Stereotypically, there are several classification problems that have been anticipated to organize formerly disregarded observations, which will be situated, or recognized set to be tested by application of a classifier is then trained by earlier prearranged observations called training dataset. Numerous typical classifiers are anticipated to deal with this type of snags such as tree-based classifiers, discriminant analysis and logistic regression.

Unbalanced data cause problems in many of the learning algorithms. This is due to irregular quantity of cases that is posed by each class of the problem. Synthetic Minority Over-Sampling Technique algorithm (SMOTE) is used for handling these unbalanced classification problems.

The Smote function can be called as defined, when it discourses the unbalanced problems with the creation of a new smote data set. Alternatively, it returns the ensuing model by routing a classification algorithm on the new data set [3].

Smote (form, data, perc. over = 200, k = 5, perc. under = 200, learner = NULL, ...)

Definition of the arguments-

Form designates the prediction problem. *Data* holds the actual unbalanced dataset. *Perc. Over* is method of over-sampling that finds a figure that initiatives the verdict of how many further cases from the minority class are generated. *Perc. Under* is an under-sampling where among each case made from the minority class, it specifies an amount that initiate the choice of the number of further cases from the majority classes are designated [4,5]. *K* is a quantity signifying the number of adjoining neighbors that is further used to produce the new instances of the minority class. *Learner* is set to Null by default. It acts as a string with a tag of a function that outfits a classification procedure that will be useful in the ensuing smote data set.

The two important constraints that switch the quantity of over-sampling of the minority class and under-sampling of majority class are perc. Over and perc. Under respectively. Perc. Over will approximately a numeral above 100, thereby perc. Over/100 innovative samples of this class are considered for the minority class. If perc. Over value is below 100 then for an arbitrarily selected proportion of the cases, a single case is created and fit into the minority class on the original dataset. The perc. Under constraint panels part of the cases of majority class that erratically selected as the final balanced dataset. With respect to the count of newly engendered minority class cases, the result is obtained [3], [5].

Designed for each existing minority class, ‘n’ new-fangled instances will be formed which is measured by the parameter perc.

Over. The instances will be generated by using the parameter K that holds the count of neighbours [3], [6].

We arrive directly to the classification model from the resulting balanced dataset by using the above-mentioned function [5]. Overall, this function will either return Null value or a new dataset depending on the usage of smote function. If not, the learner parameter will return the classification model [5].

4. Rose: A Package for Binary Imbalanced Dataset

Imbalanced learning signifies the problematic of supervised classification if a class behave erratically over the sample dataset. The Rose, Random Over Sampling Example [7] tackles these problems with its on functions embedded in the package. The class imbalance circumstances are persistent in the multiplicity of applications and fields; this issue had received considerable attention recently [8]. There originate the scarcity of software and procedures clearly meant to handle imbalanced data so to have the non-expert users adopt it. In the R environment, there exist Caret package to validate as well as select classification and regression complications. It highlights the issue of imbalance class as down-sample and up-sample [6][8]. It is worth indicating DMwR (Torgo,2010) which gives an estimation of any classifier, thereby handles imbalanced learning.

The *ROSE* package was motivated to enhance the performance of an imbalanced setting of binary classification providing both standard and more refined tools [7]. Menardi and Torelli at 2014 had developed the smoothed bootstrap-based method. By aiding the phases of model estimation and assessment ROSE [7] relieved the gravity of the effects of an unbalanced distribution of classes.

5. Theoretical Background

5.1. Ensemble Classifiers

An ensemble contains a set of independently trained classifiers whose predictions are combined for categorizing new instances [2].

Bagging [9] and Boosting (Robert E Schapire,2003) are two popular methods for producing ensembles. Bootstrap gathering samples stands for the process called Bagging. As portion of ensemble, if "n" individual classifiers are to be produced from a given original dataset of size "m" then n distinct training set of size m is engendered using sampling. In bagging multiple classifiers created are not dependent on each other. In boosting, from the training dataset each sample is allotted weights. The classifiers generated by boosting is dependent on each other.

5.2 Definition of Random Forest

Random Forest classifier comprise group of tree-structured classifiers $t(x, \Theta_n)$ n=1,2…. , where the Θ_n are self-regulating identical scattered random vectors and every tree casts a unit vote for the most popular class at input x, [2][10].

Once the forest is trained or constructed, each tree give rise to new instance which is recorded as vectors and is joined. The new instance is taken by considering the class having the maximum votes. Nearly one-third of original instances are left, after sampling with replacement of every tree the bootstrap sample set is drawn. The new instances obtained is the out of bag (OOB) data. Out-of-bag error estimation is calculated considering every individual tree's OOB dataset in the forest.

Illustrating Accuracy of Random Forest:

The Generalization error (Pe^*) of Random Forest is Use "(1)",

$$Pe^*=P_{x,y}(mg(X, Y))<0 \quad (1)$$

where mg (X, Y) is margin function. The margin function measures the level to which the average count of votes at the point (x, y) for the exact class surpasses the average votes of any further class. Here x is the predictor vector and y is the classification.

The Margin function is Use "(2)",

$$mg\ (X, Y) =\alpha v_k I(h_k(X)=Y)\ \max j_{=y}\alpha v_k I(h_k(X)=j) \quad (2)$$

Here, I is the indicator function.

Boundary is directly proportional to confidence in the classification.

Benefit of Random Forest is specified in terms of the predictable value of Margin function Use"(3)".

$$B=E_{X,Y}\ (mg\ (X, Y)) \quad (3)$$

A function of mean correlation amongst base classifiers and average strength results in the generalization error of ensemble classifier (Prenger. R, et al,2010). If the mean value of correlation is low an upper bound for generalization error is Use"(4)",

$$Pe^* \leq \rho\ (1- B^2) / B^2 \quad (4)$$

6. Aggrandized Random Forest.

For this work, we have used large dataset of about three lacs of credit card transactions. The classification algorithm is built in the R platform. The proposed algorithm is named Aggrandized Random Forest, which have an increase in its accuracy by 3.06 % for balanced data and an increase of 3.30% for imbalanced data, compared to the previous work as shown in Table.2.

Aggrandized Random Forest is proposed by considering the random forest as the base classifiers with bagging approach and compared with the existing random forest. It is analyzed that Bagged Random Forest gives better results.

Here, we have used the ROSE package of R, to train the imbalanced data set. The functions in ROSE [7,8] have improved the capacity of generalization and reduced the risk conceded by other oversampling methods. As will be expounded, the ROSE technique can be truly considered, which reduces the repetition of instances. In accuracy evaluation step, the overall accuracy may yield misleading results, thus the aggrandized random forest has been evaluated in rapports of class -independent extents such as precision, recall, F-measures etc., as mentioned in the Table.1.

The required library functions in R,

```
library(caret)
library(caTools)
```

library (ROSE)
library (random Forest)

6.1. The Usage of ROSE Function:

ROSE (formula, data, N, subset = options("subset") $subset, seed)

Defining the arguments:

Formula represents the object of class formula where the class label representing the route is allotted with a sequence of routes thru the predictors. The interaction among predictors or their transformations is mentioned by a message. *Data* argument when not specified the variables are taken from environment. It is an optional argument. *N* indicates the anticipated trial proportions of the ensuing dataset. By default, the length of the response variable in formula is considered. *Seed* argument is assigned a single integer value to indicate seeds and preserve the trace of the produced sample [7].

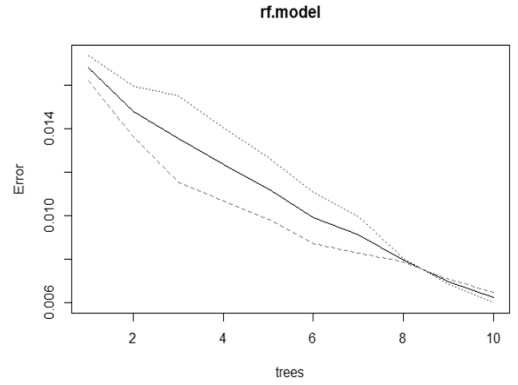

Figure 2(a). Represents the rf. model on Balanced Data

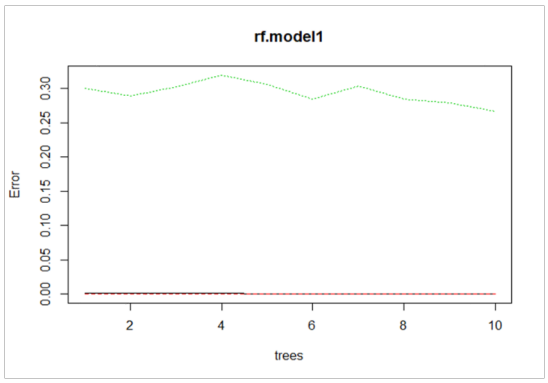

Figure 2(b). Represents the rf. Model on unbalanced data.

6.2. Coding for Imbalanced to Balanced Dataset

###imbalanced classification

creditcard$Class<- as. factor(creditcard$Class)
table (is.na (credit card)) ##-is.na-indicates missing elements.
creditcard$Time
str (credit card)
###
split<-sample. split (creditcard$Class, Split Ratio = 0.7)
train<-subset (credit card, split==T)
test<-subset (credit card, split==F)

###removing unbalanced classification problem and making data balanced
train. rose <- ROSE (Class ~., data = train, seed = 1) $data
table (train. rose$Class)
test.rose <- ROSE(Class ~ ., data = test, seed = 1)$data
table(test.rose$Class)
####Applying random forest on Balanced data
rf.model<-randomForest(Class~., data = train.rose ,ntree=10)
rf.model "As in Figure.2(a)".
####Applying random forest on unbalanced data####
rf.model1<-randomForest(Class~., data = train ,ntree=10)
rf.predict1<-predict(rf.model1,newdata = test)
plot(rf.model1) as plotted "As in Fig.2(b)".

6.3. Confusion Matrix.

After the performance of a classifier, we can engender confusion matrix grounded on the prediction results where each column of the matrix represents the instances in a predicted class, while each row represents the instances in an actual class.

The table consists of two rows and columns that gives the count of true positives (TP), false positives (FP), true negatives (TN) and false negatives (FN). The minority class is the positive class and the majority class is the negative class "As in Figure.3".

	Predicted Positive	**Predicted Negative**
Actual Positive	True Positives	False Negatives
Actual Negative	False Positives	True Negatives

Figure 3. Confusion matrix representation.

6.3.1 The Confusion Matrix for The Proposed Algorithm.

Confusion matrix to evaluate OOB error rate "As shown in Figure.4".

Actual class	**Predicted class**		**Class error**
	0	1	
0	97821	648	0.006580751
1	639	98186	0.006465975

Figure 4. OOB estimate of error rate: 0.65%.

6.3.2. Confusion matrix for balanced dataset and imbalanced dataset

The "Figure 5 (a)" represents the confusion matrix for the balanced dataset, and "Figure 5 (b)" represents the confusion matrix for imbalanced dataset, where we could get true positive value, false positive, false negative and true negative value to calculate the parameters precision, recall, f-measure, sensitivity and specificity. Thereafter, the analytical measures are calculated accordingly.

Actual class	Predicted class	
	0	1
0	42468	42
1	201	42732

Figure 5(a). For balanced data.

Actual class	Predicted class	
	0	1
0	85284	31
1	11	117

Figure 5(b). For unbalanced data.

6.4. Analytical Measures Used for Comparing the Proposed and Existing.

There are several factors which is used to the detect the best performance of the algorithm. The presentation of the proposed system is evaluated using the analytical measures such as precision, recall, f-measure etc. [1].

- Precision = TP/(TP+FP)
- Recall = TP/TP+FN)
- F-Measure = 2 *(precision * recall) / (precision + recall)
- Sensitivity= TP/FP
- Specificity=TN/FN

Along with the above-mentioned factors, the other evaluated factors are Accuracy, Kappa, prevalence, detection rate, detection prevalence, P -value, Positive Pred. value, Negative Pred. value, Mcnemar's Test P- Value, AUC etc.

Precision measured by the count of true positives divided by the sum of true positives and false positives.

Recall measures the figure of the true positives divided by the sum of true positives and false negatives.

The *F-Measure* indicates the stability between precision and recall values.

Kappa statistics characterize the range to which the data is collected correctly.

Sensitivity refers to the comparison of the count of acceptably recognized as fraud to the amount incorrectly listed as fraud. It is the ratio of true positives to false positives.

Area Under the Curve (AUC) is used to analyze the performance of classification models capable to predict the classes accurately [11,12].

Detection rate is mainly reflected in confusion matrix. This parameter will vary according to the dataset.
Detection rate=TP/(TP+FP+FN+TN).

Specificity indicates the same concept with genuine transactions, or the assessment of true negatives to false negatives.

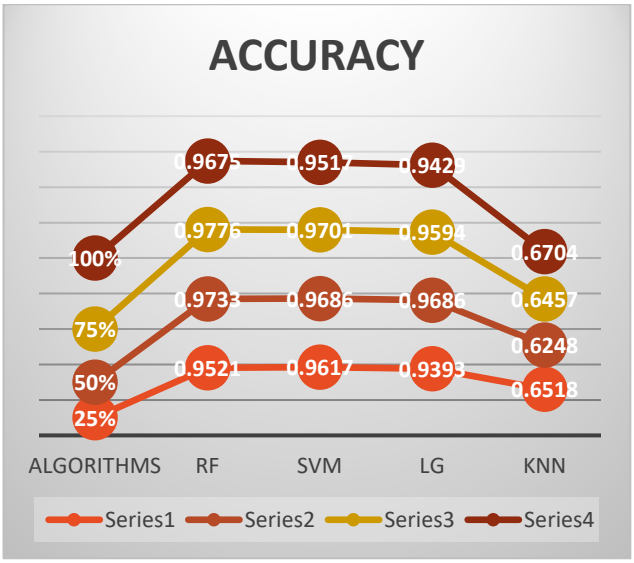

Figure 6. Accuracy of the comparative study of previous work for detecting 100% fraud in the dataset [1].

The previous work was a comparative study of different classification algorithms such as Random Forest [12-15], SVM, K-nearest neighbor and Logistic Regression [1] to detect fraud from credit card transaction. It was found that the Random Forest Algorithm [15] is best in detecting the fraud with an accuracy of 0.9675 "As shown in Figure.6".

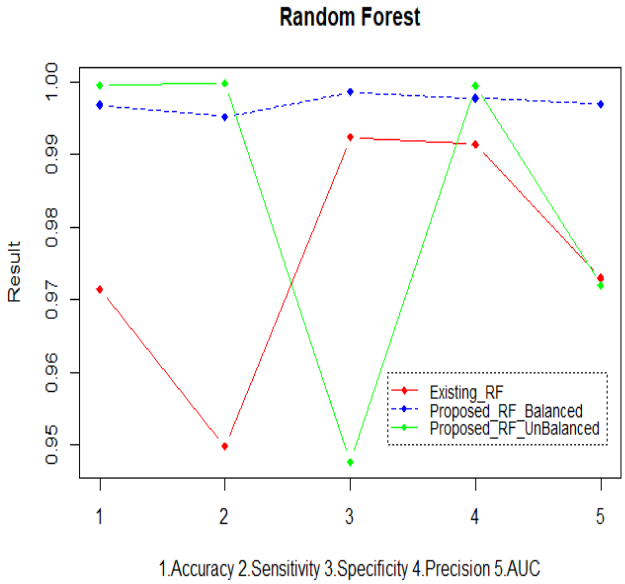

Figure 7. Performance of the proposed Random Forest

Table 1. Comparison of Analytical Measures for the Aggrandized Random Forest Results with Those of the Existing Random Forest.

Factors	Existing Random Forest	For Balanced Dataset	Imbalanced Dataset
Accuracy	0.9675	0.9972	0.9995
95% CI	0.9562, 0.9766	0.9968, 0.9975	0.9993, 0.9996
No Information Rate	0.5182	0.5006	0.9983
P-Value	< 2.2e-16	< 2.2e-16	< 2e-16
Kappa	0.9348	0.9943	0.8476
Mcnemar's Test P-Value	5.806e-07	< 2.2e-16	0.00337
Sensitivity	0.9391	0.9953	0.9999
Specificity	0.9939	0.9990	0.7905
Pos. Predc Value	0.9930	0.9990	0.9996
Neg. Predc Value	0.9461	0.9953	0.9141
Prevalence	0.4818	0.4994	0.9983
Detection Rate	0.4525	0.4970	0.9981
Detection Prevalence	0.4556	0.4975	0.9985
Balanced Accuracy	0.9665	0.9972	0.8952
'Positive' Class	Yes	0	0
AUC	0.970	0.997	0.957
Precision	0.9915	0.9978	0.9995
F-measure	0.9645	0.9965	0.9996

The comparison of the Aggrandized Random Forest with the existing Random Forest "As shown in Figure.7". The analytical measures considered to detect the performance of the new proposed random forest; Aggrandized Random Forest "As shown in the Table 1".

The Analytical measures for the Proposed and the existing is represented by chart diagram "As in Figure.8". The ROC curve which is the receiver operating characteristics of the proposed Random Forest "As shown in Figure 9(a) and Figure 9(b)" for the balanced and imbalanced dataset respectively.

Table 2. Performance of Aggrandized RF.

Dataset	Accuracy	Sensitivity	Specificity	AUC	Precision	Kappa	F-Measure
Existing RF	0.9675	0.9391	0.9939	0.970	0.9915	0.9348	0.9645
Proposed RF Balanced	0.9972	0.9953	0.9990	0.997	0.9978	0.9943	0.9965
Improvement (%)	3.06	5.98	0.51	2.78	0.63	6.36	3.31
Proposed RF Imbalanced	0.9995	0.9999	0.7905	0.957	0.9995	0.8476	0.9996
Improvement (%)	3.30	6.47	-20.46	-1.34	0.80	-9.32	3.63

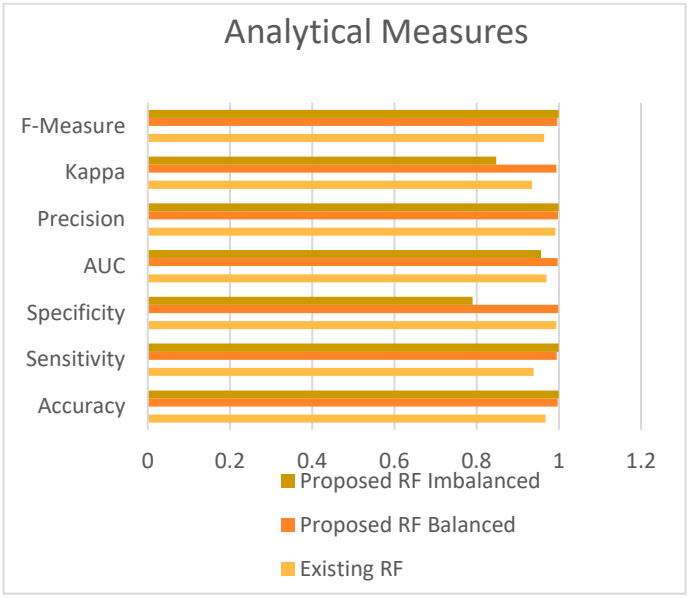

Figure 8. Chart Diagram signifying the comparative recital of Aggrandized Random Forest with Balanced and Imbalanced Dataset to the existing Random Forest Algorithm.

The overall performance of the Aggrandized Random Forest with balanced and imbalanced dataset is evaluated with the existing random Forest, and found to have more accuracy, sensitivity, F-measure, precision, etc. The Table 2 gives the improvement of the proposed algorithm.

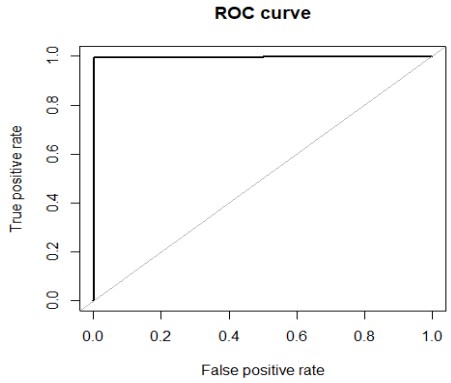

Figure 9(a). ROC of balance dataset.

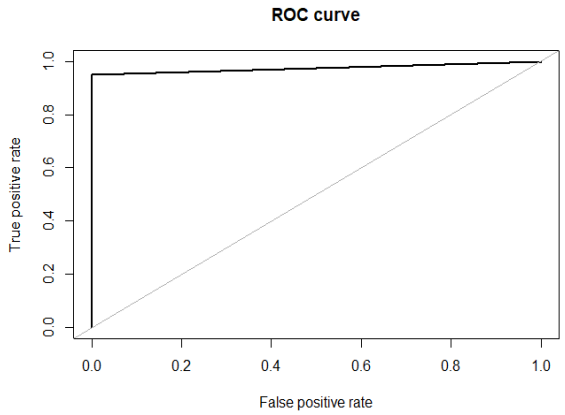

Figure 9(b). ROC of imbalanced dataset.

7. Conclusion

In this paper, our proposed algorithm Aggrandized Random Forest is developed in R platform, having a better accuracy of 0.9972 for balanced and 0.9995 for imbalanced data. The results show that for an imbalanced data, Random Forest outstrips other classification techniques and henceforth stays excessive scope for developing improved Random Forest. Using random forest as a base learner can achieve good outcome in the domain of Imbalanced data.

Acknowledgement

We author thank all the contributors of this journal for considering the article. I would like to thank my guide for giving his support and encouragement in my work. Also, thank the authors of the references giving me the privilege to cite their article and enhance my knowledge. With the responsibility as Ph.D. scholar at Nehru arts and science college, I thank all the teachers and my friends in giving their valuable ideas and support. Wish this article will be beneficial for future scholars.

References

[1] M.V. Jisha., D. Vimal Kumar, "An Efficient Credit Card Fraud Classifier of the four data mining classification algorithms- "A Comparative Analysis."(JETIR)Journal of Emerging Technologies and Innovative Research. Nov.2018, vol 5, issue 11, Pno- 371-378. https://jetir1811656.pdf.

[2] Bernard S Heutte L, Adam S, "Dynamic Random forests, Pattern Recognition Letters", 33 (2012),1580-1586.

[3] Tianxiang Gao, "Hybrid classification approach of Smote and instance selection for imbalanced Datasets". Iowa University, Iowa. Thesis work, 2015.

[4] Vrushali Y, Kulkarni, Pradeep K Sinha. Pruning of Random Forest Classifiers: A survey and future directions."2012 international Conference on Data Science & Engineering (ICDSE), 2012.

[5] R Documentation[online]Http://www.rdocumentation.org.

[6] M.Kuhn. caret: Classification and Regression Training,2014. URL http://CRAN.R-Project.org/package=caret.

[7] N. Lunardon, G. Monardo, and N.Torelli, R package ROSE: Random Over Sampling Examples(version0.0-3). Universität di Trieste and Universität di Padova, Italia ,2013.URL http://CRAN.Rproject.org/web/packages/ROSE/inedx.html.[p79][online].

[8] ROSE:A package for Binary Imbalanced/Balancing data, Https://journal.r-project.org/archieve/2014-008/RJ-2014-008.pdf.

[9] Breiman L, Bagging Predictors, Technical Report No 421, (1994).

[10] Breiman L, Random Forests, Machine Learning, 45,5-32, (2001).

[11] D.Vimal Kumar, M.V. Jisha, "Analytical Measures for Detecting Fraud Using Classification Algorithms". International Journal of Innovative Technology and Creative Engineering (Ijitce), February 2019, vol 9, No.2 636-644. https://ia601504.us.archive.org/19/items/IJITCEFEB19/IJITCE_vol9no202.pdf

[12] Bernard s. Heutte L, Adam S Using Random Forest for Handwritten Digit Recognition, International Conference on Document Analysis and Recognition 1043-1047, (2007).

[13] Bernard S Heutte L Adam S, Towards a Better Understanding of Random Forests Through the Study of Strength and Correlation, ICIC Proceedings of the Intelligent Computing 5th International Conference on Emerging Intelligent Computing Technology and Applications, (2009).

[14] Bernard S Heutte L Adam S, Forests-RK; A new Random Forests Induction Method, Proceedings of 4th International Conference on Intelligent Computing: Advanced Intelligent Computing Theories and Applications – with Aspects of Artificial Intelligence, Springer – Ver lag, (2008).

[15] Bernard S Heutte L Adam S, On the Selection of Decision Trees in Random Forests, Proceedings of International Joint Conference on Neural Networks, atlanta, Georgia, USA, June 14-19,302-307, (2009).

ASTES

Advances in Science, Technology and Engineering Systems Journal Vol. 4, No. 4, 128-132 (2019)

www.astesj.com

Special Issue on Advancement in Engineering and Computer Science

ASTESJ

ISSN: 2415-6698

Experimental Evaluation of Transmission between Two XBee Modules Using Radio-over-Fiber Technique

Luis Alejandro González Mondragón[1], Leidy Johana Quintero Rodríguez[1], Ana Gabriela Correa Mena[1], Jorge Rodríguez Asomoza[2], Alejandro García Juárez[3], Ignacio Enrique Zaldívar Huerta*,[1]

[1] *Instituto Nacional de Astrofísica, Óptica y Electrónica, Depto. de Electrónica, Calle Luis Enrique Erro No. 1, Tonantzintla, Puebla, México, 72840*

[2] *Universidad de las Américas, Depto. de Ing. Electrónica, Ex-hacienda Sta. Catarina Mártir, Cholula, Puebla C.P. 72820, México*

[3] *Universidad de Sonora, Depto. de Investigación en Física, Blvd. Luis Encinas y Rosales S/N, Hermosillo, Sonora, 83000, México.*

ARTICLE INFO

Article history:
Received: 05 April, 2019
Accepted: 04 July, 2019
Online: 17 July, 2019

Keywords:
Microwave signals
Radio over fiber
Optical communications
XBee

ABSTRACT

An experimental transmission between two XBee modules using Radio over Fiber technique is demonstrated. Data issued from an XBee module coded on a wireless microwave carrier at 2.44GHz is transmitted through an optical link of 25.24 km. The optical transmission is based on an external modulation scheme over a dispersive channel. Frequency response of the external modulation scheme is determined by simulation and experimentally. In particular, the chromatic dispersion of the optical fiber associated to its length allow the generation of a pass-band filter whose bandwidth is used to code the RF signal. The recovered RF signal exhibits a SNR of 27dB. Obtained results allow proposing this RoF scheme as a good contender for data transmission.

1. Introduction

This paper is an extension of the work originally presented at the 15th International Conference on Electrical Engineering, Computing Science and Automatic Control [1]. Now, the main contribution of this extended work resides in the fact that we are describing the mathematical procedure that allows determining the frequency response of the electro-optical system used for the transmission. Besides, the theoretical behavior of the optical communication system is validated by simulations. This work is situated on the field of Radio-over-Fiber (RoF), a technique that allows joining radio frequency and electro-optic methods. RoF emerges as a promising solution to fulfill the capacity and mobility of access networks providing high data rate, high capacity and a mobility proposal to transmit information [2-4]. Given that the transmission of information is via light through optical fibers, it is evident that its inherent advantages are exploited, such as low losses, immunity to electromagnetic interference and especially the huge bandwidth available. Figure 1 shows a basic RoF scheme composed by a RF-to-Optical stage, an optical link and an Optical-to-RF stage. The RF signal modulates the light (either directly or externally). The modulated light travels across the optical channel. Finally, the light is turned into its electrical form where it can be radiated by an antenna providing wireless coverage in zones of difficult connection such as shopping centers and subterraneous places [5].

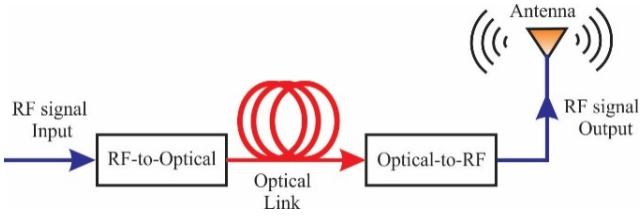

Figure 1. Basic diagram of a RoF system

RoF technology is a candidate that aims to alleviate the bandwidth restrictions for 5G Mobile, delivering wireless data signals via optical fiber channels. [6]. Thus, RoF allows supporting secure, cost-effective coverage as well as excellent capacity mobile-wireless access for oncoming services. Some drawbacks inherent to RoF are due to the distortion and noise derived by the non-linear features of the components employed in the optical network as the optical sources, the chromatic dispersion and photodetectors. For this reason, to mitigate sources of noise and

*Ignacio Enrique Zaldívar Huerta , Luis Enrique Erro #1, Sta. María Tonantzintla, Puebla, México, zaldivar@inaoep.mx

misstatement, intensity-modulation-direct-detection is advisable [7]. In this regard, we propose and experimentally demonstrate a RoF scheme using an optical communication system in the modality of external modulation for the transmission and distribution of a RF-signal. Furthermore, it is demonstrated that the chromatic dispersion (considered as a drawback in this type of systems), is used in an advantageous manner to the generation of notch filters. On the other side, it is known that an XBee is an electronic device whose operation is based on the network transport protocol IEEE 802.15.4, it is able to generate wireless paths to establish communication between devices (http://xbee.cl/que-es-xbee, https://www.digi.com/products/xbee-rf-solutions/xctu-software/xctu). In this sense, XBee modules that use the ZigBee protocol find applications in RoF networks [8, 9]. In this experimental proposal, a wireless signal delivered by an XBee module is used as test signal. A baseband modulation Gaussian Frequency Shift Keying (GFSK) signal at 2.44GHZ is generated by an XBee. This electrical signal modulates an intensity electro-optic modulator. This work is structured as follows. In Section 2, is given the principle of operation of the optical communication system at external modulation and also numerical simulations are presented. In Section 3, experimental set-up of the RoF is described. At the end, a short conclusion is given in Section 4.

2. Principle of Operation

Figure 2 depicts the block diagram the optical communication system in the modality of external modulation used in this work. Basically, it is constituted by a single-mode laser diode as optical source, a Mach Zhender-Intensity Modulator (MZ-IM), a Single Mode-Standard Fiber (SM-SF), as well as a Photodiode (PD).

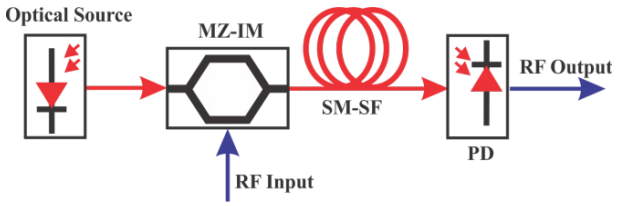

Figure 2. Block diagram of the model used

In the following, a full mathematical analysis explaining the behavior of the model is given. In order to exploit the chromatic dispersion exhibited by the SM-SF, it is necessary to assume that the single-mode laser diode emits at 1550nm. It is demonstrated that the chromatic dispersion (D) and the length (L) of the optical link play an important role that allow the system to act as photonic notch filter.

Mathematically, the optical spectrum of a single-mode laser diode (for example a DFB) can be modeled by a Gaussian envelope centered at an angular frequency ω_0 as [10]

$$S_0(\omega-\omega_0)=\frac{2S_{max}}{\Delta_\omega\sqrt{\pi}}exp\left(\frac{-4(\omega-\omega_0)^2}{\Delta_\omega^2}\right) \quad (1)$$

where S_{max} is the maximum power emission and Δ_ω is the Full Width at Half Maximum of the spectrum that can be expressed in terms of $\Delta\lambda$. Eq. (1) can be simplified, defining $a=4/\Delta_\omega^2$ and $W=\omega-\omega_0$, resulting in

$$S_0(W)=\sqrt{\frac{a}{\pi}}S_{max}exp(-aW^2) \quad (2)$$

The Fourier Transform (FT) of Eq. (2) is the spectral density of the optical source, thus

$$\{S_0(W)\}=\int_0^\infty S_0(W)exp(-j2\pi ZW)dW \quad (3)$$

Defining $Z=v_m\beta_2L$, and expressing the propagation constant $\beta_2=-D\frac{\lambda^2}{2\pi c}$, defining $\omega_m=2\pi v_m$, and $dW=d\omega$, then

$$\mathcal{F}\{S_0(W)\}=\int_{-\infty}^{\infty}\sqrt{\frac{a}{\pi}}S_{max}exp(-aW^2)\,exp(-j2\pi ZW)dW \quad (4)$$

Equation (4) is solved considering that the FT of a Gaussian function $f(t)=exp(-at^2)$ is [11]

$$\mathcal{F}[exp(-at^2)]=\sqrt{\frac{\pi}{a}}exp\left(-\frac{\omega^2}{4a}\right) \quad (5)$$

Rewriting Eq. (4) and considering a, and Z we find

$$\mathcal{F}\{S_0(W)\}=S_{max}exp\left(-\frac{(\pi v_m\beta_2L\Delta_\omega)^2}{4}\right) \quad (6)$$

When $S_0(W)$ is narrow, the frequency response of the system is

$$H(v_m)=cos\left(\frac{\pi v_m^2\lambda^2DL}{c}\right) \quad (7)$$

The squared of the modulation frequency v_m^2 makes the system behave like a non-periodic notch filter.

The notch frequencies f_i, for which Eq. (7) becomes zero, are determined by

$$f_i=\frac{1}{\lambda}\sqrt{\frac{1}{2}\frac{(2i-1)c}{DL}} \quad (8)$$

where λ is the central wavelength in nm, D is in ps/nm·km, c is speed of light in nm/s, and L is the length of the optical link in km.

Equation (7) is numerically evaluated by using MATLAB for the frequency range 0-25GHz, considering: λ=1550nm, c=2.9979x10^{17}nm/seg, L=25.24km, D=15.81ps/nm·km.

Moreover, substituting λ, c, L, and D in Eq. (8), the first and second notch frequency values are f_1=12.50GHz and f_2=21.65GHz, respectively.

Figure 3 shows the result of this numerical evaluation. The result of this evaluation is corroborated by a block level simulation using VPIphotonics software® (http://www.vpiphotonics.com/index.php), and plotted on the same graph. This software is provided with a full library of electro-optics components whose properties can be easily manipulated, therefore, the degree of reliability for the results is high.

From this graph, it is clearly appreciable that the separation between consecutive notches is not constant and decreases as the frequency increases. The bandwidth at -3dB for the low-pass band and for the first lobe (band-pass) are in the order of GHz. The common point between both curves is their tendency. Note that both curves converge to the values of 12.50GHz and 21.65GHz

as stablished by Eq. (8). The justification to use 25km is because the current transmission lengths are designed to meet 20 km, as is determined by an international standard [12].

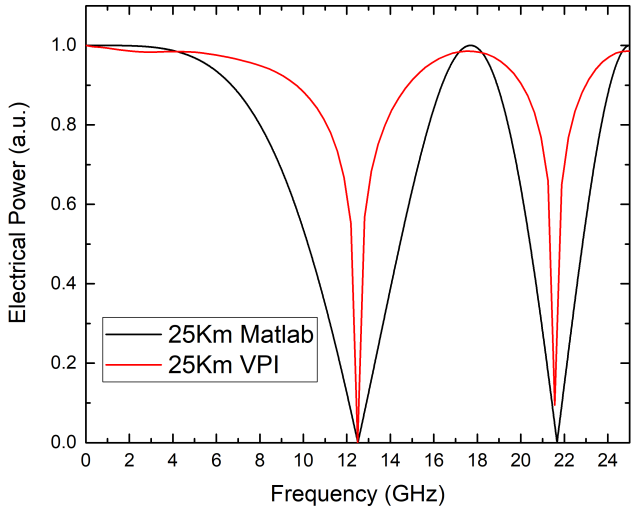

Figure 3. Simulated frequency response using MATLAB and VPI photonics software.

3. Experimental Results

Initially, a test communication between two XBee devices is carried out. Later, a characterization of the optical communication system is done. Finally, the performance of the system composed by a couple of XBee modules over a RoF link is accomplished.

3.1 Test of the XBee devices

XBee is a trademark of radio devices capable of supporting communication protocols as ZigBee, 802.15.4, and Wi-Fi, among others [9]. Figure 4 depicts an XBee network. One module plays the role of Coordinator whereas the other of an End Device.

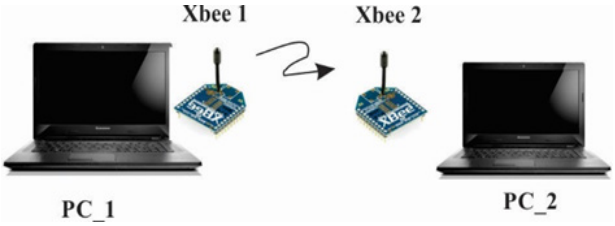

Figure 4. Network generated by using two XBee modules.

The Coordinator handles out addresses and manages the network The End Device is responsible for joining existing networks, transmitting and receiving information. In this work, two XBee modules (XBee-PRO model ZNet 2.5 OEM, indoor range 100m, operating frequency 2.4GHz, transmit power output 18dBm) are used. Both devices are provided with an omnidirectional antenna (Gain 2.15dBi, frequency range from 2.4 to 2.4835GHz) and an USB adapter (Sparkfun XBee Explorer Dongle) that allows the connection via serial communication. The communication between these devices is achieved by using the platform XCTU. Figure 5 shows this interface (https://www.digi.com/products/xbee-rf-solutions/xctu-software/xctu). Data to be transmitted by PC_1 (Coordinator) are coded at the frequency of 2.44GHz and then radiated via an antenna and decoded by PC_2 (End Device).

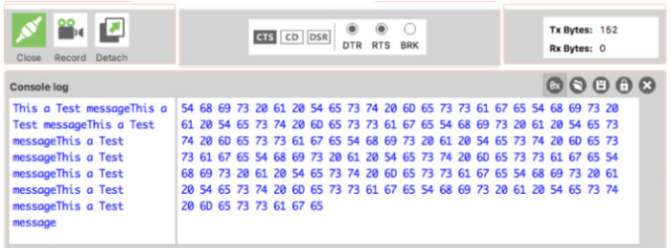

Figure 5. Screenshot showing the interface to control the Coordinator.

Figure 6 shows the spectrum of the emitted radio frequency signal at 2.44GHz measured by an Electrical Signal Analyzer (ESA) exhibiting a SNR value of 55dB. The baseband data is coded within the side lobes.

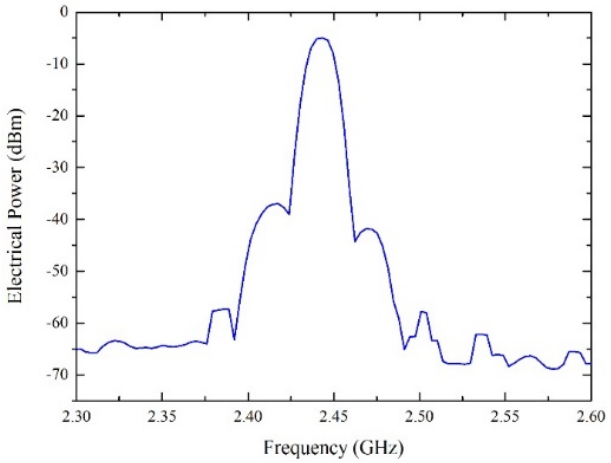

Figure 6. Electrical spectrum corresponding to the Coordinator

3.2 Experimental Frequency Response

Figure 7 illustrates the experimental bench used in this work. It is well known that the use of multimode optical fibers is reserved for short distances, such as in local area networks. Because, we are interested to emulate a FTTH-PON, whose typical length is in the order of 20km [12], thus the use of single-mode optical fiber is mandatory, due to its characteristics of extremely low-losses. Furthermore, most of commercial electro-optical devices (optical sources, optical modulators, photodetectors, etc.) operating at the commercial wavelengths of 1300 and 1550 nm, are supplied with this type of fiber. From the comments above described, SM-SF is used in this experiment. In the next sub-section, a detailed description of the optical communication system is given.

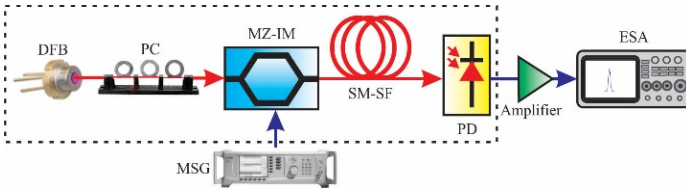

Figure 7. Optical communication system externally modulated

First, the optical spectrum of a DFB (NX8508-55, Side Mode Suppression Ratio SMSR=40dB, linewidth 0.1nm) is recorded by means of an Optical Spectrum Analyzer. According to the datasheet, this optical source has its own internal optical isolator to avoid reflections, therefore a good optical stability is guaranteed. Figure 8 shows the optical spectrum for an operation current of

20mA exhibiting a central wavelength λ_0=1553.5nm. The shape of the optical spectrum corresponds to Eq. (1).

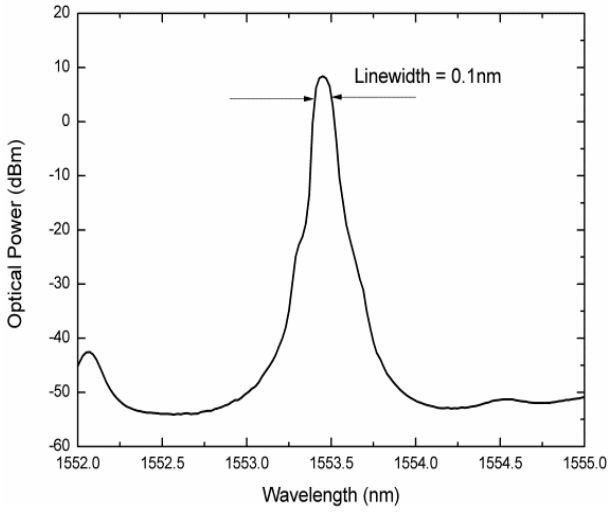

Figure 8. Optical spectrum of the DFB laser source used

Once the characteristics of the optical source are known, the light generated by the DFB is modulated via the electro-optic MZ-IM (insertion loss of 2.7dB, BW-20GHz, operating wavelength 1530-1580 nm, Vπ=7.5 V). The Polarization Controller (PC) device allows optimizing the optical power level at the output of the modulator. The RF signal used to modulate the light is provided by a Microwave Signal Generator (MSG) through a sweep in frequency range of 0.01-13 GHz at a power of 0 dBm. The modulated beam is injected to a reel of SM-SF (D=15.81ps/nm·km @ 1550nm, α=0.22dB/km, L=25.24 km). The light that emerges of the optical fiber is turned to its corresponding electrical signal by the PD (Miteq, BW-13GHz, Responsivity=0.9Amp/Watt). This signal is submitted to a process of amplification (Minicircuits, ZVA-183-S+ Ultra-Wideband Amplifier, 0.7-18GHz, Gain 26dB) and finally visualized in the screen of the ESA. Figure 9 corresponds to the measured frequency response where the simulation curves have been superimposed. Since the frequency emitted by the XBee Module is at 2.44GHz, the low-pass band will be used to code the transmission of the RF signal.

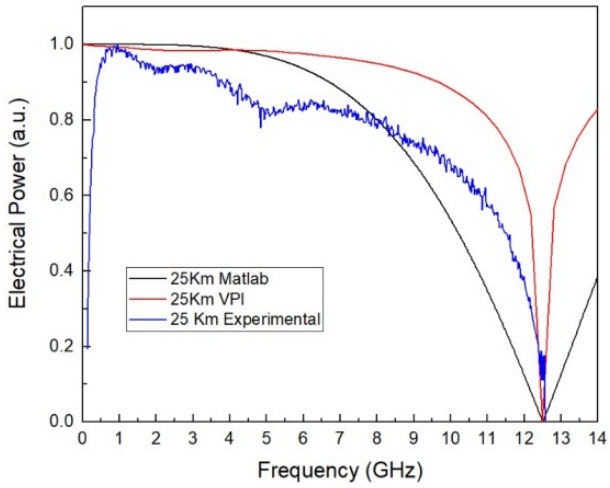

Figure 9. Comparison between simulated and experimental results

From this graph, it is noticeable that the response is restricted by the BW of the PD.

3.3 *Experimental RoF Transmission*

Figure 10 shows the test bench for carry out the transmission of the signal issued from the XBee module. The main difference to the scheme shown in Fig. 7 is that now the MSG is replaced by the coordinator module connected to PC_1 generating the information to be sent (an electrical signal at 2.44GHz at -6dBm) that is emitted from Antenna 1. Antenna 2 receives this signal which is amplified and launched to the RF port of the MZ-IM to modulate the optical signal. The modulated light is injected to the SM-SF. At the end of the link, the modulated light is converted into electric signal by the PD. Subsequently, amplified and separated by a power divider. A percentage of the recovered signal is evaluated by the ESA and the remainder is connected to the Antenna 3 where is emitted. An anechoic chamber is used to guarantee isolation between the signals emitted by antennas 1 and 3. Lastly, antenna 4 captures the signal to be handled by the second XBee module coupled to computer number 2 (PC 2), recovering in this manner the original transmitted message. Figure 11 corresponds to the measured electrical spectrum corresponding to the recovered signal with a SNR of 27dB.

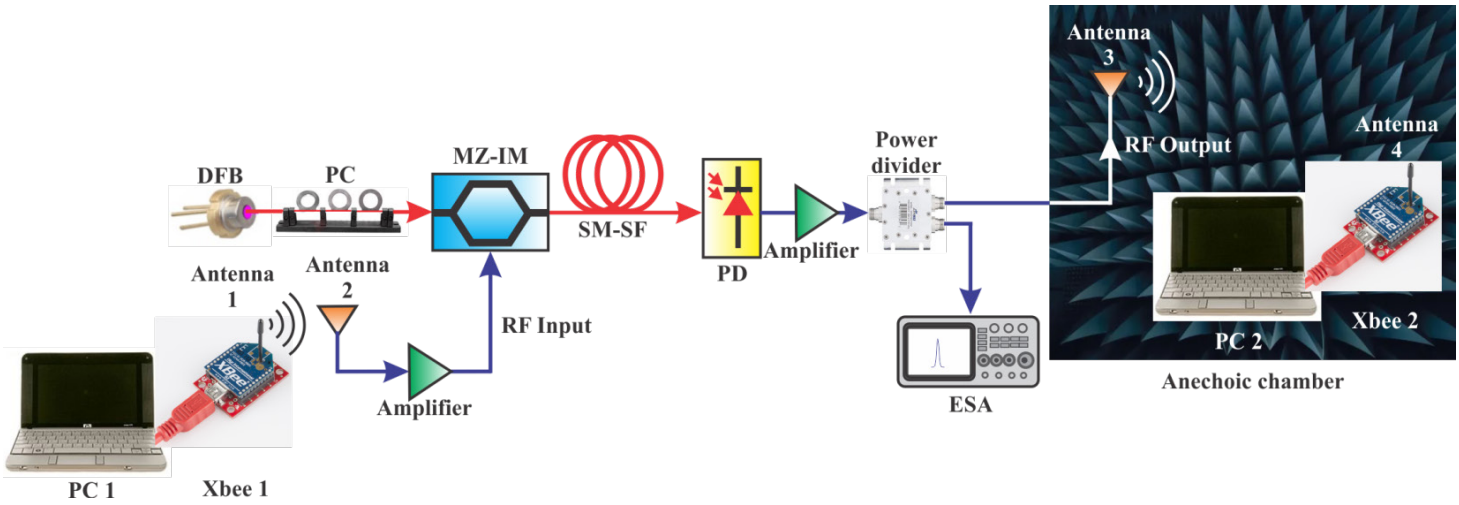

Figure 10. Experimental scheme assembled to test the RoF XBee transmission system

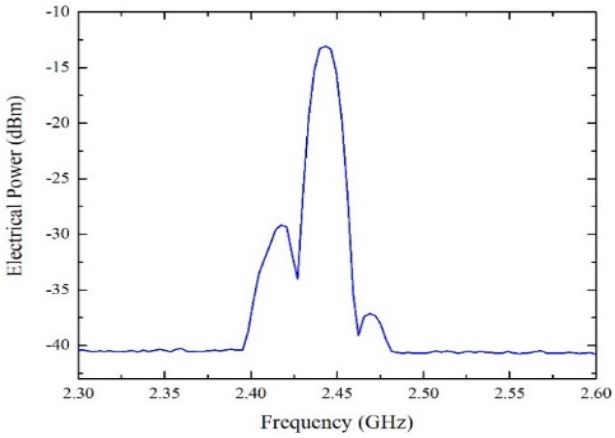

Figure 11. Recovered spectrum corresponding to the output of the system

4. Conclusion

In this work, we have experimentally demonstrated an efficient communication between two XBee modules using the RoF technique. The optical transmission was carried out by using an external modulation scheme. A full mathematical analysis explaining the principle of operation of an optical communication system was given. The relationship that allows determining the frequency response of the optical communication system was evaluated by a numerical simulation achieved in Matlab. Later, a block level simulation of the optical system was carried out by using VPIphotonics software corroborating the previous results. One thing to keep in mind is that the usage of an optical source whose central wavelength is 1310nm associated with SMSF allows the cancellation of the chromatic dispersion effect [12]. However, in this work, we have used a DFB laser whose central wavelength is around 1550nm and SM-SF; thus, the chromatic dispersion value was considerable. This effect, as well as, the length of the optical link has an important role to determine the electrical bandwidth of the system as it was evident in Eq. (7) and Eq. (8). The frequency response was composed by a low-pass band as well as a series of bandpass or notches. In particular, the first lobe was used for the transmission of a wireless signal of 2.44GHz issued by the XBee module. Optical transmission was successfully achieved through an optical link of 25.24Km. The recovered RF signal exhibits a SNR of 27dB. Considering that the electrical bandwidth can be tailored in function of the length of the optical link, it is possible to assure the possibility to accommodate future services distributed by means of RoF schemes using a larger bandwidth. Furthermore, another interesting feature of this RoF system is that, at the end of the link, data can be distributed by antennas to several customers. Direct and external modulation can be used to implement a D-RoF system in our case we have opted for external modulation using a Mach Zehnder modulator (MZM) to modulate a DFB laser in order to generate a simpler configuration [13]. As future work, we propose the use of a VCSEL as optical source in order to benefit of its properties as threshold currents of very few mA and facilitate the coupling with optical fibers [14].

Acknowledgments

L. A. González-Mondragón, L. J. Quintero-Rodríguez, and A. G. Correa-Mena, wish to thank the CONACyT for the student scholarships number 553921, 465594 and 335148, respectively.

References

[1] L. A. González-Mondragón, L. J. Quintero-Rodríguez, A. G. Correa-Mena, J. Rodríguez-Asomoza, A. García Juárez, I. E. Zaldívar-Huerta, “Performance Evaluation of Transmission Between Two Wireless Devices Based on Radio-over-Fiber Technology”, in 2018 15th International Conference on Electrical Engineering, Computing Science and Automatic Control (CCE), Mexico City , MX, 2018. https://doi.org/10.1109/ICEEE.2018.8533916

[2] A. M. Zin, M. S. Bongsu, S. M. Idrus, and N. Zulkifli, “An overview of Radio-over-Fiber Network Technology”, in 1st International Conference on Photonics 2010 (ICP 2010), Langkawi, Malaysia, 2010. https://doi.org/10.1109/ICP.2010.5604429

[3] A. K. Vyas, N. Agrawal, “Radio over Fiber: Future Technology of Communication”, International Journal of Emerging Trends & Technology in Computer Science, 1(2), 233-237, 2012.

[4] J. Beas, G. Castañon, I. Aldaya, A. Aragón-Zavala and G. Campuzano, “Millimeter-Wave Frequency Radio over Fiber Systems: A Survey”, IEEE Communications Surveys Tutorials, 15(4), 1593-1619, 2013 https://doi.org/10.1109/SURV.2013.013013.00135

[5] S. Kaur, M. Srivastava, K. Singh Bhatia, “Radio over Fiber Technology–A Review,” International Conference of Technology, Management and Social Sciences, Special Issue ICTMS-15, 85-89, 2015.

[6] D. Apostolopoulos, G. Giannoulis, N. Argyris, N. lliadis, K. Kanta, and H. Avramopoulos, “Analog Radio-over Fiber Solutions in Support of 5G”, in 2018 International Conference on Optical Network Design and Modeling (ONDM), Dublin, Ireland ,2018. https://doi.org/10.23919/ONDM.2018.8396143

[7] Pooja, Saroj, Manisha, “Advantages and Limitations of Radio over Fiber System”, International Journal of Computer Science and Mobile Computing, 4(5), 506-511, 2015.

[8] Li Zonglei, Yan Lianshan, Jiang Hengyun, Chen Zhiyu, Guo Yinghui, “Simultaneous transmission of RFID, WIFI and ZigBee over fiber”, in 22nd Wireless and Optical Communication Conference (WOCC), Chongqing, China, 2013. https://doi.org/10.1109/WOCC.2013.6676438

[9] Z. Li, L. Yan, W. Pan, B. Luo, J. Ye, H. Jian, “Simultaneous transmission of multiple wireless services over fiber with reduced network complexities”, IEEE/OSA Journal of Optical Communications and Networking, 6(1), 26-32, 2014. https://doi.org/10.1364/JOCN.6.000026

[10] J. P Goedgebuer, A. Hamel, ,H. Porte, and N. Butterlin, “Analysis of optical crosstalk in coherence multiplexed systems employing a short coherence laser diode with arbitrary power spectrum”, IEEE Journal of Quantum Electronics, 26(7):1217-1226, 1990. https://doi.org/10.1109/3.59661

[11] B. Saleh and M. Teich,. Fundamentals of photonics. Wiley Interscience, 1991.

[12] C. Lee, W. V. Sorin and B. Y. Kim, "Fiber to the Home Using a PON Infrastructure," in Journal of Lightwave Technology, 24(12), 4568-4583, 2006. doi: 10.1109/JLT.2006.885779

[13] M. U. Hadi, H. Jung, S. Ghaffar, P. A. Traverso, G. Tartarini, “Optimized digital radio over fiber system for medium range communication”, Optics Communications, 443, 177-185, 2019. https://doi.org/10.1016/j.optcom.2019.03.037

[14] M. U. Hadi, P. A. Traverso, G. Tartarini, O. Venard, G. Baudoin and J. Polleux, "Digital Predistortion for Linearity Improvement of VCSEL-SSMF-Based Radio-Over-Fiber Links", IEEE Microwave and Wireless Components Letters, 29(2), 155-157, 2019. doi: 10.1109/LMWC.2018.2889004

ASTES

Advances in Science, Technology and Engineering Systems Journal Vol. 4, No. 4, 133-140 (2019)

www.astesj.com

Special Issue on Multidisciplinary Sciences and Engineering

ASTESJ

ISSN: 2415-6698

Effects of Using Fuzzy Material Handling Inputs in the Genetic Algorithm for Machine Layout

Wanwanut Boongsood*, Chiranuwat Jadram

School of Manufacturing Engineering, Suraneree University of Technology, 30000, Thailand

ARTICLE INFO

Article history:
Received: 28 April, 2019
Accepted: 26 June, 2019
Online:17 July, 2019

Keywords :
Machine layout
Fuzzy numbers
Genetic algorithm

ABSTRACT

This study introduces the implementation of fuzzy set theory to solve machine layout design issues, in order to handle vague information, using a genetic algorithm with tournament selection as the selection operator. The material handling inputs, including frequency and volume of materials that move between machines, were the parameters regarded as fuzzy numbers. The experimental results came from 2 case studies in a manufacturing system. In the first case, examining the difference in shapes of the triangular membership functions of input data, the total distances were reduced from 38.45 m to 29.72 m, a 22.71% reduction in distance. In the second case, examining the uncertainty of fuzzy data by an expert, the total distances were reduced from 103.45 m to 82.45 m, a 20.03% reduction in distance. It was found that given the uncertainty in input data, a shorter total material handling distance might not give a lower cost. The selection operator of tournament selection can compete effectively to converge to near the optimum solution. This can, therefore, be an alternative technique in managing manufacture.

1. Introduction

Facility layout design plays a large part in business competition. Facilities can be machines, workstations, construction sites or departments, depending on the type of business. Costs can be reduced by having an appropriate layout. However, it is a complex problem. One of the essential goals of the design is to minimize total material handling costs, which are affected by many factors, such as types of materials, processing and production flow. Especially in the manufacturing industries, some produce not just one product but a variety of goods.

Moreover, in reality, the factors that affect material handling costs are vague and fuzzy. In a manufacturing system, they are dependent generally on the seasons, product variety and business growth. In order to engage with this ambiguity, there are levels of the vagueness of information, and the decision is usually made under uncertainty [1]. Fuzzy sets theory is a suitable concept to deal with this situation [2-6]. Therefore, this paper extends the research to understand the effects when the values in fuzzy sets are predictable and if they are extremely vague.

In many manufacturing industries, there can be several products manufactured in a factory, and each product can have different routes through machines or workstations. Production efficiency depends highly on this kind of problem in production planning [7]. Production costs can be reduced by 10–30% when the facility layout is more effective [8]. Shorter handling distances of materials' flow between workstations are required for faster transfer times within a factory floor.

The inputs necessary to design a facility layout for an actual production system are usually imprecise. Besides, the issue is considered a complicated situation because of the choice of products, materials, processes and other factors involved with the business. These factors are also time-dependent, such as customer orders and product growth, so the cost of material handling between machines usually changes. Different methods [9-12] have been presented for solving these kinds of problems; however, uncertain and ambiguous data inputs have been paid little attention [13]. Therefore, the fuzzy set theory is applied in this paper.

Many researchers have proposed different ways to solve this complex problem. In choosing the solution, the aim should be to achieve maximum efficiency, and there should be a simple method for finding the answer. Drira, et al. [14] gathered techniques and methods used for solving machine layout problems. Several methods can be used in the analysis of these problems, such as branch and bound, dynamic programming, simulated annealing, tabu search, genetic algorithms, ant colony, intelligence methods.

To find a solution with accurate answers to a complex problem, the costs of solving are very high [15]. Thus, it is better, rather, to have a method that can solve the vague problem obtaining an

*Wanwanut Boongsood, Email: wanwanut@sut.ac.th

acceptable answer with less time and cost than that with high accuracy and high cost. Since mathematical modeling techniques used to solve the facility layout design problem are complicated, challenging, and time-consuming, the issues require a powerful technique [5].

For the problems of machine layout design, the genetic algorithm is one popular method for finding answers, or approximate answers [16]. The Simple Genetic Algorithm (SGA) applies the principle of evolution and natural selection, by which the best individuals are selected to generate answers for the next generation. To calculate the answer by SGA is fundamental to solving the optimization problem. Many studies adopting this method have been released [14].

Conventionally, Genetic Algorithm (GA) includes these steps: generate an initial population, select high potential chromosomes to be parents, crossover and mutate parents' chromosomes to produce offspring chromosomes. Since there are a couple of genetic operators used in GA steps, improving the results fulfilling genuine applications can be achieved by adopting some of these operators (see [17-19] and [20]). The action of selecting high potential chromosomes to be parents called the selection process is the operation that has been broadly studied. Tournament Selection (TOS) and Roulette Wheel Selection (RWS) are general ways for making a selection. It was suggested that TOS is more effective than RWS [21-23]; the consequence is that a reasonable answer can be reached faster.

The research of Vitayasak [24] on fuzzy methods is interesting. The fuzzy approach can help manage uncertainty in practice, which may arise from a lack of information, not having enough data for the application, or the data not yet being available [25]. The experience of experts in reasoning or decision making in the human situation can help analysis and help manage uncertainty. The fuzzy theory is a theory of uncertain boundaries. Currently, it is widely used in the study of problems containing uncertain information [26].

It is important for machine layout design decision making and an efficient way to deal with inaccurate and vague information. Kritwattanakorn, et al. [27] used the RWS method for the selection approach in GA and suggested not to apply mutation for machine layout problems. However, based on the suggestions given by some research [21-23], the TOS method seems to be superior in finding a solution qualitatively (for instance, minimizing the total material handling cost) and obtain answers faster and closer to the optimum. In our paper presented initially to a conference [28], we related to the research of Kritwattanakorn, et al. [27] that not to apply mutation, used TOS for selection, and showed how to deal with the vagueness of information and assist solving problems taken from earlier research works [25, 26]. Our proposed method performed corresponding to the work presented by Jinghui, et al. [21] that using TOS is competitive in terms of solution quality and achieving minimization faster.

However, realistically, there are also levels of the vagueness of information. To understand the effects when the values in fuzzy sets are predictable and if they are extremely vague, in this study, the tournament method was used in the selection process for the genetic algorithms solving the machine layout problem. Material handling information was considered employing fuzzy uncertainty. An original layout and new layouts constructed from three GA based approaches were compared for 2 case studies. The first was the case where fuzzy information was thought predictable, examining different forms of skewed shapes. In the second case, the fuzzy data was obtained from a process expert in a new factory when asked to give the possible values for each variable. Thus the fuzzy sets were utterly formless. Every approach in the study was programmed and run with Visual Basic for Applications in Microsoft Excel for determining the layout, distance, and cost.

2. Methods

The fitness function, which is a particular type of objective function, is required for the GA algorithm to execute optimization. In this paper, the objective (1) is to minimize the total costs of material handling. This objective has been chosen by many researchers [29-31] in determining facility layouts. The function can be written as

$$Minimize\ C = \sum_{i=1}^{M} \sum_{j=1, i \neq j}^{M} f_{ij} c_{ij} d_{ij} \quad (1)$$

$$f_{ij} = \mathrm{F_{ij}} \times \mathrm{V_{ij}} \quad (2)$$

where C represents the total cost of the material handling system.

f_{ij} is the flow of materials in the production system.

c_{ij} is the unit cost of material handling between machines *i* and *j*.

d_{ij} is the rectilinear distance between the centroids of machines *i* and *j* (see for instance Fig. 1, where the distance between machines B to E is equivalent to $\Delta x + \Delta y$).

M is the total number of machines.

F_{ij} is the frequency flow between machines *i* and *j*.

V_{ij} is the volume flow between machines *i* and *j*.

In the calculation, minimize C is the objective, the variables used in consideration in this paper, $\mathrm{C_{ij}}$ and $\mathrm{d_{ij}}$ are considered as crisp numbers, and f_{ij} is information that is uncertain.

In general, $f_{ij} = \mathrm{F_{ij}} \times \mathrm{V_{ij}}$. However, in this study the information was considered both as if it is fuzzy to compare with the conventional idea, and as if it is crisp. Thus, when the frequency and the volume of material flows are considered as fuzzy numbers, they will be represented as $\mathrm{F'_{ij}}$ and $\mathrm{V'_{ij}}$, respectively, and the material handling flow as a fuzzy number is f'_{ij} (3).

Since the total cost, C, is a crisp number, f'_{ij} needs to be converted back to be an exact number. This method is called defuzzification, see (4).

$$f'_{ij} = \mathrm{F'_{ij}} \otimes \mathrm{V'_{ij}} \quad (3)$$

$$\mathrm{Defuzzification}(f'_{ij}) = f_{ij} \quad (4)$$

However, in some cases, the materials frequency and volume flow information are exact numbers, so they need to be converted

to a fuzzy number. This method is called fuzzification (5) when X is a number.

$$Fuzzification(X_{ij}) = X'_{ij} \quad (5)$$

The framework:

- Data input: the data input includes the production routing of each product (P_I, P_{II}, P_{III} ...), number of machines (N), sizes of machines (width, w_n, and length, l_n), shop floor area (W is width and L is length), frequency of material flow per round (F'_{ij}), volume flow per unit (V'_{ij}), unit material handling cost between locations of machines (c_{ij}) and distance between machines (d_{ij}), population size (v) and the number of generations to simulate (G).
- Step 1) Fuzzification: The uncertain flow frequency of materials, f_{ij} which is the function of F_{ij} and V_{ij} , was converted to fuzzy numbers (f'_{ij}).
- Step 2) Fuzzy computing: Fuzzy arithmetic was used.
- Step 3) Defuzzification: In order for the next step following the GA approach, crisp numbers are essential for calculation. The fuzzy number f'_{ij} was required to be transformed into crisp numbers.
- Step 4) Genetic algorithm: The sub-processes in the adapted GA are shown in Fig. 2.
- Stop: The calculation stops when conditions are met as in Fig. 2.

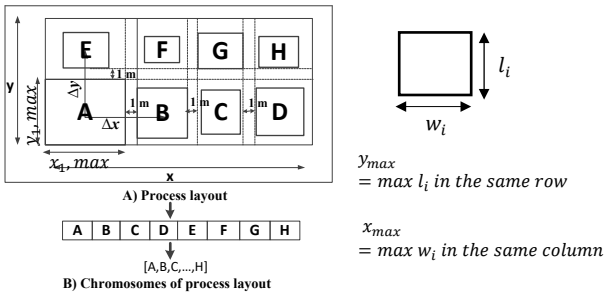

Figure 1: Chromosomes representation.

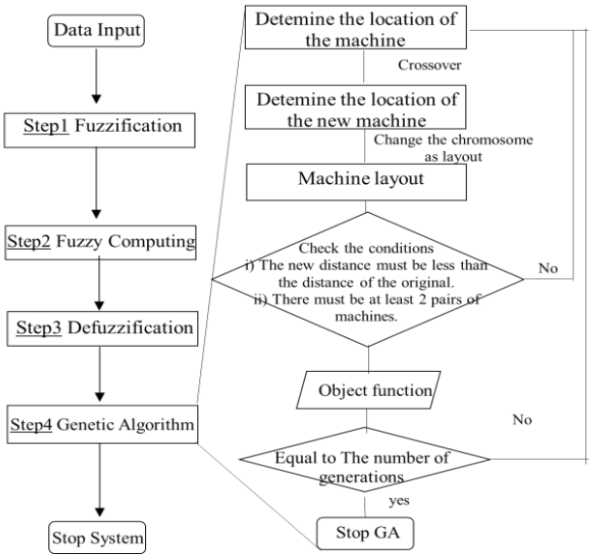

Figure 2: The framework.

2.1. Fuzzy number

Fuzzy numbers are the foundation of fuzzy set theory [2]. They are an extended form of real numbers that do not refer to one single value, but a set of possible crisp numbers. The fuzzy technique is used to represent data with uncertainties.

2.1.1. The shape of membership: Triangular fuzzy numbers (TFNs), graphically represented as Fig. 3, are used in this research. They are suitable because of their computational advantages and commonly used for subjective description [6].

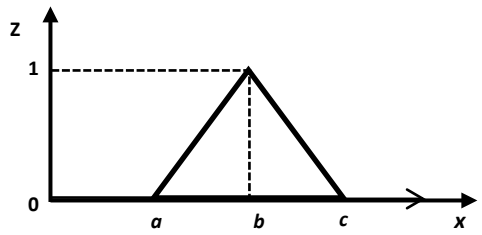

Figure 3: Triangular fuzzy number.

The membership function of a TFN can be explained by:

$\mathbf{Z(x)}$ is the grade of membership,

where $Z(x) > 0$ when $a < x < c$

$Z(x) = 0$ when $x \leq a$ *or* $x \geq c$

$Z(x) = 1$ when $x = b$ *"highest grade of membership at the modal value."*

Therefore,

a = the lowest possible value,

b = the most likely possible value,

c = the highest possible value in the fuzzy set.

2.2.2. Fuzzification: First, it is necessary to convert the input information to fuzzy numbers and calculate them using fuzzy operators. For input data F_{ij} and V_{ij}, the fuzzy sets of F'_{ij} and V'_{ij} are

$$F' = [\mathrm{F_L}, \mathrm{F_M}, \mathrm{F_H}] \quad (6)$$

$$V' = [\mathrm{V_L}, \mathrm{V_M}, \mathrm{V_H}] \quad (7)$$

$\mathrm{F_L}, \mathrm{F_M}$ and $\mathrm{F_H}$ are the lowest, most likely, and highest possible values of the frequency flow and $\mathrm{V_L}, \mathrm{V_M}$ and $\mathrm{V_H}$ are the lowest, most likely and highest possible values of the volume flow, and their grades of membership are between 0 and 1. If, for example, the total material flow frequency of all products is possibly 20 times and the total material flow volume is approximately 5 units each time, the material flow F could be a set of numbers with the most likely value of 18 such as [16, 18, 19] as well as V could be [3, 5, 6].

2.1.3. Fuzzy arithmetic: The operations [32] can be indicated by

Fuzzy addition $\oplus$:

$$\mathrm{F} \oplus \mathrm{V} = [\mathrm{F_L} + \mathrm{V_L} \ , \ \mathrm{F_M} + \mathrm{V_M} \ , \ \mathrm{F_H} + \mathrm{V_H}] \quad (8)$$

Fuzzy multiplication $\otimes$:

$$F \otimes V = [\min(F_L V_L, F_L V_H, F_H V_L, F_H V_H), F_M V_M, \max(F_L V_L, F_L V_H, F_H V_L, F_H V_H)] \quad (9)$$

With the above example values

$$F \otimes V = \begin{bmatrix} \min(16\times 3,\ 16\times 6, 19\times 3,\ 19\times 6), 18\times 5, \\ \max(16\times 3,\ 16\times 6, 19\times 3,\ 19\times 6) \end{bmatrix}$$

$$= \begin{bmatrix} \min(48, 96, 57, 114), 90, \\ \max(48, 96, 57, 114) \end{bmatrix}$$

$$= [48, 90, 114]$$

2.1.4. Defuzzification: Before entering the GA procedure, the fuzzy numbers for the material flow must be changed to crisp numbers using the fuzzy weight method [33].

$$f_{ij} \cong f'_{ij} \quad (10)$$

$$f_{ij} \cong \{[(0.5 \times (a + c)) + b]/2\} \quad (11)$$

therefore, $f_{ij} = \{[(0.5 \times (48 + 114)) + 90]/2\}$

$=85.5$

2.2. Genetic algorithm

The objective function (1) is used in this paper to find the optimum value by applying the genetic algorithm. The suggested GA has been modified from the Simple Genetic Algorithm (SGA) [16]. It begins with an initial set of random solutions for the problem being considered. The set of these alternatives is called the population. The population's individuals are called chromosomes. The objective function evaluates the results from the chromosomes. The chromosomes showing high potential is then carried out to be a part of the new generarion. In the crossover phase, a chromosome is chosen, along with the checking conditions, to produce the offspring. The details follow.

2.2.1. Initialization: GA approach begins with creating an initial population, $\boldsymbol{v}$. In our cases for solving machine layout problems, the genes represent the machines, and the chromosomes are for the layouts. Thus, the initial population can be converted from the "prior to improvement" process layout, see Fig. 1 (B) for an example.

2.2.2. Fitness evaluation: This is the procedure for assessing the chromosome's value. The chromosome that is more likely to be selected for the reproduction process would be selected by taking the proportionate fitness into consideration. The objective function of the fitness function, as presented in (12), can be described by total distance, in order to minimize the total costs of the material handling in the machine design issue.

$$\text{Total distance: } d_{ij} = \sum P_I + P_{II} + \cdots + P_k \quad (12)$$

Every material handling distance of product P is computed from the machine routing when each row or column of the machines is 1 m apart, as shown in Fig. 1. Assuming that there are 3 products required to be manufacture in a plant, as shown in Table 2, thus k=3. The machines have to be arranged on the floor plan to determine the total distance derived for a chromosome. The machines were arranged onto a certain floor area of W × L. The difference between the number of columns and rows of the machines was 1 at most.

2.2.3. Selection: This step decides which chromosomes should be parents in the reproduction process to generate offspring for the next generation.

Tournament selection (TOS): The simple tournament selection method [14] was used in this research. First, it divides the population into groups. Next, in each group, n chromosomes are randomly selected. The next generation of parents shall then be assigned from the chromosomes that make the most efficient solution in their groups. There were 2 groups in a tournament in this work. Each group had 3 chromosomes (n = 3), then the best chromosomes in each group were chosen as the next generation of parents.

2.2.4. Crossover: A new solution, namely offspring, is created by the crossover process. In this work, a crossover point, as shown in Fig. 4, was randomly chosen. After the crossover process, 2 conditions were checked. For condition 1, at least 2 pairs of machines in the chromosome must be operated side-by-side. For condition 2, after simulating the machines onto the shop floor area, and the new distance derived from the offspring must be reduced in comparison to the distance achieved by the layout of the parent.

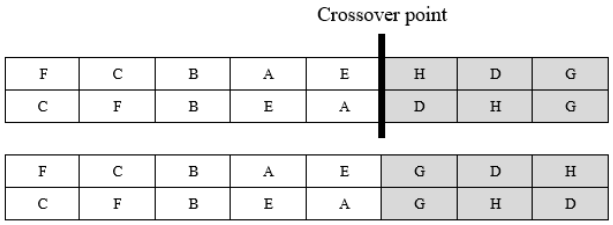

Figure 4: One point crossover process.

2.2.5. Mutation: The mutation process is one in which genes are randomly selected and their positions in the chromosome are swapped to generate additional offspring. It is a traditional step in conventional GA. Kritwattanakorn et al. [27], however, proposed that the mutation should be disregarded in this kind of problem. They have found it produced machines positioned further away while they should be put side by side when considering routing and lastly produced poor outcomes.

2.2.6. Stop: The proposed GA procedure was looped until the given number of generations was met, see Fig. 2.

3. Example

Two layout problems were studied in this research. The details are as follows:

- Case 1: This case uses original information from the manufacture of plywood furniture. There were 3 products and 8 machines in the same shop floor area. Table 2 shows the production routing for each product. Table 3 exhibits the sizes of the machines. The material handling information was initially received as crisp numbers.
- Case 2: This case studied a bus manufacturer. The fuzzy material handling information was given when their

process experts were asked for the values in the fuzzy sets of material flow between machines. There were 12 products and 8 machines. Table 4 shows the production routing of each product, and the machine sizes are shown in Table 5.

Since GA is widely applied for solving machine layout problems, the layouts constructed by different approaches were compared as listed. A summary of GA based approaches is shown in Table 1.

1. Initial layout (unknown approach)
2. SGA [16]
3. Modified GA with RWS and additional conditions (Kritwattanakorn et al. [27])
4. Modified GA with TOS and additional conditions (proposed approach)

Table 1: Summary of GA based approaches.

No	Information	Selection	Crossover	Mutation	Special Conditions
1	Crisp	Unknown (Initial layout)			
2	Crisp	RWS	One point	One point swap	No
3	Crisp	RWS	One point	No	Yes, see 2.2.4
4	Fuzzy	TOS	One point	No	Yes, see 2.2.4

Here the proposed GA approach used Thai Baht (32.50 THB = 1 USD), the number of the initial population, v, was 10, and the number of generations, G, was 100 given to stop the loop. The machine layout design problems were solved using VBA in MS Excel running under Windows 8 OS, on an Intel (R) Core (TM) i7-4500U 1.8GHz Ram 4 GB device.

Table 2: Products and production routing for case 1.

Product	Production Routing
1	A-B-C-D
2	A-E-F-G
3	A-H

Table 3: Sizes of the machines for case 1.

Machine	Dimensions	
	Width (m)	Length (m)
A	2.00	2.00
B	1.35	1.30
C	1.30	1.25
D	1.35	1.30
E	1.22	1.25
F	1.00	1.00
G	1.22	1.25
H	1.20	1.22

4. Results and Discussion

4.1. Case 1: When the level of fuzziness was considered predictable.

In case 1, the costs from layouts exposed by the existing methods including: from the SGA method [16], the adapted GA that applied GA with RWS selection and without mutation [27], and the proposed method in this study using 6 different fuzzy data sets combined with the GA approach (Fig. 5). The case studies used various fuzzy set differences of 0%, 15%, 30%, and 50% fuzziness for the frequency flow and volume flow. The fuzzy set with the difference of 0% represents a crisp number.

Table 4: Products and production routing for case 2.

Product	Production Routing
1	A - F
2	B - C
3	A - F
4	B - D
5	A - G
6	B - H
7	A – G – H
8	B – G – H
9	A – E – F
0	B – E – C
11	A – E – F
12	B – E – D

Table 5: Sizes of the machines for case 2.

Machine	Dimensions	
	Width (m)	Length (m)
A	1.20	1.50
B	1.20	1.50
C	1.70	1.50
D	1.20	1.40
E	1.50	1.20
F	1.30	6.00
G	1.20	1.00
H	3.50	2.00

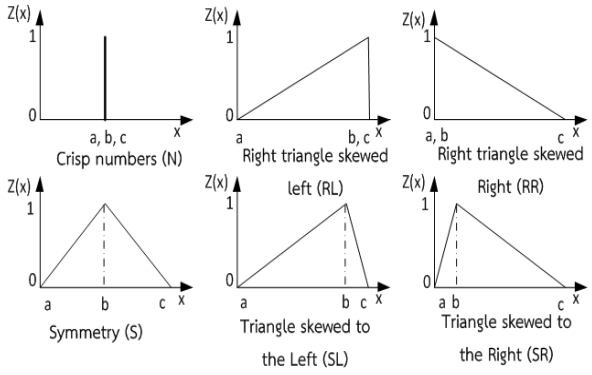

Figure 5: Data sets representing fuzzy numbers.

The results in Fig. 6 show that the total costs vary if the input information is uncertain or fuzzy. If there is the high difference between the lowest and highest possible values, the total costs increase or decrease considerably, such as for the right triangle skewed right (RR), the highest possible value gives a high total cost, but the lowest possible value gives a low total cost. The costs increase or decrease depending on the nature of the skew. If the input information is skewed fully to one side (such as RR and SR), it is likely to make the total costs higher, but if the input is skewed to the minimal side (such as RL and SL), it shows the opposite impact.

Table 6: Results of case 1 with different fuzzy types.

Difference	Fuzzy Type	F', V'	Total Cost (USD)
0% [a]	N	[20, 20, 20], [5, 5, 5]	914.46
15%	S	[18, 20, 22], [4, 5, 6]	923.61
	RL	[17, 20, 20], [4, 5, 5]	841.30
	RR	[20, 20, 23], [5, 5, 6]	1,001.34
	SL	[18, 20, 21], [4, 5, 5]	861.88
	SR	[19, 20, 22], [5, 5, 6]	976.19
30%	S	[17, 20, 23], [4, 5, 6]	955.61
	RL	[14, 20, 20], [3, 5, 5]	781.86
	RR	[20, 20, 26], [5, 5, 7]	1,101.93
	SL	[16, 20, 22], [3, 5, 6]	868.74
	SR	[18, 20, 24], [4, 5, 7]	1,005.91
50%	S	[15, 20, 25], [3, 5, 7]	960.18
	RL	[10, 20, 20], [2, 5, 5]	731.57
	RR	[20, 20, 30], [5, 5, 8]	1,234.52
	SL	[13, 20, 23], [2, 5, 7]	884.74
	SR	[17, 20, 27], [3, 5, 8]	1,067.63

a. Crisp number

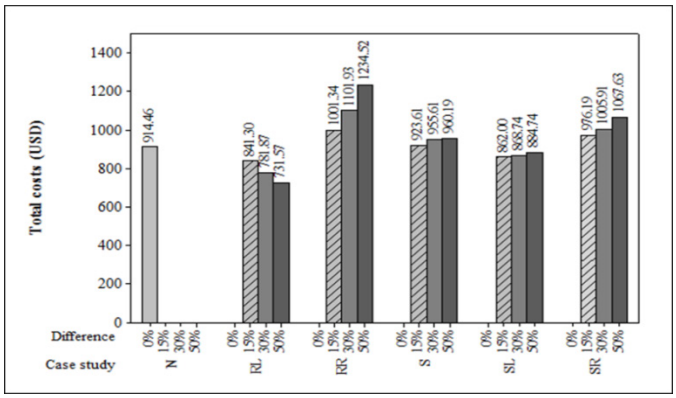

Figure 6: The relationship between various fuzzy data sets and the total cost.

From the findings of this case, it can be seen that the suggested technique shows total costs that increase or decrease depending on the flow of the material handling system in the production. These findings agree with the existing research works [9-12] that information is essential for making a decision on layout planning and design, and fuzzy sets is an appropriate idea in dealing with imprecise information [25, 26].

Table 6 shows the outcomes of the 4 different methods and their layouts for the machines are shown in Fig. 7. Table 6 demonstrates the results of total costs and distances. Before arranging the layout, the total cost initially was 1,179 USD and the total distance was 38.45. The proposed method with a different variation of 15% in fuzzy data input (due to natural associated vagueness) has a total cost of 923.61 USD and a total distance of 29.72 m. It can reduce the total cost by 21.66% and the distance by 22.71%. Both the traditional GA (SGA) method [16] and the Kritwattanakorn et al. method [27] give total costs and distances greater than the proposed method.

Table 7: Comparison of the different approaches in case 1.

Approach	Total cost (USD)	Total Distance (m)
Unknown (initial layout)	1,179.00	38.45
SGA	1,060.92	34.48
Modified GA+RWS+Conditions	978.46	31.80
Modified GA+TOS+Conditions *	923.61	29.72

* Fuzziness at 15 % difference

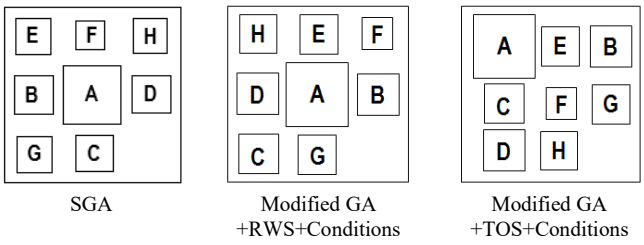

SGA | Modified GA +RWS+Conditions | Modified GA +TOS+Conditions

Figure 7: Layouts of machines obtained using different methods for case 1.

4.2. Case 2: When the level of fuzziness was extremely vague.

In fact, the shape of fuzzy sets might not be specific. This study used a bus manufacturer as an example. They are a family run business. Machines were laid out based on the experience of the systems expert, not an analysis of manufacturing data. Table 8 shows the frequency and volume of material transport between machines, by letting the expert respond what were the minimum, modal, and maximum values, as for the machine layout design input.

Table 8: Fuzzy data input of case 2.

Machine	Frequency flow (F')	Volume flow (V')
M1-M5	[3, 10, 16]	[5, 16, 22]
M1-M6	[6, 8, 14]	[7, 10, 24]
M1-M7	[3, 4, 7]	[8, 12, 18]
M2-M3	[1, 1, 1]	[0, 2, 2]
M2-M4	[3, 6, 8]	[6, 8, 14]
M2-M5	[2, 2, 4]	[7, 8, 13]
M2-M8	[1, 3, 4]	[1, 2, 2]
M5-M3	[3, 6, 8]	[6, 8, 14]
M5-M6	[2, 2, 5]	[6, 11, 15]
M7-M8	[2, 2, 2]	[3, 4, 6]

Table 9 shows the results that the totals cost of material handling can be considerably lowered. The costs generated from the layouts obtained from the method described in this paper were compared competitively with the initial machine layout and 2 existing methods. The machine layouts can be seen in Fig. 8. Table 9 compares the approaches. The total cost and the total distance before arranging being 84.22 USD and 103.10 m, respectively. The proposed method, with fuzzy data input acknowledged from the product experts, has a total cost and distance of 66.40 USD and 82.45 m, correspondingly. The total cost and distance can be reduced by 21.16% and 20.03%.

Even if the total cost obtained from the proposed method was higher than SGA [16] and the method with RWS (Kritwattanakorn et al. method [27]), the total distance was the shortest. This emphasizes the effect of fuzziness of information on decision making. More attention should be paid to uncertainties of data.

Table 9: Comparison of the different approaches in case 2

Approach	Total cost (USD)	Total Distance (m)
Unknown (initial layout)	84.22	103.10
SGA	48.56	92.40
Modified GA+RWS+Conditions	41.24	90.25
Modified GA+TOS+Conditions	66.40	82.45

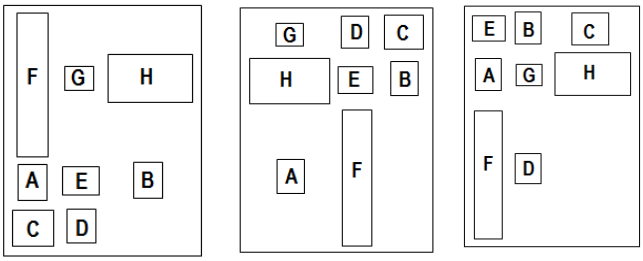

SGA | Modified GA+RWS+Conditions | Modified GA+TOS+Conditions

Figure 8: Layouts of machines obtained using different methiods for case 2.

5. Conclusion

Acknowledgment

This research was supported by grants funded by the Graduate School of Manufacturing Engineering, Suranaree University of Technology, and the Ministry of Science and Technology, Thailand.

References

[1] L. A. Zadeh, "Fuzzy Sets as a Basis for a Theory of Possibility," Fuzzy Sets and Systems, 100, 9-34, 1999. https://doi.org/10.1016/S0165-0114(99)80004-9

[2] L. A. Zadeh, "Fuzzy Sets," Information and Control, 8, 338-353, 1965. https://doi.org/10.1016/S0019-9958(65)90241-X

[3] İ. Kaya, M. Çolak, and F. Terzi, "A Comprehensive Review of Fuzzy Multi Criteria Decision Making Methodologies for Energy Policy Making," Energy Strategy Reviews, 24, 207-228, 2019. https://doi.org/10.1016/j.esr.2019.03.003

[4] A. L. Guiffrida and R. Nagi, "Fuzzy Set Theory Applications in Production Management Research: A Literature Survey," Journal of Intelligent Manufacturing, 9, 39-56, 1998. 10.1023/a:1008847308326

[5] B. K. Wong and V. S. Lai, "A Survey of the Application of Fuzzy Set Theory in Production and Operations Management: 1998–2009," International Journal of Production Economics, 129, 157-168, 2011. https://doi.org/10.1016/j.ijpe.2010.09.013

[6] S. Balin, "Parallel Machine Scheduling with Fuzzy Processing Times Using a Robust Genetic Algorithm and Simulation," Information Sciences, 181, 3551-3569, 2011. https://doi.org/10.1016/j.ins.2011.04.010

[7] M. Ficko, M. Brezocnik, and J. Balic, "Designing the Layout of Single- and Multiple-Rows Flexible Manufacturing System by Genetic Algorithms," Journal of Materials Processing Technology, 157–158, 150-158, 2004. http://doi.org/10.1016/j.jmatprotec.2004.09.012

[8] J. A. Tompkins, J. A. White, Y. A. Bozer, and J. M. A. Tanchoco, Facilities Planning: Wiley, 2010.

[9] F. M. Defersha and A. Hodiya, "A Mathematical Model and a Parallel Multiple Search Path Simulated Annealing for an Integrated Distributed Layout Design and Machine Cell Formation," Journal of Manufacturing Systems, 43, 195-212, 2017. https://doi.org/10.1016/j.jmsy.2017.04.001

[10] P. B. G. S. N. Murthy, J. Ranganayakulu, K. P. Vidhu, and K. V. Rao, "Heuristic Search Algorithm for the Single-Row Machine Layout in an Automated Manufacturing System," Procedia Technology, 25, 1088-1095, 2016. https://doi.org/10.1016/j.protcy.2016.08.213

[11] Y. Ojaghi, A. Khademi, N. M. Yusof, N. G. Renani, and S. A. H. b. S. Hassan, "Production Layout Optimization for Small and Medium Scale Food Industry," Procedia CIRP, 26, 247-251, 2015. https://doi.org/10.1016/j.procir.2014.07.050

[12] M. A. El-Baz, "A Genetic Algorithm for Facility Layout Problems of Different Manufacturing Environments," Computers & Industrial Engineering, 47, 233-246, 2004. https://doi.org/10.1016/j.cie.2004.07.001

[13] S. Safarzadeh and H. Koosha, "Solving an Extended Multi-Row Facility Layout Problem with Fuzzy Clearances Using Ga," Applied Soft Computing, 61, 819-831, 2017. https://doi.org/10.1016/j.asoc.2017.09.003

[14] A. Drira, H. Pierreval, and S. Hajri-Gabouj, "Facility Layout Problems: A Survey," Annual Reviews in Control, 31, 255-267, 2007. https://doi.org/10.1016/j.arcontrol.2007.04.001

[15] F. Karray, E. Zaneldin, T. Hegazy, A. Shabeeb, and E. Elbeltagi, "Computational Intelligence Tools for Solving the Facilities Layout Planning Problem," in Proceedings of the 2000 American Control Conference. ACC (IEEE Cat. No.00CH36334), 3954-3958, 2000.

[16] J. H. Holland, Adaptation in Natural and Artificial Systems: An Introductory Analysis with Applications to Biology, Control, and Artificial Intelligence: MIT press, 1992.

[17] N. M. Razali and J. Geraghty, "Genetic Algorithm Performance with Different Selection Strategies in Solving Tsp," in World congress on engineering 2011, London, U.K., 1134-1139, 2011.

[18] M. Gen, K. Ida, and C. Cheng, "Multirow Machine Layout Problem in Fuzzy Environment Using Genetic Algorithms," Computers & Industrial Engineering, 29, 519-523, 1995. https://doi.org/10.1016/0360-8352(95)00127-M

[19] R. Tavakkoli-Moghaddain and E. Shayan, "Facilities Layout Design by Genetic Algorithms," Computers & Industrial Engineering, 35, 527-530, 1998. https://doi.org/10.1016/S0360-8352(98)00150-8

[20] H. M. Pandey, "Performance Evaluation of Selection Methods of Genetic Algorithm and Network Security Concerns," Procedia Computer Science, 78, 13-18, 2016. https://doi.org/10.1016/j.procs.2016.02.004

[21] Z. Jinghui, H. Xiaomin, Z. Jun, and G. Min, "Comparison of Performance between Different Selection Strategies on Simple Genetic Algorithms," in International Conference on Computational Intelligence for Modelling, Control and Automation and International Conference on Intelligent Agents, Web Technologies and Internet Commerce (CIMCA-IAWTIC'06), Vienna, Austria, 1115-1121, 2005. 10.1109/cimca.2005.1631619

[22] H. Kılıç and U. Yüzgeç, "Tournament Selection Based Antlion Optimization Algorithm for Solving Quadratic Assignment Problem," Engineering Science and Technology, an International Journal, 22, 673-691, 2019. https://doi.org/10.1016/j.jestch.2018.11.013

[23] H. Kılıç and U. Yüzgeç, "Improved Antlion Optimization Algorithm Via Tournament Selection and Its Application to Parallel Machine Scheduling," Computers & Industrial Engineering, 132, 166-186, 2019. https://doi.org/10.1016/j.cie.2019.04.029

[24] S. Vitayasak, "Facility Layout Problem: A 10-Year Review and Research Perspectives (in Thai)," Naresuan University Engineering Journal, 5, 46-62, 2010.

[25] Z. Güngör and F. Arıkan, "Application of Fuzzy Decision Making in Part-Machine Grouping," International Journal of Production Economics, 63, 181-193, 2000. https://doi.org/10.1016/S0925-5273(99)00010-9

[26] S. K. Deb and B. Bhattacharyya, "Fuzzy Decision Support System for Manufacturing Facilities Layout Planning," Decision Support Systems, 40, 305-314, 2005. https://doi.org/10.1016/j.dss.2003.12.007

[27] S. Kritwattanakorn, K. Chamniprasart, and W. Boongsood, "A Permutation-Based Genetic Algorithm for Solving the Machine Layout of Manufacturing System," in The 10th SEATUC Symposium, Tokyo, Japan, 2016.

[28] C. Jadram and W. Boongsood, "Application of Fuzzy Materials-Handling Inputs with the Genetic Algorithm for Machine Layout," in 2018 7th International Conference on Industrial Technology and Management (ICITM), Oxford, UK, 265-269, 2018. 10.1109/icitm.2018.8333958

[29] R. G. Askin and C. R. Standridge, Modeling and Analysis of Manufacturing Systems: Wiley, 1993.

[30] C. K. H. Lee, "A Review of Applications of Genetic Algorithms in Operations Management," Engineering Applications of Artificial Intelligence, 76, 1-12, 2018. https://doi.org/10.1016/j.engappai.2018.08.011
[31] W. Yi, H.-L. Chi, and S. Wang, "Mathematical Programming Models for Construction Site Layout Problems," Automation in Construction, 85, 241-248, 2018. https://doi.org/10.1016/j.autcon.2017.10.031
[32] S. Gao and Z. Zhang, "Multiplication Operation on Fuzzy Numbers," Journal of Software, 4, 331-338, 2009.
[33] W. Dong and F. S. Wong, "Fuzzy Weighted Averages and Implementation of the Extension Principle," Fuzzy Sets and Systems, 21, 183-199, 1987. https://doi.org/10.1016/0165-0114(87)90163-1

ASTES

Advances in Science, Technology and Engineering Systems Journal
Vol. 4, No. 4, 141-146 (2018)
www.astesj.com
Special Issue on Advancement in Engineering and Computer Science

ASTES Journal
ISSN: 2415-6698

Optimal Discrete-time Sliding Mode Control for Nonlinear Systems Subject to Input Constraints

Olfa Jedda[*,1], Ali Douik[2]

[1]*National Engineering School of Monastir, University of Monastir, Monastir, Tunisia*

[2]*National Engineering School of Sousse, University of Sousse, Sousse, Tunisia*

ARTICLEINFO

Article history:
Received: 04 March, 2019
Accepted: 01 July, 2019
Online: 22 July, 2019

Keywords:
Discrete-time sliding mode control
Particle swarm optimization
Control input constraints
Chattering phenomenon
Inverted pendulum system

ABSTRACT

In this paper, an optimal discrete-time sliding mode control is proposed for single-input single-output nonlinear systems with input constraints. The sliding surface is designed on the basis of particle swarm optimization algorithm in order to optimize the system response characteristics while ensuring the follow-up of reference model in presence of constraints. Moreover, the controller is developed such that the elimination of chattering phenomenon, the finite-time convergence and the stability of the closed-loop system are guaranteed. Performed on an inverted pendulum system, simulation results demonstrate the effectiveness of the proposed approach over the discrete-time sliding mode controller using the saturation function and the discrete-time second order sliding mode controller in terms of fast response.

1 Introduction

This paper is an extension of work originally presented in 2018 15th International Multi-Conference on Systems, Signals and Devices (SSD) [1]. Due to the increasing use of computers in control applications, discrete-time sliding mode control (DSMC) has been extensively developed since its appearance with Milosavljevic in 1985 [2]; see, for example, [3–9]. However, the finite sampling time negatively impacts the robustness of continuous-time sliding mode control to external disturbances, parametric uncertainties and modeling errors [10–12]. In fact, the control input remains constant during the sampling period so that it can not be changed when the trajectory of system state crosses the sliding surface. This is at the origin of chattering phenomenon that may badly affect control devices and system performances [13].

Introduced by Gao in 1995 [14], the quasi-sliding mode concept consists to drive the state trajectory to cross the sliding hyperplane in finite-time, to move with a non-increasing zigzag motion and to remain within a specified layer. Thus, the above-mentioned drawback can be reduced but not eliminated. Several approaches was proposed in the literature to overcome it. In [15–17], the saturation function is used as smooth one instead of the sign function which is the origin of discontinuity. In [18–20], discrete-time second order sliding mode control (DSOSMC) was proposed for linear and nonlinear systems. In [21, 22], a piecewise-constant control is used to generate the discrete-time sliding mode. It ensures that the chatter effect is avoided and the system state trajectory convergences to the sliding surface after a finite-time interval.

In the following, an optimal discrete-time sliding mode control (ODSMC) is proposed for single-input single-output (SISO) nonlinear systems with input constraints. Particle swarm optimization (PSO) algorithm is employed to search the sliding vector to which corresponds the optimal response characteristics of the closed-loop system and its behavior follows the reference model. Developed by Eberhart and Kennedy in 1995 [23], PSO algorithm is based on food searching behavior of animals societies having no leaders in their swarm such as bird flocks and fish schools. Its main advantages are the easiness of implementation, the robustness in controlling parameters and the good efficiency in solving nonlinear, nondifferentiable and large search space problems [24, 25]. Regarding the control law, it is designed in such a way that chattering phenomenon is eliminated, the convergence to the sliding manifold is ensured in finite-time and the system dynamics are stable while respecting constraints.

The efficiency of the proposed controller will be demonstrated by applying it to an inverted pendulum system and by comparing it to DSMC controller using the saturation function and to DSOSMC controller with an arbitrary choice of control parameters and without taking into account the

[*]Corresponding Author: Olfa Jedda, olfa_jedda@outlook.com

input constraints.

This paper is organized as follows. The DSMC and DSOSMC controllers are developed for SISO nonlinear systems in sections 2 and 3. Section 4 is devoted for the design of the proposed ODSMC controller. The inverted pendulum system is represented in section 5. Section 6 illustrates numerical simulation results. Concluding remarks are given in section 7.

2 Discrete-time Sliding Mode Control

Consider a class of discrete-time SISO nonlinear system described by

$$\begin{cases} x(k+1) = F(x(k)) + H(x(k))\,u(k) \\ y(k) = Cx(k) \end{cases} \tag{1}$$

where $x(k) \in \mathbb{R}^{n\times 1}$ is the state vector, $u(k) \in \mathbb{R}$ is the control input, and $y(k) \in \mathbb{R}$ is the system output. $F(x(k)) \in \mathbb{R}^{n\times 1}$ and $H(x(k)) \in \mathbb{R}^{n\times 1}$ are vectors of nonlinear functions and C is the output matrix. Let's admit that H and its pseudo-inverse H^{+} are both bounded.

The sliding function is defined as follows

$$s(k) = c^T e(k) \tag{2}$$

where $e(k) = x(k) - x_d(k)$ is the tracking error and $c^T \in \mathbb{R}^{1\times n}$ is the sliding vector chosen such that the sliding dynamic $s(k) \equiv 0$ is asymptotically stable.

The reaching law is given by

$$s(k+1) = (1 - qT_s)\,s(k) - \varepsilon T_s \,\mathrm{sat}(s(k), \varphi) \tag{3}$$

where $0 < 1 - qT_s < 1$, $\varepsilon > 0$, T_s is the sampling period and sat is the saturation function defined as follows

$$\mathrm{sat}(s, \varphi) = \begin{cases} \frac{s}{\varphi} & \text{if } \left|\frac{s}{\varphi}\right| \le 1 \\ \mathrm{sign}(s) & \text{else} \end{cases} \tag{4}$$

with $\varphi > 0$ is the boundary layer width of s and sign is the sign function.

Using the reaching law (3) and the forward expression of the sliding function (2), the control law $u(k)$ is given by

$$\begin{aligned} u(k) = \left(c^T H(x(k))\right)^{-1} (& (1 - qT_s)\,s(k) \\ & - \varepsilon T_s \,\mathrm{sat}(s(k), \varphi) - c^T F(x(k)) + c^T x_d(k+1)) \end{aligned} \tag{5}$$

3 Discrete-time Second Order Sliding Mode Control

The sliding function defined in [19, 20] is given by

$$\sigma(k) = s(k) + \beta s(k-1) \tag{6}$$

with $\beta \in [0, 1[$ in order to ensure the stability of $\sigma(k)$.

The control law is given by

$$u(k) = u_{eq}(k) + u_d(k) \tag{7}$$

where $u_{eq}(k)$ is the equivalent control used to force the system state to evolve on the sliding manifold and $u_d(k)$ is the discontinuous control used to ensure the robustness.

Setting $\sigma(k+1) = \sigma(k) = 0$, the equivalent control $u_{eq}(k)$ is determined from the following relation

$$s(k+1) + \beta s(k) = 0 \tag{8}$$

Hence, It is given by

$$\begin{aligned} u_{eq}(k) = \left(c^T H(x(k))\right)^{-1} (& - c^T F(x(k)) \\ & + c^T x_d(k+1) - \beta s(k)) \end{aligned} \tag{9}$$

The discontinuous control $u_d(k)$ is expressed as follows

$$u_d(k) = u_d(k-1) - \varepsilon T_s \mathrm{sign}(\sigma(k)) \tag{10}$$

4 Optimal Discrete-time Sliding Mode Control

4.1 Design of Sliding Surface

The sliding vector c^T is determined using the PSO algorithm in order to ensure the optimization of the closed-loop system response characteristics and the follow-up of the reference model in the presence of constraints on control input.

PSO algorithm starts with population of np n-dimensional particles. The i^{th} particle of the swarm has a position $x_i = [x_{i,1}, \ldots, x_{i,n}]$ and a velocity $v_i = [v_{i,1}, \ldots, v_{i,n}]$. Its previously best visited position and the global best particle in the swarm are denoted by $pbest_i = [pbest_{i,1}, \ldots, pbest_{i,n}]$ and $gbest$ respectively. The velocity and the position of each particle are updated as follows

$$v_{i,j} = w\,v_{i,j} + \alpha_1 r_1 \left(pbest_{i,j} - x_{i,j}\right) + \alpha_2 r_2 \left(gbest_j - x_{i,j}\right) \tag{11}$$

$$x_{i,j} = x_{i,j} + v_{i,j} \tag{12}$$

with $i = 1, \ldots, np$ and $j = 1, \ldots, n$. w is the inertia weight, $\alpha_{1,2}$ are positive constant so-called the acceleration coefficients and $r_{1,2}$ are random parameters uniformly distributed within $[0, 1]$ at each generation.

PSO is used to generate the sliding vector that minimizes the following cost function

$$cost = \lambda_1 t_r + \lambda_2 t_s + \lambda_3 M_p + \lambda_4 E_{ss} \tag{13}$$

where t_r is the rise-time, t_s is the settling-time, M_p is the overshoot, E_{ss} is the steady-state error and λ_q , $q = 1, \ldots, 4$, are their corresponding weights.

As illustrated in Table 1, the iterative process is repeated until stopping criterion is met.

Table 1: Description of PSO algorithm

Step 1	**Parameter settings**
	Set the population size np, the minimum and maximum bounds $x_{min} = [x_{min,1}, \ldots, x_{min,n}]$ and $x_{max} = [x_{max,1}, \ldots, x_{max,n}]$, and the acceleration coefficients $\alpha_{1,2}$.
Step 2	**Initialization**
	Initialize the particle's position x_i^0, $i = 1 \ldots np$, randomly and uniformly within bounds.
	Initialize the particle's velocity v_i^0 and the particle's best position to its initial position, i.e. $pbest_i^0 = x_i^0$.
	Set $gbest$ equal to the global best particle.
Step 3	**PSO algorithm**
	WHILE stopping criterion is not met DO
	Update the particle's velocity and position
	FOR $i = 1$ to np
	FOR $j = 1$ to n
	$v_{i,j} = w\, v_{i,j} + \alpha_1 r_1 \left(pbest_{i,j} - x_{i,j}\right) + \alpha_2 r_2 \left(gbest_j - x_{i,j}\right)$
	END FOR
	$x_i = x_i + v_i$
	END FOR
	Update the particle's best position
	FOR $i = 1$ to np
	IF $f(x_i) \prec f(pbest_i)$
	$pbest_i = x_i$
	END IF
	END FOR
	Update the global best position
	FOR $i = 1$ to np
	IF $f(pbest_i) \prec f(gbest)$
	$gbest = pbest_i$
	END IF
	END FOR
	END WHILE

4.2 Design of Control Law

The control law is designed such that the chatter effect is avoided, the state trajectory convergences to the sliding surface after a finite-time interval and the closed-loop system is stable while respecting control constraints.

The forward expression of the sliding function (2) can be rewritten as follows

$$\begin{aligned} s(k+1) = s(k) &+ c^T \left(x_d(k) - x_d(k+1)\right) \\ &+ c^T \left(F(x(k)) - x(k)\right) + c^T H(x(k)) u(k) \end{aligned} \tag{14}$$

Setting $s(k+1) = 0$, the equivalent control u_{eq} is expressed by

$$\begin{aligned} u_{eq}(k) = -\left(c^T H(x(k))\right)^{-1} &\left(s(k) + c^T \left(x_d(k) - x_d(k+1)\right)\right. \\ &\left. + c^T \left(F(x(k)) - x(k)\right)\right) \end{aligned} \tag{15}$$

Consider that $\|u(k)\| \leq u_{max}$, the constrained control is given by

$$u(k) = \begin{cases} u_{eq}(k) & \text{if } \left\|u_{eq}(k)\right\| \leq u_{max} \\ \frac{u_{eq}(k)}{\left\|u_{eq}(k)\right\|} u_{max} & \text{else} \end{cases} \tag{16}$$

Suppose that

$$\left\|c^T \left(x_d(k) - x_d(k+1)\right) + c^T \left(F(x(k)) - x(k)\right)\right\| \leq \delta,$$
$$\left\|\left(c^T H(x(k))\right)^{-1}\right\| \leq \eta$$

and

$$u_{max} > \delta\eta \tag{17}$$

with $\delta > 0$ and $\eta > 0$.

It follows that

$$\begin{aligned} &\left\|u_{eq}(k)\right\| \leq \left\|\left(c^T H(x(k))\right)^{-1}\right\| \\ &\left\|s(k) + c^T \left(x_d(k) - x_d(k+1)\right) + c^T \left(F(x(k)) - x(k)\right)\right\| \\ &\qquad \leq \eta \left(\|s(k)\| + \delta\right) \end{aligned} \tag{18}$$

For $\|u(k)\| > u_{max}$, the forward expression of the sliding function (14) is expressed by

$$\begin{aligned} &s(k+1) = s(k) + c^T \left(x_d(k) - x_d(k+1)\right) \\ &+ c^T \left(F(x(k)) - x(k)\right) + c^T H(x(k)) \frac{u_{eq}(k)}{\left\|u_{eq}(k)\right\|} u_{max} \\ &= \left(s(k) + c^T \left(x_d(k) - x_d(k+1)\right)\right. \\ &\left. + c^T \left(F(x(k)) - x(k)\right)\right) \left(1 - \frac{u_{max}}{\left\|u_{eq}(k)\right\|}\right) \end{aligned} \tag{19}$$

For stability analysis, the Lyapunov function is chosen as follows

$$V(k) = \|s(k)\| \tag{20}$$

Thus, the Lyapunov difference is given by

$$\Delta V(k) = \|s(k+1)\| - \|s(k)\| \tag{21}$$

Using (17)

$$\begin{aligned} &\|s(k+1)\| \\ &= \left\|s(k) + c^T \left(x_d(k) - x_d(k+1)\right) + c^T \left(F(x(k)) - x(k)\right)\right\| \\ &\left(1 - \frac{u_{max}}{\left\|u_{eq}(k)\right\|}\right) \\ &\leq \|s(k)\| + \left\|c^T \left(x_d(k) - x_d(k+1)\right) + c^T \left(F(x(k)) - x(k)\right)\right\| \\ &- \frac{u_{max}}{\left\|\left(c^T H(x(k))\right)^{-1}\right\|} \\ &\leq \|s(k)\| + \delta - \frac{u_{max}}{\left\|\left(c^T H(x(k))\right)^{-1}\right\|} \\ &< \|s(k)\| \end{aligned} \tag{22}$$

Hence, $s(k)$ decreases monotonically. From (18), the equivalent control $u_{eq}(k)$ will belong to the constrained domain, i.e. $\left\|u_{eq}(k)\right\| \leq u_{max}$, in finite time and therefore it will bring the system trajectory to the sliding manifold $s(k) = 0$ on which the dynamics of the closed-loop system are stable.

5 Inverted Pendulum System

As shown in Figure 1, the inverted pendulum system consists of a pendulum amounted on a cart at a frictionless pivot point. The pendulum is of mass $m = 0.1$kg and length $2l = 1$m and the cart is of mass $M = 1$kg [26]. u is the force applied to the cart that lies within the range of ± 10N and $g = 9.81\text{m/s}^2$ is the gravity acceleration. The generalized coordinates are x and θ which represents the horizontal movement of cart and the rotation of pendulum respectively [27].

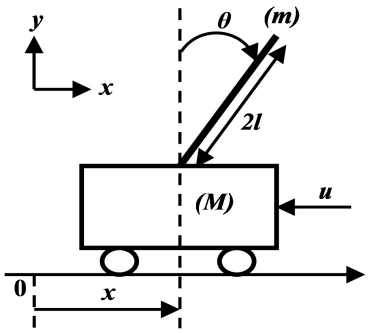

Figure 1: Schematic of the inverted pendulum system

Let $x = \begin{bmatrix} x_1 & x_2 \end{bmatrix}^T = \begin{bmatrix} \theta & \dot{\theta} \end{bmatrix}^T$ be the state vector. The dynamic equations are given by

$$\begin{cases} \dot{x}_1 = x_2 \\ \dot{x}_2 = f(x_1, x_2) + h(x_1, x_2)\, u \\ y = x_1 \end{cases} \tag{23}$$

with

$$f(x_1, x_2) = \frac{(M+m)\, g \sin x_1 - mlx_2^2 \sin x_1 \cos x_1}{\frac{4}{3}(M+m)\, l - ml\cos^2 x_1}$$

and

$$h(x_1, x_2) = \frac{\cos x_1}{\frac{4}{3}(M+m)\, l - ml\cos^2 x_1}$$

Using for discretization the Euler forward method defined by

$$\dot{x} \cong \frac{x(k+1) - x(k)}{T_s},$$

the discrete-time model of the inverted pendulum system is expressed as follows

$$\begin{cases} x_1(k+1) = x_1(k) + T_s x_2(k) \\ x_2(k+1) = x_2(k) + T_s f(x_1(k), x_2(k)) \\ \qquad\qquad + T_s h(x_1(k), x_2(k))\, u(k) \\ y(k) = x_1(k) \end{cases} \tag{24}$$

6 Numerical Simulation Results

For $T_s = 0.05$s, the reference model is chosen as follows

$$x_d(k) = \begin{bmatrix} \frac{\pi}{30} \sin(kT_s) & \frac{\pi}{30} \cos(kT_s) \end{bmatrix}^T \tag{25}$$

The initial conditions are given by

$$x(0) = \begin{bmatrix} 0.2 & 0 \end{bmatrix}^T, x_d(0) = \begin{bmatrix} 0 & \frac{\pi}{30} \end{bmatrix}^T \tag{26}$$

The sliding vector and the reaching law parameters for DSMC controller are respectively

$$\begin{gathered} c^T = \begin{bmatrix} 5 & 1 \end{bmatrix}, \\ q = 2,\ \varepsilon = 10,\ \varphi = 0.5 \end{gathered} \tag{27}$$

The parameters of DSOSMC controller are chosen as follows

$$\varepsilon = 0.02,\ \beta = 0.5 \tag{28}$$

Using the PSO algorithm, the cost function to minimize is the following

$$cost = 0.9t_s + 0.1t_r \tag{29}$$

The population size, the acceleration coefficients, and the minimum and maximum bounds of particle's position are given respectively by

$$\begin{gathered} np = 100,\ \alpha_{1,2} = 2, \\ c_{min}^T = \begin{bmatrix} 0.5 & 0.5 \end{bmatrix},\ c_{max}^T = \begin{bmatrix} 10 & 10 \end{bmatrix} \end{gathered} \tag{30}$$

The following linear decreasing inertia weight is used [28, 29]

$$w = w_{max} - (w_{max} - w_{min})\, \frac{iter}{iter_{max}} \tag{31}$$

where $w_{max} = 0.9$ and $w_{min} = 0.4$ are the initial and final values of the inertia weight respectively, $iter$ is the current iteration, and $iter_{max}$ is the maximum number of iterations.

Figure 2 illustrates the evolution of the cost function (29) corresponding to ODSMC controller. It shows that PSO algorithm ensures a rapid convergence of the cost function to its minimum value of 0.236s corresponding to the following sliding vector

$$c^T = \begin{bmatrix} 7.085 & 0.5 \end{bmatrix} \tag{32}$$

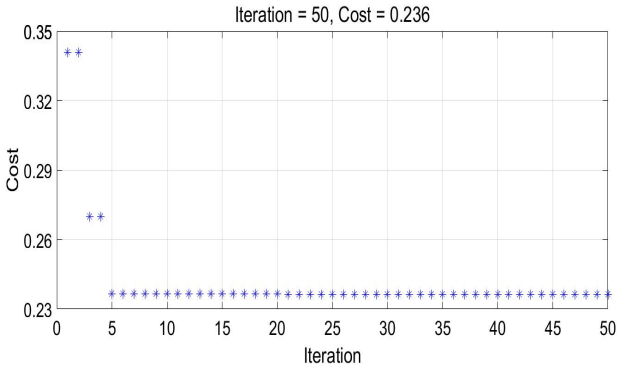

Figure 2: Evolution of the cost function for ODSMC

Figure 3 shows numerical simulation results of ODSMC controller using the sliding vector (32). Figures 3a-3b present the state variables $x_{1,2}(k)$ and their corresponding references $x_{d1,2}(k)$. They show that the developed controller ensures the follow-up of the reference model and the stability of the closed-loop system in the presence of control input constraints. Figure 3c depicts the constrained control input $u(k)$. It shows that chatter effect is avoided. Figure 3d illustrates the sliding function $s(k)$. It shows that the state trajectory converges to the sliding surface in finite time.

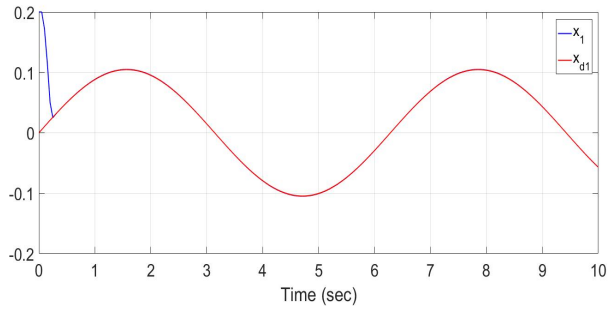

(a) State variable $x_1(k)$ and its reference $x_{d1}(k)$

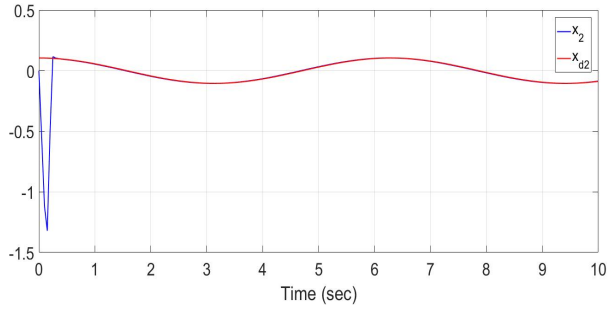

(b) State variable $x_2(k)$ and its reference $x_{d2}(k)$

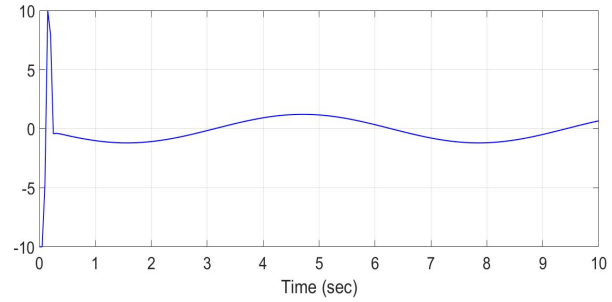

(c) Control input $u(k)$

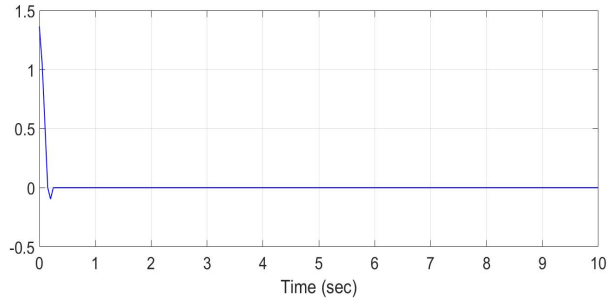

(d) Sliding function $s(k)$

Figure 3: Simulation results for ODSMC controller.

Figure 4 illustrates a comparison between DSMC with saturation function, DSOSMC and ODSMC controllers. Figure 4a presents a comparison of system responses $y(k)$. It shows that all controllers ensure the follow-up of the reference model. Yet, the ODSMC controller ensures the fastest response time while respecting input constraints. Figure 4b depicts a comparison of control inputs $u(k)$. It shows the effectiveness of the applied controllers in avoiding the chattering phenomenon. Moreover, the developed algorithm has lower values of control input in the initial phase than DSOSMC controller.

The results are summarized in Table 2. Actually, It shows that the developed ODSMC ensures the best results with the least rise and settling times of 0.14s and 0.24s respectively, and with lower values of control input than DSOSMC controller whose corresponding minimum and maximum input values are −20.6N and 12.18N respectively. Figure 4 and Table 2 demonstrate that ODSMC controller outperforms DSMC and DSOSMC controllers.

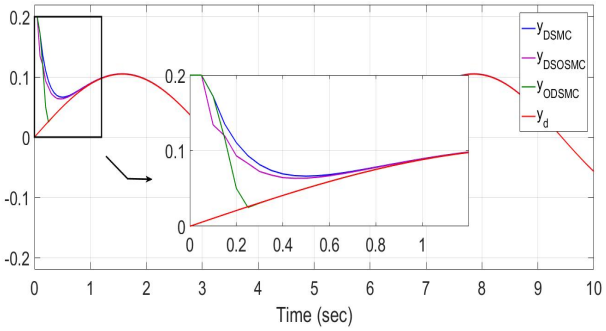

(a) Comparison of system responses

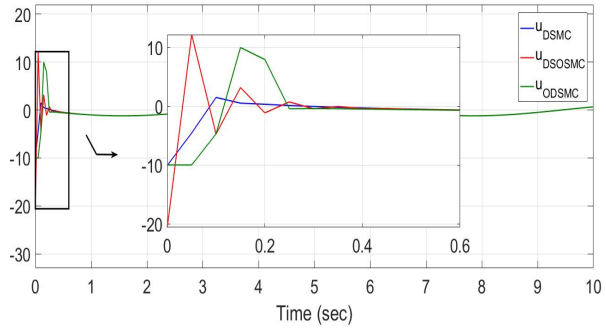

(b) Comparison of control inputs

Figure 4: Comparison between DSMC with saturation function, DSOSMC and ODSMC controllers.

Table 2: Summary table of numerical results

	Settling time (s)	Rise time (s)	u_{min}	u_{max}
DSMC	1.07	0.39	-10.07	1.5
DSOSMC	1.03	0.37	-20.6	12.18
ODSMC	0.24	0.14	-10	10

In this study, Matlab 2016a was used for the implementation of all algorithms.

7 Conclusion

This work presents an optimal discrete-time sliding mode controller for nonlinear SISO systems subject to input constraints. The particle swarm optimization algorithm is employed to determine the sliding vector for which the response characteristics are optimal and the closed-loop system model follows the reference model. Furthermore, the control law which is designed based on the equivalent control concept guarantees the avoidance of chattering phenomenon and the finite-time convergence of system trajectory to the sliding

manifold on which the system dynamics are stable while respecting constraints. Simulation results demonstrate the efficiency of the developed controller in ensuring the fastest response comparing to discrete-time sliding mode controller using the saturation function and to discrete-time second order sliding mode controller. Future work will be to develop the proposed controller to multi-input multi-output nonlinear systems and to verify its effectiveness by experiments.

Conflict of Interest The authors declare no conflict of interest.

References

[1] O. Jedda, A. Douik, "Optimal Discrete-Time Sliding Mode Control for Nonlinear Systems" in 15th International Multi-Conference on Systems, Signals & Devices (SSD), Hammamet Tunisia, 2018. 10.1109/SSD.2018.8570376

[2] C. Milosavljevic, "General Conditions for the Existence of a Quasi-Sliding Mode on the Switching Hyperplane in Discrete Variable Structure Systems" Autom. Remote Control, 14(3), 307-317, 1985.

[3] K. Furuta, "Sliding Mode Control of a Discrete System" Systems & Control Letters, 14(2), 145-152, 1990. https://doi.org/10.1016/0167-6911(90)90030-X

[4] G. Golo, C. Milosavljevic, "Robust Discrete-time Chattering Free Sliding Mode Control" Systems & Control Letters, 41(1), 19-28, 2000. https://doi.org/10.1016/S0167-6911(00)00033-5

[5] S. Z. Sarpturk, Y. Istefanopulos, O. Kaynak, "On the Stability of Discrete-time Sliding Mode Control Systems" IEEE Trans. Autom. Control, 32(10), 930-932, 1987. 10.1109/TAC.1987.1104468

[6] Y. Niu, D. W. Ho, Z. Wang, "Improved sliding mode control for discrete-time systems via reaching law" IET Control Theory Appl., 4(11), 2245-2251, 2010. 10.1049/iet-cta.2009.0296

[7] J. Hu, Z. Wang, H. Gao, L. K. Stergioulas, "Robust H sliding mode control for discrete time-delay systems with stochastic nonlinearities" J. Frankl. Inst., 349(4), 1459-1479, 2012. https://doi.org/10.1016/j.jfranklin.2011.05.018

[8] M. C. Pai, "Discrete-time sliding mode control for robust tracking and model following of systems with state and input delays" Nonlinear Dyn., 76(3), 1769-1779, 2014. https://doi.org/10.1007/s11071-014-1245-0

[9] H. Du, X. Yu, M. Z. Chen, S. Li, "Chattering-free discrete-time sliding mode control" Automatica, 68, 87-91, 2016. https://doi.org/10.1016/j.automatica.2016.01.047

[10] B. Bandyopadhyay, F. Deepak, K. S. Kim, Sliding Mode Control Using Novel Sliding Surfaces, Springer, 2009.

[11] I. U. VADIM, "Survey paper variable structure systems with sliding modes" IEEE Trans. Autom. Control, 22(2), 1977.

[12] K. D. Young, V. I. Utkin, U. Ozguner, "A Control Engineers Guide to Sliding Mode Control" IEEE Trans. Control Syst. Technol., 7(3), 328-342, 1999. 1063-6536(99)03275-3

[13] W. Perruquetti, J. P. Barbot, Sliding Mode Control in Engineering, M. Dekker, 2002.

[14] W. Gao, Y. Wang, A. Homaifa, "Discrete-time Variable Structure Control Systems" IEEE Trans. Ind. Electron., 42(2), 117-122, 1995. 10.1109/41.370376

[15] J.-h. Kim, S.-H. Oh, J. K. Hedrick, "Robust Discrete-time Variable Structure Control Methods" J DYN SYST-T ASME, 122(4), 766-775, 2000. 10.1115/1.1320448

[16] J.-h. Kim, D.-i. D. Cho, "Discrete-time Variable Structure Control using Recursive Switching Function" in Proceedings of the 2000 American Control Conference, Chicago IL USA, 2000. 10.1109/ACC.2000.876673

[17] O. Jedda, A. Douik, "Discrete-time Integral Sliding Mode Control with Anti-windup" Studies in Informatics and Control, 27(4) 413-422, 2018. https://doi.org/10.24846/v27i4y201805

[18] A. Y. Alanis, N. Arana-Daniel, C. Lopez-Franco, E. N. Sanchez, "PSO-gain Selection to Improve a Discrete-time Second Order Sliding Mode Controller" in IEEE Congress on Evolutionary Computation, Cancun Mexico, 2013. 10.1109/CEC.2013.6557672

[19] M. Mihoub, A. S. Nouri, R. B. Abdennour, "The Multimodel Approach for a Numerical Second Order Sliding Mode Control of Highly non Stationary Systems" in American Control Conference, Seattle WA USA, 2008. 10.1109/ACC.2008.4587240

[20] M. Mihoub, A. S. Nouri, R. B. Abdennour, "Real-time Application of Discrete Second Order Sliding Mode Control to a Chemical Reactor" Control Eng. Pract., 17(9), 1089-1095, 2009. https://doi.org/10.1016/j.conengprac.2009.04.005

[21] G. Bartolini, A. Ferrara, V. I. Utkin, "Adaptive Sliding Mode Control in Discrete-time Systems" Automatica, 31(5), 769-773, 1995. https://doi.org/10.1016/0005-1098(94)00154-B

[22] B. Castillo-Toledo, S. Di Gennarob, A.G. Loukianov, J. Rivera, "Discrete time Sliding Mode Control with Application to Induction Motors" Automatica, 44(12), 3036-3045, 2008. doi:10.1016/j.automatica.2008.05.009

[23] J. Kennedy, R. Eberhart, "Particle Swarm Optimization" in Proceedings of IEEE International Conference on Neural Networks, Perth Australie, 1995. 10.1109/ICNN.1995.488968

[24] J. C. Bansal, P. Singh, M. Saraswat, A. Verma, S. S. Jadon, A. Abraham, "Inertia Weight Strategies in Particle Swarm Optimization" in 3rd World Congress on Nature and Biologically Inspired Computing, Salamanca Spain, 2011. 10.1109/NaBIC.2011.6089659

[25] D. P. Rini, S. M. Shamsuddin, S. S. Yuhaniz, "Particle Swarm Optimization: Technique, System and Challenges" Int. J. Comput. Appl., 14(1), 19-26, 2011. 10.5120/ijais-3651

[26] L. X. Wang, "A Supervisory Controller for Fuzzy Control Systems that Guarantees Stability" IEEE Trans. Autom. Control, 39(9), 1845-1847, 1994. 10.1109/9.317109

[27] O. Jedda, J. Ghabi, A. Douik, "Sliding Mode Control of an Inverted Pendulum" In Applications of Sliding Mode Control, Springer Singapore, 105-118, 2017.

[28] J. Xin, G. Chen, Y. Hai, "A Particle Swarm Optimizer with Multistage Linearly-Decreasing Inertia Weight" in International Joint Conference on Computational Sciences and Optimization (CSO), Sanya Hainan China, 2009. 10.1109/CSO.2009.420

[29] Y. Shi, R. C. Eberhart, "Empirical Study of Particle Swarm Optimization" in Proceedings of the 1999 Congress on Evolutionary Computation, Washington DC USA, 1999. 10.1109/CEC.1999.785511

ASTES

Advances in Science, Technology and Engineering Systems Journal Vol. 4, No. 4, 147-151 (2019)

www.astesj.com

Special Issue on Advancement in Engineering and Computer Science

ASTESJ

ISSN: 2415-6698

Multi-Restricted Area Avoidance Scenario Using Hybrid Dynamical Model and Its Predictive Controller

Sutrisno, Widowati*, R. Heru Tjahjana, Sunarsih, Kartono

Department of Mathematics, Diponegoro University, Semarang, 50275, Indonesia

ARTICLE INFO

Article history:
Received: 29 April, 2019
Accepted: 04 July, 2019
Online :21 July, 2019

Keywords:
hybrid system
mixed-logical dynamic
multi-restricted area avoidance,
piecewise-affine
predictive control

ABSTRACT

This article is addressed to show the results of hybrid dynamical modeling in the form of PWA (piecewise-affine) and equivalent MLD (mixed-logical dynamical) model for multi-restricted areas avoidance of an autonomous system. It is a problem of determining the optimal moving trajectory from plant's initial position to some desired position while avoiding some restricted areas (obstacles) between them. In order to calculate the optimal input value capable of generating the optimal trajectory, the model predictive control (MPC) approach was utilized by minimizing an objective function of state/output prediction subject to the formulated hybrid dynamical model. To illustrate the formulated model and its responses, some computational simulations were performed in a three-dimensional state using two/three box-shape restricted areas. From the simulation results, the optimal trajectory was achieved, and the plant avoided the restricted area.

1. Introduction

Dynamical equation models, which comprise of the linear, complex, and hybrid dynamical system, play an important role in engineering the control systems. There are thousands of published research articles developed to analyze the dynamical model of some new engineering systems such as the mobile robot [1, 2], autonomous vehicles, car-like robot, etc. This research deals with an independent system with some known initial state and its corresponding output value with plant's initial position. The plant utilized moves to a decided state known as target position with minimal "effort" where some restricted states are not allowed to be passed through by the plant. The term "effort" in some cases is defined as the shortest path, while an obstacle is a restriction in space movement which should be avoided by the plant. The pioneer mathematical model utilized in this state was developed in [3] by formulating a piecewise affine model which corresponds to the restricted and normal sets. There are some published articles which described the restricted use of some systems, such as vehicles and mobile robots [4–9]. The more complicated problem comprises of several plants which are controlled by applying a multi-agent concept like flocking scheme, which was used in [10,11].

In some cases, the objectives of restricted area avoidance are not only avoiding the obstacle but also determining the optimal trajectory used to determine the final or target point. In this problem, an optimal control method based on mathematical optimization was implemented to solve the technique. For example, a particle swarm algorithm was applied in [12,13]. It is reasonable to utilize an optimization-based method because it will generate the ace result to the problem. Beside of optimal control problem, numerous inconsistencies were solved using the optimization approach which was also used to describe its profitability such as facility location optimization and the colony algorithm for knapsack.

In the system theory, a newly developed strategy is the hybrid dynamical model which comprises of different types of Piecewise-affine (PWA), discrete hybrid automata (DHA) and Mixed Logical Dynamic (MLD) models [14]. To analyze and control a hybrid model, in [15], a toolbox was developed which comprises of some MATLAB functions on model formulation and controlling. For example, the PWA model written in HYSDEL programming language can be converted into MLD using the MATLAB routine "*mld"* in the hybrid system toolbox. Furthermore, the MLD model which consists of trajectory tracking problems tends to be solved by applying a classic control method scheme MPC (model predictive control) and modifying the state prediction along with its corresponding objective function which was carried out in [16,17]. Many research articles applied this control method in agriculture field [18,19], as well as in controlling mechanical vehicles [20], boiler-turbine [21], and spacecrafts [22].

This research therefore aims at solving the problem associated with the restricted area inherent the three-dimensional states. First, the PWA model was formulated to determine whether the dynamical system of the plant is in a normal or restricted area.

*Corresponding Author: Widowati, Jalan Prof. Soedarto, SH. Tembalang, Semarang, Indonesia. Email: widowati@lecturer.undip.ac.id

Next, the PWA system is converted into equivalent MLD using HYSDEL and hybrid toolbox. Furthermore, by using predictive control method for the MLD model, the optimal input was generated to obtain the moving trajectory, which was initialized at the plant's starting point to its target position. Some computational simulations are performed to illustrate and visualize the results.

2. Dynamical System

Let vector $x(k) = \left(x_1(k), x_2(k), \cdots, x_n(k)\right)' \in \mathsf{R}^n$ denotes the state of a plant where k denotes the time instantly. Therefore, the dynamical model of the observed plant is a linear time-invariant system modeled as illustrated in the equation below

$$\left.\begin{aligned} x(k+1) &= Ax(k) + Bu(k) \\ y(k) &= Cx(k) \end{aligned}\right\} \tag{1}$$

where $u \in \mathsf{R}^p$ and $y \in \mathsf{R}^m$ are input & output vectors respectively, and the notations *A, B, C,* and *D* are real constant matrices. The control method used in this paper is applicable, the controllable and observable assumptions are held by (1).

2.1. Restricted Area Avoidance Scheme

The position to the output vector *y is defined without losing the generality property*. Let the initial position of the plant is obtained by $y(0) = y_0 = Cx(0) = Cx_0$. The value of the output, i.e., plant's position *y* have to maneuver and reach some desired target position denoted by y_f which corresponds to target state x_f, $y_f = Cx_f$, where in the output's domain, some sets such as $R_1, R_2, \ldots, R_r \subset \mathbb{R}^m$ are not allowed to be utilized by *y*. Let $R = \left(R_1 \cup R_2 \cup \cdots \cup R_r\right) \subset \mathsf{R}^m$, *y* is restricted to be in *R,* then $y \notin R$ should be held. To handle this condition, the dynamics of the system is formulated as a hybrid system.

The formula is illustrated as follows, w.l.o.g., let $y(k) \in \mathbb{R}^3$ with two restricted sets, R_1 and R_2 illustrated in Figure 1. The problem is how to determine the optimal trajectory used by the plant to maneuver (or move) from its initial state to the target position. The term "optimal" is interpreted as minimal effort (or energy or work or other similar things) used by the plant. The optimal trajectory shown in Figure 1 illustrates a moving trajectory from the initial to the target point.

The non-restricted sets are known as the normal area where the dynamics of the plant corresponds to (1). Alternatively, the dynamics which corresponds to the restricted set is defined as

$$\left.\begin{aligned} x(k+1) &= x(k) \\ y(k) &= Cx(k) \end{aligned}\right\} \tag{2}$$

which means that the dynamical model is used to prevent the plant from being located in the restricted area. The formulation of the hybrid dynamical model where the plant is prevented from entering the restricted area is illustrated by Figure 2 by assuming $x(k) \in \mathbb{R}^3$ and $y(k) = x(k)$.

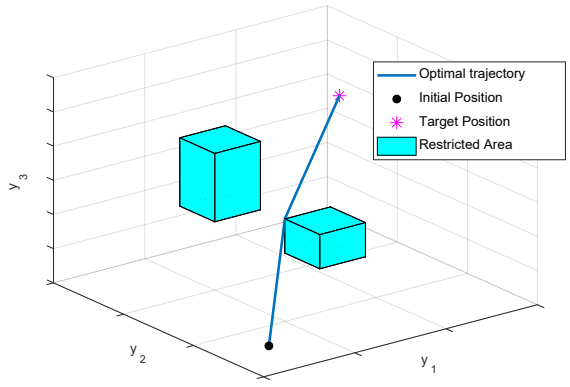

Figure 1: Two box-shape restricted areas illustration

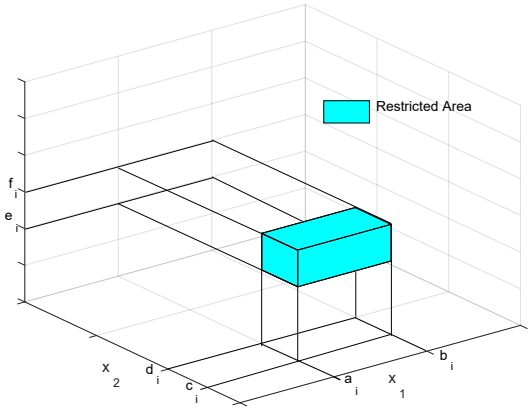

Figure 2: Restricted area labeling

Let the restricted sets (area) R_i, $i = 1, 2, \ldots, k$, and the normal set (area) denoted by *N,* then these sets are written as

$$\begin{cases} R_i : \{(x_1, x_2, x_3) : a_i \le x_1 \le b_i, c_i \le x_2 \le d_i, e_i \le x_3 \le f_i\} \\ N \ : \text{otherwise.} \end{cases}$$

2.2. PWA to MLD Hybrid Model

The hybrid model in the PWA model of the plant for restricted area avoidance purposes is formulated as

$$\left.\begin{aligned} x(k+1) &= \begin{cases} Ix(k), & x \in \text{restricted area} \\ Ax(k) + Bu(k), & x \in \text{normal area} \end{cases} \\ y(k) &= Cx(k) \end{aligned}\right\} \tag{3}$$

with *I* denotes an identity matrix with the appropriate dimension. To apply the predictive control method to this system, the MLD model is, first of all, converted into the form of

$$\left.\begin{aligned} x(k+1) &= Ax(k) + B_1u(k) + B_2\delta(k) + B_3z(k) \\ y(k) &= Cx(k) + D_1u(k) + D_2\delta(k) + D_3z(k) \\ E_2\delta(k) + E_3z(k) &\le E_1u(k) + E_4x(k) + E_5 \end{aligned}\right\} \tag{4}$$

with some initial state $x_0 = x(0)$ where $z(k)$ is an auxiliary state. The notation $\delta(k)$ is a binary valued state describing the mode of the system (mode 0 assuming it is on the normal area and 1 when restricted). The matrices A, B_i, C, D_i and E_i for all i are real constant generated by the conversion process, which is conducted using *mld* MATLAB function embedded in hybrid system toolbox given in [23] by writing the PWA system in HYSDEL, then generating the matrices for the equivalent MLD model.

2.3. Predictive Control Approach

The equation used to determine the optimal input to enable the output vector (position) reach the target point using minimal effort is represented as a terminal state optimal control problem. Furthermore, the predictive control approach is used to obtain the optimal input by letting $x(k|t)$ as the state value predicted at time instant $(k+t)$ which is resulted by applying input value $u(k+t)$ into equation (4) where the corresponding output value is predicted at time instant $(k+t)$, $y(k|t)$. The optimal input will be calculated by solving the minimal value "cost" function of output prediction as follows:

$$\min_{[u,\delta,z]^T} J = \left\| Q_y y(T|t) - y_f \right\|_w + \sum_{k=0}^{T-1} \left[\left\| Q_u u(k) \right\|_w + \left\| Q_y y(k|t) - y_f \right\|_w \right] \tag{5}$$

subject to:

$$\begin{cases} x(0|t) = x(t); y(0|t) = y(t); \\ y(k+1|t) = Cx(k|t) + D_1 u(k) + D_2 \delta(k|t) + D_3 z(k|t); \\ E_2 \delta(k|t) + E_3 z(k|t) \le E_1 u(k) + E_4 x(k|t) + E_5; \\ u_{\min} \le u(k+t) \le u_{\max}, k = 0,1,2,3,...,T-1; \\ x_{\min} \le x(k+t|t) \le x_{\max}, k = 0,1,2,3,...,T; \\ y_{\min} \le y(k+t|t) \le y_{\max}, k = 0,1,2,3,...,T-1; \end{cases}$$

where T is called the horizon control period, Q_u and Q_y are symmetric and positive definite matrices used to weight the input u and output y respectively. These symmetric and positive definite properties are applied to guarantee the objective function J is convex. This is expressed in the notation $\|Qy\|_{w=2} = y^T Qy$ where $\|Qy\|_{w=\infty} = \|Qy\|_\infty$. This predictive control scheme resulting in a mixed integer quadratic optimization problem and in our simulation, *miqp* MATLAB function, which is also embedded in hybrid system toolbox, is utilized to solve. Finally, the optimal values of $u(k)$ for all k are used by the system. For restricted area purposes, the term y_f in (5) is the final/target position where the dynamics of x is (4) which equivalents to (3).

3. Simulation Results

Given a plant with three-dimensional state

$$x(k) = \left[x_1(x), x_2(k), x_3(k) \right]^T \in \mathsf{R}^3$$

and output vector $y(k) = x(k)$ which can be described as the position in a three-dimensional Cartesian coordinate system. Let the initial state be $x_0 = x(0) = \left[1,1,1\right]^T$, which corresponds to the initial position $y(0) = \left[1,1,1\right]^T$.

```
SYSTEM pwa_obs_3d_robot {
INTERFACE { STATE { REAL x1 [-20,20];
                    REAL x2 [-20,20];
                    REAL x3 [-20,20]; }
            INPUT { REAL u [-10,10]; }
            OUTPUT{ REAL y1,y2,y3; }
            PARAMETER { REAL a1;         REAL a2;
                        REAL b1;         REAL b2;
                        REAL c1;         REAL c2;
                        REAL d1;         REAL d2;
                        REAL e1;         REAL e2;
                        REAL f1;         REAL f2; } }
IMPLEMENTATION { AUX { REAL z1,z2,z3;
                       BOOL da1,da2,db1,db2,dc1,dc2,
                            dd1,dd2,de1,de2,df1,df2; }
                 AD  {da1 = x1>=a1;      da2 = x1>=a2;
                      db1 = x1>=b1;      db2 = x1>=b2;
                      dc1 = x2>=c1;      dc2 = x2>=c2;
                      dd1 = x2>=d1;      d2 = x2>=d2;
                      de1 = x3>=e1;      de2 = x3>=e2;
                      df1 = x3>=f1;      df2 = x3>=f2; }
                 DA  {z1 = {IF
                     (da1&~db1)&(dc1&~dd1)&(de1&~df1)
                     THEN x1 ELSE x1+u }; z2 = {IF
                     (da2&~db2)&(dc2&~dd2)&(de2&~df2)
                     THEN x2 ELSE x2+u }; z3 = {IF
                     (da3&~db3)&(dc3&~dd3)&(de3&~df3)
                     THEN x3 ELSE x3+u }; }
                     CONTINUOUS {x1 = z1;
                                 x2 = z2;
                                 x3 = z3; }
                     OUTPUT { y1 = x1;
                              y2 = x2;
                              y3 = x3; } } }
```

Listing Code 1: PWA model (7) with two restricted areas in HYSDEL

Then the dynamic of the plant in the normal area is

$$\left.\begin{aligned} x(k+1) &= \begin{bmatrix} 1 & 0 & 0 \\ 0 & 1 & 0 \\ 0 & 0 & 1 \end{bmatrix} x(k) + \begin{bmatrix} 1 \\ 1 \\ 1 \end{bmatrix} u(k) \\ y(k) &= x(k) \\ x(0) &= \begin{bmatrix} 1 \\ 1 \\ 1 \end{bmatrix} \end{aligned}\right\}. \tag{6}$$

Suppose there are two restricted sets R_1 and R_2 defined visually as two boxes

$$R_1 : \left\{ (x_1, x_2, x_3) : 3 \le x_1 \le 5, 3 \le x_2 \le 4, 3 \le x_3 \le 5 \right\}, \text{ and}$$

$$R_2 : \left\{ (x_1, x_2, x_3) : 0 \le x_1 \le 3, 7 \le x_2 \le 9, 5 \le x_3 \le 7 \right\}$$

where the rest of state space is normal, then the PWA model of this system is stated as

$$x(k+1) = \begin{cases} x(k) & , x \in R_1 \cup R_2 \\ \begin{bmatrix} 1 & 0 & 0 \\ 0 & 1 & 0 \\ 0 & 0 & 1 \end{bmatrix} x(k) + \begin{bmatrix} 1 \\ 1 \\ 1 \end{bmatrix} u(k), & \text{otherwise} \end{cases} \quad (7)$$
$$y(k) = Cx(k).$$

The PWA model in HYSDEL has already been written (See Listing Code 1) and converted it into MLD model (4) resulting in the following matrices $B_2 = D_2 = zeros(3,15)$, $B_3 = C = I_3$, $A = B_1 = D_2 = D_3 = zeros(3,3)$, and E_1, E_2, E_3, E_4, and E_5 because their dimension is sufficiently large.

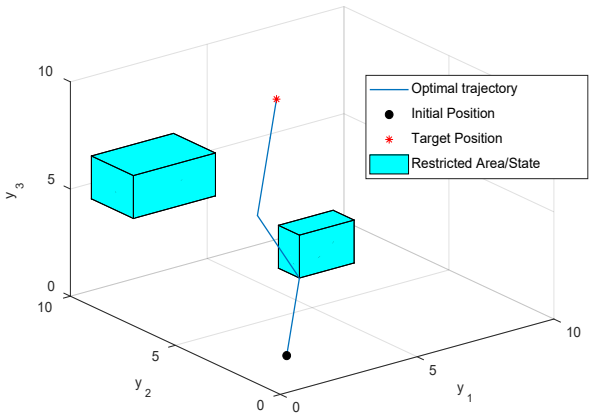

Figure 3: Optimal moving trajectory generated by the controller

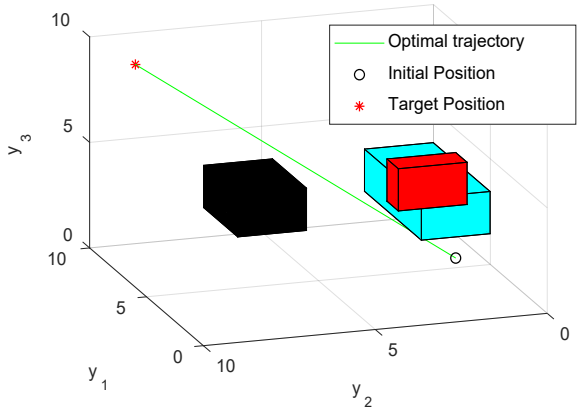

Figure 4: Optimal moving trajectory with three box-shape restricted area

By solving (5) with w=2, the optimal input values are obtained, and by applying them into (7), the optimal moving trajectory from its initial position to its target/final position as show in Figure 3 of the output values are obtained. From Figure 3, it is observed that two restricted areas were restricted and avoided by the system's moving trajectory, as illustrated in the two boxes. For further simulation, another box was added. The result is shown in Figure 4 and is similar to the optimal moving trajectory, which was generated by the controller to prevent the restricted areas.

4. Conclusions

The multi-restricted area which avoids the problem associated with the autonomous linear system was considered dynamic with the region formulated as a hybrid model and the optimal trajectory calculated. From the computational simulation, the obtained system's moving trajectory was generated by the controller, and the given restricted areas were avoided. Further research works will develop the shape of the restricted area into other shapes like polytope to control the inconsistencies associated with irregular shapes. Other control methods will be considered and compared to determine the best in performance.

Conflict of Interest

The authors declare no conflict of interest regarding this work.

Acknowledgment

This work was funded by Universitas Diponegoro under RPI 2019 research grant.

References

[1] E.S. Briskin, Y. V. Kalinin, A. V. Maloletov, N.G. Sharonov, "Mathematical Modelling of Mobile Robot Motion with Propulsion Device of Discrete Interacting with the Support Surface," IFAC-PapersOnLine, **51**(2), 236–241, 2018, doi:10.1016/j.ifacol.2018.03.041.

[2] Y.L. Kuo, "Mathematical modeling and analysis of the Delta robot with flexible links," Computers and Mathematics with Applications, **71**(10), 1973–1989, 2016, doi:10.1016/j.camwa.2016.03.018.

[3] J.J.A.M. Keij, Obstacle Avoidance with Model Predictive Control in a Hybrid Controller, 2002.

[4] Sutrisno, Salmah, E. Joelianto, A. Budiyono, I.E. Wijayanti, N.Y. Megawati, ""Model Predictive Control for Obstacle Avoidance as Hybrid Systems of Small Scale Helicopter," in 3rd International Conference on Instrumentation Control and Automation (ICA), Bali: 127–132, 2013.

[5] Z. Yan, Y. Zhao, S. Hou, H. Zhang, Y. Zheng, "Obstacle Avoidance for Unmanned Undersea Vehicle in Unknown Unstructured Environment," **2013**, 2013.

[6] R. Wang, M. Wang, Y. Guan, X. Li, "Modeling and Analysis of the Obstacle-Avoidance Strategies for a Mobile Robot in a Dynamic Environment," 2015.

[7] D.Q. Bao, I. Zelinka, "Obstacle Avoidance for Swarm Robot Based on Self-Organizing Migrating Algorithm," Procedia Computer Science, **150**, 425–432, 2019, doi:10.1016/j.procs.2019.02.073.

[8] Y. Zhao, X. Chai, F. Gao, C. Qi, "Obstacle avoidance and motion planning scheme for a hexapod robot Octopus-III," Robotics and Autonomous Systems, **103**, 199–212, 2018, doi:10.1016/j.robot.2018.01.007.

[9] Y. Gao, Y. Wu, X. Yang, C. Liao, K. Cheng, H. Luo, "Reactive obstacle avoidance of monocular quadrotors with online adapted depth prediction network," Neurocomputing, **325**, 142–158, 2018, doi:10.1016/j.neucom.2018.10.019.

[10] J. Wang, H. Zhao, Y. Bi, S. Shao, Q. Liu, X. Chen, R. Zeng, Y. Wang, L. Ha, "An Improved Fast Flocking Algorithm with Obstacle Avoidance for Multiagent Dynamic Systems," **2014**(1992), 2014.

[11] Z. Chen, L. Ding, K. Chen, R. Li, "The Study of Cooperative Obstacle Avoidance Method for MWSN Based on Flocking Control," **2014**, 2014.

[12] T. Yang, Z. Liu, H. Chen, R. Pei, "Robust Tracking Control of Mobile Robot Formation with Obstacle Avoidance," **2007**, 2007, doi:10.1155/2007/51841.

[13] G.S. Chyan, S.G. Ponnambalam, "Robotics and Computer-Integrated Manufacturing Obstacle avoidance control of redundant robots using variants of particle swarm optimization," Robotics and Computer Integrated Manufacturing, **28**(2), 147–153, 2012, doi:10.1016/j.rcim.2011.08.001.

[14] A. Bemporad, "Efficient conversion of mixed logical dynamical systems into an equivalent piecewise affine form," IEEE Transactions on Automatic Control, **49**(5), 832–838, 2004, doi:10.1109/TAC.2004.828315.

[15] A. Bemporad, Hybrid Toolbox User's Guide, Lucca, 2012.

[16] F. Borrelli, A. Bemporad, M. Morari, Predictive Control for linear and hybrid systems, Cambridge University Press, Cambridge, UK, 2014.

[17] J.M. Maciejowski, Predictive Control with Constrains, Prentice Hall, USA, 2001.

[18] Y. Ding, L. Wang, Y. Li, D. Li, "Model predictive control and its application in agriculture: A review," Computers and Electronics in Agriculture, **151**, 104–117, 2018, doi:https://doi.org/10.1016/j.compag.2018.06.004.

[19] L. Chen, S. Du, Y. He, M. Liang, D. Xu, "Robust model predictive control for greenhouse temperature based on particle swarm optimization," Information Processing in Agriculture, **5**(3), 329–338, 2018, doi:https://doi.org/10.1016/j.inpa.2018.04.003.

[20] M. Jalali, E. Hashemi, A. Khajepour, S. Chen, B. Litkouhi, "Model predictive control of vehicle roll-over with experimental verification," Control Engineering Practice, **77**, 95–108, 2018, doi:https://doi.org/10.1016/j.conengprac.2018.04.008.

[21] X. Liu, J. Cui, "Economic model predictive control of boiler-turbine system," Journal of Process Control, **66**, 59–67, 2018, doi:https://doi.org/10.1016/j.jprocont.2018.02.010.

[22] P. Li, Z.H. Zhu, "Model predictive control for spacecraft rendezvous in elliptical orbit," Acta Astronautica, **146**, 339–348, 2018, doi:https://doi.org/10.1016/j.actaastro.2018.03.025.

[23] F.D. Torrisi, A. Bemporad, "HYSDEL — A Tool for Generating Computational Hybrid Models for Analysis and Synthesis Problems," IEEE TRANSACTIONS ON CONTROL SYSTEMS TECHNOLOGY, **12**(2), 235–249, 2004, doi:10.1109/TCST.2004.824309.

ASTES

Advances in Science, Technology and Engineering Systems Journal Vol. 4, No. 4, 152-160 (2019)

www.astesj.com

Special Issue on Advancement in Engineering and Computer Science

ASTESJ

ISSN: 2415-6698

Inference Rule of Collision Risk Index based on Ship Near-Collision via Adaptive Neuro Fuzzy Inference System

Ho Namgung*

Graduate School of Maritime Transportation System, Mokpo National Maritime University, Mokpo, KS005, Republic of Korea

ARTICLE INFO

Article history:
Received: 03 June, 2019
Accepted: 17 July, 2019
Online :21 July, 2019

Keywords:
Near-collision
Ship domain
Collision Risk Index
ANFIS

ABSTRACT

Collision risk index has been studied as the required quantitative values for decision-making of collision avoidance between ships. Recently, inference methods of the collision risk were proposed on the basis of the fuzzy theory because of being possible to collect data in real time. Existing fuzzy inference system was composed of only simulation results using virtual navigation situation. In this study, we obtained the fuzzy inference rule based on ship near-collision data via the adaptive neuro fuzzy inference system. Proposed fuzzy inference rule expressed various collision risk index in order that a ship could avoid collision with an encounter ship at appropriate distance and time. It would support for navigators to make an appropriate decision for collision avoidance with encounter ships.

1. Introduction

Despite the efforts to prevent accidents, marine accidents has been occurring without interruption. According to the statistics of KMST(Korean Maritime Safety Tribunal), 10,991 marine accidents have occurred in the last five years from 2014 to 2018. Out of these accidents, 1,132 marine accidents have occurred in collision resulting from lack of look-out and violation of CORLEGs(International Regulations for Preventing Collisions at Sea) [1]. Accordingly, collision accidents can cause structural hazard, loss of human life and property, and ocean pollution due to oil and cargo spills. Thus, since the demand on system to support the safe navigation of ships has been increased, collision avoidance algorithm has been proposed.

Collision avoidance algorithm starts from assessing the collision risk. In order to assess the collision risk in the early days, the concept of a ship domain proposed by [2] was used to assess the collision risk. This concept is succeeded by [3], [4] and [5] in several shapes, the methods of determining ship domains have evolved with time [6,7,8-10]. Nonetheless, it still doesn't contain time-related information.

Since it has been possible to obtain DCPA(Distance of the Closest Point of Approach) and TCPA (Time to the Closest Point of Approach) in real time, inference method of the CRI(collision risk index) on the basis of the fuzzy theory has been proposed. In [11], the author connected DCPA and TCPA to the CRI using interviews of navigators by showing virtual navigation situation on simulator. In [12], the authors reconstructed the FIS (Fuzzy Inference System) using non-dimensionalized DCPA and TCPA. In [13], the researchers calculated the CRI by including VCD (Variance of Compass Degree) into input parameter proposed by Lee and Rhee.

On the basis of the proposed FIS [11,12,13], various studies have been conducted. In [14], the author designed an estimation algorithm of the collision risk among approaching multiple ships by using the fuzzy theory, and verified performance on the basis of the AIS (Automatic Identification System) maritime traffic data. In [15], the author proposed an evaluation algorithm of the collision risk in order that VTSO (Vessel Traffic Service Operator) was able to analyze the collision risk among ships in advance. In [16], the author proposed a model of predicting ship collision risk based on the FIS considering the general patterns of collision avoidance. Furthermore, the FIS has been applied to collision avoidance system in the field of development for an USV(Unmanned Surface Vehicle). The USV developed for multipurpose of ocean observation and surveillance could flexibly change an action space according to the collision risk, which was inferred by using obstacle information on a basis of fuzzy inference [17]. In [18], the researcher used the FIS as a point of time for generating and sending messages in order that efficient information exchange for collision avoidance was possible between autonomous ship and manned ship.

But the proposed FIS [11,12,13] had the limitation which was relied on the empirical factors of navigators. Hence, in [19], the

*Corresponding Author: Ho Namgung, Email: ngh2009@mmu.ac.kr

author suggested the FIS considering ship's characteristic in virtual navigation situation on simulator without interviews of navigators. Nonetheless, because of membership functions and rules determined by simulation results, the existing FIS still have significant limitation not reflecting on information of actual collision situation between ships.

To overcome the limitation of the existing FIS [11,12,13,19], this study proposed an improved fuzzy inference rule by learning actual near-collision data extracted from the AIS via ANFIS (Adaptive Neuro Fuzzy Inference System). Section II described inference methods of the collision risk using the FIS and decision of near-collision. Section III suggested the fuzzy inference rule obtained by learning ship near-collision data via ANFIS. Subsequently, performance of the proposed FIS comparing with the existing FIS was validated and discussed in section IV. Finally, a summary of the work and the conclusion drew in section V.

2. Materials

2.1. Calculation of the CRI using FIS

The FIS inferred the CRI based on the fuzzy theory using DCPA and TCPA. DCPA referred to a minimum distance through a target ship when own-ship and a target ship were encountered. TCPA was an expected time to arrive at the point where DCPA occurred at the ship's present location. Figure 1 is presented that ships V_1 and V_2 passed the minimum distance between ships at TCPA t_c. The time from current time to t_c was TCPA, and the distance between own-ship and a target ship at estimated time from the t_c was DCPA.

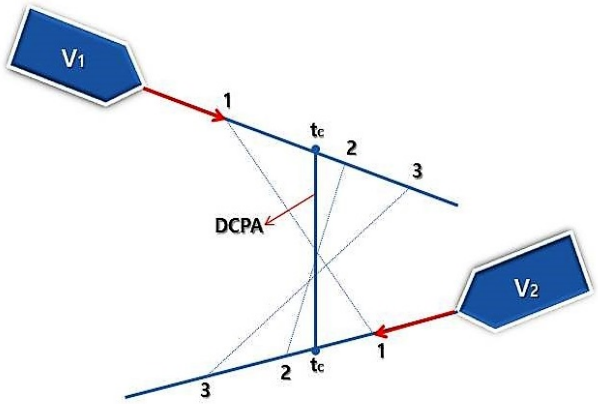

Figure 1: Calculation DCPA and TCPA

Figures 2 and 3 show the fuzzy membership function of TCPA/(L/ V) and DCPA/L, where L was a length of ship and V was a ship speed. In order to increase precise on the FIS, letting DCPA and TCPA to be dimensionless by using a length and a speed of ship was conducted[12]. The CRI can be expressed as values from -1 to 1. Negative values in TCPA mean that a target ship passed through own ship, i.e., safe situation by being out of the collision risk.

Inference rule of state variables used in the FIS are Small (S), Medium (M), B (Big), P (Positive), and N (Negative). Table 1 shows a part where collision risk was determined in order that an input and an output can express the inference rule as a two-dimensional matrix. In other words, it is determined by a condition part of the $i-$th inference rule out of all the inference rules. The CRI at the conclusion as numerals in the fuzzy inference table as show in equation (1).

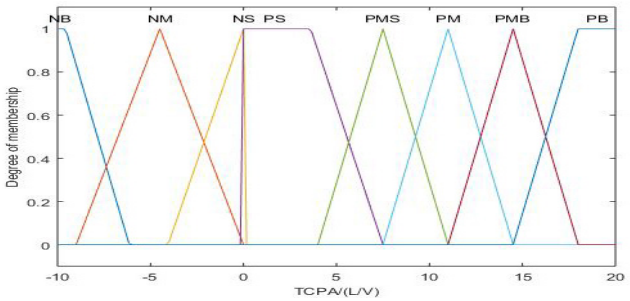

Figure 2: Fuzzy membership function of TCPA/(L/V)

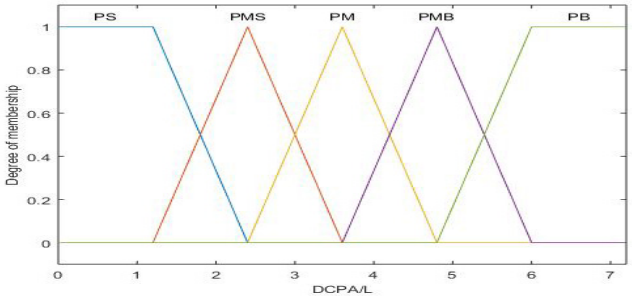

Figure 3: Fuzzy membership function of DCPA/L

$$\text{Collision Risk(CR)} = \frac{\sum_{i=1}^{n} CR_i \cdot a_i}{\sum_{i=1}^{n} a_i} \quad (1)$$

Where,

n = number of reasoning rules,

CR_i = singleton value of conclusion part of $i-$th rule,

a_i = contribution factor of conditional part of $i-$th rule.

Table 1: Fuzzy inference table

Division		TCPA/(L/V)							
		NB	NM	NS	PS	PMS	PM	PMB	PB
DCPA /L	PS	-0.2	-0.6	-1.0	1.0	0.8	0.6	0.4	0.2
	PMS	-0.2	-0.2	-0.6	0.8	0.6	0.4	0.2	0.2
	PM	-0.2	-0.2	-0.2	0.6	0.4	0.2	0.2	0.2
	PMB	-0.2	-0.2	-0.2	0.4	0.2	0.2	0.2	0.2
	PB	-0.2	-0.2	-0.2	0.2	0.2	0.2	0.2	0.2

A point of time for an action of collision avoidance[12,13,19] was determined as follows. In case of a give-away ship, more than 0.6 of the CRI mean an action of collision avoidance. A stand-on ship takes an action of collision avoidance in case of more than 0.8.

2.2. Decision of Ship Near-Collision

Because the number of actual collision accidents was very small, it was significantly difficult to construct a model for evaluating the collision risk based on previous marine accidents [20]. Therefore, near-collision, which was a situation in which there was the danger of collision between ships approaching each other, but with no collision eventually occurring, either due to

deceleration, or evasion by the change of course, was used. In order to detect a number of near-collision, ship domain was utilized for decision of near-collision as criteria not overlapped between ship domains [21,22]. Thus, in this study, near-collision was decided according to proposed methods using ship domain.

Ship domain [2] size with ellipse can be divided into two types as follows. In the sufficient sea area to freely navigate with 10 to 16 knots, the ship domain was composed of 8 L and 3.2 L, where L is ship length. In the constrained sea area such as narrow channel or harbour, the ship domain was composed of 6 L and 1.6 L by reducing speed until 6 to 8 knots. Figure 4 shows ship domain size[2].

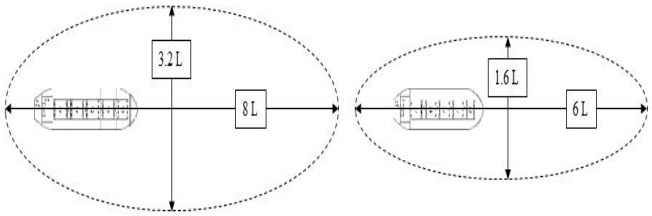

Figure 4: Ship domain size

Ship near-collision based on ship domain with ellipse can be decided in shown as Figure 5.

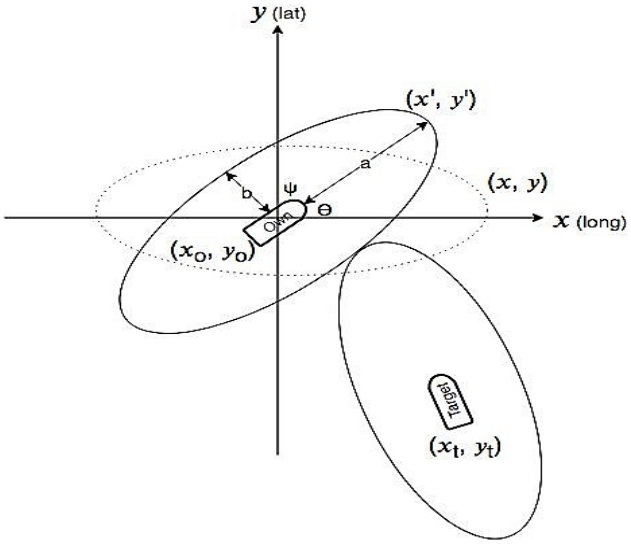

Figure 5: Near-collision between ship's ellipse dimensions

Own ship's ellipse area is parallel to the axis x at the position (x_O, y_O), and can be expressed with a long radius (a) and a short radius (b) in the shape of a dotted line. As an ellipse of position is able to be changed in accordance with own ship's course, rotation of ellipse is necessary corresponding to course. A long radius a and angle of intersection θ of bow direction on the axis x are decided according to ship course angle φ as equation (2). Calculation of rotated own ship's ellipse follows equation (3).

$$\theta = \begin{cases} |90^\circ - \varphi| \ (\varphi \leq 180^\circ) \\ |270^\circ - \varphi| \ (\varphi \geq 180^\circ) \end{cases} \quad (2)$$

$$\frac{(\cos\theta \times (x' - x_O) + \sin\theta \times (y' - y_O))^2}{(a \times L_O)^2} + \frac{(\sin\theta \times (x' - x_O) + \cos\theta \times (y' - y_O))^2}{(b \times L_O)^2} = 1 \quad (3)$$

3. Inference Rule based on Near-Collision via ANFIS

3.1. Procedure for Configuration of the Fuzzy Inference Rule

Procedure for configuration of the fuzzy inference rule presented in Figure 6 can be divided into four steps. A defined action of collision avoidance was defined in first step. Second step designated appropriate distance corresponding to an action of collision avoidance. Third step enlarged an area of the ship domain based on designated distance, and extracted DCPA, TCPA and CRI when ship domain enlarged by level was overlapped. The fuzzy inference rule by learning ship near-collision data via ANFIS was suggested in fourth step.

3.2. Set on the Collision Risk Index

The CRI was set by enlarging the ship domain corresponding to appropriate distance for collision avoidance through definition of an action of collision avoidance by level.

First step defined an action of collision avoidance corresponding to level, and set appropriate distance by level. According to the classification of encounter situations[23,25], an action of collision avoidance was divided into Collision(C), Dangerous(D), Threat(T) and Attention(A). Table 2 defines an action of collision avoidance by level.

Table 2: Definition of an action of collision avoidance by each level

Level	Definition
Collision (C)	· Both ships almost have collision
Dangerous (D)	· Both ships must conduct the best cooperation an action for collision avoidance
Threat (T)	· A give-way ship must conduct an action of collision avoidance · A stand-on ship can take an action for collision avoidance
Attention (A)	· A give-way ship must conduct an action of collision avoidance · A stand-on ship must keep own course and speed

In order to set appropriate distance according to the defined level, it is necessary to take into consideration a give-way ship and a stand-on ship's distance for an action of collision avoidance.COLREGs requested a specified light intensity to show the minimum distance of the ship lighting[23]. The mast light is 6 nm(nautical miles), side light is 3 nm and stern light is 3 nm. Comparing the minimum distance of the ship lighting with an encounter situation for an action of collision avoidance, the mast light and the side light are able to be checked on head-on and crossing situation, and the stern light are able to be checked on overtaking situation.

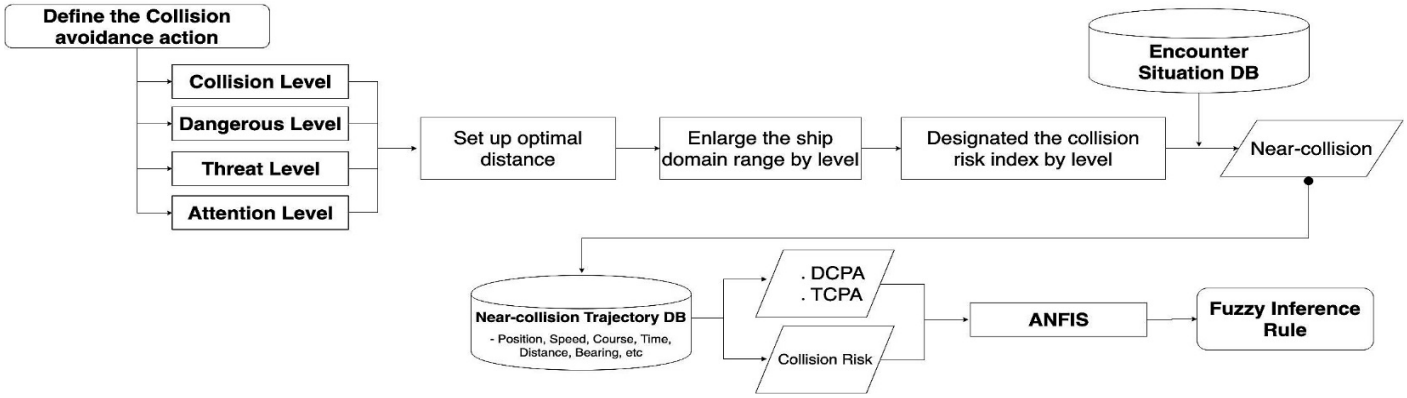

Figure 6: Procedure for configuration of fuzzy inference rule using ship near-collision data

Results of navigator's interviews[24] showed 6 nm, 3 nm and 1nm on the head-on situation, crossing and overtaking situation, and the minimum safe distance. Cockcorft, A. and Lameijer, J.N.F.,(2011) [25] advised the minimum safe distance for collision avoidance as 1 nm in sight of one another and 2 nm in restricted visibility. And, for a collision situation involving two power-driven ships, the minimum distance suggested for an action of collision avoidance were 2 to 3 nm.

Therefore, an action distance of collision avoidance for Collision(C) level was not set due to occurred situation of collision between ships. An action distance for Dangerous(D) level was set as 1 nm in order to pass safely between ships through both ship's cooperation navigation. An action distance for Threat(T) level was set as 2 nm in order that a stand-on ship takes an action of collision avoidance by continuously observing an action of a give-way ship's collision avoidance. At this distance, a give-way ship still has an obligation for collision avoidance. An action distance of Attention(A) was set 3 nm due to initial beginning of the collision risk between ships.

Second step sets the CRI corresponding to enlarged the ship domain based on designated distance by level. In order to enlarge the ship domain, we used the ship domain ($8L \times 3.2\,L$)[2] as standard, considering limited ship speed suggested in each sea area. The standard ship length was set as 70 meters due to having different lengths[2].

In case of overlapping the ship domain ($8\,L \times 3.2\,L$) set in encounter ships, each ship had extra distance 0.3 nm. At this time, the sum of extra distance was 0.6 nm. This was due to actual collision accident was not occurred. However, since distance of the overlapping ship domain was less than the minimum safe distance 1 nm, it could mean that both ships almost had collision. Hence, ship domain ($8L \times 3.2\,L$) was set corresponding to Collision(C) level. Based on this approaching methods, ship domain size was adjusted corresponding to designated distance by level.

The existing FIS had the range of the CRI from -1.0 to 1.0. But in this study, we composed of the range of the CRI from 0.0 to 1.0 except for negative sign. The CRI of Attention(A) level was set 0.0 due to initial beginning of the collision risk between ships. Other levels were designated by dividing 1.0 to the three parts. Accordingly, the CRI of Collision(C) level was 1.0 due to the meaning of having collision between ships, and Dangerous(D) level and Threat(T) level were set as 0.66 and 0.33 due to gradually increasing the CRI by times. Table 3 shows the range of the CRI, ship domain size and the minimum safe distance by proposed level. Overlapping situation between ship domains is presented in Figure 7.

Table 3: The range of the CRI, ship domain and safe distance by proposed level

Level	NM	Ship domain	CRI
C	-	$8\,L \times 3.2\,L$	1.0
D	$0.6 < \text{NM} \leq 1.0$	$13.2\,L \times 5.28\,L$	$0.66 \leq \text{CRI} < 1.0$
T	$1.0 < \text{NM} \leq 2.0$	$26.4\,L \times 10.56\,L$	$0.33 \leq \text{CRI} < 0.66$
A	$2.0 < \text{NM} \leq 3.0$	$39.6\,L \times 15.84\,L$	$0.0 \leq \text{CRI} < 0.33$

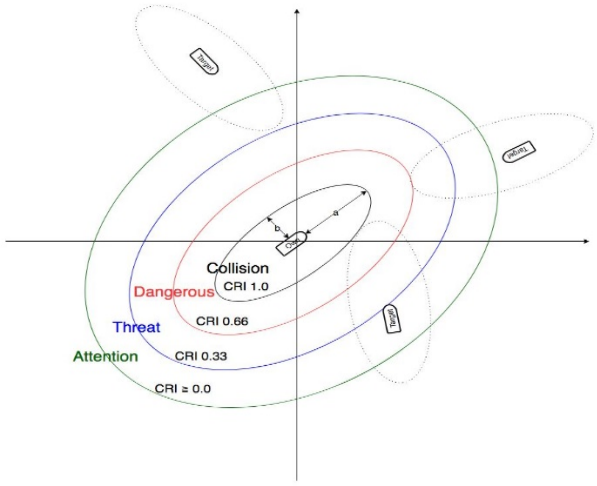

Figure 7: Overlapping situation of ship domain by proposed level

3.3. Ship's Trajectory Data by Level

By setting enlarged ship domain based on Collision(C) level to both ships, ship's trajectory data were extracted when overlapped. This was for comparing and analyzing the information generated from initial beginning of the collision risk to occurring to near-collisions. At this time, ship domain of both ships were set by having the same size in order that enlarged ship domain applied to both ships corresponded to the designated distance when overlapped. To collect ship's near-collision data, Mokpo sea area

was designated. 97 cases out of a total of 154 ships had encounter situations. Results of near-collision by setting ship domain ($8\,L \times 3.2\,L$) as Collision(C) level was a total of 49 cases. Figure 8 is shown as ship's near-collision trajectory.

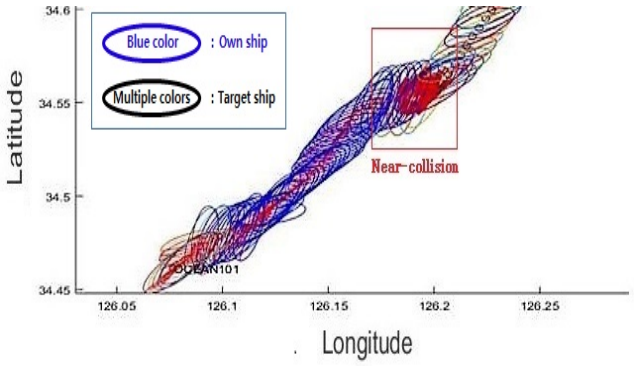

Figure 8: Ship near-collision trajectory

By extracting a total of 196 near-collision ships occurred in each level, we corresponded to the CRI of proposed level. DCPA and TCPA was extracted based on ship's trajectory near-collision data when near-collision by level occurred. At this time, the DCPA was non-dimensionalized by using ship length L, and the TCPA was non-dimensionalized by using ship length L divided by the ship speed V. Table 4 shows the trajectory data of ship near-collision by level.

Table 4: The trajectory data of ship near-collision by level

Level	DCPA/ L	TCPA/(L/V)	CRI
Collision (C)	0.12	0.74	1.0
	0.09	1.93	1.0
	0.17	1.13	1.0
Dangerous (D)	0.48	0.49	0.66
	0.41	2.98	0.66
	0.68	4.41	0.66
Threat (T)	1.07	7.28	0.33
	1.06	9.89	0.33
	0.72	0.81	0.33
Attention (A)	1.29	7.22	0.1
	1.43	3.09	0.1
	2.27	13.3	0.1

3.4. Inference Rule of Collision Risk

3.4.1. Structure of ANFIS

The ANFIS[26] is one of the neuro fuzzy systems for the fuzzy modeling and control proposed by Jang. Configuration of inference rule of the collision risk was as follows. First step designated DCPA/L and TCPA/(L/V) as input parameter, and the CRI as output parameter. At this time, DCPA/L and TCPA/(L/V) were composed of a total 4 of MF(memberships function). Table 5 shows input and output parameter set in MF.

Table 5: Categorized input and output parameter

No.	Input		Output
	DCPA/ L	TCPA/(L/V)	CRI
	Inputmf	Inputmf	Outputmf
1	Collision	Collision	Outputmf 1
2		Dangerous	Outputmf 2
3		Threat	Outputmf 3
4		Attention	Outputmf 4
5	Dangerous	Collision	Outputmf 5
6		Dangerous	Outputmf 6
7		Threat	Outputmf 7
8		Attention	Outputmf 8
9	Threat	Collision	Outputmf 9
10		Dangerous	Outputmf 10
11		Threat	Outputmf 11
12		Attention	Outputmf 12
13	Attention	Collision	Outputmf 13
14		Dangerous	Outputmf 14
15		Threat	Outputmf 15
16		Attention	Outputmf 16

Second step composed of fuzzy inference rule by learning input and output parameters via ANFIS. Figure 9 shows ANFIS structure configured by using MF of input and output parameters.

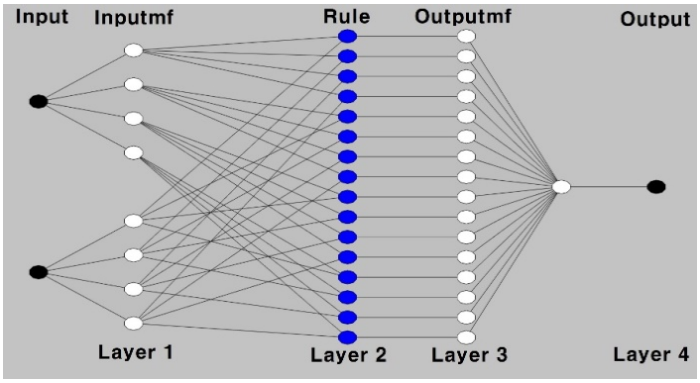

Figure 9: Structure of ANFIS

DCPA/ L and TCPA/(L/V) were designated as premise parameter x, y and CRI was designated as consequent parameter f_i. By using consequent coefficient a, b, c inference rule was composed as shown in equation (4).

$$Rule_i : If\ x\ is\ \mu_{\left(\frac{DCPA}{L}\right)i}\ and\ y\ is\ \mu_{\left(\frac{TCPA}{\left(\frac{L}{V}\right)}\right)i,}$$

$$\text{then } f_i = a_i x + b_i y + c \qquad (4)$$

3.4.2. Inference Rule through Learning Algorithm

The ANFIS can be trained by the backward propagation algorithm and the hybrid learning algorithm. In the backward propagation algorithm, the errors are propagated backward and the premise parameters are updated by gradient descent. At this time, consequent parameters are fixed. In the hybrid learning algorithm, the premise and consequent parameters are updated by least-

squares method and gradient descent. In this study, we used the backward propagation algorithm for maintaining the CRI designated by level. Therefore, surface of CRI through learning by the backward propagation algorithm was represented non-linear as shown in Figure 10.

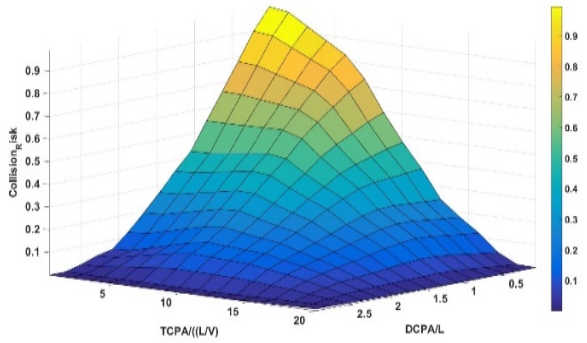

Figure 10: Surface of the CRI

Inference rule of the CRI proposed by learning near-collision data via ANFIS was presented in Table 6.

Table 6: Fuzzy inference rule for membership function

Division		DCPA/*L*			
		C	D	T	A
TCPA/(*L*/*V*)	C	0.994	0.773	0.477	0.021
	D	0.777	0.662	0.401	0.017
	T	0.395	0.423	0.335	0.015
	A	0.062	0.246	0.152	0.011

4. Result and Discussion

4.1. Result

To validate performance of the proposed fuzzy inference rule by comparing with the existing fuzzy rule, two ships navigating at Mokpo sea area were selected from AIS data. One of which was designated as own-ship and the other was designated as a target ship. An encounter situation and near-collision situation are presented in Figures 11 and Figure 12. When the encounter situation occurred within 10 nm, own-ship begun calculating the CRI with DCPA and TCPA. The CRI calculated from four types of inference rule was presented in Table 7 and Figure 13.

At the initial encounter situation between own-ship and a target ship, the FIS[12], FIS-VCD[13], FIS-SC[19] and FIS-NC proposed in section III indicated the CRI 0.29, 0.67, 0.32 and 0.11, respectively.

When it comes to TCPA and distance, the FIS-SC and the FIS-NC were gradually increased until near-collision situation according to reduction of TCPA and distance. Whereas, the FIS and the FIS-VCD were not gradually increased until near-collision situation. In case of the FIS, after it obtained the CRI until 0.94, the same CRI was kept until near-collision situation. In case of the FIS-VCD, unlike the FIS, the FIS-SC and the FIS-NC, it depended on how much the VCD was obtained due to input parameter DCPA, TCPA and VCD. As shown in Table 7, as the VCD got closer at 0, the CRI was increased.

When it comes to a point of time for action of collision avoidance of a give-way ship, distance for action of collision avoidance via the FIS, the FIS-VCD, the FIS-SC and FIS-NC represented about 7.2 nm, about 9.8 nm, about 6.1 nm and about 7.7 nm, respectively. At this time, TCPA represented about 10.7 minutes,15.8 minutes, 7.7 minutes and 11.7 minutes, respectively.

When it comes to a point of time for action of collision avoidance of a stand-on ship, distance for action of collision avoidance via the FIS, the FIS-VCD, the FIS-SC and FIS-NC represented about 5.1 nm, about 7.2 nm, about 1.7 nm and about 6.1 nm, respectively. At this time, TCPA represented about 7.4 minutes,10.7 minutes, 2.5 minutes and 7.7 minutes, respectively.

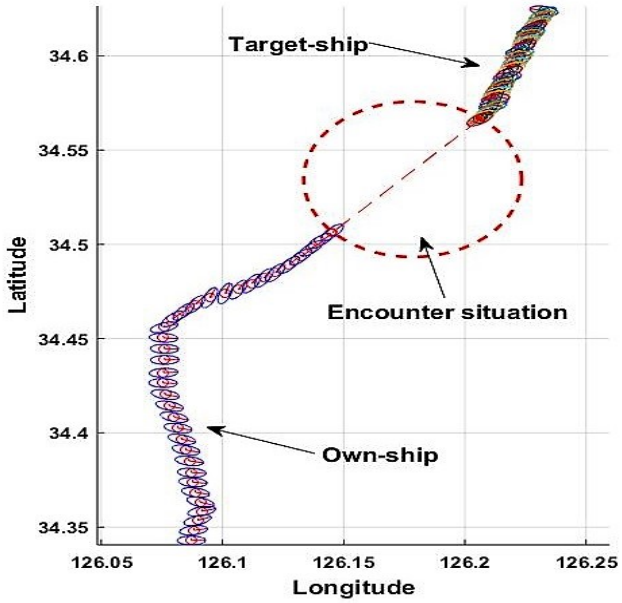

Figure 11: Encounter situation

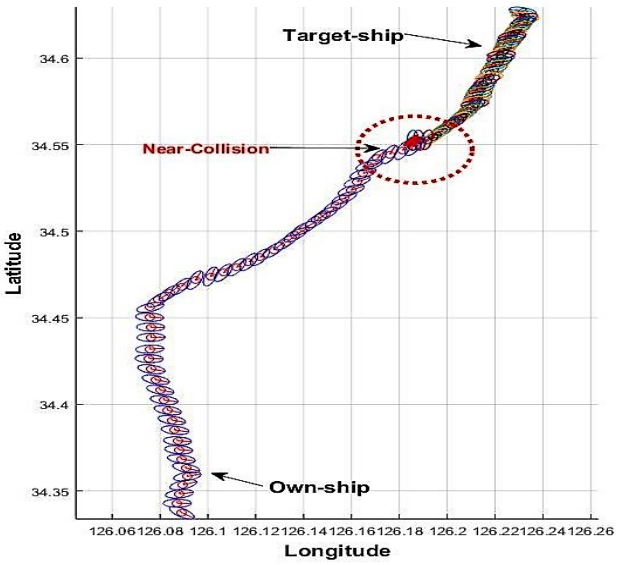

Figure 12: Near-collision situation

Table 7: Comparison with the different CRI according to TCPA and distance

Distance (nm)	TCPA (minute)	VCD (degree)	Collision Risk Index				A point of time for collision avoidance
			FIS	FIS-VCD	FIS-SC	FIS-NC	
9.8	15.8	-	0.29	0.67	0.32	0.11	FIS-VCD(give-way)
9.3	14.5	1.2	0.39	0.71	0.36	0.17	
8.9	13.6	0	0.45	0.73	0.38	0.21	
8.4	13.1	2.2	0.48	0.74	0.41	0.24	
8.1	12.4	6.5	0.51	0.77	0.44	0.31	
7.7	11.7	7.8	0.54	0.78	0.46	0.34	FIS-NC(give-away)
7.2	10.7	0.3	0.62	0.8	0.49	0.42	FIS(give-way), FIS-VCD(stand-on)
6.9	10.1	0.5	0.65	0.81	0.51	0.46	
6.4	8.3	0.3	0.74	0.84	0.58	0.61	
6.1	7.7	0.4	0.77	0.86	0.61	0.67	FIS-SC(give-way), FIS-NC(stand-on)
5.5	7.6	2.8	0.78	0.84	0.62	0.68	
5.1	7.4	0.2	0.8	0.87	0.63	0.71	FIS(stand-on)
4.6	6.8	3.5	0.8	0.83	0.66	0.77	
4.2	6.1	1.7	0.81	0.87	0.68	0.79	
3.8	5.4	2.6	0.83	0.84	0.7	0.82	
3.3	4.9	4.6	0.85	0.81	0.72	0.84	
2.9	4.4	1.3	0.88	0.88	0.75	0.86	
2.5	3.7	1.4	0.93	0.87	0.77	0.89	
2.1	3.1	6	0.94	0.81	0.79	0.92	
1.7	2.5	3.2	0.94	0.83	0.8	0.94	FIS-SC(stand-on)
1.3	2.2	0.1	0.94	0.93	0.84	0.95	
0.9	1.5	0	0.94	0.94	0.83	0.97	
0.4	0.7	2.6	0.94	0.84	0.87	0.98	
0.2	0.1	0.4	0.94	0.91	0.92	0.99	Near-Collision

FIS: Fuzzy Inference System; FIS-VCD: Fuzzy Inference System based on VCD; FIS-SC: Fuzzy Inference System based on Ship's Characteristic; FIS-NC: Fuzzy Inference System based on Near-Collision

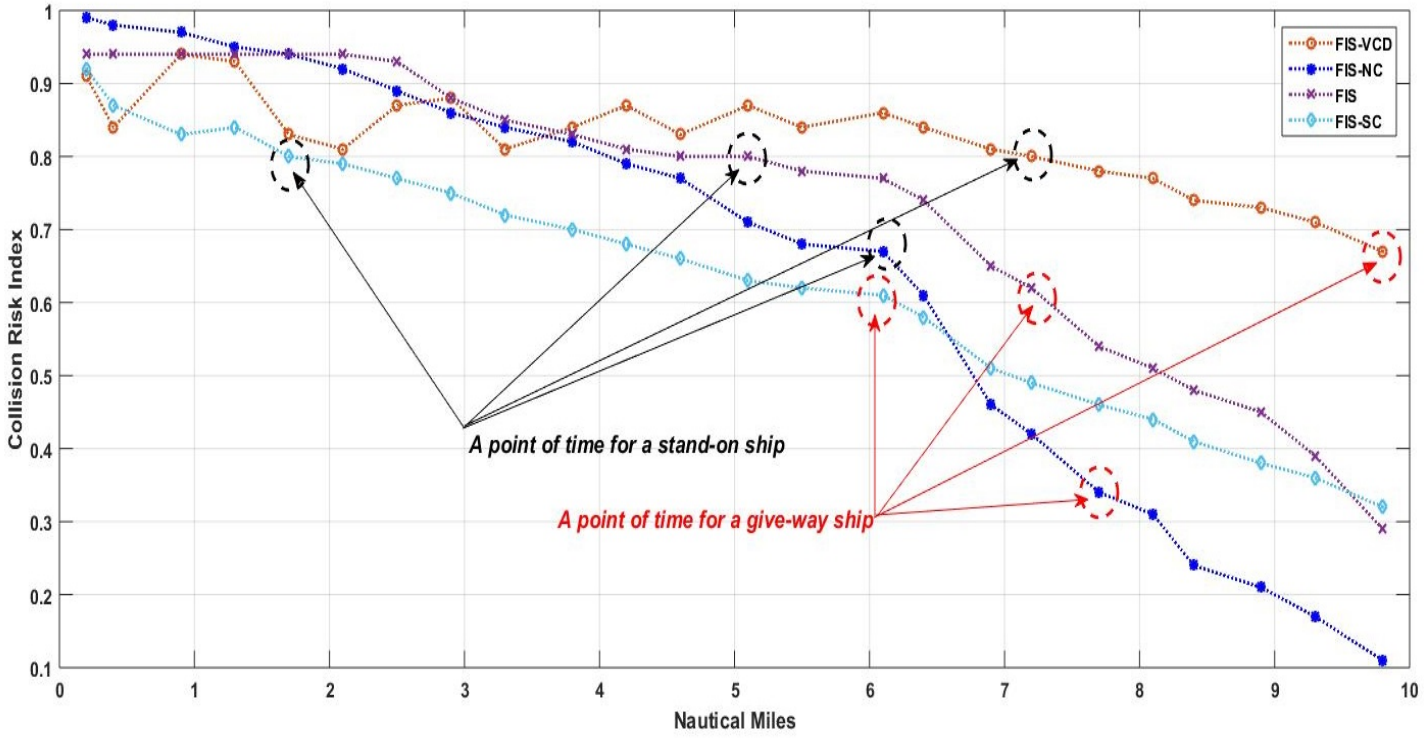

Figure 13: Comparison with the different CRI corresponding to distance

4.2. Discussion

In section 4.1, it could be seen that the exiting rule[12,13,19] and the proposed rule were able to obtain the CRI in the encounter situation between own-ship and a target ship according to values of input parameter. However, a point of time for action of collision avoidance was different according to type of the encounter situation. In case of a give-way ship, the FIS, the FIS-VCD and the FIS-SC defined that own-ship must take an action when the CRI exceeded more than 0.6. In case of a stand-on ship, own-ship must take an action for collision avoidance when the CRI exceeded more than 0.8. On the other hand, when the CRI exceeded more than 0.33, the FIS-NC proposed that a give-way ship must take an action for collision avoidance. In case of a stand-on ship in the FIS-NC, a point of time for collision avoidance was when the CRI was more than 0.66. Therefore, in this section, a point of time for action of collision avoidance via the FIS, the FIS-VCD, the FIS-SC and the FIS-NC were discussed according to the "A guide to the collision Avoidance Rules[25]", as well as a review of the various values obtained from inference rules.

According to [25], it states that ship should take an action for collision avoidance within about 5 to 10 minutes of TCPA or within about 2 to 3 nm of minimum distance. As shown in Table 7 and Figure 13, a give-way ship using the FIS, the FIS-VCD, the FIS-SC and the FIS-NC can obtain outer distance 2 to 3 nm and enough TCPA for taking an action. whereas, in case of a stand-on ship, the only the FIS-SC didn't obtain the requested distance and TCPA. it means that ship using the FIS-SC have no choice but to take into consideration collision risk at all times.

In terms of the CRI expression, even though the FIS had enough distance and TCPA until near-collision situation, it indicated the same CRI from 0.94 to near-collision situation. In case of the FIS-VCD, it relied on the only VCD. For this reason, unlike the FIS, FIS-SC and FIS-NC, the only the FIS-VCD already exceeded more than threshold at the initial encounter situation. On the other hand, the FIS-SC and the FIS-NC expressed the various CRI according to input parameters. It means that the CRI calculated from the FIS-SC and the FIS-NC reflected original information(DCPA, TCPA) well. Accordingly, because priority of multiple ships can be designated via the various CRI, these would be possible to not only take an appropriated action of collision avoidance between ships, but also among multiple ships.

For this reason, a ship using the FIS-NC can take an suitable action in any encounter situations because it reflects all of aspects, i.e., appropriated distance and TCPA according to the various CRI. However, it didn't reflect various factors, e.g., weather condition, ship size, congestion of navigation area and so on.

5. Conclusion

Although the FIS using DCPA and TCPA have been reported previously, they have largely relied on the use of either interviews of navigators or ship's characteristic in virtual navigation situation. These approaches tend to have the limitation not reflecting on information of actual collision situation between ships. Therefore, in this paper, we proposed the fuzzy inference rule based on near-collision via ANFIS by applying an action of collision avoidance corresponding to the CRI by level. For a configuration of fuzzy inference rule, steps was conducted as follows. An action of collision avoidance was defined, and distance to conduct an action of collision avoidance was set; (i). By enlarging ship domain based on designated distance by level, DCPA, TCPA and CRI were extracted when overlapped; (ii). Fuzzy inference rule was proposed by learning near-collision data via ANFIS; (iii). The results of applying proposed fuzzy inference rule to actual navigation area expressed the various CRI corresponding to the required distance and TCPA in order that navigators can make a decision appropriately. Accordingly, the proposed fuzzy inference rule not only overcame these issues, but also offered performance more outstanding than the existing fuzzy inference rule. However, it didn't reflect weather condition, ship size, congestion of navigation area, and so on. In further study, it is required to improve and validate the inference rule of the CRI taking consideration into drawbacks.

Conflict of Interest

The author declares no conflict of interest.

References

[1] Korean Maritime Safety Tribunal, "Annual Report of Marine Accident," 2018.

[2] Fujii, J., Tanaka, K., "Traffic capacity," Journal of Navigation, 24, 543–552, 1971. https://doi.org/10.1017/S0373463300022384

[3] Goodwin, E.M., "A statistical study of ship domains," Journal of Navigation, 28, 328–344, 1975. https://doi.org/10.1017/S0373463300041230

[4] Davis, P.V., Dove, M.J., Stockel, C.T., "A computer simulation of marine traffic using domains and arenas," Journal of Navigation, 33, 215–222, 1980. https://doi.org/10.1017/S0373463300035220

[5] Coldwell, T.G., "Marine traffic behavior in restricted waters," Journal of Navigation, 36, 431–444, 1983. https://doi.org/10.1017/S0373463300039783

[6] Jensen, T.K., Hansen, M.G., Lehn-Schiøler, T., Melchild, K., Rasmussen, F.M., Ennemark, F., "Free flow–efficiency of a one-way traffic lane between two pylons," Journal of Navigation, 66, 941–951, 2013. https://doi.org/10.1017/S0373463313000362

[7] Van Iperen, W.H., "Classifying ship encounters to monitor traffic safety on the North sea from AIS data," TransNav, Int. J. Mar. Navig. Saf. Sea Transp, 9 (1), 51–58, 2015. https://doi.org/10.12716/1001.09.01.06

[8] Pietrzykowski, Z., Uriasz, J., "The ship domain – a criterion of navigational safety assessment in an open sea area," Journal of Navigation, 62, 93–108, 2009. https://doi.org/10.1017/S0373463308005018

[9] Wang, N., Meng, X., Xu, Q., Wang, Z., "An intelligent spatial collision risk based on the quaternion ship domain," Journal of Navigation, 63, 733–749, 2010. https://doi.org/10.1017/S0373463310000202

[10] Wang, N., 2013. "A novel analytical framework for dynamic quaternion ship domains," Journal of Navigation, 66, 265–281, 2013. https://doi.org/10.1017/S0373463312000483

[11] Hasegawa, K., Kouzyki, A., Muramatsu, T., Komine, H., and Watabe, Y., "Ship Auto-navigation Fuzzy Expert System (SAFES)," Journal of the Society of Naval Architecture of Japan, 166, 1989. https://doi.org/10.2534/jjasnaoe1968.1989.166_445

[12] Lee, Han-Jin and Rhee, Key-Pyo, "Development of collision avoidance system by using expert system and search algorithm," Journal of International Shipbuilding Progress 48, 197–212, 2001.

[13] Eun-kyoung Kim, Il-kweon Kang, and Yong-gi Kim, "Collision Risk Decision System for Collision Avoidance," 11(6), 524-527, 2001.

[14] Nam-Sun Son, Sun-Young Kim, and Chan-Soo Lee, "On the Monitoring System of Collision Risks Among Multiple Ships," Annual of Navigation, 19(1), 2012. https://doi.org/10.2478/v10367-012-0012-x

[15] Ahmad C. Bukhari, Inara Tusseyeva, Byung-Gil Lee, and Yong-Gi Kim, "An intelligent real-time multi-vessel collision risk assessment system from VTS view point based on fuzzy inference system," Expert System with Applications, 40, 1220-1230, 2013. https://doi.org/10.1016/j.eswa.2012.08.016

[16] Mira Yi, "Design of the Neuro-Fuzzy based System for Analyzing Collision Avoidance Measures of Ships," Journal of Korean Institute of Intelligent Systems, 27(2), 113-118, 2017. https://doi.org/10.5391/JKIIS.2017.27.2.113

[17] Nam-Sun Son and Sun-Young Kim, "On the sea trial test for the validation of an autonomous collision avoidance system of unmanned surface vehicle, ARAGON," OCEANS 2018 MTS/IEEE Charleston. https://doi.org/10.1109/OCEANS.2018.8604803

[18] Ho Namgung, Jung Sik Jeong, Jo-Cheon Choi, Geun Woong Kim, and Joo-Sung Kim, "Design of Information Exchange Handling System for Safe

Navigation of Autonomous Ship," Journal of Korean Institute of Intelligent Systems, 29(1), 42-49, February, 2019. https://doi.org/ 10.5391/JKIIS.2019.29.1.42

[19] Jin-Hyeong Ahn, Key-Pyo Rhee, and Young-Jun You, "A study on the collision avoidance of a ship using neural networks and fuzzy logic," Applied Ocean Research, 37, 162–173, 2012. https://doi.org/10.1016/j.apor.2012.05.008

[20] Inoue, K. and Kawase, M., "Innovative Probabilistic Prediction of Accident Occurrence," Int. J. Marine Nav. & Safety Sea Trans., 1(1), 19-22, 2007.

[21] Zhang, W., F. Goelandt, P.Kujala, and Y.Wang, "An Advanced Method for Detecting Possible Near Miss Ship Collisions from AIS data," Ocean Eng., 124, 141-156, 2016. https://doi.org/10.1016/j.oceaneng.2016.07.059

[22] Rafal Szlapczynski, "A Framework of a ships domain-based near-miss detection method using mamdani neuro-fuzzy classification," POLISH MARITIME RESEARCH Special Issue, 25, 14-21, 2018. https://doi.org/10.2478/pomr-2018-0017

[23] IMO, International Regulations for Preventing Collisions at Sea, COLREGS, 1972.

[24] Y.S, Lee, J.M. Park, and Y.J. Lee, "A Study on the Initial Action of Navigators to Avoid Risk of Collision at Sea," Journal of Korean Navigation and Port Research, 38, 2014. https://doi.org/10.5394/KINPR.2014.38.4.327

[25] Cockcroft, A. N. and Lameijer, J. N. F., "A Guide to the Collision Avoidance Rules," Butterworth Heinemann, Oxford, UK, 2011.

[26] Jang JR, "Adaptive-network based fuzzy inference system," IEEE Transactions on systems, Man and Cybernetics, 1993.

ASTES

Advances in Science, Technology and Engineering Systems Journal Vol. 4, No. 4, 161-168 (2019)

www.astesj.com

ASTESJ

ISSN: 2415-6698

Smart Meter Data Analysis for Electricity Theft Detection using Neural Networks

Priyamvada Chandel*,[1], Tripta Thakur[2]

[1] *Central Power Research Institute, Bhopal, India*

[2] *Maulana Azad National Institute of Technology, Bhopal, India*

ARTICLE INFO

Article history:
Received: 16 June, 2019
Accepted: 11 July, 2019
Online :21 July, 2019

Keywords:
Electricity Theft Detection
Convolutional Neural Network (CNN)
Recurrent Neural Network (RNN)
Bidirectional Long Short Term Memory (BiLSTM)

ABSTRACT

The major problem in electric utility is Electrical Theft, which is harmful to electric power suppliers and causes economic loss. Detecting and controlling electrical theft is a challenging task that involves several aspects like economic, social, regional, managerial, political, infrastructural, literacy rate, etc. Numerous methods were proposed formerly for detecting electricity theft. However, the previous works considered only the one dimensional (1-D) energy consumption data which apprehended the periodicity and were found inefficient in storing and retrieving the memory that resulted in a lower accuracy rate of detection. Hence, this research study intends Convolutional Neural Network combined with Bidirectional Long Short Term Memory based Recurrent Neural Network (CNN-RNN-BiLSTM) for overcoming the aforementioned problems in the detection of electricity theft. The CNN captures the global variables of 1-D data and identifies the non-periodicity and periodicity of 2-D electricity consumption records. RNN-BiLSTM extends the memory storage capacity of the neural network with bidirectional flow of information, thereby allowing learning order dependencies. The proposed method results of the predicted values of the electricity theft show better accuracy rate with reduced time during the training phase and reduced number of epochs. The proposed model helps to discriminate the customers for preventing fraudulent activities in the usage of electric power. The validation of the proposed method is carried out by comparing the method with the existing Support Vector Machine (SVM) and multi-class SVM models. The comparative results prove that the proposed CNN-RNN-BiLSTM model of electricity theft detection works efficiently.

1. Introduction

Electricity has become a basic need in our life. Losses often occur during the transmission, generation, and distribution of electricity. The losses in the electricity supply to consumers, refer to the quantity of electricity introduced into the distribution and transmission grids that are unpaid by the users. The losses of electricity can be classified into technical losses (TLs) and Non-Technical losses (NTLs) [1]. Advanced Metering Infrastructure (AMI) they enable energy companies to obtain active energy, phase current and voltage, apparent energy, and Reactive lead from smart meter deployed at home [2]. Smart meters (SM) collect the active energy from the real-time, and reveal the user habits and behavior at home to forecast the financial loss. For example, if the daily energy is low, then the user is not at home. To disclose the theft detection is addressed in this work. Smart meters allow functions to perceive Non-Technical Loss (NTL), which was very difficult in previous days. Now SM even out functions that often measures the energy consumption (EC), and gives the better perceptive of customer consumption behavior [3].

Non-Technical losses occur due to loads and conditions when the Technical losses calculation become unsuccessful to consider or due to the triggering of the external factors. Non- Technical losses are tedious to evaluate since these losses are not frequently considered by the system operatives and therefore have no verified data existed [4]. One of the fundamental NTLs is the theft of electricity. This theft involves bypassing of the electricity meter,

* Corresponding Author: Priyamvada Chandel, Central Power Research Institute, Bhopal, India. Email Id: priyamvada@cpri.in

hacking the meter, or tampering the meter reading [5]. Electricity theft results in a great revenue fall of power company because of the surging electricity, the dense load of electrical systems, and it brings threats to public safety.

In many developing countries, at many distribution feeders, electricity theft is openly visible. In the past, indiscriminate machine learning methods have been employed for detecting electricity theft. However, convenient variables are created from meter readings, and the performance will be optimal [6]. The existing methods have some concerns that need to be addressed further. For Artificial Intelligence (AI) based methods, due to the difficulty in building a labeled dataset of electricity thefts, the application of classification methods is limited. Since the clustering algorithms are unverified, tampered load profiles with normal figures cannot be identified, ensuing in low accuracy of prediction. For the state-based methods, the measurement data and system information acquisition are much more difficult to obtain [7]. For deep learning approaches, since the scalability of the framework is arbitrary, the network can end up being unstable. Furthermore, the weights fed to the layers of the network have the underfitting of the model that tends to increase the number of epochs for training the model. Epoch is defined as the number of iterations related to the samples of the dataset. For training a network with a large dataset and a reduced number of epochs, memory storage becomes an important concern for the classification model of the network.

2. Literature Review

This section includes a survey of electricity theft detection methods proposed by researchers formerly. The studies can be categorized into hardware-based and non-hardware based solutions to the detection of electricity theft. Non-hardware based solutions include AI and machine learning techniques.

Nizar et al. applied the Extreme Learning Machine (ELM) for electricity theft detection [8]. The ELM-based technique extracts forms of customer behavior using their previous consumption data in kWh and perceives abnormal deeds. The performance of the classifier was compared with OS-ELM and SVM for validation. However, the classification rate of testing phase was found low for this approach.

In [9], the authors recommended a multi-class SVM which was trained to identify a sample of load profiles whether it is malicious or normal. This paper addressed and solved the imbalanced training by generating a synthetic dataset. The algorithm also uses silhouette plots to identify the different distributions in the dataset. One limitation of the machine learning approach is that it is vulnerable to contamination attacks.

In [10], the authors proposed an optimum-path forest (OPF) based unsupervised NTL detection methodology and compared with other popular clustering methods including k-means and GMM. OPF has attained the most accurate results while considering both the applications on two datasets composed of industrial and commercial profiles of irregular and regular consumers. However, clustering techniques are not cost-effective.

In [11], the researcher suggested for distribution lanes from current and real power measurements using linear regression technique; subsequently, NTL of all lane is measured in accordant with the estimated resistance value to find the electricity theft. Limitation of this method is that correlating more than two independent factors with dependent factor becomes complicated in the linear regression model.

In [12], the authors proposed for distribution load transformer is employed in detecting meter tampering using state estimation-based technique. The variation in the measured values and the estimated values is assessed to make suspicious details of consumers with metering issues. Customer meter data in conjunction with intelligent devices measurements in smart distribution grid are used for DSE and NTL detection without additional meter investment at points of delivery.

In [13], the researchers presented a probabilistic methodology NTL assessment in the distribution system. The sensitivity of technical loss when related to the load variation is derived, and the probabilistic distributions of total loss and technical loss are evaluated. This approach is suitable only for countries that have scarce resources and is not suitable for smart grid applications.

In [14], the authors recommended a deep-learning-based real-time technique for the finding of electricity thefts was projected. This paper utilizes real-time data and its state vector estimator (SVE), and computes the occurrence vector and state vector and the topology of the power system, and a detection scheme based on broad belief network assist the SVE identifies the false data injection (FDI). However, possible FDI attacks are not imposed on the network.

In [15], the researchers proposed Principal Component Analysis (PCA) based Theft Detection system to identify energy theft in AMI. This approach was then compared with SVM classifier to validate the supremacy of PCATD performance. But the results obtained from PCA are found to be inconsistent under change of constraints.

The study conducted in [16] detect the anomalous behavior in customer-defined patterns using an SVM classifier. However, the study relied on monthly measurements of the demand, and the detection window is approximately taken for two years. Additionally, the algorithm was found to show low performance while detecting any theft cases that are not viewed as unexpected variations.

Beyond the concept of machine-learning algorithms, techniques based on game-theory have been applied in [17], identified the fraud was executed between the utility company and fraud-committing consumers. The primary problem with these approaches is the struggle in the formulation of practical and realistic utility functions for the players involved.

In [18], the authors proposed a model that exploits the time-series nature of the customers' electricity consumption to implement a Gated Recurrent Unit (GRU)-RNN. As an improvement to RNN, random search analysis in the learning stage has been adopted. In [19], the authors suggested a deep neural network (DNN)-based customer-specific detector, that implements a sequential grid search analysis in its learning stage for tuning hyperparameters. Wide-ranging investigations are performed based on openly accessible originally energy consumption database of 5000 customers. These approaches suffer from inefficient memory for storage and retrieval.

In [20], the author proposed DNN with transfer entropy measure-based anomaly detection for both sensor measurements and innovative sequences, that can be assessed in a data-driven fashion without relying on a model of the underlying dynamic system. The results of the simulation indicated that the method takes a longer time for computation.

In [21], the authors recommended a novel data analysis method for detecting false data injection attack mitigation (FDIA) based on a data-centric model using the margin setting algorithm. The performance of the suggested methodology is presented employing the six-bus power network in a measurement system of the wide-area environment through simulation. However, it handles only a limited data for the period of the identification process.

In [22], the authors proposed to identify cyber-attacks in Cyber-Physical systems using a novel unsupervised approach, combining LSTM-RNN for behavioral-based intrusion detection. This model not only identifies the attacked sensor, but also detects the irregularities in the CPS. The limitation of this method was that the ability to validate the false positives was found less.

In [23], the authors proposed ANN-based intrusion detection. The MLP is trained to employ packet traces of internet, and then it is evaluated based on its capability to resist DoS/DDoS attacks. The study spotlight on the normal and threat patterns classification on an IoT Network. But the mean absolute error obtained for MLP was found to be high.

3. Proposed Methodology

In this section, the Electricity Theft Detection and Implementation using CNN-RNN-BiLSTM model are discussed. The advancement of the methodology proposed such work consists of the following fundamental stages:

- To construct a network for ensuring enhanced storage of memory along with cache memory and for the retrieval of the system.
- To build a balanced system for reducing the training time and epochs.
- To detect electricity theft in the Indian distribution system.

Electricity Theft Detection

Electricity Theft Detection study is categorized into two types: Data-driven solution and Hardware-based solution. The hardware-based solution met with failure due to severe weather conditions and difficulty in maintaining the devices. The data-driven solution has attained more attention

nowadays. The data-driven is planted on data fusion from sensors and AMI. The methodology uses SM data for convolution.

Data attributes

The following are the important attributes of electricity consumption behavior from 41 meters dated 1/1/2017 to 16/2/2018 with the frequency of every 15 minutes that the users consume energy daily. The attributes namely; R, Y, B phase current and voltage, active energy, apparent energy, reactive lag, reactive lead, PF, and label.

CNN

A CNN structure transforms the input work into an output work using a stack of the discrete layer. CNN comprises of an input layer, multiple hidden layers, and output layer; whereas the hidden layer embraced of pooling layer and convolutional layer [24]. The receptive field is the zone of the input matrix that influences a precise unit of the network. The convolutional layer which comprises of the less receptive field and it can extend up to full depth of

input, and it is composed of kernels or filters. Each filter is convolved using height and width of input at onward pass, and it produces the 2D activation map of the filter. The pooling layer reduces the parameters, network computation, and controls the overfitting. The pooling function employed in the proposed method is maximum pooling.

The pooling layer accepts the volume of size $W \times H \times D$, and produces a volume of size $W' \times H' \times D$.'

$$W' = \frac{W-e}{s+1} \quad (1)$$

$$H' = \frac{H-e}{s+1} \quad (2)$$

$$D' = D \quad (3)$$

Where e is the spatial extent and s is the stride. The pooling layer operates independently on every depth of the input slice and resizes it in the spatial dimension. Due to these advantages, the CNN network is used for extracting the convolution features efficiently.

RNN

In RNN the memory formed through recurrent connection. In feedforward networks, inputs are connected, and it is also independent. It exhibits vital behavior for sequential classification in a time sequence. Consider an input classification $X = (X_1, ..., X_T)$, a standard RNN evaluates the hidden vector classification $h = (h_1, ..., h_T)$ and output vector classification $Y= (Y_1, ..., Y_T)$ by repeating the below equations from t = 1 to T [25]:

$$h_t = H(W_{xh}X_t + W_{hh}h_{t-1} + b_h) \quad (4)$$

$$y_t = W_{hy}h_t + b_0) \quad (5)$$

where,

W - weight matrices (e.g., W_{xh} is the input-hidden weight matrix),

b - denote bias vectors (e.g., b_h is the hidden bias vector) and

H - hidden layer function. H is usually a sigmoid function.

Bidirectional LSTM (BiLSTM)

Long Short Term Memory (LSTM) Recurrent Neural Networks (RNN) have been solved the problem of vanishing gradients in RNNs. The LSTM structure composed of memory blocks and block consists of three multiplicative units such as input, forget and output gates and one or more self-associated memory cells. The multiplicative units afford incessant analogs of reading, write, and rearrange functions for cells. An LSTM is similar to RNN, but the main difference is the memory blocks are

used in the hidden layer instead of nonlinear units. To avoid the vanish-gradient issue and to access and store data for a long time of period, the multiplicative gates used in LSTM. Consider that the input gate rests closed (0) the cell will not be overridden by the fresh inputs, and can be set accessible for the next sequence, by opening the output gate.

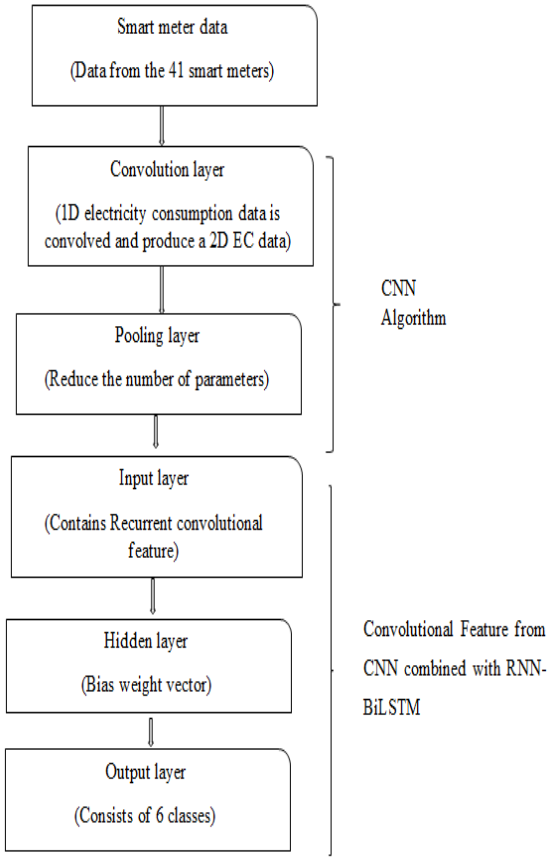

Figure.1: Methodology of CNN-RNN BiLSTM

Traditionally RNN has the problem for vanishing and exploding the gradients. The issue is due to the weight proportional to the gradient of error. During backpropagation, gradients multiply with small values leads to earning smaller values. LSTM does not suffer from any gradients, and it also controls the cell state retains in memory and passes the output. An activation function is a function that defines the output of each node. A sigmoid activation function is used in the design. A sigmoid activation function is an 'S' shaped curve function that ranges between 0 and 1.

$$\mathrm{i} = \sigma(\mathrm{xtUi} + \mathrm{st} - 1\mathrm{Wi}) \quad (6)$$

$$\mathrm{f} = \sigma(\mathrm{xtUf} + \mathrm{st} - 1\mathrm{Wf}) \quad (7)$$

$$\mathrm{o} = \sigma(\mathrm{xtUo} + \mathrm{st} - 1\mathrm{Wo}) \quad (8)$$

where,

xt is the input data sequence, the i-input gate is the gate that allows the input data to enter the network, the f-forget gate is responsible in deciding whether to keep the data or delete the data which is no longer useful, and o-output gate produces the output to be sent to the hidden state. The formula for each gate is formulated using the weight matrix (W), time sequence (U) and a sigmoidal activation function to push the values between a certain interval.

CNN-RNN-BiLSTM

This paper proposes a CNN-RNN-BiLSTM method for the detection of electricity theft. A hybrid wide and deep CNN and RNN is proposed with memory extension rendered by BiLSTM network. The Wide CNN component can capture the convolution features of 1-D electricity consumption data. And the Deep CNN module can recognize the non-periodicity and periodicity of the electricity consumption records.

BiLSTM based RNN offers enhanced memory storage with bidirectional information flow, and make the retrieval and the memory storage and recovery are possible for long term dependencies. The retrieved layer occurs with six classes.

The architecture of the proposed system

Fig 1 shows the flow diagram of the proposed CNN-RNN-BiLSTM prediction model. Data from 41 smart meters are collected and given to the Convolution layer. The convolutional layer convolves the 1-D electricity data and produces 2-D electricity consumption data. And the pooling layer reduces the number of parameters. This working flow of Convolution and Pooling layer is depicted in Fig 2. L is the number of attributes, M is the number of feature values from the convolution layer and pooling layer. Attributes considered in work are phase voltages, phase currents, active energy, apparent energy, reactive lag, reactive lead, and power factor.

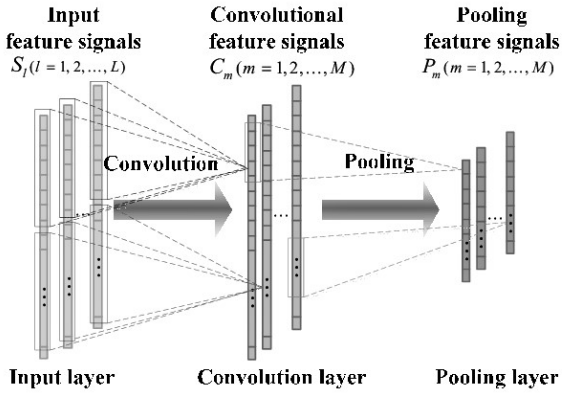

Figure. 2 Convolution and Pooling layer

The length of the input vector f is n, and that of the kernel g is m. The convolution of input vector and kernel function $f * g$ is defined as:

$$(f * g)(i) = \sum_{j=1}^{m} g(j) \cdot f(i - j + \frac{m}{2}) \quad (9)$$

These convolved values passed through max pool layer. The maximum value obtained from pooling layer is chosen as the convolution feature. The convolution features are loaded onto the input layer of RNN. The general structure of RNN is given in Fig 3.

RNN consists of 3 layers, namely, Input layer, Hidden layer, and Output layer. Input cells get convolution features and pass to the hidden or recurrent layer. It consists of neurons x1, x2, x3, etc.,

which gets the input data sequences. The hidden layer contains the hidden units h1, h2, etc., which hold the activation functions that define the output of the neurons in the recurrent layer. The neurons in the output layer y1, y2, etc., will send the predicted values of electricity theft as the output. Each cell of RNN in the proposed prediction model is a BiLSTM memory cell, whose structure is displayed in Fig 4.

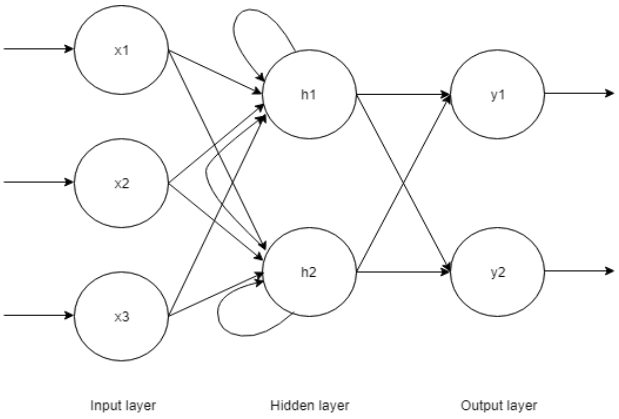

Figure 3. Structure of RNN

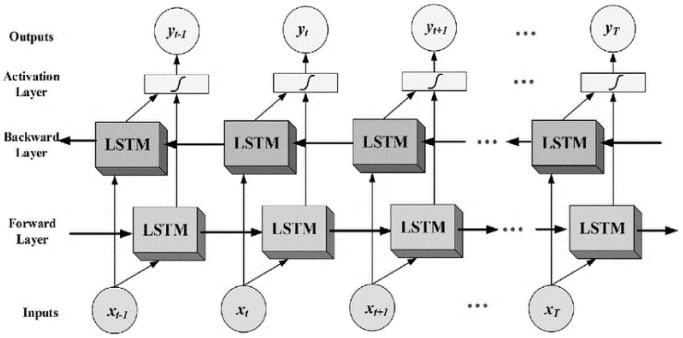

Figure 4. Structure of BiLSTM

The information flow in a BiLSTM is bidirectional, unlike the LSTM. BiLSTM cells acquire bidirectional long term dependencies among time steps or sequential data. These previous long term dependencies are useful for predicting the next state.

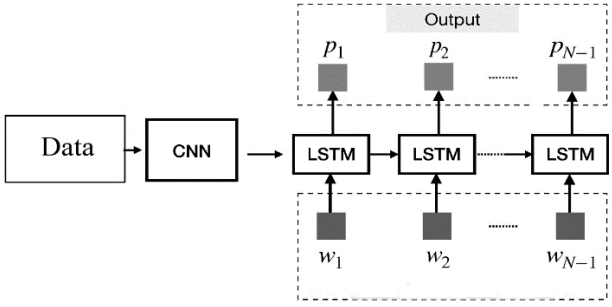

Figure. 5 CNN-RNN-BiLSTM

Fig. 5 shows the architecture of the proposed CNN-RNN-BiLSTM prediction model. Input data is sent to CNN for convolution. Convolution features extracted using CNN are sent to RNN-BiLSTM. The outputs of the model are the detected values of electricity theft.

The voltage and current threshold values for different tamper types are given in Table 1.

Table 1. Occurrence threshold values for different Tamper types

S. NO	TAMPER TYPE	OCCURRENCE THRESHOLDS
1	Link Miss phase-wise	Vx < 60 % Vref and Ix > 5 % Imax
2	CT Bypass	Iavg> 2% IBasic and Ix >2.5% IBasic
3	CT Open phase-wise	Vx > 60% Vref and Ix< 0.5% Imax
4	Current Unbalance	Vavg > 60% Vref and Iavg > 1:
5	Voltage Unbalance	Vavg > 66 % Vref
6	Current Reversal phase-wise	Vavg < 60% Vref and Net PF > -0.5:

Six classes are achieved based on Vref=240V, Ibasic=10A, Imax=40.0A, Iavg=Average of three-phase currents and the tampers are link miss-phase wire, CT bypass, CT open phase-wise, current unbalance, voltage unbalance and current reversal phase wire.

4. Result and Discussion

Evaluation of the proposed energy theft detection using abnormal conditions scheme is done using MATrix LABoratory (MATLAB) The energy usage data comes from Smart Meter Data.

Table 2. Results obtained

Class Labels	Six classes of fault types
No. of Observations	6000
Control classes	[5x1] double
Correct Rate	0.9712
Error Rate	0.0288
Classified Rate	1
Specificity	0.9929
Sensitivity	0.9990
Positive Predictive Value	0.9640
Negative Predictive Value	0.9998
Positive Likelihood	139.7162
Negative Likelihood	0.0010
Prevalence	0.1608

4.1. Experimental Data

Dataset taken for this study is the real-time data communicated by 41 numbers of three phases four-wire smart meters having a unique number, and the data is sent to the Data Collection Unit (DCU) of Chhattisgarh State Electricity Board Raipur. Totally 231637 data for every 15 minutes' interval of time from 1/1/2017 to 16/2/2018 is considered.

4.2. Testing

Then the network is tested using the 6000 data. Each label consists of 1000 data. The tested results are obtained from MatlabR2018a are given in Table 2.

The Fig.6 shows the confusion matrix accuracy of 97.1%.

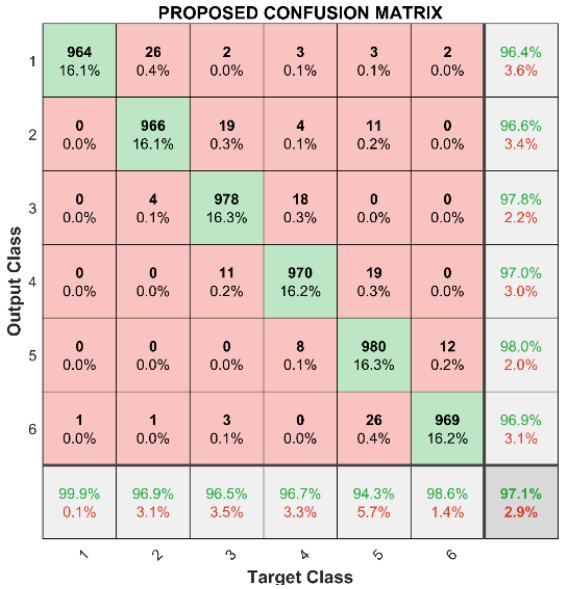

Figure 6. Proposed confusion matrix

4.3. Parameter Study

The Fig.7 shows the accuracy and loss of RNN-BiLSTM.

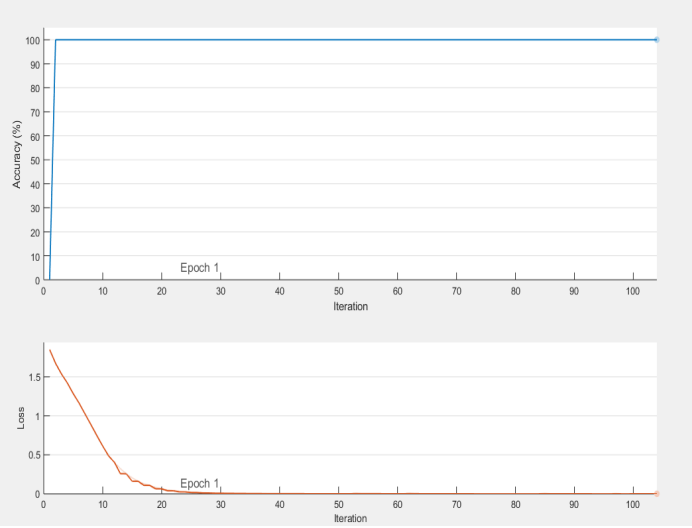

Figure 7. Accuracy and loss of RNN-BiLSTM

First Smart meter(SM) data are taken as label and balanced. Using the Convolutional Neural Network (CNN), the convolution feature of dataset is extracted. In CNN, we used two layers called Convolution and pooling layer to extract the convolution feature. Here, CNN works well for identifying simple patterns within the smart meter data, which will be employed to form higher complex patterns within higher layers. A one dimensional CNN is very efficient to derive the location of feature from shorter (fixed-length) sections of the entire data set and where the location of the feature within the section is not of high significance. The extracted feature from the convolutional feature is used in the RNN-BiLSTM network to predict the class of fault. In RNN-BiLSTM networks, information can be accessed both in forward and reverse direction. These forward and reverse feature in RNN-BiLSTM have to access the past as well as the future information. This has been effectively employed in many practical applications like language translation, future prediction, image captioning, etc., Using the Bidirectional LSTM we feed the learning algorithm with smart meter data once from the beginning to end and once from end to the beginning. There are debates here, but it usually learns faster than one-directional approach, although it depends on the task

Here the loss (error) reduces from 2 to 0, and the accuracy shows increase the value from 0 to 100. Hence it shows our proposed CNN-RNN-BiLSTM shows the efficient accuracy of 100% for the original Training Dataset.

The proposed system is compared with the existing technique and proved the accuracy of 97.1%. Table 3 given below represents the compared result of the proposed with the existing methods, and Fig. 8 represents the accuracy score of the proposed method [27]:

Table.3 Validation of proposed system

Algorithm	Arguments	Accuracy Score
Combined CNN model	100 epochs	0.9267
Single CNN model	100 epochs	0.9218
Simple DNN model	100 epochs	0.9145
Linear SVC	kernel: linear function	0.9178
Random Forest	Max depth: 7	0.9164
Logistic Regression	penalty: L2	0.9141
Proposed Model	Convolution BiLSTM	**0.9712**

The sensitivity, specificity, and accuracy for the proposed CNN-RNN BiLSTM are calculated using the confusion matrix which comprises of False Positive (FP), True Positive (TP), False Negative (FN), and True Negative (TN). Accuracy, sensitivity, and specificity are calculated using the following formulae.

$$Accuracy = \frac{TP+TN}{TN+FN+TP+FP} \quad (10)$$

$$Specificity = \frac{TN}{TN+FP} \quad (11)$$

$$Sensitivity = \frac{TP}{FN+TP} \quad (12)$$

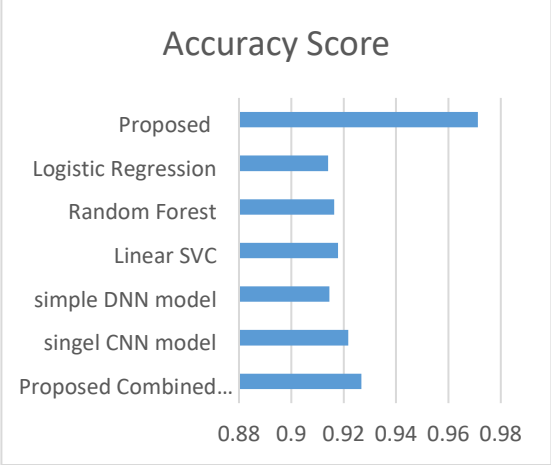

Figure 8. Accuracy score of CNN-RNN BiLSTM

The calculated values are found to be high for the proposed classifier. The specificity, sensitivity, and accuracy obtained for the proposed method are 99.29%, 99.9%, and 97.12% respectively. Fig 9 shows the performance assessment of the proposed framework:

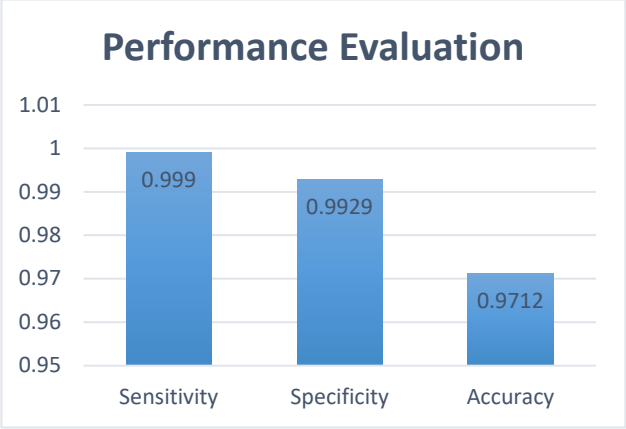

Figure 9. Performance evaluation of CNN-RNN BiLSTM

The performance of the proposed CNN-RNN-BiLSTM is compared with existing methodologies in the literature. Table 4. provides the comparative analysis of the performance parameters of the proposed model with two other models, namely, Support Vector Machine (SVM) and Multi-class SVM.

Table. 4 Performance comparison table

Method	**Accuracy (%)**
SVM [16]	60
Multi-class SVM [9]	94
Proposed	**97.1**

From the table, it is inferred that the proposed CNN-RNN-BiLSTM theft prediction model has better performance compared to the existing models.

5. Conclusion

In this paper, the detection scheme of theft using the abnormal changes in electric values measures in the smart meter is proposed. The proposed electricity theft detection model is based on the combination of CNN and RNN-BiLSTM network, which detects whether the metering data has an abnormal behavior or not. The model predicts the abnormalities in consumer's power consumption behaviors and classifies the behavior based on six classes. The proposed neural network model achieved an accuracy of 100% in training phase and 97.1% in testing phase. The use of technique proposed in this paper will help power utilities to predict theft in lesser time and higher accuracy. Hence in the future, this theoretical approach to the detection of electricity is to be tested for real time practical application. And the use of hybrid spike neural network for electricity theft detection model is presumed to improve the performance of detection effectively.

Conflict of Interest

The authors declare no conflict of interest.

References

[1] R. Jiang, R. Lu, Y. Wang, J. Luo, C. Shen, X. S. Shen, Energy-theft detection issues for advanced metering infrastructure in smart grid. *Tsinghua Science and Technology*, *19*(2), 105-120, 2004. DOI: 10.1109/TST.2014.6787363

[2] Y. Sun, L. Lampe, V. W. S. Wong, "Smart meter privacy: Exploiting the potential of household energy storage units," *IEEE Internet of Things Journal*, vol. PP, no. 99, pp. 1–1, 2017. DOI: 10.1109/JIOT.2017.2771370

[3] J. Nezhad, T. K. Wijaya, M. Vasirani, K. Aberer, "SmartD: Smart Meter Data Analytics Dashboard," Proceedings of the 5th international conference on Future energy systems. ACM, pp. 213–214, 2014. DOI: 10.1145/2602044.2602046

[4] J. P. Navani, N. K. Sharma, S. Sapra, Technical and non-technical losses in the power system and its economic consequence in the Indian economy. *International Journal of Electronics and Computer Science Engineering*, *1*(2), 757-761, 2012.

[5] S. McLaughlin, B. Holbert, A. Fawaz, R. Berthier, S. Zonouz, A multi-sensor energy theft detection framework for advanced metering infrastructures. *IEEE Journal on Selected Areas in Communications*, *31*(7), 1319-1330, 2013. DOI: 10.1109/JSAC.2013.130714

[6] R. Razavi, A. Gharipour, M. Fleury, I.J. Akpan, A practical feature-engineering framework for electricity theft detection in smart grids. *Applied Energy*, *238*, 481-494, 2019. DOI: 10.1016/j.apenergy.2019.01.076

[7] K. Zheng, Q. Chen, Y. Wang, C. Kang, Q. Xia, A Novel Combined Data-Driven Approach for Electricity Theft Detection. *IEEE Transactions on Industrial Informatics*, *15*(3), 1809-1819, 2019. DOI: 10.1109/TII.2018.2873814

[8] A.H. Nizar, Z.Y. Dong, Y. Wang, Power utility nontechnical loss analysis with extreme learning machine method. *IEEE Transactions on Power Systems*, *23*(3), 946-955, 2008. DOI: 10.1109/TPWRS.2008.926431

[9] P. Jokar, N. Arianpoo, V.C. Leung, Electricity theft detection in AMI using customers' consumption patterns. *IEEE Transactions on Smart Grid*, *7*(1), 216-226, 2016. DOI: 10.1109/TSG.2015.2425222

[10] L.A.P. Júnior, C.C.O. Ramos, D. Rodrigues, D.R. Pereira, A.N. de Souza, K.AP. da Costa, J.P. Papa, Unsupervised non-technical losses identification through the optimum-path forest. *Electric Power Systems Research*, *140*, 413-423, 2016. DOI: 10.1016/j.epsr.2016.05.036

[11] D.N. Nikovski, Z. Wang, *U.S. Patent No. 9,945,889*. Washington, DC: U.S. Patent and Trademark Office, 2018.

[12] S.C. Huang, Y. L. Lo, C.N. Lu, Non-technical loss detection using state estimation and analysis of variance. *IEEE Transactions on Power Systems*, *28*(3), 2959-2966, 2013. DOI: 10.1109/TPWRS.2012.2224891

[13] E.A.A. Neto, J. Coelho, Probabilistic methodology for Technical and Non-Technical Losses estimation in the distribution system. *Electric Power Systems Research*, *97*, 93-99, 2013. DOI: 10.1016/j.epsr.2012.12.008

[14] Y. He, G.J. Mendis, J. Wei, Real-time detection of false data injection attacks in smart grid: A deep learning-based intelligent mechanism. *IEEE Transactions on Smart Grid*, *8*(5), 2505-2516, 2017.DOI: 10.1109/TSG.2017.2703842

[15] S.K. Singh, R. Bose, A. Joshi, Energy theft detection in advanced metering infrastructure. In *2018 IEEE 4th World Forum on the Internet of Things (WF-IoT)* (pp. 529-534), 2018. DOI: 10.1109/WF-IoT.2018.8355148

[16] J. Nagi, K.S. Yap, S.K. Tiong, S. K. Ahmed, M. Mohamad, Nontechnical Loss Detection for Metered Customers in Power Utility Using Support Vector Machines. *IEEE transactions on Power Delivery*, *25*(2), 1162-1171, 2010. DOI: 10.1109/TPWRD.2009.2030890

[17] S. Amin, G.A. Schwartz, A. A., Cardenas, S.S. Sastry, Game-theoretic models of electricity theft detection in smart utility networks: Providing new capabilities with advanced metering infrastructure. *IEEE Control Systems Magazine*, *35*(1), 66-81, 2015. DOI: 10.1109/MCS.2014.2364711

[18] M. Nabil, M. Ismail, M. Mahmoud, M. Shahin, K. Qaraqe, E. Serpedin, Deep Recurrent Electricity Theft Detection in AMI Networks with Random Tuning of Hyper-parameters. In *2018 24th International Conference on Pattern Recognition (ICPR)* (pp. 740-745), 2018. DOI: https://arxiv.org/abs/1809.01774

[19] M. Ismail, M. Shahin, M.F. Shaaban, E. Serpedin, K. Qaraqe, Efficient detection of electricity theft cyber-attacks in AMI networks. In *2018 IEEE Wireless Communications and Networking Conference (WCNC)* (pp. 1-6), 2018. IEEE. DOI: 10.1109/WCNC.2018.8377010

[20] D. Shi, Z. Guo, K.H. Johansson, L. Shi. Causality countermeasures for anomaly detection in cyber-physical systems. *IEEE Transactions on Automatic Control*, *63*(2), 386-401, 2018. DOI: 10.1109/TAC.2017.2714646

[21] Y. Wang, M.M. Amin, J. Fu, H.B. Moussa. A novel data analytical approach for false data injection cyber-physical attack mitigation in smart grids. *IEEE Access*, *5*, 26022-26033, 2017. DOI: 10.1109/ACCESS.2017.2769099

[22] J. Goh, S. Adepu, M. Tan, Z.S. Lee. Anomaly detection in cyber-physical systems using recurrent neural networks. In *2017 IEEE 18th International Symposium on High Assurance Systems Engineering (HASE)* (pp. 140-145), 2017. IEEE. DOI: 10.1109/HASE.2017.36

[23] E. Hodo, X. Bellekens, A. Hamilton, P.L. Dubouilh, E. Iorkyase, C. Tachtatzis, R. Atkinson, R. (2016, May). Threat analysis of IoT networks using artificial neural network intrusion detection system. In *2016 International Symposium on Networks, Computers and Communications (ISNCC)* (pp. 1-6). IEEE.DOI: 10.1109/ISNCC.2016.7746067

[24] R. R. Varior, M. Haloi, and G. Wang, "Gated siamese convolutional neural network architecture for human re-identification," in *European Conference on Computer Vision*, pp. 791–808, 2016. DOI: https://arxiv.org/abs/1607.08378

[25] A.A. Sharfuddin, M.N. Tihami, M.S. Islam. A Deep Recurrent Neural Network with BiLSTM model for Sentiment Classification. In *2018 International Conference on Bangla Speech and Language Processing (ICBSLP)* (pp. 1-4), 2018. IEEE.

[26] C. Genes, I. Esnaola, S. M. Perlaza, L. F. Ochoa, and D. Coca, "Recovering missing data via matrix completion in electricity distribution systems," in Signal Processing Advances in Wireless Communications (SPAWC), 2016 IEEE 17th International Workshop on, 2016. DOI: 10.1109/SPAWC.2016.7536744

[27] D. Yao, M. Wen, X. Liang, Z. Fu, K. Zhang, B. Yang. Energy Theft Detection with Energy Privacy Preservation in the Smart Grid. *IEEE Internet of Things Journal*, 2019. DOI: 10.1109/JIOT.2019.2903312

ASTES

Advances in Science, Technology and Engineering Systems Journal
Vol. 4, No. 4, 169-173 (2019)
www.astesj.com

ASTES Journal
ISSN: 2415-6698

Signal-to-Quantization Noise Ratio of the Parallel Digital Ramp Analog-to-Digital Converter

Constantine Andreas Pappas*

ECE, Stevens Institute of Technology, 07030, USA

ARTICLEINFO

Article history:
Received: 05 March, 2019
Accepted: 15 June, 2019
Online: 30 July, 2019

Keywords:
SQNR
PDR ADC
Nonuniform Sampling

ABSTRACT

This work presents a theoretical analysis of the Signal-to-Quantization Noise Ratio (SQNR) of the nonuniform Parallel Digital Ramp Pulse Position Modulator Analog-to-Digital Converter (PDR-ADC) architecture. The PDR-ADC partitions the amplitude axis into P non-overlapping partitions that sample the analog input at input signal driven instances. Samples are generated when the input signal crosses a digital ramp in a partition. The parallel digital ramps operate from a single clock. For sinusoidal signals, it is shown, for uniform partitions the SQNR can be increased be increasing the number of bits in the counter or by increasing the number of partitions. A geometric partitioning scheme is then proposed where, again for sinusoids, it is shown that this quantization rule has the effect of attempting to maintain the SQNR approximately constant. For geometric partitioning, it is shown that the largest SQNR is achieved when the geometric parameter, common ratio, equals two.

1 Introduction

Many alternatives to Nyquist rate sampling systems have been proposed in the literature [1] - [8]. Of the various methods described, the nonuniform Level Crossing (LC) architectures appear to dominate the recent literature, [9] -[14]. In [15], the PDR-ADC was introduced and circuits to affect the desired response developed. A specific partitioning scheme based upon partitioning the signal amplitude axis as a geometric series was developed in terms of circuit parameters. In this communication, alternative methods to increase the SQNR of the PDR-ADC and a more general discussion of the geometric partitioning in terms of the geometric progression parameter, common ratio, are presented.

All uniform quantizers begin to lose resolution as the amplitude of the input signal decrease. To understand where information is lost in uniform quantizers, a brief review of uniform quantization is presented. Next, the SQNR of the PDR-ADC is obtained under the conditions of a uniform partitioning scheme. The SQNR for a geometric partitioning scheme with common ratio two is developed without regard to any specific circuit analysis. Lastly, the SQNR for arbitrary common ratio is presented, where is is shown that the maximum increase in SQNR for geometric partitioning is obtained for a common ratio equal to two.

2 Uniform Quantization

Figure 1 is a block diagram of an ideal, uniform, analog to digital converter. The switch represents an ideal sample and hold (S&H) operation (aperture effects are ignored), such that the output of the S&H is the 'instantaneous' analog value of the input, $f(t)$. The quantization rule is represented by the Q block. Lastly, the encoder, E, converts the quantizer output into the corresponding digital word.

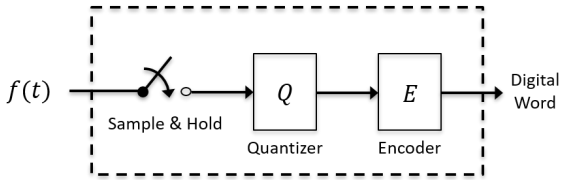

Figure 1: Ideal ADC

Let the number of bits in the digital word be, N, and let, V_{ref}, be the analog reference voltage for the ADC, then, as is well known, that the quantization step size, Δ is [15, 16]:

$$\begin{aligned} \Delta &= \frac{V_{ref}}{2^N} \\ &= \frac{V_{FS}}{2^N - 1} \end{aligned} \tag{1}$$

where V_{FS} is the *full scale* voltage: $V_{FS} = V_{ref} - \Delta$.

*Corresponding Author: Constantine Andreas Pappas, cpappas@stevens.edu

In uniform quantizers, the quantization noise power, P_{N_Q}, is well approximated by, [17, 18]:

$$P_{N_Q} = \frac{\Delta^2}{12} \tag{2}$$

The signal-to-quantization noise ratio (SQNR) is the ratio of the signal power, P_{sig}, to the quantization noise power, P_{N_Q}. For a full scale sinusoid of the form, $y = \frac{V_{FS}}{2} sin(\omega t)$, the $SQNR$ is found to be:

$$\begin{aligned} SQNR = \frac{P_{sig}}{P_{N_Q}} &= \frac{(V_{FS}/2)^2}{2} \cdot \frac{12}{\Delta^2} \\ &\approx 2^{2N} \cdot \frac{3}{2} \end{aligned} \tag{3}$$

or in decibels, the familiar "rule of thumb" for sinusoids is obtained:

$$SQNR_{dB} \approx 6.02N + 1.76\ dB \tag{4}$$

Lastly, as is well known, when the amplitude of a sinusoidal signal decreases by a factor of 2, the signal power decreases by a factor of 4 and the ADC loses 1 bit of resolution. The $SQNR_{dB}$, from 4, may be written as:

$$SQNR_{dB} \approx 6.02(N-1) + 1.76\ dB \tag{5}$$

3 PDR: Uniform Partitions

Conceptually, the PDR-ADC may initially be regarded as a parallel arrangement of uniform quantizers as shown in Figure 2. Each quantizer, in Figure 2, is referenced independently and spans a different range of possible input signal values, thus partitioning the input signal axis [19, 15].

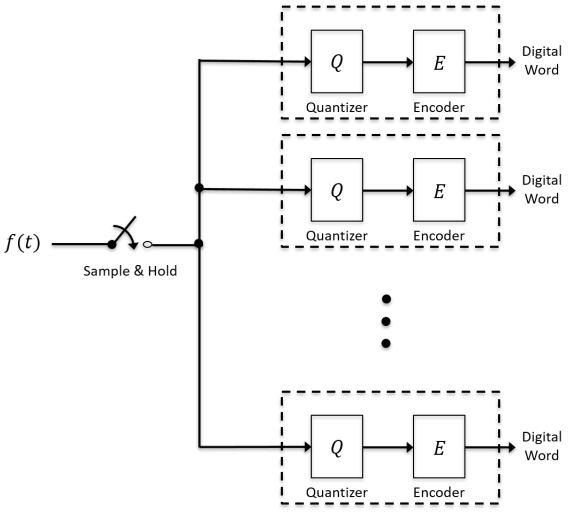

Figure 2: Parallel Quantization

In such an arrangement, if $\mathcal{P}$ is the number of partitions, and if each quantizer contains the same number of quantization levels, L, where $L = 2^N$, and if each quantizer has a dynamic range, $\frac{V_{ref}}{\mathcal{P}}$, so that together the $\mathcal{P}$ partitions span V_{ref}, then the quantization step size is given by:

$$\Delta = \frac{V_{ref}}{\mathcal{P} \cdot 2^N} \tag{6}$$

Such a parallel uniform partitioning scheme is illustrated in Figure 3 for a system with 4 partitions with 4 levels per partition.

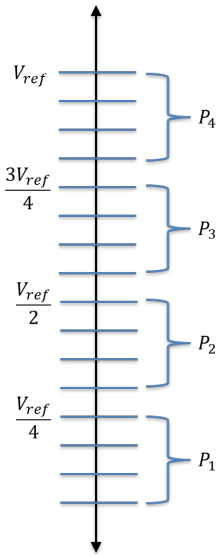

Figure 3: Parallel Uniform Partitioning

Equation (6) yields the same quantization step size as a single ADC with $L = \mathcal{P} \cdot 2^N$ levels, operating from the same V_{ref}.

The PDR-ADC, however, operates from a single N bit digital counter, that generates 2^N counts, that are scaled and shifted to generate the required number of partitions [15]. Consequently, if a single digital ramp ADC, operating with clock rate, T_{CLK}, were required to span the same dynamic range, V_{ref}, this single digital ramp would take $\mathcal{P} \cdot 2^N \cdot T_{CLK}$ seconds. The PDR-ADC however, spans the same dynamic range in $2^N \cdot T_{CLK}$ seconds, a $\frac{1}{\mathcal{P}}$ times improvement.

For a PDR-ADC, governed by (6), excited by a full scale sinusoid of the form, $y = \frac{V_{FS}}{2} sin(\omega t)$, the $SQNR$ is found to be:

$$SQNR \approx \mathcal{P} \cdot 2^N \cdot \frac{3}{2} \tag{7}$$

or in decibels:

$$SQNR_{dB} \approx 6.02N + 1.76 + 20log_{10}(\mathcal{P}) \tag{8}$$

Equation (8) states, in the PDR-ADC, with each partition operating with the identical, uniform, step size, Δ, the signal-to-quantization noise may be increased in the usual way by increasing the number of bits used in the counter, N, and/or by increasing the number of partitions, $\mathcal{P}$.

For example, the identical $SQNR$ performance of a single, 16 bit ADC can be achieved with a PDR-ADC designed with, $\mathcal{P} = 8$ partitions, operating with a 13 bit counter. Additionally, in this case, the PDR only counts to 8192, whereas a single digital ramp ADC would be required to count the full 65536 counts.

Additionally, in the PDR-ADC, the counter is not required to count, to a count value that is a power of 2. The same performance as described can be matched,

approximately, from a PDR-ADC designed with $\mathcal{P} = 10$ partitions and a counter that counts to 6554, thereby further decreasing the total time required to span the full dynamic range. A practical design constraint is that the number of partitions be even, so that the dynamic range of the PDR-DAC is symmetric about zero Volts.

4 PDR: Geometric Partitioning

In this section, the general behavior of the PDR-ADC with a geometric partitioning scheme of the amplitude axis, as illustrated in Figure 4, is presented without reference to circuit analysis[1]. For clarity, Figure 4 shows the essence of the geometric partitioning with a system of 4 partitions with 4 levels per partition. In the figure, the reference voltage of the entire system is equated to the maximum of the geometric sum, which is designated, $15V_x$, for the yet to be determined voltage, V_x.

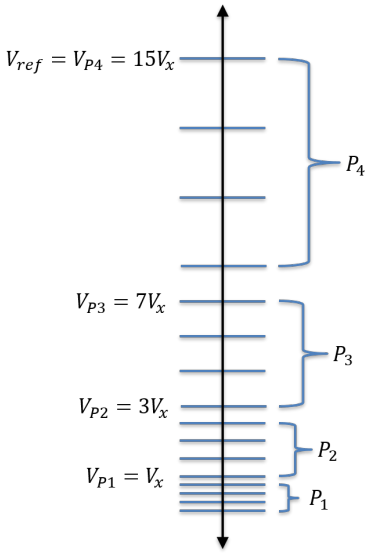

Figure 4: Parallel Geometric Partitioning

The m^{th} reference voltage, V_{P_m} for each partition is related as a geometric series, and is obtained from:

$$V_{P_m} = V_x \sum_{k=0}^{k=m-1} 2^k \tag{9}$$

Let $\mathcal{M}$ to be the maximum partition number, then, from the system reference voltage, V_{ref}, the voltage V_x may be found from:

$$V_{ref} = V_x \sum_{k=0}^{k=\mathcal{M}-1} 2^k = V_x\left(2^{\mathcal{M}} - 1\right) \tag{10}$$

from which:

$$V_x = \frac{V_{ref}}{2^{\mathcal{M}} - 1} \tag{11}$$

The ratio of the n^{th} term of a geometric progression to the $n^{th} + 1$ term is, $\frac{1}{r}$, where r is the common ratio, as is well known. If the common ratio is, $r = 2$, then as the number of partitions increases, the second to last partition is referenced to a value that *approaches* $\frac{V_{ref}}{2}$. In the case under consideration, the $\mathcal{M} - 1$ partition is referenced from:

$$\begin{aligned} V_{P_{\mathcal{M}-1}} &= \frac{V_{ref}}{2}\left(1 - \frac{1}{2^{\mathcal{M}} - 1}\right) \\ &\approx \frac{V_{ref}}{2} \end{aligned} \tag{12}$$

4.1 Geometric SQNR

In the PDR-ADC, for any adjacent partitions, the ratio of the quantization step sizes is the common ratio, which may be written as:

$$\frac{\Delta_m}{\Delta_{m+1}} = \frac{1}{2} \tag{13}$$

where this behavior can be seen in Figure 4.

From (2) and (13), it is seen, in the PDR-ADC, with common ratio, $r = 2$, the quantization noise power of adjacent partitions may be written as:

$$P_{N_{Qm}} = \frac{P_{N_{Qm+1}}}{4} \tag{14}$$

In a PDR-ADC, with geometric partitioning, the quantization noise power decreases by a factor of 4 when transitioning from a higher partition to a lower partition.

Let a full scale sinusoid of the for, $y = A_o sin(\omega t)$, be input to the PDR-ADC, the SQNR is of the form:

$$SQNR = \frac{P_{sig}}{P_{N_{Q\mathcal{M}}}} = \frac{A_o^2}{2} \cdot \frac{1}{P_{N_{Q\mathcal{M}}}} \tag{15}$$

Now, suppose the input signal amplitude decreases by a factor of 2 and let $y = \frac{A_o}{2} sin(\omega t)$ be input to the PDR-ADC, the SQNR is given by:

$$SQNR = \frac{1}{4} \cdot \frac{A_o^2}{2} \cdot \frac{1}{P_{N_{Q\mathcal{M}-1}}} \tag{16}$$

substituting (14) into (16) the SQNR is:

$$\begin{aligned} SQNR &= \frac{1}{4} \cdot \frac{A^2}{2} \cdot \frac{1}{P_{N_{Q\mathcal{M}}}/4} \\ &= \frac{A_o^2}{2} \cdot \frac{1}{P_{N_{Q\mathcal{M}}}} \end{aligned} \tag{17}$$

Equation (17) states, in the PDR-ADC, with a geometric partitioning, the signal-to-quantization noise attempts to remain approximately constant.

4.2 Constant SQNR

The constant value that the SQNR attempts to maintain can be obtained in terms of uniform ADC parameters with the aid of Figure 5. Figure 5 shows, on the left hand side, the uniform levels and the quantization step size for an 4 bit (16 Levels) uniform ADC with dynamic range, V_{FS}. The right hand side of Figure 5 shows the geometric partitioning for the same dynamic range. In the detail of Figure 5, the quantization step size of the largest partition is shown for a 4 bit counter that produces the same number of quatization

[1] A circuit realization of the geometric behavior can be found in [15].

levels (16 Levels) as the uniform quantizer shown on the left.

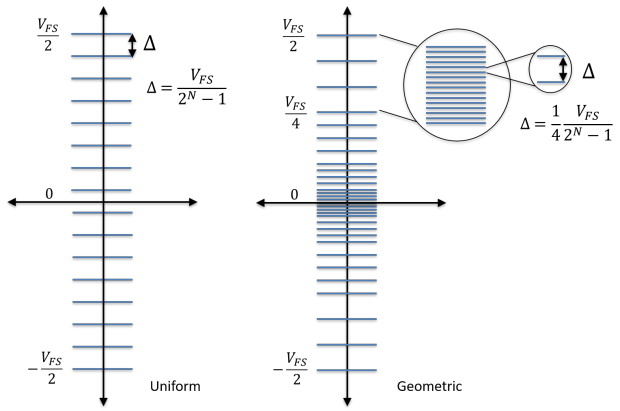

Figure 5: Constant Quantization Step Size

From (12), the dynamic range of the largest partition always approaches $\frac{1}{2}$ of the maximum voltage value, assuming a sufficient number of partitions. In the present case under consideration, as seen in Figure 5, this dynamic range is, $\frac{V_{FS}}{4}$. Consequently, when this range is divided by 2^N levels, the largest quantization step size of a PDR-ADC with geometric partitioning is:

$$\begin{aligned} \Delta_{max} &= \frac{1}{4}\frac{V_{FS}}{2^N - 1} \\ &= \frac{V_{FS}}{2^{(N+2)} - 4} \end{aligned} \tag{18}$$

Substituting (18) into (3), again assuming a full scale sinusoid of the form, $y = \frac{V_{FS}}{2} sin(\omega t)$, the SQNR is:

$$\begin{aligned} SQNR = \frac{P_{sig}}{P_{N_Q}} &= \frac{(V_{FS}/2)^2}{2} \cdot \frac{12}{\Delta_{max}^2} \\ &= \frac{12}{8} \cdot (V_{FS})^2 \cdot \frac{(2^{N+2} - 4)^2}{(V_{FS})^2} \\ &\approx \frac{3}{2} \cdot 2^{2(N+2)} \end{aligned} \tag{19}$$

or in decibels:

$$SQNR \approx 6.02\,(N + 2) + 1.76\ dB \tag{20}$$

Equation (20) states, for a full scale sinusoidal input, a PDR-ADC with geometric partitioning, operating from an N bit counter, gains 2 bits or resolution.

When the results of (20), (14) and (5) are taken together, for a PDR-ADC with geometric partitioning, operating from an N bit counter, the following behavior is deduced:

- From (20): The PDR-ADC behaves as a system with $N+2$ bits.
- From (5): When the signal amplitude drops by a factor of 2, the signal power drops by a factor of 4 and the system loses 1 bit of resolution.
- From (14): When the signal amplitude drops by a factor of 2, the quantization noise power drops by a factor of 4, and the system gains 1 bit of resolution, and the system continues to behave as a system with $N + 2$ bits of resolution.

With geometric partitioning, the PDR data converter attempts to maintain the signal-to-quantization noise ratio approximately constant.

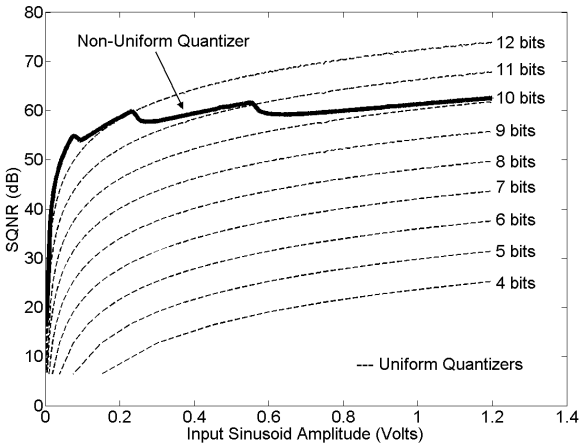

Figure 6: Approximately Constant SQNR from Geometric Partitioning

In Figure 6, the SQNR for the geometric partitioning, with common ratio $r = 2$, is shown as a function of input signal amplitude. The full scale voltage was, $V_{FS} = 2.4$ Volts and the system was driven with a sinusoid of the form, $y = A_o sin(\omega t)$, where A_o was varied from 1.2 Volts to approximately $1mV$. The PDR was modeled with $\mathcal{P} = 8$ partitions with an $N = 8$ bit counter.

For reference comparison, the SQNR for several uniform quantizers are also plotted in Figure 6. It is seen that the system performance is approximately equivalent to a system with $N = 10$ bits of resolution and that the system attempts to maintain this performance against variations in the peak signal amplitude. The peaking in the non-uniform quantizer are the locations where input signal voltage amplitude transitions from one partition to the adjacent partition.

5 Common Ratio and SQNR

Let the maximum voltage of the data converter be, $\frac{V_{FS}}{2}$, then, for any value of the common ratio, r, the maximum value of the next lower partition always approaches, $\frac{V_{FS}}{2r}$, using a geometric partitioning scheme. Consequently, the dynamic range of the largest (outer) partition, $\mathcal{M}$, is approximately:

$$\begin{aligned} \Delta V_{\mathcal{M}} &\approx \frac{V_{FS}}{2} - \frac{V_{FS}}{2r} \\ &= \frac{V_{FS}}{2} \cdot \left(\frac{r-1}{r}\right) \end{aligned} \tag{21}$$

Assuming that this voltage is spanned by an N bit counter, and if driven by a sinusoid, the SQNR becomes:

$$\begin{aligned} SQNR = &= \frac{(V_{FS}/2)^2}{2} \cdot \frac{12}{\Delta^2} \\ &= \frac{12}{8} \cdot (V_{FS})^2 \cdot \left(\frac{2r}{r-1}\right)^2 \cdot \frac{(2^N-1)^2}{(V_{ref})^2} \\ &= \frac{3}{2} \cdot \left(\frac{2r}{r-1}\right)^2 (2^N-1)^2 \\ &\approx \frac{3}{2} \cdot \left(2^{N+b}\right)^2 \end{aligned} \tag{22}$$

where $b = \frac{ln(\frac{2r}{r-1})}{ln(2)}$. Or in decibels:

$$SQNR \approx 6.02\,(N+b) + 1.76\,dB \tag{23}$$

In 23, as the common ratio, $r \to \infty$, $b \to 1$, and the system only gains 1 bit of resolution. Alternatively, as $r \to 2$, its minimum possible value, $b \to 2$, and the system gains 2 bits of resolution. It is seen, in the PDR with geometric partitioning, the largest increase in the effective number of bits occurs with the common ratio, $r = 2$.

6 Conclusion

The signal-to-quantization noise (SQNR) of the parallel digital ramp analog to digital (PDR-ADC) has been formulated using a more general analysis using the common ratio of a geometric series. It was shown that for all values of the common ratio, using a geometric partitioning scheme, the maximum possible increase in the SQNR is achieved when the common ratio, $r = 2$, and the effective increase in the number of bits of resolution provided by an N bit counter is accordingly, 2. It was shown that with geometric partitioning, the PDR-ADC attempts to maintain the SQNR approximately constant. Additionally, it was shown, using a uniform partitioning scheme provides more flexibility in the effective increase in the counters effective resolution with a trade off in the number of partitions, though in this case, the SQNR does not remain approximately constant.

Conflict of Interest The author declares no conflict of interest.

References

[1] J. Mark, T. Todd, "A Nonuniform Sampling Approach to Data Compression" IEEE T COMMUN, **29**(1), 24–32, 1981. https://doi.org/10.1109/TCOM.1981.1094872

[2] N. Sayiner, H. Sorensen, T. Viswanathan, "A Level-Crossing Sampling Scheme for A/D Conversion" IEEE T CIRCUITS SYST, **43**(4), 335–339, 1996. https://doi.org/10.1109/82.488288

[3] E. Allier, J, Goulier, G. Sicard, A. Dezzani, E. Andre, M. Renaudin, "A 120nm Low Power Asynchronous ADC" in ISLPED '05. Proceedings of the 2005 International Symposium on Low Power Electronics and Design, San Diego USA, 2005. https://doi.org/10.1145/1077603.1077619

[4] T. Wang, D. Wang, P. Hurst, B. Levey, S. Lewis, "A Level-Crossing Analog-to-Digital Converter with Triangular Dither" IEEE T CIRCUITS SYST, **56**(9), 2089–2099, 2009. https://doi.org/10.1109/TCSI.2008.2011586

[5] S. Naraghi, "Time-Based Analog to Digital Converters", Ph.D Thesis, University of Michigan, 2009.

[6] P. Maechler, N. Felber, A. Burg, "Random Sampling ADC for Sparse Spectrum Sensing" in 2011 19th European Signal Processing Conference, Barcelona Spain, 2011.

[7] S. Becker, "Practical Compressed Sensing: Modern Data Acquisition and Signal Processing", Ph.D Thesis, California Institute of Technology, 2011.

[8] M. Wakin, S. Becker, E. Nakamura, M. Grant, E. Sovero, D. Ching, J. Yoo, J. Romberg, A. Emami-Neyestanak, E. Candes, "A Nonunifom Sampler for Wideband Spectrally-Sparse Environments" IEEE J EM SEL TOP C, **2**(3), 516–529, 2012. https://doi.org/10.1109/JETCAS.2012.2214635

[9] R. Siddharth, Y. Nithin Kumar, M. Vasantha, Edoardo Bonizzoni, "A Low-Power Auxiliary Circuit for Level-Crossing ADCs in IoT-Sensor Applications" 2018 IEEE International Symposium on Circuits and Systems (ISCAS), Florence, Italy, May 2018. https://doi.org/10.1109/ISCAS.2018.8351368

[10] Marco A. Gurrola-Navarro, "Frequency-Domain Interpolation for Simultaneous Periodic Nonunifom Samples" in 2018 IEEE 9th Latin American Symposium on Circuits and Systems (LASCAS), Puerto Vallarta Mexico,, 2018. https://doi.org/10.1109/LASCAS.2018.8399937

[11] T. Wu, C. Ho, M. Chen, "A Flash-Based Non-Uniform Sampling ADC With Hybrid Quantization Enabling Digital Anti-Aliasing Filter" IEEE J Solid-State Circuits, **5**(9), 2335 - 2349, 2017. https://doi.org/10.1109/JSSC.2017.2718671

[12] S. Qaisar, M. Ben-Romdhane, O. Anwar, MTlili, A. Maalej, F. Rivet, C. Rebai, D. Dallet, "Time-domain characterization of a wireless ECG system event driven A/D converter" in 2017 IEEE International Instrumentation and Measurement Technology Conference (I2MTC), Turin Italy, 2017. https://doi.org/10.1109/I2MTC.2017.7969682

[13] M. Malmirchegini, M. Kafashan, M. Ghassemian, F. Marvasti, "Non-uniform sampling based on an adaptive level-crossing scheme" IET SIGNAL PROCESS, **9**(6), 484–490, 2015. https://doi.org/10.1049/iet-spr.2014.0170

[14] S. Qaisar, R. Yahiaoui, T. Gharbi, "An Efficient Signal Acquisition with an Adaptive Rate A/D Conversion" 2013 IEEE International Conference on Circuits and Systems (ICCAS), Kuala Lumpur, Malaysia , 2013. https://doi.org/10.1109/CircuitsAndSystems.2013.6671611

[15] C. Pappas, "A Novel Pulse Position Modulator for Compressive Data Acquisition" Adv. Sci. Technol. Eng. Syst. J. **4**(1), 171–182, 2019. https://doi.org/10.25046/aj040117

[16] R. Baker, H. Li, and D. Boyce, CMOS Circuit Design, Layout and Simulation, IEEE Press Series on Microelectronic Systems, Wiley Interscience, 1998.

[17] W.R. Bennett, "Spectra of Quantized Signals" Bell Sys. Tech. Journal, **27**(3), 446–472, 1948. https://doi.org/10.1002/j.1538-7305.1948.tb01340.x

[18] R. Gray, D. Neuhoff "Quantization" IEEE T INFORM THEORY, **44**(6), 2325–2383, 1998. https://doi.org/10.1109/18.720541

[19] C. Pappas, "A New Non-Uniform ADC: Parallel Digital Ramp Pulse Position Modulator" in 2018 IEEE Canadian Conference on Electrical & Computer Engineering (CCECE), Quebec City, Canada. https://doi.org/10.1109/CCECE.2018.8447844

ASTES

Advances in Science, Technology and Engineering Systems Journal
Vol. 4, No. 4, 174-187 (2019)
www.astesj.com
Special Issue on Advancement in Engineering and Computer Science

ASTES Journal
ISSN: 2415-6698

Model-Driven Engineering Infrastructure and Tool Support for Petrochemical Industry Automation

Thaise Poerschke Damo[*,1], Leandro Buss Becker[1], Fabio Paulo Basso[2]

[1]*Federal University of Santa Catarina (UFSC), Automation and Control Systems Department, 88066-040, Brazil*

[2]*Federal University of Pampa (UNIPAMPA), Campus Alegrete, 97546-550, Brazil*

ARTICLEINFO

Article history:
Received: 03 June, 2019
Accepted: 16 July, 2019
Online: 30 July, 2019

Keywords:
Model-Driven Engineering
Object-Orientation
Industrial Automation

ABSTRACT

The definition of equipment and components of physical plants is a necessary step towards the development of simulation, control, and supervisory applications for the petrochemical industry. Often it happens that the same plant/equipment is (re)modeled on each application, causing a waste-of-time on repetitive (re)design, besides introducing potential inconsistencies between the models. Moreover, even though each software platform normally offers a different view of the same plant, it is desirable to have some kind of interoperability between them. This paper presents a solution for such issues named M4PIA, which consists in a Model-Driven Engineering (MDE) tool support developed mainly for petrochemical industry automation. M4PIA allows representing industrial plants by means of different and interchangeable object-oriented models, providing means to perform automatic code generation from a plant specification for different software platforms. Currently, our work involves using M4PIA in high-level automation manouvers and plant simulations. Evaluations studies performed with M4PIA shows that it covers most features expected from a MDE tool suite. Besides, the use of M4PIA is expected to result in less development time and costs, while it increases efficiency, maintainability, and reliability of the developed applications.

1 Introduction

There is no doubt that todays industrial environments are highly automated, at least in the first two layers of the ISA95 automation pyramid. The most basic layer, named *Field Level*, includes devices, actuators, and sensors. The *Control level* is immediate above, and accounts with PLCs and PIDs to control such devices. Programming PLCs and PIDs is typically done by means of integrated development environments (IDEs) that comply with international standards IEC 61131-3 [1] and IEC 61499 [2]. Rarely this kind of system does not make use of SCADA (supervisory control and data acquisition) in a third *Supervisory* layer.

The IEC 61131-3 standard [1] addresses PLC programming, including four programming languages and sequential function charts (SFC). It helps migrating software developed for one PLC type to PLCs of other vendors. Targeting distributed systems, the IEC 61499 standard [2] replaces the cyclic execution model of IEC 61131 by an event-driven execution model, which allows an explicit specification of the execution order of function blocks (FB). Both standards do not address equipment specification semantics.

To cope with procedures for automating continuous process operations there is the ISA 106 standard [3], which is typically deployed at the *Supervisory level*. Examples of commercial tools therefore are *Exapilot* from Yokogawa and *GenSym G2* from Ignite Technologies. The present work stands at this layer, and makes use of a proprietary tool with similar goals named MPA [4].

Another common need in automation systems, specially when advanced control techniques come to play, is performing simulations. Examples of tools for such purposes are Labview, Matlab/Simulink, and Modelica-based (like Dymola and OpenModelica). These tools provide powerful simulation cores, and also provide a vast library of components that allow designers to build virtually every system or system element they want to. It happens, however, that there is no specific semantics for equipment specification.

Considering an automation plant, the lack of semantics for equipment specification brings difficulties for representing this same automation plant in the different software de-

[*]Thaise Poerschke Damo, DAS/CTC/UFSC, +554837217606 & thaisedamo@gmail.com

velopment tools used in all automation levels. Such repeated representation is something quite common, for instance, to implement different perspectives in the automation domain: processes operation, monitoring, simulation, and control.

The work presented in this paper targets the integration of different perspectives in petrochemical industry automation through a tool support built on the Model-Driven Engineering (MDE) paradigm [5]. MDE is built on widespread techniques in Systems and Software Engineering, presenting the following main characteristics: (1) uses models in all the phases of software development to improve understanding; (2) raises the abstraction level of software system specifications, hiding platform-specific details; (3) develops Domain-Specific Languages (DSLs) [6] and frameworks to suit a domain; and (4) applies transformations to automate repetitive activities and improve product quality derived from Software Engineering (e.g., source code, libraries, processes, etc.) [7]. In other words, MDE proposes representation of diverse artifacts through modeling and tool support.

This paper presents M4PIA (Model-Driven Engineering for Petrochemical Industry Automation), which consists of an infrastructure and tool support to help the design of advanced control applications for the Petrochemical Industry. An evaluation of the proposal is also presented. Therefore, the remainder parts of this paper are organized as follows: Section 2 presents background information that motivates this research, highlighting the application domain and related works. Section 3 details the proposed M4PIA infrastructure and tool support. Section 4 shows the evaluation method employed for assessment. Section 5 details M4PIA assessment and presented obtained results. Section 6 highlights our conclusions and future works perspective.

2 Background

2.1 Advanced Control in the Petrochemical Industry

This work targets the design of advanced control strategies for the Petrochemical Industry. The advanced control does not intend to control the automation plant devices (valves, motors, etc) located in the *Field Level* of the automation plant. This low-level control should be done by the regulatory control in the upper, *Control level*, that executes on the PLCs. The advanced control stands at the *Supervisory level*.

For example, let us analyze the design cycle of an advanced control system for oil extraction platforms. Initially, designers should create a software-in-the-loop (SIL) environment, where the phenomena to be controlled (e.g. gas compression) is "executed" within a simulation tool (Labview, Simulink, Modelica) that communicates with the control software executing in the same hardware platform that will be used in the final system. Here, the automation plant elements are represented twice: (1) in the simulation model and (2) in the control software.

Before deploying the control system under design in the operational environment (the oil extraction platform), tests are typically performed in a hardware-in-the-loop (HIL) environment. At this point, instead of communicating the control system directly with the simulation tool, it must interact with the same hardware (PLCs) and software (drivers) that are used in the operational environment - here the PLCs communicate with the simulator. The communication between control software and PLCs is typically done by means of some kind of bridge, for instance OPC drivers. Using this kind of structure brings the need of creating a third plant representation, which stands for the supervisory software. A fourth plant representation could be used if an specific simulator is adopted in the HIL environment, which is something common in the oil industry. In theory, if the HIL implementation passes all tests, the control system is ready to be implemented in the operational environment.

Given such scenario, the problem under consideration in our work concerns providing a solution to optimize the long time needed to model the equipment in different software development tools (and languages). It also should reduce possible inconsistencies generated when moving from one model to the other. It is important to provide interoperability among such plant representations.

The development starting point of the proposed infrastructure was the analysis of a system called MPA (acronym for Automated Procedures Module). MPA software platform is widely used by the development team of Petrobras in the operation and control of several oil platforms and refineries. It can be used for simulation purposes and also to control the operation of real systems. In order to maximize the gains from using a MDE approach, it was also analyzed the system called EMSO (Environment for Modeling, Simulation and Optimization), a platform used for modeling and simulating chemical processes.

2.1.1 MPA Operation and Control Software

MPA [4] software was developed for oil platforms automation in order to support the development and execution of industrial control and automation applications. This software was developed by Tecgraf/PUC-Rio Institute under request of Petrobras S.A.

Automation is performed through operation maneuvers of plant equipment. Basically, MPA consists of an execution server and a configuration and management application. In the latter, industrial plants are modeled using object-orientation and diagrams are used to define the maneuvers in the respective plant. The server is responsible for executing the configured operation maneuvers in the diagrams and handles the equipment interacting with the supervisory system through OPC (OLE for Process Control) communication bridges.

Currently, processes equipment are modeled directly in LUA programming language as classes in the application's pre-configuration phase. In this phase, attributes and methods of each class are defined, i.e., of each type of equipment. One equipment can be used to compose another, being modeled as its attribute. Equipment classes are described in a pre-configuration file and loaded at the MPA configuration stage. The developer uses such info to define the plant equipment instantiation and to model the execution diagrams, in flow language, which describes the operating maneuvers of plant equipment, i.e., the sequence of equipment functions execution. Plant and flow files are saved separately in other file formats.

The infrastructure proposed in this paper is able to simplify the pre-configuration phase by generating code automatically, reducing the time spent in conceptual modeling for new plants or even guiding the development of similar supervision and control applications, reusing existing models by including, extending, or modifying them.

2.1.2 EMSO Simulation Software

EMSO [8] is a tool for modeling and simulating dynamic processes based on equations. It is part of a project maintained by a consortium of Brazilian universities and national petrochemical companies.

The EMSO platform is composed by a graphical interface and its own object-oriented modeling/programming language. Such language was created from the combination of the best modeling characteristics found in existing languages, resulting in a simpler language with a better code reusability.

EMSO modeling language is composed of three major entities: models, devices, and flowsheets. Model is the mathematical description of a device. Device is an instance of the model and represents a real process equipment. Flowsheet represents the process to be analyzed, which is composed of a set of devices. A model development in EMSO consists of defining a class of a real equipment or a part of a process. Model can be composed of parameters, variables, equations, initial conditions, and sub-models and can be based on a pre-existing one, only adding new functionalities.

The graphical user interface allows developers to create models, build flowcharts, check project consistency, execute simulations and visualize the results. The software has several consistency analysis of the model and the whole process to be simulated, including: initial conditions consistency, measurement units, and system of equations solvability. The platform is multithread, which allows real-time simulations to run more than one simulation at the same time.

The proposed solution aims to support equipment models by generating automatic codes and to maintain a correct correspondence between plants to be controlled by other applications and their simulated processes in EMSO for tuning tests and validation of control proposals.

2.2 Challenges Related with MDE Usage

Using MDE in the present work comes from the fact that it is a software development methodology with emphasis on the domain specification models, allowing to improve productivity, system understanding, and its maintenance and evolution. MDE paradigm proposes applications described through models at different levels of abstraction using standards such as the UML (Unified Modeling Language). More than just conceptual design, the produced models can be interpreted by automation tools that can generate schemas, code skeletons, and tests for multiple platforms. Definitions of more abstract layers provide formal basis for structuring lower-layer models. Thus, it is possible to facilitate design decisions and to build artifacts automatically from models, reducing development times and costs.

Additionally, MDE has been used to support software systems development in both academia [9]–[11] and industry [12]–[19]. Among the benefits credited to MDE, Mohagheghi et al. [20] highlight the following: shortened development time and increased productivity; improved software quality; automation through generation of code and other artifacts; provision of a common framework for software development across the company and lifecycle phases; maintenance and evolution; improved communication and information sharing among stakeholders. MDE is especially interesting for scenarios involving systems that should be made available on multiple platforms [21].

However, developing software systems with MDE is not trivial. Besides the development of domain specific languages, it requires an automated process, including transformation scripts that connects MDE resources, such as refinement tools and model-based operations [22]. In special, these works need specific assessment for their pieces, such as for DSLs, as well as for their integration promoted by model transformations. In this sense, Mohagheghi et al. [14] go beyond and also expose the criteria that led companies to adopt MDE. Such criteria involve the abstraction level that hides details, communicating with non-technical staff, as well as model-based simulation, execution, and test. In other words, a feature analysis is required.

2.3 Related Works

The idea to use object-orientation towards developing industrial automation systems is not new. For instance, in [23], the authors presented an environment that allowed to make object-oriented modeling of plant equipment ir order to further make automatic code generation. Even though the proposal was conceptually very interesting, it did not make use of standard modeling languages (at that time UML was emerging), so that it could not be adapted to current standards. More up-to-date standards were used by Thramboulidis in [24], but the foccus of that work was not on the static-structure of the plants but on their their dinamic behavior, specially targeting implementation on PLCs. In fact that was an anticipation of the recent IEC-61131-3 standard [1], which covers the use of object-oriented programming on PLCs.

Other related works only covered partially the issues presented in this paper. In chemical engineering domain, for instance, Becker [25] presented an UML-based framework for building integration tools that help developers in change propagation for maintaining inter-document consistency, focusing on relationships between flow sheets, that describe chemical processes and its simulation models. MindCSP solution [26] focuses on specifying the autonomic behavior of cyber-physical systems by its sensor-actuator networks and the autonomic control loops (monitor/analyze/plan/execute). Another example of approach that supports development of industrial control applications is the AUKOTON process [27], based on the UML Automation Profile, uses profile's concepts to represent the requirements, functionality and structure of the control applications, including requirements of stakeholders, alarm events, and control algorithms such PID, fuzzy and MPC. Other relevant applications of MDE are referenced in a state-of-the-art review of software engineering in industrial automation [28]. However, so far there is no other related work on MDE application with focus

on the generic definition of industrial plants equipment for sharing between different software: control, operation, and simulation platforms. This gap is fulfilled by the proposal presented in this paper.

3 Proposed M4PIA Infrastructure

The proposed M4PIA infrastructure is composed by: 1) domain specific languages, which intents to abstract three levels that hides details from implementation; 2) two sets of model transformations supporting automated model integration between these three DSLs; and 3) two sets of code generators. Everything is developed under the same Eclipse ecosystem, including the Eclipse Modelling Framework (EMF) [29], the Acceleo model transformation engine for code generator [30], and QVTo as a mean to make transformations between different metamodels [31].

A model in MDE represents part of a function, structure, or behavior of a system. The domain knowledge necessary to design M4PIA was acquired by the analysis of a significant set of applications designed on different software platforms from the petrochemical industry, seeking to identify typical requirements and behaviors of these systems. Understanding different applications provide the ability to differentiate general structures, the invariant domain aspects, from the specific structures, the variable aspects. Successive analysis and synthesis steps converged to the generic domain design model that was created.

In a model-driven engineering method, a high level of abstraction is typically used in the application development. The system development process in MDE starts with the highest abstraction model and decreases through properly defined transformations (model refinement). There are two MDE abstraction levels used in the present work: a platform independent viewpoint, the Platform Independent Model (PIM) and specific platform viewpoints, the Platform Specific Model (PSM). The latter contains details and characteristics of specific implementations platforms.

In a new application development its PIM model is created according to the provided metamodel (constructed based on domain conceptual analysis), then the PSM model is automatically generated by a Model-to-Model transformation (M2M), based on the PIM model and according to the PSM metamodel. Lastly, the platform-specific source code is generated from the PSM through an automatic Model-to-Text transformation (M2T). This process is illustrated in Figure 1.

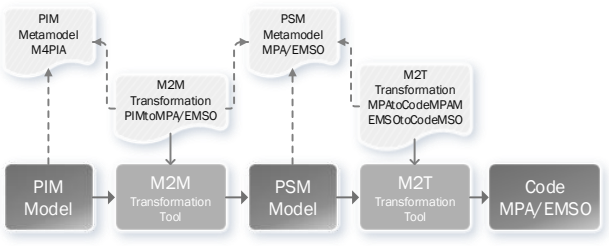

Figure 1: Development cycle using M4PIA

M4PIA infrastructure is built as support for the MDE of equipment class definition, so that applications for operation, control, and simulation platforms for the petrochemical industry can be created. The proposed solution was implemented in the EMF (*Eclipse Modeling Framework*) tool [29], in *Eclipse Oxygen* environment. The first and fundamental element built is the M4PIA metamodel, a PIM metamodel that represents the entire domain of the desired applications to be created, independently of its implementation platform. Then the PSM metamodels were constructed, defining the specificities of each supported platform. Based on metamodels, it was defined the M2M transformations from PIM model to PSM models and, at last, the M2T transformations for the automatic source code generation from each PSM model.

3.1 M4PIA Metamodel

The identification and analysis of petrochemical industry applications allowed the definition of a set of generic elements, capable of being shared by a wide range of industrial automation systems. This set of elements are materialized by means of a metamodel named *M4PIA*. Our aim is that M4PIA metamodel can contribute substantially for the implementation of new systems from such application domain, targeting reusability and facilitating automatic code generation.

The developed M4PIA metamodel is presented here through a class diagram designed using the *Eclipse Modeling Framework* and its *Ecore* metamodel, similar to UML. The proposed class diagram is shown in Figure 2. The representation shows a set of classes, interfaces, and collaborations, with their respective relationships, expressing results of the structure and requirements analysis of the problem domain and its components. Model constraints were specified using OCL (Object Constraint Language). The main metamodel elements are detailed next.

An entity is defined as the most elementary unit of the proposed model. The `Entity` class is considered abstract and only provides a basic structure for the more specialized classes in the hierarchy. A `Project` is instantiated and can be composed of several `Files`. These can be imported as libraries, `ImportedFile`, or be an entity group to have their source code generated by the infrastructure, `GeneratedFile`.

An `Equipment` is a type of entity that can contain attributes and methods, defined as specific classes to reflect physical characteristics and functions performed by the equipment in a plant.

The abstract class `Variable` represents a logical variable and can be `NonTyped` or `Typed`. Typed variables can be `EquipmentType` or `BasicType`, more specifically `Real`, `Integer`, `Boolean`, or `String`.

The `Method` class is a `Function` specialization and has exclusive connection to an `Equipment`. The `Function` class represents a logical entity that can either represent a high-level operation (in the physical domain of the plant) or a low-level (in the application domain). A function can have multiple `Variable` instances associated, acting as parameters or results, as well as may have a language and an associated code, which textually describes the instruction desired for the interpreter.

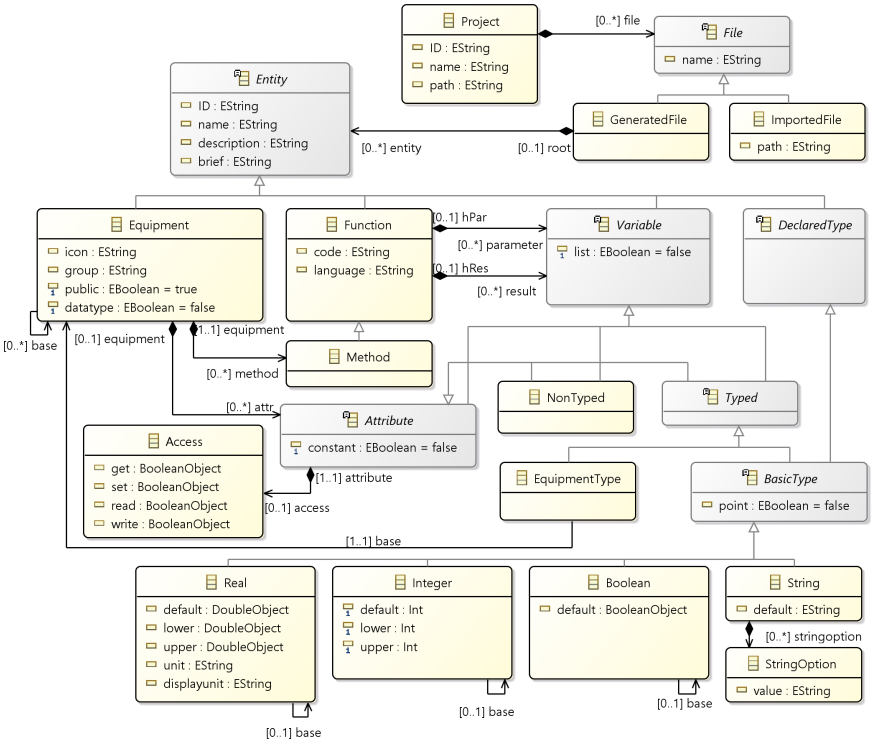

Figure 2: Elements of the proposed M4PIA metamodel

An equipment `Attribute` is a specific case of Variable which is allowed, through the relationships hierarchy, to assume a type that can be another `Equipment`. This aspect guarantees to the metamodel the ability to reproduce scenarios where there are natural recursions in relationships between equipment, i.e., an equipment or a machine that has other equipment as an attribute. For example, a specific type *Compressor* can be used as one of the attributes of a *Compression System*, both devices being instantiated by the `Equipment` class.

Furthermore in the `Attribute` context, there is a permission management for read or write operations, as highlighted in the `Access` class. New data types can be defined through the `DeclaredType` entity, based on basic types, and can be used as the basis for variables and attributes as well. For example, it is possible to declare a new type *Positive Real* and set a real type attribute *Position* of an equipment *Valve* based on the *Positive Real* type.

3.2 MPA and EMSO Metamodels

Given that the generic M4PIA metamodel was obtained through the analysis of the specific software platforms, the specific metamodels for each software are similar to the generic one and the main differences between them are further highlighted.

The PSM for MPA, or simply MPA metamodel, is depicted in Figure 3. The `Component` element corresponds to `Entities` in M4PIA. In addition to `Equipment`, the `Class` component can also be specified as `PointClass`, considered on the platform as a data type. `Variable` and `Attribute` classes are not abstract and must have an associated `Type`. Possible types are `BasicType`, point classes, and equipment. MPA basic types instances are imported automatically at the beginning of each project, they are: *Real*, *Integer*, *Logical*, and *Textual*. Four instances of native MPA point classes are also imported: *Real Point*, *Integer Point*, *Logical Point*, and *Textual Point*, each with its attributes.

In the MPA platform, codes are not exclusive related with functions, classes and files can also be composed by `Codes`. File codes are used to import components of the `DLL`, declaring the available `DLLFunctions` and their `DLLParameters`.

The second PSM developed is the EMSO metamodel, which is presented in Figure 4. Since EMSO is a simulation platform, mathematical models of the equipment, or `Devices`, are instantiated through the `Model` class. Functions are always related to a model as `Equations`. In this specific domain, `Variable` is an `Attribute` specialization and represents the variable attributes of the models and `Parameter` the constant ones. Variables cannot assume a textual type, but textual parameters can be instantiated through a `Switcher`. `Flowsheet` entities with their `Devices` and `Connections`, parameter `Estimation` and process `Optimization` were not considered primordial for the equipment description domain and are not specified at this stage of the project.

3.3 M2M and M2T Transformations

For each PSM supported by M4PIA infrastructure it is necessary to define the respective transformations. Transformations can be either model-to-model (M2M) or model-to-text (M2T). In M2M transformations the elements specified in the PIM model are mapped to elements from a specific PSM. M2M are implemented in our work using the *Eclipse QVTo* tool, an implementation of the standard

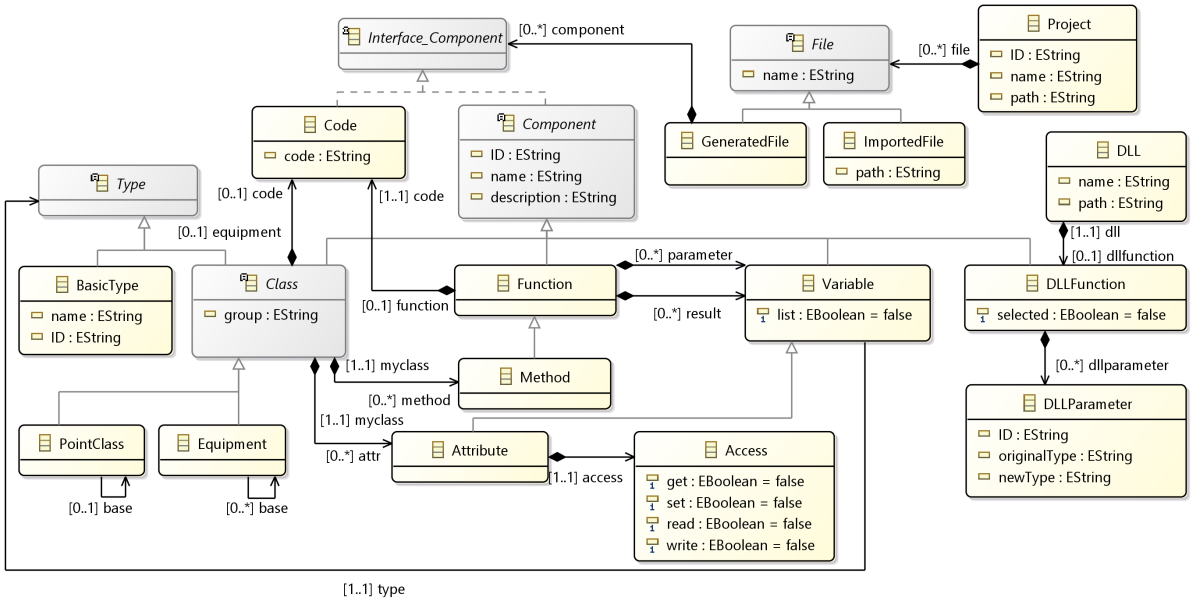

Figure 3: Elements of MPA metamodel

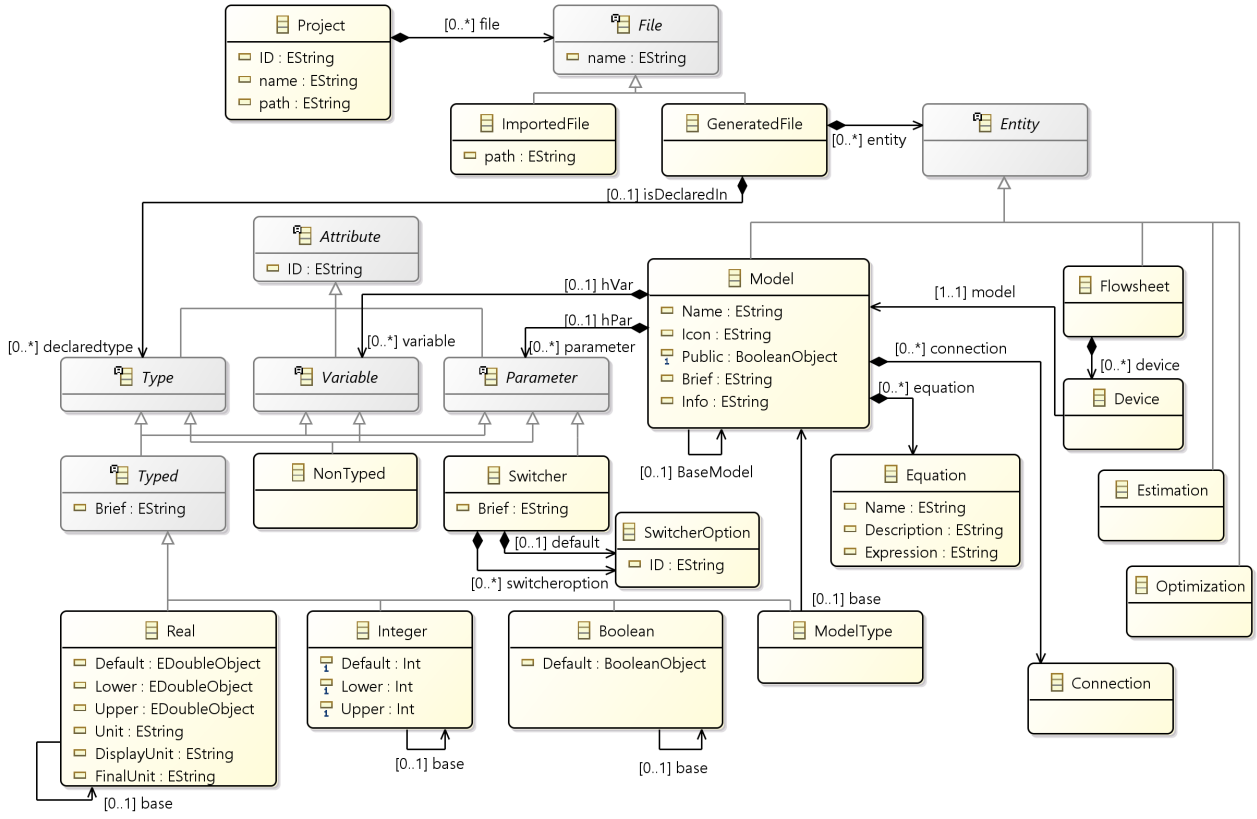

Figure 4: Elements of EMSO metamodel

OMG model transformation language QVTo (Operational Query/View/Transformation). The M2T transformations are developed specifically for each target platform. They are target in this work by using the *Eclipse Acceleo* tool for templates definitions and have as output the application source code ready to be used.

The explanation regarding each PSM metamodel provided in the previous section provide readers a good overview about the adopted M2M transformation rules, i.e., how the elements of the M4PIA metamodel (Fig. 2) map to the MPA metamodel (Fig. 3) and to the EMSO metamodel (Fig. 4). The M2T transformations are target in this work by using the *Eclipse Acceleo* tool for templates definitions and have as output the application source code ready to be used.

4 Evaluation Method

This section describes the evaluation method used to allow analyzing the completeness and applicability of the proposed infrastructure. Our goal is to capture the perception of M4PIA users in performing a characterization of the features associated with this MDE-based approach. By achieving this goal, it would allow us to understand whether the concepts introduced in M4PIA infrastructure really have potential in terms of technology, thus providing evidence of quality attributes associated with all the developed tools.

This evaluation, therefore, attempts an empirical study of type "feature analysis-experiment" [32], in a quantitative and qualitative experiment format. It allows providing evidences of suitability, very common for assessing tool support in computer science.

4.1 Context Selection

The context of this study is the academy, a first trial of in-vitro approach, with half of participants working in industry. The experiment captures the perceptions of individuals to measure the value of a technology in a real problem. It is applied with nine master students and two undergrad students from the Federal University of Pampa (Unipampa), all them with good knowledge on tool selection and software acquisition. This context configures a good sample, since students were introduced in the MDE theme, with desirable features from these tools. Therefore, it characterizes a good scenario to evaluate two main quality attributes for suitability that could be associated with the proposed tool support: completeness and applicability.

4.2 Experiment Design

No randomization and balancing: The subjects are not randomly placed into groups (not a randomized block design), so that only one design approach is performed by the same number of subjects. Thus, the goal is not to compare DSLs or code generators.

Blocking: The selected subjects for this quasi-experiment had different backgrounds in modeling systems, but no background in modeling petrochemical systems. Thus, to minimize the effect of eventual differences in experiences, the subjects received the same training. We also defined whether a subject is inexperienced or experienced, applying a survey, prior to the experiment, to qualify the subject background on the problem domain.

Instrumentation: It was provided a configured version of the Eclipse IDE with M4PIA plugins. The subjects installed this version in their notebooks in Windows or Linux. Then, we provided video tutorials in mp4 format, composed by: 1) A long duration video (75 minutes) depicting the proposed infrastructure, the needs and the proposed solution; 2) A second video (15 minutes) demonstrating how to use the Eclipse IDE, and 3) A third Video (25 minutes) demonstrating how to design a model using the proposed approach. Six other video-tutorials complement the other quantitative part of this experiment, focusing in evaluating specific design and codification tasks. However, they are irrelevant for the present evaluation, which focuses in presenting the feature analysis experiment.

4.3 Variables

Two sets of **independent variables** are used: (1) EMSO, MPA, and M4PIA; (2) Academic Experience and Industrial Experience. Besides, two **dependent variables** are used: Completeness and Applicability.

4.4 Data Analysis

Applicability: a survey to measure the quality attributes from the experience along design and transformation tasks. **Completeness**: a coverage analysis of the main features considered important in MDE including the following.

4.4.1 Desirable Features from MDE Tools

Feature 1: Platform independence: Also known as PIM support [33], it evaluates the capacity to model the PIM application at a high abstract level.

Feature 2: Multiview representation: Also known as PSM support [33], it evaluates the capacity to automatically generate a PSM model for a chosen target platform.

Feature 3: Platform adherence: Also defined in [33], it states whether multiple target platforms are supported.

Feature 4: Evolution: Also known as Application evolution (Changeability) [33] [34], observes if model changes should be done in PIM level and implies new execution of transformations.

Feature 5: Interoperability: Relates to model import/export (tool interoperability) [33], observes the support for exporting models in XMI format.

Feature 6: Flexibility: From [33], accounts for the flexibility to change the transformation process and model refinements.

Feature 7: Correctness: From [33], accounts for model validation in order to check consistency with its metamodel.

Feature 8: Expressiveness: Also called completeness [33] [35], observe if all domain concepts are needed.

Feature 9: Traceability: From [33], accounts for models traceability.

Feature 10: Reverse engineering: From [33], accounts for Code-to-model and PSM-to-PIM transformations.

Feature 11: Built on standards: From [33], accounts for the use of standarized technologies.

Feature 12: Well defined concepts: Adopted from [34], observes if there are no contradictions between concepts of the models.

Feature 13: Code generation: Feature from [35], accounts for how complete is the generated application code.

4.4.2 Metrics

Metrics for estimating the completeness of the features:

$$CFx = 1 - ((44 - Cov)/44)$$

Where CFx is the completeness for a feature x, 44 is the maximum value rank for each feature, and Cov is the computed by:

$$Cov = (TD + PD + NA + PA + TA)$$

Where Cov is the coverage for a feature, as the sum of the following values posted by each respondent: **TD** is 0 (zero) and replaces the survey value for "Totally disagree"; **PD** is 1 (one) and replaces the survey value for "Partially disagree"; **NA** is 2 (two) and replaces the survey value for "Not agree or disagree"; **PA** is 3 (three) and replaces the survey value for "Partially agree", and; **TA** is 4 (four) and replaces the survey value for "Totally agree";

Thus, at the end of the quasi-experiment, a questionnaire was filled out in a Google Forms, were the participants should rate different criteria, where those for feature analysis are built on a five point Likert scale (0=worst, 4=best) for the analysis of the proposed infrastructure.

5 M4PIA Assessment

In order to evaluate the applicability of the proposed solution, this section presents the impressions noticed by the 11 users previously mentioned. Such impressions were collected after the users modeled a simplified *Gas Compression System* (GCS). The model was further used to generate the control software in the MPA tool and the simulation software in the EMSO tool. All related development, including the PIM model design and the transformation executions, was done within the Eclipse environment.

The simplified GCS consists of one *surge tank* (a *knock-out drum* with a *flaring valve*), one *output header*, and two *one-stage compressors*. A *stage of a compressor* has one *heat exchanger*, one *suction drum*, one *compression element*, and one *recycle valve*. The *output header* has one *exportation valve* and two *gas-lift output valves*. Such system is illustrated in Figure 5. The present case study has 11 equipment, with a total of 36 attributes and 2 methods.

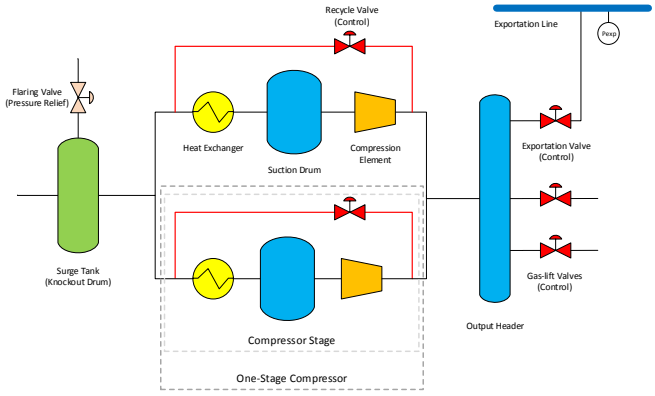

Figure 5: Simplified Gas Compression System

The work in the Eclipse tool can be summarized as follows. After creating a new project, the designer must create a PIM using the Eclipse tree structure. To illustrate how the designer interacts with Eclipse, Figure 6 shows the instantiation of three equipments from the GCS: `Compression Element`, `Compressor`, and `Compression System`. The former contains the following attributes: `Flow`, `Suction/Discharge Pressures`, and `Suction/Discharge Temperatures`. The latter has as attributes: `Power`, `Surge Tank`, `Output Header`, and a `List of Compressors`. It also has the method `Calculate Power of the Compression System`.

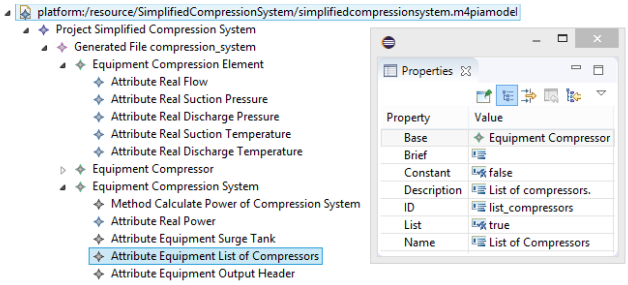

Figure 6: Illustration of the EMF tree structure

To model an equipment on both MPA and EMSO software platforms, the developers should seek out for generalization. For example, a *compression system* may have one or more *compressors* and a *compressor* may have one or more *stages*. Hierarchy is also highly desired, for example, a *valve* can be specialized in *pressure relief* or *control valve*, just as a *tank* can be specialized in *surge tank* or just a *knockout drum*. Given that in EMF the PIM is developed using a tree structure, as shown in Figure 6, the UML class diagram from Figure 7 was created to better illustrate the designed PIM.

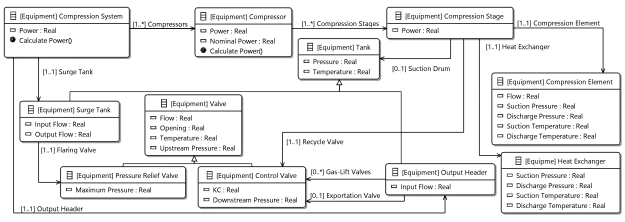

Figure 7: Class Diagram of the Simplified Gas Compression System PIM Model

After the PIM model development, the M2M transformations for MPA and EMSO platforms were performed. The PSM models were refined according to the specificity of each platform and it was possible to automatically generate the necessary source code to implement the compression system on the target platforms by applying the M2T transformations. In total, 245 effective lines of code were automatically generated for MPA and 117 for EMSO. One should recall that effective LOC means that comments and blank lines are not counted.

5.1 Preliminary Analysis

The system developed on this study can be considered small if compared to other existing applications, which can be five times bigger. In order to better illustrate the impact that the use of M4PIA can have on the development of the applications of this domain it is shown some data from a native MPA application example, which aims the detection and treatment of hydrate plug formation in gas pipelines of a floating production storage and offloading (FPSO). The numbers presented in Table 1 allow us to observe that an application with 50% more equipment classes (right on the table) can have twice the total amount of attributes and more than 12 times the number of methods. Observing the numbers regarding LOCs, the FPSO application is above 1K LOC. So it is not difficult to conclude that generating such code automatically – like M4PIA infrastructure does – can potentially save many working hours.

Table 1: Comparison of Domain Applications

	GCS	FPSO
Class of Equipment	11	17
Total Amount of Attributes	36	74
Total Amount of Methods	2	25
Effective Lines of Code (*LOC*) - MPA	245	1297
Instantiated Equipment	19	621
Instantiated Control Points	73	2428

5.2 Feature Analysis

In the following it is present data collected through a feature analysis, which allowed us to understand participants perceptions about the overall M4PIA infrastructure. The goal is to understand initial expectations of the overall approach introduced in the first video, so that their perception could help on the execution of the controlled experiment.

Figure 8 provides the answers to the analysis of Feature 1 - The approach allows to: model the application at platform independent level (PIM), at a high level of abstraction of the target problem used in the implementation (simulation, supervision, operation and control of industrial plants of the petrochemical industry. In this sense, nine from eleven students agree that this is an important feature provided in M4PIA infrastructure.

Figure 9 provides the answers to the analysis of Feature 2 - The approach allows: automatic generation of the platform-specific model (PSM) for the chosen target problem (simulation, supervision, operation and control of industrial plants in the petrochemical industry). Thus, nine from eleven students agree that this is an important feature provided by the infrastructure.

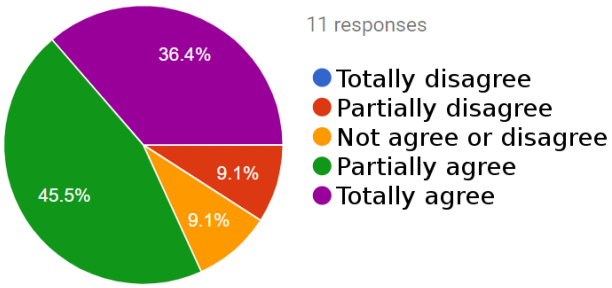

Figure 8: Analysis of Feature 1: Platform independence

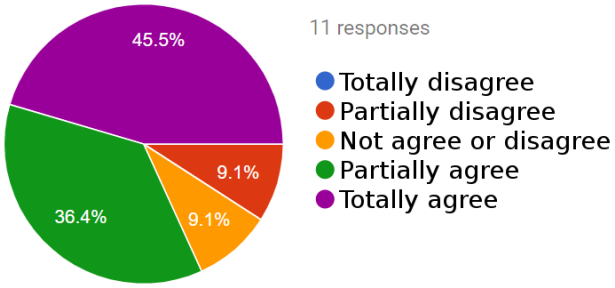

Figure 9: Analysis of Feature 2: Multiview representation

Figure 10 provides the answers to the analysis of Feature 3 - The approach allows: automatic generation of code for multiple target platforms. Seven participants agree that this is an important feature provided by the infrastructure, where five of them only partially agree. Thus, feature 3 should be planned for improvement.

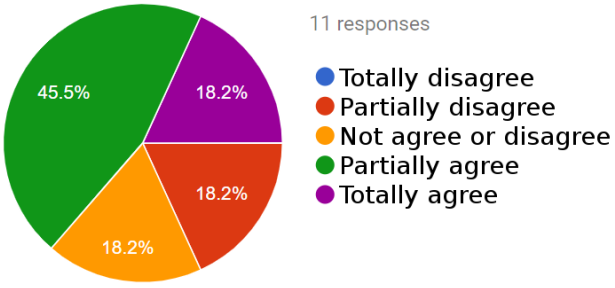

Figure 10: Analysis of Feature 3: Platform adherence

Figure 11 provides the answers to the analysis of Feature 4 - The approach supports the evolution of applications through model to model and model to code transformations. In this sense, nine from eleven students agree that this is an important feature provided by the M4PIA infrastructure. In fact, evolution is one of the greatest benefits promoted by MDE approaches for automated integration [14], and M4PIA is on a solid ground to allow this feature for their future users.

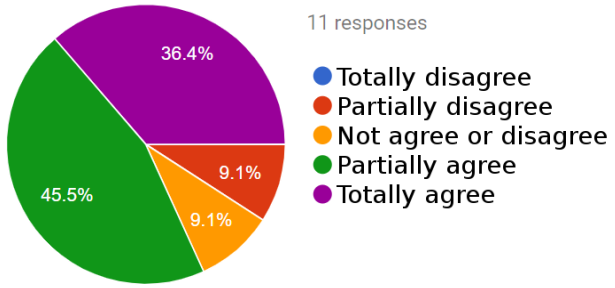

Figure 11: Analysis of Feature 4: Evolution

Figure 12 provides the answers to the analysis of Feature 5 - The approach supports model interoperability. That is, it is evaluated whether these are exported and imported in a standard way, such as those provided by OMG. Seven agree that this is an important feature provided by the infrastructure, where five of them only partially agree. Three answers were uncertain, and this is because OMG supports lots of other standards not handled in M4PIA.

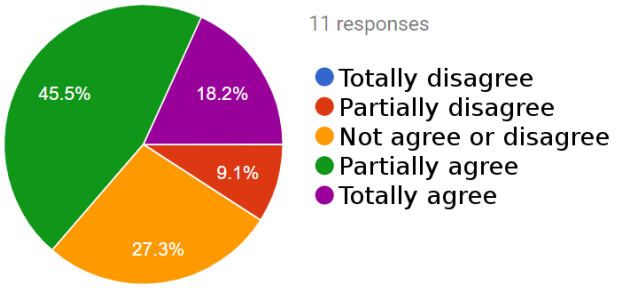

Figure 12: Analysis of Feature 5: Interoperability

Figure 13 provides the answers to the analysis of Feature 6 - The approach supports flexibility to change the transformation process and model refinements. Eight respondents agree that this is an important feature that should be provided by the infrastructure. Three answers were also uncertain, and this is because they did not scaled the problem through the demonstration.

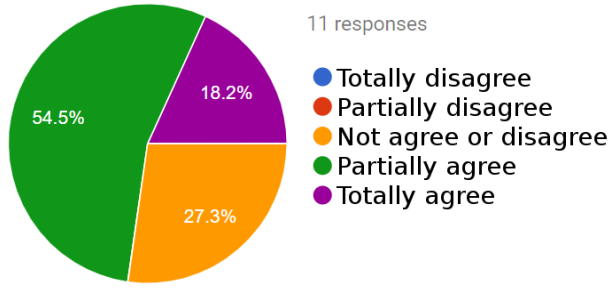

Figure 13: Analysis of Feature 6: Flexibility

Figure 14 provides the answers to the analysis of Feature 7 - The approach supports the validation of the models to verify consistency with their respective metamodels. Eight respondents agree with that statement, concluding that M4PIA provides this as an important feature for designers. Consistency in design is an essential feature in a MDE-based process that needs the correct code generation. It can only be ensured with a rich set of OCL rules [36].

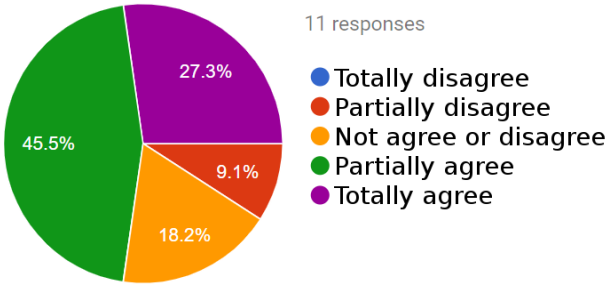

Figure 14: Analysis of Feature 7: Correctness

Figure 15 provides the answers to the analysis of Feature 8 - The approach is expressive and allows to express all the concepts of the represented problem domain. Nine from eleven respondents agree that this is a design feature associated with M4PIA. Thus, since the ability of express domain concepts is a requirement for DSL development, we conclude that the provided metamodels satisfy the modeling needs of the presented context.

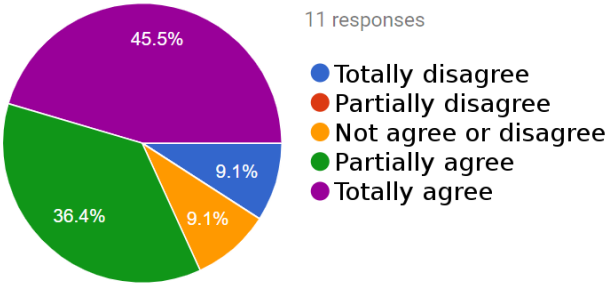

Figure 15: Analysis of Feature 8: Expressiveness

Figure 16 provides the answers to the analysis of Feature 9 - The approach supports the traceability of models. Nine from eleven respondents agree that this is a design feature associated with M4PIA. Trace is promoted through model-to-model transformations and are used for configuration management issues [37].

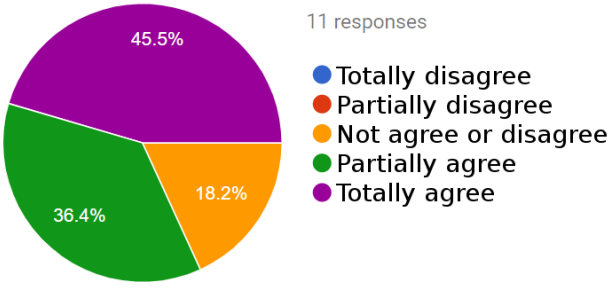

Figure 16: Analysis of Feature 9: Traceability

Figure 17 provides the answers to the analysis of Feature 10 - The approach supports reverse engineering from code to model. This statement was detected as an issue from the current version of M4PIA. first experimental trial. This feature is only implemented as a preliminary version of the infrastructure developed in ANTLr parser, not include in the provided Eclipse experimental package. In order to configure a reverse engineering into the Eclipse package, we are starting the development of reverse engineering using

MODISCO. So the answers for this feature analysis were also confused.

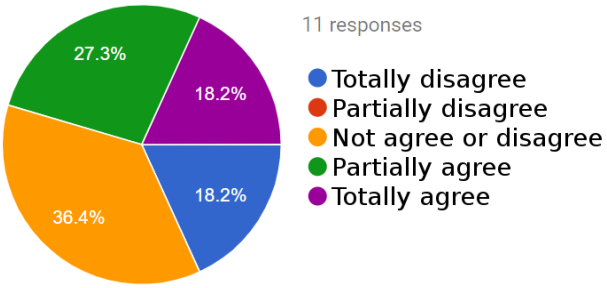

Figure 17: Analysis of Feature 10: Reverse engineering support.

Figure 18 provides the answers to the analysis of Feature 11 - The approach is heavily based on standards for building DSLs and model transformations. Nine from eleven respondents agree that this is an important feature associated with M4PIA. One of the answers reasoned that the adopted technologies is not a benefit.

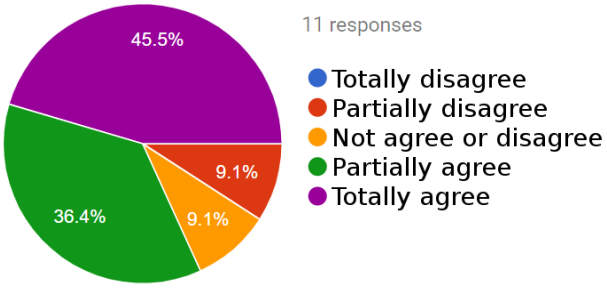

Figure 18: Analysis of Feature 11: Built on standards

Figure 19 provides the answers to the analysis of Feature 12 - There are no contradictions between the concepts of models in the M4PIA infrastructure. Here only five agree that the metamodels are well characterized, while five are still confused and suggested that they would have a stronger position with a better characterization of the context from the Petrochemical industry.

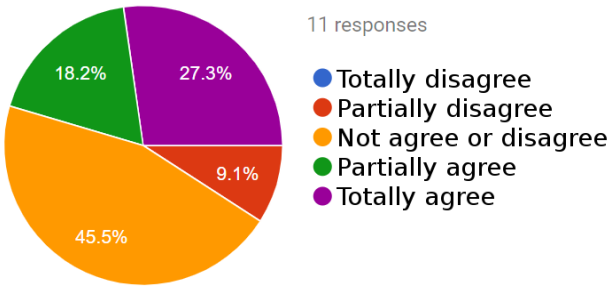

Figure 19: Analysis of Feature 12: Focused domain specific entities

Figure 20 provides the answers to the analysis of Feature 13 - The complete application code can be generated. six from eleven respondents agree that this is an important feature associated with M4PIA. Almost half the respondents or disagree or did not have sufficient information to conclude about that.

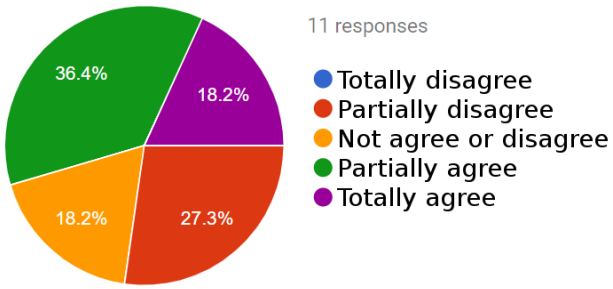

Figure 20: Analysis of Feature 13: Code generation

5.3 Final Remarks

Figure 21 presents the coverage analysis of the features after applying the metric. The highest possible score for each feature is 44. Figure 23 shows the dispersion bloxplot graph. Therefore, these graph demonstrates that M4PIA infrastructure is considered relevant for the stated problem.

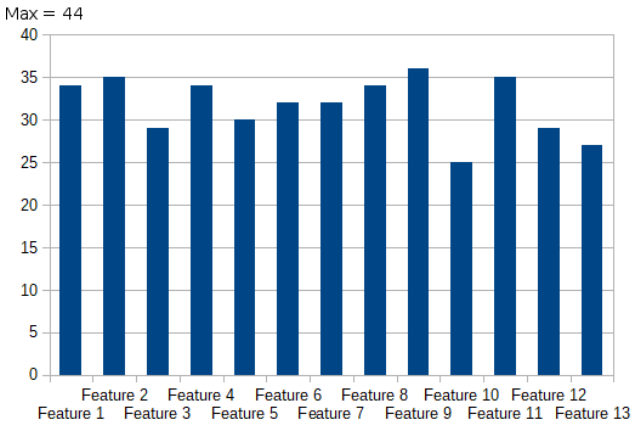

Figure 21: Coverage analysis of all the features

Finally, Table 2 presents the analysis of completeness of each analyzed feature. This data is also shown in Figure 22. The average of results from coverage is 72.73%, a good index suggesting the relevance to the MDE context. Thus, this suggests that we are on the way to achieve benefits reported by other MDE studies as well [14].

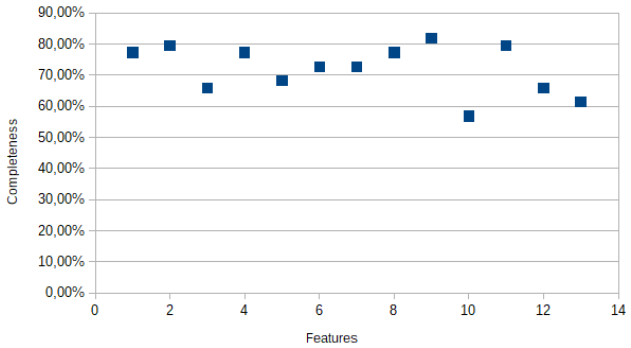

Figure 22: Completeness analysis of all the features.

5.4 Threats to Validity

As discussed by [32], studies of applicability using feature analysis experiment are usually target of the following

Table 2: Analysis of completeness after the feature analysis

	Feat 1	Feat 2	Feat 3	Feat 4	Feat 5	Feat 6	Feat 7	Feat 8	Feat 9	Feat 10	Feat 11	Feat 12	Feat 13
Uncovered	22.73%	20.45%	34.09%	22.73%	31.82%	27.27%	27.27%	22.73%	18.18%	43.18%	20.45%	34.09%	38.64%
Covered	77.27%	79.55%	65.91%	77.27%	68.18%	72.73%	72.73%	77.27%	81.82%	56.82%	79.55%	65.91%	61.36%
Total	100%	100%	100%	100%	100%	100%	100%	100%	100%	100%	100%	100%	100%

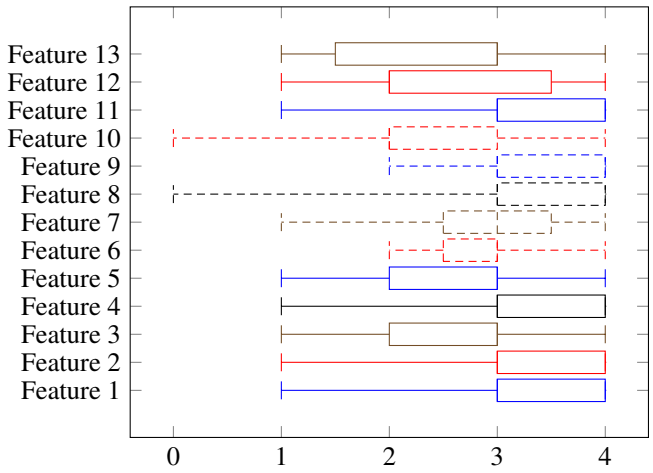

Figure 23: Boxplot of the analyzed features

threats to validity: 1) Benefits are difficult to quantify, 2) Benefits directly observable from the task output, 3) Relatively small learning time, and 4) Tool/method user population very varied. In the following, we present other threats conforming to [38].

5.4.1 Construct Validity

Feature analysis presents social threats to construct validity. In order to mitigate the Hypothesis guessing, before executing the experiment we: 1) presented the context of the problem; 2) presented the context of MDE tools; and 3) presented our goals, where we would evaluate their intuitiveness in using the M4PIA approach for each planned task along three different phases. These experimental tools were also important to mitigate the other two threats: Evaluation apprehension and Experimenter expectations. In order to mitigate the apprehension threat, an external executor for this quasi-experiment was used (the third author). This makes the study less biased, avoiding the interest in positive results, which could occur when the study is executed by the tool creators. The experiment executor also ensured the selection of subjects without any expectation about the evaluated tool, making clear their responsibility in feature analysis to rank M4PIA accordingly to the thirteen best MDE practices.

5.4.2 Internal Validity

This study was planned as a controlled experiment to be executed in three distinct phases: 1) the first one is to test the applicability of M4PIA; 2) the second one is the manual execution of the overall process, scoping design and codification tasks, performed without M4PIA; and 3) the last is the execution of the process with M4PIA. Along the execution of the first phase in the first trial, we observed that the internal validity threat called “mortality” would happen for the next phases due to the scarce available time from subjects. In order to mitigate this threat, and thus ensuring we would not loose subjects, we decided that participants could execute the experiment at home along three weeks. In this sense, they followed the video tutorials for execution of each requested task in a quasi-experiment rather than a fully controlled experiment, as initially planned. Therefore, in order to ensure the internal validity, the independent variable “time to accomplish each task” was not used.

5.4.3 External Validity

The results observed for feature analysis of M4PIA infrastructure are not generalized yet. For a such, we would need to repeat this study with, at least, three other subject profiles: 1) experts in physical plants presented on the development of simulation, control, and supervisory applications for the petrochemical industry; 2) experts both in physical plants and MDE; and 3) experts both in physical plants, MDE and software acquisition. Likewise, the threat “interaction of selection and treatment” was not mitigated, and will not gonna be while this experiment is not repeated with different subject profiles. Since our subjects are not experts in the problem domain, i.e. they are trainees in physical plants adopted by petrochemical industry, but they are experts in Software Engineering tool selection and software acquisition discipline, this study is also target of the threat “interaction of setting and treatment”. We mitigated this threat through nine video-tutorials, shared in the experimental package, which by the way are considered of high instructive quality.

5.4.4 Conclusion Validity

This study presents an associated threat, which is its low statistical power, as the evaluation presented was applied to only eleven participants. It happens that, for a feature analysis, the random heterogeneity of the subjects compensates the low statistical power, as it provides different perspectives

when evaluating the tool. Likewise, the subjects present two distinct evaluators profiles: half working on companies as professional software engineers and half characterized as students, where two of them are finishing the undergraduate school in Software Engineering. Thus, our conclusions are moderated and drawn accordingly to the statistical power provided.

6 Conclusions and Future Works

The current paper presented M4PIA, an MDE solution that facilitates the design and development of equipment classes for simulation, control, and operation of applications devoted for the petrochemical industry. It contains three metamodels, which is a rich material in respect to formalizing the representation of the elements that constitute petrochemical plants and the related control structure. These metamodels, together with the developed model transformation engines, serve to provide automatic code generation.

The conducted evaluation showed that the majority of the 13 features considered important in the scope of MDE are properly covered by the proposed M4PIA. Solutions to improve those features that were not highly ranked, like reverse engineering, are already under development. Moreover, as future work it is possible to state that M4PIA should evolve towards allowing even non-programmers (like plant engineers/designers) to describe plant structures and thereby providing additional help to develop the required applications. Therefore, a graphical modeling language might be adopted.

Conflict of Interest The authors declare no conflict of interest.

Acknowledgment Firstly we thank Cenpes/ Petrobras for the finance support that made this work possible. Thanks are also given to: (i) Tecgraf/PUC-Rio Institute team for the outstanding support in respect to MPA-related issues; (ii) Prof. Rafael de Pelegrini Soares (UFRGS) for his support in respect to the EMSO platform; (iii) the students from UNIPAMPA/Alegrete that did not measured efforts to perform the proposed evaluation protocol.

References

[1] International Electrotechnical Commission, "Iec 61131: Programmable controllers – part 3: Programming languages," standard, 2003.

[2] International Electrotechnical Commission, "Iec 61499: Function blocks standard," standard, 2005.

[3] The International Society of Automation, "Isa 106: Procedure automation for continuous process operations," standard, 2013.

[4] E. Satuf, S. F. Pinto, and B. Q. Dias, "Sistema automático de alinhamento para a plataforma de rebombeio autônomo PRA-1," in *V Congresso Rio Automação*, (Rio de Janeiro, RJ, Brasil), Inst. Brasil. de Petroleo, Gás e Biocombustíveis - IBP, 2009.

[5] R. B. France and J. M. Bieman, "Multi-view software evolution: A UML-based framework for evolving object-oriented software," in *ICSM*, pp. 386–395, 2001. https://10.1109/ICSM.2001.972751.

[6] M. Vöelter and I. Groher, "Handling variability in model transformations and generators," in *Companion to OOPSLA 2007*, pp. 1–8, ACM, 2007.

[7] P. Mohagheghi, *Evaluating Software Development Methodologies Based on their Practices and Promises*, pp. 14–35. Frontiers in Artificial Intelligence and Applications, 2008. https://doi.org/10.3233/978-1-58603-916-5-14.

[8] R. P. Soares and A. R. Secchi, "EMSO: A new environment for modelling, simulation and optimization," in *13th European Symposium on Computer Aided Process Engineering*, pp. 947–952, Elsevier Science Publishers, 2003. https://doi.org/10.1016/S1570-7946(03)80239-0.

[9] D. Batory, E. Latimer, and M. Azanza, "Teaching model driven engineering from a relational database perspective," pp. 121–137, 2013. https://doi.org/10.1007/978-3-642-41533-3_8.

[10] V. Aranega, A. Etien, and S. Mosser, "Using feature model to build model transformation chains," pp. 562–578, 2012. https://doi.org/10.1007/978-3-642-33666-9_36.

[11] R. S. P. Maciel, R. A. Gomes, A. P. F. Magalhães, B. C. da Silva, and J. P. B. Queiroz, "Supporting model-driven development using a process-centered software engineering environment," *Autom. Softw. Eng.*, vol. 20, no. 3, pp. 427–461, 2013. https://doi.org/10.1007/s10515-013-0124-0.

[12] P. Mohagheghi, M. A. Fernandez, J. A. Martell, M. Fritzsche, and W. Gilani, "Mde adoption in industry: Challenges and success criteria," vol. 5421, pp. 54–59, 2009. https://doi.org/10.1007/978-3-642-01648-6_6.

[13] J. Hutchinson, J. Whittle, M. Rouncefield, and S. Kristoffersen, "Empirical assessment of mde in industry," in *33rd International Conference on Software Engineering*, ICSE '11, pp. 471–480, 2011. https://doi.org/10.1145/1985793.1985858.

[14] P. Mohagheghi, W. Gilani, A. Stefanescu, M. A. Fernandez, B. Nordmoen, and M. Fritzsche, "Where does model-driven engineering help? experiences from three industrial cases.," *Software & Systems Modeling*, vol. 12, pp. 619–639, july 2013. https://doi.org/10.1007/s10270-011-0219-7.

[15] R. Capilla, J. Bosch, P. Trinidad, A. Ruiz-Cortés, and M. Hinchey, "An overview of dynamic software product line architectures and techniques: Observations from research and industry," *Journal of Systems and Software*, vol. 91, no. 0, pp. 3–23, 2014. https://doi.org/10.1016/j.jss.2013.12.038.

[16] R. Monteiro, G. Zimbrao, and J. Moreira de Souza, "Collaborative evolution process in mdarte: Exchanging solutions for information systems development among projects," in *Computer Supported Cooperative Work in Design (CSCWD), 2014 IEEE 18th International Conference on*, pp. 569–574, May 2014. https://doi.org/10.1109/CSCWD.2014.6846907.

[17] M. Torchiano, F. Tomassetti, F. Ricca, A. Tiso, and G. Reggio, "Relevance, benefits, and problems of software modelling and model driven techniques-a survey in the italian industry," *J. Syst. Softw.*, vol. 86, pp. 2110–2126, aug 2013. http://dx.doi.org/10.1016/j.jss.2013.03.084.

[18] G. Liebel, N. Marko, M. Tichy, A. Leitner, and J. Hansson, "Assessing the state-of-practice of model-based engineering in the embedded systems domain," pp. 166–182, 2014. https://doi.org/10.1007/978-3-319-11653-2_11.

[19] J. Whittle, J. Hutchinson, M. Rouncefield, B. Håkan, and H. Rogardt, "A taxonomy of tool-related issues affecting the adoption of model-driven engineering," *Software & Systems Modeling*, pp. 1–19, 2015. http://dx.doi.org/10.1016/10.1007/s10270-015-0487-8.

[20] P. Mohagheghi and V. Dehlen, *Where Is the Proof? - A Review of Experiences from Applying MDE in Industry*, pp. 432–443. Berlin, Heidelberg: Springer Berlin Heidelberg, 2008. https://doi.org/10.1007/978-3-540-69100-6_31.

[21] B. Selic, "On software platforms, their modelling with uml 2, and platform-independent design," in *8th IEEE International Symposium on Object-Oriented Real-Time Distributed Computing*, ISORC'05, pp. 15–21, 2005. https://doi.org/10.1109/ISORC.2005.40.

[22] L. Rose, E. Guerra, J. Lara, A. Etien, D. Kolovos, and R. Kolovos, "Genericity for model management operations," *Software & Systems Modeling*, vol. 12, no. 1, pp. 201–219, 2013.

[23] L. B. Becker and C. E. Pereira, "SIMOO-RT-an object-oriented framework for the development of real-time industrial automation systems," *IEEE Transactions on Robotics and Automation*, vol. 18, pp. 421–430, Aug 2002. https://doi.org/10.1109/TRA.2002.802933.

[24] K. C. Thramboulidis, "Using UML in control and automation: a model driven approach," in *Industrial Informatics, 2004. INDIN '04. 2004 2nd IEEE International Conference on*, pp. 587–593, June 2004. https://10.1109/INDIN.2004.1417414.

[25] S. M. Becker, T. Haase, B. Westfechtel, and J. Wilhelms, "Integration tools supporting cooperative development processes in chemical engineering," in *Proc. of Integrated Design and Process Technology (IDPT-2002), Pasadena, California*, Citeseer, 2002.

[26] C. Vidal, C. Fernández-Sánchez, J. Díaz, and J. Pérez, "A model-driven engineering process for autonomic sensor-actuator networks," *International Journal of Distributed Sensor Networks*, vol. 11, no. 3, p. 684892, 2015. https://doi.org/10.1155/2015/684892.

[27] D. Hästbacka, T. Vepsäläinen, and S. Kuikka, "Model-driven development of industrial process control applications," *Journal of Systems and Software*, vol. 84, no. 7, pp. 1100–1113, 2011. https://doi.org/10.1016/j.jss.2011.01.063.

[28] V. Vyatkin, "Software engineering in industrial automation: State-of-the-art review," *IEEE Transactions on Industrial Informatics*, vol. 9, no. 3, pp. 1234–1249, 2013. https://doi.org/10.1109/TII.2013.2258165.

[29] D. Steinberg, F. Budinsky, E. Merks, and M. Paternostro, *EMF: Eclipse Modeling Framework*. Pearson Education, Inc., 2 ed., 2008.

[30] "Acceleo mda generator," 2013. Av. at `http://www.acceleo.org`.

[31] OMG, "Meta object facility version 2.0 query/view/transformation specification," tech. rep., OMG, 2005.

[32] B. Kitchenham, S. Linkman, and D. Law, "Desmet: a methodology for evaluating software engineering methods and tools," *Computing Control Engineering Journal*, vol. 8, pp. 120–126, June 1997.

[33] "An Evaluation of Compuware OptimalJ Professional Edition as an MDA Tool," tech. rep., Department of Computer Science - The University of York and King's College London, 2003.

[34] P. Mohagheghi, V. Dehlen, and T. Neple, "Definitions and approaches to model quality in model-based software development – A review of literature," *Information and Software Technology*, vol. 51, no. 12, pp. 1646–1669, 2009. https://doi.org/10.1016/j.infsof.2009.04.004.

[35] C. F. Lange and M. R. Chaudron, "Managing model quality in UML-based software development," in *Software Technology and Engineering Practice, 2005. 13th IEEE International Workshop on*, pp. 7–16, IEEE, 2005. https://doi.org/10.1109/STEP.2005.16.

[36] P. Andersson and M. Höst, "Uml and systemc - a comparison and mapping rules for automatic code generation," vol. 10, pp. 199–209, 2008. https://doi.org/10.1007/978-1-4020-8297-9_14.

[37] J. Vara, V. Bollati, A. Jiménez, and E. Marcos, "Dealing with traceability in the mdd of model transformations," *Transactions on Software Engineering*, vol. 40, no. 6, pp. 555–583, 2014. http://dx.doi.org/10.1109/TSE.2014.2316132.

[38] C. Wohlin, P. Runeson, M. Höst, M. Ohlsson, B. Regnell, and A. Wesslén, *Experimentation in Software Engineering*. Springer, 2012.

ASTES

Advances in Science, Technology and Engineering Systems Journal
Vol. 4, No. 4, 188-196 (2019)
www.astesj.com
Special Issue on Advancement in Engineering and Computer Science

ASTES Journal
ISSN: 2415-6698

Well Balanced Multi-value Sequence and its Properties Over Odd Characteristic Field

Md. Arshad Ali[*,1], Yuta Kodera[1], Md. Fazle Rabbi[2], Takuya Kusaka[1], Yasuyuki Nogami[1], Satoshi Uehara[3], Robert H. Morelos-Zaragoza[4]

[1]*Graduate School of Natural Science and Technology, Okayama University, Okayama, 7008530, Japan*

[2]*Faculty of CSE, Hajee Mohammad Danesh Sci. and Tech. University, Dinajpur, 5200, Bangladesh*

[3]*Faculty of Environmental Engineering, The University of Kitakyushu, Fukuoka, 8080135, Japan*

[4]*Department of Electrical Engineering, San Jose State University, San Jose, CA 95192, United States*

ARTICLEINFO

Article history:
Received: 28 May, 2019
Accepted: 12 July, 2019
Online: 30 July, 2019

Keywords:
Pseudo random sequence
Trace function
Power residue symbol
Correlation
Linear complexity
Distribution of bit patterns

ABSTRACT

The authors propose a well balanced multi-value sequence (including a binary sequence). All the sequence coefficients (except the zero) appear almost the same in number, thus, the proposed sequence is so called the well balanced sequence. This paper experimentally describes some prominent features regarding a sequence, for instance, its period, autocorrelation, and cross-correlation. The value of the autocorrelation and cross-correlation can be explicitly given by the authors formulated theorems. In addition, to ensure the usability of the proposed multi-value sequence, the authors introduce its flexibility by making it a binary sequence. Furthermore, this paper also introduces a comparison in terms of the linear complexity and distribution of bit patterns properties with their previous works. According to the comparison results, the proposed sequence holds better properties compared to our previous sequence.

1 Introduction

Pseudo random sequences of having random numbers are crucial components of many cryptographic applications, for instance, key generation, session keys, masking protocol, navigation, radar ranging, and so on [1, 2, 3]. The security of these cryptographic systems deliberately depends on the randomness and unpredictability regarding the sequence. By using the non-linearity features of some mathematical functions, a pseudo random sequence of having excellent randomness characteristics can be generated. The major substances for randomness are independency of values (or lack of correlation), unpredictability (or lack of predictability), and uniform distribution (or lack of bias) [4]. Therefore, a prominent pseudo random number generator is essential to generate pseudo random sequence having good randomness property.

Most renowned pseudo random number generators are the Mersenne Twister (MT) [5], Blum-Blum-Shub (BBS) [6], Legendre sequence [7], and M-sequence [8]. Among those, the former two pseudo random number generators (MT and BBS) are well known considering their applications in cryptography rather than the theoretical aspect. On the other hand, the M-sequence and Legendre sequence are prominent geometric sequences regarding the theoretical aspect. As a result, the authors attracted in the pseudo random sequence generation research area by observing the theoretical prospect on the M-sequence and Legendre sequences.

A well balanced pseudo random signed binary sequence proposed in our previous work [9]. It is generated by utilizing a primitive polynomial, trace function, and Legendre symbol. The period and autocorrelation properties of the well balanced signed binary sequence were explained based on some experimental results. This work is actually an extension of previous works on the signed binary sequence by introducing additional two parameters k and non-zero scalar A (where k and A are responsible for generating multi-value sequence and extending the sequence period to its maximum value, respectively). It should be noted that the k-th power residue symbol is actually an extension of the Legendre symbol, therefore, this power residue symbol includes the case of the well balanced signed binary sequence. Furthermore,

[*]Corresponding Author: Md. Arshad Ali, Graduate School of Natural Science and Technology, Okayama University, 3-1-1, Tsushima-naka, Kita, Okayama, 7008530, Japan, +81-8042661986, arshad@s.okayama-u.ac.jp

this work is also an extension of our previous work on multi-value sequence [10] by considering additional two properties (linear complexity and distribution of bit patterns) and introducing its flexibility by making it binary sequence, whereas, previous multi-value sequence introduced along with its autocorrelation and cross-correlation properties (based on experimental observations only).

In this paper, the authors propose a well balanced multi-value sequence (including a binary sequence). Let $f(x)$ be a primitive polynomial of degree m and $\omega \in \mathbb{F}_q$ be its zero. Then, the sequence

$$\mathcal{S} = \{s_i\} \mid s_i = \mathrm{Tr}\left(\omega^i\right), i = 0, 1, 2, \ldots, q-2, \ldots$$

becomes a maximum length sequence whose period is $q-2$. Here, $\mathrm{Tr}(\cdot)$ is a trace function which maps an element of the extension field $\mathbb{F}_q$ to an element of the prime field $\mathbb{F}_p$. In brief, the proposed well balanced multi-value sequence generation procedure is as follows: in the beginning, a primitive polynomial generates maximum length sequence of vectors, then the $\mathrm{Tr}(\cdot)$ maps vectors to scalars, next a non-zero prime field scalar $A \in \{1, 2, \ldots, p-1\}$ added to the scalars, and finally k-th power residue symbol maps the scalars to a well balanced multi-value ($k+1$ values) sequence.

From the viewpoint of auto and cross-correlation, there are a lot of considerations to use multi-value sequence in communications [11, 12]. However, there are few papers regarding the usage of pseudo random binary sequence with a long period, high linear complexity, and good distribution of bit patterns in security applications. To make attention to the usability of the proposed sequence, the authors introduce the flexibility of their proposed well balanced multi-value sequence to make it more worthy. To do so, the authors explain how to transform their proposed sequence into a binary sequence (along with its linear complexity and distribution of bit patterns properties) due to the extensive usage of binary sequence in numerous applications (especially in cryptography).

All our previous works on sequence generation (both binary and multi-value) utilizes a mapping function during the sequence generation procedure. As a result, there exists a big difference between the appearance of sequence coefficients, which leads the distribution of bit patterns ununiform. On the other hand, the proposed sequence is a $k+1$ values well balanced multi-value sequence without applying any kind of mapping function. Therefore, all the sequence coefficients (except the 0) appear almost the same in number, thus, it is called a well balanced multi-value sequence. This balanced characteristic in the sequence coefficients contributes to low correlation (both autocorrelation and cross-correlation), high linear complexity, and almost uniform distribution of bit patterns, whereas, a suitable pseudo random sequence for cryptographic applications asks for such kinds of features.

This paper experimentally explains some prominent features regarding a sequence, for instance, its period, autocorrelation, and cross-correlation. The authors formulate theorems by which the value of the autocorrelation and cross-correlation can be explicitly given. This is one of the major contributions of this paper. Furthermore, to emphasize the usability of the proposed sequence, the authors introduce its flexibility by making it a binary sequence. In addition, a comparison result regarding the linear complexity and distribution of bit patterns properties are also included in this paper. According to the comparison results, the proposed sequence in this paper holds better properties compared to our previous sequence.

Notations

In this paper, the notation p denotes an odd characteristic prime, m be a extension degree, and q denotes the power of p, for instance, $q = p^m$. In addition, k is a prime number as well as a factors of $p-1$, such as $k \mid (p-1)$. $\mathbb{F}_q^* = \mathbb{F}_q - \{0\}$ stands for multiplicative group of $\mathbb{F}_q$ excluding the zero.

2 Preliminaries

This section briefly introduces a few mathematical fundamentals which are related to this research work such as primitive polynomial, trace function, and k-th power residue symbol. In addition, the multi-value sequence also introduced along with its properties.

2.1 Primitive Polynomial

A polynomial $f(x)$ of degree m over the prime field $\mathbb{F}_p$ is said to be irreducible if it cannot be factorized into smaller degree polynomials (including the scalar factor), then $f(x)$ is said to be an irreducible polynomial. Let e be an smallest positive integer and $f(x) \mid (x^e - 1)$. If $x = p^m - 1$, then the polynomial $f(x)$ is said to be a primitive polynomial.

Let ω be an arbitrary element in the extension field $\mathbb{F}_q$. If $f(\omega) = 0$, then ω is said to be the root of the primitive polynomial. In addition, ω becomes a primitive element in $\mathbb{F}_q$ and all the non-zero elements can be generated by the power of ω^i such as

$$\omega^0, \omega^1, \omega^2, \ldots, \omega^{q-2}.$$

The primitive element ω has a multiplicative order of $q-1$. An extension field $\mathbb{F}_q$ and its base field $\mathbb{F}_p$ holds the following property [13].

Property 1 Let ω be a generator of $\mathbb{F}_q^*$, $\omega^{(q-1)/(p-1)}$ becomes a non-zero element in prime field $\mathbb{F}_p$ and is also a generator of $\mathbb{F}_p^*$. □

2.2 Trace Function

A trace function is defined to find the sum of conjugates. Let $\mathbb{F}_q$ be an extension field and X be one of the elements (vector) of $\mathbb{F}_q$. On the other hand, let x be a prime field $\mathbb{F}_p$ element (scalar). The trace of X over $\mathbb{F}_q$ is the sum of conjugates of X with respect to $\mathbb{F}_q$. It is defined as follows:

$$x = \mathrm{Tr}(X) = \sum_{i=0}^{m-1} X^{p^i}. \tag{1}$$

Aforementioned the trace function $\mathrm{Tr}(\cdot)$ sums the conjugates in the extension field $\mathbb{F}_q$ and maps them as the prime

field $\mathbb{F}_p$ elements. As a result, it has a linearity property, which shown in the following equation.

$$\mathrm{Tr}\left(\alpha X + \beta Y\right) = \alpha \mathrm{Tr}\left(X\right) + \beta \mathrm{Tr}\left(Y\right), \tag{2}$$

where α, β are prime field $\mathbb{F}_p$ elements and X, Y are extension field $\mathbb{F}_q$ elements.

Property 2 Let $i = 0, 1, 2, \ldots, p-1 \in \mathbb{F}_p$. Then for each i the number of elements in the extension field $\mathbb{F}_q$ whose trace with regard to the prime field $\mathbb{F}_p$ becomes i be given by $q/p = p^{m-1}$. □

2.3 *k*-th Power Residue Symbol

The k-th power residue symbol with $(k > 2)$ is a generalization of the Legendre symbol to k-th powers [14]. Let a be an arbitrary element in the prime field $\mathbb{F}_p$, then the k-th power residue symbol $\left(a/p\right)_k$ can be defined as follows [15]:

$$\begin{aligned}\left(\frac{a}{p}\right)_k &= a^{(p-1)/k} \bmod p \\ &= \begin{cases} 0 & \text{if } a = 0, \\ 1 = \epsilon_k^0 & \text{else if } a \text{ is a } k\text{-th PR in } \mathbb{F}_p^*, \\ \epsilon_k^i & \text{otherwise } a \text{ is a } k\text{-th PNR in } \mathbb{F}_p^*. \end{cases}\end{aligned} \tag{3}$$

Throughout this paper, k is a prime number as well as a factor of $p-1$, such as $k \mid (p-1)$. According to the definition of the k-th power residue symbol $\left(a/p\right)_k$, a is called as the k-th Power Residue, when it has a k-th root in the base field $\mathbb{F}_p$. On the other hand, a is called as k-th Power Non-Residue. In addition, here ϵ_k is a primitive k-th root of unity belongs to $\mathbb{F}_p$ and it holds the relation $0 \le i < k$.

In Eq. (3), the value of the exponent i will be within the range of $0 \sim k-1$, since $\epsilon_k^k = \epsilon_k^0 = 1$. The k-th power residue symbol translates the scalars generated by the trace function $\mathrm{Tr}\left(\cdot\right)$ to a multi-value sequence. Thus, the sequence coefficients will be $\{0, \epsilon_k^i\}$, where $i \in \{0, \ldots, k-1\}$. In this paper, an alternate representation of the exponent i in Eq. (3) is as follows:

$$i = \log_{\epsilon_k}\left(\left(a/p\right)_k\right) = \log_{\epsilon_k}\left(a^{(p-1)/k} \bmod p\right). \tag{4}$$

Furthermore, the k-th power residue symbol holds the following property.

Property 3 For each i from 0 to $k-1$, the number of non-zero elements in $\mathbb{F}_p$ such that

$$\left(\frac{a}{p}\right)_k = \epsilon_k^i \tag{5}$$

is given by $(p-1)/k$. □

2.4 Multi-value Sequence and Its Properties

In this section, the proposed multi-value sequence introduced along with its period, autocorrelation, cross-correlation, linear complexity and distribution of bit patterns properties.

2.4.1 Notation

Throughout this paper, the proposed multi-value (more specifically, $k+1$ values) sequence $\mathcal{S}$ will be denoted as follows:

$$\mathcal{S} = \{s_i\}, i = 0, 1, 2, \ldots, n-1, \ldots, \tag{6}$$

where n denotes the period of the proposed sequence $\mathcal{S}$. In addition, here $s_i = s_{n+i}$.

2.4.2 Autocorrelation and Cross-correlation

The autocorrelation of a sequence is a measure for how much a sequence differs from its each shift value. In addition, the period and other patterns regarding a sequence can be obtained by evaluating the autocorrelation property [16]. Let $\mathcal{S} = \{s_i\}$ be a sequence and x be the shift value, then the autocorrelation $\mathrm{R}_{\mathcal{S}}(x)$ of $\mathcal{S}$ can be calculated by using the following equation as,

$$\mathrm{R}_{\mathcal{S}}(x) = \sum_{i=0}^{n-1} \tilde{\epsilon}_k^{s_{i+x} \times s_i}, \tag{7}$$

where $\tilde{\epsilon}_k$ is a primitive k-th root of unity over the complex number $\mathbb{C}$ [17] and it follows that

$$\mathrm{R}_{\mathcal{S}}(0) = \sum_{i=0}^{n-1} \tilde{\epsilon}_k^0 = n. \tag{8}$$

Furthermore, the cross-correlation property is as important as the autocorrelation property. It defines the similarities between two completely different sequences. If multiple sequences are used in an application (more specifically in any security application), then it is important to analyze their cross-correlation property to evaluate how much similar these sequences to each other. Considering this point, the cross-correlation value is preferred to be low [18, 19]. Let $\hat{\mathcal{S}} = \{\hat{s}_i\}$ and $\mathcal{S} = \{s_i\}$ be two sequences and x be the shift value, then the cross-correlation $\mathrm{R}_{\mathcal{S}}(x)$ between $\hat{\mathcal{S}}$ and $\mathcal{S}$ can be calculated by using the following equation as,

$$\mathrm{R}_{\hat{\mathcal{S}},\mathcal{S}}(x) = \sum_{i=0}^{n-1} \tilde{\epsilon}_k^{\hat{s}_{i+x} \times s_i}, \tag{9}$$

where $\tilde{\epsilon}_k$ is a primitive k-th root of unity over the complex number $\mathbb{C}$ [20, 21].

2.4.3 Linear Complexity

The linear complexity regarding a sequence is a measure of unpredictability by the length of the shortest Linear Feedback Shift Register (LFSR). In the literature, this length of the LFSR is referred to as the linear complexity [22]. The Berlekamp-Massey algorithm is an efficient method of determining the linear complexity of a sequence [23]. The forward unpredictability can be confirmed by the linear complexity property.

To calculate the linear complexity of a sequence $\mathcal{S} = \{s_0, s_1, \ldots, s_{n-1}\}$, at first, the sequence $\mathcal{S}$ needed to be represented by the polynomial expression $\mathcal{S}(x)$ as follows:

$$\mathcal{S}(x) = \sum_{i=0}^{n-1} s_i \cdot x^i, \tag{10}$$

where n denotes the period of the sequence $\mathcal{S}$. If we consider a binary sequence, then the sequence coefficients $s_i \in \{0, 1\}$, in other words, s_i belongs to $\mathbb{F}_2$. On the other hand, in case of multi-value sequence (k-values sequence), $s_i \in \{0, 1, 2, \ldots, k-1\}$, furthermore, $s_i \in \mathbb{F}_k$. After translating the sequence into polynomial, the linear complexity is evaluated by utilizing the equation in below (over $\mathbb{F}_2$ or $\mathbb{F}_k$).

$$\mathrm{LC}(\mathcal{S}) = n - \deg(\gcd(x^n - 1, \mathcal{S}(x))). \tag{11}$$

In the above equation, $\deg(f(x))$ denotes the degree of the primitive polynomial $f(x)$.

2.4.4 Distribution of Bit Patterns

The distribution of bit patterns is an important measure to judge the randomness of a sequence. As a reference, an M-sequence is well known for its uniform distribution of bit patterns. A uniform distribution of bit patterns means all the bit patterns (1-bit pattern, 2-bit patterns, 3-bit patterns, and so on) appear the same in number. Assume an M-sequence of having a period of 15 as follows and its bit distribution is shown in Table 1.

$$\mathcal{S}_{15} = \{1, 0, 0, 0, 1, 1, 1, 1, 0, 1, 0, 1, 1, 0, 0\}.$$

Table 1: Uniform distribution of bit distribution of an M-sequence [1].

n	$\mathrm{H_w}\left(b^{(n)}\right)$	$Z\left(b^{(n)}\right)$	$D_{S_{15}}\left(b^{(n)}\right)$
1	0	1	7
	1	0	8
2	0	2	3
	1	1	4
	2	0	4
3	0	3	1
	1	2	2
	2	1	2
	3	0	2

In an M-sequence, except 0 all the bit patterns appear same in number, therefore, the distribution of bit patterns of M-sequence is known as uniform.

It should be noted that the randomness and bit patterns hold a strong relationship with each other. In other words, the more uniform distribution of bits in a sequence, the sequence is more random.

3 Proposed Multi-value Sequence

The authors propose a well balanced multi-value sequence $\mathcal{S}$ by combining the features of the trace function and k-th power residue symbol. Assume that in the extension field $\mathbb{F}_q$, ω be a primitive element. Furthermore, A is a non-zero scalar which belongs to the prime field $\mathbb{F}_p$. Then, the proposed sequence $\mathcal{S}$ is defined as follows:

$$\mathcal{S} = \{s_i\},\ s_i = \left(\mathrm{Tr}\left(\omega^i\right) + A \middle/ p\right)_k, \tag{12}$$

here k is a factor of $p-1$, such as $k \mid (p-1)$. The sequence coefficients s_i in Eq. (12) can be described as the exponent of ϵ_k, such as ϵ_k^e. For instance, let $p = 7$ and $k = 3$, then the sequence coefficients in this example becomes $s_i \in \{0, 1, 2, 4\}$ and the 3-rd primitive root in $\mathbb{F}_7$ is equal to 2 or 4. In addition, let us fix 2 as a 3-rd primitive root. Then all of the non-zero sequence coefficients can be represented as an exponent of primitive root 2, this relation is developed as,

$$\epsilon_3\{1, 2, 4\} = \{2^0, 2^1, 2^2\} = \{\epsilon_3^0, \epsilon_3^1, \epsilon_3^2\}.$$

At first, the authors will focus on the autocorrelation and cross-correlation properties regarding the proposed sequence. It should be noted that the autocorrelation and cross-correlation are very close to each other. The main difference between them is the cross-correlation is calculated between two different sequences and the autocorrelation is focused in a single sequence. Thus, in the beginning, let us focus on the cross-correlation property. As mentioned earlier, using two different sequences of having the same period the cross-correlation is calculated. Let, $\mathcal{S}$ and $\hat{\mathcal{S}}$ be two different sequences which are defined as follows:

$$\mathcal{S} = \left\{ s_i \mid s_i = \left(\mathrm{Tr}\left(\omega^i\right) + A \middle/ p\right)_k \right\}, \tag{13a}$$

$$\hat{\mathcal{S}} = \left\{ \hat{s}_i \mid \hat{s}_i = \left(\mathrm{Tr}\left(\omega^i\right) + \hat{A} \middle/ p\right)_k \right\}. \tag{13b}$$

Here, A and $\hat{A}$ are non-zero elements in $\mathbb{F}_p$ can be represented by a generator $g \in \mathbb{F}_p$ such as

$$\hat{A} = g^h A, \tag{14}$$

here h satisfies the relation $0 \le h \le p-2$ and g needs to be given by $\omega^{(p^m-1)/(p-1)}$. When the value of $h = 0$, that is $\hat{A} = A$ which means $\hat{\mathcal{S}}$ and $\mathcal{S}$ becomes the same sequence. Thus, the cross-correlation becomes the autocorrelation of $\mathcal{S}$. After inspecting several experimental results, it was found that the value of the cross-correlation explicitly given by the following theorem.

Theorem 1 The cross-correlation between the two sequences $\hat{\mathcal{S}}$ and $\mathcal{S}$ is defined by the Eq. (13) is as follows:

$$\mathrm{R}_{\hat{\mathcal{S}},\mathcal{S}}(x) = \begin{cases} \left(p^m - 1 - p^{m-1}\right)\tilde{\epsilon}_k^{f_k(g^h)}, & \text{if } x = h\bar{n}, \\ -p^{m-1}\left(\tilde{\epsilon}_k^{f_k(g^j)}\right) - \tilde{\epsilon}_k^{f_k(g^h)}, & \text{else if } x = j\bar{n}, \\ -\tilde{\epsilon}_k^{f_k(g^h)}, & \text{otherwise,} \end{cases} \tag{15}$$

where $\bar{n} = n/(p-1) = (p^m - 1)/(p-1)$, h satisfies the condition in Eq. (14), and $0 \le j \ne h \le p-2$. □

If the value of $h = 0$, then $\hat{\mathcal{S}} = \mathcal{S}$ which actually means they becomes the same sequence. In this case, the cross-correlation in Eq. (15) becomes the autocorrelation after replacing the value $h = 0$.

[1] The notations $n, \mathrm{H_w}\left(b^{(n)}\right), Z\left(b^{(n)}\right)$, and, $D_S\left(b^{(n)}\right)$ means length of a bit pattern $b^{(n)}$, Hamming weight of the bit pattern $b^{(n)}$, number of zeros in $b^{(n)}$, and appearance of $b^{(n)}$ in numbers in a sequence period, respectively.

Theorem 2 The autocorrelation of a sequence $\mathcal{S}$ is given as follows:

$$\mathrm{R}_{\mathcal{S}}(x) = \begin{cases} p^m - 1 - p^{m-1}, & \text{if } x = h\bar{n}, \\ -p^{m-1}\left(\tilde{\epsilon}_k^{f_k(g^j)}\right) - 1, & \text{else if } x = j\bar{n}, \\ -1, & \text{otherwise}, \end{cases} \tag{16}$$

Corresponding to the above autocorrelation equation, the period of the proposed well balanced multi-value sequence undeniably given by $p^m - 1$. □

In the next section, the authors will introduce experimental observation regarding the period, autocorrelation and cross-correlation properties.

4 Example and Discussion

This section experimentally observes the proposed multi-value sequence properties such as its period, autocorrelation, and cross-correlation along with some examples. In this section, the notation $\mathcal{S}_2$ denotes the proposed sequence with the parameter $A = 2$. The proposed sequence in this paper is a multi-value sequence, thus its correlation is calculated over the complex number $\mathbb{C}$. To represent the absolute value of a complex number x, this section uses the notation $|x|$.

4.1 $p = 7, m = 2, k = 3$, and $A = 2, 3$

Assume, $x^2 + 4x + 5$ be a primitive polynomial over $\mathbb{F}_7$. Then, the generated sequence $\mathcal{S}_2$ having a period of 48 ($p^m - 1 = 7^2 - 1 = 48$) is shown as follows:

$$\begin{aligned} \mathcal{S}_2 = \{&2,4,1,4,4,1,1,4,4,2,2,2,4,2,1,2,2,0,4,0,4,4,2,0, \\ &0,1,2,1,4,2,4,1,1,1,0,1,4,0,2,1,1,2,1,2,4,1,0,2\}. \end{aligned} \tag{17}$$

The autocorrelation of this generated sequence $\mathcal{S}_2$ is calculated by the Eq. (7) and autocorrelation graph of $\mathcal{S}_2$ is shown in Figure 1.

$$|\mathrm{R}_{\mathcal{S}_2}(x)| = \begin{cases} 41 & \text{if } x = 0 \\ 6 & \text{else if } x = 8, 16, 32, 40 \\ 8 & \text{else if } x = 24 \\ 1 & \text{otherwise} \end{cases}.$$

To confirm the well balanced property in the proposed multi-value sequence, the authors introduce sequence coefficients appearance in the following Table 2. According to the table, it was found that in every case all of the sequence coefficients (except the 0) appears almost the same in number. This is one of the positive properties of the proposed sequence, thus, it is called as a well balanced sequence.

Table 2: Appearance of the sequence coefficients.

sequence coefficient	number of appearance
0	7
1	14
2	14
4	13

On the other hand, $\mathcal{S}_3$ is given as follows. It should be noted that the sequence $\mathcal{S}_3$ is different from the sequence $\mathcal{S}_2$, but both of them having the same period.

$$\begin{aligned} \mathcal{S}_3 = \{&4,1,4,1,2,4,0,1,1,2,4,2,2,4,4,2,2,1,1,1,2,1,4,1, \\ &1,0,2,0,2,2,1,0,0,4,1,4,2,1,2,4,4,4,0,4,2,0,1,4\}. \end{aligned} \tag{18}$$

The autocorrelation of this generated sequence $\mathcal{S}_3$ is calculated by the Eq. (7) and autocorrelation graph of $\mathcal{S}_2$ is shown in Figure 2.

$$|\mathrm{R}_{\mathcal{S}_3}(x)| = \begin{cases} 41 & \text{if } x = 0 \\ 6 & \text{else if } x = 8, 16, 32, 40 \\ 8 & \text{else if } x = 24 \\ 1 & \text{otherwise} \end{cases}.$$

The cross-correlation of $\mathcal{S}_2$ and $\mathcal{S}_3$ becomes as follows and the cross-correlation graph shows in Figure 3.

$$|\mathrm{R}_{\mathcal{S}_2,\mathcal{S}_3}(x)| = \begin{cases} 6 & \text{if } x = 0, 8, 24, 32 \\ 8 & \text{else if } x = 16 \\ 41 & \text{else if } x = 40 \\ 1 & \text{otherwise} \end{cases}.$$

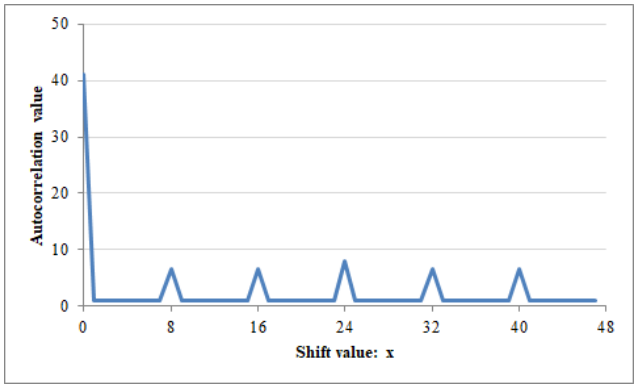

Figure 1: $|\mathrm{R}_{\mathcal{S}_2}(x)|$ with $p = 7, m = 2, k = 3$, and $A = 2$.

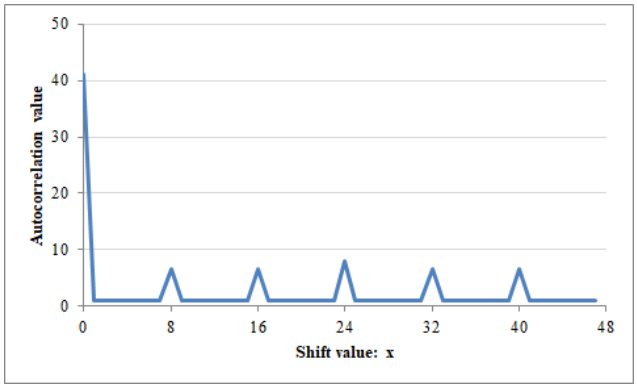

Figure 2: $|\mathrm{R}_{\mathcal{S}_3}(x)|$ with $p = 7, m = 2, k = 3$, and $A = 3$.

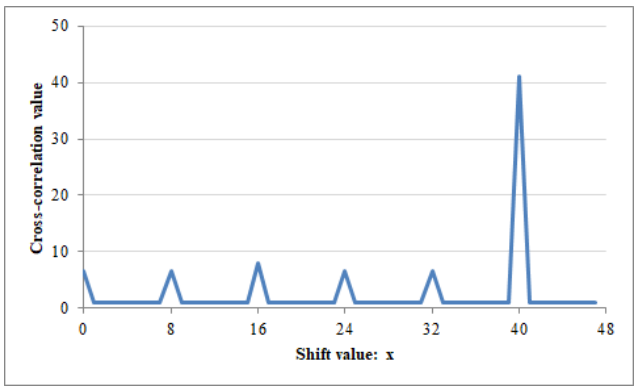

Figure 3: $|R_{S_2,S_3}(x)|$ with $p = 7, m = 2$, and $A = 2, 3$.

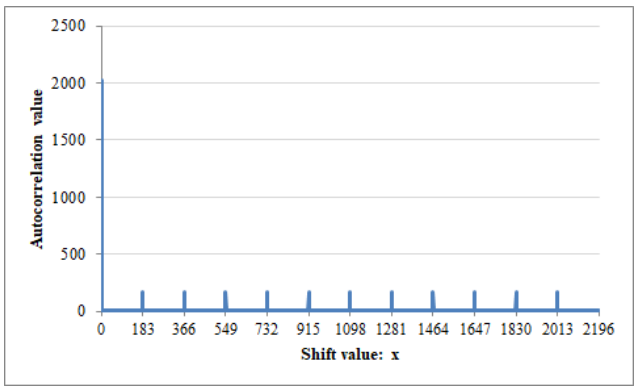

Figure 5: $|R_{S_7}(x)|$ with $p = 13, m = 3, k = 3$, and $A = 7$.

4.2 $p = 13, m = 3, k = 3$, and $A = 6, 7$

Assume, $x^3 + 6x^2 + 3x + 7$ be a primitive polynomial over $\mathbb{F}_{13}$. Then, the period of this generated sequence becomes 2196. Here, Figure 4 and Figure 5 respectively represents the autocorrelation graph of $\mathcal{S}_6$ and $\mathcal{S}_7$. Their cross-correlation graph is shown in Figure 6.

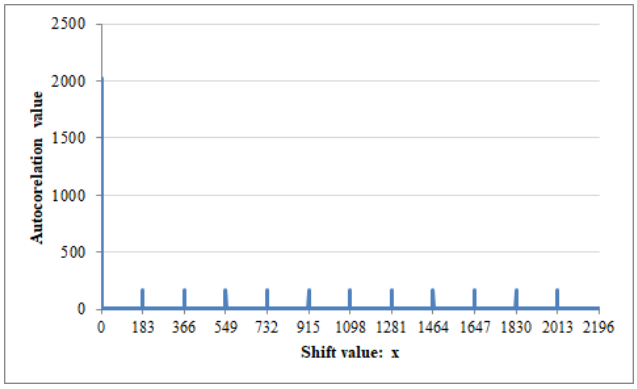

Figure 4: $|R_{S_6}(x)|$ with $p = 13, m = 3, k = 3$, and $A = 6$.

After observing the cross-correlation graphs, it was found that in each graph the number of peaks exactly is given by $p - 1$. Only a single peak has the maximum value, as an example, in Figure 3 the maximum peak value is 41 that corresponds to the first case ($x = h\bar{n}$) of Eq. (15). Remaining $p - 2$ smaller peaks conforms to the second case ($x = j\bar{n}$). Except all of these peak values, the remaining parts of the cross-correlation graph consistently having a constant value of 1, which confirms the final case of Eq. (15). It should be noted that only changing the value of non-zero scalar parameter $A \in \mathbb{F}_p$, different sequences can be generated. It is also observed that by changing all the other parameters such as primitive polynomial $f(x)$, extension degree m, non-zero scalar A, and prime factor k does not have any impact in the correlation (both autocorrelation and cross-correlation) evaluation.

Alike the cross-correlation, autocorrelation also have a $p-1$ number of peaks. Among them, only one peak hold the maximum value, while other peaks have small values and remaining parts holds a constant value of 1 and all of these values explicitly given by the Eq. (16).

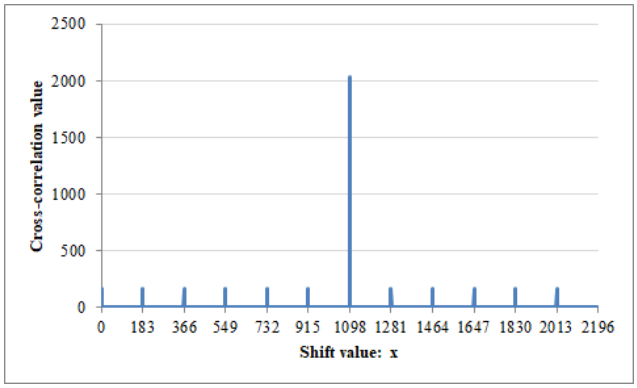

Figure 6: $|R_{S_6,S_7}(x)|$ with $p = 13, m = 3$, and $A = 6, 7$.

5 Flexibility of the Proposed Sequence and Its Application

Although nowadays multi-value sequence does not have enough application except the binary sequence especially in security applications. Therefore, the authors emphasize the flexibility of their proposed sequence to make it more worthy. To do so, the authors in this section, explains how to transform their proposed sequence into a binary sequence. In addition, this section also describes a comparison with our previous work [24] in terms of the linear complexity and distribution of bit patterns like crucial properties from the experimental viewpoint.

5.1 Proposed Binary Sequence

Binary sequences are extensively used in numerous applications (especially in cryptography). Although the authors proposed sequence is a multi-value sequence, it can be easily mapped into a binary sequence by setting the parameter value $k = 2$ and using the mapping function $M_2(\cdot)$. As mentioned previously, the proposed multi-value sequence is a well balanced sequence, in other words, all of the sequence coefficients (except the 0) appears same in number. To maintain the same property, the authors utilized the following algorithm (Algorithm 1) to make a uniform binary sequence from the well balanced multi-value sequence.

To make it binary sequence, a mapping function (intro-

duced in the following algorithm) is defined as,

$$M_2(s) = \begin{cases} 0 & \text{if } s = 0 \text{ or QR}, \\ 1 & \text{otherwise}, \end{cases} \tag{19}$$

By utilizing the parameters $p = 7$, $k = 2$, $f(x) = x^2 + 5x + 5$, and $A = 2$ the multi-value sequence becomes as,

$$\begin{aligned} \mathcal{S}_2 = \{&2,2,4,4,0,1,1,2,2,2,2,1,1,2,1,4,4,2,4,4,4,4,2,1,0,1,4, \\ &1,1,0,4,1,2,4,1,4,4,4,2,1,1,2,0,4,4,0,0,2,4,1,4,2,0\}. \end{aligned} \tag{20}$$

Algorithm 1 Generating procedure of the proposed uniform binary sequence

1: generate primitive element $\omega \in \mathbb{F}_{p^m}$
2: initialize flag $f \leftarrow 0$
3: **for** $i = 0$ to $p^m - 2$ **do**
4: compute ω^i
5: $a \leftarrow \left(\mathrm{Tr}\left(\omega^i\right) + A/p\right)$
6: **if** $a = 0$ and $f = 0$ **then**
7: $a \leftarrow 1$, $f \leftarrow 1$
8: **else**
9: $a \leftarrow p - 1$, $f \leftarrow 0$
10: **end if**
11: $s_i = M_2(a)$
12: **end for**

After using the above algorithm, the well balanced multi-value sequence in Eq. (20) can be transformed into a binary sequence as follows.

$$\begin{aligned} \mathcal{S}_2 = \{&0010000101110011111110001 \\ &1001001111000101001101 00\}. \end{aligned} \tag{21}$$

5.2 Comparison with Our Previous Work

Before applying any sequence in some security application, a lot of sequence properties needs to be well studied such as its period, autocorrelation, cross-correlation, linear complexity, distribution of bit patterns, and so on. The authors already discussed the former three properties. Additionally, this paper also includes a comparison with our previous work [24] regarding the linear complexity and distribution of bit patterns like crucial properties from the experimental viewpoint. It should be noted that from here on the authors previous sequence proposed in [24] will be called as NTU (Nogami-Tada-Uehara) sequence.

Linear Complexity

The linear complexity is an important measure to judge the unpredictability of a sequence. Thus, before recommending a sequence for any security application, its linear complexity needs to be well-studied. The linear complexity of the proposed sequence (binary case) and NTU sequence (previous sequence) having a period of 2400 are shown in Figure 7 and Figure 8, respectively. According to the comparison result, it is found that in both cases the linear complexity reaches to their maximum value. Since the M-sequence has the minimum linear complexity [25], on the other hand, the Legendre sequence has the maximum linear complexity [8]. It should be noted that the proposed sequence for being a well balanced sequence, its linear complexity reaches to its maximum value.

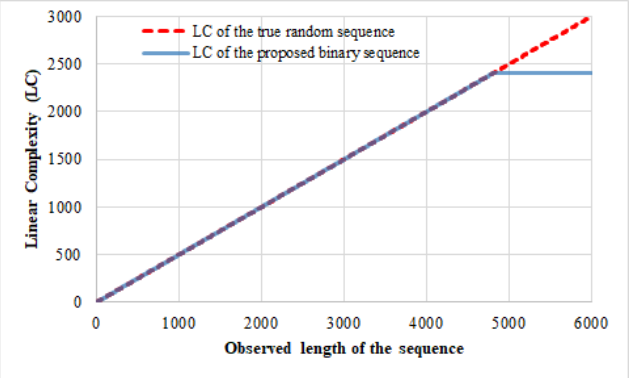

Figure 7: Linear complexity of the proposed sequence (binary case).

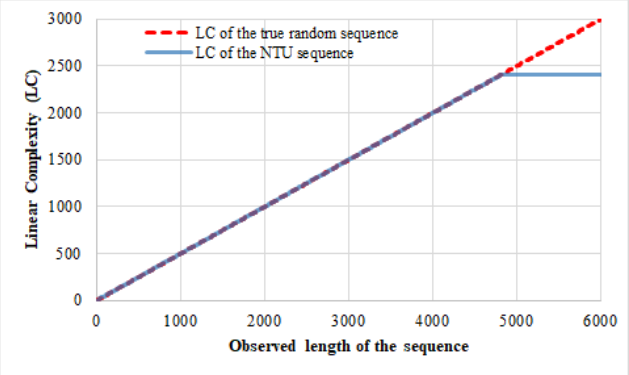

Figure 8: Linear complexity of the NTU sequence.

Distribution of Bit Patterns

The randomness of a sequence can be evaluated by observing the distribution of bit patterns of it. The bit pattern of the proposed sequence (binary case) and NTU sequence (previous sequence) having a period of 117648 are shown in Table 3. In the following table, the notations $n, b^{(n)}, Z\left(b^{(n)}\right)$, and $D_S\left(b^{(n)}\right)$ means length of a bit pattern, specific bit pattern, number of zeros in $b^{(n)}$, and appearance of $b^{(n)}$ in numbers in a sequence period, respectively. According to the comparison result, it is found that the distribution of bit pattern of the proposed binary sequence is almost uniform compared to NTU sequence.

The authors applied $k = 2$ and $M_2(\cdot)$ mapping function to make a uniform binary sequence from the well balanced multi-value sequence. It should be noted that after applying such a mapping function and uniformization algorithm, the sequence properties remains almost the same. For instance, only a small amount of change in the peak values regarding the autocorrelation, linear complexity remains the maximum, and distribution of bit patterns becomes almost uniform. In other words, they exhibit almost the same properties. It means the authors proposed sequence possesses a great flexibility.

Table 3: A comparison of distribution of 4-bit patterns between the proposed sequence (binary case) and NTU sequence.

n	$b^{(n)}$	$Z(b^{(n)})$	(proposed sequence) $D_S(b^{(n)})$	(NTU sequence) $D_S(b^{(n)})$
1	0	1	58824	67227
	1	0	58824	50421
2	00	2	28852	38415
	01	1	29972	28812
	10	1	29972	28812
	11	0	28852	21609
3	000	3	13927	21951
	001	2	14925	16464
	010	2	15066	16464
	011	1	14906	12348
	100	2	14925	16464
	101	1	15047	12348
	110	1	14906	12348
	111	0	13946	9261
4	0000	4	6680	12543
	0001	3	7247	9408
	0010	3	7391	9408
	0011	2	7534	7056
	0101	2	7402	7056
	0010	3	7664	9408
	0111	1	7631	5292
	0100	3	7275	9408
	1000	3	7247	9408
	1001	2	7678	7056
	1010	2	7675	7056
	1011	1	7372	5292
	1100	1	7523	5292
	1101	1	7383	5292
	1110	1	7275	5292
	1111	0	6671	3939

As far the authors know, there are a lot of considerations to use multi-value sequence in communications from the viewpoint of correlation [11, 12]; however there are few papers regarding the usage of pseudo random sequence with a long period, high linear complexity, and good distribution of bit patterns in security applications. The most typical security application of the pseudo random binary sequence will be the XOR-based stream cipher. First of all, in such an application, the same key is used for both encryption and decryption. Thus, each user should have a different key. In this case, these keys should have a minimum cross-correlation property compared to each other. Under this circumstance, it is important to discuss the cross-correlation property between several sequences along with linear complexity and distribution of bit patterns properties. The authors briefly introduced a use case in the following section of their proposed well balanced sequence in this paper, to emphasis on its usability.

5.3 Application

One of the most common applications of the pseudo random sequence (binary case) is in a stream cipher. Basically, a stream cipher is divided into two classes: block cipher and stream cipher. Among these a block cipher uses the same key for both encryption and decryption of each block (≤ 64 bits) of data. On the other hand, in case of a stream cipher, encryption and decryption are performed by the bit wise $\oplus$ (XOR) operation with a key stream. Here, the authors restrict the discussion of their proposed pseudo random binary sequence in a stream cipher. An image of the stream cipher is shown in Figure 9. Few important considerations during the design of a stream cipher are the key (which used for both encryption and decryption) should have a long period, good randomness, and unpredictability properties due to the usage of the same key in both encryption and decryption. Here, the encryption is carried out by applying a bit-wise $\oplus$ (XOR) operation between the plain-text of byte stream M and encryption key K. Then, the cipher-text C is transmitted through a network. On the other hand, during the decryption, after the bit-wise $\oplus$ operation between the cipher-text C and the same key K, we will get the original plain-text M. In a stream cipher, a lot of sequences are assigned to several users, respectively. If these sequences have some correlation, then it will make some security vulnerabilities. Under this circumstance, it is important to observe the cross-correlation property between several sequences. Additionally, its linear complexity and distribution of bit patterns needs to be high and uniform, respectively to confirm its randomness. Although the authors proposed sequence is a well balanced sequence, it can be easily mapped into a binary sequence with a long period, typical auto and cross-correlation, high linear complexity, and almost uniformly distributed bit patterns features. After observing the experimental and comparison results, it can be concluded that the authors proposed well-balanced sequence (binary case) can be a prominent candidate for a stream cipher like applications.

6 Conclusion

The authors have proposed a multi-value sequence (including a binary sequence) which defined over the odd characteristic field. The k-th power residue symbol utilized in this paper which is an extension of the Legendre symbol. Additionally, the proposed sequence also includes the case of the signed binary sequence. Prominent features regarding a sequence for instance, its period, autocorrelation and cross-correlation of the proposed sequence discussed based on experimental results along with a theorem (by which the value of the correlation can be explicitly given). In addition, the authors also introduced the flexibility of their proposed sequence by making a binary sequence from a well balanced multi-value sequence. Furthermore, a comparison result regarding the linear complexity and distribution of bit patterns properties are also included in this paper. According to the comparison results, the authors proposed well balanced sequence holds better properties compared to our previous sequence.

As a future work, the more efficient calculation will be introduced for instance power residue symbol needs exponentiation calculation.

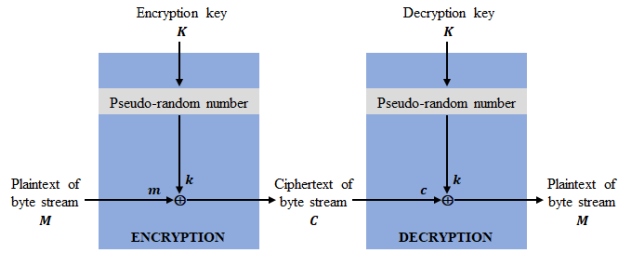

Figure 9: Application of the proposed sequence (binary case) in stream cipher.

Conflict of Interest The authors declare no conflict of interest.

References

[1] M. Luby, Pseudorandomness and Cryptographic Applications, Princeton Univ. Press, 1996. https://doi.org/10.1016/0898-1221(96)87348-2

[2] T. W. Cusick, C. Ding, and A. Renvall, Stream Ciphers and Number Theory, North-Holland Math. Library, North-Holland Publishing Co., Amsterdam, 1998. https://doi.org/10.1016/s0924-6509(98)x8001-3

[3] S. W. Golomb and G. Gong, Signal Design for Good Correlation: For Wireless Communication, Cryptography, and Radar, Cambridge University Press, NY, 2005. https://doi.org/10.1017/CBO9780511546907

[4] A. Kinga, F. Aline, and E. Christain, "Generation and testing of random numbers for cryptographic applications", Proc. of the Romanian Academy, **13**(4), pp.368–377, 2012.

[5] M. Matsumoto, and T. Nishimura, "Mersenne twister: A 623-dimensionally equidistributed uniform pseudo-random number generator", ACM Transactions on Modeling and Computer Simulation, **8**(1), pp.3–30, 1998. https://doi.org/10.1145/272991.272995

[6] L. Blum, M. Blum, and M. Shub, "A simple unpredictable pseudorandom number generator", SIAM Journal on Computing, **15**(2), pp.364–383, 1986. https://doi.org/10.1137/0215025

[7] J. S. No, H. K. Lee, H. Chung, H.Y. Song, and K. Yang, "Trace representation of Legendre sequences of mersenne prime period", IEEE Transactions on Information Theory, **42**, pp.2254–2255, 1996. https://doi.org/10.1109/18.556617

[8] C. Ding, T. Helleseth, and W. Shan, "On the linear complexity of Legendre sequences", IEEE Transactions on Information Theory, **44**, pp.1276–1278, 1998. https://doi.org/10.1109/18.669398

[9] A. M. Arshad, Y. Nogami, C. Ogawa, H. Ino, S. Uehara, and R. H. Morelos-Zaragoza, "A new approach for generating well balanced pseudo random signed binary sequence over odd characteristics field", International Symposium on Information Theory and Its Applications (ISITA), Monterey, CA, USA, 2016. ISBN 978-4-88552-309-0.

[10] A. M. Arshad, Y. Nogami, H. Ino, and S. Uehara, "Auto and cross correlation of well balanced sequence over odd characteristic field", Fourth International Symposium on Computing and Networking (CANDAR),Hiroshima, Japan, 2016. https://doi.org/10.1109/candar.2016.0109

[11] Y. K. Han and K. Yang, "New M-array sequence families with low correlation and large size", IEEE Transactions on Information Theory, **55**(4), pp.1815–1823, 2009. https://doi.org/10.1109/tit.2009.2013040

[12] N. Y. Yu and G. Gong, "Multiplicative characters, the weil bound, and poly phase sequence families with low correlation", IEEE Transactions on Information Theory, **56**(12), pp.6376–6387, 2010. https://doi.org/10.1109/tit.2010.2079590

[13] R. Lidl and H. Niederreiter, Finite Fields (Encyclopedia of Mathematics and Its Applications), Cambridge Univ. Press, 1996. https://doi.org/10.1017/CBO9780511525926

[14] E.R. Berlekamp, Algebraic Coding Theory, Aegean Park Press, Revised edition, 2014. https://doi.org/10.1142/9407

[15] M. Joye and B. Libert, "Efficient cryptosystems from 2^k-th power residue symbols", in Proceedings of Eurocrypto 2013, Johansson T. et al. Ed., ser. LNCS, vol. 7881. Berlin, Heidelberg: Springer, pp.76–92, 2013. https://doi.org/10.1007/978-3-642-38348-9_5

[16] P. V. Kumar and O. Moreno, "Prime-phase sequences with periodic correlation properties better than binary sequences", IEEE Transactions on Information Theory, **37**(3), pp.603–616, 1991. https://doi.org/10.1109/18.79916

[17] P. V. Kumar, T. Helleseth, A. R. Calderbank, and A. R. Hammons, "Large families of quaternary sequences with low correlation," IEEE Transactions on Information Theory, **42**(2), pp. 579–592, 1996. https://doi.org/10.1109/18.485726

[18] D. Hertel, "Cross-correlation properties of perfect binary sequence", in Sequences and Their Applications SETA 2004, T. Helleseth et al. Ed., ser. LNCS, vol. 3486. Berlin, Heidelberg: Springer, pp.208–219, 2005. https://doi.org/10.1007/11423461_14

[19] D. V. Sarwate and M. B. Pursley, "Cross-correlation properties of pseudorandom and related sequences", Proceedings of IEEE, **68**(5), pp.593–619, 1980. https://doi.org/10.1109/proc.1980.11697

[20] Y. T. Kim, M. K. Song, D. S. Kim, and H. Y. Song, "Properties and cross-correlation of decimated sidelnikov sequences", IEEE Transactions on Fundamentals of Electronics, Communications and Computer Sciences, **E97-A**(12), pp.2562–2566, 2014. https://doi.org/10.1587/transfun.e97.a.2562

[21] G. Gong, "New designs for signal sets with low cross-correlation, balance property and large linear span: GF(p) case", IEEE Transactions on Information Theory, **48**(11), pp.2847–2867, 2002. https://doi.org/10.1109/tit.2002.804044

[22] R. A. Rueppel, "Linear Complexity and Random Sequences", F. Pichler (Ed.): Advances in Cryptology-EUROCRYPT'85, Springer, LNCS 219, pp. 167-188, 1986. https://doi.org/10.1007/3-540-39805-8_21

[23] A. Alecu and A. Salagean, "Modified Berlekamp-Massey Algorithm for Approximating the k-Error Linear Complexity of Binary Sequences", IMA Conference on Cryptography and Coding (S.D. Galbraith, Ed.), Springer, LNCS, vol. 4887, pp. 220–232, 2007. https://doi.org/10.1007/978-3-540-77272-9_14

[24] Y. Nogami, S. Uehara, K. Tsuchiya, N. Begum, H. Ino, and R. H. Morelos-Zaragoza, "A Multi-value Sequence Generated by Power Residue Symbol and Trace Function over Odd Characteristic Field", IEICE Trans. on Fund. of Electronics, Communications and Computer Sciences, **E99.A**(12), pp.2226–2237, 2016. https://doi.org/10.1587/transfun.e99.a.2226

[25] T. Moriuchi and S. Uehara, "Periodic sequence of the maximum linear complexity simply obtained from an m-sequence", IEEE International Symposium on Information Theory (ISIT), 1991. https://doi.org/10.1109/isit.1991.695231

ASTES

Advances in Science, Technology and Engineering Systems Journal Vol. 4, No. 4, 197-205 (2019)

www.astesj.com

Special Issue on Advancement in Engineering and Computer Science

ASTESJ

ISSN: 2415-6698

Dysphoria Detection using EEG Signals

Norhaslinda Kamaruddin*,[1], Mohd Hafiz Mohd Nasir[1], Abdul Wahab[2]

[1]*Advanced Analytics Engineering Centre, Faculty of Computer and Mathematical Sciences, Universiti Teknologi MARA, 40540 Shah Alam, Selangor, Malaysia*

[2]*Kulliyyah of Information & Communication Technology, International Islamic University Malaysia, P. O. Box 10, 50728 Kuala Lumpur, Malaysia*

ARTICLE INFO

Article history:
Received: 19 May, 2019
Accepted: 14 July, 2019
Online :30 July, 2019

Keywords:
Dysphoria
EEG emotion
Affective Space Model
Multilayer perceptron

ABSTRACT

Dysphoria is a state faced when one experienced disappointment. If it is not handled properly, dysphoria may trigger acute stress, anxiety and depression. Typically, the individual who experienced dysphoria are in-denial because dysphoria is always being associated with negative connotations such as incompetency to handle pressure, weak personality and lack of will power. To date, there is no accurate instrument to measure dysphoria except using questionnaire by psychologists, such as: Depression, Anxiety and Stress Scale (DASS) and Nepean Dysphoria Scale (NDS-24). Participants may suppress or exaggerate their answers resulting in misdiagnosis. In this work, a theoretical Dysphoria Model of Affect (DMoA) is developed for dysphoria detection. Based on the hypothesis that dysphoria is related to negative emotion, the input from brain signal is captured using electroencephalogram (EEG) device to detect negative emotions. The results from analyzing the EEG signals were compared with DASS and NDS questionnaires for correlation analysis. It is observed that the proposed DMoA approach can identify negative emotions ranging from 55% to 77% accuracy. In addition, the NDS questionnaire seems to provide better distinction for dysphoria as compared to DASS and is similar to the result yielded by DMoA in detecting dysphoria. Thus, DMoA approach can be used as an alternative for early dysphoria detection to assist early intervention in identifying the patients' mental states. Subsequently, DMoA approach can be implemented as another possible solution for early detection of dysphoria thus providing an enhancement to the present NDS instruments providing psychologists and psychiatrists with a quantitative tool for better analysis of the patients' state.

1. Introduction

Stress is a condition experienced when an individual face a pressure or strain from adverse or demanding circumstances [1]. The individual life satisfaction is undermined when difficulties and challenges happen; ranging from the daily annoyances of the consequences of overstretched, time-pressured lifestyle such as traffic jams, lateness and work incompetency to the unexpected events faced in workplace, family lives, interpersonal relationship or even interaction with environment, such as road accident, bankruptcy, demise of a loved ones, loss of a pet or even handling natural disasters like flood or drought.

*Corresponding Author: Norhaslinda Kamaruddin, Advanced Analytics Engineering Centre, Universiti Teknologi MARA, Shah Alam, Selangor, Malaysia, norhaslinda@tmsk.uitm.edu.my, +603-55211163

Stress can cause positive reinforcement as it can be the source of motivation. For instance, healthy competition in workplace can boost morale of a worker to work harder and produced better results. However, if stress is not handled correctly, it can lead to other medical issues, such as; headaches, upset stomachs, anxiety, depression and other undesirable circumstances. [2]. Moreover, long term stress can contribute to other productivity issues, for example; high rate of absenteeism, high labour turnover, inefficient workforce and even high rate of accidents [3]. Hence, it is important to detect stress before it can be worse.

Generally, the number of individuals in every generation experienced stress level are increasing. This finding has been reported in a comprehensive study by American Psychological Association (APA) [4] with 23% and 37% are recorded for

millennials and older adults respectively from 2014 to 2017. The study segregated participants into four groups based on age, as follows; Millennials (18–38 years), Gen X-ers (39–52 years), Baby Boomers (53–71 years) and Older Adult (72 years and above). The survey was conducted online within the United States with participation of 3361 of adults. Figure 1(a)-(d) illustrate the American stress level by generations from 2014 till 2017.

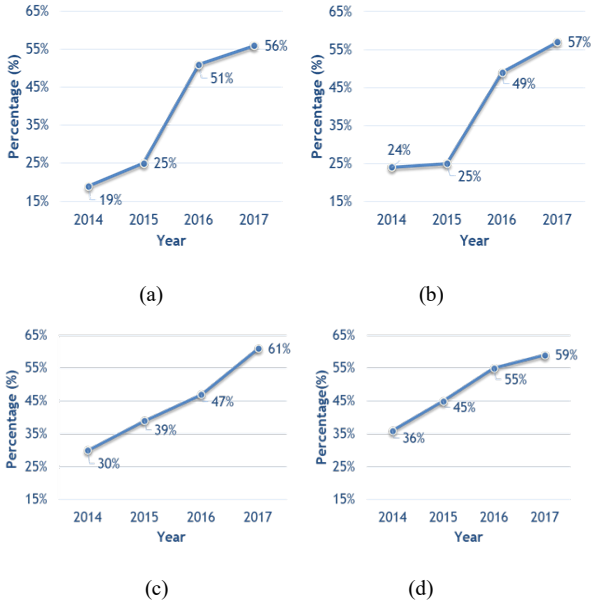

Figure 1: Graph of Stress Level Based on Generation. (a) Older Generation (b) Baby Boomers (c) Gen X-ers and (d) Millennials [4]

The survey results in Figure 1 show that higher number of younger generation experienced stress compared to Older Adult. Older Adults had the least stress levels as presented in Figure 1(a). Such trend is observed to be consistent from 2014 till 2017. This scenario may be linked to work stress as Older Adults typically have retired and are not formally working therefore their stress level is lower than younger generation who are still in employment. However, the highest change is observed in the year of 2015 to 2016 for Older Adults with 26% spike followed by 24% spike for Baby Boomers in the same duration as shown by Figure 1(b). This situation may be related to the United States Presidential Election that happened in 2016. The Baby Boomers and the Older Adults groups are highly affected as they are more in tune with the US political scenario as compared to the younger generations. Additionally, the survey revealed that a critical increment in the number of Americans who had encountered at least one symptom of stress in the previous month is observed from 71% in 2016 to 75% in 2017. Hence, the trend of stress experienced by individual is on the rise.

The finding by American Psychological Association [4] is consistent with the National Health and Morbidity Survey (NHMS) [5, 6] discovery that the trend of stress is rising, and it is reflected in the high leap of patients who suffer from mental illness as presented in Figure 2. In 2011, a total of 24,498 respondents were successfully interviewed and 6.3% reported to have mental health problem in Malaysia [5]. However, the NHMS V (2015-2018) survey [6] reported that 29.2% Malaysian adults aged 16 years and above in Malaysia experienced mental health problem. Such pattern shows a large increase over the last 4 years with almost four folds increment with factors such as younger Bumiputras female adult from low-income family is predicted to be at higher risk to experience mental health problem [5]. The report also mentioned that early recognition/detection and early treatment of depression must be enhanced.

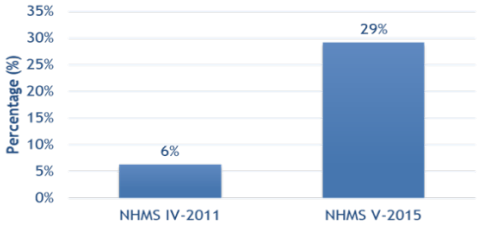

Figure 2: Mental Health Among Adult in Malaysia

Before an individual experienced stress, a state called dysphoria will be endured. Dysphoria can be defined as an emotional state with high degree of complexity and have a close relation to negative mood and in some cases can lead to frustration and dissatisfaction [7]. Dysphoria is usually connotated to anxiety, depression and stress, and can be experienced by any individuals at any time. Typically, dysphoria is viewed as everyday response once an individual face disappointment in his/her life. Figure 3 illustrates the simplified stages of mental cycle in handling disappointment [8]. Dysphoria is viewed as a starting point of either positive or negative adaptation states starting with normal condition to the circumstances when an individual faces a disappointment. When the individual cannot adapt to the dissatisfaction or disappointment, it can lead to dysphoria where the state of frustration is intense thus can lead to clinical depression or stress. On the other hand, the individual who is able to adjust and adapt to the disappointment may be able to carry out his life normally through adaptation. Since emotion indicates the mental state of an individual and is closely related to dysphoria emotion measurement methods is adopted [9]. Hence, the negative emotion that one experienced after disappointment can be empirically measured.

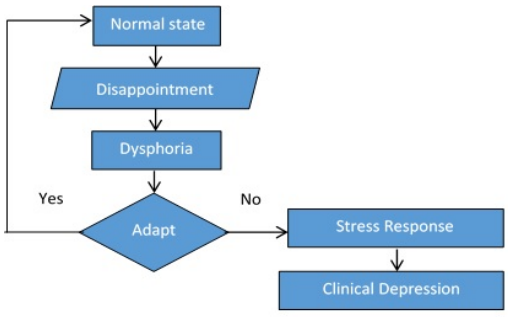

Figure 3: Mental cycle of handling disappointment

In this work, a Dysphoria Model of Affect approach is proposed to measure dysphoria from the brain signals captured using electroencephalogram (EEG) device. Such model can provide a datum for better comparative analysis with the standard psychological instruments to understand dysphoria such as DASS-21 and NDS-24 questionnaires. This is to eliminate the need to

validate the patient's answer by directly using neurophysiological input of the individual because patient have tendency to exaggerate or suppress the answers. Because dysphoria is very much related to negative emotion, emotion recognition methodology is adopted. For simplification, the working definition of dysphoria in this work is the state after disappointment of event that is prior to stress and it is always be associated with negative emotions [8].

This paper is organized in the following manner. Section literature review provides a summary of researchers concentrated efforts to recognize dysphoria and the fundamental concepts of dysphoria study are discussed. The methodology of the proposed approach of Dysphoria Model of Affect (DMoA) is presented in Section 3. The data collection, experimental result and discussion are given in Section 4. Subsequently, this paper concludes with conclusion and future work in Section 5. This paper is an extension of work originally presented in 2018 12th International Symposium on Medical Information and Communication Technology (ISMICT) [8].

2. Literature Review

2.1. Dysphoria and Psychological Instruments

Commonly, dysphoria is associated with depression, stress and anxiety [7,10,11,12]. Dysphoria is associated with depression because it shares the same features of depressive syndrome and dysphoric mood, such as sadness, despondence, despair, and others as suggested by [10]. Such notion is supported by Berner, Musalek & Walter [11] that the term dysphoria should be restricted to a condition of a morose, tense and irritated mood. It can also be recognized from stable and unstable mixed state. Moreover, anxiety may also refer to dysphoria because both have tension and the underlying hyperarousal in common. Dysphoria and anxiety can be experienced at the same time because dysphoria may happen due to long-standing stress. It is not uncommon for anxiety to arise on the background of dysphoric mood. In a certain personality disorder, dysphoria also can be incorporated such as affective instability, irritability, intense anger, and profound unhappiness [12]. These characteristics are shared or overlap with features of dysphoria. Furthermore, Starcevic et al. [7] stated that dysphoria is also associated with depression, interpersonal sensitivity, hostility and stress, reflecting broad but also complex and relatively non-specific relationship.

Dysphoria is assessed using several psychologists' instruments such as the Nepean Dysphoria Scale (NDS) [13], the Depression, Anxiety, Stress Scales (DASS) [14], the Beck Depression Inventory II (BDI II) [15], Perceived Stress Scale (PSS) [16], and the Anxiety Sensitivity Index (ASI) [17]. Typically, the participants are forced to select one answer from the fixed choice response format [18]. The participants need to respond to a series of standard measurement for attitude questions about a pre-determined topic that allow the degree of opinion rather than a simple yes and no answer. Such data enables better quantitative data analysis. The questionnaires can be provided to participants of either online or off-line dissemination method depending on the geographical availability of the participants. In summary, the PSS questionnaire is focusing on measuring the level of stress [16], the BDI-II can measure the level of depression [15] and the level of anxiety of an individual can be measured using the ASI instrument[17]. Based on the dysphoria descriptions that are being discussed earlier, dysphoria is very related to depression, anxiety and stress. All these factors can be measured using DASS [14] and NDS [13] questionnaire. It is expected to observe strong positive correlations between scores on the NDS and scores on the DASS-21. Hence, for the purpose of this work, both questionnaires are used to investigate dysphoria. The summary of the questionnaire and its focus is presented in Table 1.

Table 1: Summary of Questionnaire and Its Focus Study.

	DASS	PSS	BDI-II	ASI	NDS
Depression	√		√		√
Anxiety	√			√	√
Stress	√	√			√

The DASS-21 test is the psychological instrument to measure depression, anxiety and stress of an individual. It consists of 21 questionnaires and is able to measure the degree of depressions, anxiety and stress of the participant taking the test [14]. The participants are needed to specify indication of a symptom over the previous week based on a 4-point Likert scale. Each answer is recorded from 0 (did not apply to me at all over the last week) to 3 ('applied to me very much' or 'most of the time over the past week'). Calculation on the degree of depression (D), anxiety (A) and stress (S) is indicated is provided where every item of the questionnaire is related to either D, A or S score. The cumulative score of the D, A and S are used to indicate the level of severity, namely; normal, mild, moderate, severe and extremely severe. A trained psychologist or psychiatrist is needed to interpret the results and thus providing a more meaningful diagnostic for the patient.

The Nepean Dysphoria Scale (NDS) is a set of questionnaires to measure the severity of dysphoria [13] and expects participants to give evaluation of the frequency on a scale from 0 to 3 ranging from 'not at all', 'always', 'every day' to 'most of the time'. In this questionnaire, there are 4 factors that are being observed, namely; irritability, discontent, surrender and interpersonal resentment. Based on the summation of the score gathered from the itemized questions, the correlation matrix factor of NDS are calculated. The specified weightages are then used to get the maximum and average value of the scale. The value yielded are then compared to get the severity category of either normal, mild, moderate and severe.

2.2. Dysphoria and Negative Emotion

Dysphoria has recently been conceptualized as a complex emotional state that consists of discontent and/or unhappiness and a predominantly externalizing mode of coping with these feelings [7]. Many researchers relate dysphoria to negative emotions [10,11]. Dysphoria is also used as synonym for sadness or depression which describe a mixture of negative and unpleasant emotions [19].

A study by Caseras, Garner, Bradley and Mogg [20] examined the eye movement of the participants on negative images. The participants are grouped into dysphoric and nondysphoric group. In the experimental results, it was observed that dysphoric group have the tendency to look at the negative images longer than the control images as compared to the time taken by the nondysphoric

group. This result is in line with another work by McMakin, Santiago and Shirk [21] that observed the experiential reactivity to emotion in dynamic moment. Experimental results revealed that individual with dysphoric tendency and those who have not are equally responsive to both negative and positive film clips regardless of their dysphoric level. However, dysphoric group shows a lower ability to maintain positive emotion when they are looking at the positive film clips. Hence, it can be said that dysphoria is always associates with negative emotions.

The negative emotions are located in the negative valence axis region of Affective Space Model (ASM) [22]. The ASM consists of three main emotion primitives; namely: valance, arousal and dominance. The emotion primitives are actually the descriptive generic attributes of an emotion. These attributes function as constituents that act as a fully complementary description of the emotion. The affective space model can be divided into quadrants where each quadrant represents positive or negative value of the emotion primitives. The horizontal axis represents the valance value that indicates whether the emotion is perceived as positive or negative whereas the vertical axis representing the arousal which indicates the level of activation from passive to active. In this work, the focus is given on valence since valence is the effect of the emotion to an individual of either positive effect or otherwise. Figure 4 shows the Schlosberg's Model of Affect where dysphoria is labelled in pink rectangle in quadrant 2 and 3. Dysphoria happens at negative valance values regardless of its arousal of either active or passive.

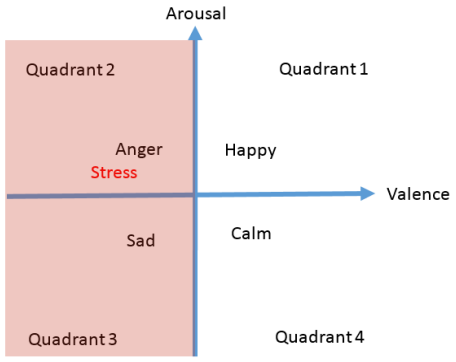

Figure 4: Model of Affect [22]

2.3. Dysphoria and Electroencephalogram (EEG)

Further reading shows that some researchers using EEG in dysphoria understanding. Siegle, Condray, Thase, Keshavan and Steinhauer [23] investigated the Gamma band in EEG signal in relating to emotional states for healthy, depressed and schizophrenia adults. The emotion condition assessment is using 3 methods; which are, never-depressed healthy controls, *Diagnostic and Statistical Manual of Mental Disorders* (DSM-IV) unipolar major depressive disorder and DSM-IV schizophrenia. During the assessment, the patients need to judge their own emotion of either positive, negative or neutral based on the words appearing on the screen of laptop. It is observed that depressed individual displayed both sustained and increased gamma-band EEG signals activity throughout the task while adults with schizophrenia displayed decreased gamma-band EEG signals activity. It is also observed that schizophrenia subjects displayed more affinity responses to negative word compared to neutral words and not significantly faster to positive than neutral words. Based on this study, it can be summarized that there are different responses towards negative words depending on either the patients suffer from schizophrenia or otherwise. Such responses can be monitored using the EEG signals produced by the depressed and schizophrenia groups.

From previous studies [7,8] it is noted that dysphoria is very much affiliated to negative emotions, thus it is proposed to use the electroencephalogram (EEG) in measuring the negative emotion of the individual and relate it the dysphoria. Lin et. al [24] applied machine learning algorithms to categorize EEG signals on emotional states during music listening. The main purpose of the research is to search emotion-specific features of the EEG signals and test the efficacy of different classifiers. The Valance-Arousal model is used as comparator of emotion. 26 subjects were instructed to keep their eyes closed and remain seated while listening to the sixteen excerpts from Oscar's film soundtracks and the EEG signals were recorded. Features are extracted using the Differential Asymmetry of 12 Electrode (DASM12), Rational Asymmetry of 12 Electrode (RASM12), Power Spectrum Density of 24 electrode (PSD24) and Power Spectrum Density of 30 electrode (PSD30) while Multi-Layer Perceptron (MLP) and Support Vector Machine (SVM) are used as classifier. As a result, SVM obtained an improvement classification performance from 81.52% ± 3.71% to 82.29% ± 3.06% compared to MLP classifier. The best result recorded were using DASMI12 using SVM as classifier. This study also concluded that the sensitivity metric for characterizing brain dynamic in response to emotional state (joy, angry, sadness and pleasure) are depending on the spectral power asymmetry across multiple frequency bands using DASM12.

Moreover, Sourina and Liu extended the work to recognize emotion from Fractal Dimension (FD) based algorithm using EEG signals [25]. The FD values are calculated from the EEG signal recorded from the corresponding brain lobes and mapped on the 2D emotion model. The International Affective Digitized Sounds (IADS) and music pieces labelled by other subjects with emotions using a questioner are used as stimuli to generate emotion to the subjects during the assessment. As a result, the FD were able to detect emotion with only using 3 electrodes and the data can be mapped into 2D Arousal–Valance model. The accuracy of 72% to 100% are recorded for arousal and valance level.

Based on the study of other researchers, we combine the understanding yielded from EEG emotion recognition and insights gathered from the DASS and NDS questionnaire to understand dysphoria. Figure 5 summarises the correlation between EEG, questionnaire and dysphoria.

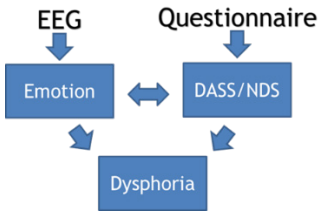

Figure 5: Overview of Correlations between DASS-21/NDS-24, Emotion and Dysphoria

3. Methodology

A theoretical framework of Dysphoria Model of Affect is presented in Figure 6. It consists of five phases, namely; data collection, pre-processing, feature extraction, classification and correlation analysis. Detailed description of each phase is presented in the next sub-sections.

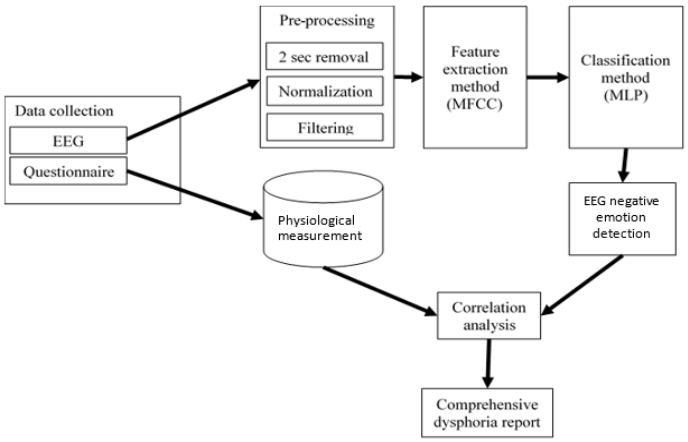

Figure 6: Theoretical Framework of Dysphoria Model of Affect (DMoA)

3.1. Data collection

In this preliminary work only four participants data were collected based on two type of inputs from the psychological instruments (DASS-21) and from the brainwave patterns using the captured EEG signals. The participants are healthy male with no medical record of experiencing acute depression, anxiety and stress with age mean of 27.5 years and variance of ±2.19 years. The participants also indicated that they are under the influence of medicine, drug or alcohol and voluntarily signed the consent form to adhere the IIUM ethic committee procedure.

Prior to taking the brainwave signal using the EEG device, all participants need to fill up two questionnaires namely; the personal information and also the DASS-21 questionnaires. This is to ensure that all four participants do not have any history of acute depression, stress or anxiety. Participants were first briefed about the experiments and were required to sign a consent form as needed by the IIUM ethics committee. To ensure consistency and to relate the study of psychological instruments to the brainwave patterns each individual was required to do the DASS-21 and the NDS-24 questionnaires prior to taking the individual brainwave pattern using the EEG device.

The DASS and NDS questionnaires results are gathered from each of all 4 subjects. The participants are asked to answer the questionnaire truthfully and to take their time to select the most appropriate answer for the questions. The participants can ask the meaning of the word in the questionnaire if they are unsure. This is to minimize misunderstanding that can lead to wrongly selected answer. The DASS questionnaire consists of 21 questions and the NDS questionnaire consists of 24 questions. The participants must answer all questions by selecting their choice in the questionnaire sheet. Once the participants finish answering the task, the questionnaire sheets are collected. Further analysis will be conducted based on the answers given by the participants.

In order to investigate the brainwave patterns signals recorded from the EEG device, the resting state of the participants need to be captured as a measurement basis. It consists of one minute of eyes close and eyes open. Then, it is followed with the reference emotion test based on the International Affective Pictures Systems (IAPS) [26] to analyse the responses of the different parts of the brain to four basic emotions of happiness, sadness, calmness and fear in one minute each respectively. In addition, sadness and fear video stimuli were presented to examine the negative emotion responses of each participant [8]. A final resting state data were collected based on a one minute each of eyes-open and eyes close after the video stimuli. The overall time taken for data collection in this work is 10 minutes without considering the pre-EEG experiment and post-EEG experiment tasks. Also note that all the EEG signals were captured and stored as numeric values to ensure compatibility of data using CSV file format. Table 2 shows the protocol that has been set for the data collection that consists of several condition which is resting state, emotional test and video stimuli.

Table 2: Protocol for EEG Experiment

Resting state (before)		Emotional test				Video stimuli		Resting state (after)	
Eye open 1minute	Eye close 1minute	Happy 1minute	Sad 1minute	Calm 1minute	Fear 1minute	Fear video 1minute	Sad video 1minute	Eye open 1minute	Eye close 1minute
2 minutes		4 minutes				2 minutes		2 minutes	

In the EEG data collection, the raw 19 channels EEG signals are captured using EEG device from BrainMarker. The device allows 19 channels EEG to be captured. However, in this work, only 6 channels are considered; namely, F3, F4, F7, F8, FP1 and FP2 to measure the negative emotion. These six channels are selected because signals from frontal brain are relevant to emotion processing according researchers [27, 28, 29] hence contains a lot of emotion information.

3.2. Pre-processing

Artifact and noise cancellation consist of three steps, namely; removing the first 2 seconds of the EEG signals, normalization and filtering. The pre-processing phase is important to ensure the analyzed data are in the region of interest and not biased or distorted by the effect of artifact and noise. Otherwise the data is regarded as inaccurate and misleading. The first 2 second of the 1-minute data of each protocol typically consists of 500 instances depending on the size of selected window size. The removal of this data is because it may not contain any useful information as the participant just starts to focus their attention to discriminate the emotion based on the presented stimuli. Then, the time vs frequency domain signals are then mapped into 19 channels to be extracted (19 channels x 14,500 instances). For the purpose of this study, only 6 channels data are considered to focus on the data of the brain frontal region.

The data from the 6 channels are normalized to [0,1] and filtered using the elliptical filter. The elliptical filters are employed to ensure to get the cut off frequency/clean signals before going

through feature extraction process. The EEG signals that are higher than 50Hz are also eliminated on the grounds that such data are usually artefacts gathered from various hand, eye and muscle movements.

3.3. Feature Extraction

Once the noise and artefacts are removed, relevant features are extracted for classification purposes. In this work, Mel Frequency Cepstral Coefficient (MFCC) feature extraction method is employed. In MFCC, window size and framing are two main components to observed. Windowing is a technique to cut the large signal into a manageable size for processing and analysis. Windowing is done for minimizing the disruptions at the starting and at the end of the frame, the frame and window function is being multiplied. If the window size selected is too large, the difference maybe too minimal for analysis whereas if the selected window size is too small, the information may not be enough for analysis. Frame is the process of dividing the signal in window into small frames to have reliable information. In the framing process, the raw EEG signals are blocked into small frames of N samples, with next frames separated by M samples (M<N) with this the adjacent frames are overlapped by N-M samples. This procedure of segregating up the signals into frames will proceed until the whole raw EEG signal is separated into small frames. Segregation of frame will make the computation more effective in term of time and processing. In this work, window type used is Hamming window with number of coefficients of 12 resulting to 12 features are extracted for each channel making it 72 features in total.

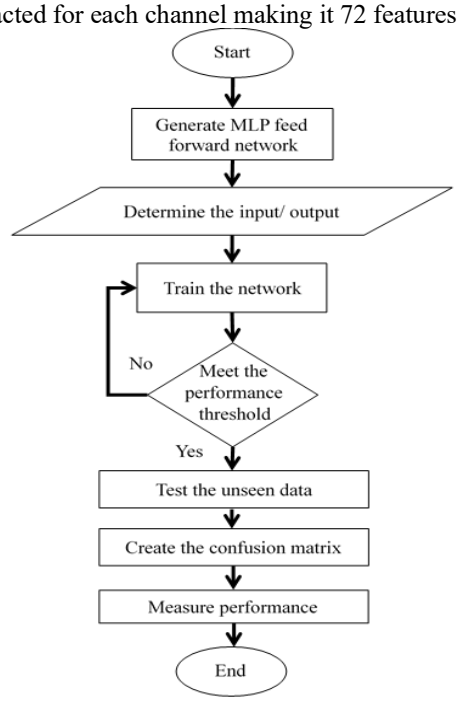

Figure 7: Flow Chart for Emotion Classification

3.4. Classification

Data are arranged according to the experimental set up needs after the relevant features are extracted. In this work, k-fold validation technique is adopted. The data are randomly partitioned into 5 groups where each approximately have an equal size. One group is used for testing while the other four groups are used for prior training. The process is iterated until all fold are used for testing.

In this work, Multi-Layer Perceptron classifier is adopted based on prior work findings [8,29]. The steps of using the MLP are simplified in the flowchart in Figure 7. Input are feed to the 72-neurons input layer before they are passed to the 10-neurons hidden layer. Then, the summation process is conducted in the output layer. The weights of the learning function of each node are iteratively improved until the performance threshold is met.

4. Result and Discussion

There are two types of experiment conducted in this work, namely; emotion recognition and emotion identification. For emotion recognition task, specific emotion is checked whether it is available or not. It is a 2-class classification task. Subsequently, the emotion identification task segregates the emotion individually and compare the intended emotion to the data pool.

4.1. Emotion Detection

The emotion detection experiment is conducted to discern the existence of specific emotion in a pool of instances. The data are arranged for two-class classification task, for instance; happy versus not happy, fear versus not fear, sad versus not sad and calm versus not calm. The emotion data consists of 67 instances and the data that opposed of the specific emotion are the combination of 1/3 of each other emotions. The total number of instances for the experiment is 134 instances. Features extracted are 72 instances gathered from 12 MFCC coefficients from the six EEG channels of F3, F4, F7, F8, FP1 and FP2. The average of the ten iterations of the experiments are presented in Figure 8(a)-(d). As a comparison, the results gathered from WEKA are also presented. Results from WEKA are used as the base result because the WEKA results are consistent. From the experimental results, it is observed that the result obtained from MLP from Matlab (denoted as MLP) gives higher accuracy as compared to WEKA with increment of 10% to 16% accuracy. The best performance was recorded by MLP for Happy vs Not Happy experiment from Subject4 with performance of 95.5%. The worst performance was recorded by Calm vs Not Calm for Subject3 with performance of 58.2%.

4.1. Emotion Identification

The emotion identification experiment is conducted to observe the ability of the classifier to predict the specific emotion given a pool of different emotion data. The data are arranged in such a way that all emotion has a similar number of instances (67 instances each) gathered from the frontal EEG signals of F3, F4, F7, F8, FP1 and FP2 for all participant. Table 3 shows the detailed MLP experimental result accuracy for emotion identification. Each experiment is repeated 10 times because the MLP performance in Matlab may have difference of ±10%.

From the result in Table 3, it is distinguished that the highest emotion identified is happy by Subject4 which achieved 97.01% accuracy. On the contrary, the lowest emotion identified is fear by Subject3 which yielded 11.94% accuracy. The result then is summarized as in Table 4. Subject4 managed to record the highest average performance for emotion identification whereas the worst

performance is yielded by Subject2 with accuracy of 64.51%. It is also observed that MLP managed to achieve accuracy ranging from 64.51% to 76.72% as compared to WEKA with accuracy ranging from 55.97% to 63.81% that show slight superiority of MLP as compared to WEKA.

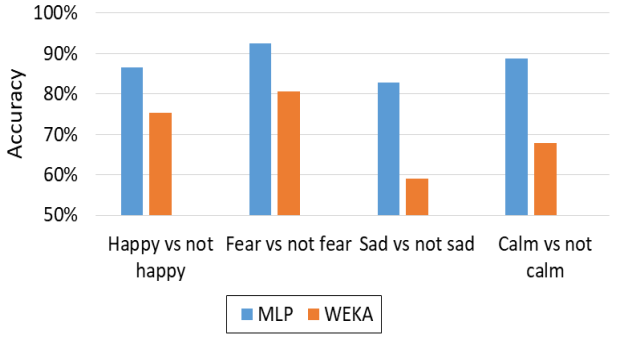

(a) Emotion Detection Result for Subject1

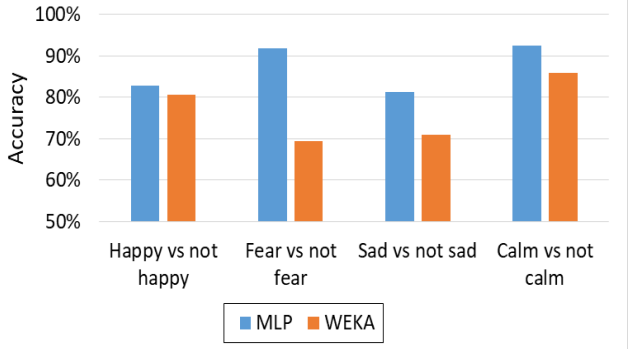

(b) Emotion Detection Result for Subject2

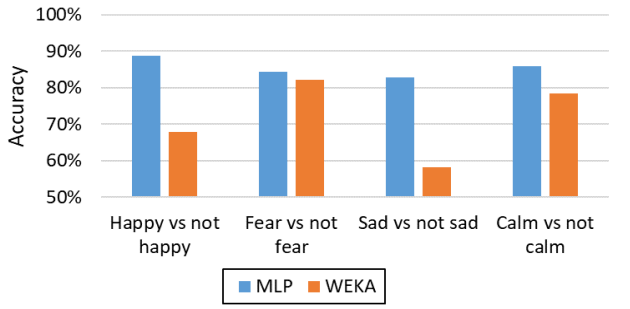

(c) Emotion Detection Result for Subject3

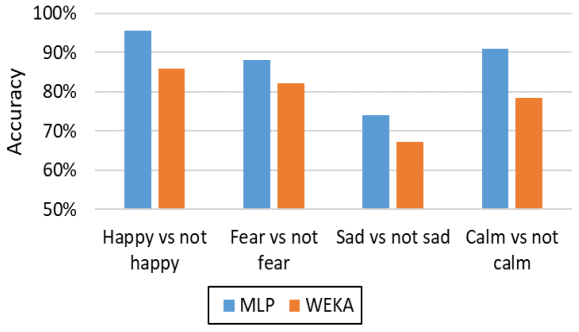

(d) Emotion Detection Result for Subject4

Figure 8: Emotion Detection Result using WEKA and MLP Classification

Table 3: Average Emotion Identification Results accuracy (%)

	Exp#1	Exp#2	Exp#3	Exp#4	Exp#5	Exp#6	Exp#7	Exp#8	Exp#9	Exp#10
Subject1	57.09	65.30	77.99	72.76	69.03	73.13	70.90	70.90	60.82	69.03
Subject2	52.99	77.61	83.58	69.40	82.84	84.33	72.01	79.10	85.45	79.85
Subject3	72.76	83.21	63.43	78.36	22.76	67.16	79.85	82.46	76.49	18.66
Subject4	86.94	61.19	72.76	70.15	73.13	54.10	70.90	68.66	74.63	68.28

Table 4: Summary of Emotion Identification Results

Participant	MLP Accuracy (%)	WEKA Accuracy (%)
Subject 1	68.69	55.97
Subject 2	76.72	63.06
Subject 3	64.51	60.45
Subject 4	70.07	63.81

4.2. Emotion Identification for Video Stimuli

Further analyses are conducted to see the difference in performance of using different media of stimuli, namely; static images and videos. For video stimuli, two videos of sad and fear videos are selected. Figure 9 and Figure 10 show the emotion identification experimental results for fear and sad videos respectively.

Figure 9 shows the bar chart of the experimental result yielded when using fear video. Based on the result, fear is consistently detected for Subject2, Subject3 and Subject4 with accuracy ranging from 33.1% to 37.1%. Subject1 recorded Calm as the highest emotion with difference of 3.5% lower than Fear. However, for the emotion experimental result Figure 10 shows the bar chart result for sad video using emotion identification network. Based on the bar chart, the highest emotion detected is fear in Subject4. Only Subject2 shows the highest sad emotion detected. This result shows inconsistency during video stimuli. This may due to the surrounding when eye open, the information enters through the eye in form of light. This information will react to the brain for visual perception.

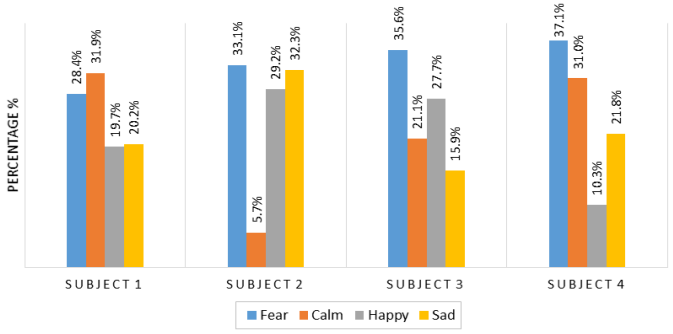

Figure 9: Emotion Identification Result using Fear Video

Extension of the comparison between the effect of emotion elicitation using dynamic emotional contents (video) and static images emotional contents (IAPS) are conducted. Figure 11(a)-(d) show the comparative accuracy of emotion recognition experiments between static images and videos for each subject.

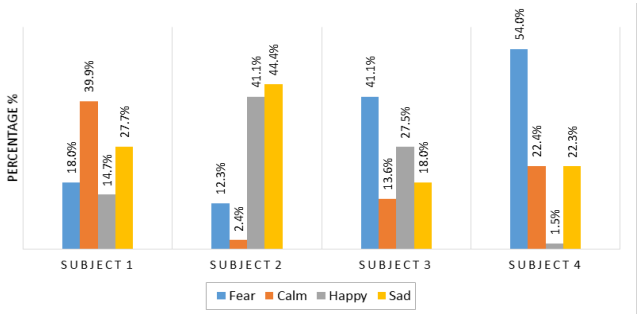

Figure 10: Emotion Identification Result using Sad Video

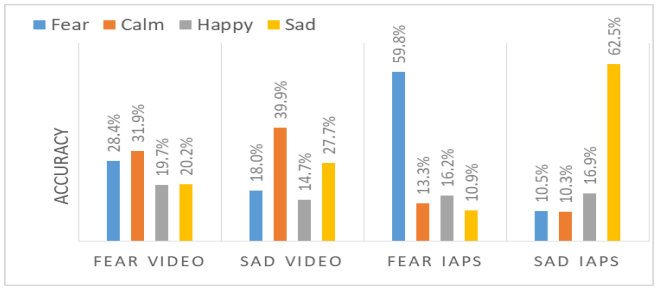

(a)

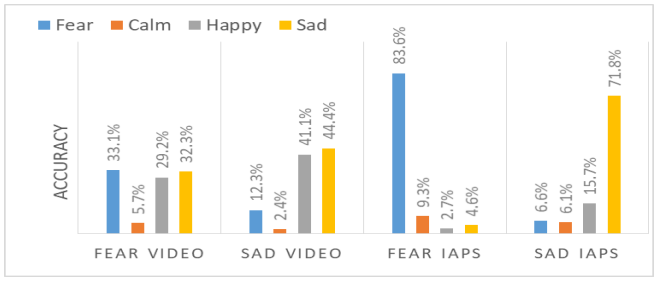

(b)

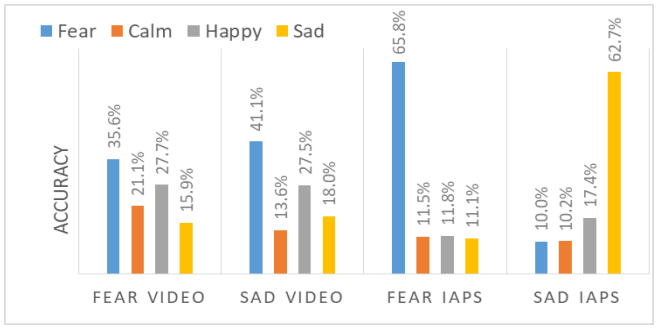

(c)

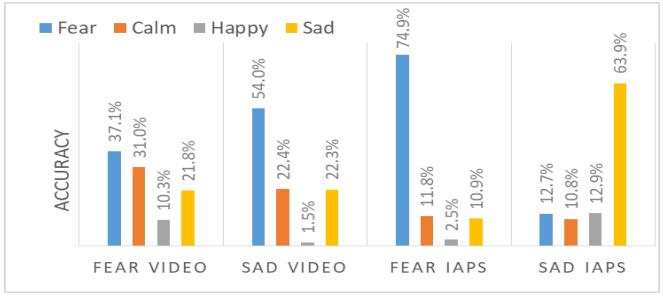

(d)

Figure 11: Result Comparison for Emotion Identification Result using Static Images and Videos for (a) Subject1 (b) Subject2 (c) Subject3 and (d) Subject4.

From the experimental results in Figure 11, the emotion identification result using static emotional contents outperformed the dynamic emotional content in all experiments. The highest accuracy achieved is fear IAPS with 83.6% for Subject2. Meanwhile the lowest accuracy is sad video for Subject4 with 1.5%. This is because the brain needs to process more information when video stimuli is exhibited instead of static images displayed in IAPS stimuli. Hence, lower performance is recorded.

4.3. Questionnaire result: DASS-21 & NDS-24

Table 5 and 6 shows the summary result of the DASS-21 and NDS-24 results respectively for all subjects. According to the depression, anxiety and stress score scale, all participants are in a normal condition. None any of them shows any negative result. However, in Table 6, Subject1 and Subject2 results indicated that they are in mild state as compared to Subject4 that recorded moderate and severe for Subject3 respectively. This result gives better insight as compared to the DASS-21 results that only indicate the participants are normal. Hence, the NDS is able to give more information about the participants' state as compared to the DASS-21 questionnaire and the DASS-21 questionnaire cannot be directly used to determine whether the subject is having dysphoria or otherwise.

Subject	DASS-21 score			Result
	Depression	Anxiety	Stress	
1	2	6	6	Normal
2	2	2	10	Normal
3	2	4	8	Normal
4	2	6	8	Normal

	Total factor Subject1	Total factor Subject2	Total factor Subject 3	Total factor Subject4
Irritability	10.8	8.68	23.2	15.2
Discontent	6.91	5.41	18.3	12.34
Surrender	5.98	5.07	12.9	8.284
Interpersonal resentment	3.41	2.14	7.39	4.55
Result	**Mild**	**Mild**	**Severe**	**Moderate**

4.4. Correlation between DASS-21, NDS-24 & EEG emotion identification

From the emotion identification experiments as in Table 7, fear is highly detected during the eye close which is in line with NDS-24 result that is severe for Subject3. There seems to be correlation between EEG emotion identification and NDS-24. However, it is not highly observable on Subject 1, 2 and 4 because NDS-24 result for each subject is only mild and moderate.

Table 7: Eye Close and Eye Open Before Experiment Training with Emotion Identification MLP Architecture

	Emotion	Before stimuli		After stimuli	
		Eye close	Eye open	Eye close	Eye open
Subject 1	fear	37.5%	43.0%	22.4%	43.0%
	calm	35.1%	25.1%	34.6%	25.1%
	happy	15.7%	24.8%	17.8%	24.8%
	sad	11.8%	7.2%	25.2%	7.2%
Subject 2	fear	41.5%	17.9%	1.2%	17.9%
	calm	10.9%	11.0%	5.4%	11.0%
	happy	31.4%	33.9%	52.0%	33.9%
	sad	16.3%	37.2%	41.5%	37.2%
Subject 3	fear	70.9%	12.2%	75.7%	12.2%
	calm	20.0%	16.4%	9.7%	16.4%
	happy	4.0%	45.7%	5.4%	45.7%
	sad	5.1%	25.7%	9.3%	25.7%
Subject 4	fear	26.4%	49.4%	1.0%	49.4%
	calm	19.6%	18.1%	16.9%	18.1%
	happy	46.3%	27.9%	76.9%	27.9%
	sad	7.8%	4.6%	5.2%	4.6%

5. Conclusion

The Dysphoria Model of Affect (DmoA) uses the neurophysiological data from the EEG devices and by extracting the emotional information from the brainwave patterns different emotions can be detected during the initial state of eyes closed. Such information are very useful in analyzing the mental state of an individual. In this preliminary study, the implementation of DmoA seems to be able to differentiate different classes of emotion fairly well thus resulting in a better tool for early detection of dysphoria as depicted by the NDS-24 results for Subject3. It is also observed that the DASS-21 questionnaire result could not differentiate dysphoria for all the subjects in this work. There are other psychological instruments that can be studied for detail analysis of dyphoria but would be expensive and require experts to interpret score. The proposed DMoA approach provides a new avenue for psychologist and psychiatrist to venture using EEG devices as tools for analyzing dysphoria, depression, anxiety and stress and can also be used in understanding personality traits or behaviour [29].

Acknowledgment

The authors would like to thank MARA University of Technology, Malaysia (UiTM) and Ministry of Education Malaysia (KPM) for providing financial support through the Fundamental Research Grant Scheme FRGS (600 – RMI / FRGS 5/3 (106/2014)) to conduct the work published in this paper.

References

[1] Kranner, I., Minibayeva, F. V., Beckett, R. P. & Seal, C. E. (2010). What is Stress? Concepts, definitions, and applications in seed science. *New Phytologist*. 188: 655–673.

[2] Edwards, J. (2015). *Fundamental facts about mental health 2015*, Mental Health Foundation, United Kingdom

[3] Mallow M. S. (2016). Occupational Stress in Malaysia: Causes, Effects and Possible Solutions, In Proceedings of 3rd International Conference on Education, Social Sciences and Humanities (SOCIOINT 2016), 82-88, Istanbul, Turkey.

[4] Poll H., American Psychological Association (APA) (2017). Stress in America: The state of our nation. Stress in America Survey.

[5] Institute of Public Health (IPH), National Health and Morbidity Survey (2011). NHMS 2011, Vol. II: Non-communicable diseases, Ministry of Health Malaysia, ISBN: 978-967-3887-68-2.

[6] Institute of Public Health (IPH), National Health and Morbidity Survey (2015). NHMS 2015, Vol II: Non communicable diseases, risk factors and other health problems, Ministry of Health Malaysia, ISBN: 978-983-2387-23-7.

[7] Starcevic, V., Berle, D., Viswasam, K., Hannan, A., Milicevic, D., Brakoulias, V., Dale, E. (2015). Specificity of the Relationships between Dysphoria and Related Constructs in an Outpatient Sample, *Psychiatr Q*, Vol 86: 459–469

[8] Kamaruddin, N., Nasir, M. H. M. and Wahab, A. (2018). EEG Affective Modelling for Dysphoria Understanding. *In 2018 12th International Symposium on Medical Information and Communication Technology (ISMICT)*, 1-6.

[9] Kamaruddin, N., Wahab, A. & Quek, C. (2012). Cultural Dependency Analysis for Understanding Speech Emotion, *Expert System with Application (ESWA)*, 39(5): 5115-5133.

[10] Snaith, R. P., & Taylor, C. M. (1985). Irritability: definition, assessment and associated factors, *The British Journal of Psychiatry*, 147(2), 127-136

[11] Berner. P., Musalek. M., Walter H. (1987) Psychopathological Concepts of Dysphoria. *Psychopathology*, 20:93–100

[12] Starcevic, V. (2007). Dysphoric about dysphoria: towards a greater conceptual clarity of the term, *Australasian Psychiatry*, Vol 15(1): 9 -12.

[13] Berle, D. & Starcevic V. (2012). Preliminary validation of the Nepean Dysphoria Scale, *Australasian Psychiatry,* 20(4) 322–326.

[14] Lovibond, P.F. & Lovibond, S.H. (1995). The structure of negative emotional states: Comparison of the Depression Anxiety Stress Scales (DASS) with the Beck Depression and Anxiety Inventories. *Behaviour Research and Therapy*, 33, 335-343.

[15] Beck, A. T., Steer, R. A. & Brown, G. K. (1996). Beck Depression Inventory manual 2nd ed San Antonio: Psychological Corporation.

[16] Cohen D., Kamarck T., & Mermelstein R. (1983). A global measure of perceived stress, *Journal of Health and Social Behavior*, 24: 386-396.

[17] Reiss, S., Peterson, R. A., Gursky, D. M. (1986). Anxiety sensitivity, anxiety frequency and the prediction of fearfulness. *Behav Res Ther*, 24: 1–8.

[18] Likert, R. (1932). A technique for the measurement of attitudes, *Archives of Psychology*, 140: 1–55.

[19] D'Agostino, A., Manganelli, E., Aportone, A., Monti, M. R., Starcevic V. (2016). Development, cross-cultural adaptation process and preliminary validation of the Italian version of the Nepean Dysphoria Scale, *Journal of Psychopathology*, 22: 149-156

[20] Caseras, X., Garner, M., Bradley, B. P., & Mogg, K. (2007). Biases in visual orienting to negative and positive scenes in dysphoria: An eye movement study. *Journal of Abnormal Psychology*, 116(3), 491.

[21] McMakin, D. L., Santiago, C. D., & Shirk, S. R. (2009). The time course of positive and negative emotion in dysphoria. *The Journal of Positive Psychology*, 4(2), 182-192.

[22] Schlosberg, H. (1954). Three Dimensions of Emotion. *Psychological Review*, 61(2), 81-88.

[23] Siegle G. J., Condray R., Thase M. E., Keshavan M. & Steinhauer S. R. (2010), Sustained gamma-band EEG following negative words in depression and schizophrenia, *International Journal of Psychophysiology*, 75 : 107–118.

[24] Lin, Y. P., Wang, C. H., Jung, T. P., Wu, T. L., Jeng, S. K., Duann, J. R. & Chen, J. H. (2010), EEG-based emotion recognition in music listening, *IEEE transactions on biomedical engineering*, Vol. 57(7).

[25] Sourina, O. & Liu, Y. (2014). A fractal-based algorithm of emotion recognition from EEG using arousal-valence model*, IEEE international conference on systems, man, and cybernetics.*

[26] Lang, P. J., Bradley, M. M. & Cuthbert, B. N. (1999). International Affective Picture System (IAPS): Technical Manual and Affective Ratings, University of Florida, Center for Research in Psychophysiology, Gainesville

[27] Cacioppo, J. T. (2004). Feelings and Emotions: Roles for Electrophysiological Markers, *Biological Psychology*, Vol. 67(1): 235-243.

[28] Asakawa, T., Hayashi, T. & Mizuno-Matsumoto, Y. (2014). Coherence Analysis of EEG under Emotional Stimuli Related to Mental States. *Electronics and Communications in Japan*, Vol. 97(8): 14-23.

[29] Wahab, A., Kamaruddin, N., Palaniappan, L. K., Li, M., & Khosrowabadi, R. (2010). EEG signals for emotion recognition. *Journal of Computational Methods in Sciences and Engineering*, 10(s1), 1-11.

ASTES

Advances in Science, Technology and Engineering Systems Journal Vol. 4, No. 4, 206-211 (2019)

www.astesj.com

ASTESJ

ISSN: 2415-6698

Predictive Modelling of Student Dropout Using Ensemble Classifier Method in Higher Education

Nindhia Hutagaol*, Suharjito

Computer Science Department, Binus Graduate Program – Master of Computer Science, Bina Nusantara University, Jakarta, Indonesia 11480

A R T I C L E I N F O

Article history:
Received: 15 May, 2019
Accepted: 06 June, 2019
Online :30 July, 2019

Keywords:
machine learning
prediction modeling
dropout
ensemble classifier method

A B S T R A C T

Currently, one of the challenges of educational institutions is drop-out student issues. Several factors have been found and determined potentially capable to stimulate dropouts. Many researchers have been applied data mining methods to analyze, predict dropout students and also optimize finding dropout variables in advance. The main objective of this study is to find the best modeling solution in identifying dropout student predictors from 17432 student data of a private university in Jakarta. We also analyze and measure the correlation between demographic indicators and academic performance to predict student dropout using three single classifiers, K-Nearest Neighbor (KNN), Naïve Bayes (NB) and Decision Tree (DT). We found indicators such as student's attendance, homework-grade, mid-test grade, and finals-test grade, total credit, GPA, student's area, parent's income, parent's education level, gender and age as student's dropout predictors. The results only get 64.29 (NB), 64.84% (DT), and 75.27%(KNN) while we tried to combine algorithms with Ensemble Classifier Methods using Gradient Boosting as meta-classifier and gets better about 79.12%. In addition, we also get the best accuracy of about 98.82% using this method which was tested by 10-fold cross-validation.

1. Introduction

Higher education tends to be a benchmark to define student education quality as a human resource. In general, higher education is considered as a reputable institute if students are qualified in their fields and get good achievements. Conversely, student's failure will impact negatively on students and universities. At present, the problem of student failure is known as an ongoing university challenges to investigate many factors that trigger the dropout, such as academic performance, demographic, financial support, and student behavior and etc. Dropout is determined as a consequence for students who cannot complete their education until the specified study period. It makes students' skills and ability of dropout students in their fields less than student retention and significantly affects institution quality [1].

Drop out is not a novelty thing but still being a serious topic which attracts researchers' attention due to its impact on decreasing higher education values and can be an adverse impact on the social environment, where other prospective students lose their opportunity to study in higher education. In the last 10 years, many research has been carried out by utilizing technology to find ways how to prevent dropout issues, which is called Education Data Mining [2]. Educational Data Mining (EDM) represents a variety of algorithmic methods to address various problems in the educational system and even generates new knowledge, to calculate student's academic performance, predict student's behavioral and especially to predict variables or indicators that influence dropout in higher education [3].

Some indicators are widely used by researchers to predict dropouts, such as cumulative grade point average (CGPA), internal assessment, student demographics, external assessment, extra-curricular activities, high school background, and social interaction network [4]. The most potentials variables are the cumulative grade point average (CGPA) and internal evaluation indicators because its value maximizes the measurement of the student's skills in present and future. [5] In the first two years of study, demographic indicators, especially gender were also influence learning qualities, not only occur on conventional higher education but also online program students. Dropout possibilities are also caused by age, financial constraints, student absence, parental influence, employment opportunities, marital status [6] [7].

In Indonesia, based on data statistics in 2017 [8], the dropout rate in higher education approximately about 195,176 students.

*Nindhia Hutagaol, Email: nindhia.hutagaol001@binus.ac.id

Data shows dropout students' percentage at private universities is greater than public universities. A related work in [9], 799 dropout students at educational institutions in Jakarta was examined and found dropouts usually occur in people aged 12 to 19 years who come from suburban and rural areas with a low average economic background. Low economic indicators trigger students to choose to get a job than continuing their studies in higher education. Another similar study as shown in [10], variable age and study program are also correlated to decide dropout students through the first-year study.

The main objective of this study is to find the best modeling solution in identifying dropout student indicators especially in the first two years of the study period. We will use student data from the Faculty of Social and Political Science in one of a private university in Jakarta and measure how many demographic data had a significant influence on student dropout predictions. In this major, students tend to leave study until dropout or expelled in the first trimester. This study will focus on the demographic and academic indicator and propose a predictive modeling concept by combine Decision Tree, K-Nearest Neighbor and Naïve Bayes which are widely used as statistical models to predict dropout students and optimize results using Ensemble Classification Method. The remainder of the paper is organized as follows. In Section 2, we review previous studies on the various prediction modelling in education field and also educational data mining research. Section 3 explains our research method to find classification techniques to find student dropout predictors. Section 4 presents a discussion of the results includes the evaluation of the Ensemble Classification Method as compared to several Decision Tree, K-Nearest Neighbor and Naïve Bayes methods. Section 5 concludes the study.

2. Literature Review

Educational Data Mining (EDM) is an interdisciplinary area which related to methods development to investigate a variety of unique data in the education area, which aims to understand the student's needs and determine properly learning methods [11]. Generally, EDM is applied to predict problems in order to improve the quality both of student performance, and teaching-learning process [12]. Its concerns about how to adapt data mining methods and find patterns that are generally very difficult to solve because of massive data in the educational dataset [13]. Data mining, as a decision-making standard, has been helped in discovering dataset with different approaches such as statistical models, mathematical methods, and also machine learning algorithms [14].

Based on a review in paper [4] some theoretical algorithms are carried out to predict student performance. In her work, she found and compare accuracy between Naïve Bayes, Neural Network and Decision Tree to predict CGPA, the students' demographics, high school, study and social network attributes as the most critical factor student passed or failed studies. Naïve Bayes has better accuracy because of attributes more significant to predict than Neural Network and Decision Tree. Another study, paper [15] compares various and appropriate data mining methods for classification in prediction, specifically to determine dominant factors in student performance predictions. It shows predictive results of Random Forest and J48 generate classification model and find the most significant factor as a determinant on student's attainment, such as study time, academic year, age and parent education.

To identify dropout, this paper [16] have been used Artificial Neural Network, Decision Tree, and Bayesian Network to explore great potential factor. Conducting empirical research on a dataset of 3.59 million student data in an online training program, Tan discovered two attribute variables as test inputs, that is, student characteristics and academic performance. As a result, the Decision Tree algorithm was more precise to prove those variables are effectively used as key factors in student dropout prediction. As shown in this study [13], Marquez proposed a new method to optimize accuracy predictive modeling, called Modified Interpretable Classification Rule Mining. Marquez held an experiment in 419 schools to find the student dropout factors. The evaluation was performed in six phases using 60 different variables from 670 students. It results in Modified Classification Rule Mining more accurate than JRip.

Currently, predictive modeling challenges are efficiency and accuracy of various prediction models which are generally due to inadequate variables with the base classifier. Related work in [17], Decision Tree, Naïve Bayes, KNN, and Artificial Neural Network applied to generate predictive student dropout model and adopt ensemble clustering on student's demographic detail, academic performance, and enrollment record. Experiment verified ensemble method which is used to transform original data to a new form can increase the accuracy of prediction models. Another similar study as shown in [18] discussed and examined the ensemble method able to reduce error and increase student performance prediction accuracy.

After reviewing background research, predictive modeling method has weakness in some way depend on attributes. In such conditions, accuracy may be misleading if we only have small attributes and data. In this study, we will compare Decision Tree, K-Nearest Neighbor, and Naïve Bayes and combine those methods to find the correlation between demographic and academic performance variables in dropout prediction. We will adopt an ensemble method to optimize accuracy results and also use Confusion Matrix to evaluate models.

2.1. Classification Methods

Decision Tree (DT) widely known as a popular and interesting machine learning algorithm, especially in classification. It can generate or measure pattern using a tree-structured rule and describes the relationship between variables by recursively partitioning inputs into two parts. Each part forms the decision node that is linked by a branch from the root node to the leaf node [19] [20]. In data mining, several well-known decision three algorithms, namely ID3, C4.5, CART, J48, and CHAID. In this study, the CART algorithm is used to generate models.

The k-Nearest Neighbor (k-NN) is a simple classification method that is measured based on the majority vote of its neighbors [21]. The best choice of k depends upon the data; generally, larger values of k reduce the effect of noise on the classification but make boundaries between classes less distinct. However, this method has a weakness with the presence of noisy or irrelevant features, or if the feature scales are not consistent with its importance in modeling.

Naïve Bayes as a simple probabilistic classifier can be developed easily on a large amount of data because it does not need complex parameter estimation which makes it outperform over another sophisticated method [2]. Naïve Bayes was also able to learn conditional probability feature separately so it also has been very effective in classifying small datasets. In this study, Bayes' theorem is used to predict probability dropout.

2.2. Ensemble Classifier Method

Ensemble method is a modeling concept with multiple learners to resolve problems which called base learners. It constructs and combines a set of hypotheses to fix weakness of training data using single-learners approach [22]. We also can find solutions and collect and combine a set hypothesis from big chance hypotheses into one single prediction. As known as Importance Sampling Learning Ensembles (ISLE) framework, it shows four classic ensemble methods, namely Bagging, Random Forest, Boosting (AdaBoost) and Gradient Boosting.

This method consists of several approaches commonly used in classification to construct models that are several approaches can be used to bagging, boosting and stacking. Based on this paper [17] [18] which has been successfully used stacking approaches (stacked generalization), this study will use Gradient Boosting as an ensemble classifier and do different things to reduce error and optimize accuracy finding.

3. Research Method

The stages of this study are four-fold as shown in Figure 1. Step 1, extract variable data related to student dropouts from Academic Information System of educational institutions, construct the training data set and do feature selection using Ensemble Bagging Tree method to get the best-correlated attribute to predict dropout. Step 2, use the data to train the prediction models that were constructed based on machine learning methods such as the Artificial Neural Network (ANN), Decision Tree (DT) and Bayesian Network (BN) to derive the samples of the prediction model. Step 3, extract another section of data as a testing data set and feed it into the actual samples of the prediction model previously generated. Step 4, apply ensemble-Decision Tree to optimize and evaluate predictive modeling accuracy of student dropout.

3.1. Data Preparation

This study used the dataset of 17.432 of student's data from the Academic Information System in Christian University of Indonesia. Sample data in this study are comprised of relevant information from students enrolled in the Faculty of Social and Political Science from 2016-2018. This dataset was purposed for classifying higher education students that potentially dropout according to academic performance. As identified from the dataset, there was a total of 17 variables associated with student's demographic data (Table 1). The first stage of data pre-processing is handling 2355 missing data by imputing relevant value and transform all values into numerical variables in order to improve the accuracy of prediction based on the algorithm's requirement.

Table 1: The attributes of Datasets

Type Variable	Variable	Description
Demographic	school.area	location student's school (urban =101, suburban =102)
	gender	student's gender (male =11, female =12)
	age	student's age (numeric)
	work.status	student's occupation (work =1, no occupation = 2)
	marital.status	student's marital status (single =110, married = 120)
	parent.education	student's parent education (no education = 0, primary school = 1, secondary school = 2, high school = 3, diploma = 4, bachelor = 5, master = 6, doctoral = 7)
	parent's income	parent's income
Academic Performance	GPA	student's grade point average (0 – 4)
	homework	homework grade (0-100)
	final.test	final test grade (0-100)
	mid.test	mid-test grade (0-100)
	student.status	student status (no dropout=0, dropout=1)
	attendance.percentage	attendance percentage (1-100)
	total.credit	total credit (1-145)

A first glimpse at the data reveals that 13856 of the data indicated students were able to successfully finish their studies, while 607 data of dropout students have been observed as dropout students. There is a big difference ratio between dropout class and retained class.

In order to tackle this problem, we do partition data into 70% training dataset and 30% testing dataset and use Synthetic Minority over-sampling Technique (SMOTE) to synthetically resampled training dataset. This method can help to improve training datasets to be optimally used in classification performance [23]. Next stage, we use algorithm Learning Vector Quantization to do feature selection with 1700 balanced data on the training dataset and performed 10-fold cross-validation with 3 repetitions to reduce bias induced by sample selection. It combines clustering and classification processes based on feed forward neural network. Inputs are propagated through a variable number of hidden layers to the output nodes.

In terms of data processing, the feature selection is the necessary steps to do because machine learning can understand data and improve prediction performance if the prediction modeling used a set of properly features. In order to select features, we use the Learning Vector Quantization algorithm to prepare some vectors in the domain of observed data samples in order to be used to classify any of the hidden vectors that are unseen. As we figured out from Figure 2, it represents the attributes selection refers to the importance level of each attribute on the dependent variable. In the feature selection process, the training process is carried out and tested using 10-fold cross-validation. It aims to calculate and measure the importance feature values based on two variables distances which are identified near or close to the variable target.

The best accuracy of this selection process is 0.9757 using the value k = 6.

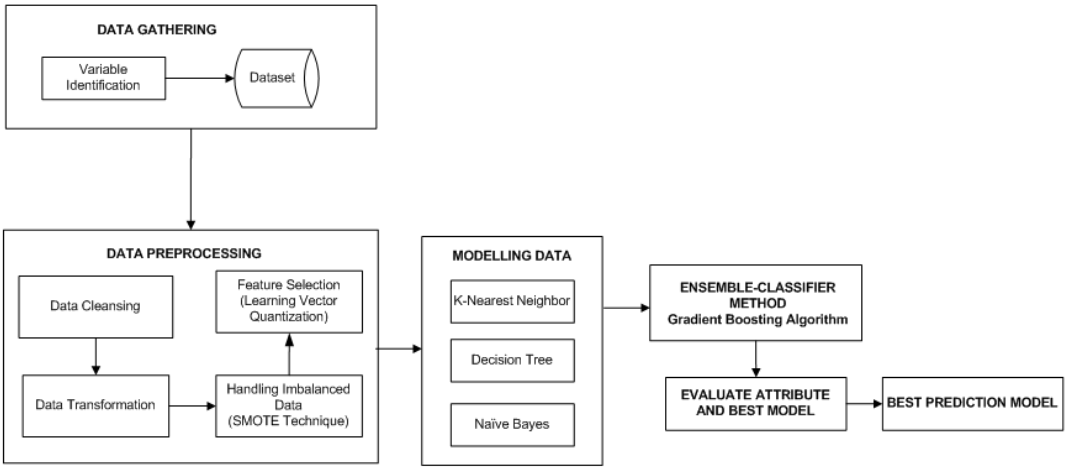

Figure 1. Research Method

The results of feature selection carried out on training data, two features of 13 variable input, including work status and marital status eliminated from the dataset.

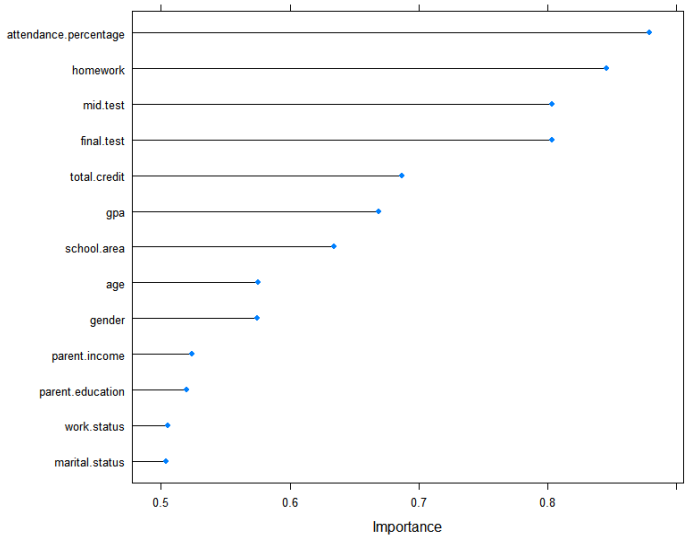

Figure 2: Feature Selection Based on Importance Score

As shown in Table. 2, the features are sorted according to importance score obtained using the Learning Vector Quantization (LVQ) technique and decide to select feature with a score greater than 50%.

Table 2. Variable Importance Value

Variable	Importance value
attendance.percentage	0.8793
homework	0.8454
mid.test	0.8033
final.test	0.8033
total.credit	0.6870
gpa	0.6691
school.area	0.6341
age	0.5752
gender	0.5747
parent.income	0.5242
parent.education	0.5195
work.status	0.5053
marital.status	0.5035

3.2. Confusion Matrix

For evaluation, we use confusion matrix to measure classifier's accuracy that is the ratio between correctly predicted results and the total number of samples. In this study, we will measure the precision rate, accuracy rate, sensitivity, and specificity.

Table 3: Confusion Matrix

		Observation Value	
		Predicted Object (Y)	**Predicted non-Object (N)**
Expectation Value	**Actual Object (Y)**	True Positive	False Positive
	Actual non-Object (N)	False Negative	True Negative

True positive (TP) is the number of students classified as dropout students, false negative (FN) value is the number of non-dropout students classified as dropout students, true negative (TN) value is the number of non-dropout students classified as non-dropout students, false positive (FP) is the number of dropout students classified as non-dropout students. Standard formula to calculate the precision rate, accuracy rate, sensitivity, and specificity defined based on confusion matrix as shown in Eq. 1-4.

$$\textbf{Precision Rate} = \frac{TP}{(TP + FP)} \quad (1)$$

$$\textbf{Accuracy Rate} = \frac{(TP + TN)}{(TP + FP + TN + FN)} \quad (2)$$

$$\textbf{Sensitivity} = \frac{TP}{(TP + FN)} \quad (3)$$

$$\textbf{Specificity} = \frac{TN}{(TN + FP)} \quad (4)$$

4. Result and Discussion

In this study, we use R language and R software package (version 1.2.13) to analyze data with several machine learning methods. First of all, we do the data cleaning process such as handling missing values in the dataset and facilitate dataset with the appropriate attributes. In this case, 2,355 rows of missing values of 'student's attendance' variable and 1221 rows of 'final-

test grade' variable have values less than zero -which are not relevant to the other variables value- were eliminated from the dataset. Next, we tested normalization or data distribution in order to determine whether data distribution was normal or balanced and also will help to minimize prediction error results during the modeling process. Furthermore, impute value technique is applied to the filled missing value in parent's income feature with its mean values in order to minimize bias in the dataset. Finally, we get 13856 data with 11 variables as variable input from the data cleaning process.

Based on distribution data, 66% of student's data was dominated by women while men were only 34% of total data. Every student generally comes from an urban area (87%), which means most students come from urban areas while the percentage of students from suburban areas are relatively small. In addition, 95% of students are dominantly 18-23 years old while others are over 23 years old. In this case, work status is not determined as predictors because its correlation is relatively small about 250 students which are only 2% of all student's data. The dataset also shown that almost 100% of students are single with the majority parent's education were 'high school' and 'undergraduate' level with parents financial is predominantly low that is less than IDR 5000000. These data distribution, especially demographic features, describe that dataset has a fairly good variation to be used during student dropout prediction.

By using 9700 training data, we demonstrated also compared and discussed 3 different common classifiers performance, which is K-Nearest Neighbor (KNN), Decision Tree (DT), and Naıve Bayes (NB) as shown in Table 4 and Table 5.

Table 4: Comparison Prediction Results

Predictive / Actual	KNN		DT - CART		NB	
	Retention	Dropout	Retention	Dropout	Retention	Dropout
Retention	3951	52	3963	76	3966	65
Dropout	23	130	11	106	8	117
Total	3974	182	3974	182	3974	182

The first prediction modeling was carried out using the K-Nearest Neighbor method. The specified k-value was used with k = 5, k = 7, k = 9, and k = 11. Its best k-value was k=5 which predict with accuracy rate about 0.9820 and recall rate of prediction was 0.8497. Next prediction model, we use the Decision Tree CART method and obtain prediction accuracy about 0.9791 and recall rate of prediction of 0.9060.

Table 5: Evaluation of Prediction Results

Evaluation Index	KNN	DT - CART	NB
Accuracy Rate	0.9820	0.9791	0.9824
Precision Rate of Retained Class	0.9942	0.9972	0.9980
Precision rate of Dropout Class	0.7143	0.5824	0.6429
Recall rate of Retained Class	0.9870	0.9812	0.9839
Recall rate of Dropout Class	0.8497	0.9060	0.9360
F-Measure	0.7761	0.7090	0.7622

The last method was Naive Bayes which is not much different from Decision Tree, its prediction accuracy is 0.9824 with recall rate about 0.9360. To improve accuracy and predictive precision values, we implement *Ensemble Stacking Classification Method* to obtain better predictive accuracy. Two things are required in build prediction model using ensemble stacking method, that is weak-learner as a base-layer classifier and meta-model as a top-layer classifier that will combine K-Nearest Neighbour (KNN), Decision Tree (DT), and Naive Bayes (NB). In this paper, the algorithm iterates to find the best rules that predict student dropout using probability results of each classification methods as describes below:

Input : Dataset S = $\{(x_1, y_1), (x_2, y_2), \dots, (x_m, y_m)\}$;
Base classifier (*k-nearest neighbor*, decision tree, naive bayes)
$H_1, \dots, H_T$
Meta-level classifier (gradient boosting algorithm) H

Process :
Step 1 : train dataset with base-level classifier
for $t = 1, \dots, T$:
$ht = H_T(S)$ % train results of base classifier
end;
Step 2 : construct new dataset of predictions
for $i = 1, \dots, m$:
$S_h = \{x'_i, y_i\}$; $x'_i = \{h_1(x_i), \dots, h_T(x_i)\}$
end;
Step 3 : train dataset with meta-level classifier
$h' = H(S_h)$ % train results of meta-classifier using new dataset S.

Output : $H(x) = h'(h_1(x), \dots, h_T(x))$

The first step, we do training data with base classifier and evaluate them with 10-fold cross-validation. Next, the predictive probability is accommodated as the new input value (x) in either training or testing data so we can use it in the next modeling stage. Three new X variables will be used as predictors on modeling using Ensemble Stacking Classification Method by combining the three base-classifiers. In the last step, prediction modeling is held by using the Gradient Boosting algorithm as a meta-classifier that will classify each prediction probabilities as predictors and variable 'student status' as a target variable. The prediction using Ensemble Stacking Classification shown in Table 6.

Table 6: Confusion matrix for Ensemble Stacking Classification

Predictive / Actual	Ensemble Stacking – Gradient Boosting		Prediction	
	Retention	Dropout	**Accuracy Rate**	0.9882
Retention	3963	38	**Precision rate of Dropout Class**	0.7912
Dropout	11	144	**Recall rate of Dropout Class**	0.9290
Total	3974	182	**Error Rate**	0.0118

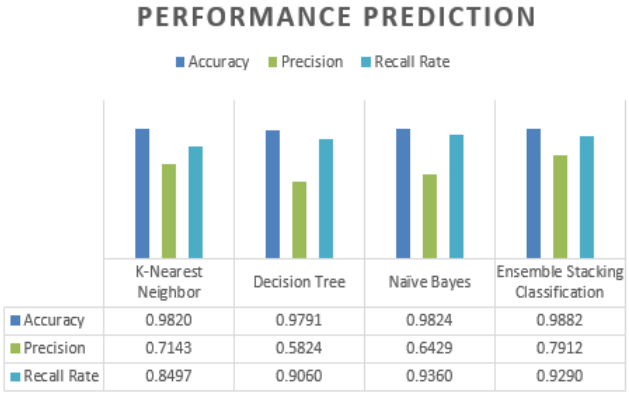

Figure 3: Comparison performance prediction between models

We get the highest accuracy rate with at 98.82%, followed by the second best method was Naïve Bayes at 98.24%. In last, the K-Nearest Neighbor method achieved an accuracy of about 98.20%, which was not much different from Naïve Bayes. As shown in Figure 3, the results of the precision predictions of the Ensemble Stacking method are not much different from the K-Nearest Neighbor even though the value was successfully increased precision percentage up to 79.12%.

Furthermore, the testing process is also found recall rates of prediction. Recall rate is a benchmark to measure modeling successfully predict rediscovering information. If we compared with its precision value, the recall rate of Ensemble Stacking method was high enough that is at 92.9%. However, the recall rate of Naïve Bayes as a single classifier is better although not much different, it gets about 93.60%.

5. Conclusion

This work aimed to describe possibilities to use data in order to help to deal with the dropout problem. Many algorithms have been involved and give a qualified insight of from simple dataset until the dataset with high complexities. In this study, the Ensemble Stacking Classification method with the Boosting Gradient algorithm as a meta-classifier can increase the accuracy of dropout predictions when it compared to a single classifier, such as K-Nearest Neighbor, Decision Tree, and Naïve Bayes. By combining those three algorithms, this method can achieve an accuracy rate of 98.82%, the precision of 79.12% and a recall rate of 92.90%. In addition, the number of false prediction called False Positive (FP) is greater than the number of false negatives (FN) prediction. It means, the performance of the Ensemble Stacking Classification method is good enough at prediction student dropouts. In this study, we also found that features that influence prediction student dropout include the percentage of student attendance, assignment scores, total credits, UTS scores, UAS scores, GPA, parental income, parent's education, gender and age of students. However, there is an indication that academic performance is not the only reason that potentially influenced student's dropout, but also the existence of external reasons such as study program selection and environmental influences.

There are still many shortcomings in this study, for further work we suggest to increase the number of variations correlative feature and large dataset so it will help to improve performance more better than this research, i.e. external assessment features. It also needs to do more research about feature selection method so each feature is more significant and very optimal to use in prediction modeling.

References

[1] Z. J. Kovačić, "Early Prediction of Student Success:Mining Students Enrollment Data," pp. 647-665, 2010.

[2] S. M. Patil and D. P. Kumar, "Data Mining Model for Effective Data Analysis of Higher Education Students Using MapReduce," *International Journal of Emerging Research in Management &Technology*, vol. 6, no. 4, pp. 177-183, 2017.

[3] K. B. Bhegade and S. V. Shinde, "Student Performance Prediction System with Educational Data Mining," *International Journal of Computer Applications*, vol. 146, no. 5, pp. 32-35, 2016.

[4] A. M. Shahiri, W. Husain and N. A. Rashid, "A Review on Predicting Student's Performance using Data Mining Techniques," *Procedia Computer Science*, vol. 72, pp. 414-422, 2015.

[5] G. S. Abu-Oda and A. M. El-Halees, "Data Mining in Higher Education : University Student Dropout Case Study," *International Journal of Data Mining & Knowledge Management Process(IJDKP)*, vol. 5, no. 1, pp. 97-106, 2015.

[6] S. Sultana, S. Khan and M. A. Abbas, "Predicting Performance of Electrical Engineering Students using Cognitive and Non-Cognitive Features for Identification of Potential Dropouts," *International Journal of Electrical Engineering Education*, vol. 54, no. 2, pp. 105-118, 2017.

[7] L. Bonaldo and L. N. Pereira, "Dropout: Demographic profile of Brazilian university students," *Procedia - Social and Behavioral Sciences*, vol. 228, pp. 138-143, 2016.

[8] Kemenristekdikti, Statistik Pendidikan Tinggi Tahun 2017, Jakarta: Pusdatin Iptek Dikti, 2017.

[9] A. Utomo, A. Reimondos, I. Utomo, P. McDonald and T. H. Hull, "What happens after you drop out ? Transition to adulthood among early school-leavers in urban Indonesia," *Demographic Research*, vol. 30, pp. 1189-1218, 2014.

[10] T. Fahrudin, J. L. Buliali and C. Fatichah, "Predictive modeling of the first year evaluation based on demographics data: Case study students of Telkom University, Indonesia," *International Conference on Data and Software Engineering (ICoDSE)*, pp. 1-6, 2016.

[11] A. K. Jain and C. K. Jha, "Dropout Classification through Discriminant Function Analysis: A Statistical Approach," *International Journal of Scientific Research in Computer Science, Engineering and Information Technology*, vol. 2, no. 4, pp. 572-577, 2017.

[12] A. Katare and S. Dubey, "A Comparative Study of Classification Algorithms in EDM using 2 Level Classification for Predicting Student's Performance," *International Journal of Computer Applications*, vol. 165, no. 9, pp. 35-40, 2017.

[13] C. Márquez-Vera, A. Cano, C. Romero, A. Y. M. Noaman, H. M. Fardoun and S. Ventura, "Early Dropout Prediction using Data Mining: A Case Study with High School Students," *Expert Systems Journal*, vol. 33, no. 1, pp. 107-124, 2016.

[14] A. Cano, A. Zafra and S. Ventura, "An interpretable classification rule mining algorithm," *Information Sciences*, vol. 240, pp. 1-20, 2013.

[15] E. Osmanbegovic, M. Suljic and H. Agic, "Determining Dominant Factor for Students Performance Prediction by Using Data Mining Classification Algorithms," *Tranzicija*, vol. 34, no. 34, pp. 147-158, 2014.

[16] M. Tan and P. Shao, "Prediction of Student Dropout in E-Learning Program Through the Use of Machine Learning Method," *iJET*, vol. 10, no. 1, pp. 11-17, 2015.

[17] N. Iam-On and T. Boongoen, "Improved student dropout prediction in Thai University using ensemble of mixed-type data clusterings," *International Journal of Machine Learning and Cybernetics*, vol. 8, no. 2, pp. 497-510, 2017.

[18] O. W. Adejo, "Predicting student academic performance using multi-model heterogeneous ensemble approach," *Journal of Applied Research in Higher Education*, vol. 10, no. 1, pp. 61-75, 2018.

[19] D. T. Larose and C. D. Larose, Discovering Knowledge in Data : An Introduction to Data Mining, 2nd ed., Canada: John Wiley & Sons, Inc., 2014.

[20] V. Kotu and B. Deshpande, Predictive Analytics and Data Mining : Concepts and Practice with Data Mining, USA: Elsevier, 2015.

[21] F. Marbouti, H. A. Diefes-Dux and K. Madhavan, "Models for early prediction of at-risk students in a course using standards-based grading," *Computers & Education*, vol. 103, pp. 1-15, 2016.

[22] Y. Pang, N. Judd, J. O'Brien and M. Ben-Avie, "Predicting Students Graduation Outcomes through Support Vector Machines," *IEEE Frontiers in Education Conference (FIE)*, pp. 1-8, 2017.

[23] A. Ramezankhani, O. Pournik and J. Shahrabi, "The Impact of Oversampling with SMOTE on the Performance of 3 Classifiers in Prediction of Type 2 Diabetes," *Ramezankhani, A., Pournik, O., Shahrabi, J., Azizi, F., Hadaegh, F., & Khalili, D. (2014). The Impact of Oversampling with SMOTE on the Performance of 3 Medical Decision Making*, vol. 36, no. 1, p. 137–144, 2016.

Advances in Science, Technology and Engineering Systems Journal Vol. 4, No. 4, 212-220 (2019)

www.astesj.com

Special Issue on Advancement in Engineering and Computer Science

ASTESJ

ISSN: 2415-6698

Providing Underlying Process Mining in Gamified Applications – An Intelligent Knowledge Tool for Analyzing Game Player's Actions

Anna Tatsiopoulou*, Christos Tatsiopoulos, Basillis Boutsinas

Management Information Systems & Business Intelligence Laboratory, Dept. of Business Administration, University of Patras, 26504, Greece

ARTICLE INFO

Article history:
Received: 30 May, 2019
Accepted: 17 July, 2019
Online :30 July, 2019

Keywords:
Semantics
Knowledge mining
Extraction
Concepts
Gamification
Education
Sequential pattern mining
Process extraction
Adoptable knowledge
Management
Behaviour prediction
User-centered prediction

ABSTRACT

This work deals with the issue of understanding a user's behaviour as this is expressed via a gamified application. The notion of ontologies and the association of concepts in relevance to decisions that have to be made is used. The current work introduces a new process-based approach, based on collected large log files and associations of underlying decisions based on them. Both of them deal with work in extracting information for intelligent use, the main difference being that the first discovers but stops on a concept relation basis, while the other based on processes, as knowledge transactions, further to the associations on a 1:1 level maybe applied on a multi associative model. The objective of the current work is to introduce the methodology into gamified environments (such as but not limited to) games, for semi-automated understanding of user behaviour and furthermore, prediction and in instances, guidance via optimal paths of decision making activities, that are useful in gamified applications in various areas like the education. Both the initial ontology based, and the extension work on it, are based on mining association rules, in one instance treated as knowledge nodes (concepts) and in the second as underlying knowledge processes, based on big log files. This may be applicable to online games, that generate big log files of user selections, that are available for study and examination for extracting user behavioural patterns. As a result, maximum length of sequential patterns and items in them, are discovered in an algorithmic based methodological approach, providing in this way a set of guidelines for designing gamified applications.

1. Introduction

The work in this paper is based on the work presented in the 9th International Conference on Information, Intelligence, Systems and Applications (IISA 2018) under the title "On Ontologies and Knowledge Associations in Gamified Environments" [1]. Its contribution is bifold (a) it extends on a more generalized manner the work so far in the above and (b) it is getting additional research by providing an additional mechanism for knowledge associations. More specifically, the case (a) above is mainly based on single concepts relations – associations and its application in mobile devices in the tourist domain, while in the part (b) contribution of additional research the notion of knowledge transaction is introduces as a set of serially associated concepts – nodes, with the presentation of its application in a gamified environment (on line game). For clarity purposes and the distinction of concepts within the domain of gamification vs. the concepts in the game domain a brief introduction is provided below.

2. Gamification – Modeling User Behaviour

Gamification is the process of applying game techniques (e.g. dynamics, feedback, badges, leveling, etc.) to non-gaming contexts [2]. It is a new methodology that flourished just after 2008 [3] and refers to understanding a user's behaviours on making decisions, made in a context of gaming and hence drive them to expected outcomes. As a process, gamification is under study within the scope of computer science, mathematics, artificial intelligence as well as psychology disciplines in the context of persuasive technology [4]. It is important to be noted here the difference between gamification and gaming itself [5]. The evolving processes in gamification are used today in various domains like education, training, marketing, health human

*Corresponding Author Anna Tatsiopoulou, & email: atatsio@upatras.gr

resources in enterprises, e-commerce and so on [6]. Understanding thus the above and applying them on involved processes on the above sectors, is of great importance. In the current work we will go through the gamification-based implications in the context of the designing educational content for computer-based learning and applications.

Designing and implementing gamification applications is an iterative process which consists of six main steps: 1) define learning objectives, 2) delineate target behaviours, 3) describe the players (either students and/or teachers), 4) device activity cycles, 5) implement fun and involve psychological factors that affect learning in it and finally, 6) deploy the appropriate tools. This process is performed so far by experience, by playtesting the designed gamification schemas, examine the corresponding KPIs, check what is working or not and in case that failures of the design and implementation are identified, return to the design phase and start the process all over [7].

Here, we attempt to formally introduce, as gamification is an emergent technology, the design of gamification applications, by analysing game player's actions stored in log files, to the domain of education as a process-based methodology. We try in other words, to study the user engagement into the knowledge acquisition cycle, in a domain agnostic way, based on a semi-formal approach, where, beneath it, underlies the concept of positive and negative reinforcement via the semantics, the mechanics and dynamics that the gamification-based applications are characterized of.

Education and gaming have many in common. Some of them are learning on achieving objectives, introduction and use as much as possible of engagement (interactivity in learning process) concept, motivation in achieving the previous, game elements, like positive and negative reinforcements, awarding and/or discouraging in specific cases and so on.

The above provided, our research was driven by the interest in studying what is a very important issue in the above context, i.e., what are the implications and the impact of the possible social and psychological factors that are being introduced by the gamification methodology to the achieving of the learning objectives. There are certain questions that have to examined. For example, is the educational content being acquired and understood better if the subject is working in such an application alone, or in an antagonistic environment (one to one or one to computer), or finally in a cooperative team-based mode? Based on this, how social media and collaboration-based environment (electronic) assist this process? Should the subject "discover" the knowledge himself, in a role-based game manner, or should be driven/directed to it? If yes, in a "strict" or a more "flexible" way?

To study the above we introduce the concept of underlying processes in the gamification application that supports the learning process. We are going to examine the model of an educational application that underneath it exists a mechanism that discovers patterns in learning and at the same time tries to understand the individual's behavioural patterns and foresee future behaviour (knowledge extraction). This mechanism gets its input from a set of log files of collected raw data, that is generated from playing a respective game.

Log files in most cases, contain structured raw data that are coming and are registered as text files, coming directly from systems' interaction activities. This either comes from the user's or from other systems' components themselves activity or both them. In most cases, this raw data, comes in a structured and in a predefined format, while in other cases, due mainly to some external reasons and abnormalities, comes as incomplete data, introducing thus "noise" to the system. Out of these log files, the important aspect and the objective of the current work is to mine hidden knowledge, that can be characterized as knowledge produced during the game play (knowledge in action, while learning), in terms of underlying processes and patterns. Such concept of getting an advanced level of knowledge out of raw data, is also currently under both research and application, known as Big Data Analysis. To have such a repository of real time produced raw data in terms of log files that registers user behaviour in a game is in this step our objective and part of presenting our design methodology, in terms of underlying techniques.

More specifically, for experimentation purposes, we have selected and dealt with log files, that are being continuously generated out of the context of a game, played worldwide on the WEB 24/7/365, by thousands of players, in real time. Therefore, the generated log files are updated, using a generalized structured data model, that in many cases has the ability to expand or to reduce itself, in a dynamic way, as it will be presented in the following sections. Due to these idiomatic data type characteristics, initial and advanced parsing techniques had to be developed for two major reasons (a) to generate clear, coherent and consistent data sets and (b) to transform them, so to be persistent and hence to be stored and aggregated in a database for further exploration and processing. What we will concentrate on also here, is the discovery of interesting and meaningful patterns that signify the underlying existence of processes, towards a predictable and modifiable behaviour, a major research topic in the field of artificial intelligence [8].

3. Ontology Based Knowledge Discovery - The ONARM+ Methodology

In the previous presented work [1], we have introduced both the theoretical as well as the technical background of the ONARM+ methodology. Based on this, we have also presented in detail an application, in the domain of tourism. For this, we have considered the case of independed users that by potentially using our platform would exchange parts of their personal concepts, based on a centralized tourism [9] concept ontology, in a semi-automated and intelligent way. The scenario to be implemented based on our methodology, required 2 major components: (a) a client component named Concept-Net, that could be able to run either on mobile and/or desktop environments and (b) the Concept-Net Back End set of modules. Both of them and their subcomponents have been implemented as the following conceptual diagrams represent them (Figure 1):

Our work dealt on the concept relevance aspects with to the transformation of raw data obtained, via user selections and decision-making actions, in a specific domain (being domain agnostic), its comparisons with others on a concept basis, represented as an ontology of a specific domain.

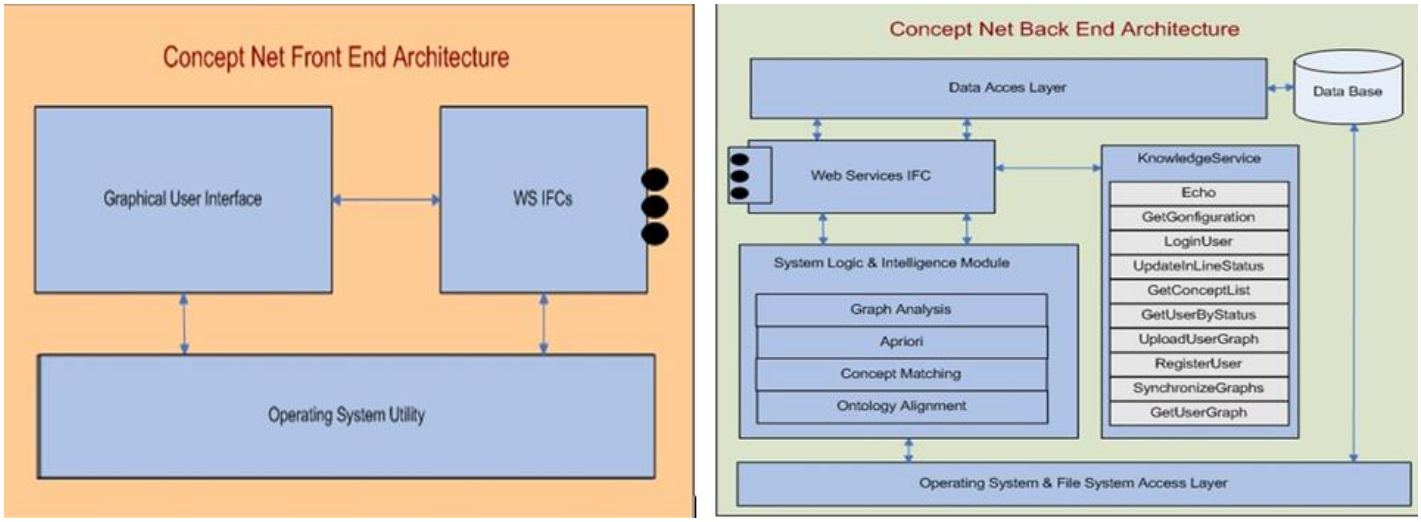

Figure 1: Left: (a) Client logical diagram, on the right (b) server-side components of the Concept-Net application

In short, during the process of knowledge extraction between the 2 users, firstly the discovery of concepts that are of common interest has to take place and then, the comparison via measures while on the final step, the merging of the parts of the specific ontology parts of each user to specific place of the ontology (aligning of them [10], [11]) takes place.

The methodology works under the assumption of existence of at least 2 user profiles, in terms of ontologies of interest. These represent the user's preferences and interests in a specific area and the categorization in a conceptual way that is depicted in a graphical way via the Protégé tool (The Protégé Ontology Editor, http://protege.stanford.edu /, last accessed on June 2, 2018). Also, there exists a central ontology that holds all concepts in the specific domain. As described in the work [1], the methodology is based on the Apriori algorithm [12], to identify. In general, the three major phases of the ONARM+ methodology are: (a) knowledge acquisition, (b) knowledge representation and (c) knowledge exchange.

While the association of concepts in terms of independent knowledge nodes, is of major significance in the discovery and exchanging knowledge processes, when we strive for understanding decision making in terms of a series of choices, then the above provide only partial information. To add value to the previous and essentially to introduce similarities and therefore predict more accurate user choices, we have introduced as an extension to this, the methodology below, which identifies similarities among processes for decision-making, in terms of generalized knowledge transaction processes. This is particularly useful, when not only we need to extract such information so to find similarities among users' profiles, but also equally significantly, to predict such patterns and in a second step, to be able to guide them, so that to trigger dynamic choices for desired user behaviour driving into.

4. Process based Knowledge Transactions Pattern Discovery

4.1. General

In this part, we go through our methodology and we provide an example for supporting the process of designing and development of educational applications based on gamification by using it. For this, we use knowledge extraction methodologies for extracting users' behavioural sequential patterns from large on-line game log files and propose to learners an optimal path or set of actions in a specific order, towards knowledge acquisition. Large game log files stored on line, are collected, processed, stored in an event data base and then transformed to appropriately format, for applying Apriori algorithm sequential pattern mining technique. Extracted patterns then are translated to set of proposed actions. The future path of user preferences in terms of decisions, can be (a) reinforced and (b) predicted by our methodology, while step by step educational/game objectives are achieved. Therefore, designers of educational gamification applications are provided with a set of means to select appropriate type of game mechanics/dynamics and offer selected action types in a user-cantered approach tailored to any individual's requirements. Following advancements in games based on electronic media and the advanced level of new generation familiarization with such environments, in conjunction with the fact that gamification has a wide application in education domain, as it is a useful mean for maintaining student participation and enhance engagement in the educational process, we focus on frequent sequential patterns extraction from game log files and transform them to powerful tools for implementing gamified educational applications.

4.2. Background

Knowledge is the ultimate resource in every enterprise's routine operations and signifies the holy grail to their success. Knowledge in human beings is better understood but not equally explained. Recent developments and technological advancement in all fields of IT technologies (hardware and software) generate on a continuous manner, on real time basis to all kind of unrelated at a first glance data, coming from simple to very complex applications and transactions. The rising need is therefore to discover underlying processes and provide meaning to them as upper level knowledge.

On the other hand, following this trend of advancements, games based on electronic media have evolved from simple applications in the very beginning, to very complex environments, many of them simulating real life experiences and scenaria. In the

domain of education, gamification has a wide application since it has been proved to be a useful mean for maintaining student participation and enhance their engagement in the educational process. Gamification is a mean that is widely used in the marketing domain targeting to foster both brand loyalty and awareness as well as to enhance customer engagement. As mentioned previously, these three key marketing concepts are relevant in the gamification context: engagement – "high relevance of brands to consumers and the development of an emotional connection between consumers and brands", brand loyalty – "the relationship between relative attitude and repeat patronage" and brand awareness, "the rudimentary level of brand knowledge involving, at the least, recognition of the brand name" [13]. Transforming these to learning processes in education, we have the students that are the consumers and the emotional connection to branding in our case the sources of educational context (humans, books, eBooks, web, Internet in general, etc). Therefore, the students can be seen as "highly engaged, emotionally driven players", in this gamified learning approach, where strategic decisions have to be made by them (intermediate learning objectives' achievements, towards the final overall knowledge acquisition, within the provided domain).

These complex gamified applications, therefore, require the track of players' actions and the estimation – calculation of potential responses to their decisions in an intelligent way. In recent years, the tracking and logging of this information and monitoring of the way that game engines and applications perform – has become widespread in the digital entertainment industry, providing sometimes very detailed and specific information on the performance of popular commercial titles with millions of players and installations in digital devices [14],[15]. It has been widely accepted in the academic and business fields that the so-called game telemetry can be a very powerful tool not only for game development but also to assist a variety of stakeholders via user modeling, behavior analysis, matchmaking and playtesting, [16] under the condition that it is processed in the right way. As a consequence, large amounts of game telemetry data are tracked, logged and stored, but not always is being correctly analyzed and used for drawing results and decisions useful to other applications. The challenge quickly became to deal with working with large-scale data, in a process based meaningful way, for extracting behavioral decisions [17]. Quickly, new methods have emerged [15] to assist analysts and decision makers to obtain the information they need to make better decisions. These included: automatic summarization of data, the extraction of the essence of the stored information, and the discovery of patterns in raw data. When datasets became very large (any dataset that does not fit into the memory of a high-end PC as large-scale, i.e. several GB and beyond) and complicated, the breakdown method to smaller sets of data was introduced. Applying on these raw data knowledge discovery processes will help identify and uncover patterns of behavior in it, whether user-derived or learning based-derived, and these, in turn, can be highly valuable.

In this work, we use sequential pattern mining to analyse game player's actions and behaviours, stored in log files.

The objective of the sequential pattern matching process is to discover patterns that take place in sequence(s), so to be used in prediction of future events that generate similar data. It has a great application domain, where human behaviour analysis plays a key role in making strategic role, that varies from students' behaviour and its impact in achieving learning objectives, customer analysis behaviour (and therefore prediction) up to security and alarm analysis, manufacturing engineering, WEB pages' prefetching and so on. In the sequential pattern matching a sequential database of records, expressed as patterns of events is provided to be analysed. The input must be sorted in absolute lexicographical order for the algorithm. The output is a subset of patterns that frequent occur within it, provided that a minimum support (at least), is entered as an expected indicator of the least desired frequency of occurrences of the patterns to be discovered within the total records of the database.

Historically, AprioriAll is the first sequential pattern mining algorithm. The authors of AprioriAll then proposed an improved version called GSP. The AprioriAll and GSP algorithms are inspired by the Apriori algorithm for frequent itemset mining [16].

4.3. Methodology Definitions and Assumptions

There are prerequisites that log files have to support to be useful for the pattern mining extraction. A non-exhaustive list of them is the "case-id", the "supporting activity", "event timestamping", "connectivity with other events, triggering or triggered by", information on resources, such the "user name", "system cost on event" and so on. These, so called event attributes, will allow the extraction of underlying processes, by associating such events and using a generalized model of event logs, consisting of cases, that in turn consist of events, consisting in turn of attributes. That introduces [18]:

1. A set of case(s) based process(es)
2. A set of events associated with processes via respective cases
3. An ordered set (tuple) of such events on a per case basis
4. A set of attributes per event (empty set allowed

As a final point to be noted, is the difficulty and the rareness of availability of user data in terms of raw data (and not in aggregated form), from the game providers, that generate and own these big data files.

At this point, the current work proposes a new methodology for discovering these meaningful patterns, using minimal human intervention (in terms of pre-processing, association and conclusions' analysis). In this section, the main steps of it are going to be presented below:

1. Data Source (Game) Selection. That was a very important step, so the proper game to be selected that conforms with the above requirements and restrictions. At the same time, the game had to offer in an open and continuous way the data being produced, in terms of log files.

2. Data Collection. Based on the fact that the previous criterion would have been met, to develop a method, that in an automatic way would be in a position to collect on a timely basis the generated data.

3. Data Maintenance. Provided the following were met, to further elaborate and develop an automatic way of synchronizing the data collection, so to avoid repeated and unnecessary steps, that

would lead in duplication of data collection. This in turn, most probably, would lead the game data provider to ban the data collection process and stop further experimentation. Unnecessary hits therefore for data collection purposes, had not only to be completely avoided, but at the same time to be carefully scheduled when to occur, avoiding Denial of Service as previously mentioned.

4. Data Transformation. This step was necessary so to introduce unique event game ids, that could be easily backwards traversed, in a meaningful way, reflecting all their attributes, that would lead to processes.

5. Data Persistence. Log files as previously explained are continuously updated in real time, as a stream of data. Out of this, chunks are not useful and have to be thrown away from mining, yet though to be identifiable in case of suspect of usefulness of it. Space and storage limitations had to be considered in the next step, being the storage in a local database.

6. Data Association. In sequence, the asynchronously generated data, has been through data cleansing and in this step, is provided in an automatic way as input to algorithms for association of it. In this step, any type of associative – rule-based algorithm could be used. It is important to be noted that since data can be easily transformed during input process to any given and expected requirement of the algorithm to be used can be applied to any type of these. For the purposes of this work the Apriori algorithm has been used [18].

7. Process Extraction via association rules. For this, the Apriori based algorithm GSP is used, with the objective to speed up the generation of interesting association rules, that will in turn lead to the mining of interesting process as proposed by [8]. The input of GSP is a sequence database and a user-specified threshold named minimum support (minsup, a value in [0,1] representing a percentage).

4.4. Technical Framework and Architecture

Based on the previous criteria, the selected game was the Alter Aeon. According to Wikipedia (https://en.wikipedia.org/wiki/Alter_Aeon), Alter Aeon was built on 1995, continuously and free provided since to thousands of people worldwide. It generates everyday thousands of lines of players' transactions, that are publicly available as streamed log files from the game developers. More details on the game and rules of playing can be found on its web site http://www.alteraeon.com.

For the specific log files, in short, the process was to download the HTML files and write them in local log files. The HTML page was created by the provider to provide the information and had to be parsed until at every entry in formation of value to be found regarding transactions. Then, the files were broken in different ways, so to match the mysqlite data base schema that was adapted. After that, the sequential files were generated and fed into the Apriori algorithm for sequential process associations.

The overall procedure from scheduled data collection from the WEB Data Source, storage of unstructured log files, transformation to structured local log files, database storage, Sequential data sets generation, Apriori as described in (Figure 2) have been implemented using Python 2.7 programming language and were tested in a distributed manner of 2 machines, connected via cloud. The first was used (a) for connection and data collection from game web site (server) of relevant data, (b) the storage of it as raw unstructured data to log files and (c) the transformation of it to local structured log files. These were implemented as a daemon set of processes, on an Ubuntu Linux server-based machine. The second part of the task was performed on a Mac Book Pro OsX with 16 GB RAM and 1 TB solid state HD.

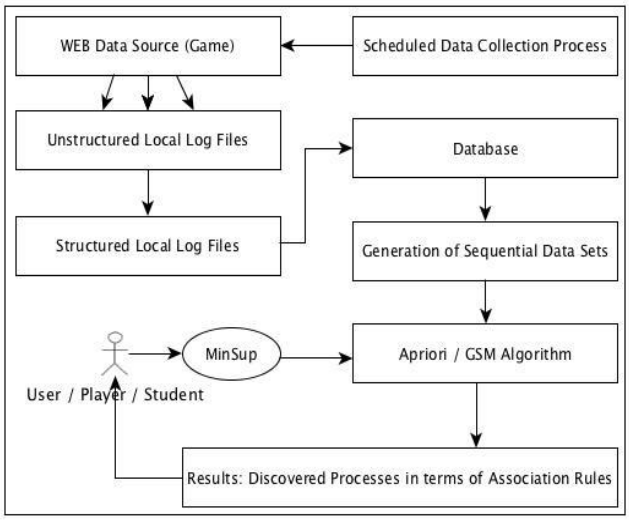

Figure 2: Overall Methodology Architecture

The separation of the overall task into two different sub tasks, in independent hardware platforms (machines), was a critical issue, since the generation of the sequential databases, as the log files were increased in size, was an intense and resources demanded issue. Additionally, the first machine has been configured to update its log files on an hourly basis (dynamically reconfigured). After this repetitive process (as many times as proper data required, here the system was collecting data for 3 consecutive months), the Apriori algorithm was applied, implemented in a Java application environment.

4.5. Results

4.5.1. Initial Results Presentation

In the diagram below (Figure 3), is shortly depicted the process for running the cleared and synthesized log files through the GSP Algorithm.

On the left-hand side of the above image, is a snapshot of the unstructured game log files, collected for a day transactional activity, from the game Web page and on the right is presented a sample of GSP process discovery outputs.

It is worth mentioned that such files were also aggregated to monthly basis and can be further aggregated to any time interval, depending on what time would like to be examined for process extraction. Initially the date / time has been registered and then event type has been recorded. Finally, on the last column, the detailed event description can be found, in a syntactically dynamic format, according the circumstances that the specific event took place.

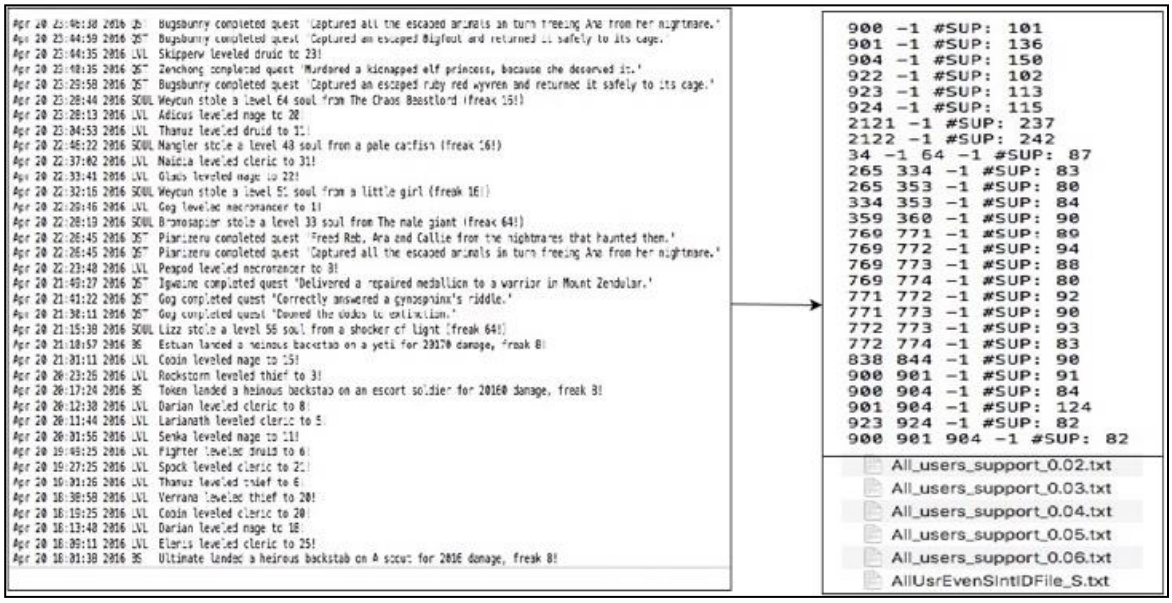

Figure 3: Initial Results Discovered by GSP algorithm.

On the right-hand side, there is (a) a sample of the process discovery after the GSP application; (b) on the lower right-hand side, the format of the filenames of the produced log files are presented, that contain the interesting associations, for processes found. It can be noted at the end of each filename, the respective minsup measure, as previously introduced, under which the process associations took place. (c) finally, on the right top, a sample of the output is presented. The (-1) stands as a separator of the frequently associated process id, that in previous steps has been uniquely composed for a player and player's activity in general to be able to be reversed tracked. As it can be seen in the sample output, there are interesting associations of frequency of 1-member, 2-member and 3-member activities. At the end, the number represents the measure of interestingness, as a measure of frequency of associated processes.

The application of the GSP Apriori implementation algorithm, provides all possible associations that could be found [12], by applying the specific minsup measure. Any sequential pattern mining algorithm could be used instead, as the VMSP [19], that works in a similar way taking the same data format as input and producing a similar file format as output, being different on the fact that provides the maximal model for the associations discovered by the sequential data files.

4.5.2. Processing of Initial Results – Extracting Behavioural Process Patterns

Sequential pattern mining is a research field studied for more than two decades, focusing now in two main areas a) Applications in the aspect of utilizing sequential pattern mining either in new applications or in new ways for existing applications and b) Algorithms either for designing more efficient algorithms or designing algorithm for handling more complex data or for finding more complex and meaningful patterns [20].

The present work contributes to the first area providing results that can be used in the design and development of new gamified applications and in the improvement of existing ones in any domain. The work performed during the experimental phase lead to the following main results:

1. The maximum length of sequential patterns varies inversely with the support value used. The finding was in line with the results stated by R. Agrawal and R. Srikant [8]

2. Sequential patterns discovered only for the events of the type "QUEST". This can be seen as the "repeated" choice of users at different "levels" to perform tasks in the game play in order to achieve certain objectives from simple to more complicated ones.

3. Sequential patterns mined were of maximum length three events for 0.02 support, of two events for support 0.03 when for support 0.04, 0.05 and 0.06 only single items were discovered, which lead to the conclusion that users for various reasons either internal (interest, resources etc.) or external (time availability etc.) are more familiar with this type of pattern.

4. Item members of two or three component sequential patterns were not present as single items in the higher support level sequential patterns mined. This fact may be interpreted and used to the design phase of the potential application(s), as a valuable hint, that helps designers combine "QUEST" elements, being at present not very popular, but of high interest, especially when associated with interaction with other facts / achievements, thus providing added value to them.

5. Single items discovered for support 0.04, 0.05 and 0.06, where not part of the maximum sequential patterns discovered with either two or three event sequence lengths, which can be seen as a cross checking point for implementing gamification strategy, where the importance is the relevance of the "QUEST" with the desired task to be performed.

The above findings are of great significance for designing gamification-based applications for behavioural prediction of users. This is because "QUEST"s can be seen as user behavioural

transactions that include events of high importance, for achieving the maximum objectives set in such applications, in any type of environments supporting well defined processes like, e.g. market(s), sales, e-learning regardless the type of gamification type applied (intrinsic or extrinsic) and so on. The current methodology overcomes the obstacle of the manual observation, association, extraction and in the end generalization, in a (semi-) manual way, based on intuitive approaches. On the contrary, the current work provides an automated algorithmic based methodological approach, for provision of a set of guidelines, to be used in the design process during the application development phase, which so far is based only on empirical findings. In the specific application selected in the current game, this is focused on using "QUEST"s, in the content of gamified applications, with the objective to drive the game user to maximal results, [6] in terms of "QUEST" usage, in a way that is familiar and transparent to him/her. Therefore, based on the fact that the maximum sequence length is 3, provides designers of gamification strategies, for the specific domain, means to select each time the appropriate "QUESTS" for achieving specific goals and drive via behavioural changes in terms of decision making in presented challenges, to the desired performance for selecting either desired actions, or products or services or education-based objectives available in a respective gamified application. On the other hand, the findings that single items gain added value when associated among other, is of great importance and can be used as guide for decision making vis-a-vis to the way that "QUESTS" are presented to the users of these specific gamified application(s).

Getting back to our case in the game selected for experimentation, as mentioned, a sample of 36.000 approximately user interactions have been collected into a respective SQLite database, categorized under 10 relevant tables of specific events types supported by the game. This data was collected on a periodic per hour and per day basis and then aggregated to a monthly based per user model. Running then the specific Apriori sequence algorithm, our methodology provided as an outcome, the conclusion that there was an interesting path of predefined processes expressed in terms of game terminology as "QUEST"s that was followed by the user as a sequence towards the game objectives. These (as all game events), have been coded as follows (processID, questID, questName):

900: q678 -> "Searched the fetid Caves of Pestilence and destroyed the weather machine"

901: q679 -> "Ruined the plans of Malkon the Plague Vampire and saved Archais from his evil machinations"

904: q682 -> "Breached the Fetid Caves of Pestilence to rescue a dwarven child"

It is important to be mentioned here, that the associations of the type (900 -> 901 -> 904) were discovered under the support measure of 0,02 and with frequency of 82 times among all possible processes interactions discovered. The number of the three (3) associated processes, is directly relevant to the sample data collected from the large log files produced by the gamified applications and they are also language/term agnostic. Finally, in the tuples discovered, the order is of significance, providing the sequence of these processes.

What this means, is that there is a significance in users' interestingness, when they use the gamified application, in getting, in a sequential way, from process 900 to 901 and to 904 by achieving their respective objectives. In other words, from the point of view of the behavioural analysis, the future path of potential user preferences getting from a point A to a point B, in terms of decisions, that can be achieved through multiple ways, can be (a) reinforced and (b) predicted by our methodology, while step by step game objectives are achieved.

This is a very important analysis and conclusion for applications that deal and are composed by decision making, based on a process-oriented approach.

5. Comparisons and Advancements – Generalizations & Potentials

The above findings, if applied in the education domain, will be of great significance and will provide initial guidance for developing gamified applications for the educational industry (eProducts, eServices and so on). Such applications need to be compliant and respect the overall model of "Input, Process and Output" (Heis, 2008) in the education domain, where input are the educational objectives that by the appropriate learning process are transformed to learning outputs that in turn are evaluated against the initial objectives (Figure 4).

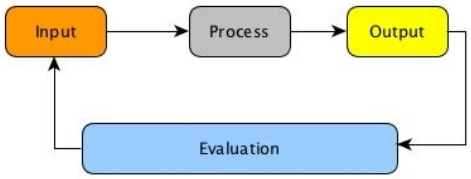

Figure 4: Input Process Output Model (Heis 2008, [220])

As a consequence, for drawing and implementing interesting, effective and challenging input for an educational application, being aware of the patterns that users are familiar with, through the "Evaluation" of their behaviour in such applications, would allow to provide to them more tailored to their needs "Input" for the educational "Process" that will allow the maximum "Output".

In terms of gamification resources, our methodology will enrich the decision process for creating and applying more personalised experience to end users and suitable quests, challenges, rewards etc. for being also compliant with the fact that designing user experience for educational applications that incorporate gamification strategies needs to facilitate the "ABCD" model educators use for writing and using learning objectives, whereas "A" means audience, "B" behaviour, "C" conditions under which the objectives have to be completed and "D" is the degree that learners have to achieve [21].

It is known that the type of proper motivation varies depending on the audience characteristics therefore for succeeding in adopting the above-mentioned model, given that learners are willing to participate in educational processes if they are subjects to appropriate education methods and resources, informed on the foreseen behavioural change and triggered enough for completing the set of achievements they are obliged to.

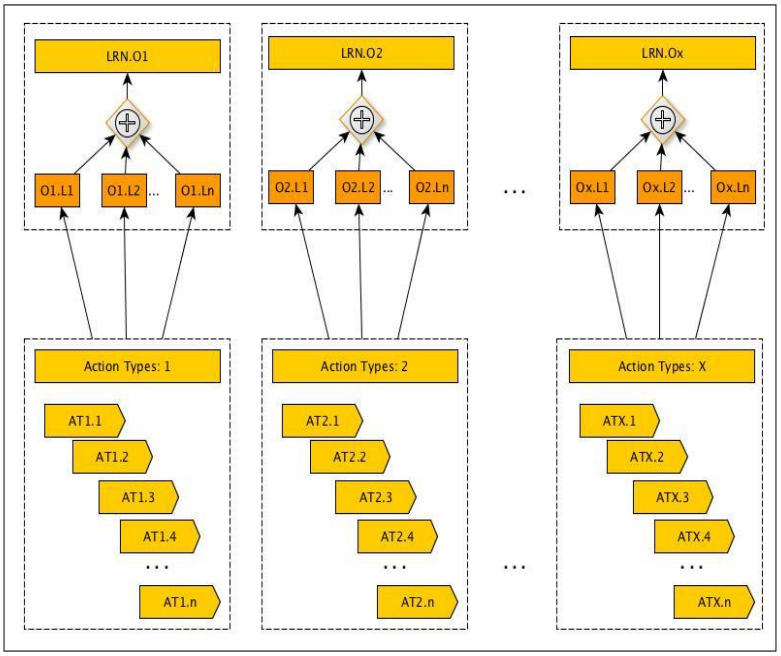

Figure 5: Design of an Educational Gamified Application

Even in Fogg's Behavior Model [22] is clearly stated that providing sufficient motivation, adequate ability and efficient activation to learners, results to the desired from the educator point of view "behaviour" achievement. As gamification contributes towards the provision of both motivation and activation of learners, it is important to employ suitable type and "portion" of them for resulting to successful applications and learning outcomes.

We select to present the potential application of our methodology to the education domain. For this purpose, we consider the education related processes, such that to be related in an input-process-output schema of relations, composing thus a system-oriented view point to it (education).

Our methodology will allow gamification applications in the above-mentioned education model, to use the "right" pattern each time, for supporting the desired behaviour for the learners, overcoming the theoretical obstacle that "the use of challenges in Information Systems though, may be limited because of a high number of monotone and standard tasks" [23]. Such strategy, hence, based on optimal path reinforcement of educational processes, will lead both teachers and students, to be informed and getting up to their educational objectives with a high degree of performance, understanding and productivity in the area.

Based on the above findings of our methodology, we attempt to design a gamified application. We consider again the educational domain for the target group of the application, that is independent of the subject that has to be introduced – taught.

The main course objectives are for the paradigm below (Figure 5), introduced as LRN.O1, LRN.O2, ..., LRNOX. It shows how action types will be connected to Learning Objectives for the design of an Educational Gamified Application. These are the necessary objectives to be achieved so that the course to be successful for the learner (or the learner group).

Every such Learning Objective Ox, in turn, can be achieved in the gamified application to be designed, by the achievement of respective objective game levels (Ox.Ln, meaning for the objective LRN.Ox, the Level n and so on). We assume that the number of levels per learning objective may vary, (but at least may have a value of 2).

On the other side, in our game design methodology we offer, the ability to the developer but at the same time to the player – learner, to design a variety of action types for the achievement of such levels, as described above and play freely by navigating and making actions – decisions through the game scenario. Such action types that are introduced by the game designer and implemented by the game developer, may be represented as a virtual library of actions, containing – being categorized further in sub-action types. For example, somebody may select to achieve the respective level, to read material, then to play a local educational game and then take a quiz to collect points towards next level. On the other hand, somebody else, may select to study much more material in sequence, so that immediately as soon as will take the quiz, to be sure that will also be awarded the next level. This model introduces the independent process in sequence selection towards one, the same objective achievement, allowing edutainment weight to be balanced by the user, on real time basis, i.e. how much game, how much, in app study, out app (text – notes) study, cooperative action types, info from social networks and so on will on demand use.

Collecting this information in large log files, as our application will run, will in turn produce frequent patterns of selected actions, where players achieved the objective much faster, as a function of selected action types. Our methodology then, when enough knowledge and processes will be collected, will propose to next player i, a proposed optimal path towards knowledge acquisition of the respective level, i.e., a set of Action Types, in a specific order, so the player – learner will be more productive. Of course,

this will be only a suggestion and the player will be always free to reject it and hence select his own path, towards the level achievement.

6. Conclusions and Future Work

As an extension to the ONARM+ previously presented work, we developed a formal methodology to support the design of gamified applications. It is based on analyzing game player's actions stored in log files to extract frequent patterns of actions. The extracted patterns are processed and classified according to the expected outcomes which can be supported in a gamification application.

This knowledge base for gamification of frequent sequential patterns of actions, along with the outcomes, they are considered as knowledge process-based transactions. Thus, given a specific domain and the expected outcomes for a gamification application, the designer could build it by selecting the proper patterns of the knowledge base above, so to drive via optimal decision making paths user behaviour changing, which is the basis for a variety of diverse domains, like marketing, learning, consumer/branding loyalty and so on. Apart from patterns, the knowledge base above. Based on this, we plan to extend our work so that the knowledge base above, to contain also meta-rules for controlling game techniques (e.g. dynamics, feedback, badges, levelling, etc.) and their relative association on a per user profile basis.

Finally, we have presented an educational game design concept, based on our proposed methodology, where the proposed application, introduces to new players – learners, accumulated optimal knowledge experience, towards game level achievements and their knowledge – learning objectives. In this game we tried to examine, using our methodology associations in user decisions and choices, as a set of concept-based processes, so based on an algorithmic approach to predict and drive choices of similar user profiles, on the same domain. While availability by developers of such real time on line games have been proven a task difficult to be achieved, future work will be focused in collecting more than an additional year's supplementary data to verify our findings vis-à-vis user behaviour.

Overall, initial interesting results of such associations were found, for specific players. Further work will concentrate also in five main directions (a) application of the maximal VMSP mining algorithm and comparison of results generate; (b) generalization of results found to a broader set of players; (c) application of the proposed methodology to other gamified domains, for mining underlying processes; (d) analysis of more other computer games (types) to extract more patterns and (e) the generalization of our work for groups of users instead of focusing to specific ones.

Conflict of Interest

The authors declare no conflict of interest.

References

[1] C. Tatsiopoulos, D.M. Katsanta, "On ontologies and knowledge associations in gamified Environments", 2018, 9th International Conference on Information, Intelligence, Systems and Applications (IISA), July 23-25, 2018, IEEE, Zakynthos, Greece, DOI: https://doi.org/10.1109/IISA.2018.8633589, e-ISBN: 978-1-5386-8161-9

[2] S. Deterding, Dixon, D. R. Khaled, L. Nacke, (2011). From game design elements to gamefulness. In Proceedings of the 15th International Academic MindTrek Conference on Envisioning Future Media Environments - MindTrek '11. http://doi.org/10.1145/2181037.2181040

[3] Z. Epstein, (2012). Enterprise Gamification for Employee Engagement. Marioherger.At.

[4] H. Oinas-Kukkonen, M. Harjumaa, (2009). Persuasive systems design: Key issues, process model, and system features. Communications of the Association for Information Systems.

[5] T. Xu, F. Feng, D. Buhalis, J. Weber, H. Zhang, (2015). Tourists as Mobile Gamers: Gamification for Tourism Marketing. Journal of Travel and Tourism Marketing, 33(8), 1124–1142. http://doi.org/10.1080/10548408.2015.1093999

[6] E. B. Passos, D. B. Medeiros, P. A. S. Neto, E. W. G. Clua, (2011). Turning real-world software development into a game. In Brazilian Symposium on Games and Digital Entertainment, SBGAMES. http://doi.org/10.1109/SBGAMES.2011.32

[7] K. Werbach, D. Hunter, (2012). The Gamification Toolkit: Game Elements. For the Win: How Game Thinking Can Revolutionize Your Business. http://doi.org/10.1017/CBO9781107415324.004

[8] R., Srikant, R. Agrawal, (1996a). Mining sequential patterns: Generalizations and performance improvements. Advances in Database Technology — EDBT '96. http://doi.org/10.1109/ICDE.1995.380415

[9] C. Tatsiopoulos, B. Boutsinas, "Automatic knowledge exchanging between tourists via mobile devices," in Journal of Hospitality and Tourism Technology, vol. 1, No2, pp.163-173, 2010.

[10] C. Tatsiopoulos and B. Boutsinas, "Ontology mapping based on association rule mining", in Proceedings of 11th International Conference on Enterprise Information Systems, vol.3, pp.33, Milan, Italy, 2009.

[11] C. Tatsiopoulos, B. Boutsinas, K. Sidiropoulos, "On aligning interesting parts of ontologies", in Proceedings of International Joint Conference on Knowledge Engineering and Ontology Development (KEOD2009), pp. 363-366, 2009, Madeira, Portugal.

[12] R. Srikant, R. Agrawal, (1996b). Mining Sequential Patterns: Generalizations and Performance Improvements. In Proc. 5th Int. Conf. Extending Database Technology, EDBT (Vol. 1057, pp. 3–17). http://doi.org/10.1109/ICDE.1995.380415

[13] A. K. B. Bharathi Gopinath, A. Singh, C. S. Tucker, H. B. Nembhard, (2016). Knowledge discovery of game design features by mining user-generated feedback. Computers in Human Behavior. http://doi.org/10.1016/j.chb.2016.02.076

[14] L. Mellon, (2009). Applying Metrics Driven Development To Mmo Costs and Risks. Versant Corporation.

[15] A. Drachen, A. Canossa, (2011). Evaluating motion: spatial user behaviour in virtual environments. International Journal of Arts and Technology. http://doi.org/10.1504/IJART.2011.041483

[16] D. Kennerly, (2003). Better Game Design Through Data Mining. In Gamasutra.

[17] A. Drachen, M. Seif El-Nasr, A. Canossa, (2013). Game Analytics – The Basics. In Game Analytics. http://doi.org/10.1007/978-1-4471-4769-5_2

[18] W.M.P. Van der Aalst, (2011). Process Mining. Process Mining. http://doi.org/10.1007/978-3-642-19345-3

[19] P. Fournier-Viger, C. W. Wu, A. Gomariz, V. S. Tseng, (2014). VMSP: Efficient vertical mining of maximal sequential patterns. In Lecture Notes in Computer Science (including subseries Lecture Notes in Artificial Intelligence and Lecture Notes in Bioinformatics). http://doi.org/10.1007/978-3-319-06483-3_8

[20] P. Fournier-Viger, J. Chun, W. Lin, R. U. Kiran, Y. S. Koh, R. Thomas, (2017). A Survey of Sequential Pattern Mining. Ubiquitous International.

[21] A. Salam, (2015). Input, process and output: System approach in education to assure the quality and excellence in performance. Bangladesh Journal of Medical Science, 14(1), 1–2. http://doi.org/10.3329/bjms.v14i1.21553

[22] B. Fogg, (2009). A behavior model for persuasive design. In Proceedings of the 4th International Conference on Persuasive Technology - Persuasive '09. http://doi.org/10.1145/1541948.1541999

[23] S. Thiebes, S. Lins, D. Basten, (2014). Gamifying information systems A synthesis of gamification mechanics and dynamics. Twenty Second European Conference on Information Systems, (August 2016), 1–17. Retrieved from http://aisel.aisnet.org/ecis2014/proceedings/track01/4/

[24] U. K. Heis, (2008). Input Process Output, 1–3. http://doi.org/10.1007/1-4020-0611-X_462

Advances in Science, Technology and Engineering Systems Journal Vol. 4, No. 4, 221-229 (2019)

www.astesj.com

Special Issue on Advancement in Engineering and Computer Science

ASTESJ

ISSN: 2415-6698

Optical Braille Recognition Software Prototype for the Sinhala Language

Shanmuganathan Vasanthapriyan*, Malith De Silva

Department of Computing & Information Systems, Sabaragamuwa University of Sri Lanka, Belihuloya, 70140, Sri Lanka

ARTICLEINFO

Article history:
Received: 31 May, 2019
Accepted: 24 July, 2019
Online :30 July, 2019

Keywords:
Braille
Visually impaired
Sinhala braille
Optical braille recognition

ABSTRACT

Braille system is purposely made for visually impaired people, to support their literal communication in order to share their knowledge. Louis Braille introduced the braille system consists of series dots which are embossed to read by touching. Early days Braille papers are made manually, but at current days braille documents are made using machines. Due to lack of perceiving on braille symbols and characters, it was highly needed fact to develop Braille system to different languages. In the Sri Lankan context, we found that the mostly inconvenience are happening inside of Sri Lankan education system. Such as in Special Education centers, Colleges, and universities. Written Braille scripts are evolution by a limited number of people who are specialized in the Sinhala braille system. Also, the process of marking braille documents are not effective and efficient. The focus of this research is to address the issue of literal communication gaps between society and the blind people in Sri Lanka. Average quality single-sided composed Braille dot characters are identified with maximum accuracy by using several novel methodologies. Obtained results denote the proposed methodologies are with the highest accuracy and system performance are more efficient as promised. The research presents executable software prototype, includes proposed methods which align with optical braille recognition in order to transpose the recognize braille characters. Introduce of new binaries cell transcription method of Braille character from a Braille document and decoding them into Sinhala characters. The proposed cost-effective system can display decoded braille characters by normalizing to Sinhala text which is in a human-understandable form.

1. Introduction

1.1. Background

Society consists of different people who have various capabilities. Among them, there are some people who are less capable of doing some daily activities due to various reasons. Visual illness is one of the causes. Blindness is a visual illness, occur due to various physical or neurological factors. It can be occurred at birth, due to an accident or due to other disabilities or diseases. Most of the time these conditions make a serious effect on their lives and change the whole lifestyle. According to WHO (World Health Organization), around 314 million people worldwide are living with serious vision impairments. Among them, 37 million people are suffering from blind and 124 million people are having low vision. Moreover, 90% of those blind people are living in low economic countries.

*Shanmuganathan Vasanthapriyan, & email: priyan@appsc.sab.ac.lk

When we consider Sri Lanka, we are having a population of 21 million. Among the population, around 150,000 people are having eye blindness and around four hundred thousand (400,000) people are having a low vision. According to the report of "*National Survey of Blindness, Visual Impairment, Ocular Morbidity and Disability in Sri Lanka*" [1], the prevalence of blindness among those aged 40+ years is 1.7% and 15.4% for moderate visual impairment.

As we all know, we all are gifted with inborn talents. It's the same for visually impaired or low sighted people. Most of the time they are searching for their capabilities. In addition rest of the people are expecting them to play an integral role in the society by using their inherited talents [2]. But in most of the cases, the blindness inhibits those talents and search other's help. Blind people need to put an extra effort than the rest in order to live normal life [3]. As they all are part of humans, we have a responsibility to make their lives easier. We have to facilitate them to socialize with the world. The key for it is communication. In

addition, we have to help them to reach universal knowledge. We should share their wiseness within the world and help them to come after in their lives.

To keep flow their lives with an ordinal pattern of the society, they need to have a clear knowledge of with other ordinal lifestyles. When they come to get to know these facts, they face the major problem in communication, knowledge sharing, and knowledge gathering. Instead of achieving everyday needs, there ought to be a few techniques to make emerged their abilities and keep up them on with their gifts by giving them information and let them impart their insight into society.

It's critical to keep data in the written format since it assumes obviously job with regards to knowledge storing and sharing. For that composed learning from easygoing note to training, recorded data to encoded figure content we need images to trade that learning and data. As ordinary individuals, we have our very own written mechanism as indicated by our languages, just as outwardly visually impaired individuals likewise need some sort of images and method for the game plan of images so as to express their emotions, contemplations, information and so forth [4]. To come up with these challenges the world has come up with several mechanisms like braille system to make it happen [5].

This issue is especially clear in the schooling framework and University frameworks, where these days' blind students are educated in standard classes. A significant number of these blind students perform the evaluation, tests, and schoolwork composing utilizing the Braille medium. Notwithstanding, most educators of these understudies are not Braille proficient [6]. One strategy by and by used to beat this trouble is that the blind students work is first sent to trained Braille transcribes, where the Braille is translated to literary text and afterward sent back to the educator before it is marked. This makes pointless postponements and cost for the blind students, educator, and government. Issues additionally exist in the working environment where any data composed by a Braille client that will be deciphered by other Braille uneducated people, should be first interpreted by the Braille client themselves [7].

Also, blind people feel helpless when it comes to situations like filling application forms. Even we don't realize, application forms play a major role in human's life from birth to death. Instances such as have a birth certificate, Death certificate, enroll to a school, to enter an university, to get an occupation, to go abroad, to have visa likewise most of the important events are linked with application forms and filling an application means we are providing our personal and confidential details to another party in order to get an opportunity or a service [8].

Even they know Sinhala, English, Tamil or other languages, they don't know how to read or write in normal characters. Also, normal people don't how to read or write in Braille characters. So there is a huge gap between normal and blind people and society make feel those people as really disable and less confident.

When it's come to knowledge gathering and knowledge sharing, literally communication is a major medium in knowledge dissemination. In order to do communication, visually impaired people have many systems to accomplish this intention. The Braille system is the reliable and most famous system for this purpose. Braille system is a communication system which is literal. It enables blind and partially sighted people to read and write through using touch stimuli. They use this braille system for calculations, menus, signs, elevator, and books [3].

Louis Braille, a French teacher invented Braille in 1825. He formulated this concept by using the military secret codes. These secret military codes are known to be night writing. This technique is used by military soldiers at dark times to communicate with each other. These secret codes have twelve dot cell six dot height and two dots wide [9]. The only problem is Louis Braille was faced on when making the Braille system that visually impaired people cannot feel all the dots at one touch. Also, the finger doesn't have that much sensitivity for recognizing dots at on time. He made it to practical by making this cell 2 dots wide and 3 dots in height. In order to make it use as character set, made up of different combinations of raised dots (tiny palpable bumps) as above mentioned. In order to represent different characters or sequences of characters, the 3-by-2 (3 rows and 2 columns) arrangement was used [10, 11].

Sinhala is known as the official native language of Sinhalese. According to the Sri Lankan context, there have been new to the braille system by comparing to other languages. The Sinhala language is often considered as two alphabets or an alphabet within an alphabet. It is because of the presence of two sets of letters. The core set, known as the "*Suddha Sinhala*" (pure Sinhalese) or "*Eḷu Hoḍiya*" (Eḷu alphabet) can represent all native phonemes [12]. In order to deliver Sanskrit and Pali words, the Misra Sinhala (mixed Sinhala), an extended set was introduced by ancient scholars. Current Sinhala alphabet uses 60 letters in the alphabet. There are 18 vowels and 42 constants contain in today's standard Sinhala alphabet. However, there are 57 characters are used in present [12].

1.2. Sinhala language braille writing style

Sinhala braille and English braille are two different alphabets. They can't be combined. We can write only single alphabets letters only at once. Numbers are recognized from a pre identification character. The numbers are identified by the braille character "⠼". If "⠼" appears before any of the braille character the following character series until space appears is considered as numeric characters

Sinhala braille system has a different way of writing comparing to the normal Sinhala writing system. As previously mentioned with the combination of 2 by 3 arrangement of the braille dots we have 64 of different combinations use when braille writing. Braille diacritics are use made up with combining constant letters along with the vowels.

In Sri Lanka, most of the blind people are not going through any kind of education mechanism. There are fewer education centers which having knowledge of Braille system in Sri Lanka. People who have knowledge of the braille system only can read the braille documents and understand what visually impaired people have written, what they try to express. Most of the normal people don't have any knowledge on how to read braille documents and as a society, we fail to understand what they express in the literal way of their feelings and knowledge. There are some people write their own braille books and exposed to the world. In Sri Lanka, most of the visually impaired people stay at home, and the parents don't have knowledge of how to read or write Braille. Even if visually impaired people have to write braille, people who are at home cannot understand the braille documents. There is a clear gap between literal communication between sighted people and visually impaired people when it's come to share their knowledge.

This identified gap is addressed through this research using the software prototype.

There is a research conducted by Perera et. al, [13] that identify Sinhala Braille characters in single-sided Braille document and translates to the Sinhala language. This system was also capable of identifying Grade1 English Braille characters, numbers, capital letters and some words in Grade 2 English Braille system.

The main objective is to make a platform to understand braille fonts and convert it to Sinhala fonts in order to formalize communication between visually impaired people and the rest of other normal people. If there is a system which can translate written braille to Sinhala, It will be an excellent communication tool for sighted people (who do not know Braille) with blind writing. And it will reduce the time and money which needed to translate such documents; also, it will secure blind people's privacy in situations like filling application forms. In order to overcome above-mentioned problems research have to follow various researches and have found there are fewer studies have done come over to address these problems. By using latest Sinhala braille alphabet [14], documents are converted with high accurate and efficiency.

2. Methodology

The overall methodological framework is shown in the following figure 1.

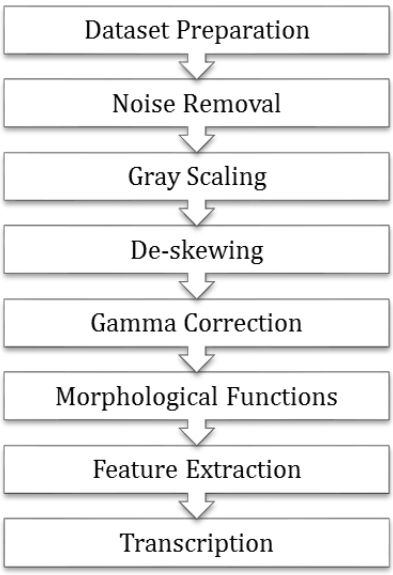

Figure 1: Methodological framework

2.1. Dataset preparation

As the first step in the research, the braille documents were collected. Both handwritten documents and typed documents were collected. The braille slate was used to write the handwritten document and braille typewriter was used for the typed documents. The size of the handwritten document was 9x12 inches and type documents were 8.5x11.8 inches and 9.5x12.5 inches.

After Braille documents have been collected, scanning was performed. In Optical Braille Recognition (OBR) scanning braille documents enable us to perform digitization which produces a digital image of the scanned Braille document. A flatbed scanner has been used for the digitization process. This is because it has been found as a cheap alternative to scan Braille images [8]. Figure 2 and Figure 3 shows the difference in light source distribution when grayscale.

Horizontal resolution and vertical resolution of 300 dpi and of 200dpi have been used for the scanning process. Most of the researches have been conducted in this area used 100 to 200 dpi resolution when scanning their documents so it is recommended to get quality images and the images are stored in JPEG format. Using this configuration Braille documents that are collected from different sources are scanned and prepared for subsequent processes.

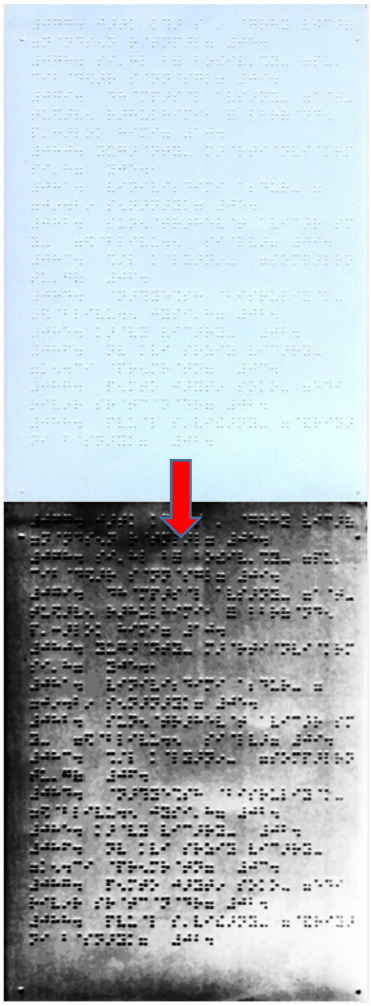

Figure 2: Braille Accusation Using Camera and After Grayscale

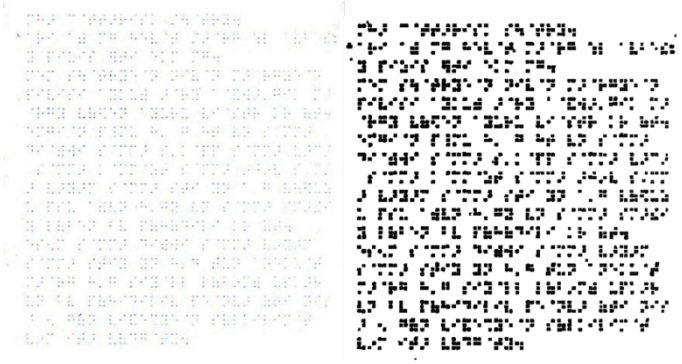

Figure 3: Braille Accusation Using Scanner and After Grayscale

Braille document property description

- Braille sheets: 12
- Resolution: 200 dpi, 300 dpi
- Digital format: Colour
- Image sizes: 9 X 12 inches, 8.5x11.8 inches, 9.5x12.5 inches
- Braille type: Single-sided
- Image format: JPEG

2.2. Pre-processing

Noise removal

Before starts to do any compilation on the scanned digital image, it's recommended to do pre-process part on the image. Before that, it's necessary to compare some technical aspects before coming to a conclusion which needs to select. There are several techniques on noise removal such as mean filtering, Median filtering, and Gaussian blur are some of it. In here research got selected the Gaussian blur for noise removal and later here it discussed why select Gaussian algorithm [15].

If the window size is small the effect of filters will reduce because it is not capable remove noise much effectively. If the window size is got increased it will remove the noise, but as well it will blur the braille bots and also the edges of the documents. Which lead to reduce the detail of the image where do not contain noise also.

There can be several ways of getting the braille document noisy. When considering the handwritten documents, according to the way of writer use the paper may lead to noise. Sometimes the environment may lead to noises. Another way of getting noise is paper may itself having some patches or print issues. However here below Figure 4 give a clear idea on how handwritten braille document have exposed for noise. Type documents are can be exposed to noise when they read by the visually impaired people because of the dust and other unnecessary things having on the fingers at the time of reading braille image [16]. Finally, in the end, there may be noise when getting through the scanner.

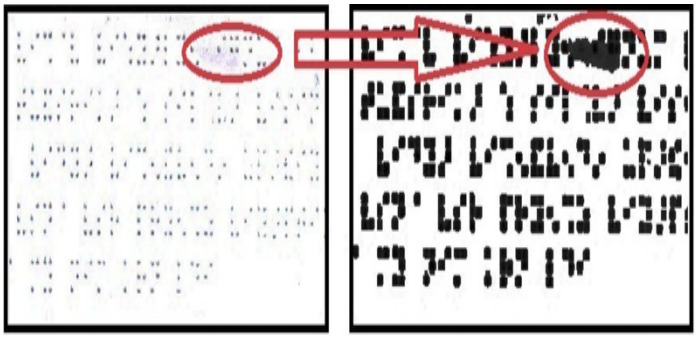

Figure 4: Noise on Handwritten Image after Pre-Processing

But in here its need to focus on both side at this stage. When using powerful noise removal algorithm to removing the noise it may affect to respective needed details on the documents which are not affected by the noise at high scale. With the above facts no need to use powerful noise removing algorithms because they may get the effect to somewhat on context [4].

Mean filter

Mean filtering is done using read pixel by pixel of the image and assign the mean value of values for its pre-defined kernel's structure center pixel. When the kernel is large, the center pixel may have a high effect through other pixel values. Even a pixel which does not contain noise also gets affected. Also, it should not affect the braille cell segmentation and features extraction. But this will lead to unnecessary complexity on future steps.

Median filter

This mechanism is a little bit ahead than the mean filter because the median filter is replacing a middle pixel with the median value of the kernel's center pixel. Which leads to damage the edges of the characters and edges of the fields [17].

Gaussian blur

Gaussian blur was used to remove the noise. Instead of utilizing other low pass filtering algorithms, Gaussian blur channel does not lessen braille dot details. However, it makes decrease noise in an incredible way. Figure 5 denotes how the Gaussian blur work on noise removing. As indicated by the Gaussian blur work it weighs more on closest pixels of the utilized kernel canter. Figure 6 shows how weight is distributed around the center pixel. Equation 1 shows Gaussian blur for one dimension.

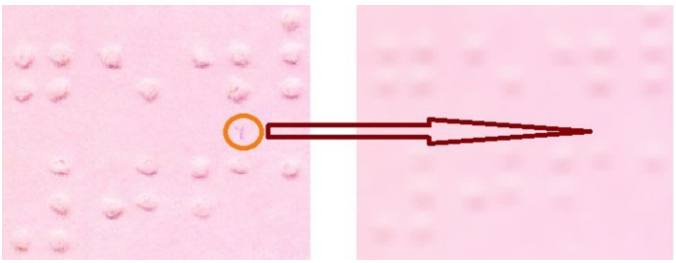

Figure 5: Gaussian Blur Apply On Noised Document

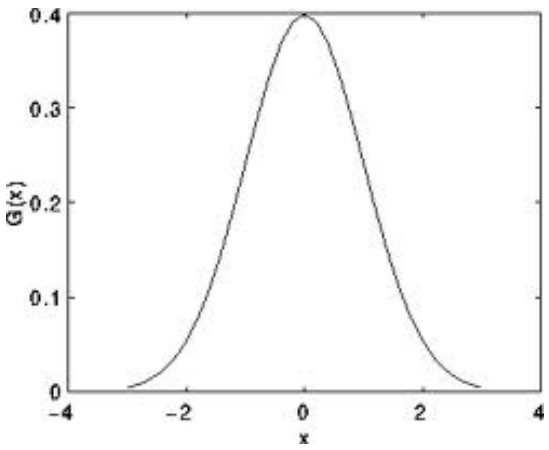

Figure 6: Pixel Weighting According To Kernel Center

$$G(x) = \frac{1}{\sqrt{2\pi\sigma^2}} e^{\frac{-x^2}{2\sigma^2}} \quad (1)$$

A filter using EmguCV was applied to the input in order to perform the smoothing function [18]. Equation 2 shows how EmguCV has done for the above mathematical operation (equation 1). Equation output pixel's value g (i, j) is determined as a weighted sum of input pixel values.

$$g(i,j) = \sum_{k,l} f(i+k, j+l)h(k,l) \quad (2)$$

The coefficients of the filter are the kernel which is represented by h (k, l). It helps to visualize a channel as a window of coefficients sliding over the image. Weighing of the pixel was done through f (i+k, j+l). Even though it is not the fasted filter it is good to filter for working with images. Gaussian filtering was done by convolving each point in the input array with a Gaussian kernel and then summing them all to produce the output array [18]. Table 1 describes the above mention details as a summary.

Table 1. Reasons Summary of Gray Scale, Mean Filter, and Gaussian Blur

Median Filter	Mean Filter	Gaussian Blur
Low Computational Cost	High Computational Cost	High Computational Cost
Preserve Image Details	Very Low Capabilities to Preserve Image Details	High Capabilities to Preserve Image Details
Low Memory Consumption	High Memory Consumption	Low Memory Consumption
Simple Implementation	Simple Implementation	Simple Implementation
Analytical Process Becomes Simpler	Analytical Process Becomes Relatively Complex	Analytical Process Becomes Relatively simple

2.3. Grayscale

The expectation of using gray scaling technology is not only for reducing noise but also several other results are expected. Since the resolution and quality of the image will higher according to the dpi of the input image. The time which takes for the process relatively large when quality is high, which is negatively affected for systems performance. But when do gray scaling it is an extremely small amount of time takes for the entire process.

On the other hand to conduct analyzing processes such as edge detection, segmentation, and feature extraction and classification techniques effectively it is necessary to reduce the intensity of the image since inputs to the system are color images. Since gray scaling contains only 0-255 values on pixels it is useful to use gray scaling such that it is easy to conduct analytical processes [19]. As the second step, convert the color image into a grayscale image. Figure 7 shows the result when the input image goes through gray scaling.

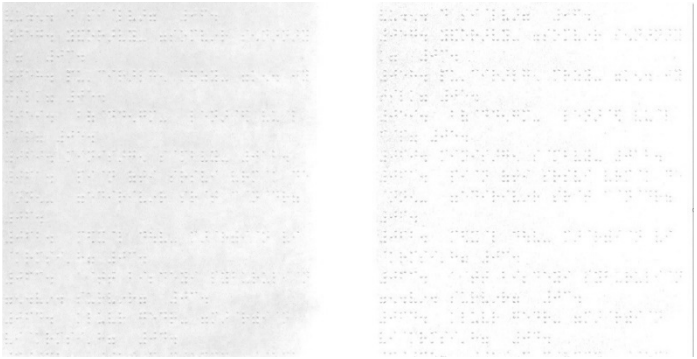

Figure 7: Gray Scale of Input Image

2.4. De-skewing

Rotation is used to de-skew braille documents in place of horizontal and vertical projection profiles.. In some cases the document may not have skewing errors but in general when braille documents are composed there is a possibility for skewing errors to occur. Instead of squandering increasingly computational capacity to de-skew documents, the work utilizes moderately fixed positions to de-skew the documents using rotation angle. Figure 8 demonstrates De-skewed image Utilizing Rotation.

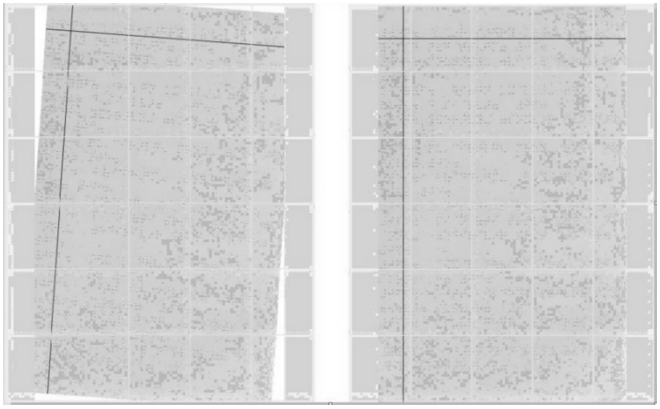

Figure 8: De-Skewed Image Using Rotation

2.5. Gamma correction

Gamma correction was done on the gray image to enhance subtleties of the braille spots. Gamma correction can be utilized in non-direct connections and in encoding or interpreting the luminance in images. Equation 3 and 4 demonstrate the calculation.

$$V_{out} = V_{in}^{\gamma} \tag{3}$$

$$\gamma = \frac{d \log (V_{out})}{d \log (V_{in})} \tag{4}$$

As this connection is nonlinear, the impact won't be equal for each pixel and will rely upon their original value. Whenever $\gamma<1$, the first original dark regions will be brighter and the histogram will be moved to one side and vice versa with $\gamma>1$. Here work utilizes the gamma= 4.0 and Figure 9 depicts the eventual outcomes on a grayscale image.

Figure 9: Gamma Correct on Gray Scale Image

2.6. Morphological erosion

Morphologic capacity disintegration is utilized to sharpen the edges of the braille spots. Unlike other methods, their morphologic capacities disregard the flaws which happen to the surface and state of the picture. Furthermore, administrators such as segregation and

joining of individual pixels and different pixels help locate the decorated braille dot. Disintegration impact as per the organizing component was utilized. In contrast to paired disintegration, grayscale disintegration improves the dot subtleties [9]. Indicating a picture by *f(x)* and the grayscale organizing component by *b(x)*, where B is the space that *b(x)* is characterized, the grayscale disintegration of *f* by *b* is given as in the equation (5). Image after Morphological Erosion is shown in Figure 10.

$$(f\theta b)(x) = \inf_{y \in B}[f(x+y) - b(y)] \quad (5)$$

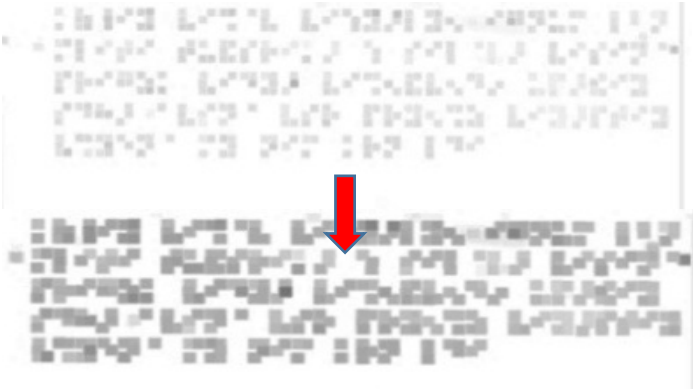

Figure 10: Image after Morphological Erosion

2.7. Feature extraction

Feature extraction is an illustrative system of the Braille image. The principle function of this procedure is to extract the Braille dots from the binaries image. The image capturing, pre-handling and division stages cause the image to be appropriate for various element extraction calculations. Some component extraction calculations are only concerned with the forms of the image while a few calculations ascertain each pixel of the image. Conversely, the underlying image might be noise influenced or obscured by different reasons..[7].

Simultaneously, the nature and the yield of the image pre-processing and division steps are determined by the picture feature and the extraction strategy. Feature extraction phase can be considered as the most important part of braille character translation because the accuracy of the translated character heavily depends on the extracted features of the cells.

Thresholding

Before the segment, the braille cell into six equal compartments, need perfect detection of braille dots. For this work have experimented on various thresholding techniques. First attempt was using straightforward thresholding strategies like Binary, To Zero thresholding and Binary inverse thresholding etc. The most intricate task was to recognize limit esteem in light of the fact that the reports have various hues and when checking, pixel luminance may change. To overcome the issue, in this research versatile thresholding Otsu strategy was utilized. Since the attempt was to make binomial pictures along the way of preparing part and it is the greatest contribution to Otsu thresholding, Otsu thresholding calculation located the bimodal qualities and attempted to discover the boundary that limits the weighted intra-class change. Bimodal picture is a picture whose histogram has two pinnacles. From the calculation, it takes the center of those histogram crests and computes the intra-class fluctuation.. Figure 11 shows the result of Otsu thresholding.

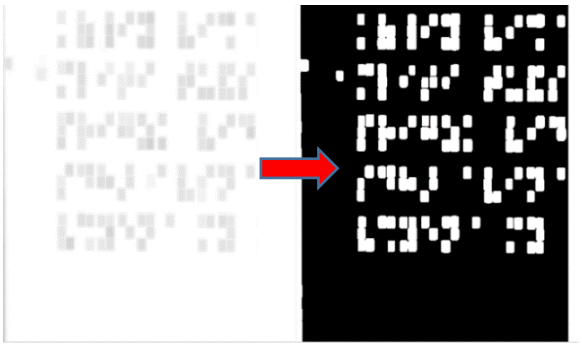

Figure 11: Image after Otsu thresholding

It actually finds a value of t which lies in between two peaks such that variances to both classes are minimum. After making thresholding, cell segmentation done using the standard braille dimensions.

The vertical as well as horizontal (however not corner to corner) separation between two focuses of neighboring dots in a specific cell is 2.5 mm. The separation between focus to focal point of relating spots in vertically contiguous cells is 5.0 mm, in the interim it is 3.75 mm for the horizontal neighboring cells.

2.8. Transcription

As presented in Figure 12 braille cells are sectioned and checked for the normal white pixels over 60%. On the off chance that the normal of white pixels is over 60%, it's perceived as substantial braille dot and marked as 1. If it's not, it is considered as there is no braille spot, which means the rate ascribed is 0.

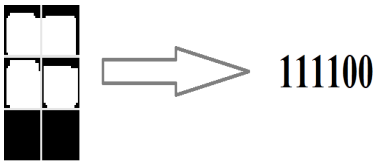

Figure 12: Cell transcription to binary values

Here below algorithm written for the binaries cell.

```
Inputs: erodeimg1, erodeimg2,
projection_x, projection_y; img,
resolutiondpi_x
For counter = projection_x to
projection and counter less than
height of erodeimg1 then
For counter = projection_x to
projection x + resolutiondpi_x and
less than width of erodeimg1 then
For counter = 0 and less than height
of img1 then
For counter =0 and less than width
of img1 then
do calculation:
Check row 1, column 1;
Check row 1, column 2;
Check row 2, column 2;
Check row 3, column 1;
Check row 3, column 2;
End for
End for
End for
End for
```

When binaries string array is extracted from the above way, the mapping to Sinhala Unicode is done using SQL Server. All the particular related string array contain it's Unicode in the database. The database connects to the system via Entity Framework in C#.

As a summary, for an example, Sinhala quote "ך ş וֹ ֿ ֽ שּׁדּ Ŕדֿ וּ" is mapped as "ךֹ וֹ ן נ שׁדּוו ד נ ּ ר ּ ד ּר ". And for the above Sinhala phase braille mapping is as follows;

3. Result and Discussion

The Final result depends on many processes. Mainly segmentation, feature extraction, and classification. These 3 processes have to perform accurately as possible so the final outcome will be more accurate.

The transformation from Braille documents into Sinhala content is a trending research area where much research has not been taken so far. The proposed framework has utilized some new strategies to perceive Braille cells utilizing a standard scanner. The framework has been tried with a wide range of sizes and diverse shading single-sided checked Braille documents written in Sinhala, and examined with various scanners.

The framework exploits the ordinary separating between Braille dabs inside a cell and the standard dividing between cells. The Braille documents can be embossed on a scope of media and with various particulars, for example, page size, dot size, bury Braille dot separation and, entomb Braille cell separation. Other than to accurately perceive Braille documents with numerous artifacts, an algorithm that effectively fragments the Braille pictures into cells is critical in Braille recognition.

Because of the idea of Braille documents, it is relied upon for most documents to have a few deformities, for example, slight varieties in background shading and few dull spots. Moreover, picture quality relies upon the degree of examining artifacts, for example, the impact of non-uniform light. These issues, for the most part, cause the softness of the feature some portion of Braille spots to be considerably less particular from the page background and could be misidentified as the feature or shadow portions of dots.

Additionally, the presence of light and dark areas that are not parts of Braille spots may prompt wrongly recognized spots on the off chance that they happen to satisfy the conditions set for true dots. Anyway, it is difficult to recognize noise regions and legitimate ones. Another factor which influences the exhibition of braille character recognition is the situation of the dots of a character in the picture. At present, if a legitimate spot lies outside the normal limits of the Braille character it won't be accepted as a component of that character. Thus, the character won't be accurately perceived.

The way that Braille characters don't have distinct contrasts in shape between them does not improve recognition. On the off chance that there is at least one spot at legitimate positions, at that point, the relating character will be perceived. It is hard to pass judgment on whether there is an additional dot or whether a spot is absent. Henceforth, on a solitary character premise, it is beyond the realm of imagination to expect to survey the rightness of the recognition result. In any case, it is conceivable to recoup from certain mistakes by performing background examination.

Generally, most of the errors can be credited to the nature of the picture of the Braille document. Additionally, it ought to be called attention to that the nature of the Braille document itself is significant. Extremely old document with a portion of the projections crushed because of substance use will offer ascent to all the more mistakenly perceived characters.

As in Table 2, it shows character-wise accuracy of the proposed programming model. With these outcomes here it demonstrates all the character recognition is above on 80% of accuracy. Table 3 and 4 indicate punctuation identification and numerical identification respectively. For that, there ought to pre-sign need to distinguish and afterward convert those into numerical. With the outcomes, numerical are additionally constantly distinguished at above 88% precision. By utilizing neural systems administration or some other profound learning calculations the precision rate can be upgraded via preparing those characters for word expectation and discover characters.

Various methods were carried out to improve the performance of the system. Experiments include scanning at different resolutions and color and grey level ranges.

However, in this system, it does not require expensive or complicated hardware. It uses a flatbed scanner, which can be shared with other applications.

The implemented method has been tested with a variety of scanned Braille documents written using standard Sinhala Braille. Documents were scanned using commercially available different scanners with 200 dpi and 300 dpi resolutions. The processing was performed on a PC with an Intel core i5, 4GB RAM, under EmguCV and.Net implementation environment.

Table 2: Character Wise Identification with Accuracy Rate

Character	Symbol	# of samples	# of samples correctly identified	Percentage (%)
අ	⠁ (braille pattern dots-1)	26	25	96.15385
ආ	⠜ (braille pattern dots-345)	90	90	100
ඇ	⠷ (braille pattern dots-12356)	22	20	90.90909
ඈ	⠻ (braille pattern dots-12456)	10	10	100
ඉ	⠊ (braille pattern dots-24)	101	96	95.0495
ඊ	⠔ (braille pattern dots-35)	18	18	100
උ	⠥ (braille pattern dots-136)	35	33	94.28571
ඌ	⠳ (braille pattern dots-1256)	15	15	100
එ	⠑ (braille pattern dots-15)	22	21	95.45455
ඒ	⠢ (braille pattern dots-26)	23	22	95.65217
ඓ	⠌ (braille pattern dots-34)	11	10	90.90909
ඔ	⠭ (braille pattern dots-1346)	10	10	100
ඕ	⠕ (braille pattern dots-135)	13	11	84.61538
ඖ	⠪ (braille pattern dots-246)	11	10	90.90909
ක	⠅ (braille pattern dots-13)	47	45	95.74468
ඛ	⠨ (braille pattern dots-46)	11	10	90.90909
ග	⠛ (braille pattern dots-1245)	30	30	100

ඹ	⠽ (braille pattern dots-126)	10	10	100
ඩ	⠳ (braille pattern dots-346)	11	9	81.81818
ච	⠨ (braille pattern dots-14)	14	14	100
ඡ	⠄ (braille pattern dots-16)	10	9	90
ජ	⠩ (braille pattern dots-245)	18	16	88.88889
ට	⠹ (braille pattern dots-23456)	20	20	100
ඨ	⠫ (braille pattern dots-2456)	10	9	90
ඩ	⠻ (braille pattern dots-1246)	13	13	100
ඪ	⠿ (braille pattern dots-123456)	10	10	100
ත	⠮ (braille pattern dots-2345)	55	53	96.36364
ථ	⠷ (braille pattern dots-1456)	10	10	100
ද	⠸ (braille pattern dots-145)	30	30	100
ධ	⠬ (braille pattern dots-2346)	17	16	94.11765
න	⠝ (braille pattern dots-1345)	72	70	97.22222
ප	⠏ (braille pattern dots-1234)	28	28	100
ඵ	⠞ (braille pattern dots-156)	11	10	90.90909
බ	⠂ (braille pattern dots-12)	22	21	95.45455
භ	⠈ (braille pattern dots-45)	12	11	91.66667
ම	⠍ (braille pattern dots-134)	73	71	97.26027
ය	⠽ (braille pattern dots-13456)	65	59	90.76923
ර	⠗ (braille pattern dots-1235)	80	79	98.75
ල	⠇ (braille pattern dots-123)	48	46	95.83333
ළ	⠌ (braille pattern dots-456)	12	12	100
ව	⠧ (braille pattern dots-1236)	70	70	100
ශ	⠯ (braille pattern dots-12346)	11	7	63.63637
ෂ	⠶ (braille pattern dots-146)	13	11	84.61538
ස	⠎ (braille pattern dots-234)	80	77	96.25
හ	⠓ (braille pattern dots-125)	30	30	100
ෆ	⠤ (braille pattern dots-124)	11	9	81.81818
ණ	⠫ (braille pattern dots-1356)	17	15	88.23529
ඟ	⠒⠶ (braille pattern dots-23)(braille pattern dots-1245)	11	9	81.81818
ඬ	⠒⠻(braille pattern dots-23)(braille pattern dots-1246)	11	10	90.90909
ඳ	⠒⠸(braille pattern dots-23)(braille pattern dots-145)	12	10	83.33333
ඹ	⠒⠂ (braille pattern dots-23)(braille pattern dots-12)	11	10	90.90909
ඥ	⠿ (braille pattern dots-12345)	10	9	90
ක්	⠁ (braille pattern dots-4)	118	113	95.76271
කං	⠲ (braille pattern dots-3)	40	34	85

Table 3: Punctuation Wise Identification Results and Accuracy Rate

Punc-tuati-on	Symbol	# of sam-ples	# of samples correctly identified	Perce-ntage (%)
.	⠲ (braille pattern dots-256)	23	21	91.30435
,	⠂ (braille pattern dots-2)	11	10	90.90909
;	⠆ (braille pattern dots-23)	12	12	100
:	⠒ (braille pattern dots-25)	10	10	100
!	⠖ (braille pattern dots-235)	12	11	91.66667
[]	⠶ (braille pattern dots-2356)	20	18	90
“	⠦ (braille pattern dots-236)	10	9	90
”	⠴ (braille pattern dots-356)	10	9	90
/	⠤ (braille pattern dots-36)	21	21	100
Space	(no braille dots)	76	73	96.05263

Table 4: Identified Numerals Results with Accuracy Rate

#	Symbol	# of sam-ples	# of samples correctly identified	Perce-ntage (%)
1	⠼⠁ (braille pattern dots-3456) (braille pattern dots-1)	25	25	100
2	⠼⠃ (braille pattern dots-3456) (braille pattern dots-12)	17	16	94.11765
3	⠼⠉ (braille pattern dots-3456) (braille pattern dots-14)	16	16	100
4	⠼⠙ (braille pattern dots-3456) (braille pattern dots-145)	16	15	93.75
5	⠼⠑ (braille pattern dots-3456) (braille pattern dots-15)	17	15	88.23529
6	⠼⠋ (braille pattern dots-3456) (braille pattern dots-124)	20	18	90
7	⠼⠛ (braille pattern dots-3456) (braille pattern dots-1245)	21	21	100
8	⠼⠓ (braille pattern dots-3456) (braille pattern dots-125)	22	22	100
9	⠼⠊ (braille pattern dots-3456) (braille pattern dots-24)	21	21	100
0	⠼(braille pattern dots-3456) (braille pattern dots-356)	70	68	97.14286

3.1. Threats to validity

With several approaches have done related to the work there is many limitations have found. Image acquisitions using different types of equipment would have an effect on results receiving. While the acquired image is not with the minimum dpi will affect results. With the lightning disturbances without equally spread on documents make the threat to results which observed. Cropping document with the desired way of the human pattern will lead to making half braille characters and direct effect on results we obtain.

4. Conclusion and Future Works

The Braille framework is a tactile technique broadly utilized by visually impaired individuals to read and write or peruse and compose. Braille documents contain lines of characters, where each character has six spots masterminded in three lines and two segments (three rows and two columns) and each dot can either be raised or be level as indicated by the corresponding character. Braille is reasonably understandable by visually impaired individuals; notwithstanding, sighted individuals need not have the option to comprehend these codes. Braille recognition system can connect the correspondence communication gap between visually impaired and sighted individuals. A ton of exertion has been made worldwide by specialists to connect this gap. In this investigation,

an endeavor has been made on the element extraction and characterization modules of Sinhala Braille acknowledgment as indicated by the Sri Lankan context.

This proposed programming model is fit for extracting Braille characters from a Braille document pursued by decoding them into Sinhala characters and after that standardization of the decoded Sinhala characters into readable Sinhala content. The transformation from Braille documents into Sinhala content is another zone where much research has not been completed.

An algorithm to distinguish dots in a picture of embossed Braille material obtained by an optical scanner was proposed. Despite the fact that the Braille dots have a similar shading as the foundation, they cast delicate shadows when checked with a standard flatbed scanner. These shadows are utilized to find the dots on the page.

In general, the methodology indicates achievability as a practical, cost-effective, quick and simple strategy to identify dots in Braille records. It doesn't require costly or complicated equipment. It utilizes a flatbed scanner which can be shared with different applications. Robustness to adapt to low-quality scans and imperfect reports are worked in at various levels. The outcomes got were promising during trials performed on single-sided embossed records, with over 95% accuracy.

The recognition rate for character recognition has the opportunity to get better. One approach to improve it is to actualize a Sinhala spell check algorithm. Any misrecognized image can be recognized since the word and sentence that the character has a place which would never again make sense.

It is important that every one of the examples in the investigations are sensibly all well-formed. A conceivable future upgrade in this undertaking is utilizing various allegations with numerous gadgets like cell phones. This may incorporate adding a few algorithms to progressively change different edges for various pieces of the framework, to represent fluctuation, for example, the shade of the paper. On account of slanted pictures, a few components to deal with the revolution will be automated. Indeed, even there are severe principles about the size of the spots utilized just as the dispersing between them, size of the braille specks in the wake of filtering is vary from record to report as indicated by its shading. If the feature extraction algorithm automatically adopted according to its color of the document there will be a much better extraction of features for classification.

Author's Contributions

Shanmuganathan Vasanthapriyan: Designing of experiment (75%), Laboratory and experiment (75%), Interpretation and data analysis (75%), Writing up (75%).

Malith De Silva: Designing of experiment (25%), Laboratory and experiment (25%), Interpretation and data analysis (25%), Writing up (25%).

References

[1] Ministry_of_Health. National Survey of Blindness, Visual Impairment, Ocular Morbidity and Disability in Sri Lanka. 2015; Available from: https://www.iapb.org/wp-content/uploads/National-Survey-of-Blindness-A-Report-2014-2015.pdf.

[2] Srinath, S. and C.R. Kumar, A novel method for recognizing Kannada Braille: Consonant-Vowels. International Journal of Emerging Technology and Advanced Engineering, 2013. 3(1): p. 596-600.

[3] Al-Salman, A.S., et al. An efficient braille cells recognition. in 2010 6th International Conference on Wireless Communications Networking and Mobile Computing (WiCOM). 2010. IEEE.

[4] Hentzschel, T. and P. Blenkhorn, An optical reading system for embossed Braille characters using a twin shadows approach. Journal of Microcomputer Applications, 1995. 18(4): p. 341-354.

[5] Mennens, J., et al., Optical recognition of Braille writing using standard equipment. IEEE Transactions on Rehabilitation Engineering, 1994. 2(4): p. 207-212.

[6] Al-Salman, A., et al., An arabic optical braille recognition system. 2007.

[7] Wajid, M., M.W. Abdullah, and O. Farooq. Imprinted Braille-character pattern recognition using image processing techniques. in 2011 International Conference on Image Information Processing. 2011. IEEE.

[8] Mousa, A., et al., Smart braille system recognizer. International Journal of Computer Science Issues (IJCSI), 2013. 10(6): p. 52.

[9] Zhang, H., J. Li, and J. Yin. A Research on Paper-Mediated Braille Automatic Extraction Method. in 2010 International Conference on Intelligent Computation Technology and Automation. 2010. IEEE.

[10] Antonacopoulos, A. and D. Bridson. A robust braille recognition system. in International Workshop on Document Analysis Systems. 2004. Springer.

[11] Li, J. and X. Yan. Optical braille character recognition with support-vector machine classifier. in 2010 International Conference on Computer Application and System Modeling (ICCASM 2010). 2010. IEEE.

[12] Educational_Publications_Department, සිංහල භාෂාව හා සාහිත්‍යය. 2018. 1 - 213.

[13] Perera, T. and W. Wanniarachchi, Optical Braille Translator for Sinhala Braille System: Paper Communication Tool Between Vision Impaired and Sighted Persons. The International Journal of Multimedia & Its Applications (IJMA) Vol, 2018. 10.

[14] Sinhalese Braille. 2016; Available from: https://ipfs.io/ipfs/QmXoypizjW3WknFiJnKLwHCnL72vedxjQkDDP1mXWo6uco/wiki/Sinhalese_Braille.html.

[15] Dubus, J., et al. Image Processing techniques to perform an autonomous System to translate relief Braille back into ink called LectoBraille. in IEEE 10th International Conference in Medicine and Biology Society, New Orleans. 1988.

[16] Falcon, N., et al. Image processing techniques for braille writing recognition. in International Conference on Computer Aided Systems Theory. 2005. Springer.

[17] Hu, Y. and H. Ji. Research on image median filtering algorithm and its FPGA implementation. in 2009 WRI Global Congress on Intelligent Systems. 2009. IEEE.

[18] Moshnyaga, V.G. and K. Hashimoto. An efficient implementation of 1-D median filter. in 2009 52nd IEEE International Midwest Symposium on Circuits and Systems. 2009. IEEE.

[19] Padmavathi, S., S.S. Reddy, and D. Meenakshy, Conversion of braille to text in english, hindi and tamil languages. arXiv preprint arXiv:1307.2997, 2013.

ASTES

Advances in Science, Technology and Engineering Systems Journal Vol. 4, No. 4, 230-238 (2019)

www.astesj.com

Special Issue on Advanced Electrical and Communication Technologies

ASTESJ

ISSN: 2415-6698

A Perceptually Optimized Embedded Image Coder and Quality Assessor Based Both on Visual Tools

Abderrahim Bajit[*,1], Mohammed Najid[2], Ahmed Tamtaoui[3], Abdellah Lassioui[1]

[1]*Ibn Toufail University, GERST Electrical Engineering Department, National School of Applied Sciences, Kénitra, Morocco*

[2]*Hassan II University, Electrical Engineering Department, Faculty of Sciences and Technologies, Mohammedia, Morocco*

[3]*Mohammed V University, SC Department, INPT Institute, Rabat, Rabat, Morocco*

ARTICLE INFO

Article history:
Received: 31 May, 2019
Revised: 24 July, 2019
Accepted :30 July, 2019

Keywords:

Human Visual System HVS,
Discrete Wavelet Transform,
Contrast Sensitivity Function,
Just Noticeable Difference,
Luminance & Contrast masking,
SPIHT embedded Coder,
Objective Quality Metric,
Subjective Quality Metric,
Mean Opinion Score MOS

ABSTRACT

In this paper, we propose a new Perceptually Optimized Embedded Zero Tree Image Coder EVIC and its improved version MEVIC. The coder presents a new perceptual model to weight wavelet coefficients to enhance SPIHT embedded coding. The new visual coder aims to improve the visual quality obtained by the reference SPIHT coder for a given targeted bit rate. In addition, the paper presents three-evaluation approaches (Objective, Subjective and Quantitative) based all on a quality score PS given by the objective visual quality metric named MWVDP which is an optimized version of Daly Visible Difference Predictor VDP. It incorporates the human visual system HVS properties, correlates largely well with the mean opinion score known as MOS and provides an important feature in image coding quality assessment. The visual coders EVIC/MEVIC are fully dependent to the HVS properties, from which, they include various masking effects and visual models. Based on this model, the visual coders weight the original wavelet coefficients and reshape their spectrum to optimize the perceptual quality coding for a given observation distance and bit rate. The visual weighting model processes within all wavelet sub-bands: 1) the contrast sensitivity filter CSF to mask invisible frequencies, 2) the threshold elevation to correct the luminance and elevate the contrast, 3) the Just Detectable Distortions JND to quantize visually the wavelet coefficients according to their corresponding thresholds. The visual coder EVIC and its optimized version MEVIC have the same software complexity as their reference SPIHT. However, they perform qualitatively and quantitatively excellent results experimentation and features improvement either in image coding and quality assessing.

1. Introduction

Recently increasing works effort made in embedded wavelet based image coder [1], which not only improves features in image compression, but also has the ability to truncate the bit stream at any desired bit budget and still capable to decode and reach an enhanced quality image. Embedded Wavelet Zero Tree coding (EZW) initiated first by J. M. Shapiro [2] and optimized next by A. Said and W. A. Pearlman [3] performs an algorithm that Sets Partitioning In Hierarchical Trees (SPIHT) the wavelet coefficients. These embedded coders have proven to be a very effective image compression and distortion measurement using spatial metrics like PSNR. Reducing such spatial errors does not necessarily guarantee the preservation of good perceptual quality of the decoded images and may result in visually annoying artifacts despite good PSNR measures. This is naturally true in low binary budget applications where we aim eliminating increasingly more redundant information while still minimizing visual distortions. Consequently, these exigencies obliged us to provide more efforts to develop a new wavelet based perceptual quality metric named MWVDP. This metric inspired from the Daly model known as Visible Difference Predictor and related to a psychometric function computes the probability of detecting errors in frequency domain and yields a score called PS serving for quality evaluation.

In computer vision, great successes are obtained by a class of wavelet based embedded visual image coders, such as PEZ, EZW, SPIHT and many others. Some coders did not compress the original wavelet coefficients with respect to the Just Noticeable Distortion JND thresholds like the optimal ones proposed by Watson model. The model experiments a psycho-visual tests

[*]Abderrahim BAJIT, National School of Applied Sciences ENSA, Ibn Toufail University, Kénitra Morocco, abderrahim.bajit@gmail.com

applied to the 9/7 biorthogonal wavelet basis [4] which offers an optimal quantization threshold that ensures a visually lossless compression quality improvement [5-8]. In other works, the use of many interesting HVS features were not adopted like, contrast sensitivity function CSF [9-12], luminance and Contrast Masking [13-16] whose special aim is to mask spatially the image spectrum invisible frequency contents according to HVS features. Implementing these properties, we may control image contrast, reduce considerable invisible information, quantize visually its frequency contents, and still efficiently improve its coding quality.

In this work, we propose a new visual optimized version MEVIC, which is a Visually Optimized version of EVIC [17] relative to its older version POEZIC introduced in [18] and its foveal one POEFIC presented in [19]. This scheme is fully dependent to the HVS properties, which, before coding the original wavelet coefficients it previously applies perceptual weights according to their visual importance. The visual model weights the original wavelet coefficients, reshapes their spectrum to optimize the final quality coding for a targeted viewing and bit budget conditions and finally assesses its reached quality to its reference SPIHT version. Although the latter reduces effectively the MSE, it is not explicitly deployed to compensate perceptual distortions that match the HVS capacities. The visual weighting model processes within all wavelet sub-bands: Contrast Sensitivity Function, Luminance and Contrast Masking and Threshold Elevation according to its perceptual thresholds JND that we employ to reduce the human observer detect ability of compression errors.

We organize the paper as follow: in section two, we will develop the visual coder scheme and flow diagram and will explain briefly its main components. Then in section three, four and five, we will detail the deployed visual models and demonstrates their important role in reshaping the original wavelet coefficients spectrum so that it keeps and encodes the necessary information and eliminates as much as possible all redundant ones. Next in the sixth section, we will introduce a new wavelet-based image quality assessor; itself is based on visual models, which takes an interesting role in optimizing and measuring objectively the image coding quality. Our new wavelet assessor, named Modified Wavelet based Visible Difference Predictor MWVDP and its versions employ all a psychometric function used to compute the probability of detecting errors in frequency domain and provide a score called PS aiming for quality assessment. Finally, in section seven, we will discuss in more detail the obtained results with respect to the qualitative, quantitative and subjective approaches and will compare them to the mean opinion score known as MOS derived experimentally from subjective tests.

2. Visual Wavelet Based Image Coding Flow Diagram

In this paper, we propose a visual coder as shown in figure 1 combines the following stages, successively: Discrete Wavelet Transform DWT, Contrast Sensitivity Filter CSF, Luminance correction, contrast adaptation known as threshold elevation more detailed in Figure 2 and set-up according to optimal wavelet visual thresholds JND, and finally SPIHT embedded coding. The visual coder MEVIC's flow diagram, in the first step, based on Daubechies biorthogonal wavelet filter (Watson model) decomposes discretely the candidate image to perform a cortical-like representation [20] despite its channel limitation. Having some special mathematics features, this wavelet ensures a perfect reconstruction, which urges the image compression standard JPEG2000 committee to recommend the filter to be the most used in image vision lossless-based compression.

The perceptual model Setup reshapes the original wavelet coefficients spectrum in order to eliminate much more redundant information and keep only important one regarding to some entered constraints exclusively the targeted bit budget with respect to a given observation distance. These constraints play an important role in evaluating objectively and subjectively both the image coder and the quality assessor. The weighting model as schematized in Figure 2 and detailed next, apply the contrast sensitivity filter, within all spatial-frequency sub-bands, to maintain perceptible frequencies and eliminate all invisible ones according to the SVH properties (Section III). In addition, we apply the wavelet-based perceptual thresholds JND that we derive from Watson experimental model to compute the wavelet coefficients threshold elevation. Applying these thresholds, the quantization distortions are under visibility control and the targeted perceptual lossless compression is achieved (section IV).

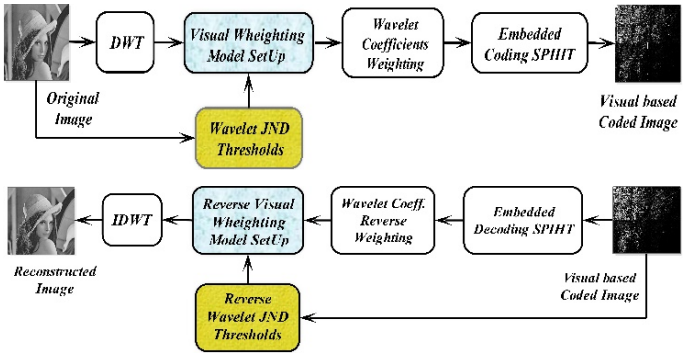

Figure 1: Visual-based Embedded Wavelet Image Coder Flow Diagram.

In the second stage, we compute the contrast masking known as the contrast thresholds elevation. Its process begins first on calculating the luminance masking related the image filtered wavelet coefficients. Then it deploys the perceptual thresholds required for contrast correction computation, known as contrast threshold elevation. This operation shadows invisible contrast components and elevates perceptible ones with respect to the level of the Just Noticeable Difference JND thresholds (Section IV).

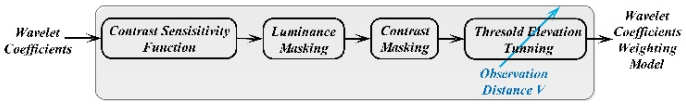

Figure 2: Wavelet-based weighting model diagram.

The main purpose of this optimized visual-based weighting model employed exclusively to MEVIC (optimized version of EVIC [17]) is the ability to tune none linearly the image spectrum shape depending on the observation distance. In this optic, as the observation distance grows from low level to the greatest ones the shape intends to cover the important frequencies. For low distances the visual models cover much more the low frequencies. In the opposite way -higher observation distances- the visual weighting model covers this case much more frequencies.

In the final step, we apply an embedded coder to encode progressively with scalable resolution the visual based wavelet coefficients until reaching the targeted resolution related to a given bit rate. In our paper, we have adopted the standard SPIHT embedded coding. The latter itself is an optimized version that belongs to the set of the wavelet-based embedded Zero Tree EZW

image coders initiated exclusively by Shapiro and optimized thereafter by A. Said and W. A. Pearlman.

3. Contrast Sensitivity Filtering Approaches

Rather than coding directly the image wavelet-based coefficients spectrum and optimize the perceptual quality of its reconstructed version, we apply the contrast sensitivity function CSF [9-12] benefits. This filter implies, quantitatively, how much the HVS perceives a pattern located spatially in image region of interest. It sets the contrast perception related to spatial frequency usually represented in cycles per optical degree. This feature makes the CSF filter spectrum shape, as plotted in Figure 3, specifically independent to the observation distance. Common to classical compression techniques focus efforts in optimizing their coding efficiency and reducing computational complexity, which is not sufficiently complete in improving its perceptual quality.

The mathematical property of the CSF filter reshapes the spectrum of the wavelet-based transformed image to perceptual domain, which gives the ability to remove significantly all imperceptible frequencies regarding the human cortical domain. In the context, we suppose that the viewing conditions (spatial resolution: r, and observation distance: r) are fixed. In reality, this is not a fortiori true, because an observer can see the image from any distance. Nevertheless, specifying the spatial resolution r and observation distance v is mandatory to apply a visual weighting. Therefore it is observed, that modifying slightly the CSF frequency spectrum shape and the assuming the ”worst case of viewing conditions”, a CSF masking filter that works perfectly for varying viewing conditions and scalable resolution devices must be conform to JPEG2000 adopted model we plotted in Figure 3.

In lossless compression applications, the CSF filter weights the original wavelet coefficients to reshape their previous spectrum, and code weighted version. In the opposite way, in non-visual coding algorithms, encoder codes classically the perceptible frequencies and many other redundant residues proved to be unusual to the human visual system, which consumes additional coding bits budget and increases significantly computational time.

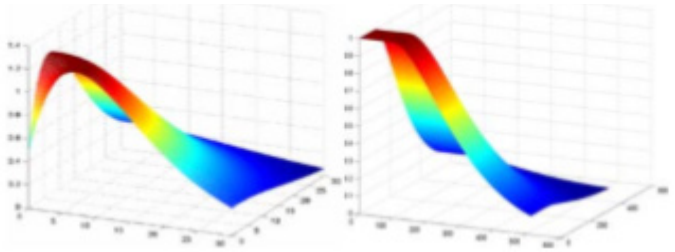

Figure 3: Mannos contrast Sensitivity filter in the left, and Daly in the right.

To implement the CSF and apply it to wavelet image spectrum, there exits many strategies. Conventional implementation weights all wavelet coefficients belonging to one sub-band adopting a single invariant weighting factor [11]. This strategy named Invariant Single Factor (ISF). It assigns one weight factor across wavelet channel. This strategy is very simple and still an excellent weighting approach. Filtering implementation weights the original wavelet spectrum matching exactly the shape of the CSF. This approach keeps the possibility of an orientation dependent weighting inside the sub-band and is adapted locally to image contents properties. Adaptive approach mixes both strategies. We apply the ISF approach to low frequency spectrum and we match the rest (higher frequencies) using adaptive strategy.

4. Luminance Masking and Threshold Elevation

The main step adopted in our visual coding process is the contrast masking-weighting filter, which we exclusively adopt in this work. In fact, we apply this operation to the original wavelet spectrum. Its conception is based on three psychophysical properties we model to implement and setup the visual weighting filter, successively: first, we determine the perpetual thresholds JND experienced by Watson, then we apply light adaptation [13-14] (also known as, luminance masking), Contrast correction [15-16] known as threshold elevation. Once computed, the model is applied to wavelet coefficients after ensuring a cortical-like decomposition, then compared to the real model processed by the famous Human Visual System cortical decomposition which we finally verify their perfect correlation.

To reach this aim, we first compute the JND thresholds using a base detection related to wavelet sub-bands. We derive its model from the psychophysical experiments processed by Watson. The experienced model corresponds exclusively the Daubechies biorthogonal wavelet filter. Modeling thresholds in image compression, depends on the mean luminance over a selected region in the image. To calculate the contrast sensitivity we take into account its variation that we may tune using luminance masking correction factor. In our paper, we adjust the luminance masking with a factor exponent of 0.649, based on the power function, adopted seemly in JPEG2000 image coder.

In addition, contrast correction or contrast threshold elevation, is a second factor that affects significantly the detection threshold. This elevation keeps in mind the idea that the visibility of one image pattern component changes significantly with the presence of an image masker compound [13-16]. Contrast masking corrects the variation of the detection threshold of a pattern component as a function of the masker compound. The masking result refers to us as contrast function of a target threshold versus a masker. In this paper, wavelet coefficients represent the masker signal he input image to code visually, while the quantization distortion represents the target signal. In figure 4, we display the final wavelet based visual weighting model process. We plot in 3D dimension the shape of the visual models. The figure presents successively the visual masking effects, applied to the image spectrum, the original image wavelet coefficients, their corresponding weights, and their weighted visual-based version.

In the beginning, the process decomposes the original image to provide wavelet coefficients -first step-. Then calculates their corresponding perceptual thresholds JND -second step-. These later stages rely both to Daubechies biorthogonal filter. Next, it computes the contrast sensitivity function CSF filter to reshape the image wavelet spectrum by weighting their coefficients –third step-. After that, it adapts the image corresponding luminance -fourth step-, and elevates the contrast according to perceptual thresholds. Finally, -fifth stage-, it applies the designed filter to weights the wavelet coefficients and progressively encode them according to SPIHT embedded coding philosophy.

We illustrate in 3D plotting demo, the visual weighting process applied to Lena test image with respect to a given viewing distance **V=4**. This process shows how we reshape the image wavelet spectrum with our designed visual weights, and shows how the filter affects the wavelet distribution across sub-bands. It reshapes considerable medium and low frequencies that constitute naturally the main image contents. Note that, one may tune and refine the spectrum shape dependently to a varying observation distance.

5. Wavelet Visual-Based Weighting Model Process

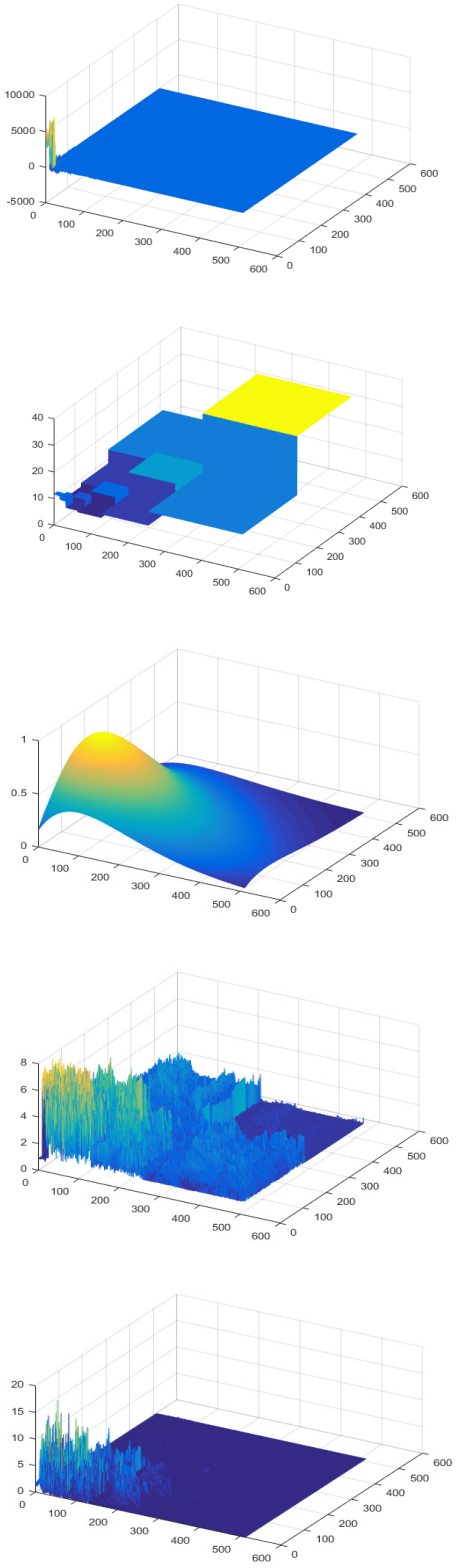

Figure 4: Visual weighting model stages process designed for LENA test image. We display from the top to bottom, its components as follow: Original Wavelet Coefficient DWT, Wavelet perceptual thresholds JND, Contrast Sensitivity Function CSF, Threshold Elevation (Contrast Masking), and the Visually Weighted Wavelet Coefficients to encode progressively by SPIHT coder.

6. Wavelet Visual Based Objective Quality Assessor

To assess the image coding quality and evaluate compression techniques we compare reliably measure the image compression quality according subjectively the mean opinion score (MOS) reference factor. The use of mathematical model such as the mean squared error (MSE) and its optimized version the peak signal to noise ratio (PSNR) are simple and computed spatially. However, these metrics correlate poorly with the mean opinion score MOS depending on advantages that offer the HVS properties.

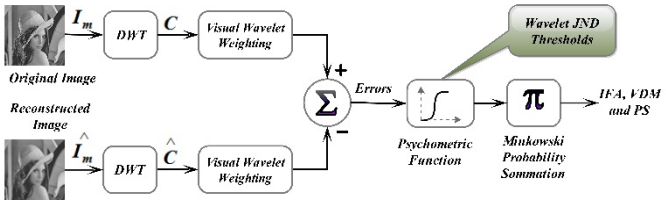

Figure 5: Modified Wavelet Visible Difference Predictor Flow Diagram.

Recently, we apply a cortical-like metrics based on the HVS properties to optimize the correlation factor with the Mean Opinion Score MOS. it predict the introduced errors in a degraded image naturally invisible to human observer [21-33]. The VDP metric [28] behaves like such assessors, which inspired on cortical models provides an indication degree of visual errors as a function of image location. Adaptive metrics based on wavelet transform becomes efficient in image coding, because of its similarity to human cortical channels. Despite their channels limitation, the wavelet-based assessors still provide an excellent quality measure and contribute in optimizing the image compression schemes.

In this paper, we have developed a new wavelet based image quality metric; named Modified Wavelet-based Visible Difference Predictor MVDP shown in figure 5. This visual metric is an optimized version of the WVDP we used in [34-36]. The later computes the visible errors summation using the Minkowski unit to reach the visible difference map and yields of course the quality factor PS using the psychometric function. The former, first, weights both the original image and its visual image using the same visual model we deployed in section 3. This way it eliminates all invisible information and compare only the important ones. Then it transfers these errors to the Minkowski summation unit to reach the visible difference map and the quality factor PS using the psychometric function. This factor contributes efficiently in visual-based image encoders aiming to enhance their performance. It expresses the ability of perceiving distortions within wavelet channels. In the following formula, we express detection probability:

$$P(\lambda,\theta,i,j)=1-\exp\left(-\left|\frac{D(\lambda,\theta,i,j)}{JND(\lambda,\theta,i,j)}\right|\right)$$

Where $D(\lambda,\theta,i,j)$ is the quantization distortion detection, is the location (λ,θ,i,j), $JND(\lambda,\theta,i,j)$ is the perceptual thresholds, β denotes a refining parameter the correspondence location(λ,θ,i,j), and P the probability summation. Inspired from Minkowski summation, we sum within all wavelet sub bands all computed probabilities to reach the evaluation score. The final objective score is computed as follow:

$$P=\exp\left(-\sum\left|P(\lambda,\theta,i,j)\right|\right)$$

Note that as more and more this factor approaches the unit the quality becomes better. In addition, this factor ranges from '0' for poor quality to '1' for excellent coding quality.

7. Quality Results Discuss

In vision, the visual coders are fully dependent to visual quality metrics which theoretically and practically correlate well with visual reference known as the mean opinion score MOS. In this paper, we tested the visual EVIC and its optimized version MEVIC coders using 8 bits monochrome test images. We assessed their quality using the wavelet visual-based objective metric WVDP for the former and its modified version MWVDP for the later. In this purpose, we compare EVIC and MEVIC quality coding with respect to their reference, respectively SPIHT for the former and EVIC for the later. In this optic, we deployed three evaluation approaches: OBJECTIVE, SUBJECTIVE, and QUANTATIVE, both according to bit budget and viewing distance conditions.

The first approach depends in the factor quality PS values are obtained from the evaluation of the visual quality coding EVIC vs SPIHT and MEVIC vs EVIC applied to ZELDA and GOLDHILL test images. As shown in figures 5 and 6, the results are given for increasing bit rates varying from 128:1 which corresponds to 0.0078125bpp till 1:1 synonymous to 1bpp and a fixed viewing distance of values V=1, 3, 6 and 10. As a results, all approaches approve that for very low binary budget (less than 0.0625bpp), many spatial patterns are hardly perceivable in SPIHT coded image, however visual coders EVIC and MEVIC exhibit much more interesting information in those regions. Similarly, at medium bit rate less than 0.25bpp, the reference still providing blurred images, while the concurrent EVIC/MEVIC coders show significant quality across the whole image. On the other hand, for bit rates around 0.5bpp, the concurrent EVIC/MEVIC quality still always superior than its reference SPIHT. Finally, when the bit-rate reaches very high bit rate more than 1bpp, visual coder approaches uniform resolution and all mentioned coders (reference SPIHT, visual EVIC, and its optimized version MEVIC) decode indistinguishable images difference.

The second strategy performs an averaged subjective assessment notation scores applied to both reference visual coders. As shown in Figures 7-8, we evaluate subjectively the EVIC versus SPIHT and MEVIC versus EVIC coding qualities of ”Barbara” test image for varying bit budget and still observation distance V and approve the subjective quality notation to the objective values related to the measured probability score PS. The second approach approves that, at low binary budget, visual coders EVIC/MEVIC maintain considerable quality across the whole image. Similarly, for intermediate binary budget, the gazed patterns are weakly recognizable in reference coded images; however those regions are strongly perceivable in visual coders and exhibits much more interesting information across image. At higher binary budget and viewing distance, the visual coder behaves perfectly over all image contents whereas the standard one becomes significant.

The last strategy (QUANTITATIVE approach), the quality gain provided by the visual coder relative to the reference coder SPIHT is calculated according to these formulas:

$$100*(PS_{EVIC} - PS_{SPIHT})/PS_{SPIHT}$$

$$100*(PS_{MEVIC} - PS_{EVIC})/PS_{EVIC}$$

We can conclude as filled in tables 1, 2 and 3, that with increasing binary budget and viewing observation conditions the quality gain grows progressively up. This constitute the aim of our visual coder and its intimate quality assessors, which are able of enhancing coding performances and avoiding errors introduction.

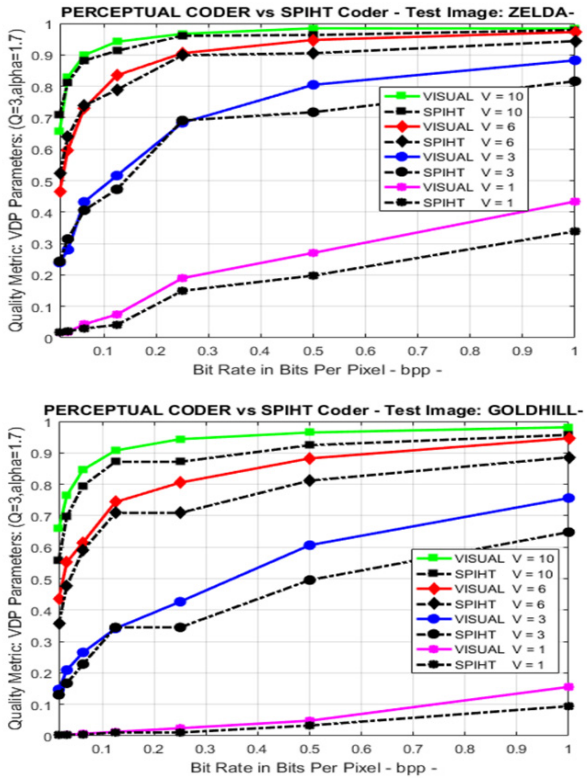

Figure 5: Visual coder EVIC vs standard SPIHT, WVDP-based visual quality metric applied to test images ZELDA (top) and GOLDHILL (bottom) for varying targeted bit rate and a given viewing distances 1, 3, 6, and 10.

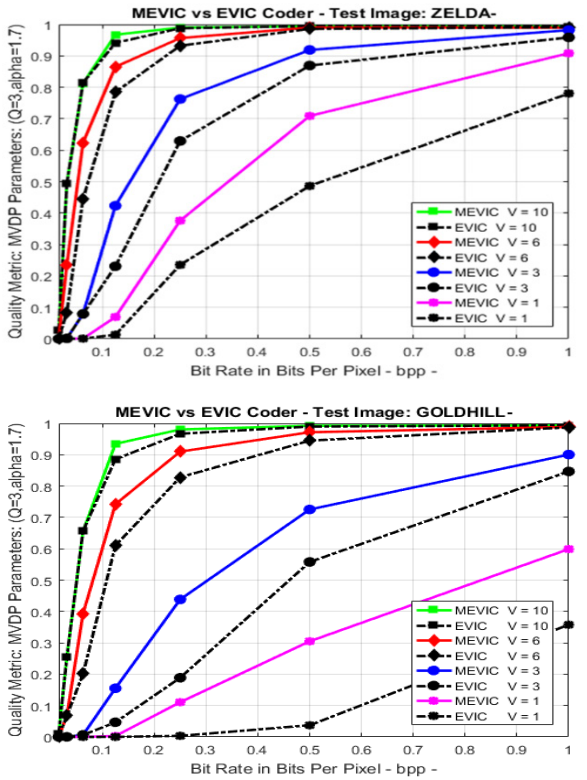

Figure 6: Visual coders MEVIC vs EVIC Quality measures, MWVDP-based visual quality metric applied to test images ZELDA (top) and GOLDHILL (bottom) for varying targeted bit rate and a given viewing distances 1, 3, 6, and 10.

Figure 7: Barbara EVIC visual coding images (left column) versus the standard SPIHT coding images (right column) and their quality scores PS using visual WVDP assessor given for varying bit rate and fixed observation distance. The bit rate varies, respectively as follow: a. 0.0313 bpp, b. 0.0625 bpp, c. 0.15 bpp, d. 0.25 bpp, and e. 0.5 bpp. Moreover, the viewing distance is tuned to V= 4.

ISAECT19 ORIGINAL RESULTS

Figure 8: Barbara visual coding images EVIC (left column) versus its optimized version MEVIC (right column) and their quality scores PS using visual MWVDP assessor given for varying bit rate and fixed observation distance. The bit rate varies, respectively as follow: a. 0.0313 bpp, b. 0.0625 bpp, c. 0.15 bpp, d. 0.25 bpp, and e. 0.5 bpp. Moreover, the viewing distance is tuned to V= 4.

ASTESJ EXCLUSIVE RESULTS

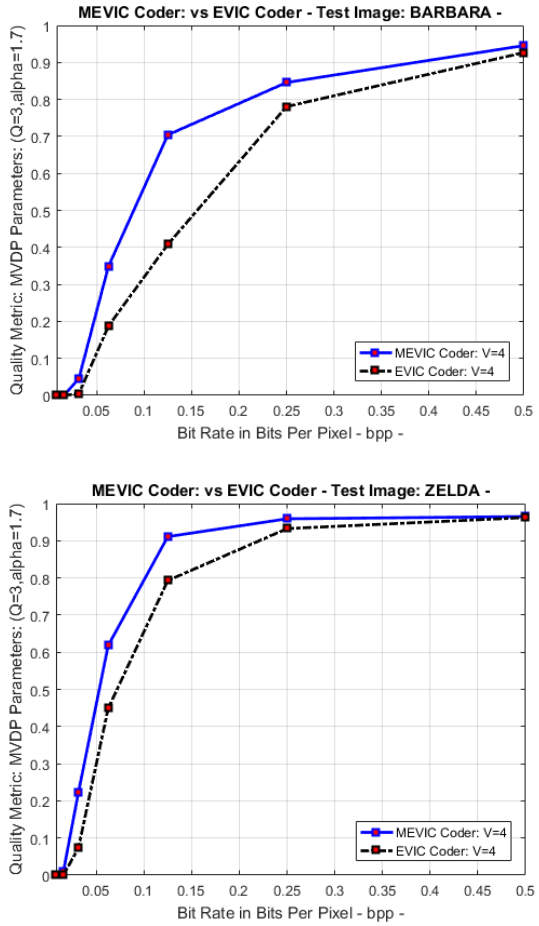

Figure 9: MEVIC vs EVIC Quality measure for varying binary budget and given observation distance 4 for images BARBARA (top) and ZELDA (bottom).

Table 1: EVIC vs SPIHT WVDP-based metric quality gain for varying bit rates and still viewing conditions. ***ISAECT19 ORIGINAL RESULTS***

Targeted Bit Rate	Quality Gain (%)			
	LENA	BARBARA	MANDRILL	BOAT
BPP = 0.0625	6.4562	0.7250	24.6382	17.3908
BPP = 0.25	3.8569	19.6639	32.9948	48.4490
BPP = 1	5.2489	2.9949	9.8373	1.8828

Table 2: EVIC vs SPIHT WVDP-based metric quality gain applied to images: LENA, BARBARA, MANDRILL and BOAT for varying viewing distances and static binary budget. ***ISAECT19 ORIGINAL RESULTS***

Observation Distance	Quality Gain (%)			
	LENA	BARBARA	MANDRILL	BOAT
V = 1	15.1549	29.6901	45.1232	78.9933
V = 3	7.6339	12.1079	18.0167	24.8798
V = 6	4.7876	10.9930	14.7008	12.1474
V = 10	6.1027	8.8758	10.1884	8.2992

Table 3: MEVIC vs EVIC MWVDP-based metric quality gain applied to images: LENA, BARBARA, MANDRILL and BOAT for varying viewing distances and static binary budget. ***ASTESJ EXCLUSIVE RESULTS***

Observation Distance	Quality Gain (%)			
	LENA	BARBARA	MANDRILL	BOAT
V = 1	166	2367	1687	3420
V = 3	2972	59	344	8862
V = 6	6	5	15	50
V = 10	9	8	7	15

8. Subjective quality metric

In this section, we will introduce a new method of assessing coding quality. This method is based on a subjective approach as it was used in the previous section. It provides a quality factor called MOS (Mean Opinion score) which averages the subjective measures applied on images coded by MEVIC for different compression rates. The measurements are collected on the basis of a study established by a group of observers of different class, sex and age on a subjective scale ranging from very poor to excellent quality. We applied the MOS factor to validate the use of the MEVIC visual coder and that of the MWVDP visual metric.

8.1. Conditions to be met in Subjective Quality Metrics

The subjective quality evaluation is normalized by the CCIR recommendations [33-38], originally designed for television images without taking into account the introduced degradations in the original image. We aim to evaluate the detected distortions between degraded image and its reference and adopt comparative measures tests. In addition, we suppose that the images can be edited, zoomed and viewed from nearest observation distance. Therefore, we assume that the evaluation conditions experienced by Fränti, as recommended in the CCIR and defined in Table. 4, are partially respected. In addition, we normalize the evaluation range so that we avoid introducing additional errors that depends naturally to the environment tests. To reach an excellent environment, we must avoid additional light sources unless those initially used for the room lighting. In worst case, significant degradation will the image quality. In addition, the screen monitor position must avoid external light source, and the observer's vision, or disturb the monitor reflections.

Test Images	Standard Test Images
Viewing Conditions	Environment of Normal Desk
Observation Distance V	This parameter is left to the observer's choice
Viewing Duration	Unlimited
Observers Number	From 15 up to 39
Quality Scale Range	Varies from 0 up to 10

Table 4: Conditions to met when using Subjective Quality Evaluation

8.2. Subjective versus Objective Metrics Correlation Score

To compute the correlation factor between the objective measures (vector X) and the subjective measures (observation vector Y), we apply the correlation's score defined as follow:

$$\rho(X,Y) = \frac{\sum_{i=1}^{n}\left(X_i - \overline{X}\right)\left(Y_i - \overline{Y}\right)}{\sqrt{\sum_{i=1}^{n}\left(X_i - \overline{X}\right)^2}\sqrt{\sum_{i=1}^{n}\left(Y_i - Y\right)^2}}$$

Where X_i and Y_i, i = 1 to n, denote respectively the vector components of X and Y. n denotes the number of components. $\overline{X}$ and $\overline{Y}$ perform, respectively, the average of the vectors X and Y values, with respect the following formula:

$$\overline{X} = \frac{1}{n}\sum_{n=1}^{n} X_i$$

And determines the variance value, as follow:

$$Var(X) = \frac{1}{n}\sum_{i=1}^{n}\left(X_i - \overline{X}\right)^2$$

8.3. Subjective Metric MOS Assessment Experimental Results

To experiment the MOS calculation, the test images are displayed on a CRT screen of a Personal computer PC, according to 10.5cm x 10.5cm size (512x512 image resolution) [33-38]. The MOS factor varies from 0 up to 10 (2: very annoying degradation, 4: annoying, 6: a little bit annoying, 8: perceptible, but not annoying, 10: Imperceptible). In addition, we allow the observers to adjust their obtained scores and note their marks by half-values. To compute the subjective score for a given distorted image, we average all noted marks provided by the observers. Finally, we perform a correlation coefficient for a single kind of image. The index n it adjusted to 8 (JPEG2000, 512x512 images).

Figure 10 shows the MOS subjective measures vs the probability scores PS given by the MWVDP metric applied to some test images degraded by the reference JPEG2000 image coder. Let assume that the probability score PS evaluate according to MOS score applied especially to highly textured images at lower bit rates. This proves a better correlation between objective and subjective measures. The correlation factor reaches 0.9529 and 0.9396 respectively for "Barbara" and "Mandrill" test images.

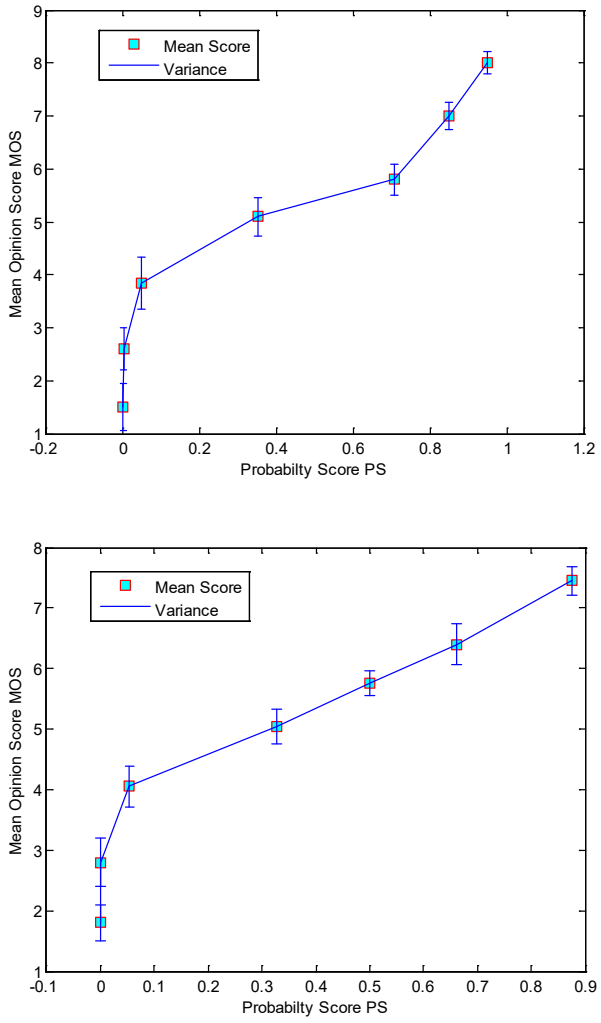

Figure 10: Subjective notes MOS vs Objective scores PS applied to "Barbara" (top) and "Mandrill" (bottom) according to the following setup: 512x512 coded images JPEG2000, observers=24, image-degraded versions=24, .V=4.

9. Conclusion

We proposed in our paper a new visual image coder named a Modified Embedded Visual based image coder MEVIC based on its previous version Embedded Visual based image coder EVIC. We derived the proposed coders from their predecessor POEZIC and its foveal version POEFIC. We also introduced a new visual image coding quality metric named Modified Wavelet Visible Difference Predictor MWVDP. Both of visual coder and quality assessor applies a battery of perceptual tools, and exploits both various visual weighting masks according to the human psychophysical properties HVS. The visual based weighting model incorporates successively the CSF filter, the perceptual thresholds JND, the Luminance adaptation and the thresholder contrast elevation. The provided model reshapes the original wavelet coefficients spectrum, keeps the important information and eliminates all invisible and redundant ones.

By doing so, we encoded and assessed the useful information, which according to a given binary budget and observation distances we reached more enhanced image quality compared to its reference version that coded directly the original wavelet spectrum. The visual coder and quality assessor compute both a cortical-like decomposition, which despite its frequency channels limitation enhances the image decomposition, minimizes perceptually more relevant distortion, reaches the targeted bit rate and optimizes the visual quality compared to its reference SPIHT. It also has the ability to tune non-linearly the image spectrum shape depending on the coding and viewing conditions. In this optic, as the observation distance grows up from low level to the greatest ones the shape intends to cover the important wavelet channels.

Moreover, we developed in this present work, a new wavelet-based image quality assessor named MWVDP, which applies the designed visual weighting model, provides a probability score PS, which takes an important place in optimizing and evaluating objectively the image coding quality. The provided factor deploys a Minkowski probability summation according to a psychometric function across wavelet channels. We applied this to the reference SPIHT, also to its visual version EVIC and MEVIC to predict the perceptual differences between each other. Note that the greatest this factor is, the best the coding quality is. Also, note that this metric plays an important role in our visual based coders, whose experimental results show very exciting performance and powerful quality improvement. In addition, we gathered, discussed and compared the obtained results with different evaluation strategies we meant objective, subjective and quantitative approaches to approve and validate our work.

To finalize our modest work, note that either visual coder and its quality intimate evaluator constitute both an interesting single task belonging a research work that designs a real time embedded system that we will integrate in an Automotive Embedded ARM-based System On Chip -SoC- applied to artificial intelligence ***AI-based antonymous driving assist and security systems –ADAS***-.

References

[1] N. Jayant, J. Johnston, and R. Safranek, "Signal compression based on models of human perception," Proc. IEEE, vol. 81, no. 10, pp. 1385– 1422, Oct. 1993.
[2] J. M. Shapiro, "Embedded image coding using zerotrees of wavelet coefficients", IEEE Trans. Signal Processing, vol. 41, pp. 3445-3462, 1993.
[3] A. Said and W. A. Pearlman, "A new, fast and efficient image codec based on set partitioning in hierarchical trees", IEEE Trans. Circuits and Systems for video Technology, vol. 6, pp. 243-250, June 1996.

[4] Michael Unser, Fellow, IEEE, and Thierry Blu, Member, IEEE Mathematical Properties of the JPEG2000 Wavelet Filters [39], IEEE TRANSACTIONS ON IMAGE PROCESSING, VOL. 12, NO. 9, SEPTEMBER 2003
[5] A. B. Watson, "DCT quantization matrices visually optimized for individual images," in Proc. Hum. Vis., Visual Process. Digital Display IV, 1993, pp. 202–216.
[6] Watson and J. A. Solomon, "A model of visual contrast gain control and pattern masking," J. Opt. Soc. Amer., vol. 14, pp. 2397–2391, 1997.
[7] T. Pappas, T. Michel, and R. Hinds, "Supra-threshold perceptual image coding," in IEEE Int. Conf. Image Processing, 1996, pp. 237–240.
[8] A.B Watson, G.Y.Yang, J.A.Solomon, and J.Villasonor, ``Visisbility of Wavelet Quantization Noise, `` IEEE Trans. Image Processing, vol.6 no, 8, pp. 1164-1175 1997.
[9] J. M. Foley and G. M. Boynton, "A new model of human luminance pattern vision mechanisms: analysis of the effects of pattern orientation, spatial phase and temporal frequency," in Comput. Vis. Based Neurobiol, vol. 2054, 1994, pp. 32–42.
[10] J. M. Foley, "Human luminance pattern-vision mechanisms: masking experiments require a new model," J. Compar. Neurol., vol. 11, no. 6, pp. 1710–1719, 1994.
[11] S. Daly, W. Zeng, J. Li, S. Lei, Visual masking in wavelet compression for JPEG 2000, in: Proceedings of IS&T/SPIE Conference on Image and Video Communications and Processing, San Jose, CA, Vol. 3974, January 2000.
[12] Marcus J. Nadenau, Julien Reichel, and Murat Kunt,`` Wavelet-based Color Image Compression: Exploiting the Contrast Sensitivity Function`` 2000.
[13] G. E. Legge and J. M. Foley, "Contrast masking in human vision," J. Opt. Soc. Amer. A, vol. 70, no. 12, pp. 1458–1471, 1980.
[14] D. G. Pelli, "Effects of Visual Noise," Ph.D. dissertation, Cambridge Univ., Cambridge, U.K., 1981.
[15] J. Ross and H. D. Speed, "Contrast adaptation and contrast masking in human vision," in Proc. Roy. Soc. Lond. B, 1991, pp. 61–69.
[16] R. J. Safranek, "A comparison of the coding efficiency of perceptual models," Proc. SPIE, vol. 2411, pp. 83–91, 1995.
[17] Bajit, A., Nahid, M., Tamtaoui, A, Lassoui, A, "A Perceptually Optimized Embedded Image Coder and Quality Assessor Based on Visual Tools" 2018, ISACET 2018 -IEEE-International Symposium on Advanced Electrical and Communication Technologies, 2018.
[18] A. Bajit, M. Nahid, A. Tamtaoui, and E. H. Bouyakhf, "A Perceptually Optimized Wavelet Embedded ZeroTree Image Coder" International Journal of Computer and Information Engineering Vol:1, No:6, 2007
[19] A. Bajit, M. Nahid, A. Tamtaoui, and E. H. Bouyakhf, "A Perceptually Optimized Foveation Based Wavelet Embedded ZeroTree Image Coding" International Journal of Computer Science Volume 2 Number 4, 2008
[20] I. Honsch and L. J. Karam, "Adaptive image coding with perceptual distortion control," IEEE Trans. Image Process., vol. 11, no. 3, pp. 213222, Mar. 2002.
[21] A. B.Watson, "Probability summation over time," Vis. Res., vol. 19, pp. 515–522, 1979.
[22] J. G. Robson and N. Graham, "Probability summation and regional variation in contrast sensitivity across the visual field," Vis. Res., vol. 21, pp. 409–418, 1981.
[23] P. C. Teo and D. J. Heeger, "Perceptual image distortion," in Proc. IEEE Int. Conf. Image Processing, 1994, pp. 982–986. [21]
[24] J. G. Robson and N. Graham, "Probability summation and regional variation in contrast sensitivity across the visual field," Vis. Res., vol. 21, pp. 409–418, 1981.
[25] S. J. P. Westen, R. L. Lagendijk and J. Biemond, "Perceptual Image Quality based on a Multiple Channel HVS Model," Proceedings of ICASSP, pp. 2351-2354, 1995.
[26] C. Zetzsche and G. Hauske, "Multiple Channel Model Prediction of Subjective Image Quality," SPIE, Human Vision, Visual Processing, and Display, 1077, pp. 209-215, 1989.
[27] S. Daly, "The visible differences predictor: An algorithm for the assessment of image fidelity," in Digital Images and Human Vision (A. B. Watson, ed.), pp. 179-205, Cambridge, MA: MIT Press, 1993W.-K. Chen, Linear Networks and Systems (Book style). Belmont, CA: Wadsworth, 1993, pp. 123–135.
[28] Andrew P. Bradley "A Wavelet Visible Difference Predictor" Member IEEE Transactions on Image Processing Vol. 8. No. 5. May 1999.
[29] X. Zhu, S. Yao, B. Sun, Y. Qian" Image quality assessment: Combining the characteristics of HVS and structural similarity index May 2018, Harbin Gongye Daxue Xuebao/Journal of Harbin Institute of Technology 50(5):121-128.
[30] C, Hillar ; S, Marzen, "Revisiting Perceptual Distortion for Natural Images: Mean Discrete Structural Similarity Index", IEEE Xplore, 4-7 April 2017.
[31] E. F. Navarro, M. C. Hernandez, M. N. Miyatake, H. M. P. Meana "Visible Watermarking Assessment Metrics Based on Just Noticeable Distortion" November 2018, IEEE Access PP (99):1-1.
[32] Yim and A. C. Bovik, "Quality assessment of deblocked images, "IEEE Transactions on Image Processing, vol. 20, no. 1, pp. 88–98, 2011.
[33] Zhou Wang, Qiang Li", Information Content Weighting for Perceptual Image Quality Assessment, IEEE TRANSACTIONS ON IMAGE PROCESSING, VOL. 20, NO. 5, MAY 2011.
[34] M. Nahid, A. Bajit, A. Tamataoui, El. Bouyakhf "A New Image Psychovisual Coding Quality Measurement based Region of Interest", World Academy of Science, Engineering and Technology World Academy of Science, Engineering and Technology 32 2007ol 32 2007
[35] M. Nahid, A. Bajit, A. Tamataoui, El. Bouyakhf " Wavelet Image Coding Measurement based on System Visual Human", Applied Mathematical Sciences, Vol. 4, 2010, no. 49, 2417 - 2429
[36] Nahid, M., Bajit, A., Baghdad, "A., Perceptual quality metric applied to wavelet-based 2D region of interest image coding" SITA 2016 - 11th International Conference on Intelligent Systems: Theories and Applications, 2016.
[37] C. Deng, Z. Li, W. Wang, S. Wang, L. Tang, A. C. Bovik "Cloud Detection in Satellite Images Based on Natural Scene Statistics and Gabor Features" IEEE Geoscience and Remote Sensing Letters, 2018.
[38] H. Kalva, A. Bovik, H. Chen, K. Egiazarian, Z. Wang, "Introduction to the Issue on Perception Inspired Video Processing", IEEE Journal of Selected Topics in Signal Processing, 2014, Vol. 8 , Issue 3, pp : 355- 357

Advances in Science, Technology and Engineering Systems Journal Vol. 4, No. 4, 239-243 (2019)

www.astesj.com

ASTESJ

ISSN: 2415-6698

An Enhanced Fuzzy Clustering with Cluster Density Immunity

Hun Choi, Gyeongyong Heo *

Department of Electronic Engineering, Dong-eui University, 47340, Busan, Korea

ARTICLE INFO

Article history:
Received: 17 June, 2019
Accepted: 27 July, 2019
Online :30 July, 2019

Keywords:
Fuzzy Clustering
Euclidean Distance
Cluster Density
Density Immunity

ABSTRACT

Clustering is one of the well-known unsupervised learning methods that groups data into homogeneous clusters, and has been successfully used in various applications. Fuzzy C-Means(FCM) is one of the representative methods in fuzzy clustering. In FCM, however, cluster centers tend leaning to high density area because the sum of Euclidean distances in FCM forces high density clusters to make more contribution to clustering result. In this paper, proposed is an enhanced clustering method that modified the FCM objective function with additional terms, which reduce clustering errors due to density difference among clusters. Introduced are two terms, one of which keeps the cluster centers as far away as possible and the other makes cluster centers to be located in high density regions. The proposed method converges more to real centers than FCM, which can be verified with experimental results.

1. Introduction

Clustering, one of the representative unsupervised learning methods, is a method for partitioning data into groups of similar objects and is one of the major techniques in pattern recognition. Since Zadeh [1] proposed the fuzzy set that represents the idea of partial membership described by a membership function, fuzzy clustering has been widely studied and applied in various areas [2]. Clustering combined with deep learning also has attracted much attention in recent years [3].

In clustering, Fuzzy C-Means (FCM), generalized by Bezdek [4], is one of the most well-known methods. Although FCM is a simple and effective method, one of the shortcomings is that low-density cluster center moves towards high-density clusters because of the sum of Euclidean distances used in FCM. In real world data, it is more common that the data consist of clusters having different densities. Preventing the cluster distortion due to density difference is, therefore, one of the main problems to be solved in clustering especially in real world applications.

If the centers of some clusters are distorted, test data may belong to wrong clusters, which affects, in particular, the data points placed near the cluster boundary, and may cause a decrease in overall performance even with a small number of mis-clustered points.

There have been several variants of FCM that use cluster density, but most of the methods introduce an additional step to estimate cluster density and density estimation is performed independently from clustering, which has a disadvantage of additional computation [5, 6]. Even worse the estimation itself cannot be accurate as real world data do not follow any known distribution in general.

In this paper, a new clustering method that can solve the bias of cluster centers due to density difference is proposed. The proposed method has little increase in computational complexity and density estimation proceeds simultaneously with clustering. The proposed clustering method adds two terms to the objective function of FCM to reduce the sensitivity to cluster density. The first term represents the sum of distances between two cluster centers. This reduces the phenomenon that a low-density cluster center is attracted to a high-density cluster center by keeping cluster centers as far away as possible. However, if the centers are simply scattered and placed on the feature space boundary, the first term may have a small value. Therefore, the second term that represents the sum of the distances between data points and cluster centers is added so that cluster centers are located in high density regions.

Clustering error decreases with a large value in the first term, while it decreases with a small value in the second term. Experimental results show that FCM-CDI (FCM with Cluster Density Immunity), the enhanced FCM with two additional terms, is more likely to converge to real cluster center than FCM does.

*Gyeongyong Heo, Department of Electronic Engineering, Dong-eui University, 47340, Busan, Korea, +82-51-890-1675, hgycap@deu.ac.kr

In the next section, fuzzy clustering, especially FCM is summarized. Section 3 is devoted to develop an enhanced new clustering method through the introduction of new terms in the objective function of FCM. Experimental results are given in Section 4 and discussion in Section 5.

2. Fuzzy C-Means

Clustering is a method to make data belong to a specific cluster based on the concept of similarity. Fuzzy clustering is a way to extend this further, introducing the concept of incomplete membership in fuzzy so that data can be partly belonged to more than one clusters. Various methods for clustering has been proposed for a long time and one of the representative methods is FCM proposed by Bezdek [4]. FCM can be represented as a constrained optimization problem [7, 8]. Given N d-dimensional data points $X = \{x_i | 1 \le i \le N, x_i \in R^D\}$, the objective function of (1) should be minimized to divide data points into C clusters.

$$J_{FCM} = \sum_{i=1}^{N}\sum_{j=1}^{C} u_{ij}^{m}\left\|v_j - x_i\right\|^2 = \sum_{i=1}^{N}\sum_{j=1}^{C} u_{ij}^{m} d_{ij}^2 \quad (1)$$

where u_{ij} is the membership of the ith data point x_i to the jth cluster, v_j is the center of the jth cluster, m is a fuzzifier constant, usually 2 ($1 < m$). d_{ij} is the distance between the ith data point x_i and the center of the jth cluster v_j. In this paper, Euclidean distance is used to calculate the distance between a data point and a cluster center.

One data point x_i can be belonged to more than one cluster in FCM. However, the degree of belonging to each cluster, that is, the membership is different from each other, and the degree of belonging to C clusters should satisfy the constraint that the sum of total membership should be one, often called sum-to-one constraint.

$$\sum_{j=1}^{C} u_{ij} = 1 \quad (2)$$

The membership values and cluster centers that minimize the objective function of (1) while satisfying the constraint of (2) can be obtained by iterative optimization method using the update equations in (3) and (4) derived from a Lagrange equation.

$$v_j = \frac{\sum_{i=1}^{N} u_{ij}^2 x_i}{\sum_{i=1}^{N} u_{ij}^m} \quad (3)$$

$$u_{ij} = \frac{\frac{1}{\left\|v_j - x_i\right\|^2}}{\sum_{k=1}^{C}\frac{1}{\left\|v_k - x_i\right\|^2}} \quad (4)$$

FCM has been successfully used for many problems in its original or modified form for a given problem since it was firstly introduced, but the existence of numerous variants is a proof that FCM is not good for all problems. This paper also proposes a modified FCM to solve the problem of finding wrong cluster centers when FCM is applied to the data composed of clusters with different densities.

3. FCM with Cluster Density Immunity

In the presence of clusters with different densities in FCM, some cluster centers moves toward a high density cluster because FCM is based on the sum of Euclidean distances (or variations) between cluster centers and data points [9, 10]. That is, each data point $x_i (1 \le i \le N)$ has the same effect on FCM objective function. There are methods of assigning different weight to each data point according to its density, but estimating densities of all data points require a lot of computation and it is not possible to estimate the density accurately. Therefore, in this paper, two terms are added to the objective function of FCM so that the density can be effectively reflected with small increase in computation compared to FCM.

The first one is the term that makes the distance between two cluster centers as far away as possible. The objective function of adding the sum of distances between two cluster centers is shown in (5) [11].

$$J_1 = \sum_{i=1}^{N}\sum_{j=1}^{C} u_{ij}^2\left\|v_j - x_i\right\|^2 - \alpha\sum_{a=1}^{C}\sum_{b=1}^{C}\|v_a - v_b\|^2 \quad (5)$$

where α (> 0) is a constant indicating the rate at which the center sparsity is included in the objective function. The second term in (5) is the sum of the distances between two cluster centers. The larger the distance is, the smaller the objective value becomes. The cluster centers obtained by optimizing the objective function J_1 are located as far away as possible, but there can be one problem. As the value of α increases, cluster centers may move away from the actual cluster centers, and in the extreme case, cluster centers may be located in data-independent regions.

In order to reduce the side effect of the second term in (5), there is a need for a method defines candidate regions where cluster centers can come in addition to making cluster centers far away. In this paper, it is assumed that the candidate regions' densities are high. However, as mentioned before, the computational complexity is high and the accuracy is low in direct density estimation, sum of distances between a data point and a cluster center is used to estimate the density indirectly. As cluster center moves to a high density region, the sum of distances between a cluster center and a data point becomes small. The new objective function where the sum of distances between a cluster center and a data point is added to the objective function of FCM can be written as (6) [12].

$$J_2 = \sum_{i=1}^{N}\sum_{j=1}^{C} u_{ij}^2\left\|v_j - x_i\right\|^2 + \beta\sum_{i=1}^{N}\sum_{j=1}^{C}\left\|v_j - x_i\right\|^2 \quad (6)$$

where β (> 0) represents the ratio of reflecting the degree to which cluster centers are located in high density regions to the objective function. The second term, added to the objective function of FCM, is the sum of distances between a cluster center and a data point. The smaller the distance is, the smaller the objective function becomes. The cluster centers obtained by optimizing the objective function J_2 are located in high density regions, but there is one problem. In the extreme case, if all the cluster centers are located at one position with the highest density, (6) can be minimized.

As explained above, it is difficult to effectively remove the influence of cluster density difference by using only one of the two proposed terms. Therefore, this paper proposes FCM-CDI (FCM with Cluster Density Immunity) using two terms together. The

objective function of FCM-CDI is shown in (7), which allows cluster centers to be located in high density regions while keeping cluster centers as far away as possible.

$$\begin{aligned} J_{FCM-CDI} = & \sum_{i=1}^{N}\sum_{j=1}^{C} u_{ij}^2 \|v_j - x_i\|^2 \\ & -\alpha \sum_{a=1}^{C}\sum_{b=1}^{C} \|v_a - v_b\|^2 \\ & +\beta \sum_{i=1}^{N}\sum_{j=1}^{C} \|v_j - x_i\|^2 \\ = & \sum_{i=1}^{N}\sum_{j=1}^{C} (u_{ij}^2 + \beta)\|v_j - x_i\|^2 \\ & -\alpha \sum_{a=1}^{C}\sum_{b=1}^{C} \|v_a - v_b\|^2 \end{aligned} \quad (7)$$

The Lagrange equation [13] can be obtained from (7) and the sum-to-on constraint in (2).

$$\begin{aligned} L = & \sum_{i=1}^{N}\sum_{j=1}^{C} (u_{ij}^2 + \beta)\|v_j - x_i\|^2 \\ & -\alpha \sum_{a=1}^{C}\sum_{b=1}^{C} \|v_a - v_b\|^2 \\ & -\sum_{i=1}^{N} \lambda_i \left(\sum_{j=1}^{C} u_{ij} - 1\right) \end{aligned} \quad (8)$$

where $\lambda = [\lambda_1, \lambda_2, \dots, \lambda_N]$ is a Lagrange multiplier vector. By taking a partial derivative with respect to u_{ij}, one can obtain

$$\frac{\partial L}{\partial u_{ij}} = 2u_{ij}\|v_j - x_i\|^2 - \lambda_i \quad (9)$$

One can obtain (10) by equating (9) to zero and solving it for u_{ij}.

$$u_{ij} = \frac{\lambda_i}{2\|v_j - x_i\|^2} \quad (10)$$

(10) must satisfy the constraint in (2). Substituting (10) into (2) and solving it for λ_i gives (11).

$$\frac{\lambda_i}{2} = \frac{1}{\sum_{j=1}^{C} \frac{1}{\|v_j - x_i\|^2}} \quad (11)$$

Using (10) and (11), one can obtain (12), which is the update equation for u_{ij} in FCM-CDI.

$$u_{ij} = \frac{\frac{1}{\|v_j - x_i\|^2}}{\sum_{k=1}^{C} \frac{1}{\|v_k - x_i\|^2}} \quad (12)$$

The update equation in (12) is the same as the one in FCM. In FCM-CDI, the membership is determined based on the Euclidean distance between a cluster center and a data point, as in FCM.

The Lagrange equation can be partially differentiated with respect to v_j to obtain the update equation for a cluster center.

$$\frac{\partial L}{\partial v_j} = 2\sum_{i=1}^{N}(u_{ij}^2 + \beta)\|v_j - x_i\| - 2\alpha \sum_{\substack{b=1 \\ b\neq j}}^{C} \|v_j - v_b\| \quad (13)$$

(13) can be converted into (14) with the introduction of $2\alpha\|v_j - v_b\|$ which values zero.

$$\frac{\partial L}{\partial v_j} = 2\sum_{i=1}^{N}(u_{ij}^2 + \beta)\|v_j - x_i\| - 2\alpha \sum_{b=1}^{C} \|v_j - v_b\| \quad (14)$$

(14) is more simple to use than (13) as a condition $b \neq j$ is removed. One can obtain (15) by equating (14) to zero and solving it for v_j.

$$v_j = \frac{\sum_{i=1}^{N}(u_{ij}^2+\beta)x_i - \alpha\sum_{b=1}^{C} v_b}{\sum_{i=1}^{N}(u_{ij}^2+\beta) - \alpha\sum_{b=1}^{C} 1} = \frac{\sum_{i=1}^{N}(u_{ij}^2+\beta)x_i - \alpha\sum_{b=1}^{C} v_b}{\sum_{i=1}^{N}(u_{ij}^2+\beta) - \alpha C} \quad (15)$$

When compared (15) with (3), cluster center update equation in FCM, it can be seen that the two new terms are applied in denominator and numerator respectively. The update equation obtained when β = 0 in (15) corresponds to the update equation for the objective function J_1 in (5). In addition, the update equation obtained when α = 0 in (15) corresponds to the update equation for the objective function J_2 in (6). That is, the objective functions in (5) and (6) correspond to special cases of FCM-CDI.

FCM-CDI can be expressed as shown in Figure 1 using the update equations in (12) and (15). The convergence condition in Figure 1 is that the maximum difference of two center positions between two successive iterations is smaller than or equal to $\epsilon_1 (= 10^{-3})$ and the maximum difference of two membership values between two successive iterations is smaller than $\epsilon_2 (= 10^{-4})$.

U : membership $(u_{ij}, 1 \le i \le N, 1 \le j \le C)$ V : cluster center $(v_j, 1 \le j \le C)$
1: initialize V and U with random values 2: initialize $t = 0$ 3: **do** 4: $t \leftarrow t + 1$ 5: calculate U using (12) 6: calculate V using (15) 7: **while** $\exists\left\|u_{ij,t-1} - u_{ij,t}\right\| > \epsilon_1$ or $\exists\left\|v_{j,t-1} - v_{j,t}\right\| > \epsilon_2$ 8: **return** U and V

Figure 1: FCM-CDI Algorithm

4. Experimental Results

Although there are various FCM variants, there is no way to reduce the clustering error due to density difference through the modification of FCM itself. Therefore, in this paper, FCM and FCM-CDI are compared, and three different objective functions in (5), (6) and (7) are used to demonstrate the effect of each term on clustering result.

Figure 2 shows the typical results of FCM and FCM-CDI. The data were randomly generated with Gaussian distributions with the centers provided in advance. The cluster on the upper right has 500 data points and the other 2 clusters have 100 data points to make density difference.

As shown in Figure 2-(a), the cluster center is shifted toward a high density cluster in FCM, but the cluster center is approaching to the actual cluster center in FCM-CDI. Since clustering is an unsupervised learning method, it is difficult to quantitatively compare the results. Therefore, in this paper, an error function is defined as the sum of distances between the actual cluster center used for data generation $V_R = \{v_{R,j} | 1 \le j \le C\}$ and the cluster

center obtained through clustering $V_C = \{v_{C,j} | 1 \le j \le C\}$ as in (15).

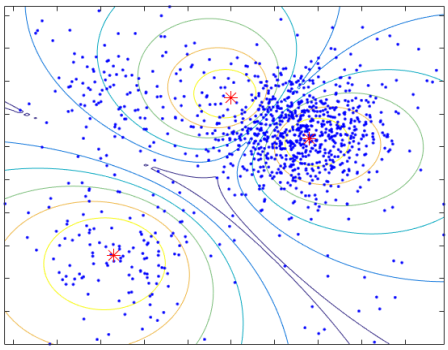

(a) FCM

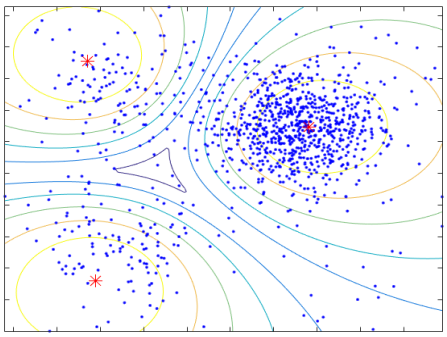

(b) FCM-CDI

Figure 2: Clustering results with data having 3 clusters

$$E = \sum_{j=1}^{C} \left\| v_{R,j} - v_{C,j} \right\|^2 \quad (15)$$

The objective function in (7) requires two constants α and β to be determined. In order to determine these constants, ① the α value with the smallest average error was experimentally determined with the objective function J_1 in (5) first. After that ② the β value with the smallest average error was experimentally determined with the objective function $J_{FCM\text{-}CDI}$. In the second step, the α value was fixed to the value obtained in the first step. ③ When J_2 is used as the objective function, the value obtained in the second step is used as the β value.

Figure 3 shows the average error obtained by varying α value for the data in Figure 2. The values shown in Figure 3 are obtained by averaging 50 experimental results with the same value of α.

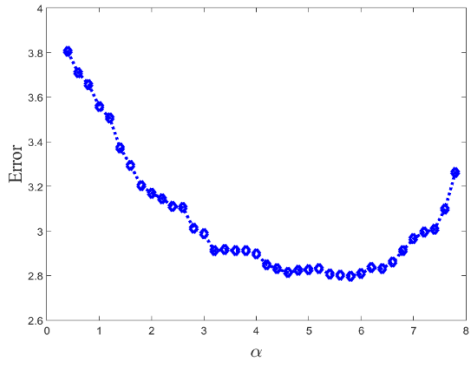

Figure 3: Clustering error with respect to α on the data having 3 clusters

As shown in Figure 3, the error decreases as the value of α increases. However, if the value of α becomes larger than some value, the cluster centers pushed to the place where no real cluster centers as well as data points exist and the error increases. The α value with the smallest error for the data in Figure 2 was 5.8.

Figure 4 shows the average error obtained by varying the β value. The values shown in Figure 4 are also averages over 50 experiments.

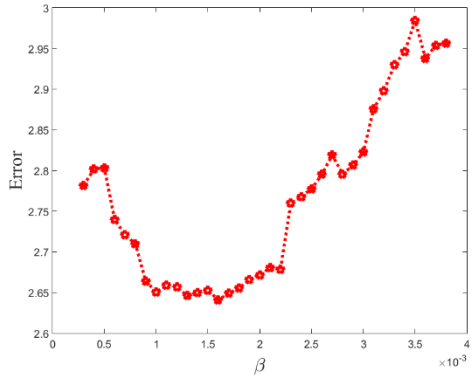

Figure 4: Clustering error with respect to β on the data having 3 clusters

Figure 4 also looks similar to Figure 3. As the β value increases, the error decreases, but when the β value becomes larger, the cluster center shifts to the higher density region. Although the candidate region where the cluster center can be located is a high density one, high density only is not enough to be a candidate for center. The β value with the smallest error for the data in Figure 2 was 0.0016.

Table 1 summarizes the results of applying four objective functions to the data in Figure 2. The average error is the error averaged over 500 experiments using randomly generated data. For α and β, the values obtained in the previous experiments were used.

Table 1: Clustering results with data having 3 clusters

Method	Objective Function	Average Error
FCM	J_{FCM}	3.3142
FCM-CDI	J_1	2.8012
	J_2	3.4021
	$J_{FCM\text{-}CDI}$	2.6934

In FCM-CDI, the first term to make the cluster centers far away and the second term to place the cluster center in a high density region are introduced. As can be seen from Table 1, FCM-CDI showed better results than FCM in data consisting of clusters with large difference in density. However, FCM-CDI showed a larger error than FCM when only the second term (α = 0) was used. This is because cluster centers were randomly initialized [14, 15]. When one randomly initialized cluster center is close to another, the two cluster centers tends to move to the same position due to the second term. Therefore, a larger average error was obtained when only the second term was used. However, when both terms were used, the best results were obtained among the four methods. In addition, as the comparison with respect to initialization methods is completely different from the topic covered in this paper, only random initialization is considered.

Figure 5 shows clustering results applying FCM and FCM-CDI to the data composed of four clusters. In the data, the upper right cluster has 400 data points and the remaining 3 clusters have 100 data points.

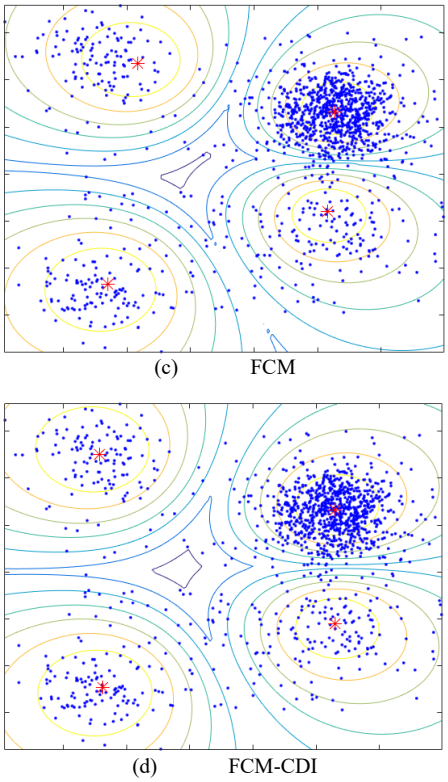

(c) FCM

(d) FCM-CDI

Figure 5: Clustering results with data having 4 clusters

Table 2 summarizes the results of applying four objective functions to the data having four clusters as in Figure 5. As before, the average error is the error averaged over 500 experiments using randomly generated data.

When there are four clusters, the randomly initialized cluster centers are more likely to be close to each other. Therefore, compared to FCM, the result with the second term only was much worse than that of the previous one.

Table 2: Clustering results with data having 4 clusters

Method	Objective Function	Average Error
FCM	J_{FCM}	1.5130
FCM-CDI	J_1	1.3012
	J_2	1.7218
	$J_{FCM\text{-}CDI}$	1.1026

5. Conclusion

In this paper, proposed is a new clustering method to reduce the deviation of a cluster center from the actual center due to the density difference. The proposed clustering method is based on the fact that the centers should be as far away as possible and that the cluster center should be located in a high density region. Two new terms reflecting these considerations are added to the objective function of FCM, which results in more convergence to real centers.

It is true that the proposed method is robust against cluster density compared to FCM, but the existence of two constants α and β can be an obstacle to its application. Since the ground truth is known in this paper, the optimal value was found experimentally. However, since clustering is a kind of unsupervised learning, it is difficult to evaluate the performance by clustering itself and it should be indirectly evaluated by the performance of the whole system. Therefore, a method that can determine the optimal α and β according to the data given is needed and this is under study. In addition, cluster center initialization affects the performance as shown in the result, initialization method for the proposed method should be examined carefully, which is left as a future study.

References

[1] L. A. Zadeh, "Fuzzy sets," Information and Control, 8(3), 338-353, 1965. https://doi.org/10.1016/S0019-9958(65)90241-X

[2] D. Xu and Y. Tian, "A Comprehensive Survey of Clustering Algorithms," Annals of Data Science, 2(2), 165-193, 2015. https://doi.org/ 10.1007/s40745-015-0040-1

[3] E. Min, X. Guo, Q. Liu, G. Zhang, J. Cui, and J. Long, "A Survey of Clustering With Deep Learning: From the Perspective of Network Architecture," IEEE Access, 6, 39501-39514, 2018. https://ieeexplore.ieee.org/document/8412085

[4] J. C. Bezdek, Pattern Recognition with fuzzy Objective Function Algorithms, Springer, 2013.

[5] C. H. Cheng, J. W. Wang, M. C. Wu, "OWA-weighted based clustering method for classification problem," Expert Systems with Applications, 36(3), 4988-4995, 2009. https://doi.org/10.1016/j.eswa.2008.06.013

[6] C. Lu, S. Xiao, X. Gu, "Improving fuzzy C-means clustering algorithm based on a density-induced distance measure," The Journal of Engineering, 2014(4), 137-139, 2014. https://doi.org/10.1049/joe.2014.0053

[7] S. Muyamoto, Handbook of Computational Intelligence, Springer, 2015.

[8] J. Nayak, B. Naik, H. S. Behera, "Fuzzy C-means(FCM) Clustering Algorithm: A Decade Review from 2000 to 2014," Computational Intelligence in Data Mining, 2, 133-149, 2015. https://doi.org/10.1007/978-81-322-2208-8_14

[9] Z. Zainuddin, O. Pauline, "An effective Fuzzy C-Means algorithm based on symmetry similarity approach," Applied Soft Computing, 35(C), 433-448, 2015. https://doi.org/10.1016/j.asoc.2015.06.021

[10] B. Abu-Jamous, R. Fa, A. K. Nandi, Integrative Cluster Analysis in Bioinformatics, Wiley, 2015.

[11] B. H. You, W. W. Kim, G. Heo, "An Improved Clustering Method with Cluster Density Independence," Journal of The Korea Society of Computer and Information, 20(12), 15-20, 2015. https://doi.org/10.9708/jksci.2015.20.12.015

[12] S. H. Kim, G. Heo, "Improvement on Density-Independent Clustering Method," Journal of the Korea Institute of Information and Communication Engineering, 21(5), 967-973, 2017. https://doi.org/10.6109/jkiice.2017.21.5.967

[13] I. M. Gelfand, S. V. Fomin, Calculus of Variations, Dover Publications, 2000.

[14] K. Zou, Z. Wang, M. Hu, "An new initialization method for fuzzy c-means algorithm," Fuzzy Optimization and Decision Making, 7(4), 409-416, 2008. https://doi.org/10.1007/s10700-008-9048-8

[15] A. Stetco, X. J. Zeng, J. Keane, "Fuzzy C-means++: Fuzzy C-means with effective seeding initialization," Expert Systems with Applications, 42(21), 7541-7548, 2015. https://doi.org/10.1016/j.eswa.2015.05.014

ASTES

Advances in Science, Technology and Engineering Systems Journal Vol. 4, No. 4, 244-250 (2019)

www.astesj.com

Special Issue on Advancement in Engineering and Computer Science

ASTESJ

ISSN: 2415-6698

Automatic Service Orchestration for e-Health Application

Anatolii Petrenko, Bogdan Bulakh*

System Design Department, National Technical University of Ukraine, Igor Sikorsky Kyiv Polytechnic Institute, 03056, Ukraine

ARTICLE INFO

Article history:
Received: 31 May, 2019
Accepted: 13 July, 2019
Online :30 July, 2019

Keywords:
Service orchestration
Semantic technologies
e-Health

ABSTRACT

This paper describes an architectural approach to the development of dynamic service-oriented systems for e-Health using the service orchestration mechanism and semantic technologies. The main idea is the dynamic synthesis of the complex functionality required by user or by software agent. This idea should help to build and easily extend the applied loose-coupled systems without strict dependencies on concrete web services and their invocation details. A sample scenario of such dynamic orchestration is covered and analyzed, possible ways of further improvement of this approach are given.

1. Introduction

This paper is an extension of work originally presented at the 2018 IEEE First International Conference on System Analysis & Intelligent Computing (SAIC) [1]. Since then the original research has been continued in the direction of development of service-oriented e-Health application. This paper covers more details of dynamic service orchestration and how it can be applied to the e-Health software design.

2. Problem Overview

Modern network applications widely use web service interaction to retrieve or update data. There may be a lot of interconnected services of different types (like SOAP or REST) interacting with each other and external third-party services, thus forming so called "service ecosystem". The interaction of these services may be implemented in different ways (see Figure 1):

- "Hard-coded" interaction: direct invocation of the service at specific URL is fixed in source code with all the invocation details. In this case even simple relocation of services to another URLs requires changing (and consequent recompiling, redeployment, retesting) of all dependent software modules (other web services, for instance).
- Services could use service discovery mechanism by means of some registry (in its simplest case by using some "name server" to translate service name to concrete URL. UDDI registry is an advanced example). This makes it easier to modify and scale the service ecosystem, but services are still tightly coupled by data formats and interaction patterns.
- Service choreography approach (e.g. "publisher-subscriber" model) could be implemented by means of some message broker. This event-driven service architecture consists of loosely coupled services that can be dynamically connected to each other through a subscription to different message types.
- Service orchestration approach: all interactions are controlled by external orchestration software. In such system services could be truly agnostic to their environment while publishing only their interface description.

It must be noted that in many real-life systems composed of hundreds of services all of these approaches may be implemented within a single service ecosystem (forming "heterogeneous" service ecosystem).

In any case it is only skilled developer who is capable to organize the inter-service communication to bring some functionality to the system. It is almost never possible for the end users to create new functionality without skills and knowledge in programming. This problem is partly solved by so called "workflow management systems" (like scientific workflow systems [2] or engineering ones [3]). Most of service-oriented workflow systems typically rely on the orchestration approach.

* Bogdan Bulakh, Email: bogdan.bulakh@gmail.com

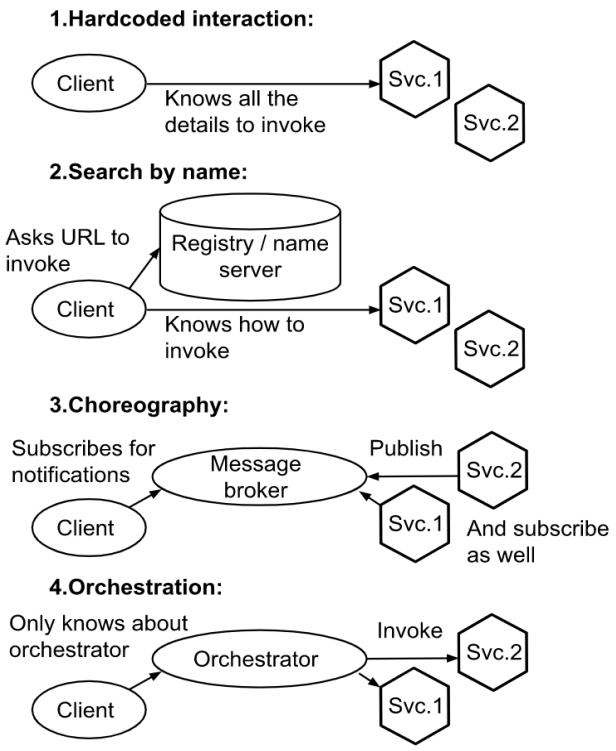

Figure 1: Some existing service interaction patterns (client could be implemented as another service as well)

2.1. Problem Definition

This paper focuses on a slightly different issue: how to make it possible for *both users and program agents* to request and execute the desired functionality *without any service-level knowledge* (existence of specific services and their interfaces' details)? In other words, dependencies between the clients and web services are forcing developers to update clients when service ecosystem changes. This costs time and extra QA efforts. We propose an approach that helps to avoid the update of the clients in case of changes in service ecosystem and thus makes it easier to maintain and improve the overall system.

Instead of making calls to specific services, or even "constructing workflows of services", software clients can issue "functionality requests" to some broker. While these requests can be fulfilled, the clients need no updates. The fulfilment of these requests could be organized using the orchestration approach, if there is no single service capable to provide the requested functionality. This is what we call here a "*dynamic semantic-based orchestration*": the automatic synthesis of a service workflows to provide the requested functionality (including some goal and output data). One of the main benefits of the dynamic orchestration is that service clients and services themselves are not coupled in any way except the functionality semantics. There is no need to keep track of web service interface changes on each client, it's only a knowledge base about services (which binds functionality semantics with service invocation details) that should be kept updated instead.

3. Possible Application Scenarios

There are a lot of application fields for dynamic semantic-based orchestration. Some of them are listed below.

Scientific and engineering workflows

There are a lot of existing 'Scientific workflow systems' and many of them support invocation of the remote services (Taverna workflows [4], Apache Airavata [5] etc.). The main problem there is a high complexity of constructing the service workflows for non-IT-domain specialists and scientists, because the workflow elements are bound to concrete services, their operations, and data formats. With the dynamic semantic-based orchestration the end users could just set the goals of the orchestration and receive the automatically built workflow. No need to deal with service-level details for the end users.

Performance monitoring dashboards

This feature can be implemented in medical (see further), scientific, engineering, industry production, financial and other domains. Given the ecosystem of services to fetch different parameters of the objects to monitor (patients' health data, the status of lab equipment or industrial equipment etc.). User needs a tool that can be used to easily construct and customize the KPIs. Possible solution: a user describes the functionality he needs in terms of some knowledge base, and new dashboard indicator will get its values from the dynamically orchestrated services providing the functionality requested.

Business analytics and data mining

Same as previous kind of scenario but it also involves the services for mining new knowledge from existing data helping to improve existing business processes. These workflows are more complex, compute intensive and provide valuable information (insights). It is a service-oriented analytics solution for business enterprises of different scale. In [6] a workflow management system for 'big data' mining is described. But its workflows are still composed manually by the end user.

Smart house and IoT

The dynamic semantic-based service orchestration can be used in controlling IoT devices, e.g. as a part of smart house. For example, anyone in the smart house environment can easily add new automation scenario, e.g. to control lighting, climate or heating or water supply in a smart way, just by describing the desired functionality. In a similar way this approach can be applied, say, to control production processes on factories or for stock management. The PROtEUS++ [7] is a promising example of a specialized workflow engine for IoT tasks, and by the way it supports dynamic service discovery using the semantic service description.

Workflows for e-Health

Workflows for patient's diagnostics and treatment (DTWf) could also be implemented with the help of automatic semantic-based service orchestration. The DTWf typically can contain invocation of basic services for diagnostics (like service to check blood pressure, controlling blood pressure data received from devices or manually entered by the patient), services of patient's health status prediction (based on the data provided by other services) and so on [8]. This application field will be mainly referred further as it is studied by authors in scope of implementation of the project of the mobile e-Health platform development.

4. Implementation

The main idea of the proposed solution is to hide as much low-level service interface specifics as possible from the client (functionality consumer), allowing the client to operate only with its goals and data. It is similar to how declarative programming languages (like SQL or SPARQL) differ from imperative ones: when working in a declarative style you need to specify what goal to reach but not how it should be reached. You actually don't worry about implementation details. Ideally the client just declares the new computational goal (e.g. "to get specific output results from specific input data" etc.) without referencing particular services. He only operates with terms and facts from the knowledge base that can help him to express his goal. The rest process is automated by means of automatic service discovery and automated orchestration.

The solution proposed is based on the following three main components (also implemented as services), as shown on Figure 2:

- *Service for execution* (SE) of functionality requests, which serves as a kind of broker and the single point of access for clients. It does not only find some concrete web services able to fulfil the client's request, but also is responsible for execution of any service operations and results provision. In other words, clients don't ask SE to find some services, they ask to do some actions, provide input data and wait for output. In order to fulfill client's request SE communicates with other two components.
- *Service registry* (SR). This service searches for available services that could provide the requested functionality (according to registered service's semantic annotations). In fact, it is an interface to the knowledge base containing facts about services and their functions. The second mission of SR is to find the possible service orchestration scenario if no single service matches the requested functionality. Then this scenario is passed to the Service orchestrator.
- *Service orchestrator* (SO). This service is responsible for execution of service workflows, created by SR. Workflows actually can consist either of a single service, or describe the orchestration scenario involving multiple services. This service complies with a SaaS model: new workflows can be deployed in a cloud infrastructure and can be interacted via the REST interface (invoked, queried about status and results, canceled, disposed etc.). It should be noted that today there are a lot of orchestration tools available. The orchestrator engine is a core part of SO and it can be implemented on top of many of existing tools, for example: BPEL engine, Taverna Workflows, Netflix Conductor (a microservices orchestration engine).

4.1. Service Registry and Knowledge Base

The SR has an extended functionality compared to UDDI registries. Instead of binding to standard fields and database schema, it is based on flexible knowledge base. Administrator-level users can add new facts or modify existing facts about services registered and extend the ontology with new classes. The SR can be queried about services in a similar way like Triple stores are queried with SPARQL queries. But the functionality of SR is not limited by simple querying the triple store. It includes the matchmaking logic helping to construct the complex service workflow according to the goals set and inputs provided. To do this the SR should contain the formalized knowledge on web service interaction details (protocols, procedures, interfaces), and the knowledge on basic data formats used and how to extract and transform the data from them (xml, JSON, CSV etc.). That's why the knowledge base should consist of domain ontology (to set goals, to describe services functionality and operations, inputs and outputs), service ontology (to allow automatic invocation, see Figure 3), and data formats ontology (to allow automatic data flow building).

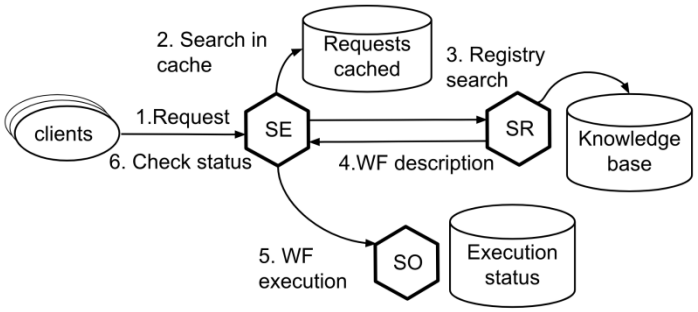

Figure 2: Main components of the proposed solution

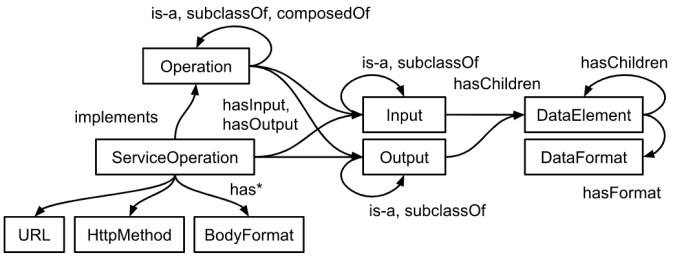

Figure 3: Service ontology (fragment)

4.2. Service Matchmaking

Existing standard solutions in service registration like UDDI are not enough for advanced semantic search. Instead it is proposed to rely on service ontologies, similar to OWL-S ontology [9], which will give more relevant results. Service matching can be done using the semantic proximity of the service ontology elements (from registry knowledge base and those from the "request for functionality" query) [10]. In order to compare these ontology elements, the following elementary proximity estimations are needed to be computed: proximity of classes, proximity of classes and instances, proximity of instances, proximity of predicates. Some service A can be called 'relevant' to some search query R only in case the proximity estimate is higher than some threshold value M_T (see further).

Another aspect is to choose what information should be included into comparison. It is proposed to use the following information categories: C (context), IOPE (inputs, outputs, preconditions, effects) and QoS.

The context C form search query can be formally defined as any information that could implicitly and explicitly impact the query generation by user (it can be profile-oriented, history-oriented, process-oriented, other context). An explicit context is

directly provided by user, while implicit one is that being gathered by any automated tool.

The service functionality can be matched by use of IOPE attributes. The *hasInput*, *hasOutput*, *hasPrecondition* and *hasEffects* query attributes (R) are matched against the corresponding ones from each service's description (A). Matching can be estimated as a one of following outcomes: "exact match", "plug-in" match when R is a subclass of A, "subsume" when R and A have common partial match, "failure" is A and R have nothing common.

QoS attributes include service price, performance, reliability, stability, scalability, security etc. The total match level estimation combines those estimations mentioned above:

$$M(R, A) = K_C M_C + K_I M_I + K_O M_O + K_P M_P + K_E M_E + \\ + K_{QoS} M_{QoS} > M_T$$

If we group IOPE and C requirements as functional requirements (FR) and QoS we refer to as non-functional requirements (NFR), and if we use mismatch-level (or level of matching error) as an indicator of matching failure (for practical reasons: to be able to use mismatch penalties instead of proximity estimations), then we'll have the following general matching error function:

$$E(R, A) = K_{FR} E_{FR} + K_{NFR} E_{NFR} < E_T$$

Both measures M and E could be used combined. First, we look for the single service with the highest M(R,A). If $M(R,A) > M_T$ then we accept it as a service providing requested functionality. If $M(R,A) < M_T$ then we need to compose a workflow of services with less possible $E(R,A) < E_T$. In order to estimate E for a workflow of services {A} we can use this general approach:

$$E(R, \{A\}) = K_{FR} E_{FR}^* + K_{NFR} E_{NFR}^*,$$

where * marks summary values for a workflow, for instance, internal inputs and outputs that are connecting services are excluded from error estimation.

During the practical implementation of a e-Health product with less than hundreds of service operations and without third-party services we found it sufficient to consider only IOE requirements (E for effects in form of functionality requested), without NFR. So, we used the following brief construct for the functionality request:

$$R = (F, \{I\}, \{O\}),$$

where F (function) – action to perform, I (input) – available inputs specification, O (output) – requested outputs specification. In a practical implementation we used JSON format, flexible enough to express complex I and O descriptions (see Figure 4). Here is a simple example of request to SE to get user name by ID:

```
{
  "operation":"get",
  "input":[
    {
      "name":"user",
      "properties":[
        {
          "name":"id",
          "value":"user001"
        }
      ]
    }
  ],
  "output":[
    {
      "name":"user",
      "properties":[
        {
          "name":"firstname"
        },
        {
          "name":"lastname"
        }
      ]
    }
  ]
}
```

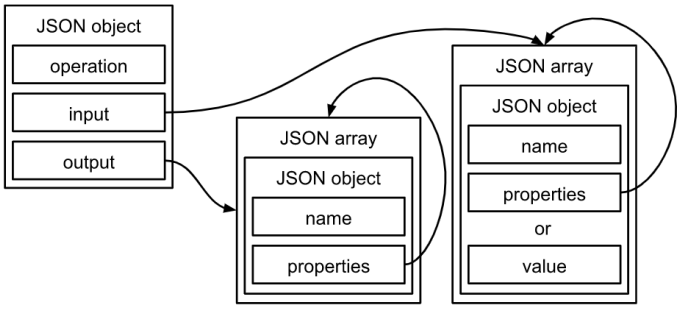

Figure 4: Inputs and outputs specification format

4.3. e-Health Application

The are many research papers studying the use of service-oriented architecture for medical software [11,12], and some of them mention service orchestration as a part of medical software, but this paper focuses on slightly different things, related to orchestration mechanism itself.

Workflow composition or, in other words, automatic semantic-based orchestration scenario synthesis, makes is easier to extend existing functionality of the system. It could be possible to get this new functionality even without development of new services: when the new functionality request could be satisfied with an orchestration scenario involving existing services. Before describing an example of such scenario, let us briefly describe the e-Health application that uses the proposed approach.

The e-Health application we develop is a system providing a virtual office for doctors and patients as an online point of their communication. It is useful in conditions when the nearest medical center is far from patient's home. In this situation the initial diagnostics can start online, and in many cases, it could be enough to help patient without real-life visit to the hospital. Also, the virtual doctor's office remembers all the patient treatment history and can provide some intelligent tool helpful for doctors and patients, like prediction of the crisis state of patients' health based on ordinary indicators like blood pressure, glucose level or complains about pain. This is an example of extended functionality that can be built by re-using the existing functions. The general

architecture blocks of this e-Heath application are presented on Figure 5.

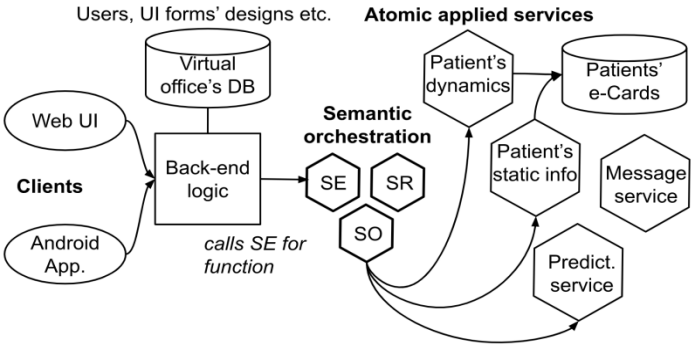

Figure 5: Virtual doctor's office using the dynamic semantic-based orchestration

Most of the office's functionality is not implemented just by back-end logic querying the database. There is a separate layer called "applied services" which is actually an API to do everything on patient's record. Conversations with doctors, diagnoses, treatment prescriptions, health indicators, reports – all of this is implemented with atomic REST services (we can call them microservices). The back-end logic's responsibility is to serve front-ends' requests and gather all necessary data for displaying to the user. Any call to operate patient's data is made as a "functionality request" with function, inputs and outputs provided to SE. This way we can truly separate back-end development and microservice API development, and only need to reflect important changes in a knowledge base of SR.

4.4. Service Workflow Composition Example

One of the examples where the dynamic orchestration takes place is the prediction of diabetes, heart problems and so on based on the last entered health indicators. This prediction is just a hint for the doctor and should only attract his attention to some possible problems (by displaying a warning), so there was no need to achieve very high accuracy of prediction. To develop such "intelligent" hint test datasets were analyzed, prepared and used for neural network training. This ended up as a separate service with one single output (binary warning flag) and a number of inputs (like weight, insulin and glucose level and much more) developed by separate team with machine learning background. In order to get the diabetes warning flag, the back-end developers just made a simple request: "given patient's ID and current date, run diabetes prediction and return warning flag". At the same time the SR's knowledge base contains information about inputs and outputs of all services, including the diabetes predictor.

Let's take a look at the process of execution of that request mentioned above. After JSON describing this request is accepted and parsed by SR, the SR itself starts to search for single service capable to satisfy the request. It founds the service operation with function briefly described like "Diabetes prediction". But this service operation has a lot of inputs, despite it has the output and function matching the request. So, no single service is found, and SR tries to build the workflow. It finds a lot of combinations of atomic services, but the best one (according to matching error penalties) is presented on Figure 6. It is executed, and the result is returned to the back-end caller (the client).

The Figures 7 and 8 shows two screens of a mobile client developed using the described diabetes prediction workflow to display a warning icon (the application's language is Ukrainian). The first screen is a menu screen for a doctor with a following action on a selected patient: indicators, chat, log, complains, diagnosis, treatment. The second screen shows some sample conversation between a doctor and his patient in a chat mode.

When a doctor selects someone of his patients, the diabetes prediction workflow is called, and the client displays or hides the warning icon (a circle with Ukrainian letter "D" inside) at the top of the screen related to that patient (seen on both screens on Figures 7 and 8). In a similar way any other predictor (e.g. for heart problems) is called via the dynamic semantic-based orchestration.

4.5. Evaluation of Results

The performance penalties for this sophisticated process of services invocation (compared with direct REST services calls) could be estimated through the workflow execution time T_{exec} :

$$T_{exec} = T_M + T_V + T_{WF} + T_S$$

where T_M is a matchmaking time, T_{WF} is a workflow execution related overhead (depends on workflow execution engine speed), T_S is a total time for the execution of the longest sequence of service invocations in a flow (web services execution time). There is also T_V which is a validation time of the composed workflow. Currently we don't use any validation technique, and fully rely on the consistency of the knowledge base during the automated workflow synthesis ($T_V = 0$). But there is a risk of the incorrect behavior of the composed workflows (like infinite loops) even if they were constructed without any inconsistency with the knowledge base, so we need formal modeling techniques. Petri nets [13] and process calculus [14] could be successfully used to model web service workflows and related tools will be further integrated to the system to improve its reliability.

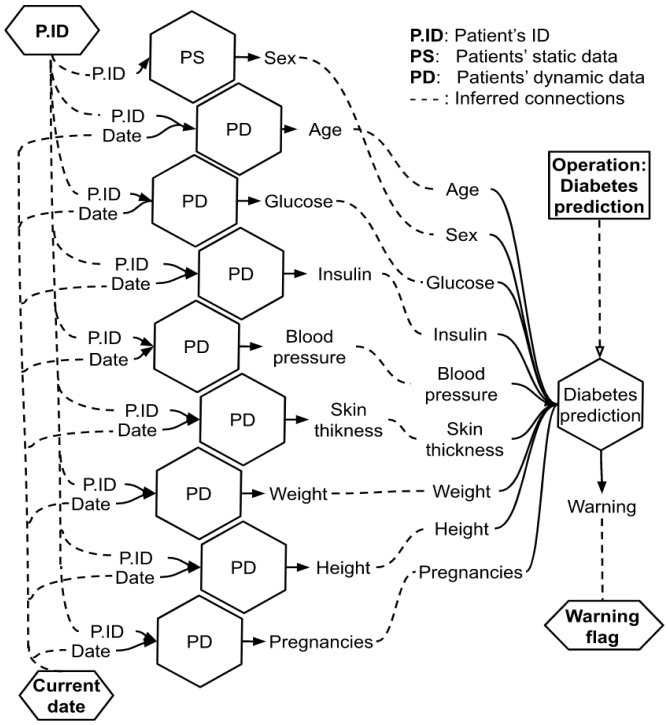

Figure 6: Diabetes prediction workflow (inputs and output are marked bold)

When comparing hard-coded scenario execution ($T_{exec}' = T_S$) with dynamic orchestration T_{exec}, the dynamic and flexible approach lasts longer by $T_{exec} - T_{exec}' = T_M + T_{WF}$, which was 3 to 5 seconds in case of small service registry (about 30 service operations) we used for diabetes prediction scenario. It should be noted that this time is seriously affected by the knowledge base facts quantity and quality (seriously impacts T_M).

In order to avoid same process of workflow synthesis each time a doctor needs a hint, the resulting workflow is cached in SR's knowledge base. The overhead is minimal and almost equal to ($T_{WF} + T_S$) because in this case $T_{exec}'' = T_C + T_{WF} + T_S$, where T_C is a cache search time and $T_C << T_M$). But in case of any changes in the knowledge base the cache should be cleared. This is a trade-off we get instead of updating the clients: the knowledge base update leads to reasoning on the updated facts and repeating the service matchmaking again from scratch. But found these knowledge base related activities less time-consuming then updating, redeploying and QA of all client applications.

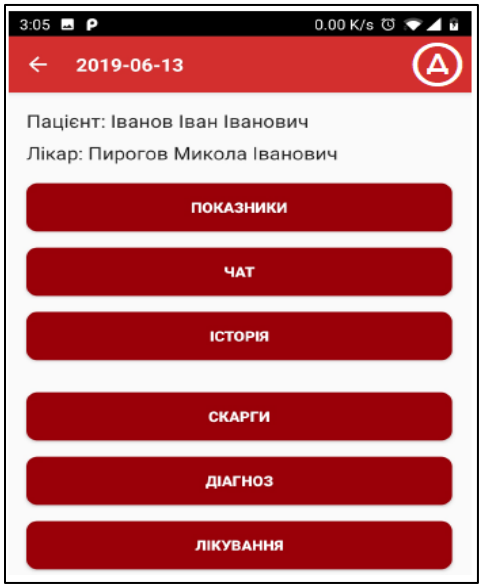

Figure 7: A 'patient menu' sample screen of the mobile e-Health application with diabetes warning icon at the top.

Figure 8: Chat screen of the mobile e-Health application, with diabetes warning icon at the top.

5. Conclusions and Future Work

This paper presented a description of a software architectural approach that aims to bring more flexibility to service-oriented systems and make service dependencies weaker. The main idea is to provide additional "abstract request layer" to the well-known service orchestration mechanism. The abstract request for functionality is being matched with the knowledge base of available web services to perform actual calculations.

The approach described has been successfully applied to the e-Health system, and it gives promising results for this application field, since e-Health applications typically have a lot of functions and data sources that could be accesses with the web service interfaces.

In our opinion this approach has the following benefits not only for e-Health domain but for other application fields as well:

- Service clients and web services are fully separated and could be developed independently by the teams of different development tools and background. The only dependency is the knowledge base (and service registry that uses it). Service ecosystem can be easily updated without changes to its clients. Only the knowledge base needs to be updated.
- It is possible to develop the UI for users to allow them easily construct the functionality requests and thus extend the functionality without help from software developers. This is one direction for our future work. It includes the development of workbench where users can test their requests and development of UI editor to control the displaying of requested results.
- In case of small service registries, the matchmaking process and workflow synthesis will not harm performance. This is true in case of avoiding usage of some existing heavyweight tools for orchestration like BPEL engines as the core for service orchestrator. The problem is that these tools like BPEL engines were basically designed for static workflows, not dynamic ones.

Of course, this vision has its drawbacks:

- The e-Health software must be very robust. But it has to be noted that the absence of hard-coded reference to concrete services there is a non-zero probability that SR will find wrong services or does not find anything thus producing wrong results returned by SE. From this point of view the only way in assuring the correct behavior is continuous testing of functions used by clients. When client gets updated with new functionality request call, this call should be added to the test plan. The improvements in QA of the solution presented are planned for our further work. At the same time formal models like Petri nets or process calculus can help to test the behavior of the dynamically generated workflows automatically.
- Another option to make sure correct services are matched to a request is to make only strict logical assertions by SR. No partial matching possible, service or workflow is either matching the request or not. In this case the clients will

need to use only strict request constructs and only correct ontology terms it their requests, thus making the new programming language to express the functionality requests. This will make it harder to add the new requests and make them work by end users and even programmers.

- In case of large registries of services, the matchmaking process could be time-consuming, since a lot of services could be "paired" according to their inputs and outputs and their functionality. So this solution will not work as expected in a system with hundreds of service operations and third-party services. And there will be problems if there are too many fine-grained microservices in the ecosystem even if it does not include external third-party services. In this case the matchmaking process should be restricted of simplified since e-Health software should operate without lags.
- Another problematic issue is the correct management of the knowledge base. Each time a new service is developed and should be registered in the system, there are a lot of work to do in the knowledge base. In fact, the knowledge base is the most important component of such system and requires very accurate updates, permanent logging of changes and intensive QA. Together with service registry it forms the fragile bottleneck of the system.
- Such complex interaction patterns could bring additional problems in security and data privacy. This is very important for e-Health applications working with personal medical data. But this aspect is out of scope of this paper.

Other possible directions for the future work are: research on the specifics of orchestrating services that control IoT devices and moving orchestrator service to the cloud infrastructure.

Acknowledgment

This paper describes partial results of the ongoing fulfillment of the project "The development of the modern service systems by the example of mobile medical system for a front-line settlements in the military conflict zone" by the National Technical University of Ukraine "Igor Sikorsky Kyiv Polytechnic Institute".

References

[1] A.I. Petrenko, B.V.Bulakh, "Intelligent service orchestration as a service", Proc. of 2018 IEEE First International Conference on System Analysis and Intelligent Computing (SAIC), 8-12 October, 2018, Kyiv. - pp 201-205. https://doi.org/10.1109/saic.2018.8516723

[2] B. Ludäscher, M. Weske, T. McPhillips, S. Bowers, "Scientific Workflows: Business as Usual?", Lecture Notes in Computer Science. (2009) 31-47. https://doi.org/10.1007/978-3-642-03848-8_4.

[3] V. Ladogubets, B. Bulakh, V. Chekaliuk, O. Kramar, "Employing BPEL Engines for Engineering Calculations", The Experience of Designing and Application of CAD Systems in Microelectronics: 12-th Intern. Conf. «CADSM'2013», 19-23 February 2013, Polyana-Svalyava (Zakarpattya), Ukraine: proc. – Lviv, 2013. – P. 427–430. – ISBN 978-617- 607-393- 2

[4] K. Wolstencroft, R. Haines, D. Fellows, A. Williams, D. Withers et al. "The Taverna workflow suite: Designing and executing workflows of Web Services on the desktop, web or in the cloud". Nucleic Acids Research. 41 (Web Server issue): W557–W561. doi:10.1093/nar/gkt328. PMC 3692062. PMID 23640334.

[5] M. Pierce, S. Marru, L. Gunathilake, T. A. Kanewala et al., "Apache Airavata: Design and Directions of a Science Gateway Framework," 2014 6th International Workshop on Science Gateways, Dublin, 2014, pp. 48-54. doi: 10.1109/IWSG.2014.15

[6] J. Kranjc, R. Orač, V. Podpečan, N. Lavrac, M. Robnik-Sikonja.. "ClowdFlows: Online workflows for distributed big data mining". Future Generation Computer Systems 68, 2017. pp. 38-58. doi:10.1016/j.future.2016.07.018.

[7] R. Seiger, S. Huber, P. Heisig. "PROtEUS++: A Self-managed IoT Workflow Engine with Dynamic Service Discovery". 9th Central European Workshop on Services and their Composition (ZEUS). 2017. pp 90-92.

[8] O.O. Petrenko, A.I. Petrenko. "Cyber-Physical Medical Platform for Personal Health Monitoring", Journal of Scientific Achievements (JSA), Australia, vol. 2, issue 8, 2017, pp. 24-28. ISSN: 2207-4236

[9] OWL-S: Semantic Markup for Web Services. [online] Available https://www.w3.org/Submission/OWL-S/.

[10] Петренко І.А., Петренко О.О. "Автоматизовані методи пошуку і відкриття необхідних сервісів", Вісник Університету «Україна», Серія «Інформатика, обчислювальна техніка та кібернетика», №1(17), 2015, С. 55-64

[11] S. Rodriguez Loya, K. Kawamoto, C. Chatwin, and V. Huser, "Service Oriented Architecture for Clinical Decision Support: A Systematic Review and Future Directions". Journal of Medical Systems, December 2014, 38(12): 140. https://doi.org/10.1007/s10916-014-0140-z

[12] A. Celesti, M. Fazio, F. Galán Márquez, A. Glikson, H. Mauwa, A. Bagula, F. Celesti, and M. Villari. How to Develop IoT Cloud e-Health Systems Based on FIWARE: A Lesson Learnt. Journal of Sensor and Actuator Networks. 2019, 8(1), 7; https://doi.org/10.3390/jsan8010007

[13] W. van der Aalst, K.M. van Hee. Workflow management: models, methods, and systems. MIT press, 2004. 368 p.

[14] M. Weidlich, G. Decker, M. Weske. "Efficient Analysis of BPEL 2.0 Processes using pi-Calculus". Proceedings of the IEEE Asia-Pacific Services Computing Conference (APSCC'07). – Japan, 2007. – P. 266-274.

ASTES

Advances in Science, Technology and Engineering Systems Journal Vol. 4, No. 4, 251-255 (2019)

www.astesj.com

Special Issue on Advancement in Engineering and Computer Science

ASTESJ

ISSN: 2415-6698

Exchange Rate Modeling: Medium-Term Equilibrium Dynamics

Anton Kuzmin*

The Financial University under the Government of the Russian Federation, Department of Data Analysis, Decision-Making and Financial Technologies, Moscow, Russian Federation

ARTICLE INFO

Article history:
Received: 14 June, 2019
Accepted: 24 July, 2019
Online :30 July, 2019

Keywords:
Exchange Rate
Equilibrium Dynamics
Modeling
Export-Import Operations
Capital Flows
The Terms Of Trade

ABSTRACT

In this study, we develop the author's approach, based on the principles of modeling of the International Flows Equilibrium Exchange Rate (IFEER). As a result, a new model is built, depending on the main macroeconomic factors in the medium term. The model presents a wide system of basic factors, but many of the intermediate factors in the modeling were eliminated. The results are discussed in the context of the previously known results of economic theory.

1. Introduction

This paper is an extension of work originally presented in Eleventh International Conference "Management of large-scale system development" (MLSD 2018, IEEE Russian section) [1] .

In the scientific literature the nominal and real exchange rate models are widely represented in conditions of the dynamic general equilibrium (DSGE-models), the founders of which is the model Obstfeld-Rogoff [2] of monopolistic competition of two open economies. At the same time, the previous approaches to fundamental factors modeling were developed by Mussa [3] and Dornbush [4] in conditions of both the monetarist and Keynesian approaches.

Many authors emphasizes the effectiveness of fundamental factors models of nominal and real exchange rates (e.g., [5]).

Conditions for the existence of the equilibrium rates were allocated in 1945 by R. Nurkse [6], which paid considerable attention to the balance of payments equilibrium, the lack of restrictions on export-import operations and capital flows and internal stability of the economy.

However, from the standpoint of structural modeling, the known models of economic theory cannot provide adequate results for assessing of the equilibrium real or nominal rates level. In a significant majority the exchange rates are not expressed in terms of the equilibrium of the financial market, but in terms of the theory of purchasing power parity (PPP). Structurally, the exchange rate analysis is limited by the current balance. Herewith, it should be emphasized the role of the exchange rates in the process of regulating the external balances and the role of the indicator of competitive advantages in foreign trade flows.

To solve these problems, we propose to use the author's approach, based on the principles of the international flows equilibrium exchange rate (IFEER) modeling [1, 7].

2. Conceptual Bases of Modeling

It should be noted, that in this article we develop the IFEER-approach and the new equilibrium exchange rate model will be presented as a result.

Initially, we suppose that the world consists of two equal rights open economies and international trade flows take into account the trading competitive position of these countries. In this context, international trading bilateral competitive position is determined by the real exchange rate. It should be noted here, that approach "small open economy - the rest of the world" under IFEER-concept was used by the author in modeling of the Russian ruble exchange rate (e.g., [7]).

We consider all real market transactions at nominal exchange rates $e_i, i \in (1, L)$ on the domestic currency market that occurred in a certain period of time.

*Anton Kuzmin, Moscow, Russian Federation, a_kuzmin@rambler.ru

Then e_i, D_i, R_i in *i-th* transaction are: the bilateral nominal exchange rate, the amount in the determined foreign currency and the amount in the national currency respectively.

In this context, these variables are linked by ratios:

$$e_i D_i = R_i, \text{ and therefore, } e_i = R_i / D_i .$$

So, we define the synthetic value of the bilateral nominal exchange rate in conditions of varying degrees of free floating for the certain period as the sum of exchange rates, weighted by amounts in determined foreign currencies:

$$e \equiv \sum_{i=1}^{L} \frac{D_i}{\sum_{j=1}^{L} D_j} \times e_i , \quad (1)$$

Using the definition of the exchange rate in *i-th* transaction, we get from (1):

$$e = \sum_{i=1}^{L} \frac{D_i}{\sum_{j=1}^{L} D_j} \times \frac{R_i}{D_i} = \sum_{i=1}^{L} R_i \Big/ \sum_{j=1}^{L} D_j . \quad (2)$$

Next, on a conceptual level, we can disaggregate balance of payments flows:

$$e_t = 1 \Big/ e_t^* = (I_t + K_t^-) \Big/ (E_t + K_t^+) = \\ = (E_t^* + K_t^{*+}) \Big/ (I_t^* + K_t^{*-}), \quad (3)$$

where I_t - the demand in the national currency on imports,

E_t - the supply in the foreign currency from exports,

K_t^+ - the capital inflows in the foreign currency,

K_t^- - capital outflows in the national currency.

This formula takes into account such important components as export revenue, demand for imports, demand for foreign assets and so on.

Therefore,we are developing two-period model in the dynamics in times *t* and *t-1*.

Herewith, at time *t* value of the functions of export-import operations and capital flows will be directly determined by the international competitive position represented by the real exchange rate at the time *t-1*:

$$e_{t-1}^R = e_{t-1} P_{t-1}^* \Big/ P_{t-1} , \quad (4)$$

where P_{t-1}^* - the exernal prices index,

P_t - the internal prices index.

For the model verification the price indices can be represented by consumer prices index (CPI), GDP-deflator and so on.

In the analysis of exchange rates, many authors (e.g., M. Bahmani-Oskoee and G. Goswami [8]) determine the terms of trade, reflecting the effectiveness of export-import operations in world trade, as one of the determining factors of the dynamics.

For example, F. Caramazza [9] explored the expectations of investors of German mark against French franc dynamics – one of the main cross-rates in the world at that time. He explained the change in parity by largely fundamental macro-variables, including terms of trade and relative inflation differential. L. Bartolini [10] similarly revealed the relationship between market expectations of devaluation and CPI-indicator of trading international advantages.

In the author's model of the ruble exchange rate [11], the use of trade terms by micro-agents as the main determinant of foreign trade operations is proved and justified on the statistical series of import and export of Russia. However, they are expressed in adjusted nominal exchange rates at price levels, including actual export prices.

3. Exchange Rate Modeling: Medium-Term Equilibrium Dynamics

In the domestic foreign exchange market at time *t* export earnings as part k_E of the average real gross domestic output $(Q_t^{\frac{1}{x+1}} Q_{t-1}^{\frac{x}{x+1}})^{\delta}$ in foreign prices P_t^* depend on the decision of producers-exporters and the state of international trade conditions e_{t-1}^R at time *t-1*:

$$E_t = P_t^* k_E (Q_t^{\frac{1}{x+1}} Q_{t-1}^{\frac{x}{x+1}})^{\delta} (e_{t-1}^R)^z , \quad (5)$$

where $k_E = const$,

Q_t - real gross domestic output.

In a function (5) $k_E (Q_t^{\frac{1}{x+1}} Q_{t-1}^{\frac{x}{x+1}})^{\delta}$ says, that the produced exports are part of averaged real gross domestic output (e.g., real GDP).

Due to the stability Q_t, the averaging method does not give a significant contribution to the fluctuations of the functional dependence (5).

The parameter *z* is the response to change in international trading position and the index *x* is associated with indexes *z* and *y* in the functions (5) and (6): *x=(z-y).*

In a functional dependence (5) the parameter δ reflects the fact that the growth rate of export exceeds the growth of gross domestic product because of a limitation of domestic demand: $\delta \geq 1$.

In the framework of the simulation because of equal rights and symmetry of flows the export of a country is an import of counterparty.

By analogy with a functional dependence (5):

$$E_t^* = P_t^* k_I (Q_t^{*\frac{1}{x+1}} Q_{t-1}^{*\frac{x}{x+1}})^{\lambda} (e^{*R}_{t-1})^{-y} , \quad (6)$$

where $k_I = const$.

The parameter y also is the response to change in real international trading position.

So, using the formula (4) and $e_t = 1/e_t^*$, functional dependency (6) can be rewritten

$$E_t^* = I_t = P_t\, k_I (Q_t^{*\frac{1}{x+1}} Q_{t-1}^{*\frac{x}{x+1}})^{\lambda} (e_{t-1}^R)^y .$$

As can be seen from formula (3), capital flows and export-import operations directly affect the exchange rate dynamics.

It should be noted that many well-known models of economic theory have serious difficulties with formalizing of the impact of capital flows on the exchange rates. However, within the framework of the proposed IFEER-concept, we can directly determine these functional dependencies.

At the same time, the mechanism of formation of functional dependencies of capital flows is very similar to the mechanisms of formation of export-import operations regarding the chosen factor system. More details can be found in the author's work [1]. For example, at time t we suppose that non-residents buy part of the real averaged domestic product $k_{K^+}(Q_t^{\frac{1}{x+1}} Q_{t-1}^{\frac{x}{x+1}})^{\theta}$ in their prices:

$$K_t^{+} = P_t^* k_{K^+} (Q_t^{\frac{1}{x+1}} Q_{t-1}^{\frac{x}{x+1}})^{\theta} (e_{t-1}^R)^z , \qquad (7)$$

where $k_{K^+} = const$, $\theta \geq 0$.

Capital inflows are capital outflows of its counterparty:

$$K_t^{*+} = P_t\, k_{K^-} (Q_t^{*\frac{1}{x+1}} Q_{t-1}^{*\frac{x}{x+1}})^{\rho} (e^{*R}_{t-1})^{-y} , \qquad (8)$$

where $k_{K^-} = const$.

We can rewrite a functional dependence (8):

$$K_t^{*+} = K_t^{-} = P_t\, k_{K^-} (Q_t^{*\frac{1}{x+1}} Q_{t-1}^{*\frac{x}{x+1}})^{\rho} (e_{t-1}^R)^y .$$

Let's substitute dependences (5) - (8) in (3):

$$e_t = \Big[P_t k_I (Q_t^{*\frac{1}{x+1}} Q_{t-1}^{*\frac{x}{x+1}})^{\lambda} (e_{t-1}^R)^y + \\ + P_t k_{K^-} (Q_t^{*\frac{1}{x+1}} Q_{t-1}^{*\frac{x}{x+1}})^{\rho} (e_{t-1}^R)^y \Big] \times \\ \Big[P_t^* k_E (Q_t^{\frac{1}{x+1}} Q_{t-1}^{\frac{x}{x+1}})^{\delta} (e_{t-1}^R)^z + \\ + P_t^* k_{K^+} (Q_t^{\frac{1}{x+1}} Q_{t-1}^{\frac{x}{x+1}})^{\theta} (e_{t-1}^R)^z \Big]^{-1} =$$

$$= \Big[P_t (Q_t^{*\frac{1}{x+1}} Q_{t-1}^{*\frac{x}{x+1}})^{\rho} (e_{t-1}^R)^y \times \\ \times (k_I (Q_t^{*\frac{1}{x+1}} Q_{t-1}^{*\frac{x}{x+1}})^{\lambda-\rho} + k_{K^-}) \Big] \times \\ \times \Big[P_t^* k_E (Q_t^{\frac{1}{x+1}} Q_{t-1}^{\frac{x}{x+1}})^{\theta} (e_{t-1}^R)^z \times \\ \times (k_E (Q_t^{\frac{1}{x+1}} Q_{t-1}^{\frac{x}{x+1}})^{\delta-\theta} + k_{K^+}) \Big]^{-1}$$

Due to the significant stability of the members $(Q_{t-1}^{\delta/\delta+} Q_t^{1/\delta+1})$ and $(Q_t^{*\frac{1}{x+1}} Q_{t-1}^{*\frac{x}{x+1}})$, compared to price indicators P_{t-1}^* and P_t, we can consider as a constant the construct:

$$\frac{(k_I (Q_t^{*\frac{1}{x+1}} Q_{t-1}^{*\frac{x}{x+1}})^{\lambda-\rho} + k_{K^-})}{(k_E (Q_t^{\frac{1}{x+1}} Q_{t-1}^{\frac{x}{x+1}})^{\delta-\theta} + k_{K^+})} = k^{x+1} = const . \qquad (9)$$

Further, it can be rewritten as:

$$e_t = k^{x+1} \frac{P_t (Q_t^{*\frac{1}{x+1}} Q_{t-1}^{*\frac{x}{x+1}})^{\rho}}{P_t^* (Q_t^{\frac{1}{x+1}} Q_{t-1}^{\frac{x}{x+1}})^{\theta} (e_{t-1}^R)^{\delta}} =$$

$$= k^{x+1} \frac{P_t (Q_t^{*\frac{1}{x+1}} Q_{t-1}^{*\frac{x}{x+1}})^{\rho}}{P_t^* (Q_t^{\frac{1}{x+1}} Q_{t-1}^{\frac{x}{x+1}})^{\theta} (e_{t-1} P_{t-1}^* / P_{t-1})^{\delta}} = .$$

$$= k^{x+1} \frac{P_t (Q_t^{*\frac{1}{x+1}} Q_{t-1}^{*\frac{x}{x+1}})^{\rho}}{P_t^* (Q_t^{\frac{1}{x+1}} Q_{t-1}^{\frac{x}{x+1}})^{\theta} (e_{t-1})^{\delta}} \left(P_{t-1} / P_{t-1}^* \right)^x$$

So after regrouping we get:

$$e_t (e_{t-1})^x = \left(k \frac{P_t}{P_t^*} Q_t^{*\rho/x+1} Q_t^{-\theta/x+1} \right) \times \\ \times \left(k \frac{P_{t-1}}{P_{t-1}^*} Q_{t-1}^{*\rho/x+1} Q_{t-1}^{-\theta/x+1} \right)^x . \qquad (10)$$

After intertemporary separation of the fundamental economic variables in formula (10):

$$e_t = k \frac{P_t}{P_t^*} Q_t^{*\rho/x+1} Q_t^{-\theta/x+1} .$$

And after the designation $\theta' = \theta/x+1$ and $\rho' = \theta/x+1$ for convenience, we get:

$$e_t(P(t),Q(t),P^*(t),Q^*(t)) = k\frac{P_t}{P_t^*}Q_t^{*\rho'}Q_t^{-\theta'}. \quad (11)$$

4. Setting the Model Parameters and Verification

The starting point of the study of the medium-term exchange rate dynamics should be characterized by stability, both internal and external economic situation. More details can be found in the author's work [1].

We suggest that setting of the parameters ρ' and θ' can use the least squares method with a normalized differences of the nominal theoretical $e_t(\theta,\rho)$ and nominal market exchange rates under constraints $\rho' \geq 0$ and $\theta' \geq 0$:

$$ND(e)_t = \frac{e_t(\theta,\rho) - e_t(\text{nominal})}{e_t(\text{nominal})}. \quad (12)$$

At the starting point of the selected period it must be put: *P(start)=1, Q(start)=1, P*(start)=1, Q*(start)=1*. Coefficient k must be equal to the nominal market exchange rate at the starting point.

Next, the sum of normalized squared deviations (12) minimizes:

$$\begin{cases} \min\limits_{\theta',\rho'} \sum\limits_t \left(ND(e)_t\right)^2 \\ \theta' \geq 0 \\ \rho' \geq 0 \end{cases}. \quad (13)$$

In order to verify the model, it is advisable to consider the results in the context of the known results of economic theory of determination of the exchange rates.

For these intentions, let us rewrite formula (11) in logarithms:

$$\log e_t = \log k + (\pi_t - \pi_t^*) + \rho'\log Q_t^* - \theta'\log Q_t = \\ = \log k + (\pi_t - \pi_t^*) + \rho' q_t^* - \theta' q_t \quad . \quad (14)$$

Using the I.Fischer equation $PQ=MV$, where M is the money supply, V is the velocity of money, we present this in logarithms:

$$\pi = m + v - q\,.$$

Assuming in the medium term the rate of the velocity of money is constant and substituting (14) symmetrically for both countries, we obtain (with $a = \log k = const$)

$$\log e_t = \log k + (m_t + v - q_t - \\ -(m_t^* + v^* - q_t^*)) + \rho' q_t^* - \theta' q_t = \quad (15) \\ = a + (m_t - m_t^*) + (\rho'+1)q_t^* - (\theta'+1)q_t = \\ = a + (m_t - m_t^*) + \rho'' q_t^* - \theta'' q_t\,.$$

Verification of dependencies of a similar type (15), having the same system of fundamental macroeconomic factors, has been successful within the framework of verification of the monetary model. Of the works on this topic it should be noted econometric studies of models of fundamental determinants of B. R. Clarida et al. [12], J. Cheung, M. Chinn, and A. Pascual [13], I. Chowdhury [14].

It is also interesting to consider predictive abilities of dependencies of a similar type. One of the most famous is the study of J. Chen and N. Mark [15]. The forecasts for the formula of type (15) at $\rho'' = \theta''$ on different time horizons gave a significantly better result than in accordance with a random walk. And it was in the medium and long term.

5. Results and Conclusion

Exogenous variables are the total products Q and Q^* and the levels of external and internal prices P^*, P in the countries of the bilateral exchange rate in this model. Other basic intermediate determinants, such as export-import operations, capital flows, the terms of trade in the modelling process have been eliminated.

It should be noted here, that author's IFEER-concept of Equilibrium Exchange Rate (EER) correlates with the widely known economical concepts: behavioural EER (BEER) [16, 17] and fundamental EER (FEER) [18].

Using national consumer price and real domestic product indices and oil prices, the main research formula (11) was applied by the author to the study of the dynamics of the Russian ruble against the US dollar in the period 2013-2015. The results of econometric verification showed a very high quality of the model.

Thus, we can state the high practicality of models of fundamental determinants in relation to different currency pairs, based on both "real" (Russian ruble, US dollar, Canadian dollar, etc.) and "past" (German mark, French franc) currencies.

Conflict of Interest

The author declares no conflict of interest.

References

[1] A. Kuzmin, "Equilibrium Exchange Rate Modeling" in Eleventh International Conference "Management of large-scale system development" (MLSD 2018), Moscow, Russian Federation, https://ieeexplore.ieee.org/document/8551843/metrics#metrics, Publisher: IEEE, 2018, Electronic ISBN: 978-1-5386-4924-4. DOI: 10.1109/MLSD.2018.8551843.

[2] M. Obstfeld, K. Rogoff, "Exchange Rate Dynamics Redux" Journal of Political Economy, **103**(3), 624-660, 1995.

[3] R. Dornbush, "Expectations and Exchange Rates Dynamics" Journal of Political Economy, Vol.84, December, 1161-1176, 1976.

[4] M. Mussa, "The Exchange Rate, the Balance of Payments and Monetary and Fiscal Policy Under Regime of Controlled Floating" Scandinavian Journal of Economics, May, **78** (2), 229-248, 1976.

[5] C.M. Engel, N.C. Mark and K.D. West, Exchange Rate Models Are Not As Bad As You Think, NBER Macroeconomics Annual, Vol. 22, 2007, revised in 2011.

[6] R. Nurkse, Conditions of International Monetary Equilibrium, 1945 in The International Monetary System: Highlights from Fifty Years of Princeton's Essays in International Finance, Kenen P.B. (ed.), Boulder, Colorado: Westvie Press, 1993.

[7] A. Kuzmin, "Exchange Rate Modeling: The Case of Ruble" Review of Business and Economics Studies, **3**(3), 39-48, 2015.

[8] M. Bahmani-Oskoee, G. Goswami, "Exchange Rate Sensitivity of Japan's Bilateral Trade Flows" Japan and the world economy, **16**(1), 1–15, 2004.

[9] L. Bartolini, Devaluation and Competitiveness in a Small Open Economy: Ireland 1987-1993, IMF Working Paper WP/93/82, Washington: IMF, November, 1993.

[10] F. Caramazza, French-German Interest Rate Differentials and Time-Varying Realignment Risk, Washington: IMF Staff Papers, Vol.40, September, 1993.

[11] A. Kuzmin, "A Structural Model of Exchange Rate Dynamics" Review of Business and Economics Studies, **2**(3), 86-92, 2014.
[12] R. H. Clarida, L. Sarno, M.P. Taylor, G. Valente, The Out-of Sample Success of Term Structure Models as Exchange Rate Predictors: A Step Beyond, NBER Working Paper, № 8601, Cambridge, Massachusetts: National Bureau of Economic Research , 2001.
[13] Y.-W. Cheung, M. Chinn, A.G. Pascual, Empirical Exchange Rate models: Are any Fit to Survive?, IMF Working Paper WP/04/73, Washington: IMF, 2004.
[14] I. Chowdhury, "Sources of Exchange Rate fluctuation: empirical evidence from six emerging market countries" Applied Financial Economics, **14**(1), 697-705, 2004.
[15] J. Chen, N.C. Mark, "Alternative Long-Horizon Exchange-Rate Predictors" International Journal of Finance and Economics, 1, 229–250, 1996.
[16] P.B. Clark, R. MacDonald, Exchange Rates and Economic Fundamentals: A Methodological Comparison of BEERs and FEERs, IMF Working Paper 98/67, Washington: International Monetary Fund, March, 1998.
[17] P.B. Clark, R. MacDonald, Filtering the BEER a permanent and transitory decomposition, IMF Working Paper 00/144 - Washington: International Monetary Fund, 2000.
[18] J. Williamson, Estimates of FEERs, In Estimating Equilibrium Exchange Rates, Williamson J. (ed.), Washington: Institute for International Economics, 1994.

ASTES

Advances in Science, Technology and Engineering Systems Journal
Vol. 4, No. 4, 256-264 (2019)
www.astesj.com
Special Issue on Advancement in Engineering and Computer Science

ASTES Journal
ISSN: 2415-6698

Event Monitoring using Distributed Pattern Recognition Approach on Integrated IoT-Blockchain Network

Anang Hudaya Muhamad Amin[*,1], Nazrul Muhaimin Ahmad[2], Subarmaniam Kannan[2]

[1]*Computer Information Sciences Division, Higher Colleges of Technology, United Arab Emirates*

[2]*Centre of Intelligent Cloud Computing (CICC), Multimedia University, Malaysia*

ARTICLEINFO

Article history:
Received: 12 June, 2019
Accepted: 17 July, 2019
Online: 08 August, 2019

Keywords:
Event Monitoring
Internet-of-Things (IoT)
Blockchain Technology

ABSTRACT

With the advancement in the field of Internet-of-Things (IoT), event monitoring applications have rapidly evolved from a simple event data acquisition towards predictive event analytics involving multi-sensory data aggregation in a distributed environment. Existing event monitoring schemes are mainly relying on inefficient centralized processing mechanism, which may lead to the common single-point of failure for the entire system. In addition, there is no proper method for verifying the event data generated by the monitoring system. In this paper, we present a distributed event monitoring scheme using a Hierarchical Graph Neuron (HGN) distributed pattern recognition algorithm. HGN is a single-cycle learning graph-based recognition scheme that is modelled for in-network deployment. In this work, event data retrieved from multi-sensory IoT devices within a distributed event monitoring network is converted into pattern. To address the event data verification problem, we integrate our proposed scheme with blockchain technology. Combining this IoT event monitoring capabilities with blockchain-based data storage and verification could leads towards a scalable event detection and monitoring model for large-scale network. The results obtained from our simulation shows that the proposed scheme offers high event detection accuracy and capable of minimizing the event storage requirements on blockchain network.

1 Introduction

Since a decade ago, Internet-of-Things (IoT) has been extensively explored as a common platform for event monitoring. In industrial manufacturing applications, IoT plays an important role in monitoring and controlling processes. The monitoring systems designed for such applications require seamless interoperability between heterogeneous distributed IoT sensor devices and processing nodes, as well as an ability to analyze different types of sensor data.

The importance of such systematic interoperability may be conceptualized through an industrial scenario, wherein the plant maintenance is automatically scheduled by coordinating and synchronizing different sub-systems including distributed engineering, control, and maintenance sub-systems. Once a maintenance event is detected, the system can directly generate suitable downstream process controls, computed according to the applications requirements as to generate a correct response within the entire system.

A conventional way of performing event detection and monitoring usually involves a set of interconnected sensor devices that are linked to a centralized processing node (sink). These sensor devices made up the IoT infrastructure, enabling data acquisition process. With this method of implementation, common issues are related to communication and processing latency. Edge computing [1] is a form of computing model that enables data acquisition and processing to be performed within the close proximity of IoT devices.

Event monitoring involving critical applications such as environmental and disaster monitoring usually requires spatio-temporal data analysis for detecting unusual events or incidents. Machine learning and neural network algorithms are commonly being applied for such use cases. Nevertheless, these approaches involve complex computational procedures to be performed on resource-abundant processing nodes. In the context of large-scale and highly distributed IoT network, these approaches may not be suitable due to the resource-constrained specification of most IoT devices. Furthermore, massive data transmission may occur between the

[*]Anang Hudaya Muhamad Amin, Higher Colleges of Technology, P.O.Box 15825, Dubai, United Arab Emirates, +9712-2064772 & aamin@hct.ac.ae

sensor nodes and the processing node, due to large volume of data to be processed continuously.

A number of approaches have been carried out to enable complex machine learning and neural network algorithms to perform in a fully-distributed manner. However, most of the existing schemes suffer from the tightly-coupled processing mechanism in detecting and classifying event/non-event. Distributed algorithms that implement a graph-based approach show a promising way towards achieving purely-distributed processing mechanism.

Graph Neuron (GN) [2] is a distributed pattern recognition algorithm that follows the principles of graph theory with (vertex, edge) representation. GN algorithm has been implemented in several different case studies, including event recognition in wireless sensor networks (WSNs). GN performs a single-cycle in-network processing in its learning mechanism. As such, this improves its scalability against other graph-based pattern recognition schemes.

This paper is an extension of work originally presented in ICIAS 2018 [3]. In this paper, we extend our proposed idea on integrating a distributed pattern recognition algorithm and blockchain technology for event monitoring in IoT network. GN-based algorithm known as Hierarchical Graph Neuron (HGN) [4] is chosen as the distributed pattern recognition algorithm to be incorporated in the proposed IoT-blockchain infrastructure, enabling event detection and monitoring to be performed in a distributed manner, close to the event data acquisition point. Integrating blockchain network and IoT infrastructure allows the event signal or data from IoT devices to be stored and verified by blockchain nodes in the form of transaction using the distributed ledger mechanism. This approach provides a way to collect and preserve significant series of events that were captured and monitored by the IoT devices. Within this infrastructure, distributed pattern recognition could be implemented by identifying patterns of multiple sensor activation on IoT devices, and thus allowing complete transactions of event data to be recorded within the blockchain network.

The outline of this paper is as follows: Section 2 provides an overview on the current approaches towards distributed event monitoring. Section 3 focuses on the Graph Neuron (GN) based approach for event detection in a distributed environment. The model for integrated IoT-Blockchain platform for event monitoring is presented in Section 4. The proposed IoT-blockchain scheme with distributed pattern recognition for event monitoring is presented in Section 5. This section also includes description of the simulation works that have been performed. Finally, Section 6 concludes the paper.

2 Distributed Event Monitoring

A typical setup for distributed event monitoring network is shown in Figure 1. In this model, each IoT device act as an observer, which observe a stream of events. These observations would then be used for analysis involving either a simple function as collecting the number of observations or other complex computations such as identifying anomalies in the input distributions. Such computations usually being carried out by the coordinator node, who is overseeing the entire observations within the network.

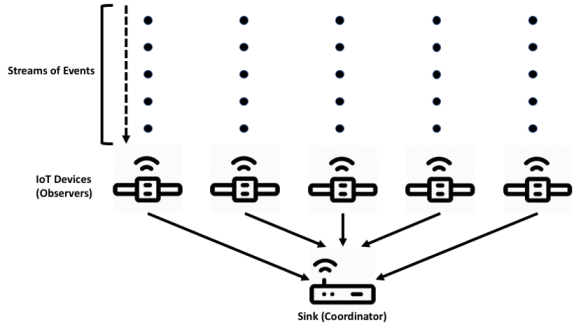

Figure 1: Distributed event monitoring setup with series of IoT devices as observers and processing node as coordinator.

There are a number of related works that demonstrate the distributed event monitoring activities carried out in different kinds of applications. These include the work by Wu et al. [5] and Ahmad Jan et al. [6].

In the survey conducted by Cormode [7], there are two approaches in deriving useful computations for the observations obtained from the sensor/IoT network. The first approach involves all the observers to simply send all the observations to a single and centralized coordinator. A drawback of such approach is such that it burdens the communication network between the coordinator and the observers. A second approach implements a periodic polling, in which at a particular time interval, the coordinator polls each observer for information on the observations and collates this information to get a snapshot of the current status since the last poll. A limitation of this approach is that it does not fit well, when considering event analysis using a non-linear computational model as in the continuous event monitoring applications.

The current centralized event monitoring systems that implement such coordinator-observer model can be seen in the works recorded by Ahmad Jan et al. [6] usually suffer from several limitations. Firstly, centralized event data processing can lead towards single-point of failure whereby failure of centralized node basically fails the entire event monitoring activity. Secondly, magnitude of data transmission to a central repository would be significantly increased as a result of massive number of IoT devices connected. This phenomena creates a connection gridlock from IoT devices to the centralized server.

Apart from the coordinator-observer model, other scheme such as presented by Basirat and Khan [8] utilizes the in-network processing capabilities that enable each IoT device to perform computation on observations within the body of the network, without relying on a centralized data processing node. With the in-network processing model, each IoT node is responsible for collecting the observations, as well as performing data aggregation. Analysis is carried out within the collaborative effort by each node, in exchanging critical information obtained from the observations.

Event monitoring with pattern recognition approach is widely applied in different application fields such as health informatics, manufacturing automation, and structural monitoring. Distributed pattern recognition algorithms such as Graph Neuron (GN) [9] and Vector Symbolic Architecture (VSA) [10] offer better schemes towards improved event

monitoring capability that runs on a distributed processing environment.

The proposed Graph Neuron (GN) based approach for event monitoring utilizes the in-network processing model that enables event identification to be conducted within the body of the network, rather than complex analysis and computations being performed at the processing node (coordinator). Discussion on how GN implements such processing model will be discussed in the next section.

3 GN-Based Approach for Event Monitoring

Graph Neuron (GN) is a single-cycle learning distributed pattern recognition algorithm that utilizes the in-network processing model [11]. The main characteristic of any distributed pattern recognition is such that it requires recognition of patterns to be implemented in a decentralized manner. Graph Neuron with similar feature, has been designed for fully-decentralized event detection scheme.

GN algorithm utilizes the graph-like pattern representation with each element of the pattern is represented with a *(value, position)* format. A variation of GN algorithm with hierarchical structure, known as Hierarchical Graph Neuron (HGN) was later developed by Nasution and Khan [4] that eliminates the crosstalk issue in GN implementation. In this paper, we present our proposed approach of utilizing HGN algorithm for distributed event monitoring on multi-sensor IoT devices.

3.1 Hierarchical Graph Neuron (HGN)

Hierarchical Graph Neuron (HGN) algorithm extends the functionality of Graph Neuron (GN) algorithm by increasing the pattern matching accuracy for highly-distorted patterns. HGN has been proven to eliminate the crosstalk issue found in GN implementation. The neuron firing in GN relies on the comparative function between stored and input elements on each neuron, which is called bias entry. These entries composed of *(value, position)* pairs that represent pattern elements. The approach is completely different from conventional neural network schemes whereby firing of neuron is based upon weight adjustment and calibration. Figure 2 shows a typical HGN network composition.

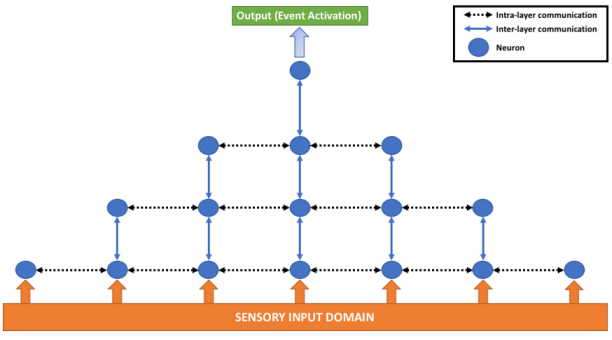

Figure 2: HGN network composition in a pyramid-like formation. Each neuron at the base layer corresponds to each input element within the sensory domain.

As shown in the figure, neurons composition in HGN network are arranged in a pyramid-like structure with base layer neurons act as input neurons to the network.

3.2 HGN Learning Mechanism

The neurons composition in each HGN network, n_{hgn} is represented by the following equation:

$$n_{hgn} = \left(\frac{p+1}{2}\right)^2 \tag{1}$$

Where p represents the number of input elements within the sensory input domain.

Following the graph-based structure, each neuron in HGN network composition forms a vertex that contains pattern element information (value or identification (ID)) while the adjacent inter-neuron communication is represented by the edge of a graph.

The HGN learning mechanism involves finding matched indices between input and stored patterns. In performing this comparison, each neuron compares its input pattern with the inputs obtained from its adjacent neurons. Adjacency information for each neuron is represented using the *(left, right)* formation. This adjacency information is known as bias entry and each neuron maintains an array of such entries. Each neurons bias array only stores the unique adjacency information derived from the input patterns. The pattern storage process involving N bias array sizes is represented in the following equation:

$$E^B = (\langle x, y \rangle; x \in N, y \in N) \tag{2}$$

Where E^B, comprises the sets of two-element ordered pair respectively, while x and y are the inputs within each entry. E^B can also be formed as one- or three-element ordered pair, depending upon the neuron location within the HGN hierarchical structure.

In retrieving matched bias entry, a linear search method is used on the adjacency information obtained for a given input pattern within each neuron through the bias array composition. The bias array entry is unique. Thus, the following equation shows a function to estimate the required number of comparisons for each input entry C_i, given n_{bEnt} number of bias entries in the array and r number of occurrences for each entry:

$$C_i = \frac{n_{bEnt} + 1}{r + 1} \tag{3}$$

In principle, HGN implements a single-cycle learning for recognizing patterns, through implementation of a graph-matching scheme on its pattern representation. Within HGN network composition, each neuron performs a forward propagation of index values obtained from the matching process as shown in Figure 3, from the base layer neurons towards the top neuron. The top layer neuron will decide on the event/non-event status based on the entire pattern recall search on the bias array composition. The procedures only involved a one-pass cycle for each input pattern, without any iterations involving value alteration as to obtain a recognition output.

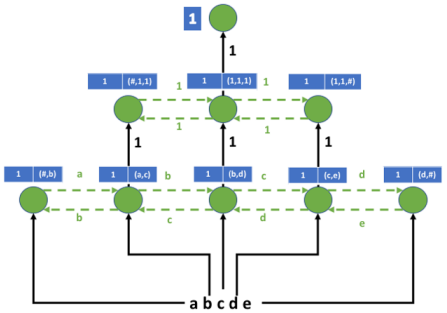

Figure 3: Neuron firing mechanism within the HGN network composition. Neuron activation is achieved through value comparison between adjacent neurons.

3.3 HGN for Event Monitoring

With distributed and lightweight features of HGN, an event detection scheme for IoT network can be carried out at the IoT device level. It could act as a front-end middleware that could be deployed within each IoT nodes in the network, forming a network of event detectors. Hence, the processing scheme minimizes the processing load at the sink and provides near real-time detection capability. Preliminary work on distributed HGN integration for distributed networks such as wireless sensor network (WSN) has been conducted by Muhamad Amin and Khan [12].

In integrating HGN within event monitoring, we have considered mapping each HGN processing cluster into each IoT node, with the assumption that each node is having more than one sensor inputs. Our proposed scheme is composed of a collection of IoT nodes and a sink. We consider a deployment of IoT network in two dimensional plane with M sensors, represented by a set $M = (m_1, m_2, ..., m_n)$, where m_i is the ith sensor. The placement for each of these sensors is uniformly located in a grid-like area, $A = (x \times y)$, where x represents the x-axis coordinate of the grid area and y represents the y-axis coordinate of the grid area. Each IoT node is assigned to a specific area of the grid as shown in Figure 4. The location of each sensor node is represented by the coordinates of its grid area (x_i, y_i).

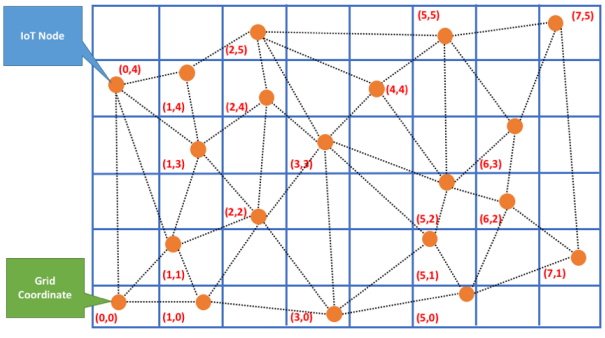

Figure 4: Cartesian grid layout used to identify location of IoT nodes in a two-dimensional space.

For communication model, HGN uses a single-hop mechanism for data transmission from IoT node to the sink. The use of *autosend* approach has been selected following the work by Saha and Bajcsy [13], to minimize error due to the loss of packets during data transmission. HGN event processing scheme involves minimal transmission of event data from IoT nodes to the sink, due to the ability for the front-end processing.

4 Integrating Blockchain in Distributed Event Monitoring

In this section, we present an overview of blockchain and its integration with the distributed event monitoring framework on IoT network.

4.1 Blockchain Technology

Blockchain provides a capability for verification of credentials and transactions using a distributed ledger mechanism. Such capability is of interest, especially when considering its integration with event monitoring system in IoT network.

Implementation of blockchain is not strictly limited to cryptocurrencies. In fact, there are many differences between cryptocurrency implementation and blockchain for industrial applications [14], including immutability and provenance. Blockchain has also been a point of interest in the field of shared economy applications (e.g. Uber, AirBnB) [15]. Nevertheless, past implementations of blockchain come with several limitations, including slow block generation period as mentioned in the Ethereum White Paper [16] and lack of loop implementation (Turing incomplete) [17]. Blockchain enables a decentralized mechanism for verification that allow participating nodes in the network to validate unique transactions through a distributed ledger (block). Figure 5 shows the decentralization approach in blockchain, in comparison with existing centralized approach.

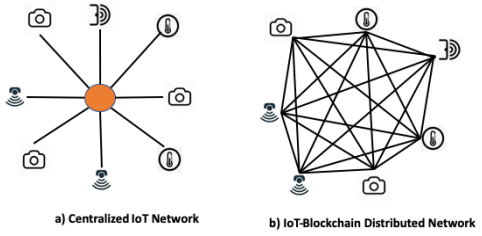

Figure 5: A comparison between conventional IoT network with IoT-Blockchain distributed network.

One of the important requirements for IoT integration on blockchain network is such that it requires fast validation and verification to be performed on blockchain network. Existing blockchain network such as Ethereum [18] has made this possible. Ethereum offers a smart contract deployment, as shown in Figure 6. It captures details of transactions including the value and its corresponding state. Developers can write a program that runs on top of Ethereum. With Ethereum as a blockchain platform, we can configure IoT devices to connect to this main network. This infrastructure would allow authentication of IoT devices through public key

infrastructure. IoT devices can utilize Ethereum platform for updating their action and behavior.

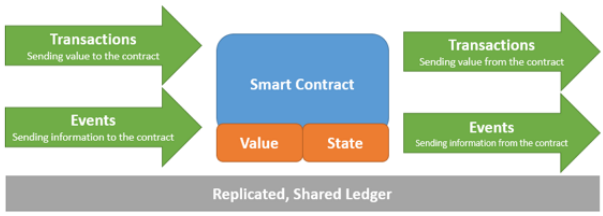

Figure 6: Smart contract deployment on Ethereum platform that captures details about transactions and events.

4.2 Device Synchronization

One of the important issues to be addressed in IoT network implementation within the IoT-Blockchain environment is device synchronization. As the number of devices increased, the need for proper synchronization mechanism is important. A work presented by Huh et al [19], demonstrated the synchronization of IoT devices on Ethereum blockchain network can be obtained using smart contract feature, which specify certain action and behavior of IoT devices. The smart contract can be used to place a code to indicate the detection of event by the IoT device.

In this paper, we demonstrate the use of blockchain network for the purpose of event data monitoring and verification. Blockchain offers immutability to the event data being captured from IoT network. Within the proposed model, sensor data are converted into activation patterns as shown in Figure 7.

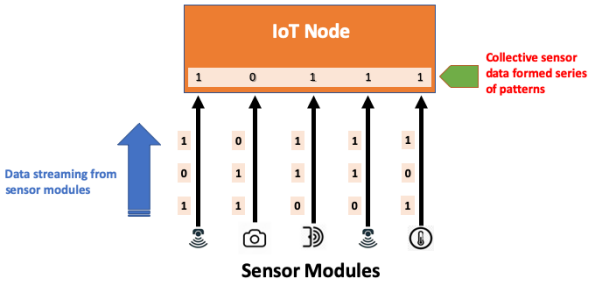

Figure 7: Inputs from sensor modules are treated as a pattern, to be processed by the IoT node.

From the temporal perspective, this sensor data patterns vary across time. Our aim is to capture unique event data to be stored and verified on blockchain network. HGN distributed pattern recognition scheme is used to detect unique event, prior to storage and verification on blockchain network. In this work, similar data patterns would be treated as non-event and will be discarded. The hypothesis for this work is such that the block generation could be minimized accordingly.

5 Proposed Infrastructure

In this section, we present our proposed IoT-blockchain with distributed pattern recognition framework for event detection and monitoring. In addition, this section will also include details on the simulation works and corresponding results involving forest fire detection using HGN distributed pattern recognition scheme.

5.1 System Model

The proposed event monitoring infrastructure incorporates a distributed pattern recognition on IoT- blockchain network. Hierarchical Graph Neuron (HGN) has been selected as the distributed pattern recognition algorithm to be used in our model. In this implementation, assumption is made as such that each IoT node is capable of performing event data collection. Each IoT node is linked to a blockchain-edge (BC-Edge) node that hold a distributed ledger, as part of the blockchain network. Figure 8 shows the proposed infrastructure for HGN deployment in IoT-blockchain network.

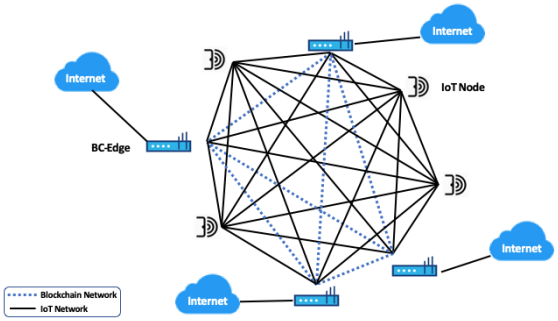

Figure 8: IoT-Blockchain network infrastructure for distributed event monitoring.

Note that the proposed scheme considered the use of multi-sensory IoT devices. Event monitoring is basically carried out at the device level, in which each device is capable of performing event detection using the HGN distributed pattern recognition algorithm. Figure 9 shows the detail event detection and verification procedures on IoT-blockchain network.

The network configuration used in this work is based upon the premise that all the nodes acquired communication capability with low latency in a full-mesh network structure.

In the proposed design, an IoT node N will establish its identity, and broadcast it to the BC-Edge nodes, B. For a given specific time interval T, the IoT nodes will communicate the event data (result from event activation using HGN scheme). This will then be processed by the BC-Edge node as event data for T. The analysis produces an output in the form of combined pattern index, event status, and event pattern as shown in the examples in Table 1. The event status contains information on the event, whether it is classified as new or recalled. Using this approach, only newly-recorded event will be stored and verified in the blockchain network.

As shown in Table 1, at T_2, event detected by IoT node *X02* is recalled and will be discarded. Similarly, at T_3, event

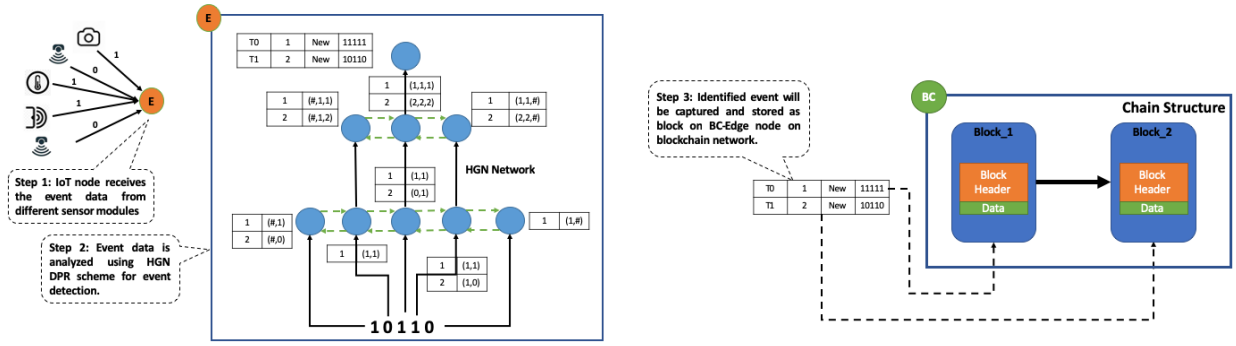

(a) Event data monitoring and detection.

(b) Unique event storage and verification on blockchain network.

Figure 9: Event monitoring with HGN distributed pattern recognition on integrated IoT-blockchain network.

Table 1: Outputs recorded by BC-Edge node, retrieved from the IoT nodes. Note that only unique event pattern will be stored in the blockchain network

Timestamp	IoT Node ID	Event Pattern	Index	Status
T_1	X01	10101	1	new
T_1	X02	11111	1	new
T_2	X01	10111	2	new
T_2	X02	11111	1	recall
T_3	X01	10111	2	recall
T_3	X02	11110	2	new

recorded by *X01* is recalled. Only unique event pattern will be captured and stored in the distributed ledger.

5.2 Event Monitoring Simulation

To demonstrate our proposed distributed event monitoring scheme, we designed a simulation work on event data analysis using the HGN algorithm. The analysis was conducted on the data related to forest fire, which contains 517 records as reported by Cortez and Morais [20]. Each event pattern detected was stored and verified using the SHA-256 secure hash algorithm on blockchain network.

We extracted five important features that contribute towards possibility of fire ignition, namely the ISI index, temperature, relative humidity (RH), wind and rain. For the purpose of simulation, the dataset is transformed into a binary representation using an interactive binning method. The range of values for each bin was specified according to the potential event (binary value 1) and non-event (binary value 0) as shown in the Table 2.

Table 2: Data values in different range used to identify each parameter as event.

Parameter	Data Range 1	Data Range 2
ISI	$x \geq 42.075$	$x \leq 14.025$
Temperature	$x \geq 23.325$	$x \leq 7.775$
Relative Humidity (RH)	$x \geq 63.75$	$x \leq 21.25$
Wind	$x \geq 6.75$	$x \leq 2.25$
Rain	$x \geq 4.8$	$x \leq 1.6$

Our assumption is such that the event data is continuous and recorded in a timely manner from T_0 till T_{516}, respectively.

5.3 Results and Discussion

In this section, we present the results of our simulation on event pattern recognition using the Hierarchical Graph Neuron (HGN) approach. The proposed scheme capable of detecting 19 unique events from the total of 517 event records. Consequently, the number of data blocks generated is reduced by 97%. This was made possible by identifying unique event patterns from the dataset. Figure 10 shows the event count distribution based on the 19 unique events detected using the proposed HGN distributed pattern recognition scheme.

Table 3 shows samples of event data for each corresponding unique event detected using our proposed HGN recognition scheme.

Apart from implementing the event data classification using HGN approach, we extended our analysis to examine the accuracy of our proposed recognition scheme on the simulated dataset. Based on the observation made, there were 40 event data that were misclassified as false positive (duplication of indices). As a result, the recognition accuracy for HGN in this simulation is at the rate of 92.3% with error rate of 7.7%. Further details on the misclassification can be seen in [21].

The simulation work that has been carried out demonstrate a high recall accuracy for HGN distributed pattern recognition implementation. The error rate for the event classification obtained is considerably low, as it only indicates value around 7.7%.In addition, the results prove that the number of unique events detected is significantly reduced. This is critical for ensuring efficient data block generation

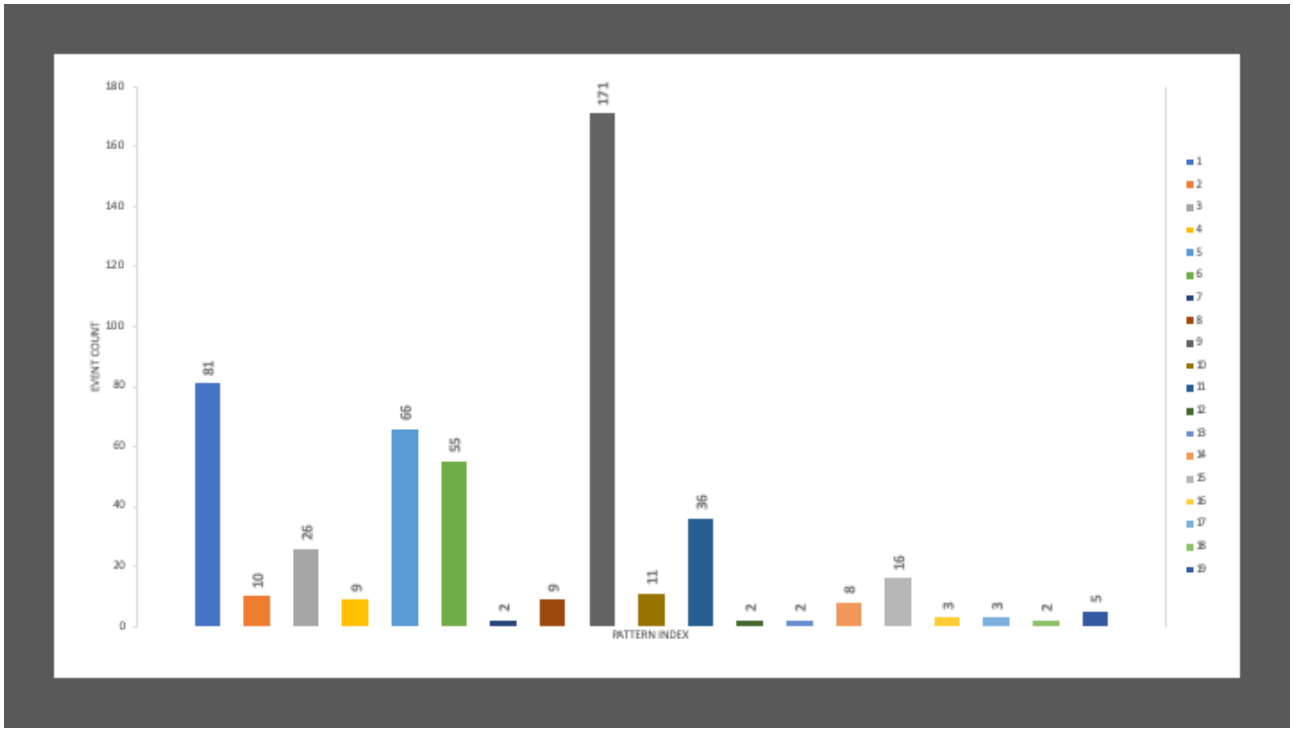

Figure 10: Unique event patterns detected using HGN distributed pattern recognition algorithm from the total of 517 event data recorded.

Table 3: Samples of forest fire event data that has been classified as unique event using HGN distributed pattern recognition algorithm.

Event ID	ISI Index	Temperature (°C)	Rel. Humidity (RH) (%)	Wind (km per hour)	Rain (mm per m^2)
1	5.1	8.2	51	6.7	0
2	7	21.3	42	2.2	0
3	5.8	23.4	22	2.7	0
4	6.2	12.9	74	4.9	0
5	17	20.1	40	4	0
6	7	21.6	33	2.2	0
7	8.9	18.4	42	6.7	0
8	15.9	25.9	24	4	0
9	10.7	10.3	74	2.2	0
10	7.8	17.4	24	5.4	0
11	3.8	15.2	51	2.7	0
12	8.1	29.6	27	2.7	0
13	6.7	18.4	25	3.1	0
14	14.3	19.1	53	2.7	0
15	14.1	33.1	25	4	0
16	10.8	26.4	35	2.7	0
17	14	30.8	30	4.9	0
18	17.7	26.4	34	3.6	0
19	14.3	27.3	63	4.9	6.4

within the blockchain network.

5.4 Future Work

Based on the simulation work that has been carried out, it was clearly indicated that the HGN distributed pattern recognition scheme is able to provide accurate classification of unique events. Our future work is basically to fully integrate the event classification module with blockchain network for event data storage and verification. The use of open-source hyperledger fabric platform [22] under the Linux Foundation Projects will be considered.

We intend to expand our research into effective scheme for data storage on blockchain. As the amount of data arises from events monitored on IoT network, the need for efficient data storage mechanism is important. At a preliminary stage, we propose a two-type storage mechanism, comprising event digest and event data. Event digest will be permanently stored in the blockchain network in the form of recorded blocks (on-chain), while the event data will be stored in conventional databases (off-chain). In implementing this scheme, it is expected that the storage requirement for event data could be further reduced.

In addition to the storage optimization, we would also aim to study on different consensus mechanisms for data verification on blockchain network. These include the proof-of-work (PoW) and proof-of-stake (PoS). The consensus mechanism enables peers and users within the network to verify the authenticity of the data that is stored on the blockchain network. Results of the study would assist us in implementing more efficient IoT-blockchain infrastructure for event monitoring on ioT network.

6 Conclusions

In this paper, we presented our on-going work on distributed event monitoring using a distributed pattern recognition algorithm on integrated IoT-Blockchain network. The proposed scheme implements a HGN recognition algorithm that performs a distributed event detection. Accuracy of HGN pattern recognition may improves the efficiency of distributed ledger storage mechanism in blockchain network. This enables unique event data to be stored and verified in a distributed environment. The simulation work being carried out shows that HGN algorithm exerts high recall accuracy with one-cycle learning. Furthermore, the algorithm is highly-suitable for in-network deployment.

HGN recognition approach also minimizes the needs for storing large amount of continuous event data on blockchain network. The detection mechanism in the proposed scheme also consider the entire state of the IoT network, rather than examining individual sensor input values.

For our future development, we intend to look into several aspects of IoT-blockchain integration, including the efficiency and effectiveness of the proposed scheme, through the scalability factor of the system in implementing multi-heterogeneous IoT-blockchain network. Apart from this, different consensus mechanisms in blockchain technology will be reviewed to analyze their effectiveness in the proposed IoT-blockchain scheme.

References

[1] Weisong Shi, Jie Cao, Quan Zhang, Youhuizi Li, and Lanyu Xu. Edge computing: Vision and challenges. *IEEE Internet of Things Journal*, 3(5):637–646, 2016.

[2] Mohamed Baqer, Asad I Khan, and Zubair A Baig. Implementing a graph neuron array for pattern recognition within unstructured wireless sensor networks. In *International Conference on Embedded and Ubiquitous Computing*, pages 208–217. Springer, 2005.

[3] Anang Hudaya, Muhamad Amin, Nazrul Muhaimin Ahmad, and Subarmaniam Kannan. Integrating distributed pattern recognition technique for event monitoring within the iot-blockchain network. In *2018 International Conference on Intelligent and Advanced System (ICIAS)*, pages 1–6. IEEE, 2018.

[4] Benny B Nasution and Asad I Khan. A hierarchical graph neuron scheme for real-time pattern recognition. *IEEE Transactions on Neural Networks*, 19(2):212–229, 2008.

[5] Kangheng Wu, Xiaokang Xiong, Bert W. Leung, Jihyoun Park, and Zhibin Lei. Event processing of monitoring data of large hi-tech manufacturing equipment: Debs grand challenge. In *Proceedings of the 6th ACM International Conference on Distributed Event-Based Systems*, DEBS '12, pages 387–392, New York, NY, USA, 2012. ACM. ISBN 978-1-4503-1315-5. doi: 10.1145/2335484.2335535. URL `http://doi.acm.org/10.1145/2335484.2335535`.

[6] Mian Ahmad Jan, Priyadarsi Nanda, Xiangjian He, and Ren Ping Liu. A sybil attack detection scheme for a forest wildfire monitoring application. *Future Generation Computer Systems*, 80:613 – 626, 2018. ISSN 0167-739X. doi: https://doi.org/10.1016/j.future.2016.05.034. URL `http://www.sciencedirect.com/science/article/pii/S0167739X16301522`.

[7] Graham Cormode. Continuous distributed monitoring: a short survey. In *Proceedings of the first international workshop on algorithms and models for distributed event processing*, pages 1–10. ACM, 2011.

[8] Amir H Basirat and Asad I Khan. Graph neuron and hierarchical graph neuron, novel approaches toward real time pattern recognition in wireless sensor networks. In *Proceedings of the 2009 International Conference on Wireless Communications and Mobile Computing: Connecting the World Wirelessly*, pages 404–409. ACM, 2009.

[9] Asad I Khan and Patrik Mihailescu. Parallel pattern recognition computations within a wireless sensor network. In *Proceedings of the 17th International Conference on Pattern Recognition, 2004. ICPR 2004.*, volume 1, pages 777–780. IEEE, 2004.

[10] Simon D Levy and Ross Gayler. Vector symbolic architectures: A new building material for artificial general intelligence. In *Proceedings of the 2008 Conference on Artificial General Intelligence 2008: Proceedings of the First AGI Conference*, pages 414–418. IOS Press, 2008.

[11] Ram Kumar, Vlasios Tsiatsis, and Mani B Srivastava. Computation hierarchy for in-network processing. In *Proceedings of the 2nd ACM international conference on Wireless sensor networks and applications*, pages 68–77. ACM, 2003.

[12] A. H. M. Amin and A. I. Khan. Parallel pattern recognition using a single-cycle learning approach within wireless sensor networks. In *2008 Ninth International Conference on Parallel and Distributed Computing, Applications and Technologies*, pages 305–308, Dec 2008. doi: 10.1109/PDCAT.2008.47.

[13] Sunayana Saha, Peter Bajcsy, et al. System design issues in single-hop wireless sensor networks. *Proc. of 2nd IASTED ICCIIT 2003*, 2003.

[14] Gideon Greenspan. Four genuine blockchain use cases. *MultiChain [blog]*, 10, 2016.

[15] Steve Huckle, Rituparna Bhattacharya, Martin White, and Natalia Beloff. Internet of things, blockchain and shared economy applications. *Procedia computer science*, 98:461–466, 2016.

[16] Vitalik Buterin et al. Ethereum white paper. *GitHub repository*, pages 22–23, 2013.

[17] Vitalik Buterin. Toward a 12-second block time. *Ethereum Blog*, 2014.

[18] Gavin Wood et al. Ethereum: A secure decentralised generalised transaction ledger. *Ethereum project yellow paper*, 151:1–32, 2014.

[19] Seyoung Huh, Sangrae Cho, and Soohyung Kim. Managing iot devices using blockchain platform. In *2017 19th international conference on advanced communication technology (ICACT)*, pages 464–467. IEEE, 2017.

[20] Paulo Cortez and Aníbal de Jesus Raimundo Morais. A data mining approach to predict forest fires using meteorological data. 2007.

[21] Anang Hudaya Muhamad Amin, Sujni Paul, Fred N Kiwanuka, Imtiaz Ahmad Akhtar, et al. Improving event monitoring in iot network using an integrated blockchain-distributed pattern recognition scheme. In *International Congress on Blockchain and Applications*, pages 134–144. Springer, 2019.

[22] Hyperledger fabric - hyperledger. `https://www.hyperledger.org/projects/fabric`. Accessed: 2019-07-12.

ASTES

Advances in Science, Technology and Engineering Systems Journal
Vol. 4, No. 4, 265-270 (2019)
www.astesj.com
Special Issue on Advancement in Engineering and Computer Science

ASTES Journal
ISSN: 2415-6698

A Novel Strategy For Prompt Small Cell Deployment In Heterogeneous Networks

Dorathy Abonyi*

Department of Electrical and Electronic Engineering, Enugu State University of Science and Technology, Nigeria

ARTICLEINFO

Article history:
Received: 27 May, 2019
Accepted: 11 July, 2019
Online: 08 August, 2019

Keywords:
Heterogeneous networks
RSSI
Direction-of-arrival estimation

ABSTRACT

Popularity and affordability of smart phones and other data hungry devices add exponentially to the traffic demand of existing cellular networks. Cell densification and small cell deployment over existing macrocell has been identified as an effective solution to high traffic demand predicted for future wireless networks like 5G. Small cells are deployed over existing macrocells in a Heterogeneous network to offload traffic, ensure balanced load and good quality of service in the network. To achieve the purpose of HetNet, small cells are deployed in locations of high user concentration. Operators are required to be able to identify these locations for optimum small cell deployment. Presently, this decision is based on long term traffic data which create latency in small cell deployment especially in areas of unexpected hotspots. The work presented in this paper is a new strategy that can practically help operators to promptly identify locations for small cell deployment based on user cluster. This strategy involves a monitoring system that can be easily incorporated in a mobile cellular network base transceiver station (BTS) to monitor the coverage area and periodically identify positions for prompt and optimum small-cell deployment in HetNets. The monitoring system is a two element array system that uses RSS data to resolve DoA, range, user cluster and identify positions for small cell deployment. At any point in time, the network operator can visualize cluster locations relative to the base station and is able to identify hotspots. When small cells like micro-, pico-, or femto-cells are promptly deployed in areas of higher user concentration, high data rates and good quality of service in the network are maintained at all times. The network coverage area is divided into a series of azimuthal and range sectors, and users are located into the sectors where they belong. The strategy was simulated in MATLAB environment for WiFi networks with thirty users and results indicate 100% *accurate DoA estimation and MAE in range estimation of* 6*m for a known environment. Optimum positions for small cell deployment based on user clusters were correctly determined. Simulation was validated with experiment and result indicate close relationship between experiment and simulation with MAE difference in range estimation of* 1*m.*

1 Introduction

The exponential growth in data traffic demand on cellular networks and the promising solution offered by heterogeneous network and small cell deployment has triggered a lot of research interest in this area. It is obvious that homogeneous networks involving macro- only cells are insufficient in solving the capacity requirement of the present and future networks like 5G. This is due to high cost of macrocell BTS and the unavailability of cell sites especially in city centers. Small cells like micro-, pico- and femtocells are therefore deployed within the existing macrocell and integrated as a heterogeneous network. These small cells are cheaper to implement and site acquisition is also easier to get since even an existing electric pole or building roof is a potential site. Deploying small cells within existing macrocell gives rise to a big umbrella cell with a number of small cells, each positioned to serve a smaller coverage area within the big

*Department of Electrical and Electronic Engineering, Enugu State University of Science and Technology, Nigeria, +2348037576332 & abonyi.dorathy@esut.edu.ng

cell as shown in Figure 1.

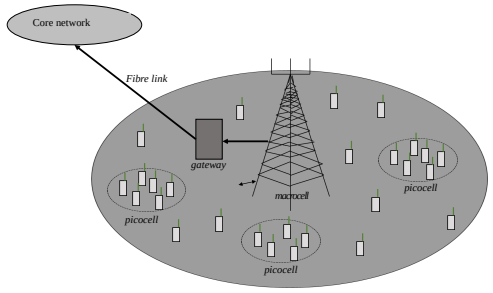

Figure 1: Heterogeneous network showing an umbrella macrocell with deployed picocells forming a 2-tier HetNet

Three main aim of heterogeneous network are (1) To offload traffic from macrocell, (2) Ensure balanced load in the network and (3) Ensure good quality of service to users. To achieve these objectives, small cells are deployed in a well targeted manager in most cases within locations of high user concentration (HUC). This therefore requires the network operators to be able to identify locations of HUC. Presently, these locations are determined using collected traffic data over a period of time and locations with high traffic demand is taken as HUC and position for small cell deployment. This approach does not give opportunity for prompt traffic offload, balanced load and good QoS using small cells especially in unexpected hotspot cases. This paper is an extension of the work originally presented in International Workshop on Computer Aided Modeling and Design of Communication Links and Networks (CAMAD) [1] which introduced the system based on simulation only. The work presented in this paper presents the application of the previous work as a strategy for prompt identification of optimum position for small cell deployment. Both simulation and experimental validation are presented to demonstrate the applicability of proposed strategy.

Strategies for small cell deployment can broadly be classified as Random Deployment Strategy (RDS) and Deterministic Deployment Strategy (DDS). RDS in most In RDS, small cells are randomly deployed within the macrocell while in DDS, the position for small cell deployment is determined based on some standing factors. Network performance for DDS and RDS was compared in [2] and their result indicate that DDS is a better option. Well targeted small cells has been shown to enhance QoS, offload traffic from macro-cell [3], ensure balance network load [4], improve energy saving capability and generally optimize performance [5] of the network. DDS can further be classified into uniformly distributed strategy (UDS), Cell edge strategy (CES) and user aware strategy (UAS). In UDS, a predetermined pattern of small cell deployment is followed for all macrocells owned my the network operator [6]. For CES approach, Small cells are arranged around the macrocell edge [7]. In UAS, locations of users are considered for small cell deployment based on usage or population. Normally, these data are obtained from long term traffic information [8] which does not provide prompt response to capacity requirement of hotspots especially when they are unexpected. Hotspots are locations of high demand characterized by high user concentration. A mobile small cell deployment strategy for unexpected hotspots which will ensure prompt response to traffic was proposed in [9] but with the assumption that network operators are able to promptly identify hotspot locations. To the best of our knowledge, there is no existing small cell deployment strategy with hotspot identification which is the contribution of this paper.

2 Problem Statement and Proposed Strategy

Considering a macrocell of a cellular network with 360° coverage. Looking at only 180 degrees coverage of this network as illustrated in Figure2 with base station (BS) located as indicated with red dot. Assuming there are so many users causing traffic overload on the existing macrocell and low quality of service (QoS) resulting to customer dissatisfaction. Some locations in this network are characterized with obvious clusters of users within the cell causing an overload on the macrocell base transciever station servicing this area. The strategy proposes a monitoring system to be deployed on the BS tower to monitor the coverage area so that it divides the area into azimuthal and range sectors as shown in Figure 2. By locating users into the individual azimuth-range classes, positions with HUC can be identified for small cell deployment. With blind or random placement of small cells in this network, the uncertainty of achieving the objective of HetNet will be high but with a monitoring system, it is almost certain that optimal placement of small cell based on user concentration will be achieved.

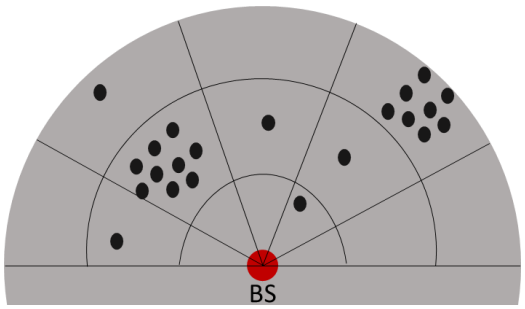

Figure 2: The proposed strategy for prompt small cell deployment

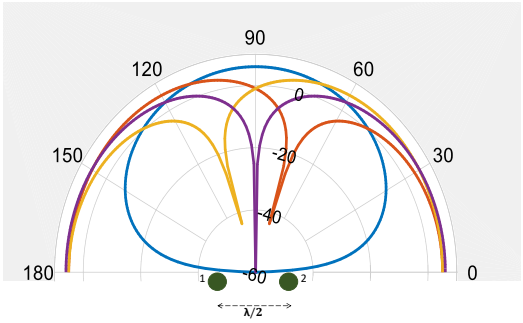

Figure 3: The proposed strategy for prompt small cell deployment

Assuming a two element array system is used for monitoring so that a directional main beam is produced on az-

imuth and steered to other azimuth locations as shown in Figure 3. This creates azimuth locations differentiated by main beam positions for angle of arrival localization of network users. By sharing the network coverage into range classes relative to the BS and estimating user range, users are located into different azimuth-range classes and users clusters can be identified.

3 User Cluster Localization and Optimum Position for Small Cell Deployment

To localize users by cluster, the system first estimates the DoA of each user. This is based on the azimuth position from where the maximum RSS was calculated when compared with measured RSS from other beam steered azimuth positions. It should be noted that the estimated DoA is not a precise estimate but considering the application, only a sector estimate is required. Second the system estimates range of each user using a range estimation model that is based on RSS-distance relationship. By fitting a curve in least square sense, a mathematical model that is applied for user range estimation is obtained. Combining estimated DoA and range, users are classified into created azimuth-range classes of the network.

3.1 Simulation

To test the proposed strategy, thirty users were randomly distributed within a simulated network coverage area as shown in Figure 4. The aim is to determine locations of user cluster and optimum positions for small cell deployment based on number of users in each cluster.

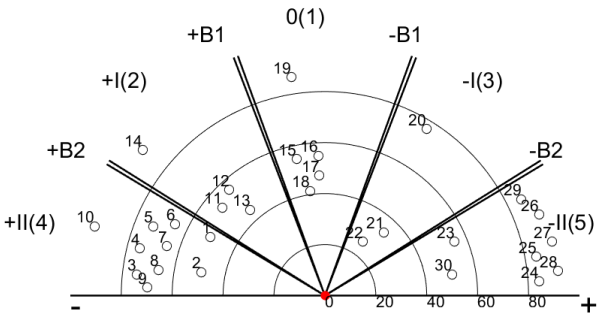

Figure 4: Actual location of users before localization

Assuming the network channel to be FSPL environment, the system acquires data for localization by calculating user RSS from all four main azimuth positions. Figure 5 is a plot of calculated RSS from all four main beam positions. From the calculated RSS data, it can be seen that different RSS values are measured from each azimuth position with a unique maximum value for each user. Using the calculated RSS, user DoA is calculated based on the azimuth position with highest calculated RSS for each user. Estimated DoA result of each user is shown in Figure 6.

Comparing the result of Figure 6 with the actual user locations of Figure 4, it can be seen that all users were correctly located to the azimuth position where they belong. Considering the accuracy of DoA estimation as the ability to locate users into each of the created azimuth sectors, this result gives 100% DoA estimation accuracy.

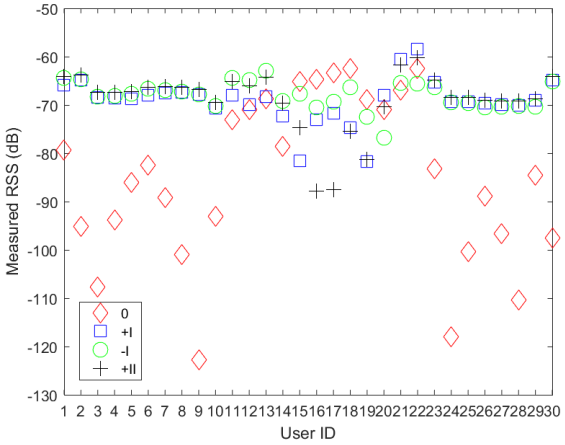

Figure 5: System simulated RSS from user devices in four main azimuth positions showing possibility of classifying DoA based on maximum RSS

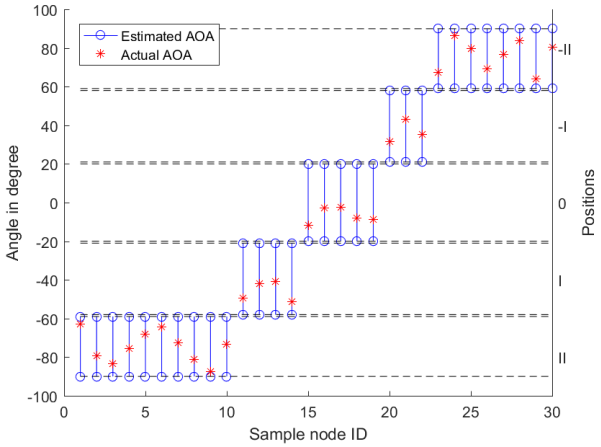

Figure 6: Estimated user DoA showing correct azimuth position localization of all users in the Network

To test the range estimation, four different environments, FSPL, HATA, ITU and WINNER defined by their empirical pathloss models of Equations 1, 2, 3 and 4 respectively were considered.

$$PL_{FSPL} = -27.5 + 20\log(f) + 20log(d) \quad (1)$$

$$PL_{HATA} = -35.4 + 20\log(f) + 26log(d) \quad (2)$$

$$PL_{ITU} = -28 + 20\log(f) + 20log(d) \quad (3)$$

$$PL_{WINNER} = -29.8 + 20\log(f) + 21.5\log(d) \quad (4)$$

where f is radio wave frequency in MHz, d is distance between BTS and user in meters. These environments were modeled and range estimation model developed for each environment. Using the measured RSS from FSPL environment, the four range estimation models for FSPL, HATA, ITU and WINNER were applied to estimate user range. Figure 7 shows the actual user range with the result of estimated range using these range models. To determine which of

the network location area is the optimum position for small cell deployment, users are classified into each of the sectors based on the estimated DoA and range. By counting the number of users in each class, user population per class is determined. Based on a preset threshold of number of users for small cell deployment depending on the type of small cell for the network, the optimum position for small cell deployment is determined. Assuming a micro-picocell network where a picocell is deployed in positions with atleast six users, optimum positions for small cell deployment in the simulated network are obtained as shown in Figure 8.

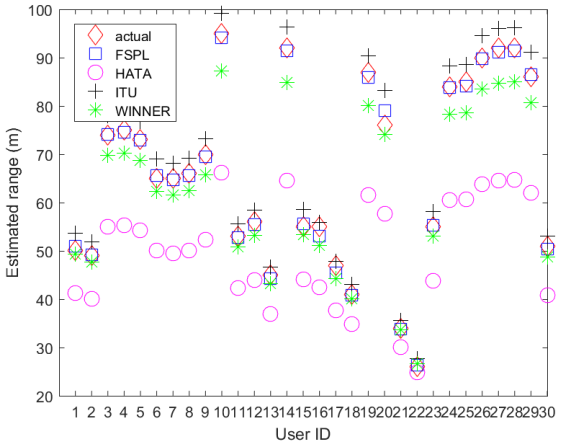

Figure 7: Estimated range of users using all four environment range estimation models for calculated RSS in FSPL environment

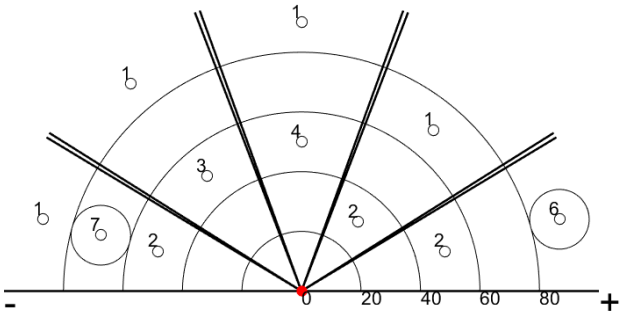

Figure 8: User cluster localization and optimum small cell deployment position identification

The range estimation result of Figure 7 gives a mean absolute error (MAE) of approximately 6m, 16m, 10m and 7m using FSPL, HATA, ITU and WINNER range models respectively. FSPL environment has given the least error in estimation because RSS was calculated in FSPL environment. This means that if the environment is known, the system is able to determine range estimation up to an accuracy of 6m but if the environment is unknown, the error in range estimation can increase up to 16m. By visually observing the result of Figure 7 and considering range estimated using FSPL range estimation model, it can be seen that users with ID numbers 1 to 10 and 23 to 30 located at azimuth positions +II and -II respectively were located with error in range estimation lying between 0 and 1m. Users with ID 11 to 14 and 20 to 22 located at azimuth positions +I and -I respectively were located with range estimation error between 1m and 37m. This is an indication that in a switched beam based localization systems, range estimation is azimuth position dependent. This will further be investigated in future work. Result of Figure 8 shows that user cluster and positions for small cell deployment can be determined.

3.2 Experimental Validation

Experiment was performed outdoor in the open field space of Ponderosa park in Sheffield, UK using a network of WiFi nodes as users. Figure 9 is a picture of the experimental setup. Figure 10 shows a model of the experimental environment with deployed users in their actual positions.

Figure 9: Outdoor experimental setup showing some of the distributed users on red and deployed observer system on yellow

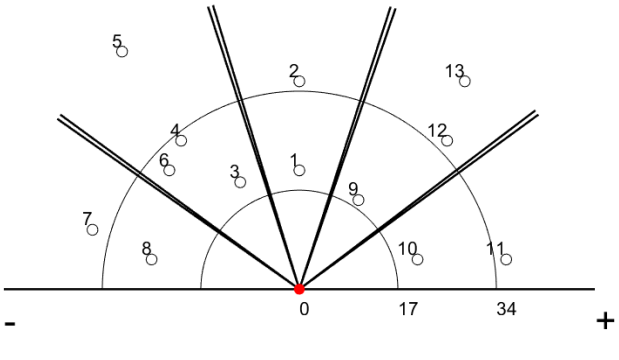

Figure 10: A model of the actual user position before localization

Ten RSS of these users were measured from a reference point where the monitoring system was positioned. Mean of the experimental measured RSS for each user from four main azimuth positions were obtained and plotted as shown in Figure 11. Using the measured RSS, DoA of users were estimated and result shown in Figure 12. Using the same measured RSS, user range were estimated using four range models representing four different environment scenarios. Result of Figure 13 shows actual, ITU simulated and experimental estimated range of users using all environment models. Next is to locate user clusters and identify locations for small cell deployment based on set threshold. Since only few (thirteen) users were used in this experiment, it was assumed that locations with up to two users are qualified for small cell deployment. Due to the small experimental area, coverage area was shared into three range sectors. Combining the estimated DoA and range, users are classified into

clusters by counting the number of users in each azimuth-range sectors of the coverage area. Figure 14 is result of experimental localized user clusters.

4 Result Analysis and Discussion

Comparing the actual user azimuth positions and the DoA estimation result of Figure 12, it can be seen that all users were correctly localized to their azimuth positions. Result has shown 100% accuracy for the used sample of users which validates the simulation DoA estimation result.

Result of range estimation shown in Figure 13 gives a mean absolute error (MAE) between actual and experiment of 2.51m, 3.56m, 2.19m and 2.54m for FSPL, HATA, ITU and WINNER open space range models respectively. This shows that the environment of RSS measurement is closely related to ITU model than other used range models. Comparing simulation and experiment, MAE in range estimation between experiment and simulation in ITU environment is 1.36m. This means that the mean deviation of experiment from simulation is approximately 1m and 2m from actual range. This shows that range estimation is achievable with manageable error levels. Apart from HATA which has a model that is well deviated from others, all other models are on the average, about 2.5m close to actual range. Deviation of experiment from simulation is just approximately 1m which means that this strategy is applicable and would work as modeled in simulation with a mean difference of $\leq$ 1.5m of range estimation in most known environments.

Comparing result of Figures 14 with the actual user positions, four small cell deployment locations were identified instead of two. This is due to over estimation of two of the users as a result of noise in measurement. This error may have been caused by the drizzling weather condition during this experiment. Also with few users and small number of users for small cell deployment as used here, this is expected but with a practical higher number of users required for small cell deployment in a real cellular network, this discrepancies will be reduced. The possibility of user cluster and small cell deployment position identification is promising with the results obtained from this experiment.

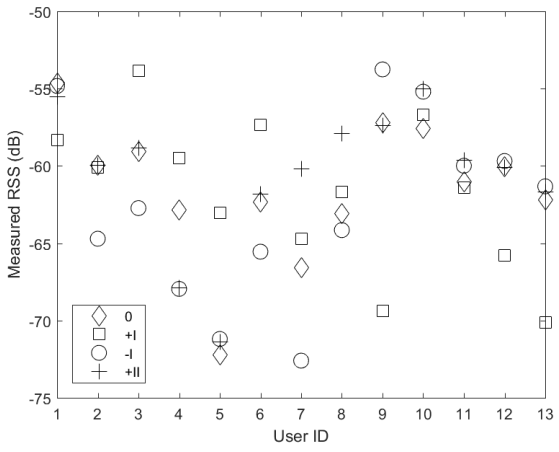

Figure 11: Measured RSS from user devices at all azimuth positions

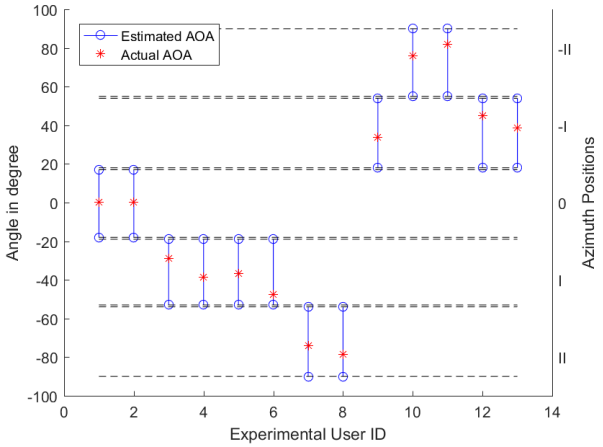

Figure 12: Experimental estimated DoA of users

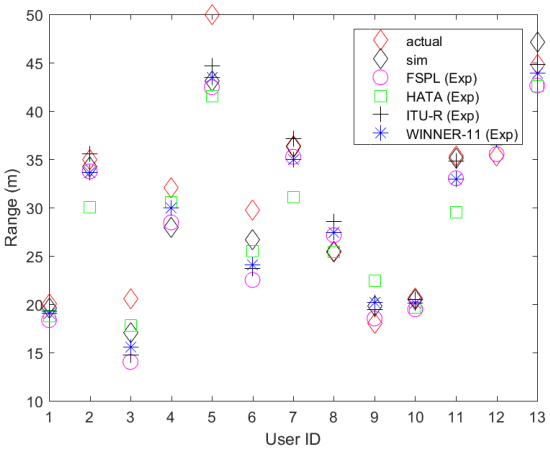

Figure 13: Experimental range estimation showing actual, simulated and experimental estimate

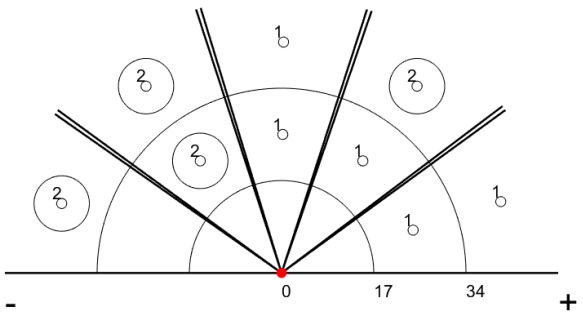

Figure 14: Experimental user cluster localization and optimum small cell deployment position identification

5 Conclusion

The work presented in this paper describes a novel and practical strategy for prompt small cell deployment in a heterogeneous network. This strategy involves using a monitoring system to periodically monitor the network coverage area of a wireless network and identify locations for small cell deployment based on user cluster localization. The entire

network coverage area is shared into azimuth and range locations for user cluster localization. By applying DoA and range estimation, user relative position is estimated. Number of users in each class is determined to identify optimum positions for small cell deployment. Both simulation and experimental results have shown that this strategy is applicable and user clusters can be correctly identified with minimal error.

Conflict of Interest The authors declare that there is no conflict of interest.

Acknowledgment I wish to acknowledge Enugu State University of Science and Technology and the Federal Government of Nigeria through Tertiary Education Trust Fund (TETF) for sponsoring this research.

References

[1] D. Abonyi and J. Rigelsford, "A System for Optimizing Small-Cell Deployment in 2-Tier HetNets," in *2018 IEEE 23rd International Workshop on Computer Aided Modeling and Design of Communication Links and Networks (CAMAD)*. IEEE, sep 2018, pp. 1–6. [Online]. Available: https://ieeexplore.ieee.org/document/8514981/

[2] G. Su, L. Li, X. Lin, and H. Wang, "On the optimal small cell deployment for energy-efficient heterogeneous cellular networks," in *2014 Sixth International Conference on Ubiquitous and Future Networks (ICUFN)*. IEEE, jul 2014, pp. 172–175. [Online]. Available: http://ieeexplore.ieee.org/lpdocs/epic03/wrapper.htm?arnumber=6876775

[3] A. Nika, A. Ismail, B. Y. Zhao, S. Gaito, G. P. Rossi, and H. Zheng, "Understanding data hotspots in cellular networks," in *10th International Conference on Heterogeneous Networking for Quality, Reliability, Security and Robustness*. IEEE, aug 2014, pp. 70–76. [Online]. Available: http://ieeexplore.ieee.org/document/6928662/

[4] M. H. Qutqut, H. Abou-zeid, H. S. Hassanein, A. M. Rashwan, and F. M. Al-Turjman, "Dynamic small cell placement strategies for LTE Heterogeneous Networks," in *2014 IEEE Symposium on Computers and Communications (ISCC)*. IEEE, jun 2014, pp. 1–6. [Online]. Available: http://ieeexplore.ieee.org/document/6912536/

[5] S. Landstrom, H. Murai, and A. Simonsson, "Deployment Aspects of LTE Pico Nodes," in *2011 IEEE International Conference on Communications Workshops (ICC)*. IEEE, jun 2011, pp. 1–5. [Online]. Available: http://ieeexplore.ieee.org/document/5963602/

[6] Y. Park, J. Heo, H. Kim, H. Wang, S. Choi, T. Yu, and D. Hong, "Effective Small Cell Deployment with Interference and Traffic Consideration," in *2014 IEEE 80th Vehicular Technology Conference (VTC2014-Fall)*. IEEE, sep 2014, pp. 1–5. [Online]. Available: http://ieeexplore.ieee.org/lpdocs/epic03/wrapper.htm?arnumber=6965951

[7] J. Hoadley and P. Maveddat, "Enabling small cell deployment with HetNet," *IEEE Wireless Communications*, vol. 19, no. 2, pp. 4–5, apr 2012. [Online]. Available: http://ieeexplore.ieee.org/document/6189405/

[8] I. Bahceci, "On femto-cell deployment strategies for randomly distributed hotspots in cellular networks," in *2014 IEEE Wireless Communications and Networking Conference (WCNC)*. IEEE, apr 2014, pp. 2330–2335. [Online]. Available: http://ieeexplore.ieee.org/document/6952713/

[9] N. E, X. Chu, and J. Zhang, "Mobile Small-Cell Deployment Strategy for Hot Spot in Existing Heterogeneous Networks," in *2015 IEEE Globecom Workshops (GC Wkshps)*. IEEE, dec 2015, pp. 1–6. [Online]. Available: http://ieeexplore.ieee.org/document/7414060/

ASTES

Advances in Science, Technology and Engineering Systems Journal Vol. 4, No. 4, 271-275 (2019)

www.astesj.com

ASTESJ

ISSN: 2415-6698

Research on Dynamic Vehicle Model Equipped Active Stabilizer Bar

Anh Nguyen Tuan*, [1], Binh Hoang Thang[2]

[1]*Mechatronics-Automobile Department, Ha Noi University of Business and Technology, Viet Nam*

[2]*Automotive Engineering Department, Ha Noi University of Science and Technology, Viet Nam*

ARTICLE INFO

Article history:
Received: 30 May, 2019
Accepted: 27 July, 2019
Online: 07 August, 2019

Keywords:
Active stabilizer bar
Rollover
Anti-roll moment
Roll angle
Dynamic vehicle model

ABSTRACT

Vehicles are rollover when steering at high speed, this phenomenon is limited by increasing the anti-roll moment of the suspension system. This research focuses on analyzing and establishing the dynamic model of vehicle when steering and describes the dependence of the vehicle body's roll angle on other factors. Research has shown that when equipped a stabilizer bar it will significantly reduce the roll angle of the vehicle body. Besides, this research shows the outstanding advantages of active stabilizer bar with other stabilizer bars. Therefore, most of the vehicle should be equipped active stabilizer bar to ensure stability and safety when moving.

1. Introduction

1.1. Rollover of the vehicle

When the vehicle goes on the road with high speed and the driver suddenly changes the direction, the centrifugal force appears. This force tends to go out of the rotating arc, cause the center of sprung mass to change, the moment causes the rolled vehicle will appear, denoted by M_1 [1].

$$M_1 = M_F + M_P \quad (1)$$

Where:

M_F: Moment of centrifugal force.

M_P: Moment of gravitation.

Assume that M_2 is the anti-roll moment of the vehicle, this moment is caused by the suspension system.

If:

$M_2 < M_1 \leq M_{2max}$: The vehicle body is tilted.

$M_1 > M_{2max}$: The vehicle is rollover.

Therefore, to limit the rollover of the vehicle is necessary to reduce the moment M_1. In fact, this value can't control, the alternative solution is to increase the value of anti-roll moment M_2 by adding an extra elastic part [2].

The problem of horizontal instability of the vehicle has been studied by foreign scientists as well as proposed many options, one of the solutions offered is to use stabilizer bar [3, 4]. However, previous studies often concentrate on the passive stabilizer bar on the vehicle with a linear single-track model and a half model [5]. This paper focuses on establishing space dynamic vehicle model equipped active stabilizer bar to limit the roll angle of the vehicle when steering.

1.2. Equipped stabilizer bar on the vehicle

To increase the value of the anti-roll moment M_2 is necessary to increase the stiffness of the suspension system. Today, vehicles are often equipped the stabilizer bar to link the two wheels of an axle [6]. The stiffness and size of the stabilizer bar are proportional to the vehicle's mass, the larger vehicle requires a stabilizer bar with a larger diameter and harder. Therefore, it will have a significant impact on the smoothness of the vehicle when moving on the road.

With the above problem, instead of using normal mechanical stabilizer bar, some middle-class and high-class vehicles were equipped stabilizer bar with electric or hydraulic control. The active stabilizer bar has the advantage of reducing the roll angle when steering and limiting the impact to the smoothness when moving on the bumpy road.

*Anh Nguyen Tuan, Email: taae177@gmail.com

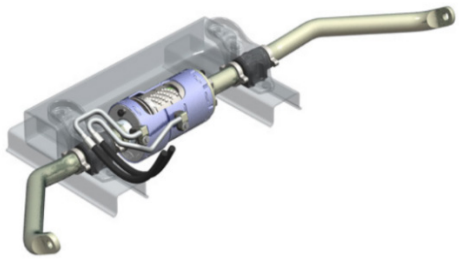

Figure 1: Active stabilizer bar

2. Dynamic vehicle model

2.1. Dynamic vehicle model 7 DOF

Consider the model of the vehicle to show in Figure 2. This section, the oscillation includes the vertical oscillation (z) and the horizontal oscillation (φ_x) because the vehicle steers at a stable velocity and the road surface are considered to be flat, it is possible to ignore longitudinal oscillation of the vehicle (φ_y).

Suppose that:

$$F_1 = F_{C11} + F_{K11} + F_{C21} + F_{K21}$$

$$F_2 = F_{C12} + F_{K12} + F_{C22} + F_{K22}$$

Using the method of separation of objects, according to [7] equations describing vertical displacement and roll angle of suspended mass:

$$m\ddot{z} = F_1 + F_2 \tag{2}$$

$$\left(I_x + mh_1^2\right)\ddot{\varphi}_x = \left(F_1 - F_2\right)b + M_1 - M_{SB} \tag{3}$$

Where:

M_1: Moment of roll vehicle.

$$M_1 = \left(a_y cos^2\varphi_x + gsin\varphi_x\right)mh_1 \tag{4}$$

M_{SB}: Moment of the stabilizer bar.

$$M_{SB} = mgh_1 sin\varphi_x \tag{5}$$

I_x: Moment of inertia around the x-axis.

h_1: The distance from the center of gravity to the roll axis.

The equation describes the vertical displacement of unsprung mass:

$$m_{ij}\ddot{\xi}_{ij} = F_{KLij} - F_{CLij} - F_{Kij} \tag{6}$$

According to [8, 9]

The elastic force of spring:

$$F_{Kij} = K_{ij}\left(\xi_{ij} - z \pm b\varphi_x\right) \tag{7}$$

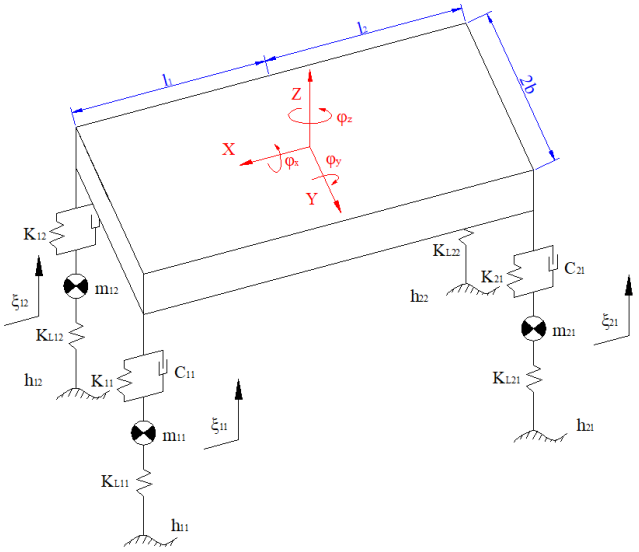

Figure 2: Dynamic vehicle model 7 DOF

The resistive force of damping:

$$F_{Cij} = C_{ij}\left(\dot{\xi}_{ij} - \dot{z} \pm b\dot{\varphi}_x\right) \tag{8}$$

The elastic force of tire:

$$F_{KLij} = K_{Lij}\left(h_{ij} - \xi_{ij}\right) \tag{9}$$

2.2. Double track dynamic vehicle model

The body vehicle is tilted caused by lateral acceleration when steering. Place the dynamic vehicle model 7 DOF on the road plane (Oxy), the vehicle performs 3 movements include longitudinal movement (x), lateral movement (y) and movement around the vertical axis (φ_z). For each of the above unknowns, there will be a corresponding equation describing the movement of the vehicle.

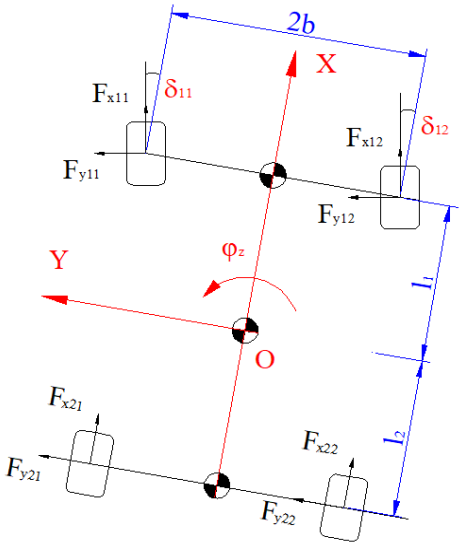

Figure 3: Double track dynamic vehicle model

Assume that the steering wheel angle δ is very small and ignore M_z at the wheel. According to [10] the equation describes the movement of the vehicle in the case of constant velocity in the form:

$$M\left(\dot{v}_y + \dot{\varphi}_z v_x\right) = F_{y1} + F_{y2} \quad (10)$$

$$I_z \ddot{\varphi}_z = F_{y1} l_1 - F_{y2} l_2 \quad (11)$$

With:

$$F_{y1} = F_{y11} + F_{y12}$$

$$F_{y2} = F_{y21} + F_{y22}$$

If the deformation wheel is considered in the linear domain, the lateral force of the wheel is determined by the following formula:

$$F_y = -C_\alpha \alpha \quad (12)$$

Where:

C_α: Side stiffness of the tire.

α: Slip angle of the tire.

Table 1: Specifications of the vehicle

Description	Symbol	Value
Distance from center to front axle	l_1	1110 (mm)
Distance from center to rear axle	l_2	1655 (mm)
Base width	2b	1500 (mm)
Distance from center of gravity to roll center	h_1	480 (mm)
Sprung mass	m	1700 (kg)
Unsprung mass	m_{ij}	45 (kg)

3. Simulate the oscillation of the vehicle

3.1. The dependence of the roll angle on the velocity

Steering angle I as shown in Figure 4, the simulation is carried out when the vehicle is moving with velocities v_1 = 60 km/h and v_2 = 90 km/h.

From the graph in Figure 5, it can be seen that at v = 60 km/h, when the equipped with passive stabilizer bar, the roll angle decreases from 3.8^0 to 3.1^0. If the velocity increases to 90 km/h, this value, in turn, decreases from 5.2^0 to 4.3^0. Therefore, it can be concluded that the vehicle's roll angle depends on velocity.

3.2. The dependence of the roll angle on the central height

For vehicles with a high center of gravity, the distance from the center of gravity to roll center is changed, this affects the vehicle's roll angle when steering. In the condition of the vehicle moving at the velocity v = 60 km/h, the steering angle is as shown in Figure 4, the correlation between the roll angle φ_x and the distance h_1 is described through the graph below.

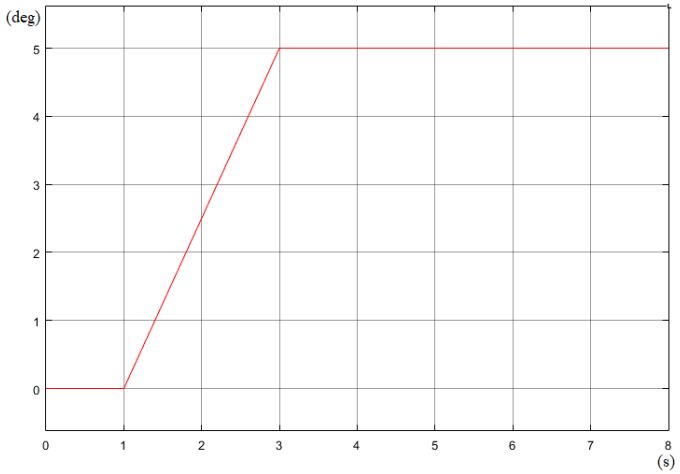

Figure 4: Steering angle I

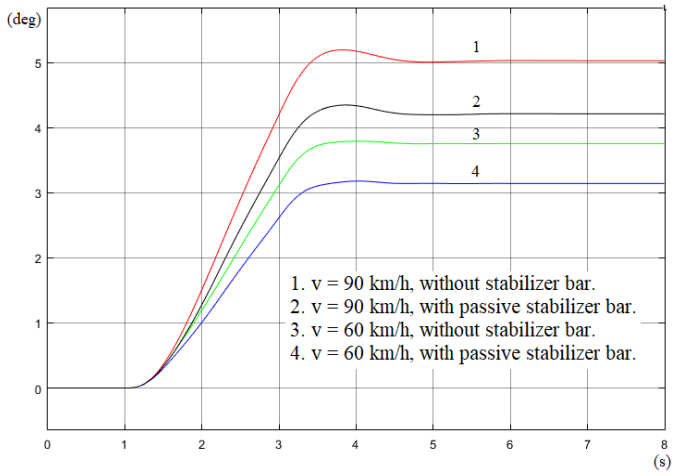

Figure 5: Roll angle depends on velocity

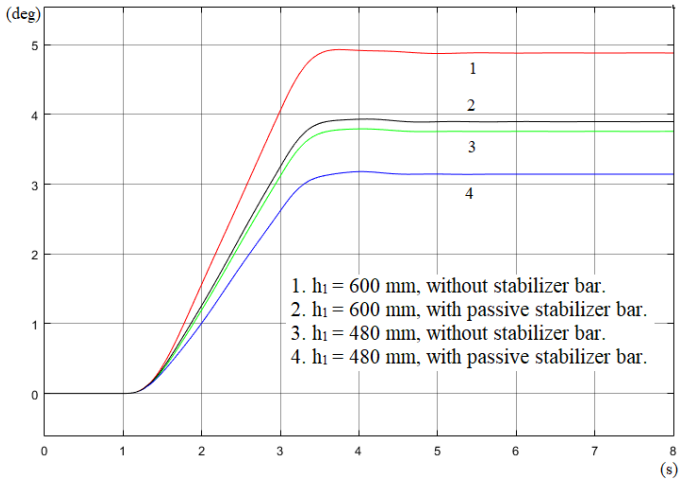

Figure 6: Roll angle depends on h_1

In the graph in Figure 6, when the vehicle is equipped the stabilizer bar is the vehicle's roll angle φ_x decreases from 3.8^0 to 3.1^0 with the distance h_1 = 0.48 m. When the height of vehicle increases, the distance between the center of gravity and roll center h_1 = 0.6 m, the corresponding angle value is 4.9^0 and 3.9^0.

Therefore, large-sized vehicles are often unstable when steering at high velocity.

3.3. The dependence of the roll angle on the steering angle

In the condition of driving with a larger angle δ as shown in Figure 7 at v = 60 km/h, the dependence between the vehicle's roll angle and steering angle is shown in Figure 8.

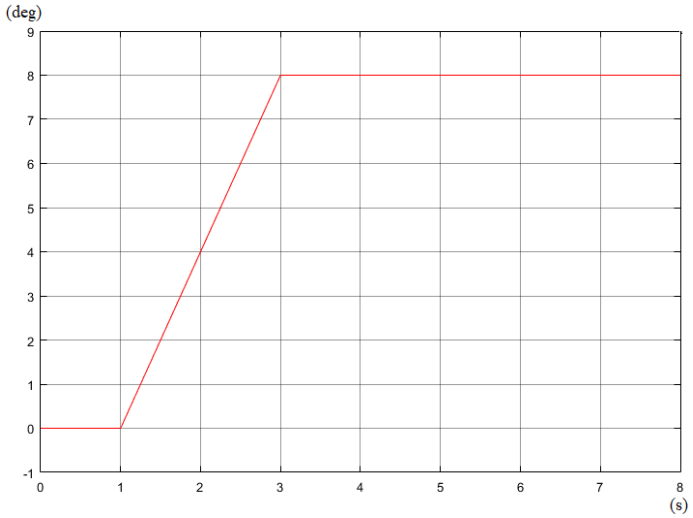

Figure 7: Steering angle II

When the value of steering angle δ increases, it also means that the roll angle of the vehicle φ_x increases. If the vehicle has the stabilizer bar, it will greatly reduce this value.

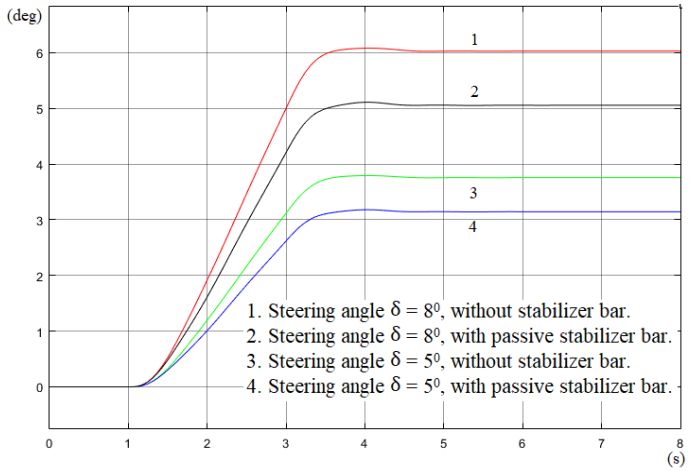

Figure 8: Roll angle depends on steering angle

From the graph in Figure 5, Figure 6 and Figure 8, it can be seen that when the vehicle has a stabilizer bar, the vehicle's roll angle will decrease depending on the working mode. If equipped with a passive stabilizer bar, there will be some disadvantages as follows:

+ The small size bar will not be able to withstand the constant load change, especially for high-mass, high-velocity vehicles.

+ The big size bar will be difficult to arrange in the vehicle and increase the mass isn't suspended. Therefore, it causes strong fluctuations when entering the bumpy road.

+ The ability to minimize the vehicle's roll angle is limited in dangerous situations.

For these reasons, today active stabilizer bar is gradually put to use in the middle-class and high-class vehicle.

3.4. The vehicle equipped active stabilizer bar

The active stabilizer bar is controlled based on input parameters such as vehicle's roll angle, center height, displacement of the suspension system,... Control rules are established based on basic mathematical models such as linear models, nonlinear models, static models, dynamic models,... In this study, the moment by the active stabilizer bar is controlled according to the following rule:

At the first mode

$$M_A = C_t C_{k1} \sin(\varphi_x - 2) \sin\varphi_x$$
$$\varphi_x - 2 = \begin{cases} \varphi_x - 2, \varphi_x \geq 2 \\ 0, \varphi_x < 2 \end{cases} \quad (13)$$

At the second mode

$$M_A = C_t \left[1.3 + C_{k2} \sin(\varphi_x - 4)\right] \sin\varphi_x$$
$$\varphi_x - 4 = \begin{cases} 2, \varphi_x \geq 6 \\ \varphi_x - 4, \varphi_x < 6 \end{cases} \quad (14)$$

where:

M_A: Moment of the active stabilizer bar.

C_t: Control coefficient; C_t = 11000.

C_k: Activation coefficient.

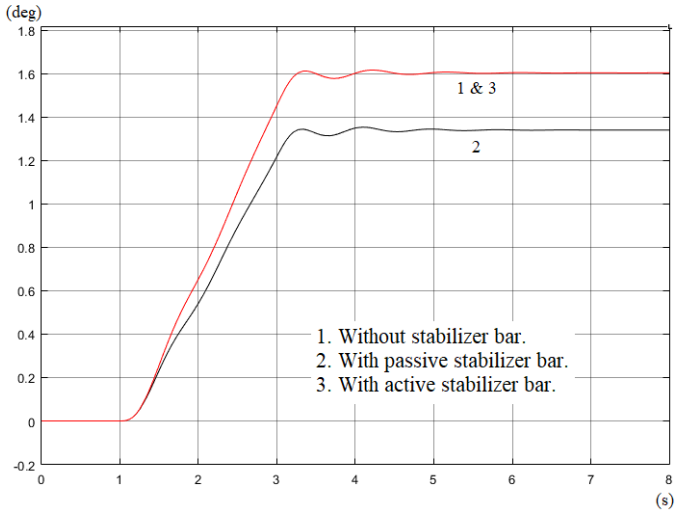

Figure 9: Roll angle at v = 30 km/h

When the vehicle's roll angle $\varphi_x < 2.0^0$, the stabilizer bar will not activate. If the roll angle exceeds this value, it will activate at (1) corresponding to the coefficient C_{k1} = 27. In case of vehicle's roll angle value $\varphi_x > 4.0^0$, the active stabilizer bar will activate at (2) corresponding to the coefficient C_{k2} = 45, the value of the anti-

roll moment that the bar providers is increased more so that the vehicle's roll angle is significantly reduced.

The steering angle is shown in Figure 4 and v = 30 km/h, the vehicle's roll angle is determined through the figure above.

Since the car moves at low velocity, the vehicle's roll angle is not large, so the active stabilizer bar hasn't been activated. With the above conditions, if the velocity increases to 60 km/h, the active stabilizer bar will be activated. At this time, the electric motor (hydraulic) will produce the torque impacting to two parts of the bar, reducing the vehicle's roll angle. However, at v = 60 km/h, the stabilizer bar is only activated at mode 1, so the angle φ_x, when equipped active stabilizer bar, is only equivalents to the passive stabilizer bar (Figure 10).

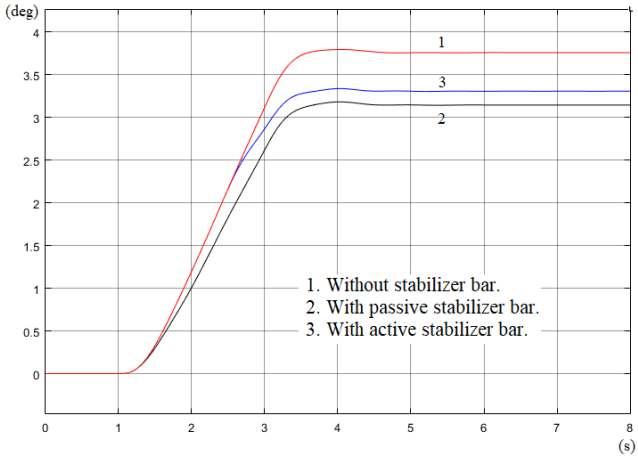

Figure 10: Roll angle at v = 60 km/h

In case the vehicle moves at v =120 km/h and the center height is also increased, the value of h_1 = 0.6 m. The active stabilizer bar is activated at mode 2, the vehicle's roll angle φ_x is significantly reduced (Figure 11).

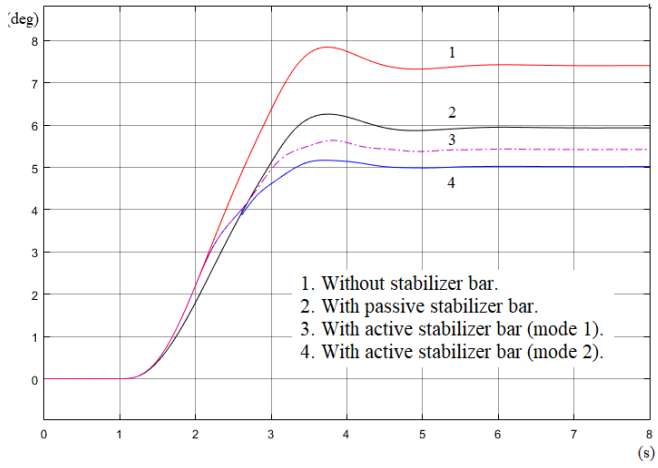

Figure 11: Roll angle at v = 120 km/h

With the above moving conditions, if the vehicle isn't equipped with a stabilizer bar, the vehicle can rollover. When the passive stabilizer bar is equipped, the vehicle's roll angle can be reduced, but because the stiffness of the bar is constant, it hasn't fully utilized the effect of the bar. In case, it can be seen that the active stabilizer bar has superiority over both cases.

4. Conclusion

The rollover phenomenon usually occurs when the roll angle is too large. This value depends on the velocity, center height, and steering angle of the vehicle. When the vehicle steers with high velocity, it is very easy to appear in this situation, the vehicle needs to be equipped stabilizer bar to limit this phenomenon. Research has shown that the vehicle's roll angle is significantly reduced when equipped stabilizer bar and shown the outstanding advantages of the active stabilizer bar compared to the passive stabilizer bar.

In the case of the vehicle's roll angle is small, the active stabilizer bar doesn't activate, so the smoothness of the vehicle will not be affected. When the value φ_x reaches the required threshold, the bar will activate and act as active stabilizer bar. In the case of roll angle is too big, the bar will switch to the second mode to significantly reduce the vehicle's roll angle, thereby making the vehicle more stable.

The study only focused on establishing the dynamic vehicle model equipped stabilizer bar and conducting simulation by Matlab – Simulink software. The parameters are referenced based on actual vehicles, the simulation was conducted under ideal conditions and not to mention the influence of external factors. Therefore, it is necessary to have empirical verification to make accurate statements.

References

[1] N. T. Anh, T. T. Tran, H. T. Binh, P. H. Nam, L. T. Dung, "Study on the Method of Calculating and Designing Stabilizer Bar on the Vehicle Using Solidworks Software", Viet Nam Mechanical Engineering Journal, 7(12), 92–99, 2018.

[2] N. K. Trai, N. T. Hoan, H. H. Hai, P. H. Huong, N. V. Chuong, T. M. Hoang, Structure Vehicle, Bach Khoa Ha Noi Publishing, 2010.

[3] P. Bravin, T. Kshitijit, P. Amit, K. Ganesh, "Design, Analysis and Optimization of the Anti-roll Bar", Journal of Engineering Research and Applications, 4(9), 137–140, 2014.

[4] A. N. Khartode, M. U. Gaikwad, "Design and Analysis of Anti-roll Bar for Automotive Application", International Journal on Recent and Innovation Trends in Computing and Communication, 4(6), 340–345, 2016.

[5] P. H. Dong, "Establish on the Lateral Roll Model of the FAW 29 Seats, Produce and Assemble in Viet Nam", Master Thesis, Ha Noi University of Science and Technology, 2015.

[6] J. N. Husen, A. M. Naniwadekar, "Analysis of Anti-roll Bar of a Passenger Car for its Nonlinear Behavior with Help of CAE", International Journal of Science Technology & Engineering, 2(1), 133–136, 2015.

[7] V. V. Huong, N. T. Dung, D. N. Khanh, D. H. Phuc, Dynamics Vehicle, Viet Nam Educational Publishing, 2014.

[8] G. A. Hassaan, N. A. Mohdsamin, "Vehicle Dynamics Response to Road Hump Using a 10 Degrees of Freedom Full-car Model", International Journal of Computer Techniques, 2(1), 56–62, 2015.

[9] V. Muniandy, P. Mohdsamin, H. Jamaluddin, R. A. Rahman, S. A. Abubakar, "Double anti-roll bar hardware-in-loop experiment for the active anti-roll control system", Journal of Vibroengineering, 19(4), 2886–2909, 2017.

[10] N. T. Anh, "Research the Dynamic Vehicle Model Equipped Active Stabilizer Bar", Master Thesis, Ha Noi University of Science and Technology, 2019.

ASTES

Advances in Science, Technology and Engineering Systems Journal Vol. 4, No. 4, 276-284 (2019)

www.astesj.com

Special Issue on Advancement in Engineering and Computer Science

ASTESJ

ISSN: 2415-6698

Localization of Emerging Leakages in Water Distribution Systems: A Complex Networks Approach

Matteo Nicolini[*,1,2]

[1]*Polytechnic Department of Engineering and Architecture, University of Udine, 33100 Udine, Italy*

[2]*Idrostudi, AREA Science Park, 34149 Padriciano, Trieste, Italy*

ARTICLE INFO

Article history:
Received: 12 May, 2019
Accepted: 20 July, 2019
Online: 07 August, 2019

Keywords:
Correlation
Degree centrality
Pressure gage
Water loss

ABSTRACT

Water distribution networks are infrastructural systems designed for providing potable water to consumers. In these last decades, the importance of assessing and identifying emerging leakages has become a primary issue, because of the high level of water loss characterizing such systems worldwide. In this paper, a new approach aimed at the prompt localization of leakages occurring in water distribution systems is introduced. The methodology relies on the analysis of real-time pressure measurements and on Complex Networks Theory. Starting from a collection of nodes representing the locations of pressure sensors, links of a virtual, complex network are created on the basis of the values assumed by correlation coefficients between pressure measurements: if such values are above a given threshold, relevant nodes are considered to be connected to each other. In this way, information about the structure and topology of the complex network is easily derived. In particular, the degree centrality of the nodes is a key parameter allowing to identify the position of a leakage. The paper first analyzes a well-known literature example, and then proves the high reliability of the methodology for a real water distribution system.

1. Introduction

Water distribution systems (WDSs) are strategic infrastructures for the transport and the delivery of potable water to various types of customers [1]. However, the deterioration of ageing components (especially pipes and pumps), the rapid growth of urbanization and the statutory and contractual quality standards that have to be guaranteed to customers are playing a fundamental role in the decision-making process, especially for the increasing costs due to the operational management. In particular, water loss is a widespread problem in all the countries of the world: for a well-managed and controlled WDS, the level of water leakage can be less than 10% [2], but percentages of 40-50% are not uncommon even in developed countries [3,4].

Water utilities have to continuously monitor and control the functioning of the system: besides financial aspects and issues related to the interruption of service, energetic costs and environmental impacts are a major concern, making water loss identification and reduction one of the most challenging tasks [5].

[*]Matteo Nicolini, via del Cotonificio, 114, +39 0432 558742;
Email: matteo.nicolini@uniud.it

In this paper, a new approach for the early identification of emerging leakages in a WDS is presented. The novelty of the methodology resides in the analysis of pressure measurements through Complex Networks Theory [6]. The reliability of the method increases with the number of installed pressure gages, up to the ideal situation of having one sensor at every node of the WDS.

In this work, the assumption that pressure data are available at every junction of the system is made (a simulation model has actually been used in order to calculate them). In a real situation, such signals arrive from pressure gages properly installed in the field, and correlations between them should provide the information about the emergence of leakages to be detected. The aim of the study is to show the capability of the methodology of localizing a leakage since its first formation, provided the above hypotheses are satisfied. However, the methodology is still valuable even in real cases, characterized by a limited amount of measure points: in such situations, the zone with the most likely presence of a leakage can be identified.

Anyway, the proposed approach does not intend to solve the problem of precisely localizing a leakage in a real WDS. Instead,

the methodology represents a valuable alternative to other prelocalization techniques, or a useful tool to be adopted in conjunction with other approaches.

The rest of the paper is organized as follows: section 2 contains a literature review, section 3 describes the methodology, which is applied to a literature system in section 4; section 5 shows the results obtained from the application to a real WDS, and section 6 draws some concluding remarks.

2. Literature Review

Leakages in WDSs are usually classified into two main categories [7]: bursts, which are characterized by sudden activation and high flows, and background leakages, which do not surface and are low, background flows that can persist for years without being detected.

Since bursts can be identified by instrumentation (sometimes they are visible on the ground), they are repaired in a short period of time, leading to a small amount of water lost. In this context, several technologies are available: step-tests, noise correlators, gas-injections, acoustic sensing through conduit pigging, and others: see [8] for a review.

Instead, background leakages can determine huge volumes of water lost, unless some dedicated leakage identification and repairing activities are performed. In these last years, many water utilities have implemented pressure management, an approach consisting in the introduction and regulation of some pressure reducing valves (PRVs) with the aim to control the piezometric surface. The selective reduction of pressure in a WDS (typically during the nighttime) may result in considerable water and energy savings [9,10].

Other approaches rely on proactive identification of water leakages, in order to keep the level of water loss always under control. To this end, District Metered Areas (DMAs) are created, consisting in the subdivision of a WDS in continuously monitored portions [11]. The installed instruments (flow and pressure gages) allow to provide a nearly real-time estimation of water loss on a 24-hour basis, by analyzing the minimum night flow (MNF) occurring in the lowest consumption interval, that is, between 2:00 a.m and 4:00 a.m.. Such minimum demand conditions determine the maximum values of pressure in the system, and hence the highest values of leakage.

A totally different approach relies on transient methods, consisting in high-frequency analysis of pressures transients in a WDS after some surge has been created [12]. Others rely on a transient network simulation model, usually very difficult to calibrate [13].

In these last years, the rapid improvement in sensor technology and in data transfer and communication systems has greatly enhanced the activity of real-time control of water losses, although many problems remain unsolved: first of all, the possibility of identifying a leakage since its first formation [14].

Several researchers have been focused on the comparison between actual field measurements and the results obtained by a calibrated numerical model [15–17]. In such cases, the key-point is the level of accuracy of the simulation model, which can hardly be optimal, since it should also contain information on the leakages to be discovered. In particular [18] have introduced a methodology for leak-detection and localization coupled with demand calibration.

More recently, Complex Networks Theory (CNT) has received increasing attention for the comprehension of a wide spectrum of real systems, ranging from physical infrastructures to social communities [19,20]. Successful examples include functional (correlation) network approaches [21], to infer hidden statistical inter-relationships between macroscopic regions of the human brain [22] or the Earth's climate system [23], difficult to uncover with traditional non-linear time series analysis techniques [24].

The application of CNT to the design and operation of WDSs has attracted a growing number of researchers, because its inherent capability of unveiling hidden properties, not grasped by traditional analyses or modelling approaches [25]. CNT has been adopted for evaluating the topological characteristics and the resilience of a system [26], or for expansion strategies [27]. Several authors investigated vulnerability-related issues, like node vulnerability under cascading failures [28–30], spectral methods to establish vulnerability areas [31,32], or for evaluating robustness under random or intentional attacks [33]. Other studies focused on the analysis of the formation of isolated communities [34], on the segmentation of WDSs for the identification of District Metered Areas (DMAs) using general metrics and modularity [35,36]. The optimal sampling design has also been addressed with the modularity concept [37] and through a combination of classical optimization and CNT [38]. More recently, Complex Networks Theory has been adopted for a systematic classification of WDSs [39], and for their optimal design through a tradeoff between network cost and reliability, measured in terms of flow entropy [40].

All such studies have been mainly focused on the topological aspects of WDSs, deriving their main characteristics from the analysis of the real system. Actually, many hidden properties may be uncovered looking at functional or correlation ties between nodes, especially when simulation or field data are available.

3. Methodological Approach

Starting from a given WDS whose topological, geometrical and hydraulic characteristics are known, the simulation model of the system can be built. In this work, the software Epanet has been adopted, being an open-source and a standard toolkit for such kind of numerical analyses [41].

The two sets of equations the software solves at the generic time t_k are the continuity equation for each junction i:

$$\sum_j Q_{ij}(t_k) - D_i(t_k) = 0 \qquad (1)$$

and the flow-headloss relationship in every pipe connecting junctions i and j:

$$H_i(t_k) - H_j(t_k) = h_{ij}(t_k) = rQ_{ij}^n(t_k) + mQ_{ij}^2(t_k) \qquad (2)$$

where Q_{ij} is the flow in pipe ij, D_i is the demand at node i, H_i and H_j are nodal heads at junctions i and j, h_{ij} is the headloss between nodes i and j; r, n and m are, respectively, the resistance coefficient, the flow exponent and the minor loss coefficient. For each time t_k,

starting from known heads at the fixed grade junctions (typically, reservoirs or tanks), the software uses the gradient method [42] in order to solve the set of equations (1) and (2) for determining all the heads and flows. Once the head is known at each junction, the pressure is directly calculated as the difference between head and the elevation of that junction (the velocity head at each junction is neglected).

The simulation model allows to determine the variability of pressure, provided a user demand pattern is defined. A pressure 'signal', $p_i(t)$, may be associated at each junction i, and the correlation coefficient c_{ij} between every pair of pressures signals at junctions i and j can be calculated. In this paper, the Pearson correlation coefficient has been adopted; it is given by the following expression:

$$c_{ij} = \frac{\sum_{k=1}^{T}(p_i(t_k)-\bar{p}_i)(p_j(t_k)-\bar{p}_j)}{\sqrt{\sum_{k=1}^{T}(p_i(t_k)-\bar{p}_i)^2 \cdot \sum_{k=1}^{T}(p_j(t_k)-\bar{p}_j)^2}} \qquad (3)$$

in which t_k represents the discretized time of the numerical module, T is the number of time steps of the simulated time horizon, and $\bar{p}_i$ is the average pressure at the i-th junction.

The temporal variability of pressure depends mainly on the fluctuation of the customers' demand: the higher the request of water, the lower is the pressure. Usually, distribution systems supplying water to residential areas are subjected to an almost spatially-uniform user demand. In this way, the temporal variability of pressure is very similar at all junctions, and the correlation coefficient c_{ij} is very close to the value of one. In other words, there is a strong linear relationship between pressure at junctions, properly described by the (linear) Pearson correlation coefficient.

However, the presence of many tanks or control devices, such as pressure regulating valves, inverter of pumps and other facilities, may introduce non-linearities in the relationships between pressures, and the correlation coefficient may not represent an appropriate measure. The more general case, which will be evaluated in future research, can be analyzed through non-linear correlation parameters or, more simply, looking for subsets of the considered time horizon for which linear correlations exist between pressure signals.

The methodology starts by creating a similarity matrix in which every element c_{ij} is the Pearson correlation coefficient between real-time measurements of pressure sensors (or pressures calculated by the simulation model) at i and j.

From the similarity matrix, an adjacency matrix representing a virtual, undirected complex network may be built (Figure 1). In this network, the nodes are the points of measurement and the links are created if the correlation coefficient between pressure signals is high enough. In other words, if c_{ij} is above a chosen threshold, θ, the related element a_{ij} of the adjacency matrix is 1, and zero otherwise (elements in the diagonal are set to zero).

In an ideal system with no leakages and characterized by a spatial uniform demand pattern, that is, the same typology of customers' consumption, there is a strong correlation between pressure signals, and the related complex network is heavily connected (it is a complete graph). As an example, Figure 1 (left) shows the situation in which four sensors are installed at junctions 3, 9, 28 and 31. In the case of no leakage, the similarity matrix presents very high values of correlation coefficients, and the adjacency matrix is that typical of a complete graph (Figure 1, top right).

The formation of a leakage starts to 'break' correlations among the node nearest to the leakage and the others, inducing a progressive link removal, depending on the amount of water loss. This is due to the fact that only the time-varying flow out of the leakage is a function of pressure, with different dynamics from customer's demand.

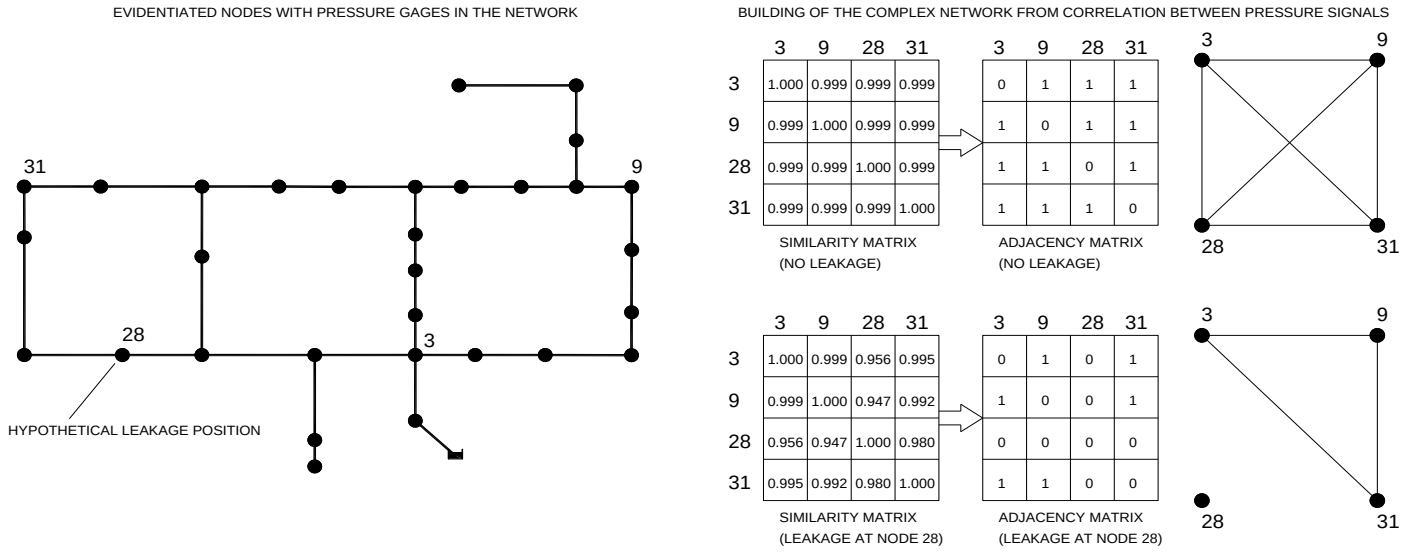

Figure 1: Difference between similarity matrix, made by Pearson correlation coefficients, c_{ij}, and adjacency matrix, in which the value of 0 or 1 assumed by each element depends on the threshold chosen for c_{ij} (in the example θ = 0.990). In this case, the size of matrices is less than the number of junctions of the water distribution system, being equal to the number of installed pressure gages (indicated on the left of the figure). The hypothetical position of a leakage is also shown, together with its impact on the matrices and the resulting virtual network.

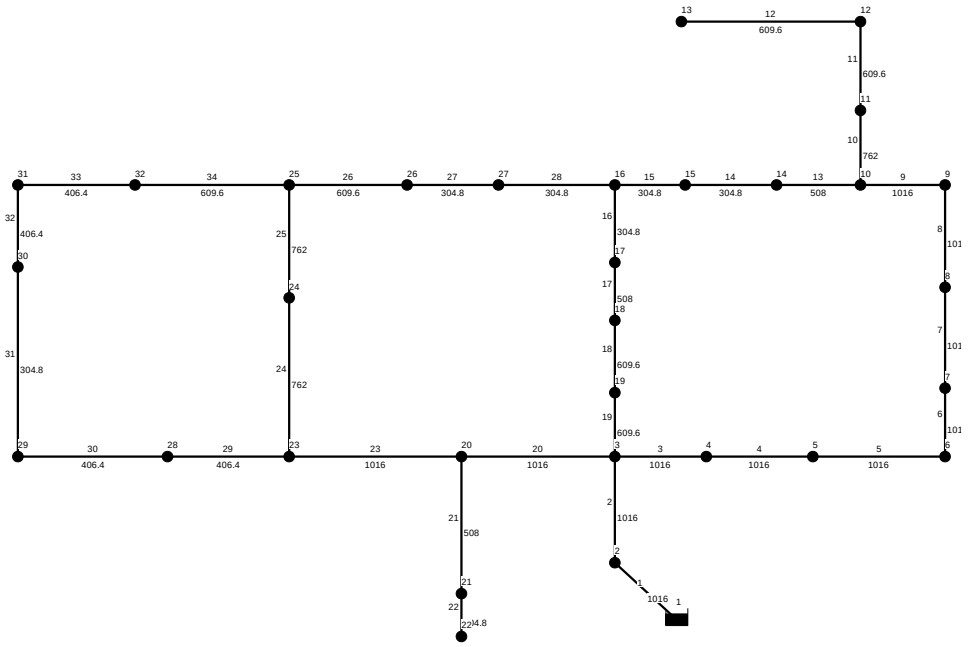

Figure 2: *Hanoi WDS adopted for the analyses. Link number and diameter (in mm) are indicated along the pipes*.

If a leakage is formed at the *i*-th junction of a WDS, the total discharge $Q_i(t_k)$ outflowing at time t_k equals the nodal demand, and can be expressed as the sum of consumer's request and pressure-dependent water loss:

$$D_i(t_k) = Q_i(t_k) = \alpha(t_k) q_i + c[p_i(t_k)]^u \qquad (4)$$

in which q_i is the average demand at node i, $\alpha(t_k)$ is the multiplier coefficient characterizing the demand pattern at time t_k (Figure 3), $p_i(t_k)$ is the pressure at node i, and c and u are the leakage coefficient and the leakage exponent: they determine, respectively, the leakage entity and its dependence on the pressure (for an ideal leakage of circular shape on a steel pipe, $u = 0.5$).

Figure 1 (bottom right) shows the example of a leakage present at junction 28: it is easily seen that the values of the correlation coefficient in the similarity matrix decrease when the position with the leakage is involved in the calculation, giving rise to a less connected network.

The parameter adopted for the identification of the junction in which a leakage is forming is the degree centrality: the degree of a node represents the number of its nearest neighbors (in other words, the number of its connections). For an undirected network (as in this case) the column vector of node degrees' **k** is given by (the symbol **1** represents an all-one column vector):

$$\mathbf{k} = (\mathbf{1}^T \mathbf{A})^T = \mathbf{A}\,\mathbf{1} \qquad (5)$$

in which **A** is the adjacency matrix [17]. Thus, the junction in which the leak is emerging is the one characterized by the lowest correlation with respect to all the others, and the related node in the complex network has the lowest degree centrality.

4. Application to a Literature System

The methodology has been applied to the Hanoi WDS (Vietnam), since it represents a well-known literature example (Figure 2): it was introduced for the first time by [43] and then analyzed by many authors [44]. The model of the main system consists of 32 junctions and 34 pipes, organized in three loops (see [43] for the data). The numerical simulation model has been used to artificially create pressure signals at every junction of the main system, where a pressure sensor is considered to be available.

Figure 3 shows the pattern assumed for customers' demand: its variability is typical of residential consumption, with two peaks during the day, respectively in the morning and in the evening, and a minimum during the nighttime. The time resolution adopted is 5 minutes.

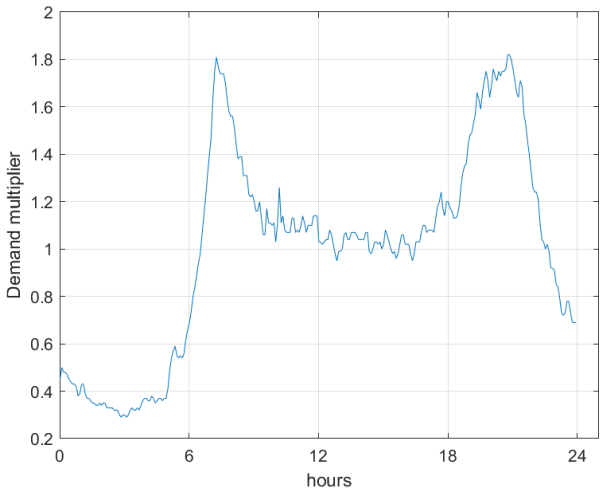

Figure 3: Temporal variability of demand multiplier $\alpha(t_k)$ in (4), describing customers' demand.

In Figure 3, the typical oscillations due to the stochastic nature of demand are evident. In the present paper, the simple case of uniform spatial distribution of demand pattern has been assumed. Due to the importance of correctly simulating users' demand variability, future research will focus on such issue: to this end, the

approach adopted by [45,46] appears the most suitable for real-time analyses. The time variability of pressure in the case of no leakage in the system is shown in Figure 4.

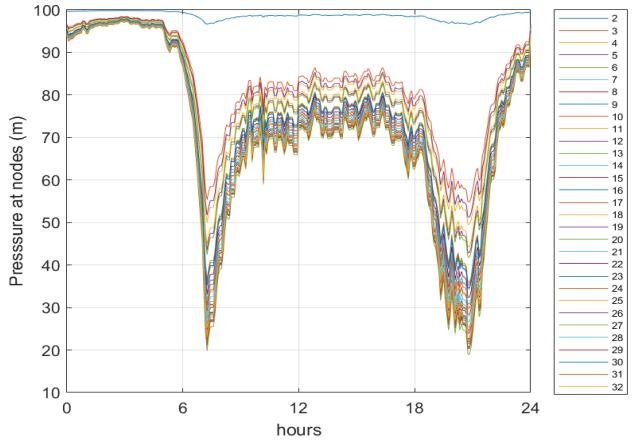

Figure 4: Pressure variability over 24 hours for the junctions of Hanoi WDS.

The results have been obtained by simulations performed with Epanet software [39], with a hydraulic time step of 5 minutes and a Hazen-Williams roughness coefficient of 130 for all pipes.

The correlation between signals is evident, and may be confirmed by the plot of Figure 5, where the relationship between pairs of nodes keeping junction 2 in abscissa are shown. Similar results may be plotted for other pairs of junctions. Such behavior confirms the validity of linearity assumption between pressures

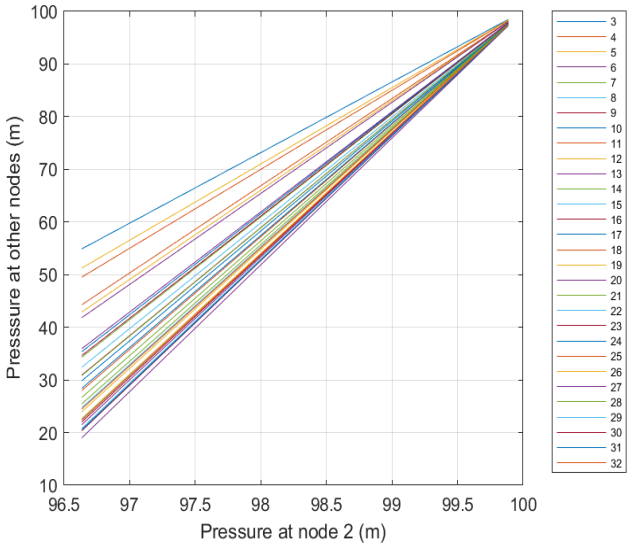

Figure 5: Correlation plot for pairs of pressures between junction 2 and others

Figure 6 is a heatmap plot of the global results obtained with reference to one leakage in all possible positions, and characterized by an average outflow of 5 l/s, which may appear to be large, but actually is a relatively small value if compared to the user demand at junctions (100 l/s on average). For each column, representing an assumed position of a leakage, the figure shows the degree centrality of the nodes on a blue-tone basis, i.e., the darkest the color, the bigger is the degree of a node.

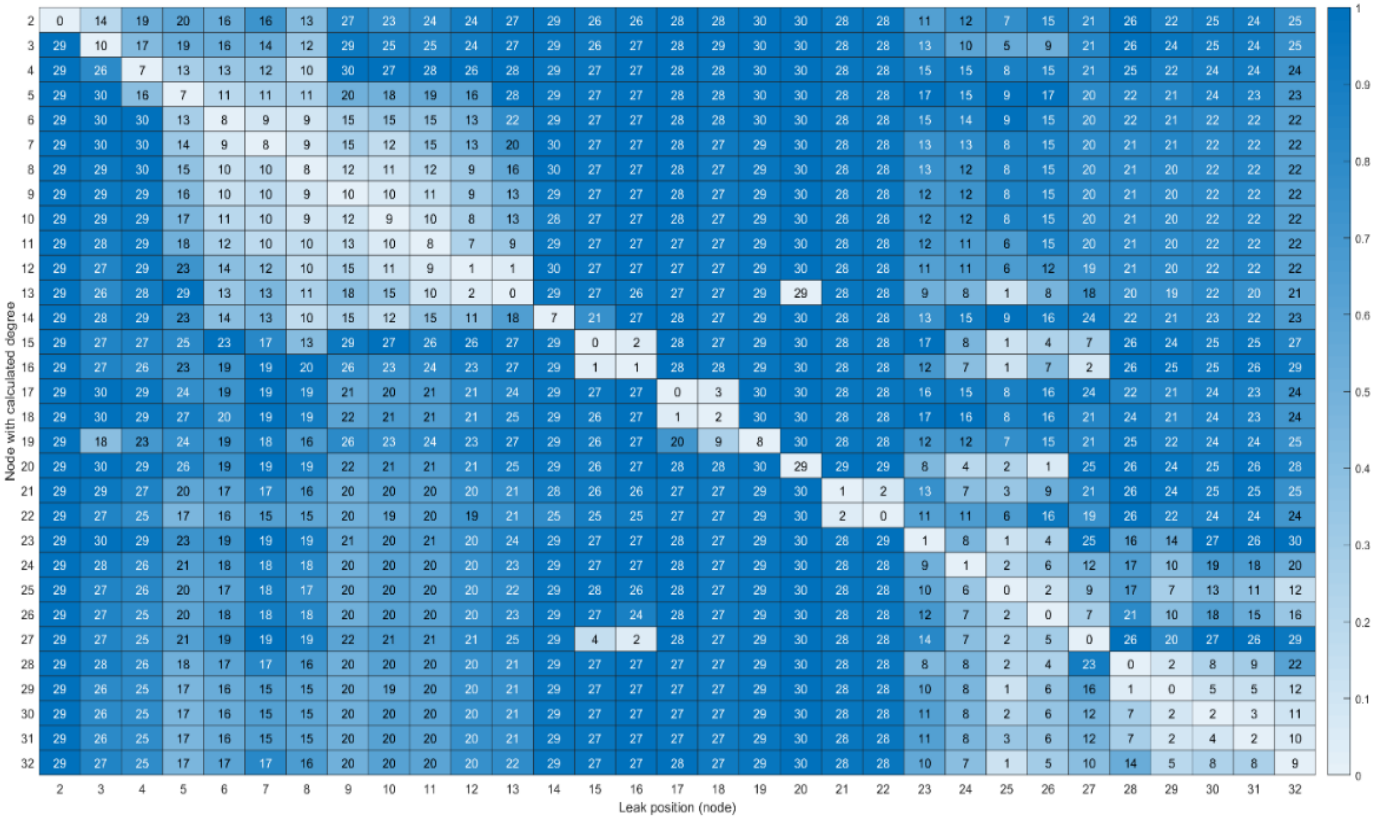

Figure 6: Heatmap representation of degree centralities when varying the position of one leakage of 5 l/s in Hanoi WDS. Number in columns are the node degrees for a fixed leakage position

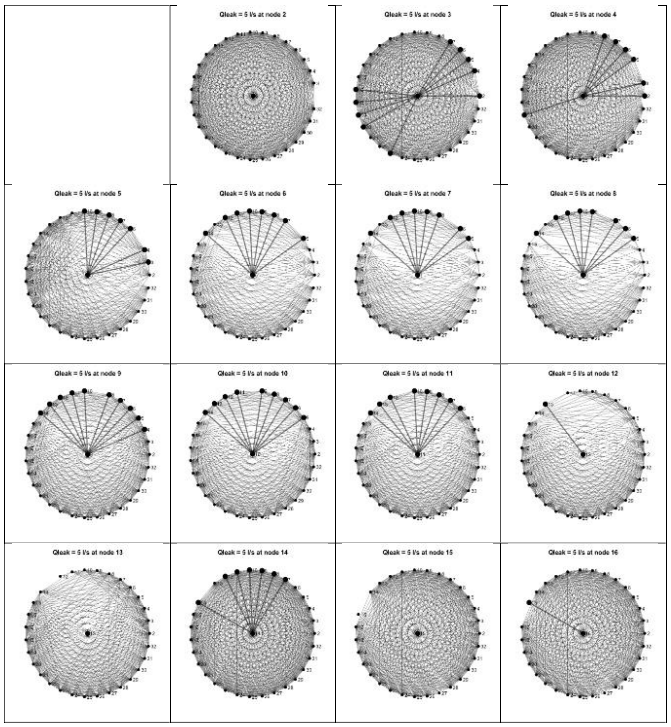

Figure 7: Round plots of virtual correlation networks obtained when varying leakage position (nodes 2 to 16). The junction where the leakage is activated is drawn at the center of each plot. Thick lines are the links connecting the central node to others, while other connections are indicated with thin lines.

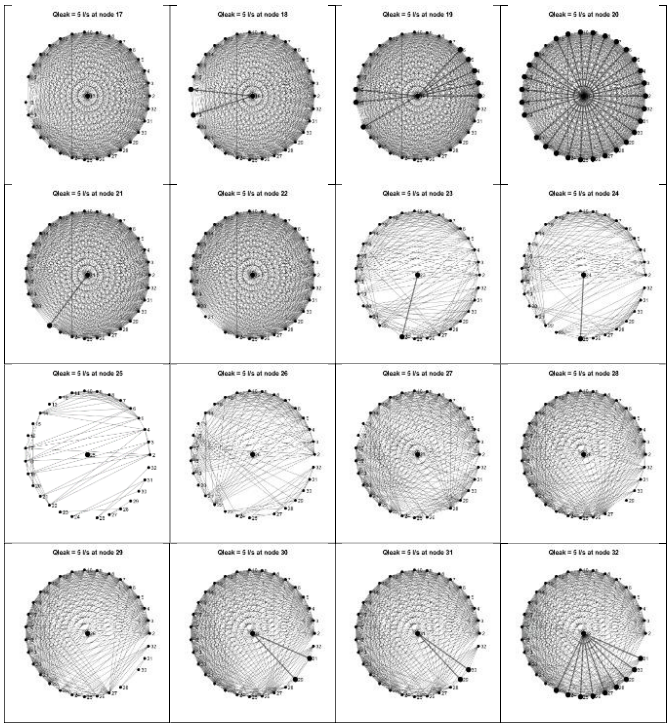

Figure 8: Round plots of virtual correlation networks obtained when varying leakage position (nodes 17 to 32). The junction where the leakage is activated is drawn at the center of each plot. Thick lines are the links connecting the central node to others, while other connections are indicated with thin lines.

In this way, the lightest cell represents (for each column) the node with the least degree centrality, that is, that affected by the leakage. This is confirmed by the number indicated in each cell, giving the degree centrality. Only simulations with one leakage at a time have been considered.It is evident that, in all the cases analyzed, the node with the smallest degree is that one in which the leakage is present.

Figure 7 and Figure 8 show round plots of the virtual networks in which the node where the leakage is activated is drawn at the center. Thick lines represent the connections the central node has with others, while thin lines indicate those between other nodes.

For each plot, the number of thick lines is the degree centrality of the node with the leakage. Such figures provide a pictorial representation of the absence of connections for the central node due to the presence of a leakage. In other words, such node is the most 'isolated'

5. Application to a real system

In order to test the reliability of the methodology, it has been applied to the western district of Tobruk city, Libya (Figure 9, left).

Figure 9: Left: layout of the city of Tobruk (Libya), and of the western district WDS (right), where the junctions characterized by the highest frequency values reported in Figure 10 are also indicated.

It covers a surface of 8 km^2 and serves a population of 54600 inhabitants. The average flow supplied is 240 l/s. The model of the system includes all the details of the network, and is made of 1139 junctions and 1621 pipes (Figure 9, right).

In this case, the performance of the methodology has been evaluated as the percentage of success in identifying the junction affected by the leakage (or its neighbors, according to a predefined tolerance of 200 m, representing the average length of the pipes), varying several parameters like threshold, θ, leakage coefficient, *c*, and leakage exponent, *u* (4).

Table 1 reports the results obtained for a tolerance distance of 200 m (in other words, it is considered a good result whenever the junction with the smallest degree centrality falls within 200 meters from that in which the leakage is activated). It can be observed that, independently of the parameters assumed, the rate of success of the methodology is around 90%. This is due to the fact that there are some junctions having the minimum value of degree centrality when leakages are activated at their surroundings.

To this end, the results in terms of frequency of occurrence of the nodes have been analyzed: Figure 10 shows several cases obtained with two values of the leakage exponent (u = 0.5; 1.0) and five values for the leakage coefficient (c = 0.1,…0.5), which are typically encountered in real situations.

Table 1: Performance indicator (PI) giving the percentage of success of the methodology when applied to Tobruk WDS, with varying threshold, θ, leakage coefficient, *c*, and exponent, *u*. (The threshold number, θ, indicated as 1-10^{-4} means 0.9999.)

θ	*c*	*u*	PI (%)
1-10^{-4}	0.5	0.5	90.34
1-10^{-6}	0.5	0.5	75.94
1-10^{-7}	0.1	0.5	86.65
1-10^{-6}	0.1	0.5	90.61
1-10^{-6}	0.1	1.0	90.61
1-10^{-5}	0.1	0.5	88.85
1-10^{-5}	0.2	0.5	90.17
1-10^{-5}	0.3	0.5	90.87
1-10^{-5}	0.4	0.5	91.83
1-10^{-5}	0.5	0.5	92.01
1-10^{-5}	0.1	1.0	88.85
1-10^{-5}	0.2	1.0	90.17
1-10^{-5}	0.3	1.0	90.87
1-10^{-5}	0.4	1.0	91.83
1-10^{-5}	0.5	1.0	92.01

In an ideal situation, all nodes should be characterized by a frequency of one, and the frequency plots would be uniform. However, from Figure 10 it can be observed that some of them exhibit very high frequency values, indicating that their minimum degree centrality occurs not only when a leakage is present there, but also when it is activated at several other surrounding junctions. When analyzing in more detail the nodes characterized by the highest values of frequency, it can be noted that they represent particular situations of 'bottlenecks' of the WDS (Figure 9, right). In these cases, their minimum degree centrality hinders some other non-linear property not captured by the linear Pearson correlation coefficient, which is still under investigation.

6. Discussion and Concluding Remarks

The paper has presented the results of a new methodology introduced for the localization of leakages emerging in water distribution systems. The main advantage of the approach is that it relies only on the measurements of pressure and on cross-correlations between signals, thus avoiding the need of comparing such data with a 'reference' (and not well defined) scenario given by a simulation model, whose optimal calibration is generally very difficult to attain. In this paper, the simulation model has been adopted with the only purpose of generating the pressure signals.

The novelty of the research resides in the fact that it analyzes pressure measurements through Complex Networks Theory, its reliability increasing with the number of installed pressure sensors. However, the proposed approach does not represent a final solution to the problem of leakage identification, but it has to be considered a further support in the process of leakage prelocalization, that is, a fast method to assess the integrity of a WDS and, eventually, to identify areas where prompt interventions should be planned.

Two test cases have been considered: the first, representing a well-known literature system, proved the best performance of the methodology in precisely localizing the node where the leakage is emerging (which is characterized by the least degree centrality with respect to all the others); the second, a real-world network, showed a high rate of success (around 90%). The difference between the results obtained can be ascribed to the fact that, in the first case, only the main transport pipes are included in the model (in other words, the model simulates the principal 'skeleton' of the water distribution system). In the second case, given by a real WDS, all the pipes have been modeled, and hence the flows in the links may arrange in such a way that the conditions of minimum degree centrality do not always occur at the junction where the leakage is present, but rather in some other surrounding nodes. Actually, this is not a problem in real situations, since water managers are interested in quickly identifying the area where the leakage is forming.

Other issues still under investigations are represented by the influence on the spatial distribution of demand pattern and the presence of several reservoirs and tanks, which actually limit the performance of the methodology. In any case, the current trend in WDS management is to divide such systems in DMA (District Metered Areas), for a better control of water leakages: thus, each DMA (which is often supplied by at most one reservoir, or may be modeled in such a way through appropriate boundary conditions) can be considered as a single system and the proposed methodology applied accordingly.

The requirement of linear correlation between pressure variability is fundamental for the success of the methodology. However it is only a necessary condition, as proved by the second test case, for which the linearity in correlation is not sufficient to always guarantee the minimum degree centrality at the node with the leakage, hindering some other non-linear property not captured by the linear Pearson correlation coefficient. Also this issue is currently under investigation.

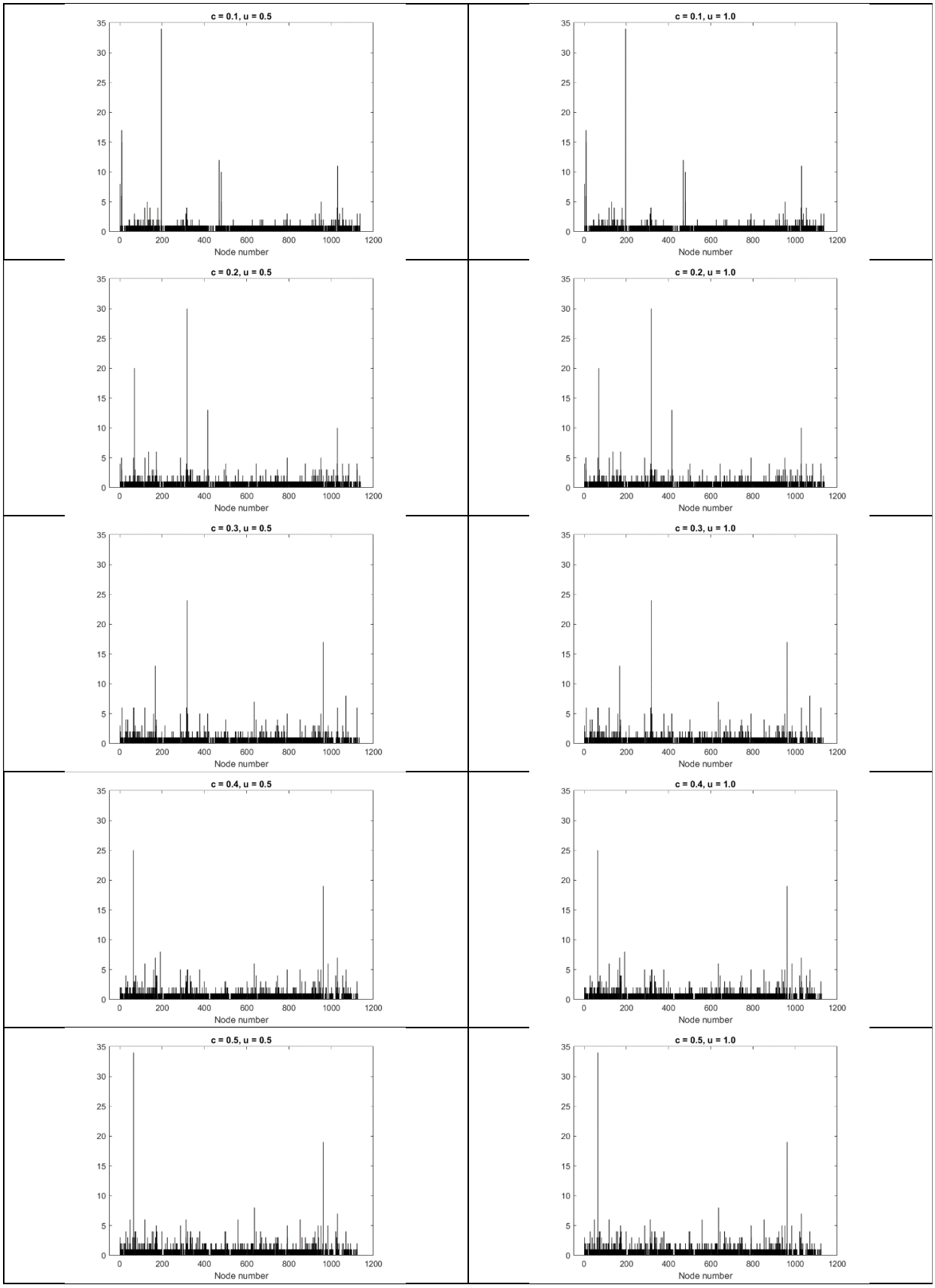

Figure 10: Frequency plots of junction occurrences in minimum degree centrality when varying leakage position and for different values of leakage coefficient, *c*, and exponent, *u*. Correlation threshold of $1\text{-}10^{-5}$ has been assumed.

Acknowledgment

The Author would like to thank the anonymous Reviewers for their comments and suggestions, which resulted in a considerable improvement of the paper.

References

[1] P. Swamee, A. Sharma, Design of Water Supply Pipe Networks, John Wiley & Sons, 2008.
[2] R. Beuken, C. Lavooij, A. Bosch, P. Schaap, Low leakage in the Netherlands confirmed, in Proceedings of the Water Distribution Systems Analysis Symposium 2008 (WDSA 2008), Kruger National Park, South Africa, 2008. DOI: 10.1061/40941(247)174
[3] A. Lambert, International Report: Water Losses Management and Techniques, Water Science and Technology: Water Supply, 2(4), 2002, 1–20. https://doi.org/10.2166/ws.2002.0115
[4] R.S. McKenzie, Z. Siqalaba, W. Wegelin, The State of Non-Revenue Water in South Africa; Report No. TT522/12, Water Research Commission: Lynnwood Manor, Pretoria, South Africa, 2012.
[5] A.F. Colombo, B.W. Carney, "Energy and costs of leaky pipes: toward comprehensive picture", J. Water Resour. Plann. Manage., 128(6), 441–450, 2002. DOI: 10.1061/(ASCE)0733-9496(2002)128:6(441)
[6] M. Nicolini, Leakage Identification in Water Distribution Systems with a Complex Networks Approach, in Proceedings of the 1st IEEE International Conference on Knowledge Innovation and Invention (ICKII 2018), Jeju Island, South Korea, 2018. DOI: 10.1109/ICKII.2018.8569182
[7] J. Thornton, R. Sturm, G. Kunkel, Water Loss Control, 2nd Ed, McGraw-Hill, New York, 2008.
[8] R. Puust, Z. Kapelan, D.A. Savic, T. Koppel, "A review of methods for leakage management in pipe networks", Urban Water Journal, 7(1), 25–45, 2010. https://doi.org/10.1080/15730621003610878
[9] M. Nicolini, L. Zovatto, "Optimal location and control of pressure reducing valves in water networks", J. Water Resour. Plann. Manage., 135(3), 178–187, 2009. DOI: 10.1061/(ASCE)0733-9496(2009)135:3(178)H.
[10] M. Nicolini, C. Giacomello, K. Deb, "Calibration and optimal leakage management for a real water distribution network", J. Water Resour. Plann. Manage., 137(1), 134–142, 2011. https://doi.org/10.1061/(ASCE)WR.1943-5452.0000087
[11] S. Alvisi, M. Franchini, "A procedure for the design of district metered areas in water distribution systems", Procedia Engineering, 70, 41–50, 2014. https://doi.org/10.1016/j.proeng.2014.02.006
[12] B. Brunone, M. Ferrante, "Detecting leaks in pressurized pipes by means of transients", J. of Hydraulic Research, 39(5), 539–547, 2001. https://doi.org/10.1080/00221686.2001.9628278
[13] D. Misiunas, J. Vitkovsky, G. Olsson, A. Simpson, M. Lambert, "Pipeline break detection using pressure transient monitoring", J. Water Resour. Plann. Manage., 131(4), 316–325, 2005. DOI: 10.1061/(ASCE)0733-9496(2005)131:4(316)
[14] M. Nicolini, A. Patriarca, Model Calibration and System Simulation from Real Time Monitoring of Water Distribution Networks, in IEEE 3rd Int.l Conf. on Computer Research and Development (ICCRD 2011), Shangai, China, 2011. DOI: 10.1109/ICCRD.2011.5763972
[15] R. Perez, V. Puig, J. Pascual, J. Quevedo, E. Landeros, A. Peralta, "Methodology for leakage isolation using pressure sensitivity analysis in water distribution networks", Control Engineering Practice, 19(10), 1157–1167, 2011. https://doi.org/10.1016/j.conengprac.2011.06.004
[16] M. V. Casillas Ponce, L. E. Garza Castañón, V. Puig Cayuela, "Model-based leak detection and location in water distribution networks considering an extended horizon analysis of pressure sensitivities", Journal of Hydroinformatics, 16(3), 649–670, 2013. https://doi.org/10.2166/hydro.2013.019
[17] D. Perfido, T. Messervey, C. Zanotti, M. Raciti, A. Costa, Automated leak detection system for the improvement of water network management, in 3rd Int.l Electronic Conf. on Sensors and Applications, 2016. https://doi.org/10.3390/ecsa-3-S5002
[18] G. Sanz, R. Perez, Z. Kapelan, D. Savic, "Leak detection and localization through demand components calibration", J. Water Resour. Plann. Manage., 142(2), 2016. https://doi.org/10.1061/(ASCE)WR.1943-5452.0000592
[19] M.E.J. Newman, Networks: An Introduction, Oxford University Press, Oxford, 2010.
[20] A.L. Barabási, "The network takeover", Nature Physics, 8, 14–16, 2012.
[21] R. Donner, E. Hernández-García, E. Ser-Giacomi, "Introduction to Focus Issue: Complex network perspective on flow systems", Chaos, 27, 2017. https://doi.org/10.1063/1.4979129
[22] C. Zhou, L. Zemanová, G. Zamora-López, C. C. Hilgetag, J. Kurths, "Structure-function relationship in complex brain networks expressed by hierarchical synchronization", New J. Phys. 9:178, 2007. doi:10.1088/1367-2630/9/6/178
[23] L. C. Carpi, P. Saco, O. Rosso, M. Gómez Ravetti, "Structural evolution of the Tropical Pacific climate network", Eur. Phys. J. B, 85:389, 2012. DOI: 10.1140/epjb/e2012-30413-7
[24] H. Kantz, T. Schreiber, Nonlinear Time Series Analysis, 2nd Ed., Cambridge University Press, 2004.
[25] O. Giustolisi, A. Simone, L. Ridolfi, "Network structure classification and features of water distribution systems", Water Resources Research, 53(4), 3407–3423, 2017. https://doi.org/10.1002/2016WR020071
[26] A. Yazdani, P. Jeffrey, "A complex network approach to robustness and vulnerability of spatially organized water distribution networks". arXiv Prepr. arXiv1008.1770, 2010.
[27] A. Yazdani, R. A. Otoo, P. Jeffrey, "Resilience enhancing expansion strategies for water distribution systems: A network theory approach", Environ. Model. Softw., 26(12), 1574–1582, 2011. DOI:10.1016/j.envsoft.2011.07.016
[28] Q. Shuang, M. Zhang, Y. Yuan, "Node vulnerability of water distribution networks under cascading failures", Reliab. Eng. Syst. Saf., 124(C), 132–141, 2014. DOI: 10.1016/j.ress.2013.12.002
[29] L. Berardi, R. Ugarelli, J. Rostum, O. Giustolisi, "Assessing mechanical vulnerability in water distribution networks under multiple failures", Water Resour. Res., 50(3), 2586–2599, 2014. https://doi.org/10.1002/2013WR014770
[30] F. Chaoqi, W. Ying, W. Xiaoyang, "Research on complex networks' repairing characteristics due to cascading failure", Physica A, 482, 317–324, 2017. DOI: 10.1016/j.physa.2017.04.086
[31] J.A. Gutiérrez-Pérez, M. Herrera, R. Pérez-García, E. Ramos-Martínez, "Application of graph-spectral methods in the vulnerability assessment of water supply networks", Math. Comput. Model., 57(7-8), 1853–1859, 2013. https://doi.org/10.1016/j.mcm.2011.12.008
[32] J.A. Gutiérrez-Pérez, M. Herrera, J. Izquierdo, R. Pérez-García, An approach based on ranking elements to form supply clusters in Water Supply Networks as a support to vulnerability assessment, in International Environmental Modelling and Software Society (iEMSs) Conference, Leipzig, Germany, 2012.
[33] A. Yazdani, P. Jeffrey, "A note on measurement of network vulnerability under random and intentional attacks", 2010. arXiv:1006.2791
[34] N. Sheng, Y.W. Jia, Z. Xu, S.L. Ho, C.W. Kan, "A complex network based model for detecting isolated communities in water distribution networks", Chaos, 23(4), 2013. doi: 10.1063/1.4823803
[35] O. Giustolisi, L. Ridolfi, "A novel infrastructure modularity index for the segmentation of water distribution networks", Water Resour. Res., 50(10), 7648–7661, 2014. https://doi.org/10.1002/2014WR016067
[36] O. Giustolisi, L. Ridolfi, L. Berardi, "General metrics for segmenting infrastructure networks", Journal of Hydroinformatics, 17(4), 505–517, 2015. DOI: 10.2166/hydro.2015.102
[37] A. Simone, O. Giustolisi, D.B. Laucelli, "A proposal of optimal sampling design using a modularity strategy", Water Resources Research, 52(8), 6171–6185, 2016. https://doi.org/10.1002/2016WR018944
[38] R. Nazempour, M.A.S. Monfared, E. Zio, "A complex network theory approach for optimizing contamination warning sensor location in water distribution networks", arXiv preprint arXiv:1601.02155, 2016
[39] C. Giudicianni, A. Di Nardo, M. Di Natale, R. Greco, G.F. Santonastaso, A. Scala, "Topological Taxonomy of Water Distribution Networks", Water, 10(4), 444, 1–19, 2018. https://doi.org/10.3390/w10040444
[40] G.F. Santonastaso, A. Di Nardo, M. Di Natale, C. Giudicianni, R. Greco, "Scaling-Laws of Flow Entropy with Topological Metrics of Water Distribution Networks", Entropy, 20(2), 95, 1–15, 2018. https://doi.org/10.3390/e20020095
[41] L. A. Rossman, EPANET 2 Users Manual, USEPA, Cincinnati, OH, 2000.
[42] E. Todini, S. Pilati, A gradient method for the analysis of pipe networks, in Int.l Conf. on Computer Applications for Water Supply and Distribution, Leicester Polytechnic, UK, 1987.
[43] O. Fujiwara, D. B. Khang, "A two-phase decomposition method for optimal design of looped water distribution networks", Water Resources Research, 26(4), 539–549, 1990. https://doi.org/10.1029/WR026i004p00539
[44] A. Marchi, G. Dandy, A. Wilkins, H. Rohrlach, "A methodology for comparing evolutionary algorithms for the optimization of water distribution systems, J. Water Resour. Plann. Manage., 140(1), 786–798, 2014. https://doi.org/10.1061/(ASCE)WR.1943-5452.0000321
[45] E. Creaco, G. Pezzinga, D. Savic, "On the choice of the demand and hydraulic modeling approach to WDN real-time simulation", Water Resources Research, 53(7), 6159–6177, 2017. https://doi.org/10.1002/2016WR020104
[46] E. Creaco, E.J.M. Blokker, S.G. Buchberger, "Models for generating household water demand pulses: literature review and comparison", J. Water Resour. Plann. Manage., 143(6), 2017. https://doi.org/10.1061/(ASCE)WR.1943-5452.0000763

ASTES

Advances in Science, Technology and Engineering Systems Journal Vol. 4, No. 4, 285-291 (2019)

www.astesj.com

Special Issue on Advancement in Engineering and Computer Science

ASTESJ

ISSN: 2415-6698

DSTATCOM-Fuel Cell System on Radial Low-voltage Distribution Network for Mitigating Voltage Rise Caused by High Penetration of Photovoltaic Systems

Dylon Hao Cheng Lam, Jianhui Wong*, Yun Seng Lim, Jimmy Chin Yong Hee

Department of Electrical and Electronic Engineering, Universiti Tunku Abdul Rahman, Selangor, Malaysia

ARTICLE INFO

Article history:
Received: 31 May, 2019
Accepted: 27 July, 2019
Online: 07 August, 2019

Keywords:
Grid-connected
DSTATCOM
Fuel cell
Distribution Network
Voltage rise

ABSTRACT

The Malaysian government has recently announced to increase the share of renewable energy generation from 2% to 20% of the total electricity consumption by year 2030. However, integrating a significant level of renewable energy sources on the distribution network without proper coordination will cause adverse effects that leads to unnecessary operation costs to the stakeholders. Various solutions including energy storage system are proven to be an effective way to overcome the issues caused by the integration of renewable energy sources. However, energy storage system using batteries have limitations such as limited life cycle and environmental hazards. As such, alternative source such as fuel cell which is well known for its zero pollutant can be considered. In this paper, a distributed static synchronous compensator integrated with a hydrogen system (DSTATCOM-Fuel cell) is proposed. The hydrogen system consists of fuel cell and electrolyzer to perform power exchange within the grid for regulating the voltage magnitude at 1 p.u. Various case studies have been conducted to validate the efficacy of this proposed combination and the results have shown that the DSTATCOM-Fuel cell can effectively mitigates the voltage rise up to 12.3% while maintaining high penetration of the photovoltaic systems.

1. Introduction

This paper is an extension of work originally presented in the International Conference on Smart Grid and Clean Energy 2018 [1]. Malaysia is expected to receive significant growth of the grid-connected renewable energy sources as the government has recently set a new target to commit on increasing the renewable energy generation from the current 2% to 20% of the total electricity consumption by year 2030 [2]. However, the growth of renewable energy sources on the electrical networks without proper coordination can create technical challenges that lead to the malfunction of power electronic devices, reduction of network efficiency, and improper operation of power protection system which gives high operating cost impact to the stakeholders. Curtailing and limits the amounts of grid-connected renewable energy have always been applied in order to avoid the deterioration of electrical power quality [3] despite these measures can greatly reduce the generation of clean energy and affect the commitment to increase the share of renewable energy generation [4]. Many solutions have been research, and realized that integrating large-scaled energy storage system by manipulating the real and reactive power exchange within the system can be used to regulate the network voltage [5–9]. Besides, energy storage system integrated with STATCOM are used to enhance the transient stability [10–14], improve voltage sags [15], smoothen wind farm power output and terminal voltage by incorporates real and reactive power control ability [16–18]. Although these combinations have proven useful, however, batteries have few disadvantages such as limited life cycle, voltage and current limitation and environmental hazards [19–21]. Therefore, more exploration on new alternative solutions and their corresponding control strategies become obligatory. Unlike the other batteries, fuel cells is an environmental friendly and well known for its zero pollutant, high efficiency, modularity, high power and reliable [22] which has the capability of high charge and discharge cycles. In this paper, a distributed static synchronous compensator integrated with a hydrogen system (DSTATCOM-Fuel cell) is proposed for active and reactive power compensation. In this combination, the DSTATCOM regulates reactive power output to maintain the voltage at 1 p.u. with the hydrogen system operates through the discharging and charging of the fuel cell and electrolyzer respectively to regulate active power based on the PV power output and voltage magnitude. Various case studies are conducted

*Jianhui Wong, Universiti Tunku Abdul Rahman, wongjh@utar.edu.my

to validate the performance of the proposed solution to mitigate the voltage rise issues while allowing high penetration from grid-connected PV systems.

2. Typical Malaysian Low-voltage Distribution Network in Radial Topology

The paper begins with a preliminary study to investigate the impact on system voltage with the integration of grid-connected PV systems on the radial distribution network. It is followed by an efficacy analysis using MATLAB Simulink to validate the performance of the proposed DSTATCOM-Fuel cell system to regulate the system voltage at 1 p.u while maximize the capacity of the grid-connected PV systems on the distribution network.

2.1. Modeling Electrical Network

A typical Malaysian low-voltage distribution network for small sub-urban area as shown in Figure 1. This network can be categorized into three sections according to its voltage level; (i) 132 kV incoming supply, (ii) 33 kV distribution substations, (iii) 11 kV distribution substations. The 132 kV incoming supply is the sub-transmission network of the national grid, the voltage is then stepped down to 33 kV by the 132/33 kV power transformers installed in the 33 kV distribution substations. The 33 kV is further stepped down to 11 kV using the 33/11 kV power transformer to a suitable voltage level for utilization. In this network, feeder 4 being the longest feeder will be modelled and the proposed DSTATCOM-Fuel cell system is integrated on feeder 4 to validate the efficacy.

There are 11 distribution substations across the radial feeder 4 with each of them are rated at 11/0.4 kV. The distance between each substation is indicated in Figure 1. The primary sides of the 11/0.4 kV transformers are labelled as 1, 2, 3 … and 11, while the secondary sides of the 11/0.4 kV transformers are labelled as 1a, 2a, 3a … and 11a. Table 1 and Table 2 show the technical specifications of the power transformer and conductor respectively. The locations of the distribution substations, the typical load characteristics and photovoltaic system power output were collected from the utility company.

A three-phase PV system is placed at the terminals 1a, 2a, and 3a in case 1 and 9a, 10a, and 11a in case 2 to investigate the impact of PV systems towards voltage rise on the network. Equation 1 shows sizing of the PV system is based on the penetration levels as follows:

$$PL = \frac{E_{PV}}{E_{load}} \times 100\% \quad (1)$$

where,

PL is the penetration level of the PV system (%)
E_{PV} is the total PV energy yield for the day (kWh)
E_{load} is the daily energy consumption at the load (kWh)

Based on the PV power output profile and load profile used in this study, it is determined that for 100% PV penetration level, the PV system should be sized at 500 kW. Thus, the PV system capacity for 60%, 70%, 80%, and 90% PV penetration are 300 kW, 350 kW, 400 kW, and 450 kW respectively.

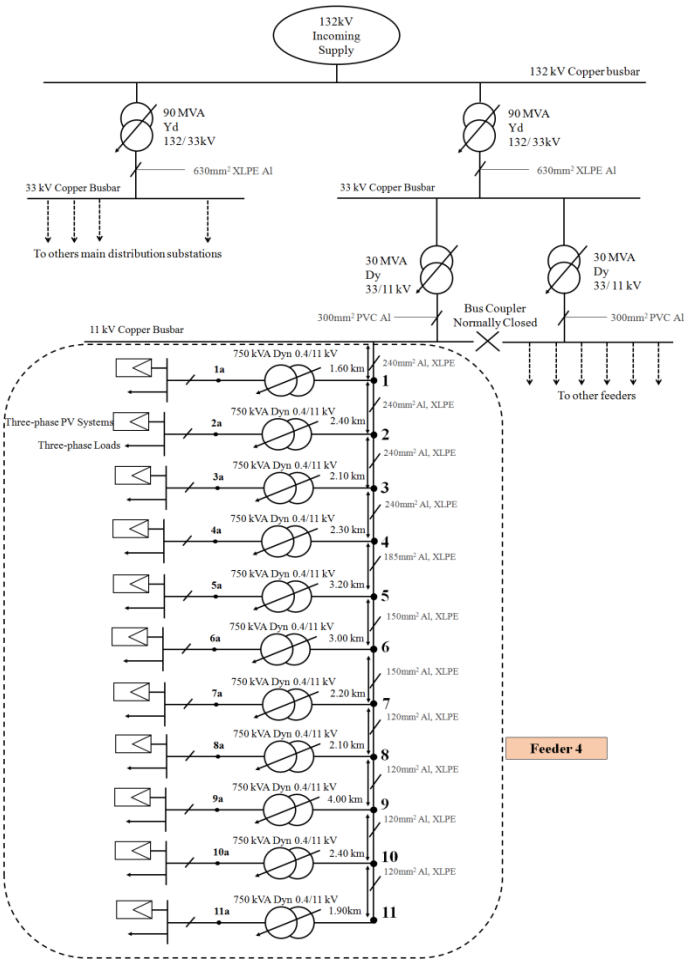

Figure 1: Typical Malaysian low-voltage distribution network in a sub-urban area.

Table 1: Technical Specification of the oil-immersed power transformers

Descriptions	Voltage Level (kV)	Rated Power (MVA)	Vector Group	Percent Reactance (%X)
Three-phase power transformers	132/33	90.00	Yd11	13.50%
	33/ 11	30.00	Dyn11	10.00%
	11/ 0.4	0.75	DYn11	4.75%

Table 2: Technical Specification of the conductors

Voltage Level (kV)	Cross-sectional Area (mm2)	Material	Insulator	R (Ω/km)	X_L (Ω/km)
0.4	300	Al	PVC	0.1300	0.0720
11.0	120	Al	XLPE	0.2990	0.0873
	150	Al	XLPE	0.2645	0.1603
	185	Cu	PILC	0.1950	0.0829
	240	Al	XLPE	0.1610	0.1524
33.0	630	Al	XLPE	0.0627	0.1070

2.2. Modeling DSTATCOM-Fuel Cell System

The proposed DSTATCOM-Fuel cell system is shown in Figure 2. The system consists of a DSTATCOM with an integrated hydrogen system. The hydrogen system consists of a fuel cell, an

electrolyzer, and a hydrogen storage tank. The hydrogen system is connected to the DC capacitor of the DSTATCOM through a boost converter which regulates the DC voltage from the hydrogen system to the desired level. The DSTATCOM consists of a DC capacitor, a three-phase pulse-width-modulated voltage source converter (VSC), and a coupling transformer. The coupling transformer connects the VSC to the network and functions to provide galvanic isolation and voltage regulation at the point of common coupling (PCC). The DSTATCOM, fuel cell, and electrolyzer are rated at 500 kVAr, 500 kW, and 500 kW respectively to match the PV system capacity at 100% PV penetration.

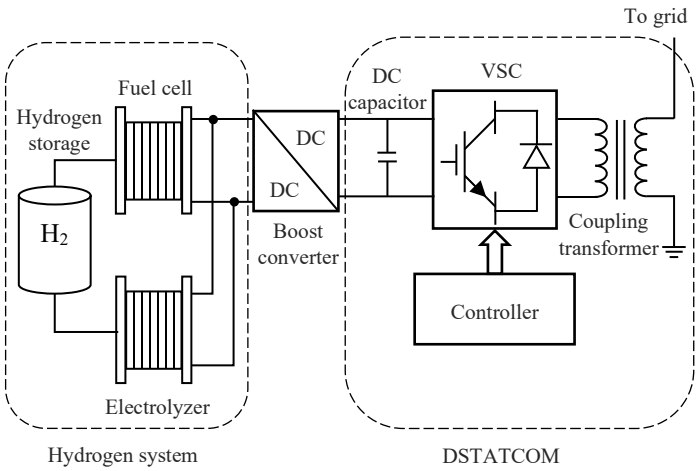

Figure 2: Schematic diagram of DSTATCOM-Fuel cell

The proton membrane exchange fuel cell (PEMFC) is used for the hydrogen system as it has a low operating temperature of 60-80°C, a high electrical efficiency range of 40-50%, a fast start up time, and high power density which makes it suitable for use in distribution networks [23,24]. A 500 kW PEMFC is modelled based on the NedStack PS6 datasheet. The parameters of the 500 kW PEMFC stack is shown in Table 3. The voltage-current (V-I) and power-current (P-I) curve of the fuel cell stack is shown in Figure 3.

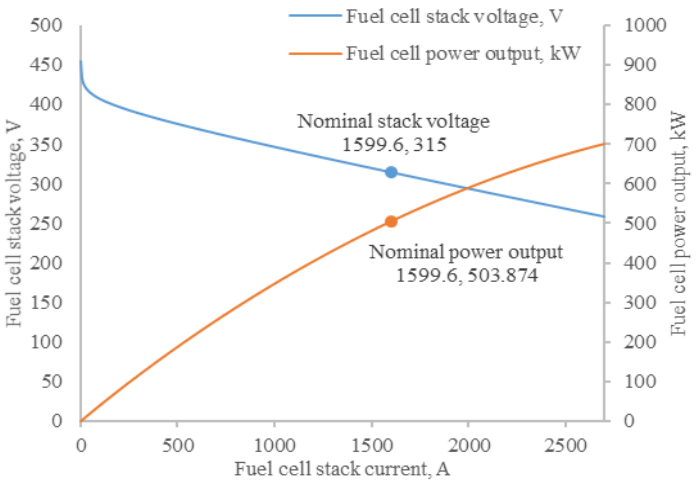

Figure 3: V-I curve and P-I curve of the fuel cell stack.

Table 3: Technical specification of the PEMFC stack

Rated capacity	504 kW
Nominal voltage	315 V
Nominal current	1333 A
Number of cells connected in series	455
Number of strings connected in parallel	12
Total number of cells in the fuel cell stack	5460

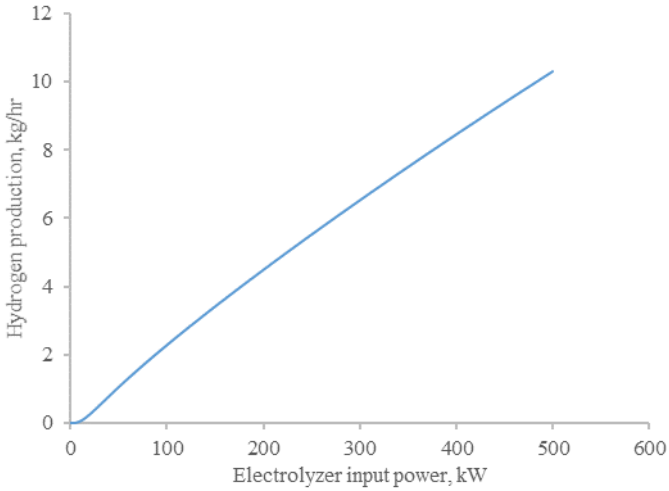

Figure 4: Hydrogen production of electrolyzer stack.

An alkaline electrolyzer stack is modelled based on the Photovoltaik, Elecktrolyse, Brennstoffzelle Und Systemtechnik (PHOEBUS) plant installed at Julich, Germany as reported in [25]. In order to create a 500 kW electrolyzer system, 19 electrolyzer stacks each rated at 26 kW are modelled and connected in parallel. The voltage-current relationship and hydrogen production of the electrolyzer system are modelled as described in [26,27]. The hydrogen produced by the electrolyzer is stored into a hydrogen storage tank without compression. The hydrogen storage tank capacity is 30 kg of hydrogen. The hydrogen production of the electrolyzer model is shown in Figure 4.

2.3. Control Strategies for Voltage Regulation

Figure 5 shows the control scheme for the DSTATCOM-Fuel cell. The objective of the controller is to mitigate voltage rise issue on the network by active and reactive power compensation. The voltage at the PCC, V_{PCC}, is measured and DSTATCOM performs reactive power compensation to regulate the voltage at 1 p.u. The voltage rise on the network occurs mainly due to high PV penetration. Hence, controller will initiate the hydrogen system charging operation when the PV power output, P_{PV}, is higher than the load consumption, P_{load} and the hydrogen tank level is less than 100%. If P_{PV} is less than P_{load}, the control will check if V_{PCC} is below the statutory limit of 1.1 p.u. If yes, the control will initiate the hydrogen system discharging operation if the hydrogen tank level is more than 20%. A minimum threshold of 20% for the hydrogen tank level is set to ensure a safe operation of the fuel cell.

If V_{PCC} exceeds the 1.1 p.u. limit, the control will stop the charging and discharging of the hydrogen system and only reactive power compensation will be used to regulate the voltage.

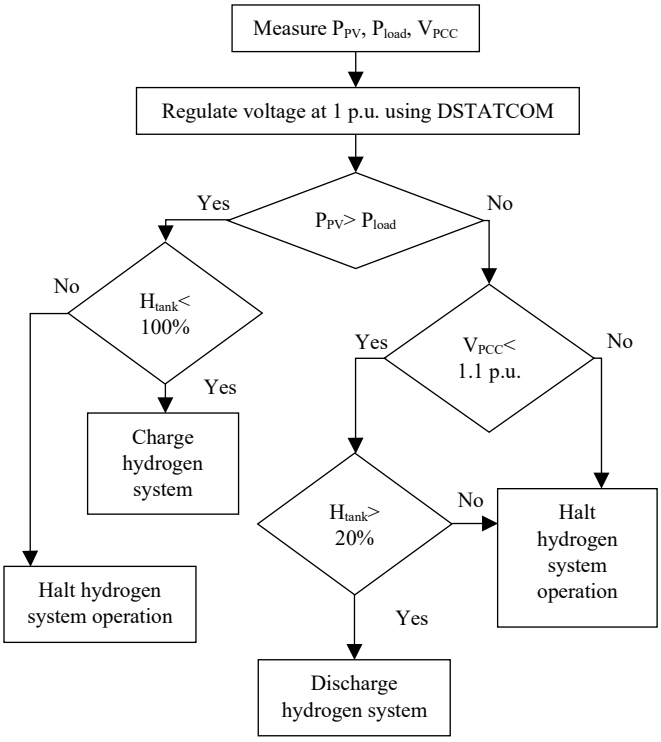

Figure 5: Flow chart of the DSTATCOM-Fuel cell controller.

3. Simulation Results

3.1. Impact of PV system allocation on voltage rise severity:

In this case study, the impact of PV system allocation on the system voltage is studied. Two cases are considered; i) Case 1 where a PV system is connected at terminals 1a, 2a, and 3a respectively, ii) Case 2 where a PV system is connected at terminals 9a, 10a, and 11a respectively. The PV power output profile used in this case study is the average hourly PV power output measured at Selangor, Malaysia during the month of April, 2018. The network is simulated for a period of 24 hours to determine the maximum voltage rise that occur within one full day.

Figure 6 shows the voltage magnitude of the load terminals 1a, 2a, and 3a for case 1. Figure 7 shows the voltage magnitude of the load terminals 9a, 10a, and 11a for case 2. In both cases, the maximum voltage is measured when there is 0%, 60%, 70%, 80%, 90%, and 100% PV. The voltage magnitudes shown in these two figures are the maximum voltage measured within the 24-hour period.

In case 1, the maximum voltage at terminal 1a, 2a, and 3a violates the 1.1 p.u. statutory limit when PV penetration exceeds 70%, 80% and 90% respectively. The maximum voltages at 1a, 2a, and 3a when PV penetration is 100% are 1.12 p.u., 1,12 p.u. and 1.11 p.u. respectively. It is noticed that in this case, the voltage rise severity reduces at terminals further away from the 11 kV main substation.

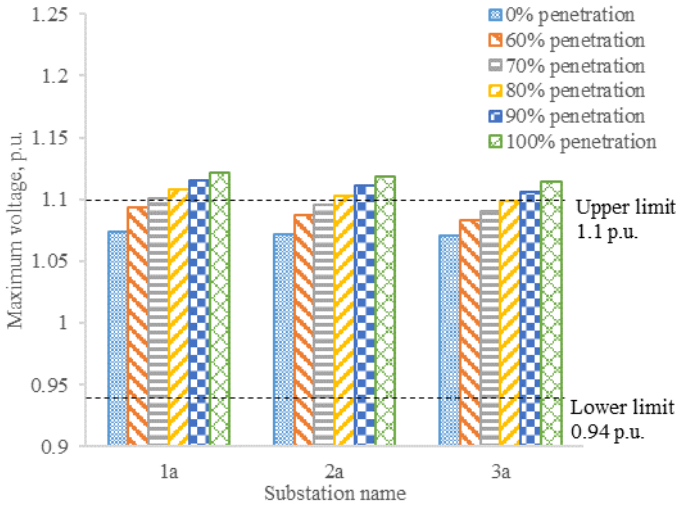

Figure 6: Maximum voltage magnitude of the load terminals when the PV system is connected at the terminals 1a, 2a, and 3a.

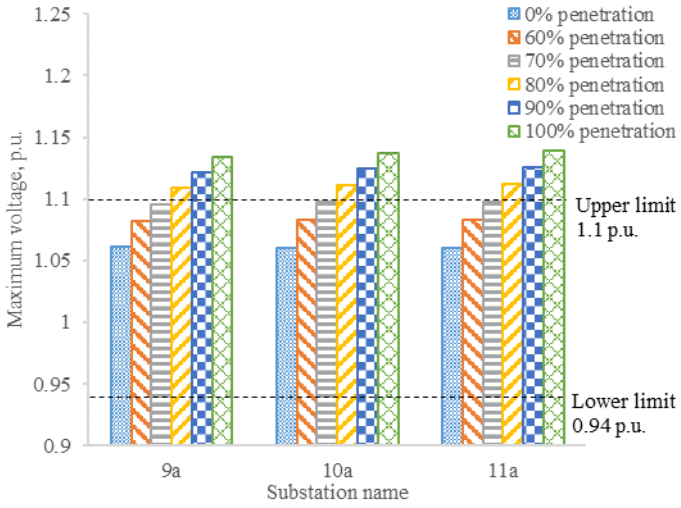

Figure 7: Maximum voltage magnitude of the load terminals when the PV system is connected at the terminals 9a, 10a, and 11a.

In case 2, the maximum voltage at terminal 9a, 10a, and 11a violates the 1.1 p.u. statutory limit when PV penetration exceeds 80%. The maximum voltages at 9a, 10a, and 11a when PV penetration is 100% are 1.13 p.u., 1.14 p.u., and 1.14 p.u. respectively. It is noticed that in this case, the voltage rise severity increases at terminals further away from the 11 kV main substation.

Comparing case 1 and case 2, it is noticed that when several PV systems are placed near the 11 kV substation, the voltage rise impact is greatest at the terminal located nearest to the main substation. Conversely, when multiple PV systems are placed at the end of the load terminals, the voltage rise is most severe at the terminal located furthest from the main substation.

Overall, it is observed that the voltage rise is more severe when multiple PV systems are placed at terminals furthest to the 11 kV main substation. The voltage increase as PV penetration increases is also more significant when the PV system is connected to the last three terminals compared to the first three terminals.

3.2. Efficacy Analysis for DSTATCOM-Fuel Cell System:

In order to determine the effectiveness of the proposed system for mitigating voltage rise caused by PV systems, a DSTATCOM-Fuel cell system is connected to terminals 1a, 2a, and 3a in case 1 and to terminals 9a, 10a, and 11a in case 2.

Figure 8 and Figure 9 show the comparison of the voltage rise for both cases when the PV system penetration level is 100%. It is observed that in both cases, the maximum voltage is maintained at 1 p.u when DSTATCOM-Fuel cell is connected. The regulation of voltage at the terminals with a connected PV system also affects the voltage at the other terminals. This effect is more significant in case 2 where the voltage at the neighboring terminals is reduced by as much as 2%. Overall, by using DSTATCOM-Fuel cell voltage rise can be reduced by as much as 10.7% in case 1 and 12.3% in case 2.

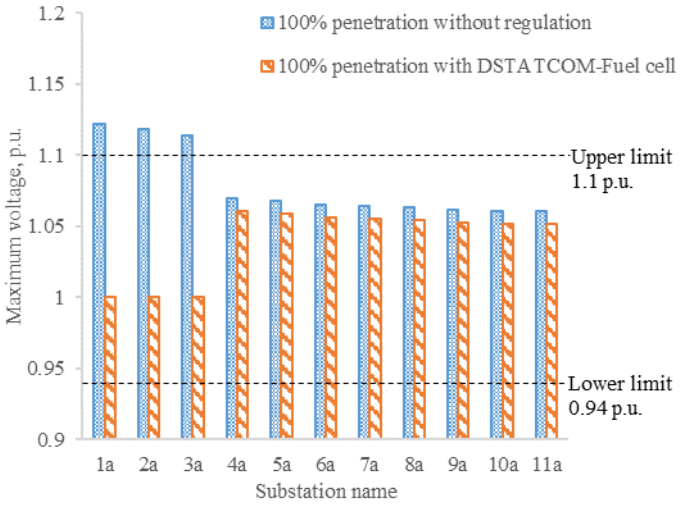

Figure 8: Comparison of voltage rise at 100% with and without regulation by DSTATCOM-Fuel cell in case 1.

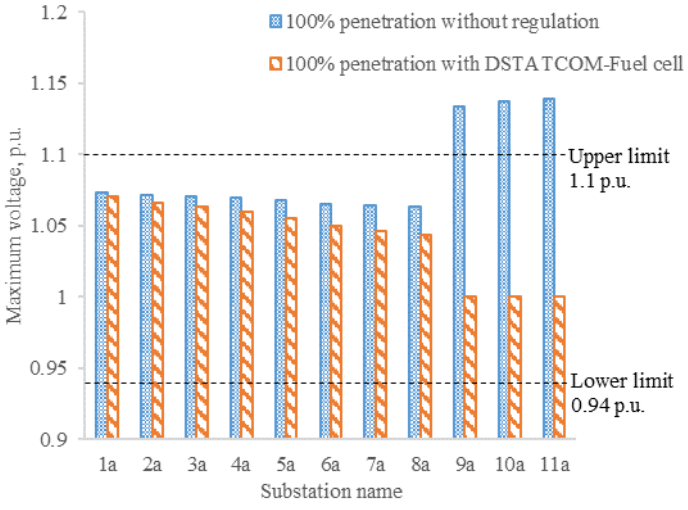

Figure 9: Comparison of voltage rise at 100% with and without regulation by DSTATCOM-Fuel cell in case 2.

Figure 10 shows the regulated power output at terminal 11a in case 3 after active power compensation by the DSTATCOM-Fuel cell system relative to the PV power output and load consumption. In order to mitigate voltage rise issues caused by reverse power flow, a combination of active and reactive power compensation is used depending on the PV power output and hydrogen tank level. When the PV power output is less than the load consumption, the hydrogen system in the DSTATCOM-Fuel cell will supply active power to the network to match the load consumption if the voltage does not exceed the statutory limit of 1.1 p.u. and the hydrogen tank level is not less than 20%. When the PV power output exceeds the load consumption, the hydrogen system charging operation is initiated if the hydrogen tank level is not full and the excess power is absorbed by the hydrogen system and converted to hydrogen.

It is observed that from 3:45:00 to 7:15:00 and 21:30:00 to 0:00:00, the regulated power is 0 kW. This is due to the hydrogen tank level being below 20%. Hence, the hydrogen system does not carry out the discharging operation during this period.

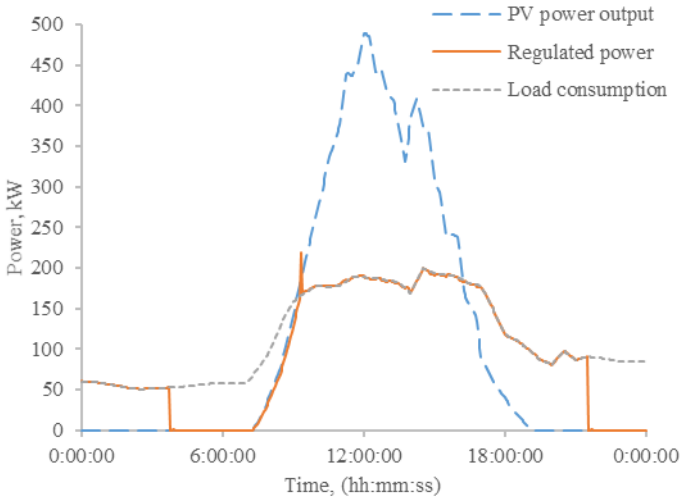

Figure 10: Regulated power output relative to PV power output and load consumption at terminal 11a in case 2.

Figure 11 shows the voltage levels throughout the day at terminal 11a in case 3. It is observed that there is significant voltage rise up to 1.14 p.u. which coincides with the peak output of the PV system. When the DSTATCOM-Fuel cell system is connected, the voltage is regulated at 1 p.u. throughout the day.

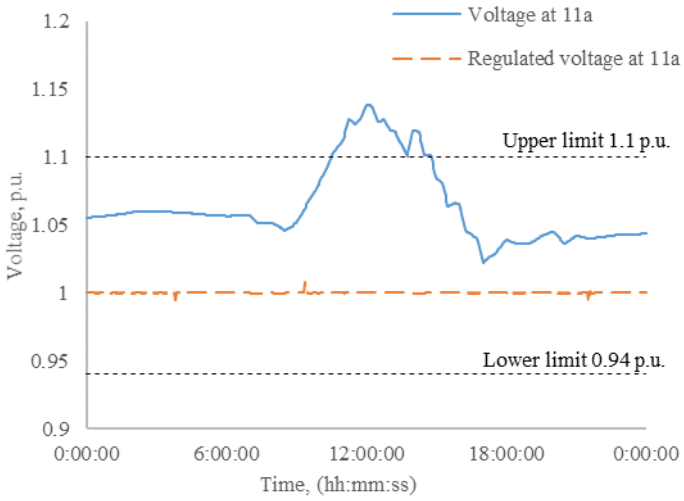

Figure 11: Regulated and unregulated voltage using DSTATCOM-Fuel cell at terminal 11a when a photovoltaic system generates 100% of the total consumed power.

Figure 12 shows the active power compensation by the fuel cell and electrolyzer and the reactive power compensation of the DSTATCOM. It is noticed that the DSTATCOM is constantly absorbing reactive power to reduce voltage level and regulated the voltage at 1 p.u. The hydrogen system charging and discharging operation depends on the PV power output. When the PV power output is high and exceeds the load consumption, the electrolyzer absorbs active power and converts it to hydrogen. When the PV power output is low and is less than the load consumption, the fuel cell supplies active power if the voltage magnitude is within the statutory limit of 1.1 p.u. It is noticed that from 3:45:00 to 7:15:00 and 21:30:00 to 0:00:00, the fuel cell does not supply any active power due to low hydrogen tank levels.

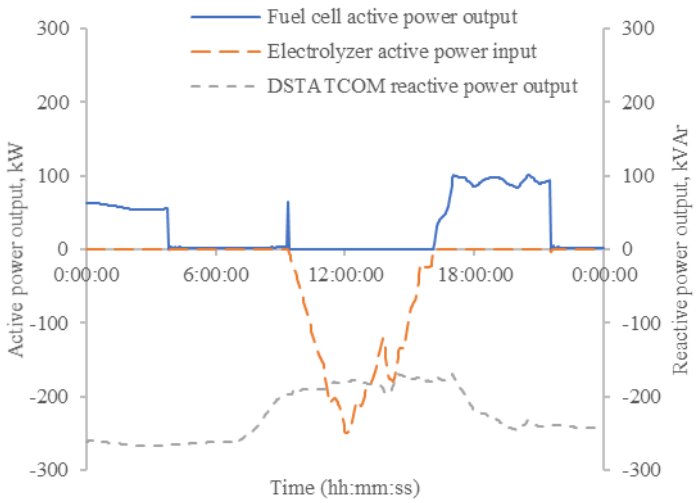

Figure 12: DSTATCOM-Fuel cell active and reactive power output at terminal 11a.

Figure 13 shows the hydrogen tank levels throughout the day. For this study, a starting level of 50%, which is 15 kg of hydrogen, has been assumed in this simulation. It is noticed that when the hydrogen tank level reaches 20%, the discharging operation of the system is turned off. Hence, only a minimal amount of hydrogen is consumed by the fuel cell to maintain the DC voltage in the DSTATCOM.

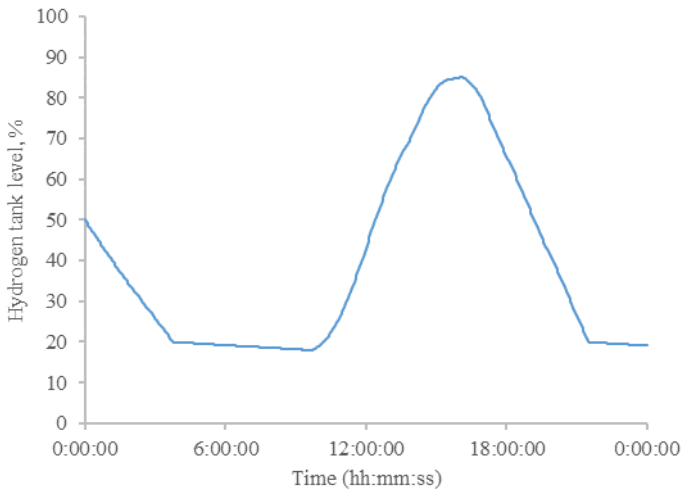

Figure 13: Hydrogen tank levels throughout the day.

4. Conclusion

Integrating large amount of renewable energy sources without suppressing the power quality always has been a challenge to the utility company. The voltage rise issues become severe when large amount of PV systems are installed across the end of a long feeder in a radial distribution network. This paper presented a DSTATCOM-Fuel cell system to perform power exchange within the grid for mitigating the voltage rise issues without curtailing the high penetration of PV systems. Excess power generated from the PV system will be converted into hydrogen and store in a hydrogen tank via an electrolyzer. In the event of high load consumption during low renewable energy generation, fuel cell will generate electricity using the hydrogen stored in the tank. Various case studies are conducted in this paper to validate the efficacy of the proposed DSTATCOM-Fuel cell system and the results have shown that this combination can mitigate the voltage rise issues up to 12.3%, maintaining the voltage at 1 p.u. while allowing high penetration of PV systems presence in the network.

Conflict of Interest

The authors declare no conflict of interest.

Acknowledgment

This work was supported by the Ministry of Higher Education (MOHE) Fundamental Research Grant Scheme (FRGS) under the grant number FRGS/1/2017/TK04/UTAR/02/2 and Universiti Tunku Abdul Rahman (UTAR) Research Fund.

References

[1] J. C. Y. Hee, J. Wong, Y. S. Lim, J. H. Tang, "Assessment on Various Allocations of Energy Storages Systems on Radial Distribution Network for Maximum PV Systems Penetration" in 2018 Int. Conf. Smart Grid Clean Energy Technol. ICSGCE, 2018. https://doi.org/10.1109/ICSGCE.2018.8556803.

[2] N. S. Eusoff, "Malaysia sets new goal of 20% clean energy generation by 2030" The Edge, 2018. https://www.theedgemarkets.com/article/malaysia-sets-new-goal-18-clean-energy-generation-2030.

[3] A. Shafiu, T. Bopp, I. Chilvers, G. Strbac, "Active management and protection of distribution networks with distributed generation" in IEEE Power Eng. Soc. Gen. Meet. 2004, 2004. https://doi.org/10.1109/PES.2004.1373011.

[4] L. Kane, G. Ault, "A review and analysis of renewable energy curtailment schemes and Principles of Access: Transitioning towards business as usual" Energy Policy, 72, 67–77, 2014. https://doi.org/10.1016/j.enpol.2014.04.010.

[5] T. Mahto, V. Mukherjee, "Energy storage systems for mitigating the variability of isolated hybrid power system" Renew. Sustain. Energy Rev., 51(Supplement C), 1564–1577, 2015. https://doi.org/10.1016/j.rser.2015.07.012.

[6] M. S. Ali, M. M. Haque, P. Wolfs, "A review of topological ordering based voltage rise mitigation methods for LV distribution networks with high levels of photovoltaic penetration" Renew. Sustain. Energy Rev., 103, 463–476, 2019. https://doi.org/10.1016/j.rser.2018.12.049.

[7] P. Ariyaratna, K. M. Muttaqi, D. Sutanto, "A novel control strategy to mitigate slow and fast fluctuations of the voltage profile at common coupling Point of rooftop solar PV unit with an integrated hybrid energy storage system" J. Energy Storage, 20, 409–417, 2018. https://doi.org/10.1016/j.est.2018.10.016.

[8] F. H. M. Rafi, M. J. Hossain, J. Lu, "Hierarchical controls selection based on PV penetrations for voltage rise mitigation in a LV distribution network" Int. J. Electr. Power Energy Syst., 81, 123–139, 2016. https://doi.org/10.1016/j.ijepes.2016.02.013.

[9] E. L. Ratnam, S. R. Weller, "Receding horizon optimization-based approaches to managing supply voltages and power flows in a distribution grid with battery storage co-located with solar PV" Appl. Energy, 210, 1017–1026, 2018. https://doi.org/10.1016/j.apenergy.2017.08.163.

[10] Z. Yang, C. Shen, L. Zhang, M. L. Crow, S. Atcitty, "Integration of a StatCom and battery energy storage" IEEE Trans. Power Syst., 16(2), 254–260, 2001. https://doi.org/10.1109/59.918295.
[11] M. A. Rahman, M. H. Shawon, S. K. Ghosh, S. K. Nath, "Transient stability enhancement of fuel cell system using D-STATCOM" in 2014 3rd Int. Conf. Dev. Renew. Energy Technol. ICDRET, 2014. https://doi.org/10.1109/ICDRET.2014.6861663.
[12] M. Stella, M. A. G. Ezra, A. Peer Fathima, C. Khang Jiunn, "Research on the efficacy of unified Statcom-Fuel cells in improving the transient stability of power systems" Int. J. Hydrog. Energy, 41(3), 1944–1957, 2016. https://doi.org/10.1016/j.ijhydene.2015.11.130.
[13] S. Morris, M. Ezra, Y.-S. Lim, "Multi-machine power transmission system stabilization using MPSO based neuro-fuzzy hybrid controller for STATCOM/BESS" Int. Rev. Electr. Eng., 7, 2012.
[14] M. A. Bhaskar, D. Sarathkumar, M. Anand, "Transient stability enhancement by using fuel cell as STATCOM" in 2014 Int. Conf. Electron. Commun. Syst. ICECS, 2014. https://doi.org/10.1109/ECS.2014.6892553.
[15] A. Hajizadeh, M. A. Golkar, "Control of hybrid fuel cell/energy storage distributed generation system against voltage sag" Int. J. Electr. Power Energy Syst., 32(5), 488–497, 2010. https://doi.org/10.1016/j.ijepes.2009.09.015.
[16] S. M. Muyeen, R. Takahashi, T. Murata, J. Tamura, Mohd. H. Ali, "Application of STATCOM/BESS for wind power smoothening and hydrogen generation" Electr. Power Syst. Res., 79(2), 365–373, 2009. https://doi.org/10.1016/j.epsr.2008.07.007.
[17] S. W. Mohod, M. V. Aware, "A STATCOM-Control Scheme for Grid Connected Wind Energy System for Power Quality Improvement" IEEE Syst. J., 4(3), 346–352, 2010. https://doi.org/10.1109/JSYST.2010.2052943.
[18] S. W. Mohod, S. M. Hatwar, M. V. Aware, "Grid Support with Variable Speed Wind Energy System and Battery Storage for Power Quality" Energy Procedia, 12, 1032–1041, 2011. https://doi.org/10.1016/j.egypro.2011.10.135.
[19] A. Lenka, A. Papachen, A. P. Fathima, "Three Area AGC of An Interconnected Power System with Superconducting Magnetic Energy Storage" Int. J. Ind. Electron. Electr. Eng., 2, 54–58, 2014.
[20] A. A. K. Arani, H. Karami, G. Gharehpetian, M. Akhavanhejazi, "Review of Flywheel Energy Storage Systems structures and applications in power systems and microgrids" Renew. Sustain. Energy Rev., 69, 2017. https://doi.org/10.1016/j.rser.2016.11.166.
[21] E. MacA. Gray, C. J. Webb, J. Andrews, B. Shabani, P. J. Tsai, S. L. I. Chan, "Hydrogen storage for off-grid power supply" Int. J. Hydrog. Energy, 36(1), 654–663, 2011. https://doi.org/10.1016/j.ijhydene.2010.09.051.
[22] M. Jouin, R. Gouriveau, D. Hissel, M.-C. Péra, N. Zerhouni, "Prognostics and Health Management of PEMFC – State of the art and remaining challenges" Int. J. Hydrog. Energy, 38(35), 15307–15317, 2013. https://doi.org/10.1016/j.ijhydene.2013.09.051.
[23] E. G. T. Services, Fuel Cell Handbook, Seventh Edition, 2004.
[24] H. R. Ellamla, I. Staffell, P. Bujlo, B. G. Pollet, S. Pasupathi, "Current status of fuel cell based combined heat and power systems for residential sector" J. Power Sources, 293(Supplement C), 312–328, 2015. https://doi.org/10.1016/j.jpowsour.2015.05.050.
[25] H. Barthels, W. A. Brocke, K. Bonhoff, H. G. Groehn, G. Heuts, M. Lennartz, H. Mai, J. Mergel, L. Schmid, P. Ritzenhoff, "Phoebus-Jülich: An autonomous energy supply system comprising photovoltaics, electrolytic hydrogen, fuel cell" Int. J. Hydrog. Energy, 23(4), 295–301, 1998. https://doi.org/10.1016/S0360-3199(97)00055-4.
[26] M. H. Nehrir, C. Wang, Modeling and Control of Fuel Cells: Distributed Generation Applications, John Wiley & Sons, 2009.
[27] Ø. Ulleberg, "Modeling of advanced alkaline electrolyzers: a system simulation approach" Int. J. Hydrog. Energy, 28(1), 21–33, 2003. https://doi.org/10.1016/S0360-3199(02)00033-2.

ASTES

Advances in Science, Technology and Engineering Systems Journal Vol. 4, No. 4, 292-299 (2019)

www.astesj.com

ASTESJ

ISSN: 2415-6698

Prototype of a Security Architecture for a System of Electronic Voting for the Ecuador

Segundo Moisés Toapanta Toapanta[*,1], Gabriel Enrique Valenzuela Ramos[1], Félix Gustavo Mendoza Quimi[1], Luis Enrique Mafla Gallegos[2]

[1]*Departamento of Computer Science, Universidad Politécnica Salesiana (UPS), Guayaquil, Ecuador*

[2]*Facultad of Systems Engineering, Escuela Politécnica Nacional of Ecuador (EPN), Quito, Ecuador*

A R T I C L E I N F O

Article history:
Received: 08 July, 2019
Accepted: 26 July, 2019
Online: 07 August, 2019

Keywords:
Electronic voting.
Security architecture
Cryptography

A B S T R A C T

To be able to perform a better voting system, it is important to go to ICT and its various platforms designed for electoral purposes, which are being used in several countries in Latin America. In Ecuador are being used digital mechanisms during the process, but with certain errors and he is being considered to implement electronic voting, although it remains a project. The objective of this study is to analyze the prototype of a security architecture for a system of electronic voting for the Ecuador. In this study applied a quantitative, deductive, non-experimental descriptive criteria allowing to analyze the documents of reference. It was observed that the laws governing the franchise in the country have been well designed to provide facilities to the greatest number of voters, whether people with certain physical disabilities or with deprivation of liberty; In addition gives to know how to vote and the rapid counting system. It is concluded that architecture deserves a protocol that protects information throughout the electoral process and also the use of cryptographic algorithms with special software, that allows to work quickly and provide security properties, integrity and authenticity.

1. Introduction

Electronic voting is a challenge for Latin American countries and Ecuador is not far behind, we aimed to start with a pilot plan 2018, but budget cuts could not be achieved; This situation is similar to what happens in other countries of South America, because they have implemented new technologies for rapid counting and transmission of final results, but only two countries used it in its entirety, Brazil and Venezuela. This happens also in other continents; in Asia only India, uses it throughout the country, changing us, France and Canada are used in some areas or States. Other countries have been unwilling to use it, despite having the required platform. This situation reflects the complexity in the implementation of electronic voting, due to the infrastructure, as well as by the education which they must venture, both for those who wish to implement, such as citizenship, for correct use.

According to the author Pacheco, combining access to information technologies with the confidence and security in the electoral process is not an easy task; but with the increase in the recent years, Internet applications, telecommunications and audiovisual and electronic technologies, has been given a gradual change in these [1].

There are two major categories of electronic voting: face-to-face and not face to face.

Non-Presential vote. -Is that which can be done through the use of electronic devices such as the internet the computer, cell phone or other device near or far site.

Presential vote. -Is done directly in the electronic ballot box is where managed vote in traditional places.

The two types of voting are effective, but require their respective care and security protocols. So also this kind of gathering of electronic votes is done is through two ways:

- The direct recording electronic voting.
- Collection by reading eye. -Storage and automation is given up to the counting of votes and then rapid publication of results.

* Segundo Moisés Toapanta Toapanta, Email: stoapanta@ups.edu.ec

This leads to plant the idea of a security architecture that provides confidence to users, that the results of the elections will be not changed at the end or during the process.

2. Materials and Methods

2.1. Materials

To carry out this study we considered several scientific articles, documentary bibliography and projects inside and outside the country, which provided a contribution to the proposed topic. The author Garcia-Barrera believes that ubiquitous, cyberspace, netizens, homo digitalis, virtual communities, telematic networks, e-democracy, e-elections politica.com are terms that are presented in the glorifier speech of the new technologies, corresponding to this era post-industrial.

Al Gore, from the American Vice President, announced "the new era of democracy" and the Internet guarantees direct, global, virtual, interactive democracy by survey and electronic voting [2].

The use of ICT, platforms and knowledge of those involved in the issue, make it possible that applies a security architecture in e-voting. Also the Constitution of Ecuador provides several articles of law for the benefit of citizens, but this requires that the Government invested in different platforms, training and search for the appropriate use of these resources, to avoid results unexpected, as well as the untimely intervention of persons unrelated to the National Electoral Council (CNE) who wish to affect the system.

The articulated in the Constitution of the Republic of Ecuador, designated the duties and rights for voters, as article 62 which says: "people enjoyment of political rights have right to vote universal, equal, direct, secret and counted publicly"[3].

Likewise it is the electoral function, which is responsible for ensuring the correct fulfilment of the rights of every citizen to vote. You could also be observed that the electoral function has three bodies that are involved in electoral processes, security and the respective protocol in each vote: The National Electoral Council, the Electoral contentious Tribunal and the receiving voting together.

2.2. Methods

This study maintains an approach to quantitative, deductive logic, correlation criteria and qualitative, conducted analysis to the various revised texts. Considering the important aspects regarding e-voting, can be established a prototype of a relevant to electronic voting security architecture in the country.

The Constitution expresses the popular will or the will of the people in the electoral system, which requires certain Protocol, protection, allocation of seats and organisation so that it complies.

The author Aguirre Board, notes that in the coincidences of some forms of participation it affects the State, either because the proposed citizens obtain recognition, transform some public policy or, if possible, institutionalize procedures e instruments of political participation, to ensure the permanence or regularity of a desirable action, such as voting, require transparency in public spending and obtain accountability of rulers, etc. [4], allowing that is expand the visibility of the instruments of social expression, with the encouragement of citizen participation.

Likewise the articulated in the Constitution indicate that people with disabilities also have the indispensable right of participation in electoral processes, even new ways in which they can vote, have adapted According to their condition. At the same time they also have legislation which protects their right to suffrage adapted to his condition.

The Convention on the rights of persons with disabilities, according to the legal norms in disability in Ecuador, are local or foreign, require direct their chance to vote. The author Quesada believes that the decision of one or another form of registration is not exclusive, on the other hand, are recommended in various ways so that between them they are complementary and, in this way, to achieve greater inclusiveness of voters abroad, so is privileged that it idea previously mentioned the principle of universality [5].

Similarly, the Constitution of the Republic of Ecuador, the code of democracy and also the rules for the participation of people with disabilities, have articles which guarantee the right of the political exercise of each person. To implement electronic voting in these cases, required instruments enabled for this purpose, as well as security protocols that take care of the decision of the voters.

I) Digital voting (electronic)

Digital voting is being implemented in several States, as noted by VALVERDE, who refers to that in several countries there are three modalities for the vote: by post, personally, in the embassies or consulates or online, through internet [6]. However, according to Legorreta, the issue of the security of electronic voting may be the aspect where the lack credibility is more evident. In this sense, the technologies of e - vote are not exempt from problems [7].

The experience in Ecuador has been through phases, first implemented new technologies for the rapid count and emission results.

There was carried out a project to start e-voting and had great reception, but the plan did not continue due to high costs that demanded. There was carried out a project to start e-voting and had great reception, but the plan did not continue due to high costs that demanded. But it has not ruled out the continuity of the project, since the benefits are large.

II) Stages of e-voting

According to Montes the stages of the process of voting on a modern voting system, can be distinguished into three stages:

- Creation of the vote: the voter selects somehow among the options available and 'creates' vote, in any format.
- Anonymous receipt of voting: the vote is sheltered along with other votes to anonymize.
- Vote count: after completed the time available for voting, count the guarded votes [8].

To use the vote Electronics is required to work with citizenship and thus obtain the expected results, therefore, is important to have several requirements, such as those set out below.

3. Requirements of electronic voting

There are two prerequisites:

- The voter confidence in the proper functioning of the system.
- The ease, comfort and simplicity that present.

In addition, a digital voting system must have other requirements that must be met, among those are: guarantee the anonymity and privacy of who exercise the vote, so that each one can be done with total freedom.

Another requirement that should have a digital voting system is to be eligible and genuine, is that they can make the vote of those who are authorized, in addition to this be done only once.

Another need is that it is full, it there is no fraud in the process, i.e. that the votes may not be disposed of or much less modified.

Electronic voting is synonymous with integrity, but not during the electoral process, but before, since the pre vote also has its own requirements, which should be considered as part of the process, not in isolation, so the results will be more optimal.

Objectives of the electronic vote, should be established so that it can be evaluated, but the participation of persons designated for such purposes, must be fundamental, so will keep the integrity of the information, you can review processes and will contain limitations of access for people that are not part of the electoral institution of the country.

Table 1: Objetives

Objectives of the electronic voting	
Data Integrity	During and after the electoral process.
Audit	It may be auditable completely at any stage of the process.
Confidentiality	Integrity and no-denegation.
Security in the user interface	That the interface can be subsequently used by anyone.

The system should be, also, accurate and verifiable. All information that will be recorded along with the votes made must be very well stored. It is reliable, is to say that all data and votes that you enter are not lost that this effective operation is essential.

Which is easy to use is other requirements you must have the system so that it can be used by all persons without complications, including persons who are responsible for the scrutiny of the data.

Another proposed requirement is to not be coaccionable, i.e. that people who exert the vote may not reveal by whom or who they have voted. The author Charles Leija the vote represents the form of most widespread citizen participation and, in many cases, the only exerted by population [9].

Finally, another requirement is to be verifiable by the voter, i.e. it must verify that it exercised their right to vote.

4. Functional requirements for electronic voting: Software, network, and security.

4.1. Software requirement

They must be grouped into modules of authentication, voting, counting and results; so make your application more feasible. Each of these modules will have certain functions. Then mentioned the functions of each module, among them are:

Authentication functions:

- Regularize the participants receiving the vote tables, to verify if those who vote enabled are to cover.
- Verify that the personal data of the user (ID, name, and precinct numbers) match those registered in the database.
- Compare the list of people who have voted with those recorded in the database of the receiving Board vote.
- Generate verified lists of those who exercised their right to vote.
- Verify that the voter has enabled access to digital ballots.
- Others.

Vote modules consist of the following functions:

- Facilitate access to the candidates in the voting, also have a braille system for visually disabled people so that they can also vote.
- There should be the option to vote blank or null and that count as valid decision for the voter.
- The encryption of data and voting should be included as part of the security.
- You must include an endorsement with digital signature enabled and authorized voter.
- Availability of authentication that do not have access to vote those who are not registered.
- Have assistance of the vote in the case of people with reduced mobility.
- Immediate impression of the vote.

Counting modules consist of the following functions:

- Decoding and transfer of the feedback received.
- Generate reports of the vote that it could not decrypt.
- Do blank votes count.
- Creating reports automated with the results of the votes.
- Generate and print digital reporting based on the final results of the voting process.
- Export of results information to be able to be checked in other platforms.

All these functions must be carried out so that it can fulfil the requirement of software.

4.2. Network requirement

You need a high-performance network, also must take into account population growth, to provide vote receiver boards which may be necessary; It is necessary to consider the bandwidth and also the fault tolerance.

4.3. Security requirement

Within the safety features, Jeff Schmidt points out that while there are many important aspects that guided development, should highlight the following general characteristics of e-voting:

- Separation of the identification of the voter and the urn; both systems must be independent. All the information needed to operate must be previously loaded.
- All functions of the system should be stored in blogs that can be extracted later for audit purposes. These logs can also be used as duplicates of the documents required by the legislation in force.
- Absence of communication between devices (URN and Padrón). This prevents that you handling a system from the other and that gives greater assurance and confidence in the secrecy of the vote.
- Print proof of voting. Once the voter manifests his election will proof, that voter will see to confirm its decision to be printed and then this is deposited automatically in an urn.
- Use of free software. While it is true that access to the source code is not a guarantee of reliability, yes we can make what an application of electronic voting whose source code not be auditable must be ruled out entirely. This decision covers also the operating system on which applications will be implemented to develop [10].

There are institutions that apply systems SAFE created by CISCO, which provides defense in depth and a modular design and architecture is aimed to detect threats in the network systems.

5. Voting Counting

Incorporated by electronic vote counting systems, these, are a hit at the time of results, since the automation of data, speeds up the query and display of information. Valverde Loya opinion has as alternative of internet voting is considered fast, low cost, through a website with restricted access with individual password for each voter in each election [11].

This technological mechanism requires the review of institutions to increase confidence in the process.

5.1. Traditional and remote voting systems

According to the storage system one of the best known and currently do not use traditional calls ballots, they are DRE and OCR systems. Among the most commonly used types today are buttons, mini switches and those who have a touch screen.

It is important to consider that electronic voting poses stages to be followed, as Chungata suggests, Jussibeth (2017), raises a sequence in the Presential vote and a system of remote that it is not very different to the traditional methodology, this being the following:

5.2. Traditional or face-to-face system

This system uses your voter from locally and face-to-face, where picks up their vote by means of different methods and issued a check, this environment is completely controlled or supervised by the responsible authority that checks your process.

Within this system are used different methods, such as perforated card, electronic ballots, machines of levers or camshaft and electronic ballot boxes; These different technologies:

- Optical character recognition, or OCR readers.
- DRE electronic record direct, using touch screens for receiving and storing the chosen option. Each one differs in the form that stores the information received, directly by optical scanning or directly in memory. These systems are usually applied in developing countries, with low levels of literacy, extensive geography and ethnic diversity.

5.3. Remote system:

This method is what allows that the voter is not specifically directed at the electoral college, this often performs it in a place other than tables, this often works with a connection to internet, intranet, or any other mobile device, as the cell phone through an SMS.

With this system there is no control by the authorities at the time of issue or receive votes, so the reliability of this is highly questionable, in turn, is considered an obstacle is the lack of total internet access in households not fully Universal [12].

Finally, in accordance with the established schedule of receipt of votes, the authorities of each table will be electronic urns can be counts and issue findings in the case thus required with proper safety of the case.

6. Prevent threats on electronic voting

E-voting while it has high safety standards, however, these can become to be also violated and present certain threats.

Among them are human threats, natural and environmental threats.

According to Bast in electronic voting systems, it is necessary to protect:

- Indefinitely the privacy of the voter: even after after the election, given that where any intruder get a digital copy of rows that allow to relate the voter with their vote, would have all the time to try to figure it out. All people want to maintain their privacy assured indefinitely, and it would be very serious to be know by a voter who voted in particular. For example, knowing the trajectory as a current candidate voter could influence the electorate.

- The security of the data of the votes while lasts the electoral process: the protection of the information of the votes issued only must support the length of time that corresponds to the voting process, given that the proposed model only records the data of the votes and voters and after the scheduled time not publicly known [13], the resulting count information, i.e. the results of the election.

The characteristics of use of security processes in the use of electronic voting, being the data those who agree are vulnerable, you can see in table 2.

Table 2: Data requiring security and/or privacy

	Confidentiality	Integrity	Availability
Electoral Padron	NO	YES	YES
Votes	YES	YES	YES
Candidates	NO	YES	YES
Charges	NO	YES	YES

6.1. Encryption of data

Data are the most important elements to the moment of electronic voting, there is very personal, sensitive information that must be cared for and protected. So says Garcia that the same is true in the field of computer security in general, and on cryptography in particular. One of the reasons for this phenomenon, passes by the large increase in the volume of information available.

Any new method that appears is quickly made available a huge critical mass that assesses and generates any changes it deems necessary.

Simultaneously the geometric growth of the ability to attack a cryptanalyst required a cryptographic system to show security so undeniable, and must apply rigorous formal mathematical techniques.

- One of the applications with highest demands in this regard is the electronic voting. The results of a vote define important power relations and the management of important economic resources. Consequently, it is essential to make two key points.
- Scrutiny must reflect the will of citizens in a transparent manner.
- A voter must have the guarantee that your vote will be kept anonymous indefinitely [14].

This deals with such aspects in such a way to ensure the security of this process. Currently asymmetric cryptography, symmetric cryptography, and figures can be uses several types of cryptography, which are crypto algorithms. The first are mathematical functions that are structured as a finite set of steps, which help to encrypt and to decrypt the data.

In symmetric cryptography is commonly used the same password or key to be able to encrypt and decrypt the information, here comprise the DES (Data Encription Standard) triple DES, AES (Advanced Encription Standard), IDEA (International Data Encription Algorithm).

In asymmetric cryptography two keys, one public and private, are used here comprise the RSA, DSA, and elliptic curves.

So that cryptographic systems work, requires a Protocol, allowing follow the respective steps, to avoid the manipulation of some external agent and allowing to achieve the proposed objectives. It should not underestimate any level of security, so we must be aware of some weakness filed with any steps that are not fulfilled as expected.

6.2. Multi-layered security architecture

The development of an architecture, there are several methods, the sequential and progressive; the sequential stipulates the collection of requirements, development, testing and delivery; in the progressive are the requirements, design, implementation and review.

In this case, it is recommended a system that uses components to the highest levels, such as authorization, access controls, authentication and audit models; These require an architecture specific and adapted to these elections.

Applications use multilayer systems and each communicates with the previous layer according to their functionality via a defined interface.

Table 3: levels of a safety mechanism

Authorization and Access Control	
Authentication	Supervision
Safe Communication	
Cryptography	

The electronic protection relies on several features that must be fulfilled and protected:

1. Inviolability: Strict access code.
2. Usability: For benefit to its social environment.
3. Monitoring/audit: Quality assurance and compliance processes.
4. Software development: Creates and builds the software according to the needs of the nation.
5. Scalability: That the Software has the ability to grow.
6. Protocol attacks: Decrease the likelihood of malicious attacks.
7. Versatility: Making the system very flexible and adaptable.
8. Maintenance: To ensure the proper functioning of the software and its infrastructure.

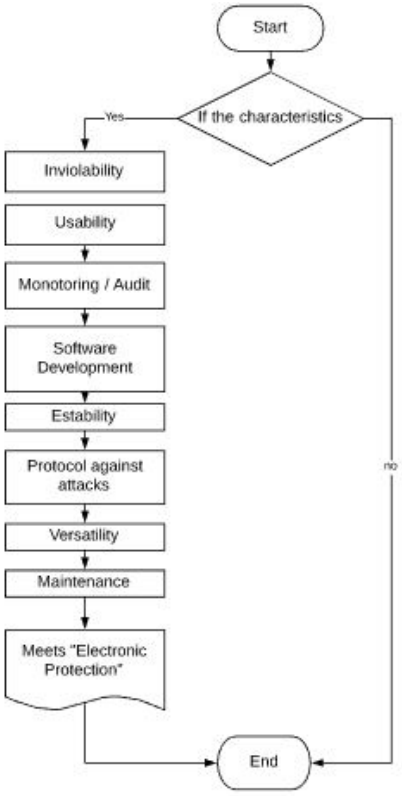

Figure 1: Electronic protection

6.3. Encryption algorithm using Diskcryptor:

This software presents tools that allows to determine the speed of encryption and decryption in megabytes per second of AES algorithms and combinations with other algorithms.

6.4. Audit

Importantly go monitoring and verifying the operation of the components during the electoral process, using blogs, reviewing the minutes of opening, the generated receipts and analyzing the final acts.

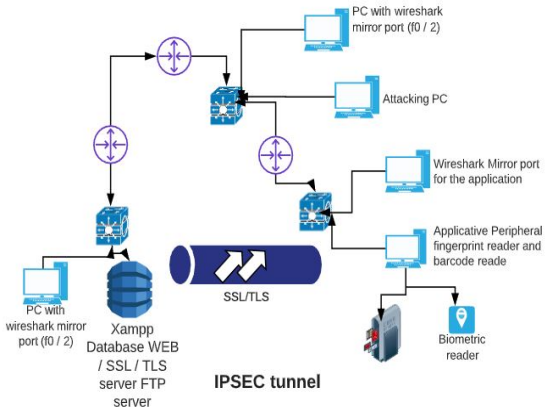

Figura.2. Security and Audit Protocol

The audit becomes a valuable requirement to establish a security architecture, but requires care processes are fulfilled accurately and avoid the intrusion of strangers and Protocol problems before, during and after of the electoral votes. the CNE must then combine aspects of the audit and security technology in the electoral process.

7. Results

For the design of a security architecture is needed of the law, as first articulated, then establish the process by software and its application to the respective vote.

Combined encryption makes possible the security of electronic voting. The use of the Diskcryptor system for a quick and appropriate encryption and decryption of the information on the electoral process.

There are systems that are used by some institutions, but only apply to identify threats in the network modules, then fight them. But also complementary procedures that complete security architecture is needed.

During the process is required to conduct audits allowing to know if the mechanism used is fulfilling their purposes, if the vote of voters is being protected and if the results are being provided Correct and timely.

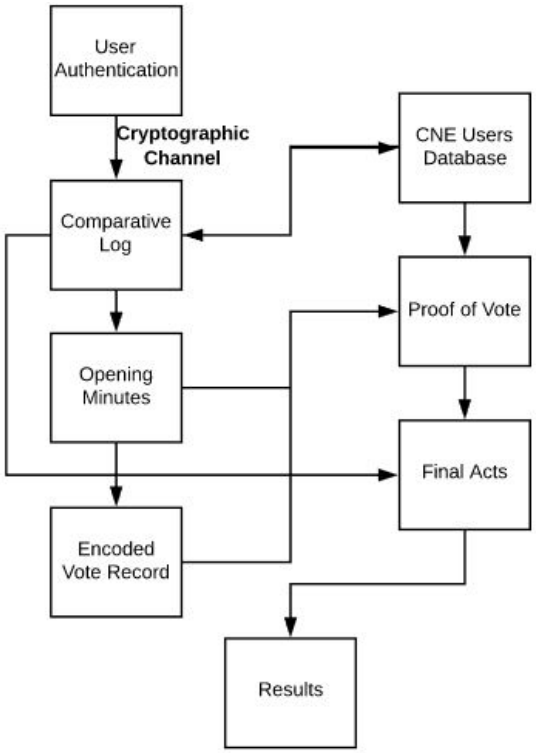

Figure 3: Prototype

1. User Authentication.
2. It encrypts the information through a cryptographic channel.
3. It decrypts the information and it occurs in the middle of a comparative log, is the comparison of the information in the database of the CNE.

4. If the data are correct, it gives way to the Act of opening which allows you to create proof of e-voting.
5. To generate the proof of e-voting, you must find the user in the Act of opening and have registered their electronic vote.
6. Once approved the above steps generates the final act and demonstrates the results.

8. Discussion

E-voting is an alternative used in few countries of Latin America and in Ecuador even these proposals not materialize by lack of decision or budget or mistrust in the political parties. With a good program, following protocol, their implementation could guarantee security, speed and efficacy, before, during and after the electoral process.

All voting system either digital or traditional will need prerequisites for its execution. However, there is a voting system that provides the security and integrity of the information; most, however, there are aspects which may be taken into consideration so as to prevent certain attacks.

In accordance with article "e-voting considerations" Miguel Montes, Daniel Penazzi and Nicolás Wolovick quoted in Nardi & Maenza, mentioned several requirements for the use of electronic voting and their respective security measures:

1. Reinsurance Individual, i.e. that not disclosed the identity of the voter.
2. Transparency, meaning that access to the code must be opened in such a way that any person can be inspected by other.
3. Separation of functions, i.e. the electronic count must be carried out by another different machine.
4. Non-electronic auditability, the vote must be printed on a paper in machine-readable form for all persons for verification and possible conduct of audit.
5. Independence of voter identification, i.e. that the identification of the elector occurs independently to the electronic ballot box.
6. Protection against unauthorized, i.e. readings that there is protection against attacks that want to be from some other device, whether this person or not.
7. Backup of keys [15].

These suggestions proposals are relevant to the proper use of the electronic medium. There is extensive coverage in relation to the information and the care of the system, but it will be necessary to maintain updated programs.

In a complementary manner, it is suggested to complete security architecture, adding an audit during the process, allowing you to monitor the compliance of each stage of scrutiny, this is relevant, at the discretion of specialists that may emit criteria to the logs of information that has been used.

9. Conclusions and Future Works

9.1. Future Works

Design of security measures in the voting systems that provide immediate feedback to the user in case present a computer plagiarism in your vote.

Audit of security technology, allowing to go to monitor the implementation of phases during electoral processes.

9.2. Conclusions

E-voting requires a security architecture that allows to avoid that the citizen decision be changed to benefit of any candidate. For this, you must set the fulfillment of the articulated law, which consists of the Constitution of Ecuador, also is needed to implement technological structures effective, with symmetrical or asymmetrical, encryption systems that prevent the manipulation of results, using the Diskcryptor software; Finally the participation of public bodies in the company of international participants will audit stages of scrutiny and give its approval to the processes and the different mechanisms implemented in the votes, which handles the electoral institution of the nation.

As indicated us Aguilar soul: analyzing the reasons for voting, are mostly reasons of trust, usefulness and interest. Level country established themselves confidence and technical reasons. These contrast with their respective visions of the situation in the country [16]. But electronic voting is not yet run, used modern technological structures in the count, and communication of results.

Acknowledgment

The authors thank the University Politécnica Salesiana of the Ecuador, to the research group of the headquarters of Guayaquil "Computing, security and Informatics for a globalized world" (CSITGW) created in accordance with resolution 142-06-2017-07-19 and the Secretariat education higher science, technology and innovation (Senescyt).

References

[1] S. L. Pacheco, "towards electronic voting in the State of Mexico electoral practice: elementary considerations," pp. 51-81, 2015.
[2] M. e.. García Barrera, "paperless Court, one step of the e-Justice TT - Paperless Courts, One More Step of Electronic Justice," Rev. IUS, vol. 12, no. 41, pp. 133-154, 2018.
[3] Constitución de la República del Ecuador. (s.f.). Organización de los Estados Americanos. Obtenido de https://www.oas.org/juridico/mla/sp/ecu/sp_ecu-int-text-const.pdf.
[4] J. F. Aguirre Sala, "The potential of digital media to traditional civic participation and in the participatory budget", new era, no. 22, pp. 211-229, 2014.
[5] P. A. Quesada, "Costa Rican vote abroad: a new national challenge," pp. 85-112, 2013.
[6] V. Loya, "reflections / REFLECTIONS."
[7] P carolina, G. Legorreta, P. Carolina, and G. Legorreta, "available at: http://www.redalyc.org/articulo.oa?id=211032011004," 2014.
[8] M. Montes, D. Penazzi, and N. Wolovick, "Considerations on the vote electronic," 10° Simp. about computer science in the State, pp. 297-307, 2016.

[9] H. A. Charles Leija, A. J. Torres García, and L. M. Colima Valadez, "socio-demographic characteristics of the voting members by 2015: an analysis of spatial Econometrics," Rev. Col. San Luis, vol. 8, no. 17, p. 107, 2018.
[10] J Schmidt-Peralta y J. Gutierrez - Alfaro, "towards the development of a prototype system of electronic voting for Costa Rica," Rev. Tecnol. in March, vol. 29, no. 3, p. 146, 2016.
[11] M. O. Gómez, "Vote of the Mexicans in the outdoors," Mexico before and after political alternation, pp. 133-138, 2018.
[12] J T. Places Chungat, E. R. Portilla Lopez, o. D. León Granizo, and M. Botto-Tobar, "reliability and considerations of electronic voting, a global vision", J. Sci. Res. Rev. Cienc. e research., vol. 2, no. 5, pp. 26-38, 2017.
[13] S. Bast, "model of data of the system of voting electronic classroom OTP-Vote", pp. 23-37.
[14] P Garcia, G. Montejano, S. Bast and E. Fritz "Seguridad Incondicional para el Anonimato en Sistemas de e-Voting", pp. 2-5.
[15] J. Leandro and r.. Rita, "electronic voting, vulnerabilities and solutions to prevent attacks," pp. 61-71.
[16] D. E. Aguascalientes, A. Lilia, S. Aguilar, C. Gutiérrez, L. Cristina, and P. Howlet, “Electronic voting : reliability and implementation of technology,” pp. 77–83, 2017.

ASTES

Advances in Science, Technology and Engineering Systems Journal Vol. 4, No. 4, 300-307 (2019)

www.astesj.com

Special Issue on Advancement in Engineering and Computer Science

ASTESJ

ISSN: 2415-6698

Investigating The Detection of Intention Signal During Different Exercise Protocols in Robot-Assisted Hand Movement of Stroke Patients and Healthy Subjects Using EEG-BCI System

Maryam Butt*,[1], Golshah Naghdy[1], Fazel Naghdy[1], Geoffrey Murray[2], Haiping Du[1]

[1] *School of Electrical Computer and Telecommunications Engineering, University of Wollongong (UOW), 2522, Australia*

[2] *School of Medicine, University of Wollongong (UOW), 2522, Australia*

Article history:
Received: 17 May, 2019
Accepted: 20 July, 2019
Online: 07 August, 2019

Keywords:
Intention detection
EEG
Brain-computer interfaces
MRCP
AMADEO hand robot
Support vector machines
Stroke

A B S T R A C T

Improving the hand motor skills in post-stroke patients through rehabilitation based on movement intention derived signals from the brain in conjunction with robot-assistive technologies are explored. The experimental work is conducted using Electroencephalogram based Brain-Computer Interface (EEG-BCI) system and the AMADEO hand rehabilitation robotic device. Two protocols using visual-cues and then using a 2-Dimensional (2D) interactive game is presented on a computer screen to healthy subjects as well as post-stroke patients performing the hand movements. The movement intention signals during hand movement are detected through the Support Vector Machine (SVM) classifier. The intent signals produced at six distinct electrodes are investigated to determine electrodes contributing most to the SVM classifier's performance. Overall, the game protocol shows better classification results for both healthy and stroke patients compared to the visual-cues protocol. FC3 is found to be the most consistent electrode site for the detection of the motor intention of the hand for both protocols. In the experimental work, average classification accuracy for the visual-cues protocol of 67.56% for healthy subjects and 56.24% for stroke patients were obtained. For the game protocol, the classifier accuracy produced for healthy participants was 79.7% and for the post-stroke patients was 66.64%. The results confirm that the intention signal is more pronounced during more engaging activities, such as playing games, for both healthy and stroke subjects. Therefore, the effectiveness of rehabilitation therapy for post-stroke patients could be significantly enhanced using interactive and engaging exercise protocols.

1. Introduction

This paper is an extension of work presented in 18th IEEE International Conference on Bioinformatics and Bioengineering (BIBE) [1]. Stroke is the main cause of prolonged disability among adults [2]. The most common impairment occurs when a stroke victim has a motor loss of limb(s) on one side of the body causing difficulty with walking and ability to perform activities of daily living. There are many types of rehabilitation therapies currently being practiced, and others being investigated. One of the therapies types being investigated and coming into clinical practice is Robot-Assisted therapy. Advancement in robotic technology over the last decade has led to increasing interest in this type of therapy. For example, Ang et al. [3] used the MIT-Manus robot for a randomized control study with 26 stroke patients to restore their arm movement. Similarly, a haptic knob robot is being used for arm rehabilitation of stroke survivors with positive outcomes [4]. A state-of-the-art robotic device called AMADEO, designed for fine finger motor skill improvement was tested on eight cortical stroke patients and resulted in a 35% increase in their hand movement after multi-session training [5]. All these strategies of post-stroke rehabilitation depend on some neurological adaption that occurs in the patient's brain to restore the impaired function of the limb. The brain's ability to adapt to new neural changes, even in adulthood, is called the neuroplasticity or brain plasticity [6].

Brain-Computer Interface (BCI) has an ability to utilize neuroplasticity mechanisms to improve motor function of post-stroke patients during their rehabilitation process [7]. Enhanced motor intention improves motor execution which in turn is fed back to the rehabilitation process. The mechanism of neuroplasticity reinforces the neural pathways which control the movement, leading to functional and motor recovery of the

*Corresponding Author: Maryam Butt, mb077@uowmail.edu.au

patients [8]. Brain signals that have been used in BCI systems include Electroencephalogram (EEG), Magnetoencephalography (MEG), ElectroCorticoGraphy (ECoG), as well as functional Near-InfraRed Spectroscopy (fNIRS). Amongst these modalities, EEG is the most common modality employed to drive various BCI systems [9]. It is popular because it is not an invasive approach to record the brain's electrical activities, and because EEG signals have the highest resolution in time-domain [10].

Many studies demonstrate applications of EEG-BCI systems to detect movement intention for various upper-limbs, such as movements of the arm [11-15], elbow [16], [17] and wrist [18] and hand [19-23] for post-stroke rehabilitation.

A self-paced reaching arm movement with the help of a haptic device has been studied in [11] and [12]. In a single-trial EEG protocol, the intention of reaching movement was detected about 500 ms before the actual limb movement [11]. In the follow-up study, the movement directions were decoded up to 76% accuracy for healthy subjects and up to 47% accuracy for stroke patients performed with their impaired arm [12]. Ibanez et al. [13] recruited six healthy subjects and six stroke patients to detect the movement onset of voluntary arm reaching action. The results showed that the True Positive Rate (TPR) of the classifier for healthy participants was 74.5±13.8% while for stroke patients, TPR was 82.2±10.4%. In another study, four chronic post-stroke patients participated in eight training sessions based on arm reaching actions [14]. The intention for the movement was decoded using an EEG-BCI system which then triggered Functional Electrical Stimulation (FES) for further assistance to perform the task. The authors stated that their protocol correctly classified about 66% of movements with an average detection latency of 112±278 ms. Moreover, clinical tests and kinematics results proved the feasibility of the designed intervention for post-stroke recovery.

Among many classifiers, Support Vector Machine (SVM) classifier is commonly used in intent detection of limb movement. For example, Frisoli et al. [15] proposed a gaze-based robot-assisted arm movement protocol in which the real-time movement of a robotic device was controlled by the intended signal of subjects. A Motor Imagery (MI) based EEG-BCI system was used to detect the intention signal through SVM. The authors reported a classification accuracy rate of 89.4±5% for robot-based movement mode. Similarly, Hortal et al. [16] measured the classification performance of SVM by designing a hybrid EEG-BCI system composed of an exoskeleton device and FES for elbow movement. The hybrid BCI system was tested using two training protocols which were MI-based training protocol and a training protocol based on motor intention detection. In the first training protocol, the authors achieved a classification accuracy of about 83% for healthy subjects and 65.3% for stroke patients, while in the second training protocol, the accuracy achieved was approximately 77% and 71.6% for healthy and patient groups, respectively.

Asynchronous EEG-BCI systems are also being deployed for motor intent detection of upper limbs. The triggering of a robotic device through intention signal was studied by Bhagat et al. [17] for elbow joint movement using an asynchronous EEG-BCI robot-assisted system. The motor intent signal of four chronic stroke patients was detected which then triggered an exoskeleton device called MAHI-EXO-II to encourage and guide the active participation of subjects. The intention signal was detected on average −367±328 ms before the actual motor execution. Bai et al. [18] also developed an asynchronous BCI protocol for real-time and online prediction of the self-paced movement of the wrist. Seven healthy subjects were recruited in the study to perform an extension of their wrist whenever they wanted. The authors successfully predicted the voluntary movement at approximately 0.6 s before the real execution of the movement.

The latest applications of EEG-BCI systems have been in detecting intention for movement of the hand, which has a greater complexity of movement than other upper limbs. The hand occupies the largest cortical representation in the motor cortex of the brain [24] as well as playing the most vital role in our daily life activities. Muralidharan et al. [19] distinguished resting state from the extension of fingers by using an open-loop EEG-BCI system. They detected attempted finger extension by post-stroke patients at about 200 to 600 ms before the actual movement onset. Only one EEG channel has been used by Jochumsen et al. [20] to detect motor intent signal during palmar grasp action using handgrip dynamometer. The signal was then decoded into speed and force. They showed that approximately 75% of the movements were detected 100 ms before movement onset, and approximately 60% of task-related movements were accurately decoded into the force and speed levels according to the performed task movements. In a separate study, Jochumsen et al. [21] also distinguish between the intention for three types of grasp tasks (palmar, pinch and lateral) achieving accuracy of 79%, 76%, and 63% respectively during 1-class, 2-class and 3-class classification problems. Ofner et al. [22] classified several arm movements which include hand-opening, hand-closing, forearm supination, forearm pronation, elbow extension as well as elbow flexion. The authors state that one movement can be classified from another with 55% classification accuracy. This research group achieved the classification accuracy of 93% while classifying grasping actions of hand from its rest state compared to the classification results stated by Jochumsen et al. in [21] [23].

In this study, we combine detection of motor intention signals using EEG-BCI system with robot assistive technologies to improve the effectiveness of the hand motor skills in post-stroke patients. Our first stage of research based on an EEG-BCI system and the AMADEO finger-hand rehabilitation robotic device (Tyromotion GmbH, Graz, Austria) is reported. The experimental setup is designed for classification of movement intention of hand-closing versus rest state. It consists of two distinct protocols, which we refer to as protocol A and protocol B. Protocol A, termed as visual-cues protocol, consists of hand-opening and hand-closing pictures which are presented to subjects. In protocol B subjects played an AMADEO game called Shoot-out. We utilize SVM, which is the most common supervised learning algorithm used for these classification problems. Intention signal produced at different single electrodes' positions during hand movement is analyzed to determine the electrode that is most consistent for the accuracy of SVM classifier.

The rest of the paper is organized as follows. In section 2, the experimental platform and experimental set up are introduced. In section 3, the pre-processing of the signals produced in the experimental work and the classifications method, the classification performance metrics are described. In section 4, the

results of the validation of the approach on stroke patients and benchmarking against the healthy subjects are presented. Some conclusions are finally drawn in section 5.

2. Experimental Design and Platform

2.1. Participants

The participants in the experimental work consisted of healthy subjects and post-stroke patients. The healthy subjects consist of four male participants with a mean age of 28 years and no history of any neurological disorder. Two post-stroke patients both right hand dominant were initially assessed through two commonly used clinical tests, namely the Motor Assessment Scale (MAS) and Fugl-Meyer Assessment (FMA) scale. Table I shows each patient's demographic details as well as their clinical tests scores. The Ethics committee at the University of Wollongong approved all methods and procedures performed in this experiment (Ethics application number: 2014/400). All participants provided written informed consent before this study commenced.

2.2. AMADEO Finger-Hand Rehabilitation Device

The AMADEO finger-hand rehabilitation device is an end-effector robot-assistive system specifically developed for hand movement recovery of post-stroke patients as shown in Figure 1 [25]. It has five Degrees-of-Freedom (DoF) allowing both passive and active movements of fingers as well as the thumb. The robot can generate various patterns of fingers and thumb movements as well as subjects can interact with the robotic device through 2D games.

(A) (B)

Figure 1: (A) AMADEO Finger-Hand Rehabilitation Unit (B) Hand-Arm Adjustment Support

2.3. Acquisition of EEG Signal

The EEG signals were acquired by deploying a 32 electrodes Ag/AgCl Quick-Cap (Compumedics-Neuroscan) in accordance to the 10-20 system for positioning electrodes. The electrode positioning diagram of the Quick-Cap is given in Figure 2. The Grael 4K EEG amplifier was employed in this study which has been set to 2048 Hz of sampling frequency. Of the 32 channels, the FPz electrode was used as the ground electrode and the CPz was set as the reference electrode. Thirty remaining electrodes were used for the acquisition of brain signal. In addition, the two electrodes were placed below the left eye and on the supraorbital ridge to record vertical eye movements and eye-blinks. Moreover, two other electrodes placed over the outer canthus of both eyes were used to monitor horizontal movements of eyes.

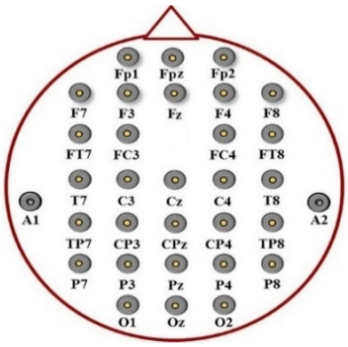

Figure 2: Quick-Cap Electrodes Positions

2.4. Experimental Setup

Participants were seated upright on a comfortable chair with their right arms attached to the AMADEO hand-arm adjustment support unit. During protocol A, each participant was trained to focus on visual-cues displayed on a computer screen. Visual-cues displaying hand-opening and hand-closing pictures to alert subjects to perform these specific hand movements. The hand-closing pictures were displayed every 5 s, followed by the hand-opening pictures 1 s later with a 4 s waiting period. This resulted in 5 s gap between any two hand-closing visual-cues. Each set comprised 23 trials of hand movements during this protocol.

Of the games available on the AMADEO system, the 'Shoot-out' was chosen for use in protocol B. The playing screen of Shoot-out game is shown in Figure 3. In this game, the subject closes their hand to shoot the drum coming out at equal time intervals. Subjects have up to 23 trials of the hand movements in each block.

Figure 3: AMADEO Shoot-out Game

Table 1: Stroke Patients' Details and Clinical Test Scores

Gender	Age	Stroke type	Time since stroke (months)	Lesion location	Paretic Hand	MAS Hand Score (0-6)	FMA Hand Score (0-14)
Female	64	Ischemic	7	Left pons	Right	2	9
Male	60	Ischemic	4	Left pons & left frontal regions	Right	2	8

All participants performed 6 blocks consisting of 23 trials (6 x 23 = 138) for both protocols. At each hand-closing event, manual event markers were sent to the CURRY 8 (Compumedics, Neuroscan) software which was used for EEG acquisition. Protocol B was the Shoot-out game of AMADEO, which was more interesting and interactive compared to protocol A. We explored the hypothesis in this study that whether a stronger motor intention signal can be produced and detected through SVM during protocol B than protocol A.

3. Signal Processing for Motor Intention Detection

The intention signal during hand-closing movements was detected by offline analysis of the data for both healthy and stroke subjects. The movement intention of a limb produces special EEG patterns in specific parts of the brain and such slow event-related potential is called Movement Related Cortical Potential (MRCP). It appears in the delta frequency band of EEG signal as a direct-current shifts up to 2 s prior to cue-based as well as self-initiated movements [26]. When the person performs the required motor action, the MRCP disappears. The continuous EEG signal at the selected electrodes is divided into two types of epochs. The first, containing MRCP signal is called Move epoch and the second, which does not have an MRCP signal, is named as No-Move epoch. Different time-domain features of MRCP signal are extracted from both these epochs. SVM algorithm is then employed to classify Move and No-Move epochs and, therefore, detecting intention signal of the hand movement.

3.1. Pre-processing

The first step in pre-processing is to filter the EEG signal for the frequency range between 0.1-1 Hz [17] as this narrow range of delta band best captures the anticipatory based MRCP [27]. This band-pass filtering was applied in three steps: first, a high-pass filter with cut-off frequency (f_c) of 0.1 Hz was applied; second, for re-referencing of signals, a Common Average Reference (CAR) filter was applied to all signals; and third, a low-pass filter with f_c of 1 Hz was applied. Both low-pass and high-pass filters were 4th order Butterworth causal filters. After filtering, the signals were down-sampled from 2048 Hz to 20 Hz to increase computational efficiency [17]. The CURRY 8 (Compumedics-Neuroscan) software was used to perform all the aforementioned pre-processing steps.

3.2. Epoch Extraction & Channel Selection

For further processing, the data were imported into a MATLAB toolbox known as 'EEGLAB'. Generally, MRCP signal does not exist 2 s before the onset of movement, all Move epochs were extracted from continuous EEG data between -2 s to 0 s with 0 s indicating the instance of actual motor execution. Between 0.5 s to 2.5 s, No-Move epochs were extracted when subjects opened or relaxed their hands. Therefore, epoch length was fixed at 2 s for both epochs. All Move epochs were inspected visually for artifacts, for instances eye-blinks, head movement, and other movement-related artifacts, and then these were removed from the data.

The EEG electrodes located over the left hemisphere of the brain were only chosen because the right-hand movement was considered in this experiment. The electrodes selected were C3, FC3, CP3, Cz, T7 and a Short Laplacian (SL) channel calculated using the C3-(FC3+Cz+CP3+T7)/4 formula [28]. In literature, the C3 channel is most commonly used for right-hand motor intention detection using the MRCP signal. The four neighboring electrodes of the C3 channel and their linear combination were also investigated to determine the best electrode choice for each protocol. It is possible that the negative peak of the MRCP exists before -1.5 s is due to artifact presence. Therefore, every Move epoch was again visually inspected and such Move epochs and their counter-part No-Move epochs were deleted to get the final processed data which was then used to extract features of MRCP signal.

3.3. Feature Extraction & Classification

The two time-domain features from both the Move and No-Move epochs were extracted. These features were the negative peak and the slope of the MRCP signal. The Move epochs have prominent negative peak and slope of MRCP signal compared to No-Move epochs. Based on these time-domain features, the SVM classifier differentiates between both epochs. These were plotted and outliers were removed (along with their counter-class features) before applying the SVM. This prevented biasing the results of SVM due to outliers. In each protocol, an average of 10±2 epochs was rejected per subject. The Move class was marked with a label of '1' and the No-Move class was marked with a label of '0'. Depending on these input features, the SVM classified between class 1 and 0. Three-fourths of the dataset was utilized for training data while one-fourth was used as test data for classification.

3.4. Evaluation of SVM Classifier Performance

The SVM classifier's performance was determined based on classification accuracy percentage, True Positive Rate (TPR)–also known as sensitivity and True Negative Rate (TNR)–also called specificity. They were calculated using the relationships given in (1), (2) and (3) where True Positive, False Positive, True Negative and False Negative were abbreviated as TP, FP, TN, and FN respectively.

$$\text{Accuracy}=(TP+TN)/(TP+TN+FP+FN) \quad (1)$$

$$TPR=TP/(TP+FN) \quad (2)$$

$$TNR=TN/(TN+FP) \quad (3)$$

Receiver Operating Characteristics (ROC) curve was analyzed to determine the classifier's performance during protocol A and B. Moreover, Area Under the Curve (AUC) for the ROC curve was calculated for both protocols. In the end, all these performance metrics were compared to find out which protocol helps better to maintain stronger motor intention level in both healthy subjects and stroke patients and therefore, obtaining better classification results. In addition, these results also could show which electrode was the best choice for intent detection during protocol A and protocol B.

4. Results & Discussion

The experimental work demonstrated the utility of the AMADEO device for rehabilitation of post-stroke patients, while also performing the motor intention detection using the described SVM algorithm.

Six electrodes which include C3, FC3, CP3, Cz, T7, and SL were chosen to determine the importance of electrode selection in intent detection during each protocol. Performance metrics were calculated after the SVM application on test data, including classification accuracy, TPR, TNR and AUC for ROC.

4.1. Intent Detection of Stroke Patients

The performance of the SVM algorithm for detection of hand motor intention signal produced by the stroke patients is studied in this sub-section. Table II presents the accuracy of the SVM classifier at all six selected electrodes for protocols A and B. For protocol A, the FC3 electrode shows the maximum accuracy of the SVM classifier of about 72%. Whereas, the same electrode shows classification accuracy of 89% for intent detection when stroke patients perform the hand movement during protocol B. This supports our hypothesis that during protocol B, subjects are more involved in performing hand movement and are likely to have greater classification accuracy as compared to protocol A. The same trend is demonstrated by the results of C3, CP3, T7, and SL electrodes. However, for electrode Cz, protocol B is showing lower classifier's accuracy than that for protocol A. The list of electrodes based on the classification accuracies from high-to-low for protocol A is FC3, Cz, SL, C3, T7, and CP3. A similar list for the protocol B is FC3, SL, C3, CP3, T7, and Cz. It is clear from the classifier accuracy results that for both protocols, FC3 shows the maximum classifier performance. However, for protocol B the classifier's accuracy is higher than that for protocol A at all electrode sites except Cz.

4.2. Intent Detection of Healthy Subjects

The results of the classifier accuracy for healthy subjects for protocols A and B are presented in Table III. The analysis of data for healthy subjects shows that protocol B has better accuracy of SVM classifier than protocol A, except for the channels Cz and T7. With respect to the results acquired for FC3, protocol B has an accuracy of SVM classifier of 98% while the classification accuracy of protocol A is 86%. From Table III, it is clear that the classifier's accuracy varies in accordance with the selected electrode. For protocol A, the electrodes can be listed as FC3, Cz, C3, T7, SL, CP3 electrodes can be ranked in order of their effectiveness in determining the intent signal. Similarly, for protocol B, the ranking is FC3, C3, SL, CP3, Cz, T7.

Table 2: Accuracy of SVM Classifier for Post-Stroke Patients

Channel	SVM Classifier's Accuracy (%)	
	Protocol A	Protocol B
C3	52.88	81.01
CP3	26.25	60.16
FC3	72.22	88.89
Cz	70.45	34.56
T7	49.29	51.43
SL	66.33	83.78

Table 3: Accuracy of SVM Classifier for Healthy Subjects

Channel	SVM Classifier's Accuracy (%)	
	Protocol A	Protocol B
C3	64.58	92.86
CP3	57.7	76.3
FC3	86.25	98.0
Cz	73.81	70.0
T7	63	57.69
SL	60.0	83.33

When the Cz electrode from stroke patients' data as well as the Cz and T7 electrodes from healthy subjects' data were chosen, protocol A had slightly better classification accuracy than protocol B. There could be many possible reasons for this apparent contradiction. The artifact removal is performed using visual inspection method so it might be possible that the data at Cz and T7 electrodes still contain some artifacts in the test data used for protocol B that made the classifier accuracy for protocol B less than protocol A. Moreover, the outlier values removal form Cz and T7 electrodes might cause loss of large data points for protocol B and due to fewer test data values, the performance of protocol B has deteriorated.

4.3. Other Performance Metrics of the SVM Classifier

The accuracy alone cannot justify the performance of the classifier, therefore, sensitivity (TPR) and specificity (TNR) parameters should be also considered. The TPR and TNR values show whether the extracted features in Move and No-Move classes are distinct enough to be classified accurately by SVM. Figure 4 shows bar graph representations of TPR and TNR using stroke patients' data from protocol A at all six electrodes. Similarly, Figure 5 shows TPR and TNR values at all selected electrodes for protocol B. For protocol A, Figure 4 shows that

TNR for CP3, FC3, Cz, and SL is significantly lower than its corresponding TPR. On the other hand, in the case of T7, TNR is slightly higher and slightly lower for C3. However, for protocol B, TNR is higher than TPR for each choice of electrode except for CP3 and T7 as shown in Figure 5.

Similarly, TPR and TNR values using data of healthy subjects for both protocols is shown in Figure 6 and Figure 7. In the case of protocol A, Figure 6 demonstrates that TPR obtained for C3, Cz and FC3 is higher than its corresponding TNR, whereas, for CP3, T7, and SL, the reverse is the case. Figure 7 shows that TPR, for all six electrodes, is higher than its corresponding TNR for protocol B indicating that the Move class contains the adequate features to correctly detect motor intention signal.

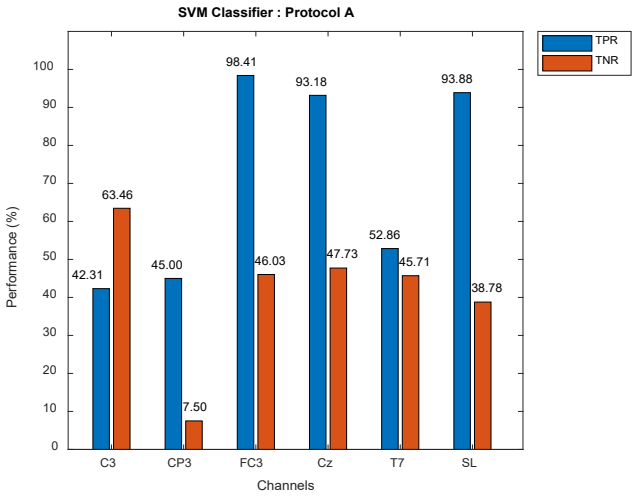

Figure 4: Protocol A Stroke Patients Data

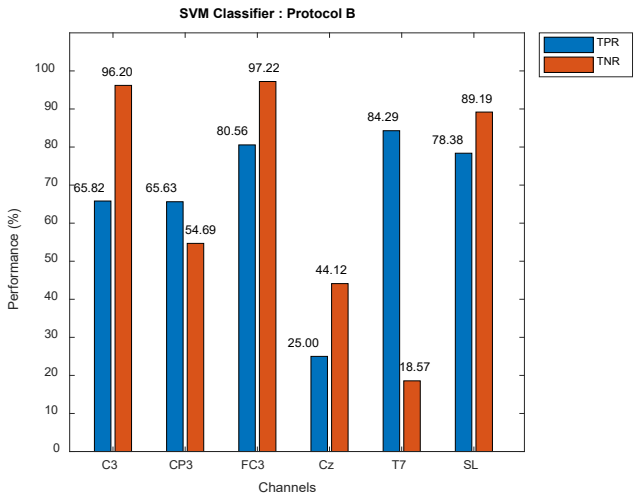

Figure 5: Protocol B Stroke Patients Data

ROC curve is another way of comparing the performance of the SVM classifier for protocols A and B. Figure 8 shows the ROC curve for the FC3 channel, the most appropriate channel for intent detection of hand movement for this experiment, for healthy participants which shows that protocol B has superior performance.

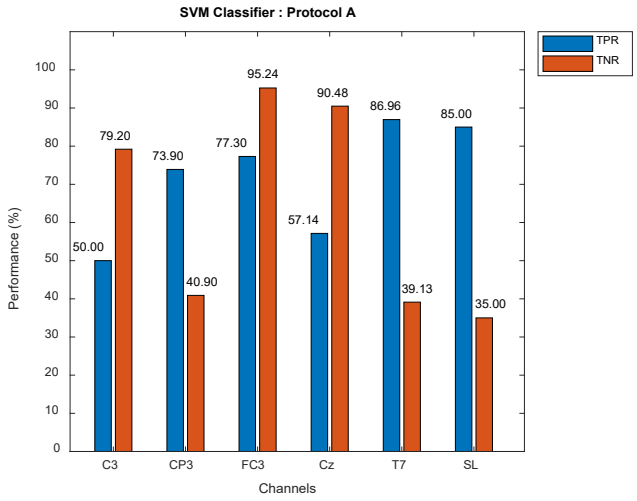

Figure 6: Protocol A Healthy Subject Data

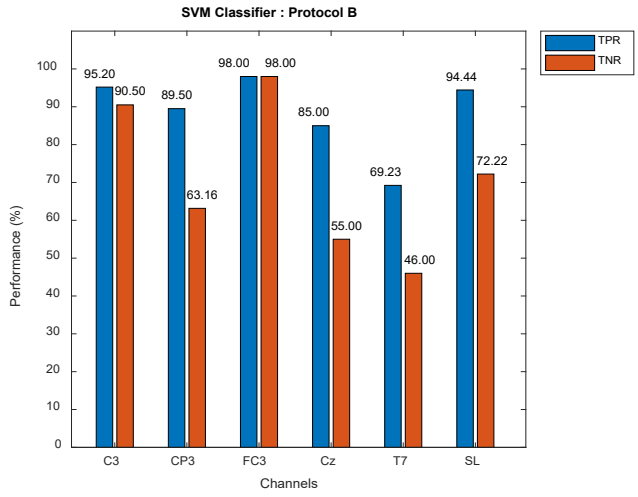

Figure 7: Protocol B Healthy Subject Data

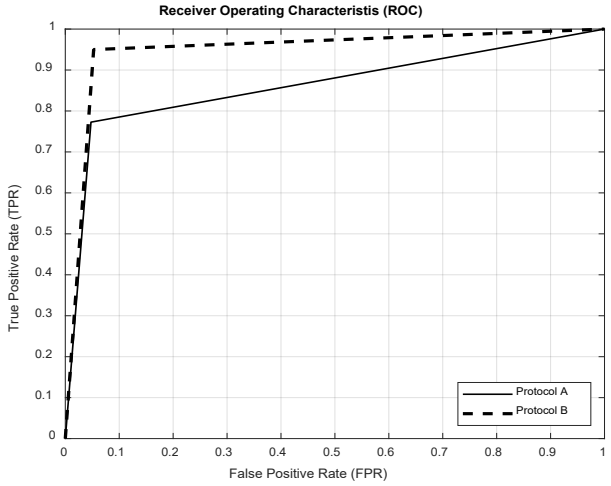

Figure 8: ROC Curve Using FC3 Channel

The Area Under the Curve (AUC) for ROC is also an important factor in assessing the classifier performance. The excellent classifier has an AUC value of 1 whereas 0.5 value

shows its random guessing behavior. The AUC values for FC3 channel for both healthy subjects and stroke patients are listed in Table IV. It is found that AUC for protocol B is greater than protocol A for both healthy subjects and stroke patients which was the expected outcome. Moreover, AUC value for protocol B in the healthy group is ~0.95 which is approximately equal to ideal AUC value for the classifier.

Table 4: Area Under the ROC Curve for FC3 Channel

Group	AUC for FC3 Channel	
	Protocol A	Protocol B
Stroke	0.7222	0.8889
Healthy	0.8626	0.9487

5. Conclusion

The utilization of EEG-BCI system together with AMADEO robotic rehabilitation system for the functional recovery of the hand of the post-stroke patients was reported as the first stage of our work. The movement intention for both healthy participants as well as post-stroke patients was detected using SVM classifier. Two protocols that were based on simple visual-cues and the AMADEO 2D game were used to detect the hand-closing movement intention vs the resting state. This was followed by an evaluation of the SVM classifier performance by selecting different single electrodes. The average classifier accuracy of 67.56% for the visual-cue protocol and 79.7% for the gaming protocol was achieved for healthy subjects. Similarly, for stroke patients, the classifier accuracy obtained was 56.24% and 66.64% for the visual-cue and the game protocols respectively. The results demonstrated that the 2D games, for example, AMADEO Shoot-out were better activities in retaining concentration compared to static pictures using visual-cues. We conclude that gaming scenarios are preferable for robot-based rehabilitation exercises to promote the active participation of the patients. The FC3 electrode was found to be the best single electrode for the designed experiment with both protocols. Both TPR and TNR were important in determining the performance of the classifier, as these parameters could indicate whether good results of the classifier were obtained either by detecting positive class or negative class accurately. In addition to TPR and TNR, it was shown that the ROC plot and AUC parameters of the classifier could also be used as the performance metric evaluators for the classifier.

Conflict of Interest

There is no conflict of interest among authors.

Acknowledgment

This work is performed by joint support by The University of Wollongong and Higher Education Commission (HEC) Pakistan.

References

[1] M. Butt, G. Naghdy, F. Naghdy, G. Murray, and H. Du, "Investigating Electrode Sites for Intention Detection During Robot Based Hand Movement Using EEG-BCI System," in 2018 IEEE 18th International Conference on Bioinformatics and Bioengineering (BIBE), 2018, pp. 177-180: IEEE.

[2] J. Adamson, A. Beswick, and S. Ebrahim, "Is stroke the most common cause of disability?," Journal of stroke and cerebrovascular diseases, vol. 13, no. 4, pp. 171-177, 2004.

[3] K. K. Ang et al., "A Randomized Controlled Trial of EEG-Based Motor Imagery Brain-Computer Interface Robotic Rehabilitation for Stroke," Clinical EEG and Neuroscience, Article vol. 46, no. 4, pp. 310-320, 2015.

[4] K. K. Ang et al., "Brain-computer interface-based robotic end effector system for wrist and hand rehabilitation: Results of a three-armed randomized controlled trial for chronic stroke," Frontiers in Neuroengineering, Article vol. 7, no. JUL, 2014, Art. no. 30.

[5] X. Huang, F. Naghdy, H. Du, G. Naghdy, and G. Murray, "Design of adaptive control and virtual reality-based fine hand motion rehabilitation system and its effects in subacute stroke patients," Computer Methods in Biomechanics and Biomedical Engineering: Imaging & Visualization, vol. 6, no. 6, pp. 678-686, 2018.

[6] B. B. Johansson, "Brain plasticity and stroke rehabilitation: the Willis lecture," Stroke, vol. 31, no. 1, pp. 223-230, 2000.

[7] U. Chaudhary, N. Birbaumer, and A. Ramos-Murguialday, "Brain–computer interfaces for communication and rehabilitation," Nature Reviews Neurology, vol. 12, no. 9, pp. 513-525, 2016.

[8] M. Grosse-Wentrup, D. Mattia, and K. Oweiss, "Using brain–computer interfaces to induce neural plasticity and restore function," Journal of neural engineering, vol. 8, no. 2, p. 025004, 2011.

[9] H.-J. Hwang, S. Kim, S. Choi, and C.-H. Im, "EEG-based brain-computer interfaces: a thorough literature survey," International Journal of Human-Computer Interaction, vol. 29, no. 12, pp. 814-826, 2013.

[10] J. S. Kumar and P. Bhuvaneswari, "Analysis of Electroencephalography (EEG) signals and its categorization–a study," Procedia engineering, vol. 38, pp. 2525-2536, 2012.

[11] E. Lew, R. Chavarriaga, S. Silvoni, and R. Millan Jdel, "Detection of self-paced reaching movement intention from EEG signals," (in eng), Front Neuroeng, vol. 5, p. 13, 2012.

[12] E. Y. L. Lew, R. Chavarriaga, S. Silvoni, and J. D. Millan, "Single trial prediction of self-paced reaching directions from EEG signals," (in English), Frontiers in Neuroscience, Article vol. 8, p. 13, Aug 2014, Art. no. 222.

[13] J. Ibanez et al., "Detection of the onset of upper-limb movements based on the combined analysis of changes in the sensorimotor rhythms and slow cortical potentials," (in English), Journal of Neural Engineering, Article vol. 11, no. 5, p. 12, Oct 2014, Art. no. 056009.

[14] J. Ibáñez et al., "Low latency estimation of motor intentions to assist reaching movements along multiple sessions in chronic stroke patients: a feasibility study," Frontiers in neuroscience, vol. 11, p. 126, 2017.

[15] A. Frisoli et al., "A new gaze-BCI-driven control of an upper limb exoskeleton for rehabilitation in real-world tasks," IEEE Transactions on Systems, Man and Cybernetics, Part C (Applications and Reviews), vol. 42, no. 6, pp. 1169-1179, 2012.

[16] E. Hortal, D. Planelles, F. Resquin, J. M. Climent, J. M. Azorin, and J. L. Pons, "Using a brain-machine interface to control a hybrid upper limb exoskeleton during rehabilitation of patients with neurological conditions," Journal of Neuroengineering and Rehabilitation, vol. 12, Oct 2015, Art. no. 92.

[17] N. A. Bhagat et al., "Design and optimization of an EEG-based brain machine interface (BMI) to an upper-limb exoskeleton for stroke survivors," Frontiers in Neuroscience, Article vol. 10, no. MAR, 2016, Art. no. 122.

[18] O. Bai et al., "Prediction of human voluntary movement before it occurs," Clinical Neurophysiology, vol. 122, no. 2, pp. 364-372, 2011.

[19] A. Muralidharan, J. Chae, and D. Taylor, "Extracting attempted hand movements from EEGs in people with complete hand paralysis following stroke," Frontiers in neuroscience, vol. 5, p. 39, 2011.

[20] M. Jochumsen, I. K. Niazi, D. Taylor, D. Farina, and K. Dremstrup, "Detecting and classifying movement-related cortical potentials associated with hand movements in healthy subjects and stroke patients from single-electrode, single-trial EEG," Journal of neural engineering, vol. 12, no. 5, p. 056013, 2015.

[21] M. Jochumsen, I. K. Niazi, K. Dremstrup, and E. N. Kamavuako, "Detecting and classifying three different hand movement types through electroencephalography recordings for neurorehabilitation," Medical & biological engineering & computing, vol. 54, no. 10, pp. 1491-1501, 2016.

[22] P. Ofner, A. Schwarz, J. Pereira, and G. R. Müller-Putz, "Upper limb movements can be decoded from the time-domain of low-frequency EEG," PloS one, vol. 12, no. 8, p. e0182578, 2017.

[23] A. Schwarz, P. Ofner, J. Pereira, A. I. Sburlea, and G. R. Müller-Putz, "Decoding natural reach-and-grasp actions from human EEG," Journal of neural engineering, vol. 15, no. 1, p. 016005, 2017.

[24] A. Nakamura et al., "Somatosensory Homunculus as Drawn by MEG," NeuroImage, vol. 7, no. 4, pp. 377-386, 1998.
[25] Z. Yue, X. Zhang, and J. Wang, "Hand rehabilitation robotics on post stroke motor recovery," Behavioural neurology, vol. , 2017.
[26] H. Shibasaki and M. Hallett, "What is the Bereitschaftspotential?," Clinical neurophysiology, vol. 117, no. 11, pp. 2341-2356, 2006.
[27] G. Garipelli, R. Chavarriaga, and J. d. R. Millán, "Single trial recognition of anticipatory slow cortical potentials: the role of spatio-spectral filtering," in 2011 5th International IEEE/EMBS Conference on Neural Engineering, 2011, pp. 408-411: IEEE.
[28] D. J. McFarland, L. M. McCane, S. V. David, and J. R. Wolpaw, "Spatial filter selection for EEG-based communication," Electroencephalography and clinical Neurophysiology, vol. 103, no. 3, pp. 386-394, 1997.

ASTES

Advances in Science, Technology and Engineering Systems Journal Vol. 4, No. 4, 308-313 (2019)

www.astesj.com

Special Issue on Multidisciplinary Sciences and Engineering

ASTESJ

ISSN: 2415-6698

Enhancing Bodily Movements of the Visually Impaired Children by Airflow

Fang-Lin Chao[1,*], Hung-Chi Chu[2], Liza Lee[3]

[1]*Department of Industrial Design, Chaoyang University of Technology, Chaoyang University of Technology, 436, Taiwan R.O.C.*

[2]*Department of Information and Communication Engineering, Chaoyang University of Technology, 436, Taiwan R.O.C.*

[3]*Department of Early Childhood Development & Education, Chaoyang University of Technology, 436, Taiwan R.O.C.*

ARTICLE INFO

Article history:
Received: 22 June, 2019
Accepted: 02 August, 2019
Online: 07 August, 2019

Keywords:
Airflow
Interaction
Bodily movement
Visually impaired

ABSTRACT

This study involved three departments of teachers and students. The concept of the flow-motivated exercise implemented with a set of flow nozzles. A computer-controlled airflow with specific music introduced, and the motion responses from the participants were analyzed during the initial test and field study. During the initial examination, we adjusted the magnitude and distance setting of the flow and allowed the children to grab the air without music. Structural design, magnetic valve, and interface were implemented based on the insights from the initial test. The redesign performed in a sitting position to reduce the need for students to deviate from the location and fit for physical disabilities during exercise. Four times of visually impaired students were arranged to observe the changes in the movements of students after being guided by the airflow during the teaching process. The performance of the fourth week is better than the previous three weeks. Almost all blind children can make movements in the right position. The cross-domain cooperation experience was beneficial to the facility design.

1. Introduction

Most of the visually impaired education is established using state funds, and many subjects are integrated with the existing school to incorporate them into society. There are not many schools for the visually impaired students in Taiwan, and some children attend the school for the mainstream setting. Under the guidance of special education teachers, the content of the textbooks for visually impaired students is designed the same as the content for mainstream students.

The core curriculum includes compensatory or functional academic skills, orientation and mobility, social interaction, independent living skills, recreation and leisure skills, technology, and visual efficiency skills [1]. Some activities provided independent in dealing with his environment at a residential school. The students with visual impairment cannot comprehend the entire picture by extracting a lot of information. Visual impairment has complex experience with the spatial world. Study [2] involving fieldwork in everyday life situations to gain insight of their experienced. The allocation of limited instructional hours and the shortage of qualified specialists are significant factors that influence effective instruction.

*Corresponding Author: Fang-Lin Chao, flin@cyut.edu.tw

Experienced teachers are scarce; thus, teaching aid facilities have to be developed on an immediate basis. Teaching aids reduce the problem of repeated guidance and allow students to obtain knowledge in a safe environment. Specialized schools in Taiwan for the visually impaired accommodate students with multiple barriers, such as slow limb movements and cerebral palsy. We observed the activities of these students after class. The students do not have much language communication with each other. When they are bored, they lie on the table or unconsciously tamper with the objects around them. Therefore, the involvement of the management is required. Once the rhythm teaching aids are placed on the table, they are engrossed in playing with the device and have a will to explore (Figure 1). The major mode of teaching is oral instructions. Some students cannot keep up with the progress when they are not attentive. They can explore and feel based on the teacher's instructions by using teaching aids. Rhythm and music-related teaching aids help students, especially in terms of instrument appearance- and rhythm-related learning. Learning through teaching aids, which cannot be easily expressed in words, presented its unique benefits.

1.1. Physical education

The physical education classes of most students include competitive events, such as running, long jump, or ball-related

games. However, these types of games do not help in enhancing the skills required by the visually impaired students for living. Physical movement and rhythm are necessary skills for the visually impaired students to keep them healthy and to help them obtain higher self-confidence.

Figure 1: Behavior observation of visually impaired children in an ordinary kindergarten classroom with their teacher [3].

The performance of the visually impaired individuals in physical education is directly associated with the severity of visual impairment, activities performed, the ability to ambulate, and family attitudes [4]. Postmenopausal changes significantly decrease the body's mechanisms for maintaining postural stability. Another study [5] analyzes the effect of sensorimotor exercise on changes in postural stability of visually impaired women. "Late blind persons had a slower walking speed, shorter stride length, and the longer time of gait" [5]. Their gait represents an attempt to adapt to maintain a stable posture during walking.

We must know the students' characteristics (limitations, abilities, and needs) in physical education programs. A school should also be aware of the teaching burden. Visually impaired children face a barrier in being integrated into the general physical education classes [6]. These children display lower physical activity levels because of the lack of instruction and practice.

Teachers sometimes lack sufficient knowledge pertaining to the method of including students. Inadequate preparation, lack of appropriate equipment and curricula, and insufficient teaching hours caused dominant barriers. Consequently, children demonstrated delays in reaching developmental milestones. A sample of 125 visually impaired children was observed [7]. The self-personality and prosocial behavior of the children were explored with respect to their mobility training. The personality well-being and social ability are correlated with the ability to be mobile.

1.2. Actuator and sensor

Technology-assisted learning has been a trend in the recent years. People use many apps to explore data, and visually impaired students can expand the scope of activities and overcome physiological limitations through the assistive technology. A study [8] developed smart connected devices for playfulness by using littleBits and Loaded Dice. Authors conducted experiments using visually impaired students and engaged in playful exploration and investigated the extent of providing imaginative design concepts. Another study [9] provided a visually impaired user interface by using embossed two-dimensional patterns that can be read using haptic sensing. In [10], a researcher introduced a haptic device that can notice the presence of obstacles inside an environment. A prototype that was implemented using a short cane and an embedded smart sensing strategy was presented.

The engineers used senses other than the visual sense to transmit a message to the visually impaired. For example, tactile pressure, temperature field, airflow field, and sound can be reconsidered for such applications that are focused on the visually impaired people. When these applications are aimed at the visually impaired population, we must reduce the cost and complexity of the technology because a high price renders the technology unaffordable and a complicated technology cannot be used reliably.

Kraus [11] designed teaching tools that are appropriate for exploring the solar system and different astronomical subjects. The magnetic field, temperature drop, and airflow connector presented physical space for the visually impaired people. The availability of the tactile constellation presents apparent magnitudes and displays the star distribution in the Cassiopeia constellation.

1.3. Flow-Motivated Interactions

This study focuses on three considerations: (1) providing haptic attention of airflow, (2) encouraging natural response from children, and (3) engaging to relate the body motion based on the excitation. Although the target users are visually impaired children, ordinary people or the elderly can follow the rhythm and find the pattern to play. The flow-motivated game uses a set of flow nozzles that can generate segmented air flow through a compressor. An air compressor is readily available in a shop. The compressor increases the pressure in the air-intake system [12] and generates a mass flow. The intensity of the mass flow can be sensed by the skin.

The airflow should be sensed by the skin; however, a very strong airflow causes discomfort. A small pipe sends the jet stream, and the high-speed air stream simultaneously causes a concomitant acoustic field with a sharp sound. Moreover, the time required for a child to respond to the airflow by performing actual body action should be considered. The response to the airflow varies from person to person. Some people move in the direction of the airflow, and some people grab the source of the airflow. This design encourages a spontaneous response and does not force the user to respond in specific manner. When a user is not pressurized to act in a specific manner, he or she can easily respond spontaneously.

The third design consideration was engagement to relate the body motion based on the excitation. The stimulation of the airflow cannot be too frequent and unpredictable and within a reasonable reaction time. The rhythmic stimuli are matched with the rhythm of the tones, thus promptly providing airflow guidance while providing the advice using the sounds. We provided four–six airflow spouts at appropriate body parts. The upper body and the lower body have three spouts each. The airflow field of each spout could be felt and was used based on the position of the person standing.

2. Materials and methods

At initial test, we used four impingement spouts without music. Teacher controls the gas flow and let the children try to grab the air. The four heads are connected to the air compressor respectively, and we control the opening and closing of the airflow by hand. We need to understand the impact of the height, position, and distance of the nozzle on the child before design. Teacher fixed the spout with a height-adjustable bracket, which was initially located at the waist of the children.

During test the position was adjusted to avoid being touched. Students listen to the teacher's introduction before they start. We

found that at the beginning, they were a bit nervous and the action was not very casual. The mentality may be a bit like facing the exam, not in a state of play.

2.1. Initial test

The experimental design used four of airflow without music. Most subjects stood still in the center without body movement and facial expression at the beginning (Figure 2).

When the airflow came out from the four ventilators at the same time, subject A,C,E,F,G,K,L,M,N,O didn't move at all.

They stood still until the air stopped. (O-A,C,E,F,G K,L,M,N,O -0325-1,2,3,4) (O-A, C, E, F, G, K,L, M, N, O-0325-R)

When subject K, L, M, N, O felt the airflow, they didn't know how to move because they are too young.(I-0325-T)

A few subjects didn't do any movement but did smile. Subject B and D didn't do any bodily movement but a few seconds later, they started smiling. (O-B, D -0325-1, 2, 3, 4) (O-B, D -0325-R)

A few subjects didn't show any expression, but moved their hands. Subject B and D didn't do any bodily movement but a few seconds later, they started smiling. (O-H, I, J -0325-1, 2, 3, 4) (O-H, I, J -0325-R)

Figure 2: Initial test setup for evaluating how visually impaired children respond to gas spreading

2.2. Discussion of initial test

This test revealed some problems.

(1) Some children did not know how to respond and became frustrated. When the students asked "Why am I coming?", they intended to tell the teacher "what should I do in this situation?". Formal learning habits constrain the mood of participation.

(2) Although some children were attracted to the flow in the first few rounds, they became bored because the same motions were repeated. Simple physical movements allowed them to respond only mechanically. The lack of self-inherent motivation reduces their interest.

(3) Some children paid so much attention to others' opinions that they became distracted and began playing. The students should be integrated in the event with a relaxed mood.

(4) The airflow produces a sharp sound. The air flow must be moderate. The motor generated considerable noise when the air pressure of the air compressor reduced. Children can get scared because of the sudden changes in the outside world.

(5) We determined whether a garment blocks airflow and found that the students did not rely solely on the airflow sprayed on the skin. When the airflow ejected, the turbulence air generated a sharp sound. Visually impaired children are sensitive to hearing, and they can determine the source of the airflow based on the noise.

Design of Flow Control

For realizing a simplistic design and the lowest price for the visually impaired, we avoided the complicated design to reduce possible failures. A central computer with touch panel controls the progress of the song and direction of the gas. Figure 3 displays the structure of the system. In the concept proposal, we suggested that the ground has a pressure sensor to determine the user's position and that infrared sensors can be installed on the bracket to know how the user moves.

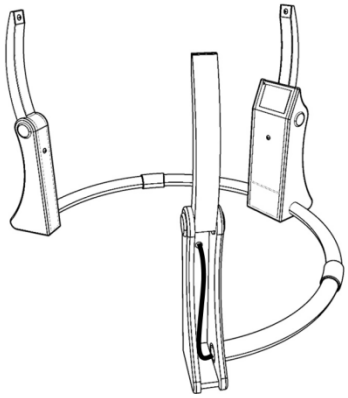

Figure 3: Diagram of the flow-motivated game with a magnetically controlled valve. Based on the problems found from the test model, a setup model with three nozzle arms was selected.

The initial test model was arranged with an air compressor and four nozzles. When the air compressor was switched on, the air reservoir of the air compressor was gradually pressurized. At this time, the control valve was opened to eject air. We used a magnetic valve to control the air outlet switch, which can be controlled remotely using an electrical signal.

The height of the three brackets was set based on the height of the children, and part of the gas was transmitted from above. Thus, the height of the bracket was set at 160 cm (Figure 3). There is an air outlet at the upper and middle sections of the bracket. The central part contains a rotating shaft, and the top arm can be folded into the lower feet. The circular frame in series was placed on ground to stabilize the three main arms. Control wires and airflow conductors were routed from the central computer through those tubes.

2.3. Circuit Design

Prototypes involving the control circuit and user interfacing software were developed. A USB interface control panel and solid-state relay (SSR) were placed on the circuit board (Figure 4). The Phidget Interface Kit [13] was utilized intangible user interfaces; the interface kit screen controller provides accurate results. We used the Phidget Interface 8/8/8 input–output board servers as a communication channel with the host computer.

The program controls the switching of the gas nozzles by using a preset sequence. The USB interface board cannot provide sufficient electrical current to switch the magnetically controlled valve. We constructed an external power board to ensure adequate current supply. An SSR has neither moving parts nor arcing contacts, which are often the primary cause of failure [14]. This provides a high degree of reliability and a long service life.

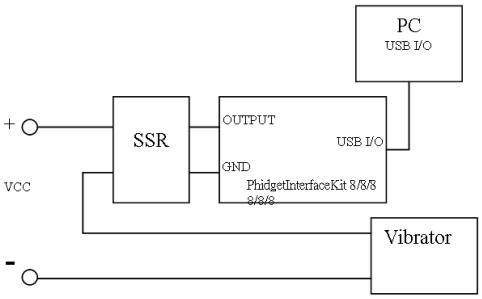

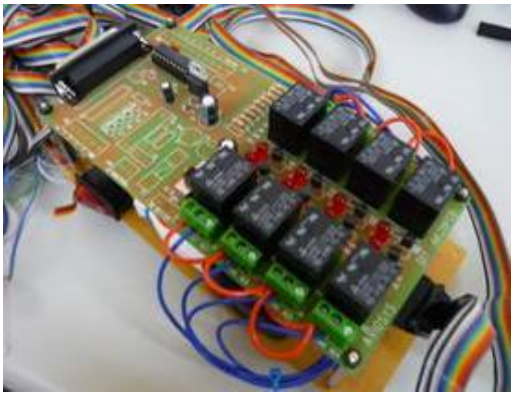

Figure 4: Circuit diagram and SSR circuit board with an external power supply [14].

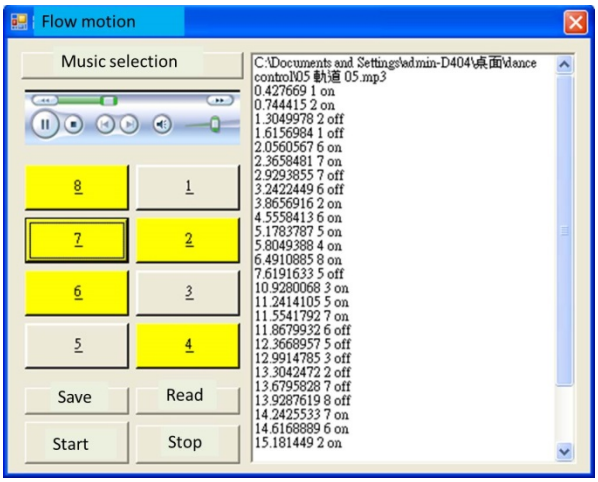

Figure 5: Software interface layout design with a sequential setting of the gas outlet and music control. The yellow blocks indicate active channels.

2.4. Dancing control editor and graphical user interface

As displayed in Figure 5, the interface control program has a graphical user interface that was developed on Microsoft Visual Studio 2005. The graphical user interface displays the current state of each switch. The button with the yellow background color indicates that it is currently activated. The text area on the right-hand side lists the sequence of the switching actions. A user can manually control the switching by directly clicking on the buttons at the specific time while the music is playing.

The status indicator, file read, and start–stop buttons are above the music editor. We can see the blocks 8, 7, 6, 2, and 4 in yellow, which implies that five nozzles are switched on. In the subsequent tests, we found that when most of the spouts simultaneously ejected, the students got confused while determining the source.

2.5. Multidisciplinary

This study comprises three departments of teachers and students. The Department of Industrial Design is responsible for proposing the structure of the concept. The students of the computer communication department are familiar with the circuits and programs and can construct the control circuit and the software to develop a working model. The students from the Department of Early Childhood Education invited children to try out prototypes in special education schools and found the areas of improvement in trial teaching.

In the past, industrial design paid more attention to the performance of modeling pursuit; computer students' interest in the pursuit of technology, they often prefer multifunctional betting into products. In the course of teaching, we understood that the function of a product is not the main part, and the user is the main part. A teacher has to adopt the story-telling method in the guiding process to allow the users to accept the taught content wholeheartedly. The experience of integrated research can adjust the design parameters and get an appropriate product design.

3. Field Study Results

The purpose of the field study was to examine a combination of music and airflow to enhance the bodily movement of visually impaired people. The methodology of this study was based on a qualitative study using interviews with students and the classroom teacher and observation reports from four observers and the researcher. Fifteen 4–19-year-old visually impaired students who enrolled in a school for the visually impaired in Central Taiwan were selected through purposive sampling for the study.

3.1. Materials and methods

The assessment instruments included structured observation forms to gather data on the reaction of the subjects from the researcher and four observers who were trained graduate students, interview reports from the teacher and the subjects at school. All interview sessions were recorded on video, and these were viewed and reported by four observers. The following is the coding symbol of the study:

Table 1: Coding symbol for music and flow activities

Coding	Meaning
O-A-0325-4	Observation of subject A on March 25, 2016 by observer 4
O-B-0325-R	Observation of subject B on March 25, 2016 by the researcher
I- 0325-T	Interview with the teacher on March 25, 2016
I-C-0325-R	Interview with subject C on March 25, 2016 by the researcher

The experimental design utilized four ventilators of airflow simultaneously with music. While revised experimental design from airflow only to play with music simultaneously, some of the subjects smiled but did not do too much movement, especially the five preschoolers. Most subjects' bodily movement was hand movement only.

Figure 6: Children interacting with the airflow

3.2. Results

In order to facilitate identification, we use the English symbol A B C D... to represent the participating students. While subject A, B, C, D, E, F, G, H, I and J listened to the music and felt the airflow, they didn't have any bodily movement but a few seconds later, they started smiling. (O- A, B, C, D, E, F, G, H, I, J-0415-1, 2, 3, 4) (O-A, B, C, D, E, F, G, H, I, J -0415-R)

The younger subject K said "It's music" while listening to the music. He also used his hands to feel the airflow. (O-K-0415-1, 2, 3, 4) (O-K -0415-R)

The subjects L, M, N and O all moved their hands to feel the airflow while the music played. (O-L, M, N,O-0415-1, 2, 3, 4) (O-L, M, N, O -0415-R)

When the researcher asked the subject K, L, M, N, O "Do you like music?" they all answered "Like." (O-K, L, M, N,O-0415-1, 2, 3, 4) (O- K, L, M, N, O -0415-R)

The subject K smiled. He said he liked the music and airflow. (O-K-0415-1, 2, 3, 4) (O-K -0415-R)

Due to the limited movement, the study changed the dynamics of airflow and music. Some subjects did not like the ventilators with strong airflow simultaneously with loud music. Some subjects said it was hard to feel anything from the four ventilators with weak airflow simultaneously with soft music.

When the four switches of airflow were opened, the researcher asked subject K "Would you like to move?" He said "Yes." But subject K needed to be held with the researcher. He wanted to find the airflow with the researcher. (O-K-0415-1, 2, 3, 4) (O-K -0415-R)

When the four switches of airflow were opened, subject L moved his body to face the air and moved his hands to touch the tube, (O-L-0415-1, 2, 3, 4) (O-L -0415-R)

When the four switches of airflow were opened, subject M stuck out his tongue and opened his mouth to feel the air. (O-M-0415-1, 2, 3, 4) (O-M -0415-R)

During four ventilators of weak airflow simultaneously with soft music, the subject O liked it and smiled. (O-O-0415-1, 2, 3, 4) (O-O -0415-R)

When the researcher asked the subject P "Do you like the air and music?" he said "like." (O-P-0415-1, 2, 3, 4) (O-P -0415-R)

When the ventilators were opened randomly, most older subjects could find the direction to adjust and move their hands and feet to feel it. (O- A, B, C, D, E, F, G, H, I, J -0415-1, 2, 3, 4) (O-A, B, C, D, E, F, G, H, I, J -0415-R)

3.3. Discussion of field test

The visually impaired children like music; thus, music it could be a good motivator for them to exercise. The study also found that children enjoy catching the flow. Sometimes their hand touched the air outlet, and this disturbed the original setup of the gas flow direction (Figure 6). This free exploration usually occurred in the first class and should be encouraged. With the teacher's guidance, the students gradually responded to such airflow with their body. Giving the students freedom to explore is also an essential factor. When students reflect based on specific rules, they lose their interest. Moreover, the interaction between peers affects an individual's attitudes. Peers' experience of trying can also stimulate the willingness of the students to try.

The results suggest avoiding frequent changes in the direction of the airflow. Students give up when they are unable to respond appropriately. The design was such that the students could be guided using a small amount of airflow from above or below depending on the characteristics of the music. Students become familiar with it by gradual learning.

The sound of the motor is loud when the air compressor is on, which scares the children. One of the solutions is to move the air compressor to another space or use a small air compressor. Then, the air volume ejected by the device can be reduced once the students are familiar with the device.

4. Redesign

The redesign adopted sitting position (Figure 7) to reduce the need for students to deviate from the location and fit for physical disabilities during exercise. The air outlet is located at the lower edge of the table to avoid being deflected by the student. Infrared sensors arranged on the side of the air outlet end, and a variable resistor provided for adjusting the distance of infrared emission and reception. Visually impaired students with physical disabilities sit in the middle and shift their bodies with the direction of the airflow; this prevents them from falling due to instability during the shift. Four times of visually impaired students were arranged to observe the changes in the movements of students after being guided by the airflow during the teaching process. There were six subjects under test, and Professor Li was composing music for visually impaired children. The TA will fill in the average performance (1-5 points), range of action, and emotional response of the children.

The first week found that due to the experience of no contact airflow in daily life, there was rejection at the beginning of the test. Subject A needs the teacher to encourage him to find the outlet point actively. Subject B can actively touch after the teacher's

guidance, but the body does not move when the air jets. After the guides explained, they were able to proactively find the airflow, but the movements did not change much (Figure 7a). The performance of the fourth week is better than the previous three weeks. Almost all blind children can make movements in the right position (Figure 7b) and can feel the way the airflow interacts. The test results show that the overall average performance is increasing from 1.6 to 4.3. The average number of follow-up airflows was 4.31. In the magnitude of the action (can swing the limb) up to 3.12. When the music and the rhythm of the airflow match, it is more inspiring to the children's movements.

(a) (b)

Figure 7: Response of the respondent (a) First week, (b) the Fourth week - Encourage students to respond with a silk scarf.

5. Conclusions

We presented a flow-motivated facility that adopts noncontact techniques for enhancing the exercising behavior. The airflow reinforces active participation of visually impaired children and increases positive interactions. The results of the study revealed that visually impaired children like music; thus, music could be a good motivator for them to exercise. They were beneficial to develop more holistic equipment for the visually impaired. Brief comparisons of the results against previous findings in [4] and [6], the decreasing of the body's mechanisms for maintaining postural stability can gradually improve after systematic learning and stimulation. Children enjoy catching the airflow; thus, sometimes their hand touched the air outlet and disturbed the original setup of gas flow direction. The study comprised three departments of teachers and students. This cross-domain cooperation experience was quite rare for us. Appropriate guidance during the teaching process is vital for the user to accept the product. The integrated research can adjust the design parameters and obtain a proper product design. The use of appropriate technology solves user problems and reduces the user's frustration.

References

[1] Hatlen, P., "The core curriculum for blind and visually impaired students, including those with additional disabilities" Review 28(1), 25-32, 1996.

[2] Cecilie H. Anvik, "Embodied spaces in the making: visually impaired people, bodies and surroundings" Scandinavian Journal of Disability Research, 11(2), 145-157, 2009. DOI: 10.1080/15017410902830710

[3] Chao, F.L., Lee, L., Chu, H.C. & Wu, W.T., "A Pilot Study on Applying Combination of Music and Airflow to Enhance Bodily Movement of Visually Impaired" in P. Resta (Ed.), Proceedings of Society for Information Technology & Teacher Education International Conference, 3564-3569, Austin, Texas, USA, 2012.

[4] Winnick, J.P., "The performance of visually impaired youngsters in physical education activities: Implications for mainstreaming" Adapted Physical Activity Quarterly, 2(4), 292-299, 1985.

[5] Zuzanna Maćkowiak, Wieslaw Osiński,"The Effect of Sensorimotor Training on the Postural Stability of Visually Impaired Women Over 50 Years of Age" Journal of Women & Aging, 27(1), 68-80, 2015. DOI: 10.1080/08952841.2014.928140

[6] Wiskochil, B. et al. "The effects of trained peer tutors on the physical education of children who are visually impaired" Journal of Visual Impairment & Blindness, 101(6), 339-350, 2007.

[7] Malik, S. et al., "Orientation and mobility training in special education curriculum for social adjustment problems of visually impaired children in Pakistan" International Journal of Instruction, 11(2), 185-202, 2018.

[8] Bischof, A. et al. "Exploring the playfulness of tools for co-designing smart connected devices: a case study with blind and visually impaired students" Proceedings of the 2016 Annual Symposium on Computer-Human Interaction in Play Companion,. ACM, 2016.

[9] Lefeuvre, K. et al. "Loaded dice: exploring the design space of connected devices with blind and visually impaired people" Proceedings of the 9th Nordic Conference on Human-Computer Interaction, ACM 2016.

[10] Ando, B. et al. "A haptic solution to assist visually impaired in mobility tasks" IEEE Transactions on Human-Machine Systems, 45(5), 641-646, 2015.

[11] Kraus, S. "Astronomy for the blind and visually impaired" Bringing the Universe to the World, 36, 2016.

[12] Gibby, D. G. U.S. Patent No. 9,133,759. Washington, DC: U.S. Patent and Trademark Office. 2015.

[13] Bagwan, F. et al. "Tangible user interface based descriptor for appliances" National Conference NCPCI, 2016.

[14] Verma, N., Gupta K., & Mahapatra S. "Implementation of solid state relays for power system protection" International Journal of Scientific & Technology Research 4(6), 65-70, 2015.

ASTES

Advances in Science, Technology and Engineering Systems Journal Vol. 4, No. 4, 314-322 (2019)

www.astesj.com

Special Issue on Advancement in Engineering and Computer Science

ASTESJ

ISSN: 2415-6698

The Role of Information Technology Human Capability in the Implementation of Information Technology Governance (ITG): A Systematic Literature Review on Malaysian Organizations

Nor Aziati Abdul Hamid[*,1], Chin Wei Liew[1], Nor Hazana Abdullah[2], Siti Sarah Omar[3]

[1]*Faculty of Technology Management and Business, University Tun Hussein Onn Malaysia, 86400, Malaysia*

[2]*Department of Technology Management, FPTP, University Tun Hussein Onn Malaysia, 86400, Malaysia*

[3]*Department of Business, FPTP, University Tun Hussein Onn Malaysia, 86400, Malaysia*

ARTICLE INFO

Article history:
Received: 13 May, 2019
Accepted: 08 July, 2019
Online: 07 August, 2019

Keywords:
Information technology governance (ITG)
Information technology human capability
Systematic literature review
Governance issues
Malaysia organizations

ABSTRACT

This study reviewed articles on information technology governance (ITG) in the Malaysian context and categorized the issues found in ITG implementation according to organizational-related and human-related issues. It further analysed the impact and role of information technology (IT) human capability in ITG implementation in developing countries like Malaysia, which is still in the infancy stage of ITG. This study found that most organizations in Malaysia are not only facing organizational-related issues but also human-related issues as well. However, there are insufficient studies on how implementation issues between organization and humans are interrelated. The roles of IT human capability in ITG implementation has been heavily underrated as most studies focused on ITG mechanisms and the impact of ITG on firm performance. Issues highlighted in past studies were summarized and used to explain the roles of IT human capability in ITG implementation. The findings revealed that the number of issues reported in the human-related category was slightly more than organizational-related issues. This study explains the role of IT human capability in ITG and reduces the ambiguity of IT human capability in ITG for future research activities.

1. Introduction

Since the beginning of the 21st century, organizations worldwide have been focusing on integrating Information Technology (IT) into organizational business processes. IT has emerged as one of the most important tools for organizations to retain and improve their competitive advantage. Rapid development in IT has enabled organizations to streamline their operations by improving organizational agility and information flow throughout the entire organization. Strategic alignment between business & IT strategies has become one of the main focuses of organizations in order to ensure that IT tools can be fully utilized to support business decisions. However, organizations have encountered more IT investment failures than expected. According to Aziz *et al*., [1], the number of IT failures has been growing since the last decade. Despite all the attention given, the implementation of IT governance (ITG) has not been easy, especially for developing country.

*Corresponding Author: Nor Aziati Abdul Hamid, aziati@uthm.edu.my

2. Problem Statement

The ITG concept has become increasingly well-known to worldwide organizations due to the importance of good IT governance that is constantly developing at a rapid pace in support of business decisions. The ITG concept has garnered increased attention from scholars and practitioners around the globe but the concept is still relatively new to Malaysia. There are numerous ITG frameworks that are readily available for adoption, such as Control Objectives for Information and Related Technologies (COBIT 5.0) and Information Technology Infrastructure Library (ITIL v3). The ITG concept has been constantly evolving as the COBIT and ITIL frameworks have already seen multiple updated versions up till now. Organizations have been trying to adopt various practices and frameworks for governance purposes. However, the implementation of ITG is a difficult process especially for organizations in developing country like Malaysia as there are various barriers to the adoption of ITG practices [2]. In addition, the number of studies on factors that inhibit the positive implementation of ITG has been less than ideal, and even

worse for developing countries. ITG awareness and practices are severely lacking in the Asian region [3]. For a developing country like Malaysia, where ITG implementation is still at the infancy stage, more studies should be conducted to increase the understanding of ITG. Lacks of ITG awareness, guidelines and practices have also been reported concerning the public sector in Tanzania [4]. Therefore, this study attempted to examine and categorize ITG issues that are consistently faced by Malaysian organizations. This study also explained why most issues are interrelated and emphasized on how IT human capability can mitigate ITG implementation issues.

3. Research Context

3.1. Information Technology Governance (ITG)

Due to the massive amount of attention given to the field of ITG, researchers and experts have given various definitions and expectations of ITG. One of the most accepted definition of ITG is "the distribution of decision rights and accountability in order to induce positive behaviour or patterns in managing and using IT resources" [5]. ITG is also defined as the "utilization of organizational capacity by the board, executives and IT management team to formulate and implement IT strategy as well as achieve strategic alignment between business and IT" [6]. ITGI defined ITG as an integral part of corporate governance aided by adequate leadership, structures and processes to ensure IT sustainability and act as an extension of an organization's strategies and objectives [7].

3.2. Information Technology Capability

Although IT capability has seen various definitions in previous studies, the definitions have been centred on "the ability to manipulate IT resources and costs" [8]. The definition was extended by stating that IT resources have been combined to support business-related decisions [9]. Both definitions referred to the ability to utilize and manipulate IT-related resources and other complementary resources to support businesses in value-added ways [10]. Aside from controlling IT resources, IT capability is specifically referred to as the ability to affect organizational goals through the control of IT-related costs [11].

IT capability is placed in between technical capabilities and IT-related organizational capabilities. However, most of the classifications included three of the following, namely IT infrastructure capabilities, IT human capabilities, and IT-enabled intangibles [8, 10-13]. IT infrastructure capabilities is defined as the ability to provide sustainable infrastructure services to support business-related processes or IT-related tangible assets that include IT systems, gadgets, and various tools and applications that form the very base of IT infrastructure and shared throughout the firm [8,12,14]. IT human capabilities refer to the combination of technical and managerial skills of IT professionals in solving and attending various organizational needs [8,12]. IT-enabled intangibles are referred to as intangibles made available due to the utilization of IT resources. These intangibles include knowledge assets, synergy, relationship assets, responsiveness and others [8,10]

3.3. ITG Issues in Malaysia

Since the sources of information for ITG implementation issues were found to be lacking in the review process, data collected for this study included those from studies concerning various sectors, such as public, financial and higher education sectors. Most organizations in Malaysia are still in the infancy stage of ITG implementation, as reported by [2]; hence, the factor of sector diversity is expected to have minimal effect on the barriers to initially accept the basic implementation of ITG. This study has classified issues faced by organizations that implement ITG into two main categories. The first category is organizational-related, and the second category is human-related. Further details on the categorization and issues found will be discussed in the section on findings.

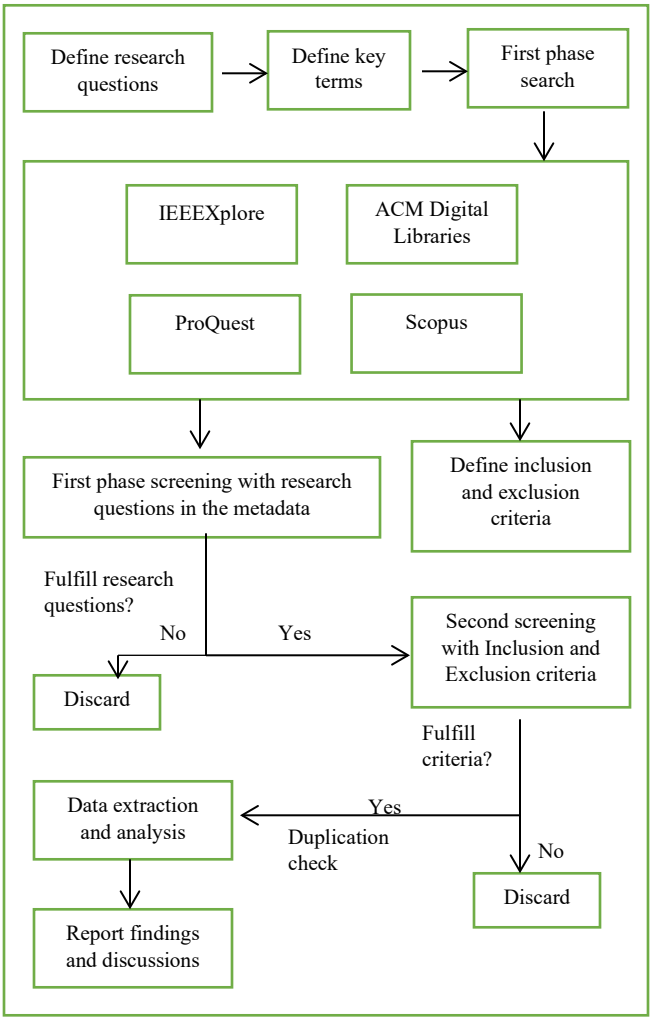

Figure 1: Systematic Literature Review Process

4. Systematic Literature Review

The methodology used in this study was the systematic literature review method. The guidelines for a systematic literature review were provided by Kitchenham [15]. This type of review is mostly used when the study intends to identify any research gap or interpret any area of interest in a span of time. This methodology helps the researcher to be better positioned for future research activities according to the research gaps found in the review process. The steps undertaken for systematic literature review in this study are as follows: i) Define the research questions; ii) Define key terms for searching the database; iii) First phase literature search and selection process; iv) Define

inclusion and exclusion criteria for the second phase selection process; v) Data extraction and analysis; and vi) Report findings and discussions. Figure 1 illustrates the systematic literature review process undertaken in this study.

The first step in the systematic literature review is to define the research questions for the literature screening process involving the metadata in the first phase. The research questions set for literature screening are as follows:

i) Is the article related to information technology governance?

ii) Are there any primary findings on the implementation of information technology governance?

iii) Did the study take place in developing countries or Malaysia?

The literature searches were conducted on 6 databases, which were IEEEXplore, ACM Digital Libraries, Scopus, Science Direct, Springer Link, and ProQuest. The initial search began in November 2018 and was updated in June 2019. Some of the terms used for literature searches only in the metadata are "information technology governance", "information and communication technology governance", "IT governance", and "ICT governance". Thus, if the initial search presented 500 or more hits, the term "Malaysia" is added to the search results, if available, or in the full text to limit the search results to the context of this study. Moreover, if the results yield less than 50 hits, the newly added term "Malaysia" is deleted, and the previous results are considered. As for the literature search in Science Direct, there were 1,297 hits after the term was added. The results were then filtered according to articles with open accessibility. The results of the literature searches are listed below:

i) IEEEXplore – 454

ii) ACM Digital Libraries – 158

iii) SCOPUS – 97

iv) ProQuest – 25

Next, initial screenings were carried out by referring to the research questions. After the initial screenings, the breakdown in the number of qualified articles were 16 articles from IEEEXplore, 7 from ACM Digital Libraries, 47 from SCOPUS, and 1 from the ProQuest database. The inclusion and exclusion criteria for the second phase of screening were then determined, as shown in Table 1 below.

Table 1: Inclusion and Exclusion Criteria

Inclusion Criteria	Exclusion Criteria
Paper written in English	Paper not written in English
Full accessibility	Partial/No accessibility
Findings related to organizations in Malaysia	Findings unrelated to organizations in Malaysia
Findings reveal IT governance implementation issues and causes	Findings did not reveal IT governance implementation issues
Primary study	Non primary study

In the second phase, the criteria were used in the literature selection process after reading the full text. Finally, 11 articles were selected, and after removing redundant articles, 10 articles had fulfilled the criteria, and 2 additional articles outside the database were found from previous studies and referred by related authors in the qualified articles. A total of 12 articles had qualified for this study. As the study focused only in the context of Malaysian organizations, the number of qualified articles was low. Figure 2 illustrates the number of articles published per year.

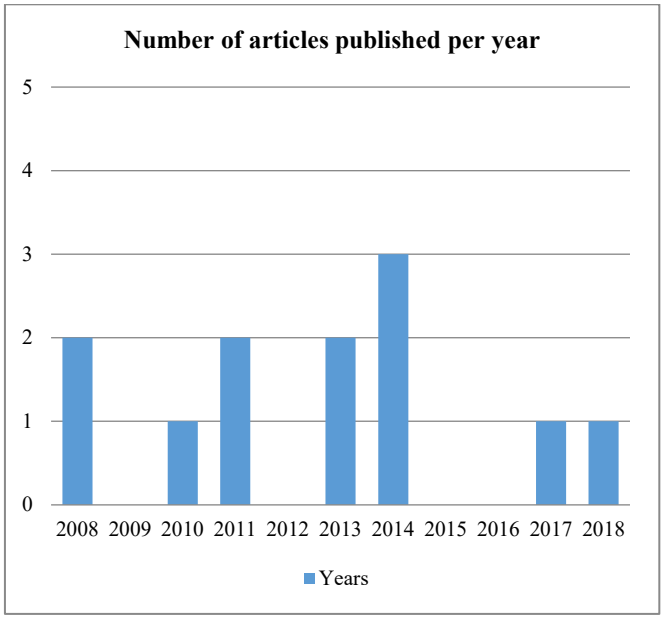

Figure 2: Number of articles published per year

As shown in Figure 2, the number of articles published per year is unusually low, especially after 2014. This might be because most studies on ITG had focused on the benefits and impact of ITG on firm performance instead of barriers to ITG implementation. As reported in [16], most organizations that participated in the study had a low ITG maturity level. Therefore, this study attempted to summarize issues that consistently inhibited the process of ITG implementations and adoption, as well as to propose potential solutions for future studies.

Table 2 reveals that most of the articles reviewed had both organizational and human-related issues in ITG implementation with the exception of 2 papers where one focused solely on IT practitioners and the other focused more on structural issues, such as the lack of defined roles and responsibilities. Human-related issues were mentioned 21 times and organizational-related issues were mentioned 18 times in all 12 articles. Table 3 shows the issues that were found in each category, while Table 4 shows the classifications of key issues found in articles after the reviewing process.

4.1. Organizational-related Issues

The issues in this category are regarded as issues faced during ITG implementation due to organizational decisions pertaining to the structure, guidelines and practices, as well as the support from top management. Organizational issues are related to top-down decision making where structures, responsibility and accountability, policy, guidelines and practices as well as

direction and goals are determined by the top management to be implemented by the entire organization. Hence, organizational-related issues are mostly related to the upper level of an organization. The subcategories proposed by this study pertaining to organizational-related issues are structure, guidelines and practices and top management.

4.1.1. Structure

Structure issues defined in this study refer to issues developed due to lack of assignation in accountability and responsibility in ITG. Structural issues are one of the most commonly found issues faced by newcomers to ITG implementations [4, 17-20]. As ITG is still a relatively new concept in Malaysia, organizations often struggle to develop appropriate structures or hierarchy of power in terms of ITG implementation. More often, a IT steering committee and IT strategy committee should be established by involving the Chief Information Officer (CIO). It was reported that structural issues were not functioning well as the CIO did not understand his/her role and responsibility in ITG [18]. Without an appropriate structure in place, there would be lack of transparency in the governance process and even difficulties in justifying IT-based decisions [19]. In addition, lack of structure can lead to communication issues [2]. Organizations will find it difficult to refer to the personnel in-charge as no one will assume the responsibility for related issues without a structure in place [18]. Similar issues were reported as there was a lack of a platform for management to discuss IT-related issues [21].

4.1.2. Guidelines and Practices

Guidelines and practices issues arise due to the lack of ITG guidelines and practices in the organization. Guidelines and practices are complementary factors to a reliable governance structure, which also contributes to the creation of transparency for justifying the ITG implementation processes [19]. The lack of strategic guidelines for IT funding in public universities was reported in [18]. It was revealed that IT projects that were initially approved or agreed by the IT committee were rejected eventually due to financial issues.

Miscommunication and improper guidelines led to a lack of coordination between departments and facilities regarding the utilization of IT resources. Guidelines and practices together with a reliable ITG structure prevent information disparity between the expectations of the CIO and implementation on the ground [21]. A study on Malaysia's public sector revealed that 76.19% of organizations had a low ITG maturity level. Findings also showed that IT managers expected at least an average level of ITG practice despite the lack of proper mechanisms and exposure to ITG practices [16].

4.1.3. Top Management

ITG should be driven and initiated from the organization's top level [19]. Top management support is classified as an organizational issue because top level executives are responsible for deciding organizational initiatives for moving forward in the right direction. Successful ITG implementation often depends on the top management's initiative to offer sufficient support. In addition, ITG implementation is also influenced by internal organizational cultures and politics. It is important for top management to recognize the needs for ITG and assign appropriate accountability according to initiatives, beginning from the top of the organization [3].

Lack of support and commitment from top management is one of the current issues faced by Malaysia organizations when implementing ITG [2, 22]. Similar situations where the top management was lackadaisical in supporting ITG was also reported [1], which then resulted in a lack of adequate resources to manage assigned controls as the top management willingness to incorporate ITG into the organization's future strategy is highly dependent on the recognition and knowledge about the importance of ITG.

Table 2: Key Findings

No.	Authors	Context	Key findings/Issues					
			①	②	③	④	⑤	⑥
1	[17]	Malaysia Ministry of Education	√	√		√	√	
2	[18]	Malaysia public university	√	√		√	√	√
3	[3]	Malaysian senior management		√	√		√	
4	[1]	Malaysian organizations			√	√		
5	[2]	Malaysian organizations	√	√	√	√	√	
6	[25]	Malaysian IT practitioners				√	√	
7	[20]	Malaysian universities	√					
8	[21]	Malaysian public universities	√	√		√	√	√
9	[26]	Malaysian public sector	√	√			√	
10	[19]	Malaysian public sector	√					√
11	[16]	Malaysian public sector		√		√	√	√
12	[22]	Malaysian financial sector			√	√	√	

Legend	
Organizational-related	Human-related
① Structure ② Guidelines and Practices ③ Top Management	④ Competencies ⑤ Awareness and Understanding ⑥ Leadership

Table 3: ITG Issues According to Categories

No.	Key Findings/ Issues					
	Organizational-related			Human-related		
	①	②	③	④	⑤	⑥
1	Lack of steering committee	Lack of documented practices		IT skills at basic level	Lack of understanding	
2	Communication breakdown and lack of commitment	Lack of approach for funding strategy		Lack of skills and knowledge in CIO and staffs	Lack of CIO with adequate ITG understanding	Lack of CIO presence in ITG and lack of IT initiative
3		Lack of exposure in ITG practices	IT accountability for top management		Recognition and knowledge from top management required	
4			Lack of top management support	Lack of adequate human resource		
5	ITG affected by culture and politics	Communication issues	Lack of top management support	Lack of time, training, knowledge and skills	Lack of ITG awareness	
6				ITG requires continuous commitment	ITG requires special knowledge	
7	Weak structure and lack of clear roles and responsibilities					
8	Communication breakdown	Lack of coordination and alignment		Lack of capable human resources	ITG responsibilities placed on IT only	Lack of CIO presence and effort to create awareness
9	Lack of governance in collaboration	Lack of governance in collaboration			Lack of understanding towards the importance of ITG	
10	Lack of accountability and transparency	Lack of justification on expense and resources	ITG should be driven from top management			ITG requires leadership
11		Lack of exposure on proper guidelines and mechanisms		Insufficient proficient IT personnel	Lack of consistent understanding on ITG	Lack of official directive
12			Lack of top management support	Complexity in ITG practices		

Table 4: Classification of Key Issues

Key Findings/Issues					
Organizational-related			Human-related		
Structure	Guidelines and Practices	Top Management	Competencies	Awareness and Understanding	Leadership
• Lack of adequate structure and accountability	• Lack of documented practices and guidelines • Lack of guidelines for collaborations • Lack of exposure	• Lack of top management support • Lack of top management accountability	• Lack of adequate IT-related skills • Lack of adequate managerial skills • Lack of human resources	• Lack of awareness and understanding on ITG • Lack of recognition of ITG	• Lack of role in CIO • Lack of IT initiative

4.2. Human-related Issues

Human-related issues refer to issues originating from human resources caused by the lack of quality, competency, and understanding required for managing and completing tasks required by organizations. Specifically, human-related issues in this study refer to barriers to ITG implementation due to insufficient personnel with quality to manage and govern IT-related resources and issues. In human-related issues, the personnel included in this study were the CIO and other personnel involved in ITG from the middle to the top management level. Three subcategories in human-related issues are competencies, awareness and understanding as well as leadership quality.

4.2.1. Competencies

Competency issues are often overlooked by organizations since most of the attention is placed on ITG frameworks and practices. Competency in this study refers to the ability of ITG personnel to manage and complete assigned responsibilities and practices related to ITG. The terms competency and capability are often used interchangeably due to how closely their interpretations are. Competence is defined as having the ability to utilize skills, knowledge and the capacity to satisfy or achieve current needs. Capability is defined as qualities, abilities, and the potential to develop accordingly to meet future needs by adapting to changes in a dynamic environment while generating new knowledge for improving working performance [23]. Therefore, in order to fit in the context of this study, where current ITG issues can be safely regarded as current ITG needs, the term competency is used in this subcategory. Most senior management and CIOs lack knowledge and experience in ITG because ITG is a relatively new concept compared to working skills and experience [1,3,17-18]. In addition, it was reported that the complexity of ITG practices was the highest ranked barrier from the technical aspect [22]. The prerequisites for ITG personnel have been elevated as ITG committees are required to plan, manage, and monitor IT initiatives. ITG personnel also need to master non-technical skills such as business strategic planning, leadership, and communication [16]. Hence, due to the increased prerequisites for ITG personnel, organizations have been lacking human resources equipped with proficient skills in technical and non- technical aspects to resolve ITG issues and challenges.

4.2.2. Awareness and Understanding

As mentioned previously, top and senior management need to recognize the need for ITG to ensure smooth top-down implementation [3]. Such recognition requires adequate awareness and understanding about ITG. Awareness and understanding issues refer to issues that occur due to the lack of experience and understanding on the potential benefits of ITG in organizations. Awareness can elevate performance and allow accurate understanding of situations that can further lead to better decision making by leaders [3]. The authors had further revealed 3 level of ITG awareness in reference to Endsley's theory of awareness [24]. The first level of awareness includes gathering perceptual information from the surrounding and focusing on elements that are beneficial and relevant. One example of this is to understand the availability of resources, infrastructure, and skills required to achieve current tasks. The second level of awareness includes integrating perceptual information with experiences and knowledge to assess the significance of the context, which is the role of ITG in organizations [25]. The third level of awareness includes projecting future elements by anticipating the changes that can be brought to the operational environment. Examples of third level awareness are management of IT resources that meet organizational needs, lead the initiative in addressing IT issues, ensure continuous alignment between business and IT, and leverage IT potentials to enhance business growth. It was found that top management perceives that there is no need for ITG as there is a lack of awareness and knowledge [2]. There were no efforts by the top management to create awareness about ITG adoption [21]. Instead, all the issues were thought to be an IT-only responsibility, which further leads to a disoriented alignment between strategic business and IT planning. Business executives did not understand the strategic value of IT as it was thought to be insignificant [26]. Business executives failed to understand IT issues and there was a severe lack of collaboration between business and IT. IT managers assumed a high-level of maturity for ITG but in reality, 76.19% of the organizations were still in position of low ITG maturity [16]. This could be due to different levels of understanding regarding the definitions of ITG and ITG itself. Most implementations were highly dependent on instructions, and there was a lack of initiative to actively seek improvement. All the issues mentioned above indicate that most

organizations in Malaysia still lack ITG awareness and understanding.

4.2.3. Leadership

Leadership quality in this study refers to the ability of top and senior management to spearhead the IT initiative in ITG implementation. As most of the organizations are still at the infancy stage of ITG, lower levels of the organization hierarchy need to be guided by top management. This requires top management to lead using the IT initiative and provide direction from the highest level of the organization [19]. For top management to lead, adequate knowledge about ITG is required. Therefore, a lot of issues arise because even the top management has a low understanding of ITG itself [18]. There is a possibility of a lack of official directives concerning ITG, which causes the lack of collaboration between business and IT [16]. Top management should always initiate the active involvement of stakeholders in ITG, while providing sufficient guides and empowering key personnel with expectations and support. As most personnel lack ITG knowledge and experience, top management plays a major role in ensuring the continuity and sustainability of ITG. Presence of the CIO was insignificant because the responsibilities were not up to a respectable standard [21]. There was no effort to create awareness and liaison between business and IT. Hence, the IT department assumed all responsibility for issues identified. Leadership in ITG is especially vital for organizations at the infancy stage as the top management is responsible for setting the guidelines and directions for organizations to move forward. Newcomers to ITG need explicit guidance or they would just become simple rule followers instead of skilled personnel actively seeking continuous innovation and improvement.

5. Role of IT Human Capability

IT human capability mentioned in this study refers to technical capabilities, business capabilities and behavioural capabilities [12]. Technical capabilities refer to technical skills and knowledge in a specific area of expertise. Business capabilities refer to the IT personnel's ability to understand and manage overall business processes and environments. Behavioural capabilities refer to the IT personnel's interpersonal ability to interact effectively with others. The results show that both organizational-related and human-related issues are major factors that help organizations to implement ITG in Malaysia. It is undeniable that both issues need unwavering attention from organizations in order to implement ITG and move it in the right direction.

ITG is more than just following rules and guidelines. ITG requires continuous commitment from organizations to ensure sustainability, and having competent human resources is one of the prerequisites for future sustainability, whether in business or ITG [25]. It has been stated that organizations might be governing IT with less than adequate prerequisites in terms of IT capabilities [10]. Development of ICT personnel has been one of the focuses of the Malaysian Strategic IT Plan 2011 [26]. However, findings indicate that there is a lack of effort or mechanisms for developing IT personnel in the area of ITG. Although issues have been categorized into organizational-related and human-related categories, both issues are interrelated as one issue can cause the other to surface.

One of the primary issues in organizational-related issues is the lack of adequate structure and accountability in ITG. The lack of organizational structure is not directly related to IT human capability, but it should be taken into consideration when forming the ITG structure. When forming the ITG structure, organizations should assess whether there are qualified personnel available and accountable for ITG implementation. It is undeniable that collaboration issues [21,26] have consistently emerged during ITG implementation. In the selection of qualified personnel for ITG, there is no doubt that at least certain levels of business and behavioural capability should be considered as ITG often requires collaborative efforts for strategic alignment purposes. This requires personnel to possess some level of business acumen and the capability to work well with other units when needed. It raises further questions on whether business or IT executives should be held accountable, as most business executives possess business capabilities without IT skills, and most IT executives possess IT capabilities without business skills. It does not mean that business executives are required to possess IT capabilities but at least they should be aware of the importance of ITG since IT executives are now required to extend their understanding of business knowledge [27]. It was also revealed that business and IT, which act in collaboration, can lead to ITG effectiveness and strategic alignment as knowledge sharing between business and IT executives lead to a better understanding of each other's environment [28-29]. For example, it has been revealed that a web-based system developed in a university aligns the entire existing or new program with the Malaysian Qualification Framework (MQF) [30]. Similar web-based systems can be designed to monitor and align ITG prerequisites pertaining to certain personnel involved. Training should be given for those who do not meet the prerequisite capabilities for ITG.

Guidelines and practices are some of the most common issues faced when implementing ITG. Guidelines and practices are available through frameworks like COBIT 5.0 and ITIl.v3. However, despite the availability of frameworks in the market, not all practices and mechanisms are suitable for every organization. One main purpose of guidelines and practices is to help and give direction to organizations intending to implement ITG. It is also important to practice the relevant mechanisms that help develop positive IT behaviours throughout the entire organization. One of the common issues with the availability of frameworks is the lack of instructions on how to perform tasks with the right mind-set. ITG is more than just simply following rules and guidelines. Organizations must also implement various ITG mechanisms that help to develop individuals with adequate capabilities so that ITG efforts are sustainable in the future. It is important for organizations to develop enough ITG awareness among IT personnel through various practices and mechanisms. As reported, organizations with awareness imbue governance-related mind-sets into daily routines and practices [3]. Personnel with the ability to actively lead and think using IT initiatives are better than rule followers. Guidelines and practices provide the basis for incorporating ITG into daily routines, but it depends on the personnel's capability to understand and manage tasks effectively. In addition, only qualified IT personnel who are aware of the importance of ITG will actively think of the processes and

guidelines that need to be improved and adapted to the changing business process. Therefore, IT human capability is important for the continuous improvement of ITG implementation in an organization.

Gaining top management support has been an issue for organizations in Malaysia as top management lack the understanding of the importance of ITG. Moreover, lack of top management support directly affects the outcome of ITG implementation as resources are often procured with the approval of the top management. It is important to convince the top management about the implementation of ITG in order to gain their support. It has been proven that new IT deployment is easier with firm commitment from the top management [30]. However, it is not easy to convince the top management as ITG is a long-term project that requires various resources to succeed. Therefore, having capable human resources that are knowledgeable in ITG can ensure the continuity and success of ITG implementations, especially in the future. The CIO plays an important role in convincing top management as the CIO often acts as a liaison between business and IT executives. The CIO who is capable of recognizing, understanding, and relaying the importance of ITG to the top management ensures better allocation of resources for a smoother implementation process.

Unlike organizational-related issues, human-related issues are directly related to IT human capability. As mentioned before, competencies refer to the ability to satisfy current needs with skills and knowledge. Therefore, organizations need to develop current competencies into capabilities in order to adapt to future challenges. Currently, ITG is presented as a brand-new challenge that requires human resources with proficient skillsets and capabilities for organizations in Malaysia. Most Malaysian organizations lack competent human resources for implementing ITG. The lack of competency generally includes IT as well as managerial skills and knowledge, which are part of technical and business capabilities. The issues are especially troubling for the public sector as most public sectors have a more or less fixed number of staffs. Therefore, a recruitment of additional experts or capable personnel was less likely to occur unless external expertise is specifically consulted. Hence, organizations need to develop human resources that are proficient in ITG supplemented by the help of various practices and mechanisms. However, competency issues consistently emerge from organizations suggesting that organizations are more focused on setting rules and guidelines rather than developing capable human resources that are supposedly accountable for ITG tasks. This creates the culture of passive governance where actions are only taken based on rules and instructions. As mentioned earlier, personnel involved in ITG should be equipped with business knowledge and ITG awareness. This can be achieved with job rotations and cross training between business and IT units [27]. A web-based system can be developed to record all qualifications and skills of related personnel. All training and rotations should be provided based on specific skills that are lacking. Qualified personnel with cumulated experience in the task can improve the efficiency of the process and are more inclined to offer and seek improvements for ITG.

Another factor of passive governance comes from the lack of awareness and understanding of ITG. ITG requires leaders with enough understanding and knowledge about the ITG concept to lead with IT initiative and active thinking in order to create a good culture of governance. Results revealed that the importance of ITG was severely underestimated by organizations. Few cases reported that senior management did not recognize the importance of ITG and felt that ITG was unnecessary [3,26]. There was also a case where ITG was thought to be only as an IT responsibility [21]. Issues like this clearly show that the roles of ITG in organizations were ambiguous to entire organizations, or at least to the top management and business executives. For ITG implementation to be successful, ITG awareness must be spread throughout the organization so that strategic alignment between business and IT can be achieved. Organizations must reach consensus on the role of ITG, and how it can affect organizations moving forward. As mentioned previously, awareness allows organizations to imbue certain mindset into daily practices. For this case, ITG awareness prevents the culture of passive governance and allows personnel to be actively involved in the governance process moving forward. In this case, awareness and understanding must be included as part of IT human capability as both play a big role in adapting to new challenges.

In this study, leadership is listed under behaviour capability since leadership is an essential ability to lead and interact with others. From the leadership aspect, the CIO is expected to be in the midst of ITG implementation. However, previous articles reveal that CIOs in Malaysian organizations lacked leadership qualities, especially in terms of IT initiative [16, 18-19]. In ITG's infancy stage, leadership plays one of the most important roles in ITG implementation as beginners in the organization need more guidance than ever. The CIO is seen by practitioners as the main driver in ITG [27]. However, the CIO should not be the only one to be held responsible for leadership issues. Anyone in the organization who is aware of the importance of ITG should be leading-by-example in order to create more ITG exposure. As mentioned previously, ITG should be driven from the top management downwards. Therefore, the top management must take responsibility in leading the IT initiative by recognizing the importance of instilling a successful ITG.

Finally, as mentioned by [10], the use of IT capability has been ambiguous in the ITG literature. Therefore, this study attempted to clear the ambiguity by exploring and explaining the role of IT human capability in ITG implementation. This study can contribute to future studies on the relation between ITG and IT human capability.

6. Conclusion

In conclusion, this study explained the interrelated relations between organizational-related and human-related issues by justifying the role of IT human capability. This study also clarified the ambiguity concerning the use of IT capability on ITG literature. Through systematic literature review, it has become clear that structure and guidelines help ITG to consistently move in the right direction. However, without specific capabilities, such as business, technical, and behavioural capabilities possessed by related personnel, ITG cannot be implemented effectively since most ITG implementation and practice requires collaboration from both business and IT units for the sake of strategic alignment. Therefore, it can be concluded that both organizational and human

factors are important for the consistency, efficiency and effectiveness of ITG. Additionally, researchers are encouraged to commit further studies on IT human capability and ITG implementation in Malaysia in order to compensate the lack of proven ITG studies in the Malaysian context. This study also attempted to further highlight the importance and role of IT human capability in the midst of ITG implementation and mechanisms in order to garner more attention toward human-related issues since developing countries like Malaysia are affected by issues such as the lack of qualified human resources. Therefore, organizations should pay equal attention to both organizational and human-related issues in order to create a well-built structure, framework, and environment that are well-suited for ITG implementation at the infancy stage.

Conflict of Interest

The authors declare no conflict of interest.

Acknowledgment

Special thanks to University Tun Hussein Onn Malaysia (UTHM) for assisting in the completion of the paper.

References

[1] K. A. Aziz, M. B. Norhashim, E. M. Halim, "Information security and information technology governance: a Malaysian case study" International Journal of Management Practice, 4(4), 331, 2011. https://doi.org/10.1504/ijmp.2011.039204

[2] M. F. I. Othman, T. Chan, E. Foo, "IT Governance Adoption in Malaysia : A Preliminary Investigation" in 2011 22nd Australasian Conference on Information Systems (ACIS), Sydney, Australia http://aisel.aisnet.org/acis2011/69

[3] Y. M. Lin, N. H. Arshad, H. Haron, Y. B. Wah, M. Yusoff, A. Mohamed, "IT Governance Awareness and Practices: an Insight from Malaysian Senior Management Perspective" Journal of Law and Governance, 5(1), 2010. https://doi.org/10.15209/jbsge.v5i1.177

[4] E. N. Nfuka, L. Rusu, "Critical Success Factors for Effective IT Governance in the Public Sector Organizations in a Developing Country: The Case of Tanzania" in 2010 ECIS 18th European Conference on Information Systems, Pretoria, South Africa, 2010. https://doi.org/10.1080/1097198X.2013.10845642

[5] P. Weill, J. W. Ross, "It Governance on One Page" MIT Sloan Working Paper No. 4517-04; Research Working Paper No.349, 2004. http://dx.doi.org/10.2139/ssrn.664612

[6] W. V. Grembergen, S. D. Haes, "Exploring the relationship between IT governance practices and business/IT alignment through extreme case analysis in Belgian mid-to-large size financial enterprises" Journal of Enterprise Information Management, 22(5), 615-637, 2009. http://doi.org/10.1108/17410390910993563

[7] ITGI, Board Briefing on IT Governance, 2nd Edition, 2003.

[8] A. S. Bharadwaj, "A Resource-based perspective on information technology capability and firm performance: an empirical investigation" MIS Quarterly, 24(1), 169-196, 2000. http://dx.doi.org/10.2307/3250983

[9] V. Sambamurthy, W. Zmud, "Arrangements for information technology governance: A theory of multiple contingencies" MIS Quarterly, 23(2), 261-290, 1999. http://dx.doi.org/10.2307/249754

[10] K. Hiekkanen, J. Korhonen, E. Patricio, M. Helenius, J. Collin, "IT Governance, Decision-Making and IT Capabilities in 2013 Proceedings of The 9th European Conference on Management Leadership and Governance, Klagenfurt, Austria, 2013.

[11] Z. Aiqun, "An IT capability approach to informatization construction of higher education institutions" Procedia Computer Science, 131, 683–690, 2018. https://doi.org/10.1016/j.procs.2018.04.312

[12] D. Ko, D. Fink, "Information technology governance: An evaluation of the theory-practice gap" Corporate Governance: The international journal of business in society, 10(5), 662–674, 2010. https://doi.org/10.1108/14720701011085616

[13] J. S. Chen, H. T. Tsou, "Performance effects of IT capability, service process innovation, and the mediating role of customer service" Journal of Engineering and Technology Management, 29(1), 71-94, 2012. https://doi.org/10.1016/j.jengtecman.2011.09.007

[14] L. Fink, S. Neumann, "Gaining agility through IT personnel capabilities: The mediating role of IT infrastructure capabilities" Journal of the Association for Information System, 8(8), 440-462, 2007. https://dx.doi.org/10.17705/1jais.00135

[15] B. Kitchenham, S. Charters, Guidelines for Performing Systematic Literature Review in Software Engineering, Software Engineering Group, University of Durham, 2007.

[16] R. A. Razak, M. S. Zakaria, "The Information and Communication Technology Governance Maturity Level for Malaysian Public Sector" in Proceedings of the Second International Conference on Internet of Things, Data and Cloud Computing, Cambridge, United Kingdom, 2017. https://dx.doi.org/10.1145/3018896.3018967

[17] S. Ismail, R. A. Alias, A. A. Rahman, "IT Governance Implementation in the Malaysian Ministry of Education" in 2008 Postgraduate Annual Research Seminar (PARS '08). Johor Bahru, Malaysia, 2008.

[18] N. A. Ismail, "Information technology governance, funding and structure" Campus-Wide Information Systems, 25[3], 145-160, 2008. https://dx.doi.org/10.1108/10650740810886321

[19] R. A. Razak, M. S. Zakaria, "The critical success factors for effective ICT governance in Malaysian public sector : A Delphi study. International Journal of Economics and Management Engineering" 8(11), 2014. http://www.waset.org/publications/9999698

[20] A. R. Ahlan, B. A. Ajayi, H. Hussin, "Roles of Governance, Ethics and Integrity in Managing Information Technology Resources: Muslim Practitioner's View" in 2013 5th International Conference on Information and Communication Technology for the Muslim World (ICT4M), Rabat, Morocco, 2013. https://doi.org/10.1109/ICT4M.2013.6518926

[21] A. R. Ahlan, Y. Arshad, and B. A. Ajayi, "IT governance in a Malaysian public institute of higher learning and intelligent decision making support system solution," Engineering and Management of IT-based Service System, 19(33), 2014. https://doi.org/10.1007/978-3-642-39928-2_2

[22] M. F. I. Othman, "Using analytical hierarchy process (AHP) to evaluate barriers in adopting formal IT governance practices" Journal of Telecommunication, Electronic and Computer Engineering (JTEC), 10, 35-40, 2018.

[23] R. Nagarajan, R. Prabhu, "Competence and capability- a new look" International Journal of Management (IJM), 6(6), 7-11, 2015.

[24] M. R. Endsley, "Measurement of situation awareness in dynamic systems." Human Factors, 37(1), 65-84, 1995. https://doi.org/10.1518/001872095779049499

[25] W. L. Teo, A. A. Manaf, P. L. F. Choong, "Perceived effectiveness of information technology governance initiatives among IT practitioners. International Journal of Engineering Business Management, 5(1), 1–9, 2013. https://doi.org/10.5772/56661

[26] J. Kaur, S. A. H. Bahri, "Implementation of Information Technology Governance in the Malaysian Public Sector Practice" in Pacific Asia Conference on Information Systems (PACIS), Chengdu, China, 2014. http://aisel.aisnet.org/pacis2014/119

[27] B. A. Ajayi, H. Hussin, "IT governance from practitioner's perspective: sharing the experience of a Malaysian university" Journal of Theoretical and Applied Information Technology, 88(2), 219-230, 2016.

[28] J. Kaur, N. Mohamed, A. R. Ahlan, "A Confirmatory Factor Analysis of the Information Technology Governance Effectiveness: Evidence from Malaysia" in 2011 International Conference on Research and Innovation in Information Systems, Kuala Lumpur, Malaysia, 2011. http://dx.doi.org/10.1109/ICRIIS.2011.6125666

[29] M. A. J. Sabegh, S. M. Motlagh, "The role and relevance of IT governance and IT capability in Business- IT alignment in medium and large companies" Business and Management Review, 2(6), 16-23, 2012.

[30] N. Musa, D. H. A. Ibrahim, N. A. Bolhassan, J. Abdullah, N. Kulathuramaiyer, M. N. Khairuddin, "An IT Governance Framework for Achieving the Development of Academic programme in Higher Institutions: A Case of Universiti Malaysia Sarawak (UNIMAS)" in The 5th International Conference on Information and Communication Technology for the Muslim World (ICT4M), Kuching, Malaysia, 2014. http://dx.doi.org/10.1109/ICT4M.2014.7020673

ASTES

Advances in Science, Technology and Engineering Systems Journal
Vol. 4, No. 4, 323-327 (2019)
www.astesj.com

ASTES Journal
ISSN: 2415-6698

Long-term Traffic Flow Forecasting Based on an Artificial Neural Network

Alimam Mohammed Karim*,[1], Alimam Mohammed Abdellah[1], Seghuiouer Hamid[2]

[1]*Abdelmalek Essaâdi University, Avenue Khenifra, Tétouan 93000, Morocco*

[2]*École nationale des sciences appliquées de Tétouan, ENSA de Avenue de la Palestine Mhanech I. Tétouan, Morocco*

ARTICLEINFO

Article history:
Received: 01 June, 2019
Accepted: 20 July, 2019
Online: 19 August, 2019

Keywords:
Traffic forecasting
Neural network
Supervised learning algorithm
Highway

ABSTRACT

There is no doubt that a good knowledge of traffic demand has a direct impact on improving traffic management. Road traffic is strongly correlated with many factors such as day of week, time of day, season and holidays which make it suitable for prediction. In this paper, we develop a neural network model for hourly traffic prediction that makes full use of these temporal characteristics. The proposed algorithm is tested on a real-world case, and the experiment results is presented to evaluate its accuracy.

1 Introduction

Accurate traffic volume prediction plays a significant role in traffic management and control. Estimate the number of vehicles passing per unit time can help traffic managers make the right decisions. Up to now a variety of traffic flow prediction algorithms have been proposed. These methods can be arranged into two categories: parametric approach and non-parametric approach.

Since the early 1980s, a wide range of parametric techniques have been studied such as historical average algorithms, smoothing techniques, linear regression, filtering techniques [1], and autoregressive integrated moving average (ARIMA)[2] family. Later on, researchers began to explore the potential of non-parametric techniques in traffic forecasting, including neural networks [3, 4, 5, 6, 7], support vector machines [8, 9], k-nearest neighbor [10, 11], etc. These methods have gained more attention compared to parametric techniques considering that they can capture the stochastic and nonlinearity of the traffic flow. They are flexible in their use and are generally quite robust.

The rest of the paper is structured as follows. Following this introductory section, a description of the proposed methodology is provided. The dataset for the numerical experiments is introduced in section 3 along with the results and performance evaluation. Finally, concluding remarks are stated in section 4.

2 Methodology

In this section, a description of the Artificial Neural Network structure is presented. Artificial Neural Networks (ANNs) are one of the recent methods employed for traffic forecasting. They have the ability to approximate almost any function due to their properties of self-learning and self-adaptive capabilities.

2.1 Prediction logic with artificial neural network

A neural network consists of a set of interconnected processing elements, called neurons, which are arranged in a series of layers: an input layer, one or more hidden layers and an output layer.

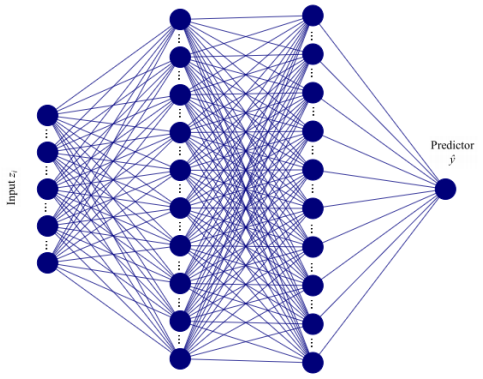

Figure 1: Architecture of a neural network prediction model

There is no connection between neurons in the same layer. However, each neuron in a layer is fully connected to all neurons in the next layer. Those connections are uni-

*Alimam Med Abdellah, Morocco, Tangier, karim.alimam@gmail.com

directional: information from the inputs pass through the hidden units to eventually reach the output units. This type of architecture is called feedforward neural network (Fig. 1).

Neural networks are able to perform different categories of tasks, including regression. ANN can be trained to model the relationship between a number of input variables and a set of continuous results (target variables).

The inputs z_i reach the neuron through connection links, each with an associated weight w_i. The higher the value of a weight, the stronger the intensity of the incoming signal. When the signals are received, a weighted sum of the inputs plus a bias b, called the net input, is calculated:

$$net_i = \sum_i (w_i z_i) + b_i \tag{1}$$

The output is then determined by applying a transfer function f to the net input. The transfer function can be any differentiable non-linear function.

$$output_i = f(net_i) \tag{2}$$

This output will serve as input to other neurons in the next layer and so on. When the entire network has been executed, the neurons in the output layer become the outputs of the entire network (predicted values).

3 Experiments

In this section, the real-world data used in this study is described and the forecasting model along with the results are presented. The forecasting model is implemented using Python and Keras.

3.1 Data preparation and description

Data on the volume of traffic on hourly basis has been collected from the Melloussa Toll plaza. This traffic represents the number of vehicles passing through the system during each hour of the day. The Toll Lane Controller collects data from the lanes and transmits it to a server where all transaction data are stored.

The Melloussa Toll plaza is one of the major toll highways in Tangier. It is located on a North-South motorway axis that leads directly to The Port of Tangier, Africa's biggest port, allowing the toll plaza to become an important transit point between Morocco and the European continent, with a throughput volume that could approach 900 vehicles per hour during summer peak periods.

Collected data for experiments spans for two years ranging from 2017/01 to 2018/12. The first 80% of the observations was selected to train the forecasting model, while the remaining 20% was treated as the testing dataset.

Missing and abnormal data are almost inevitable in practice. Their presence can affect the quality of data and can lead to incorrect results and conclusions. Therefore, missing and abnormal data were removed and repaired by estimating values from historical data.

To fit into the ANN model, the data was arranged in the following format (see Tab. I):

Table 1: Data structure used in the experiment

Year	Month	Day	Hours	Holiday	Traffic
2017	January	Sunday	1	Yes	61
2017	January	Sunday	2	Yes	32
2017	January	Sunday	3	Yes	17
2017	January	Sunday	4	Yes	16
2017	January	Sunday	5	Yes	33
...	...	...	...	...	...
...	...	...	...	...	...
2018	December	Monday	23	No	83
2018	December	Monday	24	No	47

Before being able to model a problem with a machine learning algorithm, it is often necessary to perform a number of transformations on the data, so that the problem can be easily understood and interpreted by the machine learning algorithm.

Therefore, the data, including Hours, Day, Month, and Holiday were converted into binary variables (for example, "Day of Week" feature 2 is transformed to 001000).

3.2 The forecasting model

Artificial neural networks are characterized by two main parameters: the number of hidden layers and the number of neurons per hidden layer.

There is no general method for determining the appropriate values of these parameters. Thus, it is usually necessary to proceed by trial and error in order to find the optimal structure.

In our approach, a three-layer ANN with 100 hidden neurons in each layer was found to achieve the lowest error rates. ReLU(Rectified Linear Unit) was used as the activation function for the hidden layers while the linear function was used for the output layer.

3.3 Model Evaluation

The mean square error (MSE) was used as the indicator of the accuracy of the prediction method, defined as:

$$MSE = \frac{1}{N}(\sum_{i=0}^{n}(f_i - y_i)^2 \tag{3}$$

Where,

- N is the number of data points
- f_i is the predicted value (the network's output)
- y_i is the target value for the ith observation

3.4 Forecasting results

As we mentioned earlier, the traffic flow data is divided into two parts: the first part is the training sample and the second part is the testing sample. The training data is used to identify the pattern of data and the test data is used for checking the performance. The forecasting results of the testing data set are shown in Fig. 2.

The error is quantified using Mean Square Error (MSE) and the values obtained for each iteration are shown in Fig. 2(b).

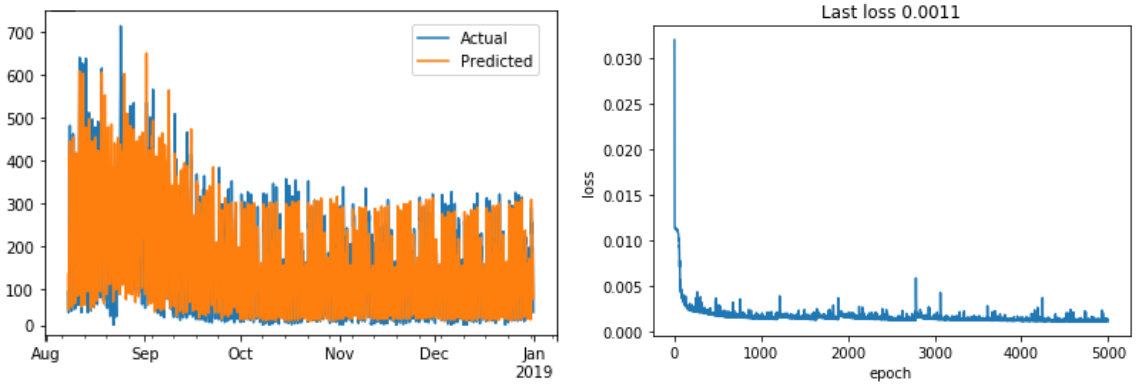

(a) Line plot of ANN forecast vs original values

(b) Model loss

Figure 2: The forecasting results

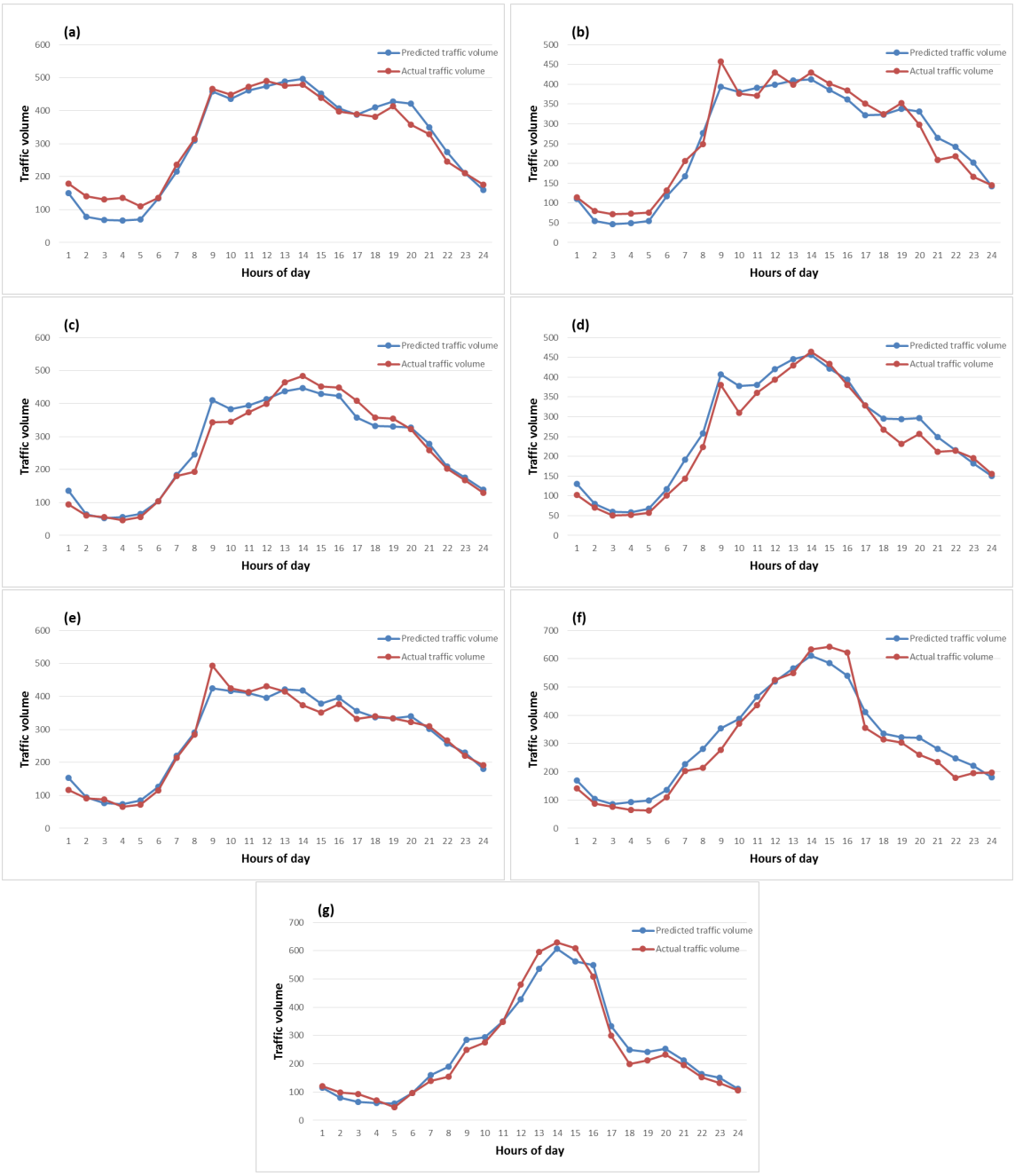

Figure 3: The hourly traffic volumes of different days in a week: (a) Monday, (b) Tuesday, (c) Wednesday, (d) Thursday, (e) Friday, (f) Saturday, and (g) Sunday

From Fig. 2(a), it can be seen that the line graph is divided into two parts: the first part is the one with the highest traffic volume and varying traffic patterns, which corresponds to the month of August. The second part presents the remaining months of the year, which shows a relatively stable traffic patterns. The model perform reasonably well in predicting the second part compared to the first one. This could be explained by the following reasons:

- During this time period, the variations of traffic flow are high. Traffic patterns are not the same comparing day with day, which makes it hard to capture pattern similarities.
- The shifting nature of Eid festivals had a direct impact on the traffic flow pattern. In this particular period, Eid Al-Adha, one of the most important festivities of the year, coincides with the end of the summer holidays and the start of the school year, which help increase the variability in traffic demand.
- The proposed method is trained to learn the behavior and predict future outcomes using historical data. Therefore, a larger training set provides better results. Here in this study, we only have August of 2017 as historical data.

In order to better underline the predictive accuracy of the ANN model, a comparison of estimated and actual traffic values for different times of the day and week is presented in Fig. 3.

We can observe that the ANN model performs well in capturing the data patterns on hourly and daily basis.

The same results has been obtained for the next year (see Fig. 4).

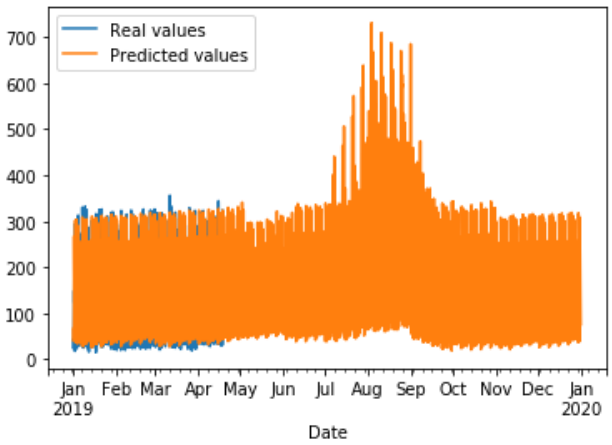

Figure 4: Prediction results of the hourly traffic volume for the first four months of 2019.

On a seasonal basis, the proposed model was able to accurately capture the behaviour of traffic over time as can be seen in Fig. 5. Traffic tends to pick up heavily during the summer months compared to other time of the year.

4 Conclusion

By visually exploring the traffic data, we observe that traffic is affected by a number of temporal features. In this paper, we developed an ANN algorithm for the prediction of hourly traffic volume that model the relationship between the traffic and these temporal features. The suggested model is tested on real world traffic volume, collected from The Melloussa toll plaza and the results showed that the method was able to identify the changes in traffic pattern at different period of time.

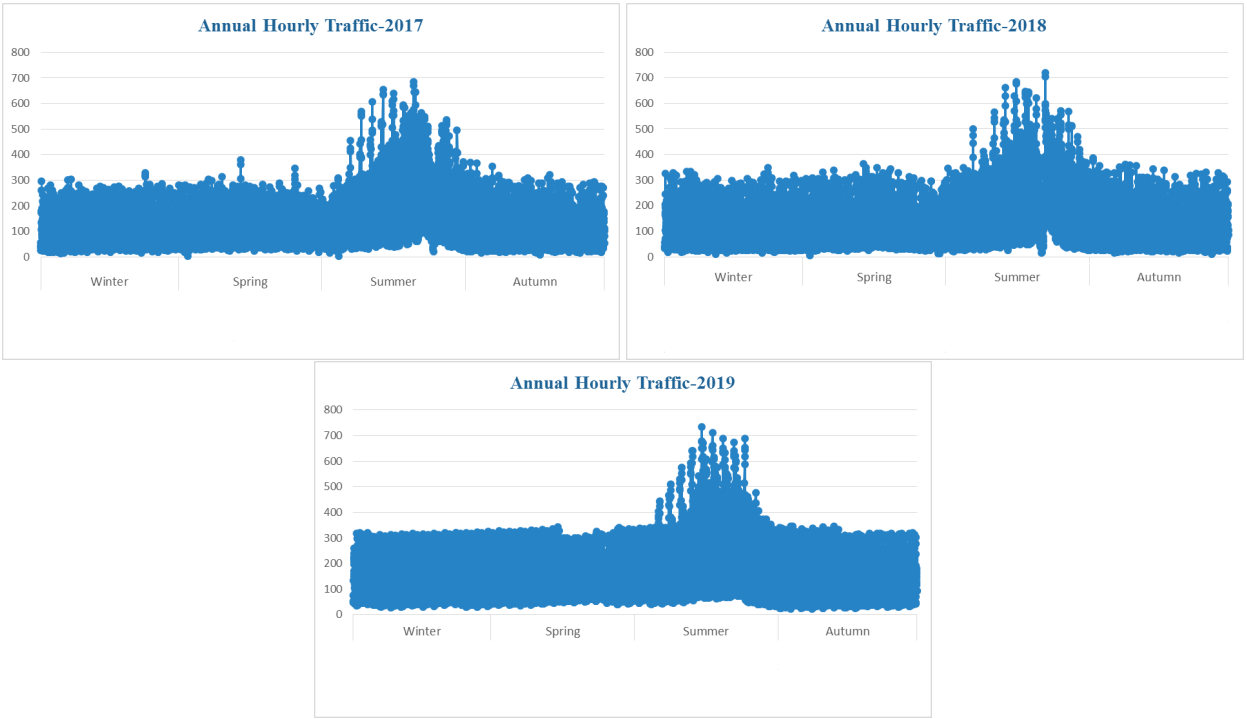

Figure 5: Seasonal variation in traffic flows

Special events are also one of the factors that can greatly affect traffic pattern. Adding this feature to the model is worth studying.

References

[1] Okatuni, I., and Y. J. Stephanedes.(1984) "Dynamic Prediction of Traffic Volume Through Kalman Filtering Theory," *Transportation Research Part B,* Vol. 18, No. 1, pp. 1–11.

[2] M. Levin and Y. D. Tsao. , "On forecasting freeway occupancies and volumes (Abridgment)," *Transportation Research Record,* No. 722, 1980, pp. 47-49.

[3] Centiner, B. G., Sari, M., and Borat, O. (2010). "A neural network based traffic-flow prediction model," *Mathematical and Computational Applications*, 15, 269-278.

[4] Licheng Qu, Wei Li, Wenjing Li, Dongfang Ma, Yinhai Wang (2018). "Daily long-term traffic flow forecasting based on a deep neural network," Expert Syst. Appl. 121: 304-312.

[5] Kranti Kumar, M.Parida, V.K.Katiyar. "Short term traffic flow prediction for a non urban highway using artificial neural network,"*Procedia - Social and Behavioral Sciences, 2013*, Vol. 104. P. 755-764.

[6] M.S.A Siddiquee, S. Hoque. "Predicting the daily traffic volume from hourly traffic volume using Artificial Neural Network," 2017.

[7] Melinda Barabas, Georgeta Boanea, Andrei B. Rus, Virgil Dobrota, Jordi Domingo-Pascual. "Evaluation of network traffic prediction based on neural networks with multi-task learning and multiresolution decomposition," *2011 IEEE 7th International Conference on Intelligent Computer Communication and Processing*.

[8] Sapankevych, N., Sankar, R., et al, 2009. "Time series prediction using support vector machines: a survey. Comput," Intell. Mag., IEEE 4 (2), 24–38.

[9] Amanda Yan Lin, Mengcheng Zhang. "Highway Tollgates Travel Time and Volume Predictions using Support Vector Regression with Scaling Methods," Department of Applied Mechanics CHALMERS UNIVERSITY OF TECHNOLOGY Gothenburg, Sweden 2017.

[10] Zheng, Z., Su, D., 2014. "Short-term traffic volume forecasting: a k-nearest neighbor approach enhanced by constrained linearly sewing principle component algorithm," *Transport. Res. Part C : Emerg. Technol,* 43, 143–157.

[11] F. Habtemichael, and M. Cetin. "Short-Term Traffic Flow Rate Forecasting Based on Identifying Similar Traffic Patterns," *Transportation Research Part C,* 66, pp. 61-78, 2016.

[12] Van Der Voort, M., M. Dougherty, and S. Watson. "Combining Kohonen Maps with ARIMA Time-Series Models to Forecast Traffic Flow," *Transportation Research Part C*, Vol. 4, No. 5, 1996, pp. 307–318.

[13] Ahmed, M. S., and A. R. Cook. "Analysis of Freeway Traffic Time-Series Data by Using Box–Jenkins Techniques," *Transportation Research Record 772,* TRB, National Research Council, Washington, D.C., 1979, pp. 1–9.

[14] Williams, B. M. "Multivariate Vehicular Traffic Flow Prediction: Evaluation of ARIMAX Modeling," *Transportation Research Record: Journal of the Transportation Research Board,* No. 1776, TRB, National Research Council, Washington, D.C., 2001, pp. 194–200.

[15] Mario Cools, Elke Moons, and Geert Wets. "Investigating the Variability in Daily Traffic Counts Through Use of ARIMAX and SARIMAX Models," *Transportation Research Board of the National Academies,* No. 2136, Washington, D.C., 2009.

[16] Williams, B. M., and L. A. Hoel. "Modeling and Forecasting Vehicular Traffic Flow as a Seasonal ARIMA Process: A Theoretical Basis and Empirical Results," *Journal of Transportation Engineering (ASCE)*, Vol. 129, No. 6, 2003, pp. 664–672.

[17] Blaž Kažič, Dunja Mladenić and Aljaž Košmerlj (2015). "Traffic Flow Prediction from Loop Counter Sensor Data using Machine Learning Methods," *Proceedings of the 1st International Conference on Vehicle Technology and Intelligent Transport Systems (VEHITS-2015),* pages 119-127.

ASTES

Advances in Science, Technology and Engineering Systems Journal
Vol. 4, No. 4, 328-346 (2019)
www.astesj.com
Special Issue on Advancement in Engineering and Computer Science

ASTES Journal
ISSN: 2415-6698

Overview on 5G Radio Frequency Energy Harvesting

Sanae El Hassani*[1], Hind El Hassani[2], Noureddine Boutammachte[3]

[1] *LTI Laboratory, ENSA El Jadida, Chouaib Doukkali University, 24 000, Morocco*

[2] *LISA Laboratory, ENSA Fès, Sidi Mohamed Ben Abdellah University, 30 000, Morocco*

[3] *3ER Team, ENSAM Meknès, Moulay Ismail University, 50 000, Morocco*

ARTICLEINFO

Article history:
Received: 21 May, 2019
Accepted: 02 August, 2019
Online: 19 August, 2019

Keywords:
Energy Harvesting
5G
Green technologies
SWIPT
Rectenna

ABSTRACT

The current industrial landscape is becoming increasingly aware of the need to optimize energy use and management for all domains, including telecommunications. Among others, RF Energy Harvesting is a promising technique for 5G systems as an alternative to traditional energy supply sources. This paper presents 5G landscape and ecosystem. It positions RF-Energy Harvesting in 5G context and reviews its techniques. It also considers constraints and research trends for different aspects needed to make RF energy harvesting ready for deployment along with 5G enabling technologies.

1 Introduction

This paper is an extension of the overview originally presented in 2017 about *RF Energy Harvesting For 5G* at the International Renewable and Sustainable Energy Conference (IRSEC) [1]. In fact, due to the rapid evolution of new technologies, the world faces new challenges concerning Energy Efficiency (EE). The transformation in users habits, driven by the installation of new services and the creation of new needs, especially in telecommunication, resulted in a significant rising in volume demand and requirements diversity. These transformations are leading the development of the fifth Generation (5G) of mobile systems, expected by 2020 [2], and research is being conducted to issue this new generation. In addition to the growing number of subscribers, new applications as for smart cities, smart grids, Internet of Things (IoT) and Machine-2-Machine (M2M) communications imply an increasing number of sensors, and thus the need of reviewing the system design. The sophisticated power hungry future handsets, the very large number of simpler sensors, and the dense network architecture necessary to respond to the growing needs are all factors to make energy management an urgent issue for future systems. EE appears thus as a major development key of 5G systems, as pointed in many 5G visions by telecommunication industry actors [3, 4, 5]. In order to enhance the energy consumption and management, techniques like Radio-Frequency Energy Harvesting (RF-EH), virtualized network functionalities, cloud technologies, etc. are proposed.

Energy aspects in 5G systems have attracted a lot of attention in the last years, and many studies, reviews and tutorials have considered these aspects. For example, in [6], authors provide a survey on energy-efficient wireless communications, with a discussion on the most relevant challenges at that time. General energy efficient technologies are discussed iwith no specific interest in EH solutions. Authors in [7] give an overview of EH techniques, in particular on EH power management policies optimizations, with specific stress on Wireless Sensor Networks (WSNs) and on ambient RF harvesting. In their survey [8], authors discuss 5G green network EE and promising technologies and architecture for its optimizations. Among these techniques, EH is discussed as well as other key enabling techniques, but specific EH integration is not detailed. The authors in [9] also consider EH from a circuit design point of view, particularly for embedded systems, and authors in [10] research RF-EH for IoT from an implementation perspective, including the design of antennas, rectifiers, and matching networks.

This paper aims to give a general review of EH in 5G systems, which includes both ambient and dedicated EH. In addition, considering the imminent commercial launching of 5G, and the ongoing standardization of 5G New Radio (5GNR) [11], an updated overview of RF-EH techniques is needed taking into account the standardization landscape. To this end, 5G requirements and use cases, as well as 5G ecosystem and some of the key 5G enabling technologies, are

*Corresponding Author: Route d'Azzemour Nationale N1 ELHAOUZIA BP 1166 El Jadida 24002 Morocco, (+212) 5 23 34 48 22 & elhassani.s@ucd.ac.ma

presented in the first section. In addition, a special subsection is dedicated to IoT, as one of the most RF-EH appealing 5G enabled use cases. The second section discusses EE in 5G networks from both network and terminal sides, while RF-EH implementation challenges and candidate solutions are reviewed in the the third section. The fourth section presents RF-EH in 5G ecosystem, giving a literature review of combinations between RF-EH and some of the most important 5G key enabling technologies. A conclusion of the paper is then given.

2 5G general technological landscape

2.1 5G Requirements

Compared to current mobile generation, 5G mobile data rate volume per area is expected to be multiplied by 1000, and user data rate as well as the number of connected devices are expected to be multiplied by 10 to 100. Battery life should also be 10 times longer, and latency 5 times shorter. 5G requirements are summarized in Figure 1, and the International Telecommunication Union (ITU), which has established an R&D programme worldwide on International Mobile Telecommunications for 2020 and beyond values(IMT-2020), has established a 5G framework as illustrated in Table 1 [12].

Table 1: 5G requirements

Requirements	Desired Value
Data Rate	1 to 10 Gbps
Data Volume	9 GB/h (busy period) and 500GB/month/user
Latency	Less than 5 ms
Battery Life	One decade
Connected devices	300000 devices/AP
Reliability	99.999%

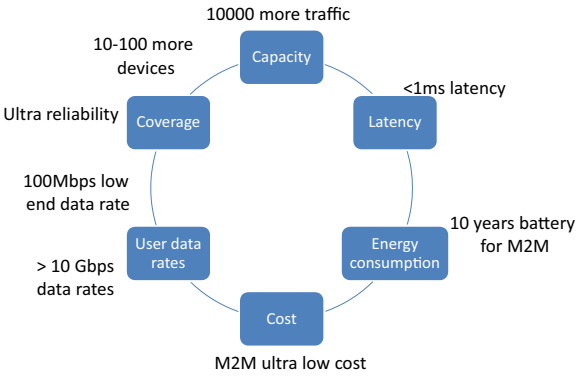

Figure 1: 5G key requirements summary (Source [13])

5G systems are meant to manage at the same time very low cost devices, such as sensors, and advanced ones, such as smartphones and tablets. For example, simple devices may choose not to use large bands. Thus, in the same system, and in some frequency bands, smart devices will use a band of 100 MHz while sensors only 10 MHz. Note that 5G will have to manage much denser networks than today, around 1 million connections/km^2, and the more predominant design parameter will thus be the cost/area.

2.2 5G use cases

Traditional as well as new use cases are addressed in 5G, and this implies new challenges. The corresponding requirements are specified by several organizations and research actions.

Each use case has its own requirements, such as throughput, delay, reliability, etc. and consequently uses different techniques. Hence, a wide range of devices, such as smartphone, wearable, MTC, etc., are being all expected to use 5G systems in a diverse heterogeneous environment. A categorization example of use cases has been developed by the Next Generation Mobile Networks (NGMN) Alliance through representative examples, which leads to 8 families of use cases [14], illustrated in Figure 2.

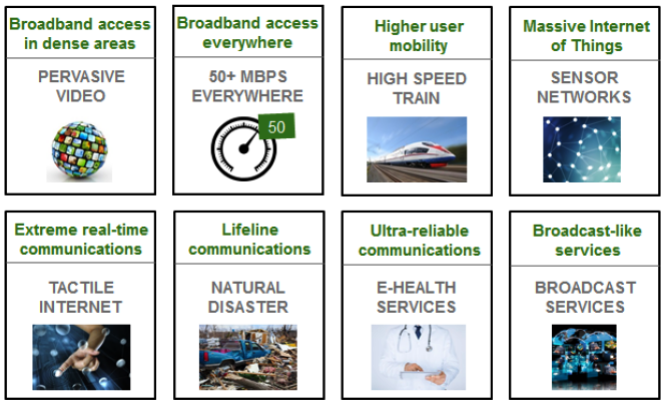

Figure 2: Families of use cases identified by NGMN (Source[14])

For example, smart cities applications including metering, city or building lights management, environment monitoring, and vehicle traffic control can be deployed as WSNs. These services, when aggregated, form a high density devices environment with heterogeneous technologies that need to be managed in a common communication and interworking framework, where very low cost devices with very long battery life may exist. 5G may provide platform for such deployments. Another example of 5G use cases is the mobile Video Surveillance, which is expected to be deployed almost everywhere. This means an automated analysis of the video footage with constraints, though relatively reduced for battery life, but high for reliability and security of the network as well as performance and interactivity with remote systems.

Note that the 3rd Generation Partnership Project (3GPP) issued and approved four Technical Reports on 2016, which outlined new Services and Markets Technology Enablers (SMARTER) [15], and contained more than 70 different use cases categorized into different groups :

- Massive Internet of Things, particularly relevant to the new vertical services, such as smart home and city, smart utilities, e-Health, and smart wearables.
- Critical Communications, for which there is more need for latency, reliability, and availability. Use case

examples are industrial control applications and tactile Internet.

- Enhanced Mobile Broadband, including use case families related to higher data rates, higher density, deployment and coverage, higher user mobility, devices with highly variable user data rates, fixed mobile convergence, and small-cell deployment.

- Network Operation, addressing functional system requirements, including for example flexible functions and capabilities, new value creation, migration and interworking, optimizations and enhancements, and security.

Example of projects exploring EE and EH in 5G systems is Sustainable Cellular Networks Harvesting Ambient Energy (SCAVENGE) [16], which is a project funded from the European Union's Horizon 2020. It defines among others an architecture framework for EH networks for Core Network (CN) and Radio Access Network (RAN).

2.3 5G ecosystem

5G systems cover a large span of use cases, with different data rates, latencies, reliabilities, densities, required powers, etc. This implies many tradeoffs, and a highly scalable architecture. As described in [17], the new 5G ecosystem is complex and involves many participants, including manufacturers for components, chipsets, network equipments and wireless devices, in addition to mobile networks operators, application developers and even users themselves, all overlaid by different standardization entities. As stated in [18], the first mover of 5G is the wireless part as it establishes foundations for the feasibility of final products and services. Many connectivity options are considered in 3GPP, which allows several deployment alternatives. However, as highlighted in [18] the focus for initial deployments is on non-standalone NR and standalone NR, as the deployment of several options may make the whole 5G ecosystem too complex. The simplification of 5G through reduction of deployment options is also adopted by other industry actors, such as Ericsson [19].

2.4 Examples of 5G key enabling technologies

5G systems require an important change in the cellular architecture as well as key wireless technologies. The requirement for massive network capacity along with the increased user experience suggest research in numerous dimensions. In particular, the RAN appears as one of the biggest challenges. For example, the increase in bandwidth demand implies the optimization of current systems spectrum use, unlicensed spectrum use and the allocation of new bands, starting with the move to millimeter wave (mmWave) bands. The optimization of spectrum use also means that, among others, new waveforms and advanced Multiple Input Multiple-Output (MIMO) will be used. Extreme densification and offloading are also key elements to enhance capacity, which implies an urgent need for virtualization and softwarization of the network. As presented in [4], the Figure 3 illustrates these needs in three distinct dimensions.

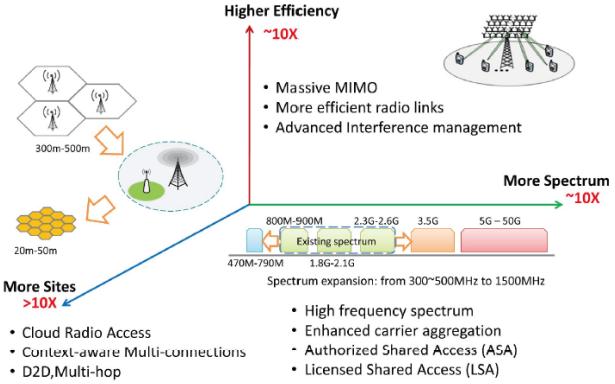

Figure 3: 5G technological research in three different dimensions (Source: [4])

Examples of key 5G enabling technologies are given in the remainder of this subsection.

2.4.1 Spectrum allocation

5G is a convergence of previous and new systems, and its spectrum is expected to be a combination of allocated and new bands. Some of the spectrum below 6GHz is thus being re-purposed for use with newer technologies; it is the primary 5G band, as decided in WRC 2015. Complementary 5G bands above 6GHz, are expected to be allocated in the 2019 World Radiocommunication Conference (WRC 2019) [20] (October). Illustration of these bands is given in Figure 4. On the The 3rd Generation Partnership Project (3GPP) Release-15, the New Radio-Unlicensed spectrum (NR-U) work item supports both the existing 5GHz unlicensed band and the new "greenfield" 6GHz unlicensed band. Other unlicensed and shared spectrum bands, including mmWave, can be expected in coming releases [11], even though it is not as mature as current frequency bands. In fact, mmWave has rather hostile propagation characteristics, as well as a current comparatively high equipment cost, which has limited its use so far. However, 5G mmWave mobile technology have been already demonstrated, as first by Samsung in May 2013 [21], and later by others, as for Huawei [22]. A more accomplished 5G pilot system was demonstrated in 2018 Winter Olympics [23].

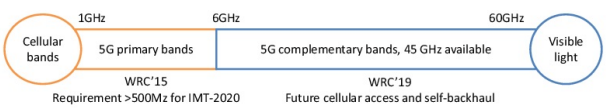

Figure 4: WRC-15 and WRC-19 5G spectrum allocation

Integration of many bands for the same transmission can be made through Cognitive Radio (CR), motivated by the underutilization of many frequency bands. In fact, CR allows dynamic allocation of underutilized resources, after their sensing, in an opportunistic way without altering the other users, and thus to expand the spectrum of a cellular networks on demand and at a relatively low cost [24, 25].

2.4.2 Carrier Aggregation (CA)

As 5G is a convergence of many systems, the 5G radio access uses simultaneously many technologies, with possibly different frequency bands. This may enable a more effective use of the crowded and fragmented spectrum, a simultaneous use of different Radio Access Technologies (RATs) and more flexibility of resource allocation. However, this implies also the need to aggregate different carriers. CA is already used in Long Term Evolution (LTE) since 3GPP Release 10 for inter and intra LTE-LTE contiguous carriers aggregation. Release 11 presented Intra-band non-contiguous CA, and Release 12 presented CA for Frequency Division Duplex (FDD) and Time Division Duplex (TDD). Release 13 presented CA for 5 GHz WiFi bands, called Licensed Assisted Access, and Release 14, which starts 5G standardization, defines more cases following the 5G adopted bands [26]. Some issues should be considered for Internet Protocol (IP) configuration, interference coordination and time synchronization. Moreover, resource scheduling over the aggregated bands should be optimized and may use advanced tools, such as game theory [27].

2.4.3 Massive MIMO

Many techniques used to enhance spectrum efficiency are surviving in 5G, while other new techniques are proposed. MIMO antennas techniques is already used for LTE and LTE-Advanced (LTE-A), and 5G proposes massive MIMO as one of its most important enabling techniques. In fact, thanks to multiple antennas at the Base Station (BS), the energy in downlink can be focused to form beams towards the User Equipment (UE). In 5G, a large number of antennas, i.e. massive MIMO, can enable the serving of many users in an accurate way. Moreover, when combined with other 5G techniques, like small cells and mmWave, it provides significant capacity, as required for 5G systems [28]. Note that massive MIMO can also be used for backhauling [29].

2.4.4 Channel modeling

In 5G systems, the expected bands to be used, especially above 6GHz, are not addressed by current models, and accurate models are needed to enable many of the physical layer techniques. Thus, research is already conducted for mmWave characterization in several environments [30]. As indicated in [31], the new channel model extends the existing 3GPP 3D channel model, and handles frequencies up to 100 GHz in several mobility scenarios. In this optic, 3GPP RAN Meeting for example was held in Busan Korea in June 2016 and approved the first standard for the mobile broadband 5G high-frequency ($6 - 100$ GHz) channel model.

2.4.5 Signal waveforms

Multicarrier modulation, particularly Orthogonal Frequency Division Multiplexing (OFDM), is adopted in LTE and enables good spectrum efficiency. However, it still presents some drawbacks, as it inserts a Cyclic Prefix (CP) that reduces the efficiency, in addition to its large sidelobes, and thus considerable Out-Of-Band (OOB) emission, resulting from the rectangular pulse shaping,as well as its high Peak to Average Power Ratio (PAPR). Most popular candidates waveform for 5G, in addition to OFDM, include :

- Filtered OFDM, which removes OOB emissions by filtering the signal [32].
- Filter Bank based MultiCarrier-Offest Quadrature Amplitude Modulation (FBMC-OQAM), which is a modified OFDM requiring no CP and thus enhancing spectrum efficiency [33]. Sub-carriers are filtered at both transmitter and receiver sides, and this reduces OOB and makes the signal more robust against Doppler effect, Inter-Symbol Interference (ISI), synchronization imperfections, spectrum fragmentation, etc. This also results in self-equalization, which can reduce the number of unused subcarriers, and blind channel tracking, reducing pilot contamination and thus enhancing massive MIMO functioning.
- Universal Filtered Multi Carrier (UFMC), which filters subbands rather than subcarriers [34]. This gives more flexibility to the design. The use of a prefix in this case depends on filters design.
- Generalized Frequency Division Multiplexing (GFDM), which also provides a flexible structure via adjustable pulse shaping and subcarrier filtering. In addition, data symbols are grouped both in time and frequency domains. However, filtering flexibility implies self-created interference, which is dealt with using iterative interference cancellation at the receiver [35].

2.4.6 Multiple access

The multiple access technique used in 4G is OFDMA, which may survive for 5G. However, massive MIMO in a dense network context, multi-user MIMO (MU-MIMO) can be enabled using Spatial Division Multiple Access (SDMA). For higher capacity, Non-Orthogonal Multiple Access (NOMA) schemes are also proposed for 5G, as it allows more than one user to share the same subband without coding or spreading redundancy [36, 37, 38]. For this scheme, users are superposed in time and frequency, and have different powers following their channel conditions. Differentiation of the users is then performed using Successive Interference Cancellation (SIC), which uses joint processing combined with subcarrier and power allocation algorithm [39, 40]. An illustration of NOMA mechanism is given in Figure. 5. So far, 3GPP NR has specified flexible technology framework that can be tuned to enable a wide range of 5G scenarios, and more specifications are expected for Release 16 [41].

2.4.7 Ultra Dense Network (UDN)

5G brings a substantial network architecture redesign, particularly through densification, in order to support the expected heavy traffic. Networks densification has been used since the second generation (2G) for capacity scaling, but the ultra densification for future networks can provide an extreme and user-centric reuse of system bandwidth on the spatial domain, and improve propagation conditions by reducing the distance between the end user and the BS. It implies

an increased spatial reuse of system resources, a large node density and irregular deployments. Challenging issues about UDN include among others interference management, heterogeneous multi-RAT optimization, the possibly high cost of a dense infrastructure, the cell-edge effect, and the backhauling.

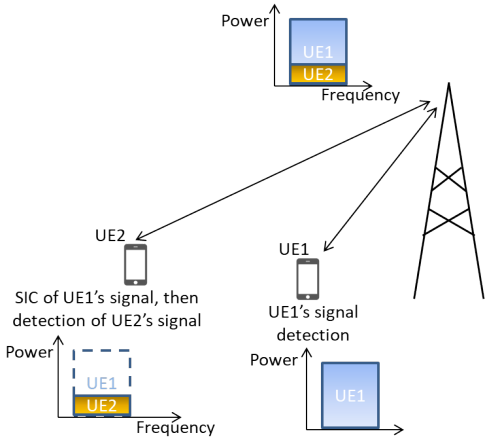

Figure 5: Downlink NOMA in a simple scenario with one BS and two UEs

2.4.8 Cloud-Based Radio Access Network (C-RAN)

As network densification is a key 5G networks enabler, it is expected that BSs will have to handle a heavy radio processing. A suggested solution in this case is the Cloud-based RAN (C-RAN). In fact C-RAN dissociates the Base-Band processing Unit (BBU) from the Remote Radio Heads (RRHs); For resource optimization, the BBU part is moved to a pool, or to the cloud, which is a virtualized cluster connected to the core network through the backhaul, and the transmission of the radio signal is performed by RRHs based on computed signals from the cloud. On the otehr hand, RRH is connected with the cloud BBU pool via a fronthaul.

RRHs are cheaper and simpler if cloud based computations are used. This allows thus more scalability and densification opportunities. It can also reduce the delay for inter-cell coordination and permits more joint optimization of processing, e.g. for cooperative interference management, scheduling, Coordinated Multi-Point, etc. [42].

C-RANs can also be self-organizing; intelligent smart cells are deployed in the area covered by a macro BS, and can enable advanced clustering and coordination schemes to enhance mobility and handovers. In addition, C-RAN in Heterogenous context lead to H-CRAN, where different types of nodes, including low power and high power nodes, use the same computing pools. The H-CRAN is illustrated in Fig. 6.

2.4.9 Network architecture

5G cellular networks are expected to be multi-RAT and multi-layer. Considering emerging 5G use cases, current network architecture is relatively incompetent to address 5G requirements. Thus, one of the central objectives in 5G architecture is network flexibility. Logical core and RAN have to be split to allow their evolution and to ease their deployment. To this end, the European Telecommunications Standards Institute (ETSI) adopted the separation of User Plane (UP) functions and Control Plane (CP) functions, and modularization of the function design, e.g. to enable flexible and efficient network slicing [44]. Similarly, a 5G architecture made of three layers and a management entity is presented by NGMN [45]. It is based on a central cloud and typically comprises multiple data centres which may be very distant, and connected to each other or to the central cloud or edge clouds. Figure 7 illustrates this topology as viewed by the project 5G NOvel Radio Multiservice Adaptative network architecture (5G NORMA), which is one of the 5G Public Private Partnership (5G PPP) projects under the Horizon 2020 framework [45].

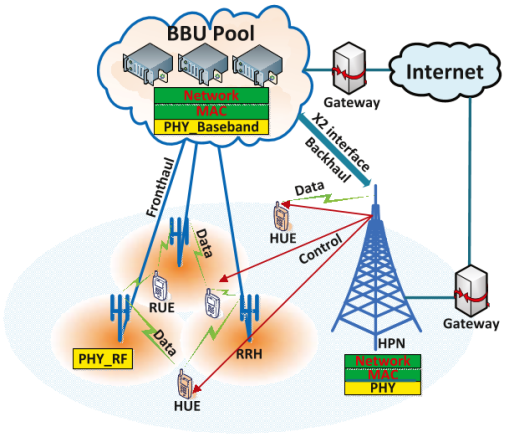

Figure 6: H-CRAN : Heterogeneous Cloud Radio Access Networks (Source [43])

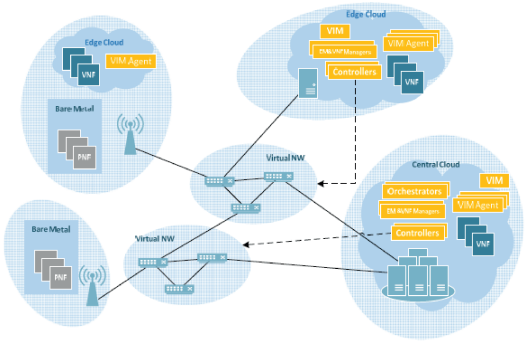

Figure 7: 5G NORMA topology view on architecture

As suggested in [46], in order to avoid redundancy, low layer functionalities are insured by radio logical network while a network cloud provides all higher layer functionalities. In addition, functions can be dynamically deployed in the network cloud through Software Defined Networks/Network Functions Virtualization (SDN/NFV).

In addition to layers, 5G uses network slicing to deliver services with different performance characteristics. It is a network technique, initially for the core network but extended to an End-to-End (E2E) concept including also RAN part. For example, massive IoT service, connecting fixed sensors that measure humidity, temperature, etc. to mobile networks, does not require advanced mobility features, critical in serving mobile phones. In contrary, a mission-critical IoT service, like autonomous driving or remote controlled

robots, requires a very low E2E latency. To avoid building a dedicated network for each service, multiple logical networks over a single physical network can be insured through network slicing. The physical network is sliced up into different virtual E2E slices, with specific network functions and RAT parameters, following the requirements of the use case or business model. Note that network slicing also limits error propagation between slices.

2.4.10 NFV/SDN

An important trend for 5G networks is virtualization, as it enables resource sharing. In addition, hardware and software have to be dissociated, and network functions to be moved towards software. Assuming separation between control and data, NFV is an important 5G architecture driver. It provides network adaptability and scalability [44], boosted by automated mechanisms; simple and fast operations will be needed to deploy new network features, and resources can be easily shared through the abstraction of physical resources to a number of virtual resources. An illustration of wireless network virtualization is given Figure 8.

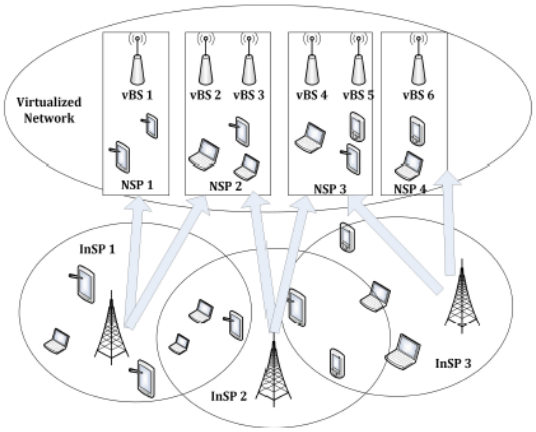

Figure 8: An example of wireless network virtualization (Source [47])

NFV uses a virtualized commercial server to set up network function software in virtual machines. RAN works thus as edge cloud while core works as core cloud. Connectivity among virtual machines located in edge and core clouds is insured by SDN. This makes thus the network architecture ultra-flexible; NFV processes network functions in the cloud, and SDN creates and exposes private virtual networks, linking thus the cloud back to the network. SDN enables the orchestration of the NFV physical and virtual infrastructure resources, through supporting provisioning and configuration of network connectivity and bandwidth.

2.4.11 Mobile Edge Computing

The diversity of 5G applications and the density of the network may lead to congestion, which may be solved by Mobile Edge Computing (MEC), mainly standardized by ETSI, 3GPP and ITU-T. MEC provides Information Technologies (IT) and cloud computing functions in the RAN, in close proximity to mobile subscribers. This enhances responsiveness to content, services and application requests, and enables thus ultra-low latency, high bandwidth radio network information.

MEC introduces new processing capabilities in the BS for new applications, with a new functions separation and a new interface between BBU and Remote Radio Unit (RRU). This is linked to C-RAN as C-RAN implements baseband processing capabilities in distributed locations. A demonstration for a 5G MEC proof-of-concept was conducted by Ericsson and Vodafone [48].

Note that MEC is currently deployed in LTE networks as an add-on to offer services in the edge. However, 5G system specifications provide new functionalities for edge computing [44].

2.4.12 Device to Device communications (D2D)

High-density expected for 5G networks can also be solved by D2D communication. In fact, unlike voice-centric systems, where no spatial proximity is assumed between communication parties, some data communication cases may imply collocated devices which try to wirelessly share content. In this case, it can be more efficient to use proximity-based D2D communication, which may also enhance capacity and coverage when devices act as transmission relays. Note that D2D is already used in 4G, and presents some challenges for 5G. Figure 9 presents typical downlink D2D scenario.

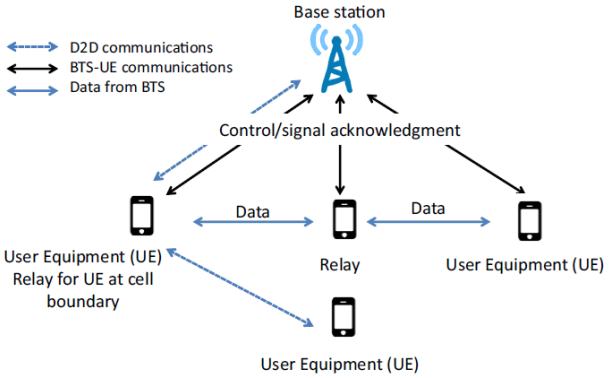

Figure 9: D2D typical scenario (Source [49])

2.5 IoT applications landscape

2.5.1 IoT characteristics

In IoT applications, a large variety of devices is implied, from small devices to big data centres. The devices can be self-empowered, battery-empowered or connected to the grid. For IoT specific applications, most devices, in number, are battery-empowered or self empowered, i.e. using EH.

IoT is distinct from WSN as it has specific characteristics. In particular, IoT energy sources have the following characteristics [50]:

- Scalability, as IoT often imply large deployments in possibly variable locations with different accessibilities. In this case, batteries are not ideal.
- Maintenance-free, as the deployments often imply a large number of devices. Wired empowering would be thus impossible and battery-based one would be costly.

- Mobility support, as for many applications, the devices are mobile.
- Long life-time, as in some applications, and because of difficult maintenance, devices are supposed to work autonomously up to several decades.
- Flexibility, as capacity and size of energy sources may vary following the IoT application.
- Low-cost, as IoT are usually deployed in a large scale, which means that a small difference in the unit cost may limit affordability of the application.
- Sustainability, as large scale deployments may imply significant power consumption, requiring thus sustainable power solutions.
- Environment-friendly, as IoT popularity may imply serious environmental impact, especialy if disposable batteries are used for devices powering.

Currently, solutions meeting these characteristics with very low power consumption are standardized, but having energy autonomy is even more attractive. EH-enabled nodes techniques, as well as batteries storing harvested energy and optimized low power circuits, have to be thus combined with power saving mechanisms and network resource management. Note that for traditional wireless networks, many factors are important in the design. For example, the acceptable latency of the transmission can lay from some milliseconds to some days. Transmission rate is also generally low, mostly some kilobytes per second. Similarly, the distance between nodes is critical, as it contributes in the definition of the transmission power. Depending on the application, the distance can range from centimeters to kilometers, and it can vary over time when mobility of the nodes is considered.

2.5.2 IoT standards and solutions

RF-EH globally provides little energy compared to other energy sources. Thus, it is more suitable for low power IoT applications. These are hence one of the most interesting motivations for RF-EH technologies development. It is also one of the vectors in international standardization bodies. Even though solutions exist since many years for low-power applications, including Wi-Fi, Bluetooth, and ZigBee, these are unsuitable for long-range cellular and M2M, which are essential for IoT. Low-Power Wireless Area Networks (LPWANs) aim to respond to such requirements. In fact, in order to achieve a low-power long-range communication, high receiver sensitivity is needed, as fine as to −130 dBm against −90 to −110 dBm in traditional technologies. This means that a higher energy per bit is needed, and thus that the modulation rate should be slower.

One of the major issues for M2M communications is the low-power long-range communication. LPWAN technologies, in order to achieve a long range capability, need to use high receiver sensitivities, up to −130 dBm compared with the −90 to −110 dBm in many traditional wireless technologies. This implies a higher energy per bit and thus a slower modulation rate. The two most popular solution for LPWAN are Sigfox and LoRaWAN. The first one is a global IoT network, aiming a low deployment cost of long-range, small-message device communication. It is a narrowband technology using extremely slow Binary Phase Shift Keying (BPSK) modulation. The second one is an LPWAN specification for long-range low-datarate wireless battery operated devices communication, promoted by LoRa Alliance, which coverage is comparable to a cellular network.

3GPP addressed categories and new standards for IoT requirements [51]. New users categories (cat1-6) are introduced starting from LTE Release 8. Release 10 defines 6-8 categories, and Release 12 defines LTE Cat-0. This category suits IoT applications and general M2M applications needs with low data rates in short bursts. This results in a reduced complexity and power. NarrowBand-IoT (NB-IoT) and LTE-M (or eMTC for enhanced Machine-Type Communications), are two complementary technoogies for IoT applications. NB-IoT is a direct candidate of Sigfox and LoRa, as it is less energy consuming and can address a large amount of connected devices. It can be deployed as a standalone solution or inside an LTE carrier, and will have more in-band deployment flexibility in 5G NR. LTE-M addresses another connected devices category which is more constrained in latency, mobility and density. Application examples are e-health, security, object tracking, etc. LTE-M however is more energy consuming. An illustration of LTE IoT evolution is given in Figure 10.

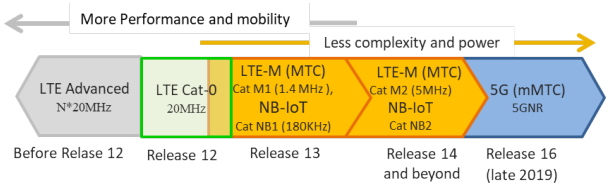

Figure 10: 3GPP IoT solutions standards

Note that many 5G technologies are specified to support IoT deployment, such as include D2D, SDN, NFV and MEC. For example, C-RAN reduces the cost of ultra-dense networks, expected especially with IoT deployments, through the simplification of BSs. This enables flexible and adaptable deployment.

3 5G Energy considerations

Today, energy is a major issue in all industries, including telecommunications. For example, the Mobile and wireless communications Enablers for Twenty-twenty Information Society (METIS) project considers EE as an important 5G topic [52]. The objectives of the project lead to technical goals with in particular a much denser network, containing low-power devices requiring higher battery life, up to 10 times longer than current batteries.

3.1 Energy efficiency on network side

5G will densify the network in order to increase the coverage and the capacity of the system. However, as power consumption is expected to increase at the same time, a challenging issue for 5G is the EE. For example, considering

data centres in the network, the author in [53] examines the variety of clusters and clouds that implies the need for power-saving control mechanisms. He presents network and cluster resources control algorithms, as well as an integrated and hierarchical control of the resources. Similarly, as treated by the project EARTH [54], improving EE at BS level need a variety of technologies. For example, it is proposed in [55] to use Cellular Partition Zooming (CPZ) to reduce energy consumption; following the present users in the area, the BS zooms in for coverage or out for sleep mode, which is energy saving.

Optimizations, categorized on green energy researches, aim BS energy use reduction [56]. In fact, the power consumption in the Operation Expenditure (OPEX) in today's mobile systems is dominated by networks, up to 90%, and only 10% is for mobile user. The network electricity supply is thus a critical issue in mobile industry, especially for regions with difficult grid power connection. Alternative energy sources, light, wind, vibrations, etc. are considered. However, alternative energies, especially renewable ones, present some challenges regarding availability and volumes. In particular, combining renewable energy sources at BS is critical. For example, the japanese operator NTT DoCoMo launched in July 2004 the *DoCoMo Eco Tower* [57], which is an experimental an self-powered 3G BS. Thid BS uses solar and wind power at once. Similarly, Alcatel proposed *Eco-sustainable Wireless Networks* to replace current generators [58]; Alcatel has an Alternative Energy Program combining alternative energy sources and energy-efficient equipments and networks.

Note that RF-EH appears as a candidate technology to further optimize energy management in 5G. In particular, EH from RF signals is actively studied and mathematical models are made in order to make it possible in the near future, as proposed in [59]. In the same scope, researches are interested in several scenarios, as cooperative multicast communication in [60]; EH relays harvest energy from the BS transmissions following two power splitting strategies at the relays for EH, and analytical expressions of outage probability are given for these strategies.

3.2 Energy efficiency on terminals side

Battery life is a major constraint for equipments' design. In fact, it can be lengthened through enhancement of its capacity, use and recharge process. The overall EE of the network would be consequently improved. 5GPPP establishes requirements for future 5G systems considering ultra-efficient 5G hardware, especially in terms of energy consumption, flexibility and compatibility with heterogeneous environments [61]. The interface between network and terminal can use massive MIMO technique to enhance EE, in addition to new waveforms and to network radio resources optimization. The air interface, procedures, and signaling can also be enhanced in terms of energy consumption through sleep modes, simplified procedures access schemes, and more efficient modulation, spreading and coding that allow low transmission powers. Energy consumption can be reduced using EH from environmental energy sources, such as light, heat and vibration [62]. However, as they vary along location, time, weather conditions, etc., it can be difficult to guarantee a given Quality of Service (QoS) that is required in some wireless applications. A possible solution for this problem is ambient radio signals harvesting, i.e. RF-powered energy-harvesting network (RF-EHN) [63, 64].

Note that circuit design has also to be coherent with EE optimization. Many technologies are discussed to prepare 5G-ready handsets, as in [65]. The research areas for that purpose include RF design, mobile cooperation, context awareness and seamless roaming among multiple technologies. New techniques for power amplification, antenna and filter design, and RF architecture are being studied for future handsets design. For example, M2M and D2D communications may use wireless power transfer technologies and optimization of sleep mode switching in order to have a battery-less sensor operation.

4 RF Energy harvesting implementation

4.1 Energy harvesting sources

EH has been already widely deployed using several energy sources. It consists on absorbing ambient energy in order to utilize it instantly or later. The most popular harvested energy sources are solar energy, wind energy, tidal waves energy, mechanical energy, electromagnetic energy, thermal energy, etc. EH sources and their corresponding sensors are illustrated in Figure. 11 [10].

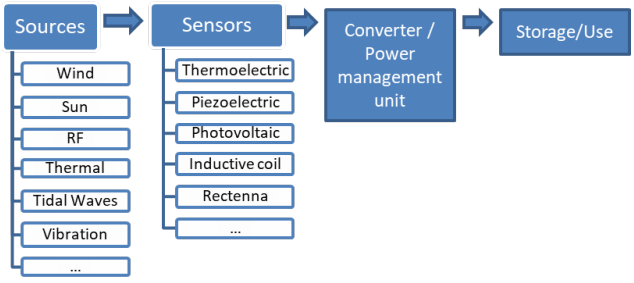

Figure 11: Energy harvesting sources and sensors

- RF sources have a power density ranging from 0.1 μW/cm^2 for ambient RF to 1000 μW/cm^2 for dedicated RF [10]. Electricity in that case is produced through magnetic inductive coupling: a loop with time varying current induces a receive loop with an open circuit voltage, and the resulting voltage can thus be directly used or stored in a battery for later use.
- Harvesting energy from heat is based on thermal energy generator, which uses the difference of temperatures to generate electricity. However, it has a low efficiency(5-10%) [50] and needs a temperature difference of 30°C. The power density in this case is about 135 mW/cm^2 at 10°C [66].
- Sun and light EH, i.e. solar and photovoltaic energy, is very popular nowadays due to its power density, efficiency, and flexibility. The light is collected by a semiconductor material, usually silicon, that produces DC power by the movement of electrons in the

semiconductor. The electricity is then stored in batteries or supercapacitors. The power density is about 100 mW/cm^3, but it requires direct exposure to light, which limits its use indoor [66].

- Mechanical energy is by the other hand harvested from vibration, pressure, etc. Among others, piezoelectric material, when exposed to a mechanical force, makes a polarization of ions in the crystal. This has a high energy density, which is about 50 μJ/N [66]. An example of piezoelectric EH for IoT applications can be found in [50].

4.2 Energy Harvesting constraints

EH presents an interesting solution to current energy consumption issues. However, it also presents some design constraints, as ambient RF waves figure among the most challenging energy sources. It suffers more particularly from :

- Causality, so that when harvested in the present, the energy is only available in the future, .
- Difficulty of concurrent EH and information transmission, at least for current designs.
- Efficiency loss when converting RF harvested signal to Direct Current (DC).
- Finite nature of energy storage.

For some applications, difficult environment access, connection cost and mobility makes it difficult to charge sensors or, at least, with a certain periodicity. In addition, if EH is used, for some EH sources, harvested energy depends on time and/or location and may not be enough for terminal's needs. Examples of time dependance are stillness time for vibration energy and night time for solar energy. Electromagnetic Radiation appears thus as an interesting stable and predictable energy source.

A cellular system can integrate EH using a standalone technique, hybrid technique or Simultaneous Wireless Information and Power Transfer (SWIPT) technique [67]. For the first technique, it allows to equip only some entities with EH. Hybrid EH empowers the system by both grid and EH, which may solve occasional unavailability of EH. SWIPT empowers the devices with harvested radio wave frequencies through which data is being received, as developed in 4.4.1.

Most of current mobile systems broadcast RF signals, carrying energy that presents a true opportunity as a source. At the same time, considering this possibility, the RF energy can supply devices. This implies the use of Wireless Power Transfer (WPT), and promising techniques are studied in order to implement such systems. The most significant examples are :

- Magnetic resonance coupling, which uses near-field signals and covers an extent ranging from some centimeters to some meters. This makes this technique adapted for charging mobile phones and hybrid electric vehicles, and its efficiency is 30% to 90% for a Tx-Rx distance ranging from 0.75m to 2.25m [68].
- Resonant inductive coupling, which exploits near-field signals and can also be used suitable for mobile phones charging, passive RF IDentification (RFID) cards and contactless cards. Frequency bands for this technique range from 10 KHz and 30 MHz and have an efficiency from 6% to 90% respectively [69].
- RF energy transfer, which uses far-field waves. Its coverage ranges from few meters to several kilometers and is suitable for wireless body and WSNs. Its efficiency is 0.4% to over 50% for −40 and −5 dBm input power, respectively [70]. This technique is being increasingly researched these last years and is gaining growing maturity, which promises new networks concepts, such as Wireless Powered Communication Networks (WPCN) [71].

The circuit suggested in [72] for ambient RF energy battery charge, as may be used in IoT-like applications, is made of a rectifier circuit and an impedance matching network. It converts RF waves to Direct Current (DC). Unlike EH circuit, information decoding uses down-conversion and sampling to process the baseband signal. For EH, a dedicated circuit directly connected to a receiving antenna, called a rectenna (rectifier antennas), captures energy which is converted then into functional DC voltage. This operation is called RF-to-DC conversion.

A rectenna has five main components: an antenna, the network matching the output impedance of the antenna to the rest of the circuit, a low pass filter that eliminates higher-order harmonics, the rectifier which is a diode, and DC filter load (peak detector). Such rectennas are designed in [73], operating at 27.5GHz, and achieve rectification with coupling between the input and output microstrip lines in the design. Note that EH-Oriented transceivers, especially rectennas, can be adopted in most cases for both indoor and outdoor applications and provide an efficient RF-to-DC conversion, reaching 80% in some configurations [74].

Figures 12 and 13 illustrate separately respectively energy and information receivers, which have to be combined for an EH scenario.

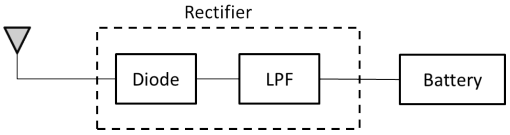

Figure 12: Simplified energy receiver scheme

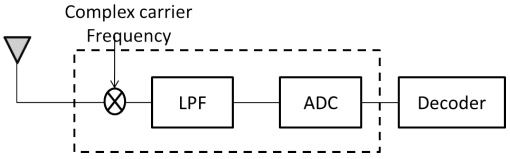

Figure 13: Simplified information receiver scheme

In the case of a receiver combining both EH and information decoding, the received power is split between the two either statically or dynamically. The splitting depends on the variations of RF energy and information, and also in the

needs of the receiver. The combined receiver can separate information and energy circuits [75], as illustrated in Figure 14, or it can integrate both in the same circuit, as illustrated in Figure 15.

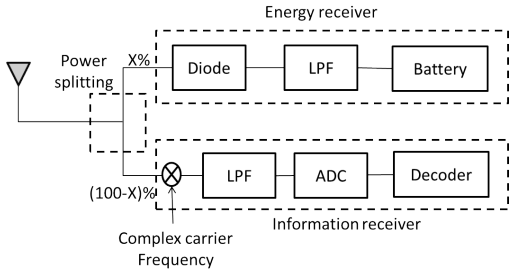

Figure 14: Separated information and energy receiver

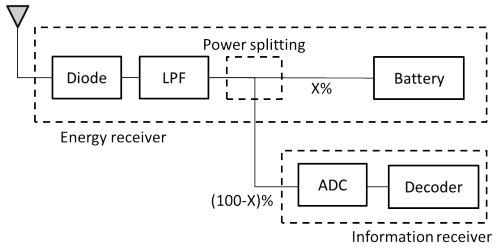

Figure 15: Integrated information and energy receiver

Authors in [75] show that there is a tradeoff exists between harvested energy and achievable rate, so that either integrated or separate receivers are selected depending on the harvested energy.

In teh remainder of this paper, RF-EH is considered. Note that RF energy by nature implies a relative time variability, as well as a sporadic aspect. On the other hand, this technology at mobile networks' scale is much younger than other energy sources harvesting, and accumulates thus less technology mastering and experience.

4.3 RF Energy Harvesting hardware

Several 5G use cases announce the need for self-sufficient and self-sustaining equipments. This energy chase covers the network as a whole including terminal devices, network elements and data centres, and EH can bring a solution for such requirements [72]. However, implementation of RF-EH presents many challenges, including, in some scenarios, the conception of rectennas to collect RF energy and the WPT [73]. Two categories can be cited for WPT: generation of electric power within few meters, i.e. near-field, and generation in an extent that can reach few kilometers, i.e. far-field. The efficiency of energy transfer in near-field case can reach up to 80% [76]. The WPT in far-field appears as RF or microwave signal and uses antennas for transmission and reception then converts it to power by rectifier circuits.

From a hardware point of view, antenna designs already exist for EH from interference signals issued from GSM, WLAN, UMTS and related applications, where antennas are designed with the potential to be used in EH systems. Several categories are also proposed in the literature for different frequency bands such as 900MHZ, 940MHz, 1.95GHz and 2.44GHz, 0,8 to 12GHz [77, 78, 79, 80, 81]. The designed antennas can be integrated in an antenna array to increase the gain and preserve a very high frequency bandwidth.

Though the harvested energy remains suitable for low power electronics, as it is rather low compared to other EH sources. However, a major challenge for RF-EH is still the low power sensitivity and legal restrictions of maximum authorized RF power radiation.

n the other hand, following [82], the global EH market is expected to reach 974.4 Million USD in 2022 when it was only 268.6 Million USD in 2015. This growth is driven by electronic sensors with ultra low-power and by embedded systems, which involve an energy issue. EH can be used to solve this issue, as suggested in [83], and EH relays can be considered, especially when the devices use WPT through RF signals. These signals carry both information and energy, and suggest for relays to charge themselves by extracting energy from the signals they overhear.

Note that RF-EH chips are already being developed as indicated in [84], where a startup has raised 30 million USD in funding to develop chips that can be powered by ambient radio frequencies. More generally, EH from other sources is also coming to reality, as the market for EH chips will approach 3.4 billion USD by 2022 according to the report in [85]. The mentioned report cites some companies that are in the race for EH chip market, and include for example Apple, National Instruments, Analog Devices, STMicroelectronics, Powercast, Renesas, Microchip Technology, Texas Instruments, Mentor Graphics, etc. An example of optimizations for RF Energy in a WSN using Powercast can be found in [86].

4.4 RF Energy harvesting approaches

In order to supply power to the nodes through WPT, it is possible to use either BSs already present in the network, or dedicated Power Beacons (PBs) specifically deployed, as illustrated in Figures 16 and 17. The latter has the advantage of being easy to deploy as it doesn't need backhauling. In both cases, energy beamforming can improve the EH efficiency, and distributed cooperative beamforming can be used to provide data rate fairness [87].

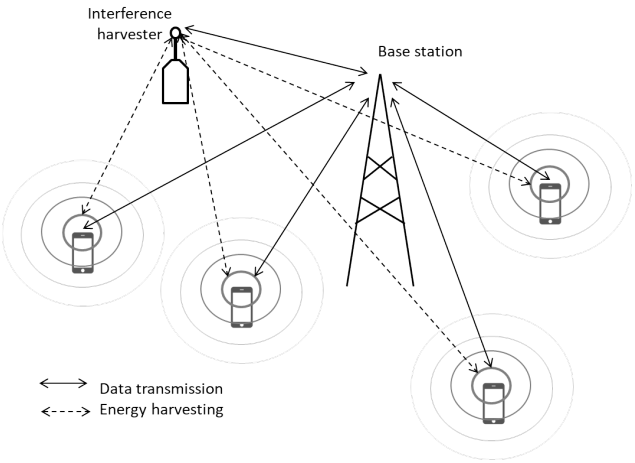

Figure 16: Illustration of the dedicated energy sources to supply RF energy

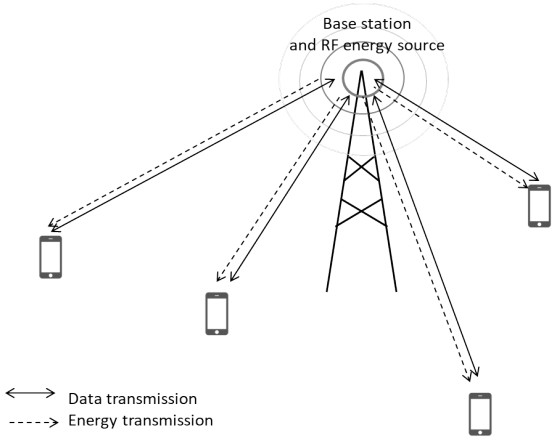

Figure 17: Illustration of the use of existing BSs to supply RF energy

4.4.1 Simultaneous Wireless Information and Power Transfer

Many suggestions for EH receiver architectures are inspired from the use of WPT in wireless networks. Actually, the same electromagnetic field can be used both for information and energy transfer to the end users and/or devices. This case is called Simultaneous Wireless Information and Power Transfer (SWIPT).

Two different tasks have to be completed by an EH receiver: decoding information and harvesting energy. The ideal case would integrate in the same receiver both functions with no power loss. However, realistic case dedicate a circuit for each task, so that EH and information decoding are performed separately. Authors in [75] suggest an intermediate solution that partially combines EH and information decoding circuits in a manner that the rectifier performs a part of the information decoding.

In a SWIPT configuration, a time slot, or a received signal power portion, are used for EH. The rest of time, or of power, are intended for decoding information. Nevertheless, time sharing scheme is more interesting as energy receivers and information receivers, which are usually distinct, have different power sensitivities. Note that there is a tradeoff between energy transfer rate and information transmission rate following the channel. For example, in an Additive White Gaussian Noise (AWGN) channel, maximum information rate target and maximum power transfer efficiency target are compatible.

There are technological issues that still need to be addressed in order to enable SWIPT use for wireless network deployment. For example, if we consider the nature of the transfers in SWIPT, the variation detection in RF signal by the receiver defines the information amount it can decode. The relationship between the two can be described by the Signal to Interference plus Noise Ratio (SINR), i.e. ratio between the power of the signal power and the disturbance power, including interference, noise and eventually any other disturbance affecting the decoding. In practice, even though a signal power can be low, its information rate could be very high. This is however not true for energy amount carried by an RF signal, which depends on its magnitude only. Hence, in a SWIPT, there is a trade-off between transferred energy amount and information rate, as it is not possible to maximize the "rate" of the two transfers simultaneously. Consequently, there is a need to adapt te network design for SWIPT implementation, leading to research issues on the design, analysis and optimization of SWIPT-based networks architectures and protocols. For example, in [88], the wireless powering of terminals in an UDN considers game theoretical approach of power allocation in a network of Full-Duplex (FD) BSs which serve an area highly dense of half-duplex (HF) user equipments. Considering EE and coverage optimization problem for such network as a mean field game gives an optimal strategy to adapt BSs for this type of network settings. SWIPT can also be considered in cooperative communication networks, as proposed in [89], where relays harvest powers to be able to amplify and forward data. An optimization, such as maximum ratio combining, can be then operated considering direct and relayed signals.

Note that there are many variants of SWIPT schemes following the integration in the model of other 5G techniques or the consideration of specific use case. An example is given in [87], where a cooperative communication network is considered with a distributed energy beamforming and simultaneous communication with several users. Moreover, when used with NOMA, efficient EH can be performed, and EE can be enhanced with the use of EH pilots for channel estimation.

4.4.2 Dedicated RF sources powering

Many tools are proposed in case of powering through dedicated RF energy source, as in [90] where optimal power allocation is suggested for frequency division multiplexing, meaning that data transmission and EH can be performed simultaneously, and time division multiplexing, meaning that data transmission and EH are implemented in different time slots but in the same frequency band. Optimal EH and information transmission strategy is then given and long-term throughput can be optimized. Note that authors in [91] considered the possible optimizations in the case of dedicated energy sources for WPT as in IoT applications. Authors showed that power control is critical for system achievable rate improvement in the case of a finite blocklength, and when the Tx power is asymptotically optimum, performance is nearly optimum.

PBs provided by the network, can be integrated in a relay network. For example, [92] suggests that relay nodes harvest transmitted power from the PB station to forward signals to destination. The information can be relayed but also power, following adequate protocols to optimize power splitting, especially in the presence of multi-antennas. Another example using dedicated RF charging in the case of smart wearables, where the energy consumption is very low, is discussed in [93]. This implies a mix of operator-deployed and user-deployed systems that will need to cooperate. Authors in fact highlight through system-level evaluation the preference for omnidirectional energy transmission in this case.

4.4.3 Interference harvesting

An increasing number of users are actively using mobile systems and demanding continuously improved quality of

experience. In addition to the diversity of end devices and of applications, each with its own constraint, 5G uses a heterogeneous UDN to respond to the current landscape, which already implies the coexistence of many RF signals on different bands. In fact, as illustrated in Figure 18, today's current deployments imply the presence of many signals, which can be harvested to power devices. In particular, GSM bands present a higher RF power density, while other sources may also be exploited for energy harvesting, such as Amplitude Modulation (AM) radio stations and Ultra High Frequency (UHF) RFID.

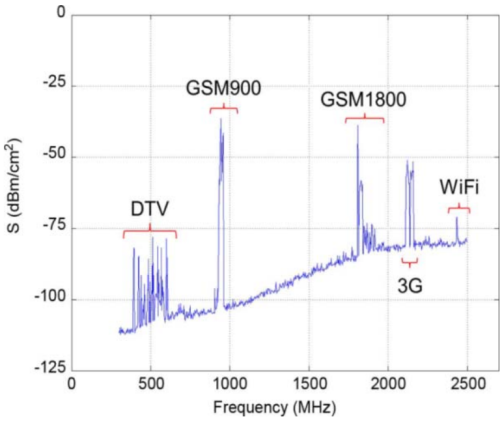

Figure 18: Example of measured RF power densities of main RF energy sources in an urban outdoor location (Source [94])

A given device using a given system is exposed to signals intended for other users in the same network, signal from other networks, or signals on other bands. These signals are usually seen as interference and many techniques and resources are used to mitigate it. It has to be carefully dealt with in an EH context for different types of channels, including broadcast channels, multicast channels, multiple access channels, and multi-user interference channels, as reviewed in [95]. However, they can also be seen as an energy source to harvest.

Figure 19 illustrates the case where signal from the user can be harvested by an interference harvester, which is a node capable of communicating itself with the BS. The harvesting and transmitting are usually sequential.

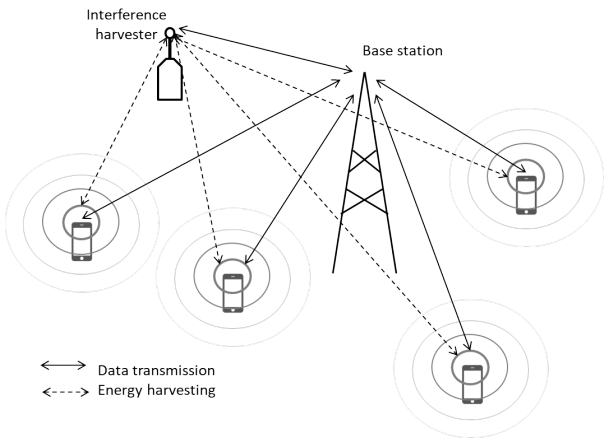

Figure 19: Example of an interference Harvesting scenario

The authors in [96] present opportunistic communication for devices that can reconfigure according to the the band they use, which makes them able to separate useful signal from possibly harvestable OOB interference. Nevertheless, interference harvesting from the same band requires additional processing, and strategies to realize this harvesting are currently being researched, and promising to be a key enabling factor for self-sustainable transmissions in 5G networks [97]. Similarly, authors in [98] present a cooperative wirelessly powered communication network protocol, where distant users overhear uplink signals of users and downlink access point broadcast signals, and time allocation for uplink and downlink are jointly optimized, which increases users rate and improves user fairness and transmission delay. Actually, the analysis of RF-EH performance has been considered in works such as [99], where the harvested energy mean, transmission outage probability and power outage probability are studied.

The energy can be also harvested from parts of the signal of the same user. An example with multicarrier modulations, as in [74], considers the fact that the Cyclic Prefix (CP) is used when still analog and thus, its energy can be harvested. The CP would remove inter-symbol interference, and at the same time contribute in SWIPT implementation, especially for WPT in downlink.

A backscatter communication architecture is suggested in [100], which combines ambient EH and reflection of this same energy modulated, with all its related signal processing aspects and multiple access techniques.

4.5 RF Energy harvesting scenarios

Globally, as enumerated in [95], three EH and transmission protocols can be identified:

- Harvest-Use (HU), for which the device is powered by EH directly, without using any buffer. Data transmission is thus possible only when harvested energy can cover the processing energy cost.

- Harvest-Store-Use (HSU), for which a storage device, typically a battery, is used to gather harvested energy. This energy is then available for use only in the next time slot. This case has to consider carefully possible storage inefficiency during the charging and leakage during the storage. For example, only about 70% of the energy is stored in Ni-MH rechargeable batteries while 95% can be reached with a supercapacitor. However, a battery implies less leakage than a supercapacitor.

- Harvest-Use-Store (HUS), which uses two energy storage devices : a supercapacitor storing the harvested energy for immediate use, and a buffer storing the remaining energy for later use.

The energy buffer is critical when using one of these protocols. Other schemes in a different optimization perspective can consider storage constraints, QoS requirements or capacity achieving targets. An example is the introduction of a sleep-and-awake mechanism to enhance the achievable rate [95].

4.6 RF Energy harvesting scheduling

In order to have an efficient EH system, and depending on the used EH protocol used, the energy consumption has to be adapted to the EH. This is to prevent energy outage or overflow. Thus, the design of energy use scheduling is critical. It can be offline or online, following the case where channel state information is available at the beginning of the transmission or only on the fly.

Energy scheduling depends on many parameters, such as data throughput, transmission competition time, mean delay, outage probability, quality of coverage, message importance, grid power consumption when there is a hybrid power supply, etc. For instance, the scheduling of RF harvested energy optimizes the time duration of information processing and EH. A tradeoff between the minimum information outage probability and the maximum average harvested energy defines the optimal mode switching between the two functions at the receiver. A review of scheduling techniques can be found in [95].

The signaling in wirelessly empowered communication networks has also to be carefully designed. In fact, if wireless powered communication networks control is centralized, signaling overhead, as well as optimizations in case of large number of devices can be prohibitively complex. Thus, a distributed EH random access protocol can be adopted, as in [101], where a slotted ALOHA is used a harvest-until-access protocol. The proposed algorithm optimizes the average channel throughput without knowledge of full channel state information, especially when the number of devices is large, which reduces the complexity and overhead of a centralized management.

Integrated spectrum and energy control mechanisms are presented for a typical heterogeneous 5G network in [102]. In this work, the authors consider the network where the devices have different EH capabilities and perform a cooperative resource sensing for CR implementation. In this case, both energy and spectrum are *"harvested"*. This leads to an architecture and model with specific spectrum and energy control mechanisms in many 5G scenarios, and consequently a Medium Access Control (MAC) protocol for this context. Another energy and spectrum efficiency optimized MAC protocol for 5G EH can be found in [103], where SWIPT is considered for cooperative and non-cooperative schemes with EH capabilities in a CR aided 5G networks.

5 RF Energy harvesting in 5G ecosystem

5G ecosystem integrates a wide range of use cases, using established and new technologies. EH is researched to be integrated with key 5G enablers, and examples of these researches are given in the remainder of this section.

5.1 UDN RF-EH-enabled

UDN are among main 5G enablers for many use cases, including IoT. Considering ambient RF-EH in dense networks, many implementation and operation challenges arise including energy availability, EH mode selection, cooperation between BSs and devices. In particular, there are tradeoffs between EE, SINR and outage probability, as highlighted in [104], where it is found that co-channel interference EH can bring efficiency improvement, especially if combined with an optimization of BSs parameters.

When the capacity is limited, the H2020 project SCAVENGE [105] suggests that cells can be split so that some are master Access Nodes (AN) while the others are EH AN. In case of heavy traffic, all ANs would be enabled to provide required capacity, while for light traffic, a part of EH AN can be switched off. This can be possible as UDN have high probability of Line-of-Signt, making the access easier for devices without the need of EH ANs. Backhauling the cells, if using wireless connection, makes the deployment cheaper and more flexible. In particular, EH ANs backhauling can use mmWave or be self-backhauling. In the second case, the access and the backhauling use the same link, shared in time and/or frequency. In the first case, mmWave can provide EH capabilities for rapid AN installation. In particular, for some deployment scenarios, micro cells with low power can be used, for which an EH powering and a wireless backhaul are suitable. The use of EH in this case, as indicated in [105], can be cost-effective. It can also provide an easy coverage and deployment in rural areas, easy cell planning, reduced environmental impact and cost saving in long-term.

Note that WPT can be used between BSs in addition to terminals. This will imply a new cell planning based for example on energy balancing connection and QoS-aware BS planning.

5.2 RF-EH in C-RAN

C-RAN and H-CRAN aim to provide a high data rate, energy efficient network. However, because of its heterogeneous nature, H-CRAN is more energy consuming as it has a larger number of RRHs than C-RAN. When the network is dense, the energy requirements become critical and several adaptations and optimizations have to be made. EH can bring thus a solution as in [106], where BSs are suggested to be powered with EH, and can also power devices. A throughput optimization in that case can be performed under receiver charged energy constraint. The grid energy consumption in the case H-CRAN downlink with one grid-powered BS and many RRHs EH-powered is studied in [67] and a model and optimization of user association, power allocation and EH constraints are given. In this scenario, the EE optimization is modeled as a fractional mixed integer nonlinear programming problem, which can be solved in few iterations. This improves the number of users, who are mostly associated to EH-RRHs, and thus decreasing the grid energy consumption.

In a UDN deployment, the implementation cost can be high due to infrastructure and small cells backhauling, and C-RAN can en be used to reduce this cost, especially for low data rate traffic as in IoT. The fronthauling then can use EH for an energy efficient deployment [105]. Similarly, the energy cost in an RF-EH combined with an energy management and scheduling in H-CRAN context is considered in [107]. RRHs in that case are EH-powered, and a hierarchical framework based on economical model and using energy sharing and energy trading between 5G actors, and more specifically internet service providers, can provide a

framework for the system design.

5.3 RF-EH enabled MEC

In MEC, computing resources are available at the edge of the mobile network, i.e. BSs, in order to ensure low latency and to reduce core network traffic. Globally, two main scenarios are considered for EH and MEC combination. Either EH capability is deployed at the MEC BS (or resource server) to prevent possible grid energy absence or unavailability in some scenarios, like natural disasters or remote areas, or it is implemented on device side, which is more suitable in case, for example, of IoT. Study of the state of the art for these two scenarios can be found in [108]. For the first scenario, energy forecast and EH enabled BSs load balancing have to be controlled. An example considers BSs equipped with EH capabilities and may reduce thus by the same occasion energy consumption. The authors in [109] suggest to optimize the BSs and virtual MEC resources use following traffic load and forecasted harvested energy parameters. The heuristic optimization employs sleep mode for BS and soft-scaling for Virtual machines. The authors announce up to 69% energy saving in single BS case, that can be enhanced by up to 16% in BSs cluster. Similarly, an illustration of the second scenario can be found in [110] and present a low-complexity dynamic computing offloading strategy for MEC with EH. This strategy decides computation offloading power and device transmit power, without the need of distributed information, and is easily implementable, besides being asymptotically optimum.

5.4 D2D with EH

D2D communication suffers from a major constraint, which is energy. EH can be thus integrated to devices in order to solve this issue, and many studies consider this case and provide theoretical performance derivation for different scenario. For example, in [111], the authors consider the scenario where UEs in a traditional cellular network assisted with relays use decode-and-forward cognitive D2D communication and EH. They provide analytical expression for main performance parameters, which helps to optimize link robustness. Another scenario can consider D2D in large-scale cognitive cellular networks as by authors in [112], where D2D transmitters harvest energy from dedicated multi-antenna PBs. A power transfer model with three possible power transfer policies can be proposed, in addition to an information signal model with two considered receiver selection cases. In addition to outage probability, secrecy is also considered in the analysis conducted by the authors and complete the framework for secure D2D communication.

5.5 RF-EH with key 5G RAN techniques

Spectral efficiency is critical in current mobile systems, particularly in RAN. Thus, spectrum optimizations have to be considered, in combination with RF-EH techniques. Reviewed techniques in the rest of this section include cooperative communications and cognitive radios, in addition to massive MIMO, NOMA and D2D. The combinations and optimizations usually consider many of these techniques at a time, in order to prepare its integration on practical systems.

5.5.1 Cooperative communications

In an EH network, nodes may have different channel and energy conditions, which may enhance performance using a cooperative approach. Transmission schemes for cooperative networks, multi-user networks, cognitive radio networks and cellular networks are thus to be considered.

Multi-user environment is an example of scenarios with EH, where interference management mechanisms have to be effective. Moreover, this environment presents spatial diversity gains that offer an opportunity to enhance system performances through collaboration between network nodes, which form a virtual MIMO system. Among studied aspects for cooperative networks, the power allocation is to be optimized under EH models, as well as throughput in delay constrained environment, and joint power allocation and time scheduling with EH.

Another example of EH integration issues is the joint optimizations of EE and frequency bands in the design of wireless-empowered transceivers, as presented in [74] where in-band interference harvesting is designed so to realize self-sustainable communication architecture.

5.5.2 NOMA

The adaptation of EH with 5G coming techniques, such as NOMA or CR networks, is an important issue to address for RF-EH deployment. In fact, there is a need for more comprehensive design for both new technologies, NOMA and RF-EH. Such combination may if established provide an efficient use of the energy and radio spectrum in energy efficient and sufficient networks, as in [113]. Other examples of issues are modeling and analysis of large scale EH networks and relay-based EH networks, as well as the design of energy cooperative strategies between harvesting devices. Note that in addition to energy and power transfers, it is fundamental to consider energy storage at end nodes, which ideally would consume harvested energy immediately within a transmission cycle.

Analysis tools for EH NOMA are intensively investigated, as in [114] where users outage probability under imperfect channel state information and imperfect SIC in a cooperative EH NOMA network is derived. Another example of mathematical modeling for user grouping, power and time allocation can be found in [115], which adopts a mesh adaptive direct search algorithm to optimize data rate and transmit power for each user with reasonable complexity. Similarly, outage probability is calculated for relay systems with NOMA and EH in [116], where the multiuser downlink is considered and BSs use multiple antennas to beamform information and energy.

NOMA use in specific wireless powered IoT relay systems with RF-EH capabilities can be found in [117], where RF-EH and information transmission system with time switching and power splitting relaying are considered. Due to the constrained nature of IoT nodes, the authors propose for IoT nodes to first harvest energy from the source node, either with time switching relaying or power splitting relaying

protocol. After that, the information of the source node is transmitted by the relay node as well as its own information using NOMA. The description of this system is mathematically derived by the authors, allowing several optimizations of system parameters.

5.5.3 Massive MIMO

Massive MIMO is a key 5G enabler, and its integration with EH schemes has been studied by many researchers. In [118], the authors explore the use of massive MIMO in heterogeneous networks. The deployment considers macrocells where users harvest energy to maximize their uplink power by minimizing uplink pathloss. It is found that user association should be optimized to maximize both harvested energy and information transfer. In this case, the downlink received power and the uplink received power should be both considered in the optimization. The stochastic model for the harvested energy and its link to uplink achievable performance demonstrates the added value of massive MIMO on that point, though the gain may deteriorate with network density. The proposed model enables however the study of massive MIMO and RF-EH integration with other technologies.

Another example of 5G techniques integration can be found in [119], where the downlink of a C-RAN enabled scenario with distributed large-scale MIMO is considered. Each RRH is powered EH and the grid in order to secure the RRHs from possible EH unavailability. The problem problem of BS energy consumption minimization under QoS constraints in this scenario can be solved using linear programming or an online energy management algorithm.

SWIPT in massive MIMO systems is studied in [120], where an analytical study of hybrid and full-dimensional processing is performed. It considers hybrid precoding and beamforming BS and derives expressions for harvested energy, achievable rates and energy-rate tradeoff for growing number of BS antennas and network nodes. A hybrid precoding and combining is proposed which optimizes harvested energy with little energy-rate tradeoff degradation.

5.5.4 mmWave

mmWave is attractive for EH as it is intended to be integrated for large antenna arrays and a dense network, presenting thus interesting harvesting opportunities. However, it propagation characteristics, i.e. poor penetration and diffraction, may limit its use to some scenarios. Many studies though consider RF-EH for mmWave communications. For example, authors in [121] consider a scenario where mmWave signal provides energy and/or information to low power devices and derive key information and EH performance parameters as well as overall coverage performance. This establishes an analytical framework to design network and device parameters, for example for antenna geometry optimization.

A study on combination of NOMA with massive MIMO using mmWave can be found in [122], where SWIPT is used to enhance EE. Hybrid precoding is used for mmWave massive MIMO, and information and energy can both be *"harvested"* by users thanks to a power splitting receiver. Algorithms are proposed to select a user per beam, and an analog precoding is then performed to all beams, then users grouping is performed and a digital precoding is applied. An iterative joint optimization of power allocation and power splitting reaches finally a maximized achievable sum-rate.

Note that antennas design for mmWave specific applications are also a challenge, as investigated in [123], where the authors consider ambient RF-EH antenna on textile for wearable in mmWave, and provides up to 40% on-body and 60% off-body radiation efficiency.

5.5.5 Cognitive Radio

Cognitive radio environment needs to be adapted with EH. As already mentionned, CR is often considered with other 5G enabling technologies. In fact, the spectrum usage is optimized as Secondary Users (SUs) use the spectrum of Primary users (PUs), following different priorities and cooperation strategies. These strategies may incorporate information transmission and spectrum sharing among nodes, but also EH strategies. In this case, both PU and SU get benefits as the PU improves his throughput through SU as relay node, and SU gets more spectrum usage opportunities from PU's spectrum. In addition, PU's bands access can be supported by SU's harvested energy. Conventional cognitive radio networks, e.g., spectrum allocation and management, spectrum sensing and handover, spectrum sharing, are reconsidered to enhance the network reliability in an EH context where, in addition, harvesting, spending or conserving energy have to be optimized.

An example of transmission CR schemes in RF-EH network can be found in [124], where an analytical study characterizes dedicated PBs. Information transfer and EH operate asynchronously in different bands. Another example considers a two-way relay assisted CR NOMA network [125]. In this example, a joint optimization of power allocation, transmit power and power splitting ratio is proposed. Similar throughput maximizations under QoS constraints can be found in [126] for a CR context.

6 Conclusion

This paper is a reflection of the increasing interest on new techniques to make energy use more efficient in 5G systems. It aims to provide a comprehensive review on RF-EH-enabled 5G networks. To this end, 5G standardization, requirements, use cases, ecosystem and key enabling technologies were reviewed, and particularly their energy aspects. RF-EH was then highlighted as a promising technique to solve energy supply and/or optimization. Different aspects of EH were exposed, including implementation and network protocols. The paper then presents literature review of RF-EH integration with 5G enabling technologies, as well as some research trends and challenges following the integrated technologies.

Conflict of Interest The authors declare no conflict of interest.

References

[1] S. El Hassani, H. El Hassani, and N. Boutammachte, "Rf energy harvesting for 5g: An overview," in *2017 International Renewable and Sustainable Energy Conference (IRSEC)*, Dec 2017, pp. 1–6.

[2] Cisco, "Cisco, visual networking index: Global mobile data traffic forecast ,update 2013-2018," Tech. Rep., 2014.

[3] "5g energy performance, ericsson white paper," Ericsson, Tech. Rep., apr 2015.

[4] "Driving the convergence of the physical and digital world - white paper on next generation mobile technology," ZTE Corp, Tech. Rep., 2014.

[5] "Sktelecom 5g white paper (white paper,version 1.0)," SKTelecom, Tech. Rep., oct 2014.

[6] S. Buzzi, C. I, T. E. Klein, H. V. Poor, C. Yang, and A. Zappone, "A survey of energy-efficient techniques for 5g networks and challenges ahead," *IEEE Journal on Selected Areas in Communications*, vol. 34, no. 4, pp. 697–709, April 2016.

[7] Y. He, X. Cheng, W. Peng, and G. Stuber, "A survey of energy harvesting communications: models and offline optimal policies," *Communications Magazine, IEEE*, vol. 53, no. 6, pp. 79–85, June 2015.

[8] I. B. Sofi and A. Gupta, "A survey on energy efficient 5g green network with a planned multi-tier architecture," *Journal of Network and Computer Applications*, vol. 118, pp. 1 – 28, 2018. [Online]. Available: http://www.sciencedirect.com/science/article/pii/S1084804518302029

[9] T. Soyata, L. Copeland, and W. Heinzelman, "Rf energy harvesting for embedded systems: A survey of tradeoffs and methodology," *IEEE Circuits and Systems Magazine*, vol. 16, no. 1, pp. 22–57, Firstquarter 2016.

[10] S. Divakaran, D. D. Krishna, and N. Nasimuddin, "Rf energy harvesting systems: An overview and design issues," *International Journal of RF and Microwave Computer-Aided Engineering*, p. e21633, 12 2018.

[11] "3gpp commits to 5g nr in unlicensed spectrum in its next release," https://www.qualcomm.com/news/onq/2018/12/13/3gpp-commits-5g-nr-unlicensed-spectrum-its-next-release, Press News, Tech. Rep., Dec 2018, accessed: 2019-07-26.

[12] "FP7 ICT project : Mobile and Wireless Communications Enablers for the Twenty-Twenty Information Society 5G," https://www.metis2020.com/, Tech. Rep., 2012, accessed: 2019-05-11.

[13] "White paper - 5g use cases and requirements future works," Nokia Networks, Tech. Rep., 2014.

[14] "5G White Paper," NGMN Alliance, Tech. Rep., 02 2015.

[15] "5g and energy," https://5g-ppp.eu/wp-content/uploads/2014/02/5G-PPP-White_Paper-on-Energy-Vertical-Sector.pdf, 5G PPP, Tech. Rep., 2015, accessed: 2017-12-16.

[16] M. S. C. A. H2020-MSCA-ITN-ETN, "Sustainable cellular network harvesting ambient energy," http://www.scavenge.eu/, Tech. Rep., accessed: 2019-07-28.

[17] "Follow the leaders on technology, tools, and techniques : Understanding and testing the 5g ecosystem," http://literature.cdn.keysight.com/litweb/pdf/5992-3144EN.pdf, Keysight TECHNOLOGIES, Tech. Rep., jul 2018, accessed: 2019-07-30.

[18] M. Medin and G. Louie, "The 5g ecosystem: Risks & opportunities for dod," https://media.defense.gov/2019/Apr/03/2002109302/-1/-1/0/DIB_5G_STUDY_04.03.19.PDF, Defense Innovation Board, Tech. Rep., apr 2019, accessed: 2019-07-30.

[19] M. CAGENIUS, A. RYDE, J. VIKBERG, and P. WILLARS, "Simplifying the 5g ecosystem by reducing architecture options," https://www.ericsson.com/48f8e1/assets/local/publications/ericsson-technology-review/docs/2018/etr-5g-core-radio-migration.pdf, Ericsson Technology review, Tech. Rep., nov 2018, accessed: 2019-07-30.

[20] J. A. Manner, "Wrc-19 — an opportunity to bridge the digital divide for 5g: Opinion," https://news.itu.int/wrc-19-opportunity-to-bridge-digital-divide-5g/, ITU News, Tech. Rep., May 2019.

[21] "Samsung announces world's first 5g mmwave mobile technology," https://news.samsung.com/global/samsung-announces-worlds-first-5g-mmwave-mobile-technology, Samsung Corp., Tech. Rep., May 2013, accessed: 2019-07-26.

[22] "Huawei to bring 73ghz mmwave mu-mimo live demo to deutsche telekom," http://www.huawei.com/en/news/2016/2/73GHzmm-Wave-Mu-MIM-live-demo, Huawei press, Tech. Rep., Feb 2016, accessed: 2019-07-26.

[23] A. Bleicher, "First intercontinental 5g trial begins at winter olympics," http://www.huawei.com/en/news/2016/2/73GHzmm-Wave-Mu-MIM-live-demo, IEEE Spectrum, Tech. Rep., Feb 2018, accessed: 2019-07-26.

[24] X. Hong, J. Wang, C. Wang, and J. Shi, "Cognitive radio in 5g: a perspective on energy-spectral efficiency trade-off," *IEEE Communications Magazine*, vol. 52, no. 7, pp. 46–53, July 2014.

[25] E. Paulson, M. KAMALUDIN, S. Kamilah, and U. Dauda, "Cognitive radio in 5g - a smart city perspective-," in *The 2017 Malaysia-Japan Workshop on Radio Technology*, 01 2017.

[26] R. Alkhansa, H. Artail, and D. M. Gutierrez-Estevez, "Lte-wifi carrier aggregation for future 5g systems: A feasibility study and research challenges," *Procedia Computer Science*, vol. 34, no. 0, pp. 133 – 140, 2014, the 9th International Conference on Future Networks and Communications (FNC'14)/The 11th International Conference on Mobile Systems and Pervasive Computing (MobiSPC'14)/Affiliated Workshops. [Online]. Available: http://www.sciencedirect.com/science/article/pii/S1877050914009235

[27] M. Alam and M. Ma, "Resource matching in carrier aggregation enabling 5g networks," *Wireless Personal Communications*, 10 2016.

[28] H. PAPADOPOULOS, C. Wang, O. BURSALIOGLU, X. Hou, and Y. Kishiyama, "Massive mimo technologies and challenges towards 5g," *IEICE Transactions on Communications*, vol. E99.B, pp. 602–621, 03 2016.

[29] Z. Gao, L. Dai, D. Mi, Z. Wang, M. A. Imran, and M. Z. Shakir, "Mmwave massive-mimo-based wireless backhaul for the 5g ultra-dense network," *IEEE Wireless Communications*, vol. 22, no. 5, pp. 13–21, October 2015.

[30] T. Rappaport, S. Sun, R. Mayzus, H. Zhao, Y. Azar, K. Wang, G. Wong, J. Schulz, M. Samimi, and F. Gutierrez, "Millimeter wave mobile communications for 5g cellular: It will work!" *Access, IEEE*, vol. 1, pp. 335–349, 2013.

[31] "5g channel model for bands up to100 ghz," *IEEEGC*, dec 2015.

[32] X. Zhang, M. Jia, L. Chen, J. Ma, and J. Qiu, "Filtered-ofdm - enabler for flexible waveform in the 5th generation cellular networks," in *2015 IEEE Global Communications Conference (GLOBECOM)*, Dec 2015, pp. 1–6.

[33] A. Farhang, N. Marchetti, F. Figueiredo, and J. P. Miranda, "Massive mimo and waveform design for 5th generation wireless communication systems," in *1st International Conference on 5G for Ubiquitous Connectivity*, Nov 2014, pp. 70–75.

[34] F. Schaich, T. Wild, and Y. Chen, "Waveform contenders for 5g - suitability for short packet and low latency transmissions," in *2014 IEEE 79th Vehicular Technology Conference (VTC Spring)*, May 2014, pp. 1–5.

[35] N. Michailow, M. Matthé, I. Gaspar, A. Navarro Caldevilla, L. Mendes, A. Festag, and G. Fettweis, "Generalized frequency division multiplexing for 5th generation cellular networks (invited paper)," *IEEE Transactions on Communications*, vol. PP, pp. 1–18, 08 2014.

[36] A. Benjebbour, K. Saito, A. Li, Y. Kishiyama, and T. Nakamura, "Non-orthogonal multiple access (noma): Concept, performance evaluation and experimental trials," in *2015 International Conference on Wireless Networks and Mobile Communications (WINCOM)*, Oct 2015, pp. 1–6.

[37] S. Timotheou and I. Krikidis, "Fairness for non-orthogonal multiple access in 5g systems," *IEEE Signal Processing Letters*, vol. 22, no. 10, pp. 1647–1651, Oct 2015.

[38] M. Al-Imari, P. Xiao, M. A. Imran, and R. Tafazolli, "Uplink non-orthogonal multiple access for 5g wireless networks," in *2014 11th International Symposium on Wireless Communications Systems (ISWCS)*, Aug 2014, pp. 781–785.

[39] M. Vaezi, Z. Ding, and H. V. Poor, *Multiple Access Techniques for 5G Wireless Networks and Beyond*. Springer International Publishing, 2018.

[40] S. R. Islam, M. Zeng, and O. Dobre, "Noma in 5g systems: Exciting possibilities for enhancing spectral efficiency," 06 2017.

[41] M. Aldababsa, M. Toka, S. Gokceli, G. K. Kurt, and O. Kucur, "A Tutorial on Nonorthogonal Multiple Access for 5G and Beyond," *arXiv e-prints*, p. arXiv:1902.08992, Feb 2019.

[42] C. Mobile, "C-ran the road towards green ran (white paper,version 3.0)," Tech. Rep., dec 2013.

[43] J. Li, M. Peng, Y. Yu, and Z. Ding, "Energy-efficient joint congestion control and resource optimization in heterogeneous cloud radio access networks," *CoRR*, vol. abs/1602.05351, 2016. [Online]. Available: http://arxiv.org/abs/1602.05351

[44] G. T. . version 15.3.0 Release 15) Technical specification, "System architecture for the 5g system," https://www.etsi.org/deliver/etsi_ts/123500_123599/123501/15.03.00_60/ts_123501v150300p.pdf, Tech. Rep., sep 2018, accessed: 2019-07-28.

[45] D. d3.1 : Functional network architecture and security requirements, "5g novel radio multiservice adaptive network architecture (5g norma)," https://5gnorma.5g-ppp.eu/wp-content/uploads/2016/11/5g_norma_d3-1.pdf, Tech. Rep., dec 2015, accessed: 2019-07-28.

[46] P. K. Agyapong, M. Iwamura, D. Staehle, W. Kiess, and A. Benjebbour, "Design considerations for a 5g network architecture," *IEEE Communications Magazine*, vol. 52, no. 11, pp. 65–75, Nov 2014.

[47] Z. Chang, Z. Zhou, S. Zhou, T. Chen, and T. Ristaniemi, "Towards service-oriented 5g: Virtualizing the networks for everything-as-a-service," *IEEE Access*, vol. 6, pp. 1480–1489, 2018.

[48] R. Wireless, "Vodafone, ericsson connect german labs in 5g mobile edge poc," http://www.rcrwireless.com/20160701/europe/germany-5g-mobile-edge-poc-tag17, Tech. Rep., jul 2016, accessed: 2019-07-28.

[49] V. K. Singh, H. Chawla, and V. A. Bohara, "A proof-of-concept device-to-device communication testbed," *CoRR*, vol. abs/1601.01398, 2016. [Online]. Available: http://arxiv.org/abs/1601.01398

[50] M. Shirvanimoghaddam, K. Shirvanimoghaddam, M. M. Abolhasani, M. Farhangi, V. Z. Barsari, H. Liu, M. Dohler, and M. Naebe, "Towards a Green and Self-Powered Internet of Things Using Piezoelectric Energy Harvesting," *arXiv e-prints*, p. arXiv:1712.02277, Dec 2017.

[51] 3GPP, "Standards for the iot," https://www.3gpp.org/news-events/3gpp-news/1805-iot_r14, Tech. Rep., dec 2016, accessed: 2019-07-28.

[52] J. F. Monserrat, G. Mange, V. Braun, H. Tullberg, G. Zimmermann4, and O. Bulakci, "Metis research advances towards the 5g mobile and wireless system definition," *EURASIP Journal on Wireless Communications and Networking*, 2015.

[53] P. Arabas, "Energy aware data centers and networks: a survey," *Journal of Telecommunications and Information Technology*, no. 4, pp. 26–36, 2018.

[54] "Final report on green radio technologies, earth project delivrable d4.3," https://www.ict-earth.eu/publications/deliverables/deliverables.html, accessed: 2017-12-16.

[55] S. Zhang, X. Xu, Y. Wu, L. Lu, and Y. Chen, "A survey on 5g new waveform: From energy efficiency aspects," pp. 1939–1943, Nov 2014.

[56] L. C. Wang and S. Rangapillai, "A survey on green 5g cellular networks," in *2012 International Conference on Signal Processing and Communications (SPCOM)*, July 2012, pp. 1–5.

[57] "Ntt docomo launches eco-friendly cell phone station," http://www.japanfs.org/en/news/archives/news_id025703.html, accessed: 2017-06-28.

[58] R. Garafola, "Eco-sustainable wireless networks: Ready for prime time," *Alcatel-Lucent*, 2009.

[59] F. Mukhlif, K. A. B. Nooridin, Y. A. AL-Gumaei, and A. S. AL-Rassas, "Energy harvesting for efficient 5g networks," in *2018 International Conference on Smart Computing and Electronic Enterprise (ICSCEE)*, July 2018, pp. 1–5.

[60] M. Ashraf, J. W. Jang, J.-K. Han, and K.-G. Lee, "Video multicast cooperative communication in 5g systems with radio frequency energy harvesting," *Computer Communications*, vol. 118, pp. 60 – 68, 2018. [Online]. Available: http://www.sciencedirect.com/science/article/pii/S014036641730508X

[61] "5g ippp (2014) 5g infrastructure ppp: The next generation of communication networks will be 'made in eu'," http://ec.europa.eu/information_society/newsroom/cf/dae/itemdetail.cfm?item_id=14424, accessed: 2017-12-16.

[62] J. Paradiso and T. Starner, "Energy scavenging for mobile and wireless electronics," *Pervasive Computing, IEEE*, vol. 4, no. 1, pp. 18–27, Jan 2005.

[63] X. Lu, P. Wang, D. Niyato, D. I. Kim, and Z. Han, "Wireless networks with rf energy harvesting: A contemporary survey," *Communications Surveys Tutorials, IEEE*, vol. 17, no. 2, pp. 757–789, Secondquarter 2015.

[64] S. Devasenapathy, R. Venkatesha Prasad, V. Rao, and I. Niemegeers, "Impact of antenna directionality and energy harvesting rate on neighbor discovery in eh-iots," in *Consumer Communications and Networking Conference (CCNC), 2013 IEEE*, Jan 2013, pp. 302–307. [Online]. Available: http://www.es.ewi.tudelft.nl/papers/2013-Devasenapathy-EHND.pdf

[65] A. Radwan and J. Rodriguez, *Energy Efficient Smart Phones for 5G Networks*, ser. Signals and Communication Technology. Springer International Publishing, 2016. [Online]. Available: https://books.google.co.ma/books?id=jCkTvgAACAAJ

[66] Z. Kausar, A. Reza, M. U. Saleh, H. Saleh, and H. Ramiah, "Energizing wireless sensor networks by energy harvesting systems: Scopes, challenges and approaches," *Renewable and Sustainable Energy Reviews*, vol. 38, pp. 973–989, 07 2014.

[67] N. Chughtai, "Energy harvesting in 5g networks," Ph.D. dissertation, 08 2018.

[68] A. Kurs, K. A.S., R. Moffatt, J. Joannopoulos, P. Fisher, and M. Soljai, "Wireless power transfer via strongly coupled magnetic resonances," *Science*, Jul 2007.

[69] R. Zhang and C. K. Ho, "Mimo broadcasting for simultaneous wireless information and power transfer," *IEEE Transactions on Wireless Communications*, vol. 12, no. 5, pp. 1989–2001, May 2013.

[70] C. Mikeka and H. Arai, "Sustainable energy harvesting technologies—past, present and future, hap. design issues in radio frequency energy harvesting system," *InTech*, 2011.

[71] H. Ju and R. Zhang, "Throughput maximization in wireless powered communication networks," in *2013 IEEE Global Communications Conference (GLOBECOM)*, Dec 2013, pp. 4086–4091.

[72] T. Kaźmierski and S. Beeby, *Energy Harvesting Systems: Principles, Modeling and Applications*, ser. SpringerLink : Bücher. Springer New York, 2010. [Online]. Available: https://books.google.co.ma/books?id=e4QQc6AEG1IC

[73] P. EFTHYMAKIS, "A rectenna for 5g energy harvesting," 2014.

[74] M. Maso, *Energy Harvesting Oriented Transceiver Design for 5G Networks*. Cham: Springer International Publishing, 2016, pp. 67–95.

[75] X. Zhou, R. Zhang, and C. K. Ho, "Wireless information and power transfer: Architecture design and rate-energy tradeoff," *IEEE Transactions on Communications*, vol. 61, no. 11, pp. 4754–4767, November 2013.

[76] S. Kim, R. Vyas, J. Bito, K. Niotaki, A. Collado, A. Georgiadis, , and M. M. Tentzeris, "Ambient rf energy-harvesting technologies for selfsustainable standalone wireless sensor platforms," in *Proc. IEEE*, November 2014, pp. 1649–1666.

[77] H. Kanaya, S. Tsukamaoto, T. Hirabaru, D. Kanemoto, R. K. Pokharel, and K. Yoshida, "Energy harvesting circuit on a one-sided directional flexible antenna," *IEEE Microwave and Wireless Components Letters*, vol. 23, no. 3, pp. 164–166, March 2013.

[78] B. Pham and A. Pham, "Triple bands antenna and high efficiency rectifier design for rf energy harvesting at 900, 1900 and 2400 mhz," 06 2013, pp. 1–3.

[79] L. M. Borges, N. Barroca, H. M. Saraiva, J. Tavares, P. T. Gouveia, F. J. Velez, C. Loss, R. Salvado, P. Pinho, R. Gonçalves, N. B. Carvalho, R. Chavéz-Santiago, and I. Balasingham, "Design and evaluation of multi-band rf energy harvesting circuits and antennas for wsns," in *2014 21st International Conference on Telecommunications (ICT)*, May 2014, pp. 308–312.

[80] N. A. Zainuddin, Z. Zakaria, M. N. Husain, B. M. Derus, M. Z. A. A. Aziz, M. A. Mutalib, and M. A. Othman, "Design of wideband antenna for rf energy harvesting system," in *2013 3rd International Conference on Instrumentation, Communications, Information Technology and Biomedical Engineering (ICICI-BME)*, Nov 2013, pp. 162–166.

[81] J. SCHNEIDER1, M. MRNKA, J. GAMEC, M. GAMCOVA, and Z. RAIDA, "Vivaldi antenna for rf energy harvesting," *RADIOENGINEERING*, vol. 25, pp. 666–671, 12 2016.

[82] "Energy harvesting system market by technology (light, vibration, electromagnetic, thermal), application (building and home automation, consumer electronics, industrial, transportation, security), and geography - global forecast to 2022," http://www.marketsandmarkets.com/Market-Reports/energy-harvesting-market-734.html, Apr 2016, accessed: 2019-05-19.

[83] K. hao Liu and P. Lin, "Toward self-sustainable cooperative relays: state of the art and the future," *Communications Magazine, IEEE*, vol. 53, no. 6, pp. 56–62, June 2015.

[84] J. Morra, "Startup's energy harvesting chips run on radio frequencies," https://www.electronicdesign.com/analog/startups-energy-harvesting-chips-run-radio-frequencies, January 2019, accessed: 2019-05-19.

[85] R. Pell, "Boom time for energy harvesting chip market," https://www.eenewseurope.com/news/boom-time-energy-harvesting-chip-market-0, September 2018, accessed: 2019-05-19.

[86] A. M. Zungeru, L. Ang, S. R. S. Prabaharan, and K. P. Seng, "Radio frequency energy harvesting and management for wireless sensor networks," *CoRR*, vol. abs/1208.4439, 2012. [Online]. Available: http://arxiv.org/abs/1208.4439

[87] A. Rajaram, R. Khan, S. Tharranetharan, D. N. Jayakody, R. Dinis, and S. Panic, "Novel swipt schemes for 5g wireless networks," *Sensors*, vol. 19, p. 1169, 03 2019.

[88] X. Ge, H. Jia, Y. Zhong, Y. Xiao, Y. Li, and B. Vucetic, "Energy efficient optimization of wireless-powered 5g full duplex cellular networks: A mean field game approach," *IEEE Transactions on Green Communications and Networking*, pp. 1–1, 2019.

[89] S. Mahama, D. K. P. Asiedu, and K. Lee, "Simultaneous wireless information and power transfer for cooperative relay networks with battery," *IEEE Access*, vol. 5, pp. 13 171–13 178, 2017.

[90] Q. Li, J. Gao, H. Liang, L. Zhao, and X. Tang, "Optimal power allocation for wireless sensor powered by dedicated rf energy source," *IEEE Transactions on Vehicular Technology*, vol. 68, no. 3, pp. 2791–2801, March 2019.

[91] T. A. Khan, R. W. Heath, and P. Popovski, "Wirelessly powered communication networks with short packets," *IEEE Transactions on Communications*, vol. 65, no. 12, pp. 5529–5543, Dec 2017.

[92] T. Do, "Optimal energy harvesting scheme for power beacon-assisted wireless-powered networks," *Indonesian Journal of Electrical Engineering and Computer Science*, vol. 7, pp. 802–808, 09 2017.

[93] O. Galinina, H. Tabassum, K. Mikhaylov, S. Andreev, E. Hossain, and Y. Koucheryavy, "On feasibility of 5g-grade dedicated rf charging technology for wireless-powered wearables," *IEEE Wireless Communications*, vol. 23, pp. 28–37, 2015.

[94] A. Nechibvute, A. CHAWANDA, N. Taruvinga, and P. LUHANGA, "Radio frequency energy harvesting sources," *Acta Electrotechnica et Informatica*, vol. 17, pp. 19–27, 12 2017.

[95] M. L. Ku, W. Li, Y. Chen, and K. J. R. Liu, "Advances in energy harvesting communications: Past, present, and future challenges," *IEEE Communications Surveys Tutorials*, vol. 18, no. 2, pp. 1384–1412, Secondquarter 2016.

[96] N. Zhao, F. Yu, and V. Leung, "Wireless energy harvesting in interference alignment networks," *Communications Magazine, IEEE*, vol. 53, no. 6, pp. 72–78, June 2015.

[97] M. Maso, S. Lakshminarayana, T. Q. S. Quek, and H. V. Poor, "The price of self-sustainability for block transmission systems," *IEEE Journal on Selected Areas in Communications*, vol. 33, no. 8, pp. 1549–1562, Aug 2015.

[98] W. Shin, M. Vaezi, J. Lee, and H. V. Poor, "Cooperative wireless powered communication networks with interference harvesting," *IEEE Transactions on Vehicular Technology*, vol. 67, no. 4, pp. 3701–3705, April 2018.

[99] H. Kong, I. Flint, P. Wang, D. Niyato, and N. Privault, "Exact performance analysis of ambient rf energy harvesting wireless sensor networks with ginibre point process," *IEEE Journal on Selected Areas in Communications*, vol. 34, no. 12, pp. 3769–3784, Dec 2016.

[100] M. L. Memon, N. Saxena, A. Roy, and D. R. Shin, "Backscatter communications: Inception of the battery-free era—a comprehensive survey," *Electronics*, vol. 8, no. 2, 2019. [Online]. Available: https://www.mdpi.com/2079-9292/8/2/129

[101] H. Choi and W. Shin, "Harvest-until-access protocol based on slotted aloha for wireless powered dense networks," in *2019 International Conference on Electronics, Information, and Communication (ICEIC)*, Jan 2019, pp. 1–6.

[102] Y. Liu, Y. Zhang, R. Yu, and S. Xie, "Integrated energy and spectrum harvesting for 5g wireless communications," *Network, IEEE*, vol. 29, pp. 75–81, 06 2015.

[103] J. Ghosh and Z. Jakó, "Mac protocol operation in energy harvesting for 5g networks," *ICST Transactions on Mobile Communications and Applications*, vol. 3, p. 153554, 01 2018.

[104] A. Ghazanfari, H. Tabassum, and E. Hossain, "Ambient RF energy harvesting in ultra-dense small cell networks: Performance and trade-offs," *CoRR*, vol. abs/1512.03122, 2015. [Online]. Available: http://arxiv.org/abs/1512.03122

[105] M. S. C. A. H2020-MSCA-ITN-ETN, "Sustainable cellular network harvesting ambient energy, deliverable d3.1 : Wp3 - sustainable networking, d3.1 - intermediate report," http://www.scavenge.eu/wp-content/uploads/2018/02/D3.1.pdf, Tech. Rep., jan 2018, accessed: 2019-07-28.

[106] Z. Chen, Z. Chen, L. X. Cai, and Y. Cheng, "Energy-throughput tradeoff in sustainable cloud-ran with energy harvesting," in *2017 IEEE International Conference on Communications (ICC)*, May 2017, pp. 1–6.

[107] G. Qiao, S. Leng, Y. Zhang, M. Zeng, and L. Xu, "Multiple timescale energy scheduling with energy harvesting aided heterogeneous cloud radio access networks," in *2016 IEEE/CIC International Conference on Communications in China (ICCC)*, July 2016, pp. 1–6.

[108] Q. Pham, F. Fang, H. Vu, M. Le, Z. Ding, L. B. Le, and W. Hwang, "A survey of multi-access edge computing in 5g and beyond: Fundamentals, technology integration, and state-of-the-art," *CoRR*, vol. abs/1906.08452, 2019. [Online]. Available: http://arxiv.org/abs/1906.08452

[109] T. Dlamini, Ángel Fernández Gambín, D. Munaretto, and M. Rossi, "Online supervisory control and resource management for energy harvesting bs sites empowered with computation capabilities," *Wireless Communications and Mobile Computing*, p. 17, 2019.

[110] Y. Mao, J. Zhang, and K. B. Letaief, "Dynamic computation offloading for mobile-edge computing with energy harvesting devices," *IEEE Journal on Selected Areas in Communications*, vol. 34, no. 12, pp. 3590–3605, Dec 2016.

[111] H.-S. Nguyen, T.-S. Nguyen, and M. Voznak, "Wireless powered d2d communications underlying cellular networks: design and performance of the extended coverage," *Automatika*, vol. 58, no. 4, pp. 391–399, 2017. [Online]. Available: https://doi.org/10.1080/00051144.2018.1455016

[112] Y. Liu, L. Wang, S. A. R. Zaidi, M. Elkashlan, and T. Duong, "Secure d2d communication in large-scale cognitive cellular networks: A wireless power transfer model," *IEEE Transactions on Communications*, vol. 64, 11 2015.

[113] L. S. Mohjazi, M. Dianati, G. K. Karagiannidis, S. Muhaidat, and M. Al-Qutayri, "Rf-powered cognitive radio networks: technical challenges and limitations," *IEEE Communications Magazine*, vol. 53, no. 4, pp. 94–100, 2015.

[114] D. Do, M. Vaezi, and T. Nguyen, "Wireless powered cooperative relaying using NOMA with imperfect CSI," *CoRR*, vol. abs/1810.00276, 2018. [Online]. Available: http://arxiv.org/abs/1810.00276

[115] M. Basharat, "Joint user grouping and time allocation for noma with wireless power transfer," 2017.

[116] P. T. Hiep and T. M. Hoang, "Non-orthogonal multiple access and beamforming for relay network with rf energy harvesting," *ICT Express*, 2019. [Online]. Available: http://www.sciencedirect.com/science/article/pii/S240595951930150X

[117] A. Rauniyar, P. E. Engelstad, and O. N. Østerbø, "Rf energy harvesting and information transmission based on noma for wireless powered iot relay systems," in *Sensors*, 2018.

[118] Y. Zhu, L. Wang, K. Wong, S. Jin, and Z. Zheng, "Wireless power transfer in massive mimo-aided hetnets with user association," *IEEE Transactions on Communications*, vol. 64, no. 10, pp. 4181–4195, Oct 2016.

[119] R. Hamdi, E. Driouch, and W. Ajib, "Energy management in large-scale mimo systems with per-antenna energy harvesting," in *2017 IEEE International Conference on Communications (ICC)*, May 2017, pp. 1–6.

[120] R. Shrestha and G. Amarasuriya, "Wireless energy harvesting in massive mimo with low-dimensional digital precoding," in *Proc. IEEE Global Communication Conference (GLOBECOM)*, 12 2018, pp. 1–7.

[121] T. A. Khan, A. Alkhateeb, and R. W. H. Jr., "Millimeter wave energy harvesting," *CoRR*, vol. abs/1509.01653, 2015. [Online]. Available: http://arxiv.org/abs/1509.01653

[122] L. Dai, B. Wang, M. Peng, and S. Chen, "Hybrid precoding-based millimeter-wave massive mimo-noma with simultaneous wireless information and power transfer," *IEEE Journal on Selected Areas in Communications*, vol. 37, no. 1, pp. 131–141, Jan 2019.

[123] M. Wagih, A. S. Weddell, and S. Beeby, "Millimeter-wave textile antenna for on-body rf energy harvesting in future 5g networks," in *Wireless Power Week 2019, IEEE Wireless Power Transfer Conference. (21/06/19)*, June 2019, pp. 1–4. [Online]. Available: https://eprints.soton.ac.uk/431955/

[124] N. I. Miridakis and T. A. Tsiftsis, "A new interweave cognitive radio scheme for out-band energy harvesting systems," *IEEE Access*, vol. 6, pp. 72 225–72 232, 2018.

[125] W. Zhao, R. She, and H. Bao, "Energy efficiency maximization for two-way relay assisted cr-noma system based on swipt," *IEEE Access*, vol. 7, pp. 72 062–72 071, 2019.

[126] B. Alzahrani and W. Ejaz, "Resource management for cognitive iot systems with rf energy harvesting in smart cities," *IEEE Access*, vol. 6, pp. 62 717–62 727, 2018.

ASTES

Advances in Science, Technology and Engineering Systems Journal
Vol. 4, No. 4, 347-358 (2019)
www.astesj.com
Special Issue on Advancement in Engineering and Computer Science

ASTES Journal
ISSN: 2415-6698

Using Privacy Enhancing and Fine-Grained Access Controlled eKYC to implement Privacy Aware eSign

Puneet Bakshi*, Sukumar Nandi

Department of Computer Science and Engineering, Indian Institute of Technology, Guwahati, 781039, India

ARTICLE INFO

Article history:
Received: 28 May, 2019
Accepted: 23 July, 2019
Online: 19 August, 2019

Keywords:
eSign
eKYC
Electronic Signature
Privacy
Access Control
Authentication
Token
BAN logic

ABSTRACT

eSign is an online electronic signature service which is recently gaining more prominence in India. eSign is based on two online services from UIDAI, viz. a viz., Aadhaar based authentication and retrieval of resident's eKYC information after taking his/her consent. With increased adoption of Aadhaar based services, privacy of user data has become more and more important. Present method of taking boolean consent from resident through non-UIDAI entity may not be acceptable for two main reasons, first is that the consent does not include in itself a proof from resident that the consent is indeed taken from him/her and second is that the resident may wish to have better privacy and fine grained access control rules to access his/her eKYC data. Bakshi et.el have introduced a mechanism to improve amortized performance of eSign using a digital access token. In this work, the digital access token is enhanced to include Privacy Enhancing and Fine-Grained Access Control (PEaFGAC) Statements for facilitating Privacy Aware eSign. These tokens can be used by other entities to access eKYC data of the resident with better access controls enforced by the resident. This paper briefly describes the present model of eSign, the earlier proposed model of eSign followed by the proposed model of Privacy Aware eSign. The proposed model of Privacy Aware eSign is also analyzed using BAN logic assuming Dolev-Yao security environment.

1 Introduction

eSign is an online electronic signature service in India which is being promoted by Government of India as part of its Digital India Initiative. As opposed to traditional dongle based electronic signature, *eSign* provides benefits such as less cost, no manual authentication, no requirement of special hardware device and no requirement for the end user to keep any key secret. With the passage of *Information Technology Act (ITA-2000)*, an electronically signed digital document is considered equivalent to a handwritten signed paper document. In India, *eSign* is being regulated by *Controller of Certifying Authority (CCA)* and is being operated by certain designated empaneled agencies known as *eSign Service Providers (ESP)*. *ESP* provides its services to application specific agencies known as *Application Service Providers (ASP)*. *ASP* provides *eSign* service to the end users. *eSign* is governed by *Public Key Infrastructure (PKI)* which is further governed in legal matters by the national legislature of the country.

To avail *eSign* service, a resident needs to enroll with *Unique Identification Authority of India (UIDAI)* and receive a 12-digit identity number called *Aadhaar* [1] [2]. As part of the enrollment process, resident needs to provide information about his/her identity and address to *UIDAI* such as *Name*, *Date of Birth*, *Address*, *Phone number*, *Email-id*, *Biometric (fingerprint-scan, iris-scan)* etc. The process of obtaining this information from the end user is known as *Know Your Customer (KYC)* and is initially introduced by *Reserve Bank of India (RBI)* for financial banks [3]. Traditionally, this process involves submission of a self-attested physical form along with necessary physical documents, followed by verification and approval by receiving organization. eKYC is an online service which facilitates completion of KYC process electronically. eKYC has some significant benefits over traditional KYC, eKYC eliminates submission of physical documents by customer, is faster and is less error prone. *UIDAI*'s eKYC service facilitates a third entity to retrieve resident's identity, address and other details after taking explicit consent and authorization from the resident.

With increased adoption of *Aadhaar* based identification,

*Corresponding Author: Puneet Bakshi, IIT Guwahati, b.puneet@iitg.ac.in

many online services are now using *Aadhaar* based services and with its such wide adoption, privacy of user data has become even more important. Although *Aadhaar* based eKYC service provides access to eKYC data only after taking an explicit consent from the resident, this way of taking consent from resident has two shortcomings. First is that the consent is taken by *non-UIDAI* entity and does not encode in itself a proof from resident that the consent is indeed given by the resident. Second is that providing a boolean consent is too broad, either an unconditional access is given to the whole eKYC information or no access is given at all. A resident may wish to have a better privacy enhancing fine-grained access control to his/her eKYC data. Resident may wish to define a privacy and access control policy dictating the *scope* of information which can be provided, the *purpose* for which the information can be provided and *recipients* to whom the information can be provided. For example, a resident may wish to disclose only his/her name and address, only for electronic signature purpose and only to a specific *eSign* Service Provider.

In [4], the author explained two limitations of present *eSign* model. The first limitation is that the eKYC data access reflects a restrictive *self-only*, *full-resource* and *unlimited* access control. Author pointed out that a resident may wish to have a better access control mechanism which allows third entities to access part of a resource which is to be used for a specific purpose and for a limited time period. The second limitation is that for each *eSign* request, resident has to authenticate itself each time and to include the authentication proof in each such request. Author pointed out that if a resident needs to *eSign* multiple times, time taken by initial authentication phase will be a major bottleneck. The author proposed that amortized performance of eSign can be improved using *digital access token* which encodes in itself the authentication proof and other information such as how many *eSign* requests can be made using this token and the expiry time of the token.

This paper is an extension of [4] and the digital access token is enhanced to implement *Privacy Aware eSign*. Our main contribution in this paper is to introduce a method to implement *Privacy Aware eSign* using *Privacy Enhancing and Fine-Grained Access Control (PEaFGAC) Statements*. A resident can encode these statements in digital access token for better access to his/her eKYC data. This token can be provided to third entities so that they can present this token for claiming protected resource from *UIDAI*. This paper also presents security analysis of the proposed scheme using *Burrows-Abadi-Needham (BAN)* logic. The analysis shows that in the proposed scheme, even if the network is unreliable, the exchanged information is reliable and is secured against eavesdropping.

The remainder of this paper is organized as follows. Section 2 presents related work. Notations used in the paper are reported in figure 1. Section 3 presents Aadhaar based eKYC service. Section 4 presents *eSign* version 2.0 model. Section 5 presents *eSign* model proposed in [4] to improve amortized performance of *eSign*. Section 6 presents proposed *Privacy Aware eSign* model using privacy enhancing and fine-grained access controlled eKYC. Section 7 presents formal security analysis of the proposed model using *BAN logic* and finally section 8 concludes the paper.

$\{X\}_Y$	X is signed by key Y
SK_Y	Symmetric key of entity Y
SK_{Y_Z}	Symmetric key shared by entities Y and Z.
PR_Y	Private asymetric key of entity Y
PB_Y	Public asymetric key of entity Y
R_i	Resident
ASP_i	Application Service Provider
ESP_i	eSign Service Provider
$UIDAI$	Unique Identification Authority of India
ID_{R_i}, ID_{ASP_i} ID_{ESP_i}	Identities of R_i, ASP_i and ESP_i
TID_{ESP_i}, TID_{ASP_i}	Unique transaction identifiers generated by ESP_i and ASP_i
PW_{R_i}	Password of R_i for login to ASP_i portal
$AadhaarNo_{R_i}$	Aadhaar No of R_i
C_{R_i}	Cookie associated with R_i's logged-in session, assigned by ASP
PR_{B_i}, PR_{ASP_i} PR_{ESP_i}, PR_{UIDAI}	Private keys of R_i browser, ASP_i, ESP_i and $UIDAI$
PB_{B_i}, PB_{ASP_i} PB_{ESP_i}, PB_{UIDAI}	Public keys of R_i browser, ASP_i, ESP_i and $UIDAI$
$n*_!$	nonces such as $n1_{ASP_i}$, where $*$ is any integer and ! can be R_i, ASP_i, ESP_i or $UIDAI$
$DataR_i(DataA_i,$ $DataE_i, DataU_i)$	Intermediate data in plaintext to be send by R_i (ASP_i, ESP_i, $UIDAI$)
$SignR_i(SignA_i,$ $SignE_i, SignU_i)$	$\{H(DataR_i)\}_{PR_{Ri}}$
$consent_{use\_ekyc}$	Consent from resident whether his/her eKYC can be used
$consent_{genuse\_at}$	Consent from resident whether a digital access token can be generated for later use
$License_{ASP_i}$ $License_{ESP_i}$	License for ASP_i (ESP_i) to use services from ESP (UIDAI)
M_i	Message (in plaintext) to be eSign
DSC_{Ri_Mi}	Digital Signature Certificate generated for message M_i for resident R_i
$\{M\}_{eSign\_R_i\_ESP_i}$	eSigned message (by R_i) through ESP_i
$H()$	One way cryptographically secure hash fn
$\|\|$	Concatenation operator
$\oplus$	XOR operator

Figure 1: Notations used in this paper

2 Related Work

Digital tokens are increasingly being used in many cryptography related applications to achieve varied objectives.

U-Prove [5] is an identity management solution based on blind signatures [6] which uses digital tokens to achieve objectives of privacy and anonymity. *U-Prove* consists of two protocols, viz., issuance protocol and presentation protocol. In issuance protocol, identity provider issues digital token to the subscriber which (s)he can later present to the verifier in presentation protocol so that the service provider can grant resource access to the subscriber. A *U-Prove* token consists of a unique token identifier, a public key of the token which aggregates information in the token, a token information field which encodes token specific information, a prover information field which is opaque to the issuer, issuer signature on all the other token contents and a boolean value which indicates whether the token is protected by a device. *U-Prove* uses digital tokens effectively by encoding necessary information in it in cryptographically secure way to achieve objectives such as privacy and anonymity.

OAuth2 [7] is an authorization framework which allows delegation of access to protected resources to a third party by using digital tokens referred to as access tokens. Access tokens are issued to Clients by *Authorization Server* after taking permission from *Resource Owner*. An access token can be of two types, viz., a bearer token and a MAC token. A bearer token is an opaque string which can be used to claim access to a resource by any entity who presents the

token. A MAC token is essentially a shared symmetric key which is used to sign a challenge by the client to prove its possession of the token to authorization server. *OAuth2* uses digital tokens effectively for access delegation and is used by many organizations for data sharing.

Bitcoin [8] is a decentralized digital currency which can be transacted over peer-to-peer bitcoin network. A bitcoin network is composed of cryptographically secure linear chains of blocks with each block containing a header and a collection of transactions. A transaction is essentially a digital token that changes ownership of bitcoins from one entity to another. Each transaction in bitcoin network is broadly composed of three parts, viz., input, output and amount. Input refers to the previous owner of the bitcoins, output refers to the new owner of the bitcoins and amount refers to the amount of bitcoin that is transacted. Bitcoins uses cryptographically secure digital information containers (similar to digital tokens) effectively for the realization of digital currency.

Although Attribute Based Encryption (ABE) is also evolved to protect privacy of user data, it is based on Identity Based Encryption (IBE). An agency may not shift from PKI to IBE framework for a number of reasons.

3 Aadhaar based e-KYC service (v2.1)

Aadhaar based eKYC service is available to general citizens only through certain empaneled agencies such as *eSign Service Provider (ESP)* and the infrastructure network is secured by certain designated agencies known as *Authentication Service Agency (ASA)* and *KYC User Agency (KUA)*. eKYC service is hosted as a stateless REST based web service over HTTPS and the details are sent as input data encoded in XML. Figure 2 depicts Aadhaar's eKYC webservice as specified in eKYC v2.1 specification [9]. The specification provides following information about element *rc* which represents the resident consent.

"rc – (mandatory) Represents resident's explicit consent for accessing the resident's identity and address data from Aadhaar system. Only valid value is "Y". Without explicit consent of the Aadhaar holder application should not call this API [9]."

As can be seen from the specification, *rc* is a boolean consent and assumes that it has been transferred from resident to *UIDAI* unaltered. Although intermediate communication channels between various entities from resident to *UIDAI* are well secured and access to eKYC data is provided only after receiving explicit consent from resident, this way of taking consent from resident has two shortcomings. First is that the consent is taken by a *non-UIDAI* entity and does not encode in itself a proof from resident that it is (s)he who provided the consent. This is because residents do not have any registered tamper proof crypto device which can be used to encrypt user consent using resident specific PIN or password. Second is that providing a boolean consent is too broad, either an unconditional access is given to the whole eKYC information or no access is given at all. A resident may wish to have a better privacy enhancing fine-grained access control to his/her eKYC data indicating details on *scope*, *purpose* and *recipient*.

```
URL:
  https://<host>/kyc/<ver>/<ac>/<uid[0]>/<uid[1]>
        /<asalk>

Input Data:
  <Kyc ver="" ra="" rc="" lr="" de="" pfr="">
       <Rad>base64 encoded fully valid Auth XML for
           resident
       </Rad>
  </Kyc>

Response Data:
  <Resp status="" ko="" ret="" code="" txn="" ts=""
        err=""> encrypted and base64 encoded KycRes
        element
  </Resp>

  <KycRes ret="" code="" txn="" ts="" ttl="" actn=""
      err="">
      <Rar>base64 encoded fully valid Auth response
          XML for resident
      </Rar>
      <UidData uid="">
          <Poi name="" dob="" gender="" />
          <Poa co="" house="" street="" lm="" loc=""
               vtc="" subdist="" dist="" state=""
               country="" pc="" po=""/>
          <LData lang="" name="" co="" house=""
               street="" lm="" loc="" vtc=""
               subdist="" dist="" state=""
               country="" pc="" po=""/>
          <Pht> base64 encoded JPEG photo of the
               resident
          </Pht>
          <Prn type="pdf"> base64 encoded signed
               Aadhaar letter for printing
          </Prn>
      </UidData>
      <Signature/>
  </KycRes>
```

Figure 2: Aadhaar's eKYC 2.1 API

4 Present model of eSign in India

In *eSign* version 2.0 [10], a resident first registers itself with a front end application specific agency viz. a viz., *Application Service Provider (ASP)*. A resident can use either OTP based authentication or biometric based authentication. In case of OTP based authentication, OTP generation request is forwarded to *UIDAI* via *ASP* and *ESP*. *UIDAI* generates an OTP and sends it to resident's registered mobile number. In case of biometric based authentication, resident gets his fingerprint/iris scanned through a registered device. After authentication phase, resident now initiates an eSign request through *ASP* by providing it the consent to use his/her eKYC, the document to be signed and his/her *Aadhaar* number. *ASP* calculates cryptographic hash of the document and sends it along with the resident's consent and resident's *Aadhaar* number to *ESP*. *ESP* takes authentication proof from resident, creates a random symmetric key SK_{ESP_UIDAI} and a

Personal Identity Data Object (*PID*). *PID* encodes in itself the resident's authentication proof and the cryptographic hash of the *PID* object ($SHA256(PID)$). *ESP* first encrypts *PID* with SK_{ESP_UIDAI}, second encrypts cryptographic hash of *PID* ($SHA256(PID)$) with SK_{ESP_UIDAI} and third encrypts SK_{ESP_UIDAI} with public key of *UIDAI* (PB_{UIDAI}). *ESP* now wraps them in a new object called "Auth" and sends it to *UIDAI* in eKYC request. *UIDAI* provides eKYC information to *ESP*. Using received eKYC information, *ESP* generates a Digital Signature Certificate (DSC) and provides it to *ASP*. *ASP* provides the digitally signed document to the resident.

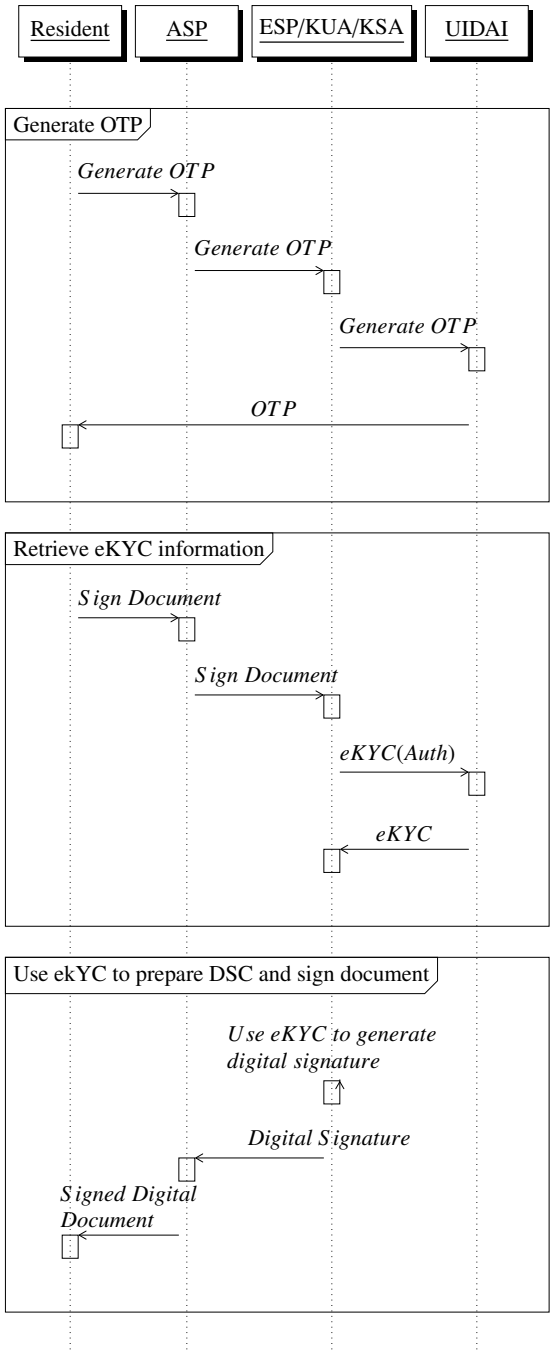

Figure 3: Sequence diagram of eSign 2.0

In practice, the initial authentication phase in *eSign* request is most time consuming since it involves either the manual text input (in case of OTP based authentication) or the physical scan of the fingerprint/iris (in case of biometric based authentication). Other than that, in some use cases such as *Create Birth Certificate*, *Create Death Certificate*, *Student Enrollment*, etc., the application is most heavily used during a certain time period (nearing the end of a deadline) which puts a sudden nationwide load on *UIDAI* services.

5 eSign model as proposed in [4]

In [4], author explained two limitations of present *eSign* model and proposed a mechanism to address the same. The first limitation is that in present model of *eSign*, eKYC data access reflects a restrictive *self-only*, *full-resource* and *unlimited* access control. Author pointed out that the resident may wish to have a better access control mechanism reflecting *third-entity-also*, *partial resource*, *use-limited* and *time-limited*.

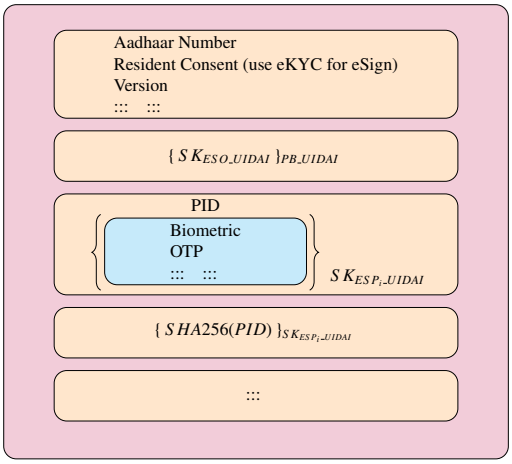

Figure 4: Auth Object (eSign 2.0)

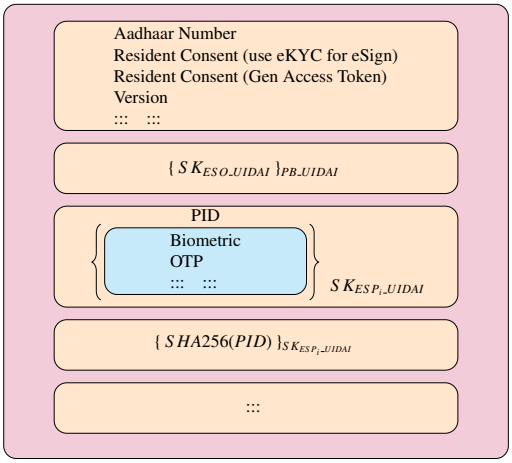

Figure 5: Auth Object as proposed in [4]

The second limitation is that a resident has to authenticate himself/herself for each *eSign* request and include the corresponding authentication proof in each *eSign* request.

If a resident wishes to *eSign* a large number of documents, the initial authentication phase will comprise most of the overall *eSign* time. After taking necessary consent from the resident, his/her authentication proof be stored with *ESP* in first request and is reused in rest of the requests.

A digital access token [figure 6] can be used to include claims from participating entities (*ESP* and *UIDAI*). A new service named *GenerateAccessToken* is proposed to be introduced by *UIDAI*.

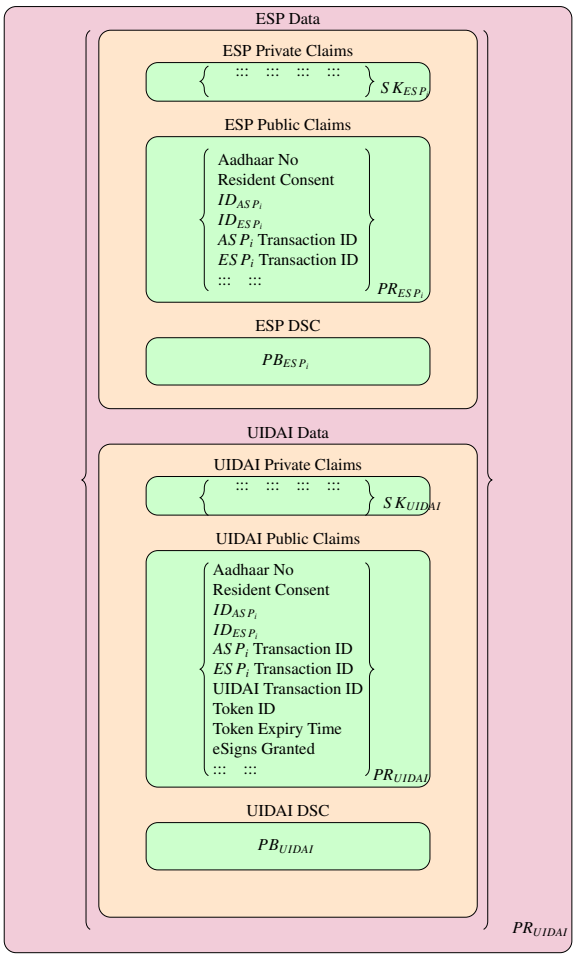

Figure 6: Access Token Structure as proposed in [4]

In this proposed model of eSign [figures 7, 8], resident first authenticates himself/herself using OTP or biometric based authentication and sends *eSign* request to *ASP*. *ASP* forwards this *eSign* request to *ESP*. *ESP* takes OTP and permission to generate access token from resident and creates an "Auth" object. This "Auth" object is created as before but additionally including *ESP* claims as well. *ESP* sends *GenerateAccessToken* request to *UIDAI* including "Auth" object. After receiving this request, *UIDAI* creates an access token including its own claims as well as claims received from *ESP*. *UIDAI* sends this access token back to the *ESP*. Now, *ESP* sends eKYC request to *UIDAI* including this access token instead of the "Auth" object. After receiving eKYC information from *UIDAI*, *ESP* generates *Digital Signature Certificate (DSC)* from it and provides the same to *ASP*. *ASP* embeds DSC in the document and sends the digitally signed document to the resident. For all rest of the *eSign* requests, *ESP* can reuse the same access token in eKYC requests and avoid the initial authentication phase.

The paper also presented two usability scenarios, based on whether the eKYC information can be cached by *ESP* or not. If *ESP* is permitted to reliably and securely store eKYC information of the resident, even the repeated eKYC requests from *ESP* to *UIDAI* can be avoided.

The paper also presented performance comparison analysis of proposed model with present model and found substantial improvement in amortized performance of *eSign*.

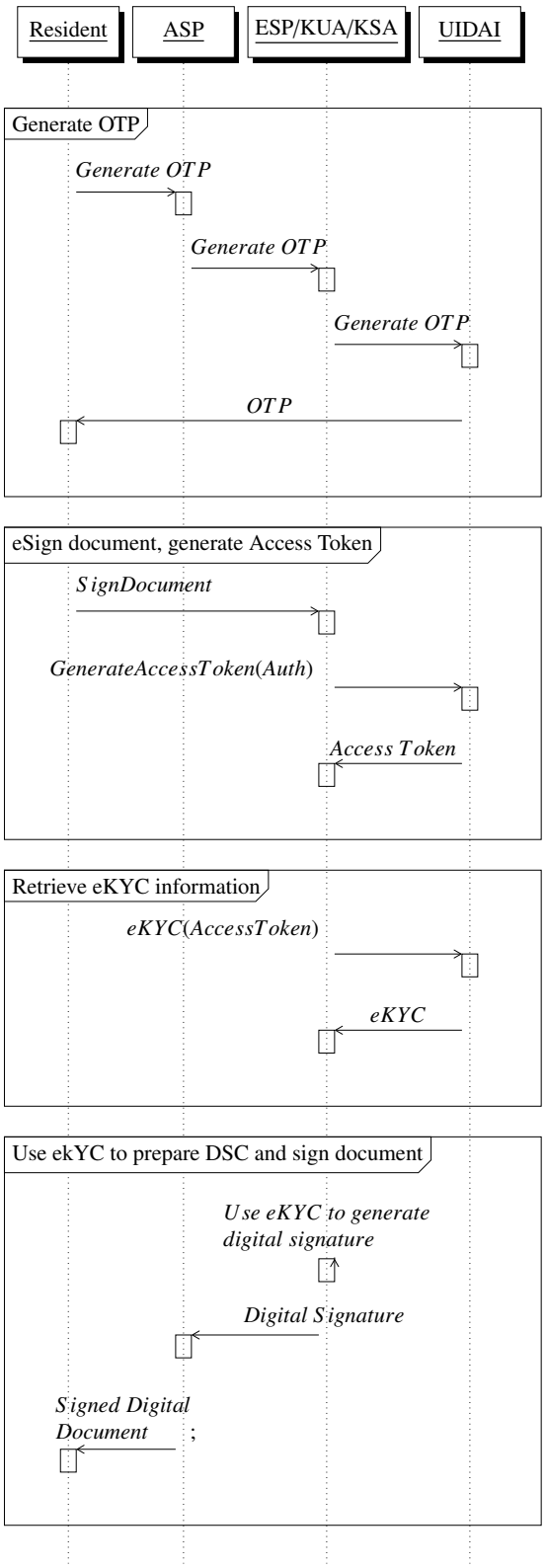

Figure 7: First call to eSign in eSign model proposed in [4]

6 Privacy Aware eSign model

In earlier proposed model [section 5] digital access token is used to increase amortized performance of *eSign* by storing necessary claims from *UIDAI* and *ESP*. The same token can be enhanced to include claims from resident as well. A resident can encode claims related to privacy and fine grained access control of his/her eKYC data. A stricter *PEaFGAC* statements may be enforced centrally at *UIDAI* level and an

overriding less strict rule can be supplied with each eKYC request to grant access to the requesting entity.

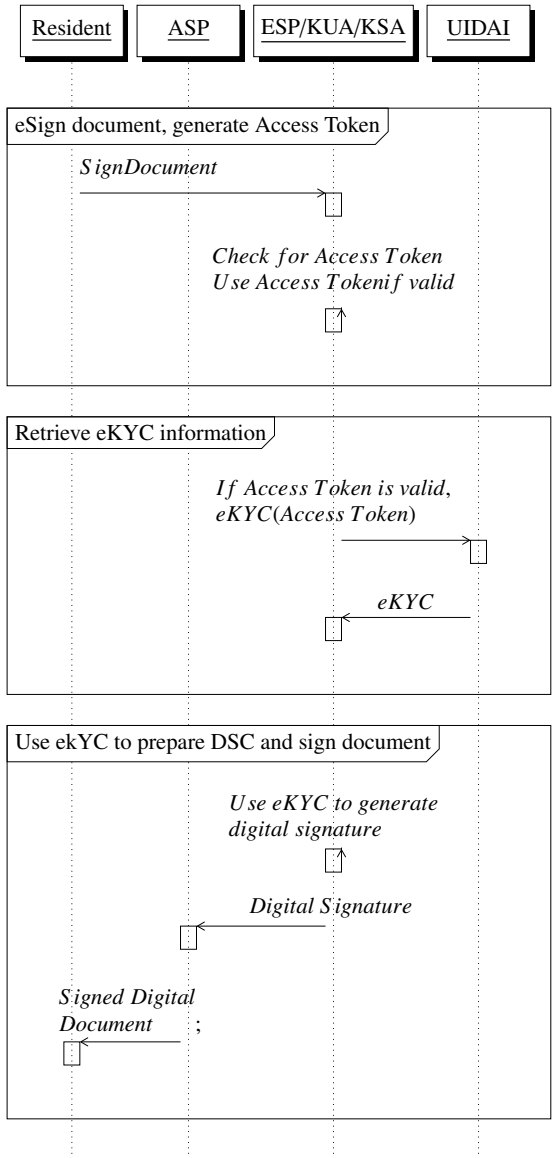

Figure 8: Second call to eSign in case eKYC needs to be fetched again

6.1 Privacy and Fine-Grained Access Control (PEaFGAC) Statements for eKYC data

A *PEaFGAC* statement encodes in itself the *scope* of information which can be provided, the *purpose* for which the information can be provided and attributes of *recipients* to whom the information can be provided. These statements are comprised of small sub-statements which are combined using relational operators. Each statement is identified by a numeric *id* and an alphanumeric *tag*.

An example of a *PEaFGAC* statement is presented in figure 10. This statement encodes in it that the purpose for seeking eKYC information should be *eSign*, seeking entity must either have the email in domain *finance.iitg.ac.in*, or must be working in *finance* department of *Indian Institute of Technology, Guwahati (IITG)*, or must have a designation of *director* or above. The statement is uniquely identified by a statement identifier (*ID*) and has a small alphanumeric representational string (*TAG*). Other than these, the staement also encodes in it the purpose for which eKYC can be accessed (*Purpose*), required (*eKYC*) attributes of information seeker (*AP*) and eKYC information which can be provided to the requester (*scope*). If required, a user can have multiple privacy statements for his/her eKYC data represented by different tags.

```
AadhaarNo
POI:
  name, dob
POA:
  co, house, street, lm, loc, vtc, subdist, dist,
  state, country, pc, po
LData:
  lang, name, co, house, street, lm, loc, vtc,
  subdist, dist, state, country, pc, po
Pht:
  <Base64 encoded JPEG photo of resident
Org:
  dep, desig
Other:
  email
```

Figure 9: Least information assumed to be available from eKYC for this paper

```
PS.ID:
  5
PS.Tag:
  eSignDoc
PS.Purpose:
  eSign
PS.AP:
  (email = *@finance.iitg.ac.in)       OR
  (org = IITG AND org.dep = finance)   OR
  (desig >= director)
PS.Scope:
  poi.name, poi.dob, poa.country, Ldata.lang
```

Figure 10: Example of a PEaFGAC statement

It is assumed that all entities which request eKYC data also have their eKYC information available with *UIDAI*. This include not just the users but the organizations such as *ESP*s as well. To better know an entity (both users and organizations), it is proposed that eKYC fields are expanded to include more details such as entity type (indicating whether the subject is a human or an organization), resident's organization, resident's department, resident's designation, etc. When an entity attempts to access eKYC data of a resident, entity's eKYC data and purpose for which the eKYC data is sought are verified against *PEaFGAC* statement protecting eKYC data to decide whether the requisite access can be granted or not. Only if the access can be granted, will the eKYC data be provided to the requesting entity. The eKYC data provided to the entity is limited in scope by *PEaFGAC* statement. For rest of this paper, eKYC data is assumed to consists of at least the information presented in figure 9.

6.2 PEaFGAC Token

The token structure introduced in [4] can be enhanced to include resident claims including *PEaFGAC* statement [fig-

ure 11]. Before sending an *eSign* request, resident creates a *PEaFGAC* token by sending a token generation request to *UIDAI* through *ASP* and *ESP*. During token generation process, resident is redirected to *UIDAI* web page where (s)he provides OTP value for authentication and *PEaFGAC* statement for privacy and fine-grained access to his/her eKYC data. Subsequently *UIDAI* verifies the OTP value and signs cryptographic hash of the statement with its private key and stores the signed hash in resident's private claims and stores the statement in plaintext in resident's public claims section of *PEaFGAC* digital access token.

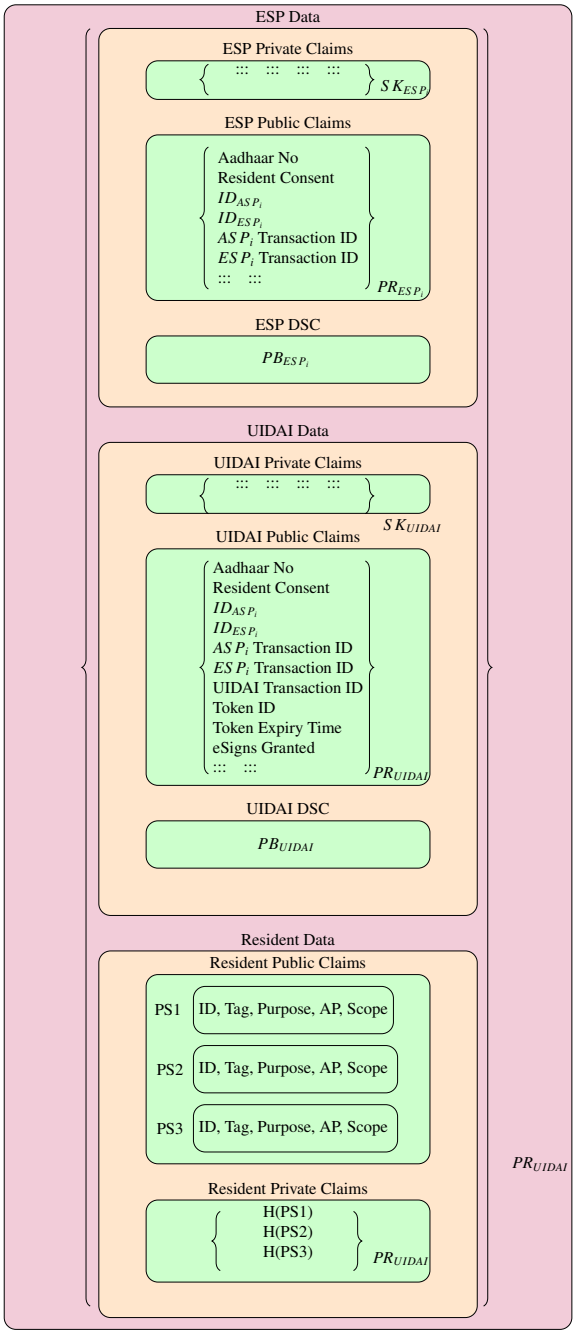

Figure 11: Proposed PEaFGAC Token Structure

Figure 12 depicts the sequence and details of communication messages among participating entities for generation of a token. First column indicates the message identifier, second column indicates the participating entities and the direction of communication and third column indicates what message is sent and how it is constructed.

Login to ASP		
$TGM1$	$R \rightarrow ASP$	$Generate\ nonce\ n1_{R_i}$ $DataR_1 = ID_{R_i} \| PW_{R_i} \| PB_{B_i} \| n1_{R_i}$ $SignR_1 = \{H(DataR_1)\}_{PR_{B_i}}$ $\{\ loginReq(DataR_1, SignR_1)\ \}_{PB_{ASP_i}}$
$TGM2$	$R \leftarrow ASP$	$DataA_1 = C_{R_i} \oplus (n1_{R_i} + 1)$ $SignA_1 = \{H(DataA_1)\}_{PR_{ASP}}$ $\{\ loginRes(DataA_1, SignA_1)\}_{PB_{B_i}}$
Generate OTP		
$TGM3$	$R \rightarrow ASP$	$Generate\ nonce\ n2_{R_i}$ $DataR_2 = AadhaarNo_{R_i} \| C_{R_i} \| n2_{R_i}$ $SignR_2 = \{H(DataR_2)\}_{PR_{B_i}}$ $\{\ getotpASPReq(DataR_2, SignR_2)\ \}_{PB_{ASP_i}}$
$TGM4$	$ASP \rightarrow ESP$	$Generate\ nonce\ n1_{ASP_i}$ $DataA_1 = AadhaarNo_{R_i} \| ID_{ASP_i} \|$ $License_{ASP_i} \| TID_{ASP_i} \| n1_{ASP_i}$ $SignA_1 = \{H(DataA_1)\}_{PR_{ASP_i}}$ $\{\ getotpESPReq(DataA_1, SignA_1)\ \}_{PB_{ESP_i}}$
$TGM5$	$ESP \leftarrow UIDAI$	$Generate\ nonce\ n1_{ESP_i}$ $DataE_1 = AadhaarNo_{R_i} \| ID_{ESP_i} \|$ $License_{ESP_i} \| TID_{ESP_i} \| n1_{ESP_i}$ $SignE_1 = \{H(DataE_1)\}_{PR_{ESP_i}}$ $\{\ getotpReq(DataE_1, SignE_1)\ \}_{PB_{UIDAI}}$
$TGM6$	$R \leftarrow UIDAI$	$\{\ OTP\ \}_{SecureCellularNetwork}$
$TGM7$	$ESP \leftarrow UIDAI$	$DataU_1 = returnStatus \| TID_{ESP_i} \|$ $MaskedMobileNo \| (n1_{ESP_i} + 1)$ $SignU_1 = \{H(DataU_1)\}_{PR_{UIDAI}}$ $\{\ getotpRes(DataU_1, SignU_1)\}_{PB_{ESP_i}}$
$TGM8$	$ESP \leftarrow ASP$	$DataE_2 = returnStatus \| TID_{ASP_i} \|$ $MaskedMobileNo \| (n1_{ASP_i} + 1)$ $SignE_2 = \{H(DataE_2)\}_{PR_{ESP_i}}$ $\{\ getotpESPRes(DataE_2, SignE_2)\}_{PB_{ASP_i}}$
$TGM9$	$ESP \leftarrow R$	$DataA_2 = returnStatus \|$ $MaskedMobileNo \| (n2_{R_i} + 1)$ $SignA_2 = \{H(DataA_2)\}_{PR_{ASP_i}}$ $\{\ getotpASPRes(DataA_2, SignA_2)\}_{PB_{B_i}}$
Generate Token		
$TGM10$	$R \rightarrow ASP$	$Generate\ nonce\ n3_{R_i}$ $DataR_3 = C_{R_i} \| n3_{R_i}$ $SignR_3 = \{H(DataR_3)\}_{PR_{B_i}}$ $\{\ gentokASPReq(DataR_3, SignR_3)\ \}_{PB_{ASP_i}}$
$TGM11$	$ASP \rightarrow ESP$	$Generate\ nonce\ n2_{ASP_i}$ $DataA_3 = AadhaarNo_{R_i} \| ID_{ASP_i} \| License_{ASP_i} \|$ $TID_{ASP_i} \| n2_{ASP_i}$ $SignA_3 = \{H(DataA_3)\}_{PR_{ASP_i}}$ $\{\ gentokESPReq(DataA_3, SignA_3)\ \}_{PB_{ESP_i}}$
$TGM12$	$ESP \rightarrow UIDAI$	$Generate\ nonce\ n3_{ESP_i}$ $DataE_3 = AadhaarNo_{R_i} \| ID_{ESP_i} \|$ $License_{ESP_i} \| TID_{ESP_i} \|$ $n3_{ESP_i}$ $SignE_3 = \{H(DataE_3)\}_{PR_{ESP_i}}$ $\{\ gentokUIDAIReq(DataE_3, SignE_3)\ \}_{PB_{UIDAI}}$
$TGM13$	$UIDAI \leftarrow ESP$	$Generate\ nonce\ n1_{UIDAI}$ $DataU_1 = UIDAIRedirectURL$ $(ForTakingPrivacyStatements) \|\|$ $PB_{UIDAI} \| TID_{ESP_i} \| n1_{UIDAI}$ $SignU_1 = \{H(DataU_1)\}_{PR_{UIDAI}}$ $\{\ genpsUIDAIReq(DataU_1, SignU_1)\ \}_{PB_{ESP_i}}$
$TGM14$	$ESP \leftarrow ASP$	$Generate\ nonce\ n4_{ESP_i}$ $DataE_4 = UIDAIRedirectURL$ $(ForTakingPrivacyStatements)$ $\| PB_{UIDAI} \| TID_{ASP_i} \| n4_{ESP_i}$ $SignE_4 = \{H(DataE_3)\}_{PR_{ESP_i}}$ $\{\ genpsESPReq(DataE_4, SignE_4)\ \}_{PB_{ASP_i}}$
$TGM15$	$ASP \leftarrow R$	$Generate\ nonce\ n4_{R_i}$ $DataA_4 = \{\ Present\ UIDAIRedirectURL\ to$ $Resident\ which\ requests\ him$ $to\ provide\ OTP\ Value\ and\ Privacy$ $statements \| PB_{UIDAI} \| n4_{R_i}\}$ $SignA_4 = \{H(DataA_4)\}_{PR_{ASP_i}}$ $\{\ genpsASPReq(DataA_4, SignA_4)\ \}_{PB_{B_i}}$
$TGM16$	$R \rightarrow UIDAI$	$\{\ PEaFGACPrivacyStatements\ \}_{PB_{UIDAI}}$
PEaFGAC Token Generation Request		
$TGM17$	$R \rightarrow ASP$	$DataR_4 = C_{R_i} \| (n4_{R_i} + 1)$ $SignR_4 = \{H(DataA_4)\}_{PR_{B_i}}$ $\{\ genpsASPRes(DataA_4, SignA_4)\ \}_{PB_{B_i}}$
$TGM18$	$ASP \leftarrow ESP$	$DataA_5 = (n4_{ESP_i} + 1)$ $SignA_5 = \{H(DataA_4)\}_{PR_{ASP_i}}$ $\{\ genpsESPRes(DataA_4, SignA_4)\ \}_{PB_{ESP_i}}$
$TGM19$	$ESP \leftarrow UIDAI$	$DataE_5 = (n1_{UIDAI} + 1)$ $SignE_5 = \{H(DataE_5)\}_{PR_{ESP_i}}$ $\{\ genpsUIDAIRes(DataE_5, SignE_5)\ \}_{PB_{UIDAI}}$
$TGM20$	$ESP \leftarrow UIDAI$	$Create\ PEaFGACTokenAT_{Ri}$ $DataU_2 = AT_{Ri} \| (n3_{ESP_i} + 1)$ $SignU_2 = \{H(DataE_5)\}_{PR_{ESP_i}}$ $\{\ gentokUIDAIRes(DataE_5, SignE_5)\ \}_{PB_{UIDAI}}$
$TGM21$	$ASP \leftarrow ESP$	$DataE_6 = (n2_{ASP_i} + 1)$ $SignE_6 = \{H(DataE_5)\}_{PR_{ESP_i}}$ $\{\ gentokESPRes(DataE_6, SignE_6)\ \}_{PB_{ASP_i}}$
$TGM22$	$R \leftarrow ASP$	$DataA_5 = (n3_{R_i} + 1)$ $SignA_5 = \{H(DataE_5)\}_{PR_{ASP_i}}$ $\{\ gentokESPRes(DataA_5, SignA_5)\ \}_{PB_{B_i}}$

Figure 12: Proposed PEaFGAC Token Generation protocol

6.3 Proposed Privacy Aware eSign model using PEaFGAC statement for eKYC data and PEaFGAC token

This section presents how *PEaFGC* statement for eKYC data and *PEaFGAC* token can be used to implement *Privacy Aware eSign*. It is assumed that *PEaFGAC* token has already been generated as explained in section 6.2. It is also assumed that the communication channel between resident and *ASP* is secured using SSL/TLS, between *ASP* and *ESP* is secured using SSL/TLS and between *ESP* and *UIDAI* is secured using dedicated secure leased lines.

Figure 13 depicts the sequence and details of communication messages transferred in *eSign* request in case eKYC needs to be fetched again.

Login to ASP		
$M1$	$R \rightarrow ASP$	$Generate\ nonce\ n1_{R_i}$ $DataR_1 = ID_{R_i} \| PW_{R_i} \| PB_{B_i} \| n1_{R_i}$ $SignR_1 = \{H(DataR_1)\}_{PR_{B_i}}$ $\{\ loginReq(DataR_1, SignR_1)\ \}_{PB_{ASP_i}}$
$M2$	$R \leftarrow ASP$	$DataA_1 = C_{R_i} \oplus (n1_{R_i} + 1)$ $SignA_1 = \{H(DataA_1)\}_{PR_{ASP}}$ $\{\ loginRes(DataA_1, SignA_1)\}_{PB_{B_i}}$
Initiate eSign request		
$M3$	$R \rightarrow ASP$	$Generate\ nonce\ n2_{R_i}$ $DataR_2 = M_i \| consent_{use\_ekyc} \|$ $consent_{genuse\_at} \| C_{R_i} \| n2_{R_i}$ $SignR_2 = \{H(DataR_2)\}_{PR_{B_i}}$ $\{\ signdocASPReq(DataR_2, SignR_2)\ \}_{PB_{ASP_i}}$
$M4$	$ASP \leftarrow ESP$	$Generate\ nonce\ n1_{ASP_i}$ $DataA_3 = H(M_i) \| AadhaarNo_{R_i} \| ID_{ASP_i} \|$ $License_{ASP_i} \| TID_{ASP_i} \|$ $consent_{use\_ekyc} \| consent_{genuse\_at} \|$ $n1_{ASP_i}$ $SignA_3 = \{H(DataA_3)\}_{PR_{ASP_i}}$ $\{\ signdocESPReq(DataA_3, SignA_3)\ \}_{PB_{ESP_i}}$
Retrieve eKYC (reusing access token) and sign document		
$M5$	$ESP \rightarrow UIDAI$	$Generate\ nonce\ n1_{ESP_i}$ $If\ AT_{R_i}\ is\ valid\ use\ it$ $DataE_5 = AT_{R_i} \| H(M_i) \| n1_{ESP_i}$ $SignE_5 = \{H(DataE_5)\}_{PR_{ESP_i}}$ $\{\ kycESPReq(DataE_5, SignE_5)\ \}_{PB_{UIDAI}}$
$M6$	$ESP \leftarrow UIDAI$	$Retrieve\ eKYC_{ESP_i}$ $Retrieve\ AT_{R_i} \rightarrow UC \rightarrow AP$ $Verify\ whether\ access\ can\ be\ granted$ $based\ on\ above\ two\ parameters.$ $eKYC_{R_i} = eKYC\ of\ resident\ scoped$ $by\ AT_{R_i} \rightarrow UC \rightarrow scope$ $DataU_3 = eKYC_{R_i} \| (n1_{ESP_i} + 1)$ $SignU_3 = \{H(DataU_3)\}_{PR_{UIDAI}}$ $\{\ kycESPRes(DataU_3, SignU_3)\ \}_{PB_{ESP_i}}$
$M7$	$ASP \leftarrow ESP$	$Generate\ key\ pair\ PB_{R_i}\ PR_{R_i}\ using\ eKYC_{R_i}$ $SignChain = \{\ PB_{R_i}\ \}_{PR_{ESP_i}} \|$ $\{\ PB_{ESP_i}\ \}_{PR_{CCA}}$ $DSC_{R_i\_M_i} = \{\ eKYC_{R_i} \| H(M_i)\ \}_{PR_{R_i}} \|$ $PB_{R_i} \| SignChain$ $Delete\ PR_{R_i}$ $DataU_2 = DSC_{R_i\_M_i} \| TID_{ASP_i} \| (n1_{ASP_i} + 1)$ $SignU_2 = \{H(DataU_2)\}_{PR_{ESP_i}}$ $\{\ signdocESPRes(DataU_2, SignU_2)\ \}_{PB_{ASP_i}}$
$M8$	$R \leftarrow ASP$	$\{M_i\}_{eSign\_R_i\_ESP_i} = M_i \| DSC_{R_i\_M_i}$ $DataA_6 = \{M_i\}_{eSign\_R_i\_ESP_i} \| (n2_{R_i} + 1)$ $SignA_6 = \{H(DataA_6)\}_{PR_{ASP_i}}$ $\{\ signdocASPRes(DataA_6, SignA_6)\ \}_{PB_{B_i}}$
$M9$	$R \leftrightarrow R$	$Verify\ correctness\ of\ eKYC,\ H(M)\ and$ $SignChain\ in\ \{M_i\}_{eSign}$

Figure 13: Proposed Privacy Aware eSign model

7 Formal Security Analysis of the proposed model using BAN Logic

This section presents formal security analysis of the proposed scheme using *Burrows-Abadi-Needham (BAN) logic* [11]. Because of space limitation, it is assumed that PEaFGAC token has already been generated securely.Analysis of the token generation request can be done similarly.*BAN logic* is a well-known model used to find beliefs of participants in a cryptographic protocol.

Operator Usage	Description
$P \models X$	P believes statement X
$P \lhd X$	P sees statement X
$P \mapsto X$	P controls X
$\#(X)$	Message X is fresh
$P \overset{K}{\leftrightarrow} Q$	P and Q share key K
$\overset{K}{\mapsto} P$	P has K as its public key
$P \overset{X}{\rightleftharpoons} Q$	Formula X is a secret known only to P and Q
$\{X\}_K$	Formula X is encrypted using K
$\langle X \rangle_Y$	Formula X is combined with formula Y

Figure 14: Fundamental BAN operators

Operator Usage	Description
$M_{eSign\_R\_ESP\_CCA}$	eSign of message M is done by Resident R through ESP approved by CCA $M_{eSign\_R\_ESP\_CCA}$ $= M \| DSC_{R\_M}$ $= M \| \{eKYC_R \| H(M)\}_{PR_R} \|$ $PB_R \| SignChain$ $= M \| \{eKYC_R \| H(M)\}_{PR_R} \|$ $PB_R \| \{PB_R\}_{PR_{ESP}} \|$ $\{PB_{ESP}\}_{PR_{CCA}}$
$P \models E_i \overset{secure}{\longrightarrow} E_j$	P believes that communication from entity E_i to E_j is secure
$P \models E_i \overset{secure}{\longleftarrow} E_j$	P believes that communication from entity E_j to E_i is secure
$P \models E_i \overset{secure}{\longleftrightarrow} E_j$	P believes that communication between entities E_i and E_j is secure in both directions
$P \models E_i \overset{ACTPerm}{\longleftrightarrow} E_j$	P believes that entity E_i has given permission for action ACT to entity E_j
$P \models C_R \rightsquigarrow E_i$	P believes that cookie C_R is associated with logged-in entity E_i
$E_R \models E_R \overset{C_{E_R} \rightarrow ID_{E_R}}{\longrightarrow} E_R$	E_R believes that it has securely communicated its identity ID_{E_R} to entity E_R through cookie C_{E_R}

Figure 15: Extended BAN operators

The security environment is assumed to be based on *Delev-Yao model* in which all messages are communicated over public channels and an attacker can see, modify, compose and replay messages but cannot break cryptographic principles. The security environment also assumes that an attacker can decipher messages if he has a valid decryption key. Some of the fundamental operators used in *BAN logic* are defined in figure 14. An extension to *BAN* logic, defined in figure 15 is required to analyse the proposed model.

Rules of Inference

[R1:] *Message meaning rules* concern the interpretation of messages. They all derive beliefs about the origin of messages.

For shared secrets, the inference rule is

$$\frac{P \models Q \overset{Y}{\rightleftharpoons} P,\ P \lhd \langle X \rangle_Y}{P \models Q \rhd X}$$

That is, if P believes that the secret Y is shared with Q and sees $\langle X \rangle_Y$, then P believes that Q once said X.

[R2:] The *nonce-verification* rule expresses the check that a message is recent, and hence, that the sender still believes in it:

$$\frac{P \models \#(X),\ P \models Q \rhd X}{P \models Q \models X}$$

That is, if P believes that X could have been uttered only recently and that Q once said X, then P believes that Q believes X.

[R3:] The *jurisdiction* rule states that if P believes that Q has jurisdiction over X, then P trusts Q on the truth of X:

$$\frac{P \models Q \Rightarrow X,\ P \models Q \models X}{P \models X}$$

[R4:] The *seeing* rule states that if a principal sees a formula, then he also sees its components, provided he knows the necessary keys:

$$\frac{P \lhd (X,Y)}{P \lhd X},\quad \frac{P \lhd \langle X \rangle_Y}{P \lhd X},\quad \frac{P \models Q \overset{K}{\leftrightarrow} P(.) P \lhd \{X\}_K}{P \lhd X},$$

$$\frac{P \models \overset{K}{\mapsto} P,\ P \lhd \{X\}_K}{P \lhd X},\quad \frac{P \models \overset{K}{\mapsto} P,\ P \lhd \{X\}_{K^{-1}}}{P \lhd X}.$$

Note that if P sees X and P sees Y it does NOT follow that P sees (X, Y) since that means that X and Y were uttered at the same time.

[R5:] The *fresh* rule states that if one part of the formula is fresh, then the entire formula must be fresh.

$$\frac{P \models \#(X)}{P \models \#(X, Y)}.$$

[R6:] The *belief* rule states that if P believes one part of the formula, then it also believe part of the formula.

$$\frac{P \models (X, Y)}{P \models (X)}.$$

Extended Rules of Inference

[R7:] If receiver entity E_R believes that C_R is a cookie associated with a unique session from resident R, PB_B is public key with browser used by resident R, PB_{E_R} is public key of receiver entity E_R, n_R is a fresh nonce generated by R, E_R receives message of the form $\{CommMsgReq(X||C_R||n_R, \{H(X||C_R||n_R)\}_{PR_{B_i}})\ \}_{PB_{E_R}}$, then E_R believes that X is sent by entity R and communication channel from R to E_R is secure and no message is observed, modified or replayed by an intruder.

$$\begin{array}{lll} E_R & \models & \overset{PB_{E_R}}{\longmapsto} E_R, \\ E_R & \models & C_R \rightsquigarrow S, \\ E_R & \models & \#n_R, \\ E_R & \models & \{\{Y\}_{PR_R}\}_{PB_R} = Y \\ E_R & \lhd & \{\ CommMsgReq\ (\\ & & \quad X||C_R||n_R, \\ & & \quad \{H(X||C_R||n_R)\}_{PR_{R_i}})\ \}_{PB_{E_R}} \\ \hline E_R & \models & R \xrightarrow{Secure} E_R, \\ E_R & \models & R \rhd X \end{array}$$

[R8:] If receiver entity E_R believes that PB_{E_R} is public key of receiver entity E_R, n_{E_R} is a fresh nonce generated by E_R, E_R receives message of the form $\{\ CommMsgReq\ (X||n_{E_R}, \{H(X||n_{E_R})\}_{PR_{E_R}})\ \}_{PB_{E_R}}$, then E_R believes that X is sent by entity E_R and communication channel from E_R to E_R is secure and no message is observed, modified or replayed by an intruder.

$$\begin{array}{lll} E_R & \models & \overset{PB_{E_R}}{\longmapsto} E_R, \\ E_R & \models & \{\{Y\}_{PR_{E_R}}\}_{PB_{E_R}} = Y, \\ E_R & \models & \#n_{E_R} \\ E_R & \lhd & \{\ CommMsgReq\ (\\ & & \quad X||n_{E_R}, \\ & & \quad \{H(X||n_{E_R})\}_{PR_{E_R}})\ \}_{PB_{E_R}} \\ \hline E_R & \models & E_R \xrightarrow{Secure} E_R \\ E_R & \models & E_R \rhd X \end{array}$$

[R9:] If receiver entity E_R believes that communication from all possible sender entities E_{R_i} to E_R $(\forall i = 1...n)$ is secure, then E_R believes that communication channel to E_R is secure and no message is observed, modified or replayed by an intruder.

[R10:] If resident R believes that C_R is a cookie associated with a unique session from resident R, PB_{E_R} is public key of entity E_R, n_R was a fresh nonce generated by R and used in a previous request call from R to E_R, R receives a message of the form $\{CommMsgRes(X||(n_R+1), \{H(X||(n_R+1)\}_{PR_{E_R}})\}_{PB_{E_R}}$, then E_R believes that X is sent by entity R and communication channel from R to E_R is secure and no message is observed, modified or replayed by an intruder.

[R11:] If sender entity E_R believes that PR_{E_R} is private key of sender entity E_R, PB_{E_R} is public key of receiver entity E_R, n_{E_R} was a fresh nonce generated by R and used in a previous request call from E_R to E_R, E_R receives message of the form $\{CommMsgRes\ (X||(n_{E_R}+1), \{H(X||(n_{E_R}+1)\}_{PR_{E_R}})\}_{PB_{E_R}}$, then E_R believes that X is sent by entity E_R and communication channel from E_R to E_R is secure and no message is observed, modified or replayed by an intruder.

[R12:] If sender entity E_R believes that communication from all possible receiver entities E_{R_i} $(\forall i = 1...n)$ is secure, then E_R believes that communication channel to E_R is secure and no message is observed, modified or replayed by an intruder.

[R13:] An electronic signature (M_{ieSign}) is a valid signature only when resident verifies that three main parts in signature, viz., $eKYC$, $H(M)$ and $SignChain$ are as expected.

Assumptions

The protocol makes several assumptions. The assumptions relevant for the discussion of this paper are listed below.

[A1:] It is assumed that all sessions from all residents R_i keeps their cookie C_{R_i} secret.

[A2-A6:] The scheme makes several assumptions about public keys. For example, R_i believes that PB_{ASP_i} is public key of ASP_i. Similar to this, other entities also make similar assumptions. These assumptions are listed below.

$$\begin{array}{llll} R_i & \models & \overset{PB_{ASP_i}}{\longmapsto} & ASP_i \quad ...(A2) \\ ESP_i & \models & \overset{PB_{ASP_i}}{\longmapsto} & ASP_i \quad ...(A3) \\ ASP_i & \models & \overset{PB_{ESP_i}}{\longmapsto} & ESP_i \quad ...(A4) \\ UIDAI & \models & \overset{PB_{ESP_i}}{\longmapsto} & ESP_i \quad ...(A5) \\ ESP_i & \models & \overset{PB_{UIDAI}}{\longmapsto} & UIDAI \quad ...(A6) \end{array}$$

[A7:] ASP_i assumes that all valid cookies C_{R_i} are associated with a valid ongoing session from a unique valid user R_i already logged in to ASP_i portal.

$$ASP_i \models C_{R_i} \rightsquigarrow ID_{R_i} \quad \forall i = 1..n$$

[A8-A15:] R_i and ASP_i assumes that all nonce $n*_{R_i}$ (where $*$ is any integer used in the scheme) are fresh. Similar to this, other entities also make similar assumptions. These assumptions are listed below.

$$\begin{array}{lll} R_i & \models & \#n*_{R_i} \quad ...(A8) \\ ASP_i & \models & \#n*_{R_i} \quad ...(A9) \\ ASP_i & \models & \#n*_{ASP_i} \quad ...(A10) \\ ESP_i & \models & \#n*_{ASP_i} \quad ...(A11) \\ ESP_i & \models & \#n*_{ESP_i} \quad ...(A12) \\ UIDAi & \models & \#n*_{ESP_i} \quad ...(A13) \\ UIDAI & \models & \#n*_{UIDAI} \quad ...(A14) \\ ESP_i & \models & \#n*_{UIDAI} \quad ...(A15) \end{array}$$

[A16:] It is assumed that when ASP_i receives message of the form $CommMsg(DataA_j, SignA_j)_{PB_{ASP_i}}$ from ESP_i, it has verified the validity of data, i.e., $\{SignA_j\}_{PB_{ESP_j}} = H(DataA_j)$. The same assumption is made for all entities receiving messages of this form.

Goals to be achieved.

Following are the goals which are envisaged to be achieved by the proposed model.

[G1-G6:] Sender entity must be sure that the data received by receiver entity is same as what was sent by it and is not modified, observed or replayed by an intruder after it was sent by the sender entity. Similarly, receiver entity must be sure that the data received by it is same as what was sent by sender entity and is not modified, observed or replayed by an intruder after it was sent by the sender entity.

$$\begin{array}{llll} ASP_i & \models & R_i & \overset{secure}{\longleftrightarrow} \quad ASP_i \\ R_i & \models & R_i & \overset{secure}{\longleftrightarrow} \quad ASP_i \\ ASP_i & \models & ASP_i & \overset{secure}{\longleftrightarrow} \quad ESP_i \\ ESP_i & \models & ASP_i & \overset{secure}{\longleftrightarrow} \quad ESP_i \\ ESP_i & \models & ESP_i & \overset{secure}{\longleftrightarrow} \quad UIDAI \\ UIDAI & \models & ESP_i & \overset{secure}{\longleftrightarrow} \quad UIDAI \end{array}$$

[G7:] Resident R_i must be sure that at the end what he receives is indeed a digital signature on message M_i, signed by resident's private key and generated by the genuine ESP_i. $R_i \models M_{ieSign} = M_{eSign\_R_i\_ESP_i\_CCA}$

Idealization

BAN idealization of communication messages in communication phase is shown in table 1

Table 1: BAN Idealization of Proposed Protocol (Part I: M1-3) and (Part II: M4-8)

$M1$	ASP_i	$\lhd$	$\{login\ ($ $ID_{R_i} \| PW_{R_i} \| PB_{B_i} \| n1_{R_i}$ $\{H(ID_{R_i} \| PW_{R_i} \| PB_{B_i} \| n1_{R_i})\}_{PR_{B_i}}$ $)\}_{PB_{ASP_i}}$
$M2$	R_i	$\lhd$	$\{loginRes\ ($ $C_{R_i} \oplus (n1_{R_i}+1)$ $\{H(C_{R_i} \oplus (n1_{R_i}+1))\}_{PR_{ASP_i}}$ $)\}_{PB_{B_i}}$
$M3$	ASP_i	$\lhd$	$\{signdocASPReq\ ($ $M_i \| consent_{use\_ekyc} \| consent_{genuse\_at} \| C_{R_i} \| n2_{R_i})$, $\{H(M_i \| consent_{use\_ekyc} \| consent_{genuse\_at} \| C_{R_i} \| n2_{R_i})\}_{PR_{B_i}}$ $)\}_{PB_{ASP_i}}$
$M4$	ESP_i	$\lhd$	$\{signdocESPReq\ ($ $H(M_i) \| AadhaarNo_{R_i} \| ID_{ASP_i} \| License_{ASP_i} \| TID_{ASP_i} \| consent_{use\_ekyc} \| consent_{genuse\_at} \| n1_{ASP_i}$, $\{H(H(M_i) \| AadhaarNo_{R_i} \| ID_{ASP_i} \| License_{ASP_i} \| TID_{ASP_i} \| consent_{use\_ekyc} \| consent_{genuse\_at} \| n1_{ASP_i})\}_{PR_{ASP_i}}$ $)\}_{PB_{ESP_i}}$
$M5$	$UIDAI$	$\lhd$	$\{kycESPReq\ ($ $AT_{R_i} \| H(M_i) \| n1_{ESP_i}$, $\{H(AT_{R_i} \| H(M_i) \| n1_{ESP_i})\}_{PR_{ESP_i}}$ $)\}_{PB_{UIDAI}}$

$M6$	ESP_i	$\triangleleft$	$\{kycESPRes\ ($ $eKYC_{R_i} \| (n1_{ESP_i} + 1)$ $\{H(eKYC_{R_i} \|$ $(n1_{ESP_i} + 1))\}_{PR_{UIDAI}}$ $\}_{PB_{ESP_i}}$
$M7$	ASP_i	$\triangleleft$	$\{signdocESPRes\ ($ $\{eKYC_{R_i} \| H(M_i)\}_{PR_{R_i}} \|$ $PB_{R_i} \| \{PB_{R_i}\}_{PR_{ESP_i}} \|$ $\{PB_{ESP_i}\}_{PR_{CCA}} \|$ $TID_{ASP_i} \| (n1_{ASP_i} + 1),$ $\{H(eKYC_{R_i} \| H(M_i)\}_{PR_{R_i}} \|$ $PB_{R_i} \| \{PB_{R_i}\}_{PR_{ESP_i}} \|$ $\{PB_{ESP_i}\}_{PR_{CCA}} \|$ $TID_{ASP_i} \|$ $(n1_{ASP_i} + 1))\}_{PR_{ESP_i}}$ $)$ $\}_{PB_{ASP_i}}$
$M8$	R_i	$\triangleleft$	$\{signdocASPRes\ ($ $M_i \| \{eKYC_{R_i} \| H(M_i)\}_{PR_{R_i}}$ $\| PB_{R_i} \| \{PB_{R_i}\}_{PR_{ESP_i}} \|$ $\{PB_{ESP_i}\}_{PR_{CCA}} \| (n2_{R_i} + 1)$ $\{H(M_i \| \{eKYC_{R_i} \| H(M_i)\}_{PR_{R_i}}$ $\| PB_{R_i} \| \{PB_{R_i}\}_{PR_{ESP_i}} \|$ $\{PB_{ESP_i}\}_{PR_{CCA}} \|$ $(n2_{R_i} + 1))\}_{ASP_i}$ $)$ $\}_{PB_{B_i}}$

Analysis

[P1-P6:] Using messages M1, M3 and rule R7, it can be deduced that ASP_i believes that communication from R_i to ASP_i is secure. Using messages M2, M8 and rule R11, it can be deduced that ASP_i believes that communication from ASP_i to R_i is secure. From these two deductions, it can further be deduced that ASP_i believes that communication between R_i and ASP_i is secure in both directions.

Using M1, M3, R7, R8,
$ASP_i \models R_i \xrightarrow{secure} ASP_i$ ($I1$)

Using M2, M8, R11,
$ASP_i \models R_i \xleftarrow{secure} ASP_i$ ($I2$)

Using I1 and I2,
$ASP_i \models R_i \xleftrightarrow{secure} ASP_i$ ($G1$: *Proved*)

Using M1, M3, R10, R11
$ASP_i \models R_i \xrightarrow{secure} ASP_i$ ($I3$)

Using M2, M8, R8,
$ASP_i \models R_i \xleftarrow{secure} ASP_i$ ($I4$)

Using I3 and I4,
$ASP_i \models R_i \xleftrightarrow{secure} ASP_i$ ($G2$: *Proved*)

Using M4, R7,
$ESP_i \models ASP_i \xrightarrow{secure} ESP_i$ ($I5$)

Using M7, R11,
$ESP_i \models ASP_i \xleftarrow{secure} ESP_i$ ($I6$)

Using I5 and I6,
$ESP_i \models ASP_i \xleftrightarrow{secure} ESP_i$ ($G3$: *Proved*)

Using M4, R11,
$ASP_i \models ASP_i \xrightarrow{secure} ESP_i$ ($I7$)

Using M7, R8,
$ASP_i \models ASP_i \xleftarrow{secure} ESP_i$ ($I8$)

Using I5 and I6,
$ASP_i \models ASP_i \xleftrightarrow{secure} ESP_i$ ($G4$: *Proved*)

Using M5, R7,
$UIDAI \models ESP_i \xrightarrow{secure} UIDAI$ ($I7$)

Using M6, R11,
$UIDAI \models ESP_i \xleftarrow{secure} UIDAI$ ($I8$)

Using I7 and I8,
$UIDAI \models ESP_i \xleftrightarrow{secure} UIDAI$
($G5$: *Proved*)

Using M5, R11,
$ESP_i \models ESP_i \xrightarrow{secure} UIDAI$ ($I9$)

Using M6, R8,
$ESP_i \models ESP_i \xleftarrow{secure} UIDAI$ ($I0$)

Using I9 and I10,
$ESP_i \models ESP_i \xleftrightarrow{secure} UIDAI$ ($G6$: *Proved*)

[P7:] Using message M9 and rule R13, it can be deduced that R_i believes that $\{M_i\}_{eSign}$ is a valid electronic signature.

Using M9 and R13,
$R_i \models \{M_i\}_{eSign} = \{M_i\}_{eSign\_R_i\_ESP_i\_CCA}$
($G7$: *Proved*)

8 Conclusion

This work is an extension of the work [4] on enhancing amortized performance of *eSign* by using digital access tokens including claims from *ESP* and *UIDAI*. In this work, the digital access token introduced in [4] is extended to include privacy and fine-grained access control statements for access to resident's eKYC data. This enhanced token can be used by third entities to access the protected eKYC data with better privacy and fine-grained access control rules enforced by the resident. A formal security analysis of the proposed model using *BAN logic* is also presented.

References

[1] UIDAI, "Unique Identification Authority of India", [Online]. Available: https://uidai.gov.in (2017).

[2] Wikipedia, "Aadhaar", [Online]. Available: https://en.wikipedia.org/wiki/Aadhaar (2017).

[3] Reserve Bank of India, "Master Direction - Know Your Customer (KYC) Direction, 2016", [Online]. Available: https://rbidocs.rbi.org.in/rdocs/notification/PDF s/18MDKYCD8E68EB1 3629A4A82BE8E06E606C57E57.PDF, 2018.

[4] Bakshi, Puneet, Neelakantan Subramanian, and Sukumar Nandi. "Using digital tokens to improve amortized performance of eSign." 2018 IEEE 16th Intl Conf on Dependable, Autonomic and Secure Computing, 16th Intl Conf on Pervasive Intelligence and Computing, 4th Intl Conf on Big Data Intelligence and Computing and Cyber Science and Technology Congress (DASC/PiCom/DataCom/CyberSciTech). IEEE, 2018.

[5] Paquin, Christian, and Greg Zaverucha. "U-prove cryptographic specification v1. 1." Technical Report, Microsoft Corporation (2011).

[6] Chaum, David. "Blind signatures for untraceable payments." Advances in cryptology. Springer, Boston, MA, 1983.

[7] Hardt, Dick. The OAuth 2.0 authorization framework. No. RFC 6749. 2012.

[8] Nakamoto, Satoshi. "Bitcoin: A peer-to-peer electronic cash system." (2008).

[9] UIDAI, "Aadhaar e-KYC API Specification - Version 2.1", [Online]. Available: http://www.cca.gov.in/cca/sites/default/files/files/eSign-APIv2.1.pdf, 2017

[10] CCA, "eSign Service", [Online]. Available: http://cca.gov.in/cca/?q=eSign.html (2017).

[11] Burrows, Michael, Martin Abadi, and Roger Michael Needham. "A logic of authentication." Proceedings of the Royal Society of London. A. Mathematical and Physical Sciences 426.1871 (1989): 233-271.

[12] Rivest, Ronald L., Adi Shamir, and Leonard Adleman. "A method for obtaining digital signatures and public-key cryptosystems." Communications of the ACM 21.2 (1978): 120-126.

[13] Merkle, Ralph C. "A digital signature based on a conventional encryption function." Conference on the theory and application of cryptographic techniques. Springer, Berlin, Heidelberg, 1987.

[14] Paquin, Christian, and Greg Zaverucha. "U-prove cryptographic specification v1. 1." Technical Report, Microsoft Corporation (2011).

[15] Chaum, David. "Blind signatures for untraceable payments." Advances in cryptology. Springer, Boston, MA, 1983.

[16] Hardt, Dick. The OAuth 2.0 authorization framework. No. RFC 6749. 2012.

[17] Nakamoto, Satoshi. "Bitcoin: A peer-to-peer electronic cash system." (2008).

[18] PKIA2017, "Development of Smart Authentication and Identification in Asia", [Online]. Available: http://pkiindia.in/pkia/#preceding, 2017.

[19] CCA, "Pki framework in India", [Online]. Available: http://www.cca.gov.in/cca/?q=pki˙frame work.html (2015).

[20] CCA, "Public key certificate classes", [Online]. Available: http://www.cca.gov.in/cca/?q=node/45 (2017).

[21] CCA, "Empanelled eSign Service Providers", [Online]. Available: http://www.cca.gov.in/cca/?q=service-providers.html (2017).

[22] Jones, Michael, John Bradley, and Nat Sakimura. Json web token (jwt). No. RFC 7519. 2015.

[23] Jones, Mike, et al. Cbor web token (cwt). No. RFC 8392. 2018.

ASTES

Advances in Science, Technology and Engineering Systems Journal
Vol. 4, No. 4, 359-365 (2019)
www.astesj.com
Special Issue on Advancement in Engineering and Computer Science

ASTES Journal
ISSN: 2415-6698

Hidden Surface Removal for Interaction between Hand and Virtual Objects in Augmented Reality

Takahiro Ishizu[1], Makoto Sakamoto[*,1], Masamichi Hori[1], Takahiro Shinoda[1], Takaaki Toyota[1], Amane Takei[1], Takao Ito[2]

[1]*Department of Computer Science and System Engineering, University of Miyazaki, 889-2192, Japan*

[2]*Institute of Engineering, Hiroshima University, 739-8511, Japan*

ARTICLEINFO

Article history:
Received: 31 May, 2019
Accepted: 27 July, 2019
Online: 19 August, 2019

Keywords:
Augmented Reality (AR)
Virtual object
Occlusion problem
Canny edge detection
Hidden surface removal
Hand area

ABSTRACT

Recently, augmented reality (AR) technology has been applied to the interaction technology between human and virtual objects. In AR interaction technology, it is necessary for users to be able to manipulate virtual objects intuitively. Thus, we focus on manipulating virtual objects directly with the user's bare hands in this study. On the other hand, in AR technology, since the 3-dimensional (3D) model is superimposed on the image of the real space afterwards, it is always displayed on the front side than the user's hand (occlusion problem). Thus, it becomes an unnatural scene in some cases. In this study, this system detects hand area of the user by extracting depth information, color information and using canny edge detection in the user's hand. Thus, this system performs hidden surface removal along the area of the user's hand by considering the object-context relations between the user's hand and the virtual object. In the evaluation experiment, it is confirmed that the hidden surface removal in this study make it possible to distinguish between finger boundaries and to clarify and process finger contours. This work is an extension of the paper entitled "Hidden Surface Processing for Interaction of Hand and Virtual Objects Using Leap Motion Controller" published in 2018 International Conference on Information and Communication Technology Robotics (ICT-ROBOT).

1 Introduction

Augmented reality (AR) is used in many fields including education, medicine and entertainment, and its applications became widespread [1, 2, 3]. Also, the interaction with the virtual objects is required in those papers. Therefore, we think that more precise virtual object manipulations in AR will be performed in the future.

On the other hand, since hands are our main means of interaction with objects in real life, AR interfaces should also be able to be for free hand interaction with virtual objects.

Furthermore, it is important to be able to adapt to more detailed tasks by hand in order to handle a wide range of fields such as medical care and education.

In the conventional study [4], by putting a marker, a special glove, etc. on a user, the user's position information was acquired and interaction with a virtual object was realized. However, these methods may give the user a sense of discomfort such as weight due to wearing. Therefore, bare hand interaction is required.

However, since the 3-dimensional (3D) model displayed by the AR is superimposed on the image of the real space afterwards, the 3D model is always displayed on the front side and user's hand is hidden by virtual objects. Thus, the scene may become an unnatural scene, and the user cannot see the object-context relations of the virtual object and his/her hand, and feels that it is difficult to manipulate the virtual objects.

In the existing study [5], the system used transparent 3D models and the 3D models followed each fingers of the user based on the depth information of the user's hand. In this way, they performed hidden surface removal and tackled the occlusion problem. However, since the 3D models which follow the user's fingers are larger than the finger, a wider range than the actual finger was displayed on the front (see Figure 1). In addition, no description has been given of a case where there is a multiple virtual objects in the existing study.

In other related study [6], using the Kinect sensor in order to obtain depth information of the user, hidden surface removal was realized when an arm was inserted between multiple virtual objects. Also, it was the same even when

*Corresponding Author: Makoto Sakamoto, 1-1, Gakuen-Kibanadai-Nishi, Miyazaki City, Miyazaki, 889-2192, Japan, sakamoto@cs.miyazaki-u.ac.jp

it came to deformable virtual object. However, the Kinect sensor is a sensor that roughly recognizes human motion and depth information, and the study didn't focus on the interaction between hands and virtual objects.

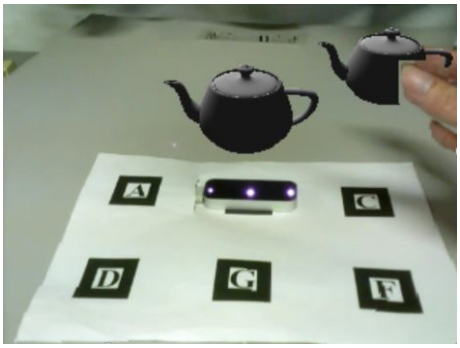

Figure 1: Hidden surface removal in existing study

In this study, we use Leap Motion Controller to acquire depth information of the user's hand. Additionally, this system acquires RGB (Red, Green and Blue) information from the web camera. Based on these pieces of information, the contour of the hand is extracted to realize hidden surface removal along the contour of the hand.

In this study, we aim to cope with more detailed virtual object manipulations by conducting hidden surface removal along the outline of the user's hand. Moreover, we conduct a manipulation of grasping a virtual object of primitive model by hand and confirm whether it works properly.

2 Proposal

In order to conduct hidden surface removal along the contour of the user's hand, this system detects hand area of the user by extracting depth information, color information and edge detection in the user's hand.

First, in order to extract hand area, we use the RGB image based on color information. Next, based on the depth information of the hand, a blue point group is created on the thumb, and a green point group is created on the other fingers. These point groups are displayed at their positions only when the hand is in front of the virtual object. In addition, the hidden surface removal along the fingers is realized by using the hand area extracted first and the result of edge detection. Also, in order to cope with multiple virtual objects and distinguish the object-context relations of the blue point group and the green point group, we use the Z-buffer method.

In this way, when the user's hand is near from camera than the virtual object, the user's hand is correctly displayed on the front side of the virtual object, and the user can grasp the anteroposterior relationship between the user's hand and the virtual object.

2.1 System Component

This system consists of a Web camera, the Leap Motion Controller, PC and AR marker. In this study, since this system needs accurate position information of user's fingers, we use the Leap Motion Controller that can acquire various data relating to user's hand with high accuracy.

The purpose of use of each of the devices shown above is as follows:

- Web camera: Acquisition of real image and recognition of marker.
- The Leap Motion Controller: Obtaining 3D coordinates of the user's fingers.
- Monitor: Video output.
- AR marker: Acquisition of position and tracking of virtual objects.

The Leap Motion Controller and the webcam both use camera features, which causes the camera features to interfere with each other. Therefore, this system addresses this problem by using network programming. This system acquires data of 3D coordinates of the user's fingers with the Leap Motion Controller on the server side. In addition, this system sends the data to the client side. On the other hand, this system acquires images with the Web camera, and conducts image processing and video output using the data which received from the server side on the client side.

This system controls the position and orientation of the virtual objects is by recognizing the AR marker. Therefore, the AR marker needs to be recognized by the web camera. However, when the user manipulates virtual objects, the AR marker may be covered by his/her own hand. Therefore, this system adopts a method of treating Marker A to Marker F as one marker (see Figure 2). Thus, even when a part of the marker is covered, the virtual objects can be displayed properly.

We place the Leap Motion Controller on the position of Marker B. This system displays the virtual objects on the position of Marker C and Marker G (see Figure 2).

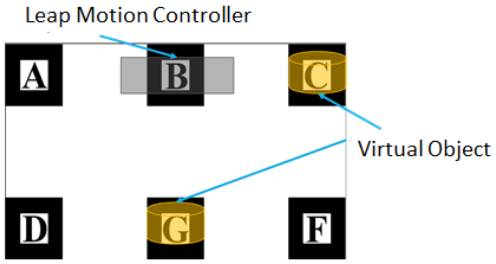

Figure 2: AR marker

2.2 Development Environment

We use ARToolKit for AR marker recognition and camera control. And, we develop this system using OpenGL for displaying virtual objects and OpenCV for various image processing. Here, the resolution of the camera is 320×240 pixels.

2.3 Flow of Image Processing

The processing flow comprises of several steps as shown in Figure 3. In Figure 3, the block of light red background indicates that it is generated image.

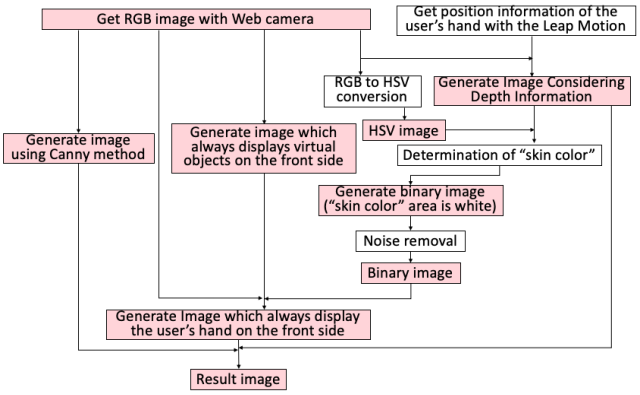

Figure 3: Flow of image processing in this system

2.4 Processing of Camera Image

This system gets RGB image with the web camera (see Figure 4). In this study, in order to use the HSV (Hue, Saturation and Value) color space often used in the processing of color images, this system converts RGB images to the HSV color space.

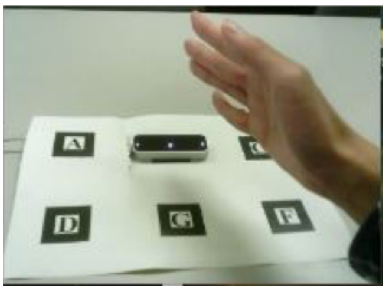

Figure 4: RGB Image

2.5 Generation of Binary Image

2.5.1 Determination of "skin color"

This system needs to extract the area of skin color for detection of the user's hand area. At first, this system puts red point on the finger which are the closest to the camera (see Figure 5). A certain range is given to the HSV value obtained from the pixel of that point, and it is defined as "skin color".

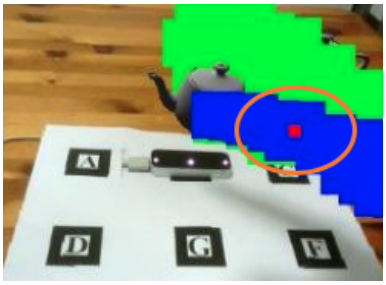

Figure 5: Red point

Next, this system detects the user's hand area as binary images.

The procedure is shown below.

1. Get the 3D coordinates of the proximal phalanx of the finger which are the closest to the camera with the Leap Motion Controller.
2. Generate images that red point is plotted around the acquired position.
3. Obtain the 2D coordinate value of pixel units in the red point.
4. In Figure 4, this system gets average values of HSV in the pixel values corresponding to the coordinates acquired in step 3.
5. Apply an appropriate range to each value of Hue, Saturation, Value and decide it as "skin color".

2.5.2 Noise removal

The binary image generated by this system contains salt and pepper noise at first. Therefore, this system conducts erosion and dilation twice in 8-neighbor in order to remove noise.

However, that alone cannot remove the noise sufficiently (see Figure 6). This is because, in this method, this system has to conduct erosion and dilation multiple times in order to remove loud noise. However, it needs complicated calculation.

Therefore, regarding to the loud noise, this system removes the noise in the area of the hand by conducting the following processing (see Figure 7).

1. Determine white area including red point (which is put on the finger which is closest to the camera) as hand area.
2. Fill the inside of the hand area with black and the outside of the hand area with white.
3. Invert white and black.

In this way, all noise in the hand area is removed (see Figure 8).

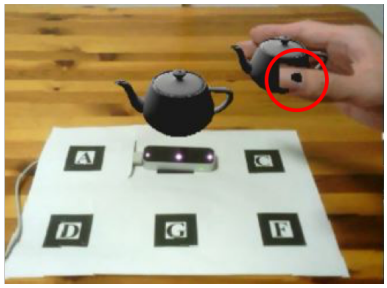

Figure 6: Result image including noise

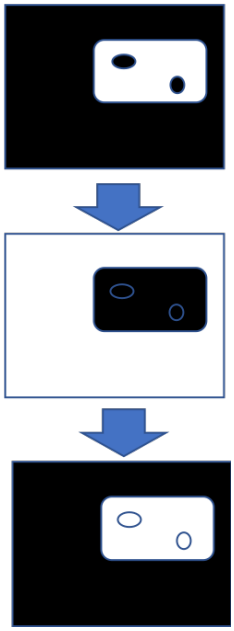

Figure 7: Noise removing process

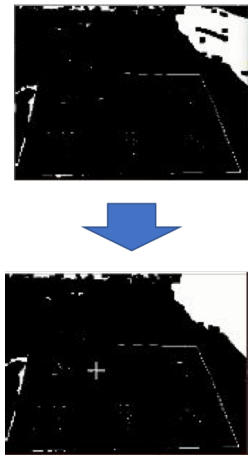

Figure 8: Noise removing

2.6 *Generate Image Considering Depth Information*

This system acquires 3D coordinates of the distal bone, middle phalanx, basal bone and metacarpal bone of the user's hand (see Figure 9) with Leap Motion Controller.

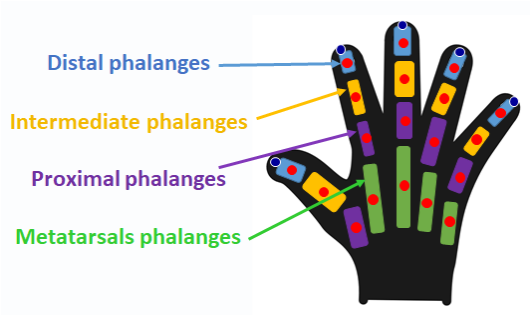

Figure 9: Hand joint

Based on the acquired position information of the fingers, this system generates images plotting blue point group (following the position of the thumb) and green point group (following the position of a finger other than the thumb).

Blue point group displays at the positions of each joint of the thumb when the user's thumb is front of the back object (see Figure 10).

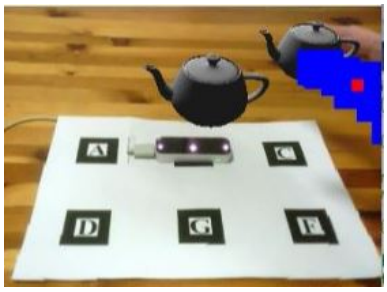

Figure 10: Blue point group following the thumb

In addition, green point group displays at the positions of each joint of the fingers except thumb when the user's fingers except thumb are front of the back object (see Figure 11).

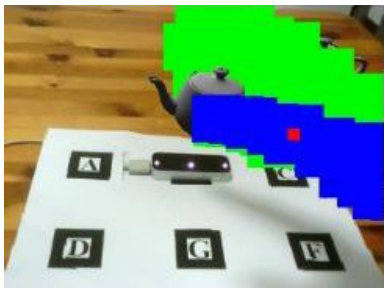

Figure 11: Blue point group and green point group following the whole hand

Furthermore, this system makes it possible to handle multiple virtual objects of different depths. The object-context relations between the back virtual object and the hand of the user is determined depending on whether or not blue point group and green point group are displayed. On the other hand, the object-context relations between the virtual object on the near side and the user's hand is determined by using the Z-buffer method. Using the Z-buffer method, when a finger is positioned behind the virtual object, blue point group and green point group following the position of the finger are hidden by the virtual object. In this way, this system can determine the object-context relations between the user's hand and the virtual objects even if there are multiple virtual objects.

2.7 *Generate Images which Always Display The Hand in Front of Virtual Objects*

This system synthesizes the original RGB image (see Figure 12-a) only in the white area in Figure 13 to the image in Figure 12-b. Thus, this system generates images that the user's hand is always displayed on the front of the virtual object (see Figure 12-c).

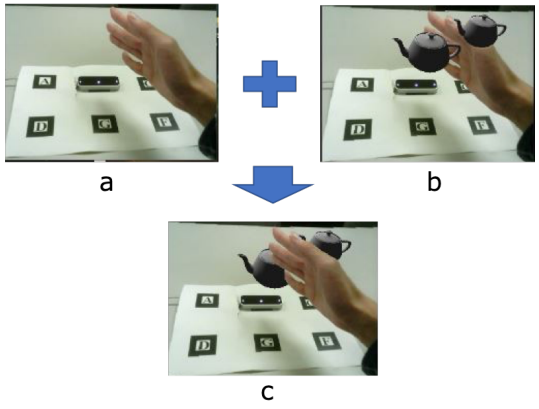

Figure 12: Generation of images which hand is displayed front

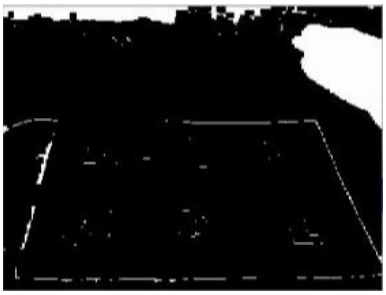

Figure 13: Binary image

2.8 Generate Result Images

The area in Figure 12-b corresponding the area of the blue point group, the green point group and the red point group (in the case where the position of the proximal phalanges of thumb is in front of the virtual object) of Figure 14-a are replaced with the image shown in Figure 14-b (Figure 12-c). Thus, based on the depth information, this system generates images that the hand is displayed in front of the virtual object (see Figure 14-c).

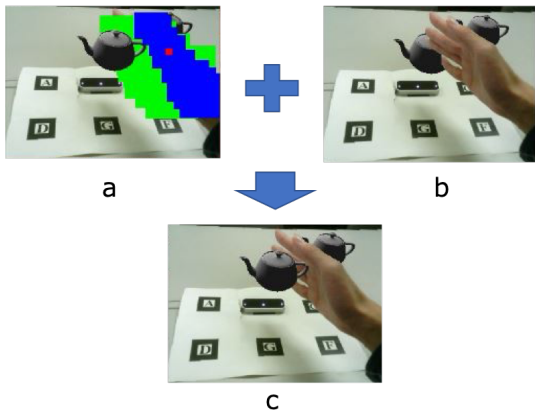

Figure 14: Generation of result images

2.9 Distinction between Fingers Using Canny Edge Detection

The white area in Figure 13 indicates the hand area. However, no distinction between fingers is made from this image. Therefore, if hidden surface removal is conducted based on this image, even if only the thumb should be subjected to hidden surface removal like Figure 15, other fingers are involved and processing is conducted.

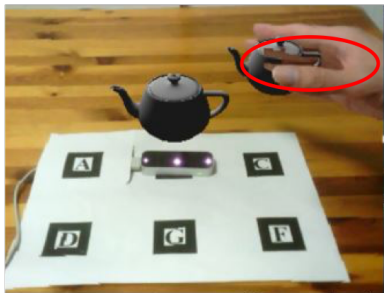

Figure 15: Involved other fingers

Therefore, we need edge detection of the user's thumb in order to solve this problem.

Edge detection is the name for a set of mathematical methods which aim at identifying points in a digital image at which the image brightness changes sharply or more formally, has discontinuities. The point at which image brightness changes sharply are typically organized into a set of curved line segments termed as edges.

We need to detect finger edge in order to distinguish between thumb and other fingers. Furthermore, at the time of the edge detection, the edge must be one clear line, since the area of the thumb extracted by edge detection is filled in the area surrounded by the edges in the later processing.

In this study, we use Canny edge detection algorithm [7] to find an edge of the user's thumb. Because it provides better results and efficiency than other available algorithm when we want to detect clear edges [8].

Canny edge detector uses two thresholds and if the intensity of that pixel is below that lower threshold than it is assigned "0" value that can be none edge and if the intensity of any pixel is above that the higher threshold than it is assigned "1" value and can be edge.

In this study, we distinguish the thumb from the other fingers. In order to detect the thumb, the thumb is surrounded by an ellipse, and the inner area surrounded by it and the boundary displayed by edge detection is extracted. The area is the thumb area (see Figure 16).

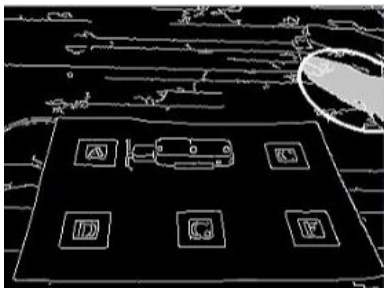

Figure 16: Extraction of the thumb area

The following process is conducted to detect the thumb.

1. Get two coordinates of upper left end and lower right end of blue point group (see Figure 17-a).

2. Make an ellipse based on a line connecting the two points (which are the coordinates acquired in step 1).

3. Overlap the ellipse surrounding the thumb on the image generated based on the Canny edge detection (see Figure 17-b).

4. Fill the area surrounded by the ellipse and the edge in Figure 17-b which corresponding to the position including the red point group in Figure 17-a with gray.

5. Regards this gray area as the thumb area.

In this way, this system generates result image (see Figure 17-c).

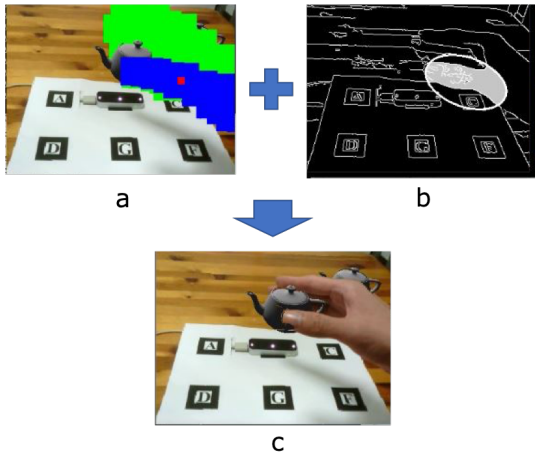

Figure 17: Distinction between the thumb and the other fingers

3 Experimental Results

We executed this system to confirmed whether hidden surface removal along the fingers is possible or not.

First, we checked whether this system can cope with multiple virtual objects. In this system, the object-context relations between the back virtual object and the hand of the user is determined depending on whether or not blue point group and green point group are displayed. In order to confirm whether this is properly processed, we placed the virtual object at position C in Figure 2 and performed manipulation that a user grabs the virtual object. On the other hand, the object-context relations between the virtual object on the near side and the user's hand is determined by using the Z-buffer method. In order to confirm whether this is properly processed, we placed the virtual object at position G in Figure 2 and performed manipulation that a user grabs the virtual object.

Furthermore, we performed grasping manipulations on virtual objects of 3D primitive figures from various directions in order to confirm whether this system is applicable to virtual objects of various shapes.

3.1 In the case of an object behind

Since only the thumb comes to front side than Marker C, the blue point group follows only the thumb (see Figure 10) and draw the thumb properly on the front of the virtual object (see Figure 18).

Figure 18: Result at the position of C in the AR marker

3.2 In the case of an object in front

This system conducted the hidden surface removal considering multiple virtual objects by the Z-buffer method. The blue point group follows only the thumb and the green point group follows the other fingers (see Figure 11). Besides, only the point group of the thumb was drawn on the front of the virtual object by the Z-buffer method. As a result, it was possible to draw only the thumb on the front (see Figure 19).

The blue point group and green point group in Figure 11 are based on the depth information of the user's fingers. Also, the anteroposterior relationship between the blue point group and the green point group is correctly displayed by the Z-buffer method. In this way, when the thumb is positioned behind the other fingers, the green point group is displayed on the front side of the blue point group.

Figure 19: Result at the position of G in the AR marker

3.3 Various trials

We tested three movement patterns for each 3D objects. Here, we use cube (see Figure 20), cone (see Figure 21) and torus (see Figure 22) as 3D primitive objects.

In this section, we display the virtual object at position B.

Each movement is as follows.

1. Grip the virtual object from the side.

2. Grip the virtual object from the top.

3. Grip the virtual object while the user's thumb is behind the other fingers.

The results are shown below. Here, "Grip the virtual object from the side", "Grip the virtual object from the side", and "Grip the virtual object from the side" in order from the left in Figure 20 - Figure 22.

Figure 20: Cube

Figure 21: Cone

Figure 22: Torus

4 Consideration

We confirmed that this system can perform correctly hidden surface removal even when a user manipulates multiple virtual objects by Z-buffer method from the experiment result. In addition, we also confirmed that this system is effective for virtual objects of various shapes.

The distinction between the virtual object and the user's hand was not clear when using the Z-buffer method when considering the depth between the virtual object and the user's hand. Therefore, if there is only one virtual object or if the depth coordinates of the virtual objects are all at the same position, it is better to have blue point group follow the thumb of the user only than to have blue point group and green point group follow the palm of the user's hand.

Regarding gripping the virtual object from the side (see Figure 20), it was confirmed that the hidden surface removal was accurately distinguished without involving a nearby finger.

Regarding gripping the virtual object from the top (see Figure 21), sometimes the hidden surface removal of the base of the thumb did not work well, and a virtual object was displayed superimposed on the thumb. This is because the area of the thumb extracted by the Canny method is smaller than the area of the real thumb.

Regarding gripping the virtual object while the user's thumb is behind the other fingers (see Figure 22), it was confirmed that the hidden surface removal was properly treated even when the fingers other than the thumb were on the near side. This is an effect of the present system because the determination of the skin color is conducted on the foremost finger. Also, at this time, since the blue point group is moved to the back from the green point group, processing such as the Canny method for the thumb is ignored.

5 Conclusion

The future of AR as interaction technology in users and virtual objects looks bright. In recent years, AR has been applied to a wide range of fields such as education, medicine, entertainment and a guide for various tasks. Among them, the user directly manipulates virtual objects with their bare hands. In the future, we expect further development of interaction manipulation, and more detailed virtual object manipulation will be required.

Thus, we proposed and implemented hidden surface removal along the fingers, aiming at being able to apply to more detailed works about interaction manipulation in AR. In this study, we paid attention to detection the contour of the hand to realize hidden surface removal along the user's fingers. In this system, processing based on hand depth information, color information and edge detection is conducted to detect hand contours.

As for edge detection, the Canny method was used to reduce noise and obtain a clear contour. By these processes, appropriate hidden surface removal was realized without involving other fingers.

In the evaluation experiment, it was shown that it can cope with multiple virtual objects. In addition, we tested various grip methods for virtual objects of various shapes, and showed that they manipulate normally.

As future works, since the generation of binary images is not stable at the time of skin color detection, it needs the solution. Moreover, since the contour of the thumb is interrupted at the time of the Canny edge detection, it needs to set more appropriate threshold in Canny edge detection.

References

[1] Kangdon Lee, "Augmented Reality in Education and Training", TechTrends, vol.56, no.2, pp.13-21, 2012.

[2] Carmigniani J, Furht B, Anisetti M, Ceravolo P, Damiani E, Ivkovic M, "Augmented reality technologies, systems and applications", Multimedia Tools and Applications 51:341-77, 2011.

[3] Abdelkader Bellarbi, Christophe Domingues, Samir Otmane, Samir Benbelkacem and Alain Dinis, "Underwater augmented reality game using the DOLPHYN", Proceedings of the 18th ACM symposium on Virtual reality software and technology, ACM, 2012.

[4] Buchmann V, Violich S, Billinghurst M, Cockburn A. "FingARtips – Gesture Based Direct Manipulation in Augmented Reality", 2nd international conference on computer graphics and interactive techniques, ACM Press, pp.212–221

[5] R. Katahira, M. Soga. "Development and Evaluation of a System for AR enabling Realistic Display of Gripping Motions using Leap Motion Controller", Procedia Computer Science 60:1595–1603, 2015.

[6] J. Adrián Leal-Meléndrez, Leopoldo Altamirano-Robles, and Jesus A. Gonzalez. "Occlusion Handling in Video-based Augmented Reality Using the Kinect Sensor for Indoor Registration", Progress in Pattern Recognition, Image Analysis, Computer Vision, and Applications: 18th Iberoamerican Congress, CIARP 2013, Proceedings, Part II, 2013.

[7] J. Canny. "A Computational Approach to Edge Detection", IEEE Trans. Pattern Analysis and Machine Intelligence, vol.8, no 6, pp.679-698, 1986.

[8] Abhinandan Julka and Sandeep Bhargava. "A Static Hand Gesture Recognition Based on Local Contour Sequence", International Journal of Advanced Research in Computer Science and Software Engineering, Volume 3, Issue 7, 2013.

ASTES

Advances in Science, Technology and Engineering Systems Journal
Vol. 4, No. 4, 366-379 (2019)
www.astesj.com
Special Issue on Advancement in Engineering and Computer Science

ASTES Journal
ISSN: 2415-6698

Evaluation of the Effects of Bidding Strategy with Customized Pricing on the Individual Prosumer in a Local Energy Market

Borislava Spasova[*,1,2], Daisuke Kawamoto[1], Yoshiyasu Takefuji[2]

[1]*Sony Computer Science Laboratories Inc.,141-0022, Japan*

[2]*Keio University, Graduate School of Media and Governance, 252-0882, Japan*

ARTICLE INFO

Article history:
Received: 31 May, 2018
Accepted: 27 July, 2019
Online: 19 August, 2019

Keywords:
Energy trading
Microgrid
Heterogeneous power sources

ABSTRACT

Peer-to-peer (P2P) energy trading is a mechanism that allows people to share locally the energy they have generated from distributed renewable resources (DER), to generate profit form the unused resources and to reduce the cost for electricity for the household and in the community itself. This calls for the design of new energy markets, accompanied with the development of comprehensive exchange strategies, which reflect both the consumer?s preferences and the heterogeneity of the renewable sources. The paper presents a study of the behavior patterns of individual prosumers using bidding strategies based on the State-of-Charge of the battery and two different pricing algorithm, one with fixed prices and one based on the battery price of each standalone system as well as the effect such patterns have on a local energy market with solar panels, fuels cells and batteries. The evaluation is achieved by the use of a prototype based on the Open Energy Systems (OES), a community in Okinawa, Japan, made of 19 interconnected houses with residential storage, photovoltaic cells and AC grid connection. In order to simulate heterogeneity, a fuel cell, modeled after Ene-Farm, is added to the original configuration. Each house has a power flow management system, which uses a priority-based algorithm to maintain demand-response efficiency, capable of scheduling the operating hours of the available fuels cells. The energy market is based on Zaraba, a continuous double auction algorithm used by the Japanese Stock Exchange, in which prosumer can bid for a desired amount and price of electricity for a 30-minutes time slot in the future The preliminary numerical evaluation is based on the results from several simulations using different versions of the bidding agent.

1 Introduction

This paper is written as an extension of the work titled "Energy exchange strategy for local energy markets with heterogeneous renewable sources", presented at the 2018 IEEE International Conference on Environment and Electrical Engineering and 2018 Industrial and Commercial Power Systems [1] in Palermo, Italy.

In the recent years a huge surge in the usage of renewables worldwide [2]. The growth of the solar photovoltaic capacity installations in particular is remarkable, nearly double those of wind power and adding more net capacity than coal, natural gas and nuclear power combined. This trend can be seen not only on global scale since the dropping prices for energy storage and Feed-In Tariffs(FIT) [3] has led to an increase in the adoption of solar energy by individual consumers. Additionally, the efforts of countries like Japan, have contributed to the improvement of the efficiency and reducing of the cost for Distributed Renewable Resources (DER), making on-site energy sources such as fuel cells more popular with consumers [4]. However, the current centralized nature of both the grid infrastructure and the electricity markets is preventing residential customers from participating and taking full advantage of cheaper renewables. The successful implementation of blockchain technology for peer-to-peer (P2P) trading in the Brooklyn Microgrid [5], has not only led to a surge in the adoption of the technology in the development of local energy markets but to new and innovative approach towards designing such markets. Still the increased heterogeneity of the microgrids as well as the needs of the individual prosumers are yet to be addressed.

The paper [1], on which the research presented here is based, studied the impact of introducing a new power source,

[*]Borislava Spasova, 3-14-13 Higashigotanda, Tokyo 141-0022, Japan, +818044094144, b.spasova@gmail.com

in this case a hydrogen fuel cells, on already existing on a local energy market with renewables and batteries. The prototype, used for the analysis was built upon and existing system, the Open Energy Systems (OES) [6], operating it real world microgrid in Okinawa, Japan. OES consists of 19 autonomous subsystems, equipped with photovoltaic cells, energy storage and loads and interconnected via DC power bus. The system, currently used by the OES microgrid, has a well-defined exchange algorithm [7], designed to enable energy exchanges between all of the connected subsystems. However, no financial rewards are attributed to the prosumers and the energy is essentially exchanged for free.

The subsequently developed prototype aimed to change that by developing a market-based trading platform which can provide financial incentives for trading and thus enabling all the prosumers to be active participants in the local energy market and to make better use of the generated renewable energy. Such approach contributes to the an increase in the self-sufficiency and the sustainability of the community itself and expands the possibility for developing decentralized energy market to reflect on the decentralized nature of the P2P exchange. Usually trading platforms require the submission of an order bid, using an internal bidding strategy, which may or may not be fully matched, or be matched only partially, with someone else?s bid using a perviously agreed matching method. The matching can be done centrally by aggregating all requests, determining a common market clearing price (MCP) in order to maximize trading volume for a given timeslot. Another approach is to use auctions, a method often used for trading goods, mainly non-fungible goods e.g. E-bay. Continuous or real-time trading, characteristic for spot markets, is used in this prototype as it provides both speed and liquidity. The bids, used here, require for the desired amount and price of the energy for exchange to be set in advance. Both parameters are determined by the individual prosumer's exchange strategy, which is based on the State of Charge (SoC) of the available battery. A version of the algorithm was already in operation in the OES system, proving to be working well for the for subsystems with solar panels and batteries. In order to further test the SoC-based exchange strategy, a hydrogen fuel cell was added to the original configuration of the subsystems in simulated environment. The fuel cell came to the attention of the authors, due to it rising popularity among Japanese households. Unlike the the fluctuating output of the solar panels, it provides stable generation level which coupled with well devised prediction of consumption patterns can contribute to the building of off-grid communities, completely self-sufficient and independent from the utility grid.

The study presented 2018 IEEE EEEIC and I&CPS showed the broader effects of the SoC-based exchange strategy have on a community with heterogeneous power sources and the strategy itself has a very simplistic pricing algorithm which didn't account for the actual price of the energy being exchanged. As a result, a new pricing method was added, based on the price of the energy, stored in the battery of each individual subsystem. This paper presents a quantitive evaluation of the effects of this change on the developed market as well as on the behavior of predetermined prosumers' groups, created based on the daily consumption average. Examining more detailed behavioral patterns allows for better understanding of each prosumer's needs which can enhanced the development of more customized bidding strategies. Moreover, it opens the possibilities to design a more diverse community, where each standalone system can use different set of power sources, to serve as testing environment in order to achieve more realistic results.

The evaluation, presented in this paper, is based on a study of the effects of SoC-based bidding strategy with simple pricing algorithm and pricing algorithm based on the current price of the energy, contained in the battery of each standalone subsystem, on the local market and on the individual prosumer. It is achiebed by comparing the results, obtained by the simulation with the OES community, with the two bidding strategies. Furthermore, the presented strategies are evaluated in the context of a single member of a prosumers' group to better understand how changes in the bidding system can affect the individual prosumer.

Section 2 of this paper introduces the basic concepts used in the development of the solution and provides a look into the current state of P2P energy trading and existing blockchain based markets. Section 3 gives a more detailed information about the observed community and the selected prosumers' groups. Section 4 provides an overview of the prototype's design and the concrete implementation which is used for the quantitative evaluation. Finally, Section 5 will focus on the analysis of the simulations' results followed by final remarks and discussion of future works.

2 Research background

This paragraph will introduce existing solutions for energy exchange between interconnected subsystems. Many studies focus on the exchange strategies between interconnected microgrids and the main grid. The research, presented by Asimakopoulou [8], suggests a Leader-Follower strategy for energy management of Multi-Microgrids, achieved with the use of bilateral contracts between microgrids and a large production unit. Wang [9] proposes a control strategy for networked microgrids and distribution systems. Other authors such as Matamoros and Gregoratti [10, 11] has focused on developing an optimization framework for a distributed energy trading algorithm between islanded microgrids. They were also among the first researchers to give a solution for direct trading between microgrids although due to the lack of clear separation between the microgrids' internal power management strategy and their exchange strategy the proposed system didn't offer many possibilities of implementing self-interest-based internal strategies.

Such opportunity was offered by Wang [12, 13, 14] who proposed a two-layered optimization method that separates internal and external strategy and helps avoiding undesired power injections and reduces peak consumption. This proposal creates new opportunities for collabotation between self-interest microgrids. Other papers [16, 17] prefer the use of Game Theory for the trading algorithm, while Nunna [18] came up with an multi-agent approach for power trading between microgrids using demand-response and distributed storage.

Dimeas' paper [19] proposed a *multiagent system* (MAS) approach, that allows independent agents,*Buyers* and *Sellers*, to submit *Bids* for *EnergyPackages* according to *GridPrices*. Other papers also discussed this kind of approaches [20, 21, 22] but mainly from a theoretical point of view without physical prototype.

Starting with Nakamoto's white paper on Bitcoin [23], Blockchain has received both academic and industry interest for being the first scalable method to successfully decentralize P2P exchanges. It can be applied not only for cryptocurrencies, but also for various other use cases as for instance in the energy sector, notably the here-addressed P2P energy trading [24]. Using Blockchain for trading was first address by Transactive Grid Project [25] which demonstrated the concept of the Brooklyn Microgrid [26], [5]. Later many projects such as Grid+ [25], NRGCoin [27], Bankymoon, Daisee, D3A and Energo Labs [28] followed but so far few pilots and prototypes are completed and the one that are focus more on developing functioning energy market from the perspective of retailers and producers and not from the customer's perspective.

As stated in previous works [1], a prototype, following the Wang's approach was developed, which focuses on developing a platform for trading between members of one microgrid. The base concept design allows in the future to expand the market by trading with neighbouring microgrids as well. For research purposes, a prototype was developed, having explicit separation between the internal strategy for energy management and the trading algorithm, defined in the external strategy built-in in its base design. Such division aims to address both the lack of incentive and the decision coupling issue which is particularly affects cases where blockchain is used without separating external and internal logic beforehand. The systems aims to create environment where different energy exchange strategies can be used to better reflect the different targets set by prosumers when using renewable energy. The internal strategy, is tasked with managing the demand-response efficiency of each subsystem and with evaluating the system needs for buying and selling energy, implemented by the priority-based internal agent and the bidding agent, respectfully. The external strategy is the software implementation of the local energy market, used in this study.

Moreover, unlike the other studies, introduced in the paragraph, this research focuses on the small prosumers and aims to create local energy market where each player can use a customized bidding strategy that is best suited to their needs. In order to achieve that, a better understanding of the behavior of different types of prosumers is needed. This paper deepens the study of the market by observing the effects a small change in the bidding strategy can have on the individual prosumer.

3 Application in real world microgrid

This section will provide more detailed information on the real world microgrid, used for the evaluation and on the prosumers' groups, designed based on the recorded consumption data in the microgrid for the year 2015.

3.1 Microgrid Architecture

The OES is a bottom-up, distributed electric power system that mainly uses renewable energy sources. It presents an alternative way of exchanging energy in-between energy subsystems in order to manage energy fluctuations within the community. Supply and demand are balanced autonomously without impacting the utility grid and thus energy autonomy is increased with minimal infrastructure costs. The concept and feasibility of OES have been demonstrated in a decentralized, peer-to-peer microgrid in Okinawa, Japan. The microgrid has been operating there since late 2014 and consists of 19 houses, each equipped with their own subsystem with photovoltaic cells, residential energy storage in a form of 4.8 kWh batteries, dc nanogrid and loads. All the subsystems are connected via dedicated, shared DC power bus as well as communication line which allows energy exchanges within the community. The subsystem use a direct current (DC) procedure for exchange, combined with pure peer-to-peer (P2P) communication infrastructure and exchange algorithm [7]. All the houses also have connection to the utility (AC) grid, which can be used as an auxiliary power supply when no other energy supply is available. Bidirectional dc-dc converters are used as an interface between subsystems: they allow for an effective control of the power flow and can be used as an abstraction of the internal subsystem design. This way, dc power can be exchanged within a community to help balancing demand-response requirements without requiring global knowledge or control.

In order to test the system capabilities in simulated environment with heterogeneous power sources, a fuel cell is added to the to the configuration of each standalone subsystem. The fuel cell, used here is largely based on Ene-Farm, a hydrogen fuel cell for home use, that has been gaining popularity in Japan. Ene-Farm is an energy system that can extract hydrogen from natural gas, usually supplied though underground pipes in most major cities in Japan, or propane gas (LPG), usually supplied to a residence via external tanks part of the building design. The hydrogen is then used in combination with ambient oxygen to generate electrical power and at the same time to capture the residual heat which in turn is used to heat up water. Ene-Farm was chosen here for both its wide spread use and its high efficiency ratio.

The extended topology of the observed microgrid, very similar to the real world one, can be seen on Figure 1.

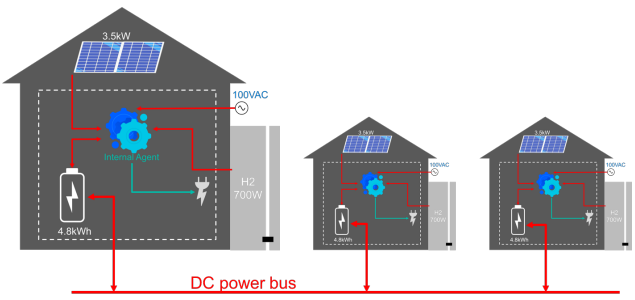

Figure 1: Sample subsystem configuration and general microgrid architecture of the chosen microgrid

3.2 Prosumers' groups in the OES community

During the process of design and development of the prototype the daily consumption of all 19 members of the OES community for the entire year of 2015 was examined in detailed. Furthermore the solar generation patterns we also mapped for the same period of time. Based on the analysis, the OES consumers were divided into three main groups, defined by their individual average daily consumption for the observed period, using the generated output from the fuel cell and the solar panels patters a baseline indicator. The groups are as follows:

1. Group 1: High consumers, with observed daily average consumption of more than 700 watts;
2. Group 2: Average consumers, with daily average consumption in the range of 350 to 700 watts;
3. Group 3: Low consumers, with daily average consumption of less than 350 watts.

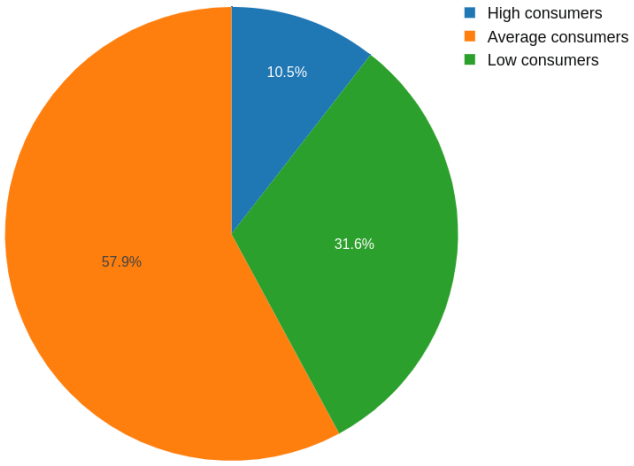

Figure 2: OES prosumers distribution, based on their consumption

Figure 2, shows that more than 50% of the consumers in the OES community are in the second category, a trend that remained unchanged for the entire year 2015. Moreover, no noticeable changes in the members of Group 2 was observed throughout the year. One notable exception was registered in April 2015 when a user moved from Group 3 to Group 1 due customers moving into previously uninhabited house.

Dividing the community into categories, based on such a crucial factor as consumption, helps further the understanding of the community and the prosumers themselves because it provides an effective way to analyze the behavior of different types of consumer since members of one category tend to exhibit similar behavior within an acceptable margin of error. That will allow for the development of different strategies aimed to satisfy the needs of variety of customers.

4 Prototype design and implementation

The prototype, presented here, is developed based on the Open Energy Systems (OES), a real world microgrid operating in Okinawa, Japan. This section will provide an overview of the basic premises and concrete algorithms used in the development of the proposed solution.

4.1 Design assumptions and limitations

During the development of the prototype, presented here, several simplification were incorporated in the design. The following paragraph focuses only on the ones that have major implication for the research, subject of this paper. For more detailed list, please refer to the cited paper [1].

1. No losses, including conversion and transmission losses, are taken into account during the powerflow management;
2. Projected transmission losses, however, are taken into consideration in the pricing algorithm;
3. Initial investment in the renewable source is disregarded when calculating the energy price;
4. Each subsystem is equipped battery, used for absorbing imbalances in the network;
5. The price of the battery is calculated for $\forall t \in \mathcal{T}$, where $\mathcal{T}$ is time series.
6. The price of the battery is calculated as a sum of the amount charged in the battery from each power source multiplied by the predefined energy price of the source and then divided by the current amount of energy in the battery. The formula can be seen bellow.

$$bp = \frac{\sum_{i \in \mathcal{N}} \mathrm{PS}_{i,t}^{\mathrm{amount}} * \mathrm{PS}_{i}^{\mathrm{price}}}{currentcapacity} \quad \forall t \in \mathcal{T} \qquad (1)$$

7. Users are charged when storing energy in the battery, not when discharging the stored energy for the consumption
8. It is presumed that the data, provided by the power meters and the controllers, can be trusted;
9. The DC line capacity is set as 2.5 kw for all subsystems;
10. Japanese yen is selected as main currency for all the financial transactions, due to the microgrid location;
11. The battery is charged solely from the renewable sources;
12. There is no Feed-in to the utility grid

4.2 Prototype design

The following paragraphs will give a short description of the internal and externals strategies, focusing on the bidding component of the former. For more information about the chosen algorithms, please refer to the cited paper [1].

4.2.1 *Internal strategy*

The internal strategy, used in this paper, is tasked with managing the demand-response efficiency of each subsystem and with evaluating the system needs for buying and selling energy. It is comprised of two main components: priority-based agent and bidding agent, each implementing different side of the internal agent. They are designed to work independently using only the same data in order to increase encapsulation. More information about the basis of the algorithms cam be found in the paragraphs bellow.

Priority-based internal agent: The internal agent is responsible for scheduling the power flows to and from the modules, configured for each individual subsystem. It is designed for standalone house equipped with residential storage, energy sources and loads. The fundamental premise built into the design of the system is inherent flexibility when it comes to changing the number and types of the installed power sources. Essentially the system allows for various sources such as photovoltaic and fuel cells, wind turbines, standard electricity grid, etc. to be added to the configuration at any moment, given that each source is a assigned a priority level, a parameter used to control when it is going to be used, and a price for electricity for kWh. The priority is normally determined by factors such as energy price and cost for curtailment. In the current system the priority is set as follows: fuel cell output; solar generation; battery; utility grid. In this case power sources with what is considered an expensive curtailment, like fuel cells, are given higher priority in order to fully utilize their generation even though the cost for electricity for other sources such as solar tends to be much lower. Once the priority is defined, the algorithms uses it to satisfy the demand-response requirements by accessing the available energy from each source until the demand is satisfied. If after using all the power from the renewables, the demand is still not satisfied, the system gets the remaining necessary power from the AC grid. If there is still available renewable energy after the demand-response requirements are satisfied, it is charged to the battery if there is enough capacity, the remaining energy is curtailed. As it can be seen, in this system, the battery plays a dual role as both a power source and a load. The role of the agent is to maintain internal power balance at any moment:

$$P^{batt}_{i,t} = \sum_{n=1}^{\infty} P^{ps}_{n,i,t} + P^{ac}_{i,t} + P^{trade}_{i,t} - P^{load}_{i,t} \quad \forall t \in \mathcal{T}, i \in \mathcal{Z} \qquad (2)$$

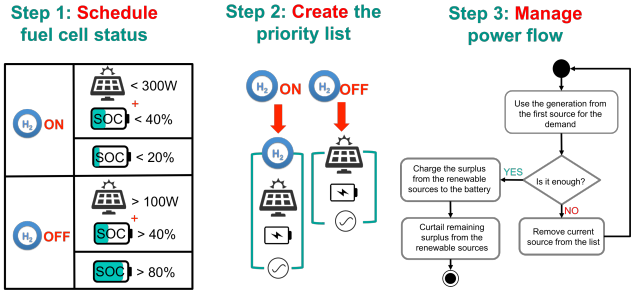

Figure 3: Scheduling conditions and simplified workflow of the internal agent.

Following the research presented in previous works [1] a scheduling component was added to the functionality of the internal agent. This software module is tasked with scheduling the operating hours of power sources with constant output like a fuel cell. The module analyzes the future energy requirements and gives command to shut down or turn on the fuel cell. Fuel cells of the Ene-Farm type require 30 minutes to stop and start operation therefore the default conditions are set based on the solar generation output and the SoC of the battery to take into account the future state of the system.

Figure 3 shows the basic workflow of the priority-based internal agent with the defined configuration. As shown the fuel cell is scheduled to shut down when the SoC of the battery is higher that 80%, which is more than enough to satisfy any upcoming changes in the consumption and to reduce to risk of curtailment from this power source. Even if the SoC is lower, if there is an observed spike in the solar generation, the fuel cell also turn off to enable the solar generation to be fully absorbed by the battery, thus utilizing better the generation and lowering the bidding price. In the opposite scenario, the fuel cell is scheduled to resume operations, when the SoC falls under 20% in order to prevent the activation of the connection to the utility grid, which has much higher price than the fuel cell generation. For the same reasons, the fuel cell turns on, when there is a decline in solar generation whether due to reduced solar radiation caused by weather conditions or during nightfall. This conditions help reduce the electricity cost for the household by decreasing the reliance on the utility grid.

Bidding agent: The bidding agent is a module that is installed together with the internal agent and is tasked with generating a sell or buy bid for the next timeslot and dispatching it for matching. Each bid consists of desired amount of electricity for a certain price for kWh. The amount is determined based on a detailed analysis of the status of each subsystem which includes the number and type of configured power sources, e.g. batteries, PV, fuel cell, etc., and current consumption and generation patterns. This is then used by a pricing function to determine the future need for electricity and is reflected in the bids that follow.

The bidding strategy, subject to evaluation of this paper, uses the State-of-charge (SoC) of the installed battery to predict the amount of electricity that will be needed for the next 30-minute timeslot but with two different pricing algorithms. The ***base*** amount, seen in Figure 4a,b, refers to the minimum amount of electricity available for exchange, calculated as a function of the DC line capacity and the trading timeslot duration to avoid line congestion.

In the case of the previously used bidding strategy, the prices are fixed based on the prices for the electricity, paid by the customer, as seen on Figure 4a. It is assumed that the lower the SoC level, the more inclined is the prosumer to buy electricity. Since all systems are connected to the AC-grid, the highest price for the electricity in the market was designed to always be less than the price of the grid. Similarly, there is a higher incentive to sell the generated renewable energy when the battery is getting full. The price in this case is set as a minimum price at which electricity can

be sold while still generating profit. This pricing, although well designed for the original OES configuration, is not as effective in the presence of a stable power source such as fuel cell, because of the difference in the price for energy, generated from the solar panels and from Ene-Farm.

Battery SoC (%)	Sell Bid		Buy Bid	
	price (yen/kWh)	amount(watt-hour)	price (yen/kWh)	amount(watt-hour)
<=20			25	(base) x4
20 - 40	30	base	20	(base) x3
40 - 60	20	(base) x2	10	(base) x2
60 - 80	15	(base) x3	5	base
>= 80	10	(base) x4		

a)

Battery SoC (%)	Sell Bid		Buy Bid	
	price (yen/kWh)	amount(watt-hour)	price (yen/kWh)	amount(watt-hour)
<=20			25	(base) x4
20 - 40	bp + 40%	base	20	(base) x3
40 - 60	bp + 35%	(base) x2	10	(base) x2
60 - 80	bp + 30%	(base) x3	5	base
>= 80	bp + 25%	(base) x4		

b)

Figure 4: Bidding prices and amounts for State of Charge (SoC)-based bidding strategy with simple pricing algorithm(**a**) and pricing algorithm based on battery price (**b**).

The new pricing algorithm, shown on Figure 4b, takes into account the price of the electricity, currently stored in each individual subsystem, noted as ***bp*** in the table. It currently affects only the sell bid with the price similarly decreasing with the increased incentive to sell. The percentage is based on a projected transmission loss of nearly 15% which in the case of the studied community is paid by the Seller.

4.2.2 *External Strategy:*

The external strategy represents the software implementation of the local energy market, used in this study. At the core of the market is the matching algorithm, a simplified version of the Zaraba method, which is a continuous double auction algorithm used by the Japanese Stock Exchange. The trading is done in real time, with multiple sell and buy bids received for the duration of each 30-minute timeslot. They are match on on first-come first-served basis with the most beneficial counter bid being chosen each time as a counterpart. At the end of the timeslot the agreed deals are sent to the internal agent to execute the physical exchange and all the unmatched bids are invalidated.

Since the DC losses are neglected, we assume that the sum of all energy trading must be equal to zero:

$$\sum_{i \in \mathcal{Z}} \mathrm{P}_{i,t}^{\mathrm{trade}} = 0 \quad \forall t \in \mathcal{T} \tag{3}$$

4.2.3 *Virtual Wallet:*

In order to keep an accurate record of all financial transaction, including detailed information about the used energy from the renewable sources and from the grid, cost of the energy charged to batter and cost/revenue from the energy trading, each subsystem has a virtual wallet. The data, kept in the wallet, is accessible via simple user interface which provides basic analysis and monthly reports.

5 Simulation Setup and Results

For numeric evaluation purposes, this study uses the results of multiple simulations, obtained using prototype, comparatively similar to the OES Simulator [7], written in Python 3.6. The prototype provides a software approximation of the internal power flow of each system and of the community. All the implemented algorithms are consistent with the descriptions given in the previous section and in other works [1]. The following subsection will display the general configuration of studied subsystems, the data, provide information of the scope of the data used as an input for the simulator and will discuss the results of the performed tests.

5.1 *Input Data and Configuration*

In order to further the research, shown in previous works [1], the simulation uses the same dataset for the consumption and solar radiation, recorded for 19 houses, part of OES in Okinawa, Japan, in the duration of year 2015 with 10 minutes granularity. The bidding is done for a 30-minutes timeslot in the future, which amounts in total to 48 trading timeslots per day.

Each subsystem in the community has the following configuration of modules:

1. ***Solar panels*** with average area of 20 m^2, with estimated panel yield of 19% and 75% performance ratio. Since the initial investment is not taken into consideration in the estimate, the price for solar energy is set to 0 yen for kWh.

2. ***Fuel cell*** with factory output of 700 watts and predefined price for electricity of14 yen for kWh, based solely on the price of the fuel used, since the initial investment is also disregarded during calculations.

3. ***Utility grid,*** used as an auxiliary power source with no power limitations. The price for electricity is considered 30 yen for kWh, which is an approximation of the real price of the electricity in Japan. This is necessary due to the varying prices for different regions as well as different usage categories.

4. ***Battery*** with capacity of 4.8kWh, charged at 50% with energy price of 10 yen for kWh, used only in the first iteration of the algorithm. For the remaining of the simulation, it is calculated in the beginning of each iteration, how much energy was charge it in the previous cycle and from which renewable source.

5. ***Wallet*** with 100,000 Japanese yen available.

5.2 Results

In order to evaluate the added functionality presented in this paper, two simulations are performed, each using different bidding strategies as listed below:

1. SoC-based bidding strategy, described in the cited paper [1].

2. SoC-based bidding strategy with pricing algorithm based on the battery price of each standalone system, presented in this paper.

All simulations are performed using a only selected potion from the available dataset with length of 1 calendar month, in this case August 2015. To simplify the visualization of the results, only one week, from August 2nd to August 9th, is taken for the analysis of the whole market. That particular week is chosen because of the variety of weather conditions that occurred during that period. The selected timeframe consisting of several sunny days and two partially cloudy day is chosen. In order to better study the behavior pattern of the individual participants, only data from 1 day, August 5th 2015, with daily generation close to the month's average is examined.

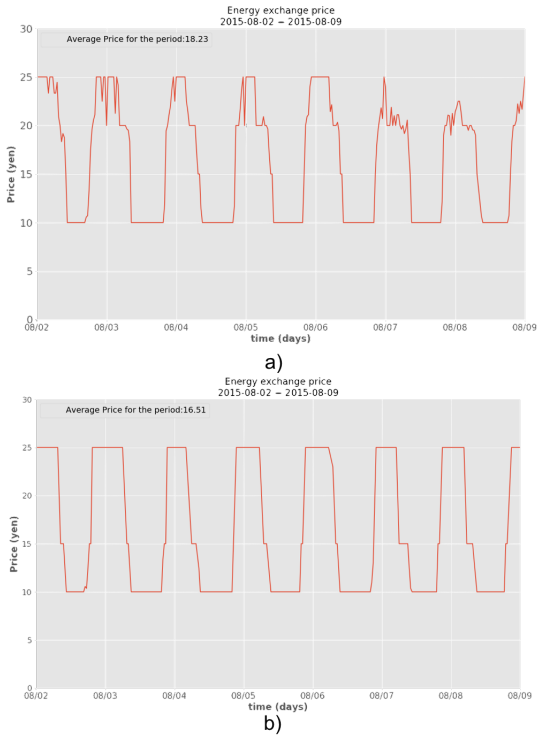

Figure 5: Market price within a community, comprised of standalone houses with solar panels and fuel cells, SoC-based bidding strategy with fixed pricing(**a**) and SoC-based bidding strategy with pricing algorithm based on the battery price (**b**)

5.2.1 Community overview

This section will provide a detailed analysis of the effects of the new bidding strategy on the entire community before focusing on selected members of the predefined prosumers' groups. The second portion of the analysis can be seen in the next section. Detailed analysis of the results of the simulations showed 55% decrease in the number of deals with the new bidding strategy. This is due to less available matches in the preferable price range of the prosumers which makes them less willing to either sell or buy energy if it is not beneficial for them. This has had an effect on the market price as well as seen on Figure 5.

Fig. 5b shows that the pricing algorithm, has led to predictable patterns for market price, with stable peaks that indicate higher prices in comparison with the case of fixed pricing, Fig. 5a. Most influenced by the new pricing algorithm are the high consumers which show 10% decrease in energy spending. Average consumers and low consumers with daily average consumption more than 100 watts spent 7% less for electricity for the same period of time while systems with daily average consumption of less than 100 watts registers a surplus increase of 10%.

Despite the lower number of deals, there has been observed in 10% increase in the utilization of solar generation due to a drop in the consumption of electricity from the AC grid. The numbers are based on the numeric evaluation of the results though a slight reduction the curtailment peaks can be seen on Figure 6. The increase is due to more customized bidding strategy and shows that better focus on customers' energy requirements and implementing them into individual bidding strategy can be used as a foundation for building self-sustainable community. There is no visible curve for the Fuel cell curtailment since it remains 0 for the entire period due to the efficiency of the scheduling component of the internal agent.

5.2.2 Analysis of individual prosumers from the predefined groups

The analysis of a selected members of the groups, described above, provides a deeper understanding of the results shown above. Consumers of all groups showed slight in the usage of the energy stored in their battery which is a contributing factor for the slight decrease in the solar curtailment.

For a Group 1 consumer the increase has led to lowering the usage of the AC grid, shown on Fig. 7, while for consumer from Groups 2 and 3, the difference is compensated by using less electricity directly from the Fuel cell, shown on Fig. 8 and Fig. 9 respectively. The solar usage remained unchanged. Since solar energy is considerable cheaper than the one from AC or Fuel cell it can be considered as a factor in the general lowering of the energy cost.

Deeper analysis of the sources of energy for the battery further shows that the new pricing algorithm has contributed to the higher utilization of the solar energy. Although the results shows very little change for customers of Group 1, Fig. 10, in the case of customers from both Group 2 and 3, Fig. 11 and Fig. 12 respectively, shows increased charging from the solar generation while the no energy has been bought from the market. That scenario shows better management of the energy and of the trading which is more consistent with the system requirement of this two types of consumers since both should have enough energy so be entirely self-sufficient and participate in the market only to sell their excess energy. The graph of the energy exchanged through the DC bus gives even better idea of what is happening. As we can see on Fig. 14 for customers of Group 2 and Fig. 15 for customers of Group 3, there is a distinctive

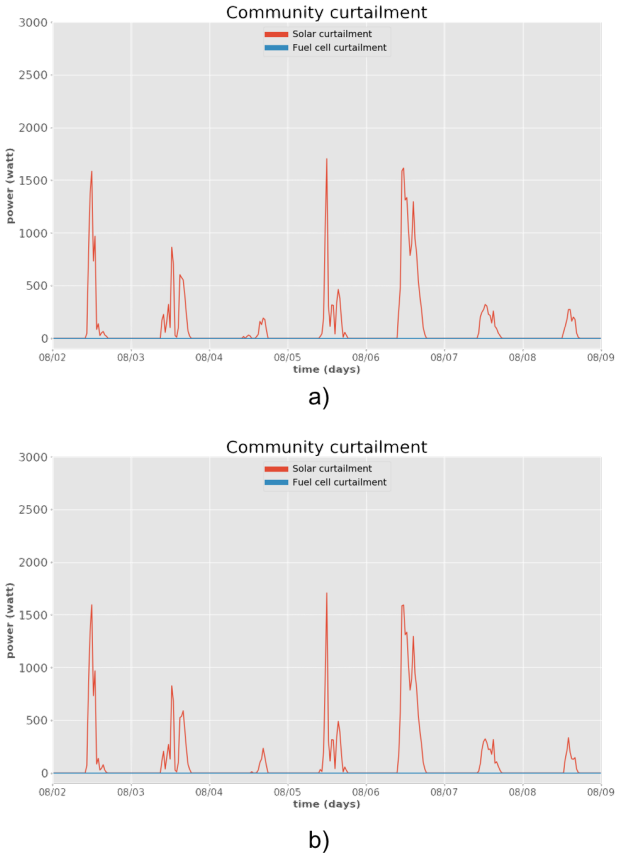

Figure 6: Average curtailment in community, comprised of standalone houses with solar panels and fuel cells, SoC-based bidding strategy with fixed pricing(**a**) and SoC-based bidding strategy with pricing algorithm based on the battery price (**b**)

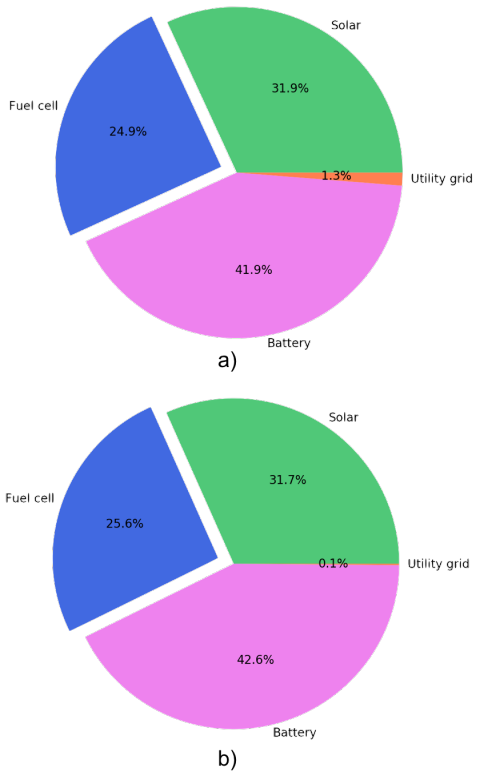

Figure 7: Energy usage by power sources for ***Group 1*** consumer that use SoC-based bidding strategy with fixed pricing(**a**) and SoC-based bidding strategy with pricing algorithm based on the battery price (**b**)

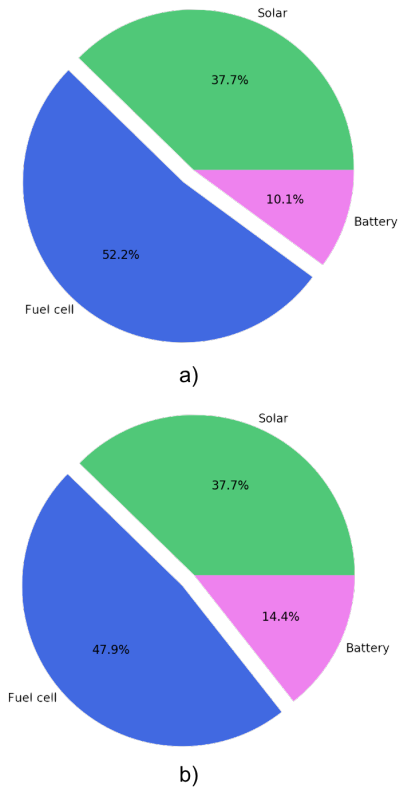

Figure 8: Energy usage by power sources for ***Group 2*** consumer that use SoC-based bidding strategy with fixed pricing(**a**) and SoC-based bidding strategy with pricing algorithm based on the battery price (**b**)

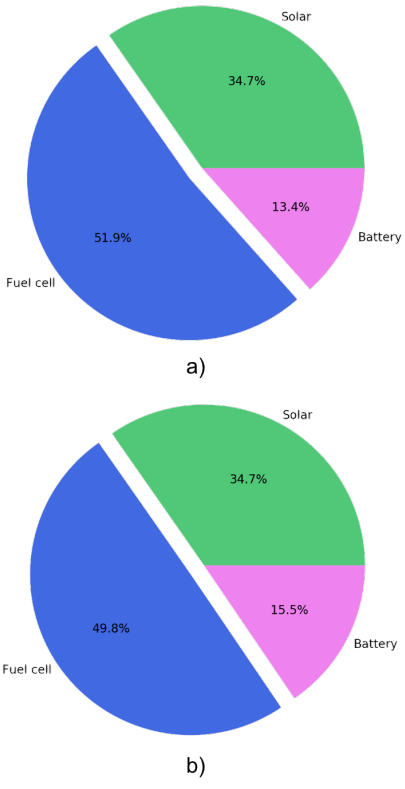

Figure 9: Energy usage by power sources for ***Group 3*** consumer that use SoC-based bidding strategy with fixed pricing(**a**) and SoC-based bidding strategy with pricing algorithm based on the battery price (**b**)

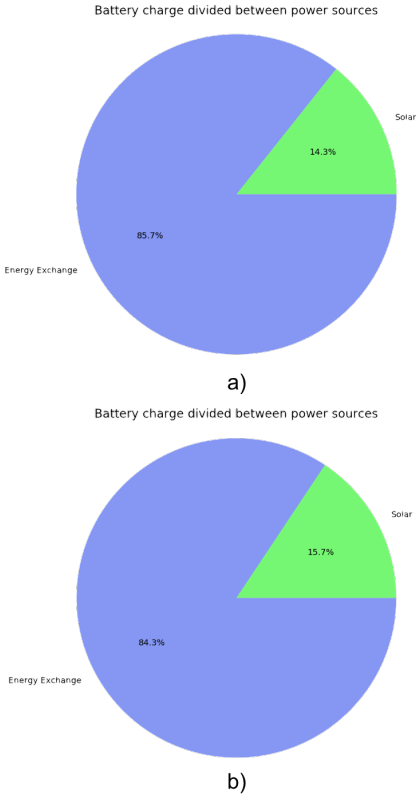

Figure 10: Energy charged to the battery by power sources for ***Group 1*** consumer that use SoC-based bidding strategy with fixed pricing(**a**) and SoC-based bidding strategy with pricing algorithm based on the battery price (**b**)

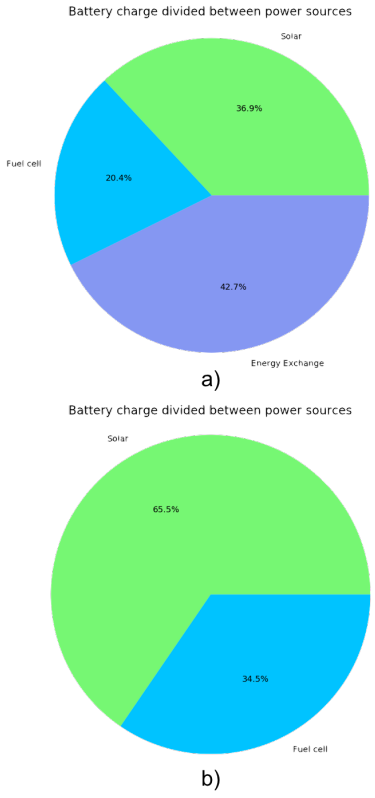

Figure 11: Energy charged to the battery by power sources for ***Group 2*** consumer that use SoC-based bidding strategy with fixed pricing(**a**) and SoC-based bidding strategy with pricing algorithm based on the battery price (**b**)

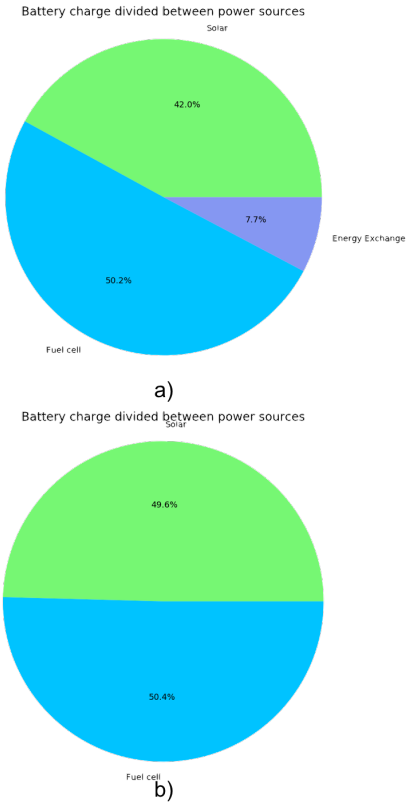

Figure 12: Energy charged to the battery by power sources for ***Group 3*** consumer that use SoC-based bidding strategy with fixed pricing(**a**) and SoC-based bidding strategy with pricing algorithm based on the battery price (**b**)

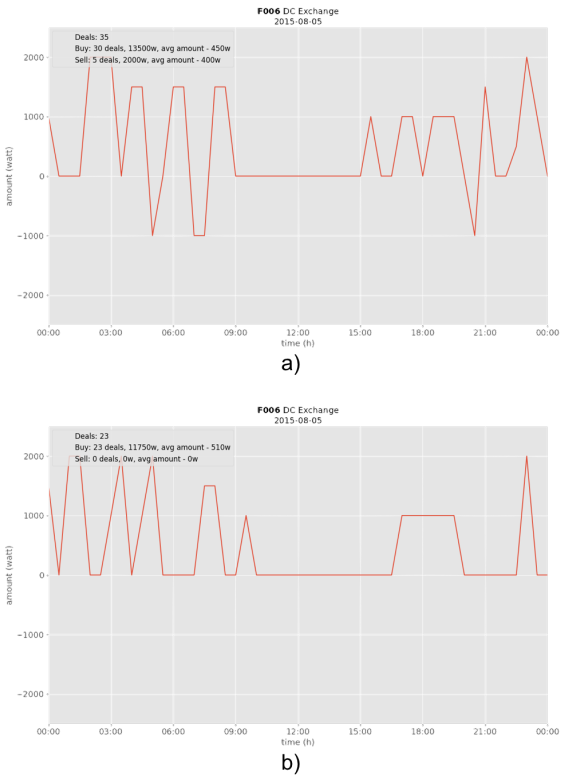

Figure 13: Deals distribution for ***Group 1*** consumer using SoC-based bidding strategy with fixed pricing(**a**) and SoC-based bidding strategy with pricing algorithm based on the battery price (**b**)

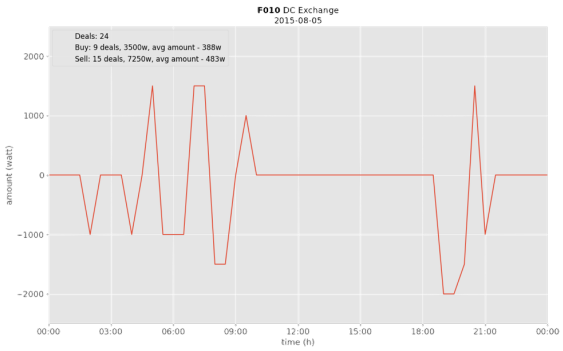

a)

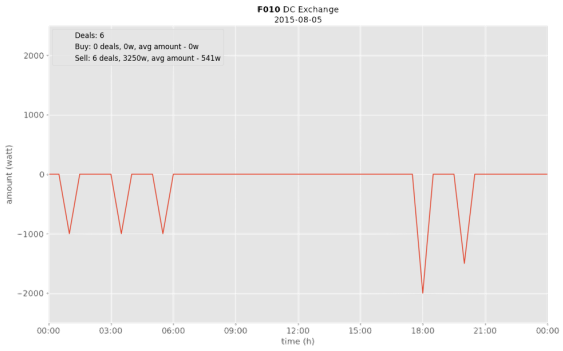

b)

Figure 14: Deals distribution for ***Group 2*** consumer using SoC-based bidding strategy with fixed pricing(**a**) and SoC-based bidding strategy with pricing algorithm based on the battery price (**b**)

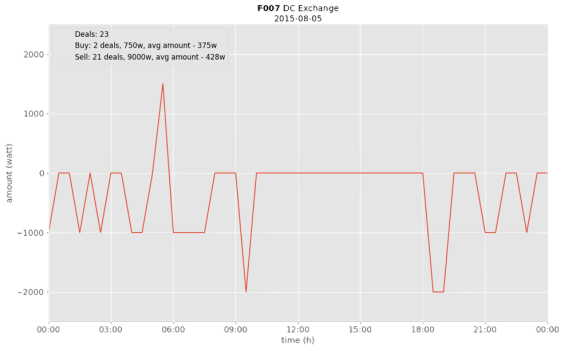

a)

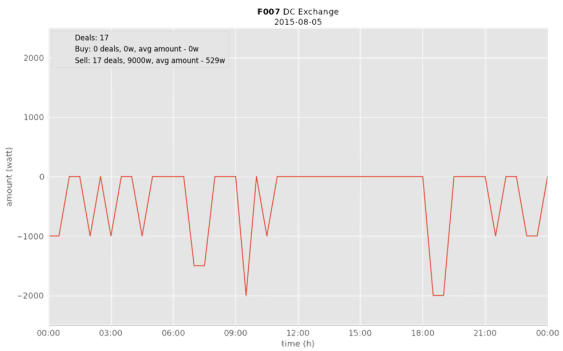

b)

Figure 15: Deals distribution for ***Group 3*** consumer using SoC-based bidding strategy with fixed pricing(**a**) and SoC-based bidding strategy with pricing algorithm based on the battery price (**b**)

lack of spikes that indicate buy deals, which shows that in the case of the simple SoC strategy we have moments early morning and late evening where prosumers with enough energy are forced to buy from other prosumers electricity on higher prices because they have previously sold their for lower price. Reversed pattern can be observed for customers of Group 1, Fig. 13, because their have electricity demand that on average exceeds their generation by 50% so they should not be selling energy in those periods of time as well.

Although the effects on the community are only marginal, the new pricing method had shown significant shift in the patters of all of the observed individual customers. Further customization can provide better results and can make the prosumers more competitive in the market but in the context of their individual needs.

6 Conclusion

This study shows the impact of enhanced pricing algorithm, which accounts for the price of the electricity contained in the battery of standalone systems, part of a local energy market with renewables and batteries. The evaluation is done by analyzing the results, generated by a prototype with the use of real data from a full-scale microgrid in Okinawa, Japan. The microgrid represents a community of 19 houses each equipped with residential storage, photovoltaic cells, fuel cell and AC grid connection. All the houses are connected via dedicated, shared DC power bus which allows them to exchange energy with their neighbors. A continuous double-auction algorithm, used by the Japanese Stock exchange, is used for the implementation of the trading platform. Each house can bid on the local market, using a State-of-Charge based bidding strategy. Similar to previous works [1], some simplifications were taken during the development of the simulation platform, including neglecting all losses and ignoring the price of the energy, stored in the battery when calculating the desired exchange price. The effects of the incorporation of the losses in the algorithm are yet to be studied but it is expected that such change will cause an increase in the market price. The topic is currently being investigated and will be a subject to future works.

This paper focuses on studying how including the battery price in the pricing algorithm affects different types of consumers and the community as a whole. The results show that increasing the customization leads to higher utilization of the renewables and further reduces the cost of electricity for consumers with daily average consumption higher than 100 wats. Since this was achieved with customizing a single parameter, it is the opinion of the authors that further analysis of the behavior of the individual system is need in order to create bidding strategy, tailored to each prosumer. It is the opinion of the authors that a well design exchange strategy should allow for the customers to set individual goals such as maximizing profit, maintaining independence from the utility grid, reducing energy waste, etc. It should implement a prediction algorithm which accounts for consumption and generations patterns and include weather predictions for better evaluation of the energy needs. Furthermore, with the wide spread of renewables and distributed renewable resources (DER), more diverse communities are likely to appear so further tests in the community with standalone systems with various configuration power sources can serve as a testing environment to achieve more realistic results.

Conflict of Interest The authors declare no conflict of interest.

Acknowledgment This paper would not have been possible without the continuous support of the Okinawa Institute of Science and Technology and H.Kitano. The authors would like to thank A.Werth and M.Hoshino, for their contribution in forming these ideas.

References

[1] B. Spasova, D. Kawamoto, Y. Takefuji, "Energy exchange strategy for local energy markets with heterogenous renewable sources", 2018 IEEE International Conference on Environment and Electrical Engineering and 2018 Industrial and Commercial Power Systems, 12-15 June 2018, Palermo, Italy. https://doi.org/10.1109/eeeic.2018.8494458

[2] Renewable energy policy network for the 21st century REN21, "Renewables 2018 Global Status Report (GSR)", http://www.ren21.net/gsr-2018/

[3] A. Brautigam, T. Rothacher, H. Staubitz, and R. Trost, "The Energy Storage Market in Germany", 2017.

[4] P. De Martini, K.M. Chandy and N.A. Fromer, "Grid 2020: Towards a Policy of Renewable and Distributed Energy Resources", Technical Report, California Institute of Technology, Resnick Institute: Pasadena, CA, USA, 2012.

[5] E. Mengelkamp, J. Garttner, K. Rock, S. Kessler, L. Orsini, and C. Weinhardt, "Designing microgrid energy markets. A case study: The Brooklyn Microgrid", Applied Energy, vol. 210, pp. 870?880, 2017. https://doi.org/10.1016/j.apenergy.2017.06.054

[6] A. Werth, N. Kitamura, and K. Tanaka, "Conceptual Study for Open Energy Systems: Distributed Energy Network Using Interconnected DC Nanogrids", IEEE Transactions on Smart Grid, vol. 6, pp. 1621–1630, jul 2015. https://doi.org/10.1109/tsg.2015.2408603

[7] A. Werth, A. Andre, D. Kawamoto, T. Morita, S. Tajima, M. Tokoro, D. Yanagidaira, and K. Tanaka, "Peer-to-peer Control System for DC Microgrids", Smart Grid, IEEE Transactions on, pp. 1–8, 2016. https://doi.org/10.1109/tsg.2016.2638462

[8] G. E. Asimakopoulou, A. L. Dimeas, and N. D. Hatziargyriou, "Leader- follower strategies for energy management of multi-microgrids", IEEE Transactions on Smart Grid, vol. 4, no. 4, pp. 1909–1916, 2013. https://doi.org/10.1109/tsg.2013.2256941

[9] Z.Wang, B.Chen, J.Wang, M.M.Begovic,and C.Chen, "Coordinated energy management of networked microgrids in distribution systems", IEEE Transactions on Smart Grid, vol. 6, no. 1, pp. 45–53, 2015. https://doi.org/10.1109/tsg.2014.2329846

[10] J. Matamoros, D. Gregoratti, and M. Dohler, "Microgrids energy trading in islanding mode", 2012 IEEE 3rd International Conference on Smart Grid Communications, SmartGridComm 2012, pp. 49–54, 2012. https://doi.org/10.1109/smartgridcomm.2012.6485958

[11] D. Gregoratti and J. Matamoros, "Distributed Energy Trading: The Multiple-Microgrid Case", IEEE Transactions on Industrial Electronics, vol. 62, no. 4, pp. 2551–2559, 2015. https://doi.org/10.1109/tie.2014.2352592

[12] H. Wang, "Economic Mechanisms for Integrating Smart Grid Technologies into Power System", PhD thesis, The Chinese University of Hong Kong, 2016.

[13] H. Wang and J. Huang, "Bargaining-based energy trading market for interconnected microgrids", IEEE International Conference on Communications, vol. 2015–Septe, pp. 776–781, 2015. https://doi.org/10.1109/icc.2015.7248416

[14] H. Wang and J. Huang, "Cooperative Planning of Renewable Generations for Interconnected Microgrids", IEEE Transactions on Smart Grid, vol. 7, no. 5, pp. 2486–2496, 2016. https://doi.org/10.1109/tsg.2016.2552642

[15] A. Werth, N. Kitamura, I. Matsumoto, and K. Tanaka, "Evaluation of centralized and distributed microgrid topologies and comparison to Open Energy Systems (OES)", 15th International Conference on Environment and Electrical Engineering (EEEIC), pp. 492–497, IEEE, June 2015. https://doi.org/10.1109/eeeic.2015.7165211

[16] L. Zhang, Z. Li, C. Wu, "Randomized Auction Design for Electricity Markets between Grids and Microgrids", SIGMETRICS '14 The 2014 ACM International Conference on Measurement and Modeling of Computer Systems, pp. 99–110. https://doi.org/10.1145/2591971.2591999

[17] W. Saad, Z. Han, and H. V. Poor, "Coalitional game theory for cooperative micro-grid distribution networks", IEEE International Conference on Communications, pp. 6–10, 2011. https://doi.org/10.1109/iccw.2011.5963577

[18] H. S. V. S. Kumar Nunna and S. Doolla, "Energy management in microgrids using demand response and distributed storage - A multiagent approach", IEEE Transactions on Power Delivery, vol. 28, no. 2, pp. 939–947, 2013. https://doi.org/10.1109/tpwrd.2013.2239665

[19] A. Dimeas and N. Hatziargyriou, "A multiagent system for microgrids", in IEEE Power Engineering Society General Meeting, 2004., vol. 2, pp. 55–58, IEEE, 2004. https://doi.org/10.1109/pes.2004.1372752

[20] A. Amato, B. D. Martino, M. Scialdone, and S. Venticinque, "A Negotiation Solution for Smart Grid Using a Fully Decentralized, P2P Approach", 2015 Ninth International Conference on Complex, Intelligent, and Software Intensive Systems, pp. 527–534, 2015. https://doi.org/10.1109/cisis.2015.78

[21] J. Lagorse, D. Paire, and A. Miraoui, "A multi-agent system for energy management of distributed power sources", Renewable Energy, vol. 35, pp. 174–182, jan 2010. https://doi.org/10.1016/j.renene.2009.02.029

[22] H. Algarvio and F. Lopes ,"Multi-agent Retail Energy Markets : Bilateral Contracting and Coalitions of End-use Customers", 12th International Conference on the European Energy Market (EEM), p. 5, 2015. https://doi.org/10.1109/eem.2015.7216750

[23] S. Nakamoto, "Bitcoin: A Peer-to-Peer Electronic Cash System", Consulted, pp. 1–9, 2008. https://bitcoin.org/bitcoin.pdf

[24] M. Swan, "Blockchain: Blueprint for a New Economy", O'Reilly, 2015.

[25] Consensys, "GRID+ Welcome to the Future of Energy", 2017.

[26] J. Lilic, "Building the Decentralized Utility on the Ethereum Blockchain", in EcoSummit Berlin, 2016.

[27] M. Mihaylov, S. Jurado, N. Avellana, K. Van Moffaert, I. M. De Abril, and A. Nowe, "NRGcoin: Virtual currency for trading of renewable energy in smart grids", International Conference on the European Energy Market, EEM, 2014. https://doi.org/10.1109/eem.2014.6861213

[28] E. Labs, "White Paper: Decentralized Autonomous Energy System", 2017.

ASTES

Advances in Science, Technology and Engineering Systems Journal Vol. 4, No. 4, 380-387 (2019)

www.astesj.com

Special Issue on Advancement in Engineering and Computer Science

ASTESJ

ISSN: 2415-6698

An Analysis of Social Media Usage in Winery Businesses

Constantina Costopoulou[1,*], Maria Ntaliani[1], Filotheos Ntalianis[2]

[1]*Informatics Laboratory, Department of Agricultural Economics & Rural Development, Agricultural University of Athens, 75 Iera Odos, 118 55 Athens, Greece*

[2]*Department of Business Administration, University of Piraeus, Karaoli & Dimitriou 80, 185 34 Piraeus, Greece*

A R T I C L E I N F O

Article history:
Received: 31 May, 2019
Accepted: 23 July, 2019
Online: 16 August, 2019

Keywords:
Social Media
Social Media Analytics Tools
Wine Industry
Greece
Germany
Facebook

A B S T R A C T

Although social media is used by an ever-increasing number of businesses, its benefits have not yet been fully exploited. Social media analytics tools can prove helpful in this regard, since they comprise a unique information source for business intelligence. As the social media environment rapidly evolves, various social media analytics tools are emerging. This research examines the usefulness of social media analytics tools for assessing corporate websites and Facebook pages. Two social media analytics tools, Website Grader and LikeAlyzer, are selected to evaluate the wine industry in Greece and Germany. A comparative study of the two countries is subsequently presented. The paper suggests that researchers and practitioners can easily use these analytics tools to acquire valuable quantitative data for a fast, effective and efficient assessment of corporate websites and Facebook pages and thus improve their social media usage. The results show that the two countries present similarities, but there is great potential for improvement in their use of social media.

1. Introduction

Digital marketing is transforming the very nature of business through the implementation of digital technologies which serve the marketing goals of businesses. Digital marketing is classified into various categories, including search engine marketing (e.g. Bing, Google), influencer marketing, social media (SM) marketing, online display advertising, mobile marketing, affiliate marketing (e.g. Amazon), email marketing, and content marketing.

SM marketing provides an innovative way of communicating with the public, attracting new and maintaining old customers, improving customer relationships, creating brand awareness, increasing market share and return of investment, gaining business revenue from sales, and engaging more customers in charities, corporate social responsibility activities and other issues [1]. Nowadays, more firms are gradually adopting SM, for example, YouTube, Twitter, Pinterest, Google+, Facebook, Instagram, and Flicker, setting aside their initial doubts regarding their effectiveness [2].

As the digital environment evolves, SM hold a substantial position in the next generation business intelligence platform. Effective SM use can have a decisive impact on a digital marketing campaign [3]. Thus, more and more SM analytics tools are emerging. Understanding SM usage in the context of digital marketing through analytics tools is critical for both academic and business communities. These tools have become a unique information source for assessing a business's presence in the SM environment as they collect, monitor, analyze, summarize and visualize a vast amount of SM data [4]. However, businesses from various sectors, including the food and beverage industry, have not yet exploited the full potential of these tools.

Wine may be considered a social product, as it is included in the top eight product categories involved in discussions over the internet. Thus, the internet provides an ideal medium for wine promotion and sale. Surveys have shown that in comparison to many other consumer products, wine appears more often as a search engine keyword [5]. In the past wine consumers sought information from specialized magazines, books, and newsletters. Lately more and more consumers are consulting SM connoisseurs, sommeliers and the wine-loving audience in order to help them decide on a satisfactory wine purchase. On the other hand, businesses have a lot to gain from the feedback provided by customers through SM. Professionals in the wine industry are

*Corresponding Author: Constantina Costopoulou, tina@aua.gr, +302105294183

trying to understand consumer behavior and preferences through the opinions and criticism diffused through various SM [6].

Today competition in the wine market is at its highest level to date. Around the world the vineyard surface area covers 7.4 million hectares and the production of wine has reached 292.3 million hectoliters. The exact number of wine producers cannot be safely estimated since, in addition to professional winemakers, there are hobbyists, family micro-businesses and single producers. In 2018 Italy, France and Spain were the dominant global wine exporters. Specifically, in terms of volume Spain is the largest exporter and the three countries together represent half of the world market. In terms of value, France – maintaining a successful strategy for high quality products – is the leader; France and Italy together hold a share of the global market of approximately 30% [7].

However, this intense competition requires new strategies which go beyond the production of high quality wine, leading wineries to strive for differentiation [8]. Towards this end, SM have succeeded the geographic decoupling of wine customers and wineries affecting data collection and sharing, communication, and the overall wine purchasing experience.

Despite the significant impact of SM on wine customers and winery businesses [9, 10] digital marketing for wine is still complex [11]. Wineries are increasingly adopting SM [12] but at a slow pace, as most lack the knowledge to incorporate and exploit SM effectively in their marketing strategy [13-16]. A study of Italian wineries has shown that it is principally large wineries with a number of employees with SM knowledge and skills that are highly motivated for adopting SM [17].

The current study aims to shed light on the usefulness of SM analytics tools for helping businesses to evaluate SM usage, plan their SM efforts and revise them regularly. It focuses on the wine industry in Greece and Germany. Two freely available online tools are used to extract useful data for both countries. The German market holds the largest share of wine imports in Europe, becoming a target for wine exporting countries, such as Greece. In addition, Greek wine exporters are trying to become more active in the German market [18].

The article is structured as follows. We begin with a discussion of SM analytics tools. We then outline the methods and tools used for assessing German and Greek wineries' websites and Facebook pages. The SM analytics tools, Website Grader and LikeAlyzer, are selected as these offer an accurate/comprehensive and quick assessment. Next, we present the evaluation for the two countries – 105 Greek and 100 German wineries. Finally, we provide the survey results and draw some conclusions.

2. SM Marketing

SM regard communication means among people, allowing content to be created and shared in the digital networking environment [19]. SM can be described as an online platform for participation, discussion, and sharing; its use encourages the exchange and diffusion of opinion and information among users [20]. [21] argues that the revolutionary role of content publishers provided to SM users contributes to a democratization of information. Although SM comprise sources of information, they also provide social and emotional support, as within the SM context there is emphasis on the interaction rather than on the content itself [22, 23]. [24] distinguishes five main categories of SM: collaborative projects (e.g. Wikipedia); social networking sites (e.g. Facebook); content communities (e.g. YouTube, Pinterest, and Flickr); blogs (e.g. Blogger, Tumblr, and Twitter); and virtual worlds (e.g. Second Life). SM reflect daily life discussions, occurring at work or at home, at a restaurant or supermarket, which travel far away from the place they happen and are communicated to the public through the digital world [25]. According to the definition by [26], SM can be considered an interactive dialogue. This "dialogue is often triggered by consumers/businesses and/or products/services that circulate among them to set in motion a revealing communication on promotional information, so that it allows learning from one another's use and experiences, eventually benefitting all of the involved parties" [p. 290].

While for individuals SM serve as a means of communication for users with similar interests, businesses can leverage user conversations about their products, services and brand, and engage in discussions for using the relevant information to make better business decisions [27]. [28] designates SM marketing as an interdisciplinary and interoperable concept that uses SM to achieve business aims by adding value for the parties involved. [29] defines it as the use of SM technologies (e.g. Web 2.0, Web 3.0) and software for creation, communication, delivery and sharing of offers that have value for business owners.

SM marketing focuses on producing attractive content for customers and promoting the use and sharing of this content through the various social networks they follow. In this way "word-of-mouth" marketing is practiced, establishing a strong relationship between consumers and products, with a limited cost for businesses [5]. Although the general public uses SM primarily to develop social contacts rather than for shopping, the success of SM marketing is based on a more indirect approach. More specifically, instead of offering products for sale, the company encourages members of a community to discuss and disseminate the use and benefits of these products [30]. Several businesses try to exploit consumers' opinions expressed through SM by involving them in product design choices [31] using SM analytics tools. In light of this, a significant number of data services, platforms and tools have been developed [32]. Some of the most popular examples are: Buffer, Hootsuite, Google Analytics, Talkwalker, TapInfluence, Brand24, Klear, Keyhol, Quintly, IBM Watson Personality analytics, BuzzSumo, Funnel.io, nTuitive.social, Sprinklr, Website Grader, MeetEdgar, MavSocial, ZohoSocial, Lithium, Social report, SumAll, Social Mention, Cyfe, Sendible, Eclincher, SproutSocial, AgoraPulse, Bit.ly, Everypost, Socedo, Socialoomph, and Fanpage Karma. However, there are also analytics tools for specific SM, for example weepi, Followerwonk, Postchup, Twitonomy and Tweetdeck for Twitter; Komfo, Sociograph.io, LikeAlyzer and AdEspresso for Facebook; Owlmetrics, Storyheap and SocialDrift for Instagram; and ViralWoot and Tailwind for Pinterest. Table 1 presents a literature review of the use of SM analytics in various business sectors. The review was based on the Google Scholar search engine.

3. Methods and Tools

The approach used for the evaluation of the corporate wineries' websites and their Facebook pages can be analyzed in three phases:

Table 1. Social media analytics tools review

Social Media Analytics Tools	Paper	Sector
Facebook: Sociograph.io	[33]	Traded firms
	[34]	Radiology
LikeAlyzer	[35]	Hotel
	[36]	Tourism
Pinterest: ViralWoot	[37]	Academic libraries
	[38]	Data management & analytics of big data
Twitter: Followerwonk	[39]	Most influential emergency physicians
	[40]	Hospital pharmacy
Twitonomy	[41]	Communication tool in congress
	[42]	SM marketing
All SM Hootsuite	[43]	SM marketing
Google Analytics	[44]	Usability of e-commerce sites
	[45]	Libraries
	[46]	Tourism
Talkwalker	[47]	Business and market research
	[48]	Fashion
Brand24	[49]	Start-up companies
Quintly	[50]	Tourism
BuzzSumo	[51]	Health
	[52]	SM marketing in higher education institutions
Website Grader	[53]	Website evaluation tools
	[54]	Universities' websites
MavSocial	[55]	Tourism
SumAll	[56]	Engaging library users
Social Mention	[48]	Fashion
	[57]	SM networking
Sendible	[58]	SM management tools
	[59]	SM marketing
AgoraPulse	[60]	Fitness
Fanpage Karma	[61]	Brand communication
	[62]	SM marketing
	[63]	Wine tourism

- Determination of the sample of winery businesses.
- Selection of appropriate SM analytics tools for assessing websites and Facebook pages.
- Data collection and analysis.

The survey was conducted in 2019 and the sample for Greek and German wineries was identified through the Google search engine. For the Greek market the keywords used were: "winery", "retail sale winery", "Greek winery", "wine", "wine trade", "winemaking", "wine in Greece". For the German market the keywords used were: "Wein", "Weingut", "Deutscher Wein", "Wein Online-Shop", "German wineries", and "German wines". 105 Greek and 100 German wineries were identified, which have a corporate website and/or a Facebook page.

The selection of the appropriate SM analytics tools was based on the aforementioned literature review (Table 1) and free online availability of tools. Website Grader (website.grader.com) was selected for corporate websites and the LikeAlyzer (likealyzer.com) was selected for Facebook pages [35, 54, 64-67].

Website Grader is a comparative online tool, which evaluates a website based on a standard rating (from 0 to 100) in relation to other sites. The rating indicates whether the website works well for the company and helps to improve website quality. More specifically, the features that Website Grader evaluates are:

- *Performance:* evaluates the overall appearance of a website, the size of web pages and its speed. Performance is probably one of the most important features, as it is associated with the visitor's first impression and experience of the website. This can help increase the visibility and impact of the business. The value of this feature ranges from 0 to 30. The *performance* feature includes the following characteristics: page size, page requests, page speed, browser cashing, page redirects, compression, and render blocking.
- *Mobile readiness:* refers to the capacity to view the website on any mobile device, for example smart phones, in terms of response and viewer settings. As a large portion of the purchasing community visits pages and makes extensive use of the internet and SM from their mobile device, the flexibility of a website to work efficiently on these devices is important. Its value ranges from 0 to 30. Responsiveness and viewport are the characteristics included in this feature.
- *Search Engine Optimization (SEO):* relates to the ranking of the website by search engine users. The short title of a website, short descriptions and keywords can help improve the rankings. Its value ranges from 0 to 30. The *SEO* feature includes the following characteristics: page titles, sitemap, headings, and meta description.
- *Security:* checks the existence of a security certificate, such as a Secure Sockets Layer (SSL), for ensuring security and authentication of information submission. The value of this feature ranges from 0 to 10.

The LikeAlyzer tool was selected for the evaluation of wineries' Facebook pages. It is a popular analysis tool [66], which provides monitoring and feedback on an organization's Facebook presence and impact, allowing the comparison and exploration of Facebook potential. More specifically, it assesses any Facebook page, provides suggestions for improvement and compares it with other Facebook pages. The features that the LikeAlyzer evaluates are the following:

- *Frontpage:* refers to the visitor's first impression of the page. This includes information about the business, for example, about, username, profile picture and cover photo, and call to action.
- *About:* regards more detailed business information, such as milestones, contact information, location and products.
- *Activity:* concerns the activity of the page and how often it occurs. It evaluates the number of pages liked, native

Facebook videos, the number of posts per day, and the average post length.

- *Response:* refers to the response to visitors, either through comments on posts or through personal messages. It evaluates whether visitors can post.
- *Engagement:* evaluates visitors' activity on the page, and some features that can only be accessed by the page developer. The number of people who have interacted with the page and the total page likes are measured.

It is worth noting that LikeAlyzer does not provide an overall score, but each feature is graded from 0 to 100%.

4. Results

4.1. The Greek Case

Europe is a leader in global wine exports. In Greece the importance of the winemaking sector is reflected in its potential for promoting traditional products abroad [18]. As one of Greece's main export products, wine comprises more than 50% of the total export value of the Greek beverage industry. Fragmentation of domestic production and the large number of businesses that are exclusively active in winemaking, mainly small and medium sized companies, are the main characteristics of the sector [3]. There are also large wineries with extensive distribution networks throughout Greece, which are responsible for a significant proportion of wine production. Moreover, although the Greek economic crisis has resulted in a decrease in demand, recently it has generated an increased interest in non-bottled wines [68].

Of the 105 Greek wineries in the sample, 86% have a corporate website for promoting and advertising their products/services, 72% support a Facebook page, 37% use Instagram, 38% use Twitter, 17% use YouTube, and 10% use Pinterest. This leads to the conclusion that Greek wineries use and trust SM, and especially Facebook, Instagram and Twitter, for marketing activities [3]. It is evident that Greek wineries have turned to the digital environment for success in the market. The wine industry has been among the slowest to adopt SM [69]. As regards the year the winery established its internet presence, 24% established between 1999 and 2005, 22% between 2006 and 2011, while 54% between 2012 and 2018. Turning to the languages supported by corporate websites, 82% are both in Greek and English and 18% only in Greek, indicating that the majority are interested in export activities.

Greek winery websites were evaluated with Website Grader. The overall mean score was 66.42%. The overall mean score for each of the Website Grader features is: (a) *performance:* 19.45/30; (b) *mobile readiness:* 23.62/30; (c) *SEO:* 17.06/30 and (d) *security:* 6.12/10. Figure 1 shows the scores of *performance* characteristics of a Greek winery website.

Figure 2 shows the overall recommendations of the Website Grader tool for the improvement of the particular website. The recommendations refer only to *performance* and *SEO* features, which scored lower than satisfactory values.

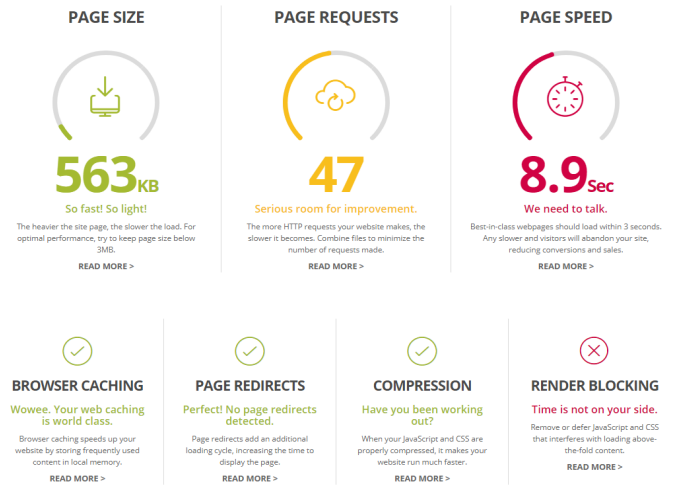

Figure 1. Website Grader Results for performance characteristics of a Greek winery website

Figure 2. Website Grader recommendations for performance and SEO characteristics of a Greek winery website

Next, the results from the LikeAlyzer evaluation are presented. The *Frontpage* feature mean score for the sample is 97% and is analyzed according to the following attributes:

• Profile picture and cover photo: 92.81% of the wineries use a profile picture/cover photo in their profile.

• Username: 93.75% use a shortened page address to promote their business more easily.

• About: 89.06% provide information about the page and what someone can expect when starting to follow the page.

• Call to Action: 100% use "Call to Action" buttons (e.g. "Message Now", "Call Now", "Sign Up Now", "Shop Now") to support interaction with users and promote the business' main objectives.

The *About* feature mean score is 72% and is analyzed according to the following attributes:

• Milestones: only 3.13% use milestones to tell the story of their business.

• Contact information: 64.06% of all contact information (telephone, email, website) is provided on the Facebook page. The percentage is quite low compared to the usefulness and convenience of this information for users. In addition, the lack of

such information has a negative impact on the reliability and safety of the page.

• Location: 70.31% provide the location of their headquarters.

• Products: 26.56% promote their products on their page.

The *Activity* feature mean score is 54% and is analyzed according to the following attributes:

• Posts per day: 0.24 are the daily posts made by businesses, which needs improvement to enhance user engagement.

• Average post length: 192.88 characters is the average length of the posts, which can be improved as it has been noted that posts with 40-100 characters generate more user engagement.

• Pages liked: 42.06 is the average number of "Likes" made by the businesses in the sample to other businesses. Increasing this average will positively affect the cross-sector dialogue and interest, as well as the overall engagement.

• Native Facebook videos: 1.56 is the average number of videos published. Given that video is considered the most engaging format on Facebook, this feature needs to be improved.

The *Engagement* feature mean score is 3% and is analyzed according to the following attributes:

• People talking about this: on average 163 users accessed the page or interacted with its content within the past week.

• Total page likes: 5,840 is the average number of "Likes" by users per business. A larger number of likes corresponds to the business' wider reach.

The *Response* feature mean score is 85% and is analyzed according to the following attribute:

• Users can post: 52.38% of businesses offer their users the option of posting on their page.

4.2. The German Case

German businesses have a long history in the wine sector. For the last forty years Germany has been a leader in global wine imports. Most of the Greek wine imports are made by Germany. Despite the maturity of the German wine sector, it is currently undergoing structural changes. In the near future it is expected that expenditure for marketing will increase, as consumer habits change and new marketing approaches and channels (e.g. blogs and electronic auctions) are required on the basis of a strategic path for sustainability [71,72]. The German Wine Institute, which comprises the country's wine industry marketing organization for the generic promotion of German wines domestically and abroad, already uses SM tools, including Twitter, Instagram, YouTube and Facebook [73].

In 2012 German wineries' SM usage was explored in two research studies [6, 74]. In [6], a sample of 321 German wineries was studied to identify winemakers' SM preference. Facebook was found in this study to be German winemakers' favorite platform. In [74] the SM usage of German wineries and its impact on a sample of Facebook and non-Facebook users was assessed. The turnover of purchases of Facebook users was higher than that of non-users as they are interested in sales offers from wineries they support through SM. 87% of the sample purchased wine from a specific winery and 15% purchased wine from this winery on a regular basis.

All 100 German wineries have a corporate website and 53% also have a Facebook page. Concerning the year the winery established its internet presence, 61% established between 1998 and 2005, 15% between 2006 and 2011, and 24% in 2018. As regards the languages supported by corporate websites, 29% are only in German, 71% are available both in German and English, and 7% support a third language.

Data collected from the German wineries indicate that they engage in SM marketing practices to a high degree. Regarding SM usage, 96% of wineries use Facebook, 28% use Instagram, 8% use Twitter, and 1% use YouTube and Pinterest.

German winery websites were evaluated with Website Grader, achieving an overall mean score of 70.58%. Specifically, the scores for each feature are presented as follows: (a) *performance:* scores reached an average of 23.61/30; (b) *mobile readiness*: 23.27/30; (c) *SEO*: 16.79/30; and (d) *security*: 7.65/10.

Next, the results from the LikeAlyzer evaluation are presented. The *Frontpage* feature mean score of the sample is 94.30% and is analyzed according to the following attributes:

• Profile picture and cover photo: 86.79% of the wineries use a profile picture/cover photo in their profile.

• Username: 94.34% use a shortened page address.

• About: 81.13% provide information about the page.

• Call to Action: 100% use "Call to Action" buttons.

The *About* feature mean score is 82.90% and is analyzed according to the following attributes:

• Milestones: only 9.43% use milestones.

• Contact information: 85% of all contact information is provided on the Facebook page. The percentage is not extremely high, offering scope for improvement for the German wineries.

• Location: 90.56% provide the location.

• Products: 9.43% promote their product, showing low exploitation of Facebook for promotion.

The *Activity* feature mean score is 42.50% and is analyzed according to the following attributes:

• Posts per day: 0.09 are the daily posts.

• Average post length: 186.74 characters is the average text size of the posts.

• Pages liked: 28.91 is the average number of "Likes".

• Native Facebook videos: 0.91 is the average number of videos published.

The *Engagement* feature mean score is 3% and is analyzed according to the following attributes:

• People talking about this: on average 70 people have interacted with a page.

• Total page likes: 4,515 is the average "Likes" made by users per business.

The *Response* feature mean score is 90.56% and is analyzed according to the following attribute:

• Users can post: 90.56% of businesses allow users to post on their page.

In the following figures an example of a German winery assessed with LikeAlyzer is presented. Figure 3 presents the overall impression of the Facebook page, and Figures 4 and 5 show the assessment of Frontpage and Activity features respectively.

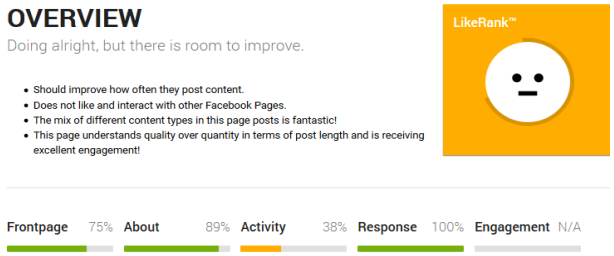

Figure 3. Overview of the Facebook page of a German winery assessed by LikeAlyzer

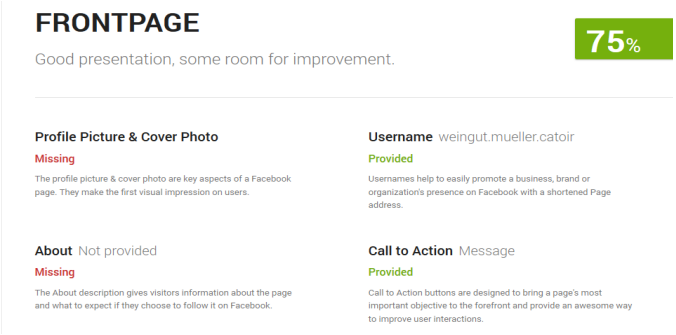

Figure 4. Frontpage feature assessment by LikeAlyzer

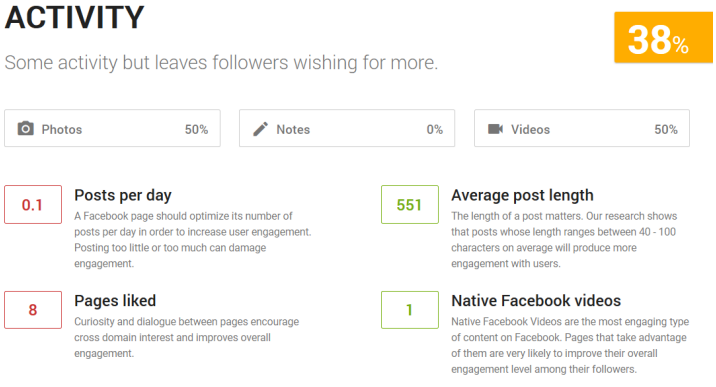

Figure 5. Activity feature assessment by LikeAlyzer

4.3. Discussion

The assessment results of the Greek and German wine industry using Website Grade and LikeAlyzer tools are presented in Table 2. According to the Website Grader evaluation, the *performance* rating for Greece is 19.45 out of 30, and for Germany 23.61. This slight difference in *performance* of German corporate websites shows that they create a better first impression and experience for users. However, Greek winery websites enrich their content with many images and videos in addition to a standard description of their products, which significantly reduces their speed. Regarding *mobile readiness*, Greek and German websites have similar scores, though flexibility and responsiveness for mobile devices have to be further improved. Moreover, according to [4], 60% of users are unlikely to return to a website with accessibility problems from a mobile device, while 40% of users choose to visit a competitor's site. It is therefore essential for winery websites to offer customers an optimized experience for their smart phones and tablets. SEO was 17.06 for Greek wineries and 16.79 for German. Greece seems to be ranked more highly when customers search through a search engine. As regards security, Greek websites scored 6.12, while German websites are ahead with a score of 7.65. Security seems to be moderate for both countries; Greek websites in particular need immediate improvement with the implementation of security protocols such as SSL.

Table 2. Greek and German winery assessment results from Website Grader and LikeAlyzer

Features	**Countries**	
	Greece	**Germany**
Website Grader		
Overall	66.42 %	70.58 %
Performance	19.45/30	23.61/30
Mobile readiness	23.62/30	23.27/30
SEO	17.06/30	16.79/30
Security	6.12/10	7.65/10
LikeAlyzer		
Frontpage	97.00	94.30
About	72.00	82.90
Activity	54.00	42.50
Engagement	3.00	3.00
Response	85.00	90.56

Well-designed corporate websites provoke customers' emotional reactions while browsing [76]. From the study of German and Greek wineries' corporate websites, there is an overall impression that the website design presents some differentiation. In particular, Greek wineries' homepages have rich, impressive and colorful photos with people celebrating food and wine, experiences from product use, and information on the winery's history, showing a better understanding of how to project customers' ideal experience. In contrast, the appearance of German wineries' websites is less meticulous, generating less positive or even negative comments/impressions among users [3]. A German study conducted in 2016 showed that websites with large-sized, high-quality photos of joyful people or inspired moments, such as a panoramic view of the vineyard, can potentially create an emotional impact on users/customers [75]. Customers' emotional influence and engagement can be taken forward when wineries try to tell their own business story, allowing customers to get to know the winemakers better and identifying similar values that connect them.

Our research also provides data on extroversion to foreign customers. Specifically, 83% of Greek wineries and 71% of German wineries provide their websites in at least two languages. This indicates that Greece constitutes a dynamic player in wine exports and endeavors to develop its export activities further, and highlights Germany's position as the largest importer of wine.

The LikeAlyzer evaluation shows that Greek and German winery Facebook pages are in general terms at similar levels. However, both countries have prospects for further improvement.

Regarding the *Frontpage* feature that shapes visitors' first impressions, Greece's score of 97% is higher than Germany's score of approximately 94%. Concerning the *About* feature, German pages provide a satisfactory amount of business information. However, it is worth mentioning that Greek wineries exploit Facebook more effectively than Germany by providing more product information. The *Activity* feature scores are low for both countries although Greek pages have more posts per day, pages liked and native videos. The *Engagement* feature has the same score (3%) for both countries since only Facebook page administrators have access to the specialized data. Finally, Germany scores more highly for *Response*, showing that German wineries allow more user interaction.

5. Conclusions

Enterprises recognize the value of SM analytics in innovation and product development, and customer service operations and strategy. Social media analytics are recently used by business managers and professionals.

SM analytics are easier to use than traditional media analysis and can provide a fast, effective and efficient assessment of corporate websites and Facebook pages. This is verified by the current research. Two freely available SM analytics tools were used to assess the corporate websites and Facebook pages of the winery industry in Greece and Germany. Few studies to date have focused on the implementation of SM analytics in the food and beverage industry. In this research the use of such tools has proved easy and effective, providing specialized data which can offer valuable insights into the wine industry in both countries. The websites of German wineries are of higher quality – from a technical perspective – than those of Greek wineries. However, the latter have a stronger Facebook presence. This can be explained by the overall attitude of Greek internet users and businesses towards SM usage. According to the Digital Economy and Society Index 2019 [77], the percentage of internet users that uses SM is 73%, 57% and 65% for Greece, Germany and the European Union respectively; the percentage of businesses that uses SM is 21%, 16% and 21% for Greece, Germany and European Union respectively.

The key contribution of this paper lies in the use of simple standard analytics to help winery managers and practitioners to plan their SM efforts and revise them regularly, using inexpensive open source tools. A limitation of this paper regards the exclusive focus on Facebook. Assessing the overall SM strategy of wineries requires the study of other SM, for example, Pinterest, Instagram, and Twitter. Such platforms can have additional potential for online visibility and direct sales by linking to corporate websites or electronic shops [75]. Future work will focus on the use of free SM analytics tools for Twitter and Instagram for retrieving data that can be used to build an overall assessment of the wine industry, as well as other food and beverage sectors. It is expected that this research will give researchers and practitioners an assessment of the wine industry and motivate them to use SM analytics tools to improve digital marketing strategies in the wine and other industries, for example, tourism, health and entertainment. This in turn can help to create a roadmap for exploitation of SM benefits.

References

[1] L. Weber, Marketing to the social web: How digital customer communities build your business. John Wiley & Sons, 2009.

[2] M. Armara, Digital Marketing: the effectiveness of advertising through Social Media. Master Thesis. University of Piraeus, Department of Industrial Management and Technology, 2015.

[3] C. Costopoulou, M. Ntaliani, F. Ntalianis, "Social Media in Greek and German Wineries' Websites" in 2018 9th International Conference on Information, Intelligence, Systems and Applications (IISA), Zakynthos, Greece, 2018. https://ieeexplore.ieee.org/abstract/document/8633596

[4] D. Zeng, H. Chen, R. Lusch, S. H. Li, "Social media analytics and intelligence" IEEE Intelligent Systems, 25(6), 13-16, 2010.

[5] I. Fabiatou, "Greek and German Wineries' Websites", B.Sc. Thesis, Supervisor: C. Costopoulou, Dept. of Agricultural Economics and Development, Agricultural University of Athens, 2018.

[6] G. Szolnoki, H. Dieter, "Online, face-to-face and telephone surveys-Comparing different sampling methods in wine consumer research" Wine Economics and Policy, 2(2), 57-66, 2013. https://doi.org/10.1016/j.wep.2013.10.001

[7] OIV, Organization Internationale de la Vigne et du Vin, State of the Vitiviniculture World Market, State of the sector in 2018. http://www.oiv.int/public/medias/6679/en-oiv-state-of-the-vitiviniculture-world-market-2019.pdf

[8] A. Morrison, R. Rabellotti, "Gradual catch up and enduring leadership in the global wine industry" Research Policy, 46(2), 417-430, 2017. https://doi.org/10.1016/j.respol.2016.09.007

[9] L. Thach, T. Lease, M. Barton, "Exploring the impact of social media practices on wine sales in US wineries" Journal of Direct, Data and Digital Marketing Practice, 17(4), 272-283, 2016. https://doi.org/10.1057/dddmp.2016.5

[10] D. Kolb, L. Thach, "Analyzing German winery adoption of Web 2.0 and social media" Journal of wine research, 27(3), 226-241, 2016. https://doi.org/10.1080/09571264.2016.1190324

[11] N. A. Viana "Digital wine marketing: Social media marketing for the wine industry" in BIO Web of Conferences 7, 03011, EDP Sciences, 2016. https://doi.org/10.1051/bioconf/20160703011

[12] G. Szolnoki, D. Taits, M. Nagel, A. Fortunato, "Using social media in the wine business: An exploratory study from Germany" International Journal of Wine Business Research, 26(2), 80-96, 2014. https://doi.org/10.1108/IJWBR-09-2013-0031

[13] D.A. Laverie, W.F. Humphrey, N. Velikova, T.H. Dodd, J.B. Wilcox "Building wine brand communities with the use of social media: a conceptual model" in 6th AWBR International Conference, Bordeaux, France, 2011.

[14] R. Dolan, S. Goodman, C. Habel "How (and why) are wineries using Facebook for marketing?" Grapegrower & Winemaker, 595, 85-86, 2013.

[15] G. Szolnoki, R. Dolan, S. Forbes, L. Thach, S. Goodman, "Using social media for consumer interaction: An international comparison of winery adoption and activity" Wine Economics and Policy, 7(2), 109-119, 2018. https://doi.org/10.1016/j.wep.2018.07.001

[16] T. Pucci, E. Casprini, C. Nosi, L. Zanni, L. "Does social media usage affect online purchasing intention for wine? The moderating role of subjective and objective knowledge" British Food Journal, 121(2), 275-288, 2019. https://doi.org/10.1108/BFJ-06-2018-0400

[17] A. Galati, S. Tinervia, A. Tulone, M. Crescimanno, "Drivers affecting the adoption and effectiveness of social media investments: The Italian wine industry case" International Journal of Wine Business Research, 2019. https://doi.org/10.1108/IJWBR-04-2018-0016

[18] I. Eleftheriadis, "The competitiveness of Greek exports of wine to the markets of Germany and China" Master Thesis, School of Agriculture, Aristotle University of Thessaloniki, 2012.

[19] T. Ahlqvist, A. Bäck, M. Halonen, S. Heinonen, Social media roadmaps, Helsinki: Edita Prima Oy, 2008.

[20] R. Jones, "Social Media Marketing 101, Part 1", 2009. http://searchenginewatch.com/article/2064413/Social-Media-Marketing-101-Part-1

[21] W. D. Evans, "Social marketing campaigns and children's media use" The Future of Children, 18(1), 181-203, 2008. https://doi.org/10.1353/foc.0.0009

[22] D. Nazan, I. Menevi, R. Eyyam, "What is the motivation for using Facebook?." Procedia-Social and Behavioral Sciences 15, 2642-2646, 2011. https://doi.org/10.1016/j.sbspro.2011.04.162

[23] J. Zhang, "Social Media and distance education", 2010. http://deoracle.org/online-pedagogy/emerging-technologies-social-media-and-distance-education.html.

[24] A. M. Kaplan, M. Haenlein, "Users of the world, unite! The challenges and opportunities of Social Media" Business Horizons, 53(1), 59-68, 2010. https://doi.org/10.1016%2Fj.bushor.2009.09.003

[25] S. Tsartsaflis, E. Kletsios, "How social media influence the branding of mass catering and entertainment companies in a period of economic crisis", B.Sc. Thesis, Alexander Technological Educational Institute of Thessaloniki, Department of Marketing, 2013.

[26] Y. K. Dwivedi, K.K. Kapoor, H. Chen, "Social media marketing and advertising" The Marketing Review 15(3), 289-309, 2015. https://doi.org/10.1362/146934715X14441363377999

[27] S. Falkow, "Social media strategy" E+ White paper 2400 (2009).

[28] R. Felix, P. A. Rauschnabel, C. Hinsch, "Elements of strategic social media marketing: A holistic framework" Journal of Business Research, 70, 118-126, 2017. https://doi.org/10.1016%2Fj.jbusres.2016.05.001
[29] T. L. Tuten, M. R. Solomon, Social Media Marketing, Sage, 2017.
[30] G. Schneider, Electronic Commerce, Cengage Learning Editions, 2015.
[31] J. Mahoney, S. Lawson, R. Stone, "What do you Think of the Return of Dunga-Rees?" Social Media Interactions Between Retail Locations and their Customers" in the 32nd annual ACM conference on Human factors in computing systems, ACM, Toronto, Canada 2014. http://dx.doi.org/10.1145/2559206.2581299
[32] B. Batrinca, P. C. Treleaven, "Social media analytics: A survey of techniques, tools and platforms" AI & Society, 30(1), 89-116, 2014. doi:10.1007/s00146-014-0549-4
[33] B. Kaushik, H. Hemani, P.V. Ilavarasan, "Social media usage vs. stock prices: an analysis of Indian firms" Procedia computer science, 122, 323-330, 2017. https://doi.org/10.1016/j.procs.2017.11.376
[34] R. L. Seidel, A. Jalilvand, J. Kunjummen, L. Gilliland, R. Duszak, "Radiologists and social media: do not forget about Facebook" Journal of the American College of Radiology, 15(1), 224-228, 2018. https://doi.org/10.1016/j.jacr.2017.09.013
[35] V. S. Kumbhar, "Hotel Websites Facebook Data Analysis Using Weka" in Second International Conference of Commerce and Management (ICCM) on Development through Transformation: Prospects for Inclusive Growth, Shivaji University, Kolhapur, 2017.
[36] R. McGee, "The Use of Facebook to Promote Tourist Destinations: A Case of the Middle East" Doctoral dissertation, University of New Haven, 2016.
[37] L. Bingle, "Pinterest in Academic Libraries: Social media policy on visual social networks". https://ojs.library.ubc.ca/index.php/seealso/article/view/188985/186518
[38] R. Saravanakumar, C. Nandini, "A survey on the concepts and challenges of big data: Beyond the hype" Advances in Computational Sciences and Technology, 10(5), 875-884, 2017.
[39] J. Riddell, A. Brown, I. Kovic, J. Jauregui, "Who are the most influential emergency physicians on Twitter?" Western Journal of Emergency Medicine, 18(2), 281, 2017. https://dx.doi.org/10.5811%2Fwestjem.2016.11.31299
[40] J. M. Delgado, J. T. De Pourcq, E. M. Boquet, J. M. Sesmero, F.M. Alonso, "Social authorities concerning# hospital pharmacy on twitter", Eur J Hosp Pharm, 2019.
[41] J. Straus, R. Williams, C. Shogan, M. Glassman, "Social media as a communication tool in Congress: Evaluating Senate usage of Twitter in the 113th Congress" in APSA 2014 Annual Meeting Paper, Washington, D.C., 2014.
[42] P. E. Lutu, "Data analytics to support social media marketing: challenges and opportunities" in CONF-IRM, Cape Town, South Africa, 54, 2016.
[43] P. R. Geho, J. Dangelo, "The evolution of social media as a marketing tool for entrepreneurs" The Entrepreneurial Executive, 17, 61, 2012.
[44] L. Hasan, A. Morris, S. Probets, "Using Google Analytics to evaluate the usability of e-commerce sites" in International Conference on Human Centered Design, Springer, Berlin, Heidelberg, 2009. https://doi.org/10.1007/978-3-642-02806-9_81
[45] W. Fang, "Using Google Analytics for improving library website content and design: A case study" Library Philosophy and Practice, 1-17, 2007. https://doi.org/doi:10.7282/T3MK6B6N
[46] B. Plaza, "Google Analytics for measuring website performance" Tourism Management, 32(3), 477-481, 2011. https://doi.org/10.1016/j.tourman.2010.03.015
[47] S. A. Parnsup, D. Tancharoen, N. Phaphoom, A. Kongthon, "An Adoption of Social Media Monitoring Tools for Business and Market Research" TNI Journal of Business Administration and Languages, 4(1), 1-4, 2016.
[48] S. Ranfagni, M. Faraoni, "Be Social and be Tuned: Evaluate your Brands in Online Communities" in 2017 Global Fashion Management Conference at Vienna, Austria, 2017. https://doi.org/10.15444/GFMC2017.03.06.01
[49] E. Gheribi, A. Kotnicka, A. Klemens, M. Klepacz, R. Kwiatkowski "Analysis of Financing Sources for start-up Companies" Management and Education, 14(1), 22-27, 2018.
[50] S. Asongu, N. Odhiambo, "Tourism and social media in the world: An empirical investigation" African Governance and Development Institute, Working Paper, 2018.
[51] P. M. Waszak, W. Kasprzycka-Waszak, A. Kubanek, "The spread of medical fake news in social media–the pilot quantitative study" Health Policy and Technology, 7(2), 115-118, 2018. https://doi.org/10.1016/j.hlpt.2018.03.002
[52] K. Aman, N. Hussin, "The Effectiveness of Social Media Marketing in Higher Education Institution" International Journal of Academic Research in Business and Social Sciences, 8(9), 827-834. http://dx.doi.org/10.6007/IJARBSS/v8-i9/4657
[53] S. S. Khandare, S. Gawade, V. Turkar, "Survey on website evaluation tools" in 2017 International Conference on Recent Innovations in Signal processing and Embedded Systems (RISE), IEEE, Bhopal, India, 2017.
[54] S. Kaur, K. Kaur, P. Kaur, "An empirical performance evaluation of Universities Website" International Journal of Computer Applications, 146(15), 10-16, 2016. https://doi.org/10.5120%2Fijca2016910922
[55] R. Ribeiroae, T.Florentino, "Digital Transformation in Tourism: a high level analysis of the impact that social networks and mass collaboration concept is having at tourism service providers" in 7th International Conference on Cinema and Tourism-ICCT, Porto, 2016.
[56] E. Ramsey, A. Vecchione, "Engaging library users through a social media strategy" Journal of Library Innovation, 5(2), 71-82, 2014.
[57] J. H. Kietzmann, K. Hermkens, I. P. McCarthy, B. S. Silvestre, "Social media? Get serious! Understanding the functional building blocks of social media" Business horizons, 54(3), 241-251, 2011. https://doi.org/10.1016/j.bushor.2011.01.005
[58] S. Thapa, G. Skinner, "Review of Social Media Management Tools and Related Literature" International Journal of Advanced Trends in Computer Applications, 2(1), 89-99, 2015.
[59] I. Gasparini, "Social Media Marketing: Facebook e le Banche", Ph.D Thesis, Università di Modena e Reggio Emilia, 2015.
[60] J. García-Fernández, A. Elasri-Eijaberi, F. Pérez-Tur, X. M. Triadó-Ivern, L. Herrera-Torres, P. Aparicio-Chueca, "Social networks in fitness centres: the impact of fan engagement on annual turnover" Journal of Physical Education and Sport, 17(3), 1068-1077, 2017.
[61] A. Huertas, E. Marine-Roig, "Destination brand communication through the social media: What contents trigger most reactions of users?" Information and Communication Technologies in Tourism, 295-308, Springer, 2015.
[62] S. A. Movsisyan, "Social media marketing strategy of Yerevan brandy company", Annals of Agrarian Science, 14(3), 243-248, 2016. https://doi.org/10.1016/j.aasci.2016.08.010
[63] M.M. Rodriguez-Fernandez, E. Sanchez-Amboage, V.A. Martinez-Fernandez, "The emergent nature of wine tourism in Ecuador and the role of the Social medium Facebook in optimising its positioning" Revista ESPACIOS, 38(14), 24-37, 2017.
[64] S. Kaur, K. Kaur, P. Kaur, "Analysis of website usability evaluation methods" in 3rd International Conference on Computing for Sustainable Global Development (IEEE), New Delhi, India, 2016.
[65] B. F. Canziani, D. H. Welsh, "Website quality for SME wineries: Measurement insights", Journal of Hospitality and Tourism Technology, 7(3), 266-280, 2016. http://dx.doi.org/10.1108/JHTT-02-2016-0009
[66] M. M. Rodríguez-Fernández, E. Sánchez-Amboage, C. Rodríguez-Vázquez, M. D. Mahauad-Burneo, "Galician Spas in Facebook, Media and Metamedia Management", Advances in Intelligent Systems and Computing, 503, Springer, 2017. https://doi.org/10.1007/978-3-319-46068-0_43
[67] M. Teijeiro-Álvarez, C. Rodríguez-Vázquez, F. Blázquez-Lozano, "The Importance of Social Capital in Higher Education. A Study of The Facebook Fan Pages", New Advances in Information Systems and Technologies. Advances in Intelligent Systems and Computing, 445, 2016. https://doi.org/10.1007/978-3-319-31307-8_48
[68] S. Tsitos, "Empirical investigation of Greek winemaking enterprises in international markets", Master Thesis. Department of Economics, University of Piraeus, 2016.
[69] O. Notta, A. Vlachvei, "Web site utilisation in SME business strategy: The case of Greek wine SMEs" in 6th International Business and Social Sciences Research Conference, Dubai, UAE, 2013.
[70] M. Machill, C. Neuberger, F. Schindler, "Transparency on the Net: functions and deficiencies of Internet search engines", Info 5(1), 52-74, 2003.
[71] M. Dressler, "The German wine market: A comprehensive strategic and economic analysis" Beverages, 4(4), 92, 2018. https://doi.org/10.3390%2Fbeverages4040092
[72] A. G. Goncharuk, "Wine business performance benchmarking: A comparison of German and Ukrainian wineries" Benchmarking: An International Journal, 25(6), 1864-1882, 2018. https://doi.org/10.1108%2Fbij-06-2017-0131
[73] DWI, Deutsches Weininstitut/ The German Wine Institute. www.germanwines.de, 2019
[74] C. Hoffmann, G.Szolnoki, L. Thach, "Cross-Cultural Comparison of Social Media Usage in the Wine Industry: Differences between the United States and Germany" Successful Social Media and Ecommerce Strategies in the Wine Industry. Palgrave Macmillan, New York, 154-166, 2016.
[75] P. Merdian, E. Rüger-Muck, G. Raab, "Emotional impact of wine selling websites: An investigation of the online perception of wine web stores" in 9th Academy of Wine Business Research Conference, Adelaide, Australia, 2016.
[76] S. Wilhelm, "Erfolgsfaktor Online-Handel: Tipps für die E-Commerce-Praxis - von der Gründung bis zur Expansion, Frankfurt am Main, Deutscher Fachverlag, 2012.
[77] DESI, "The Digital Economy and Society Index (DESI) for 2019", European Commission, Brussels, 2019 https://ec.europa.eu/digital-single-market/en/de

ASTES

Advances in Science, Technology and Engineering Systems Journal Vol. 4, No. 4, 388-393 (2019)

www.astesj.com

Special Issue on Advancement in Engineering and Computer Science

ASTESJ

ISSN: 2415-6698

A Proposal of Control Method Considering the Path Switching Time of SDN and Its Evaluation

Kosuke Gotani[1], Hiroyuki Takahira[1], Misumi Hata[1, 2], Luis Guillen[1], Satoru Izumi[*, 1], Toru Abe[1, 3], Takuo Suganuma[1, 3]

[1]*Graduate School of Information Sciences, Tohoku University, 980-8577, Japan*

[2]*Japan Society for the Promotion of Science, 980-8577, Japan*

[3]*Cyberscience Center, Tohoku University, 980-8577, Japan*

ARTICLE INFO

Article history:
Received: 17 June, 2019
Accepted: 31 July, 2019
Online: 16 August, 2019

Keywords:
Software Defined Network
OpenFlow
Path Switching Time

ABSTRACT

Recently, communication demands often change because of the various network services in companies and individuals. Software Defined Networking (SDN) has emerged as a viable control paradigm that allows flexible communication, using OpenFlow as its default standard and enabler. However, when changes happen frequently in SDN networks due to unforeseen reasons -such as a network failure or topology changes- it takes a long time to perform all the operations. For instance, to change a routing path, first new paths must be calculated, then the controller must transmit the commands to the network elements, which has to process those commands. This process can cause a delay, or even disruption, in the communication service. Therefore, this paper proposes a network control method to reduce the time to change a path using OpenFlow.

1. Introduction

1.1. Background and Overview

This paper is an extension of a previous work originally presented at the 5th International Conference on Information and Communication Technologies for Disaster Management (ICT-DM2018) [1]. Recently, the spread of cloud services has led to the diversification of communication [2], as well as the demand for frequent changes on the communication demand.. Thus, it is necessary to respond promptly to such demands, e.g., unexpected network failure. In particular, a technology that can control the network flexibly is needed.

Therefore, SDN [3,4] and OpenFlow [5,6] have recently attracted attention. SDN can control the network flexibly by software and OpenFlow is one of the most popular southbound implementation protocols of SDN. The OpenFlow architecture consists of an controller and OpenFlow-enabled switches which are centrally managed by the controller. In this OpenFlow network, when a failure or server configuration change occurs, all the paths of the traffic that is passing by through the involved switches from a source to a destination (also known as flow) must be changed.

To change the path of a flow, a new flow entry must be installed in all the switches' memory. A flow entry is represented by a condition part and an action part. The condition part includes specific values on fields within the flow header, such as MAC address or IP address. The action part includes how to route the flow when the values of its header match the values of the condition part.

However, it takes a long time to change various paths of the several flows.Specifically, it takes around 10 ms to change a single path due to the influence of the transmission time of a flow entry form the controller to the switch, and the processing time to add flow entry into the switch [7, 8, 9]. Therefore,in time-sensitive situations, such as disasters, in which several paths must be changes in a short period of time, not all the flow changes will be successful . For example, SONET (Synchronous Optical Network) needs to be recovered within 50 ms, but, it will be challenging to change more than six flows within that time [10]. This time constraint can lead to delays or even service outage. In this way, a technique to switch many flows in a short time is needed.

The main goal of this research is to reduce the delay or service outage in OpenFlow networks, with particular focus on the time needed to change the path of a flow. The proposal consists of a network control method that considers the time needed to change a path in each switch. In this method, the initial assumption is that

[*]Satoru Izumi, 2-1-1, Katahira, Aoba-ku, Sendai, 980-8577, +81-22-217-5453, izumi@ci.cc.tohoku.ac.jp

the network model consists of OpenFlow-enabled switches with different processing time, linked by connections with different bandwidth. Then, the paths with the shortest switching time and the least bandwidth requirements are selected. The basic design was described in [1], and the preliminary simulation experiments presented in [11]. In this paper, the authors evaluate the effectiveness of the proposed method using emulated environments. Based on the obtained results, we confirmed that the proposed method can reduce the switching time for all paths, so that it can realize the reduction of communication delay and network services outages.

1.2. Novelty and Contribution

In this work, a novel approach which chooses communication paths considering not only the processing time to add flow entry of the switch, but also the available bandwidth in the links. Existing approaches mainly focus on the reduction of the calculation time of the paths, or using a backup path in advance. However, they do no deal with the processing time of the switch.

By considering both the processing time and the bandwidth, it can shorten the path switching time and improve the amount of data transferred in a short period. Moreover, tt can also contribute to the reduction of the packet-loss due to the communication interruption during the network failure. This method is effective for services that require lowdelay communication. Furthermore, it is possible to improve the amount of data transfer between two sites in the situation where path change frequently, such as is the case in a disaster situation.

1.3. Paper Organization

In the following Section 2, we explain the related work on fast path switching and the target problem. In Section 3, we describe the proposed control method. The design of the algorithm is shown in Section 4. Then, Section 5 shows the evaluation of the proposed method and its effectiveness. Finally, we conclude this paper in Section 6.

2. Related Work

2.1. Related Work on Fast Path Switching

There are several authors that studied fast path switching in OpenFlow networks, which are mainly categorized in two approaches. The first approach, consists of switching to a backup path registered in advance in a proactive manner [13,14,15], while the second one reactively calculates a new path when a request occurs [10,16,17,18]. These authors select the paths considering a variety of single parameters, e.g., switching time, bandwidth of the link between the controller and the switch, and power consumption. However, all of them largely depend on the available amount of memory (TCAM) to hold the flow table. In this research, we deal with methods for calculating and switching the path reactively.

Cascone et al. [13] proposed a recovery mechanism based on fast reroute of paths in disaster situations. Mohan et al. [14] investigated algorithms to choose a backup path to decrease the number of flow entries. Stephens et al. [15] showed a mechanism to compress the flow table for fast recovery from link failure.

Astaneh et al. [10] proposed a path selection method to reduce the path switching time while considering the communication bandwidth. They reduced the cost of the path switching compared to the traditional approach of using Dijkstra's algorithm. Sharma et al. [16] proposed an in-band based path switching method for failure recovery. Paris et al. [17] showed a dynamic control scheme for network reconfiguration. Malik et al. [18] proposed a method to reduce the path calculation and switching time by partially reusing the route before the change of path. Therefore it can reduce the number of added flow entries.

2.2. Target Problem

The related work presented in the previous section did not take into account environments in which there are heterogeneous switches. Many organizations often build their network by combining switches with various specifications because of budget constraints and differences on the time of purchase [12]. Moreover, the processing time is also different in these switches, causing large delays when there is a heavy traffic on low-processing time switches. Therefore, it is necessary to create a network control method to cope with the difference in processing time when adding flow entries.

3. A Proposal of Control Method Considering Path Switching Time

3.1. Overview

In this section, to solve the problems mentioned above, the authors of this paper propose a network control method that considers the path switching time of each switch. In this method, the network model is designed with different processing time for each switch, and the proposed algorithm selects paths with the shortest time for all paths. Our proposed method considers both the processing time of the switch and the network bandwidth.

The proposed method chooses a path with enough bandwidth, and that goes through high-performance switches to add a flow entry, so that the overall path switching time is reduced when there are several flows. In addition, the proposed method also selects paths sequentially without considering the combination of paths, so that the computational time per path is reduced.

3.2. Path Selection Considering Path Switching Time

This section presents the basic concept of the path-selection mechanism that considers the path switching time as shown in the example depicted in Figure 1. In this example, there are four switches (S_1 to S_4) and the processing time to add a flow entry in each switch is different. Now, there is a communication flow from S_1 to S_4, and for some reason the path must be changed. In this case, there are two candidate paths; p_1 ($s_1 \rightarrow s_2 \rightarrow s_3$) and p_2 ($s_1 \rightarrow s_4 \rightarrow s_3$). The overall path switching time of the flow is the processing time for the switch on the path that has the maximum processing time. For instance, the path switching time of p_1 is 4.0 ms and that of p_2 is 6.0 ms. Thus, the proposed method chooses p_1 which has the shortest switching time.

3.3. Path Selection Considering Available Bandwidth

The path cost, which is used to choose the path with enough communication bandwidth, is calculated by the available bandwidth of the links on the path. Such that when the link with a larger communication bandwidth is used in the path, the path cost

is smaller. Conversely, when the link bandwidth of the path is smaller, the path cost is larger. In the example shown in Figure 2, the path cost of the upper path is smaller because the bandwidth of the links on that path are larger than the ones in the lower path, and therefore the former is selected.

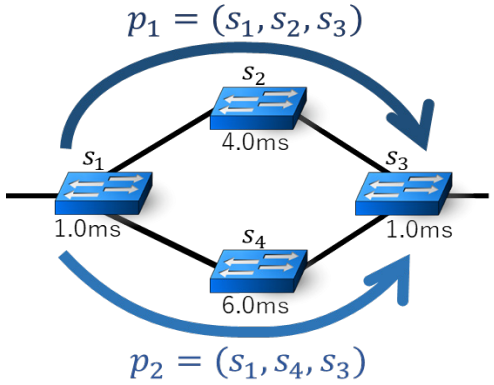

Figure 1: Example of Path Selection Considering Path Switching Time

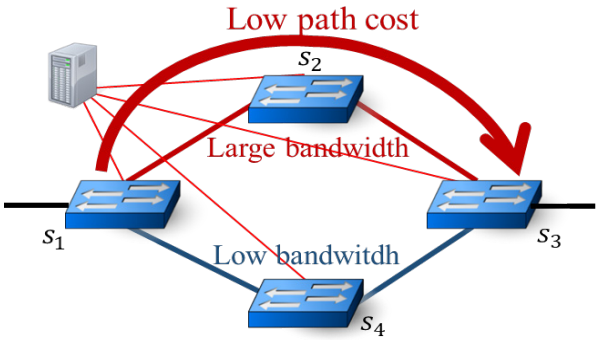

Figure 2: Example of Path Selection Considering Available Bandwidth

4. Design

4.1. Network Model

The network model is defined as below.

- $s_i \in S\ (i = 1, 2, ..)$: Switch
- t_i : Processing time for adding one flow entry into s_i
- $e_{i,j} \in E$: Link between s_i and s_j
- $B_{i,j}$: Available bandwidth of $e_{i,j}$
- p_k : Path (list of switches)
- $c_{i,j}$: Link cost of $e_{i,j}$ (= 1Gbps/$B_{i,j}$)

4.2. Definition of Path Switching Time

The path switching time is defined as:

"The time from the arrival of the first additional flow entry from the controller to the switch until the completion of the path switching on all switches"

Figure 3 shows an example. Suppose that tthere are three flows (flow 1, 2, and 3) assigned to the paths shown in Figure 3. In this case, t_1 is 1 ms, and s_1 needs to switch the three flows. Thus, the time to complete the processing of the additional flow entry is 1 ms * 3 = 3 ms. Then, t_2 is 4 ms and the s_2 needs to switch two flows (flow 1 and 2). Therefore, the time to complete the processing of the additional flow entries is 8 ms (4 ms * 2). For the other switches, the time is calculated in the same way. Finally, the path switching time in this example is 8 ms, which is the longest time to complete the process.

The path switching time $T(P_m)$ for a set of paths (P_m) is defined as in (1)

$$T(P_m) = \max_{\{i|s_i \in S\}} \{t_i \times \sum_{p_k \in P_m} z_i(p_k)\} \quad (1)$$

Here, $z_i(p_k)$ means whether the list of p_k includes s_i.

$$z_i(p_k) = \begin{cases} 1\ (s_i \in p_k) \\ 0\ (otherwise) \end{cases} \quad (2)$$

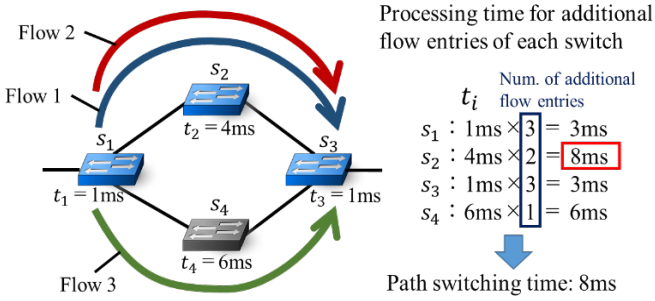

Figure 3: Example of Path Switching Time

4.3. Link Cost

The proposed method prioritizes the path switching time rather than the path cost, and chooses paths sequentially. The overview of the sequential path selection method is as follows:

- Choose a path for one flow at a time.
- Substract the required bandwidth of the flow from the link bandwidth on the path, and update the link cost every time the path is selected.
- Assign a flow to the path until there is no available bandwidth left for the flow.

Figure 4 shows an example of the link cost update. If the link bandwidth is 1 Gbps, the link cost is 1. Then, when a flow requires 300 Mbps of bandwidth, it is inserted into the link. The available bandwidth of the link becomes 700 Mbps, and the link cost increases to about 1.4.

Figure 4: Example of Link Cost Update

4.4. Flow of Path Selection

This section explains the process of path selection. In order to consider both the processing time of the switch and the path cost, the proposed method chooses paths as detailed below.

1. Compute the paths with the smallest increase in the path switching time.
2. Choose the path with the lowest path cost form the computed paths.
3. Repeat process 1 and 2 for the number of flows that needs to change.

5. Experimentation

5.1. Overview

The proposed method was evaluated in an emulated environment. The network used in the experiment is shown in Figure 5. Here, the available bandwidth $B_{i,j}$ of all links is set as 1 Gbps. Also, the processing time of the source switch, and destination switch was set to 1 ms; while remaining switches were randomly set from 1 to 10 ms.

Several flows with different required bandwidth were inserted, and randomly shutdown links. After the link is down the paths of the flows are switched. To compare the effectiveness of the proposal, the obtained throughput is obtained and compared with an existing method, which selects paths considering only path cost.

In this experiment, Mininet (ver. 2.2.2) [19] was used as a network emulator on a single computer, whose specification is as below:

- CPU: Intel (R) Xeon (R) CPU E5-2650 v4 @ 2.20 GHz) x 8 cores
- Memory: 16 GB

We also used OpenDaylight (0.3.3-Lithium-SR3) [20] as the OpenFlow controller, and OpenVSwitch (ver. 2.5.5) [21] as the OpenFlow switch.

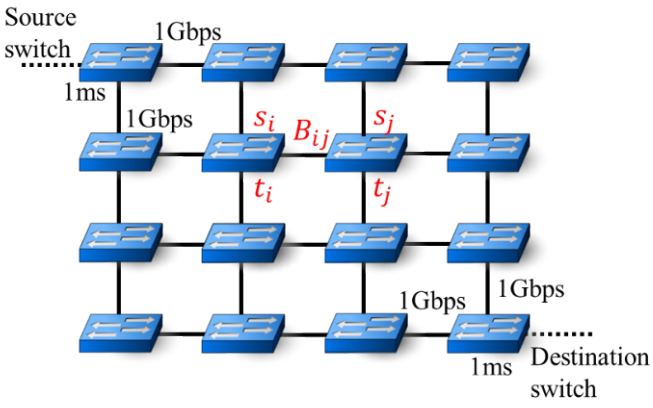

Figure 5: Network Topology Used in the Experiment

5.2. Results

The authors categorize the throughput comparing the proposed method with the existing method into the following three patterns:

- The proposed method always dominates (Win).
- The proposed method dominates until a certain time (Win[time]).
- The proposed method is equal to the existing method (Eq).

Examples of graphs of the three patterns are shown in Figures 6, 7, and 8. The comparison of the data transfer amount between the proposed method and the existing method is shown in Table 1. From the table, it is observed that when the total bandwidth of the flows is 1,800 Mbps or more, and the number of disconnected links is large, the data transfer amount of the proposed method is always better. However, when the total bandwidth of the flows is 1,800 Mbps or more, and the number of link disconnections is small, then the amount of transferred data of the proposed method is larger within 0.1 to 0.2 seconds.

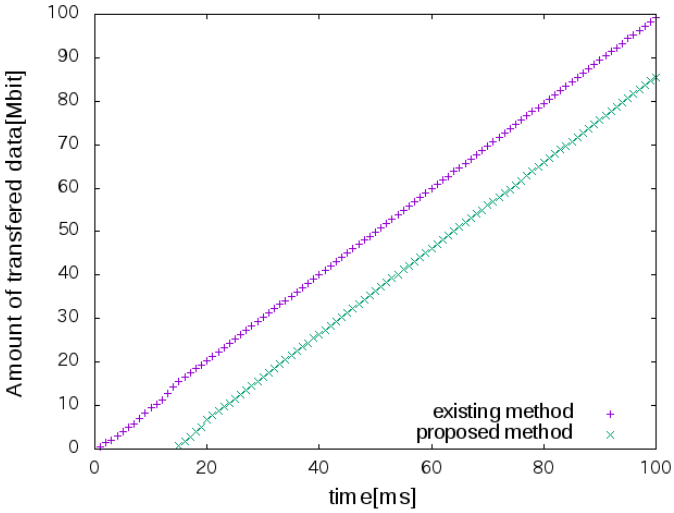

Figure 6: The Proposed Method Dominates Always (Win)

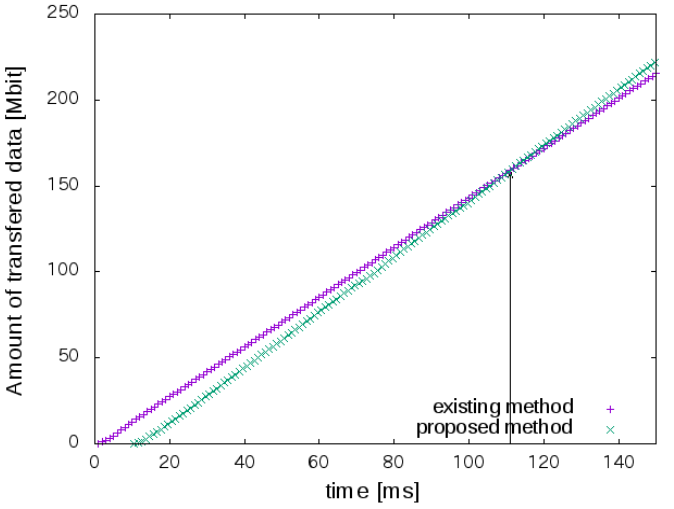

Figure 7: The Proposed Method Dominates Until A Certain Time (Win[112s])

Moreover, when the total bandwidth of flows is less than 1,400Mbps, and the amount of transferred data of the proposed method is larger is within 1.5 seconds, the proposed method is larger regardless of the number of disconnected links. Finally, when the total bandwidth of flows is less than 1,200 Mbps, the proposed method is always better.

Table 1: Comparison of the data transfer amount between the proposed method and the existing method

		Total bandwidth of the flows [Mbps]										
		1,000	1,200	1,400	1,600	1,800	2,000	2,200	2,400	2,600	2,800	3,000
Number of down links	0	Win	Win	Win [1.5ms]	Win [0.3ms]	Win [0.1ms]	Win [0.1ms]	Win [0.1ms]	Win [0.1ms]	Win [0.1ms]	Win [0.1ms]	Win [0.1ms]
	4	Win	Win	Win [1.5ms]	Win [0.3ms]	Win [0.2ms]	Win [0.2ms]	Win [0.2ms]	Win [0.1ms]	Win	Win	Win
	8	Win	Win	Win	Win [0.2ms]	Win [0.1ms]	Win	Win	Win [0.1ms]	Win	Win	Win
	12	Win	Win	Win	Win [0.1ms]	Win	Win	Win	Win	Win	Win	Win
	16	Win	Win	Win	Win	Win	Win	Win	Win	Win	Win	Eq
	18	Eq	Eq	Eq	Eq	Eq	Eq	Eq	Eq	Eq	Eq	Eq

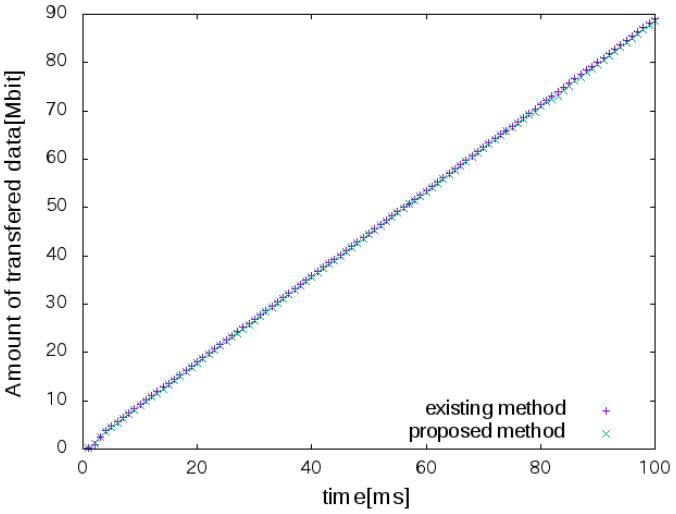

Figure 8: The Proposed Method Is Equal To The Existing Method (Eq)

5.3. Discussion

From the experimental results in the previous sections, the authors of this paper confirm that the proposed method is more effective than the existing method, since the amount of transferred data is equal or larger to the existing method while the path switching time is shortened. Morever, the path switching process is more effective than the existing method when these events occurs frequently and there is not enough bandwidth.

6. Conclusion

This paper presents a network control method considering the path switching time in SDN. We designed the path selection method and evaluated with an emulated experimentation. From the experimental results, it is confirmed that the proposed method is effective in situation where changes occurs frequently in a short time due to link disconnection and restoration (e.g., disasters).

As future work, we will extend the proposed method by introducing other parameters and experiment with real networks. Currently, we focused on the time from the arrival of the first additional flow entry from the controller to the switch until the completion of the path switching on all switches. Thus, we will evaluate the total time of changing paths from the moment some events occur until they complete changing the paths in comparison with related work.

Conflict of Interest

The authors declare no conflict of interest.

References

[1] K. Gotani, H. Takahira, M. Hata, L. Guillen, S. Izumi, T. Abe, and T. Suganuma, "OpenFlow Based Information Flow Control Considering Route Switching Cost," Proc. the 5th International Conference on Informationand Communication Technologies for Disaster Management (ICT-DM 2018), pp.1-4, 2018.

[2] Ministry of Internal Affairs and Communications, ahttp://www.soumu.go.jp/johotsusintokei/whitepaper/ja/h30/html/nd252140.html (Accessed 2019).

[3] S. H. Yeganeh, A. Tootoonchian, and Y. Ganjali, "On Scalability of Software-Defined Networking," IEEE Communication Magazine, Vol. 51, No. 2, pp.136-141, 2013.

[4] "Software-Defined Networking (SDN) definition," Open Networking Foundation, https://www.opennetworking.org/sdn-resources/sdndefinition, (Accessed 2019).

[5] N. McKeown, T. Anderson, H. Balakrishna, G. Parulkar, L. Peterson, J. Rexford, S. Shenker, and J. Turner, "OpenFlow: Enabling Innovation in Campus Networks," ACM SIGCOMM Computer Communication Review, Vol. 38, Iss. 2, pp.69-74, 2008.

[6] Open Networking Foundation, "OpenFlow Switch, Specification (Version 1.5.1)," https://www.opennetworking.org/wp-content/uploads/2014/10/openow-switch-v1.5.1.pdf (Accessed 2019).

[7] A. Nguyen-Ngoc, S. Lange, S. Gebert, T. Zinner, P. Tran-Gia, and M. Jarschel, "Performance Evaluation Mechanisms for FlowMod Message Processing in OpenFlow Switches," Proc. of IEEE Sixth International Conference on Communications and Electronics (ICCE2016), pp.40-45, 2016.

[8] C. Rotsos, N. Sarrar, S. Uhlig, R. Sherwood, and A. Moore, "OFLOPS: An open framework for openflow switch evaluation," Proc. of Passive and Active Measurement (PAM2012), LNCS 7192, pp.85-95, 2012.

[9] R. Bifulco and A. Matsiuk, "Towards Scalable SDN Switches: Enabling Faster Flow Table Entries Installation," Proc. of 2015 ACM Conference on Special Interest Group on Data Communication (SIGCOMM 2015), pp.343-344, 2015.

[10] S. A. Astaneh and S. Shah Heydari, "Optimization of SDN Flow Operations in Multi-Failure Restoration Scenarios," IEEE Transactions on Network and Service Management, Vol.13, No.3, pp.421-432, 2016.

[11] K. Gotani, H. Takahira, M. Hata, L. Guillen, S. Izumi, and T. Abe, "OpenFlow Based Information Flow Control Considering Route Switching Cost," Proc. the 2nd IEEE International Workshop on Information Flow Oriented Approaches in Internet of Things and Cyber-Physical Systems (InfoFlow 2019), pp.527-530, 2019.

[12] A. Feldmann, P. Heyder, M. Kreutzer, S. Schmid, J.P. Seifert, H. Shulman, K. Thimmaraju, and M. Waidner, "NetCo: Reliable Routing With Unreliable Routers," Proc. of the 46th Annual IEEE/IFIP International Conference on Dependable Systems and Networks Workshop (DSN-W), pp.128-135, 2016.

[13] C. Cascone, L. Pollini, D. Sanvito, A. Capone, and B. Sanso, "SPIDER: Fault resilient SDN pipeline with recovery delay guarantees," Proc. of IEEE NetSoft Conference Workshops (NetSoft), pp. 296-302, 2016.
[14] P. M. Mohan, T. Truong-Huu, and M. Gurusamy, "TCAM-Aware Local Rerouting for Fast and Efficient Failure Recovery in Software Defined Networks," Proc. of 2015 IEEE Global Communications Conference (GLOBECOM 2015), pp.1-6, 2015.
[15] B. Stephens, A. L. Cox, and S. Rixner, "Scalable Multi-Failure Fast Failover via Forwarding Table Compression," Proc. ACM SIGCOMM Symposium on SDN Research Article (SOSR 2016), no. 9, pp.1-12, 2016.
[16] S. Sharma, D. Staessens, D. Colle, M. Pickavet, and P. Demeester, "In-Band Control Queuing and Failure Recovery Functionalities for OpenFlow," IEEE Network, vol. 30, no. 1, pp. 106-112, 2016.
[17] S. Paris, G. S. Paschos, and J. Leguay, "Dynamic Control for Failure Recovery and Flow Reconfiguration in SDN," Proc. International Conference on the Design of Reliable Communication Networks (DRCN 2016), pp.152-159, 2016.
[18] A. Malik, B. Aziz, M. Adda, and C. Ke, "Optimization Methods for Fast Restoration of Software-Defined Networks," IEEE Access, Vol.5, pp.16111-16123, 2017.
[19] Mininet, http://mininet.org/
[20] OpenDaylight, https://www.opendaylight.org/
[21] Open vSwitch, http://openvswitch.org/

ASTES

Advances in Science, Technology and Engineering Systems Journal Vol. 4, No. 4, 394-403 (2019)

www.astesj.com

ASTESJ

ISSN: 2415-6698

Comparing the Scientific Production of Peruvian Universities with Equitable Indexes

Avid Roman-Gonzalez[*,1], Antony Ciriaco-Susanibar[1], Natalia I. Vargas-Cuentas[2]

[1]*Universidad Nacional Tecnológica de Lima Sur, Aerospace Sciences and Health Research Laboratory (INCAS-Lab), 15314, Peru*

[2]*Universidad de Ciencias y Humanidades, Image Processing Research Laboratory (INTI-Lab), 15834, Peru*

ARTICLE INFO

Article history:
Received: 17 June, 2019
Accepted: 27 July, 2019
Online: 16 August, 2019

Keywords:
University ranking
SCOPUS
Published papers
Research measurement
Research

ABSTRACT

In recent years, research has been taking an important role in Peru. There are different sources of funding for research projects, research internships, the publication of scientific articles, scholarships for postgraduate studies, among others. This importance of research has resulted in an interest in being able to measure and compare universities according to their scientific production. One of the main factors to be used to make these comparisons is the number of articles published and indexed in SCOPUS. However, this measure is not entirely fair, since it is not equitable to compare a large university with a small university since large universities have more human resources to publish scientific articles. Seeing this reality, in the present work, we present a comparison of scientific production in Peruvian universities, taking into account the size of the institutions. Among the results obtained, we can observe a change in the ranking of small universities that invest heavily in research.

1. Introduction

Research is essential for the development of a country. It has already been seen during the Second World War; the main advances were made thanks to the scientists [1]. One of these advances, for example, is the development of the atomic pump thanks to the work of Albert Einstein [2].

According to what is argued by Roman-Gonzalez in [3], the research should be supported by a tripod composed of the university, the government, and the private enterprise, as shown in Figure 1.

The university is an essential support of the tripod since the university is not only called to train new professionals, but also is hoped to contribute with human knowledge, and this is achieved through research. Professors are the main actors of the investigation, but it is also the students who can collaborate in the publication of scientific articles.

The government is another significant support because it is called to define the policies and laws that promote research in a country. One of these policies that encourage research is, for example, the tax benefit for companies investing in research and technological development that currently applies in Peru [4].

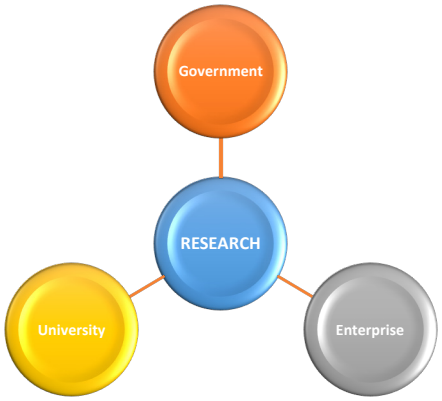

Figure 1: Tripod of the research

The private company completes the tripod since they are called to finance the research. This financing can mainly be oriented to solve problems or challenges of the same company.

In developed countries, the private sector has many challenges to solve and relies on the university (professors and students) and their capacity to face these challenges. In this way, the company finances the different research projects under a political framework established by the government.

Unfortunately, this scenario is not replicated in developing countries, mainly because companies do not trust in the

[*]Avid Roman-Gonzalez, Universidad de Ciencias y Humanidades, Image Processing Research Laboratory (INTI-Lab), +51984904763, avid.roman-gonzalez@ieee.org

university's abilities to solve problems, and because the government does not have adequate policies to motivate the research activities.

In Peru, we are in the process of transition from one panorama (the second) to the other (the first), hoping to obtain good results.

The research is a process that follows the scientific method, and that must end in the publication of one or several scientific articles. The scientific article is nothing more than a report of the research work carried out under a pre-established format. The release of scientific articles is critical because it is necessary to let the world know about what one is researching because whatever the subject one is investigating, one is sure that on the other side of the world more research groups are working on the same subject and/or similar topics. Thanks to the publications one can get in touch with other research groups, collaborative works are achieved, joint efforts to obtain better results, scholarship opportunities, and research stay, among other benefits.

Because the research is so essential, different rankings have been established that evaluate the universities in the function of the investigation and scientific production they carry out. Among these rankings we can mention the ones elaborated by SCIMAGO [5], America Economia [6], National Superintendency of Higher University Education (SUNEDU - Superintendencia Nacional de Educacion Superior Universitaria) of Peru [7], Academic Ranking of World Universities (ARWU) [8], Webometrics [9], QS World University Ranking [10], among others. For the elaboration of these rankings, different parameters are used such as scientific production, scientific talent pool, citations by document, web size, international collaboration, domain's inbound links, percentage of publication in journals of the first quartile, average scientific quality, among others [3] [6] [11].

The universities carry out and implement different strategies to improve their position in the rankings. Some use new methodologies in their teaching processes as in [12], and others develop a whole program of formative research to get undergraduate students to start publishing scientific articles, as mentioned in [13].

One of the most critical rankings developed as a function of scientific production is the one produced by the SCIMAGO group [5] [11].

SCIMAGO generates two types of ranking, one is the SIR World, which is a worldwide raking in which only institutions that have publications indexed in SCOPUS equal to or higher than 100 per year are included. Peru has had a growth in the number of institutions that enter in this ranking since 2009. In Figure 2, we can see this evolution where one can see that Peru went from 1 institution in 2009, passed through 4 institutions in 2012 and reached seven institutions in 2018. In Figure 2, one can also see the evolution of the best positioned Peruvian university in the ranking.

Apart from the SIR World, there is also the SIR Iber ranking that includes only Ibero-American countries. For entering into this ranking, it is only necessary to have at least one article published and indexed in SCOPUS. In Figure 3, one can see the evolution of the number of Peruvian institutions included in the SIR Iber ranking. One can see that by 2009 there were 50 Peruvian institutions and by 2018 the number increased to 77.

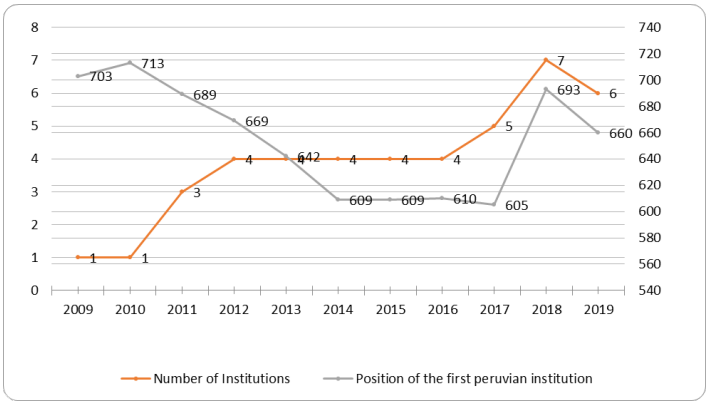

Figure 2: Evolution of the number of Peruvian institutions in the SIR World rankings [5] [11]

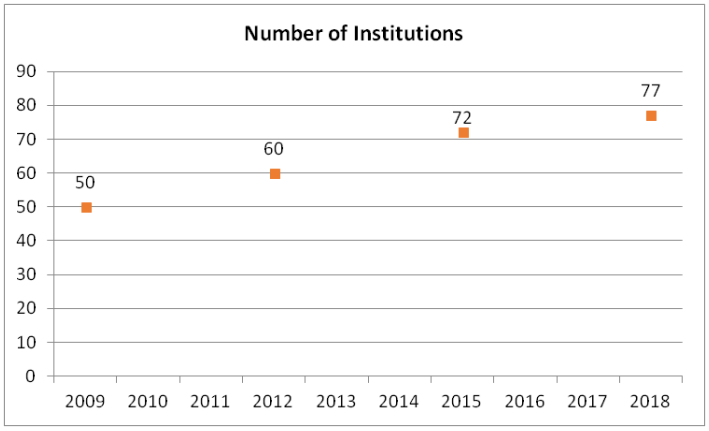

Figure 3: Evolution of the number of Peruvian institutions in the SIR Iber ranking [5] [11]

Among all the parameters mentioned above, one of the most used for the elaboration of the rankings of universities that evaluate scientific production is the number of published scientific articles. While it is true that it is an important parameter, it is not the most appropriate way to compare large universities that have many professors and students, compared to small universities with fewer professors and students. The universities with the most significant number of professors and students have more considerable human resources to carry out research and therefore, to have higher scientific production.

Faced with this situation, some proposals try to use more equitable parameters to compare scientific production in large and small universities. One of these works is the one presented in [14], where the authors use the ratio between the number of publications and the number of professors.

In this paper, one proposes other parameters that can also be used to develop rankings more equitably when comparing universities of different sizes and ages.

The continuation of this work is structured as follows: Section II shows the data source for the analysis carried out as well as the methodology followed. Section III presents the rankings obtained as a result. Finally, in Section IV, these results will be analyzed as part of the discussion and conclusions

2. Methodology

In Peru, due to the new University Law 30220, the majority of universities are investing more in research. Likewise, different analyzes on scientific production are being prepared, such as the one presented in [15].

The most equitable way to compare the scientific production of universities is taking into account their size. One way to include the size of the university in the elaboration of the rankings is to use the number of students. Another idea of having reference to the size of the university is to consider the amount of professor, as was done in [14].

There is a discrepancy due to the fact of considering the number of students or the number of professors since the students are not the main ones involved in the formal research process. Professors are called to do research; however, it is debatable to take into account the total number of professors or only take the number of full-time professors. It is arguably to say that just full-time professors do research.

Faced with this situation, in the present work, one takes into account the number of professors qualified as REGINA researchers. REGINA is the National Registry of Researchers by its initials in Spanish (Registro de Investigadores en Ciencia y Tecnología del Sistema Nacional de Ciencia, Tecnología e Innovación Tecnológica). REGINA is a proposal of CONCYTEC (National Council of Science, Technology and Technological Innovation) that takes into account a set of parameters to evaluate the professionals who research to qualify them as researchers [16]. When considering the number of REGINA researchers per university, we will be sure to take into account those who are involved in scientific activity.

Likewise, in the present work, one will also consider the number of authors identified in SCOPUS to measure with an equitable way the scientific production in large and small universities.

In this section, the methodology followed for the elaboration of the proposed equitable rankings will be described.

2.1. Data Collection

The data analyzed in the present work correspond to the articles published by each university. For this, the SCOPUS database belonging to ELSEVIER will be taken as a reference. The publications of 2017, 2018 will be analyzed, and the total papers will also be taken into account.

The analysis of the present work will be carried out on all the Peruvian universities that have an ID in the SCOPUS database. According to the SUNEDU biennial report [17], in Peru, there are 142 universities of which ten did not provide services at the date of publication of the mentioned report, besides there are four graduate schools and the Facultad de Teología Pontificia y Civil de Lima that has university rank.

To access the SCOPUS data, CONCYTEC provides access to all the people registered in CTI Vitae (bio-sketches related to Science and Technology) through the credentials created for that purpose. In this sense, there will be direct access to SCOPUS, as shown in Figure 4. CTI Vitae is a database that allows people who carry out science, technology, and innovation (CTI) activities to register their resumes.

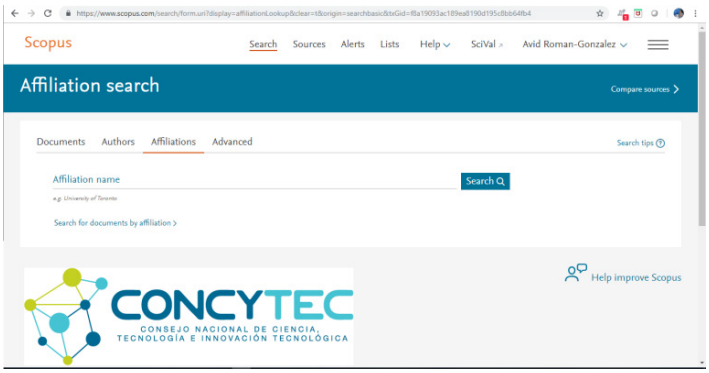

Figure 4: Access to the SCOPUS database

Likewise, the information will be collected regarding the number of professors qualified as REGINA that each university has. For this purpose, the portal created by CONCYTEC will be accessed, as shown in Figure 5

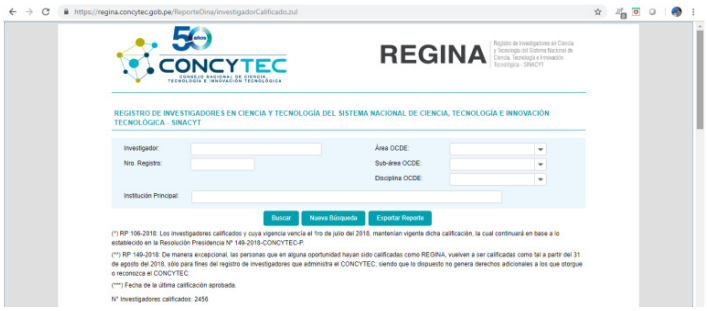

Figure 5: Access to the portal to identify the REGINA researchers for each university

All data were collected on 31st March 2019.

2.2. The ratio between the number of publication and number of researches and authors

For the elaboration of equitable rankings when comparing large universities with small universities, we propose to use two ratios. The first ratio will be considering the number of publications in a given year, divided by the number of REGINA researchers for each university (Equation 1). The second ratio considers the total number of publications divided by the number of authors identified in SCOPUS by each university (Equation 2).

$$R_{p/r} = P / R \quad (1)$$

$$R_{p/a} = P / A \quad (2)$$

Where:

- $R_{p/r}$ is the ratio between the number of paper indexed in SCOPUS and the number of REGINA researchers that will be used to elaborate the ranking.

- $R_{p/a}$ is the ratio between the number of paper indexed in SCOPUS and the number of authors identified in SCOPUS that will be used to elaborate the ranking.
- P is the total number of published paper indexed in SCOPUS.
- R is the number of REGINA researchers for each university, according to CONCYTEC.
- A is the number of total authors that publish papers with the affiliation of the university under analysis, according to SCOPUS.

3. Results

Of all the Peruvian universities, at the date of data collection, only 66 universities have their ID in SCOPUS, have at less one publication in 2017 and 2018, and have REGINA researchers.

After the calculation of the ratios mentioned in Section II, the following results are obtained and compared with the classical ranking based only on the number of publications.

Table I and Table II show the rankings only according to the number of paper for the years 2017 and 2018, respectively.

Table 1: Ranking based on the number of papers published in 2017

N°	University	Papers SCOPUS 2017 (*P*)
1	Pontificia Universidad Católica del Perú	415
2	Universidad Peruana Cayetano Heredia	402
3	Universidad Nacional Mayor de San Marcos	366
4	Universidad Peruana de Ciencias Aplicadas S.A.C.	138
5	Universidad de San Martín de Porres	101
6	Universidad Nacional de San Agustín de Arequipa	76
7	Universidad Nacional Agraria La Molina	76
8	Universidad Nacional de Ingeniería	65
9	Universidad Científica del Sur S.A.C.	64
10	Universidad Nacional de San Antonio Abad del Cusco	54
11	Universidad Católica San Pablo	51
12	Universidad del Pacífico	50
13	Universidad de Piura	46
14	Universidad Privada Antenor Orrego	44
15	Universidad San Ignacio de Loyola S.A.	44
16	Universidad Nacional de Trujillo	41
17	Universidad de Ciencias y Humanidades	39
18	Universidad Privada del Norte S.A.C. -	36
19	Universidad Continental S.A.C. (*7)	36
20	Universidad ESAN	30
21	Universidad Ricardo Palma	29
22	Universidad Nacional Federico Villarreal	27
23	Universidad Nacional San Luis Gonzaga	24
24	Universidad Nacional de Piura	23
25	Universidad de Ingeniería y Tecnología	22
26	Universidad Católica de Santa María	19
27	Universidad Nacional del Altiplano	17
28	Universidad de Lima	17
29	Universidad Nacional Pedro Ruiz Gallo	14
30	Universidad Nacional de la Amazonía Peruana	13
31	Universidad Católica Los Ángeles de Chimbote (*4) -	13
32	Universidad Católica Santo Toribio de Mogrovejo -	13
33	Universidad Nacional de San Cristóbal de Huamanga	10
34	Universidad César Vallejo S.A.C.	10
35	Universidad Señor de Sipán	10
36	Universidad Nacional del Centro del Perú	9
37	Universidad Privada San Juan Bautista S.A.C. (*6)	9
38	Universidad Nacional Micaela Bastidas de Apurímac	8
39	Universidad Nacional de Tumbes	7
40	Universidad Nacional de Cajamarca	6
41	Universidad Nacional Santiago Antúnez de Mayolo	6
42	Universidad Privada de Tacna	5
43	Universidad Alas Peruanas	5
44	Universidad Privada Norbert Wiener	4
45	Universidad Católica Sedes Sapientiae	4
46	Universidad La Salle	4
47	Universidad Nacional del Callao	3
48	Universidad Nacional de Ucayali	3
49	Universidad Nacional de Huancavelica	3
50	Universidad Nacional Toribio Rodríguez de Mendoza de Amazonas	3
51	Universidad Nacional José María Arguedas	3
52	Universidad Andina Néstor Cáceres Velásquez	3
53	Universidad Andina del Cusco	3
54	Universidad Autónoma del Perú	3
55	Universidad Nacional Agraria de la Selva	2
56	Universidad Nacional Daniel Alcides Carrión	2
57	Universidad Nacional de San Martín	2
58	Universidad Nacional del Santa	2
59	Universidad Nacional Intercultural de la Amazonía	2
60	Universidad Nacional Autónoma de Chota	2
61	Universidad Peruana Los Andes	2
62	Universidad Peruana Unión	2
63	Universidad Tecnológica del Perú	2
64	Universidad Nacional Jorge Basadre Grohmann	1

Table 2: Ranking based on the number of papers published in 2018

N°	University	Papers SCOPUS 2018 (*P*)
1	Pontificia Universidad Católica del Perú	456
2	Universidad Nacional Mayor de San Marcos	427

3	Universidad Peruana Cayetano Heredia	411
4	Universidad Peruana de Ciencias Aplicadas S.A.C.	221
5	Universidad de San Martín de Porres	126
6	Universidad Nacional de Ingeniería	116
7	Universidad Nacional de San Agustín de Arequipa	115
8	Universidad Científica del Sur S.A.C.	101
9	Universidad de Ciencias y Humanidades	86
10	Universidad Nacional Agraria La Molina	83
11	Universidad Nacional de San Antonio Abad del Cusco	74
12	Universidad del Pacífico	66
13	Universidad San Ignacio de Loyola S.A.	63
14	Universidad Nacional de Trujillo	53
15	Universidad Continental S.A.C. (*7)	51
16	Universidad Privada del Norte S.A.C. -	47
17	Universidad de Piura	41
18	Universidad Católica San Pablo	34
19	Universidad Privada Antenor Orrego	31
20	Universidad de Ingeniería y Tecnología	31
21	Universidad Nacional Federico Villarreal	27
22	Universidad de Lima	27
23	Universidad Nacional de la Amazonía Peruana	26
24	Universidad ESAN	26
25	Universidad Nacional Pedro Ruiz Gallo	20
26	Universidad Nacional del Centro del Perú	19
27	Universidad Nacional del Altiplano	19
28	Universidad Católica de Santa María	18
29	Universidad Nacional de Piura	17
30	Universidad César Vallejo S.A.C.	17
31	Universidad La Salle	16
32	Universidad Nacional San Luis Gonzaga	14
33	Universidad Privada San Juan Bautista S.A.C. (*6)	13
34	Universidad Nacional de San Cristóbal de Huamanga	10
35	Universidad Peruana Unión	9
36	Universidad Católica Los Ángeles de Chimbote (*4) -	9
37	Universidad Alas Peruanas	9
38	Universidad Nacional Agraria de la Selva	8
39	Universidad Nacional del Santa	8
40	Universidad Nacional Santiago Antúnez de Mayolo	7
41	Universidad Nacional de Ucayali	7
42	Universidad Nacional Micaela Bastidas de Apurímac	7
43	Universidad Privada de Tacna	7
44	Universidad Nacional de Cajamarca	6
45	Universidad Nacional Toribio Rodríguez de Mendoza de Amazonas	6
46	Universidad Católica Santo Toribio de Mogrovejo -	6
47	Universidad Señor de Sipán	6
48	Universidad Nacional Jorge Basadre Grohmann	5
49	Universidad Peruana Los Andes	5
50	Universidad Autónoma del Perú	5
51	Universidad Nacional del Callao	4
52	Universidad Nacional de Huancavelica	4
53	Universidad Nacional Intercultural de la Amazonía	4
54	Universidad Ricardo Palma	4
55	Universidad Privada Norbert Wiener	4
56	Universidad Tecnológica del Perú	4
57	Universidad Nacional de San Martín	3
58	Universidad Nacional José María Arguedas	3
59	Universidad Andina Néstor Cáceres Velásquez	3
60	Universidad Andina del Cusco	3
61	Universidad Católica Sedes Sapientiae	3
62	Universidad Nacional Daniel Alcides Carrión	2
63	Universidad Nacional Autónoma de Chota	2
64	Universidad Nacional de Tumbes	1
65	Universidad Nacional Tecnológica de Lima Sur (*1)	1
66	Universidad Antonio Ruiz de Montoya	1

As indicated, these rankings are not equitable with small universities. In this sense, in Table III and Table IV, we can observe new classifications based on the $R_{p/r}$ ratio described in Section II for the years 2017 and 2018, respectively.

Table 3: Ranking using the ratio *Rp/r* for the year 2017

N°	University	REGINA Researchers (*R*)	Papers SCOPUS 2017 (*P*)	Paper 2017 / REGINA (*Rp/r*)
1	Universidad Nacional Federico Villarreal	1	27	27,00
2	Universidad Señor de Sipán	1	10	10,00
3	Universidad Continental S.A.C. (*7)	5	36	7,20
4	Universidad Católica Los Ángeles de Chimbote (*4) -	2	13	6,50
5	Universidad Nacional San Luis Gonzaga	4	24	6,00
6	Universidad Peruana de Ciencias Aplicadas S.A.C.	23	138	6,00
7	Universidad Privada del Norte S.A.C. -	8	36	4,50
8	Universidad Católica Santo Toribio de Mogrovejo -	3	13	4,33
9	Pontificia Universidad Católica del Perú	98	415	4,23
10	Universidad La Salle	1	4	4,00
11	Universidad Peruana Cayetano Heredia	104	402	3,87
12	Universidad Privada Antenor Orrego	12	44	3,67
13	Universidad ESAN	9	30	3,33
14	Universidad de Ciencias y Humanidades	13	39	3,00

15	Universidad Científica del Sur S.A.C.	23	64	2,78
16	Universidad de San Martín de Porres	42	101	2,40
17	Universidad Nacional de Piura	10	23	2,30
18	Universidad Ricardo Palma	13	29	2,23
19	Universidad Nacional de San Antonio Abad del Cusco	27	54	2,00
20	Universidad Nacional Daniel Alcides Carrión	1	2	2,00
21	Universidad del Pacífico	25	50	2,00
22	Universidad Católica Sedes Sapientiae	2	4	2,00
23	Universidad de Ingeniería y Tecnología	12	22	1,83
24	Universidad Nacional Pedro Ruiz Gallo	8	14	1,75
25	Universidad Nacional de San Cristóbal de Huamanga	6	10	1,67
26	Universidad Privada de Tacna	3	5	1,67
27	Universidad Católica San Pablo	32	51	1,59
28	Universidad Andina Néstor Cáceres Velásquez	2	3	1,50
29	Universidad de Piura	34	46	1,35
30	Universidad Privada San Juan Bautista S.A.C. (*6)	7	9	1,29
31	Universidad San Ignacio de Loyola S.A.	35	44	1,26
32	Universidad Nacional Mayor de San Marcos	303	366	1,21
33	Universidad Nacional de San Agustín de Arequipa	69	76	1,10
34	Universidad Nacional de Ucayali	3	3	1,00
35	Universidad Peruana Los Andes	2	2	1,00
36	Universidad Andina del Cusco	3	3	1,00
37	Universidad Privada Norbert Wiener	4	4	1,00
38	Universidad Nacional Micaela Bastidas de Apurímac	9	8	0,89
39	Universidad Nacional Agraria La Molina	88	76	0,86
40	Universidad de Lima	20	17	0,85
41	Universidad Nacional de Ingeniería	80	65	0,81
42	Universidad Nacional de Tumbes	9	7	0,78
43	Universidad Nacional Santiago Antúnez de Mayolo	8	6	0,75
44	Universidad Nacional José María Arguedas	4	3	0,75
45	Universidad Católica de Santa María	27	19	0,70
46	Universidad Nacional de Cajamarca	9	6	0,67
47	Universidad Nacional Intercultural de la Amazonía	3	2	0,67
48	Universidad Nacional Autónoma de Chota	3	2	0,67
49	Universidad Alas Peruanas	8	5	0,63
50	Universidad Nacional del Centro del Perú	15	9	0,60
51	Universidad Nacional de Huancavelica	5	3	0,60
52	Universidad Autónoma del Perú	5	3	0,60
53	Universidad Nacional de la Amazonía Peruana	22	13	0,59
54	Universidad Nacional de Trujillo	70	41	0,59
55	Universidad Nacional del Callao	6	3	0,50
56	Universidad Nacional de San Martín	5	2	0,40
57	Universidad Nacional del Altiplano	44	17	0,39
58	Universidad César Vallejo S.A.C.	29	10	0,34
59	Universidad Nacional del Santa	7	2	0,29
60	Universidad Peruana Unión	8	2	0,25
61	Universidad Tecnológica del Perú	9	2	0,22
62	Universidad Nacional Agraria de la Selva	10	2	0,20
63	Universidad Nacional Toribio Rodríguez de Mendoza de Amazonas	18	3	0,17
64	Universidad Nacional Jorge Basadre Grohmann	7	1	0,14

Table 4: Ranking using the ratio *Rp/r* for the year 2018

N°	University	REGINA Researchers (*R*)	Papers SCOPUS 2018 (*P*)	Paper 2018 / REGINA (*Rp/r*)
1	Universidad Nacional Federico Villarreal	1	27	27,00
2	Universidad La Salle	1	16	16,00
3	Universidad Continental S.A.C. (*7)	5	51	10,20
4	Universidad Peruana de Ciencias Aplicadas S.A.C.	23	221	9,61
5	Universidad de Ciencias y Humanidades	13	86	6,62
6	Universidad Señor de Sipán	1	6	6,00
7	Universidad Privada del Norte S.A.C. -	8	47	5,88
8	Pontificia Universidad Católica del Perú	98	456	4,65
9	Universidad Católica Los Ángeles de Chimbote (*4) -	2	9	4,50
10	Universidad Científica del Sur S.A.C.	23	101	4,39
11	Universidad Peruana Cayetano Heredia	104	411	3,95
12	Universidad Nacional San Luis Gonzaga	4	14	3,50
13	Universidad de San Martín de Porres	42	126	3,00
14	Universidad ESAN	9	26	2,89
15	Universidad Nacional de San Antonio Abad del Cusco	27	74	2,74
16	Universidad del Pacífico	25	66	2,64
17	Universidad Privada Antenor Orrego	12	31	2,58
18	Universidad de Ingeniería y Tecnología	12	31	2,58
19	Universidad Nacional Pedro Ruiz Gallo	8	20	2,50
20	Universidad Peruana Los Andes	2	5	2,50
21	Universidad Nacional de Ucayali	3	7	2,33
22	Universidad Privada de Tacna	3	7	2,33

23	Universidad Nacional Daniel Alcides Carrión	1	2	2,00
24	Universidad Católica Santo Toribio de Mogrovejo -	3	6	2,00
25	Universidad Privada San Juan Bautista S.A.C. (*6)	7	13	1,86
26	Universidad San Ignacio de Loyola S.A.	35	63	1,80
27	Universidad Nacional de Piura	10	17	1,70
28	Universidad Nacional de San Cristóbal de Huamanga	6	10	1,67
29	Universidad Nacional de San Agustín de Arequipa	69	115	1,67
30	Universidad Andina Néstor Cáceres Velásquez	2	3	1,50
31	Universidad Católica Sedes Sapientiae	2	3	1,50
32	Universidad Nacional de Ingeniería	80	116	1,45
33	Universidad Nacional Mayor de San Marcos	303	427	1,41
34	Universidad de Lima	20	27	1,35
35	Universidad Nacional Intercultural de la Amazonía	3	4	1,33
36	Universidad Nacional del Centro del Perú	15	19	1,27
37	Universidad de Piura	34	41	1,21
38	Universidad Nacional de la Amazonía Peruana	22	26	1,18
39	Universidad Nacional del Santa	7	8	1,14
40	Universidad Peruana Unión	8	9	1,13
41	Universidad Alas Peruanas	8	9	1,13
42	Universidad Católica San Pablo	32	34	1,06
43	Universidad Andina del Cusco	3	3	1,00
44	Universidad Privada Norbert Wiener	4	4	1,00
45	Universidad Antonio Ruiz de Montoya	1	1	1,00
46	Universidad Autónoma del Perú	5	5	1,00
47	Universidad Nacional Agraria La Molina	88	83	0,94
48	Universidad Nacional Santiago Antúnez de Mayolo	8	7	0,88
49	Universidad Nacional Agraria de la Selva	10	8	0,80
50	Universidad Nacional de Huancavelica	5	4	0,80
51	Universidad Nacional Micaela Bastidas de Apurímac	9	7	0,78
52	Universidad Nacional de Trujillo	70	53	0,76
53	Universidad Nacional José María Arguedas	4	3	0,75
54	Universidad Nacional Jorge Basadre Grohmann	7	5	0,71
55	Universidad Nacional de Cajamarca	9	6	0,67
56	Universidad Nacional del Callao	6	4	0,67
57	Universidad Nacional Autónoma de Chota	3	2	0,67
58	Universidad Católica de Santa María	27	18	0,67
59	Universidad Nacional de San Martín	5	3	0,60
60	Universidad César Vallejo S.A.C.	29	17	0,59
61	Universidad Tecnológica del Perú	9	4	0,44
62	Universidad Nacional del Altiplano	44	19	0,43
63	Universidad Nacional Toribio Rodríguez de Mendoza de Amazonas	18	6	0,33
64	Universidad Ricardo Palma	13	4	0,31
65	Universidad Nacional Tecnológica de Lima Sur (*1)	8	1	0,13
66	Universidad Nacional de Tumbes	9	1	0,11

Likewise, in Table V, one can see the ranking developed using the $R_{p/a}$ ratio also described in the previous section.

Table 5: Ranking using the $R_{P/A}$ ratio

N°	University	Papers SCOPUS (*P*)	Authors SCOPUS (*A*)	Paper / Authors (*Rp/a*)
1	Universidad Católica Los Ángeles de Chimbote (*4) -	35	10	3,50
2	Universidad Nacional Tecnológica de Lima Sur (*1)	3	1	3,00
3	Universidad Privada del Norte S.A.C. -	111	37	3,00
4	Universidad La Salle	39	13	3,00
5	Universidad Científica del Sur S.A.C.	430	154	2,79
6	Universidad San Ignacio de Loyola S.A.	181	76	2,38
7	Universidad Peruana Cayetano Heredia	4742	2088	2,27
8	Universidad Nacional José María Arguedas	9	4	2,25
9	Universidad del Pacífico	267	128	2,09
10	Universidad ESAN	200	98	2,04
11	Universidad Continental S.A.C. (*7)	116	59	1,97
12	Pontificia Universidad Católica del Perú	2899	1515	1,91
13	Universidad de Ciencias y Humanidades	170	90	1,89
14	Universidad de San Martín de Porres	558	310	1,80
15	Universidad Nacional Micaela Bastidas de Apurímac	32	18	1,78
16	Universidad Nacional Mayor de San Marcos	4378	2471	1,77
17	Universidad Andina Néstor Cáceres Velásquez	7	4	1,75
18	Universidad Antonio Ruiz de Montoya	7	4	1,75
19	Universidad Nacional Toribio Rodríguez de Mendoza de Amazonas	13	8	1,63
20	Universidad Nacional Autónoma de Chota	8	5	1,60
21	Universidad Católica San Pablo	187	121	1,55
22	Universidad Nacional de Ingeniería	687	447	1,54
23	Universidad Ricardo Palma	234	155	1,51
24	Universidad Peruana Unión	31	21	1,48
25	Universidad Nacional de Ucayali	22	15	1,47

26	Universidad Nacional de Piura	122	84	1,45
27	Universidad Nacional de la Amazonía Peruana	219	151	1,45
28	Universidad Nacional de San Antonio Abad del Cusco	523	361	1,45
29	Universidad Privada de Tacna	23	16	1,44
30	Universidad Privada Antenor Orrego	160	112	1,43
31	Universidad de Lima	125	88	1,42
32	Universidad Alas Peruanas	31	22	1,41
33	Universidad Nacional Santiago Antúnez de Mayolo	39	28	1,39
34	Universidad Nacional Agraria La Molina	641	462	1,39
35	Universidad Nacional Federico Villarreal	172	126	1,37
36	Universidad César Vallejo S.A.C.	47	35	1,34
37	Universidad Andina del Cusco	16	12	1,33
38	Universidad Católica Sedes Sapientiae	16	12	1,33
39	Universidad Nacional de Cajamarca	78	59	1,32
40	Universidad de Ingeniería y Tecnología	89	68	1,31
41	Universidad Autónoma del Perú	12	10	1,20
42	Universidad de Piura	285	239	1,19
43	Universidad Nacional Agraria de la Selva	48	41	1,17
44	Universidad Peruana Los Andes	14	12	1,17
45	Universidad Nacional Daniel Alcides Carrión	15	13	1,15
46	Universidad Privada Norbert Wiener	15	13	1,15
47	Universidad Nacional de San Martín	24	21	1,14
48	Universidad Nacional Jorge Basadre Grohmann	30	27	1,11
49	Universidad Nacional de San Agustín de Arequipa	475	429	1,11
50	Universidad Nacional San Luis Gonzaga	94	85	1,11
51	Universidad Privada San Juan Bautista S.A.C. (*6)	42	38	1,11
52	Universidad Nacional de Trujillo	364	330	1,10
53	Universidad Nacional del Altiplano	111	101	1,10
54	Universidad Nacional del Santa	20	19	1,05
55	Universidad Señor de Sipán	20	19	1,05
56	Universidad Católica de Santa María	117	113	1,04
57	Universidad Nacional Pedro Ruiz Gallo	98	95	1,03
58	Universidad Nacional Intercultural de la Amazonía	11	11	1,00
59	Universidad Tecnológica del Perú	27	27	1,00
60	Universidad Nacional de San Cristóbal de Huamanga	41	44	0,93
61	Universidad Peruana de Ciencias Aplicadas S.A.C.	875	953	0,92
62	Universidad Nacional del Centro del Perú	56	73	0,77
63	Universidad Nacional del Callao	16	21	0,76
64	Universidad Nacional de Huancavelica	34	48	0,71
65	Universidad Nacional de Tumbes	22	36	0,61
66	Universidad Católica Santo Toribio de Mogrovejo -	46	76	0,61

Through these results can be observed that small universities rise in position when we compare the results of Table I and Table II with the results of Table III and Table IV.

4. Discussion and Conclusions

From Table I and Table II, it can be seen that most universities have a growth in the number of publications from 2017 to 2018. This growth is mainly due to the increasing importance that has been given to research in Peru due to many factors, among them, the new University Law, the accreditation process, and the competitive funds to finance research projects. It can be seen that the universities with the highest growth are Universidad Nacional Jorge Basadre Grohmann with 400 percent growth and Universidad Peruana Unión with 350 percent growth. Likewise, it can be seen that there are universities that show a decrease, these being the universities Universidad Ricardo Palma with 86.21 percent of regression and Universidad Nacional de Tumbes with 85.71 percent of regression. One can see in Figure 6, all publication evolution from 2017 to2018 for the Peruvian universities.

The fact of using the number of REGINA researchers as a reference to taking into account the size of the university responds to the fact that there are opinions that indicate that not all professors carry out research, while REGINA investigators are called to carry out research. However, it is also true that some professors are not REGINA and publish scientific articles, as well as students who have publications. In that sense, the use of the number of authors identified in SCOPUS could be the best option.

In Figure 7, the distribution of the best 20 universities can be observed according to the different parameters considered in this study.

Finally, one can conclude that when one not only take into account the number of published scientific articles but also the size of the university, the ranking changes drastically resulting in great surprises, mainly in small universities that invest in research

References

[1] L. Medic, and J. Cieza, “Design projects in the first three years of a computing program”, III IEEE World Engineering Education Conference – EDUNINE 2019, March 2019, Lima - Peru.

[2] Einstein, Albert. Einstein on politics: His private thoughts and public stands on nationalism, Zionism, war, peace, and the bomb. Princeton University Press, 2013.

[3] Gonzalez, Avid Roman. "Investigación: Oportunidad de Desarrollo."; XIII Congreso Nacional de Computacion, Informatica y Sistemas-CONACIS 2010. 2010.

[4] Lastra, Javier Ulises Solis. "Tax Incentive to Promote Research Development and Innovation in Peru." 2018 IEEE Sciences and Humanities International Research Conference (SHIRCON). IEEE, 2018.

[5] De-Moya-Anegón, Félix; Herrán-Páez, Estefanía; Bustos-González, Atilio; Corera-Álvarez, Elena; Tibaná-Herrera, Gerardo (2018). Ranking Iberoamericano de instituciones de educación superior. SIR Iber 2018. Barcelona, España: Ediciones Profesionales de la Información SL. ISBN: 978 84 09 03911 1. https://doi.org/10.3145/sir-iber-2018.

[6] Ránking Universidades Perú | AméricaEconomía. (2017). Rankings.americaeconomia.com. Retrieved 26 January 2017, from http://rankings.americaeconomia.com/2016/universidadesperu/metodologia.

[7] SUNEDU, “Informe Bienal Sobre la Realidad Universitaria Peruana”, First Edition, 2018. https://www.sunedu.gob.pe/informe-bienal-sobrerealidad-universitaria/.

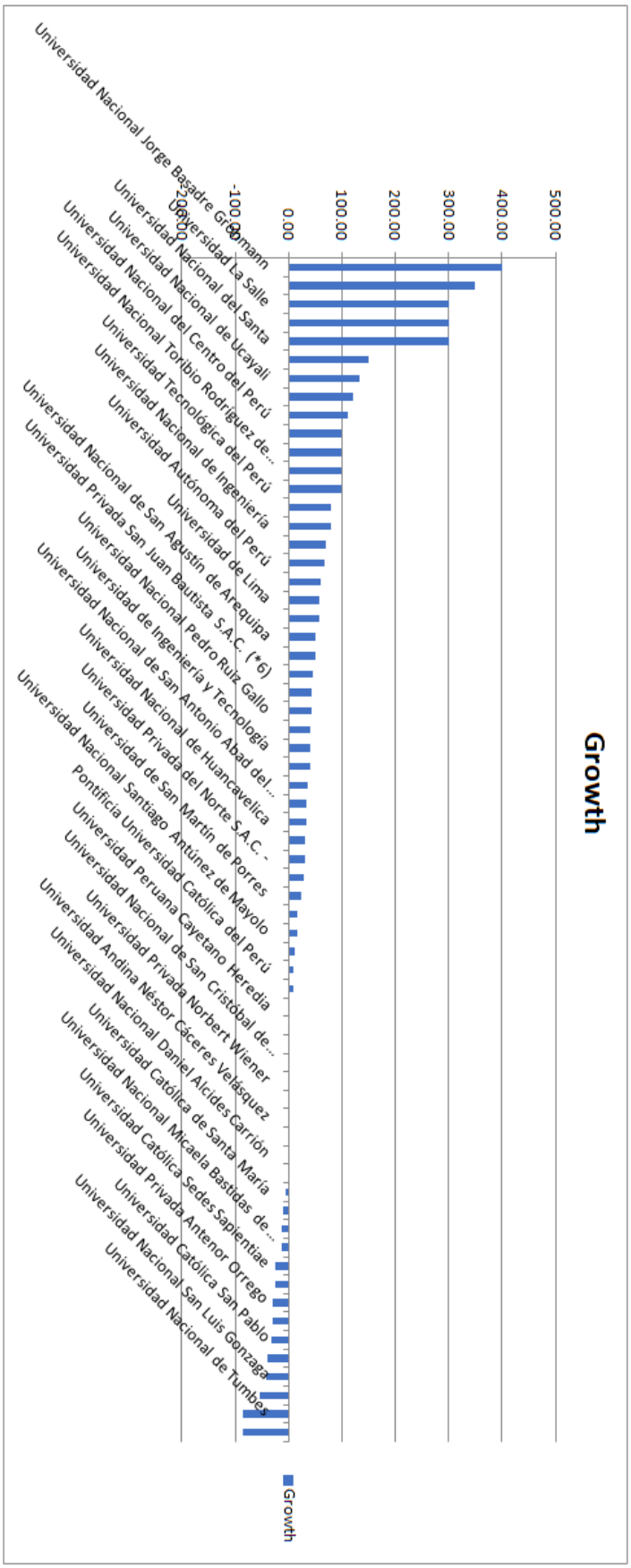

Figure 6: Distribution of the top 20 universities according to the number of publications and the ratios *Rp/r* and *Rp/a*

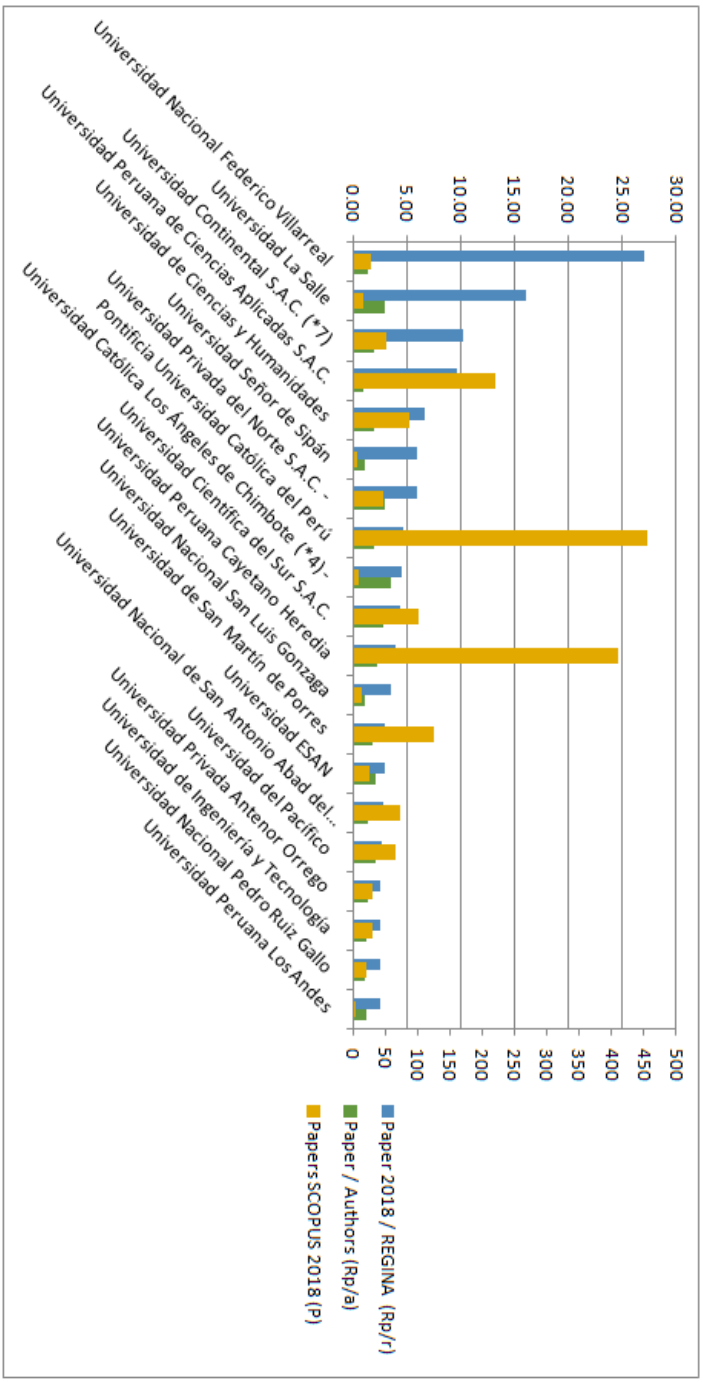

Figure 7: Distribution of the top 20 universities according to the number of publications and the ratios *Rp/r* and *Rp/a*

[8] Docampo, D.; Herrera, F.; Luque-Martínez, T.; Torres-Salinas, D. (2012). Efecto de la agregación de universidades españolas en el Ranking de Shanghai (ARWU): caso de las comunidades autónomas y los campus de excelencia. El Profesional de la Información, 21 (4), 428-432. https://doi.org/10.3145/epi.2012.jul.16.

[9] Webometrics, "Ranking de Universidades", Edition 2018 2.1.2, http://www.webometrics.info/.

[10] QS, "Top Universities", https://www.topuniversities.com/qs-worlduniversity-rankings.

[11] SIR Methodology. (2017). Scimagoir.com. Retrieved 26 January 2017, from http://www.scimagoir.com/methodology.php.

[12] Ahmad, Mohammad Esmail, et al. "The Role of Information Technology on Teaching Process in Education; An Analytical Prospective Study at University of Sulaimani." INTERNATIONAL JOURNAL OF ADVANCED COMPUTER SCIENCE AND APPLICATIONS 9.11 (2018): 512-521.

[13] U. Lapa-Asto, G. Tirado-Mendoza, and A. Roman-Gonzalez, “Impact of Formative Research on Engineering Students”, III IEEE World Engineering Education Conference – EDUNINE 2019, March 2019, Lima - Peru.
[14] Roman-Gonzalez, Avid, and Natalia I. Vargas-Cuentas. "Scientific Production in the 50 First Universities Licensed by SUNEDU." 2018 IEEE Sciences and Humanities International Research Conference (SHIRCON). IEEE, 2018.
[15] Mayta-Tristán, Percy, et al. "Producción científica y licenciamiento de escuelas de medicina en el Perú." Revista Peruana de Medicina Experimental y Salud Pública 36.1 (2019): 106-15.
[16] Estrada-Cuzcano, Alonso, and Karen Lizeth Alfaro-Mendives. "A propósito de REGINA: los investigadores de la Facultad de Letras y Ciencias Humanas." (2017).
[17] SUNEDU. "Informe Bienal Sobre la realidad Universitaria Peruana", Impresión Arte Peru SAC, Primera Edicion, 2018

ASTES

Advances in Science, Technology and Engineering Systems Journal
Vol. 4, No. 4, 404-413 (2019)
www.astesj.com
Special Issue on Advancement in Engineering and Computer Science

ASTES Journal
ISSN: 2415-6698

Supporting Better Physical Activity in a Smart City: a Framework for Suggesting and Supervising Walking Paths

Mário Rodrigues[*,1], Rita Santos[2], Alexandra Queirós[1], Anabela Silva[3], João Amaral[1], Patrícia Simões[3], Jorge Gonçalves[4], Ciro Martins[1], António Pereira[5], Nelson Pacheco da Rocha[6]

[1]*ESTGA & IEETA, University of Aveiro, 3810-193 Aveiro, Portugal*

[2]*ESTGA & DigiMedia, University of Aveiro, 3810-193 Aveiro, Portugal*

[3]*ESSUA & CINTESIS.UA, University of Aveiro, 3810-193 Aveiro, Portugal*

[4]*ESTGA & GeoBioTec, University of Aveiro, 3810-193 Aveiro, Portugal*

[5]*ESTG & CIIC, Polytechnic Institute of Leiria, 2411-901 Leiria, Portugal*

[6]*DCM & IEETA, University of Aveiro, 3810-193 Aveiro, Portugal*

ARTICLEINFO

Article history:
Received: 01 June, 2019
Accepted: 27 July, 2019
Online: 20 August, 2019

Keywords:
mHealth
Smart City
Walk Paths
Mobile App
Health Professional Back-Office

ABSTRACT

The increase of elderly population creates the need to promote healthy aging, with autonomy and independence, for preserving the functional capacity and quality of life as much as possible. To achieve this goal the recommendations include walking a certain amount of steps daily, given that the exact amount of steps changes with age, lesions, and chronic health conditions that can affect health and well-being.
Understanding how much exercise is adequate for an individual requires specialized knowledge and training. It is important to avoid risks that include: (1) be too aggressive in exercising and increase injuries, create new ones, and later refrain in exercising more; or (2) be too conservative and in the long run have an activity level under each one's potential and below what is recommended.
In this article is proposed and discussed a framework that aims to support people having an adequate level of activity for its particular condition and to do it without disrupting daily routines. The framework is supported by a software system built for monitoring well-being and physical activity in the context of Smart Cities. The system is composed by: (1) smartphone applications that interact with the end-user for showing possible exercises and walk routes, and that collects some relevant data; (2) a back-office application that collects and presents data obtained from the smartphone applications. The back-office application is designed for health professionals to follow users' progression over time, to recommend new exercises or to correct less optimal situations.
The first tests with a system implementing this framework show that the solution is robust and able to be used in a large scale.

1 Introduction

This paper is an extension of work originally presented in 2018 2nd International Conference on Technology and Innovation in Sports, Health and Wellbeing (TISHW) [1].

Active and healthy aging is important as individuals should have the best life possible and this usually means a long and healthy life. It is important for individuals as well as for communities since a political concern is the mounting pressure on national health services of aging societies due to the ever larger proportion of elderly population. Therefore it is important to minimize costs associated to assistance to people and digital technologies can give an important contribution. As healthier aging benefits both individuals and societies, there is a growing awareness of the importance of promoting it, with autonomy and independence, and preserving each one's functional capacity.

The question is thus: how to help people aging with good health? Several studies suggest that monitoring people's level of activity has the potential to foster health and well-

[*]Mário Rodrigues, IEETA – Campus Universitário de Santiago, Aveiro, Portugal, Tel. +351 234 370 500 & mjfr@ua.pt

being by transforming it from an individual goal towards a collective and social goal [2, 3]. Some experiments have concluded that the use of information and communication technology (ICT) enabled devices to collect individual performance data, a communication network for sharing those data, can contribute to increase the activity levels and to promote community building. Other studies go further ahead and infer that connecting residents and municipal health professionals through digital applications can decrease ansiety levels thus increasing well-being and promoting a sense of comfort as for instance to reassure young parents that a nurse is as close as a click of a button [2]. Mobile health (mHealth) is a paradigm that refers to medical and health practice supported by mobile devices. Despite the rapid growth of mHealth, mainly due to the significant growth in mobile device penetration [4], there are still a number of challenges including the need of having a high degree of security, reliability, quality, and effectiveness. Technological advances (e.g. accelerometers) have allowed for the objective measurement and characterization of physical activity and sedentary behavior in terms of volume, duration, intensity and frequency. This helps to personalize strategies and interventions aiming to increase physical activity and decrease sedentary behavior as well as goal setting [5]. Most mobile applications (apps) related to health, well-being, and physical exercise are not properly validated or under the supervision of health professionals, even though some are quite popular and well rated by users [6]. Privacy concerns also arise when apps collect and store data. The importance and potential impact on people's life of health related advices and personal information makes it a quite sensitive topic to be explored without proper validation and supervision.

In this paper we discuss and present a framework for a monitoring system of wellbeing and physical activity in the context of Smart Cities. The framework is more than a single mHealth app as it is designed for health professionals take control and operate the system, having access to user specific information as well as to contextual information about users' environment.

Although the proposed framework is more than an app, as it will have health professionals operating the system and will take into consideration contextual and user specific information, the app is a key component as it will be the interface for end users. The back-office component is designed to work with a range of alternative apps however it is important to provide a default app that, at least, works as a showcase of good practices and helps to illustrate the framework potential.

The framework is designed for the global Smart City, in the sense that its technical solutions and its conceptual approach take advantage of sensor and city state information. The framework is deployed in a concrete Smart City: the Smart City of Águeda that is a member of the Open and Agile Smart Cities. Águeda was selected for two reasons: (1) it is recognized nationally and internationally as one of the most dynamic Smart Cities of Portugal; (2) it belongs to a region where the proportion of elder population is increasing, as in many other Portuguese and European areas. The Portuguese census of 2011 showed that 22,5% of the population of in this region was 65 years old or more.

From the city authorities perspective, collecting information where people usually practice outdoor exercise, or stroll, is valuable for planning public spaces. More and better infrastructures like fitness equipment, benches for people to seat and rest for a while, children's playgrounds, sports equipment as Basketball fields, among other, can be better located if city officials posses such information. Also, concerning mobility, is important to know here people concentrate when deciding the location of bicycle parking structures, electrical vehicle's chargers, bus stops, and so on and so forth [7].

After the introduction in this section, section II presents the relevant background and related work on smart city projects and on mHealth and related mobile applications. The third section explains the developed work, discussing the relevant implementation details and presenting the interface of the system. The following section, Section IV, discusses the main features of the proposed framework and explains how it helps to mitigate known shortcomings in current mHealth solutions. The paper ends with the conclusions in section V.

2 Background and Related Work

This section will first provide some background information on smart cities followed by recent relevant projects on this topic. Then, the section introduces background information on mHealth ending with a description of three of the most popular apps for mHealth.

2.1 Smart Cities

Smart City has become a key marketing term for researchers and politicians to justify technological investments in urban areas. Several cities and less dense urban areas in quite different stages of development claim to be smart, with no clear definition of what a Smart City is. One universally accepted aspect is that ICT are the smartness enabler. With this reality in mind, some researchers have identified a minimal set of features that must fulfilled for an urban area be able to claim its smartness [8]. It is widely accepted that to be considered smart an urban area must: (1) have an explicit agenda about the development of its smartness; (2) providing open data about itself; (3) provide software services or mobile applications that may be used widely; and (4) have some kind of digital infrastructure that allow data communication in its area of actuation.

As a measurement of the order of magnitude of smart city initiatives, a study from 2017 [8] found that "more than 300 cities of all types and sizes participate in approximately 40 coalitions, thinking tanks and forums or are being advised by organizations, in their attempts to co-define their innovative future, while most of them claim to be smart, and almost all cities want to engage in this era". Smart cities aim to improve the quality of life for residents and visitors. As such, most of the city's intelligence indicators are defined with respect to the potential impact on people's lives. The study conducted in [9] lead to the observation that "a Smart City is quintessentially enabled by the use of technologies (especially ICT) to improve competitiveness and ensure a more sustainable future by symbiotic linkage of networks of peo-

ple, businesses, technologies, infrastructures, consumption, energy and spaces".

The European Union (EU) adopted an indicator that measures the city's smartness according to six dimensions [9, 10]. This indicator is also adopted here because of its relevance and because the proposed framework will be implemented in an EU city, and the dimensions are:

1. Smart Governance - relates to the degree of citizen participation in public life, transparency of governance, and the quantity and quality of public and social services.
2. Smart Economy - how competitive is the economy measured by its innovative spirit, entrepreneurship, international insertion, among other.
3. Smart Mobility - addresses concerns such as the existence of transport infrastructure considering (inter-)national and local accessibility, availability of IT infrastructure, and sustainability of the transportation system.
4. Smart Environment - what is the concern level about natural resources, including environmental conditions, air quality, sustainable resource management and ecological awareness.
5. Smart People - is about human and social capital, including the level of qualification, the promotion of lifelong learning and ethnic plurality, and the openness of minds.
6. Smart Living - is relative to the quality of life, including cultural and educational facilities, health conditions, quality of housing and tourist attractiveness, among other.

Smart City initiatives can address any combination of these six dimensions, and can be quite distinct in terms of goals and technical solutions adopted. For example, innovation in Smart Living includes transformations in construction, urban planning and renovation of facilities whereas innovation in Smart Mobility may involve tracking systems, and in Smart Governance may just entail a change in official procedures without further material investment. Overall, solutions that drive initiatives may involve cyber-physical integration of sensors and other hardware, or be primarily a software engineering challenge to generate new applications and services, or be more closely related to data science and analysis of big data. Considering the six dimensions of the EU smart city indicator, the framework proposed is aligned with the Smart Living dimension. As such, here will be described works that contribute to Smart Living and that are ready to be deployed in a real context.

2.1.1 i-SCOPE

The i-SCOPE project – interoperable Smart City services through an Open Platform for urban Ecosystems [11] covers four dimensions of the Smart City indicator: Living, Environment, Mobility, and People. In the context of the project was developed an open platform that supports three services: (1) optimization of buildings energy consumption through the precise evaluation of the potential and loss of solar energy; (2) environmental monitoring through real-time noise mapping, leveraged by the involvement of citizens, as citizens and their mobile devices can act as sensors, thus being able to measure noise levels throughout the city in a distributed way; and (3) a service more related to this work, which aims to improve the inclusion and personal mobility of elderly citizens and mobility difficulties. In this context, the platform presents a detailed urban layout, with features and barriers, to allow a precise and personalized routing service that takes into account the characteristics of individuals and the city [11]. The i-SCOPE had pilots implemented in the cities of Wien (Austria), Newcastle (United Kingdom), Indjija (Serbia), Lázio Region (Italy), and Zadar County (Croatia).

2.1.2 Amsterdam Smart City Platform

The Amsterdam Smart City Platform [12, 13] is an initiative that includes several projects developed and implemented in Amsterdam (The Netherlands). Being a comprehensive initiative, it contributes to the various profiles of the Smart City indicator. From the set of projects that contribute to the profile of Living, two are related more related to the framework discussed in this work: VITAMINE [14] and PAUL - Active Urban Living based on playful data [15].

The VITAMINE project, dubbed the Dutch word for vitamin, was created to help the elderly who are looking for a suitable lifestyle [14]. The idea is to increase the frequency of training activities by providing and supporting an additional home workout program. The absence of an exercise supervisor or instructor is mitigated by the availability of online support. In addition, it also focuses on the diet of its users and the example given is to examine whether the use of extra protein has or does not effect on exercise.

The PAUL project aims to understand how the physical activity of city dwellers can be increased using custom apps [15]. It is observed that different apps to stimulate people to exercise exercise use different strategies [6]. The way to encourage more exercise, or at least maintain the same level of activity, varies and can be motivational messages, games, or peer comparison. The project assumes that the type of app that works best for a particular person is a highly individual choice. Thus, the project studies how to make the best match between the user and the app.

2.2 mHealth

Health Apps are a good option for the elderly especially because of its mobility and portability. However, some important issues need to be addressed since older people often find it difficult to use new technologies including smartphones and respective apps [16]. However, the Internet and the use of smartphones among the elderly population will increase in the near future, as the elderly in the future will be more likely to use the Internet to search information than the elderly today. In addition, they are concerned about health and are likely to use the Internet for health-related issues [17]. Thus, there seems to be a potential interest in older adults to use mHealth apps, which is essential for these systems to be adopted by that group.

The development of new ICT applications, especially those that need mobile devices or the Internet, should help reduce the digital divide. This suggests that, in order to have an application accessible to a large group of older adults, it is appropriate to opt for a human-centered design process whose key premises are the active involvement of users in the development process as well as in the evaluation of interactive systems [18]. In addition, a human-centered design choice also appears to be a valuable approach when developing a mobile health application for other stakeholders, such as health professionals.

Experiments exist with context-aware recommender system that offers personalized recommendations of exercise routes to people according to their medical condition, and real-time information from a smart city [19]. This recommender has predefined routes and selects the best route based on a memory-based method that employs neighborhood search (to determine groups of similar users) and on information such as air quality, ultraviolet radiation, wind speed, temperature, and precipitation. The user can then select the best course according to their profile (age, effort, distance) and can inform the system about unexpected situations that could affect other users. Users can also propose new routes [19].

There are dozens of fitness apps and discussing a representative set here would not bring further insights into discussion. Nevertheless, here will be described three popular and feature-full apps selected from dozens due to their higher ratings voted by hundreds of users, for better understanding of what is being made and the real potential of such applications. The first application was developed for iOS and Android, the second one just for iOS, and the third one just for Android.

2.2.1 Pacer Pedometer & Step Tracker

This app uses a set of parameters based on the smartphone sensors and usage patterns to classify the user's lifestyle from sedentary to highly active [20]. It contains a step counting algorithm, and allows to check the performance over a certain period of time, presenting results using graphics for easier reading. The historical data is recorded and can be used to check whether or not the user has progressed against their goal, in terms of number of steps per day as well as calorie and weight loss. A set of predefined objectives are defined to give users a sense of progression. The app encourages users to exercise in case of a long period of poor activity, and it has a social component in which users, besides being able to share the number of steps taken, can also encourage friends to exercise as well.

2.2.2 The Walk: Fitness Tracker Game

This app was created in conjunction with United Kingdom's National Health Service and essencially is a game to stimulate people to walk more often [21]. The apps monitors the activities of the user to verify if the user is walking, provides several stories and users are required to move for progressing in the story. So this app is masked in a game for encouraging people to reach the adequate number of steps per day thus improving their health. As such, it motivates users to follow the story and not so much to take into account the number of steps or distance traveled.

2.2.3 Pedometer - Step Counter

The main feature of this app is a step counter. As a secondary functionality, it computes several metrics acquired through specifically designed exercises [22]. The application records the evolution of the metrics over time. Users can have training plans focused on each part of the body with the purpose of achieving their own goals more efficiently, addressing more specifically the part of the body they intend to exercise. It includes several other tests possible using the smartphone sensors such as hearing test and color blindness test.

3 Developed Work

The objective of this framework is to explain how mHealth can be further improved by making sure that health professionals are at the core of the decisions, without hindering the vibrant existing mHealth app market. Having health professionals at the core of the decisions means that users are followed by health professionals, and not just by algorithms or predefined generic reference values, and that they are in control of the recommendations passed to users having the ability to take into account the individual health history or recent changes in its health conditions. Health professionals also have access to contextual information such as weather conditions, points of interest and sidewalk conditions, among others, to obtain an accurate perspective of the real environment where users will develop their walks. They are able to recommend (new) exercises and walk paths, or introduce the necessary changes to correct less optimal situations.

3.1 Framework Description

Figure 1 depicts the proposal overview. Distinct type of mHealth apps are able to interact with the back-office application. At the top of the figure is represented a health professional analyzing the users' data and assuring that they have the best possible walk program, at the bottom of the picture are represented some users doing their exercises, and between them is a system composed by the communication networks and by the back-office.

Two health professionals helped defining the requirements of the framework, of the back-office application, and helped to define personas to guide the user experience requirements. The requirements identified for the back-office application are discuss in detail in [1]. The back-office application is composed by five main modules:

1. Health professional interface - is a web based graphical user interface that integrates information from the other components, presenting it to health professionals in an intuitive and organized way. The interface is multi-user as distinct health professionals can follow distinct sets of end-users. Also there is the ability to share users to accommodate events such as vacations or planned leaves. It is considered particularly important providing an area where health professionals can

find all essential information to support their decision-making process, making it easier, faster and less prone to errors. The two interface panels presented as Figures 2 and 3 will be explained next.

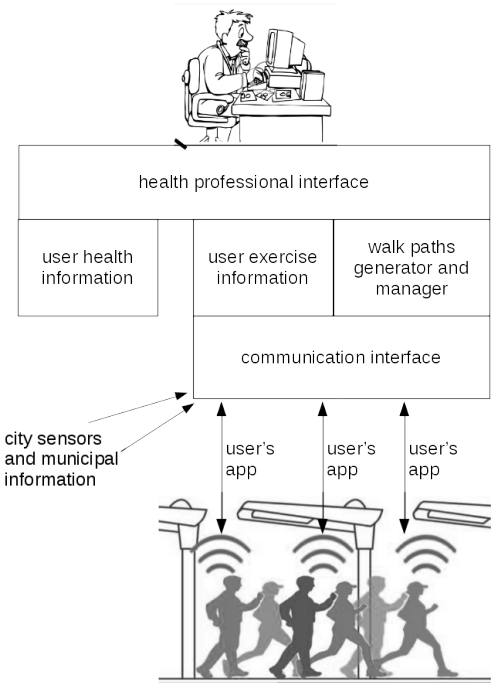

Figure 1: Depiction of the core actors of the system with details regarding the dataflow and the main system modules.

2. User health information module - manages health information that is private and sensitive. This information is never accessible to the mobile app or to any other module than the health professional interface. The informaton is stored in a specific and isolated database and it is inserted by the health professional when the user subscribes the service. This information is updated whenever the user meets with the health professional responsible for its follow up. Fig. 2 presents a screen-shot of the health professional interface relative to this module. The left panel contains generic information such as user's name, contacts, weight and height, and education. The right panel contains the user's medical record that includes heart rate, blood pressure, six minute walking test (6MWT), regular medication, and a medical record of some relevant conditions. No special concern about data security – other than stock data encryption - was taken care in the prototype development as, when deployed, these part of the system needs to comply to the specific norms of each instituion and/or can just be a reference to an already existing database.

3. Exercise information module - manages user exercise information that, being private information, is not as sensitive as the one managed by the user information module. Since this module interacts with the communication interface that, by its turn, interacts with the (third party) apps, there exists an increased factor of vulnerability. For that reason this module does not explicitly have information about the user. The user is referred by a code that does not encode personal information. This code is for the health professional interface query the user health information module about which user corresponds to a given code. When this happens the user health information module just replies if that health professional is authorize to view such data. Fig. 3 presents the health professional interface relative to the exercise information. In the left panel is visible the resume of the user, at the center a map showing the walk routes suggested to the user and, at the right panel, the amount of times the user walked those courses.

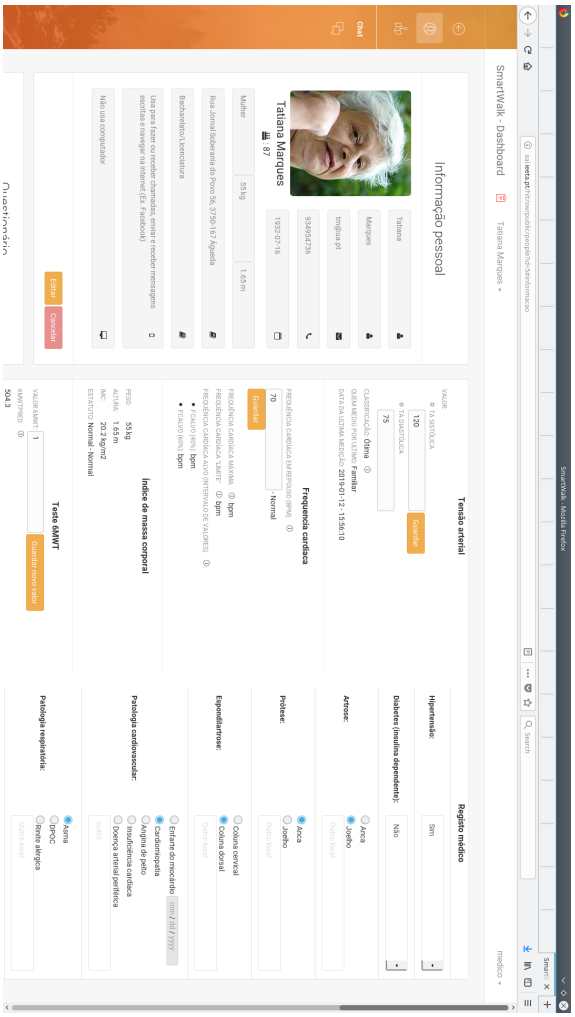

Figure 2: The back-office screen to insert and visualize health information of one user.

4. Walk paths generator and manager - this module allows to generate paths using multi-criteria [23]. It is possible ask for path of a given distance, to force paths to include given places - like rest areas or streets without cars - and also to exclude some areas such as more polluted areas or less safe. Then the algorithm optimizes the rest of the path by preferring streets with larger sidewalks, avoid the busiest roads, etc [23]. The interface of this module is a contextual menu that

pops up by right-clicking at the map of the exercise interface (see menu inside the map in Figure 3).

5. Communication interface - is handles all data received from or passed to the apps, receives data from the city sensors (temperature, wind, air quality,...) and from the municipality information systems (roads/streets under maintenance, social events,...). This interface is implemented as a RESTful Web Service and so it does not start a communication by its initiative. When the system has to pass information to someone, that information is stored and later sent when the mobile app initiates a communication with the system and ask for such information. If the health professional needs to contact the user the contact request goes by alternative ways such as short message service (SMS) or e-mail.

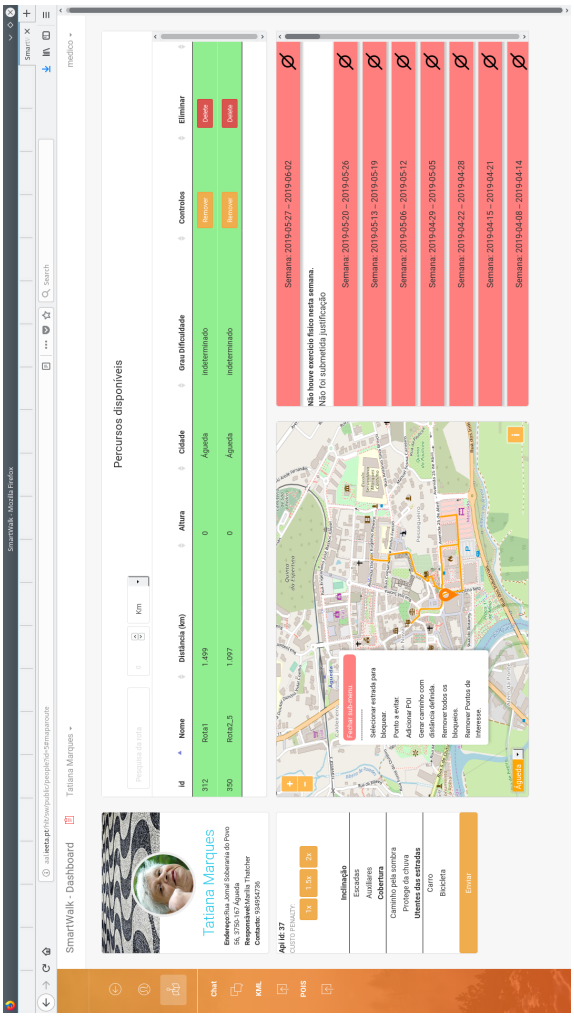

Figure 3: The back-office screen to define a walk plan for a given person, and to see how often that plan was executed.

3.2 Data Transport

The ability to allow distinct apps to interact with the back-office application implies a public definition of the data to be passed between the apps and back-office, besides the implementation of the communication interface.

The back-office sends to the app free text messages for users' information in JavaScript object notation (JSON). To send the walk paths, the back-office application generates a file in keyhole markup language (KML) format, places that file in an externally acessible universal resource location (URL), and sends that URL in the JSON message.

The data transport is made by JSON and a data package can contain one or more of the following sections: (1) user messages, (2) physical activity, (3) heart data, (4) inactivity justification.

All data packages include a code that represents the user. This code does not contain personal information as mentioned before, is used for the back-office associate the received data with the respective user. As such, in case of communication interception is not possible to identify the user just by looking to the data package.

All pieces of information have a timestamp representing when that information was generated. These timestamps are used for correctly build the events timeline at the back-office. As users can use apps without an active data link the time when the information arrives at the back-office can be quite distinct of when it was generated.

The section "User Messages" contains information written by users. It can have any free text message the user wants to share with the health professionals, namely questions regarding any concern he may have. This specific part of the package is bi-directional in the sense that the healt professional can use it to send messages (questions) to users. It also includes information about medications the user is taking. Table 1 presents an example of a message.

Table 1: Example of a "user messages" section.

```
"User Messages": [{
  "Message": {
    "Text": "Everything is OK",
    "Time Stamp": "2019-01-09  15:56:10"
  }},{
  "Medications": [{
      "Name": "Placebo 1",
      "Time Stamp": "2019-01-09  15:56:10",
      "Amount": 10,
      "Reason": "Arrhythmia"
    }, {
      "Name": "Placebo 2",
      "Time Stamp": "2019-01-09  15:56:10",
      "Amount": 4,
      "Reason": "Headache"}]}]
```

The section "Physical Activity" includes information of routes walked by users and how was the experience in terms of satisfaction, polution, etc. It includes information about how many stops the user has made during the course because it is an indicator of problems - it should be considered a stop if the user remains at the same place for a minute or more. It is also collected information about if any pain was felt and its location, the total duration of the walk, and a list of global positioning system (GPS) coordinates representing the actual path made. Table 2 presents an example of this data section.

Table 2: Example of a "physical activity" section representing that the route 305 was walked during 40 minutes with two stops, the first during 1 minute and the second for 10 minutes.

```
"Physical Activities": [{
  "Physical Activity": {
    "Active": {
      "Start": "2019-01-09 15:56:10",
      "Stop": "2019-01-09 16:36:10",
      "Route": {
        "Other": "No Comments",
        "Satisfaction": {
          "Pleasure of Course": 3,
          "Pollution Level": 2,
          "Luminosity": 8,
          "State of the tours": 6,
          "Population Density": 4
        },
        "Difficulty": 4,
        "RouteId": 305 },
      "StopDuringActivity":[{
          "Start": "2019-01-09 16:06:10",
          "Stop": "2019-01-09 16:07:10",
          "Coords": "40.575423,-8.446624"
        }, {
          "Start": "2019-01-09 16:09:10",
          "Stop": "2019-01-09 16:19:10",
          "Coords": "40.575612,-8.446191"
        }],
      "Pain Condition": {
        "Hands": 0,
        "Feet": 0,
        "Ribcage": 0,
        "Thigh": 4,
        "Head": 7,
        "Shoulders": 0,
        "Lumbar": 3,
        "Neck": 1,
        "Knee": 0,
        "Arms": 0,
        "Hip": 0 },
      "Duration": 40,
      "Path": ["40.575320,-8.446634",
               "40.575320,-8.446639",
               ...]}}}]
```

Two very important measures of effort, that have implications on the helth and well-being, are the heart rate and the blood pressure. This are reported in a "heart data" section illustrated in Table 3. These values are stored in the "exercise information" module and not in the "user health information" module since there is no guarantee that is was correctly obtained. These values are used just for monitoring and, if a consistent anomaly is verified, the next time the health professional meets the user he will try to understand the reason of the anomaly.

When some user is inactive for a long period of time, the back-office issues an alert for the health professional. If he finds appropriate it can question the user the reason of its inactivity. An example is presented in Table 4.

Table 3: Example of a "heart data" section representing that the values were obtain by a familiar. Other options could be a drug store or a health professional.

```
"User Heart Data": {
  "Blood Pressure": {
    "Diastolic": 70,
    "Systolic": 120
  },
  "Time Stamp": "2019-01-09  15:56:10",
  "Heart Rate": 68,
  "Who Measured": "Familiar" }
```

3.3 Mobile App

As mentioned before, the data transport of the framework is open and standardized for allowing third party apps to integrate the framework seamlessly. Nevertheless it was found important to provide a default app that, at least, helps to illustrate the potential of the framework.

Table 4: Example of a "inactivity" section. The main purpose is to allow helath professional understand if users were just busy and did have time to use the system or if it is a situation that need proper attention.

```
"Justification of inactivity": [{
  "Justification": {
    "Other": "None",
    "Time Stamp": "2019-01-09  15:56:10",
    "Absence": true,
    "Disease": false
  }
}, {
  "Justification": {
    "Other": "None also",
    "Time Stamp": "2019-01-09  15:56:10",
    "Absence": false,
    "Disease": true }}]
```

The devices that run the app are required to have wifi capabilities in order to send the data for the back-office and, to receive from it, the walk paths in KML format. They also need to have a GPS sensor for helping users complete the walk paths assigned to them, and acquiring information about the paths users actually did for subsequent analysis by health professionals.

The devices are not required but are strongly encouraged to have a heart beat sensor. This recommendation is due to the heart beat rate is strongly correlated with physical effort, and thus should be monitored by health professionals to assess if exercises are adequate to the given persons. It is not mandatory as heart beat rate and blood presure can be measured after the exercise by a health professional, or in a publicly available machine or at home, and then the values can be inserted manually. Even if the app is running on a device with a heart beat sensor, such as in the case of smartwatches, current technology is not accurate if a person is moving, thus the exercise should be finished before the value is measured.

3.4 Default App Implementation

Apps can run on devices such as smartphones and/or smartwatches. Apps running on smartphones have the advantage of benefiting from a bigger screen for the grphical user interface and longer energy autonomy, alongside these devices are well widespread troughtout population. Apps running on smartwatches have the advantage of benefitins from a heart beat sensor and being less intrusive as these devices are smaller. The default app runs combined on both types of devices: it runs on a smartwatch that acquires heart beat data and passes it by bluetooth low energy (BLE) to the smartphone, which combines that data with its own (GPS, user inputs, ...) and sends alltoghether to the back-office.

A default app was thus designed taking usability considerations adequate for older people [24, 25], and fully developed to show how each framework feature is accionable from the app. The user interface was designed with the support of three personas and two usage scenarios specifically developed to foster discussion and reflection [25]. Those three personas were characterized in terms of age, personality behaviour, and interests. One usage scenario was elaborated including one of the three personas while in the other scenario the other two personas interacted with which other.

The findings obtained from the personas and scenarios development lead the designed decisions of the app including: the way it was designed, how it works, and why it is easy to use for an elderly user who may not be used to the technology or has health impediments that make its use difficult [26]. The automatically app provides help if it is waiting for user's input and no activity is detected. Figure 4 presents a screen capture of such event in the home screen.

When the app does not detect an available heart beat sensor it will prompt users about the heart rate. Such form is presented in Figure 5. The fields DATE and HOUR will have as default values the current date and hour, respectivelly.

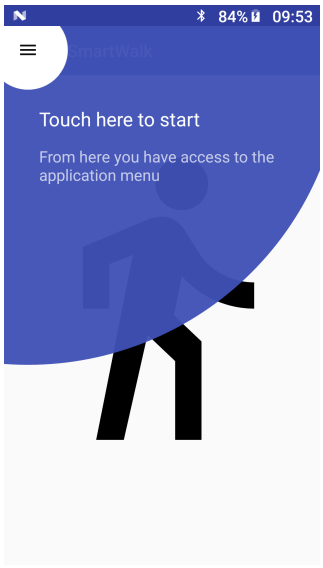

Figure 4: Screen capture of the default app home screen. The app provides contextual help when user action is required and no user activity is detected.

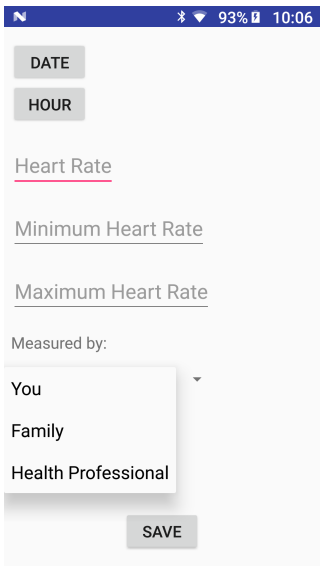

Figure 5: Screen capture of the default app. The app allows manual insertion of data if sensors are not available or if users prefer to measure themselves or ask someone else.

4 Discussion

Projects that conform to this framework can contribute to the challenges associated with the Smart Living profile. This profile is about lifestyles, behavior and consumption made through ICT, healthy and safe living in a culturally vibrant city with diverse cultural facilities, and good quality accommodation. Smart Living also promotes tourist attractiveness and high levels of social cohesion and social capital [9].

In particular, these types of systems described here can contribute to a healthy ICT-based lifestyle, as it aims to support people to maintain an adequate level of physical activity by advising them with a walk plan defined by a professional and transmitted using an ICT-based solution. In addition, health professionals, by knowing the places where people walk, can propose the most popular places to walk, thus being safer and more appealing. As it includes contextual information such as climatic conditions, points of interest, and temporary events among other, it has the potential to contribute to increase tourist attractiveness. One possibility that this type of system offers is also to propose joint walking plans, thus contributing to increase social cohesion.

Placing health professionals at the center of the decision allows individualized and quite different paths for individuals who, even if at first glance may seem to have the same profile, may have very different needs among themselves. [27] states that physical activity among the older population differs widely. According to studies that gathered information from ethnographic studies and interviews with health professionals, it is necessary to create different profiles of the elderly, with respect to physical activity and health conditions, and consequently create and adapt different routes to a specific profile. Adequate physical activity levels vary with health conditions and lifestyle [28]. Considering this, it is necessary to evaluate the health of users, namely the elderly. Thus it is of utmost importance to allow health professionals evaluate and define the profile of the user, and adapt the path of the walk to their state of health, physical activity level,

and personal preferences.

Regarding health conditions, the first thing to evaluate is whether the user needs to see a doctor before becoming more physically active. This can be reported using the Physical Activity Readiness Questionnaire - PAR-Q [29]. Then the 6-minute walk test - 6MWT [30] will be used to assess the user's level of physical activity. Other health information should be requested, such as an existing medical diagnosis, location and intensity of pain, usual medication, heart rate, and usual physical activity. With this package of health professional information can define the profile of the elderly.

A characteristic highlighted by one of the personas created was the need to make periodic evaluations face to face. For example, if a user as a health problem as breaking a leg, there is a need to make a new health assessment, or if the user leaves the city for a period of time and does not engage in any physical activity. Health information is needed to define the profile of the elderly and to customize the routes for the health conditions of the users, so it is necessary to have different routes. This also allows us to adapt the routes to personal information about the user, for example, a user who prefers routes integrated in a natural environment or if he prefers to pass in a local market. Finally, to induce and motivate the practice of physical activity, it is necessary to maintain face-to-face contact through periodic health assessment and to maintain the adaptability and personalization of the routes.

A system conforming to the proposed framework was implemented and tested with simulated users. The simulated users asked for walking courses and sent information regarding their physical activities (see Table 2), and sometimes other data relative to the other parameters, using distinct combinations of the four information sections. Users also sent information sections that were not defined and that should be silently ignored. The system handled efectivelly the distinct combinations of information sections and the information sections not defined. These results show that this design should cope well with upgrades since one major difficulty for upgrading systems is when distinct versions with distinct features coexist in the same environment. Although just one instance (and thus one version) of the back-office is expected in one usage environment, regarding the mobile applications one should expect a variety of implementations and with different versions. The system was also tested for temporary loss of connectivity and didn't show problems in such cases. The option of having a back-office connectivity module implementing a RESTful web service proved quite robust to the loss of connectivity events.

To extend the system in the future is necessary to define the JSON format of the message to be passed between the back-office and the apps, and implement the respective code and extend the database if necessary. These are the miminum things to do in any case. There is no necessity to change the lower level communication mechanisms between the back-office and the apps as the extension is just in the semantic part of the content.

In this stage of the work there is no automation (e.g. no artificial intelligence methods involved). This work was about designing and validating a monitoring platform that could be used by mobile apps with the benefit of having health professionals supervising the exercises. Without this stage consolidated this framework would be like alternatives already available: fully automated solutions not necessarily validated by health professionals.

A possible future extension would be provide some statistics as the places most visited by users, for instance for city planning purposes. This can be readilly available and it was not addressed since since third parties didn't yet identified those needs.

5 Conclusion

This article presented a framework to help people to have a more adequate physical activity, using the infrastructure of smart cities when it exists. As people age, because of their individual health history, it is more difficult to know what the proper level of physical exercise is, and therefore they should have the support of a professional with specialized knowledge and training. If people are left alone by deciding their own level of activity, they may be too aggressive and aggravate their injuries, create new ones and refrain from exercising more, or be very conservative and, in the long run, have a level of activity under their potential.

For this, information about chronic conditions, previous surgeries and current injuries, among others, is needed, raising concerns about privacy, and people are often reluctant to share these details. As such, the framework is designed to be operated by people who already know this information, or who are already legally authorized to own it, health professionals and probably the local public health unit. Also, special care was taken to make sure that health sensitive information remains private.

The back-office application was designed for health professionals be able to make fast, error-free decisions and minimize the risk of overloading them with much more work. In addition, the end user application can be made by third parties. One default app was designed and developed considering that some people are able to easily operate the smarphone and some have difficulties in using ICT, some may have problems of vision, etc. The best guidelines for the interfaces of the elderly were considered.

The project is implemented in Águeda, a city of about fifty thousand inhabitants, and ready for large-scale testing. The municipality of Águeda is a stakeholder in the project and it is expected that the project will be implemented definitively after all the tests and eventual corrections. All the technology planned for use is available in the market, such as smarphones and wristband models. This is important because the project is being deployed locally, but it has been carefully designed to be deployed (easily) in any other city.

Conflict of Interest The authors declare no conflict of interest.

Acknowledgment Not displayed due to anonymity purposes.

References

[1] M. Rodrigues, R. Santos, A. Queirós, A. G. Silva, J. Amaral, L. J. Gonçalves, A. Pereira, N. P. Rocha. "Meet smartwalk, smart cities

for active seniors." In 2018 2nd International Conference on Technology and Innovation in Sports, Health and Wellbeing (TISHW). IEEE, 2018. https://doi.org/10.1109/TISHW.2018.8559493

[2] G. Trencher, A. Karvonen, "Stretching ŝmart: advancing health and well-being through the smart city agenda", Local Environment, Taylor and Francis Group, 2017. https://doi.org/10.1080/13549839.2017.1360264

[3] T. Miura , K. Yabu, A. Hiyama, N. Inamur, M- Hirose, T. Ifukube, "Smartphone-Based Gait Measurement Application for Exercise and Its Effects on the Lifestyle of Senior Citizens". in 2015 Human-Computer Interaction, INTERACT, 2015. https://doi.org/10.1007/978-3-319-22698-9_7

[4] S. R. Steinhubl, E. D. Muse, E. J. Topol, "The emerging field of mobile health", Science Translational Medicine, **7**(283), 2015. https://doi.org/10.1126/scitranslmed.aaa3487

[5] P. Husu, J. Suni, H. Vähä-Ypyä, H. Sievänen, K. Tokola, H. Valkeinen, T. Mäki-Opas, T. Vasankari, "Objectively measured sedentary behavior and physical activity in a sample of Finnish adults: a cross-sectional study", BMC Public Health, **16**(1), 920, 2016. https://doi.org/10.1186/s12889-016-3591-y

[6] P. Simões, A. G. Silva, J. Amaral, A. Queirós,N. P. Rocha, M. Rodrigues, "Features, Behavioral Change Techniques, and Quality of the Most Popular Mobile Apps to Measure Physical Activity: Systematic Search in App Stores", JMIR Mhealth Uhealth, **6**(10), 2018. https://doi.org/10.2196/11281

[7] M. Batty, "Big data, smart cities and city planning", Dialogues in Human Geography, **3**(3), 274-–279, 2013. https://doi.org/10.1177/2043820613513390

[8] L. Anthopoulos, "Smart utopia VS smart reality: Learning by experience from 10 smart city cases", Cities, **63**, 128 – 148, 2017. https://doi.org/10.1016/j.cities.2016.10.005

[9] C. Manville, G. Cochrane, J. Cave, J. Millard, J. K. Pederson, R. K. Thaarup, A. Liebe, M. Wissner, R. A. Massink, B. Kotterink, "Mapping smart cities in the EU", European Parliament; Directorate General for Internal Policies. Policy Department Economic and Scientific policy A, 2014.

[10] M. Kullman, J. Campillo, E. Dahlquist, C. Fertner, R. Giffinger, J. Grosse, N. B. Groth, G. Haindlmaier, A. Kunnasvirta, F. Strohmayer, et al., "Note: The PLEEC Project-Planning for Energy Efficient Cities", Journal of Settlements and Spatial Planning, **5**, 89–92, 2016. https://doi.org/10.19188/09JSSPSI052016

[11] D. Patti, R. De Amicis, F. Prandi, E. D'Hondt, H. Rudolf, P. Elisei, I. Saghin, "iScope smart cities and citizens", in REAL-CORP, 2013.

[12] R. P. Dameri, "Comparing Smart and Digital City: Initiatives and Strategies in Amsterdam and Genoa. Are They Digital and/or Smart?", Smart City: How to Create Public and Economic Value with High Technology in Urban Space, Springer International Publishing, 2014. https://doi.org/10.1007/978-3-319-06160-3_3

[13] Amsterdam project, "Amsterdam Smart City platform", https://amsterdamsmartcity.com, accessed 20 May 2019

[14] J. Helder, M. Schets, "VITAMINE – Active senior citizens in Amsterdam", https://amsterdamsmartcity.com/projects/vitamine, accessed 17 May 2019.

[15] Y. Slaats, "PAUL – Playful data-driven Active Urban Living", https://amsterdamsmartcity.com/projects/playful-data-driven-active-urban-living, accessed 17 May 2019.

[16] R. Gudjonsdottir, "Personas and Scenarios in Use", PhD dissertation, KTH, Stockholm, 2010.

[17] A. Blomquist, M. Arvola, "Personas in Action: Ethnography in an Interaction Design Team", in 2002 Nordic Conference on Human-computer Interaction, NordiCHI '02, 2002. http://doi.acm.org/10.1145/572020.572044

[18] J. Pruitt, A. Tamara, "The persona lifecycle: keeping people in mind throughout product design". Elsevier, 2010.

[19] F. Casino, C. Patsakis, E. Batista, F. Borràs and A. Martínez-Ballesté, "Healthy Routes in the Smart City: A Context-Aware Mobile Recommender", IEEE Software, **34**(6), 42–47, 2017. https://doi.org/10.1109/MS.2017.4121209

[20] Pacer Health, "Pacer Pedometer & Step Tracker (Play Store)", https://play.google.com/store/apps/details?id=cc.pacer.androidapp&rdid=cc.pacer.androidapp, accessed 17 May 2019

[21] Six to Start, "The Walk: Fitness Tracker Game", https://itunes.apple.com/us/app/the-walk-fitness-tracker-game/id678971662?mt=8& app=itunes& ign-mpt=uo%3D4, accessed 17 May 2019.

[22] Guava Studio, "Pedometer – Step Counter", https://play.google.com/store/apps/details?id=com.guava.pedometer.stepcounter&rdid=com.guava.pedometer.stepcounter, accessed 17 May 2019

[23] J. Amaral, M. Rodrigues, L. J. Gonçalves, C. Teixeira, "Customized Walk Paths for the Elderly", in 2019 Information Technology and Systems, ICITS, Quito, Peru, 2019. https://doi.org/10.1007/978-3-030-11890-7_71

[24] A. I. Martins, A. Queirós, A. G. Silva, N. P. Rocha, "ICF Based Usability Scale: Evaluating Usability According to the Evaluators' Perspective About the Users' Performance", in 2016 International Conference on Software Development and Technologies for Enhancing Accessibility and Fighting Info-exclusion, DSAI, Vila Real, Portugal, 2016. http://doi.acm.org/10.1145/3019943.3019997

[25] A. Queirós, A. G. Silva, P. Simões, C. Santos, C. Martins, N. P. Rocha, M. Rodrigues. "Smartwalk: personas and scenarios definition and functional requirements." In 2018 2nd International Conference on Technology and Innovation in Sports, Health and Wellbeing (TISHW). IEEE, 2018. https://doi.org/10.1109/TISHW.2018.8559574

[26] D. Bastos, J. Ribeiro, F. Silva, M. Rodrigues, R. Santos, C. Martins, N. Rocha, A Pereira. "SmartWalk Mobile–A Context-Aware m-Health App for Promoting Physical Activity Among the Elderly." In World Conference on Information Systems and Technologies. Springer, Cham, 2019. https://doi.org/10.1007/978-3-030-16184-2_79

[27] F. Sun, I.J. Norman, A.E. While, "Physical activity in older people: a systematic review", BMC public health, **13**(1), 2013. https://doi.org/10.1186/1471-2458-13-449

[28] I. Bautmans, M. Lambert, T. Mets, "The six-minute walk test in community dwelling elderly: influence of health status", BMC geriatrics, **4**(1), 2004. https://doi.org/10.1186/1471-2318-4-6

[29] D. Warburton, V. Jamnik, S. Bredin, D. McKenzie, J. Stone, R. Shephard, N. Gledhill, "Evidence-based risk assessment and recommendations for physical activity clearance: an introduction", Applied Physiology, Nutrition, and Metabolism, **36**(S1), 2011. https://doi.org/10.1139/h11-060

[30] R. E. Rikli, C. J. Jones, "The reliability and validity of a 6-minute walk test as a measure of physical endurance in older adults", Journal of aging and physical activity, **6**(4), 363–375, 1998.

Advances in Science, Technology and Engineering Systems Journal Vol. 4, No. 4, 414-420 (2019)

www.astesj.com

Special Issue on Advancement in Engineering and Computer Science

ASTESJ

ISSN: 2415-6698

Development of Wavelet-Based Tools for Event Related Potentials' N400 Detection: Application to Visual and Auditory Vowelling and Semantic Priming in Arabic Language

Nadia Mountaj[1], El-Mehdi Hamzaoui[2,*], Mohamed Majid Himmi[1], Mireille Besson[3]

[1]*LIMIARF Laboratory, University Mohammed V, Faculty of Sciences, Rabat 10000, Morocco.*

[2]*National Centre for Nuclear Energy, Science and Technology (CNESTEN), Rabat 10001, Morocco.*

[3]*Cognitive Neurosciences Laboratory, CNRS — Aix-Marseille University, Pôle 3C, Marseille 14000, France.*

ARTICLE INFO

Article history:
Received: 04 May, 2019
Accepted: 31 July, 2019
Online: 16 August, 2019

Keywords:
Daubechies
ERP signals
N400
Wavelets
Vowelling priming
Semantic priming

ABSTRACT

Neurological signals are generally very weak in amplitude and strongly noisy. As a result, one of the major challenges in neuroscience is to be able to eliminate noise and thus exploit the maximum amount of information contained in neurological signals (EEG...). In this paper, we aimed at studying the N400 wave of the Event-Related Potentials (ERPs) that may reflect the effects of vowelling and semantic priming in Arabic language. To improve the quality of the recorded ERP signals, we considered a nonlinear filtering method based on 10th order Daubechies discrete wavelet transform combined to principal component analysis (PCA). Among all tested wavelets, the Daubechies one showed high values of the used signal processing metrics. Thus, it allowed a significant enhancement of the signal to noise ratio while using only 10 ERP trials. In addition, we confirm its effectiveness while comparing the filtered outputs to those obtained using the averaging technique implemented in the conventional EEGLab toolbox. In a second step, the Mexican Hat function was used to achieve continuous wavelet analysis of the filtered signals. This time-scale analysis method permitted to get an alternative representation of the ERPs and to detect the N400 wave with significantly greater accuracy.

1. Introduction

The Event Related Potential (ERP) N400 wave is a negative deflection or component elicited by the brain as a reaction to semantically unexpected words in sentence contexts [1]. The N400 component has been found in many languages, such as English, French, Mandarin Chinese..., but to our knowledge, only a few studies have examined the occurrence of an N400 in the Arabic language [2].

The shallow or deep character (i.e vowelled or unvowelled words respectively) of written depends on how its phonology is reflected by the orthography of the language. Indeed, Arabic written words are composed from consonant and long vowels in addition to diacritics. These last reflect the vowellisation of the written word in order to enable inferring specific pronunciation. Also, Arabic is characterized by a non-concatenative morphology whereby every surface form is analyzable into a consonantal root, that conveys semantic meaning, and a word pattern (made up of vowels and of a subset of consonants) conveying morphosyntactic and phonological information.

In the present experiment, we recorded and analyzed ERP, in particular the N400 component, while participants performed a semantic judgment task with Arabic words. As many neural signals, ERPs are very weak signals and strongly corrupted by noise. Thus, previous studies aimed at improving the quality of ERP signals using statistical methods [3,4], linear and nonlinear adaptive filtering [5], neural network based techniques [6] and wavelets denoisng techniques [7,8].

In the present study, our aim was to go one step further to improve the quality of ERP signals. We used discrete wavelet combined with principal component analysis (PCA) as nonlinear filtering tools. This allowed us to enhance the signal to noise ratio and thereby to highlight the N400 component. In addition, we used

* El-Mehdi Hamzaoui, Email: hamzaouielmehdi@gmail.com

the Mexican hat function to achieve the time-scale analysis of the filtered ERPs in order to detect the N400 with more accuracy.

2. Material and methods

2.1. Experiment

In our experiment, which was approved by the Ethics Committee of the Mohammed V University, a total of 20 Master MSc and PhD students (10 women), aged between 20 and 34 years old, were tested after giving their written consent to participate in the experiment. They were all right-handed and without neurological disorders. They all use Arabic daily.

Each participant was comfortably seated in a Faradized room and was asked to silently read two words that were successively presented at the center of a computer screen. A total of 256 Arabic prime-target word pairs were used as stimuli with 128 pairs presented in the vowelled condition and 128 pairs presented in the unvowelled condition. For each condition, 64 pairs were semantically related and 64 pairs were semantically unrelated. For both vowelled and unvowelled pairs, two lists were constructed so that across lists, the same target word was paired once with a semantically related prime and once with a semantically unrelated prime [2]. The order of presentation of the two lists was balanced across participants.

EEG data was continuously recorded using 24 electrodes (impedance < 5kΩ) mounted on an elastic head cap according the 10/20 International EEG System [9]. The signals were amplified using SAI amplifiers (San Diego) and recorded at a sampling frequency of 250 Hz. The Electro-Occulogram (EOG) was recorded from an electrode placed under the right eye to detect eye blinks. Finally, two reference electrodes were placed on the left and right mastoids. The experiment was conducted in a Faraday's cage in order to reduce external interference [10].

The analyzed ERP signals correspond to the electrodes F3, F4, C3, C4, P3, P4, Fz, Cz and Pz. Previous results have shown that the N400 component is larger over centro-parietal regions of the right hemisphere than over frontal regions.

At the end of the experiment, three participants have been excluded because they present too many ocular and muscular artifacts contaminating the EEG signal.

2.2. Data analysis

Since the creation of wavelets, scientific and technical applications based on this mathematical tool have continued to be developed [11,12], exploiting their power and their efficiency for to perform multiresolution data analysis [13,14]. In the present work, we used a filtering technique developed by AminGhafari M. et al., [15] in order to denoise multivariate signals. This method combines both univariate wavelet decomposition of the signal and the principal component analysis (PCA) of the resulting wavelet coefficients in order to evaluate the correlation structure of the noise.

According to AminGhafari M. et al., [15], the algorithm performs the filtering task in four main steps. First, for a matrix X (nxp) of p observed signals, we achieve the wavelet decomposition at a defined level K. This results into two matrices D_k and A_k that contain respectively the details and approximation coefficients up to the level K of the p signals. Second, using the matrix Dj of finest details, a minimum covariance estimation is calculated and used for the diagonalization of a robust estimate of the noise covariance matrix. The obtained diagonal matrix is then used for changing the basis at each level 1<i<K. In the third step, the matrix D_k undergoes a classical one-dimensional soft thresholding. We then apply the PCA to both the detail and approximation coefficients matrices in order to choose the appropriate number of useful principal components. The best number is automatically defined using the Kaiser distance criterion which retains components associated with eigenvalues higher than the mean of all eigenvalues.

From the simplified matrices D and A, inverting the wavelet transform provides a new matrix containing the filtered signals. These lasts correspond to the main features of the original matrix X.

In our study, we tested 8 wavelet functions belonging to 5 wavelet families which are Daubechies of order 10 (db10) [16,17], Coiflets of order 5 (coif5) [18], Symlets of order 4 and 8 (sym4 and sym8 respectively) [19], Biorthogonal (bior1.1) [20] and Reverse Biorthogonal (rbio1.5) [18].

To evaluate the performance of the different wavelets, we computed the structural similarity index (SSIM), which is usually used to evaluate image quality on the basis of its luminance, contrast and structure characteristics. It is based on the comparison of an image I with a reference image [21,22]. It is known that the closer the SSIM value is to 1, the stronger the structural similarity between the evaluated image and the reference image is. By contrast, an SSIM value close to 0 indicates that there are no similarities between the 2 images [21]. To use this metric, we considered the matrix containing the wavelet based filter's output signals as an image (30 matrices of 9 analyzed electrodes x 2200 samples for each participant) and we compared it to the matrix that contained the averaged trials for each electrode.

In addition, we computed the signal-to-noise ratio (SNR) via a MATLAB® routine. This signal processing metric is commonly used to assess the performance of signal processing methods. It is often expressed in decibels as [23,24]:

$$SNR = 20.log_{10}(\frac{P_x}{\sigma^2}) \quad (1)$$

where P_x and σ^2 denote the power density of the original and the noise signals respectively.

In the case of closer SNR values, we also used the mean square error (MSE), given by the following equation 2, as second metric to evaluate the accuracy of the chosen wavelet. The value of the MSE, the closer the filtered signal is to the original one and thus the better filtering method is [6,10,21,23].

$$MSE = \frac{1}{N}\sum_{n=1}^{N}(x(n) - \hat{x}(n))^2 \quad (2)$$

where $x(n)$ and $\hat{x}(n)$ denote the original and the filtered signals respectively. N is the length of x(n).

In the second step, we used the continuous wavelet transform (CWT) as an alternative method to the classical signal time representation. This is based on the idea that wavelet analysis can provide accurate and specific time-frequency decomposition of

neurologic signals. This method has already been applied to EEG denoising [18,24,25], ERP component separation [26], spindle and spike detection [27,28,29], etc. It allowed an automatic processing of the signal and provided both qualitative and quantitative information.

The continuous wavelet transform converts a continuous signal into extremely redundant signal of dual continuous variables which are the translation and the scale. The resulting changed signal is easy to interpret and valuable for time-frequency or time-scale analysis [30]. In general, CWT of a signal s(t) is defined as:

$$S(\alpha,\beta) = \frac{1}{\sqrt{\alpha}}\int_{-\infty}^{+\infty} \psi\left(\frac{t-\beta}{\alpha}\right)^{*} . s(t)dt$$

where α and β represent the scaling and the dilation factors respectively, whereas ψ* is the complex conjugate of the mother wavelet function.

The scale α is associated to the wavelet's central frequency Fc and varies according to frequencies (in Hz) by:

$$\alpha = \frac{F_c}{f * \Delta T} \quad (3)$$

ΔT is the sampling period.

For time-scale analysis, we represented the modulus of the CWT coefficients, which corresponds to the energy density of the analyzed signal, according to $\log_2(\alpha)$ (ordinate axis) and time (abscissas axis) [12]. In this graphical representation, called scalogram, a color map is used to quantify the energy density of the transformed signal. The highest value of the energy corresponds to the white color whereas the lowest is represented by black color [31,32,33].

In our application, ψ is chosen to be the Mexican Hat (equation 4), which is the second-order derivative of the Gaussian function. This last is not a wavelet, but all its derivatives can be used as wavelets, particularly the first and the second derivatives [34,35]. In practice, the Mexican Hat is expressed by the real function of equation (5) and represented by the figure 1 below.

$$\psi(t) = \frac{2}{\frac{1}{\pi^4}\sqrt{3\delta}}\left(\frac{t^2}{\delta^2} - 1\right) exp\left(-\frac{t^2}{2\delta^2}\right) \quad (4)$$

where 0<δ<1 represents the wavelet width [35]

$$\psi(t) = (1-t)exp\left(-\frac{t^2}{2}\right) \quad (5)$$

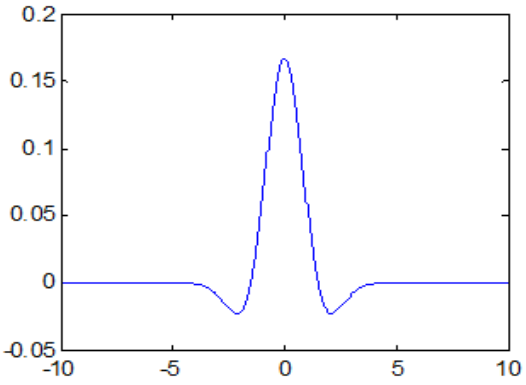

Figure 1. Plot of real function of the Mexican Hat function.

As illustrated by this figure, the Mexican Hat waveform looks like most of the waves that compose the ERPs (Figure 2). This was the reason to use it to perform the time-scale analysis of our data set. In addition, this function is easy to implement under the MATLAB environment.

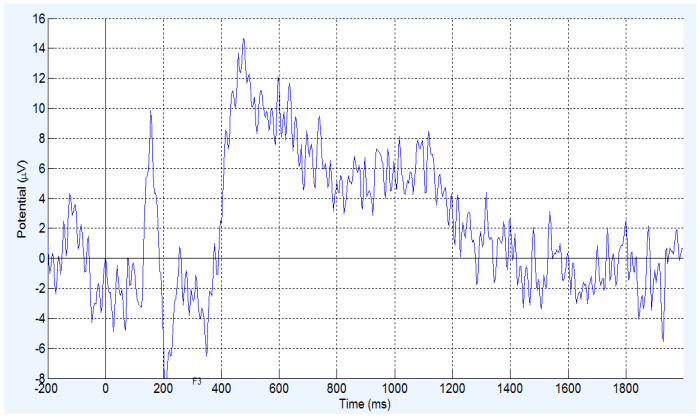

Figure 2. Example of recorded ERP.

3. Results and discussion

The averaged values of the performance metrics, SNR and MSE, corresponding to the application of the Aminghafari's algorithm with different DWT functions to our signals are presented in Table 1. As described in the Materials and Methods section, we recorded 30 ERP signals per electrode from each participant (9 electrodes and 20 participants). We processed 5, 10 and 15 trials to evaluate the efficiency of the filtering algorithm and thus to define the most accurate DWT function that allowed a good filtering of the ERPs. Results showed that the 10th-order Daubachies wavelet (db10) yielded the best results in terms of accuracy of de-noising ERP signals. In fact, this DWT function shows the highest SNR values and the lowest MSE values in all test conditions.

Importantly, and as presented in Table 2, db10 showed the highest values of the structural similarity index for all electrodes. In addition, and as illustrated on Figure 3, its application to filter the ERPs showed good improvement of the visual quality of waveforms' plots.

Visual comparison of these results to those obtained using the classical averaging method implemented in the EEGLab Toolbox showed that, for each electrode, the same visual quality of plots is obtained via our method and via EEGLab when averaging all recorded signals for SNR values of about 3.5. However, using our db10-PCA filtering method, only 5 to 10 ERP trials are sufficient to improve the SNR value and to highlight the occurrence of an N400 component. This can be explained by the fact that our filtering method is a nonlinear technique that takes into consideration some statistics of the signal and how the noise is affecting the signal. By contrast, the averaging method is a linear method that assumes that the noise is additive, white and Gaussian.

In order to still improve accuracy in N400 waveform detection, a time-scale representation of the ERP signals was performed on the basis of the Mexican hat CWT function. An example of results obtained for the 9 recorded electrodes is illustrated on Figure 4.

Table 1: Averaged values of metrics obtained using 5, 10 and 15 EEG trials.

Wavelet Name		5 ERP trials		10 EEG trials		15 EEG trials	
		MSE	SNR	MSE	SNR	MSE	SNR
Daubachies	db10	62,84	7,90	74,96	7,10	68,61	6,13
Coiflets	coif5	70,19	6,64	92,70	6,50	79,73	5,66
Symlet	sym4	67,63	7,19	86,94	6,77	78,32	5,66
	sym8	68,64	7,20	89,95	6,63	78,05	5,75
Mery	dmey	102,60	5,42	141,43	5,82	114,99	4,49
Biorthogonal wavelet	bior 1.1	73,68	6,59	84,64	6,38	85,34	5,08
Reverse biorthogonal	rbio 1.5	67,19	7,26	88,92	6,65	77,26	5,77

Table 2: Averaged values of structural similarity index metric.

Wavelet Name		Structural similarity index metric								
		F3	F4	C3	C4	P3	P4	Fz	Cz	Pz
Daubachies	db10	0,97	0,99	0,95	0,98	0,93	0,94	0,99	0,98	0,96
Coiflets	coif5	0,54	0,50	0,52	0,50	0,58	0,49	0,55	0,60	0,59
Symlet	sym4	0,28	0,26	0,23	0,28	0,3	0,31	0,29	0,23	0,31
	sym8	0,25	0,30	0,27	0,31	0,27	0,28	0,31	0,29	0,32
Mery	dmey	0,08	0,11	0,09	0,10	0,07	0,14	0,08	0,15	0,08
Biorthogonal wavelet	bior 1.1	0,18	0,22	0,20	0,17	0,21	0,22	0,26	0,22	0,23
Reverse biorthogonal	rbio 1.5	0,27	0,35	0,25	0,33	0,28	0,31	0,36	0,33	0,27

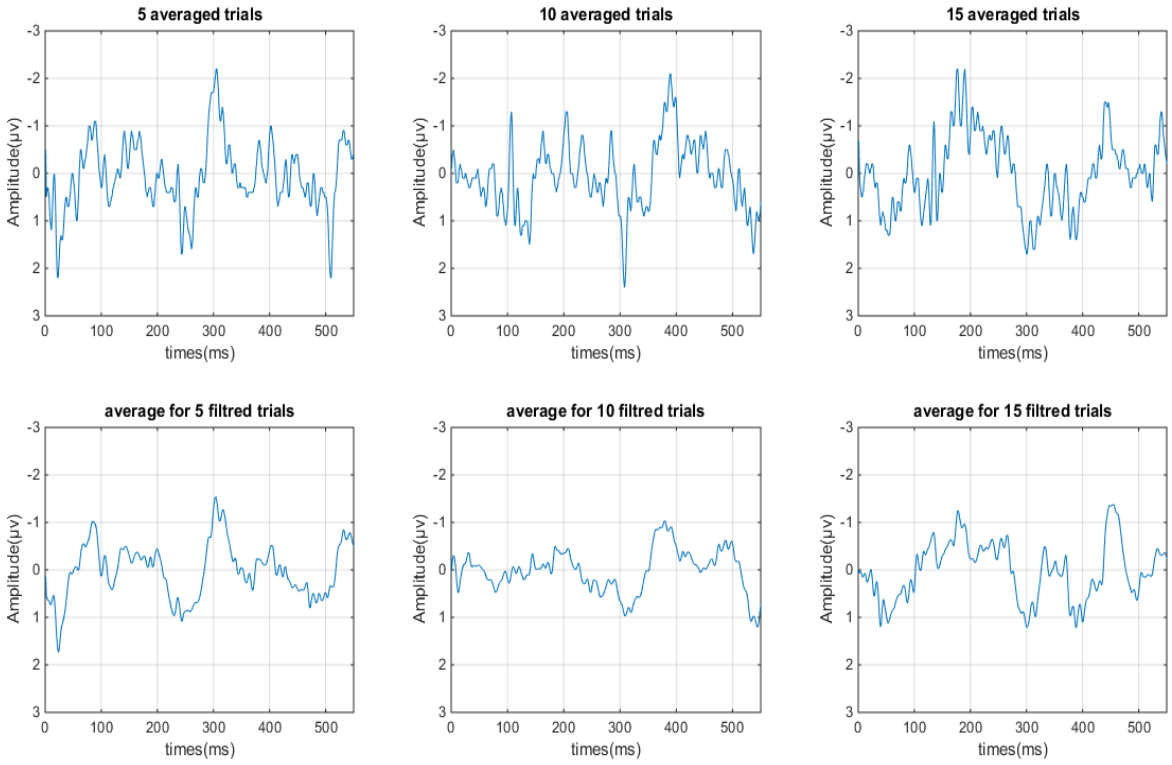

Figure 3. 5, 10 and 15 ERP trials filtered using both EEGLab Averaging technique (Up) and the developed db10-PCA filtering method (down).

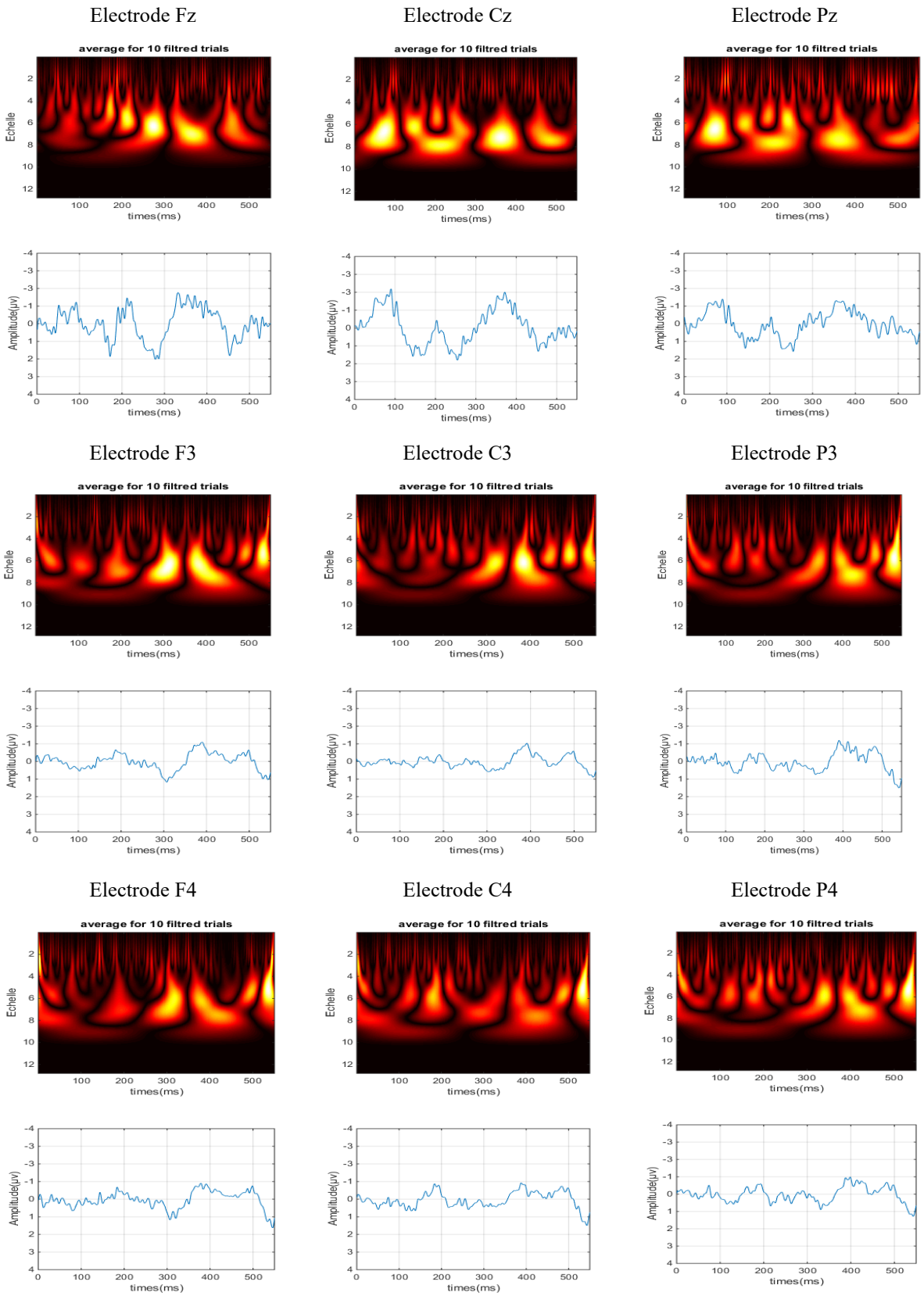

Figure 4. Scalograms of the average of 10 filtered ERP trials using db10-PCA.

Visual reading of these scalograms revealed the presence of light-colored vertical bands for medium and small scales, depicting smaller changes throughout the ERP signal. In particular, high-energy concentrations are observed in the time range of the N400 component [360; 470msec] and for scales between 3 and 8. Importantly, these regions correspond to a maximum energy around the position of the N400 component in the temporal representation of the ERP signal.

Based on these results and similar ones obtained by processing the entire set of data available for this study, the maximum energy localization in time and scale allowed us to define a qualitative criterion to detect the N400 occurrence and position. Moreover, we have demonstrated in our previous scientific works, that the primed Arabic words elicit smaller N400 components than unprimed Arabic words [2]. This result is confirmed by the use of the CWT technique. Indeed, for unprimed Arabic words, a high energy band is detected around 380 to 410 millisecond, that is, in a narrow range of about 30 milliseconds, whereas for primed words, this energy region is of very low intensity.

4. Conclusion

In this study we exploited the wavelets, as signal processing tools, to improve the quality of the ERP signals recorded during a semantic priming task in Arabic. We used the discrete wavelet transform to denoise the recorded signals. Moreover, the filtering procedure combined the DWT and the PCA methods to form a nonlinear filter that allowed us to improve the visual quality of ERP plots based on a few trials only. Importantly, using the SSIM, the SNR and MSE metrics, we demonstrated that 10th-order Daubachies wavelet of order 10, was the most efficient to improve the SNR and thus to reveal the occurrence of the N400 component. Finally, visual comparison with the results obtained using EEGLab tools, showed that our procedure allowed a clear improvement of the quality of the ERP plots.

In a second part, we used the continuous wavelet transform based on the Mexican Hat function to perform the time-scale analysis of the filtered ERPs. The resulting scalograms allowed us to define qualitative and quantitative criteria to detect the presence of the N400 component in the auditory and visual evoked signals. The qualitative criterion consists of visual reading of the energy density representation whereas the quantitative criterion is based on defining with acute precision the maximum of the N400 energy within time and scale positions. In this case, we found that, for unprimed Arabic words, a high energy band is detected between 3 and 8 on scale axis and in the time range [380; 410msec]. This last corresponds to the normal position of the N400 wave in the temporal representation of an ERP. In the case of primed Arabic words, a very low intensity energy region is present in the time range [360; 470msec].

Conflict of Interest

The authors declare no conflict of interest.

Acknowledgment

This work was supported by the French-Moroccan Research Consortium (GDRI-Neuro), coordinated by Dr Driss Boussaoud and supported by the French Government and the French Institute of Life Sciences.

References

[1] M. Kutas, S. A. Hillyard, “Reading senseless sentences: brain potentials reflect semantic incongruity” Science, 207(4427), 203-205, 1980.
[2] N. Mountaj, R. El Yagoubi, M. Himmi, F.L. Ghazal, M. Besson, S. Boudelaa, “Vowelling and semantic priming effects in Arabic” Int. J. Psychophysiol., 95(1), 46-55, 2015.
[3] G. Inuso, F. La Foresta, N. Mammone, F.C. Morabito, “Wavelet-ICA methodology for efficient artifact removal from Electroencephalographic recordings” In 2007 IEEE International Joint Conference on Neural Networks, Orlando, FL, USA, 2007.
[4] D. Kang, L. Zhizeng, “A Method of Denoising Multi-channel EEG Signals Fast Based on PCA and DEBSS Algorithm” in 2012 IEEE International Conference on Computer Science and Electronics Engineering (ICCSEE), Hangzhou, Zhejiang, China, 2012.
[5] A. Garcés Correa, E. Laciar, H.D. Patiño, H.D. Valentinuzzi, “Artifact removal from EEG signals using adaptive filters” in 2007 16th Argentine Bioengineering Congress and the 5th Conference of Clinical Engineering, San Juan, Argentina, 2007.
[6] G. Kaushik, H. Sinha, L. Dewan, “Biomedical signals Analysis by Dwt Signal Denoising with Neural Networks” J. Theor. & App. Inf. Tech., 62(1), 184-198, 2014.
[7] M. Balamareeswaran, D. Ebenezer, “Denoising of EEG signals using Discrete Wavelet Transform based Scalar Quantization” Biomed. & Pharmacol. J., 8(1), 399-406, 2015.
[8] R. Princy, P. Thamarai et B. Karthik, “Denoising EEG signal using wavelet transform” Int. J. of Adv. Res. in Comp. Eng. & Tech., 4(3), 1070-1074, 2015.
[9] H. Jasper, “The ten-twenty electrode system of the International Federation” Electroenceph. Clin. Neurophysiol., 10, 371-375, 1958.
[10] N. Fathima, K. Umarani, “Reduction of Noise in EEG Signal using Faraday’s Cage and Wavelets Transform: A comparative Study” Int. J. Eng. Sci. & Comp., 6(7), 8566-8569, 2016.
[11] S.P. Suhas, K.P. Minal, “Quality advancement of EEG by wavelet denoising for biomedical analysis” in 2012 IEEE International Conference on Communication, Information and Computing Technology (ICCICT), Hammamet, Tunisia, 2012.
[12] P. Addison, The Illustrated Wavelet Transform Handbook: Introductory Theory and Applications in Science, Engineering, Medicine and Finance, Bristol: Institute of Physics Publishing, 2002.
[13] H. Li, H. Hu, T. Kobayashi, T. Saga et N. Taniguchi, “Wavelet Multi-Resolution Analysis of Dual-plane Stereoscopic PIV Measurement Results in a Lobed Jet” in 2001 4th International Symposium on Particle Image Velocimetry, Göttingen, Germany, 2001.
[14] A. Drissi, E. Maliani, M. El Hassouni, Y. Berthoumieu, D. Aboutajdine, “multi-model approach for multi component texture classification” in 2012 5th International Conference on Image and Signal Processing (ICISPP12), 2012.
[15] M. Aminghafari, N. Cheze, J. Poggi, “Multivariate denoising using wavelets and principal component analysis” Comput. Stat. Data An., 50(9), 2381-2398, 2006.
[16] D. Sundararajan, Discrete wavelet transform: a signal processing approach, John Wiley & Sons, 2016.
[17] I. Daubechies, Ten lectures on wavelets, SIAM, 1992.
[18] S. Mallat, A wavelet tour of signal processing, Academic Press, 1999.
[19] M.S. Chavan, N. Mastorakis, M.N. Chavan, M.S. Gaikwad, “Implementation of symlet wavelets to removal of gaussian additive noise from speech signal” in 2011 Joint WSEAS International Conferences on Recent Researches in Communications, Automation, Signal Processing, Nanotechnology, Astronomy and Nuclear Physics, Cambridge, UK, 2011.
[20] C. Uyulan, T.T. ERguzel, “Comparison of Wavelet Families for Mental Task Classification” J. Neurobehavioral Sci., 3(112), 2016.
[21] R. Dosselmann, X.D. Yang, “A comprehensive assessment of the structural similarity index” Signal, Image Video P., 5(1), 81-91, 2011.
[22] A. Hore, D. Ziou, “Image quality metrics: PSNR vs. SSIM” In 2010 IEEE 20th International Conference on Pattern Recognition, Istanbul, Turkey, 2010.
[23] A. Sundar, V. Pahwa, C. Das, M. Deshmukh, N. Robinson, “A Comprehensive Assessment of the Performance of Modern Algorithms for Enhancement of Digital Volume Pulse Signals” Int. J. Pharma. Med. Biolo. Sci., 5(1), 91-98, 2016.
[24] A. Dixit, S. Majumdar, “Comparative analysis of coiflet and daubechies wavelets using global threshold for image de-noising” Int. J. Adv. Eng. Tech., 6(5), 2247, 2013.
[25] P. Khatwani, A. Tiwari, “Removal of Noise from EEG Signals Using Cascaded Filter – Wavelet Transforms Method” Int. J. Adv. Res. Electrical, Electronic Instr. Eng., 1(21-23,12), 2014.

[26] C. Yongjian, "Neural Network Based EEG Denoising" in 2008 IEEE 30th Annual International EMBS Conference, Vancouver, British Columbia, Canada, 2008.
[27] L. Yu, "EEG De-Noising Based on Wavelet Transformation" In 2009 IEEE 3rd International (ICBBE 2009), Beijing, China, 2009.
[28] J. Raz, L. Dickerson, B. Turetsky, "A wavelet packet model of evoked potentials" Brain and Language, 66(1), 61-88. 1999.
[29] T. Kalayci, O. Ozdamar, N. Erdol, "The use of wavelet transform as a preprocessor for the neural network detection of EEG spikes" in 1994 IEEE Southeastcon Conference, Miami, FL, USA, 1994.
[30] S.J. Schiff, J. Heller, S.L. Weinstein, J. Milton, "Wavelet transforms and surrogate data for electroencephalographic spike and seizure detection" Optical Eng., 33(7), 2162-2170, 1994.
[31] Z. W. Tang, and N. Ishii, "The recognition system with two channels at different resolu-tion for detecting spike in Human's EEG" IEICE Trans. Info. Sys., 76(3), 377-387, 1993.
[32] T. Kristjansson, J. Hershey, "High Resolution Signal Reconstruction" in 2003 IEEE Workshop on Automatic Speech Recognition and Understanding, St Thomas, VI, USA, 2003.
[33] T. Perez-Muñoz, J., Velasco-Hernandez, E. Hernandez-Martinez, "Wavelet transform analysis for lithological characteristics identification in siliciclastic oil fields" J. Appl. Geophys., 98, 298-308, 2013.
[34] Z. Zhou, H. Adeli, "Time-frequency signal analysis of earthquake records using Mexican hat wavelets" Comput-Aided Civ. Inf., 18(5), 379-389, 2003.
[35] E-M. Hamzaoui, F. Regragui, "Discrimination of Visual Evoked Potentials Using Image Processing of Their Time-Scale Representations" in 2013 2nd Conference in Electronics, Telecommunications, and Computer Engineering (CETC'13), Lisbon, Portugal, 2013
[36] R. M. Rao, AS. Bopardikar, Wavelet Transforms, Addison-Wesley, 1998.
[37] S.J. Schiff, "Resolving time-series structure with a controlled wavelet transform" Optical Engineering, 31(11), 2492–2496.
[38] G. Samorodnitsky, M. Taqqu, Stable non-Gaussian random processes, Chapman and Hall, 1994.

Advances in Science, Technology and Engineering Systems Journal Vol. 4, No. 4, 421-430 (2019)

www.astesj.com

Special Issue on Advancement in Engineering and Computer Science

ASTESJ

ISSN: 2415-6698

A Balanced RF Power Amplifier using the Improvement 3-dB Quadrature Hybrid Couplers for Mitigation of the Reverse Intermodulation in FM Broadcasting Systems

Panya Hantula, Rangsan Tongta*

School of Telecommunication Engineering, Institute of Engineering, Suranaree University of Technology, 111 University Avenue, Muang District, Nakhon Ratchasima, Thailand.

ARTICLE INFO

Article history:
Received: 31 May, 2019
Accepted: 29 July, 2019
Online: 16 August, 2019

Keywords:
Reverse Intermodulation
FM Power Amplifiers
Balanced RF Power Amplifiers
3-dB Quadrature Couplers
Broadside-coupler Striplines
Printed Circuit Broads (FR-4)

ABSTRACT

FM broadcast stations generate reverse intermodulation signals that cause communication problems between ATC controllers and pilots in the Air Traffic Control systems (ATC) in Thailand. In this paper proposes a balanced RF power amplifier using the improvement 3-dB quadrature hybrid couplers to reduce the reverse intermodulation of FM broadcasting systems. The mathematics analysis of the balanced RF power amplifier for two closely located FM stations shows that can reduce the reverse intermodulation products. A reverse signal from nearby FM stations travels into two amplifiers of a balanced amplifier that create intermodulation signals. The quadrature hybrid coupler in a balanced RF amplifier to provide intermodulation signals of two amplifiers have a 180˚ out-of-phase which cause reducing intermodulation signals. In this paper designs 3-dB quadrature hybrid couplers for a proposed RF balanced amplifier. The low-cost PCBs are used to make prototype couplers. The proposed couplers are provided experimental results of return losses that are lower than -15 dB. The directed port has a coupling coefficient -3.3 dB and the coupled port has a coupling coefficient -3.4 dB. The prototype couplers are applied to a balanced amplifier that obtains a maximum output power 210 watts with 17.20 dB gain. A proposed balanced RF amplifier is measured the reverse intermodulation products of with a situation of two closely located FM broadcast stations to compare with a single-stage class-C amplifier. The experimentation demonstrates of the transmitter using a balanced RF power amplifier that can reduce an intermodulation product 18.47 dBc.

1. Introduction

The RF power amplifiers are important components for wireless communication systems. The design techniques for RF amplifier can use classes A, B, C, and AB, etc. Each type of class-amplifiers has different features and performances. The class-C amplifiers are suitable for FM broadcasting systems because it has the output power and efficiency higher than other types. The disadvantage of class-C power amplifiers is non-linearity which creates harmonic and intermodulation signals. Harmonic signals are multiple of the fundamental frequency. It can be eliminated by using the Low Pass Filters. Intermodulation signals are unwanted signals of non-linear RF power amplifiers. When the power amplifier of FM station is injected by two frequencies which are generated intermodulation signal to fall into the other frequency ranges. The intermodulation products can be calculated from $2f_2$-f_1 and $3f_2$-$2f_1$ [1].

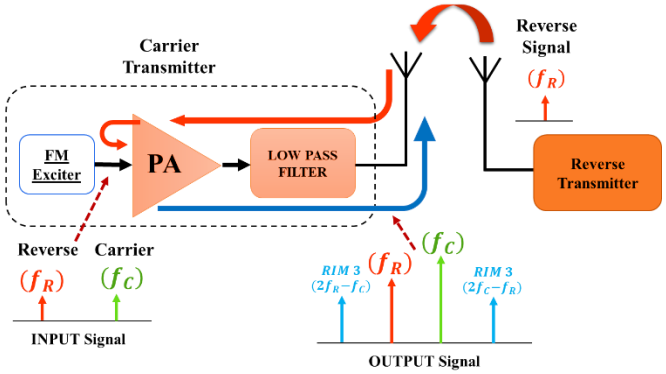

Figure 1: The reverse intermodulation products of FM broadcast stations

*Rangsan Tongta, Engineering, Institute of Engineering, Suranaree University of Technology. 111 University Avenue, Muang District Nakhon Ratchasima, Thailand. Email: tongta@sut.ac.th

Although, the FM broadcast station uses an RF power amplifier with a single frequency. In practice, the signals from nearby FM broadcast stations can radiate to the own station. In Figure 1, two closely located FM broadcasting stations, the signal from a reverse transmitter radiates into a carrier transmitter via an antenna and transmission line in the reverse direction, called "Reverse Signal". The reverse signal travels until it present at the input of a carrier transmitter. So, the station own signal and the reverse signal create intermodulation signals, called "Reverse Intermodulation (RIM)".

The FM broadcast station uses a low pass filter in the final stage to block unwanted signals, such as harmonic and intermodulation signals. A low pass filter has a wide transition band, the frequency response to change from a pass-band to a stop-band. Which frequencies of intermodulation products are very close to a cut-off frequency point of the filter that cannot eliminate intermodulation products with a low pass filter. The FM broadcast station using the frequency band is 88-108 MHz that are close to the frequency band of Air Traffic Control (ATC) systems, using the frequencies between 108-137 MHz. Therefore, reverse intermodulation signals from FM station generates may be interferences communication between air traffic controllers and pilots, as shown in Figure 2. [2]

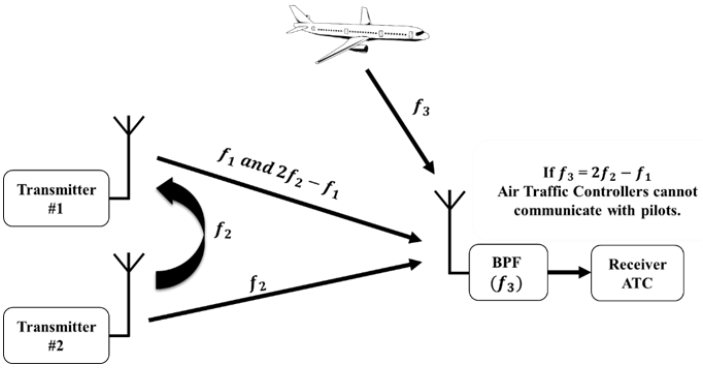

Figure 2: Intermodulation products interference to Air Traffic control systems

To overcome this problem, circulators or cavity bandpass filters are alternatives to reduce intermodulation products. It can block reverse signals from nearby stations and unwanted signals from the own station. Disadvantages of circulators and cavity bandpass filters are adding considerable cost, complexity and power loss to a system. As will be shown, none of the techniques available to reduce reverse intermodulation are particularly attractive.

This paper presents a balanced RF power amplifier using the improvement 3-dB quadrature hybrid couplers to reduce reverse intermodulation signals of FM broadcast station. The concept of balanced RF power amplifiers is structured from two identical quadrature couplers and two signal-stage amplifiers. The reverse signal from nearby FM stations radiates to the own station until it present at the input of two signal-stage amplifiers that generated intermodulation signals. The second quadrature hybrid coupler provides a 180˚ out-of-phase of two intermodulation signals from two amplifiers that can cancel intermodulation signals. The mathematics analysis of a balanced RF power amplifier for two closely located FM stations shows that can reduce the reverse intermodulation products, will be explained in section 3. In the previous work presents a design and implementation of the prototype 3-dB quadrature couplers [3]. In this work, prototype 3-dB quadrature couplers are included in a structure of a balanced RF power amplifier to reduce reverse intermodulation signals of FM broadcast station.

The quadrature hybrid couplers are an important component for a balanced RF power amplifier. Due to it can separate an input signal into two identical amplifiers and combines both output signals. The quadrature hybrid coupler has a very beneficial feature that can reduce a reverse intermodulation signal of FM broadcasting systems. The branch-line hybrid couplers are applied to traditional couplers for the balanced rf power amplifier. The branch-line is a simple type of quadrature couplers that are realized by using four transmission lines to construct a single-box coupler [4]-[5]. Each line in the single-box is a quarter-wavelength transmission line. The disadvantage of branch-line couplers is a large physical size because a quarter-wavelength transmission line determines the physical size of branch-line couplers. Especially, FM broadcasting systems use a low-frequency range that is a long transmission line that increases physical size. The large physical size is unsuitable to use for an RF power amplifier of the FM stations [6]-[10]. The quadrature hybrid couplers in this paper are structured by using the broadside-coupler stripline technique to reduce the size of couplers. Section 4 describes the design, implementation of quadrature hybrid couplers.

The prototype quadrature couplers are applied to a balanced RF power amplifier. The two identical single-stage amplifiers use a class-C RF amplifier with two MRF151 N-channel MOSFETs and operate at the frequency range of 88-108 MHz. Experimental results of the total output power, a frequency response of prototype balanced power amplifier will be presented in section 5. The situation of two closely located FM broadcast stations is used to create the reverse intermodulation signal. Two carrier transmitters that use a single-stage power amplifier and a balanced RF power amplifier have been measured. The FM broadcast station using a balanced power amplifier eliminates the intermodulation signals by using the phase-shifting property of the quadrature hybrid coupler. The reverse signals (f_R) from nearby FM stations and the intermodulation signals have a 180˚ out-of-phase which can be canceled the reverse signals and RIM signals without the cavity bandpass filters and circulators. Experimental results of the FM broadcast station using a balanced RF power amplifier comparing with single-stage RF power amplifier are presented in sections 6.

2. RF Power Amplifier for FM Broadcasting Systems

2.1. Class-C Power Amplifiers

The RF power amplifiers are an electronic circuit that transfers an input power to load such as the antenna by amplifying. FM broadcasting systems require high output power and efficiency. The Class-C amplifier offers the highest efficiency more than Class-A, Class-B, and Class-AB. The efficiency of Class-C amplifiers can be approximated about 70-80%. The disadvantage of Class-C amplifiers is non-linearity which has poor distortion qualities and generates harmonics [11]. When two signals are the input of an amplifier that creates intermodulation components (IM). The several techniques are presented reducing the intermodulation distortion by improved the RF power amplifiers, such as the feed-forward techniques [12], etc. They are

suitable to the multicarrier amplifiers which cannot eliminate the reverse signal from nearby FM broadcast stations.

2.2. Non-linear Distortion and Intermodulation Products

Non-linear distortions can be described in terms of a non-linear relationship between the input and output signals. The non-linearity creates several effects such as harmonic and intermodulation signals. Harmonic signals are unwanted signals which are included a number of integer multiples of an input frequency. Intermodulation signals occur when an input of non-linear systems are composed of two frequencies. FM broadcast stations use a Class-C amplifier that is a nonlinear system. Therefore, we can express by:

$$y(t) = \alpha_1 x(t)+\alpha_2 x(t)^2+\alpha_3 x(t)^3+\alpha_3 x(t)^4+\ldots \quad (1)$$

Where $y(t)$ represents the output, $x(t)$ represents the input and α_n represents the gain coefficient.

$$x(t) = A_1 \cos(2\pi f_1 t) + A_2 \cos(2\pi f_2 t) \quad (2)$$

If an input signal consists of two signals with different frequencies that are applied to a nonlinear system (1). The resultant of the output can be expressed as:

$$\begin{aligned} y(t) = {} & \left[\frac{\alpha_2 A_1^2}{2}+\frac{\alpha_2 A_2^2}{2}\right]+ \\ & \left[\alpha_1 A_1+\frac{3\alpha_3 A_1^3}{4}+\frac{3\alpha_3 A_1 A_2^2}{2}\right]\cos(2\pi f_1 t)+ \\ & \left[\alpha_1 A_2+\frac{3\alpha_3 A_2^3}{4}+\frac{3\alpha_3 A_1^2 A_2}{2}\right]\cos(2\pi f_2 t)+ \\ & \left[\frac{\alpha_2 A_1^2}{2}\right]\cos(2\pi 2f_1 t)+\left[\frac{\alpha_2 A_2^2}{2}\right]\cos(2\pi 2f_2 t)+ \\ & \left[\frac{3\alpha_3 A_1^2 A_2}{4}\right]\cos\left(2\pi t(2f_1+f_2)\right)+ \\ & \left[\frac{3\alpha_3 A_1 A_2^2}{4}\right]\cos\left(2\pi t(2f_2+f_1)\right)+ \\ & \left[\frac{3\alpha_3 A_1^2 A_2}{4}\right]\cos\left(2\pi t(2f_1-f_2)\right)+ \\ & \left[\frac{3\alpha_3 A_1 A_2^2}{4}\right]\cos\left(2\pi t(2f_2-f_1)\right)+\ldots \end{aligned} \quad (3)$$

From (3), the output that does not contain only the fundamental frequency. The nonlinearity gives other frequencies adding to output components. The second term of this expression shows the amplitude of the fundamental frequencies. The third term shows the second-order harmonics. The fourth and fifth terms show third-order intermodulation distortions. The terms of $2f_1$-f_2, $2f_2$-f_1 are third-order intermodulation products. The intermodulation signals are very close to fundamental frequencies which are cannot be easily filtered.

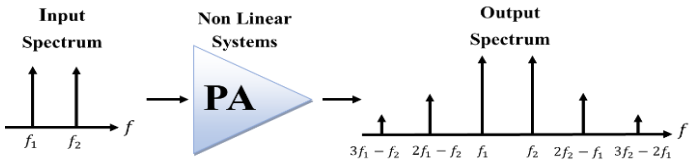

Figure 3: Intermodulation Products of nonlinear systems

3. Balanced RF Power Amplifier

The balance RF power architecture shows in Figure 4. Two identical signal-stage amplifiers are parallel connecting with two quadrature hybrid couplers. Both amplifiers share the same input signal ($x_{in}(t)$) which is fed through the quadrature hybrid coupler. The first quadrature hybrid coupler on the input is the splitter that divides an input signal (from port 1) into two equal amplitude outputs (port 2 and port 3) with a 90˚ phase difference. The input signal of the first amplifier (PA1) has been 90˚ phase-shifted and the signal of the second amplifier (PA2) has been 180˚ phase shifted. Two amplifiers have the same bias voltage that provides equal output power capability. The second quadrature hybrid coupler on the output is a combiner that is connected to the output stages of two amplifiers. which an output signal of PA1 connect to port 1 and an output signal of PA2 connect to port 4. Both output signals are in-phase on port 3 that means output signals from two amplifiers are combined. While output signals are out-of-phase at port 2 that mean the output signals from two amplifiers are canceled. A port 2 of a hybrid coupler is an isolation port that is terminated by match load 50Ω.

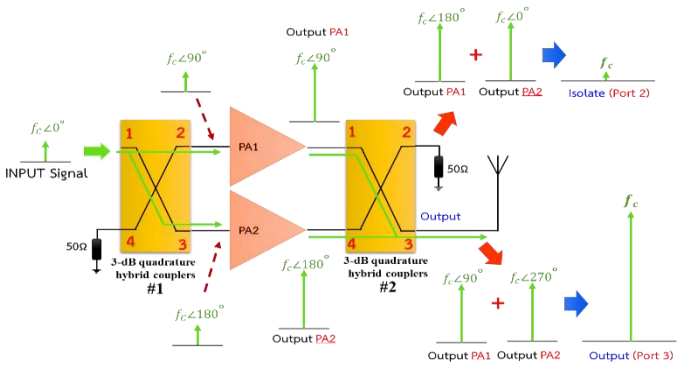

Figure 4: The balanced RF power amplifier structures

3.1. Analysis of the Balanced RF Power Amplifier to Reduce Reverse Intermodulation Products

This paper proposes the balanced RF power amplifier that reduces the reverse intermodulation products. From Figure 5, an input signal is $x_i(t)$ which represents the FM modulation signal. The input signal is fed through the first quadrature hybrid coupler which separates an input signal into two equally signals with a 90˚ phase difference, we can express by:

$$x_{i1}(t) = \frac{1}{2}\cos(2\pi f_C t+90^\circ) \quad (4)$$

$$x_{i2}(t) = \frac{1}{2}\cos(2\pi f_C t+180^\circ) \quad (5)$$

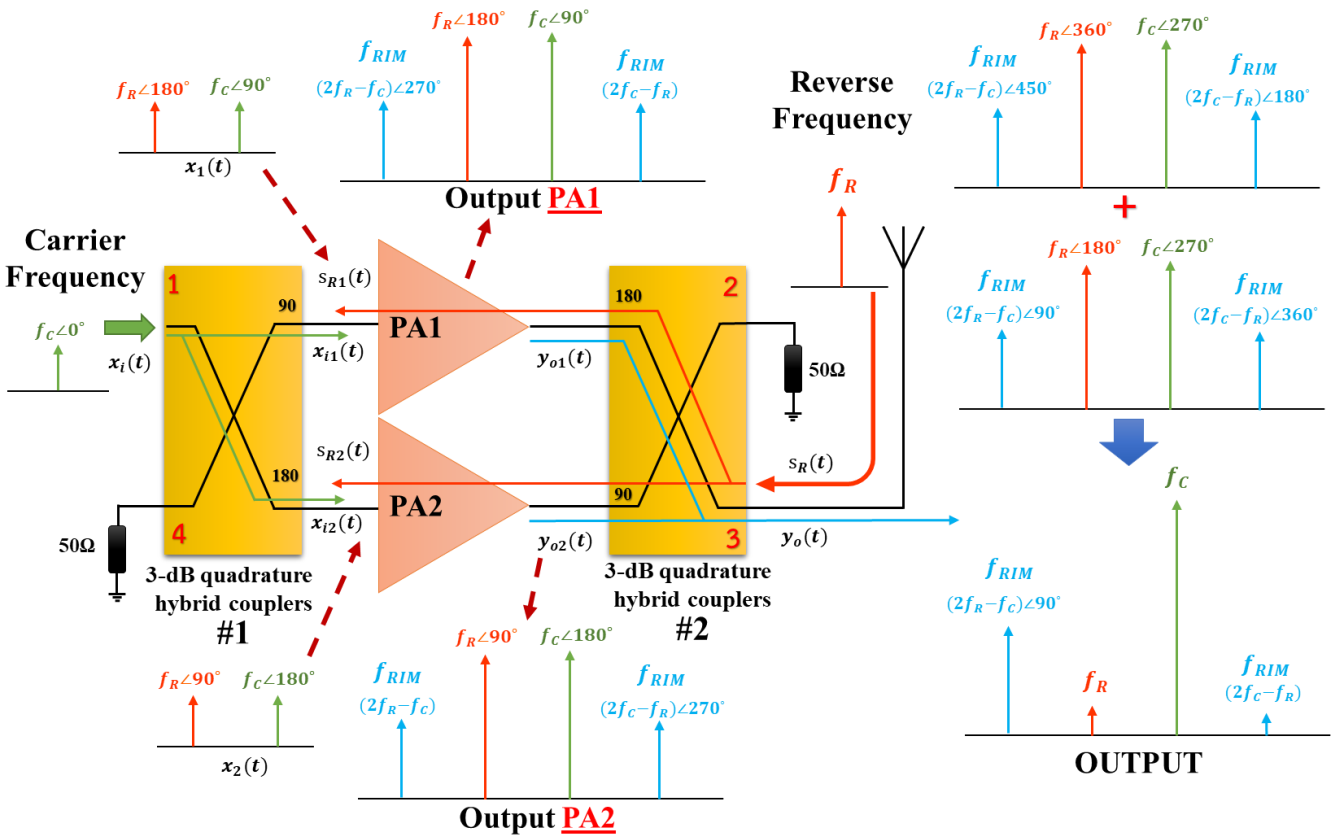

Figure 5: The analysis of a balanced RF power amplifier to reduce reverse intermodulation products

Where $x_{i1}(t)$ is an input signal for the first power amplifier and the $x_{i2}(t)$ is an input signal for the second power amplifier. The f_C represent a carrier frequency. When the reverse signal ($S_R(t)$) from nearby FM station travels in a reverse direction until it presents at the output stage, the port 3 of a second quadrature hybrid coupler. A similar expression for the output stage of a balanced amplifier, a second quadrature hybrid coupler is the symmetric 4-port microwave device that separates a reverse signal to two equally signals with a relative phase difference of 90˚. We can express both reverse signals by:

$$S_{R1}(t) = \frac{1}{2}\cos(2\pi f_R t + 180^\circ) \quad (6)$$

$$S_{R2}(t) = \frac{1}{2}\cos(2\pi f_R t + 90^\circ) \quad (7)$$

Where $S_{R1}(t)$ and $S_{R2}(t)$ are the respective reverse signals traveling into two power amplifiers and the f_R is a frequency of a reverse signal. Both reverse signals travel in the reverse direction through the coupler until they present at the input of each amplifier. Input signals ($x_i(t)$) together with the reverse signals ($S_{Ri}(t)$) present at an input of each power amplifiers, can be written as follows:

$$x_1(t) = x_{i1}(t) + S_{R1}(t) \quad (8)$$

$$x_2(t) = x_{i2}(t) + S_{R2}(t) \quad (9)$$

The $x_1(t)$ and $x_2(t)$ are the respective input signals of two power amplifiers. We use $x_1(t)$ and $x_2(t)$ to a nonlinearity equation of power amplifiers (1). Therefore, a resultant of the output can be expressed as:

$$\begin{aligned} y_{o1}(t) = {} & [\alpha_2] + \left[\alpha_1 + \frac{9\alpha_3}{4}\right]\cos(2\pi f_R t + 180^\circ) + \\ & \left[\alpha_1 + \frac{9\alpha_3}{4}\right]\cos(2\pi f_C t + 90^\circ) + \\ & \left[\frac{\alpha_2}{2}\right]\cos(2\pi 2f_R t + 180^\circ) + \\ & \left[\frac{\alpha_2}{2}\right]\cos(2\pi 2f_C t + 90^\circ) + \\ & \left[\frac{3\alpha_3}{4}\right]\cos(2\pi t(2f_R + f_C) + 90^\circ) + \\ & \left[\frac{3\alpha_3}{4}\right]\cos\left(2\pi t(2f_C + f_R)\right) + \\ & \left[\frac{3\alpha_3}{4}\right]\cos(2\pi t(2f_R - f_C) + 270^\circ) + \\ & \left[\frac{3\alpha_3}{4}\right]\cos\left(2\pi t(2f_C - f_R)\right) + \\ & \left[\frac{\alpha_3}{4}\right]\cos(2\pi 3f_R t + 180^\circ) + \\ & \left[\frac{\alpha_3}{4}\right]\cos(2\pi 3f_C t + 90^\circ) + \ldots \end{aligned} \quad (10)$$

$$y_{o2}(t) = [\alpha_2] + \left[\alpha_1 + \frac{9\alpha_3}{4}\right]\cos(2\pi f_R t + 90^\circ) + \quad (11)$$

$$\left[\alpha_1 + \frac{9\alpha_3}{4}\right]\cos(2\pi f_C t + 180^\circ) +$$

$$\left[\frac{\alpha_2}{2}\right]\cos(2\pi 2f_R t + 90^\circ) +$$

$$\left[\frac{\alpha_2}{2}\right]\cos(2\pi 2f_C t + 180^\circ) +$$

$$\left[\frac{3\alpha_3}{4}\right]\cos\left(2\pi t(2f_R + f_C)\right) +$$

$$\left[\frac{3\alpha_3}{4}\right]\cos(2\pi t(2f_C + f_R) + 90^\circ) +$$

$$\left[\frac{3\alpha_3}{4}\right]\cos\left(2\pi t(2f_R - f_C)\right) +$$

$$\left[\frac{3\alpha_3}{4}\right]\cos(2\pi t(2f_C - f_R) + 270^\circ) +$$

$$\left[\frac{\alpha_3}{4}\right]\cos(2\pi 3f_R t + 90^\circ) +$$

$$\left[\frac{\alpha_3}{4}\right]\cos(2\pi 3f_C t + 180^\circ) + \ldots$$

The $y_{o1}(t)$ and $y_{o2}(t)$ are respective output signals of two power amplifiers. Both output signals are several effects of a nonlinear distortion that contains the term of the carrier frequency, the reverse frequency, the harmonics, and the third-order intermodulation products. Both output signals are combined by a second quadrature coupler which is connected to an output signal $y_{o1}(t)$ at port 1 and an output signal $y_{o2}(t)$ at port 4. The term of a reverse frequency (f_R) and the term of intermodulation product ($2f_C$-f_R) are out-of-phase on port 3 of a second quadrature coupler. Thus, the reverse signal and the intermodulation signal are canceled. A similar expression, a term of a carrier frequency (f_C) is in-phase on port 3. So that the total output power can be increased and can be expressed as:

$$y_o(t) = 2\alpha_2 + 2\left[\alpha_1 + \frac{9\alpha_3}{4}\right]\cos(2\pi f_C t + 270^\circ) + \quad (12)$$

$$\alpha_2\cos(2\pi 2f_C t + 270^\circ) +$$

$$\left[\frac{6\alpha_3}{4}\right]\cos(2\pi t(2f_C + f_R) + 180^\circ) +$$

$$\left[\frac{6\alpha_3}{4}\right]\cos(2\pi t(2f_R - f_C) + 90^\circ) +$$

$$\left[\frac{\alpha_3}{4}\right]\cos(2\pi 3f_C t + 270^\circ) + \ldots$$

The math model of balanced RF power amplifiers with a carrier frequency (f_C) 100 MHz and a reverse frequency (f_R) 95 MHz is simulated. The line spectrums of simulation results show in Figure 6. The intermodulation signals in term of ($2f_C$-f_R) and a reverse signal are eliminated.

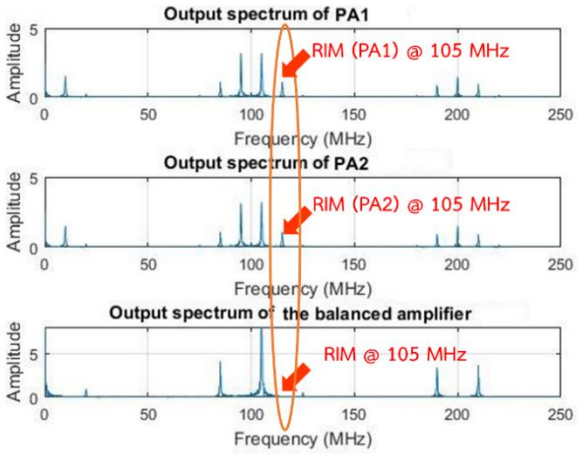

Figure 6: Simulation results of the math model based on a balanced RF power amplifier

3.2. Intermodulation Measurements

The third-order intermodulation distortion creates additional frequencies in terms of $2f_1 - f_2$ and $2f_2 - f_1$. The measurement is described by the power ratio between the power level of a fundamental frequency and intermodulation products, can be expressed as:

$$P_{IM3}(\text{dBc}) = P_C(\text{dBm}) - P_S(\text{dBm}) \quad (13)$$

Where the P_C is a power of a fundamental frequency and the P_s is the power of a third-order intermodulation product. The P_{IM3} is the intermodulation level (dBc) of an intermodulation product relative to a power level of the fundamental frequency.

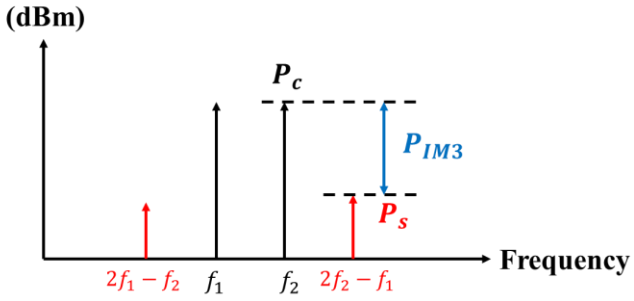

Figure 7: Intermodulation Distortion Measurement

4. Design and Implementation of 3-dB Quadrature Hybrid Couplers

The conventional couplers for balance power amplifiers use branch-line hybrid couplers because it is simple and easy to make. The size of the branch-line couplers is increased when using in an FM frequency range. The reducing of the physical size of branch-line couplers, many methods have been suggested. The slow-wave transmission line technique can make short-wavelength transmission lines by reducing phase velocity [13]-[17]. The increasing of inductances and capacitances with the same ratio causes reducing phase velocity while a characteristic impedance of the coupler is unchanged. Also, lumped-element hybrid couplers use for reducing the circuit size of branch-line hybrid couplers [18]-[19]. Lumped-element circuits are realized by using

LC-microstrip resonance circuits to replace the line sections of branch-line couplers. The lumped-element circuits have a characteristic impedance equivalent to the quarter-wavelength transmission line while the circuit size of lumped-element circuits is shorter than the branch-line couplers.

Lange couplers are two parallel microstrip lines with alternate lines on the same surface [20]- [21]. The alternate lines can reduce the occupied area of couplers. However, after the circuit of couplers have been processed, the circuit requires wire bonders for bonding the conductor spacing of coupler lines [22]. Wire bonders increase the manufacturing processes which are difficult to realize. Broadside-coupler striplines are the hybrid couplers without bonding wires [23]. The broadside-coupler structure comprises two parallel quarter-wavelength transmission lines on the opposite surface. A coupled line is a floating transmission line overlay on a signal line. The length of a coupled line determines the physical size of the hybrid couplers. It can be significantly reduced the occupied area of couplers by using symmetrical circuits of two parallel striplines with the opposite surface and using tightly stripline. The coupling coefficient of couplers is increased by using printed circuit broads with a small substrate thickness, e.g., 0.1mm substrate thickness, which has expensive cost and is difficult to find [24]-[29].

The broadside-coupled striplines in this paper consist of two parallel lines which are embedded in a dielectric between two ground planes [26]-[28], as shown in Fig. 8. The energy transfer from a signal line to a coupler line occurs at the through parallel striplines.

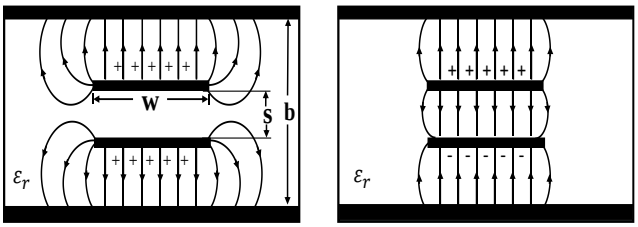

Figure 8: voltages and currents on two striplines.
(a) Even-mode field distribution.
(b) Odd-mode field distribution.

The configuration as shown in Fig. 8 is used to design a broadside coupler. The coupling coefficient can be calculated in terms of a characteristic impedance (Z_0). The voltage coupling coefficient (C) is calculated from the characteristic impedances of even-mode (Z_{0e}) and odd-mode (Z_{0o}) which can be expressed as [30]:

$$Z_{0e} = Z_0\sqrt{\frac{1+C}{1-C}} \tag{14}$$

$$Z_{0o} = Z_0\sqrt{\frac{1-C}{1+C}} \tag{15}$$

According to Cohn [31]-[33], the even-mode and odd-mode characteristic impedances with respect to ground planes can be calculated by:

$$Z_{0e} = \frac{188.3}{\sqrt{\varepsilon_r}}\frac{K(k^{\square})}{K(k)} \tag{16}$$

$$Z_{0o} = \frac{296.1}{\sqrt{\varepsilon_r}\frac{b}{s}\,tan^{\square-1}(k)} \tag{17}$$

Where $K(k)$ and $K(k^{'})$ are complete elliptic integrals of the first kind and $k' = \sqrt{1-k^2}$. The ground plane spacing (b) and the spacing between two parallel striplines (s) are used to calculate the k parameter which can be calculated by:

$$\frac{K(k')}{K(k)} \approx \frac{2}{\pi}\ln\left[\frac{4}{k}\right] \tag{18}$$

Thus, we can calculate the stripline width (w) from:

$$\frac{w}{b} = \frac{1}{\pi}\left[\ln\left(\frac{1+R}{1-R}\right) - \frac{s}{b}\ln\left(\frac{1+\frac{R}{k}}{1-\frac{R}{k}}\right)\right] \tag{19}$$

$$R = \sqrt{\left[\frac{\left(k\frac{b}{s}-1\right)}{\left(\frac{1}{k}\frac{b}{s}-1\right)}\right]} \tag{20}$$

The circuit design of a 3-dB quadrature hybrid coupler, as shown in Figure 9. The top stripline is embedded between the substrate 1 and the top ground plane. The bottom stripline is embedded between the substrate 3 and the bottom ground plane. The space between the top stripline and the bottom stripline is inserted by a substrate 2, as shown in Figure 9 (a). Assume, the input signal is injected into port 1, called "input port". The bottom stripline passes an input signal to port 3, called "directed port". Also, an input signal is coupled via the top stripline to port 2, called "coupled port". An input signal is divided by a 3-dB quadrature hybrid coupler into two equal amplitude outputs with a 90˚ relative phase difference. The input and coupled signals are canceled at the port 4 that has no signal going out from this port, called "isolated port".

The hybrid coupler is implemented at the frequency of 98 MHz, It is a center frequency of FM broadcast systems. The FR-4 printed circuit broads (PCB) are used to make prototype couplers. A dielectric constant (ε_r) of an FR-4 PCB is 4.6 and a substrate thickness (s) is 0.8 mm. Assuming the characteristic impedance (Z_0) is 50 Ω, coupling coefficients (C) is 0.707 The summarize calculated parameters from (14) – (20) are the stripline width (w) 2.54 mm. The ground plane spacing (b) is 10.4 mm. The length of a coupled line (L) is 385 mm. The circuit of a 3-dB quadrature hybrid coupler using tightly microstrip line, as shown in Figure 9(b). This circuit designed is simulated with the CST software to verify a proposed hybrid coupler.

Due to the general FR-4 PCBs have 1.6 mm and 0.8 mm substrate thickness while the dimension of ground plane spacing (b) of the proposed coupler is 10.4 mm. Thus, we choose an FR-4 PCB with 1.6 mm substrate thickness to make substrate 1 and substrate 3 which can be made by using PCBs piling up to three layers. The constructed of a prototype coupler is shown in Fig. 9. The overall physical dimension is 75×85 mm.

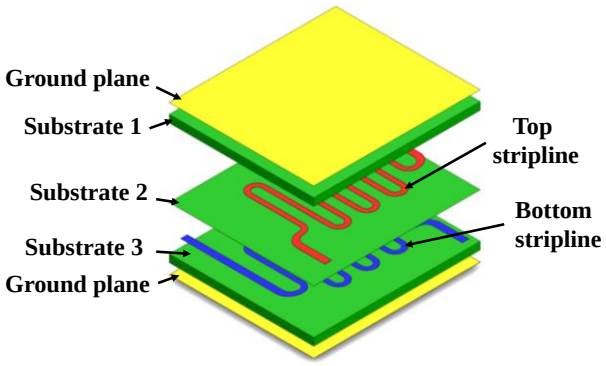

(a) Layers of the 3dB quadrature coupler

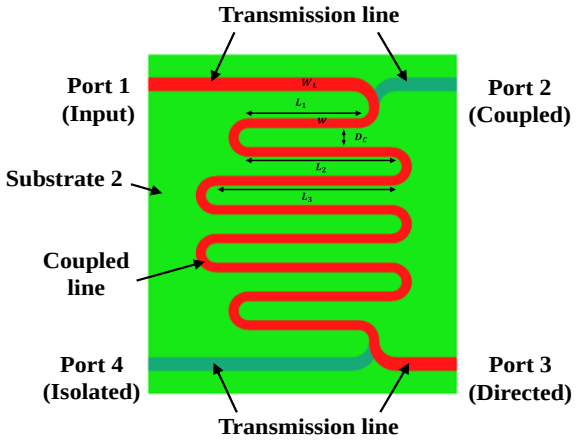

(b) Circuit layouts were designed

Figure 9: The configuration of a 3-dB quadrature hybrid coupler
(a) Layers of the 3-dB quadrature hybrid coupler
(b) Circuit layout of the 3-dB quadrature hybrid coupler

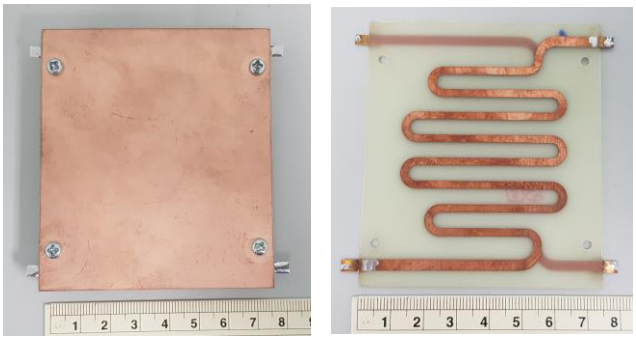

(a) Physical size of the coupler (b) Circuit layout of the coupler

Figure 10: Photographs of the prototype coupler

4.1. Measurement Results of the Quadrature Hybrid Couplers

In this section presents the experimental results of the prototype 3-dB hybrid coupler. The frequency range between 25 MHz to 150 MHz has return losses lower than -15dB, as shown in Figure 11. The center frequency of an FM broadcasting systems (98MHz) provides a maximum coupling coefficient, as shown in Figure 12. The coupling coefficient between a signal line and a coupler line is -3.4 dB (S21) and The transmitted coefficient between a signal line and a coupler line is -3.3 dB (S31). The relative phase difference between the two output ports is 90 ± 2˚, as shown in Figure 13. The measured isolations (S41) are lower than -17 dB. The input and coupled signals are canceled at the port 4.

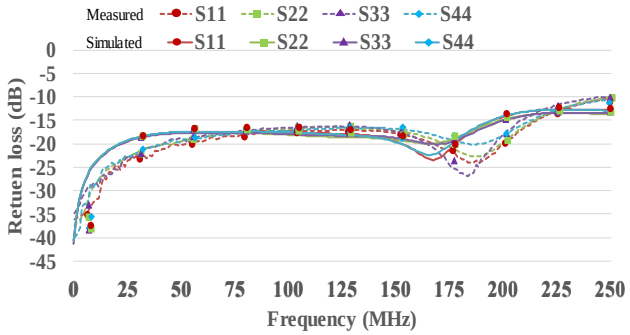

Figure 11: Measured and simulated results of the return loss

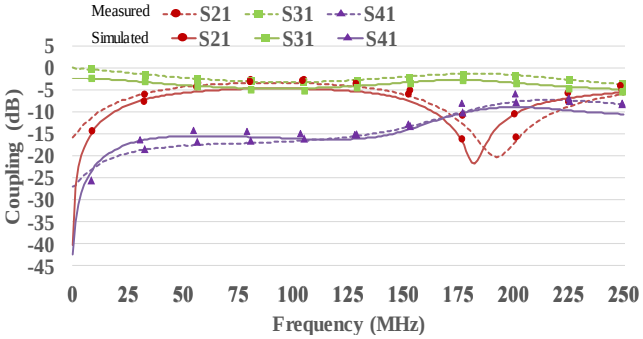

Figure 12: Measured and simulated results of the coupling coefficient

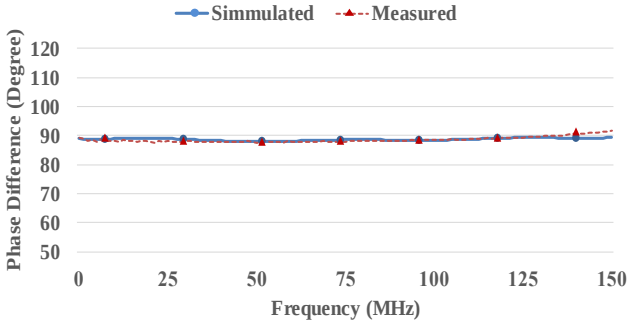

Figure 13: Measured and simulated results of the relative phase difference

5. Design and Implementation of Balanced RF Power Amplifiers

The balanced power amplifier was implemented by using two prototype 3-dB quadrature hybrid couplers. The first coupler divides an input signal into two identical single-stage amplifiers. The amplifier modules were designed for FM broadcasting systems, at 88-108 MHz frequency range, based on class-C push-pull amplifiers. The single-stage amplifier consists of 2 x MRF151 N-channel MOSFET. The bias configuration set a drain-source voltage (Vds) = 48V, drain-source current (Ids) = 0.3A and gate-source voltage (Vgs) = 2.9V. Maximum output power is 250-W with gain 14 dB. Two amplifiers have the

same bias voltage which provides an equal output power capability. The output signals from two amplifiers are combined by the second quadrature coupler. The total power is transmitted to the antenna systems.

The prototype of a balanced power amplifier shows in Figure 14. The port 1 of the first couplers is an input port and the port 3 of the second couplers is an output port. Isolated ports, port 4 of first couplers and port 2 of seconded couplers, are terminated by a dummy load 50 Ω. When the input and output impedance is poorly matched with the RF power amplifiers that are propagated signals reflected into a dummy load.

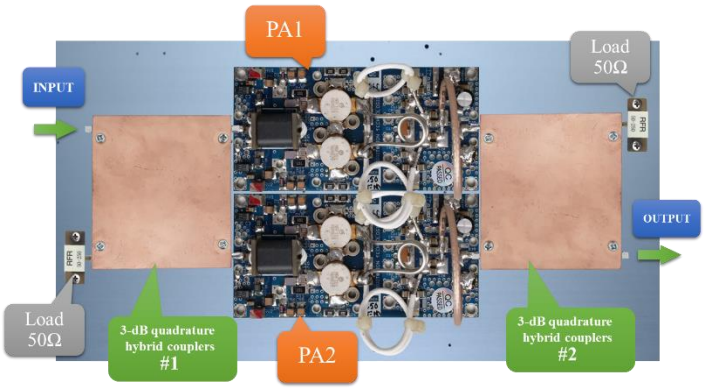

Figure 14: The configuration of a prototype balanced RF power amplifier

5.1. Measurement Results of the Balanced RF Power Amplifiers

The ROHED&SCHWARZ NRP2 Power meter is used to measure a balanced RF power amplifier. The Agilent E4421B signal generator creates an FM modulation signal and injects to the input port of a balanced amplifier. The first measurement focuses on the output power of each single-stage amplifier. The proposed balanced amplifier was tested at frequency 105 MHz that is a reverse frequency. Output powers of each amplifier module compared to the input power level displays in Figure 15. when the input power level is 4 watt that provides the output power of two amplifiers approximately 116.20 watts and 118.90 watts respectively. The line curves of two amplifiers have been overlapped. The result shows that two amplifiers are equal output power capability which can be combined.

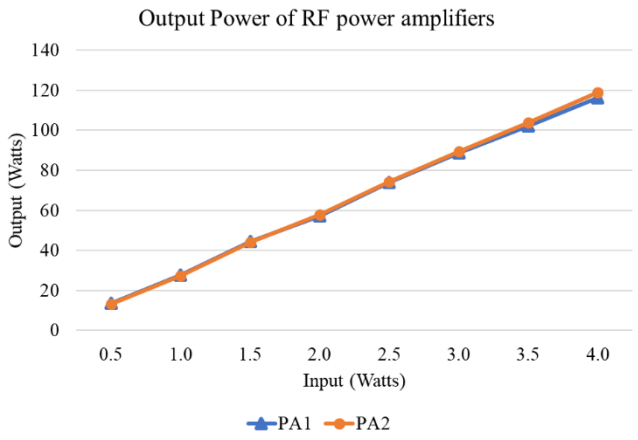

Figure 15: Measured results of the output power of each amplifier module

The second measurement focuses on the total output power of a balanced RF power amplifier. The total power is realized by the sum of two signals from two single-stage amplifiers that use the second quadrature hybrid coupler. The prototype balanced amplifier obtains an output power of 210 watts with a gain of 17.20 dB when the input power level is 4 watts. The output power has been dropped off 25.1 watts from sum signals of two amplifiers due to the insertion loss of the coupler at the output stage.

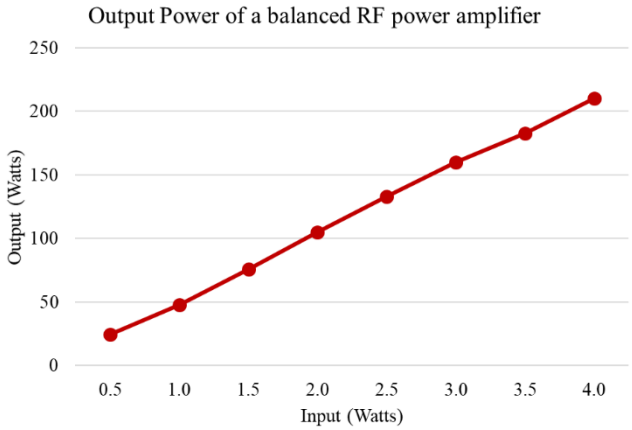

Figure 16: Measured results of the balanced RF power amplifier

6. Measurement Results of a Balanced RF Power Amplifier using to Reduce Reverse Intermodulation Products

6.1. Measurement Setup

This section presents experimental results of the FM broadcast station using a balanced RF power amplifier to reduce the reverse intermodulation. A practical setup, as shown in Figure 17, is used to demonstrate the situation of two closely located FM broadcast stations. The one FM transmitter generates a reverse frequency (f_R) that is transmitted 500 watts output power at 99.50 MHz. Another FM transmitter generates a carrier frequency (f_C) at 105.00 MHz. The two parallel antenna systems for a reverse frequency and a carrier frequency are installed in the same tower which has a height 60 meter. This configuration provides a maximum level of reverse intermodulation products. The reverse transmitter uses a cavity bandpass filter in the output stage which ensures to block unwanted signals from this transmitter.

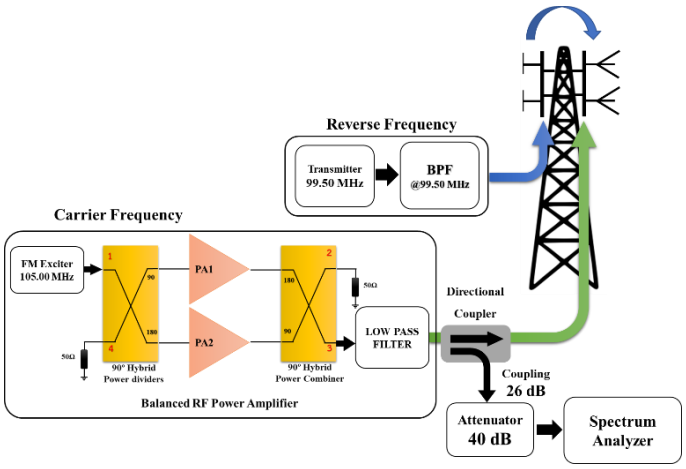

Figure 17: Measurement setup to demonstrate the situation of two closely located FM broadcast stations.

Two transmitters are measured in this research. The first transmitter uses a single-stage RF power amplifier, based on a class-C push-pull, and the second transmitter uses a prototype balanced amplifier in this research. Two transmitters are used to generate a carrier frequency (f_C) that is transmitted 200 watts output power at 105.00 MHz. Almost output signals from a transmitter is measured via a directional coupler with a coupling value of 26 dB and an attenuator of 40 dB. Intermodulation products are provided in terms of $2f_1 - f_2$ and $2f_2 - f_1$ that are a frequency of 94.00 MHz and 110.50 MHz respectively. Since the frequency of 110.50 MHz is out of an FM frequency band and falls into the frequency range of Air Traffic Control systems. Therefore, the measurement results consider the intermodulation product in terms of $2f_2 - f_1$ only.

6.2. Measurement Results of the FM transmitters using a single-stage power amplifier.

Measurement results of a carrier transmitter using a single-stage power amplifier present in Figure 18. The carrier transmitter transmits an FM modulation signal that is the frequency of 105.00 MHz without cavity bandpass filters. The signal strength of a reverse frequency, at the frequency of 99.50 MHz, is -42.35 dBm that is a signal traveling until it present at the output state of the carrier transmitter, port 3 of the second quadrature coupler. The output power of a carrier frequency at 105.00 MHz is -17.55 dBm and the intermodulation level at 110.50 MHz is 30.87 dBc.

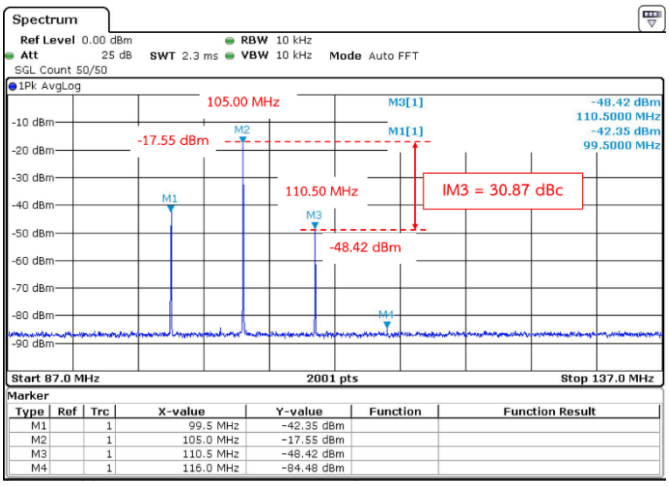

Figure 18: Intermodulation level of the FM transmitter using a single-stage RF power amplifier

6.3. Measurement Results of the FM transmitters using a Prototype Balanced RF Power Amplifier

The FM transmitter using a prototype of a balanced RF power amplifier is measured that is compared with a single-stage RF power amplifier. The output power of a balanced amplifier must be adjusted equal to a single-stage RF power amplifier. From Figure 17, the frequency spectrum shows that the signal strength of a reverse frequency at 99.50 MHz is -50.89 dBm which is decreased by 8.54 dBm. The output power of a carrier frequency at 105.00 MHz is -16.50 dBm and the intermodulation level is 49.34 dBc. Table 1 shows a comparison of the measurement results of two FM transmitters that use a single-stage RF power amplifier and a balanced RF power amplifier. It shows that both transmitters provide the same power level which is approximate -17 dBm. A power level of a reverse frequency is less than a single-stage RF power amplifier. The balanced RF power amplifier provides a good performance that improvements an intermodulation level from 30.84 dBc to 49.34 dBc. Measurement results are according to the analysis in section 3. The results show the mitigation of an intermodulation signal that is approximate 18.47 dBc without cavity bandpass filters. The mitigation intermodulation signal is difficult to obtain a maximum reduction due to the quadrature hybrid couplers have slightly different amplitudes and phases.

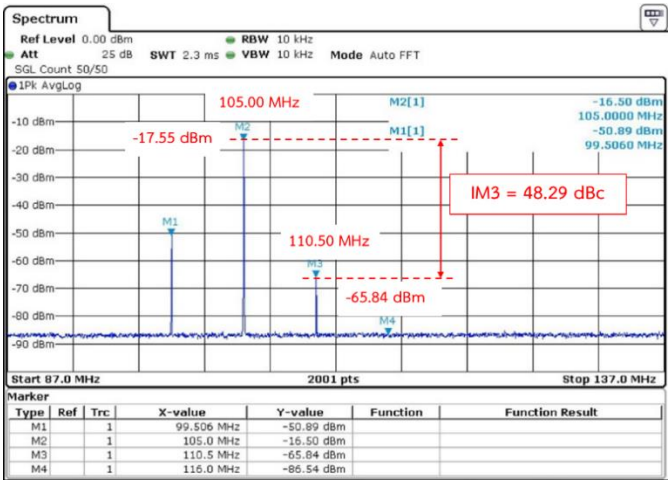

Figure 19: Intermodulation level of the FM transmitter using an FM transmitter using a Balanced RF Power Amplifier

Table 1: Measurement results of two FM transmitters.

	Signal Strength		
Frequency (MHz) / Amplifier types	99.50 (dBm)	105.00 (dBm)	110.50 (dBc)
The single-stage RF power amplifier	-42.35	-17.55	30.87
The balanced RF Power Amplifier	-50.89	-16.50	49.34
Δ	-8.54	1.05	18.47

7. Conclusions

This paper proposes a balanced RF power amplifier using the improvement 3-dB quadrature hybrid couplers to reduce the reverse intermodulation of FM broadcast stations. The balanced RF power amplifier was implemented by using the prototype 3-dB quadrature hybrid couplers. The FR-4 low-cost PCB with a broadside-coupled striplines technique is chosen to construct prototype couplers that can reduce the overall size of a hybrid coupler and suitable to use for balanced RF power amplifies. Experimental results of the prototype coupler, The return loss is lower than -15 dB. The coupled port has a coupling coefficient -3.4 dB and the directed port has a coupling coefficient -3.3 dB. The phase difference between a coupled and directed port is $90 \pm 2^{\circ}$. Isolation values are lower than -17 dB. The overall size of the prototype couplers is 75x 85 mm. We apply a prototype 3-dB quadrature hybrid couplers to a balanced power amplifier which are structured from two identical quadrature couplers and two signal-stage amplifiers. The two identical single-stage amplifiers use a class-C RF amplifier with the MRF151 N-channel MOSFET and operate at the frequency range of 88-108 MHz. A balanced

amplifier obtains an output power of 210 watts with a gain of 17.20 dB when the input power level is 4 watts.

The situation of two closely located FM broadcast stations is used to create the reverse intermodulation signal. The one transmitter generates a reverse signal (f_R) at 99.50 MHz that is transmitted 500 watts output power and another transmitter generate a carrier signal (f_C) at 105.00 MHz. The antenna systems for two frequency are installed in the same tower which has height 60 meters. Two carrier transmitters which use a balanced RF power amplifier and a single-stage RF power amplifier are measured. The carrier transmitter using a balanced RF power amplifier improvements an intermodulation level from 30.84 dBc to 49.34 dBc. The results show the mitigation of an intermodulation signal approximate 18.47 dBc without cavity bandpass filters. The mitigation intermodulation signal is difficult to obtain a maximum reduction due to the quadrature hybrid couplers have slightly different amplitudes and phases.

Acknowledgment

This work was supported by The National Broadcasting and Telecommunications Commission (NBTC) of Thailand and the Research Department Institute of Engineering, Suranaree University of Technology (SUT), Nakhon Ratchasima, Thailand.

References

[1] David Hand C.Eng MIET, “THE RF CHALLENGES OF ATC COMMUNICATIONS” Consultant Engineer - Park Air Systems Ltd.

[2] Jaiyen, N., Hantula, P., & Tongta, R. (2017, December). Real-time audio similarity comparison algorithm. In 2017 IEEE 15th Student Conference on Research and Development (SCOReD) (pp. 477-480). IEEE.

[3] Hantula, P., Jaiyen, N., & Tongta, R. (2018, August). A 3-dB Quadrature Coupler Using Broadside Striplines for FM Power Amplifiers. In 2018 IEEE International Workshop on Electromagnetics: Applications and Student Innovation Competition (iWEM) (pp. 1-2). IEEE.

[4] Alcon Garcia, P., Esparza Lopez, N., Herran Ontanon, L. F., & Las Heras Andres, F. (2016). Complex Impedance Transformers Based on Branch-Line Hybrid Couplers. Progress In Electromagnetics Research, 69, 147-157.

[5] Jung, S. C., Negra, R., & Ghannouchi, F. M. (2008). A design methodology for miniaturized 3-dB branch-line hybrid couplers using distributed capacitors printed in the inner area. IEEE Transactions on Microwave Theory and Techniques, 56(12), 2950-2953.

[6] Hussein, Ehab Abdul Razzaq, and Mohammed A. Abdulkadhim. "Performance improvement of BER in OFDM system using feed forward technique on power amplifier." International Journal of Computer Applications 75.4 (2013).

[7] Amanpreet Kaur, Rajbir Kaur “Reducing the Third-Order Inter Modulation Distortion by Feed Forward Linearization of Power Amplifier” International Journal of Advanced Research in Computer and Communication Engineering Vol. 5, Issue 1, January 2016

[8] Parsons, K. J., R. J. Wilkinson, and P. B. Kenington. "A highly-efficient linear amplifier for satellite and cellular applications." Global Telecommunications Conference, 1995. GLOBECOM'95. , IEEE. Vol. 1. IEEE, 1995.

[9] Grebennikov, Andrei. "Linearity Improvement Techniques for Wireless Transmitters: Part 2." High frequency electronics (2009): 16-26.

[10] Katz, Allen, et al. "Sensitivity and mitigation of reverse IMD in power amplifiers." Power Amplifiers for Wireless and Radio Applications (PAWR), 2011 IEEE Topical Conference on. IEEE, 2011.

[11] Berglund, Bo, Thorsten Nygren, and Karl-Gosta Sahlman. "RF multicarrier amplifier for third-generation systems." ERICSSON REV (ENGL ED) 78.4 (2001): 184-189.

[12] Ma, Hongbo, and Quanyuan Feng. "An improved design of feed-forward power amplifier." PIERS Online 3.4 (2007): 363-367.

[13] Tsai, K. Y., Yang, H. S., Chen, J. H., & Chen, Y. J. E. (2011). A miniaturized 3 dB branch-line hybrid coupler with harmonics suppression. IEEE Microwave and Wireless Components Letters, 21(10), 537-539.

[14] Sun, K. O., Ho, S. J., Yen, C. C., & van der Weide, D. (2005). A compact branch-line coupler using discontinuous microstrip lines. IEEE Microwave and Wireless Components Letters, 15(8), 519-520.

[15] Caillet, M., Clenet, M., Sharaiha, A., & Antar, Y. M. (2009). A compact wide-band rat-race hybrid using microstrip lines. IEEE Microwave and Wireless Components Letters, 19(4), 191-193.

[16] Li, H., Zhang, H. L., Hu, B. J., Wei, X. D., & Zeng, W. (2015, September). Novel wideband quadrature hybrid coupler with tunable power dividing ratio. In Signal Processing, Communications and Computing (ICSPCC), 2015 IEEE International Conference on (pp. 1-4). IEEE.

[17] de Paco, P., Verdu, J., Menendez, Ó., & Corrales, E. (2008). Branch-line coupler based on edge-coupled parallel lines with improved balanced response. IEEE Transactions on Microwave Theory and Techniques, 56(12), 2936-2941.

[18] Vijayaraghavan, A. S., & Dunleavy, L. (2011). Design and optimization of lumped element hybrid couplers. High Frequency Electronic.

[19] Moubadir, M., Aziz, H., Touhami, N. A., & Mohamed, A. (2018). A miniaturized branch-line hybrid coupler microstrip for long term evolution applications. Procedia Manufacturing, 22, 491-497.

[20] Breed, G. (2009). Transmission line and lumped element quadrature couplers. High Frequency Electronics.

[21] Kajfez, D., Paunovic, Z., & Pavlin, S. (1978). Simplified design of Lange coupler. IEEE Transactions on Microwave Theory and Techniques, 26(10), 806-808.

[22] Mao, S. G., & Wu, M. S. (2007). A novel 3-dB directional coupler with broad bandwidth and compact size using composite right/left-handed coplanar waveguides. IEEE Microwave and wireless components letters, 17(5), 331-333.

[23] Gruszczynski, S., Wincza, K., & Sachse, K. (2006). Design of compensated coupled-stripline 3-dB directional couplers, phase shifters, and magic-T's—Part I: Single-section coupled-line circuits. IEEE transactions on microwave theory and techniques, 54(11), 3986-3994.

[24] Javadzadeh, S. M. H., Majedi, S. M. S., & Farzaneh, F. (2010, September). An ultra-wideband 3-DB quadrature hybrid with multisection broadside stripline tandem structure. In International Conference on Mobile Multimedia Communications (pp. 672-681). Springer, Berlin, Heidelberg.

[25] Chang, C. P., Chiu, J. C., Chiu, H. Y., & Wang, Y. H. (2008). A 3-dB quadrature coupler using broadside-coupled coplanar waveguides. IEEE Microwave and Wireless Components Letters, 18(3), 191-193.

[26] Chiu, J. C., Lin, C. M., & Wang, Y. H. (2006). A 3-dB quadrature coupler suitable for PCB circuit design. IEEE transactions on microwave theory and techniques, 54(9), 3521-3525.

[27] Abdolhamidi, M., Mohammad-Taheri, M., & Ali-Abad, M. A. A "Design Equations for Broadside and Edgewise Stripline Couplers".

[28] May, J. W., & Rebeiz, G. M. (2008). A 40-50-GHz SiGe 1: 8 differential power divider using shielded broadside-coupled striplines. IEEE Transactions on Microwave Theory and Techniques, 56(7), 1575-1581.

[29] Bhartia, P., & Pramanick, P. (1988). Computer-aided design models for broadside-coupled striplines and millimeter-wave suspended substrate microstrip lines. IEEE transactions on microwave theory and techniques, 36(11), 1476-1481.

[30] Bahl, I. J., & Bhartia, P. (1981). The design of broadside-coupled stripline circuits. IEEE Transactions on Microwave Theory and Techniques, 29(2), 165-168.

[31] Cohn, S. B. (1960). Characteristic impedances of broadside-coupled strip transmission lines. IRE Transactions on Microwave Theory and Techniques, 8(6), 633-637.

[32] Hilberg, W. (1969). From approximations to exact relations for characteristic impedances. IEEE Transactions on Microwave Theory and Techniques, 17(5), 259-265.

[33] Raab, F. H., Asbeck, P., Cripps, S., Kenington, P. B., Popovic, Z. B., Pothecary, N. and Sokal, N. O. (2003). RF and microwave power amplifier and transmitter technologies Part 3. High Frequency Electronics, 2(3), 22-36.

ASTES

Advances in Science, Technology and Engineering Systems Journal Vol. 4, No. 4, 431-439 (2019)

www.astesj.com

Special Issue on Advancement in Engineering and Computer Science

ASTESJ

ISSN: 2415-6698

Effectiveness and Comparison of Digital Substations Over Conventional Substations

Aashir Waleed[*,1], Umar Siddique Virk[2], Muhammad Tanveer Riaz[2], Shaikh Bilal Mehmood[1], Saeed Ahmad[2], Muhammad Rameez Javed[1], Ali Raza[1]

[1]*Department of Electrical Engineering, University of Engineering & Technology, Lahore (Faisalabad Campus), 38000, Pakistan*

[2]*Department of Mechatronics & Control Engineering, University of Engineering & Technology, Lahore (Faisalabad Campus), 38000, Pakistan*

ARTICLE INFO

Article history:
Received: 06 May, 2019
Accepted: 07 August, 2019
Online: 16 August, 2019

Keywords:
Digital substations
Intelligent electronic device
Smart grids
Grid topology
Substation

ABSTRACT

The entire electrical system is changing at an abrupt speed since its beginning. With the rapid advance of renewable energies (which are constantly subject to fluctuations), the electricity generation is distributed to countless locations. The traditional model of the unidirectional flow of electricity is leaning towards multidirectional flows. This situation needs significant changes in the transport infrastructure of the electrical power system and mode of operation. Technological advancements are making a smarter and more organized management system of electricity supply and demand. This development needs to incorporate modern communication, monitoring, and control capabilities, along with the intelligent transport, generation, and storage value chain. Digital substations integrate thousands of sensors by providing greater comfort, self-reliance, availability, and safety while at the same time reducing costs, risks, and environmental damage. Conventional power system lacks digital communication, remote monitoring & control, and consumer participation. Fiber-optic cabling in digital substations will attain not only real-time data transmission but also remote maintenance. The comparison between conventional and digital substations has also been presented in this work along with latest trends in smart protection. Electronic protection and control devices based on a microprocessor, communicating with cloud servers, will enhance the flexibility to control and monitor the digital substations. A significant amount of data generated by components in the electrical substations will allow greater sophistication of the monitoring, diagnostic, protection and optimization capabilities of the facilities. The goal for the review of said advancements is to have a smart electrical system with greater efficiency and better user experience.

1. Introduction

The existing grid infrastructure seems to meet part of the expectations (from traditional and renewable generation to transport and part of the distribution), but it must improve significantly from the end user and the functionalities expected from it. The forecasts indicate moderate growth in demand, a substantial increase in renewable energies and a need for firm and flexible power [1]. Consequently, a new concept of an electrical network, i.e., "intelligent network" emerges. The basic definition of "intelligent networks" may correspond to "Electric networks that intelligently integrate the behavior and actions of all the actors connected to them (those who generate electricity, those who consume it and who perform both actions) to provide a safe, economical and sustainable electricity supply"[2]. In such networks, very advanced integrated systems are used in the process of supplying electricity at all levels. The function of these integrated systems is to protect the components of the electrical system, control of the power flow and the monitoring of the process. For example, electrical system automation devices are integrated into communication networks to exchange information between various devices, as well as with supervisory systems. The technological trends of the integrated systems in the automation of electrical systems will be determined by three different technological trends such as electronic Integration, integration of switching equipment and data communication [3].

[*]Dr. Aashir Waleed, Department of Electrical Engineering, University of Engineering & Technology, Lahore (Faisalabad Campus), 38000, Pakistan, Email:aashir.walid@uet.edu.pk

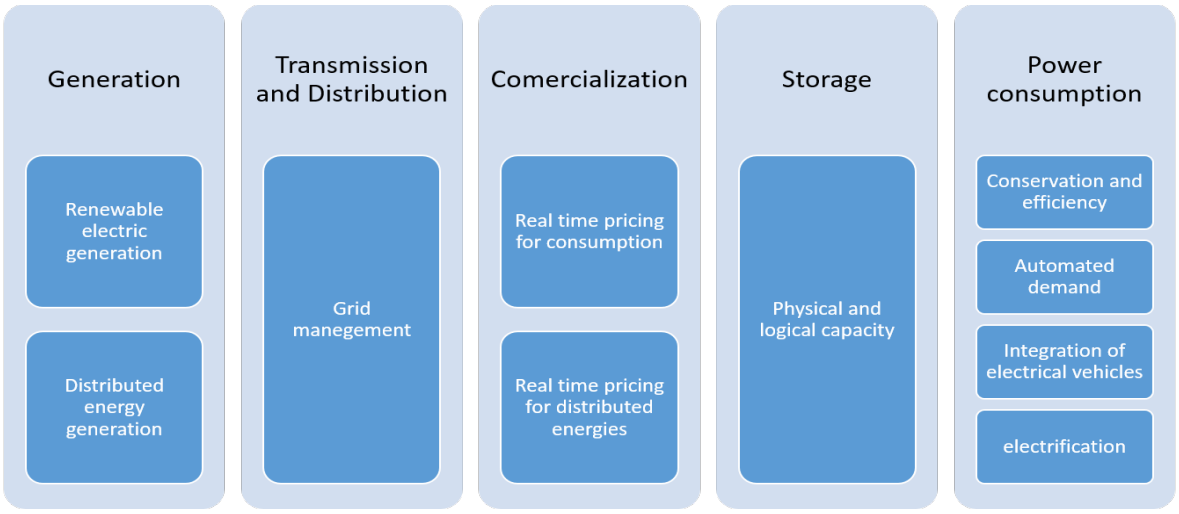

Figure 1. Challenges for current grid topology.

In the last years, an extensive research of energy production based on fossil energy sources has been performed. Fossil fuel sources have been exploited believing that there is an infinite availability of resources, but these sources cause huge damage to environment. The old energy model based on fossil fuel energy involved a chain of processes like generation, distribution, transportation, and consumption. However, to meet the consumer demand, it is necessary to upgrade the above energy model to distributed energy generation. This new energy model (Figure 1) will support variety of energy sources and an increase in the use of renewable energy and efficiency.

The main advantage of the recent energy model is distributed energy generation system. This system allows individuals to generate energy at micro-level and link to the national grid [4], which drastically reduces losses caused by the energy transport. This system facilitates the connections of all kinds of renewable energies to the system, which will ultimately improve the power system. This is possible by promoting the integration of non-manageable energies such as wind or solar power and by using energy storage devices that will be able to charge and discharge in the network. Keeping in mind the future growth and energy trends, the future projection of digital substations is provided in Figure 2.

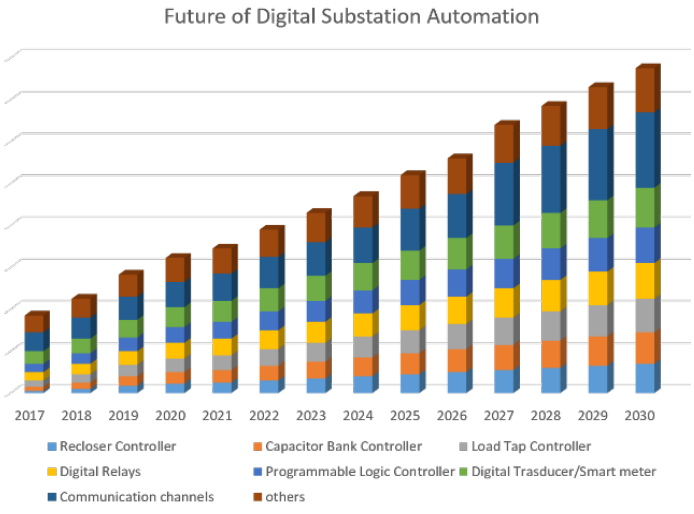

To carry out all the actions mentioned previously, the grid topology must [5], [6] have following features.

- Allow self-management of incidents, to deal with the defects that have occurred in the system and guarantee the electric flow in all the points.
- Be equipped with strength against attacks and destabilizations.
- Increase the flow of consumer participation, promoting the local generation process and providing excess energy to the network during peak hours.
- Have the capacity to supply power of adequate quality to the digital era. The higher number of generation points will allow the delivery of different energy qualities for each type of application.
- Fix a variety of generation and storage modes, thanks to the micro-grids and the generation of the energy that is distributed.
- Facilitate the flowering of markets, due to the inclusion of new elements in the network such as the electric vehicle, a more sizeable number of renewable energies, etc.
- Perform a more competent optimization of your assets and operation; this is achieved by automating all the elements that are involved.

2. Composition of Smart Grids

The Smart Grid concept refers to intelligent management of electricity using computer and communication technologies. The smart grid concept encompasses many interconnections between the different elements of the generation, transmission and distribution of electricity. In addition, the concept is strongly linked to the inclusion of unconventional renewable energies (both large-scale with large generators and household level) in the electricity grid, thus changing the current paradigm of uniqueness in generation towards a distributed generation concept.

Smart grid is smart energy network that integrates all the parameters of generation, transmission, distribution and

consumption. It also provides advanced control processes to achieve an efficient and sustainable supply (Figure 3) [7]. The motivation behind creation of smart grid is: care for the environment, reliability and quality of supply and improvement in the operation of networks.

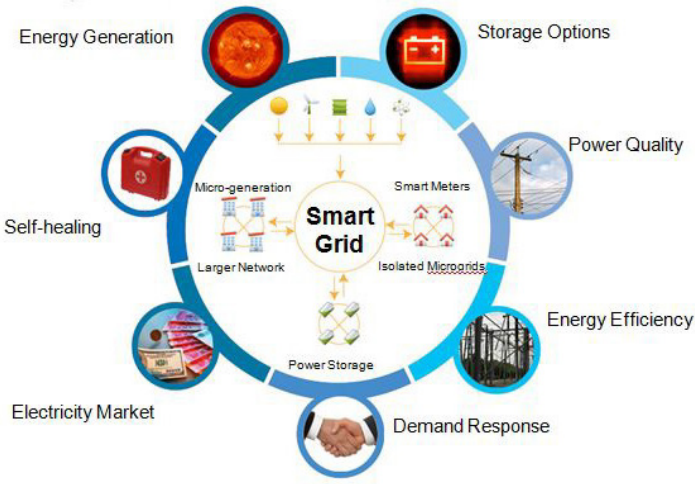

Figure 3. Different aspects that make up the smart grid

The following components must be developed to meet the above-mentioned objectives objective of smart grid:

2.1. Smart Metering:

The smart metering helps consumers to generate their own energy and inject surplus generated energy into the network at a certain price. This increases the dynamism of the system and decreases the prices of electricity [8].

2.2. Load Management:

The data delivered by the smart meters helps in effective management of load. The hourly consumption of energy as delivered by meters is the main deciding factor for the connection or disconnection management of generation sources and loads. This connection or disconnection can be automatic through intelligent controllers, which entails awareness and education of the population in general. Conclusively, this helps in developing a culture of low consumption and energy saving.

2.3. Inclusion of Renewable Energies and Electric Mobility

The smart grid also covers the issue of microgeneration in households. For that purpose, it is necessary to study the natural resources that can be used in the houses of different geographical sectors of the country and improve the technologies in their connection to the distribution lines.

2.4. Renewal of The Current Transmission Networks:

A fundamental point to achieve the above points requires the inclusion of an effective transmission network. The distributed generation and a strong increase in the amount of non-conventional renewable energies injected into the network require a transmission system that supports these bidirectional flows.

So, conclusively smart grid requires different technologies that can ensure a correct operation of this new network due to the complexity that is added to become intelligent [9].

3. Latest Developments in Smart Protection

Microgrid is normally operated parallel with utility grid and e.g. during faults in upstream network it can be separated quickly from utility grid and operated independently as an island grid. MMS will be responsible from the overall economic and energy effective operation of microgrid taking account the technical boundary conditions in both normal and island operation. In this paper only technical aspects related to LV microgrids are discussed. Technical choices made in the microgrid concept must be such that they can be justified by the needs of normal operation, but at the same time allowing and supporting the solutions needed

for implementation of island operation.

In overall the operation and control of LV microgrid is a very complex issue because there are number of things that will have influence to the behavior of microgrid in different ways. For example the dynamics of islanded microgrid, e.g. lack of inertia, is totally different when compared to the normal operation of the microgrid parallel with utility grid. Islanded microgrid is much more sensitive to disturbances and successful island operation requires fast, accurate and stable control.

In addition the protection of the future microgrid is a challenging issue and very strongly connected to the control and operation issues of a microgrid. The conventional protection in distribution networks is designed to operate for high fault current levels in radial networks, but during island operation of the microgrid high fault currents from the utility grid are not present. Also most of the DG units that will be connected to the LV microgrid in the future are converter interfaced and have limited fault current feeding capabilities. This means that the traditional fuse protection of LV network is no longer applicable and new protection methods must be developed. The developed protection scheme for microgrid must be supported by the technical choices made in the microgrid operation and control issues.

In the development of the new protection scheme for LV microgrids many things must be considered including amount of protection zones in LV microgrid, speed requirements for microgrid protection in different operation states and configurations and protection principles for parallel and island operation of the microgrid.

4. Technological Trends

Among the new technological trends of smart grids, substations are intelligent networks, which are designed to manage the consumption of each element connected to it in an "intelligent" way [10]. These networks will use innovative equipment and services, along with new communication, control, monitoring, and self-diagnosis technologies that will help to achieve the following objectives [11]:

- Reinforce and automate the network, achieving an improvement in the functionality of the system, having better quality values and less loss in the network.

- Optimize the connection between the areas that have renewable energy sources, improving the connection capacities and reducing connection costs.
- Study the decentralized generation architectures, making smaller installations (distributed generation) in balance with the system [12].
- Develop intermittent generation integration and new storage technologies
- To advance in the development of the electricity market, allowing new functionalities and services to the market.
- Allow consumers to manage their energy efficiency better through active demand management.
- Enable the penetration of the electric vehicle, accommodating these new mobiles and dispersed loads to the grid, minimizing the development of new infrastructure and enabling the energy storage features they possess [13].

4.1. Advanced Automated Distribution

Advanced distribution automation allows the electrical power distribution system to be completely controllable to increase efficiency, sustainability and reliability. Some applications for advanced automation of distribution are monitoring, data acquisition and control, voltage and reactive power control, fault localization, automatic reconfiguration, isolation and restoration service, user information, time management, asset management and remote control. The main reason for the advanced distribution automation is to guarantee the safety of the service, the quality of the energy and the efficiency of the energy system. The above is possible once the next three control processes of the distribution operation are automated [14]. These control processes are: (1) the data is arranged almost in real time, (2) the optimal decisions and (3) the coordination with the services of the different generation and distribution systems to control the distribution operations.

An automated system of advanced distribution will be able to perform data collection, along with the verification and correction of consistency of that data. Besides, the system should reconfigure the multilevel feeder. It should be pre-armed with the corrective action schemes and the organization of urgency actions in distribution. It should take care of the previous assembly of recovery schemes and coordination of corrective actions in the distribution, registration, and reports [15].

4.2. Distributed Energy Resources

Distributed energy source technologies consist of storage and power generation resources labeled as "behind the meter." These resources are installed at customer's end and are operated to supply partial or total energy consumed by the client [16]. These energy resources may also be able to inject energy into the distribution system and the transmission system or into a local network in parallel with the public network. Moreover, certain technologies such as combined heat and power (CHP) systems, photovoltaic solar energy (PV), microgrids, wind turbines, microturbines, standby generators and energy storage are included [17]. These resources represent immense importance because they can contribute to the reliability of the network. They may be able to produce energy to support the load of the host or the system. These technologies have evolved at a great pace in the years that have passed. However, the current challenges require unique planning, operation, and market management [18].

Moreover, the term that characterizes it as "behind the meter" means that it represents certain resources that are not directly connected to the commercial electric power system but are connected to the customer's access point. In this case, it is possible that the resources are acting to meet the customer's internal electrical loads, or the resources may be working to sell to the electric power system [19].

4.3. Information and Communication Technologies

Advancement in information and communication technologies (ICT) has been helping to maintain the distribution of electricity while limiting the environmental consequences. In addition to this, ICTs allow greater incorporation of renewable energy sources, allowing the transport of little carbon. ICT also includes electric vehicles and inducing changes in the structure with respect to excessive consumption of electricity [20]. Among its specific political implications, ICTs include convergent telecommunications services. These services can be the changes in connectivity requirements, changes in the roles of ICT companies as partners in the electricity sector and the development of new ability for personnel of the industry [21]. Smart electrical substations guarantee the interoperability between elements connected to the network. They ensure privacy to the critical infrastructures and commercial use of power-sharing applications.

The communication between different devices of the Transformation Center and the Control and Supervision Center has not yet had a standard that allows efficient data communication. This limitation makes it difficult to implement the SCADA systems in the transformation centers [22]. Moreover, the interface with the relays was in many cases non-existent. To resolve these problems, the International Electrotechnical Commission launched some standard protocols called as IEC 61850. This protocol defines the communication between different devices connected to a local area network. Intelligent Electronic Devices (IEDs) are replacing the old wired communication techniques.

IEDs can integrate communication elements for tele-control [23]. Out of the three main layers of smart grid technologies (energy layer, communication layer, and application layer), the communications layer enables the existence of the smart grid (Figure 4). Communication technologies act as a circulatory system to interconnect the different systems and devices. It links the energy layer with the application layer, to communicate both with the energy supply chain [24].

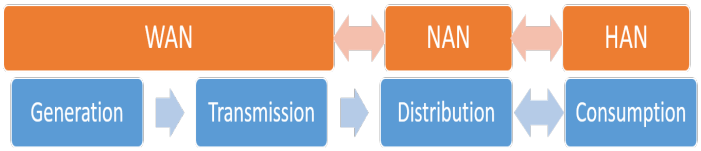

Figure 4. Smart grid topology for power flow in blue and information flow in orange

4.4. Supervisory System

The components of a supervisory system range from detection equipment, fault protection, communication, measurement, and data processing by the software. The software integrates all the intelligent devices (IED) that are part of the system [25]. However, the most relevant components of a supervisory system are the sensors of state and measurement. These sensors are installed in the field and are the base of the generation information for the supervising system. The status sensors have only two possible values zero or a logical one. These logical values reflect the states of the control elements of the system. For example, the status of a power switch can be estimated by the logical values of these sensors [26]. The protection relays that are currently manufactured are mainly IEDs. A typical IED (Intelligent Electronic Device) can contain around five to twelve protection functions and five to eight control functions. Control functions include separate devices control, an "auto-recloser" function, the self-monitoring function, and the communication functions etc. [27]. Currently, some IEDs work with the standard for the automation of IEC61850 electrical substations. This standard allows interoperability and good communications capacity (Figure 5) [28].

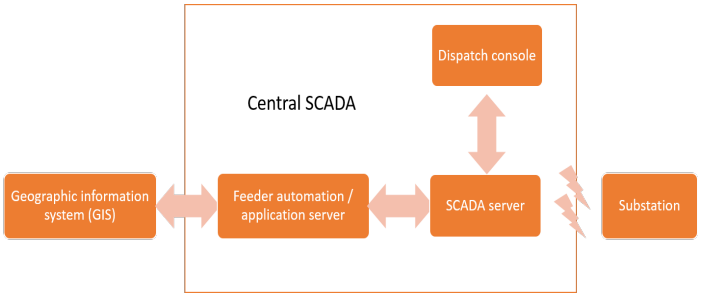

Figure 5. Feeder automation based on SCADA, current proposals in execution.

The communications network is the backbone of the entire supervisory system in real time. Its efficiency will depend on the speed and response time of the system to external events. The software is the last component that is required in the supervisory system; it is the way of representing the system [29].

4.5. Protection and Automation of the Network

The automation systems in substations for interconnecting a series of devices have existed for about 20 years, using proprietary protocols. These methods have been mainly responsible for the supervision of elements. Nowadays, this type of systems has evolved and continue to do so by following the protocols and actions declared in IEC 61850 [30]. This can be achieved by using peer-to-peer communications and enabling the exchange of data between systems at various levels and with various tools. This system also allows the supervision, control a series of devices or variables [31]. On the other hand, the increase in renewable energy generation and co-generation require the application of technologies in such a way that their management and protection is possible [32]. This impact on electrical networks is currently manifested, both in the transmission and distribution. The effect on substations, both in their protection and in their control, has been profound. This is due to the need of managing the intermittent electricity and several voltage levels [33].

The automation systems in substations for interconnecting a series of devices have existed for about 20 years, using proprietary protocols. These methods have been mainly responsible for the supervision of elements. Nowadays, this type of systems has evolved and continue to do so by following the protocols and actions declared in IEC 61850. This can be achieved by using peer-to-peer communications and enabling the exchange of data between systems at different levels and with various tools. This system also allows of supervisory control of devices or variables [34]. On the other hand, the increase in renewable energy generation and co-generation require the application of technologies in such a way that their management and protection is possible. The effect on substations, both in their protection and in their control, has been profound. This is due to the need of managing the intermittent electricity and several voltage levels. Therefore, for the development and supervision of the elements of the network, there are many emerging solutions for energy monitoring and parameters associated with it [35].

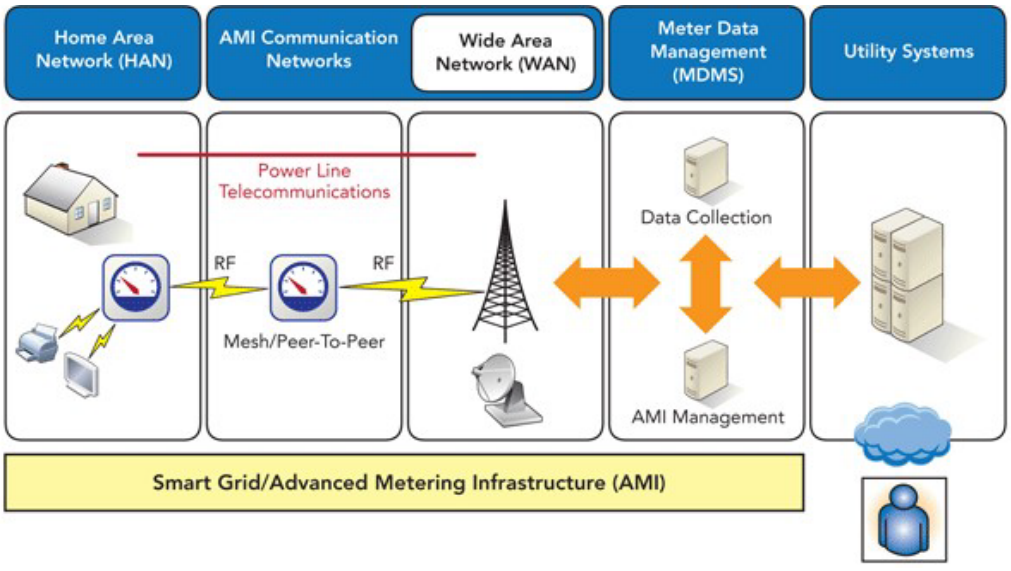

5. Digital Substations Control

To carry out and be able to develop all the functionalities that are expected from smart grids, this capacity (primarily redundant bi-directional data communications and the possibility of remote management) must be reproduced throughout the entire distribution network. It is already beginning to work in the section of the electrical consumption measurement infrastructure [36]. It must be implemented and improved in all sections of the power system.

The systems are based on bidirectional communications, technologies are associated with RF (radio frequency) wireless communications or power line carrier communications or broadband options (Figure 6) [37].

The desired functionality of smart meters could be the bidirectional communications with the electric company and with other devices (such as possible local energy managers). The other possible use of smart meter is alarms associated with quality of supply, personalization of the contract, planning, and possibility of bidding and purchase of electricity at the desired moments and control of loads, etc. [38]. This communication and monitoring capacity must be expanded to all measurement points and equipment in the electrical infrastructure. Also, it should be able to manage all distributed energy resources, considering not only the amount of energy flow but also the direction of it.

The technologies that affect smart grids are those that try to optimize and rationalize the management of electricity demand. As already mentioned, electrical energy cannot be stored (at least in enormous quantities), so it is necessary to generate it at the same time as it is needed. This situation means that at the very moment when a dedicated appliance is turned on, there must be a power plant (or any other type of electricity generator) that produces the necessary electricity [39].

5.1. Transport Network

To guarantee the electrical supply, in the absence of a line, the topology can be reconfigured to redirect the energy flows and thus avoid cutting off the supply. In this case, the systems of fault detection and reconfiguration of the network must act in small time spans for the control to be carried out in real time.

5.2. Distribution Network

The trend towards Smart Grids implies a replication or expansion of the existing capacities in the transport network to the distribution network. Considering that, unlike the conventional transport network, there are several owners and managers of the distribution networks. This situation will involve the definition of standard instruments and the creation of tools based on proven technology solutions. These tools will allow the integration of all types of generating plants, decentralized management of energy and automation of distribution and measurement services, supported by a system of communications that reaches the end user [40].

The electrical distribution companies can analyze and remotely control the electrical network by replacing meters with smart equipment. This equipment can take hourly measurements with Tele-management capacity [41]. In most cases, to guarantee interoperability, it is likely to install concentrators in the transformation centers with communication capabilities to control center of the corresponding distributor [42]. On the contrary, for the communication between the transformation center and the meters, the tendency in Europe is to use the power line carrier. The evolution of current electricity grids towards intelligent electricity networks implies the start of new intelligent equipment. This equipment will have local decision-making capacity and new communication technologies or the adaptation of existing ones. The current map of communication protocols used in the electrical system is very extensive and is regulated by the TC57 technical committee of the International Electrotechnical Commission (IEC). Thus, IECTC57 brings together several working groups to standardize the communications in the electrical system through the development of data models and generic interfaces. Each of these working groups has been responsible for defining and maintaining a communication standard based on the communication needs of each point of the electrical network [42].

Thus, it is worth highlighting:

- IEC60870-5 to communicate SCADA masters and electrical substations for the control and acquisition of data on serial lines or TPC / IP
- IEC60870-6, also known as TASE-2 for communications between powers centers over WAN networks.
- IEC61970 to interconnect energy management applications or EMSs in the environment of the control centers.
- EC61968 to communicate the control centers with the systems of the distribution network.
- IEC61334 for communications on PLC distribution lines.
- IEC62325 that defines a new interface between local utilities and the liberalized energy market.
- IEC62351 to determine security profiles to be used in all the previous ones at the TCP / MMS / 61850 level.
- IEC61850 (see fig 5) for automation in the environment of electrical substations (station and process buses) and communication between their IEDs (Intelligent Electronic Devices).

With the reference IEC61850 (see Figure 7 [43])), other similar regulations have been developed in other areas of application [44] such as:

- IEC61400-25 inherits a subset of communications services defined in IEC61850. It provides a new mapping of communications to Web Services and extends the data model modeling the functionalities, data, and attributes present in a wind turbine.
- IEC61850-7-420, which extends the data model by modeling the features, data, and attributes present in distributed generation systems such as photovoltaic systems, storage systems, diesel generators and heat exchange systems.
- IEC61850-7-410 is identical to IEC61850-7-420 for hydroelectric power plants.

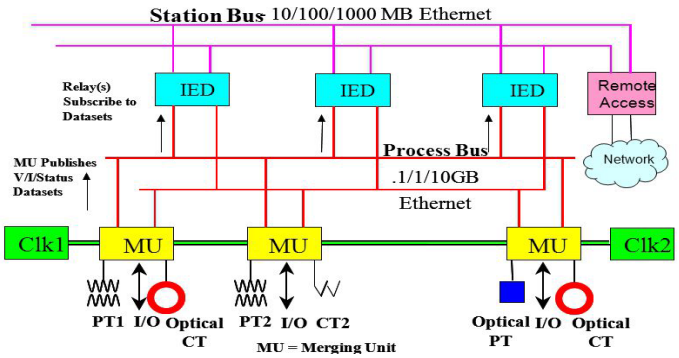

Figure 7. IEC61850 substation architecture.

6.1. Less Copper

Digital Substations utilize less copper by (1) replacing copper cables between switchyard and relay house by fiber optics, (2) replacing horizontal wiring between protection and control IEDs with IEC 61850, (3) reducing the number of connections between primary apparatus and redundant process interface modules and (4) reduction in cables for power supply and other connection for primary equipment.

6.2. Less Transport

In digital substation, more than 30 tons of material can be saved [45]. This helps in less transportation. The fiber optic installation reduces the cabling under 90% and by using optical instead of conventional CTs achieves an 80% weight reduction on CTs.

6.3. Space Reduction

IED installations require less space than conventional IOs. A space reduction around 30% to 60% for panels is possible. This results in higher integration of control and protection systems and reduction of switchyard footprint.

6.4. Less Installation and Outage Time

Digital substations cause faster installation of control systems due to reduction in number of panels for installation. There are fewer cables to be pulled, connected and tested. This causes reduction of feeder outage time by 40 to 50% during secondary system upgrades. This helps in full system test from process IO to protection, control and SCADA system offsite and Installation of new FO based system while the station is in service

6.5. Operational Cost Reduction

The Supervision of all exchanged data reduces the need for periodic maintenance testing and permanent supervision enables fast and precise actions in case of failures. IEC 61850 testing and simulation features enable fast and save isolation and testing of protection functions. Standard compliance enables efficient future retrofits of the secondary system (see Figure 5).

7. Conclusions and Recommendations

This work provides a review on digital substations importance and their working. This work emphasized on the importance of digital substations along with latest trends in modern smart grids. The provided comparison study proved the effectiveness of modern digital grids over conventional grids as well.

Apart of above-mentioned benefits, digital substations in Smart Grids provide a series of direct advantages to energy companies and end users that will help in the development of the energy market. The evolution of the electricity network provides the distribution companies with following benefits:

- Reduction of energy losses.
- Efficiency.
- Accomplish the optimization of the network infrastructure.
- Offering a better service to the client, with more commercial advantages (new rates, payment for use, etc.).

The users get the following benefits:

- Pay per use.
- Flexible rates.
- Remote management of the power supply.

Although at present, the home automation sector is in a complicated situation. It is promoting the instillation of control and automation systems in the home aimed at increasing energy efficiency, reducing energy losses, generated energy integration and accessibility to people with disabilities [46]. Currently, the number of agents involved in the electricity system has increased due to the liberalization of the energy market. The appearance of new participants is expected such as energy companies, system integrators, auditors, etc. It also predicts the development of renewable energies e.g., efficient solar cells, wind powered systems [47]-[48] and electric vehicles exponentially, in parallel with Smart Grids. So, it is necessary to keep these concepts in mind when carrying out any research or development related to the evolution of the electrical network.

R & D in the field of telecommunications for the development of new communication techniques and optimization of existing ones is still in progress. Technologies such as PLC, wireless connections or fiber optic, will provide a fundamental part of the Electrical Network of the future. Development in areas of power electronics, energy transport, electrical storage, energy efficiency, automated systems, new intelligent control techniques, etc. needs more investment and research [49]. Insofar, smart grids would play a great role in the development of smarter world having smart cities, smart homes, smart vehicles, etc. The ultimate requirement is to create systems of objects that are configured automatically and can operate autonomously [50]-[53].

Conflict of Interest

The authors declare no conflict of interest.

Acknowledgment

We would like to thank Dr. Muhammad Nasir for his assistance on data organization and guidance for writing.

References

[1] Ramie, J. 2017 “Testing requirements for intelligent electronic devices in transmission & distribution facilities”in IEEE International Symposium on Electromagnetic Compatibility & Signal/Power Integrity (EMCSI), 7-11 Aug 2017: 1-36, Washington, DC: IEEE.

[2] Salvadori, F., Gehrke, C.S., Hartmann, L.V., de Freitas, I.S., Santos, T. D., and Texeira, T.A., "Design and implementation of a flexible intelligent electronic device for smart grid applications." in IEEE Industry Applications Society Annual Meeting, 1-5 Oct 2017: 1-6, Cincinnati, OH: IEEE.

[3] Chen, J., and Fu, Q., 2016 "Design of experiment platform for digital substation based on IEC 61850." In 5th International Conference on IEEE Computer Science and Network Technology (ICCSNT), 10-11 Dec 2016: 4-8, Changchun: IEEE.

[4] Hu, J., and Vasilakos, A., 2016 "Energy Big Data Analytics and Security: Challenges and Opportunities." IEEE Transactions on Smart Grid 7(5): 2423-2436, doi:10.1109/TSG.2016.2563461.

[5] Kong, P., 2016 "Wireless Neighborhood Area Networks with QoS Support for Demand Response in Smart Grid", IEEE Transactions on Smart Grid 7(4): 1913-1923, doi: 10.1109/TSG.2015.2421991.

[6] GVR "Substation Automation Market Size, Share | Global Industry Report 2024", (Accessed: 06- Jun- 2018) https://www.grandviewresearch.com/industry-analysis/substation-automation-market/.

[7] Faheem, M., Shah, S., Butt, R., Raza, B., Anwar, M., Ashraf, M., Ngadi, M. and Gungor, V., 2018. "Smart grid communication and information technologies in the perspective of Industry 4.0: Opportunities and challenges." Computer Science Review 30: 1-30, doi: doi.org/10.1016/j.cosrev.2018.08.001.

[8] Hong, T., Chen, C., Huang, J., Lu, N., Xie, L. and Zareipour, H. 2016. "Guest Editorial Big Data Analytics for Grid Modernization." IEEE Transactions on Smart Grid 7(5): 2395-2396, doi: 10.1109/TSG.2016.2593358.

[9] Siano, P., 2014. "Demand response and smart grids—A survey." Renewable and sustainable energy reviews 30: 461-478, doi: doi.org/10.1016/j.rser.2013.10.022.

[10] Mohtashami, S., Pudjianto, D., and Strbac, G., 2017. "Strategic Distribution Network Planning with Smart Grid Technologies" IEEE Transactions on Smart Grid 8(6): 2656-2664, doi: 10.1109/TSG.2016.2533421.

[11] Noriaki, K., 2013. "Electric network innovation by digital grid." IEEJ Transactions on Power and Energy 133(2): 141–144, doi: 10.1541/ieejpes.133.141.

[12] Hayashi, K., Kato, R., Torii, R., Taoka, H., and Abe, R., 2015. "Bi-directional power flow through a digital grid router" Journal of International Council on Electrical Engineering 5(1): 42-46, doi: https://doi.org/10.1080/22348972.2015.1068511.

[13] Rahim, M., Khalid, A., Javaid, N., Alhussein, M., Aurangzeb, K., and Khan, Z., 2018. "Energy efficient smart buildings using coordination among appliances generating large data", IEEE Access: 34670-34690, doi: 10.1109/ACCESS.2018.2805849.

[14] Meng, W., Ma, R. and Chen, H-H., 2014. "Smart Grid Neighborhood Area Networks: A Survey," IEEE Network 28(1): 24–32, doi: 10.1109/MNET.2014.6724103.

[15] Mortaji, H., Ow, S., Moghavvemi, M., and Almurib, H., 2017. "Load Shedding and Smart-Direct Load Control Using Internet of Things in Smart Grid Demand Response Management", IEEE Transactions on Industry Applications 53(6), 5155-5163, doi: 10.1109/TIA.2017.2740832.

[16] Chang, K.H., 2013. "Interoperable nan standards: a path to cost-effective smart grid solutions," IEEE Wireless Communications 20(3): 4–5, doi: 10.1109/MWC.2013.6549274.

[17] Al-Fuqaha, A., Guizani, M., Mohammadi, M., Aledhari, M., and Ayyash, M., 2015. "Internet of Things: A Survey on Enabling Technologies, Protocols and Applications," IEEE Communications Surveys & Tutorials 17(4): 2015 2347-2376, doi:10.1109/COMST.2015.2444095.

[18] Luo, F., Zhao, J., Dong, Z.Y., Chen, Y., Xu, Y., Zhang, X., and Wong, K.P., 2016. "Cloud-based information infrastructure for next-generation power grid: Conception, architecture, and applications," IEEE Transactions on Smart Grid 7(4): 1896-1912, doi: 10.1109/TSG.2015.2452293.

[19] Lim, J., Doh, I., and Chae, K., 2017. "Secure and structured IoT smart grid system management", International Journal of Web and Grid Services 13(2): 170, doi: https://doi.org/10.1504/IJWGS.2017.083383.

[20] Chiu, W., Sun, H., Thompson, J., Nakayama, K., and Zhang, S., 2016. "Integrated communications, control, and computing technologies for enabling autonomous smart grid", IEEE Communications Magazine 54 (12): 58-59, doi: 10.1109/MCOM.2016.7786111

[21] Yang, C. Vyatkin, V. and Pang, C., "Service-oriented extension of IEC 61850 for model-driven smart grid automation design." in IECON 2017 - 43rd Annual Conference of the IEEE Industrial Electronics Society, 29 Oct-11 Nov 2017: 5489-5496, Bejing: IEEE.

[22] Carvalheira, E., and Coronel, E., 2014. "Testing the protection system in IEC 61850 communication-based substations." in IEEE ANDESCON, 15-17 Oct 2014: pp. 1-1, Cochabamba:IEEE.

[23] Li, Y., Cheng, X., Cao, Y., Wang, D., and Yang, L., 2018. "Smart Choice for the Smart Grid: Narrowband Internet of Things (NB-IoT)", IEEE Internet of Things Journal, 5(3): pp. 1505-1515, doi: 10.1109/JIOT.2017.2781251.

[24] Krata, J. and Saha, T., 2018. "Real-Time Coordinated Voltage Support with Battery Energy Storage in a Distribution Grid Equipped with Medium-Scale PV Generation", IEEE Transactions on Smart Grid: 1-1, doi: 10.1109/TSG.2018.2828991.

[25] Veldman, E., and Verzijlbergh, R., 2015. "Distribution Grid Impacts of Smart Electric Vehicle Charging from Different Perspectives", IEEE Transactions on Smart Grid 6(1): 333-342, doi: 10.1109/TSG.2014.2355494.

[26] Aburukba, R.O., Al-Ali, A., Landolsi, T., Rashid, M., and Hassan, R., 2016. "IoT based Energy Management for Residential Area," in IEEE International Conference on Consumer Electronics-Taiwan (ICCE-TW), 27-29 May 2016: 1–2, Taiwan:IEEE.

[27] Baimel, D., Tapuchi, S. and Baimel, N., 2016. "Smart Grid Communication Technologies", Journal of Power and Energy Engineering 4(8): 1-8, doi:10.4236/jpee.2016.48001.

[28] Konstantelos, I., Giannelos, S., and Strbac, G., 2017. "Strategic valuation of smart grid technology options in distribution networks" IEEE Transactions on Power Systems 32(2): 1293-1303, doi: 10.1109/TPWRS.2016.2587999.

[29] Rossi, M., Viganò, G., Moneta, D., and Clerici, D., 2017. "Stochastic evaluation of distribution network hosting capacity: Evaluation of the benefits introduced by smart grid technology" in International Annual Conference, 20-22 Sep 2017:1-6, Cagiliari, Italy:IEEE.

[30] Wang, H., Qian, Y., and Sharif, H., 2013. "Multimedia communications over cognitive radio networks for smart grid applications," IEEE Wireless Communications 20 (4): 125–132, doi: 10.1109/MWC.2013.6590059.

[31] Cao, Z., Lin, J., Wan, C., Song, Y., Zhang, Y., and Wang, X., 2017. "Optimal cloud computing resource allocation for demand-side management," IEEE Transactions on Smart Grid, 8(4): 1943-1955, doi: 10.1109/TSG.2015.2512712.

[32] Cheng, X., Lee, W., and Pan, X., 2017. "Modernizing Substation Automation Systems: Adopting IEC Standard 61850 for Modeling and Communication". IEEE Industry Applications Magazine 23(1): 42-49, doi:10.1109/MIAS.2016.2600732.

[33] Miswan, N.S., Ridwan, M.I., Hayatudin, A., and Musa, I.A., 2015. "Interoperability testing for Digital Substation in Smart Grid domain: A power utility perspective" in International Symposium on Technology Management and Emerging Technologies (ISTMET), 25-27 Aug 2017: 154-158, Langkawai Island:IEEE.

[34] Abe, R., Taoka, H., and McQuilkin, D., 2011. "Digital grid: communicative electrical grids of the future". IEEE Trans. Smart Grid 2(2): 399-410, doi: 10.1109/TSG.2011.2132744.

[35] Deng, R., Yang, Z., Chow, M.-Y., and Chen, J., 2015. "A Survey on Demand Response in Smart Grids: Mathematical Models and Approaches," IEEE Transactions on Industrial Informatics 11 (3): 570– 582, doi: 10.1109/TII.2015.2414719.

[36] Shen, B., Yuan, Y., Xie, L., Zeng, X., Liu, Y., and Luo, H., 2017. "Reasch on IED configurator automatic modeling based on IEC 61850" in IEEE Conference on Energy Internet and Energy System Integration (EI2), 26-28 Nov 2017 :1-5, Beijing:IEEE.

[37] Yang, Y., Xu, H., Gao, L., Yuan, Y., McLaughlin, K., and Sezer,K., 2017. "Multidimensional Intrusion Detection System for IEC 61850-Based SCADA Networks". IEEE Transactions on Power Delivery. Volume: 32 (2): 1068-1078, doi: 10.1109/TPWRD.2016.2603339.

[38] CRO "Renewable energy sources and climate change mtigation: special report of the Intergovernmental Panel on Climate Change", Choice Reviews Online, 49(11): 49-6309-49-6309, 2012, doi: https://www.ipcc.ch/report/renewable-energy-sources-and-climate-change-mitigation/

[39] Koko, S., Kusakana, K., and Vermaak, H., 2017. "Optimal energy management of a grid-connected micro-hydrokinetic with pumped hydro storage system", Journal of Energy Storage, 14: 8-15, doi: https://doi.org/10.1016/j.est.2017.09.007.

[40] Chena, W., Zhoua, K., Yanga, S., and Wuc, C., 2017. "Data quality of electricity consumption data in a smart grid environment", Renewable and Sustainable Energy Reviews, 75: 98–105, doi: https://doi.org/10.1016/j.rser.2016.10.054.

[41] Guerrero, J.L., García, A., Luque, J., and León, C., 2017. "Heterogeneous data source integration for smart grid ecosystems based on metadata mining", Expert Systems with Applications, 79: 254–268, doi: https://doi.org/10.1016/j.eswa.2017.03.007.

[42] Schett, G. 2017. "Digital substations for hydro power plants", in Proceedings of the Hydro Conference Series, Montreux, Switzerland 2017.

[43] Torbaghan, M.E., Burrow, M., Hunt, D., and Elcheikh, M., 2017. "Risk-Based Framework (RBF) for a UK Pan-European Supergrid" Energy, 124: 124-132, doi: https://doi.org/10.1016/j.energy.2017.02.058.

[44] Einfalt, A., Cejka, S., Diwold, K., Frischenschlager, A., Faschang, M., Stefan, M., and Kupzog, F., 2017. "Interaction of smart grid applications supporting Plug & Automate for intelligent secondary substations", CIRED - Open Access Proceedings Journal, 2017(1): 1257-1260, doi: 10.1049/oap-cired.2017.1080.

[45] Viswanatham, V., Chari, A., and Saritha, V., 2016. "Region-based group and hierarchical key management for secure smart grid communications." International Journal of Smart Grid and Green Communications, 1(1): 50, doi: 10.1504/IJSGGC.2016.077289.

[46] La, Q., Chan, Y., and Soong, B., 2016. "Power Management of Intelligent Buildings Facilitated by Smart Grid: A Market Approach", IEEE Transactions on Smart Grid, 7(3): 1389-1400, doi: 10.1109/TSG.2015.2477852.

[47] Waleed, A., Zhang, Q., Tavakoli, M.M., Leung, S.F., Gu, L., He, J., and Fan, Z., 2016."Performance improvement of solution-processed CdS/CdTe solar cells with a thin compact TiO2 buffer layer", Science bulletin, 61(1): 86-91, doi: https://doi.org/10.1007/s11434-015-0963-0.

[48] Waleed, A., Hassan, K.M., and Virk, U.S., 2014. "Designing a dual axis solar tracker for optimum power", Journal of Electrical Engineering 14(2): 168-173, doi: http://www.jee.ro/covers/art.php?issue=WH1375121304W51f6af987b6d1.

[49] Waleed, A., and Fan, Z., 2017. "Fabrication of stable organometallic halide perovskite NWs based optoelectronic devices" Science bulletin, 62(9): 645-647, doi: 10.1016/j.scib.2017.04.012.

[50] Tafreshi, S.M., and Lahiji, A.S., 2015. "Long-Term Market Equilibrium in Smart Grid Paradigm with Introducing Demand esponse Provider in Competition", IEEE Transactions on Smart Grid, 6(6): 2794-2806, doi: 10.1109/TSG.2015.2413951.

[51] Althaher, S., Mancarella, P., and Mutale, J., 2015. "Automated Demand Response from Home Energy Management System Under Dynamic Pricing and Power and Comfort Constraints", IEEE Transactions on Smart Grid, 6(4): 1874-1883, doi: 10.1109/TSG.2014.2388357.

[52] Kim, S-G., Hur, S-I, and Chae. Y-J., 2010. "Smart grid and its implications for electricity market design", Journal of Electrical Engineering and Technology, 5(1): 1-7, 2010.

[53] Sattarpour, T., Nazarpour, D., Golshannavaz, S., and Siano, P., 2015. "An optimal procedure for sizing and siting of DGs and smart meters in active distribution networks considering loss reduction", Journal of Electrical Engineering & Technology, 10(3): 804-811, doi:10.5370/JEET.2015.10.3.804.

ASTES

Advances in Science, Technology and Engineering Systems Journal Vol. 4, No. 4, 440-448 (2019)

www.astesj.com

Special Issue on Advancement in Engineering and Computer Science

ASTESJ

ISSN: 2415-6698

Optimized Design of PM Halbach Array Linear Generator for Sea Wave Energy Converters Operate at Maximum Power Transfer

Ahmed Elsayed ELGebaly [*], Mohamed Kamal El-Nemr

Electrical power and machines department Faculty of engineering, Tanta university, Tanta, 31527, Egypt

A R T I C L E I N F O

Article history:
Received: 31 May, 2019
Accepted: 04 August, 2019
Online: 16 August, 2019

Keywords:
Marine Renewable Energy
Halbach Array
Linear Generators
Finite Element Method
Maximum Power Transfer

A B S T R A C T

This paper proposes Halbach array PM linear generators for direct conversion of ocean or sea wave energy. This generator is proposed to be directly coupled to a reciprocating wave energy system which may be a valued alternative for pneumatic and hydraulic systems. In this research, air-cored permanent magnet PM linear generator has been optimally designed according to optimal cost and performance indices. The design depends on Halbach array PM arrangement. The design this linear generator is appropriate for direct extraction of energy from sea waves specially at small wave amplitude. The finite element method and the space harmonic analysis are used to develop the electromagnetic design of this topology. In this article, the concept of the extraction of maximum permissible power from sea waves is established according to the direct wave energy converters hydrodynamics model. The dynamic analysis of the Halbach array linear generator is investigated during the state of maximum power extraction.

1. Introduction

This paper is an extension of work originally presented in 2018 Twentieth International Middle East Power Systems Conference (MEPCON) under title (Optimal Design of Slotless PM Halbach Array Linear Generator for Wave Energy Converters at Maximum Power Transfer Condition) [1]. Nowadays, the energy sources have great importance allover the world. Because of the expected deterioration of fossil fuels accompanied with hazardous environmental impacts, it is indispensable to establish clean renewable sources of energy. Ocean and sea waves energies are considered promising alternative renewable energies resources. On the Earth, it is considered as the largest renewable energy source. The running cost of this type of energy is low. Moreover, it is clean energy source. However, is not competently employed up till now. Preliminary reviews show that marine power has the ability to significantly contribute in energy market all over the world. Experts expect that the economical visibility of ocean or sea energies is very effective. It is expected that if wave-capturing technologies become totally developed, the predicted developed wave energy may equal 750 Trillion kWh/year [2].

Recently, numerous technologies are established to extract electric energy from seas or oceans waves [3]. These technologies are called the wave energy converters (WECs). They can transfer the mechanical wave energy to electrical energy. Such types of converters utilize the concept of a water column changing or buoy body movement [4]. Some of developed converters are more and more commercially established. There are some WECs directly convert the oscillating wave motion to reciprocal vertical movement. The small reciprocating motion with a speed about 2m/s may be obtained by these devices in some seas such as Mitterrandian Sea. Some researchers suggest the usage of induction generators to produce electric energy from sea waves. Nevertheless, this technology requires a hydraulic transmission system to convert the small velocity of the vertical motion to high rotational speed[5]. The wave energy converters which depend on the direct conversion of wave energy have great advantage related to the simple construction free of mechanical transmission system. The linear permanent magnet synchronous generators LPMSG have been developed and implemented as WECs which depend on the principle of Archimedes wave swing [1, 6]. The main shortage of such linear synchronous generators is the high cogging force. On the other hand, the air-cored tubular permanent magnet linear generators are suggested to overcome such force [7]. Therefore, the elimination of cogging force reduces the stress on the machine parts so there is no need for additional structure support. These machines can be built without the usage of back-iron. Therefore, the elimination of back-iron from stator and forcer leads to the

[*]Electrical power and machines department, faculty of engineering, Tanta university, Tanta, Egypt, +201153026587, ahmed.elgebaly@f-eng.tanta.edu.eg

elimination of their corresponding core loss. Additionally, such generators have significant lightweight compared with the conventional linear synchronous generators. The improvement of flux distribution in the air-cored PM generators improve their performance from the point of view of the developed voltage and power [1]. Halbach array arrangement is applied to provide low space harmonics magnetic field, which leads to further sinusoidal waveform of induced voltage and more developed power with the same forcer current. The field uniformity leads to extracting of higher power over small time. Therefore, the Halbach arrangement is proposed to be implemented in these generators to gain its performance improvements [1, 2, 8].

The optimized design of the proposed PM Halbach array linear generators requires the fulfilment of some indices; such as cost minimization and the production of appropriate voltage and power level. The recent optimization techniques are applied to obtain the optimal design of generator which is suitable for wave energy extraction [9]. In this paper, the design details are taken into consideration to obtain the optimal design. The design variables include the generator topology, the appropriate PM arrangement, the coils design and the generator overall dimensions. Moreover, this research proposes the concept of maximum power tracking MPT to make use of the most delivered wave energy. Preliminary, the MPT concept is explained in this paper according to the hydrodynamic performance of the WEC. The application of MPT mode requires the implementation specific control technique and power electronics converter [10].

2. Modelling of hydrodynamics of direct WEC

Figure1 demonstrates the structure of air-cored tubular PM linear synchronous generator for WEC based Halbach array configuration. According to this design, the floating buoy is directly connected to the movable translator of the PM linear generator where its base is strongly fixed to the sea bottom. The generator base may be connected to the sea bottom via wires. The changing of the height of the wave is the base of the operation of the WEC. The hydrodynamic model of the direct buoy WEC has been developed previously in numerous researches [5, 11]. The difference forces act on the moving part of the translator have been modeled. Without reaction force control, the moving part are affected by three forces; the input force produced by the wave, the extracted output power and the inertia force. It is recommended to integrate a suitable mechanical spring in the WEC to develop reaction force counteracts the force of inertia developed by the movable parts. The maximum power transfer condition in the WEC systems happens when both the inertia and the spring forces are equal in value and opposite in direction [1, 2].

The buoy may take a cylindrical shape with radius r and its motion is limited to be along the vertical axis (z). The cylinder is partly immersed. When the wave acts on the buoy in x direction as illustrated in Figure (1), a force is applied on the buoy cylinder due its tendency for floating. In this study, the incident wave is considered to have sinusoidal wave for simplicity.

The buoy motion equation can be formulated as the following:

$$m\frac{d^2z}{dt^2} = F_{stf} + F_{gen} + F_{hyd} \quad (1)$$

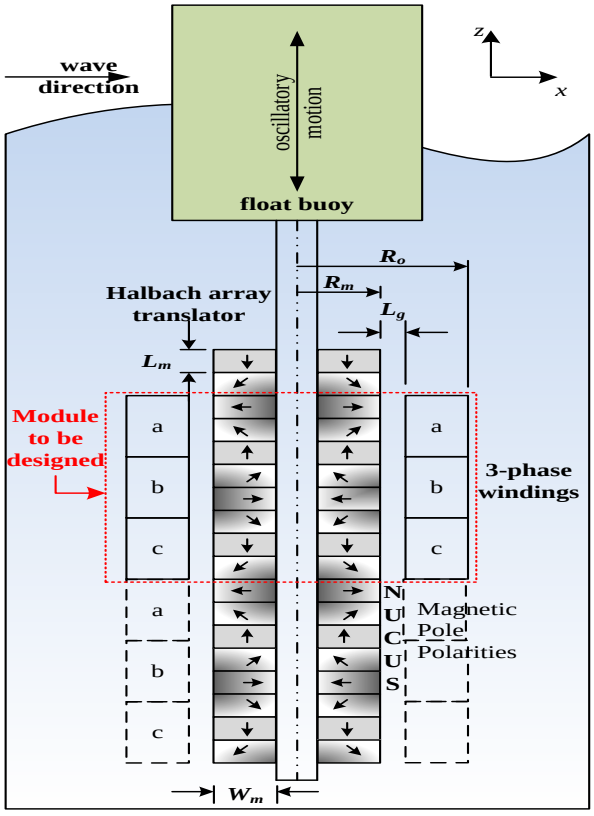

Figure 1: Proposed tubular Halbach array slotless linear generator for wave energy conversion

where m is movable parts mass i.e. buoy and Halbach array PMs. F_{stf} is the force produced by the spring, F_{gen} is the reacting generator force due to electrical power extraction, and F_{hyd} are hydrodynamic forces applied on the buoy exerted by the wave.

The stiffness or spring force is proportional to the translator displacement,

$$F_{stf} = -k_{st}\, z \quad (2)$$

where k_{st} is the constant of spring and z is the displacement on the vertical axis away from the balance point.

The force that causes the electrical power is modeled as a damping force where the produced force is proportional to the movable parts velocity. Therefore, the generated force is determined as:

$$F_{gen} = -B\frac{dz}{dt} \quad (3)$$

where B is the coefficient of damping which depends on the generated power. This coefficient should be continuously adjusted to enable the generator to extract the maximum allowable power from the wave.

The Archimedes' principle provides the equation that determine the hydrodynamic force correlated to the volume of water displaced:

$$F_{hyd} = -\rho g \pi r^2 z \quad (4)$$

To study the hydrodynamic model in steady state mode, all equation should be transfer to the frequency domain by applying Fourier transformation. At steady state, the cylinder is assumed to be exposed to sustained alternating force has a frequency ω. The output power from the generator can be maximized when the system is in the resonance where the stiffness force equals in magnitude the inertia force. Therefore, the natural frequency ω_r of the hydrodynamic system can be determined by [11]:

$$\omega_r = \sqrt{\frac{\rho g \pi r^2 + k_{st}}{m}} \quad (5)$$

The design of buoy cylinder relies on the hydrodynamic parameters which achieve the maximum power transfer condition. In this research, the proposed design is suitable for south shores of the Mediterranean Sea where the frequencies of the waves are within 3 radian per second [12]. The spring constant is determined depending on WEC rating and generator parameters [11]. Figure 2 illustrate the relation between the radius of buoy cylinder and the proper stiffness constant at different masses of movable parts. The required stiffness constant decreases with the increment of the radius. If the stiffness constant has negative values, the mass of the translator should be increased to achieve resonance condition [13]. So, the adjustment of spring constant is very vital to achieve the resonance condition; and therefore, to achieve the maximum power transfer condition. Nevertheless, the frequency of incident sea waves is continuously changed; so, the stiffness constant

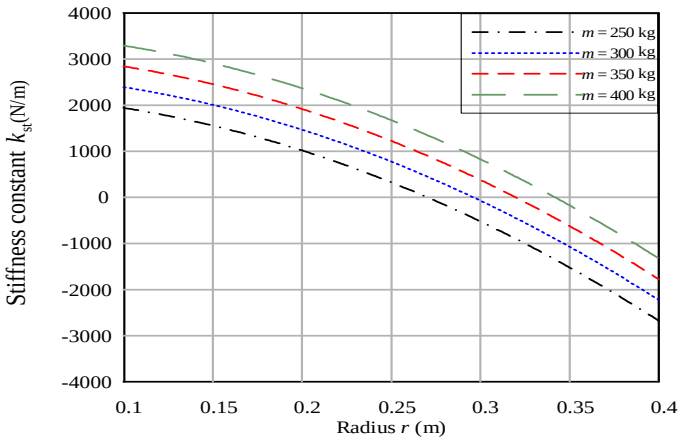

Figure 2: Variation of required stiffness constant with radius at different masses at ω_r = 3 rad/s

should be changed to change the natural frequency of the system to produce the maximum permissible power. The active adjustment of the stiffness constant is very complicated if it is mechanically implemented. Therefore, in this research, a adaptive electric spring is implemented to regulate the stiffness constant to run in resonance manner for different frequencies of the incident wave. The stiffness force or reaction force [10] can be created electrically due to certain current and voltage adjusted by power electronics converters. In this article, reaction force is applied during the operation of the generator to produce maximum power. Nevertheless, the movable parts mass should to be minimalized to reduce the reaction force and consequently, the produced generator current and its corresponding losses. Therefore, the mass of the generator movable parts is a vital index to obtain the optimized design.

3. Design of Halbach array WEC generator using FEM

Figure 1 illustrates that the proposed PM Halbach array linear generator has fixed coils surround a PM tubular Halbach array. The translator is composed of directed polarized permanent magnets for instance NdFeB. The magnets fluxes are directed with special sequence North (N) and South (S). But, the complete of the magnetic flux requires some magnets to be oriented in (C) direction. The PMs labeled (U) are oriented with 45 degrees or 135 degrees to produce smooth sinusoidal distributed flux. The resultant field tracks the translator motion, passing through the the concentrated coils. This paper studies the design of one module and the other modules have the same design parameters.

Low velocities WECs requires large reactive forces, therefore large dimension generators. In such iron-cored generators, the robust magnetic field leads to a noteworthy attraction force between the movable part and stator [14]. The structure can be significantly saved in the case when the cogging force can be decreased or even cancelled. The slotless air-cored linear generator is considered as a solution. The Halbach array has a vital advantage over the traditional air-cored related to the production of magnetic flux with less space harmonic content. The proposed generator module has the next ratings: 600 w rated power, 60 V rated phase voltage, the height of the wave about 1 m and the frequency of the wave about 3 rad/s. The ratings of the generator and wave is suitable to be applied on South Mediterranean Sea [12].

The proposed module may be repeated vertically to absorb larger amount of power from the incident wave. The overall length of generator depends on the depth of sea in the place of installation and on the stresses applied on the construction of the generator. In this research, the proposed generator has 3 kW; so, it consists of five modules. The following procedures explains the steps to obtain the optimal design of one module.

The investigation of the proposed model has been achieved by the application of finite element method by using FEMM package. Due to the slow motion of the translator in such type of generators, the analysis of the generator is considered magnetostatic problem. The problem of electromagnetic field is analyzed depending on FEM. The following equations is solved by FEM to analyze any electromagnetic problem. The vector of magnetic potential **A** is related to the vector of current density **J** by the following equation:

$$-\frac{1}{\mu}\nabla^2 \boldsymbol{A} = \boldsymbol{J} \quad (6)$$

where, (μ) is the permeability that depends the flux density for nonlinear materials. The advantage of solving FEM problem depending on the vector potential **A** is that all circumstances to be fulfilled are integrated within on equation. If **A** is determined for any geometry, the corresponding density of magnetic flux can be determined according:

$$\boldsymbol{B} = \nabla \times \boldsymbol{A} \quad (7)$$

The proposed designs of the generators are analyzed by FEM to achieve the required ratings. Figure 1 illustrates the various dimensions of the module; R_o the outer radius of the module, τ is the pole pitch, L_g is air gap length, L_m is PM segment height, W_m is PM thickness and R_m is the PMs cylinder outer diameter.

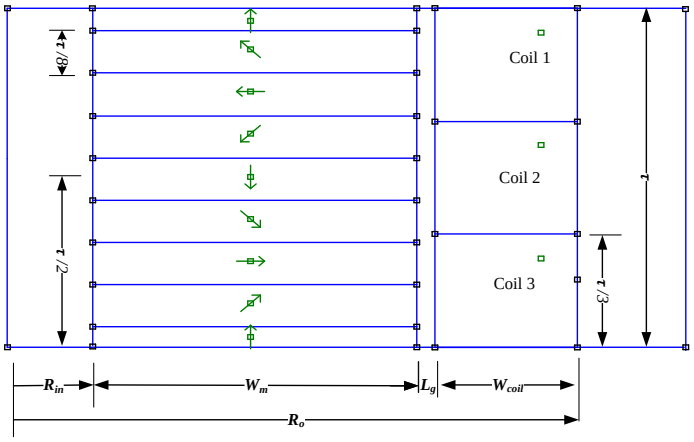

Figure 3: Full dimensions of one module of the proposed generator design

There are additional generator design parameters foi instance number of windings of each coil, the cross-section area of the copper conductors and the coil's filling factor. FEM analysis helps to determine the parameters of the design which achieve the suitable ratings. For any proposed dimensions and materials, FEM can calculate the different variables of the generator such as flux linkage, developed force overall weight. For each determined variable, the objective function is formulated to obtain the optimized design. Figure 3 illustrate the full dimensions applied in FEM for axisymmetric representation while R_{in} is the PMs cylinder inner radius, W_{coil} is the coil width and τ is the pole pitch. Along one pole pitch, the PM cylinder is divided into eight species. Along the full length of the translator, there are number of pole pitches equals N_{pit}. Over each pole pitch, the stator contains three coils where each coil presents one phase. The modularity of the proposed design allows to provide different generator ratings. Consequently, in case of 600 W module, generators of 1200, 1800 and 2400 W are developed. The control system applied for one module can be applied for the other modules without modifications.

Because of tubular shape of generator, the simulated model in FEMM is presented in axisymmetric dimensions. Several efforts have been achieved in [1], [2] and [5] which present a good guide to determine the probable ranges of design variables appropriate for the predetermined ratings demonstrated in Table.1.

The package FEMM is used to implement the finite element analysis of the proposed generator. The slow motion of the translator and the currents low frequencies which passes through coils lead to solving of the finite element problem as magnetostatic problem.

The optimization problem has some constrains; the first constrain is the filling factor of each coil should be less than 85 %; the second constrain is the losses which shouldn't exceed 50 % of the developed power. The dissipation of generator losses under water governs the description of constrains [2].

Some of post-process results of FEM present important terms which formulate the objective function. The obtained parametes are are as the following, the volume of PM segment Vol_{pm}, the volume of the coil Vol_{coil}, the produced loading force F_d, copper losses P_{cu}, and the maximum flux linkage at no-load λ_{max}. Some post-process results are essential to obtain some fitness function terms. The mass of both PMs and coils should be determined as the following:

$$M_{pm} = 8\ Vol_{pm}\ \rho_{pm} \tag{8}$$

$$M_{coil} = 3\ Vol_{coil}\ \rho_{cu}\ k_f \tag{9}$$

where M_{pm} is the mass PM cylinder for one module, ρ_{pm} is the PM material density, M_{coil} is the three-phase coils mass, ρ_{cu} is the density of copper and k_f is the filling factor. The maximum flux linkage per pole pitch λ_{max}/τ is an essential parameter should to be calculated to formulate the objective function.

The objective function is formulated to obtain the optimized design according to the next indices:

1- minimization of coils' mass
2- minimization of PM translator mass
3- achieving the rated power
4- achieving the rated voltage

Consequently, the objective function is formulated as the following:

$$O.F = k_1 M_{coil} + k_2 M_{pm} + k_3 \left| P_d - P_{dref} \right| + k_4 \left| \frac{\lambda_{\max}}{\tau} - \left(\frac{\lambda_{\max}}{\tau} \right)_{ref} \right| \tag{10}$$

and the fitness function to be maximized is:

$$fitness = -O.F \tag{11}$$

where P_d is the produced power by certain model, P_{dref} and $(\lambda_{\max}/\tau)_{ref}$ present the reference values and constants k_1 to k_4 are used as weighting factors to adjust the contribution of $O.F.$ terms.

Figure 3 illustrates the FEM presentation of one module located at the balance position where $z = 0$. With minimum number of calculations, this position has advantage related to the determination of required values of maximum flux linkage at no-load for coil 2 and developed force at loading if both coil 1 and coil 3 have maximum current. the proposed arrangement provides the benefit of obtaining the terms of objective function deprived of carrying out a complex dynamic modeling using FEM.

Table 1: the probable ranges of design variables appropriate for the proposed Halbach array generator

Variable	Symbol	Range	Unit
PM thickness	W_m	1: 9	Cm
Inner radius of PMs cylinder	R_{in}	0.5: 7	Cm
Air gap width	L_g	0.05: 0.5	Cm
Coil width	W_{coil}	2.5: 6	Cm
Pole pitch	τ	8: 15	Cm
Turns number of each phase	N	150: 300	Turn

In this research, the Genetic Algorithm (GA) is applied to obtain the optimized design with minimum weight and losses and provides voltage and power ratings.

Figure 4 demonstrates the flux produced by the Halbach array where the flux is directed out of the side area of the cylinder and partly deleted in the inner side of the cylinder. For the same generators volume, the characteristics related to providing higher power density of Halbach array linear generator is better than these of air-cored generator [2].

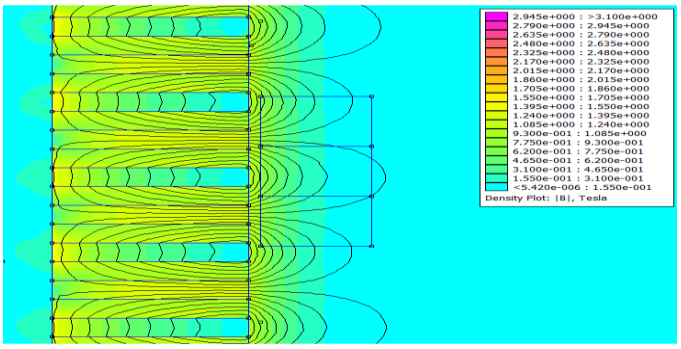

Figure 4: The Halbach array produced magnetic flux distribution and contour

To obtain the optimal values for the parameters, GA is applied to maximize the fitness function. In this study, the generation consists of 20 gene is applied. The six parameters are coded within one gene as binary string where these parameters are illustrated in Table.1. Therefore, the gene is composed of 120 bit. Then, the design parameters are passes to FEMM package to obtain their indices and design results. Then, the post-processing parameters are calculated. Therefore, the objective function and fitness value is determined for each gene. Then, GA applies its reproduction processes. The developed programs are carried out using programming language C++ and MFC library.

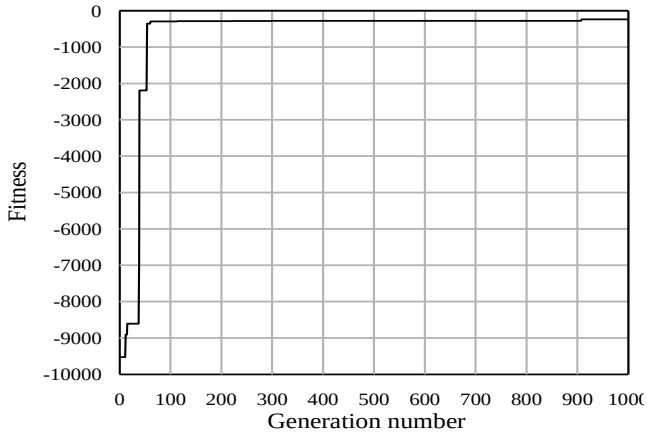

Figure 5: Fitness variation with GA generations for the optimization problem

The process of search is completed if the fitness value is stable at almost fixed value. Figure 5 demonstrates the changing of the fitness value versus the number of generation. After 1000 generation, the maximum fitness is stabilized at -270 as best vakue as shown in Figure 5. The stabilized fitness value is achieved approximately after 120 generations.

Table 2 illustrates the details of optimized design of the proposed generator topology for the specified ratings. The developed parameters of the optimized design are used in the dynamic analysis of the generator when it works in maximum power transfer state. The power density of the optimized design equals 41.6 W/kg which is more than the conventional air cored by 10% which equals 38 W/kg [15].

Table 2: The detailed parameters and dimensions of the optimized design

Dimensions		
Symbol	value	Unit
R_{in}	1.27	cm
W_m	4.37	cm
L_g	0.54	cm
τ	8.7	cm
W_{coil}	2.65	cm
Overall diameter	8.82	cm
Overall height	8.7	cm
The optimized parameters		
λ_{max}/τ	0.0676	wb/cm
M_{coil}	8.2	kg
M_{pmref}	6.2	kg
P_{dref}	600	W
Coil parameters		
N	393	turns
λ_{max}	0.588	wb
r_{in} Coil resistance	1.935	Ω
Inductance matrix $[M]$	$\begin{bmatrix} 0.033 & 0.0237 & 0.0236 \\ 0.0237 & 0.033 & 0.0237 \\ 0.0236 & 0.0237 & 0.033 \end{bmatrix}$	Henry

4. Performance assessment of Halbach array linear generator of WEC at maximum power transfer

According to the dimensions determined by the FEM, each coil of the there-phase has flux linkage over the displacement with one pole pitch illustrated in Figure 6. The flux linkage has sinusoidal waveform over τ.

Figure 7 demonstrations the equivalent circuit of the three-phase Halbach array linear generator. The there-phase equivalent

circuit model consists of three EMF supplies e_a, e_b and e_c. the phases assumed to be connected in star. Moreover, the model for each phase contains an internal winding resistance r_{in}, self-inductances L_a and the mutual induced voltage due to currents pass in the other phases is presented by two dependent sources. The load

$$\begin{bmatrix} e_a \\ e_b \\ e_c \end{bmatrix} = \frac{d}{dt}\begin{bmatrix} \lambda_a \\ \lambda_b \\ \lambda_c \end{bmatrix} = \frac{d}{dz}\begin{bmatrix} \lambda_a \\ \lambda_b \\ \lambda_c \end{bmatrix}.\frac{dz}{dt} = \frac{d}{dz}\begin{bmatrix} \lambda_a \\ \lambda_b \\ \lambda_c \end{bmatrix} v_z \quad (12)$$

$$\begin{bmatrix} v_a \\ v_b \\ v_c \end{bmatrix} = \begin{bmatrix} e_a \\ e_b \\ e_c \end{bmatrix} - \begin{bmatrix} r_{in} & 0 & 0 \\ 0 & r_{in} & 0 \\ 0 & 0 & r_{in} \end{bmatrix}\begin{bmatrix} i_a \\ i_b \\ i_c \end{bmatrix} - \begin{bmatrix} L_a & M_{ab} & M_{ca} \\ M_{ab} & L_b & M_{bc} \\ M_{ca} & M_{bc} & L_c \end{bmatrix}\frac{d}{dt}\begin{bmatrix} i_a \\ i_b \\ i_c \end{bmatrix} - \begin{bmatrix} i_n & r_n \\ i_n & r_n \\ i_n & r_n \end{bmatrix} \quad (13)$$

$$\text{where } i_n = i_a + i_b + i_c \quad (14)$$

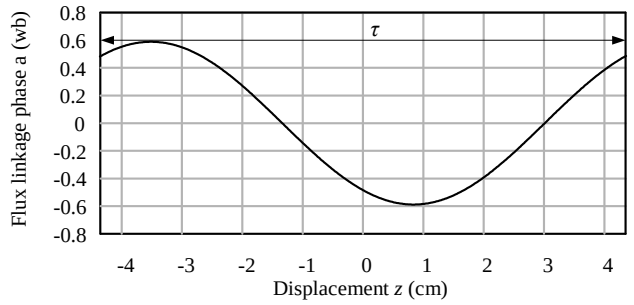

Figure 6: The changing of flux linkage with the vertical displacement over one pole pitch

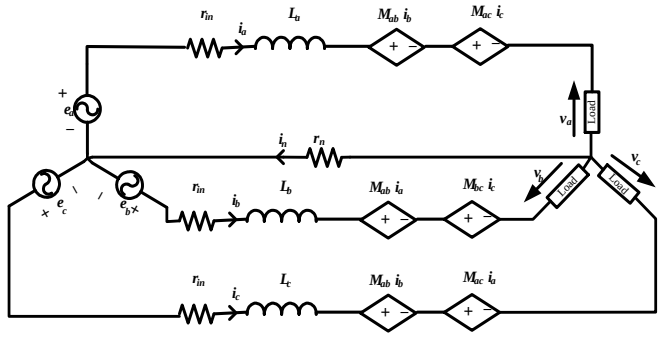

Figure 7: The equivalent circuit of the three-phase model of proposed Halbach array linear generator

To apply the maximum transfer condition from the mechanical point of view, the inertia force should be eliminated by stiffness force produced by applying current i_q* has phase shift of 90° with the induced phase voltage envelop [1]. From electrical point of view, the maximum power transfer happens when the circuit current is in phase with applied voltage. So, there is another current i_d* is in phase with voltage and therefore with the velocity. In (12), the voltage mainly relies on flux linkage and the velocity of the PM cylinder regarding the three-phase coils. In this generator, the energy is extracted from both rising and falling motions.

Now, the proposed Halbach array generator module is tested under two cases; the first when the maximum wave velocity equals 1.5 m/s and the second when it equals 1 m/s. Figure 8(a) shows the velocity applied on the floating buoy of WEC where the maximum velocity equals 1.5 m/s. This velocity is supposed to have sinusoidal waveform while its positive value means that the direction is up towards and the negative value means the reverse direction. As shown in Figure 8(b), the span of displacement ranges from 50 to -50 cm. Figure 8(c) illustrates the changing of the coils flux linkage during translator movement. As shown in Figure 8(d), the three phase voltages have 120° phase shift between each other although the voltages amplitude changes. Correspondingly, the velocity of the generator is directly related to the frequency of the induced voltages. The frequency related to speed should be considered during the voltage control of the generator output. The way of power extraction related to the value of currents passes through coils. Thus, the MPT is achieved by current regulation technique. Therefore, the MPT is achieved by allowing current i_q to pass through coils to produce stiffness force cancels the inertia force. Figure 8(e) illustrates the current i_q where its envelop has 90° phase shift with the envelop of voltage. Therefore, current i_q envelop is in phase with the translator displacement according to equation (2). The production of active power is achieved by allowing current i_d to pass through generator phases. The envelop of current id is in phase with the envelop of induced voltage as in Figure 8(e). Therefore, the maximum power transfer is achieved by allowing total current i_{tot} to be pass through each phase; where

$$i_{tot} = i_d + i_q \quad (15)$$

These currents for phase a are illustrated in Figure 8(f). The total current with its two components can cancel mechanical inertia and electrical inductances. Figure 8(g) demonstrates both the stiffness and inertia powers which have the same amplitude and opposite sign. Figure 8(h) demonstrates the total output power P_{tot} produced by the generator at MPP and the output power P_{out}.

Figure 9 illustrates the generator performance at 1 m/s maximum velocity. It can be observed that the span of movement is reduced by 36 cm. Although the flux linkage, in this case, has the same amplitude, the induced phase voltages have less amplitude because they depend on the velocity. The currents are reduced due to the reduction of reaction forces and the total and output power. According to the results at different velocity, the concept of operation of MPT can applied to obtain the maximum power from the waves.

5. Conclusion

Slotless tubular Halbach array linear generator has been developed to be used within wave energy converter system at maximum power transfer condition. The simple hydrodynamic model of the WEC have been developed to describe the hydrodynamic circumstances to achieve MPT condition. The principle of operation of the proposed Halbach array linear generator has been introduced. Moreover, the parameters affects the design of the generator have been derived to formulate the proper objective function. The FEM has been used to get the design parameters for different dimensions of the generator. The GA in combined with FEM is used to get the optimal parameters of generator design achieves the maximum fitness value. The optimized design has been modeled and simulated to study its performance in the maximum power transfer condition. The WEC system has been simulated to work with low velocity sea waves as these in the Mediterranean Sea. The MPT has been successfully achieved by using the concept of current control to cancel all system inertias.

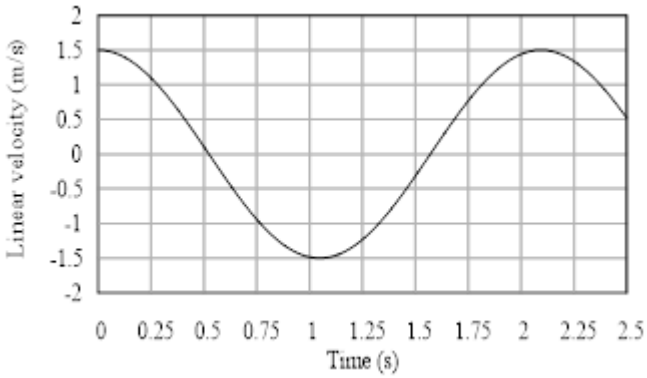

(a) Linear speed of WEC

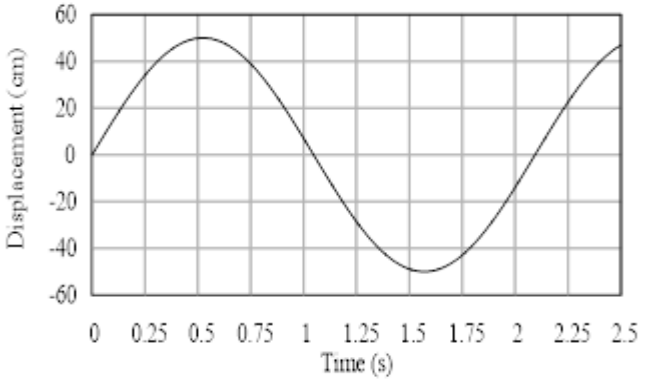

(b) Displacement of the buoy

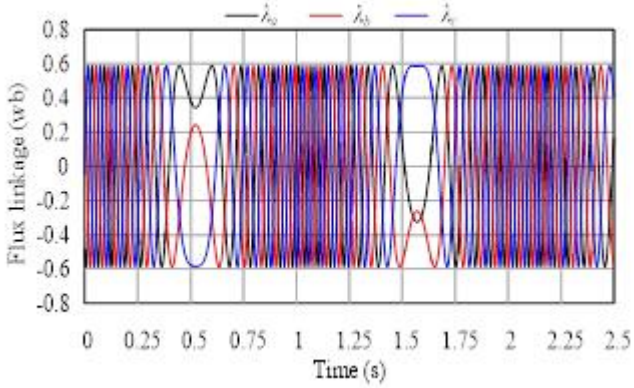

(c) Flux linkage of each phase

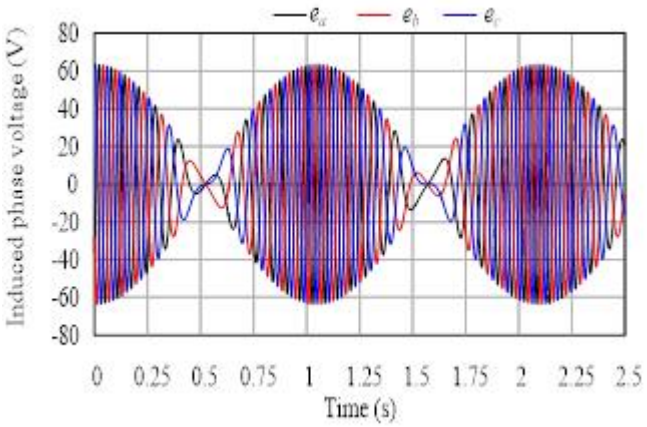

(d) Induced voltage of each phase

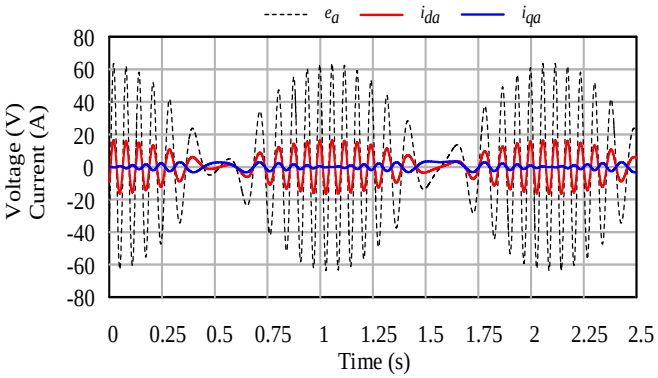

(e) Voltage and currents of phase a

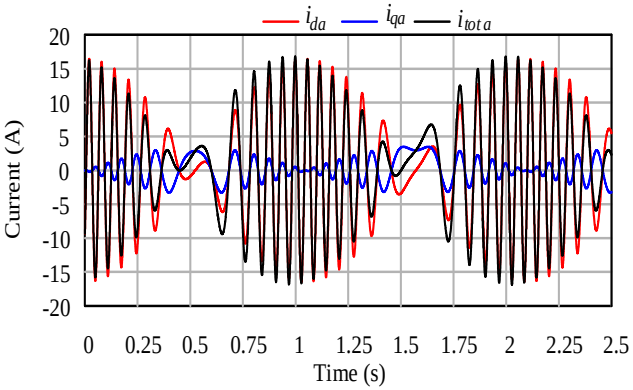

(f) direct, quadrature and total currents of phase a

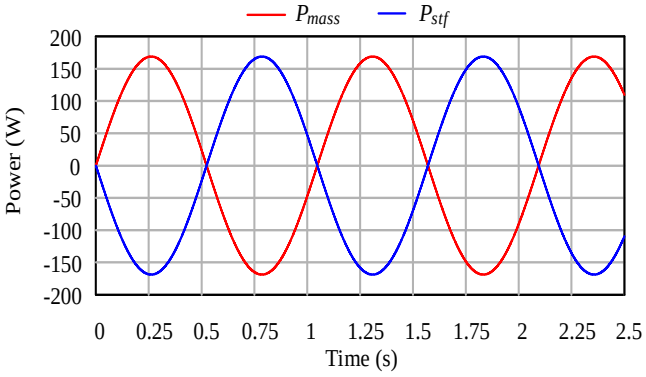

(g) Powers due to reactive forces (inertia and stiffness)

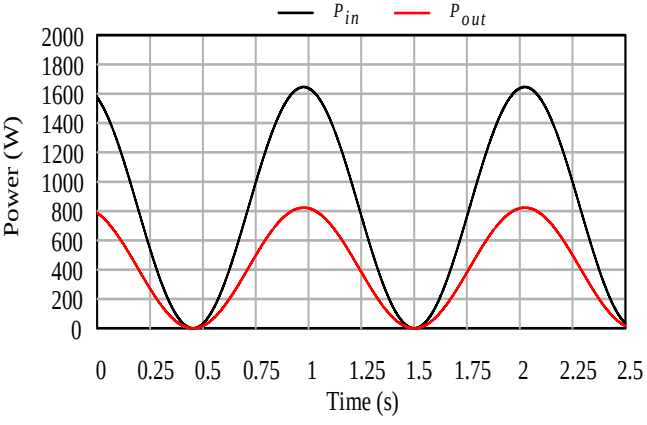

(h) Input and output power of WEC at MPT

Figure 8: The performance of Halbach array linear generator as WEC at maximum linear speed with 1.5 m/s

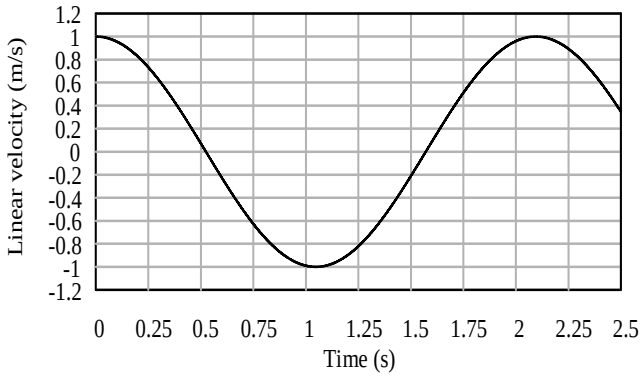

(e) Linear speed of WEC

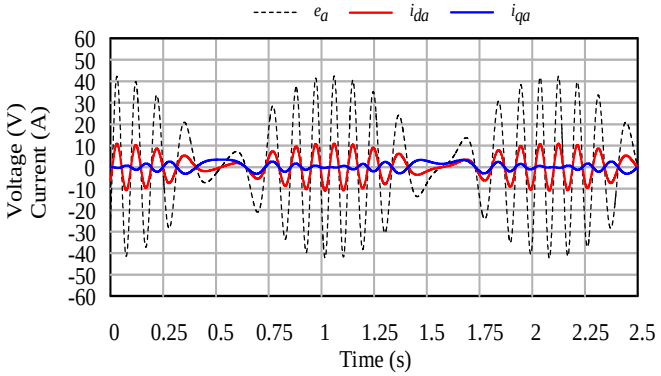

(e) Voltage and currents of phase a

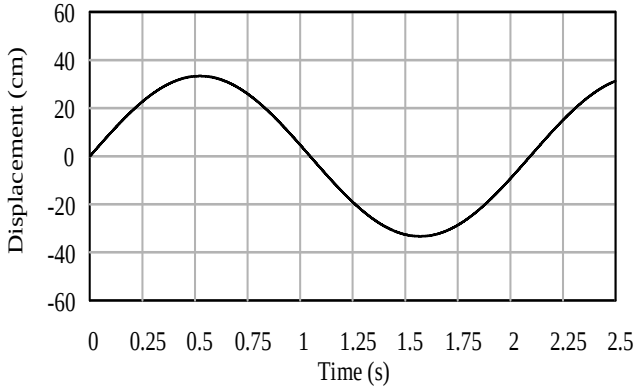

(f) Displacement of the buoy

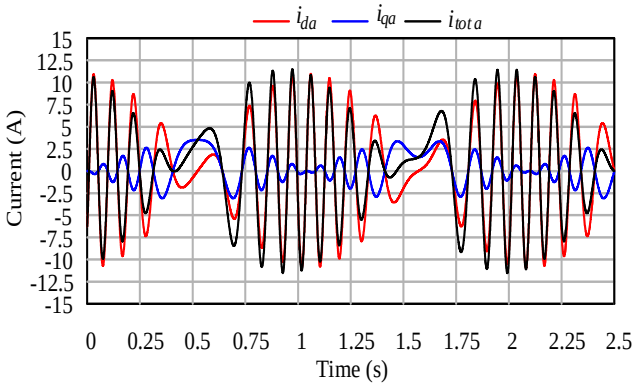

(f) direct, quadrature and total currents of phase a

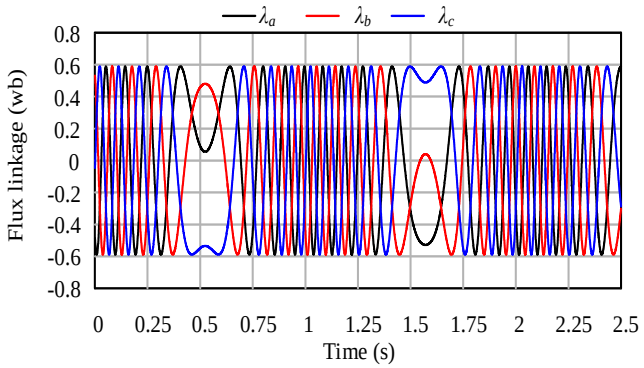

(g) Flux linkage of each phase

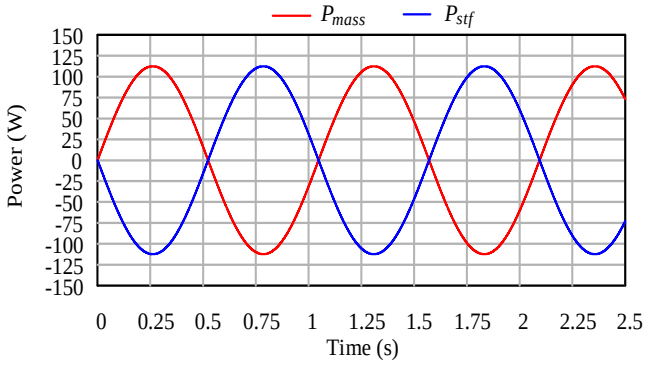

(g) Powers due to reactive forces (inertia and stiffness)

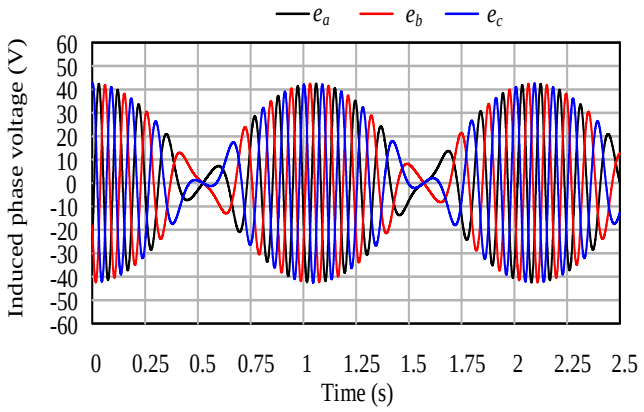

(h) Induced voltage of each phase

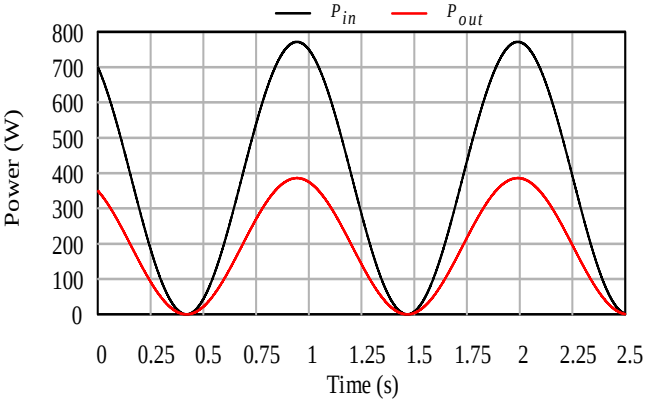

(h) Input and output power of WEC at MPT

Figure 9: The performance of Halbach array linear generator as WEC at maximum linear speed with 1 m/s

Acknowledgment

This study is performed at Energy Conversion Research Laboratory, Electrical power and Machines Department, Faculty of Engineering, Tanta University, Tanta, Egypt

References

[1] Ahmed E. ELGebaly, Mohamed K. El-Nemr, "Optimal Design of Slotless PM Halbach Array Linear Generator for Wave Energy Converters at Maximum Power Transfer Condition". in *2018* 20th International Middle East Power Systems Conference, MEPCON 2018, Cairo, Egypt, 2018. https://doi.org/10.1109/MEPCON.2018.8635113

[2] Ahmed E. ELGebaly, Mohamed K. El-Nemr, "Design and performance evaluation of halbach array linear generator for wave energy converters". in 2015 IEEE 8th GCC Conference and Exhibition, GCCCE 2015. Muscat, Oman, 2015. https://doi.org/10.1109/IEEEGCC.2015.7060035

[3] M. Mueller and H. Polinder, "Electrical Drives for Direct Drive Renewable Energy Systems. Electrical Drives for Direct Drive Renewable Energy Systems" 1–264 (Elsevier Ltd, 2013). doi:10.1533/9780857097491

[4] Bedard, R., Jacobson, P., Previsic, M., Musial, W. & Varley, R. An Overview of Ocean Renewable Energy Technologies. *Oceanography* 23, 22–31 (2011). doi: 10.5670/oceanog.2010.40.

[5] Vining, Jennifer, Tim Mundon, and Balky Nair. "Electromechanical Design and Experimental Evaluation of a Double-Sided, Dual Airgap Linear Vernier Generator for Wave Energy Conversion." *2017 IEEE Energy Conversion Congress and Exposition, ECCE 2017*. doi: 10.1109/ECCE.2017.8096926

[6] H. Polinder, B. C. Mecrow, A. G. Jack, P. G. Dickinson, and M. A. Mueller. "Conventional and TFPM Linear Generators for Direct-Drive Wave Energy Conversion" *IEEE TRANSACTIONS ON E NERGY CONVERSION*, VOL. 20, NO. 2, JUNE 2005

[7] Salauddin, M., M. A. Halim, and J. Y. Park. "A Low Frequency Vibration Energy Harvester Using Dual Halbach Array Suspended in Magnetic Springs." *Journal of Physics: Conference Series*. Vol. 660. Institute of Physics Publishing, 2015. doi: 10.1088/1742-6596/660/1/012011

[8] Zhu, Z.Q., and D. Howe. "Halbach Permanent Magnet Machines and Applications: A Review." *IEE Proceedings - Electric Power Applications* 148.4 (2002) doi: 10.1049/ip-epa:20010479

[9] Hodgins, Neil et al. "Design and Testing of a Linear Generator for Wave-Energy Applications." *IEEE Transactions on Industrial Electronics* 59.5 (2012): 2094–2103. *IEEE Transactions on Industrial Electronics* doi: 10.1109/TIE.2011.2141103

[10] B. Guo, R. Patton, M. Abdelrahman and J. Lan. " A continuous control approach to point absorber wave energy conversion 2016 UKACC 11th International Conference on Control (CONTROL), 31 Aug.-2 Sept. 2016, Belfast, UK. doi: 10.1109/CONTROL.2016.7737655

[11] Zheng, Xiong Bo, Jin Jiang, and Liang Zhang. "Power Characteristic Analysis and Optimization of Point Absorber Wave Energy Converter." *Applied Mechanics and Materials* 313–314 (2013): 837–842. https://dx.doi.org/10.4028/www.scientific.net/amm.313-314.837

[12] Kaiser, M. F.M., and O. E. Frihy. "Validity of the Equilibrium Beach Profiles: Nile Delta Coastal Zone, Egypt." *Geomorphology* 107.1–2 (2009): 25–31. doi: 10.1016/j.geomorph.2006.09.025

[13] Hazra, Samir et al. "Dynamic Emulation of Oscillating Wave Energy Converter." *2014 IEEE Energy Conversion Congress and Exposition, ECCE 2014*. Institute of Electrical and Electronics Engineers Inc., 2014. 1860–1865. *2014 IEEE Energy Conversion Congress and Exposition, ECCE 2014*. doi: 10.1109/ECCE.2014.6953645

[14] Dawande, M. S., Kanetkar, V. R. and Dubey, G. K. "Three-phase switch mode rectifier with hysteresis current control". *IEEE Transactions on Power Electronics* 11, 466–471 (1996). https://doi.org/10.1109/63.491640

[15] Farrok, Omar et al. "A New Optimization Methodology of the Linear Generator for Wave Energy Conversion Systems." *Proceedings of the IEEE International Conference on Industrial Technology*. Vol. 2016-May. DOI: 10.1109/ICIT.2016.7474965

ASTES

Advances in Science, Technology and Engineering Systems Journal Vol. 4, No. 4, 449-457 (2019)

www.astesj.com

Special Issue on Advancement in Engineering and Computer Science

ASTESJ

ISSN: 2415-6698

A Fuzzy-Based Approach and Adaptive Genetic Algorithm in Multi-Criteria Recommender Systems

Mohamed Hamada[*,1], Abdulsalam Latifat Ometere[1], Odu Nkiruka Bridget[1], Mohammed Hassan[2], Saratu Yusuf Ilu[2]

[1]*African University of Science and Technology, Department of Computer Science & Engineering, 90001, Nigeria*

[2]*Bayero University of Nigeria, Department of Software Engineering, 700231, Nigeria.*

A R T I C L E I N F O

Article history:
Received: 25 April, 2019
Accepted: 29 July, 2019
Online: 16 August, 2019

Keywords:
Recommender System
Multi-criteria Recommendation,
Adaptive Genetic Algorithm
Fuzzy Logic

A B S T R A C T

Recommender Systems (RSs) are termed as web-based applications that make use of filtering methods and several machine learning algorithms to suggest relevant user objects. It can be said that some techniques are usually adopted or trained to develop these systems that generate lists of suitable recommendations. Conventionally, RS uses a single rating approach to preference user recommendation over an item. Recently, multi-criteria technique has been identified as a new approach of recommending user items based on several attributes or features of user items. This new technique of item recommendation has been adopted to solve several recommendation problems compared to the single rating approach. Furthermore, the predictive performance of the multi-criteria technique when tested proves to be further efficient as compared to the traditional single ratings approach. This paper gives a comparative study between two models that are based on the features and architecture of fuzzy sets system and adaptive genetic algorithm. Genetic Algorithms (GAs) are robust and stochastic search techniques centered on natural selection and evaluation that are often applied when encountering optimization problems. Fuzzy logic (FL) on the other hand, is known for its wide application in diverse fields in science. This study aims to evaluate, analyze, and compare the predictive performance of both methods and present their results. The study has been accomplished using Yahoo! Movies dataset, and the results of the performance of each model have been presented in this paper. The results proved that both techniques have significantly enhanced the system's accuracy.

1. Introduction

The advancement of Internet of things together with the rapid growth of e-commerce websites has caused uneasiness for customers to choose appropriately from the overwhelming number of items offered by these websites [1]. This fast development of web-based tools and the steady accessibility of a variety of information on the web have also given rise to the problem of information overload. As such, this has led online customers to make poor choices while purchasing items online [2]. To overcome this persistent problem, there is a need to introduce an intelligent decision support system that has the potential to scan through the available items using some computational and machine learning techniques to find and recommend appropriate items to users. Hence the need for RSs. Currently, RS is a significant tool that solves problems of information overload. It solves this problem by suggesting only items that are suitable to users. Increasing the number of items sold in e-commerce sites and an increase in customers' satisfaction from buying items online is one of the key benefits of RSs [3].

RS is a web-based application that supplies users with recommendations of items that might be of interest to them. The recommendations of items to users may be personalized or non-personalized [4]. The personalized recommendations are typically presented as orderly lists of items offered to the system user. It takes into consideration users' previous history for rating and predicting items. On the other hand, non-personalized recommendation systems recommend what is popular and relevant to all the users, which can be a list of top-5 items for every new user. Consequently, RS studies the user behaviour first, which could be expressed explicitly by the user through the rating of items or implicitly by just clicking on items. After learning the user's behaviour, it suggests items that might be useful to the user based on what it has learned from the user. It further suggests an ordered list of items in a way the user will like or rate them [3].

*Mohamed Hamada, University of Aizu, Software Engineering Lab, Japan, +81 242 372617, Email: mhamada2000@gmail.com

Rating of items by the user is one of the main forms of data transaction that is collected by the RS and uses it to classify RS into traditional RS and multi-criteria RS.

Traditionally, the commonly used recommendation approach adopted is either a hybrid-based, content-based or collaborative filtering approach. These approaches, together with subdivisions of collaborative filtering approach are shown in Fig. 1 [4]. These methods obtained an overall rating of a specific user on an item. Ratings of the users over items are used by recommendation algorithms to evaluate and predict users' preferences on new items. Single criterion rating tends to be inadequate in most cases because they have been proven to offer recommendations that are not quite efficient in achieving user desires, since users are unable to define their opinions based on various attributes of the item.

Multi-criteria Recommender Systems makes use of several items attributes to define the appropriateness of user items [5]. As an example, in a Movie RS, part of the attributes sighted may be the direction, action, visual, story. Multi-criteria RSs improves the Single criterion RS by putting into consideration varied items attributes in which users may like. Unlike Single Criterion RSs, users are capable of providing individual preference ratings on various item attributes. In most cases, additional relevant information offered by multi-criteria recommender systems helps to enhance recommendation value accurately. This enhancement depicts different features that a user may like about the item. In most RSs research, accuracy has been the most extensively examined point of emphasis [3]. However, more research is mandated on the effectiveness of new methods to integrate the multi-criteria rating information into the recommendation process efficiently. Therefore, this work aims to analyze and investigate how to use genetic algorithms and fuzzy technique to improve the precision in a multi-criteria RS. The study also provides a comparative analysis of the efficiencies of the two techniques.

The current paper is separated into five distinct sections, together with section 1. Section 2 presents a summary of traditional and multi-criteria RSs. Section 3 presents the methodology and frameworks used to implement both systems. Section 4 presents the results and comparison of both methods. Finally, section 5 presents the conclusion and discusses future work

2. Concept of Collaborative Filtering (CF)

CF is among the very commonly used approaches in generating valuable recommendations due to its human nature centred approach. It mainly "use the wisdom of the crowd or what seems to be common amongst my cycle" to recommend items to me. This is centred on the connection between users of the system and the item itself. It performs well in complex object recommendations (for example movies and music), which are seen to be totally autonomous from any machine-readable prediction of the items recommended.

Various companies have used RSs by implementing numerous algorithms that cut across different area. An example of such implementation is the statistical interactive learning techniques implemented by CleverSet, and also, the classical CF implemented in Net Perceptions [6] and Amazon [7].

CF approaches are mostly categorised into Memory-based and Model-based filtering method. The latter method makes use of earlier activities of the user to acquire a predictive model. This is done either by making use of some statistical analysis or machine learning techniques in making relevant recommendations [1]. Memory-based filtering approach makes use of recommendations grounded on similarities that exist in comparing previous activities or users' stored data. According to literature, there exist two ways commonly used to achieve memory-based techniques (item-based or user-based techniques) [8]. Fig. 1 shows a summary of the recommendation techniques. Model-based techniques can be developed using algorithms, some of such algorithms include Bayesian classifiers [9], Support vector machine, Neural networks [10], Boltzmann machine, Fuzzy patterns [11], Latent features, Genetic algorithms [12] and Matrix factorizations [13].

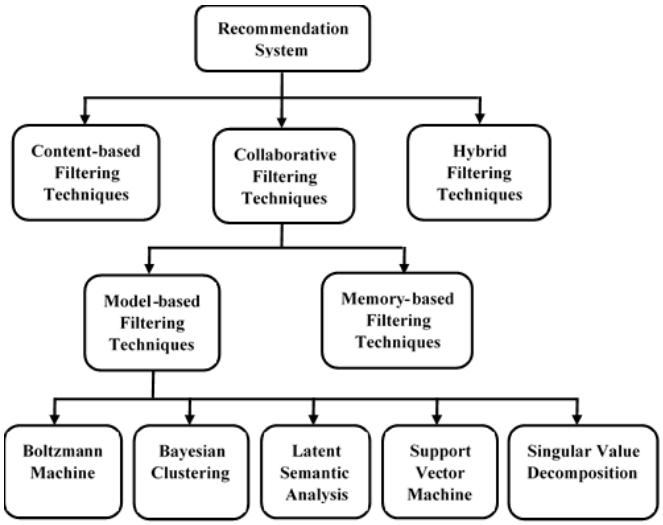

Figure. 1 Overview of existing recommendation methods

2.1. Asymmetric Singular Value Decomposition (ASVD)

ASVD is an extension of SVD. It relates to three vectors (c_i, d_i, $L_i \in \mathbb{R}^f$), also, users are signified by the objects they desire. User predictions to an item are represented in Eq. (1).

$$R'_{ui} = b_u + b_i + \mu + L_i^T(|R(u)|^{-0.5}\sum_{j\in R(u)}(R_{uj} - b_{uj})c_j + |N(u)|^{-0.5}\sum_{j\in N(u)} d_j) \quad (1)$$

by minimalizing the normalized squared error, we obtained Eq. (2).

$$\min_{b^*,L^*,c_i^*,d_i^*}\sum_{(u,i)\in K}(R_{ui} - \mu - b_u - b_i - L_i^T(|R(u)|^{-0.5}\sum_{j\in R(u)}(R_{uj} - b_{uj})c_j + |N(u)|^{-0.5}\sum_{j\in N(u)} d_j))^2 + \lambda(b_u^2 + b_i^2 + \| L_i\|^2 + \sum_{j\in R(u)}\|c_i\|^2 + \sum_{j\in R(u)}\|d_i\|^2) \quad (2)$$

where R_{ui} represent user ratings u to item i, μ represent the overall mean rating, b_u and b_i represent detected deviation of user u and observed deviation of item i correspondingly, $R(u)$ represent a set of the total items rated by the user u which are known ratings, $N(u)$ represent the set of all items which are rated by u, this can either be a known or an unknown rating and j represent an item.

The regularized squared error was minimised using stochastic gradient descent, and the boundaries λ and γ are

assigned positive real values of 0.002 and 0.005 respectively [14].

2.2. Multi-Criteria Recommender System (MCRS)

Majority of the RSs in use today are based on a single criterion rating which contains the overall user's satisfaction of an item [3]. Single criterion rating hides the users' choices and misleads the system when predicting items to the users [15]. It works in two-dimensional space of users and its utility function as expressed in Eq. (3)

$$R: Users \times Items \rightarrow R_0. \quad (3)$$

The utility function is gotten from the user inputs, e.g., transaction history or numeric ratings.

Single-criterion rating systems have shown successful recommendations in many areas. However, research in RS has identified the benefits of multi-criteria RS to enhance the prediction accuracy [16]. Multi-criteria RS does this by providing detailed information about the user ratings than a single-criterion RS and this enhances the recommendation process [5]. To determine the utility function of a user for a given item, we consider the overall rating R_0 and the user's ratings $R_1, \ldots, R_k$ for each criterion c (c = 1, 2, ..., k). Thus, the utility function R for multi-criteria RS is given as in Eq. (4)

$$R: Users \times Items \rightarrow R_0 \times R_1 \times R_2, \ldots, R_k. \quad (4)$$

2.3 Genetic Algorithm

Genetic Algorithms (GAs) are a robust and stochastic search technique centered on natural selection and evaluation that is frequently applied when encountering optimization problems. GA applications are frequently used when dealing with combinatorial optimization problems [17]. GA applies the same knowledge as any other evolutionary algorithm. It makes use of data collected from a set of individuals, represented as *G(i)*, where *G* represents the set (population), and *i* represents the number of the set (individuals). Each of the individuals is evaluated by assigning an appropriate fitness value, which is dependent on how respective individual is close to finding a solution to the problem. As its iteration continues, it finally approaches a local minima/maximum of the function.

A possible solution for a GA problem in GA is often called *chromosome or individuals*. Chromosomes are referred to as a set of genes; where each gene is represented by a distinct bit of nearby bit that encodes a part of the possible solution. Chromosomes are often scrambled as a sequence of bit string characterized abstractly in a genetic form. *Locus* is referred to as a location that has the encoding of some traits, while an *Allele* is a representation of each possible value of a locus (0 or 1) [18].

The *genotype* is referred to as a set of genes that exist in a genome, while the *Phenotype* is referred to as the physical representation of the genotype. After each encoding of the chromosome, the next step is to apply several reproduction procedures to the genotype. The genetic operators, such as the crossover, selection and mutation works on the genotype plot in other to return the value of the best chromosome.

Lastly, the stochastic nature of GA makes it challenging when trying to guarantee a solution that is optimal, and the algorithm may never stop running, which prompts for a termination condition. The algorithm is said to terminate only when the stopping criterion is met. The flowchart of a GA is shown in Fig. 2.

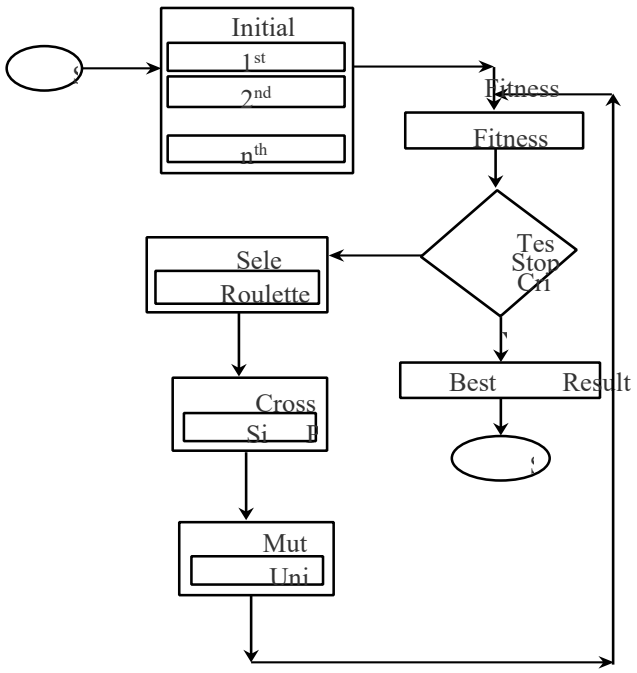

Figure 2 Flow chart of a standard genetic algorithm

2.3.1 Adaptive GA

Adaptive genetic algorithms are a subset of genetic algorithms. They provide substantial functionality improvements over the traditional GA implementations [19]. The configuration of genetic algorithms operators such as the probability of mutation and probability of crossover is a significant deterministic factor which affects the performance of a GA. The main function of GA is that, they help to modify the operators automatically, this is done by fine-tuning the operators centred on the algorithm's state [20]. These fine-tuning operations offered by GAs helps in maintaining convergence capacity and population diversity. The modification is centred on the values of the fitness solution which are, the best fitness value of the recent population and the best fitness value of the average population.

2.4 Fuzzy logic: An overview

Fuzzy Logic (FL) is a concept that is gotten from the fuzzy set theory which was developed by Lotfi Zadeh in 1975 [22]. It is a technique that can be used to mathematically express human reasoning or language by using a range of real numbers between 0 and 1. A membership function (MF) expressed as μA and defined as $\mu A: X \rightarrow [0, 1]$ is used to express the degree of membership of elements in a fuzzy set A.

2.4.1 Fuzzy logic architecture

Fuzzification

This step involves converting crispy set of inputs to a fuzzy set.

Linguistic variables

These are variables whose values are represented using ordinary language

Membership Function (MF)

It is used to represent graphically the amount of satisfaction a user got from an item.

Fuzzy Rule

It controls the output variable by applying some set of rules

Defuzzification

It is used to get a crispy value.

3. Methodology

This section presents the methods and frameworks used in the implementation of both systems.

3.1. Experimental dataset

Both systems were evaluated using Yahoo! Movie dataset collected from their website [5]. The dataset is a multi-criteria dataset that consists of user preferences ratings on movies based on four various movie features as follows: direction (c1), action (c2), story (c3), and visual (c4) effect of the movie. Each criterion ratings were considered on a 13-fold scale ranging from F through A^+ where F denotes the lowest preference, while A+ denotes the highest preference. An overall rating (c_0) denotes the total satisfaction derived by the user. The sample of the dataset is shown in Table 1.

Table 1: User Rating Obtained from *Yahoo*! Movies Rs

User ID	direction (c_1)	action (c_2)	Story (c_3)	visual (c_4)	Overall rating	Movie ID
1	10	10	10	8	9	100
	5	8	3	2	5	25
2	1	5	8	2	4	48
1	7	7	5	9	5	320
	10	13	4	13	10	360
3	7	8	10	10	9	224

For simplicity to model both systems, these categorical data were transformed to the numerical dataset as shown in Table 2.

The datasets were pre-processed to remove inconsistency that arose due to missing ratings. In the end, we achieved a total of 6078 users, 978 movies and 62,156 ratings with 0.0105 total sparsity estimate. The global median, global average, and standard deviation are 11.0000, 9.5221, and 3.5232, respectively. The summary of the records is shown in Table 3.

Table 2: User Rating Obtained from Yahoo Movies Rs (After Conversion)

Values	Frequency-rating	Percentage (%)	Cumulative-Percentage(%)
1	3395	5	5
2	1340	2	8
3	1522	2	10
4	1329	2	12
5	2051	3	16
6	2428	4	19
7	2489	4	23
8	3251	5	29
9	5586	9	38
10	7006	11	49
11	6702	11	60
12	12153	20	79
13	12904	21	100

Table 3: Rating Frequency of The $\boldsymbol{user} \times \boldsymbol{item}$ In Yahoo! Movie Datasets After Preprocessing.

User ID	direction (c_1)	action (c_2)	story (c_3)	visual (c_4)	Overall rating	Movie ID
1	B^+	B+	B+	B	B+	100
	D^-	B	D-	D	C	25
2	F	C	B	D	D+	48
1	C^+	C+	C	B-	C	320
	B^+	A+	D+	A+	B+	360
3	C^+	B	B+	B+	B-	224

3.2. Adaptive GA MCRS Methodology

The Adaptive GA method for rating approximation was divided into different stages:

1) Prediction of N multi-criteria Rating: This was done by decomposing the *k*-dimensional multi-criteria ratings into *k* single rating problem. To predict the unknown multi-criteria rating, an ASVD was used. For the next stage, the individual ratings were combined to provide an overall prediction of the ratings.

2) Acquiring the Function: This stage was aimed at approximating the connection between the original multi-criteria ratings and overall ratings of the items, such that $R_0=f(R_1,\ldots, R_k)$. An Adaptive GA was used to obtain the optimal weight of the individual benchmark for respective users over several criteria.

Feature weight is the priority a user gives to a feature, which may differ for each feature. In our method, Adaptive GA was applied to modify the weight to take user priorities for several features. User feature weight is denoted as a set, weight (u_a) = [w_i] (where i = 1, …, z, and z = number of features). Any feature with the weight zero is ignored for further calculation. Any double-valued vector strings are used to represent the genotype. The proposed adaptive GA parameters are reviewed below:

i. ***Initial Population*:** The original set of the population was created randomly with a size of 40 which consist of valid feature weights.

ii. ***Fitness Function*:** Fitness function is one of the most significant parts of GA. This function determines the success level of the individual chromosome after the population set is initialized. For a user who is active, a separate chromosome c is allocated a fitness function. The examined fitness function computes the accuracy of the predicted items using generated random weights. Eq. (5) represents the proposed fitness function.

$$fitness\ (c) = 1 - \left(\frac{\sum_{j=1}^{N_a} \left| R_{0j} - \left(\frac{w_1 R_{j1} + \cdots + w_z R_{jz}}{(w_1 + \cdots + w_z)} \right) \right|}{N_a} \right) \quad (5)$$

where N_a represent the aggregate number of times an individual chromosome c was tested, R_j represent the real ratings and R_{0j} represent the total ratings of u_a on an item, i_j.

iii. **Reproduction:** his step was solely dependent on the value of individual chromosome's fitness function. The fitness function defined for individual chromosome in the set of the population was computed and the chromosomes with the highest fitness rate were chosen as best chromosomes. The best chromosomes are reserved for the following generation.

iv. **Selection:** Roulette wheel selection technique was used, where parents are chosen according to their fitness value. Using the roulette wheel technique, each chromosome is allocated a slice of the wheel and the size of the slice is proportional to each chromosome's fitness. The wheel is then rotated and any chromosome the wheel lands each time was chosen.

v. **Crossover:** A single point crossover was selected to be implemented for the crossover. The selected crossover point was done randomly along the mated string length, then the next crossover point bits were swapped. The crossover probability was dependent on the fitness function, due to the fact that it's an adaptive GA.

vi. **Mutation:** Diversity was introduced by adopting uniform mutation. The value of the chosen gene was replaced with a uniform random value, selected between the specified upper and lower bounds for the gene by the mutation operator. The mutation probability was dependent on the fitness function, due to the fact that it's an adaptive GA.

vii. **Termination Condition:** Stopping criteria were centred on a well-defined number of initiations (100), and also on the convergence of best fit chromosomes.

3. Predicting Total rating: The calculation of the unknown total rating for test data was accomplished using the weighted sum of each predicted ratings. This was generated as depicted in Eq. (6).

$$R'_0 = \frac{\sum_{i=1}^{z} w'_i \times R'_{ji}}{\sum_{i=1}^{z} w'_1} \quad (6)$$

Where R'_j represent the predicted rating of u_a to i_j of the particular multi-criteria ratings. Developing Eq. (6) yields Eq. (7)

$$R'_0 = \frac{w'_1 R'_{j1} + \cdots + w'_z R'_{jz}}{(w'_1 + \cdots + w'_z)} \quad (7)$$

The aim of multi-criteria recommender systems is to generate a recommendation list for active users. The RS calculates the unknown total ratings by using feature weight function. Lastly, all unrated items and objects were sorted in non-increasing order with respect to the total ratings. Fig. 3 summarizes the working process of the Adaptive MCRS.

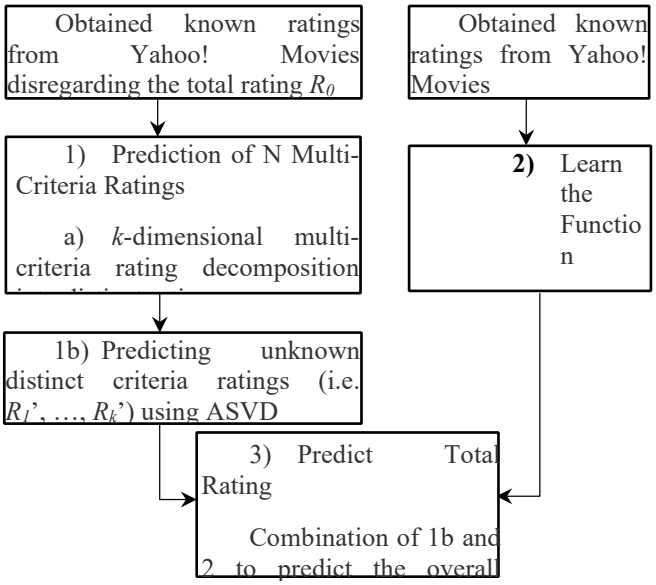

Figure 3 Structure of Adaptive Multi-Criteria Recommender System

3.3. Fuzzy-based MCRS Methodology

i. Predict N Multi-criteria rating

This step involves the decomposition of the n-dimensional multi-criteria rating space $R: Users \times Items \rightarrow Ro \times R_1 \times \ldots \times Rn$ where $(i = 1, \ldots, n)$ into n single-rating recommendation problems as $R: User \times Item \rightarrow R_c (c = 1, 2, \ldots n)$. The proposed model learns and predicts the user ratings for new items, however, we did not consider the overall rating at this stage.

$$(a, b, c) = \begin{cases} 0, & for\ x \leq a \\ \frac{x-a}{b-a} & for\ a \leq x \leq b \\ \frac{c-x}{c-b} & for\ b \leq x \leq x \\ 0 & for\ x > c \end{cases} \quad (8)$$

ii. Learn the Relationship f

This stage involves the computation of the relationship f relating to the overall rating r_0 and multi-criteria $r_1, \ldots, r_k$. Also, The aggregation function is considered as shown in the work of [21]. We integrated the FL technique to find the degree of satisfaction derived by a user from an item. Firstly, the user's ratings were represented using linguistic terms including (high, medium, low, etc.) and triangular membership function as shown

in TABLE 4. We considered a triangular membership function whose membership function is well-defined by the real numbers expressed as (a, b, c) as shown in Eq. (8).

We defined the membership function using 13 linguistic terms to represent interests of users and degrees to which each criterion was chosen. To compute the weight that determines the actual degree of membership of each criterion rating, this is calculated by dividing each user rating by n as shown in Eq. (9) below:

$$w_i = \frac{R_i}{n} \quad (9)$$

Where R_i represent user rating for each item and n represent the total number of fuzzy linguistic value.

We then derived the relationship f to learn how the user rates an item. Eq. (10) shows the aggregation function.

$$f(x_u^j) = \frac{\sum_{i=1}^{n} w_i\, c_i}{\sum_{i=1}^{n} c_i} \quad (10)$$

Where Ci is the users' criteria ratings and W_i is the weight associated with each criteria rating (for $i = 1, 2, \ldots, n$)

The relationship f for each user criteria rating for j items was computed, the function that resulted in the highest degree of membership for user u, for j ratings ($j = 1, 2, 3, \ldots n$) is chosen as the most preferred criterion for the user as shown in Eq. (11).

$$f(x_u) = max\{f(x_u^j)\}. \quad (11)$$

Table 4: Membership Function

User rating	TFN	Linguistic terms
1.0	(0,1,2)	V-V-V-V-low
2.0	(1,2,3)	V-V-V-low
3.0	(2,3,4)	V-V-low
4.0	(3,4,5)	V-low
5.0	(4,5,6)	Low
6.0	(5, 6,7)	Medium-low
7.0	(6,7,8)	Medium
8.0	(7,8,9)	Medium-high
9.0	(8,9,10)	High
10.0	(9,10,11)	V-high
11.0	(10,11,12)	V-V-high
12.0	(11,12,13)	V-V-V-high
13.0	(12,13,14)	V-V-V-V-high

i. Predict Overall rating

At this stage, the model predicts the overall rating $r'_0 = f(r'_1, r'_2, \ldots, r'_k)$ for an active user u_a. This is achieved through the integration of the trained fuzzy MCRS and the

single rating technique (Asymmetric SVD) so as to present the top-N recommendation to a user u_a. To calculate the overall rating for the user u_a, we use Eq. (12).

$$r'_0 = \frac{\sum_{i=1}^{n} w'_i \times P'_{ji}}{\sum_{i=1}^{n} w'_i} \quad (12)$$

Where

W_i represents the selected weight of the users to item i, and P_i represents the predicted rating of the users to the item i_j.

3.4. Implementation

Java programming language was used for implementing both systems. Java is a class-based, object-oriented programming language that is rich in FL and GA libraries that enhanced the process of both systems implementation,

3.4.1 Performance Metrics

To check the precision of both systems we explored the three categories of prediction precision measures [3]. As follows:

1. Rating predictions**:** Root Mean Squared Error (RMSE) and Mean Average Error (MAE) were used.

(a) RMSE: checks the precision of the predicted ratings as defined in Eq. (13) below:

$$RMSE = \sqrt{\frac{1}{|T_s|}\sum_{(u,i)}(\varepsilon T_s)\left(\widehat{P_{ui}} - r_{ui}\right)^2} \quad (13)$$

(b) MAE is defined in Eq. (14)

$$MAE = \frac{1}{T_s}\sum_{(u,i)}(\varepsilon T_s)\left|\widehat{P_{ui}} - \widehat{r_{ui}}\right| \quad (14)$$

Where: T_s = Test sets of user − item pairs (u, i) , $\widehat{P}_{ui}$ represent the predicted rating generated by the system and r_{ui} represent the actual rating of the user.

2. **Usage prediction**: This is used to measure the accuracy of the system based on how the system would predict the item a user would add to their content list. We considered Recall and Mean Average Precision (MAP) for the top-10 recommendation, which is defined in Eq. (15) and Eq. (17).

(a) $$recall = \frac{\#tp}{\#tn+\#fn} \quad (15)$$

Where tp is the number of positive useful items and fn is the number of useful predictions that are not in the top-n recommendation list.

(b) MAP: This calculates the value of Average Precision (AP) throughout the distinctive levels of recall. The value of MAP is expected to be less than or equal to 1 for a good algorithm and 0.5 for a bad algorithm. Eq. (16) and Eq. (17) was used to calculate these

$$AP = \frac{\sum_{i=1}^{N}(\text{precision(i)}\times\text{recall(i)})}{\text{number of relevant items}} \quad (16)$$

$$MAP = \frac{\sum_{u=1}^{M} AP_u}{M} \quad (17)$$

Where M represents the total number of items that are relevant in the catalogue of Top-N recommendation

3. **Ranking prediction**: This evaluates how accurate the

system would predict how a user would rank items according to their preference. Three approaches were considered, they are

(i) Area under the curve of Receiver Operating Characteristics (ROCAUC),
(ii) Fraction of Concordant Pairs (FCP),
(iii) Normalized Discounted Cumulative Gain (NDCG).

$$(a)\ ACU = \frac{1}{N}\left[\left(\sum_{i=1}^{\#tp_u} rank_{uj}^{+}\right)^{\#tp+1}_{2}\right] \quad (18)$$

where $rank_{uj}^{+}$ is the Position of the k^{th} relevant item on the top-N recommendation

$$(b)\ FCP = \frac{n_c}{n_c + n_d} \quad (19)$$

where n_c is the number of concordant pairs defined as:

$$n_c = \sum_u \varepsilon \cup |i,j| \left\{ \widehat{r_{ui}} > \widehat{r_{uj}} \Rightarrow \hat{r}_{ui} > \hat{r}_{uj} \right\} \quad (20a)$$

and n_d is the number of corresponding discordant defined as:

$$n_d = \sum_u \varepsilon \cup |(i,j)| \left\{ \hat{r}_{ui} > \hat{r}_{uj} \Rightarrow \hat{r}_{ui} \leq \hat{r}_{uj} \right\} \quad (20b)$$

4. Results and Discussion

This section discusses the results of the experiments done

4.1. Experiment

To verify the precision and efficiency of both systems, experiments were done using the Yahoo! movie dataset. An offline experiment was performed to simulate the actual system. Both systems were compared with their corresponding traditional collaborative filtering technique known as Asymmetric Singular Value Decomposition (AsySVD). We performed each test using a 10-fold cross-validation rule, which randomly divides the datasets into 10 separate subsets. The dataset was divided on a ratio of 90: 10 where 90% is used as training-sets and 10% as a test-set. The precision of both systems was checked by applying the metrics discussed in section 3.3.1. The results of evaluating the systems were compared with their corresponding traditional rating. TABLE 5 and TABLE 6 give the breakdown of the resulting performance evaluation of the system. We used Adaptive MCRS, Fuzzy-MCRS and AsySVD to represent Adaptive Genetic MCRS, Fuzzy logic model and Asymmetric SVD respectively.

Table 5: Performance Evaluation Results

Performance-measure	AsySVD	Adaptive-MCRS	%Accuracy Improvement
MAE	2.3980	1.5990	0.7990(49.9%)
RMSE	3.0900	2.1220	0.9680(45.6%)
MAP	0.0200	1.0290	1.0090(98.1%)
AUC of ROC	0.6880	0.9510	0.2630(27.7%)
FCP	0.7100	0.9460	0.236(24.9%)

It can be clearly seen from TABLE 5 above that the Adaptive MCRS outperforms the traditional AsySVD. The results proved that Adaptive MCRS achieved better predictive performance. The Adaptive MCRS approach achieved a decrease in prediction accuracy in terms of RMSE and MAE. RMSE and MAE had a value of 0.968 and 0.799 respectively, this decrease might seem minute, but it is able to generate a totally dissimilar answer and interpret into substantial enhancement on the accuracy and quality of recommendation. Adaptive MCRS achieved a MAP of 1.029, outperforming the traditional AsySVD by 50.5%. There is a necessity for recommendation algorithm to generate recommended ordering of objects or items that matches how users would have ranked the same item since users are frequently concerned of the items at the top-N recommendation list. The Adaptive MCRS achieved a more accurate and improved rank accuracy of 33.2% and 38.2% respectively for FCP and AUC when compared to the conventional AsySVD, which implies that Adaptive MCRS will provide a further precise top-N recommendation list to users. Fig. 4 is a line chart clearly demonstrating the high-performance result achieved by Adaptive MCRS as compared to AsySVD.

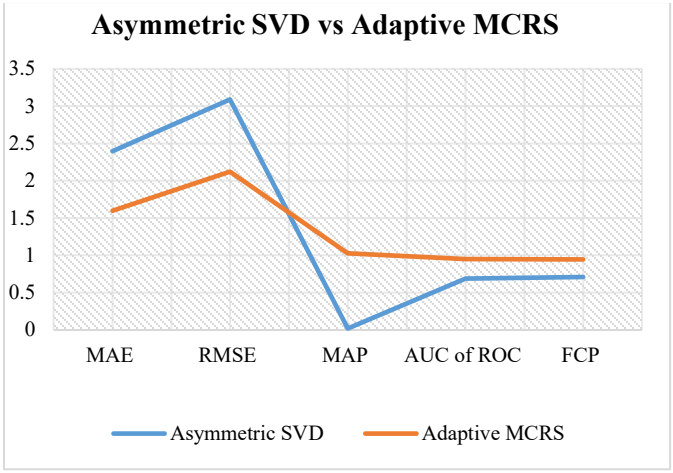

Figure. 4. The result of the evaluation of Adaptive MCRS

The result From Fig. 5 and TABLE 6, shows that Fuzzy-MCRS achieved a lower prediction error in RMSE and MAE, and similarly shows a higher-ranking accuracy in AUC and FCP. This indicates that modelling a multi-criteria RS using fuzzy logic would yield an efficient and more accurate system than the traditional AsySVD.

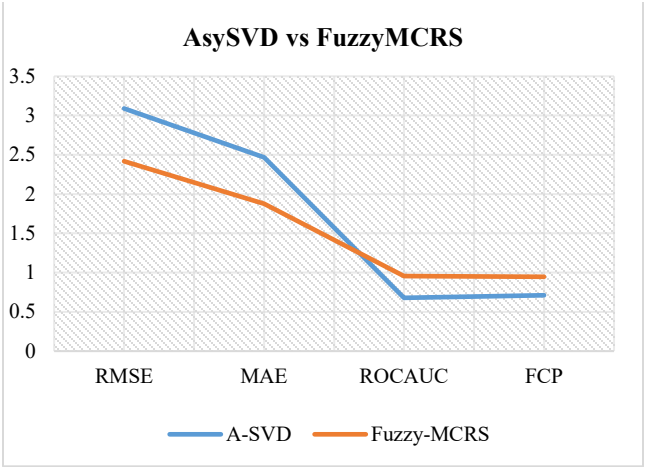

Figure 5. Comparing AsySVD and Fuzzy-MCRS

Table 6: Comparison of Result Of The Evaluation

Metrics	Fuzzy-MCRS	AsySVD	Accuracy Improvement
RMSE	2.4176	3.0895	0.6719(27.7%)
MAE	1.8753	2.4677	0.5924(31.5%)
ROCAUC	0.9558	0.6786	0.2572(26.9%)
FCP	0.9467	0.7118	0.2349(24.8%)

Table 7 and Fig. 6 clearly shows the comparison of the experimental result from both models. Adaptive MCRS resulted in lesser prediction inaccuracy in MAE and RMSE than the Fuzzy-MCRS, which implies that Adaptive MCRS yielded a better rating prediction than Fuzzy-MCRS. But both models seem to have equivalent usage accuracy, although Fuzzy-MCRS seem to have produced a higher usage accuracy level in ROCAUC and FCP than the Adaptive MCRS. This shows that Fuzzy-based model would be ideal for predicting the ranking behaviour of users for an item since it studies the exact degree to which a user will rank items to their content list and the order in which the items would be ranked. Similarly, Adaptive MCRS would be ideal to model a system that would be accurate in predicting and classifying the rate of satisfaction derived by a user from a purchased item.

Table 7: Comparison of Fuzzy-Mcrs and Adaptive-Mcrs

Metrics	Fuzzy-MCRS	Adaptive MCRS	Percentage Change
RMSE	2.4176	2.122	0.2956 (13.9%)
MAE	1.8753	1.599	0.2763 (17.3%)
ROCAUC	0.9558	0.951	0.0048 (0.5%)
FCP	0.9467	0.946	0.0007 (0.1%)

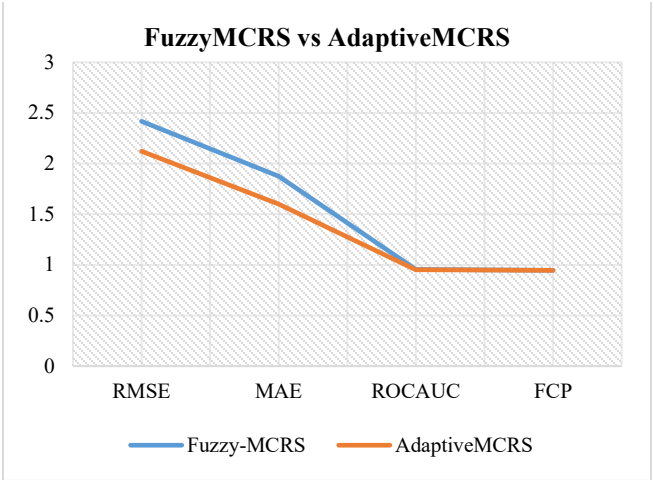

Figure. 6. Comparison of Fuzzy-MCRS and Adaptive MCRS

5. Conclusion

Providing efficient techniques for integrating the criteria ratings in multi-criteria RSs is of the utmost significance in predicting preferences of users based on several attributes of the items. Machine learning methods and other powerful techniques from the area of artificial intelligence should be the priorities, especially in product recommendations such as movies, song, and other items that could be purchased online. In this study, two important techniques (Adaptive genetic algorithm and fuzzy logic) have been proposed for developing recommendation models that could efficiently integrate the criteria ratings for making good recommendations. The experiments were conducted using a real-life dataset from Yahoo Movies, and the results have been analysed and compared. The study has shown that the two techniques realized the objectives of delivering better recommendation and predictive performance. This performance includes a reduction in error prediction and increased classification and rank accuracy. Lastly, the obtained experimental results from associating the predictive implementation of both multi-criteria recommender systems using the adaptive genetic algorithm and fuzzy logic, with existing conventional CF approach showed that the proposed system produced results that are better and also outperformed the conventional CF recommender system. Nonetheless, to achieve a better performance, it is recommended to design a hybrid model which could resolve some of the issues realized in the results of both systems.

Therefore, we propose to integrate both models to achieve higher performance. However, in the future, we plan to acquire a larger amount of data from a different domain to further certify the accuracy of the proposed system.

References

[1] L. Liu and D. Xu, "Multi-Criteria Service Recommendation Based on User Criteria Preferences," 2011.
[2] F. Ricci, L. Rokach, and B. Shapira, Recommender Systems : Introduction and Challenges. 2015.
[3] D. R. Tobergte and S. Curtis, *Recommender Systems Handbook*, vol. 53, no. 9. 2013.
[4] R. Burke, "Hybrid Web Recommender Systems," *Adapt. Web*, pp. 377–408, 2007.
[5] K. Lakiotaki, N. F. Matsatsinis, and A. Tsoukiàs, "Multi-Criteria User Modeling in Recommender Systems."
[6] J. Mo, S. Sarkar, and S. Menon, "Know When to Run: Recommendations in Crowdsourcing Contests," *MIS Q.*, vol. 42, no. 3, pp. 919–944, 2018.
[7] G. Linden and B. Smith, "Amazon-Recommendations.pdf," no. February 2003.
[8] F. O. Isinkaye, Y. O. Folajimi, and B. A. Ojokoh, "Recommendation systems: Principles, methods and evaluation," *Egypt. Informatics J.*, vol. 16, no. 3, pp. 261–273, 2015.
[9] K. Miyahara and M. J. Pazzani, "Improvement of Collaborative Filtering with the Simple Bayesian Classifier 1," pp. 1–28, 2002.
[10] M. Hassan and M. Hamada, "A Neural Networks Approach for Improving the Accuracy of Multi-Criteria Recommender Systems," *Appl. Sci.*, vol. 7, no. 9, p. 868, 2017.
[11] R. Yera and L. Mart, "Fuzzy Tools in Recommender Systems : A Survey," vol. 10, pp. 776–803, 2017.
[12] U. Marung, N. Theera-Umpon, and S. Auephanwiriyakul, "Top-N recommender systems using genetic algorithm-based visual-clustering methods," *Symmetry (Basel).*, vol. 8, no. 7, pp. 1–19, 2016.
[13] J. S. Breese, D. Heckerman, and C. Kadie, "Empirical analysis of predictive algorithms for collaborative filtering," *Proc. 14th Annu. Conf. Uncertain. Artif. Intell.*, pp. 43--52, 1998.
[14] O. Alter and G. H. Golub, "Singular value decomposition of genome-scale

mRNA lengths distribution reveals asymmetry in RNA gel electrophoresis band broadening," *Proc. Natl. Acad. Sci.*, vol. 103, no. 32, pp. 11828–11833, 2006.
[15] G. Adomavicius and Y. Kwon, "for Multicriteria."
[16] G. Adomavicius and A. Tuzhilin, "Towards the Next Generation of Recommender Systems : A Survey of the State-of-the-Art and Possible Extensions," pp. 1–43.
[17] R. P. Badoni, D. K. Gupta, and P. Mishra, "A new hybrid algorithm for university course timetabling problem using events based on groupings of students," *Comput. Ind. Eng.*, vol. 78, pp. 12–25, 2014.
[18] "Genetic Algorithms Thanks to : Much of this material is based on :," *Evol. Comput.*, 2009.
[19] L. Budin, M. Golub, and D. Jakobovic, "Parallel Adaptive Genetic Algorithm," pp. 157–163, 1998.
[20] L. Jacobson and B. Kanber, *Genetic Algorithms in Java Basics*. 2015.
[21] D. Warshawsky and D. Mavris, "Choosing aggregation functions for modeling system of systems performance," *Procedia Comput. Sci.*, vol. 16, pp. 236–244, 2013.

ASTES

Advances in Science, Technology and Engineering Systems Journal Vol. 4, No. 4, 458-461 (2019)

www.astesj.com

ASTESJ

ISSN: 2415-6698

Design and Control of Autonomous Surface Vehicle to Support Bathymetry Survey in the Coastal Environment

Ahmad Fauzan Zakki[*,1], Aris Triwiyatno[2], Bandi Sasmito[3], Krismon Budiono[2]

[1]*Naval Architecture Department, Engineering Faculty, Diponegoro University, 50275, Indonesia*

[2]*Electrical Engineering Department, Engineering Faculty, Diponegoro University, 50275, Indonesia*

[3]*Geodetical Engineering Department, Engineering Faculty, Diponegoro University,50275, Indonesia*

ARTICLE INFO

Article history:
Received: 16 July, 2019
Accepted: 16 August, 2019
Online: 21 August, 2019

Keywords:
Small Water-plane Area Twin Hull
Autonomous Surface Vehicle
Bathymetry Survey

ABSTRACT

Traditionally bathymetry survey is generally carried out using boat, research vessel, and small craft which is equipped with the echo sounding instrument and involves many persons as the vessel crew. The survey method demands an additional cost because of the extra man power and an expensive vessel operational cost. An autonomous surface vehicle (ASV) which is equipped with echo sounder was developed by adopting small water-plane area twin hull (SWATH) hull form to support bathymetry survey in the coastal environment. The paper is focused on the design of hull and control system of the SWATH-ASV, electronic device and sensor selection for control of the vehicle. The hull and control system is designed to organize the surface vehicle to perform the defined mission from ground control station. The hull form geometry, hardware and software of the SWATH-ASV and the control system are presented.

1. Introduction

Recently, the development of unmanned surface vehicle (USV) was made as an instrument that replaces the role of direct human involvement. Thus it might be useful to support the research activities such as data collection, survey and measurement in the remote and severe location with the ground control system. Many USV researches were made for oil and gas exploration, pipeline monitoring. The USV application for military operation can be found for surveillance, intelligence, search and rescue (SAR), inspection/exploration and strike missions.

In the scope of this research project, the prototype of autonomous surface vehicle was developed that will enable real time data monitoring to support bathymetry survey, especially in the coastal environment. The intact stability and the sea keeping characteristics of the developed autonomous surface vehicle were investigated in the previous study, [1]. In this paper, the study is focused on the design of the hull, propulsion system and the control system such as electronic device, sensor and data link. The SWATH hull form was selected that was expected to provide low resistance and excellent station keeping performance.

[*]Ahmad Fauzan Zakki, Naval Architecture Department, Diponegoro University, +622476480784, ahmadfauzanzakki@lecturer.undip.ac.id

2. Literature Review

Several articles which are related to the ASV design and control development can be found. An autonomous surface craft called ARTEMIS was designed by a research group in MIT for collecting the bathymetry data, [2]. ARTEMIS have two electric motors and a rudder for the propulsion system. It is equipped automatic heading and navigation control through the defined reference points that was used as the location of measurement point. Subsequently the catamaran was adopted for improving the intact stability and increasing the payload capacity.

In the other research, The DELFIM was developed as an Autonomous Underwater Vehicles (AUV), [3]. The ROAZ and ROAZ II was developed and designed for bathymetry survey, [4]-[5]. Furthermore the development of autonomous marine vehicle was represented by the SWORDFISH, MESSIN and SPRINGER. The SWORDFISH is equipped with the modular sensor for payload and a gateway for data communication from air to underwater environment, [6]-[7]. The catamaran hull form was used by MESSIN for hydrological mapping and oceanographic survey, [8]. The MESSIN able to operate in very shallow water and the autonomous navigation system was able to follow the defined route efficiently. In 2004, the SPRINGER was developed

for hydrographical survey and used as a test-bed for autonomous navigation and sensor system, [9]-[10].

The study of ASV hull form development can be found in some references. In [11], the author studies the modeling of twin hull for the USV known as SESAMO for data collection in the Antarctic region. In [12], the authors develop the catamaran hull form, propulsion and control system for the ASV prototype to survey the coastal region. The integrated system for sampling and monitoring of environmental parameters has been achieved. In [1], the authors investigate the intact stability and sea keeping performance of the SWATH hull form for the ASV development to support bathymetry survey. In [13], the researchers study the performance of SWATH and catamaran hull form using CFD analysis for geological and geophysical survey.

3. Design of ASV Hull and Drag Characteristics

Regarding the research objective is to obtain the ASV design for bathymetry survey, this will lead to the need of a reliable vessel design which would provide a good performance of stability, station keeping and hydrodynamic behavior. According to research on ThyssenKrupp Marine Systems, [14], SWATH technology able to provide the low hydrodynamic drag, high stability and good motion performance, compared with the monohull. Therefore the SWATH hull form is adopted as an appropriate solution to carry the several electronic devices and sensors that would be used for the data scanning and recording during the bathymetry survey.

The principal dimension of the ASV was determined through the design exploration process. The process was made by involving the configuration of design parameters from the modification of the existing parent model. The proposed hull form of the SWATH-ASV which is obtained from the selected principal dimension can be seen in Fig. 1.

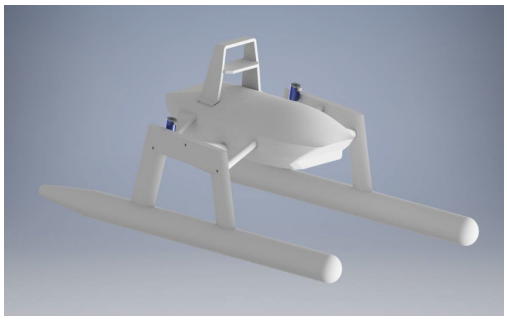

Figure 1: The hull form of the SWATH-ASV

Theoretically, the moving submerged bodies have viscous drag which is resolved into two items that is viscous pressure and frictional resistance. The viscous drag characteristic of ASV depends on the Reynolds number. In the case of surface vehicle, additional wave making resistance is provided, and it is depending on the Froude number.

The estimation of total resistance of the proposed SWATH-ASV was made through the CFD analysis for determining the power of propulsion system, [15]. The service speed, wetted surface area and simulation parameters were provided on the CFD analysis. The result shows that the total resistance force of the ASV is 5.55 N. the drag coefficient is determined using parabolic equation approach, [15], see Fig.2.

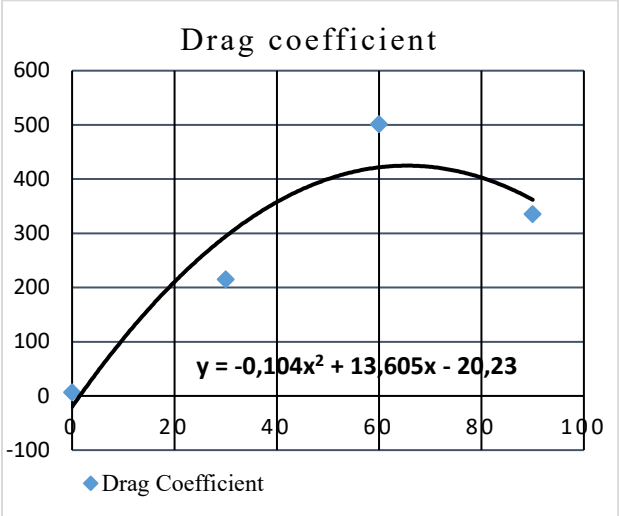

Figure 2: Drag coefficient of the SWATH-ASV, [15]

4. Control System of the SWATH-ASV

4.1. Electrical System of the SWATH-ASV

The principal electrical wiring of the SWATH-ASV is presented in the Fig. 3. Two cells LiPo batteries with an output voltage of 12.4 volts are used as the power source. Each of the batteries have a discharge rate of 30 capacity ratings which supply power for every electronic component on the SWATH-ASV, such as navigation system and data recording system.

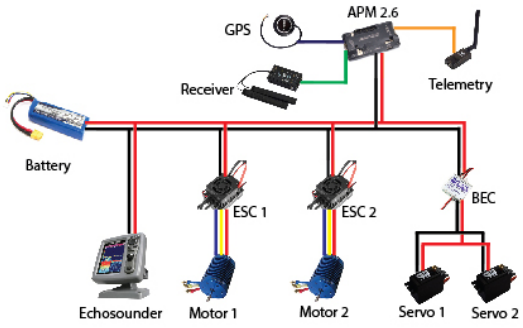

Figure 3: Wiring System

The GPS Ublox M8 is connected to the Ardupilot Mega (APM 2.6). Ardupilot Mega is an autopilot system which used inertial measurement unit (IMU) sensors. APM acts as an electronic speed controller (ESC), servo, GPS control center based on input data from mission planners and receiver. Subsequently, the data is transmitted to the ground station with the transceiver. The transmitted data are recorded using Telemetry Module 433 MHz. The direction control is made by servo motor. Otherwise the DC motor which is controlled by the ESC is adopted to control the speed of the SWATH-ASV.

When the ASV system runs in manual mode, the ship will move according to the instructions of the controller. Data will be sent to the computer in the form of ship motion direction data, GPS data and sensor data contained in the ASV. When the system runs

in automatic mode, the ship will move automatically by using the PID control as a regulator of the ship's automatic motion while monitoring the environment around the ship. The environmental conditions are monitored and measured in the form of data stored on the device, and some of the data is sent directly by telemetry to the ground station (personal computer) in real time.

PID is a controller that functions as a ship controller to be able to move automatically or commonly called autonomous. The main function of the PID control on the Autonomous Surface Vehicle is to set the direction or heading of the ship to fit the destination, see Fig. 4. PID is a combination of several elements, namely P (Proportional), I (Integral), and D (Derivatives). P, I, and D elements can quickly respond to systems to eliminate offsets. Each element has advantages to determine the appropriate value of Kp, Ki, and Kd with the manual tuning method. Kp, Ki, and Kd are proportional gain, integral gain and derivative gain.

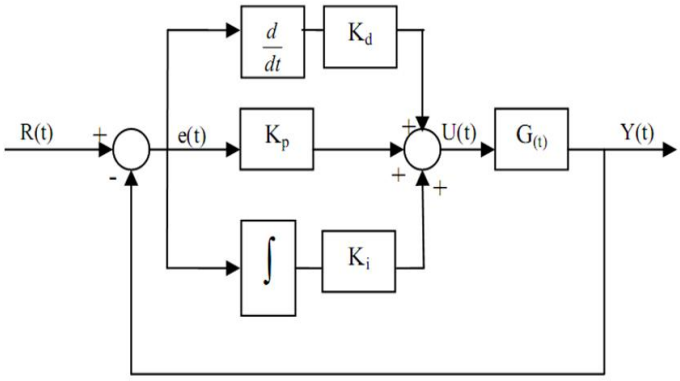

Figure 4: PID Control

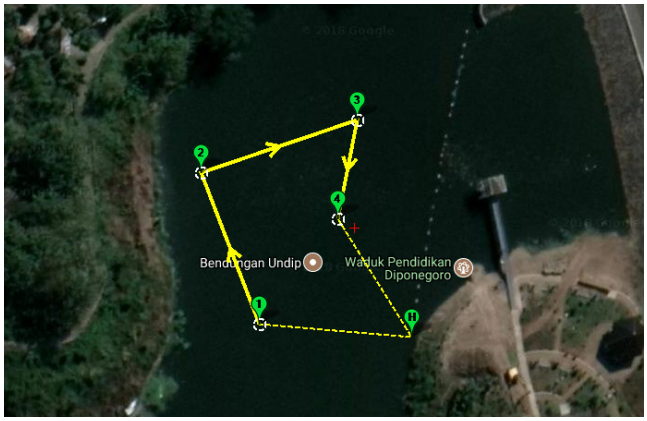

Figure 5: Waypoint Navigation System

4.2. *Navigation System of the ASV*

The Autonomous Surface Vehicle can move automatically using the GPS waypoint navigation system. Furthermore, the waypoint navigation system also able to predetermined the ASV path automatically. By importing map database from Google Map the mission planner software is adopted to define the path of the SWATH-ASV. The illustration of waypoint navigation system on the defined path of the SWATH-ASV can be seen in the Figure 5. The SWATH-ASV will run through the defined path from point to point with no obstacle along the path. Therefore the SWATH-ASV is able to follow the path relatively accurate without any difficulties.

When ASV runs automatically following a waypoint, it can be monitored using a mission planner. Some data on ASV will be sent in real time to the personal computer using the telemetry module 433 MHz. This module can transmit data like the direction of motion, ASV stability, battery capacity, current and GPS. While the echo sounder will always record the condition of the waters around the waypoint until it is finished and returns to home, see Fig. 5.

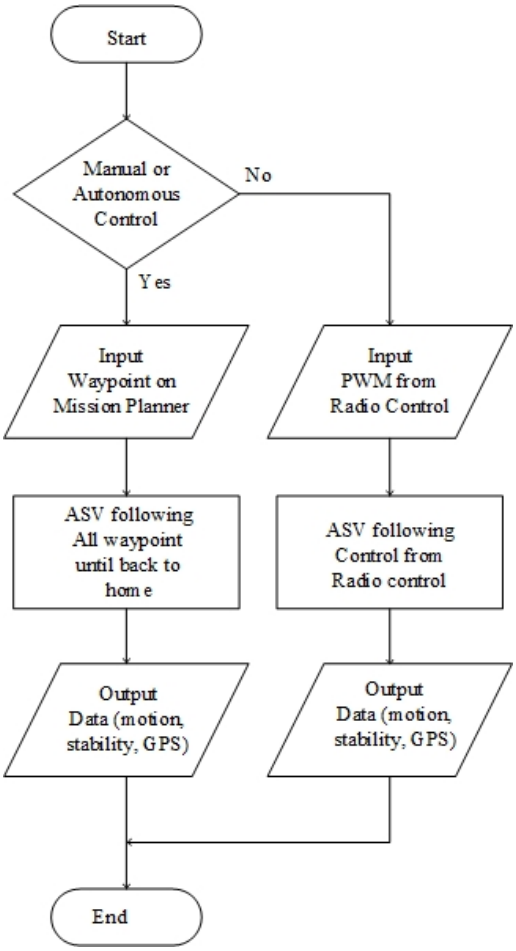

Figure 6: Flowchart System

Fig. 6 shows the flowchart of system control the SWATH-ASV. The RC is used to choose manual control or autonomous control. If an automatic control is chosen, the SWATH-ASV will need waypoint input from the mission planner to move to the specified waypoint, and the SWATH-ASV will automatically follow and send real time data to the personal computer. However, when the manual control is selected, the SWATH-ASV will be controlled by the navigation system, according to signals which is received from the radio/remote control. The autopilot system (Ardupilot) will arrange the motors to navigate the ASV through the defined path. The servo motor is used to control the direction and the DC motor is used to control the speed of the SWATH-ASV. The SWATH-ASV will always follow the received command from radio/remote control and send real time data to the personal computer.

Although the waypoint navigation system has been applied in the SWATH-ASV, however the obstacle-avoidance algorithm still not be included into this automated navigation system. The

SWATH-ASV will travel blindly without any smart system that able to detect its surrounding environment. While the defined path is blocked with an obstacle, an unavoidable collision surely can be occurred. Therefore the manual system using remote control should be used for the application of the SWATH-ASV in the actual situation during bathymetry survey activities.

5. Conclusion

The design and control of small water-plane area twin hull autonomous surface vehicle (SWATH-ASV) was made. The SWATH hull form was adopted and realized as an alternative prototype of autonomous surface vehicle which have innovative features and suitable for supporting the bathymetry survey activities.

All of the SWATH-ASV components were designed and organized in order to be able to perform the innovative bathymetry measurement activities by considering functionality and portability aspects.

The SWATH-ASV has been developed in according to the lifting capacity requirements and to execute the bathymetry measurement mission in the coastal marine regions which have complex area logistically.

Although the autonomous control system have been implemented on the SWATH-ASV, however the remote control system is still to be adopted as a secondary control system, especially when the ASV do not follow the waypoint because of the uncontrollable external disturbance.

6. Acknowledgment

The authors wish to thank the reviewers for their constructive comments and suggestions helped in improving this research paper and Ministry of Research, Technology and Higher Education, Indonesia for providing the funding in carrying out this research in the scheme of PDUPT 2018.

7. References

[1] A. F. Zakki, A. Triwiyatno, B. Sasmito, Intact stability and seakeeping characteristics of autonomous surface vehicle (asv) using swath hullform to support bathymetry survey activities on the coastal area, MATEC Web of Conferences, Vol. 177, pp. 01–06, 2018. https://doi.org/10.1051/matecconf/201817701001

[2] J. E. Manley, Development of the autonomous surface craft ACES, OCEANS '97 MTS/IEEE, Vol. 177, pp. 01–06, 2018. https://doi.org/10.1109/OCEANS.1997.624102

[3] Pascoal A., Oliveira P., Silvestre C., Sebastiao L., Rufino M., Barroso V., Gomes J., Ayela G., Coince P., Cardew M., Ryan A., Braithwaite H., Cardew N., Trepte J., Seube N., Champeau J., Dhaussy P., Sauce V., Moitie R., Santos R., Cardigos F., Brussieux M. and Dando P., Robotic ocean vehicles for marine science applications: the European ASIMOV project, OCEANS 2000 MTS/IEEE, Vol. 1, pp. 409–415, 2000. https://doi.org/10.1109/OCEANS.2000.881293

[4] Ferreira H., Almeida C., Martins A., Dias N., Dias A. and Silva E., Autonomous bathymetry for risk assessment with ROAZ robotic surface vehicle, OCEANS 2009 MTS/IEEE, 2009. https://doi.org/10.1109/OCEANSE.2009.5278235

[5] Ferreira H., Martins A., Dias A. and Almeida C., ROAZ autonomous surface vehicle design and implementation, Robotica, 2006.

[6] Ferreira H., Martins R., Marques E. and Pinto J., Marine Operations with the SWORDFISH Autonomous Surface Vehicle, Robotica, 2006

[7] Ferreira H., Martins R., Marques E., Pinto J., Martins A., Almeida J.M., Sousa J. and Silva E., SWORDFISH: an Autonomous Surface Vehicle for Network Centric Operations, OCEANS 2007 MTS/IEEE, 2007. https://doi.org/10.1109/OCEANSE.2007.4302467

[8] Majohr J. and Buch T., Modelling, simulation and control of an autonomous surface marine vehicle for surveying applications Measuring Dolphin MESSIN, IEE CONTROL ENGINEERING SERIES, 69 (Advanced in Unmanned Marine Vehicles, 2006, pp. 329-351). https://doi.org/10.1049/PBCE069E_ch16

[9] Naeem W., Sutton R. and Chudley J., Modelling and control of an unmanned surface vehicle for environmental monitoring, UKACC International Control Conference, 2006

[10] Naeem W., Xu T., Sutton R. and Tiano A., The design of a navigation, guidance, and control system for an unmanned surface vehicle for environmental monitoring, Proceedings of the Institution of Mechanical Engineers, Part M: Journal of Engineering for the Maritime Environment, Vol. 222(Issue 2): 67-79, 2008. https://doi.org/10.1243/14750902JEME80

[11] Caccia M., Bono R., Bruzzone G., Bruzzone G., Spirandelli E., Veruggio G., Stortini A.M. and Capodaglio G., Sampling Sea Surfaces with SESAMO, Robotics & Automation Magazine, 2005. https://doi.org/10.1109/MRA.2005.1511873

[12] Evangelista L., Giordano L., Di Fiore V., Lengo A., a new prototype of unmanned surface vehicles to survey the coastal marine environment: design, modelling and control, Rapp. Tec. INGV, 374: 1-22, 2017. https://doi.org/10.13140/RG.2.2.19869.82409

[13] Gursel K. T., Taner M., Unsalan D., Neser G., Design of a Marine Autonomous Surface Vehicle for Geological and Geophysical Surveys, Scientific Bulletin of Naval Academy, Vol. 21: 20-36, 2018. https://doi.org/10.21279/1454-864X-18-I1-003

[14] Schellenberger G., SWATH Technology – Advanced SWATH Design Methods, ThyssenKrupp Marine Systems, 2007.

[15] A. F. Zakki, A. Triwiyatno, B. Sasmito, I. A. C. Abar, Study on Hydrodynamics Coefficient of SWATH Autonomous Surface Vehicles (ASV) Hullform for Bathymetry Survey Activities, ARPN Journal of Engineering and Applied Sciences (submitted manuscript – status in review), 2018.

ASTES

Advances in Science, Technology and Engineering Systems Journal Vol. 4, No. 4, 462-467 (2019)

www.astesj.com

Special Issue on Advancement in Engineering and Computer Science

ASTESJ

ISSN: 2415-6698

Marginalizing Last Mile Logistics Cost through 4th Party Milk Run

Robert de Souza[1], Linda William[2,*], Cher Kian Lee[3]

[1]*The Logistics Institute – Asia Pacific, National University of Singapore, 21 Heng Mui Keng Terrace #04-01, Singapore 119613*

[2]*School of Informatics and IT, Temasek Polytechnic, 21 Tampines Ave 1, Singapore 529757*

[3]*Independent Researcher*

ARTICLE INFO

Article history:
Received: 28 May, 2019
Accepted: 28 July, 2019
Online: 21 August, 2019

Keywords:
Last mile logistics
Milk run
Excess capacity
Horizontal collaboration
Marginal cost

ABSTRACT

To reduce its high last mile logistics cost, a company may explore different options such as a horizontal collaboration with another company that has a similar logistics requirement. Traditionally, the collaboration can be conducted through an outsource contract mechanism where the company may need to guarantee a certain number of logistics demands or usage for a fixed period of time. This may incur a fixed transportation and logistics cost for the company. For a company who has more fluctuated logistics demands, it would be difficult to guarantee a certain number of logistics demands or usage for an outsourcing mechanism. The company may end up paying more than it should. Alternatively, the company may want to explore horizontal collaboration with a more flexible contract mechanism such as the "4th party milk run" (4PMR). The 4PMR model leverages on the last mile excess capacity of one company to fulfill the last mile logistics demands for another company based on a pay-per-use arrangement. Using the 4PMR model, the fixed transportation and logistics cost would be translated into a marginal cost. This paper describes the 4PMR model, including the optimization model and its computation experiment on two last mile logistics scenarios. The first scenario is a hypothetical scenario based on our field study in Jakarta, Indonesia with a small number of deliveries, while the second scenario is an actual scenario with a large number of deliveries based on existing routes of a Logistics Service Provider (LSP) in Surabaya, Indonesia. The experiment results show that 4PMR is able to provide a significant reduction in last mile logistics cost. To complement the experiment results, industry perspectives for implementing the 4PMR model is also reviewed.

1. Introduction

This paper is an extension of the work originally presented in the 2017 6th IEEE International Conference on Advanced Logistics and Transport (ICALT) in [1]. Loss of logistics efficiency becomes the highest across the supply chain at the nearest point to the aggregated or single demand point [2, 3]. This last (or sometimes first) mile logistics face significant fulfillment constraints, making it the most expensive part of the overall supply chain. For a company that moves millions of tons of materials every year, reducing the last mile logistics cost by a few cents can save tremendous amounts of money. As such, the company looks for new strategies to reduce the last mile logistics cost. Several strategies such as a horizontal collaboration with other similar companies or partners in the same level of the supply chain are now attracting the interest of those companies [4, 5, 6].

In supply chain, collaborations between companies can be grouped into two, namely: vertical and horizontal collaboration [7]. The vertical collaboration includes collaboration between companies in different level of supply chain [7], such as Vendor Managed Consignment Inventory (VMCI) model [8] and Collaborative, Planning, Forecasting and Replenishment (CPFR) model [9]. While the horizontal collaboration includes two or more

* Corresponding author: Linda William, School of Informatics and IT, Temasek Polytechnic, 21 Tampines Ave 1, Singapore 529757, Telp: +65-6780-5274, email: lwilliam@tp.edu.sg

unrelated or competing companies at the same level of the supply chain [7]. In horizontal collaboration, a company can work closely with another company that has similar logistic requirements by sharing resources and taking advantage of potential distribution synergies [10]. The benefits of horizontal collaboration are increasing vehicle utilization on the main tracking routes and vehicle efficiency as well as better improving resource management and delivery service level to the customers. Although vertical collaboration has been deeply studied and implemented [11], horizontal collaboration is still in its infancy [12, 13].

As illustrated in Figure 1, horizontal collaboration can be done in several forms. A company may explore the option of engaging one or more companies (e.g. Logistics Service Provider (LSP)) in a form of fixed outsourcing contracts to fulfill its last mile logistics demands. The company may need to guarantee a certain number of logistics demands or usage for a fixed period of time (e.g. monthly, quarterly or yearly) to the outsourcing companies. Using outsourcing, the company is able to save a substantial amount of money because the company does not need to invest in costly logistics-related assets such as transportation vehicles. Generally, this kind of outsourcing would incur a certain amount of fixed transportation and logistics costs.

For a company who has more fluctuated logistics demands, it would be difficult to guarantee a certain number of logistics demands or usage for outsourcing mechanism. The company may need to pay the fixed cost even though it has minimum logistics demands. For this kind of company, a model with a flexible (and often less binding) agreement, such as "uberization" and "4th party milk run" (4PMR) would be beneficial. These models use the pay-per-use mechanism that allows the company to pay only based on its logistics demands. It would reduce the logistics cost by translating the fixed costs to marginal costs. For example, the company does not need to pay fixed cost of 90,000/month for having only 50 last mile logistics demands.

These models use sharing economy concept to reduce the transportation costs. Uberization mainly focuses on conducting the deliveries using crowdsourcing, while the 4PMR model focuses on collaborating with one company (B2B) that has existing delivery routes/networks along the last mile delivery locations.

This paper focuses on analyzing the 4PMR model for reducing last mile logistics cost. It extends the model in [1, 14]. The 4PMR model is developed as an optimization model and solved using two metaheuristics solvers/algorithms. To investigate the cost reduction, we test the model on two scenarios. The first scenario is a hypothetical scenario based on our field study in Jakarta, Indonesia. It consists of 40 random logistics demand samples. While the second scenario is an actual scenario based on 9,622 logistics demands from an LSP in Surabaya, Indonesia. Our experiment results show that the 4PMR model is able to reduce 4.16% and 24.84% of the logistics cost in the first and the second scenario respectively. This provides a promising indication that the 4PMR model would be able to reduce the last mile logistics cost. To complement the experiment results, we also gather industry perspectives for implementing the 4PMR model in its day-to-day logistics operations.

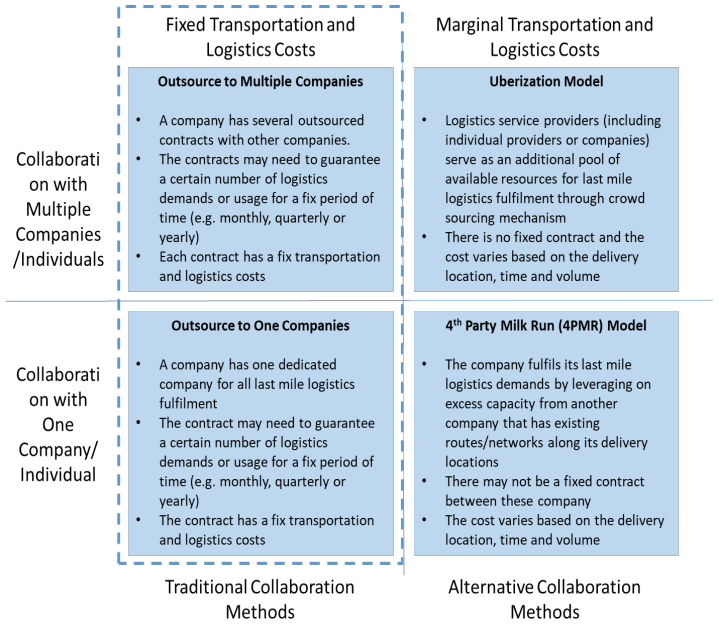

Figure 1. Horizontal Collaboration Strategies

The remainder of the paper is organized as follows. Section 2 presents the overview of 4PMR and its related works. Section 3 reviews the 4PMR optimization model. Section 4 describes the solvers/algorithms to solve the 4PMR and section 5 describes the computational experiments, including the scenarios and experiment results. Section 6 reviews the industry perspective on implementing 4PMR model. Lastly, section 7 presents the conclusions.

2. 4th Party Milk Run (4PMR) Model

2.1. Overview

The 4PMR model leverages on the excess capacities from one company that has existing designated routes along the last mile logistics demand locations of another company. The company with existing designated routes (henceforth as providing company) needs to serve those routes periodically regardless of the delivery volume. These routes may not be fully utilized and may have significant excess capacities. These unused capacities can be tapped and used by another company (henceforth as receiving company) to fulfill its last mile logistics demands.

In 4PMR model, the routing is based on the existing routes or networks from the providing company. It would stop at several locations to fulfill logistics demands from the receiving company.

2.2. Benefits of 4PMR model

The 4PMR model would bring benefits to the collaborating companies. These benefits can be categorized into three groups: costs and productivity, service and market position.

1. Cost and productivity benefits

One potential benefit of using the 4PMR model is to reduce logistics costs [15, 16]. Both collaborating companies, providing and receiving companies, would be able to achieve logistics cost reduction. By joining their delivery requirements, these companies can utilize and optimize their logistics-related assets. This can be

translated into a lower logistics cost and lower capital investment for logistics-related assets as it would need a lesser number of logistics-related assets.

One example of this cost reduction is on empty backhaul utilization. The providing company may have existing routes from area A to area B. If there is an imbalance of deliveries where all the loads come from area A to area B with no loads from area B to area A, the providing company must absorb the cost of the empty vehicle return (empty backhauls). However, if another company has last mile logistics demands in the opposite direction (from area B to area A), the company can make use of the empty backhauls. The providing company would be able to reduce its costs of absorbing empty backhaul while the receiving company would be able to negotiate a lower transportation cost.

2. Service benefits

For the receiving company, the 4PMR model would add the company capabilities to serve low demand areas. It allows the company to facilitate more frequent deliveries for wider geographic areas. The receiving company would be able to expand its area coverage by collaborating with the providing company that operates in different areas with minimum additional setup cost. It provides flexibility in providing more service and reaching more potential customers.

3. Market Position

For the providing company, the 4PMR model would enable the company to have "insinking" opportunities where the company would be able to replicate its 4PMR model to provide services to different companies and proactively select a group of companies with a strong synergy potential [10, 17]. It would create another business opportunity for the providing company. It would further increase vehicle utilization and reduce the last mile logistics cost.

2.3. Related Works

Two areas of works that is closely related to ours are the Vehicle Routing Problem (VRP) [18, 19] and Milk Run Logistics [20, 21]. VRP aims to provide optimal set of routes for a fleet of vehicles to fulfil logistics demands. It has many variants, including VRP with Time Windows [22, 23], Capacitated VRP [24, 25], green VRP [26, 27] and ride-sharing VRP [28, 29]. While Milk Run Logistics is essentially a logistics method that uses routing to consolidate the transportation of goods that has the following characteristics: small lot of transport, less than truckload, geographically sparse demands [20], as illustrated in Figure 2. As shown in Figure 2, milk run model reduces the excess capacity by consolidating the deliveries from different companies (i.e. Company X and Company Y).

3. Optimization Model

One potential concern with the 4PMR model is that the providing company may not have a direct route to fulfill the receiving company' logistics demands (direct from an origin location to a final destination location). It may need to go through several stops/hops/transit locations before it can finally deliver to the final delivery destination. There is a need to match the providing company existing routes with the receiving company logistics demand locations.

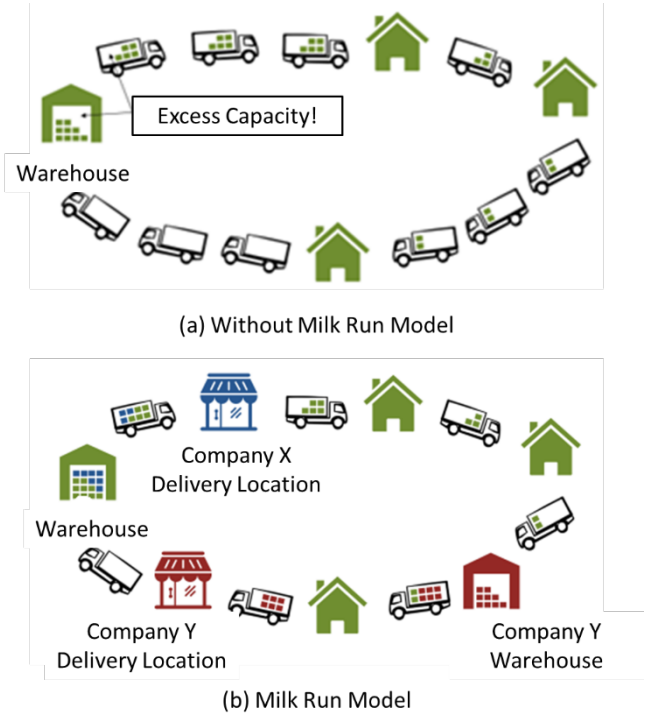

Figure 2. Milk Run Model Illustration

To match the logistics demands with the existing routes, an optimization model for the 4PMR is developed. The 4PMR model is defined as follows. Let $G = (v, e)$ be a directed graph representing the providing company existing routes. It consists of a set of locations, as vertexes or nodes (the term vertex and node are used synonymously throughout the paper), denoted by $V = \{v_1, v_2, \dots, v_n\}$, and a set of routes, as arcs E $\subseteq$ V x V, denoted by an ordered pair of nodes (u, v), where $u \in V$ and $v \in V$. e_{uv} represents a directed route from node u to node v. Each arc e_{uv} has an excess capacity Q_{uv} and time capacity T_{uv}. To simplify the problem, we consider each arc to have a fixed excess capacity Q_{uv}. For each arc e_{uv}, d_{uv}, t_{uv} and c_{uv} represent a non-negative travel distance, a non-negative travel time and a non-negative transportation cost for arc e_{uv}, respectively. A path is defined as a sequence of arc $p_{uv} = \{u = u_1, (u_1, u_2), (u_2, u_3), \dots, (u_{l-1}, u_l), u_l = v\}$.

Let $L = \{1, \dots, n\}$ be a set of logistics demands of the receiving company. Each delivery $l \in L$ has delivery load size q_l, origin node u and destination node v. $[w_u, z_u]$ denotes the time window in origin node u. While $[w_v, z_v]$ denotes the time window in destination node v. Each delivery service at origin node u and destination node v must take place between the time windows. For each logistics demand $l \in L$ from origin node u to destination node v fulfilled by 4PMR model, the delivery cost is defined as $c^l(p)$, where $c^l(p) = \sum_{(u,v)\in p} c^l_{uv}$. If the delivery fulfillment cannot be done using the 4PMR model (due to capacity or time constraints), it will use a direct delivery. The delivery cost for the direct delivery denotes as c^l_d, where in general $c^l(p) \ll c^l_d$.

There are a lot of constraints that can be included in the 4PMR model, such as capacity, transportation cost, overall cost, transportation distance, and time windows. These constraints depend on the nature of the collaboration between providing and

receiving companies and the nature of the products being delivered. In this paper, we only use one constraint, capacity. The capacity for logistics demands fulfilled by the 4PMR should not exceed the fixed weight capacity Q_{uv} for each arc. The model can be expended to include more constraints.

Using these notations, we define the 4PMR problem as:

$$Min\ Z = \sum_{l \epsilon L} \left(\min \left(\min \left(\sum_{(u,v) \epsilon E} c_{uv}^{l} \times x_{uv}^{l} \right), c_{d}^{l} \right) \right) \quad (1)$$

Subject to:

$$x_{uv}^{l} = \begin{cases} 1, if\ delivery\ request\ l\ can\ use\ arc\ (u,v) \\ 0, otherwise \end{cases} \quad (2)$$

$$\sum_{l \epsilon L} q_{l} \times x_{uv}^{l} \leq Q_{uv} \qquad \text{for every } (u,v) \in E \quad (3)$$

Constraint (2) and (3) ensures that the capacity for logistics demands fulfilled by the 4PMR model goes through a certain arc should not exceed the fixed weight capacity for that arc.

4. Solvers and Algorithms

The 4PMR optimization model is implemented in two solvers/algorithms. The first solver is designed for a small dataset with less than 50 logistics demands. It uses an evolutionary function in Microsoft Excel [30]. The function is based on genetic and evolutionary algorithm to seek "good" solutions for a limited dataset. This solver fits the purpose to provide a preliminary result for further study and exploration.

The second solver is used for large problem sizes. It is developed using a meta-heuristic algorithm that combines the Dijkstra algorithm with the Greedy algorithm [31]. The algorithm has two parts as illustrated in Figure 3. First, it uses the Dijkstra algorithm to produce all the shortest paths for each pair of delivery locations in the existing routes. It also calculates the logistics cost for each of the shortest path. Second, it runs the greedy algorithm to assign the logistics demands to the path with minimum cost. It will also re-configure the shortest paths and re-calculate the logistics cost, if necessary.

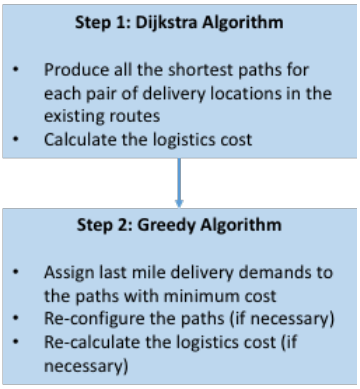

Figure 3. Meta-Heuristics Algorithm for Solving 4PMR

5. Computational Experiments

5.1. Small Problem Size

The 4PMR model was tested on a hypothetical scenario based on our field study in Jakarta, Indonesia in December 2016. The scenario comprises of a providing company with 5 existing routes. The routes connect 12 nodes. In each route, the delivery starts from and returns to the providing company' warehouse. The logistics demands are derived from a receiving company with 40 logistics demands in several locations along the providing company's routes. The receiving company produces goods and uses a hub-and-spoke model to deliver goods to all its customers within the same distribution network. The receiving company has a headquarter/main warehouse for its hub-and-spoke model. The providing company's warehouse and the receiving company's headquarter are located in different locations (represented by different nodes).

Given that the logistics demands originating from the receiving company, all the logistics demands share the same origin point – the receiving company's headquarter. For the hub and spoke distribution network, the utilization of the vehicles is 80% and that they return back to headquarter empty.

We run the first solver for this scenario. The experiment results are shown in Table 1. The results show that the 4PMR model is able to get a 4.16% reduction for the receiving company. For the no collaboration (own vehicle) model, the company will have additional costs to purchase the vehicles also (which is not included in the comparison). The detailed results for this experiment can be found in [1].

Table 1. Experiment Result of the 4PMR Model in Small Problem Size

Solution	Parameters		
	Total number of logistics demands	Number of logistics demands using 4PMR model	Logistics Cost
No collaboration (own vehicle)*	40	0	56.737
The 4PMR model	40	11	54.377

*: only logistics cost, without capital cost to purchase the vehicles

5.2. Experiment Result in Large Problem Size

To evaluate the performance of the 4PMR model in large problem size, we tested the model on scenario based on actual delivery routes from one Logistics Service Provider (LSP) in Surabaya, Indonesia. The LSP has an existing network comprising 27 nodes/locations with existing routes in Greater Surabaya, Indonesia. Each route has a certain excess capacity (around 20% of the overall capacity). The logistics demands were derived from real logistics demands from one FMCG company operated in Surabaya, Indonesia. We used 10 days of logistics demands in July

2015. It comprises of 9,622 logistics demands for different locations in Greater Surabaya.

Using the second solver, we run the 4PMR model for this scenario. In our experiment, we set the processing (i.e. execution) time to 10 second. To compare the 4PMR model with another horizontal collaboration, we also calculated the transportation cost for outsource mechanism. We assumed that the company needs to pay for 1 dollar for each delivery with minimum delivery of 1,000 deliveries/day.

The experiment results are shown in Table 2. The results show that the 4PMR model is able to get a 24.84% reduction from the no collaboration model and 29.54% reduction from the outsource model. For the no collaboration (own vehicle) model, the company will have additional costs to purchase the vehicles also (which is not included in the comparison).

6. Industry Perspective in Implementing 4PMR

While the benefits of the 4PMR model are clear, implementing it can be challenging. The challenges are varied depending on the company and also the industry. Based on our observation and close interaction with one e-commerce company in Singapore, we observe these two main challenges.

Table 2. Experiment Result of the 4PMR Model in Large Problem Size

Solution	Parameters		
	Total number of logistics demands	Number of logistics demands using 4PMR model	Logistics Cost
No collaboration (own vehicle)*	9,622	0	9,622.0
Horizontal collaboration with outsource	9,622	0	10,264
With 4PMR	9,622	2,656	7,231.6

*: only logistics cost, without capital cost to purchase the vehicles

Firstly, stakeholders of the 4PMR model (i.e. providing and receiving company) will require access to as much real-time data as possible. The providing company needs to provide information about its routes and excess capacities so that the receiving company can decide on whether to utilize those excess capacities or not. When excess capacities are eventually bought up, the providing company then has to update its information again to show the latest excess capacities and the routes to fulfill the receiving company's last mile logistics demands. Hence, software that leverages on secure and real-time data is needed. The Internet and the Internet of Things (IoT) can be used to facilitate information sharing (e.g. mobile applications to link providing and receiving companies).

For the providing company with existing the Transportation Management Software (TMS), another challenge will be to integrate the 4PMR solver/algorithm with its TMS. As TMS typically captures information about the vehicle, the cargo, the route and schedule, the logistics demands using the 4PMR model should be updated to the company's TMS.

Secondly, potential stakeholders of the 4PMR model (i.e. potential providing and receiving company) need to be convinced about the benefits of the 4PMR model. The potential providing company needs to evaluate whether the effort both in terms of IT infrastructure changes and manpower training to improve excess capacities worthwhile and whether there is an obvious return on investment. The potential receiving company needs to analyze its last mile logistics requirements and decides if the 4PMR model would be able to fulfill its business needs. For example, if a company requires trucking of large volumes (typically half to full truckload), it needs to understand that it risks its deliveries for not being fulfilled by the providing company because there are simply not enough excess capacities. Alternatively, if a company requires frequent trucking of easily forecasted volumes, it may need to evaluate the 4PMR model cost versus the traditional outsource model.

7. Summary and Key Take Away

This paper introduces the 4th Party Milk Run (4PMR) model for collaboration between similar companies in the same level of the supply chain. The 4PMR model leverages the excess capacities from one company (i.e. providing company) that has existing designated routes along the pick-up and delivery locations of another company (i.e. receiving company). The providing company needs to serve those routes periodically regardless of the delivery volume, and often these deliveries are not at full capacity. These unused capacities can be tapped and used by the receiving company to fulfill its last mile logistics needs. It would potentially bring benefits to the companies involved in terms of costs and productivity, service and market position.

Two solvers are designed to implement the 4PMR model. The solvers aim to match the providing company's existing routes with the receiving company's logistics demands. The first solver is used for small problem size scenario, while the second solver is used for large problem size scenario. We run these solvers for two scenarios – a small problem size scenario and a large problem size scenario. From the experimental result, it is also revealed that 4PMR is able to reduce logistics cost for up to 4.16% (in the small problem size scenario) and 24.84% (in the large problem size scenario).

Conflict of Interest

The authors declare no conflict of interest related to this paper.

References

[1] C. Lee, Lindawati and R. de Souza, "Utilizing Excess Capacity in Last Mile Using 4th Party Milk Run," in *6th IEEE International Conference on Advanced Logistics and Transport*, Bali, Indonesia, 2017.

[2] R. de Souza, M. Goh, H. Lau, W. Ng and P. Tan, "Collaborative urban logistics–synchronizing the last mile a Singapore research perspective," *Procedia-Social and Behavioral Sciences,* vol. 125, pp. 422-431, 2014.

[3] J. Lin, Q. Chen and K. Kawamura, "Sustainability SI: logistics cost and environmental impact analyses of urban delivery consolidation strategies," *Networks and Spatial Economics,* vol. 16, no. 1, pp. 227-253, 2016.

[4] I. Badraoui, J. G. Van der Vorst and Y. Boulaksil, "Horizontal logistics collaboration: an exploratory study in Morocco's agri-food supply chains," *International Journal of Logistics research and applications,* pp. 1-18, 2019.

[5] Y. Sheffi, M. J. Saenz, L. Rivera and D. Gligor, "ew forms of partnership: the role of logistics clusters in facilitating horizontal collaboration mechanisms," *European Planning Studies,* pp. 1-26, 2019.

[6] N. Martin, L. Verdonck, A. Caris and B. Depaire, "Horizontal collaboration in logistics: decision framework and typology," *Operations Management Research,* vol. 11, no. 1-2, pp. 1-19, 2018.

[7] L. Chen, X. Zhao, O. Tang, L. Price, S. Zhang and W. Zhu, "Supply chain collaboration for sustainability: A literature review and future research agenda," *nternational Journal of Production Economics,* vol. 194, pp. 73-87, 2017.

[8] M. Hariga, S. Babekian and Z. Bahroun, "Operational and environmental decisions for a two-stage supply chain under vendor managed consignment inventory partnership," *International Journal of Production Research,* vol. 57, no. 11, pp. 3642-3662, 2019.

[9] C. A. Hill, G. P. Zhang and K. E. Miller, "Collaborative planning, forecasting, and replenishment & firm performance: An empirical evaluation," *International journal of production economics,* vol. 196, pp. 12-23, 2018.

[10] F. Cruijssen, P. Borm, H. Fleuren and H. Hamers, "Supplier-initiated outsourcing: A methodology to exploit synergy in transportation," *European Journal of Operational Research,* vol. 207, no. 2, pp. 763-774, 2010.

[11] S.-L. D., P. Kaminsky and E. Simchi-Levi, Designing and Managing the Supply Chain: Concepts. Strategies, and Cases, McGraw-Hill, 2000.

[12] F. Cruijssen, W. Dullaert and H. Fleuren, "Horizontal cooperation in transport and logistics: a literature review," *Transportation journal,* pp. 22-39, 2007.

[13] R. Leitner, F. Meizer, M. Prochazka and W. Sihn, "Structural concepts for horizontal cooperation to increase efficiency in logistics," *CIRP Journal of Manufacturing Science and Technology,* vol. 4, no. 3, pp. 332-337, 2011.

[14] The Logistics Institute - Asia Pacific, "E-Commerce Trends and Challenges: A Logistics and Supply Chain Perspective," The Logistics Institute - Asia Pacific White Papers Series, Singapore, 2016.

[15] L. Wang, F. Kong, J. Cao and Y. Wang, "Research on the application and optimization countermeasures of auto parts milk-run logistics mode," in *IEEE 18th International Conference on Industrial Engineering and Engineering Management*, 2011.

[16] M. Jafari-Eskandari, S. Sadjadi, M. Jabalameli and A. Bozorgi-Amiri, "A robust optimization approach for the milk run problem (An auto industry Supply Chain Case Study)," in *IEEE International Conference on Computers & Industrial Engineering*, 2009.

[17] F. Cruijssen, B. Peter, H. Fleuren and H. Hamers, "Insinking: A Methodology to Exploit Synergy in Transportation," CentER Discussion Paper, 2005. [Online]. Available: https://ssrn.com/abstract=870403. [Accessed 26 03 2018].

[18] P. Toth and D. Vigo, The vehicle routing problem, Philadelphia: Society for Industrial and Applied Mathematics, 2002.

[19] B. L. Golden, S. Raghavan and E. A. Wasil, he vehicle routing problem: latest advances and new challenges, New York: Springer Science & Business Media, 2008.

[20] G. Brar and G. Saini, "Milk run logistics: literature review and directions," *Proceedings of the world congress on engineering,* vol. 1, pp. 6-8, 2011.

[21] G. S. Brar and G. Saini, "Milk run logistics: literature review and directions," in *In Proceedings of the world congress on engineering*, 2011.

[22] F. Errico, G. Desaulniers, M. Gendreau, W. Rei and L. M. Rousseau, "The vehicle routing problem with hard time windows and stochastic service times," *EURO Journal on Transportation and Logistics,* vol. 7, no. 3, pp. 223-251, 2018.

[23] Y. Niu, Z. Yang, P. Chen and J. Xiao, "Optimizing the green open vehicle routing problem with time windows by minimizing comprehensive routing cost," *Journal of cleaner production,* vol. 171, pp. 962-971, 2018.

[24] L. Wei, Z. Zhang, D. Zhang and S. C. Leung, "A simulated annealing algorithm for the capacitated vehicle routing problem with two-dimensional loading constraints," *European Journal of Operational Research,* vol. 265, no. 3, pp. 843-859, 2018.

[25] A. N. Letchford and J. J. Salazar-González, "The capacitated vehicle routing problem: stronger bounds in pseudo-polynomial time," *European Journal of Operational Research,* vol. 272, no. 1, pp. 24-31, 2019.

[26] G. Poonthalir and R. Nadarajan, "A fuel efficient green vehicle routing problem with varying speed constraint (F-GVRP)," *Expert Systems with Applications,* vol. 100, pp. 131-144, 2018.

[27] A. Shuib and N. Muhamad, "Mixed Integer Multi-Objective Goal Programming Model For Green Capacitated Vehicle Routing Problem," *Advances in Transportation and Logistics Research,* vol. 1, no. 1, pp. 356-368, 2018.

[28] L. Agussurja, S. F. Cheng and H. C. Lau, "A State Aggregation Approach for Stochastic Multiperiod Last-Mile Ride-Sharing Problems," *Transportation Science,* vol. 53, no. 1, pp. 148-166, 2019.

[29] V. F. Yu, S. S. Purwanti, A. P. Redi, C. C. Lu, S. Suprayogi and P. Jewpanya, "Simulated annealing heuristic for the general share-a-ride problem," *Engineering Optimization,* vol. 50, no. 7, pp. 1178-1197, 2018.

[30] FrontlineSolvers, "Excel Solver – Non-smooth Optimization," [Online]. Available: http://www.solver.com/excel-solver-non-smooth-optimization. [Accessed 01 05 2017].

[31] A. Benoit, R. Yves and F. Vivien, A guide to algorithm design: paradigms, methods, and complexity analysis, Boca Raton: CRC Press, 2013.

ASTES

Advances in Science, Technology and Engineering Systems Journal Vol. 4, No. 4, 468-477 (2019)

www.astesj.com

Special Issue on Advancement in Engineering and Computer Science

ASTESJ

ISSN: 2415-6698

Estimation of Target Maneuvers from Tracked Behavior Using Fuzzy Evidence Accrual

Stephen Craig Stubberud[1], Kathleen Ann Kramer[2,*], Allen Roger Stubberud[3]

[1]*Advanced Programs, Oakridge Technology, San Diego, 92121, USA*

[2]*Department of Electrical Engineering, University of San Diego, San Diego, 92110, USA*

[3]*Department of Electrical and Computer Engineering, University of California, Irvine, 92697, USA*

ARTICLEINFO

Article history:
Received: 31 May, 2019
Accepted: 06 August, 2019
Online: 21 August, 2019

Keywords:
Evidence accrual
Fuzzy logic
Kalman gain monitoring
Maneuver detection
Pattern detection

ABSTRACT

While the Kalman filter, including its many variants, has been the staple of the tracking community, it also has been shown to have drawbacks, particularly when tracking through a maneuver. The most common issue is a lag in the position of the target track compared to the true target position as the target performs its maneuver. Another more problematic issue can occur where the filter covariance collapses, requiring the filter to be reinitialized. Techniques exist to compensate for maneuvers, but generating their response relies on detection of error between the estimated trajectory and the measured target position. In this effort, a maneuver detection routine is developed that can be used in conjunction with more standard maneuver compensation approaches. This routine is able to validate the existence of a maneuver more quickly than use of the inherent detection relied upon in the other methods. Maneuver detection is performed by an evidence accrual system that uses a fuzzy Kalman filter to incorporate new information and provide a level of evidence that maneuver is occurring. The input data uses behavior characteristics of the Kalman gain vector from the tracking algorithm.

1. Introduction

Feature objection extraction [1, 2] is an evidence accrual technique that can be applied to classification problems. An undirected tree [3] with various levels of information is used to connect evidence nodes. Each node has a level of evidence and an associated level of uncertainty similar to a state in a Kalman filter. Within the tree, nodes represent levels of evidence of what might be elementary information or a complex combination of information. This paper extends work originally presented in the 2018 Conference on Innovations in Intelligent Systems and Applications [1]. In theory, every node can be measured directly or indirectly. Unlike typical evidence accrual methods [4-6], the states are not probabilistic. When evidence points to more than one solution, multiple competing solutions can each have levels of evidence. Evidence can affect nodes at the same level, with the same evidence potentially increasing one or more than one node in levels of evidence, while others may have their levels decreased, and still other nodes at the same level may not be affected at all.

Feature objection extraction (FOX) propagates information within the tree using a variety of function or function-approximation relationships. The measured information is injected using a fuzzy Kalman filter [1, 7]. As will be described in detail, the FOX evidence accrual system decomposes high-level concepts into simpler concepts until it reaches root nodes which are comprised elementary information. Figure 1 describes a basic FOX tree with different connections and a variety of level of elementary information.

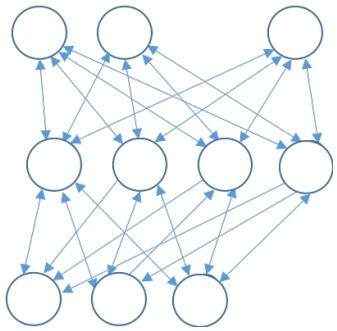

Figure 1: Feature-object extraction structure with various interconnections in a multi-level tree

* Kathleen Ann Kramer, Email: kramer@sandiego.edu

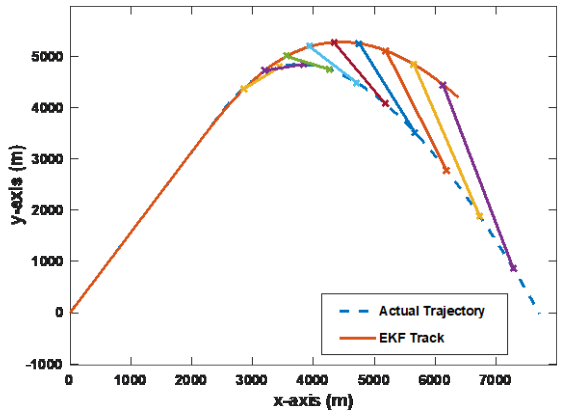

Figure 2: Ballistic target and standard tracker result in lagging of track through maneuver

FOX is incorporated into a tracking system to detect a target's maneuver and can use the computed values of the track to produce a measure of evidence that maneuver is occurring. Maneuver detection is important because, if the target dynamics are not modeled correctly for a maneuver, the tracking system can have an offset or a time-lag in its estimation of the target position and velocity. In Figure 2, an example of a maneuvering target trajectory is shown, alongside the target track from a Kalman-filter based tracking system, a more typical approach. The figure shows a track lagging the true target trajectory as the target proceeds through the maneuver. This comparative result illustrates the deleterious effects that can result when a maneuver occurs. Tracking problems also become more prevalent when the measurement lies in the unobservable space of the track kinematics, as seen in [8]. For example, if an angle-only tracker is used, the filter can become numerically unsound and require a reinitialization. In the tracking problem, losing a target or creating large target kinematic-errors can be life-or-death issue. If a maneuver can be detected, the tracking algorithm can be modified to improve performance and avoid catastrophic failures.

The Kalman filter, and its numerous variants, such as the extended Kalman filter (EKF) [9] and the unscented Kalman filter [10], have long provided the predominant core approaches for kinematic target-tracking systems [11]. To reduce the deleterious effects that maneuvers have on a tracking system, compensation approaches have been developed. The most widely used technique is the interacting multiple model (IMM) and its variants [12]. The IMM incorporates various maneuver models. The IMM system creates weighted combinations of models by comparing the residuals of each measurement to each model's prediction. The residual scores are used to interpolate between the models and create a weight for the state of each motion model to create a more accurate state estimate of the target position and velocity. Other techniques include adaptive Kalman filters such as a neural extended Kalman Filter (NEKF) [13] that also employ the Kalman filter residuals to adapt their maneuver parameters to more closely model that of the actual target dynamics.

All of these approaches rely on the residual measures to detect and make the adjustments. While the residual is an effective measure, variations in uncertainty can mask the maneuver until the residual value becomes significantly large. Fortunately, there exist other metrics as part of the Kalman filter that can detect a maneuver. Besides the residual, the behaviors of the Kalman gain can also indicate that the target is in a maneuver.

FOX can be employed to combine the disparate information and the associated uncertainty, providing for an effort at detection based upon more than one type of measure. In the problem demonstrated in this work, there is an injection of Kalman gain data provided by the aforementioned fuzzy Kalman filter, augmenting the residual measures, and the evidence is propagated using fuzzy, linear, and nonlinear relationships.

Four further sections provide an overview of the development of this approach and analyze its capability. Section 2 overviews the EKF, the most prominent variant of the Kalman filter used in tracking that provides the Kalman gains. Section 3 describes the Kalman gain behaviors that can provide information measures to indicate a target maneuver. Section 4 describes the FOX evidence accrual maneuver detection technique. In Section 5, examples of maneuvering targets are described and are used to exemplify the capabilities of FOX as a maneuver detection technique.

2. Target Tracking with the Extended Kalman Filter

For kinematic target tracking, the discrete-time dynamics of the are defined in (1).

$$\boldsymbol{x}_{k+1} = \boldsymbol{F}\boldsymbol{x}_k \tag{1}$$

The subscript k indicates discrete time, and $\mathbf{x}$ is the standard state-vector representation of the target behavior represents position and velocity. In (2), the state vector represents three dimensions

$$\boldsymbol{x}^T = [\boldsymbol{x} \quad \dot{\boldsymbol{x}} \quad \boldsymbol{y} \quad \dot{\boldsymbol{y}} \quad \boldsymbol{z} \quad \dot{\boldsymbol{z}}]. \tag{2}$$

The target dynamics $\mathbf{F}$ are often described with the straight-line motion model

$$\mathbf{F} = \begin{bmatrix} \boldsymbol{F}_{2x2} & \mathbf{0}_{2x2} & \mathbf{0}_{2x2} \\ \mathbf{0}_{2x2} & \boldsymbol{F}_{2x2} & \mathbf{0}_{2x2} \\ \mathbf{0}_{2x2} & \mathbf{0}_{2x2} & \boldsymbol{F}_{2x2} \end{bmatrix}, \tag{3a}$$

where

$$\mathbf{F}_{2x2} = \begin{bmatrix} \mathbf{1} & \boldsymbol{dt} \\ \mathbf{0} & \mathbf{1} \end{bmatrix}. \tag{3b}$$

The term dt is the time difference between the last sensor report on the target and the latest sensor report.

While the dynamics are linear, the measurements provided by sensors are often nonlinear. Using active sensors, such as radar, a complete measurement space for the three-dimensional target-track would be a report ***h(x)*** of range, bearing, and elevation, shown in (4)

$$\mathbf{h}(\mathbf{x}) = \begin{bmatrix} range \\ bearing \\ elevation \end{bmatrix} = \begin{bmatrix} \rho \\ \beta \\ \varepsilon \end{bmatrix}, \tag{4}$$

where

$$\rho = \sqrt{\left(x_{tgt} - x_{plt}\right)^2 + \left(y_{tgt} - y_{plt}\right)^2 + \left(z_{tgt} - z_{plt}\right)^2}$$

$$\beta = \arctan\left(\frac{x_{tgt} - x_{plt}}{y_{tgt} - y_{plt}}\right)$$

$$\varepsilon = \arctan\left(\frac{z_{tgt}-z_{plt}}{\sqrt{(x_{tgt}-x_{plt})^2+(y_{tgt}-y_{plt})^2}}\right),$$

and the subscript *tgt* denotes target component and the subscript *plt* denotes the platform.

Since these measurements are generated relative to the sensor platform, when they are reported to the tracking algorithm, they may be transformed to a universal coordinate system, such as earth-centered-earth-fixed (ECEF), be relative to the tracking system, or be relative to a localized flat earth [14]. To maintain the accuracy of the measurement, though, it is kept in a nonlinear-coordinate frame rather than being mapped into the track-coordinate frame which would linearize the tracking system. This is one reason the extended Kalman filter (EKF) is the most prevalent tracking algorithm [11].

These measurements are the driving inputs for the tracking algorithm. The EKF uses its estimate of the measurement and the residual between the estimated and reported measurements to correct its state-estimate of the target kinematics. The process of EKF to accomplish this is defined in (5a-e)

$$\mathbf{K}_k = \mathbf{P}_{k|k-1}\mathbf{H}_k^T\left(\mathbf{H}_k\mathbf{P}_{k|k-1}\mathbf{H}_k^T + \mathbf{R}_k\right)^{-1} \tag{5a}$$

$$\mathbf{x}_{k|k} = \mathbf{x}_{k|k-1} + \mathbf{K}_k\left(\mathbf{z}_k - \mathbf{h}\left(\mathbf{x}_{k|k-1}\right)\right) \tag{5b}$$

$$\mathbf{P}_{k|k} = \left(\mathbf{I} - \mathbf{K}_k\mathbf{H}_k\right)\mathbf{P}_{k|k-1} \tag{5c}$$

$$\mathbf{x}_{k+1|k} = \mathbf{f}\left(\mathbf{x}_{k|k}\right) \tag{5d}$$

$$\mathbf{P}_{k+1|k} = \mathbf{F}_k\mathbf{P}_{k|k}\mathbf{F}_k + \mathbf{Q}_k, \tag{5e}$$

where **H**, based on (4), provides the Jacobian of the output-coupling function:

$$\boldsymbol{H} = \begin{bmatrix} \frac{\delta\rho}{\delta x} & 0 & \frac{\delta\rho}{\delta y} & 0 & \frac{\delta\rho}{\delta z} & 0 \\ \frac{\delta\beta}{\delta x} & 0 & \frac{\delta\beta}{\delta y} & 0 & 0 & 0 \\ \frac{\delta\varepsilon}{\delta x} & 0 & \frac{\delta\varepsilon}{\delta y} & 0 & \frac{\delta\varepsilon}{\delta z} & 0 \end{bmatrix}. \tag{6}$$

The function **f** is the modeled target dynamics, and the matrix **F** in (5d-e) is the associated Jacobian. As stated previously, the target dynamics are usually defined as (3a). The subscript indicates discrete time, with $k|k$ is the estimate at the time k given all the information up to that time and $k+1|k$ is the estimate for time $k+1$, given all the information up through time k.

The process noise, **Q**, indicates the accuracy of the system dynamics, and is usually modeled as integrated white noise [15]:

$$\boldsymbol{Q} = q^2\begin{bmatrix} \boldsymbol{Q}_{2x2} & \boldsymbol{0}_{2x2} & \boldsymbol{0}_{2x2} \\ \boldsymbol{0}_{2x2} & \boldsymbol{Q}_{2x2} & \boldsymbol{0}_{2x2} \\ \boldsymbol{0}_{2x2} & \boldsymbol{0}_{2x2} & \boldsymbol{Q}_{2x2} \end{bmatrix} \tag{7a}$$

$$\boldsymbol{Q}_{2x2} = \begin{bmatrix} \frac{dt^3}{3} & \frac{dt^2}{2} \\ \frac{dt^2}{2} & dt \end{bmatrix}. \tag{7b}$$

As the process noise is increased, the dynamic model, **F**, in (5d-e) is weighted less. The measurement becomes more dominant in the processing, allowing more of the measurement noise to be passed thought the filter to the track solution. As the process noise is decreased, in contrast, the reaction of the tracking algorithm becomes less responsive to the measurement and more smoothing occurs.

While not explicit in the (5a) and often overlooked, the EKF's Kalman gain is affected by the process noise, the error covariance **P**, and the state estimate **x**. The state estimate is injected into the Kalman gain though the output-coupling Jacobian **H**. The gain is also affected by the measurement noise **R**. The measurement noise relates to the quality of the sensor. A standard radar will have its angle accuracies based on its beamwidth, for example while the range accuracy will be based on the resolution of the pulse signal. The accuracy indicates that the target can be anywhere within the beam and so-called range bin, as with airborne radar.

Since a Kalman filter is used, the accuracy is represented as a Gaussian distribution. (If the accuracy is not Gaussian, techniques such as Gaussian sums could be used to represent the measurement accuracy [16], but that is beyond the needs of these developments.) In Kalman filtering, the ratio of **Q** to **R** represents the relative belief of the target-motion model versus that of the sensor reports. If **Q** is smaller relative to **R**, the measurements will have a reduced of effect on the target track and the results from measurements over time will be smoothed, with the effects of noise less pronounced. If this ratio is reversed, the measures will dominate the track behavior, with the effects of individual measurements more pronounced in the target track. It is of note that, since the EKF is a measurement driven method, measurements will always ultimately have some effect on the target track. When the measurements noise is smaller, the measurement effects will have a faster impact on the track as sensors are viewed as more accurate.

3. Kalman Gain Monitoring

The extended Kalman filter (EKF) behaves differently than the Kalman filter for linear time-invariant systems. While the Kalman filter for such systems is predictable in nature, the EKF will vary over time. The variations in the error covariance **P** are affected by the nonlinear behavior of the system and the local estimate in both the update equation of (5c) and the prediction equation of (5e).

The behavior of the Kalman gain within the EKF, the vector **K**, often precedes the noticeable changes of the error covariance. This arises as the Kalman gain is affected both by the nonlinearities directly in (5a) and by the variations in the error covariance matrix. As the gains change over time, the filter can inherently detect changes in the actual system that vary from the estimation model. In [1], for a target tracking application of the extended Kalman filter, the Kalman gains demonstrated that over time there existed features in their behaviors that coincided with target maneuvers. The analysis of [1] looked at the individual gains, tracking both position and velocity of the targets in two-dimensional space using a range and bearing measurement. The resulting behaviors of the eight element Kalman-gain vector were used as features to identify when various maneuvers, including turns and simple linear accelerations, occurred. Another example is provided here.

The details of the scenario are shown in Figure 3. The target simulates the behavior of a submarine as it is being tracked by another vessel. The submarine maintains a straight-line trajectory with a constant speed. The trailing vessel also maintains a constant

speed and course. After some time, the target maneuvers. This represents a concept in a submarine-tracking problem where, being tracked, the target maneuvers to clear baffles to "see" the trailing ship and possibly cause a break-in-track of the enemy's tracking system. The platform ship then maneuvers, followed quickly by the submarine maneuvering again. These successive maneuvers can result in the filter becoming numerically unsound.

Figure 4 shows the behavior of the four Kalman gains related to the range over this whole scenario and is marked where the target and the sensor platform perform maneuvers. The Kalman gains show different behaviors, including a sharp transient, a significant change in the slope of the gain, and a zero-crossing.

The other four gains, which relate to the bearing measurements, are shown in Figure 5, and are larger in magnitude, but similar in relative behavior. Other test cases [1, 17], have also shown the gains to high frequency behaviors during maneuvers.

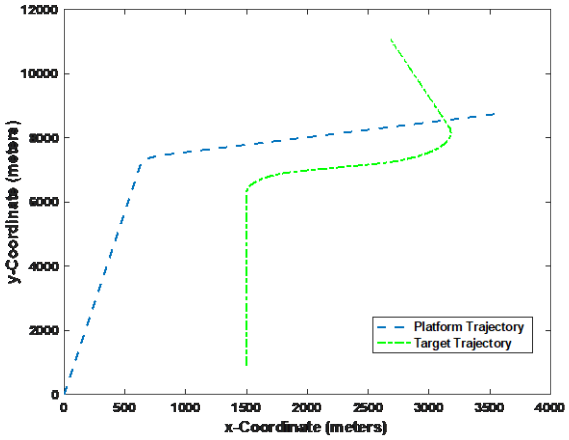

Figure 3: A manuevering target being tracked by a maneuvering sensor platform

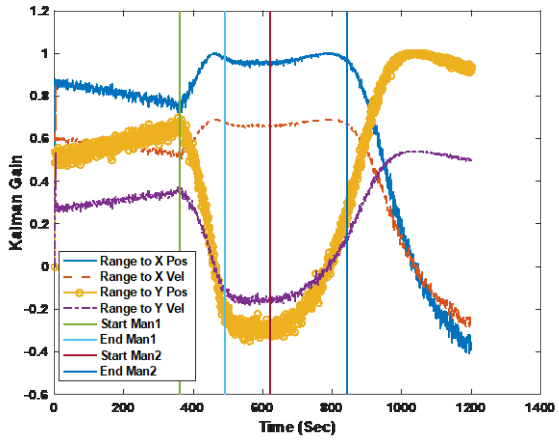

Figure 4: The behavior of the range-related Kalman gains over the course of the scenario with the target maneuvers marked

From these various test cases, the features of interest to detect a target maneuver have been determined to include monitoring the frequency behavior, the zero-crossings, the transient behavior, the slope performance, and the ownship (platform) maneuvers. It has also been determined that only a subset of the Kalman gains are necessary to observe. These include the gains related to the position states and range measurements K_{11} and K_{31} and all of the gains related to the bearing measurements K_{i2}, where those required vary by feature

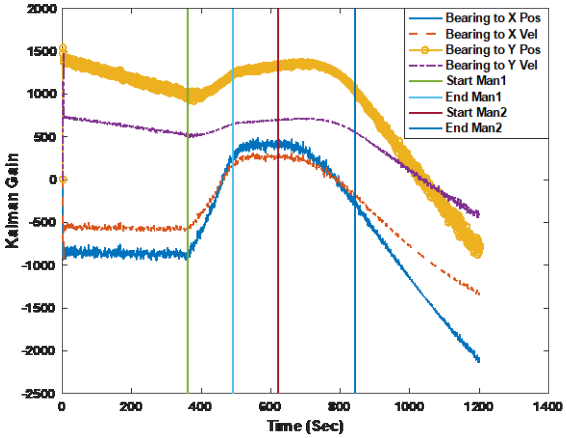

Figure 5: The behavior of the bearing-related Kalman gains over the course of the scenario with the target maneuvers marked

4. Evidence Accrual Using Feature Object Extraction

Many evidence accrual methods have been developed to combine information which, in this case, provide a level of evidence that a maneuver is occurring or has ceased to be. The primary evidence accrual techniques are the Dempster-Shafer method [5] and the Bayesian taxonomy approach [4], also referred to as the Pearl Tree. While these techniques have been utilized for decades, they have drawbacks, including that both represent the information as probabilities that update following Bayes rule. Also, uncertainty in the information that is the basis of the probabilities is not modeled easily, even with Dempster-Shafer.

FOX provides for distinct levels of evidence, such as of maneuver and for a non-maneuver separately. Since the measures of evidence are generated independently, the scores, unlike probabilities, are not related and an increasing evidence for one decision (i.e., a maneuver) need not decrease the other decision (i.e., no maneuver). Evidence can prove one or multiple decisions thus changing all or some of the decision.

FOX is also designed to provide a quality score with each level of evidence. The quality score is similar to a Kalman filter error covariance in that a high score indicates uncertainty while a low score indicates a high degree of certainty about the evidence score. The corroboration of evidence gathered from various behaviors can improve the certainty that an event occurred. Conversely, with multiple sources of evidence, maneuver events can be detected with one gain behavior being triggered while the others have not met the threshold.

For the maneuver detection problem, each of the elements of the Kalman gains' behaviors from the target tracking system can be used individually to indicate when a target maneuver is being initiated.

The FOX technique is designed to decompose a complex classification problem into a series of smaller and simpler problems. For the maneuver detection problem, a unidirectional tree is employed, as shown in Figure 6, illustrating use of FOX to accrue evidence based upon multiple behaviors of the Kalman

For maneuver detection, the top level is *Detected Maneuver.* The degree of evidence for this evidence node is limited to a range between 0 and 1. A corresponding tree for determining a level evidence for no maneuver occurring would be similar in concept with different linkages. The next level of this tree is comprised the individual-event detections of the tracking-system's Kalman gain vector: *Zero Crossing*, *Gain Frequency,* and *Slope Variation.* These three components are combined to create the *Detected Maneuver* scores. As the evidence levels in these states increase

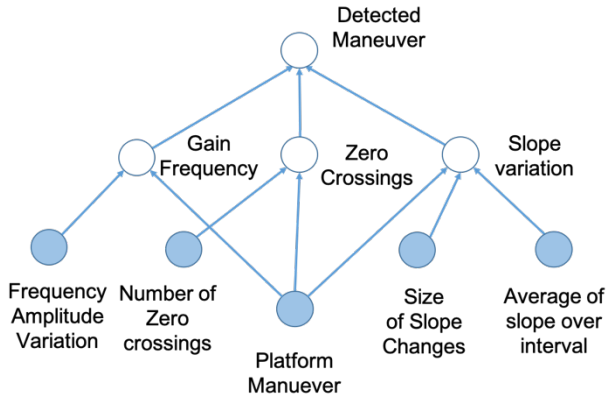

Figure 6: The proposed evidence accrual tree decomposition for Kalman gain maneuver detection approach of FOX

from 0 to 1, the overall detection-levels vary based not only on the lower-level scores but the quality level as well. Poor quality scores are weighted less than higher quality scores.

6, the shaded states indicate elementary-evidence input nodes. These represent the elemental measurements such as the measured frequencies or number of zero crossings. The unshaded nodes are referred to as states of interest. These are states of combined information.

approach is that, unlike the states of Markov chain [6], these states need not be disjoint nor do the states need be a complete representation of all the states of the system.

While the Kalman gain elements of the target tracking system provide evidence to the FOX evidence accrual system which employs a Kalman filter itself. To clarify, the Kalman filter of the FOX system in this case, actually a fuzzy Kalman filter, is different than that of the tracking system that is a source of evidence.

The level of evidence for a state of interest can be generated in two ways. The first is through direct observation, which implies a direct measurement is available, as shown with the shaded nodes. The evidence is then processed through a substate, depicted with a clear node. The tree of Figure 6 shows some substates have multiple injection nodes flowing into them. The FOX Kalman filter that injects the evidence into the tree nodes is a fuzzy Kalman filter (FKF). The FKF takes the multiple inputs and creates a single-output fuzzy measure. Substates that do not have direct evidence injection are generated using systems theory. The substates connect to state of interest through links that represent the functional relationship.

The FKF of the FOX system is based upon a development of Watkins [7] and modified in [2]. This approach was selected to allow a wide variety of measurement types and uncertainty models to be used with ease. The FKF implementation is a straightforward variant of the standard Kalman filter with a modification in the update equations. The FKF is defined in (8) with five equations, (8a) to (8e). Comparing the sets of equations, (5) and (8), two of these, the Kalman gain equation of (5a) and (8a), and the state update equation of (5b) and (8b), are the ones where counterparts differ. The fuzzy measures are incorporated by using the first moment, indicated as mom_1, of the consequent fuzzy membership function, referred to as m_{adj}, or the membership adjunct.

$$\mathbf{K} = \mathbf{P}_{k|k-1}\mathbf{H}^T(\mathbf{H}\mathbf{P}_{k|k-1}\mathbf{H}^T + mom_1(m_{adj}(\mathbf{R})))^{-1} \tag{8a}$$

$$\mathbf{x}_{k|k} = \mathbf{x}_{k|k-1} + \mathbf{K}(mom_1(m_{adj}) - \mathbf{H}\mathbf{x}_{k|k-1}) \tag{8b}$$

$$\mathbf{P}_{k|k} = (\mathbf{I} - \mathbf{K}\mathbf{H})\mathbf{P}_{k|k-1} \tag{8c}$$

$$\mathbf{x}_{k+1|k} = \mathbf{F}\mathbf{x}_{k|k}$$

$$\mathbf{P}_{k+1|k} = \mathbf{F}\mathbf{P}_{k|k}\mathbf{F}^T + \mathbf{Q}_k \tag{8e}$$

The use of fuzzy logic provides for simplified linguistic based conversion from the measurement coordinate systems to the evidence space, which has been defined as a value between 0 and 1. If the measurement and uncertainty values are crisp, the FKF devolves into the standard Kalman filter.

The nature of the measurement data determines whether the fuzzy measure or a crisp measure is used. A true measure such as the number of zero crossings or a known even as the knowledge of a platform maneuver would be a crisp value that would map into crisp groupings. The mapping of data into groupings, such as a determination based upon the frequency behavior or degree of slope change, would be fuzzy.

Once elementary evidence is injected into the tree, it can propagate another FKF process or through the use system theory process as follows. A state of interest and its direct-substates are represented in vector form as

$$\mathbf{x}_S = [x_{s1} \quad x_1 \quad x_2 \quad \cdots \quad x_n \quad x_n] \tag{9}$$

The state of interest or of the node value is the first element of the state vector.

Using first-order observer decomposition [18], the evidence dynamics are given as

$$\mathbf{x}_{k+1} = \begin{bmatrix} f(xa, x_{s1}, \ldots, x_{sn}) \\ \begin{bmatrix} 0 & f_1 & 0 & \cdots & 0 \\ 0 & 0 & \ddots & \ddots & \vdots \\ \vdots & \vdots & \ddots & \ddots & 0 \\ 0 & 0 & \cdots & 0 & f_n \end{bmatrix} \mathbf{x}_k \end{bmatrix}. \tag{10}$$

The state of interest is comprised of its substates and the previous value of the state of interest. The observer concept provides a forgetting factor. This forgetting factor and the observer updating equation are used to incorporate the quality factor of each sub-state. In (10), the uncertainty can be incorporated as a simple scaling in the state values or in the state-of-interest function, $f(\cdot)$.

The associated error covariance or uncertainty equation is propagated by (11).

$$P_k = f_a P_{a,k-1} f_a^T + f_1 P_{s1,k-1} f_1^T + \cdots + f_n P_{sn,k-1} f_n^T + q_x. \tag{11}$$

This decomposition of the problem into the individual substates reduces the complex model of the interactions of information into simplified operations. The decomposition also simplifies the incorporation of the uncertainty into the state vector.

4.1. Maneuver Detection Fuzzy Membership Functions

To generate the injection evidence, the following antecedent and consequent functions along with their associated inference engines were considered:

4.1.1. Frequency Amplitude Variation

When a maneuver occurs, some Kalman gain elements experience high frequency changes in amplitude. The high frequency behavior indicates that a maneuver could be occurring. As seen in [17], the high frequencies indicate potential issues with the Kalman filter that are a result of sharp maneuvers. The frequencies are mapped into a score using two input antecedent functions: *Max_frequency_value* and *Ratio_of_high_frequency_to_low_frequency_power.*

Figure 7 provides a four-element antecedent function that breaks the fast Fourier transform (FFT) spectrum of a time slice of the Kalman gain maps into the four trapezoidal-based functions. Figure 8 shows the five-element triangular antecedent membership functions that represents the ratio of the power of the highest-tenth of the spectrum to the lowest tenth of the spectrum. Table 1 provides the inference engine of the two sets of membership functions. These map to the consequence functions shown in Figure 9. These are defuzzified using the FKF.

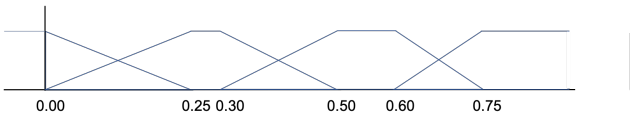

Figure 7: Kalman Gain Frequency amplitude variation FFT time slice antecedent function

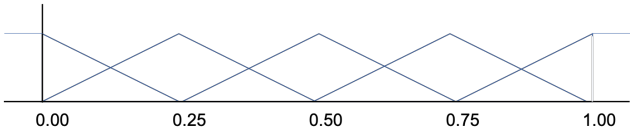

Figure 8: Kalman Gain Frequency amplitude power ratio membership function

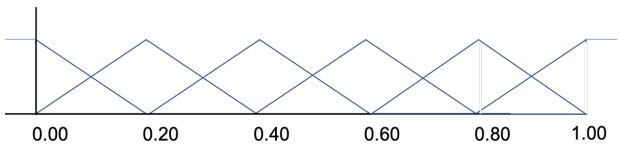

Figure 9: Kalman Gain Frequency Consquence Function

Table 1: Kalman Gain Frequency Inference Engine

	Frequency Maximum Membership Function			
Frequency Power Ratio Membership Function	1	2	3	4
1	1	2	3	4
2	1	2	4	4
3	2	3	4	5
4	2	4	5	5
5	3	4	5	5

4.1.2. Number of Zero Crossings

The number of zero crossings is a crisp value. The number of zero crossings num_{ZC} is mapped into a score ZC_{score}:

$$ZC_{score} = \begin{cases} 0 & num_{ZC} = 0 \\ 0.2 & num_{ZC} = 1 \; or \; 2 \\ 0.6 & num_{ZC} = 3, 4, or \; 5 \\ 1.0 & num_{ZC} > 5 \end{cases} \tag{12}$$

4.1.3. Slope Changes

The size of the slope changes in a given time interval is measured. The value is an absolute value of the difference between the initial slope and the ending slope compared to the maximum and minimum values. This crisp value is mapped similarly to the number of zero crossings but, are mapped evenly across four regions are mapped into the scores:

$$SC_{score} = \begin{cases} 0 & \frac{slope_{max}}{slope_{min}} \leq 0.5 \\ 0.33 & 0.5 < \frac{slope_{max}}{slope_{min}} \leq 2.5 \\ 0.67 & 2.5 < \frac{slope_{max}}{slope_{min}} \leq 4.0 \\ 1.00 & 4.0 < \frac{slope_{max}}{slope_{min}} \end{cases} \tag{13}$$

Unlike the other injection evidence mentioned here, the uncertainty is also fuzzy. The size in the slope changes creates the next score. Figures 10 depicts a five-element trapezoidal function that map the change in slopes. Table 2 provides the inference engine that maps into the consequence function represented by five triangular functions as seen in Figure 11. Again, the defuzzification is performed by the FKF.

Table 2: Kalman Gain Slope Inference Engine

	SC_{score}			
Slope Average Membership Function	0.0	0.33	0.67	1.0
1	1	1	2	3
2	1	2	3	3
3	3	3	4	4
4	5	5	5	5
5	5	5	5	5

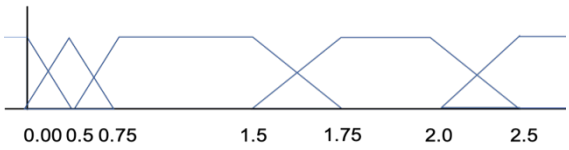

Figure 10: Changes in Kalman Gain Slope Membership Function

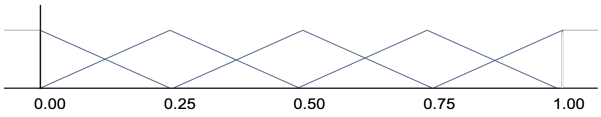

Figure 11: Changes in Kalman Gain Slope Consquence Function

Now that the direct evidence has been defined, the higher level nodes, depicted in Figure 4, can also be defined. The function relating the three sets of substate evidence to the *Detected Maneuver* state is defined with the limited linear combination in (14).

$$\boldsymbol{x_{MD}}(k) = \min\big(1, \mu(k)\big),$$

$$\mu(k) = [0.7 \quad 0.47 \quad 0.7]\, \boldsymbol{x_{MD}}(k),$$

with

$$\boldsymbol{x_{MD}} = \begin{bmatrix} x_{MDfreq} \\ x_{MDZC} \\ x_{MDslope} \end{bmatrix}, \tag{14}$$

where $\mathbf{x_{MD}}(k)$ is the estimated level of evidence at time k for detection of a maneuver state. The states that comprise $\mathbf{x_{MD}}$ are $\boldsymbol{x_{MDfreq}}$, the frequency behavior of the Kalman gain used to detect a maneuver, $\boldsymbol{x_{MDZC}}$, which is the incidence of zero-crossings for a Kalman gain value, and $\boldsymbol{x_{MDslope}}$, which is the change in slope of the Kalman gain value that indicates a manuever. For $\boldsymbol{x_{MD}}$, the score was not directly weighted by the measurement uncertainty and is solely based on the current values of the components.

The subnode x_{MDZC} is defined at time k as

$$x_{MDZC}(k) = [0.2 \quad 0.95] \cdot \begin{bmatrix} x_{MDNZC}(k-1) \\ \max\big(1, x_{lc}(k-1)\big) \cdot \big(1 - x_{pltmnv}(k-1)\big) \end{bmatrix}, \tag{15}$$

where $x_{pltmnv}(k)$ is either 1 or 0, with a 1 indicating the platform is, and a 0 indicating that it is not, in a maneuver at time k. x_{lc} is defined based upon whether the measurement is range-bearing in (16) or bearing only in (17), using elements of the Kalman gain. For range-bearing,

$$x_{lc}(k) = 0.4\, x_{K11}^{ZC}(k) + 0.4\, x_{K31}^{ZC}(k) + 0.4\, x_{K12}^{ZC}(k) + 0.4\, x_{K22}^{ZC}(k) + 0.4\, x_{K32}^{ZC}(k) + 0.4\, x_{K42}^{ZC}(k), \tag{16}$$

or, if the measurement is bearing-only

$$x_{lc}(k) = 0.67\, x_{K11}^{ZC}(k) + 0.67\, x_{K21}^{ZC}(k) + 0.67\, x_{K31}^{ZC}(k) + 0.67\, x_{K41}^{ZC}(k). \tag{17}$$

Here, the subscript *Kij* indicates the ith, jth element of the Kalman gain and $x_{Kij}^{ZC}(k)$ indicates the Kalman gain number of zero-crossings upto time *k*.

The subnode x_{MDfreq} is defined in (18) and (19) for the range-bearing measurement and in (20) and (21) for the bearing measurements.

For the range-bearing subnode $\boldsymbol{x_{MDfreq}}$,

$$x_{MDfreq}(k) = \Big[\min\Big(1, \mu_{freq}(k)\Big)\Big] \cdot \big(1 - x_{pltmnv}(k-1)\big), \tag{18}$$

where

$$\mu_{freq}(k) = [0.9 \quad 0.2 \quad 0.3 \quad 0.3 \quad 0.3 \quad 0.2]\, \mathbf{x}_{\mathrm{Krb}}^{freq}(k),$$

and

$$\mathbf{x}_{\mathrm{Krb}}^{freq}(k) = \begin{bmatrix} x_{MDfreq}(k-1) \\ x_{K11}^{freq}(k) \\ x_{K31}^{freq}(k) \\ x_{K22}^{freq}(k) \\ x_{K32}^{freq}(k) \\ x_{K42}^{freq}(k) \end{bmatrix}. \tag{19}$$

For the bearing-only measurement, the subnode x_{MDfreq} is defined similarly, but with different Kalman gains, as

$$x_{MDfreq}(k) = \Big[\min\Big(1, \mu_{freq}(k)\Big)\Big] \cdot \big(1 - x_{pltmnv}(k-1)\big), \tag{20}$$

where

$$\mu_{freq}(k) = [0.9 \quad 0.6 \quad 0.6 \quad 0.5]\, \mathbf{x}_{\mathrm{Kb}}^{freq}(k),$$

and

$$\mathbf{x}_{\mathrm{Kb}}^{freq}(k) = \begin{bmatrix} x_{MDfreq}(k-1) \\ x_{K21}^{freq}(k) \\ x_{K31}^{freq}(k) \\ x_{K41}^{freq}(k) \end{bmatrix}. \tag{21}$$

Finally, the subnode $x_{MDslope}$ is defined in (22) and (23) for range-bearing measurements and in (24) and (25) for bearing-only measurements. For range-bearing,

$$x_{MDslope}(k) = \Big[\min\Big(1, \mu_{slope}(k)\Big)\Big] \cdot \big(1 - x_{pltmnv}(k-1)\big), \tag{22}$$

where

$$\mu_{\mathrm{slope}}(k) = [0.7 \quad 0.4 \quad 0.4]\, \mathbf{x}_{\mathrm{Krb}}^{slope}(k),$$

and

$$\mathbf{x}_{\mathrm{Krb}}^{slope}(k) = \begin{bmatrix} x_{MDslope}(k-1) \\ x_{K12}^{freq}(k) \\ x_{K32}^{freq}(k) \end{bmatrix}. \tag{23}$$

For bearing only,

$$x_{MDslope}(k) = \left[min\left(1, \mu_{slope}(k)\right)\right] \cdot \left(1 - x_{pltmnv}(k-1)\right), \quad (24)$$

where

$$\mu_{slope}(k) = [0.7 \quad 0.4 \quad 0.4]\, \mathbf{x}_{\mathrm{Kb}}^{slope}(k),$$

and

$$\mathbf{x}_{\mathrm{Kb}}^{slope}(k) = \begin{bmatrix} x_{MDslope}(k-1) \\ x_{K11}^{freq}(k) \\ x_{K31}^{freq}(k) \end{bmatrix}. \quad (25)$$

5. Scenario, Example, and Analysis

In each of two examples, an EKF target tracking system is employed and the FOX system as previously described is applied. The scenario used to demonstrate the effectiveness of FOX technique as applied to the maneuver detection problem was summarized in Section 2 and is illustrated in Figure 3. The simulator was developed in MATLAB by the authors. The scenario lasts 1200 seconds. A platform is heading 5 degrees west of north for 480 seconds at 15 kts. Then, the platform changes heading and speed over 60 seconds to 65 degrees west of north and to 9 kts. The platform remains at this heading and speed for the rest of the scenario. The target heads due north for 360 seconds at 15 kts. Then the target changes course and speed over 130 seconds. The course is changed to 70 degrees west of north, and the speed is slowed to 10 kts. At 620 seconds into the scenario, the heading and speed is changed again. This time the acceleration of the target is changed over 224 seconds. The speed is changed to 15 kts while the heading is changed to 10 degrees east of north.

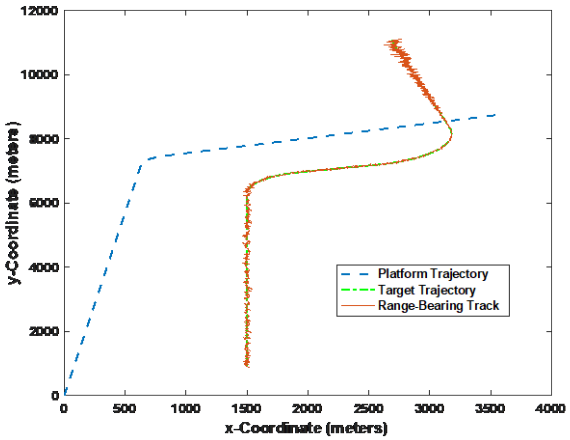

Figure 12: The test scenario with the tracked target using range and bearing meaasurements.

The platform sensor in the first example is a range-bearing sensor with a reporting time of 1 second. The range accuracy is 0.01 m while the bearing accuracy is 0.0003 radians. In the second example, the range sensor is turned off, while the bearing sensor has the same sample time and accuracy in the first example.

5.1. Example 1

The target track of the scenario when using the range-bearing measurement is shown in Figure 12. The associated Kalman filter gains associated to the range measurements are seen in Figure 4 and the gains associated to the bearing measurements were provided in Figure 5. The gains are windowed over a 20 second segment. The window continually slides until the end of the scenario. Figure 13 shows the resulting maneuver detection score.

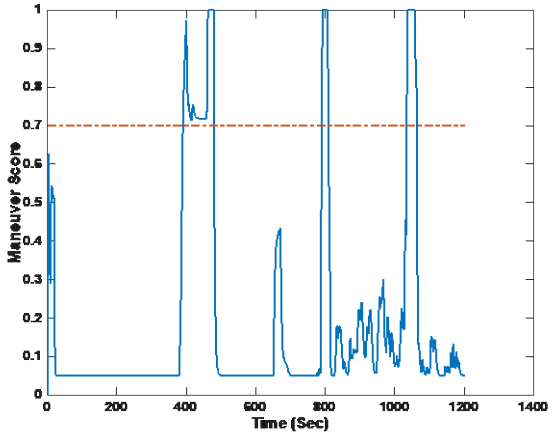

Figure 13: FOX maneuver-detection system results for the range-bearing example

The maneuver detection results indicate that the FOX maneuver detection does detect the target maneuvers when the measurements driving the tracking system contain both a range and a bearing. Using a detection threshold of 0.7, the first target maneuver is detected 31 seconds after it begins (near 400 seconds into scenario) and FOX continues to detect it until the platform begins its maneuver. The second maneuver is detected 170 seconds into its 224 second increase-in-speed and turn. When the target switches from east to west in absolute bearing, the event is detected as a maneuver for 30 seconds. The sharper maneuver (the first maneuver) is detected earlier and for a longer percentage of time of the maneuver. The maneuver has a significant effect on the range and bearing change and impacts the Kalman gain relatively more than a measurement that has little relative impact as with the second maneuver.

In the second maneuver, the effect on the Kalman gain vector values is smaller; the change in bearing and range is smaller at first, and then builds. This compares similarly to the results in [1, 17] in that the closer a target is to the platform and the sharper the maneuvers, the greater the Kalman gain behavior. When the target moves from east to west of the platform, the bearing changes from positive to negative. While the tracker handles the transition smoothly, the sign-changes affect the Jacobian of the measurement-coupling function **H**, as in Eq. (5a). This would be the same if the platform were to maneuver. The results indicate that using the Kalman gains are able to provide indication of maneuvers. The underlying scores indicate that slope behavior is important in target turns. The frequency behavior complements the zero-crossing in the last two detections.

5.2. Example 2

Figure 14 shows the target track overlaid the truth track for the scenario. The target track is, as expected, terribly inaccurate as bearing-only measurement makes the target location and velocity partially unobservable [19]. The target also maneuvers, and this exacerbates the issue [20]. The associated Kalman gains are shown in Figure 15. The Kalman gains are similar to the bearing gains of

range-bearing measurement of Example 1. The gains are windowed over a 20 second segment. The window continually slides until the end of the scenario. Figure 16 shows the maneuver detection score.

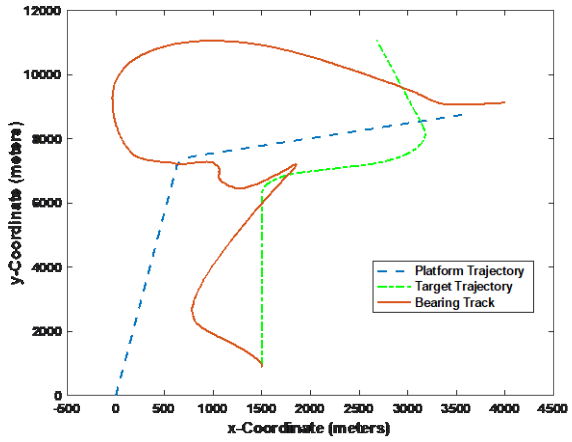

Figure 14. The test scenario with the tracked target using bearing-only measurements where the target position and velocity become unobservable

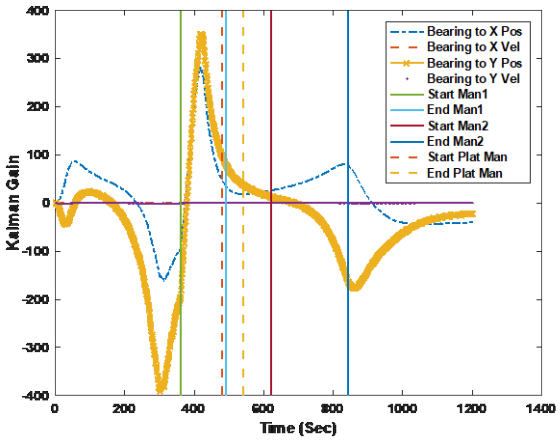

Figure 15: The bearing-only related Kalman gains as mapped over the entire scenario with target and platform maneuvers indicated

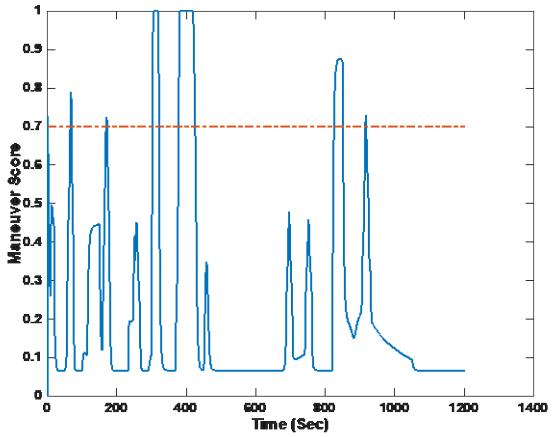

Figure 16: FOX maneuver-detection system results for the bearing-only tracker

The maneuver detection algorithm shows six detections of maneuvers. As discussed in [8], the estimations from a bearings-only track have significant observability issues. The fact that the target is moving originally parallel to the sensor platform results in the range information not being observable. This often collapses the range uncertainty covariance. Three times the target track is detected as a maneuver. In watching the tracker behavior, the Kalman gain is actually providing indications of the failure of the tracking system. When the target maneuvers, the algorithm detects this behavior as the EKF becomes more inaccurate. The platform maneuver provides a pseudo cross-fix which temporarily corrects the track but does not provide enough information to stabilize the filter. The second maneuver is detected later than the maneuver when the range-bearing tracking. For this unobservable measurement type, the FOX algorithm will detect issues with the tracker performance besides maneuvers.

5.3. Summary of Results

The two test scenarios indicate that the FOX maneuver-detection algorithm was able to provide triggers when the target is in or concluding a maneuver. The algorithm also detects other events, particularly the failure of the EKF. This would indicate that at times a reset in the tracker could be useful. It also indicates that behaviors, such as the change from east-to-west of the target, needs to be incorporated into the algorithm similar to the platform maneuver.

6. Conclusions

In this paper, the FOX evidence accrual technique was applied to the problem of detecting target maneuvers using measures from the Kalman gain behaviors from an EKF tracking routine. The algorithm was demonstrated to a variety of events most notably, when the trackign system begins to numerically collapse. Kalman gains of an EKF are important element in detecting tracking failures or changes. The results indicate that other highest-level nodes,i.e., target cross-overs and Kalman collapse, should be incorporated into the FOX system. Maneuver detection can be exploited to work with EKF tracking systems. Incorporation of the method into an interacting multiple-model (IMM) tracking system is planned to advance the applicability of the technique.

Conflict of Interest

The authors declare no conflict of interest.

References

[1] S.C. Stubberud, K.A. Kramer, and A.R. Stubberud, “Fuzzy-Based Evidence Accrual for Target Maneuver Detection,” in Proc. of Innovations in Intelligent Systems and Aplications, INISTA ’18. 2018, pp. 1-7. https://doi.org/10.1109/INISTA.2018.8466310

[2] S. Stubberud and R. Pudwill, in "Feature object extraction - a fuzzy logic approach for evidence accrual in the Level 1 Fusion classification problem," in Computational Intelligence for Measurement Systems and Applications, 2003. CIMSA '03. 2003 IEEE International Symposium on, 2003, pp. 181-185. https://doi.org/10.1109/CIMSA.2003.1227224

[3] R. Sedgewick and K. Wayne, *Algorithms*, *4th Edition*, Addison-Wesley, 2011.

[4] J. Pearl, Causality: Models, Reasoning and Inference, 2nd Edition ed.: Cambridge University Press, 2009.

[5] A. P. Dempster, "Upper and lower probabilities induced by a multivalued mapping," Annals of Mathematical Statistics, vol. 38, pp. 325-339, 1967. https://doi.org/10.1214/aoms/ 1177698950

[6] J. R. Norris, *Markov Chains*. New York: Cambridge Press; 1997.

[7] F.A. Watkins. *Fuzzy Engineering*. MS thesis, Electrical and Computer Engineering, University of California, Irvine; 1994.
[8] R. Lobbia and M. Kent, "Data fusion of decentralized local tracker outputs," in *IEEE Transactions on Aerospace and Electronic Systems*, vol. 30 (3), July 1994. pp. 787-799. https://doi.org/10.1109/7.303748
[9] R. G. Brown, P. Y. C. Hwang. Introduction to Random Signal Analysis and Kalman Filtering, 3rd Ed. New York: Wiley; 1996.
[10] S. Haykin, Kalman Filtering and Neural Networks, Prentice-Hall, Englewood Cliffs, NJ, 2002.
[11] S. Blackman and R. Popoli, Design and Analysis of Modern Tracking Systems, Artech House, Norwood, MA, 1999.
[12] H. A. P. Blom and Y. Bar-Shalom. "The interacting multiple model algorithm for systems with Markovian switching coefficients." In IEEE Trans. On Automatic Control, 33 (8), 1988, pp. 484-488. https://doi.org/10.1109/9.1299
[13] M. W. Owen and A. R. Stubberud, "A neural extended Kalman filter multiple model tracker," Proc. of OCEANS 2003, Vol 4, Sept. 2003, pp. 2111–2119. https://doi.org/10.1109/OCEANS.2003.178229
[14] P.J. Shea, T. Zadra, D. Klamer, E. Frangione, R. Brouillard, and K. Kastella, "Precision tracking of ground targets," *Proceedings of the IEEE Aerospace Big Sky Conference,* vol. 3, pp. 473-482, 2000. https://doi.org/10.1109/AERO.2000.879873
[15] Y. Bar-Shalom, X.-R.K.T. Li, Estimation with applications to tracking and navigation, Wiley, 2001.
[16] D. Alspach and H. Sorenson, (1972). "Nonlinear Bayesian Estimation Using Gaussian Sum Approximations," *IEEE Transactions on Automatic Control*, Vol. 17 , No. 4 , pp. 439 – 448, Aug., 1972.
[17] S. C. Stubberud and KA Kramer, "Monitoring the Kalman Gain Behavior for Maneuver Detection," 25th International Conference on Systems Engineering (ICSEng), 2017, pp. 39-44. https://doi.org/10.1109/ICSEng.2017.71
[18] M.S. Santina, A.R. Stubberud, G.H. Hostetter, Digital control system design, Saunders College Pub., 1994.
[19] W.S. Levine (ed.), *The Control Handbook,* CRC Press, Boca Raton, Florida, 1996.
[20] SC Stubberud, KA Kramer, "Navigation using angle measurements," Mathematics in Engineering, Science & Aerospace (MESA) 8 (2), 2017, 1-15

ASTES

Advances in Science, Technology and Engineering Systems Journal Vol. 4, No. 4, 478-484 (2019)

www.astesj.com

Special Issue on Advancement in Engineering and Computer Science

ASTESJ

ISSN: 2415-6698

Conceptual Architecture for the Continuity if Workflow in Activities on Multi-Devices: Case Study Co-Kitchen

Mirian Janeth Avalos-Viveros [1,*], Luis Gerardo Montané-Jiménez[1], Gabriela Sánchez Morales[2], Carmen Mezura-Godoy[1], Edgard Benítez-Guerrero[1]

[1]*Facultad de Estadística e Informática, Universidad Veracruzana, 91020, Mexico*

[2]*Department of instruction and knowledge management, Universidad de las Américas Puebla, 72810, Mexico*

ARTICLEINFO

Article history:
Received: 31 May, 2019
Accepted: 02 August, 2019
Online: 21 August, 2019

Keywords:
Continuity
Workflow
Multi-device

ABSTRACT

Nowadays, the realization and follow-up of a team activity takes place in different execution environments (e.g. mobile phone, PC) through the use of computer applications. This implies context changes that generate interruptions in the activity. To improve the continuity of an activity with the reduction of interruptions during the development of this activity, would help to finish a task in a shorter time. An example of interruption occurs when a user initiates an activity on a device and decides to continue working on it on a different device, thus facing additional steps that must be performed to obtain the updated information on the desired device. The interruptions can be found in several domains as in the previous example that refers to the work developed through multi-devices or collaborative systems (CS). In this article we present a proposal for a model that incorporates the continuity attribute in the CS development process, to support its users to carry out Collaborative Activities (CA) through different devices with the least possible number of interruptions, so that that way the user does not require additional steps that extend the time of the task and negatively affect the process of transferring his CA to another device.

1. Introduction

This article is an extension of a previous work, in which a Conceptual model to improve the continuity of the workflow of collaborative activities in multi-devices is presented [1]. Collaborative activities can be developed within the Collaborative Systems (CS). CS allow a team of people to work on a common task, through a user interface in a shared environment, virtually [2]. Currently, due to the increase in the capabilities of mobile devices, these are used to perform different activities, gradually replacing the need for the use of a personal computer. This allows to conceptualize that the users of a CS can interact from any of their devices. An example of this scenario is a group of people which for different reasons of time and space decide to use a tool that supports distance collaboration, such as Google Drive®, with which it is possible to give continuity to an activity from a laptop, a tablet or a mobile phone.

The flow of continuity of an activity is limited due to the additional steps that are required to perform activities in multi-devices [3, 4]. These additional steps are considered interruptions, which are presented once the user wishes to continue performing an activity in a new device, such as: saving progress made in the source device, to later log in to the target device, open the application and position to the last state or download the advances in the new device; to name a few. It is important to mention the existence of tools that offer the user a flow of activity that involves fewer steps such as Apple AirPlay®, which in conjunction with Apple TV® wirelessly transmits movies, music and photos from any IOS® device; or Google Drive® offering the creation of content and editing flow, documents, photos and videos, allowing users to access them from any device.

Due to the problem described above, in this work we propose a model that offers continuity to the workflow of CA with support to multiple devices, seeking to reduce the number of interruptions that the user faces each time he wishes to resume a task in a different device. That is, for any user, the process of transferring the last state of information from one device to another is transparent.

* Mirian Janeth Avalos-Viveros, Email: zs17000719@estudiantes.uv.mx

The structure of this article is as follows: Section 2 addresses the aspects of Collaborative Systems, Collaborative Activities, Workflow and Continuity. Section 3 presents papers that support continuity in the workflow. Section 4 shows the challenges and opportunities identified from the analysis of the state of the art. Section 5 presents the proposal of a conceptual model that offers continuity in the CA workflow in multi-devices. Section 6 shows the proposal of a conceptual architecture for the construction of a CS under the concept of continuity. In section 7 a case study is presented to be implemented under the proposed model and architecture, as well as the design of the prototype. Finally, section 8 presents the conclusions and introduces future work.

2. Collaborative activities and Workflow

2.1. Collaborative systems

CS are computer systems that support collaborative work among groups of people who share common goals [2]. These CS are classified based on space, where collaborators can be found in the same place or in different geographical spaces; also, they are classified based on time, where people work at the same time (synchronous), or at different times (asynchronous) [5].

The CS offer functionalities for communication, coordination and collaboration, also known as the 3C's. The communication is through the sending and receiving of messages between team members, as well as the way in which these users observe what the rest of their team is doing. The coordination provides the way to organize the activities to be carried out. The collaboration considers functionalities necessary for users to achieve a collaborative activity [6, 7].

2.2. Collaborative activity

In [8] the activity theory (AT) is presented, representing it in a triangular figure with the elements that intervene in a collaborative activity and its relationship. The elements that make up the triangular system of activity correspond to: subjects, tools, community, division of labor, rules, objects and results; in [9] it is described as the relationship given by the link that exists between two elements of the system with another of the same. During the development of a CA, the people who are involved are immersed in a little-explored element so far: the workflow, by means of which one can know the interruptions that are generated during the life cycle of a task; for example, an interruption to the continuity of the workflow could occur when the user is writing a text on his cell phone and receives a phone call. At this moment, the flow is interrupted and the continuity suffers pauses due to the change of context.

2.3. Workflow

The workflow of an activity is a set of actions that need to be carried out to achieve a specific purpose. The [3] workflow considers two types of activities: individual activity flow and flow of sequenced activities. In the flow of individual activity, the user carries out only one activity, for example: watching a video, reading a book, editing a text, among others, making use of different devices, where each of them takes up the activity from the same point where the previous device left it. While in the stream of sequenced activities, the task flow is composed of different activities that must be performed by users to achieve the final goal; generally, each activity is carried out in a different device according to the needs of the activity, in different contexts of space and time [10]. The flow of activity suffers interruptions in its process due to changes in context, as previously mentioned; that is, there is no continuity in the process of completing a task.

2.4. Continuity

Continuity can be defined as the execution of steps without interruptions. The duration of an activity is an important factor that allows to determine the continuity within a task that is being carried out through a device. For that purpose, it [3] shows three ways in which the flow of continuity is carried out in accordance with the duration of the activity: multiple sessions, context changes and their tasks. With multiple sessions, when an activity is extensive, the user manages to complete it in multiple steps and different devices, depending on the context. While, in context changes of an activity, the user ends session and later takes it back, perhaps in a new device depending on the context where the user is. However, in the case of subtasks, when an activity is relatively extensive, it can be divided into subtasks; which can be different from each other and require a different place of context (time, location, among others.), therefore they can be made in different devices. Figure 1 shows the example of the user John who is in different context changes during the performance of a particular activity. He begins his work at his school using a desktop computer but changes the context to work using his laptop; this generates interruptions (represented by spikes, see Figure 1) that the user faces when he decides to transfer the information to a new device. Later, the user John decides to stop using the desktop computer to continue working from his tablet or cell phone, because he needs to be in motion (in this case he is experiencing interruptions to make possible the transfer of workflow). Finally, when he returns to his work area (school kitchen), he projects the content of the activity on a screen.

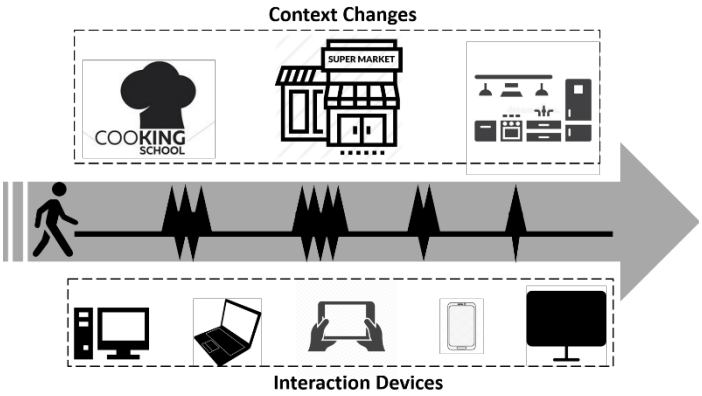

Figure 1: Continuity of a task with changes of context and devices.

3. Works on the continuity in the workflow

Currently, most people have multiple devices and interact with each other to perform their daily tasks [4, 10, 11], this because mobile devices (cell phones or tablets) have capabilities similar to those of a desktop computer or laptop, as people seek to try to keep their work at their disposal at all times. But this has brought unattractive events for users, for example: [12] discovered that when there was no storage in the cloud, people e-mailed the URLs of the websites they visited, to access them from a different device; in [11], a study finds that there are systems with an unintuitive design so that users have continuity in the interaction with multiple devices. In scenarios like this, where the user wants to work with

the devices, the transfer of the task between each device becomes a negative charge.

As a consequence of the lack of continuity in the process of carrying out the activity, there is a disconnection between the actions required of the user when he is using multiple devices [7].

As time passes, proposals have been sought to solve the lack of continuity with the aim of providing the user with the way to transfer information from one device to another without the intervention of unfavorable solutions such as: email, desktop software remote, USB drives, among others. Koren and others, in [13] propose an architecture for the mobility of the session of applications between different mobile devices, within the contributions include support for the discovery of nearby devices and the transfer of sessions with support for interactions based on the exchange of messages and files. However, they present problems in the transfer of the status of the activity.

Cabarcos and others, in [14] propose the design of an architecture for single session initiation in multi-devices (SuSSo) that includes the definition of storage formats of flow of operation session for the transfer of information in an abstract level, so that it can be easily implemented in any electronic device and guarantee interoperability of the cloud service in all devices; in this way sessions initiated from a device transfer their content to a second device without any problem.

Salminen and others, in [15], propose the implementation and evaluation of a middleware to migrate the user interface. The middleware is responsible for having control in the handling of events of the user interface and, in this way, the aforementioned component is transparent for the application. According to the tests carried out by the authors, the studies show that the preference for doing a task in a mobile device depends on the degree of familiarity that the user has with the keyboard of his cell phone, and they consider not having the need to incorporate a new method in order to finish their task before.

Cheng in [16]proposes a middleware capable of handling communication through different devices. The virtual browser facilitates operations between devices according to a predefined file. This research divides a DOM tree into multiple sub_DOM trees, to dynamically manage subviews on multiple devices and link them into a single virtual device. The author presents problems in the development of his proposal, for example: the difficulty to share events and the synchronization of elements and statuses.

Ghiani and others, in [17] present a process of migration for the permanence of status of the tasks that the user is doing in the device called source to the target device, that is, to which he wants to move the user interface to continue his interaction. The authors seek to provide: i) flexible support in several aspects taking into account the variety of possible devices that users may want to use, and ii) an accessible solution for the migration of any application developed with standard Web language, without using any specific complement. According to the tests carried out in this work, they obtained two variants as a result of user evaluations: ease of use and utility.

Pyla and others, in [18] designed a continuous user interface prototype that guarantees a seamless migration of tasks for users who try to perform a specification of requirements and collect tasks, using a tablet and a desktop computer. This system provides support for automatic migration of the task context (eg, applications that were in use) between two devices. In an evaluation carried out, the participants informed that the proposal helped to mitigate the effects associated with the disconnections of tasks, also informed that the automatic availability of the necessary data in the computers and modules contributed directly to a higher perceived reliability and lower error probability.

Currently, there are proprietary applications that offer continuity during the flow of activity, these are available for public use where some have cost and others are freely available, such as: Google Drive®, Netflix®, Office package ®, among others. In Google Drive®, the user has information availability from any device, as long as the device is linked to the same email account; the changes that are made are automatically saved by the tool. In the case of Netflix®, the user can access the exact minute in which he was watching a movie or series in his last session. In desktop systems such as the Office® parcel, if a document that has already been edited is opened, it asks the user if he wishes to continue working from the place where he was previously doing it. In [18] and [19], studies are presented to users where they interact with at least two devices to perform a task. Among the results obtained, an aspect that stands out from the others is the need to have a continuous interface design, for the process of information transfer with fewer steps towards a new device. Additionally, in [19], the authors consider that this aspect could improve the user´s experience when interacting with multi-devices in the development of tasks.

Table 1: Summary of related works

Work	Collaborative	Problems
Koren el at. (2013)	Yes	When the transfer of activity states is made to a new device, there is loss of information.
Cabarcos (2012)	No	The entire state of the task is not preserved.
Cheng (2012)	No	Conflict when several devices share information.
Ghiani et al. (2012)	Yes	Registration to the platform is required to obtain continuity in the devices.
Salmien et al. (2007)	No	Additional steps that users seek to avoid.
Pyla et al. (2009)	No	It does not allow working in parallel in a task with two devices.

In our review of the literature, limited efforts were found that seek to provide continuity in the workflow through multi-devices. Table I summarizes the problems of the papers presented in this section; it is also indicated that only two out of the six works have a collaborative approach as proposed in this research work.

4. Challenges and opportunities to support the continuity of the workflow.

In an exploratory way, we conducted a preliminary study with two teams of five members, each of which held a Collaborative

Activity that included two tasks; the Google Drive® tool was used to perform the tasks. In the first task, they used their computer; once finished this, they had to change device. The second task was developed using their cell phone. After performing the activity by teams, the users were questioned about their experience when doing the activity in multi-devices.

As a result of the exploratory study, we observed that the majority of users usually do tasks through their different devices, but they express displeasure when they need to execute a series of steps to change the device, such as opening the application in the cell phone or downloading the advance in the new device; reason why some users requested to continue the activity from their computer, to avoid extending the time of completion of the task due to interruptions.

Therefore, within the identified challenges and opportunities, is to build a mechanism for the development of Collaborative Systems that transfers information between multi-devices with the least number of interruptions, achieving so that users can work on their tasks not only from their office, school or area where they normally do it, but from any context in which they find themselves and wish to continue working through the device that best adapts to the context. In this way, the user would be provided with a way to carry out Collaborative Activities from any of their devices whenever they wish, according to their needs and interaction preferences, and without being limited to working only in specific spaces.

5. Conceptual model for the continuity of the workflow

As a consequence of the analysis of the works related in this research, this article proposes the Model 4C's, as a frame of reference to provide the Collaborative Systems developers with the continuity element.

With the Model of the 4C's, the number of interruptions can be reduced through continuity support, to minimize additional steps when the user resumes work on a new device. Another contribution of the Model of the 4C's, is to allow users to carry out collaborative activities in multi-devices without affecting the workflow of the CAs by the operating system or the user's context change.

The Model of the 4C's is an instance of the Model 3C's, which arises from the models: 3C's [2] , [19] , Mars [20] and CAMCOS [21], taking components such as: communication, cooperation, coordination, workspaces, actors, interactions; which in turn are linked to the continuity element proposed in this work. The 4C's model is shown in Figure 2.

In a Collaborative Activity, groups of actors (users) participate in a group work space to carry out joint activities; These actors also have an individual work space, a space in which each user carries out their activities independently. Within both spaces, users perform different interactions that represent actions to complete a particular activity, which are executed within the three properties of the CS: communication, coordination and cooperation; but, in addition, continuity is required to offer the user the possibility of interacting through different devices during the performance of a task.

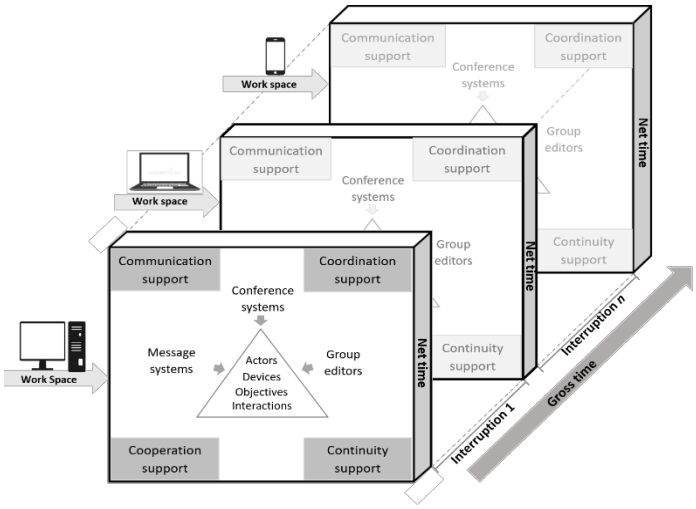

For this reason, it is necessary to include in the 3C's model of [4] the continuity element, which provides the user with permanence of the last status of the task when a context change is presented, that is, when the user for external reasons or preference of interaction is in the need of leaving the device with which he initiated the CA and requires to retake it in a different device. In order to provide continuity to the CA workflow through multi-devices, the 4C's model considers 8 elements: 1) Family of actors, 2) Actors, 3) Roles, 4) Objects, 5) Tasks, 6) Interactions, 7) Artifacts and 8) Work spaces; which are described in Table II. These elements are interrelated to propitiate an environment that minimizes interruptions in the sense that the statuses of each of them can be transferred to another device.

Table 2: Elements of the 4C′s model for collaborative applications.

Elements	Description
Family of actors	Set of names of actors where each actor has a different role.
Actors	People or software that carry out CA, through the interaction of different artifacts
Roles	Role that each user plays within the realization of an AC.
Objects	Everything that the actor can manipulate through interactions to achieve goals.
Actions	Actions that the user carries out to fulfill the collaborative activity.
Interactions	Realization of an action by a user through different artifacts within the system.
Mechanism	Hardware that the user uses to carry out his AC, within the SC, such as cell phone, tablet, laptop, desktop computer, among others.
Workspaces	Place where actors perform their actions in a group or individual way through an mechanism.

6. Conceptual architecture

Based on the 4C's conceptual model, we designed a conceptual architecture that supports the continuity of the CA workflow, through which the user can work in a collaborative activity from different mobile devices with a reduced number of interruptions in the process of information transfer and status of the task. The proposed architecture is shown in Fig. 3.

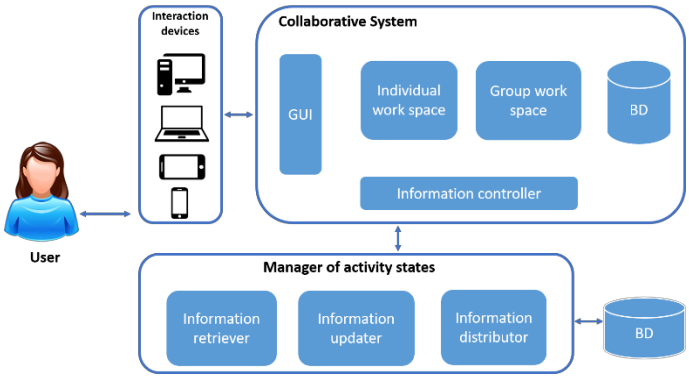

Figure 3: Conceptual architecture of the 4C's model

The continuity support starts once the user selects the device to start the CA. The interaction device is the means of communication between the application and the user. It is responsible for sending requests to the system in order to obtain updated information, and the system receives these requests through the activity's status manager.

Within the activity's status manager, three components are considered: an information retriever, an information updater and an information distributor. The information retriever obtains the last modifications of the users, in addition to the last workspace where they stopped.

The information updater is responsible for unifying the information of the individual and group workspace of the users and generates a new version of the progress of the team's work. When the user wants to resume the activity in a new device, the information distributor obtains the latest version of the work's progress and shows it to the user from the workspace in which he/she is working, supporting in this way the continuity of the workflow of the collaborative activity in multi-devices.

7. Case study

Based on the elements of the 4C's model and the conceptual architecture proposed above, a case study is being addressed through a scenario where, during the process of developing an CA, it is required to transfer the information to different mobile devices, in order to test whether the elements identified in the conceptual architecture are sufficient to provide the user with a continuous workflow, in the performance of collaborative activities in multi-devices.

The case study was modeled so that a team of actors worked on different activities for a common goal (to prepare a dish and generate a recipe). There are three types of actors: the administrator (teacher of the cooking school), the team representative and the members of the work team. Each actor plays a role within the collaborative activity; the administrator is the evaluator of the final product that each team elaborates, the team representative is the organizer of activities within the team and the member of the team is the buyer of ingredients. The actors interact with different artifacts during the collaborative work process such as: a desktop computer or a laptop to send the list of ingredients to the work team, as well as to make the recipe for the final product; a cell phone to perform tasks that require user mobility such as going to a supermarket to buy the ingredients of the dish; a tablet where users can count on a broader work space compared to the telephone, but also with mobility in the different workspaces where the actors must move to meet the objective of the activity.

The design of the Co-Kitchen system was made using the user-centered design methodology, an approach that allows iterations with the design throughout the life cycle of the product and in this way to redesign the system in order to meet the expectations and needs of end users [22]. Within the work framework for the design of human-centered interactive systems [23], the design process starts from the understanding of the context of use to specify the requirements of users, make a proposal of design solution and finally evaluate the design.

Phase one of the design process has been specified at the beginning of this section, where the modeled study case is detailed. Once analyzed and understood the context of use, we identified the requirements that the actors have in accordance with what they do within the system; in this way we knew the functionalities that the system should provide. In Table III, the functionalities of the system are described.

Table 3: Functions of the prototype Team Cooking

Function	Description
Create team	The administrator can create a work team.
Create list of ingredients	The administrator generates a list of the ingredients that the team must use to prepare a dish.
Assign tasks	The team representative is responsible for assigning tasks to each member of the team. Tasks such as buying ingredients, looking for kitchen utensils, lighting the oven, among others.
Create recipe	All the team at the end of the proposed dish, should generate a recipe for cooking it; for this each one must describe within the kitchen format the procedure for the realization of it, resulting in the recipe of the dish.

Once the requirements and functionalities that the system should provide the user in order to carry out his tasks were identified, the next step was to create the proposed design solution, which is shown and described below in Figures 4, 5, 6 and 7.

For the design of the proposal we use standard components such as: buttons, menus, text fields, etc., as well as: pointers, chat, and lists of connected users, according to [24] [25], who propose to simplify the development of groupware interfaces and to reduce the time of information search by grouping related elements in such a way that it is easy for the user to identify in which section is the element that he requires in order to perform a task.

In Figure 4, the start screen that the team representative actor displays when logging into the system is displayed. On the left side are the actions that can be executed within the system, in the center part of the screen you can see the work area and on the right

side there is the collaboration area where, through a list of connected users, the actor is kept informed of the presence of users who are collaborating during the realization of the CA and, at the top of that same side, we can also see the presence of each member, as well as the progress that each one of them has.

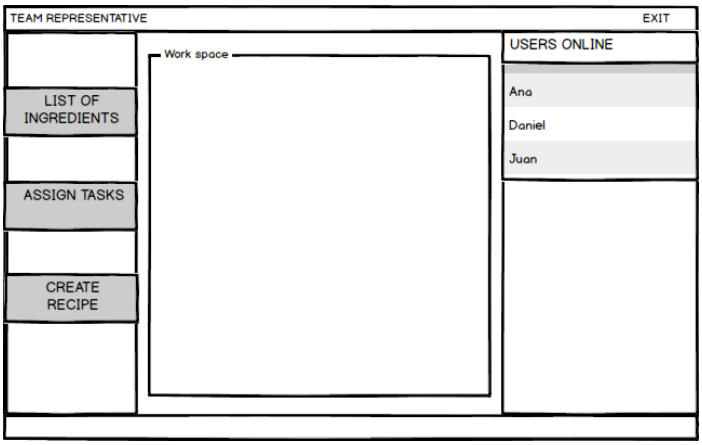

Figure 4: Team representative window.

Figure 5: Window to visualize list of ingredients.

In Figures 5, 6 and 7, what happens when the user clicks on one of the buttons on the left side is shown. When selecting "List of ingredients" (see Figure 5), in the work area the list of ingredients that was sent by the teacher of the cooking class is loaded. In case of selecting the option "Assign tasks" (see Figure 6), within the work area the team representative can enter the tasks assigned to each member of their team, which once assigned arrive as notification to the members to begin to work on them.

Finally, for the option to create a recipe (see Figure 7) within the work area, the actor works together with the rest of the team members in making the previously prepared recipe. Since it is a shared work area, each user has access to specific areas of the recipe according to the tasks previously assigned, which can be reported and described in the recipe.

The design of the solution proposal corresponds to a Web version loaded from a laptop or a tablet, but in the case of using a mobile device such as a cell phone, the design of the interface must be redesigned to fit a smaller screen, so that the work area is not affected and so the actor can work through it without complications.

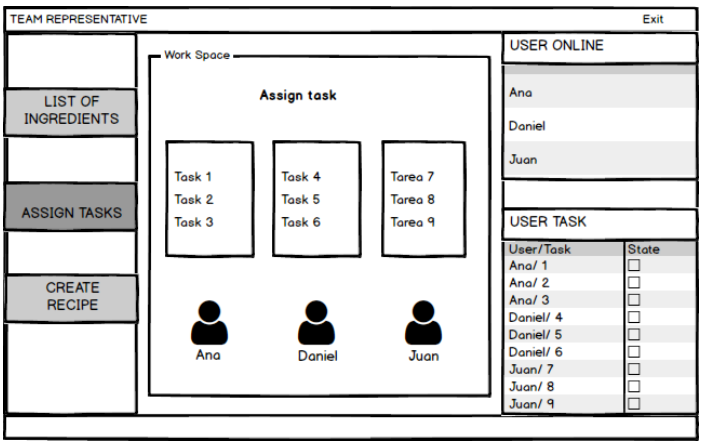

Figure 6: Window to assign tasks

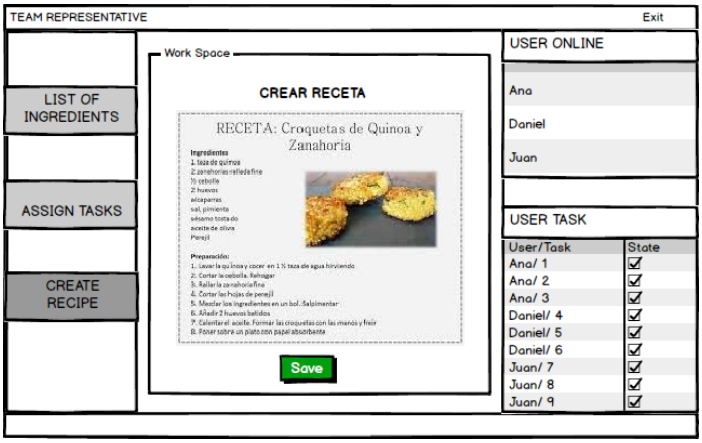

Figure 7: Window to create recipe.

8. Conclusions and future work

The advance of technology generates systems for collaboration between groups of people that interact with each other through the computer. Nowadays, it is possible to carry out an activity from different mobile devices such as: a cell phone, a tablet or a laptop, providing the user mobility to perform their activities. However, there is a gap in the conservation of the task status when moving to a new device. Therefore, this problem needs to be addressed in order to offer users systems that provide continuity to their workflow by requiring changes in the context of use during the performance of a task. That is why in this article we propose the model of the 4C's and the conceptual architecture to support users to carry out a collaborative activity in multiple devices in a shorter time. This proposal includes the continuity element of the model 3C's of [2], and the manager of states in the conceptual architecture, seeking to minimize the number of interruptions during the transfer of information from the collaborative activity through different mobile devices

As future work, we plan to continue with phase four of the framework for the design of interactive human-centered systems [23], corresponding to the evaluation of the design proposal

presented in this article, to subsequently work on a redesign under the observations and suggestions obtained from its evaluators.

Once the iterations of the design and evaluation process of the system design proposal have been finalized, we will give the appropriate follow-up to the construction of the Co-Kitchen system, to subsequently test the system and test whether our proposal effectively improves the continuity of the workflow of a collaborative activity when it is carried out through multi-devices, reducing the time in the interruptions that the user experiences when transferring and resuming the activity in a new device.

References

[1] L. G. M. -J. G. S. M. C. M.-G. a. E. B.-G. M. J. Avalos-Viveros, ""Conceptual Model to Improve Continuity of the Workflow of Collaborative Activities in Multi-Devices" International Conference on Information Systems and Computer Science (INCISCOS). IEEE, pp. 233-238, 2018.

[2] C. A. ELLIS, S. J. GIBBS y G. REIN, "Groupware: some issues and experiences" Communications of the ACM, vol. 34, n 1, pp. 39-58, 1991.

[3] M. Levin, Designing multi-device experiences : an ecosystem approach to creating user experiences across devices, O'Reilly Media, 2014.

[4] K. MAJRASHI, M. HAMILTON y A. UITDENBOGERD, "Evaluating Cross-Device Transitioning Experience in Seated and Moving Contexts" de Proceedings of the 22nd Pacific Asia Conference on Information Systems (PACIS 2018)(Yokohama, Japan2018), AISEL, Yokohama, Japan, 2018.

[5] G. GERONIMO, V. CANSECO y H. DE LEÓN, "Breve Introducción a los Sistemas Colaborativos: Groupware & Workflow" Temas-Universidad Tecnológica de la Mixteca, pp. 49-54, 2002.

[6] L. N. Yann Laurillau, "Clover architecture for groupware" In Proc. Conference on Computer supported cooperative work, ACM, pp. 236-245, 2002.

[7] C. G. a. S. G. D. Pinelle, "Task analysis for groupware usability evaluation: Modeling shared-workspace tasks with the mechanics of collaboration" ACM Transactions on Computer-Human Interaction (TOCHI), vol. 10, n 4, pp. 281-311, 2003.

[8] Y. Engeström, "Expansive learning at work: Toward an activity theoretical reconceptualization" Journal of education and work, vol. 14, n 1, pp. 133-156, 2001.

[9] L. G. M. Jiménez, Presencia social en sistemas groupware, Tesis doctoral, Facultad de Estadística e Informática, Universidad Veracruzana, Xalapa, México, 2016.

[10] D. R. J. K. M. B. S. E. V. R. a. B. M. L. J. Paay, "Investigating Croos-Device Interaction between a Handheld Device and a Large Display" In Proc. of the 2017 CHI Conference on Human Factors in Computing Systems. ACM, pp. 6608-6619, 2017.

[11] J. K. a. M. B. S. D. Raptis, "Continuity in multi-device interaction: an online study" In proc. of the 9th Nordic Conference on Human-Computer Interaction. ACM, p. 29, 2016.

[12] H. B. a. S. D. W. Jones, "Keeping found things found on the web" Tenth international conference on Information and knowledge management. ACM, pp. 119-126, 2001.

[13] D. S. a. T. S. I. Koren, "Session mobility for collaborative pervasive apps using XMPP" Pervasive Computing and Communications Workshops (PERCOM Workshop), IEEE Internacional Conference on. IEEE, pp. 169-174, 2013.

[14] F. A. M. R. S. G. A. M. L. a. D. D.-S. P. A. Cabarcos, "Susso: seamless and ubiquitous single sign-on for cloud service continuity across devices" IEEE Transactions on Consumer Electronics, vol. 58, n 4, pp. 1425-1433, 2012.

[15] S. H. a. J. R. T. Salminen, "Middleware based user interface migration: implementation and evaluation" In Proc. of the 4th international conference on mobile technology, applications, and systems and the 1st international symposium on Computer human interaction in bobile technology, ACM, pp. 358-363, 2007.

[16] B. Cheng, "Virtual browser for enabling multi-device web applications" In Proc. of the Workshop on Multi-device App Middleware. ACM, pp. 3-7, 2012 .

[17] F. P. a. C. S. G. Ghiani, "Push and pull of web user interfaces in multidevice environments" International Working Conference on Advanced Visual Interfaces. ACM, pp. 10-17, 2012.

[18] P. S. T. M. H. J. &. P.-Q. M. A. Pyla, "Continuous user interfaces for seamless task migration" International Conference on Human-Computer Interaction, Springer, pp. 77-58, 2009.

[19] E. I. B. M. D. C. M. a. E. M. L. G. Montané, "Studying Social Interactions in Groupware Systems" IEEE Latin America Transactions, vol. 13, n 10, pp. 3488-3497, 2015.

[20] M. R. a. S. T. C. Mezura-Godoy, "Mars: Modelling arenas to regulate collaborative spaces" In International Conference on Collaboration and Technology, Springe, pp. 10-25, 2003.

[21] C. M.-G. a. L. G. M.-J. E. Benítez-Guerrero, "Context-aware mobile collaborative systems: Conceptual modeling and case study" Sensors, vol. 12, n 10, pp. 13491-13507, 2012.

[22] J. R. a. D. Chisnell, Handbook of usability testing : how to plan, design, and conduct effective tests, Indianapolis: Wiley Publishing, Inc., 2008.

[23] ISO, E. N. 9241-210: Ergonomics of human-system interaction. Human-centred design for interactive systems, 2010.

[24] V. M. R. M. L. L. M. D. G. J. L. G. J. A. N. M. .. &. H. M. V. Penichet, " Una aproximación al proceso de diseño e implementación de interfaces de usuario para aplicaciones groupware" IX Congreso Internacional Interacción , pp. 19-28, 2008.

[25] C. Stephen, " A cognitive approach to the design of information graphics" CARNEGIE-MELLON UNIV PITTSBURGH PA DEPT OF PSYCHOLOGY, pp. AIP-143, 1991.

ASTES

Advances in Science, Technology and Engineering Systems Journal Vol. 4, No. 4, 485-502 (2019)

www.astesj.com

Special Issue on Advancement in Engineering and Computer Science

ASTESJ

ISSN: 2415-6698

Material, Structural Optimization and Analysis of Visible-Range Back-Illuminated OPFET photodetector

Jaya V. Gaitonde*, Rajesh B. Lohani

Electronics and Telecommunication Department, Goa Engineering College, Farmagudi-Ponda-Goa, 403401, India

ARTICLE INFO

Article history:
Received: 16 June, 2019
Accepted: 02 August, 2019
Online: 21 August, 2019

Keywords:
Material optimization
Structural optimization
Back-illuminated OPFET
Photodetector
Visible range
Visible/UV contrast ratio

ABSTRACT

High gain-bandwidth product and visible/UV contrast photodetectors are vital in Visible Light Communication (VLC) and Ultraviolet (UV) reflectance imaging applications respectively. We adopt material and structural optimization to perceive such photodetectors with back-illuminated Optical Field Effect Transistor (OPFET) wherein any potential difference in absorption coefficient of the semiconductor material between the visible and the UV range (higher in the UV region) can be explored at its full potential. The results have been analyzed using the photoconductive and the photovoltaic effects, the series resistance effects, scaling rules- induced effects, and channel length-variation effects. We consider the three most prominent and functional materials in the visible range (Si, GaAs, and InP) for material-based optimization. Structural optimization is performed employing a range of medium gate lengths. The gate electrodes utilized are Indium-Tin-Oxide (ITO) for Si and GaAs with high Schottky barrier heights of ~0.71 eV and ~0.98 eV respectively whereas the Schottky contact on InP is gold (Au) with a high barrier height of ~0.8 eV. The operating visible and UV wavelengths are 600 nm and 350 nm respectively. The results suggest that GaAs OPFET has wide bandwidth potential in the gigahertz range apart from its high sensitivity and visible/UV contrast features. The InP-based OPFET exhibits high sensitivity and sub-gigahertz frequency response; and can compete or surpass the GaAs OPFET in terms of the visible/UV contrast ratio. The Si OPFET shows bandwidth in the megahertz range along with high sensitivity but exhibits low contrast ratio. The structural parameters have a significant effect on the detector response. The results are in-line with the experiments. This paper reflects the performance of the investigated detectors towards the said applications through optimization and the associated analysis represents the dependence of the obtained response on the device material and structural parameters, thus, opening the door for further research.

1. Introduction

This paper is an extension of work originally presented in *The IEEE Conference on Emerging Devices and Smart Systems* (*ICEDSS'18*) [1].

Visible-Light Communication (VLC) is an emerging alternative to RF-based communication to suffice for the increasing demand for bandwidth. Its potential applications include Li-Fi (Light-Fidelity) Networks, vehicle to vehicle communication, robots in hospitals, underwater communication, and information displayed on sign boards [2]. The photodetectors contributing to VLC should feature high gain-bandwidth product apart from low dark current. Presently, the state-of-art photodetectors being employed in VLC include the p-i-n and the Avalanche photodiodes (APDs). p-i-n detectors provide high speed detection but without amplification whereas the APDs offer high gain but as the frequency increases, the gain reduces significantly. On the other hand, Ultraviolet (UV) reflectance imaging is a well-known application in biomedical engineering. It requires photodetectors with high visible/UV contrast ratios alongwith high visible sensitivity and low dark current. There is no much information available on the visible/UV contrast features of any photodetector. The contrast ratio should be high in order to appropriately control the ambient visible light in the presence of background UV radiation during imaging and enabling erroneous

*Jaya V. Gaitonde, Goa Engineering College, Farmagudi-Ponda-Goa-India, 403401, Mobile: (+91) 9420687029, Email: jayagaitonde46@gmail.com

operation. Low dark current improves the device performance. Both the applications have one thing in common: they need photodetectors operating in the visible range. Three most featured materials capable of operating in the visible region include Si, GaAs, and InP. These possess distinct electrical and optical properties which motivate one to conduct research using these materials. One potential candidate to cater to high gain-bandwidth product applications is a phototransistor or a photoFET. Optical Field Effect Transistor (OPFET) or optically controlled Metal-Semiconductor Field Effect Transistor (MESFET) has been a widely studied device over the past few decades for its applications as photodetectors, optically-controlled amplifiers, oscillators, and switches [3]-[13]. However, the research lacks the assessment or the impact of the OPFET device incorporating these materials from the optimization point of views i.e. material and structural optimization. Further, analysis of the attained results and the correlation of the detector responses with the material and the structural parameters can substantiate further research. Thus, in this paper, we call for material and structural optimization of the visible-range back-illuminated OPFET detector for communication and visible/UV contrast applications. The back-illuminated OPFET model (without substrate effect) is purposely chosen so that any significantly high difference in absorption coefficient at the visible and UV wavelengths is potentially used for contrast applications. The transparent gate materials considered for simulation are Indium-Tin-Oxide (ITO) for Si and GaAs whereas gold (Au) for InP. The corresponding barrier heights are ~0.71 eV, ~0.98 eV, and ~0.8 eV respectively. Possibly large barrier heights have been chosen since these can have considerable positive effect on the photovoltage and the photoconductive effect through the modulation of the depletion width.

A theoretical semi-analytical model accounting for photoconductive and photovoltaic effect is presented. The continuity equations have been solved analytically to yield the carrier densities whereas the charges are calculated numerically using the Trapezoidal method. The total drain-to-source current is estimated using the model given in [14]. The trap effects have been neglected in this work.

We begin with the theory followed by the results, discussion, and the relevant analysis. We conclude with a brief summary.

2. Theory

The back-illuminated device structure is schematically shown in Fig. 1. The gate is shorted to the source for a reduction in the number of power supplies. The channel is n-type uniformly moderately doped whereas the substrate is p-type semi-insulating. The illumination is guided by a fiber inserted from the rear side of the device through the substrate upto the active layer-substrate interface. The radiation is absorbed in the channel and the substrate regions creating electron-hole pairs. The holes contribute to photovoltage after crossing the Schottky junction which increases the drain-to-source current through a reduction in the depletion width (photovoltaic effect). On the other hand, the electrons are directed toward the channel which increases its conductivity upon the application of the drain-to-source voltage (photoconductive effect).

The device characteristics are depicted by the three regions of operation: the linear, the pinch-off, and the saturation regions. The drain-to-source saturation current depends upon the total charge, the gate width, and the saturation velocity and is limited by the voltage drop across the source series resistance. The drain-to-source conductance also depends upon the total charge (however, at zero drain-to-source voltage), the carrier mobility, and the gate width; is inversely proportional to the gate length, and is limited by the source and drain series resistances. The total drain-to-source current is given by [14]:

$$I_{ds} = I_{dss}(1+\lambda V_{DS})\tanh(\eta V_{DS})$$

where the symbols have the same meaning as stated in [14]. The parameter η is defined as the ratio of the drain-to-source conductance to the saturation current as the drain-to-source voltage tends to zero. Thus, on one hand, the drain-to-source current is directly proportional to the saturation current; on the other hand it is inversely proportional to the saturation current through the parameter η under the hyperbolic tangent expression. This shows that there is limitation on the total current that can be achieved. The parameter η also signifies that the total current is directly proportional to the conductance as V_{DS} tends to zero under the hyperbolic tangent expression. Hence, the conductance as V_{DS} tends to zero and the saturation current are the prominent factors determining the total drain-to-source current apart from the voltage, V_{DS}, and the total current is limited by the source and drain series resistances.

Under illumination, the total charge is boosted due to the photovoltaic and the photoconductive effects which enhances the saturation current and the drain-to-source conductance limited by the series resistances. In addition, with the increase in the optical power, the photovoltage increases reducing the series resistances and augmenting the current. The source and drain series resistances are calculated based on the method provided in [15]. The reader is advised to follow [1] for the modeling equations and the calculation of the carrier densities, photovoltage, and the total charge.

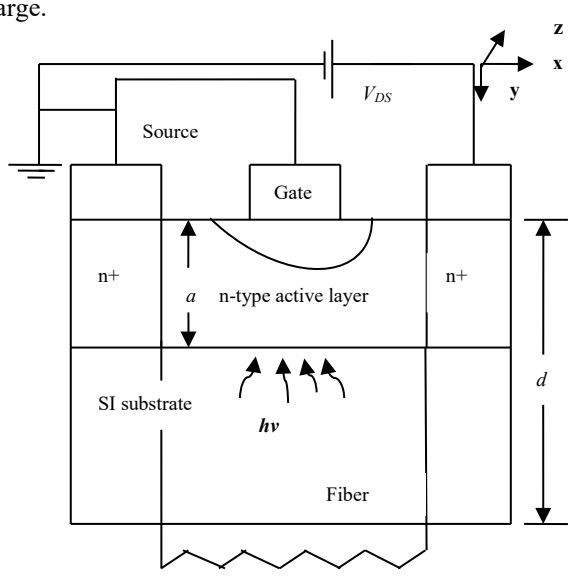

Figure 1. The schematic structure of the back-illuminated model of OPFET.

The detector parameters such as responsivity, dark current, and visible/UV contrast ratio are defined in [1]. Here we define the 3-

dB bandwidth and the unity-gain cut-off frequency (f_T) of the device. The bandwidth is the highest modulation frequency which the photodetector can detect without errors. Mathematically, it is given by the frequency at which the photocurrent response falls to 0.707 times its DC response. The unity-gain cut-off frequency is the operating frequency at which overall gain of the device falls to unity. The f_T is given by the ratio of the transconductance to 2π times the gate-to-source capacitance. The transconductance is the variation in the drain-to-source current with the variation in the gate-to-source voltage and is the amplification factor. The gate-to-source capacitance is the change in the space charge below the gate and its sidewalls with the change in the gate-to-source voltage and is a switching parameter. Thus, fT represents the amplification bandwidth of the device. The simultaneous detection-cum-amplification bandwidth is given by either of the two (3-dB bandwidth or the f_T value), whichever is smaller.

3. Results and Discussion

The simulations have been carried out in MATLAB with MEX coding feature. The results have been validated with experimental work published elsewhere [3] (Figure 2). The results have been compared with the commercially available software (Visual TCAD)-based simulations and have shown close resemblance (Figure 3) (Gate length of 4 μm, gate width of 4 μm, active layer thickness of 0.27 μm, and doping concentration of 4×10^{22} /m^3). The drain-to-source bias voltage is variable whereas the gate-to-source voltage is set to zero volts. The wavelengths used are 600 nm for the visible light and 350 nm for the UV radiation. The photon flux densities of 10^{16}, 10^{19}, and 10^{22} /m^2-s used in these simulations correspond to optical power densities of 0.33 μW/cm^2, 0.33 mW/cm^2, and 0.33 W/cm^2, respectively at 600 nm and 0.57 μW/cm^2, 0.57 mW/cm^2, and 0.57 W/cm^2 respectively at 350 nm. The structural optimization is performed over a wide range of medium gate lengths from 3 μm to 5 μm. However, only the four most relevant sets are provided here for comparison. The design variables are chosen based on the scaling rules stated in [16]. The materials being employed are Si, GaAs, and InP for the back-illuminated OPFET device with the gate electrodes being Indium-Tin-Oxide (ITO) for Si and GaAs, and gold (Au) for InP. The simulated optimization results are presented in Table I. The parameters used for calculation are given in Table II. The comparison with the state-of-art photodetectors and amplifiers is provided in Table III showing significantly enhanced response. Figure 4 depicts the drain-to-source current responses under dark and illumination for all the three devices at a gate length of 3 μm and an active layer thickness of 0.27 μm at an intensity of 10^{19} /m^2-s clearly showing the sensitivity to visible light. Figure 5 portrays the frequency responses of the three devices at a gate length of 3 μm and an active layer thickness of 0.27 μm at an intensity of 10^{19} /m^2-s demarcating that the GaAs, InP, and Si OPFET devices operate at high, moderate and low data frequency ranges respectively.

3.1 Series resistance and photovoltage analysis in Si, InP, and GaAs OPFETs

Beginning the discussion with the Si back-illuminated OPFET, this device exhibits the largest series resistances among all the material devices with similar dimensions in the visible range. With the smallest Schottky barrier height of ITO-Si junction (~0.71 eV), the series resistance ought to be the smallest due to the larger undepleted channel thickness in the spacing between the gate and the source, and the gate and the drain (depletion width is dependent upon the barrier height). This should have drawn larger current through the channel charge. However, due to the low electron mobility (~0.09 cm^2/(V.s)) and the said barrier height, upon which the current flowing in the spacing between the gate and the source, and the gate and the drain depends upon (barrier height directly affects the voltage drop across the channel), the current significantly falls. This raises the series resistance value to compensate for the fall with the increment in the depletion width through the voltage drop across the series resistance. Other materials, GaAs and InP exhibit lower and almost equal series resistances. This is attributed to the higher mobility of GaAs (~0.5 cm^2/(V.s)) and higher barrier height of ITO-GaAs junction (~0.98 eV) (through the voltage drop) which tend to increase the current in the spacing and lower the resistance. The same barrier height also tends to decrease the current (through the increment in the depletion width) and raise the resistance, however, the factors supporting the lowering of the resistance supersede those raising it, resulting in net reduction of resistance. For InP, the mobility is (~0.43 cm^2/(V.s)) and the barrier height of Au-InP junction is (~0.8 eV). In this case, the mobility is significantly high whereas the barrier height is moderate. With the moderate barrier height, the series resistance ought to be between that of Si and GaAs, but due to the high mobility the series resistance in InP features the same as that in GaAs. The series resistances play an important role in limiting the photocurrent. The series resistances decrease with illumination.

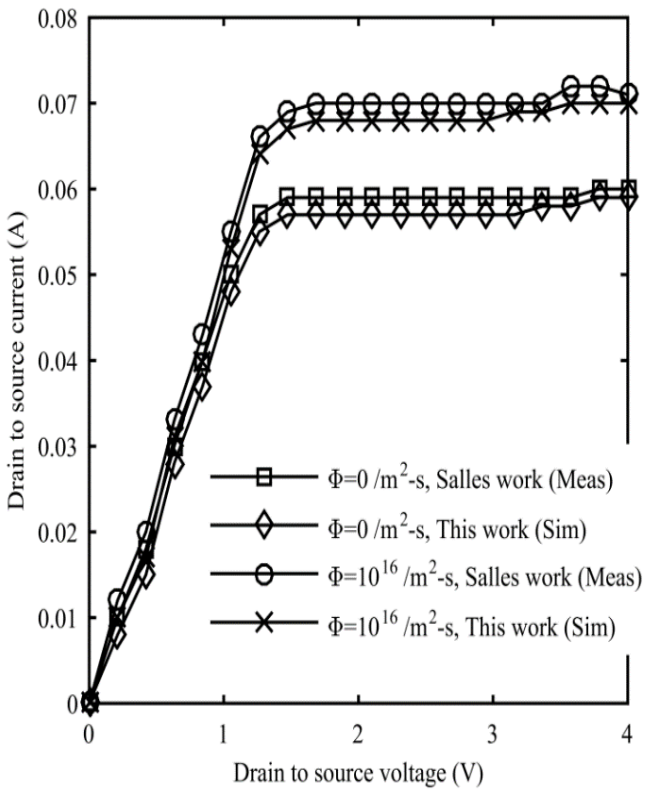

Figure 2 Comparison of the present model results with the experiments in [3].

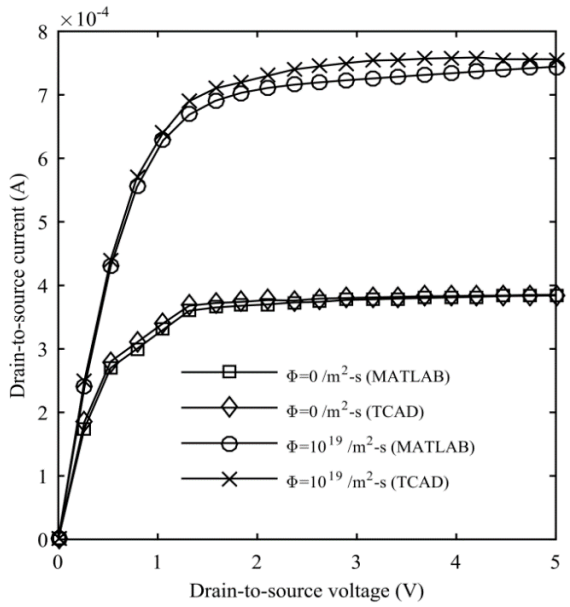

Figure 3 Comparison of the present model results with the simulations using Visual TCAD Software.

The photovoltage generated is almost the same in both Si and InP devices (~0.27 V, ~0.46 V, and 0.61 V) in the visible range considering most of the sets. This can be explained as follows: The photovoltage depends upon the photogenerated hole density crossing the Schottky junction which in turn, depends upon the absorption coefficient, the photon flux density, the hole lifetime, and the saturated hole velocity. The absorption coefficient of Si at 600 nm is 7.5×10^5 /m, the hole lifetime is 75 µs, and the saturated hole velocity is ($\sim6.3\times10^4$ m/s). On the other hand, the corresponding parameters for InP are 1×10^7 /m, 0.3 µs, and ($\sim5.6\times10^4$ m/s) respectively. The hole density is directly proportional to the absorption coefficient, the photon flux density, and the hole lifetime ($\alpha\Phi\tau_p$), whereas it is inversely related to the saturated hole velocity through ($1+\alpha v_y\tau_p$).The values suggest that the terms directly as well as inversely related to the hole density are almost the same in both the cases since any difference in individual parameters between the two material systems is cancelled out when their product is evaluated. One more parameter upon which the photovoltage is dependent upon is the reverse saturation current density through the Schottky barrier height. The photovoltage is inversely related to the saturation current density, and the saturation current density is inversely related to barrier height. Hence, the photovoltage is directly related to barrier height. Since, the barrier heights of ITO-Si andAu-InP junctions are (~0.71 eV) and (~0.8 eV) respectively, the photovoltage tends to be more in the InP device. However, since InP possesses a high absorption coefficient of 1×10^7 /m corresponding to an absorption depth of 0.1 µm, the hole density experiences an exponential decrease with distance and fewer holes cross the Schottky junction as compared to the Si device. The moderate absorption coefficient of 7.5×10^5 /m results in a large absorption depth thus, causing a lesser degradation of hole density with distance. As a result, the photovoltage developed is almost the same in both the cases. On the other hand, the photovoltage generated in GaAs OPFET is enhanced (~0.398 V, ~0.576 V, and ~0.755 V). This is due to the moderate absorption coefficient of GaAs in the visible region (4×10^6 /m), the higher saturated hole velocity ($\sim9\times10^4$ m/s), and the significantly higher Schottky barrier height of the ITO-GaAs junction (~0.98 eV) superseding the effect of lower hole lifetime (10^{-8} s). The saturated hole velocity positively affects the photovoltage through the photogenerated hole current density in the equation for photo voltage.

At the lowest gate length under consideration of 3 µm and the highest doping concentration of 5×10^{22} /m^3 (gate length-doping concentration product is constant from scaling rules [16]) with an active layer thickness of 0.15 µm, the OPFET devices exhibit the lowest dark and photocurrents among all the sets. This is ascribed to the very less active-layer thickness, as well as the low gate length and the gate width along with the reduced sensitivity at the higher doping concentrations. This proportionally decreases the current although the high doping concentration induces significant channel charge.

3.2 Analysis of Si OPFET at 3 µm gate length and 0.15 µm channel thickness

The drain-to-source currents obtained using Si OPFET are (0.36 mA, 0.9 mA, 1.7 mA, and 15.6 mA). The large series resistances owing to the small active layer thickness (0.15 µm) and significantly high barrier height (~0.71 eV) limit the said currents. At the flux density of 10^{16} /m^2-s, the photovoltaic effect is significant (0.28 V) whereas the photoconductive effect is negligible as compared to the photovoltaic effect (due to the lower power level) resulting in a current of 0.9 mA. The photoconductive effect will add to the response only when the photoconductive charge is comparable to the doping-induced charge. As the flux density is increased to 10^{19} /m^2-s, the photoconductive effect also contributes in addition to the photovoltaic effect (0.46 V) owing to the higher power level and the long electron lifetime (75 µs). Most of the photoconductive contribution emanates from the depletion region since the major portion of the channel is depleted owing to high barrier height, small channel thickness, and the large series resistance which incurs significant voltage drop across it. This results in a quite high current of 1.7 mA. At the flux density of 10^{22} /m^2-s, the current is significantly enhanced (15.6 mA) owing to the considerably high contribution from the photoconductive effect in the depletion region. There is no photovoltaic contribution; instead the device shows negative sensitivity i.e. increase in depletion width with illumination. This arises due to the substantially high current from the photoconductivity which incurs large voltage drop across the series resistance. Thus, the depletion width increments with illumination surpassing the effect of photovoltage-induced reduction of the depletion width. As such, the responsivities attained are (5.3×10^8 A/W, 1.32×10^6 A/W, and 1.49×10^4 A/W) which are significantly high owing to the above discussed phenomena and the low dark current. The 3-dB bandwidths exhibited by this device are (0.16 MHz, 0.136 MHz, and 0.57 MHz). These megahertz range bandwidths are due to the long electron and the hole lifetimes (75 µs) upon which the bandwidth is inversely related through the modulation of carrier lifetime with frequency. At the lowest flux density, the bandwidth is 0.16 MHz due to the contribution from the photovoltaic effect alone. At the higher flux density, the bandwidth falls to 0.136 MHz due to both photovoltaic and photoconductive effects adding to the response.

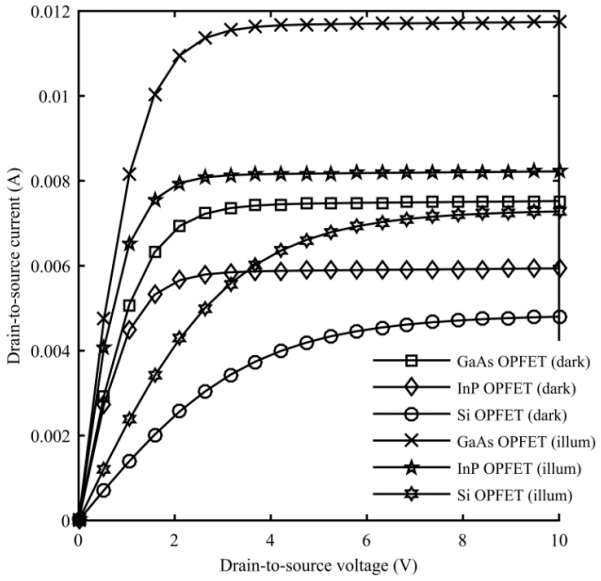

Figure 4 Comparison of the Si, InP, GaAs OPFET devices under dark and illumination.

This can be explained by the fact that when the identical frequency responses of two independent comparable effects are added, the net frequency response exhibits reduced bandwidth as compared to the individual ones. As the flux density is increased further, the bandwidth rises to 0.57 MHz. This is attributed to the sole and substantially high contribution from the photoconductive charge as compared to the previous responses. The transconductances obtained are the lowest among all the sets (1.4 mS, 2.4 mS, 3.9 mS, and 29.1 mS) due to the reduced dimensions at this gate length which decreases the overall current and the reduced sensitivity at high doping concentrations. Note that at constant photovoltage, the depletion width sensitivity is higher at lower doping concentrations. The transconductance increases with the increase in the optical power [6], [7], [9], [10] since at a constant doping concentration, the depletion width sensitivity is higher at larger photovoltages. However, at the highest flux density, this does not hold good where the device experiences negative sensitivity. In this case, it is the high photoconductive charge which results in high saturation current and is independent with the change in the gate-to-source voltage due to the complete depletion of the channel. The drain-to-source conductance evaluated at zero drain-to-source voltage also is high due to the induced charge and is sensitive to the variation in the gate-to-source voltage since the channel is undepleted (zero drain-to-source voltage). Further, the conductance is affected by the dependence of the series resistances on the gate-to-source voltage. The above reasons suffice for the observed high transconductance. The gate-to-source capacitances are also the lowest among all the sets (0.0546 pF, 0.084 pF, 0.105 pF, and 0.0076 pF) owing to the same reasons as applicable to the transconductances, however, here the gate region space charge replaces the drain-to-source current. The reasons hold good for the lower flux densities. However, at the higher flux density, the space charge is considerably reduced due to the photoconductive electrons in the depletion region de-ionizing the charged donor ions. Also, the gate-to-source capacitance is independent of the change in the photoconductive charge (which is a major contributor to the response) since it is a measure of the space charge variation with the gate-to-source voltage. These reasons explain the significant drop in the capacitance at the higher flux density. As such, the unity-gain cut-off frequency attained is (4.08 GHz, 4.53 GHz, 5.89 GHz, and 606.7 GHz). Under UV illumination of 350 nm, the photovoltage is slightly enhanced (0.31 V, 0.49 V, and 0.61 V) as compared to that under visible light since Si possesses a larger absorption coefficient of 1×10^7 /m at the UV wavelength. The smaller active layer thickness (0.15 μm) enables significant number of holes to cross the junction before the generated carriers experience degradation due to the dependence on the distance. The series resistances experienced by the device are almost the same due to the slight difference between the photovoltages. The drain-to-source current is almost the same at the lower intensity (1 mA) whereas there is a considerable boosting of the current at the higher intensities. This is attributed to the large absorption coefficient of Si under UV light which augments the photoconductive charge in the depletion region. At these intensities, the large currents develop large voltage drops across the series resistances thus inducing negative sensitivity and eliminating the photovoltaic contribution. The currents so obtained are 7.9 mA and 16.1 mA. The lesser enhancement of current at the flux density of 10^{22} /m^2-s is due to the limitation of the drain-to-source conductance (at zero drain-to-source voltage) by the series resistances and the large saturation current due to the induced charge also limiting the factor η as discussed earlier thus, restricting the total drain-to-source current. As such, the responsivities attained are (3.53×10^8 A/W, 4.33×10^6 A/W, and 9×10^3 A/W). The responsivities at the flux densities of 10^{16} and 10^{19} /m^2-s are slightly lower than the visible range responsivities. This is because the device uses more power to detect UV light than the visible light since the power is directly proportional to the photon energy. Hence the visible/UV rejection or the contrast ratios are very low (1.5, 0.3, and 1.65).

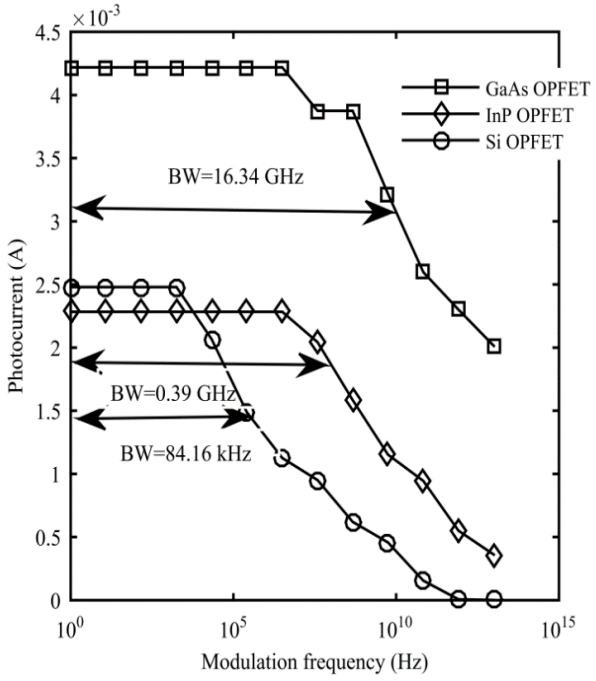

Figure 5 Frequency responses of the Si, InP, GaAs OPFET devices.

3.3 Analysis of InP OPFET at 3 μm gate length and 0.15 μm channel thickness

Discussing the InP OPFET with a gate length of 3 μm and an active layer thickness of 0.15 μm, the photovoltage is slightly enhanced (0.297 V, 0.476 V, and 0.65 V) as compared to the Si OPFET due to the small active layer thickness which eliminates the degradation of the generated carriers with distance as would occur in other cases. The series resistances are significantly lower than the Si OPFET but comparatively higher than that at higher gate length devices due to the reasons discussed earlier. The conducting photovoltaic charge is higher in the case of the InP OPFET in the presence of series resistances. This is because, the Si device possesses larger series resistances which incurs considerable voltage drop across these resistances thus, limiting the photovoltaic effect. Further, the photovoltage is slightly higher in the InP detector. This charge determines the saturation current. Hence, the saturation current is higher in the InP device. The conducting photovoltaic charge in the absence of series resistances i.e. at V_{DS}=0 V, is lower in the case of InP OPFET. The above emanates from the fact that at a fixed doping concentration and at a given gate-to-source voltage, the depletion width sensitivity to illumination is higher in both the lower barrier height and the lower dielectric constant device i.e. Si device. This charge determines the drain-to-source conductance at V_{DS}=0 which is higher in the Si OPFET however, is limited by the presence of series resistances which are larger in the case of Si detector. One more factor which differentiates the two devices is the electron mobility upon which the conductance depends upon and is substantially higher in the case of InP. The dark current is lower in the InP device due to the higher barrier height. The above factors result into slightly higher photovoltage-induced currents (1.3 mA, and 2.2 mA) in the InP OPFET than the Si OPFET. At the flux density of 10^{22} /m^2-s, the photoconductive charge from the depletion region alone contributes since the device exhibits negative sensitivity as mentioned earlier and the channel is totally depleted. The InP detector generates a current of 27.8 mA as opposed to 15.6 mA in the Si OPFET. This can be explained as follows: Since the absorption coefficient of Si is moderate (7.5×10^5 /m), there is almost uniform photogeneration throughout the fully depleted channel of 0.15 μm thickness. The absorption coefficient of InP is high (1×10^7 /m) due to which only a part of the depletion region carries significant number of carriers. Thus, the contributing charge is one order higher in the case of Si OPFET than the InP OPFET. This results in a large saturation current in the Si device. However, the conductance is lower in the Si device owing to lower electron mobility and larger series resistances. Since the saturation current appears in the numerator and as well as the denominator (through the hyperbolic tangent expression (see (1))), the large saturation current also limits the total drain-to-source current in the Si device. As a cumulative effect, the current is larger in the InP OPFET. These currents are the lowest among all the sets due to the reasons discussed earlier in the case of the Si OPFET. The 3-dB bandwidths achieved are (67.35 MHz, 0.26 GHz, and 3.84 MHz). These bandwidths are higher than that in Si OPFET owing to the shorter hole and electron lifetimes (0.3 μs) in InP as compared to 75 μs in Si. The boosting of the photovoltage as the intensity is increased from 10^{16} to 10^{19} /m^2-s also boosts the bandwidth from 67.35 MHz to 0.26 GHz. At the flux density is raised to 10^{22} /m^2-s, the bandwidth drops to 3.84 MHz due to the following: Under dc conditions or at lower frequencies, the photoconductive effect is significantly high and is the sole contributor. However, as the frequency is increased, the photoconductive contribution starts decreasing due to the dependence of the electron lifetime on frequency. This reduces the voltage drop across the series resistance thus, widening the effective channel width and increasing the photovoltaic contribution. Hence, at the juncture of the 3-dB point, both the effects effectively contribute causing the drop in the bandwidth. The responsivities attained are (9.97×10^8 A/W, 1.9×10^6 A/W, and 2.7×10^4 A/W) which are higher than that in the Si device due to larger photocurrents. The InP detector exhibits transconductances of (2.3 mS, 4.3 mS, 5.6 mS, and 6.7 mS). These values are higher than that for Si OPFET except at the flux density of 10^{22} /m^2-s. As explained earlier, the saturation currents, the drain-to-source conductances, and the mobility involved are higher in the InP device whereas the series resistances are lower in the InP device at the lower intensities. The depletion width sensitivity to the applied gate-to-source voltage with the other factors kept constant is higher in the lower barrier height and the lower dielectric constant device (Si OPFET). But, in practice, due to larger series resistances and the lower mobility of Si, the net effect is the larger sensitivity in the InP device. Further, the photovoltage is slightly larger in the InP device. Due to the above factors, the transconductances are higher in the InP OPFET at the lower flux densities. But at the intensity of 10^{22} /m^2-s, the channel is fully depleted. The depletion state does not affect the saturation current in terms of magnitude (it grows without bounds in spite of the presence of the series resistances). This is because, when the channel gets depleted (due to the large voltage drop across the series resistances), it is the photoconductivity in the depletion region which takes over role of the otherwise contributing photoconducting charge from the neutral channel region. Since the photoconductive charge in Si OPFET is very high and one order higher than that of the InP OPFET, the saturation current is considerably higher in the Si device. This current is insensitive to the applied gate-to-source voltage owing to the complete depletion of the channel. However, the drain-to-source conductance changes with the gate-to-source voltage since it is evaluated at V_{DS}=0 which means a finite undepleted channel width. This conductance is lower in magnitude as well as less sensitive to the change in the gate-to-source voltage in the Si detector due to the lower mobility and limiting effects of the series resistances. But, the effect of very large saturation current in the Si device supersedes the effect of lower conductance and its sensitivity to generate higher transconductance. The transconductance increases with the increase in the optical intensity due to the enhancement of the photovoltaic effect upto the flux density of 10^{19} /m^2-s and high contribution of photoconductive effect at the intensity of 10^{22} /m^2-s. On the whole, the transconductances obtained at this gate length are the lowest among all the sets due to the reasons stated earlier for the Si OPFET. The gate-to-source capacitances attained in the InP device are (0.034 pF, 0.0695 pF, 0.092 pF, and 0.016 pF). These values are lower than that of Si device. This is explained by the fact that at a constant or slightly varying photovoltage and a fixed doping concentration, the depletion width sensitivity to the applied gate-to-source voltage is larger for the lower barrier height (and dielectric constant) device i.e. Si OPFET. The capacitances increase with optical power and fall at the highest flux density and are lowest among all the sets due to the same reasons as described earlier in the case of Si device. The unity-gain cut-off frequencies

thus obtained are (10.76 GHz, 9.74 GHz, 9.65 GHz, and 65.4 GHz). Under UV illumination, the photovoltages developed are substantially lower (0.0943 V, 0.27 V, and 0.44 V) than that in the visible region owing to the very high absorption coefficient of InP in the UV region (7.6×10^7 /m).This generates significantly large number of carriers only upto a small distance from the absorption surface (i.e. the active layer-substrate interface). The generated carriers crossing the Schottky junction are considerably low due to the significant degradation of the carriers with distance (the active-layer thickness (0.15 μm) is much larger than the absorption depth (0.013 μm)). The drain-to-source currents obtained are (0.272 mA, 0.54 mA, 1.2 mA, and 30.1 mA). Due to the lesser photovoltages, the currents obtained are lower in the UV region upto the intensity of 10^{19} /m^2-s. At the flux density of 10^{22} /m^2-s, the current is higher (30.1 mA) owing to the substantially high contribution from the photoconductive effect in the depletion region emanating from the larger absorption coefficient of InP in the UV region. The photovoltaic effect plays no role at this intensity since the device exhibits negative sensitivity. The responsivities obtained are (1.53×10^8 A/W, 5.2×10^5 A/W, and 1.71×10^4 A/W) based on the above photocurrents and further assisted by the fact that the device uses more optical power in the UV region than the visible region. The visible/UV contrast ratios obtained are (6.516, 3.65, and 1.58).

3.4 Analysis of GaAs OPFET at 3 μm gate length and 0.15 μm channel thickness

Discussing the GaAs OPFET device possessing a gate length of 3 μm and an active-layer thickness of 0.15 μm, this device develops photovoltages of (0.41 V, 0.58 V, and 0.76 V) in accordance with [7] which are substantially higher than the Si and the InP devices. Under dark, the channel is totally depleted on account of a large Schottky barrier height of ITO-GaAs junction (0.98 eV). Thus, the current from the device channel ceases to exist but there is a small current flowing in the device due to the presence of the shunt resistance. The higher photovoltages ought to have produced larger photovoltaic charge responses as compared to the other detectors (InP OPFET). However, since the channel is deeply depleted (beyond the active-layer thickness), the developed photovoltages do not open the channel wide enough (of course, limited by the series resistances) as opposed to the InP device. The InP device is partially depleted under dark and the generated photovoltages (0.297 V, 0.476 V, and 0.65 V) are able to significantly reduce the depletion width thus yielding greater photovoltaic charges than the GaAs device. In spite of this, the drain-to-source currents (97.1 μA, 1.4 mA, 2.5 mA, and 54.9 mA) and the transconductances (0, 5.5 mS, 7.5 mS, and 67.2 mS) achieved in GaAs OPFET under illumination are higher than the InP device. This is attributed to the higher electron saturated velocity (1.2×10^5 m/s) of GaAs as compared to InP (7.6×10^4 m/s) which considerably increases the saturation current further assisted by slightly lower source series resistance in GaAs. Also, the slightly higher electron mobility of GaAs (0.5 m^2/(V.s)) as compared to InP (0.43m^2/(V.s)) and the lower source and drain series resistances in the GaAs device enhances its drain-to-source conductance even if the conductance in the absence of series resistances is almost the same in both the devices. As a result, the higher currents are attained. The larger transconductances emanate from the amplification of the charge due to the depletion width sensitivity to the applied gate-to-source voltage by the higher electron saturation velocity in GaAs producing larger change in the saturation current. Further, the amplification of the said charge under the absence of series resistance by the higher mobility of GaAs so also the lower series resistances results in larger variation in the drain-to-source conductance. This, on the whole, produces a larger change in the drain-to-source current with the applied gate-to-source voltage. Also, the photocurrents are slightly enhanced due to the lower dark current. At the flux density of 10^{22} /m^2-s, the photocurrent as well as the transconductance are considerably enhanced. This is owing to the boosting of the saturation current and the conductance due to the substantially high contribution from the photoconductive effect in the depletion region as a result of moderate absorption coefficient of GaAs and one order of magnitude higher lifetime (1 μs). The transconductance is much higher than the other two devices because of high saturation current and greater magnitude of the drain-to-source conductance as well as its higher sensitivity to the applied gate-to-source voltage. The gate-to-source capacitances under illumination (0.064 pF, 0.086 pF, and 0.018 pF), on the whole, are lower than the other devices due to the earlier stated fact that the sensitivity of depletion width to the change in the gate-to-source voltage is higher with devices bearing lower barrier height and lower dielectric constant when other factors are almost constant. The capacitance dependence upon the optical power is the same as analyzed with other devices. As such, the f_T values attained are (13.68 GHz, 13.79 GHz, and 596.5 GHz). The 3-dB bandwidths exhibited by the device are (1.5 GHz, 6.3 GHz, and 1.1 MHz) which are considerably higher than the other two detectors at the lower intensities owing to the significant photovoltaic effect and lower hole lifetime (10^{-8} s) with the photovoltage increasing with the optical power. However, at the higher intensity, the bandwidth falls due to the significant sole contribution from the photoconductive effect with a large electron lifetime of 1μs. The responsivities obtained are (1.24×10^9 A/W, 2.4×10^6 A/W, and 5.37×10^4 A/W) in line with [27] which are larger than the other two devices due to larger photocurrents. Under UV light, the response falls significantly (1.57×10^8 A/W, 6.4×10^5 A/W, and 2.56×10^4 A/W), due to the lower photovoltages (0.19 V, 0.37 V, and 0.55 V) owing to the larger absorption coefficient of GaAs (8×10^7 /m) which enables lesser hole density to traverse the Schottky junction. In this case, the significantly high generation takes place only at or near the absorption surface. Also, the larger photoconductive charge contribution at the high intensity of 10^{22} /m^2-s, emanating from more than one order of magnitude larger absorption coefficient of GaAs than that in the visible region produces large saturation current and large conductance wherein the large saturation current limits the total current. The currents obtained are as (97.1 μA, 0.37 mA, 1.2 mA, and 44.9 mA). The contrast ratios obtained are (7.9, 3.75, and 2.1).

3.5 Comparative Analysis of Si, InP, and GaAs OPFETs at 3 μm gate length and 0.27 μm channel thickness

As the active layer thickness is widened to 0.27 μm, keeping the gate length constant at 3 μm, the series resistances are significantly reduced owing to the wider thickness. However, they are still higher in the Si device as compared to the other two devices. The photovoltage remains almost the same in the Si and the GaAs OPFETs whereas it is slightly decreased in the InP OPFET explained by the possession of moderate absorption

Table 1: Comparative Studies of Si, InP, and GaAs OPFET detectors (1st set)

Si back-illuminated OPFET with ITO gate (v_{gs}=0 V, V_{ds}=10 V, λ=600 nm (visible) and 350 nm (UV) **1st set** (L=3 μm, Z=100 μm, t_{sm}=0.15 μm, N_{dr}=5×10^{22}/m^3)										
	Visible							**UV**		
Photon Flux Density (/m^2-s)	**Photo-voltage (V)**	**Drain-to-source current (A)**	**Responsivity (A/W)**	**Trans-conductance (S)**	**Gate-to-source capacitance (F)**	**f_T(Hz)**	**Band-width (Hz)**	**Photo-voltage (V)**	**Drain-to-source current (A)**	**Responsivity (A/W)**
0	0	0.36 mA	------	1.4 mS	0.0546 pF	4.08 GHz	-------	0	0.36 mA	------
10^{16}	0.28 V	0.9 mA	5.3×10^8	2.4 mS	0.084 pF	4.53 GHz	0.16 MHz	0.31 V	1 mA	3.53×10^8
10^{19}	0.46 V	1.7 mA	1.32×10^6	3.9 mS	0.105 pF	5.89 GHz	0.136 MHz	0.49 V	7.9 mA	4.33×10^6
10^{22}	0.606 V	15.6 mA	1.49×10^4	29.1 mS	0.0076 pF	606.7 GHz	0.57 MHz	0.61 V	16.1 mA	9×10^3
InP back-illuminated OPFET with Au gate (v_{gs}=0 V, V_{ds}=10 V, λ=600 nm (visible) and 350 nm (UV) **1st set** (L=3 μm, Z=100 μm, t_{sm}=0.15 μm, N_{dr}=5×10^{22}/m^3)										
	Visible							**UV**		
Photon Flux Density (/m^2-s)	**Photo-voltage (V)**	**Drain-to-source current (A)**	**Responsivity (A/W)**	**Trans-conductance (S)**	**Gate-to-source capacitance (F)**	**f_T(Hz)**	**Band-width (Hz)**	**Photo-voltage (V)**	**Drain-to-source current (A)**	**Responsivity (A/W)**
0	0	0.27 mA	------	2.3 mS	0.034 pF	10.7 GHz	-------	0	0.27 mA	------
10^{16}	0.297 V	1.3 mA	9.97×10^8	4.3 mS	0.0695 pF	9.74 GHz	67.35 MHz	0.094 V	0.54 mA	1.53×10^8
10^{19}	0.476 V	2.2 mA	1.9×10^6	5.6 mS	0.092 pF	9.65 GHz	0.26 GHz	0.27 V	1.2 mA	5.2×10^5
10^{22}	0.65 V	27.8 mA	2.7×10^4	6.7 mS	0.016 pF	65.4 GHz	3.84 MHz	0.44 V	30.1 mA	1.71×10^4
GaAs back-illuminated OPFET with ITO gate (v_{gs}=0 V, V_{ds}=10 V, λ=600 nm (visible) and 350 nm (UV) **1st set** (L=3 μm, Z=100 μm, t_{sm}=0.15 μm, N_{dr}=5×10^{22}/m^3)										
	Visible							**UV**		
Photon Flux Density (/m^2-s)	**Photo-voltage (V)**	**Drain-to-source current (A)**	**Responsivity (A/W)**	**Trans-conductance (S)**	**Gate-to-source capacitance (F)**	**f_T(Hz)**	**Band-width (Hz)**	**Photo-voltage (V)**	**Drain-to-source current (A)**	**Responsivity (A/W)**
0	0	97.1 μA	------	0 mS	0 pF	0 GHz	-------	0	97.1 μA	------
10^{16}	0.41 V	1.4 mA	1.24×10^9	5.5 mS	0.064 pF	13.7 GHz	1.5 GHz	0.19 V	0.37 mA	1.57×10^8
10^{19}	0.58 V	2.5 mA	2.4×10^6	7.5 mS	0.086 pF	13.8 GHz	6.3 GHz	0.37 V	1.2 mA	6.4×10^5
10^{22}	0.76 V	54.9 mA	5.37×10^4	67.2 mS	0.018 pF	596 GHz	1.1 MHz	0.55 V	44.9 mA	2.56×10^4

coefficient by Si and GaAs which enables significantly high hole density to cross the Schottky junction even if the channel thickness is increased.

On the other hand, the high absorption coefficient of InP results in lesser hole density to traverse the junction when the channel is widened. With the increase in active-layer thickness, the drain-to-source currents and the photocurrents are substantially enhanced due to the increment in the conducting charge as well as the reduction in the series resistances, however, with some exceptions at higher intensity of 10^{22} /m^2-s. At this flux density, in InP OPFET, due to the low series resistance, and the moderate Schottky barrier height, the increase in the channel thickness leads to the partial depletion of the channel. Hence, both the neutral channel and depletion regions contribute to the photoconductive effect significantly. However, owing to the large absorption

coefficient of InP, the contribution from the depletion region is lesser as compared to that at the lower active-layer thickness since the absorption depth is small and the most of the generated carriers in the far end of the depletion region are negligible as compared to that in the near end. But, it is still larger than the neutral channel contribution attributed to the factor in the denominator of the electron density equation in the depletion region which is absent in the equation for electron density in the neutral channel region. This results in one order higher density in the case of depletion region considering the same thicknesses for their contribution (by inspection of the two equations). At this intensity, the photovoltaic effect also contributes to the response, due to partial depletion of the channel and the device does not exhibit negative sensitivity. However, in overall, the response falls as compared to that at the lower channel thickness resulting in a lower current of 16.8 mA. In the other two detectors, these phenomena do not occur as the series resistance is sufficiently large in Si OPFET and the barrier height is considerably high in the GaAs OPFET thus maintaining complete depletion of the channel thickness at this flux density. Further, due to the moderate absorption coefficient of Si and GaAs (absorption depth is large), the photoconductive effect from the whole of the depletion region contributes significantly, thus, boosting the photocurrent. The devices exhibit negative sensitivity as usual at this intensity, thus, eliminating the photovoltaic response. The transconductances are boosted as the channel thickness is increased owing to the larger currents involved and the lesser limitation of the depletion width sensitivity due to the lower series resistances. This produces greater change in the saturation current and the drain-to-source conductance, however, again with some exceptions. In the Si OPFET, at the flux density of 10^{22} /m^2-s, the transconductance falls to 27.1 mS from 29.1 mS which is attributed to the larger photoconductive effect contribution from the depletion region induced by the greater depletion area leading to substantially high enhancement of the saturation current which is independent of the gate-to-source voltage. In this case, the channel is totally depleted sowing to the large voltage drop across the series resistance. The large saturation current limits the total current, and the only significant variation with the gate-to-source voltage is the considerable drain-to-source conductance (being evaluated at V_{DS}=0), on the whole, causing a fall in the transconductance. Similarly, in the GaAs OPFET, analogous phenomena occur, but in this case the saturation current involved is much lower than in the case of Si OPFET. This is due to the lesser contribution from photoconductivity in the depletion region since the electron lifetime in Si is more than one order of magnitude higher than that in GaAs. Also, the significant conductance variation with gate-to-source voltage is limited by the series resistances causing a substantial drop in the transconductance. These phenomena do not occur in InP OPFET, since the channel is partially depleted with a significant contribution from the photovoltaic effect, and the photoconductive effect from the depletion and the neutral channel regions with lower series resistances (as discussed earlier). However, this contribution is comparatively lower than the photoconductivity alone in the case of Si and GaAs OPFETs. This results in the rise in the transconductance from its previous value at the lower active layer thickness but exhibiting smaller values compared to that in Si and GaAs OPFETs. One anomalous behavior is observed at the flux density of 10^{19} /m^2-s in the InP OPFET, wherein the transconductance falls to 4.9 mS from its previous value of 5.6 mS at the lower active layer thickness and is also lower than its value (5.3 mS) at the flux density of 10^{16} /m^2-s. The reason behind this is still under our own investigation. The gate-to-source capacitance values increase with the increase in the channel thickness owing to the fact that at the lower channel thickness, with the applied drain-to-source voltage of 10 V, significant channel area is depleted as compared to that with the higher channel thickness. This is because the applied voltage drops itself across the channel in the form of the channel voltage which varies nearly linearly from zero at the source end to V_{DS} at the drain end. Thus, the change in the space charge with the change in the gate-to-source voltage is greater in the structure possessing larger channel thickness leading to the enhancement of the gate-to-source capacitance. As such, with the obtained tranconductance and capacitance values, the Si OPFET experiences an overall rise in f_T whereas the InP and the GaAs devices perceive a drop in the f_T with the widening of the channel thickness. With the enhanced photocurrents, on the whole, all the detectors show increased responsivities with the increment in the channel thickness. The 3-dB bandwidths obtained using Si device with the active layer thickness of 0.27 μm are as (0.66 MHz, 84.16 kHz, and 0.57 MHz) as compared to its previous values at the lower channel thickness (0.16 MHz, 0.136 MHz, and 0.57 MHz). The boosting of the bandwidth at the lower flux density is owing to the increase in the photovoltaic effect whereas the fall at the flux density of 10^{19} /m^2-s is due to the rise in the photovoltaic effect but simultaneous augmentation of the photoconductive effect due to widening of the channel thickness, thus, causing the drop. The reason for the constant bandwidth at the intensity of 10^{22} /m^2-s is still under our own study. The frequency responses of the InP device are (32.9 MHz, 0.39 GHz, and 4.156 MHz) at the higher active layer thickness as opposed to (67.35 MHz, 0.26 GHz, and 3.84 MHz) at the lower channel thickness. At the intensity of 10^{19} /m^2-s, the rise in the bandwidth is due to the increase in the photovoltaic effect. The slight increase in the bandwidth at the flux density of 10^{22} /m^2-s can be discussed as follows: At the lower channel thickness, at dc or lower frequencies, the photoconductive effect alone contributes but as stated earlier at the juncture of the 3-dB point, both the photovoltaic and the photoconductive effects are equally contributing. This results in a bandwidth of 3.84 MHz. On the contrary, at the higher channel thickness, under dc or lower frequencies, both the effects contribute significantly but the photoconductive charge is higher. But as the frequency increases, the photovoltaic charge starts incrementing whereas the photoconductive charge starts decreasing. Thus, at the juncture of the 3-dB point, the photovoltaic charge has rose to significantly high value but the photoconductive charge has decreased significantly. Hence, the non-equally contributing charges results in a wider bandwidth (4.156 MHz).The reason behind the drop in the bandwidth at the optical intensity of 10^{16} /m^2-s is still being investigated (shows anomalous behavior being contrary to the increase in the photovoltaic effect). On the other hand, the bandwidths attained using GaAs OPFET are (12.87 GHz, 16.34 GHz, and 0.72 MHz) as compared to that at the lower channel thickness (1.5 GHz, 6.3 GHz, and 1.1 MHz). At the lower flux densities, the enhancement of the photovoltaic effect results in the rise in the bandwidth whereas at the higher intensity, the device shows anomalous behavior being contrary to the increase in the photoconductive effect alone. The UV responses of the Si OPFET

device (4.8 mA, 5.9 mA, 9.9 mA, and 28.1 mA) are almost the same as that in the visible region except at the flux density of 10^{19} /m^2-s (higher in the UV region) owing to the two orders higher absorption coefficient of Si in the UV region. This significantly boosts the photoconductive effect in the depletion region at this flux density in addition to the contribution from the photovoltaic effect thus increasing the response. The photovoltages developed are almost the same as that in the visible region and slightly lower than that at the lower active layer thickness attributed to the larger absorption coefficient of Si in the UV region. This signifies that the generated carriers undergo significant degradation before these traverse the Schottky junction after travelling through the active layer thickness of 0.27 µm starting from the absorption surface. Due to the almost same photovoltages as that in the visible region, the series resistances almost remain unaltered. At the flux density of 10^{16} /m^2-s, the response remains unchanged due to similar photovoltaic effect. At the intensity of 10^{22} /m^2-s, the insensitive response to the wavelengths under consideration is because although the photoconductive effect in the depletion region is considerably enhanced in the UV region owing to the larger absorption coefficient, this leads to a larger saturation current and the conductance; the total current limited by the saturation current. As such, the responsivities attained are lower at the flux densities of 10^{16} and 10^{22} /m^2-s due to the insensitive response with the use of higher photon energy in the UV region. The slightly higher responsivity at the intensity of 10^{19} /m^2-s is due to the enhanced photocurrent. The contrast ratios obtained are (1.45, 0.826, and 1.73) which are very low signifying that the Si detector can function well in both the visible and UV regions. In the InP OPFET, there is significant degradation of photovoltage at the UV wavelength (0.105 mV, 42.1 mV, and 0.2107 V) owing to the very large absorption coefficient of InP (7.6×10^7 /m) and the higher channel thickness (0.27 µm). Due to the low photovoltages, the series resistances are higher. The photoconductive responses are negligible compared to the photovoltaic currents due to the small absorption depth and generation area. The currents involved are (5.9 mA, 5.9 mA, 6.1 mA, and 6.9 mA) leading to responsivities of (0.0764 A/W, 1.02×10^5 A/W, and 5.4×10^2 A/W). The contrast ratios thus obtained are (1.75×10^{10}, 22 and 19.7). This shows that the InP device with the structure under consideration can detect visible light with high responsivity under background UV radiation with rejection ratio of 1.75×10^{10}at the intensity of 10^{16} /m^2-s. At the higher intensities, the ratios are not high but can suffice in certain instances of applications. In the GaAs OPFET, similar situation occurs under UV illumination since the absorption coefficient of GaAs (8×10^7 /m) is identical to that of InP (7.6×10^7 /m) signifying small absorption depth. With this, the photovoltages produced are (2.6 mV, 0.12 V, and 0.3 V), the currents induced are (7.5 mA, 7.5 mA, 8.2 mA, and 9.5 mA) and the responsivities registered are (48.88 A/W, 4×10^5 A/W, and 1.15×10^3 A/W) rejecting UV wavelength with the factors of (5.21×10^7, 10.25, and 68.7).Thus, the rejection ratio is inferior to the InP OPFET at the lower intensities and vice versa at the higher intensity.

3.6 Comparative Analysis of Si, InP, and GaAs OPFETs at 4 µm gate length and 0.3 µm channel thickness

When the gate length is elongated to 4 µm from 3 µm with a proportionate increase in the active layer thickness to 0.3 µm from 0.27 µm and a corresponding increment in gate width from 100 µm to 150 µm, the doping concentration is reduced to 4×10^{22} /m^3 from 5×10^{22} /m^3 considering constant gate length-doping concentration product from scaling rules [16]. These changes in the structural parameters have a significant change in the device parameters and some of them can be correlated based upon certain basic facts and phenomena. At first, the series resistances are reduced due to the larger channel thickness. Secondly, the photovoltages remain almost unaltered owing to the materials' absorption depths which are sufficient enough to cause the hole density crossing the junction to experience very less carrier decay with distance. The drain-to-source currents proportionally increase with the gate length ascribed to the corresponding increase in the gate width, the active layer thickness, the electron saturated velocity (velocity decreases with the doping concentration) and the lower series resistance which raises the value of the saturation current although the lower doping concentration induces less conducting channel charge under dark. The increase in electron mobility (mobility also decreases with the doping concentration), the gate width to the gate length ratio, and the lower drain and source series resistances boosts the drain-to-source conductance in spite of the lower doping concentration under dark. The longitudinal increment of gate length induces more conducting charge along the gate length which increases the current under dark. Under illumination, the photocurrents introduced also increase with the gate length: Since the photovoltages are maintained at almost the same values, it's a fact that at a fixed photovoltage and a constant gate-to-source voltage, the depletion width sensitivity to the applied illumination is higher at the lower doping concentrations i.e. the structure possessing a higher gate length. However, the reduced doping concentration induces less conducting charge which supersedes the depletion width sensitivity to give lesser photovoltaic charge. Nevertheless, due to the parameters and the factors mentioned under the dark condition in addition to the above-mentioned facts, the photocurrents are enhanced as compared to their values at the lower gate length.

At the flux density of 10^{22} /m^2-s, at the most at the intensity of 10^{19} /m^2-s in Si OPFET (due to high electron lifetime), the photoconductive effect significantly contributes to the response owing to the larger channel thickness in addition to the above stated factors to produce very large response. The transconductances also rise with gate length due to the fact that at a fixed photovoltage, the depletion width sensitivity to the applied gate-to-source voltage is larger at the lower doping concentrations (higher gate length). This is assisted and limited by the other factors as mentioned earlier for the drain-to-source current and the photocurrent enhancement. The significant boost of transconductance at the intensity of 10^{22} /m^2-s is due to the significant photoconductive effect (in Si and InP OPFET) wherein the saturation current is sufficiently high but at its optimum to produce significant change in the drain-to-source current with the applied gate-to-source voltage through the drain-to-source conductance. In GaAs OPFET, there is a fall in the transconductance owing to the large saturation current limiting the conductance change with the gate-to-source voltage. The gate-to-source capacitances are also incremented with the gate length on account of the fact that at a given photovoltage, the depletion width sensitivity to applied gate-to-source voltage is higher at the lower doping concentrations.

Table 2: Comparative Studies of Si, InP, and GaAs OPFET detectors (2nd set)

Si back-illuminated OPFET with ITO gate (v_{gs}=0 V, V_{ds}=10 V, λ=600 nm (visible) and 350 nm (UV) **2st set** (L=3 μm, Z=100 μm, t_{sm}=0.27 μm, N_{dr}=5×10^{22}/m^3)										
	Visible							**UV**		
Photon Flux Density (/m^2-s)	**Photo-voltage (V)**	**Drain-to-source current (A)**	**Responsi-vity (A/W)**	**Trans-con-ductance (S)**	**Gate-to-source capacitance (F)**	**f_T(Hz)**	**Band-width (Hz)**	**Photo-voltage (V)**	**Drain-to-source current (A)**	**Responsivity (A/W)**
0	0	4.8 mA	------	3.7 mS	0.1 pF	5.72 GHz	-------	0	4.8 mA	------
10^{16}	0.28 V	5.8 mA	9.35×10^8	4.3 mS	0.12 pF	5.57 GHz	0.66 MHz	0.28 V	5.9 mA	6.43×10^8
10^{19}	0.46 V	7.3 mA	2.43×10^6	5.5 mS	0.14 pF	6.39 GHz	84.16 kHz	0.46 V	9.9 mA	2.94×10^6
10^{22}	0.606 V	28.3 mA	2.3×10^4	27.1 mS	0.0078 pF	554.3 GHz	0.57 MHz	0.59 V	28.1 mA	1.33×10^4
InP back-illuminated OPFET with Au gate (v_{gs}=0 V, V_{ds}=10 V, λ=600 nm (visible) and 350 nm (UV) **2nd set** (L=3 μm, Z=100 μm, t_{sm}=0.27 μm, N_{dr}=5×10^{22}/m^3)										
	Visible							**UV**		
Photon Flux Density (/m^2-s)	**Photo-voltage (V)**	**Drain-to-source current (A)**	**Responsi-vity (A/W)**	**Trans-con-ductance (S)**	**Gate-to-source capacitance (F)**	**f_T(Hz)**	**Band-width (Hz)**	**Photo-voltage (V)**	**Drain-to-source current (A)**	**Responsivity (A/W)**
0	0	5.9 mA	------	4.5 mS	0.098 pF	7.23 GHz	-------	0	5.9 mA	------
10^{16}	0.266 V	7.3 mA	1.34×10^9	5.3 mS	0.11 pF	7.6 GHz	32.9 MHz	0.1 mV	5.9 mA	0.0764
10^{19}	0.44 V	8.2 mA	2.2×10^6	4.9 mS	0.13 pF	5.9 GHz	0.39 GHz	42.1 mV	6.1 mA	1.02×10^5
10^{22}	0.62 V	16.8 mA	1.064×10^4	7.6 mS	0.034 pF	35.7 GHz	4.15 MHz	0.21 V	6.9 mA	5.4×10^2
GaAs back-illuminated OPFET with ITO gate (v_{gs}=0 V, V_{ds}=10 V, λ=600 nm (visible) and 350 nm (UV) **2nd set** (L=3 μm, Z=100 μm, t_{sm}=0.27 μm, N_{dr}=5×10^{22}/m^3)										
	Visible							**UV**		
Photon Flux Density (/m^2-s)	**Photo-voltage (V)**	**Drain-to-source current (A)**	**Responsi-vity (A/W)**	**Trans-con-ductance (S)**	**Gate-to-source capacitance (F)**	**f_T(Hz)**	**Band-width (Hz)**	**Photo-voltage (V)**	**Drain-to-source current (A)**	**Responsivity (A/W)**
0	0	7.5 mA	------	6.7 mS	0.088 pF	12.1 GHz	-------	0	7.5 mA	------
10^{16}	0.39 V	10.1 mA	2.55×10^9	7.6 mS	0.11 pF	10.9 GHz	12.87 GHz	2.6 mV	7.5 mA	48.9
10^{19}	0.57 V	11.7 mA	4.1×10^6	8.6 mS	0.13 pF	10.8 GHz	16.34 GHz	0.12 V	8.2 mA	4×10^5
10^{22}	0.75 V	88.1 mA	7.9×10^4	38.5 mS	0.018 pF	342 GHz	0.72 MHz	0.3 V	9.5 mA	1.15×10^3

This is further assisted by the greater gate width, gate length and active layer thickness, which offer larger transverse, longitudinal, and lateral space charges superseding the effect of lower doping concentration on the total charge. Owing to the enhancement of the transconductances and the gate-to-source capacitances, the unity-gain cut-off frequencies experience a rise with the gate length since the rate of transconductance increase is greater than that of the gate-to-source capacitance except in GaAs OPFET at the flux density of 10^{22} /m^2-s due to the fall in the transconductance. The responsivities decrease on the whole with gate length although the photocurrents are enhanced since the devices use greater optical power to produce a given photocurrent, optical power being directly proportional to the gate length and the gate width of the devices. However, in the case of Si and GaAs OPFETs, at the

intensity of 10^{22} /m^2-s the responsivity increases due to large photoconductive effects. The bandwidths exhibited by the devices are: In Si OPFET, with the elongation of the gate length, the bandwidths attained are (0.72 MHz, 44.5 kHz, and 0.41 MHz) as opposed to (0.66 MHz, 84.16 kHz, and 0.57 MHz) at the lower gate length. The slight rise in the bandwidth at the intensity of 10^{16} /m^2-s is attributed to the fact that the depletion width sensitivity increases at lower doping concentration (or higher gate length) which creates the roll-off slope of the photovoltaic charge or current frequency response curve to be gentler thus, broadening the response. The fall in the bandwidth at the flux density of 10^{19} /m^2-s in spite of the roll-off slope of the photovoltaic effect being gentler is owing to the increase in the photoconductive contribution due to larger channel thickness. The reason behind the drop in the bandwidth at the intensity of 10^{22} /m^2-s is still under study. On the other hand, in the InP OPFET, the bandwidths obtained are (92.6 MHz, 0.36 GHz, and 3.84 MHz) as compared to (32.9 MHz, 0.39 GHz, and 4.156 MHz) at the lower gate length. The same principles apply for the attained bandwidths at the flux densities of 10^{16} and 10^{19} /m^2-s, however, the slight fall in the bandwidth at the intensity of 10^{19}/m^2-s is due to the limitation by the series resistance. Whereas at the flux density of 10^{22} /m^2-s, there is slight drop in bandwidth owing to the fall in the photovoltaic charge response as compared to that at the lower gate length due to lower doping concentration but maintaining almost the same photoconductive contributions. This is owing to the contribution adjustment between the neutral channel and depletion regions signifying that at the juncture of the 3-dB point, both the effects contribute significantly resulting in the fall of bandwidth (3.84 MHz). The 3-dB bandwidths attained with the GaAs OPFET device are (4.57 GHz, 42.4 GHz, and 0.615 MHz) as compared to (12.87 GHz, 16.34 GHz, and 0.72 MHz) at the lower gate length. The reduction in the bandwidth at the lower intensity is contrary to the fact of gentler roll-off slope of photovoltaic charge frequency response (reason behind it is under study) whereas it is in line with the said fact at the intensity of 10^{19} /m^2-s. The slight drop in the bandwidth at the flux density of 10^{22}/m^2-s is contrary to the increment in photoconductive response with gate length and is under investigation. Under UV illumination, in the Si OPFET, the photovoltages are almost the same as that in the visible region since the increase in the absorption coefficient in the UV region by two orders of magnitude is neutralized by the lesser absorption depth maintaining the same values. The photocurrent is almost the same at the flux density of 10^{16} /m^2-s due to the same photovoltage. At the intensity of 10^{19} /m^2-s, the photocurrent is enhanced as compared to its value in the visible region owing to the substantial enhancement of the photoconductivity on account of the two orders of magnitude higher absorption coefficient in the UV region. At the flux density of 10^{22} /m^2-s, almost the same photocurrent is maintained although there is boost in the photoconductive effect due to the large saturation current which limits the total current. The responsivities obtained are (3.5×10^8 A/W, 2.34×10^6 A/W, and 2.4×10^4 A/W) with the visible/UV contrast ratios as (1.71, 0.8, and 1.74). This shows again that at this gate length, the Si device can detect both the visible and UV wavelengths with high sensitivities. The InP OPFET can reject very well the UV radiation and detect visible light with the rejection ratios as (Very High, Very High, and 28.556) at this gate length ascribed to the very high absorption coefficient of InP in the UV region which limits its absorption depth and the generation area. Also, due to the larger active layer thickness, the photovoltages generated are significantly degraded which produces zero response at the lower intensities whereas considerable response at the higher intensity due to somewhat moderate photovoltage owing to the higher optical power level. On the other hand, the GaAs OPFET exhibits rejection ratios of (Very High, 16.05, and 137.54). This can be explained as follows: Although the absorption coefficient of GaAs is almost the same as that of InP, the photovoltages generated in GaAs are slightly higher than that in InP owing to the larger barrier height. Hence, the GaAs device produces zero response (due to very low photovoltage) at the lower intensity whereas substantial responses (due to reasonable photovoltages) at the higher intensities which account for the obtained ratios.

3.7 Comparative Analysis of Si, InP, and GaAs OPFETs at 5 μm gate length and 0.4 μm channel thickness

As the gate is elongated to 5 μm from 4 μm, with a corresponding increase in the active layer thickness to 0.4 μm from 0.3 μm, and the gate width to 200 μm from 150 μm,thedoping concentration is reduced to 3.2×10^{22} /m^3. This tends to increase the depletion width sensitivity but is significantly limited by the voltage drop across the series resistances since the large channel thickness induces high conducting charge under dark which considerably raises the dark current. The series resistances are substantially lowered due to large active layer thickness. In the Si OPFET, the photovoltages remain almost unaltered due to the moderate absorption coefficient of Si. The currents induced in the Si OPFET are (11.9 mA, 13.8 mA, 17.5 mA, and 150.2 mA). The current increase with gate length is due to the reasons described earlier. It is the photovoltaic effect enhancement at the lower intensities whereas the photoconductive effect is boosted at the higher intensity due to larger channel thickness resulting in a larger current of 150.2 mA. The transconductances are considerably boosted (7 mS, 8.1 mS, 7.6 mS, and 100 mS) as compared to that at the lower gate length due to the principles stated earlier. The transconductance increases with illumination initially as usual, but falls at the flux density of 10^{19} /m^2-s due to the limitation by the voltage drop incurred across the series resistance owing to larger current involved (17.5 mA). At the intensity of 10^{22} /m^2-s, although the current is very large, it is due to the photoconductive effect which is insensitive to the voltage drop across the series resistance and can gain sensitivity through the change in the conductance with the applied gate-to-source voltage. The gate-to-source capacitance increases further with the gate length as usual due to the reasons explained earlier (0.18 pF, 0.216 pF, 0.23 pF, and 0.013 pF). These result in the f_T values of (6 GHz, 6 GHz, 5.2 GHz, and 1.42 THz). The Si detector shows bandwidths of (0.72 MHz, 30 kHz, and 0.41 MHz) at this gate length. The unchanged value at the lower flux density is owing to the limitation posed by the series resistance effect. The drop in the bandwidth at the intensity of 10^{19} /m^2-s is attributed to the fall in the photovoltaic charge response with gate length (due to the lower doping concentration) and the increase in photoconductivity from larger channel thickness. The reason behind the unaltered bandwidth of 0.41 MHz at the intensity of 10^{22} /m^2-s is still unknown. The responsivities attained at this gate length are (5.54×10^8 A/W, 1.63×10^6 A/W, and 4.07×10^4 A/W) which are lower than that at the previous gate length as the

Table 3: Comparative Studies of Si, InP, and GaAs OPFET detectors (3rd set)

Si back-illuminated OPFET with ITO gate (v_{gs}=0 V, V_{ds}=25 V, λ=600 nm (visible) and 350 nm (UV) 3rd set (L=4 μm, Z=150 μm, t_{sm}=0.3 μm, N_{dr}=4×10^{22}/m^3)										
	Visible							UV		
Photon Flux Density (/m^2-s)	Photo-voltage (V)	Drain-to-source current (A)	Responsi-vity (A/W)	Trans-con-ductance (S)	Gate-to-source capacitance (F)	f_T(Hz)	Band-width (Hz)	Photo-voltage (V)	Drain-to-source current (A)	Responsivity (A/W)
0	0	6.4 mA	------	4.6 mS	0.12 pF	6 GHz	-------	0	6.4 mA	------
10^{16}	0.286 V	7.7 mA	6×10^8	5.7 mS	0.145 pF	6.2 GHz	0.72 MHz	0.28 V	7.7 mA	3.5×10^8
10^{19}	0.46 V	10.3 mA	1.87×10^6	7.4 mS	0.16 pF	7.3 GHz	44.5 kHz	0.46 V	14.6 mA	2.34×10^6
10^{22}	0.607 V	91.6 mA	4.17×10^4	84.7 mS	0.011 pF	1.25 THz	0.41 MHz	0.58 V	90.2 mA	2.4×10^4
InP back-illuminated OPFET with Au gate (v_{gs}=0 V, V_{ds}=25 V, λ=600 nm (visible) and 350 nm (UV) 3rd set (L=4 μm, Z=150 μm, t_{sm}=0.3 μm, N_{dr}=4×10^{22}/m^3)										
	Visible							UV		
Photon Flux Density (/m^2-s)	Photo-voltage (V)	Drain-to-source current (A)	Responsi-vity (A/W)	Trans-con-ductance (S)	Gate-to-source capacitance (F)	f_T(Hz)	Band-width (Hz)	Photo-voltage (V)	Drain-to-source current (A)	Responsivity (A/W)
0	0	7.9 mA	------	5.7 mS	0.116 pF	7.73 GHz	-------	0	7.9 mA	------
10^{16}	0.26 V	9.4 mA	7.4×10^8	7 mS	0.13 pF	8.4 GHz	92.6 MHz	Very Less	7.9 mA	0
10^{19}	0.44 V	10.9 mA	1.47×10^6	7.9 mS	0.15 pF	8.2 GHz	0.36 GHz	10.7 mV	7.9 mA	0
10^{22}	0.61 V	24.2 mA	7.97×10^3	18.2 mS	0.044 pF	65.6 GHz	3.84 MHz	0.15 V	8.9 mA	279.1
GaAs back-illuminated OPFET with ITO gate (v_{gs}=0 V, V_{ds}=25 V, λ=600 nm (visible) and 350 nm (UV) 3rd set (L=4 μm, Z=150 μm, t_{sm}=0.3 μm, N_{dr}=4×10^{22}/m^3)										
	Visible							UV		
Photon Flux Density (/m^2-s)	Photo-voltage (V)	Drain-to-source current (A)	Responsi-vity (A/W)	Trans-con-ductance (S)	Gate-to-source capacitance (F)	f_T(Hz)	Band-width (Hz)	Photo-voltage (V)	Drain-to-source current (A)	Responsivity (A/W)
0	0	9.4 mA	------	8.3 mS	0.106 pF	12.3 GHz	-------	0	9.4 mA	------
10^{16}	0.398 V	13 mA	1.75×10^9	9.4 mS	0.13 pF	11.4 GHz	4.57 GHz	0.3 mV	9.4 mA	0
10^{19}	0.576 V	14.6 mA	2.6×10^6	10.9 mS	0.15 pF	11.5 GHz	42.4 GHz	66.2 mV	10 mA	1.62×10^5
10^{22}	0.755 V	180.5 mA	8.39×10^4	28.9 mS	0.027 pF	171 GHz	0.615 MHz	0.24 V	11.5 mA	6.1×10^2

device uses more illuminated area for achieving the said photoresponse. In the UV region, the Si OPFET device generates slightly lower photovoltages owing to the higher absorption coefficient which means a smaller absorption depth and due to the large channel thickness, slightly fewer holes make it to the Schottky junction. Due to slightly lower photovoltage, the drain-to-source current is slightly reduced as compared to that in the visible region (13.4 mA) at the flux density of 10^{16} /m^2-s. However, at the flux density of 10^{19} /m^2-s, the response is raised to 18.6 mA due to the significant photoconductive contribution from the depletion region emanating from larger absorption coefficient of Si. At the intensity of 10^{22} /m^2-s, the response falls to 143.7 mA since the photoconductivity is enhanced whereby a large saturation current limits the total current. The responsivities achieved are

(2.55×10^8 A/W, 1.14×10^6 A/W, and 2.26×10^4 A/W). As such, the contrast ratios obtained are (2.17, 1.43, and 1.8).

In the InP OPFET with a gate length of 5 μm, the currents are further enhanced at the lower intensities whereas at the higher intensity, the photocurrent drops owing to the limited sensitivity caused by the presence of large dark current. This, in addition to the photocurrent creates large voltage drop across the series resistance. Thus, with a finite channel width due to moderate barrier height of Au-InP junction and the high absorption coefficient of InP, the photoconductive effect contributes non-significantly as compared to the lower gate length. In this case, the contributions are divided between the neutral channel region and the depletion region, with depletion region still the major contributor. This induces lesser change in the photovoltaic charge as compared to that at the lower flux density. Hence, both the photovoltaic and photoconductive effects fall at this flux density at this gate length causing a drop in the photocurrent. The transconductance rises as opposed to its value at the lower gate length under dark explained by the reasons discussed earlier since the current is comparatively lower which does not significantly limit the sensitivity through the series resistance. However, as the flux density increases, significantly high drain-to-source currents are introduced which considerably limit the depletion width sensitivity due to the voltage drop across the series resistance. At the intensity of 10^{22} /m^2-s, the transconductance is nearly zero since the reduction in photovoltaic sensitivity as explained earlier is almost totally compensated by the rise in the photoconductive sensitivity with the applied gate-to-source voltage resulting in the zero transconductance. The capacitances as usual are raised above their values at the lower gate length. The limitation of the transconductance and the rise in the capacitance leads to the fall in the unity-gain cut-off frequencies (5.5 GHz, 5.6 GHz, 5.5 GHz, and 0.653 mHz). The bandwidths drop at the lower flux densities (62.2 MHz, and 0.33 GHz) owing to the series resistance limiting effects. At the higher flux density, the bandwidth is raised (6.2 MHz). This can be discussed as follows: At the lower gate length, at dc or lower frequencies, both the photoconductive and the photovoltaic effects contribute with significantly high contribution from the photoconductive effect in the depletion region (owing to the lower channel thickness). As the frequency is increased, the photovoltaic charge starts increasing since the otherwise limited sensitivity under large current is converted into non-limited sensitivity. In this case, the increment in frequency lessens the photoconductive charge in the depletion region due to the dependence of electron lifetime on frequency. This reduces the overall current and hence, the voltage drop across the series resistance. This signifies that at the juncture of the 3-dB point, both the photovoltaic and the photoconductive effects are equally contributing. Further, it is known that when two similar effects are contributing to the response with equal operating lifetimes, the net frequency response has a bandwidth which is lower than that of the individual ones. This results in a bandwidth of 3.84 MHz. On the contrary, at the gate length of 5 μm, under dc or lower frequencies, both the effects contribute significantly but here the photovoltaic effect contribution has increased and the photoconductive contribution has decreased (still photoconductive charge is higher). But as the frequency increases, as explained in the previous case, the photovoltaic charge starts incrementing whereas the photoconductive charge starts decreasing. Thus, at the juncture of the 3-dB point, the photovoltaic charge has rose to significantly high value but the photoconductive charge has decreased significantly. Hence, the non-equally contributing charges results in a wider bandwidth (6.2 MHz). The responsivities attained are (5.1×10^8 A/W, 9.3×10^5 A/W, and 3.5×10^3 A/W) which account for the generated photocurrents and the optical power used under visible light. Under UV illumination, the photovoltages are severely degraded and the photoconductive responses are negligible owing to the very large absorption coefficient of InP and the larger active layer thickness which produce zero responsivities. Thus, the visible/UV contrast ratios are very high. This shows that the InP OPFET with a gate length of 5 μm is a high sensitivity detector with a very high contrast between visible and UV wavelengths but at the expense of a larger dark current. Discussing the GaAs OPFET device with a gate length of 5 μm, this device exhibits the same photovoltages as that with other gate lengths owing to the moderate absorption coefficient of GaAs even if the channel thickness is increased to 0.4 μm. Due to the larger active layer thickness and the high photovoltages, the series resistances are substantially reduced. As usual with the elongation of the gate length, the drain-to-source currents and the photocurrents are significantly enhanced (17.5 mA, 21.5 mA, 24.2 mA, 275.4 mA), however, this time with the limitation by the series resistances owing to the larger currents involved. The transconductance drops under dark (7.9 mS) since the dark current is very high (17.5 mA) as compared to its value at the previous gate length (9.4 mA) thus, limiting the sensitivity. At the flux density of 10^{16} /m^2-s, the transconductance is enhanced (12.7 mS) due to significant photovoltaic effect. At the flux density of 10^{19} /m^2-s, the transconductance falls (10.6 mS) due to larger current involved (24.2 mA) thus inducing series resistance-limited effect. At the intensity of 10^{22} /m^2-s, the transconductance slightly rises (30 mS) due to the substantial photoconductive effect in the depletion region insensitive to the voltage drop across the series resistance, thus, inducing a large saturation current independent of the gate-to-source voltage also limiting the total current and the device gaining the sensitivity through the significant conductance change with the applied gate-to-source voltage. The capacitances are increased as usual (0.16 pF, 0.2 pF, 0.22 pF, and 0.036 pF). As such, the f_T values obtained are (7.6 GHz, 10.11 GHz, 7.65 GHz, and 133.1 GHz) which are lower than the values at the lower gate length. The 3-dB bandwidths attained are (19.15 GHz, 19.15 GHz, and 0.615 MHz). At the intensity of 10^{16} /m^2-s, the bandwidth enhancement is due to the larger sensitivity. At the flux density of 10^{19} /m^2-s, the drop in the bandwidth is due to the limitation by the series resistance. The unaltered bandwidth at the intensity of 10^{22} /m^2-s is owing to no significant change in the photoconductive charge. The responsivities achieved are (1.18×10^9 A/W, 2×10^6 A/W, and 7.59×10^4 A/W) which account for the generated photocurrents utilizing larger illuminated areas. Under UV light, the photovoltages are significantly degraded owing to the very large absorption coefficient of GaAs and wider channel thickness (0.4 μm). This produces zero photoresponses at the lower flux densities but at the higher flux density since the optical power level is high and on account of the very high absorption coefficient of GaAs, the photoconductive effect from the depletion region is large. This is because the photovoltage is very low and the high photoconductive current develops significant voltage drop across the series resistance thus, making the channel totally depleted and producing high response (4.42×10^4 A/W). Hence, the visible/UV

Table 4: Comparative Studies of Si, InP, and GaAs OPFET detectors (4thset)

Si back-illuminated OPFET with ITO gate (v_{gs}=0 V, V_{ds}=30 V, λ=600 nm (visible) and 350 nm (UV) **4th set** (L=5 μm, Z=200 μm, t_{sm}=0.4 μm, N_{dr}=3.2×10^{22}/m^3)										
	Visible							**UV**		
Photon Flux Density (/m^2-s)	**Photo-voltage (V)**	**Drain-to-source current (A)**	**Responsi-vity (A/W)**	**Trans-con-ductance (S)**	**Gate-to-source capacitance (F)**	**f_T(Hz)**	**Band-width (Hz)**	**Photo-voltage (V)**	**Drain-to-source current (A)**	**Responsivity (A/W)**
0	0	11.9 mA	------	7 mS	0.18 pF	6 GHz	-------	0	11.9 mA	------
10^{16}	0.289 V	13.8 mA	5.54×10^8	8.1 mS	0.216 pF	6 GHz	0.72 MHz	0.26 V	13.4 mA	2.55×10^8
10^{19}	0.47 V	17.5 mA	1.63×10^6	7.6 mS	0.23 pF	5.2 GHz	30 kHz	0.449 V	18.6 mA	1.14×10^6
10^{22}	0.61 V	150.2 mA	4.07×10^4	100 mS	0.013 pF	1.42 THz	0.42 MHz	0.56 V	143.7 mA	2.26×10^4
InP back-illuminated OPFET with Au gate (v_{gs}=0 V, V_{ds}=30 V, λ=600 nm (visible) and 350 nm (UV) **4th set** (L=5 μm, Z=200 μm, t_{sm}=0.4 μm, N_{dr}=3.2×10^{22}/m^3)										
	Visible							**UV**		
Photon Flux Density (/m^2-s)	**Photo-voltage (V)**	**Drain-to-source current (A)**	**Responsi-vity (A/W)**	**Trans-con-ductance (S)**	**Gate-to-source capacitance (F)**	**f_T(Hz)**	**Band-width (Hz)**	**Photo-voltage (V)**	**Drain-to-source current (A)**	**Responsivity (A/W)**
0	0	13.8 mA	------	6.2 mS	0.178 pF	5.5 GHz	-------	0	13.8 mA	------
10^{16}	0.24 V	15.5 mA	5.1×10^8	7 mS	0.197 pF	5.6 GHz	62.2 MHz	Very Less	13.8 mA	0
10^{19}	0.42 V	17 mA	9.3×10^5	7.6 mS	0.22 pF	5.5 GHz	0.33 GHz	Very Less	13.8 mA	0
10^{22}	0.596 V	25.7 mA	3.5×10^3	0 mS	0.106 pF	0.65 mHz	6.2 MHz	6 mV	13.8 mA	0
GaAs back-illuminated OPFET with ITO gate (v_{gs}=0 V, V_{ds}=30 V, λ=600 nm (visible) and 350 nm (UV) **4th set** (L=5 μm, Z=200 μm, t_{sm}=0.4 μm, N_{dr}=3.2×10^{22}/m^3)										
	Visible							**UV**		
Photon Flux Density (/m^2-s)	**Photo-voltage (V)**	**Drain-to-source current (A)**	**Responsi-vity (A/W)**	**Trans-con-ductance (S)**	**Gate-to-source capacitance (F)**	**f_T(Hz)**	**Band-width (Hz)**	**Photo-voltage (V)**	**Drain-to-source current (A)**	**Responsivity (A/W)**
0	0	17.5 mA	------	7.9 mS	0.16 pF	7.6 GHz	-------	0	17.5 mA	------
10^{16}	0.39 V	21.5 mA	1.18×10^9	12.7 mS	0.2 pF	10.1 GHz	19.1 GHz	Very Less	17.5 mA	0
10^{19}	0.57 V	24.2 mA	2×10^6	10.6 mS	0.22 pF	7.65 GHz	19.1 GHz	0.13 mV	17.5 mA	0
10^{22}	0.75 V	275.4 mA	7.59×10^4	30 mS	0.036 pF	133 GHz	0.615 MHz	0.046 V	274.8 mA	4.42×10^4

rejection ratios attained are (Very High, Very High, and 1.72). Thus, the GaAs OPFET is comparable to the InP OPFET at the lower intensities in terms of contrast ratio whereas it is inferior to the InP OPFET at the higher intensity.

Conclusion

We studied in detail the visible light and the UV photoresponses of the three efficient materials-based (Si, InP, and GaAs) back-illuminated OPFET photodetectors for VLC and UV reflectance imaging applications i.e. high gain-bandwidth product and high visible/UV contrast applications respectively. The results were analyzed based on the photoconductive and the photovoltaic effects, the series resistance effects, scaling rules- induced effects, and channel length-variation effects. The GaAs OPFET emerges

as a high-performance photodetector with higher responsivities, higher 3-dB bandwidth in the gigahertz range, and high visible/UV rejection ratios. On the other hand, the InP OPFET device can compete or even surpass the GaAs OPFET device in terms of contrast ratio with high photoresponse but inferior to the GaAs device and bandwidth in the sub-gigahertz range. Whereas the Si OPFET device exhibits high responsivities inferior to the InP device at the lower intensity and ranging between that of the InP and the GaAs devices at the higher intensities but the bandwidth is in the sub-megahertz range and the contrast ratios are very low. All the devices show significant unity-gain cut-off frequencies. On the whole, the drain-to-source currents, the photocurrents, the transconductances, and the gate-to-source capacitances increase with the elongation of the gate length and the widening of the active layer thickness. The responsivities decrease with the gate length. The photovoltages remain almost unaltered. The series resistances reduce with the gate length and the active layer thickness. Very High visible/UV rejection ratios are observed at the higher gate lengths in the case of the InP and the GaAs OPFETs. The 3-dB bandwidth under photovoltaic conditions in normal circumstances increase with the gate length but in some instances is limited by the series resistance effects. Also, with the enhancement of the photoconductive effect with gate length, the bandwidth increases. However, in other circumstances, wherein the bandwidth depends upon both the photoconductive and the photovoltaic effects, and their relative contributions, the bandwidth can either increase or decrease with gate length. The unity-gain cut-off frequency has an arbitrary dependence upon the gate length based upon the relative contributions of the transconductance and the gate-to-source capacitance. The GaAs OPFET detector exhibits the highest detection-cum-amplification bandwidth of around 11 GHz using a gate length of 3 μm and an active layer thickness of 0.27 μm at the flux densities of 10^{16} and 10^{19} /m^2-s whereas it shows a bandwidth of 11.5 GHz with a gate length of 4 μm at the intensity of 10^{19} /m^2-s, thus, showing its potential as detector-cum-amplifier in Opto-Electronic Integrated Circuits (OEICs)-based high bandwidth VLC applications such as Li-Fi (Light-Fidelity Networks). At 3 μm gate length, it exhibits the highest responsivities of 2.55×10^9 A/W and 4.1×10^6 A/W at the intensities of 10^{16} and 10^{19} /m^2-s respectively. Further, the corresponding visible/UV contrast ratios are 5.21×10^7 and 10.25. The InP OPFET attains a modest detection-cum-amplification bandwidths of 92 MHz, 0.36 GHz and 3.84 MHz at the 4 μm gate length and at the flux densities of 10^{16}, 10^{19}, and 10^{22}/m^2-s respectively with the corresponding high responsivities as 7.4×10^8 A/W, 1.47×10^6 A/W, and 7.97×10^3 A/W and contrast ratios as (Very High, Very High, and 28.5). These values suffice for moderate bandwidth VLC applications viz. hospitals and healthcare, under-water communication, defence, and security. The Si OPFET device can operate in low data rate VLC applications such as general positioning, vehicle and transportation, and smart lighting, due to its low detection-cum-amplification bandwidths of 0.66 MHz, 84.16 kHz, and 0.57 MHz at the gate length of 3 μm and an active layer thickness of 0.27 μm at the flux densities of 10^{16}, 10^{19} and 10^{22} /m^2-srespectively, with the corresponding responsivities of 9.35×10^8 A/W, 2.43×10^6 A/W, and 2.3×10^4 A/W. The Si OPFET is not suitable for visible/UV contrast applications. These devices show good prospects for communication and contrast applications. The comprehensive analyses presented here which relate the effect of the structural and the material parameters on the device parameters through physics-based discussion will aid in conducting further research.

Table 5: Parameters employed in calculation.

Parameters used in calculation (Si)			
Parameter	**Name**	**Value**	**Unit**
μ	Low field electron mobility	(~ 0.09)	(m^2/V.s
Φ_B	Schottky Barrier Height (ITO-Si)	(~ 0.71)	(eV)
v_{vn}	Saturated electron velocity	~9.4×10^4	(m/s)
v_{vp}	Saturated hole velocity	~6.3×10^4	(m/s)
τ_p	Lifetime of holes	75×10^{-6}	(s)
τ_n	Lifetime of electrons	75×10^{-6}	(s)
ε	Permittivity	1.04×10^{-10}	(F/m)
α	Absorption Coefficient @ 600 nm	7.5×10^5	(/m)
α	Absorption Coefficient @ 350 nm	1×10^7	(/m)
Parameters used in calculation (InP)			
μ	Low field electron mobility	(~ 0.43)	(m^2/V.s
Φ_B	Schottky Barrier Height (Au-InP)	(~ 0.8)	(eV)
v_{vn}	Saturated electron velocity	~7.6×10^4	(m/s)
v_{vp}	Saturated hole velocity	~5.6×10^4	(m/s)
τ_p	Lifetime of holes	0.3×10^{-6}	(s)
τ_n	Lifetime of electrons	0.3×10^{-6}	(s)
ε	Permittivity	1.11×10^{-10}	(F/m)
α	Absorption Coefficient @ 600 nm	1×10^7	(/m)
α	Absorption Coefficient @ 350 nm	7.6×10^7	(/m)
Parameters used in calculation (GaAs)			
μ	Low field electron mobility	(~ 0.5)	(m^2/V.s
Φ_B	Schottky Barrier Height (ITO-GaAs)	(~ 0.98)	(eV)
v_{vn}	Saturated electron velocity	~1.2×10^5	(m/s)
v_{vp}	Saturated hole velocity	~9×10^4	(m/s)
τ_p	Lifetime of holes	1×10^{-8}	(s)
τ_n	Lifetime of electrons	1×10^{-6}	(s)

ε	Permittivity	1.14×10^{-10}	(F/m)
α	Absorption Coefficient @ 600 nm	4×10^{6}	(/m)
α	Absorption Coefficient @ 350 nm	8×10^{7}	(/m)

Table 6: Performance comparison with state-of-art photodetectors and amplifiers.

Ref. No.	Year	Detector	Optical Power Density	Responsivity (A/W)	Bandwidth	Amplifier Type and f_T (Hz)
[17]	2004	PIN	NP (Not Provided)	0.36 A/W @ 660 nm	1.35 Hz	TIA (25 GHz)
[18]	2010	Photodiode (PD)	NP	0.21 A/W @ 660 nm	70 MHz	TIA (NP)
[19]	2012	PD	NP	0.36 A/W @ 670 nm	60 MHz	TIA (4.5 GHz)
[20]	2012	PIN	NP	0.52 A/W @ 660 nm	720 MHz	TIA (0.622 GHz)
[21]	2013	PIN	NP	0.54 A/W @ 675 nm	995 MHz	TIA (NP)
[22]	2014	APD	0.147 W/cm^2	27.9 A/W @ 670 nm	700 MHz	NP
[23]	2016	APD	0.016 W/cm^2	30 A/W @ 670nm	850 MHz	TIA (0.731 GHz)
[24]	2016	APD	NP	0.28 A/W @ 450 nm	650 MHz	NP
[25]	2017	APD	0.75 mW/cm^2	14.2 A/W @ 675 nm	960 MHz	TIA (NP)
[26]	2017	APD	NP	2.61 A/W @ 450 nm	>90 MHz	TIA (NP)
This Work	2019	**OPFET**	**0.33 mW/cm^2**	**4.1×10^{6} A/W @ 600 nm**	**16.34 GHz**	**OPFET (10.8 GHz)**

References

[1] J. V. Gaitonde, and R. B. Lohani, "Back-illuminated GaAs OPFET: A High Visible/UV Contrast Photodetector," In 2018 Conference on Emerging Devices and Smart Systems (ICEDSS), IEEE, Namakkal, Tamil Nadu, India, 2018.https://doi.org/10.1109/ICEDSS.2018.8544284

[2] L. U. Khan, "Visible light communication: Applications, architecture, standardization and research challenges," Digital Communications and Networks 3(2), 78-88, 2017. https://doi.org/10.1016/j.dcan.2016.07.004

[3] C. Baack, G. Elze, and G. Walf, "GaAs MESFET: A high-speed optical detector," Electronics Letters, 13(7), 193-193, 1977.https://doi.org/10.1049/el:19770141

[4] A. A. A. De Salles, "Optical control of GaAs MESFET's," IEEE Trans. on Microwave Theory and Techniques, 31(10), 812-820, 1983.https://doi.org/10.1109/TMTT.1983.1131611

[5] H. Mizuno, "Microwave characteristics of an optically controlled GaAs MESFET," IEEE Trans.on Microwave Theory and Techniques, 31(7), 596-600, 1983.https://doi.org/10.1109/TMTT.1983.1131551

[6] S. R. Saxena, R. B. Lohani, R. U. Khan, and B. B. Pal, "Generalized dc model of GaAs optical field effect transistor considering ion-implanted profile," Optical Engineering, 37(4), 1343-1352, 1998..https://doi.org/10.1117/1.601895

[7] P. Chakrabarti, S. K. Shrestha, A. Srivastava, and D. Saxena, "Switching characteristics of an optically controlled GaAs-MESFET," IEEE Trans. on Microwave Theory and Techniques, 42(3), 365-375, 1994.https://doi.org/10.1109/22.277428

[8] N. S. Roy and B. B. Pal, "Frequency-dependent OPFET characteristics with improved absorption under back illumination," Journal of lightwave technology, 18(4), 604-613, 2000.https://doi.org/10.1109/50.838136

[9] J. Gaitonde and R. B. Lohani, "GaAs Optical Field Effect Transistor (OPFET): A High Performance Photodetector for Automotive Applications," SAE International Journal of Passenger Cars-Electronic and Electrical Systems, 9(2016-01-0094), 204-211, 2016.https://doi.org/10.4271/2016-01-0094.

[10] N. S. Roy, B. B. Pal, and R. U. Khan, "Frequency-dependent characteristics of an ion-implanted GaAs MESFET with opaque gate under illumination," Journal of Lightwave Technology, 18(2), 221-229, 2000. https://doi.org/10.1109/50.822796

[11] M. K. Verma and B. B. Pal, "Analysis of buried gate MESFET under dark and illumination," IEEE Trans. on Electron Devices, 48(9), 2138-2142, 2001.https://doi.org/10.1109/16.944207

[12] R. Gautam, M. Saxena, R. S. Gupta, and M. Gupta, "High Sensitivity Photodetector Using Si/Ge/GaAs Metal Semiconductor Field Effect Transistor (MESFET)," in AIP Conference Proceedings, Optics: Pheneomenon, Materials, Devices, and Characetrization, 1391(1), 232, 2011.https://doi.org/10.1063/1.3646835

[13] A. Singh, A. Kumar, M. Gupta, and R. S. Gupta, "Model for dc and rf characteristics of optically biased GaN metal semiconductor field effect transistor for electronic/optoelectronic microwave applications," Optical Engineering, 41(11), 2915-2922, 2002.https://doi.org/10.1117/1.1512909

[14] T. Chen and M. S. Shur, "Analytical models of ion-implanted GaAs FET's," IEEE Trans. on Electron Devices, 32(1), 18-28, 1985.https://doi.org/10.1109/T-ED.1985.21903

[15] Y. H. Byun, M. S. Shur, A. Peczalski, and F. L. Schuermeyer, "Gate-voltage dependence of source and drain series resistances and effective gate length in GaAs MESFETs," IEEE Transactions on Electron Devices, 35(8), 1241-1246, 1988.https://doi.org/10.1109/16.2543

[16] J. M. Golio, "Ultimate scaling limits for high-frequency GaAs MESFETs," IEEE Transactions on Electron Devices, 35(7), 839-848, 1988. https://doi.org/10.1109/16.3334

[17] R. Swoboda, and H. Zimmermann, "2.5 Gbit/s silicon receiver OEIC with large diameter photodiode," Electronics Letters, 40(8), 505-507, 2004. https://doi.org/ 10.1049/el:20040346

[18] F. Tavernier, M. Steyaert, "A high-speed POF receiver with 1 mm integrated photodiode in 180 nm CMOS," In Optical Communication (ECOC), 2010 36th European Conference and Exhibition on, IEEE, 2010, Torino, Italy. https://doi.org/10.1109/ECOC.2010.5621473

[19] Y. Dong, and K. W. Martin, "A high-speed fully-integrated POF receiver with large-area photo detectors in 65 nm CMOS," IEEE Journal of Solid-State Circuits, 47(9), 2080-2092, 2012.https://doi.org/10.1109/JSSC.2012.2200529

[20] M. Atef, R. Swoboda, and H. Zimmermann, "1.25 Gbit/s over 50 m step-index plastic optical fiber using a fully integrated optical receiver with an integrated equalizer," Journal of lightwave technology, 30(1), 188-122, 2012. https://doi.org/10.1109/JLT.2011.2179520

[21] P. Brandl, and H. Zimmermann, "3 Gbit/s optical receiver IC with high sensitivity and large integrated pin photodiode," Electronics Letters, 49(8), 552-554, 2013. https://doi.org/10.1049/el.2013.0558

[22] W. Gaberl, K. Hornstein, R. Enne, and B. Steindl, "Avalanche photodiode with high responsivity in 0.35 μm CMOS," Optical Engineering, 53(4), 043105, 2014. https://doi.org/10.1117/1.OE.53.4.043105

[23] P. Brandl, T. Jukić, R. Enne, K. Hornstein, H. Zimmermann, "Optical wireless APD receiver with high background-light immunity for increased communication distances," IEEE Journal of Solid-State Circuits, 51(7), 1663-1673, 2016. https://doi.org/10.1109/JSSC.2016.2557815

[24] X. Li, N. Bamiedakis, X. Guo, J. McKendry, E. Xie, R. Ferreira, E. Gu,M. D. Dawson, R. V. Penty, and I. White, "Wireless visible light communications employing feed-forward pre-equalization and PAM-4 modulation," Journal of Lightwave Technology, 34(8), 2049-2055, 2016.https://doi.org/10.1109/JLT.2016.2520503

[25] D. Milovancev, T. Jukić, B. Steindl, P. Brandl, and H. Zimmermann, "Optical wireless communication using a fully integrated 400 um diameter APD receiver," The Journal of Engineering, 2017(8), 506-511, 2017. https://doi.org/10.1049/joe.2017.0247

[26] S. Rajbhandari, A. Jalajakumari, H. Chun, G. Faulkner, K. Cameron,R.Henderson, D. Tsonev, H. Haas, E. Xie, J. J. McKendry, and J. Herrnsdorf, "Multigigabit per Second Integrated Multiple-Input Multiple-Output VLC Demonstrator," Journal of Lightwave Technology, 35(20), 4358-4365, 2017. https://doi.org/10.1109/JLT.2017.2694486

[27] J. Luo, A. Grot and D. Psaltis, "Optical FET receivers for neural network applications," In Proc. Optoelectronic Interconnects III (Vol. 2400, pp. 355-362). International Society for Optics and Photonics, Photonics West '95, 1995, San Jose, CA, United States. https://doi.org/10.1117/12.206325

ASTES

Advances in Science, Technology and Engineering Systems Journal Vol. 4, No. 4, 503-508 (2019)

www.astesj.com

ASTESJ

ISSN: 2415-6698

An Investigative Study on Technology Impact on the Quality of Working Life in a University Healthcare and Pharmacy

Andrea Daly*,[1], Dean Richardson[2], Sean Thorpe[2]

[1]*College of Health Sciences, School of Pharmacy, University of Technology, Jamaica, Kingston, Jamaica*

[2]*Faulty of Engineering and Computing, University of Technology, Jamaica, Kingston, Jamaica*

ARTICLE INFO

Article history:
Received: 14 April, 2019
Accepted: 06 August, 2019
Online: 23 August, 2019

Keywords:
Electronic health records
Electronic medical records
Health information systems
Information systems
Change Management
Conceptual framework
Computerized provider order entry

ABSTRACT

The purpose of this study was to investigate the impact of the implementation of the Online Appointment Scheduling system and Pharm Partner system technologies on the quality of working life for users in a small healthcare environment at the University of Technology, Jamaica. Both qualitative and quantitative methods were employed. Two data collection instruments were: interviews and survey forms. The sample included Health Clinic and Pharmacy staff and users of these facilities. The investigation covered a one (1) year period. The Statistical Package for the Social Sciences software version 24.0 and NVivo software were used for data entry and analysis of the surveys and interviews respectively. Findings supported that the systems improved users' quality of working life. Reduced waiting time for patients to access doctors and receive their prescription from both facilities. Pharmacists were able to dispense drugs to patients at a faster rate. Most manual functions at both facilities were automated: the retrieval of patient's appointment scheduled information at health clinic and the retrieval of patient's records at the pharmacy. Pharmacy inventory system was automated, patients at the health clinic were able to go online and see doctors available for appointments.

1. Introduction

The University of Technology, Jamaica Health Clinic provides services in the form of general medical care, family planning, emergency care with referral to hospitals and specialists, health and grief counseling and health presentations. Prior to the implementation of the Online (internet/Computer network connectivity) Appointment Scheduling system, most of their processes were manually driven. Patients were seen on a first come basis except for emergencies and overcrowding of the facility was an issue.

This resulted in the implementation of Online Appointment Scheduling system to replace the walk-in or call-in appointment system. It took approximately nine (9) months to complete the full implementation, which was done on July 21, 2014. Due to financial concerns, an in-house software system was developed by the Enterprise. Application System office (ESA) along with the Learning Technology Support Unit (LTSU) instead of the purchasing of an off-shelf software system.

*Corresponding author: Andrea Daly, University of Technology, Jamaica, adaly@utech.edu.jm

The primary factors that drove the implementation of the Online Appointment Scheduling System were the need to reduce waiting time for patients of the health facility. There was a need also to reduce health facility processing time and stream line operations. The secondary factors were to provide real-time appointment listing, improved quality of service delivery, improved process flow, reporting and to automate some processes that were manually driven.

The University of Technology, Jamaica Pharmacy provided services (which are not limited to) dispensing of prescriptions, Over the Counter (OTC) medications, general information, blood pressure monitoring and patient counseling. Prior to the implementation of the Pharm Partner system, most of their processes were manually driven. Operations were manually intensive with the use of Cardex card system. Staff had to manually locate patient's records which were stored in cabinets, stock and dispense drugs by manually checking the shelves for available drugs and conducted manual inventory filings.

The Pharm Partner system was implemented in the University Pharmacy over ten (10) years ago to automate these processes.

The primary factors that drove the implementation of the Pharm Partner system were the length of time taken to serve patients as most of the processes were manually driven such as the processing of prescription and medical insurances; patients' records were manually stored in file cabinets and their inventory system was manual. A system was required with the following criteria, accuracy, most current version, user friendly and the cost.

Minimal research has been conducted in this area in Jamaica and the Caribbean up to the time that investigated the impact of these technologies on the university population quality of working life. The Aim of this research was to assess user's feedback on what impact to their quality of working life and what improvements were caused by the implementation of the University Online Appointment Scheduling system and the Pharmacy Pharm Partner system. The study also investigated how patients were impacted by the implementation of these technologies.

2. Related Work

The research provided the state of the art with respect to the technology adoption and the perceived impact on users' quality of working life and improvement to the customer experience of such systems within the healthcare environment.

2.1 Conceptual Framework and the Technological Impact on the Changed Management Process

Works carried out by [1], where the authors that examined the implementation of an Electronic Health Records (EHR) system in a small family medicine residency clinic in the University of Wisconsin. They used three data collection instruments to evaluate user experience, work pattern changes, and organizational changes related to the implementation and use of the EHR system. These were an EHR user's survey, interviews with key personnel involved in the EHR implementation project and a work analysis of clinic staff.

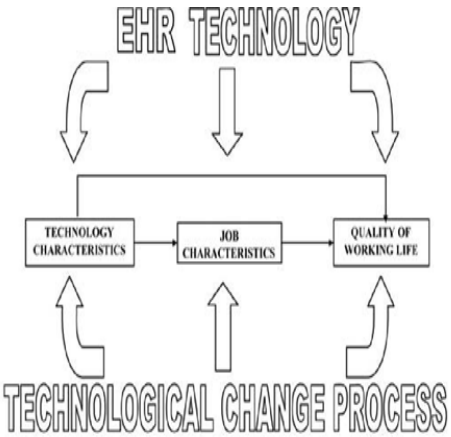

- Technology characteristics: type of technology, functionality, and usability issues
- Job characteristics: job control, workload, uncertainty/clarity, challenge, and role ambiguity
- Quality of working life: job satisfaction, stress, self-reported health, and perceived performance
- Technological change process: employee participation, feedback, project management, information and communication, and training and learning

Figure 1. Impact of EHR technology on quality of working life and performance

Both [2] and [3] examined different frameworks that were appropriate for Health Information Systems implementation and adaptation. However, [2] wanted to know if the technology implemented were actually delivering on the purpose it was implemented for. So [4] explored the present state of technology adoption, where it should be and the gaps that exist and what can be done about it, while [5] examined the benefits and barriers of the technology implementation. However, [6] believed that the technology should be investigated further to see if its implementation and use improved the quality of life. But [7] believed that it was important to investigate if the implementation of the technology impacted more than just the quality of life of users. While [8] believed in doing this the factors and influencers to the technology implementation must be examined. This was further explored by this research along with an examination of [9] change management process to assess changes in the Health Clinic and Pharmacy environment at University of Technology.

2.2 Factors and Influencers to the Technology Implementation

Accordingly [8] concluded that health system stakeholders cannot expect their health care system's performance to meet the increasing demand placed on it, unless interventions were taken. The authors believed that health information systems were seen to be one solution to the pending problem and such solutions can assist physicians in tracking patient medical history, interventions, encounters, lab test results as well as managing allergies and drug contraindications. The authors stated that implementations were not simple technical projects. Implementation as believed by the authors comes with risks, the apprehension over which can paralyze a health information systems project in its tracks or even prevent it from starting altogether. Countries studied by the authors were choosing to use health information systems as one of many strategies to alleviate concerns, these countries as stated by the authors, established policies to drive the adoption of health information systems, or even mandate them, thereby placing physician offices in a position where they were implementing systems even if they were not ready for such change.

In their discussion, [8] revealed that their literature review was a comprehensive systematic search of several sources to understand factors which affect implementations of health information systems in general practice. They provided a chart as shown Figure 2 to illustrate several factors which affect the goal of implementation success. This chart shows the "fit factor" or "socio-technical factor" directly adjacent to the project goal, as the review found it can directly influence implementation success. The authors also mentioned that implementers also had concerns over privacy, patient safety, provider or patient relations, staff anxiety, time needed to implement, quality of care, financial, efficiency, and liability. From their research the authors highlighted that these risks can be managed through sound project management, strong leadership, and implementation of standardized terminologies and staff training as stated in articles they researched. This [8] illustrated in Figure 2, by showing four

insulating factors inserted between risk factors and the project goal.

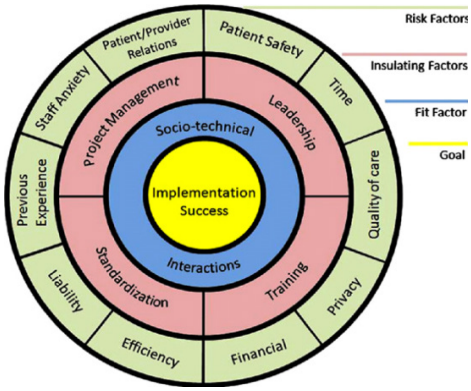

Figure 2. Insulating and Risk Factors

2.3 The Impact of Technology

The research of [7] believed that implementing an information technology system can impact more than just quality of care and patient outcomes. The authors therefore proposed a four (4) years, observational research project to examine changes in organizational culture Quality Improvement (QI) maturity, and quality of care following adoption of a single electronic health record (EHR) system within an integrated healthcare network. The authors' main results were to measure the Culture and Quality Questionnaire (CQQ), and assess the perceived culture of an organization and the degree of CQI maturity in seven quality management areas.

According to [7], the authors distributed Baseline surveys before the conversion to the EHR system. They then collected primary data over a period, 12 months post "go live" and subsequently, 24 and 36 months after the first hospital "go live". The authors used routinely collected patient satisfaction measures and standard quality indicators to abstract secondary data. [7] findings proved contrary to their expectation, the Baseline and 12 month follow-up data suggested that employees perceived the organizational culture as becoming more, rather than less, hierarchical. Also the authors had hypothesized that quality indicators would show improvement due to enhanced information flow and ease of information retrieval, this was not supported by 1-year results. According to [7], years two and three follow-up data may have provided different results. From its research, the authors revealed that IT tools, such as computerized clinical decision support systems and computerized physician order entry, can improve physician performance and patient outcomes. The authors went on to point out that, from their research it became increasingly clear that successful implementation and utilization of IT systems (and their resultant effects on care) depends on a variety of factors. Some of the factors the authors mentioned included technical, individual, and organizational variables. What [7] believed is that the ultimate shape and "success" of IT depends upon and emerges from a complex, multidimensional interaction between IT and the individual and organizational users. It was the belief of the authors that in order to more fully understand the outcome of IT implementation efforts, one should consider the relationships between systems, individual and organizational characteristics and how they affect each other. The authors reported initial (i.e. first 12 month follow-up) results from their 4 years project, evaluating changes in organizational culture and quality, during and subsequent to conversion to an electronic health record (EHR). The authors also provided some preliminary information on the relationship between one important organizational characteristic, organizational culture, and the impact of a new IT initiative, the implementation of a system wide EHR, on quality of care. Several limitations to their research [7] pointed to were:

1. The authors were only able to survey managerial level staff and above due to finite resources. They believed that employees at other levels may have answered their surveys very differently.
2. Their research was done as an observational study. They found that there were potential confounding factors within the organization and the larger healthcare arena that they were unable to control (for e.g. mandated changes in employee benefit packages, provider salary structure) and that may have influenced their results.
3. Finally, since the authors' focused on group level rather than individual-level attributes and wanted to obtain input from a large number of people in the most efficient way possible, they used only quantitative measures to assess culture and degree of CQI maturity.

4. Method

The study employed a mixed method design and used two instruments for data collection. The instruments used were 1) the random sampling survey of users impacted by the Health Clinic Online Appointment Scheduling system and the Pharmacy Pharm Partner system and 2) interviews of key personnel involved in the implementation of these systems. Both quantitative and qualitative approaches were employed. The two data type instruments that were used were the User's Survey – Online and Paper-based and Interviews of key personnel, the Health Clinic Administrator and the Pharmacy Manager. The general interview guide was structured that included implementation background, post implementation process, including goals, training, health information system support and changes in the working environment. The survey conducted was a Simple Random Sample (modeled from the Questionnaire for User Interface Satisfaction). Three Survey forms were used, one each for the Health Clinic staff, Pharmacy staff and the wider University population impacted by the Health Clinic Online Appointment Scheduling system

The university main campus is located in the Greater Kingston Metropolitan Region in Papine, in the parish of St. Andrew. The sites that were studied were the University of Technology Jamaica Health Clinic and the University of Technology Jamaica Pharmacy, both located at the University of Technology, Jamaica. The population size of approximately 13500 (Staff & students) had General Users Online Appointment Scheduling system *(n* = 153), health clinic staff (*n*= 9) and Pharmacy staff (n = 8). To have a reasonable sample from which to make suitable

generalization, 1870 students and staff were asked to participate in this survey. This gave a required sample size of approximately 374 respondents, with a margin of error of 5%, confidence level of 95% and an estimated response rate of 20%. The research survey was inclusive of University of Technology Jamaica Health Clinic staff, Pharmacy staff, Office staff, Lecturers, wider University staff, Part time and Full time students who were 18 years and older. The research excluded non University staff and students below the age of 18 years old.

5. Data Analysis

Survey data collected primarily through self-administered questionnaires & online questionnaires using Google Forms. The Statistical Package for the Social Science (SPSS) software version 24, distributive statistics frequency test and Kruskal Wallis Nonparametric Test were used to analyze the data. Interviews answers were organized through the data management tool NVivo for windows version 11.4.1.1064 software.

6. Results and findings

Structured interviews were conducted with both the University of Technology Jamaica Health Clinic and Pharmacy to answer two of the three research questions, similar to the one carried out by [1] in their research.

Table 1: Analysis of the health clinic interview

Research Question 1: How did the quality of working life for Health Clinic staff change after the implementation of the Online Appointment Scheduling System within the University of Technology health care environment?			
Health Clinic			
Question Structure	**Findings & Results**	**Question Structure**	**Findings & Results**
Post Implementation process:	Noticeable increase in the dependency of computers. Staff and patients were complimentary. General attitude of staff was that quality of work life improved.	**Changes in working environment:**	Improved flow in the work process. Less crowded waiting area. Staff excited working with the system
Issues.	Inability to logon network, inaccessible appointment slots, increased input time.		

Table 2: Analysis of the pharmacy interview

Research Question 2: How did the quality of working life for Pharmacy staff change after the implementation of the Pharm Partner System within the University of Technology Pharmacy environment?			
Pharmacy			
Question Structure	**Findings & Results**	**Question Structure**	**Findings & Results**
Post Implementation process:	Noticeable increase in the dependency of computers. Records are now kept in database. Information is retrieved by patients' ID. Search time and Processing time reduced. General attitude of staff was that quality of work life improved.	**Changes in working environment:**	Increased efficiency, improved inventory management and reduced search time. Positive attitude by staff.
Issues.	Staff reported physical problems due to prolong computer usage		

Table 3: Analysis health clinic staff survey question 1

Research Question 1: How did the quality of working life for Health Clinic staff change after the implementation of the Online Appointment Scheduling System within the University of Technology health care environment?	
Health Clinic Staff	
Survey Question	**Are you able to efficiently complete your work using this system?**
Analyze Descriptive Statistics Frequency Test	9 staff members responded to this question 77.78% said 'Most of the Time' 11.11% said 'Sometimes' 11.11% said 'Unlikely'
Surveyed Category	Online Appointment System ($P < 0.05$)
P-value	P value = 0.570
Hypothesis	H0 'The answers for each roles/positions were equal, there was statistically no significant difference in mean rank answers for the different roles/positions'.
Decision	Fail to Reject null hypothesis

Table 4: Analysis health clinic staff survey question 2

Research Question 1: How did the quality of working life for Health Clinic staff change after the implementation of the Online Appointment Scheduling System within the University of Technology health care environment?	
Health Clinic Staff	
Survey Question	**What is your overall experience using the Online Appointment System to Fulfilling a patient appointment?**
Analyze Descriptive Statistics Frequency Test	*9 staff members responded to this question* *66.67% said 'Very Good'* *11.11% said 'Excellent'* *11.11% said 'Good'* *11.11% said 'Satisfactory'*
Surveyed Category	Online Appointment System ($P < 0.05$)
P-value	P value = 0.254
Hypothesis	H0 'The answers for each roles/positions were equal, there was statistically no significant difference in mean rank answers for the different roles/positions'.
Decision	Fail to Reject null hypothesis

Table 5: Analysis pharmacy staff survey question 1

Research Question 2: How did the quality of working life for Pharmacy staff change after the implementation of the Pharm Partner System within the University of Technology Pharmacy environment?	
Pharmacy Staff	
Survey Question	**Are you able to efficiently complete your work using this system?**
Analyze Descriptive Statistics Frequency Test	8 staff members responded to this question 75.00% said 'Most of the Time 25.00% said 'Sometimes'
Surveyed Category	Online Appointment System ($P < 0.05$)
P-value	P value = 0.564
Hypothesis	H0 'The answers for each roles/positions were equal, there was statistically no significant difference in mean rank answers for the different roles/positions'.
Decision	Fail to Reject null hypothesis

Table 6: Analysis pharmacy staff survey question 2

Research Question 2: How did the quality of working life for Pharmacy staff change after the implementation of the Pharm Partner System within the University of Technology Pharmacy environment?	
Pharmacy Staff	
Survey Question	**What is your overall experience using the Pharmacy Prescription System to fill a patient prescription?**
Analyze Descriptive Statistics Frequency Test	8 staff members responded to this question 37.50% said 'Satisfactory' 25.00% said 'Very Good' 25.00%% said 'Good' 12.50% said 'Excellent'
Surveyed Category	Online Appointment System ($P < 0.05$)
P-value	P value = 0.365
Hypothesis	H0 'The answers for each roles/positions were equal, there was statistically no significant difference in mean rank answers for the different roles/positions'.
Decision	Fail to Reject null hypothesis

Table 7: Analysis general users survey question 1

Research Question 3: How did the Online Appointment Scheduling system provided improvements in appointment scheduling to the general users who were impacted by the system implementation?	
General Users	
Survey Question	**How long do you have to wait after arriving at the prescribed time given for your scheduled appointment?**
Analyze Descriptive Statistics Frequency Test	149 out f 153 persons responded to this question 36.24% said 'At least 15 minutes waiting time' 27.52% said 'More than an hour' 17.45% said 'I see the doctor according to my appointment time 8.73% said 'Sometimes Half day' 5.37% said 'I see the doctor immediately' 4.69% said 'Sometime I do not get to see a doctor'
Surveyed Category	Online Appointment System ($P < 0.05$)
P-value	P value = 0.259
Hypothesis	H0 'The answers for each roles/positions were equal, there was statistically no significant difference in mean rank answers for the different roles/positions'.
Decision	Fail to Reject null hypothesis

Table 8: Analysis general users survey question 2

Research Question 3: How did the Online Appointment Scheduling system provided improvements in appointment scheduling to the general users who were impacted by the system implementation?	
General Users	
Survey Question	**What is your overall experience using the Online Appointment System to make an appointment?**
Analyze Descriptive Statistics Frequency Test	Out of the 153 persons surveyed 147 persons responded to this question 41.50% said 'Very Good' 27.89% said 'Good' 17.69% said 'Satisfactory' 9.52% said 'Excellent' 3.40% said 'Poor'
Surveyed Category	Online Appointment System ($P < 0.05$)
P-value	P value = 0.230
Hypothesis	H0 'The answers for each roles/positions were equal, there was statistically no significant difference in mean rank answers for the different roles/positions'.
Decision	Fail to Reject null hypothesis

7. *Discussions Online Appointment Scheduling/Pharm Partner Systems*

The results revealed that the processing time on arrival at the Health Clinic/Pharmacy were more efficient and less time consuming since the implementation of the new system. Pharmacy/Health Clinic staffs depended on the technologies to better function in their jobs. Results showed that both systems automated certain manual processes/reporting procedures that were resource manual intensive. These results reflected [1], that showed that the work of clinical and office staff changed significantly (reduction in time spent distributing charts, transcription and other clerical tasks, etc.) The general users believed that their waiting time overall was shorter and over 78% believed that their overall experience using the systems were from good, very good to excellent. This was reported performance of *P-values* was 0.238. Although statistically no significant difference in answer given between the different roles/positions, this was similar [1] who reported performance *P value* = 0.800 with statistically no significant difference. This was in contrast to [7] research which *P values* were mostly below 0.05, indicating statistical significant differences.

The quality of working life indicators showed improvement since the technologies were implemented in both facilities. This was observed in reduced waiting time, automation of processes, ease of access to services and increase in employee's satisfaction. This reflected [6] and [1] work which showed improvement of quality of working life for job satisfaction.

8. Conclusion

The Technologies have improved the quality of working life of the users they impacted. The systems users have seen a vast improvement in the way they carried out their functions since the system implementation, therefore an improvement in their quality of working life. This was a perceptual study; quality of working life was greatly influenced by the personal characteristics of those who determine it. Determining the quality of working life always involved the interplay between and among the worker, the users, job content, job context and the technology. This was in keeping with the literatures of [8], [1] and [7] who believed that technology will impact the quality of life of users but also organization and human factors will impact also. It was realized that technologies improved the quality of working life of the users.

This research just like [6] was not a refutation of previous studies. It was suggested that as technology use broadens, one should not assume an automatic diffusion of improved quality of working life to users.

Conflict of Interest

The authors declare no conflict of interest.

References

[1] P. Carayon, P. Smith, A. Hundt, V. Kuruchittham, & Q. Li, Implementation of an electronic health records system in a small clinic: the viewpoint of clinic staff. Behaviour & Information Technology, 28(1), 5-20, 2009.

[2] M. Yusof., A. Papazafeiropoulou, R. Paul & L. Stergioulas, Investigating evaluation frameworks for health information systems. International Journal of Medical Informatics, 77(6), 377-385, 2008.

[3] D. Bell, S. Cretin, R. Marken, &A. Landman, A conceptual framework for evaluating outpatient electronic prescribing systems based on their functional capabilities. Journal of the American Medical Informatics Association, 11(1), 60-70, 2004.

[4] J. Ash & D. Bates, Factors and forces affecting EHR system adoption: report of a 2004 ACMI discussion. Journal of the American Medical Informatics Association, 12(1), 8-12, 2005.

[5] J. Anderson, Social, ethical and legal barriers to e-health. International Journal of Medical Informatics, 76(5), 480-483, 2007.

[6] J. Linder., J. Ma, D. Bates, B. Middleton & R. Stafford, Electronic health record use and the quality of ambulatory care in the United States. Archives of internal medicine, 167(13), 1400-1405, 2007.

[7] C. Nowinski, S .Becker, K. Reynolds, J. Beaumont, C. Caprini., E. Hahn. & B. Arnold, The impact of converting to an electronic health record on organizational culture and quality improvement. International Journal of Medical Informatics, 76, S174-S183, 2007.

[8] D. Ludwick & J. Doucette, Adopting electronic medical records in primary care: lessons learned from health information systems implementation experience in seven countries. International Journal of Medical Informatics, 78(1), 22-31, 2009.

[9] V. Rama Devi & S. Charan, Conceptual Model for Effective Change Management, 2013.

ASTES

Advances in Science, Technology and Engineering Systems Journal Vol. 4, No. 4, 509-516 (2019)

www.astesj.com

ASTESJ

ISSN: 2415-6698

Embedded Artificial Neural Network FPGA Controlled Cart

Mohamad Faiz Ahmad, Syed Sahal Nazli Alhady*, Ooi Zhu Oon, Wan Amir Fuad Wajdi Othman, Aeizaal Azman Abdul Wahab, Ahmad Afiq Muhammad Zahir

School of Electrical and Electronic Engineering, Engineering Campus, Universiti Sains Malaysia, 14300 Nibong Tebal, Pulau Pinang, Malaysia.

ARTICLE INFO

Article history:
Received: 02 June, 2019
Accepted: 16 August, 2019
Online: 23 August, 2019

Keywords:
Artificial neural network
Color code
Field programmable gate array
Mobile robot
Multilayer perceptron
Root mean square error
Verilog HDL

ABSTRACT

An artificial neural network (ANN) computing system can be significantly influenced by its implementation type. The software implemented ANN can produce high accuracy output with slow computation time performance compared to hardware implemented ANN which runs at a faster computation time but with low accuracy. Normally, software implementation reduces the proficiency and efficiency of the model. Robot performance plays an important role as it needs fast response to process information that is applied with ANN. As a consequence, the proposed research focuses on comparison between hardware and software implementation multilayer perceptron (MLP) for cart follower in Field Programmable Logic Array (FPGA). Both of the software and hardware models produced the same precision where the output distance at angles -10°, 0° and 10° shows same percentage error. Besides that, both of the models have similar root mean square error (RMSE) which are 0.469, 0.479 and 0.267 at -10°, 0° and 10° respectively. The processing time of MLP model implemented in hardware and software are at 1.91µs and 78.06µs respectively. Thus, it can be concluded that hardware implementation is better than software implementation.

1. Introduction

The concern of societies in creating a quality of life for everyone has become prevalent. Therefore, lots of research on creating infrastructures and tools to ease the daily activities of people are fostered. This has led to the research on designing and fabricating of robots. In this technological era, the world is making a great stride towards autonomous systems. An autonomous system is referred to as a system that is capable of operating in the real-world environment without any external controls. It can maintain its internal structures and processes for extended periods and capable to adapt toward environmental change. The overall architecture of the robot consists of sensors, actuators and intelligent processors [1].

Autonomous robotic vehicle is able to perform intelligent motion and action without guidance or tele-operator control. It is used for remote repair and maintenance, a motorized system for office and factory and even an intelligent wheelchair for the handicapped [2]. It is also known as a mobile robot or embedded robot. After a long research, the mobile robot today is smaller with numerous actuators and sensors controlled by inexpensive embedded computer system as a processor [3].

Visual tracking is commonly utilized in a various of robotic applications that need the localization of moving target like machine learning, human machine connection and robot navigation. It proposes object tracking through the literature and algorithm based on the particular cue observation like edges, color and feature templates. Each of the cues can provide reliable tracking under limited conditions [4].

Artificial neural network (ANN) is defined as an operation of a biological ANN system [5]. It makes the computer able to simulate a human in processing the data and behave intelligently in some ways like pattern recognition. It gathers all the information pattern based on the input data and produce a desired result. The production of ANN can be concluded as a process that gathers enough knowledge to produce a model with a correct sequence of the rules that satisfies the expected condition.

*Syed Sahal Nazli Alhady, School of Electrical and Electronic Engineering, Engineering Campus, Universiti Sains Malaysia, 14300 Nibong Tebal, Pulau Pinang, Malaysia, +604-5996019, sahal@usm.my

ANN comprises of data collection, data analysis and decision making with different approaches in each stage [6]. ANN can be used to control the physical actions of a mobile robot which enable it to navigate through the environment and manipulate items and solve other situations. The production of ANN can be characterized as a search process to search for the correct sequence of rule as control strategy with enough knowledge in a database to produce the termination condition [7].

The main purpose of this research is to perform MLP implementation into FPGA and evaluate the network performance. Therefore, the following objectives are being set to achieve the aim of this research:

- To perform MLP implementation of ANN into FPGA.
- To compare the performance of MLP implemented hardware and software in FPGA.

The embedded MLP data in FPGA is only used as a tool to implement the operating system of Cart Follower using the FPGA. So, any data from the MLP is only used as a reference. The research mainly focuses on data comparison between MLP hardware and software implementation in FPGA. Thus, an analysis on both type of implementations will be obtained and discussed.

2. Literature review

2.1. Mobile robot

There are several mobile robot-based localization methods present which can be roughly divided into 2 general classes. The first class is without its local position information. It keeps track of the robot's position to enable localization. The second class is with its local position information. It uses the global position estimate to enable localization. For the mobile robot in the second class, it is normally equipped with GPS for localization and estimate the distance (indoor positioning tracking) [8]. For the mobile robot in the first class, it can be described as following to keep track or follow object. Examples of the robot are leader following, human following, line or path following and sound following. The method to achieve the task of following might vary in the hardware or sensor used. Ghandour et al. [9] came out with a collision avoidance mobile robot based on human interaction. Kinect sensor with motion identification became an interface for humans to interact with. The robot will navigate directly to the target if there is no human around for interaction process.

CMUcam used as a tracking sensor contributed to a successful autonomous mobile robot. The taken value of camera's field of view (FOV) with several details from other sensors gathered as well to establish the robust tracking system [10-13].

Leader following robot is mobile robot that follows the command of the leader robot. It can be used as an active signal positioning machine to discover and track the leader position [14]. The leader robot works together with all its following robots to move the box. AI follower forces will synchronize with the direction of the force applied by the one leader robot although there is no communication between the follower robots [15].

Human following robot has an ability to coordinate the human motion in a populated, continuously changing, natural environment. For Prassler model, Velocity Obstacle approach is applied for motion planning amongst moving obstacles. Besides, the model also tracks the virtual target to manipulate the direction and velocity of the robot's movement according to the person it follows [16]. For ApriAttenda model by Yoshimi, it uses the image processing to define region of interest. Then it recognizes the texture and color of the subject. The specific person is then detected from the specification and the human position is calculated. Stereo vision with systemizing visual and motion control helps to grab the details on the distance to each features like color, targeted speed and point for a stable tracking in many situations [17]. Line or path following robot is route-based following robot. It uses line tracking method with the implemented Infrared Ray (IR) sensors. The IR sensors was set up and distributed according to its position and informing the line location to maneuver the navigation [18].

Another type of following robot is sound following. It can detect the presence of human based on specific sound frequency. Luo et al proposed a mobile assistive companion robot that used laser and vision sensor to follow the aimed person. The robot was made up of a laser range finder, a tracking camera and a microphone. It contains lot of sound source recording system to perform an interaction with human. This function is useful to detect the user if the robot lost its tracking path. The microphone's function was to grab the sound wave in time delay of arrival (TDOA). The laser finder was used to detect the lower part of human and the camera was used to track the upper part of human [19].

The optimization of ANN with the trajectory tracking control system proposed lead to enhancement of orientation and motion control of autonomous vehicle's performance. The trained evaluator manages to acknowledge both linear and nonlinear systems behavior due to ANN structure that allows complex variables mapping [20]. In an instance, the increment of the system performance is only temporarily boosted for a certain time.

2.2. FPGA cart follower

Field Programmable Gate Arrays (FPGA) are advanced microprocessor created to be programmed by the user [21]. It contains a sets of configurable logic blocks (CLB), multiplexers, look table and flip flops. CLB provides physical support for the program downloaded on FPGA [22]. Hence, it supports the sequential functions and complex computations [23]. ANN implementation in FPGA is possible as it preserves the parallel architecture of the neurons in a layer and offers flexibility in reconfiguration. FPGA maintains high gate density which is needed to utilize the parallel computation in an ANN [22]. Most of ANN are implemented in software. A project, "Investigation on MLP ANN Using FPGA for Autonomous Cart Follower System" [24]. This project shows that the hardware floating-point acceleration block increases the logic element resource utilization. This project focuses more on the system on chip (SOC) design but not on hardware implementation. Software configuration has the advantage of being easy to implement but with poor performance. Hardware configuration is generally more complex to be implemented but with better performance.

2.3. Artificial neural network

ANN ideas came from computer programs engineered to mimic how human brain thinking and making a decision [25].

ANN is one of the main tools used in machine learning. A simple neuron made up of three layers, which are the input layer, hidden layer, and output layer [26]. Figure 1 shows an ANN MLP model.

• Input layer: This layer is responsible for receiving signals, information (data), and features from the external environment.

• Hidden layer: These layers will extract patterns in neurons and analyzing the processor system. It transforms the data from the input layer to the output layer as a final product.

• Output layer: This layer is responsible for creating the final outputs, which the processed neurons in the hidden layer.

There are two main procedures in design ANN which are forward process and backward process. Feedforward ANN is known as data-driven. It defines the number of layers, the number of neurons in each layer, what kind of training method and activation function are selected, and then passes input data through the network. Backpropagation ANN is known as goal-driven. It defines the loss function to calculate the gap between the prediction value and the labelled values. It looks for the minimum value of the error function in weight space using gradient descent [27]. The weights will get updated to optimum weights. One feed forward and back propagation process can be called as one epoch and a trained ANN model need hundreds or thousands of epochs.

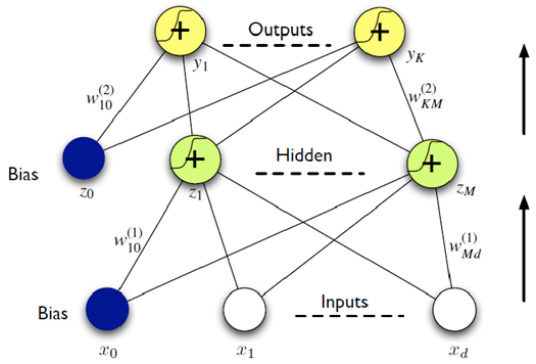

Figure 1: ANN MLP model

2.4. Hardware ANN FPGA implementation

Wibowo et al. [28] presented of the hardware implementation ANN algorithm in FPGA to solve reconfigurable computing (RC) issues. Speed and space are two main factors to be considered on performing parallel processing method. The processing speed rely on time taken by the route and logic gates meanwhile space rely on FPGAs component utilization. The ANN can be illustrated as a proportional graph composed of multiple edges. It functions as a communicator to send information to other parts through weighted connections. The FPGA has reached a successful penetration in various domains. The improvement could be made by adding activation function components to further increased the processing speed.

Gaikwad et al. [29] proposed a hardware implemented FPGA for military equipment that uses an MLP algorithm to perform classification tasks. Parallel MLP computation was implemented to reach enhanced hardware design. The evaluation of the overall system has been made by UCI dataset with 20 samples. The training, validation and testing process was held on 10 different MLP models. The time taken for classification was 270 ns and used 120 mW of power. The result shows that the performance efficiency was better than other hardware MLP implementation in FPGA in term of processing time.

Zeng et al. [30] presented a worldwide embedded hardware implementation ANN to balance the parallel connected current suppression. The focusing part is on control execution and strategy. The ANN was adapted with PID controller to yield the characteristics of the current suppression. It can be refined automatically to control the PID parameters based on various real world feedbacks and fit with linear and non-linear current. The analysis on ANN-PID shows that there was 0.023% of mean error in current control and the performance was increased up to 5.5 times as the load expanded.

2.5. Software ANN FPGA implementation

Jia et al. [31] proposed a mixed gas online detector instrument based on ANN algorithm in FPGA software implementation to detect natural gases. The proposed method can simply acknowledge the concentration of three different gases that are mixed together and separate them individually by back-propagation (BP) MLP ANN technique. The gases compositions were measured by infrared gas sensors due to its long life and fast response. FPGA has an advantage in solving parallel computation in a small size with quick response. The BP MLP ANN technique was attached with FPGA. The results show that the three gases maximum error were reduced from 0.64% to 0.27, 1.02% to 0.32 and 1.34% to 0.42% respectively. The response time taken for the proposed method to separate three gases completely is about half minute.

Cedano et al. [32] came out with a configurable architecture for ANN with FPGA in an SOC implementation. They used Multilayer Feedforward NN (MFNN) to produce the transfer functions. This architecture depends on memory blocks, multiplexers and single perceptron that enable the information collecting process. Extended kalman filter has been used to obtain the best weight values for the MFNN. The function blocks in the FPGA for configuring the MFNN was controlled with SOC microprocessor. The result shows that the generalization of root mean square error (RMSE) obtained for uncertain inputs was -32.82 dB. However, the desired resources by a custom implementation were directly proportional to the MFNN size.

3. Proposed methodology

3.1. Overall scheme

The beginning of the project started with literature review on previous researchers. This showed ANN embedded systems. After that, the proposed MLP algorithm was presented to obtain the best weights and biases throughout the network. For instance, the model for activation function was proposed to enable the learning process of complex mappings between the inputs and response variables. The sequences were proceeded with software and hardware implementation after the model was tested. The proposed model was then simulated with MATLAB. Debugging was done if the output is not close to the targeted output. At the last, an analysis was carried out on both software and hardware implementation model in FPGA and the performance for both implementations were then compared. Figure 2 shows the general flow chart of the research.

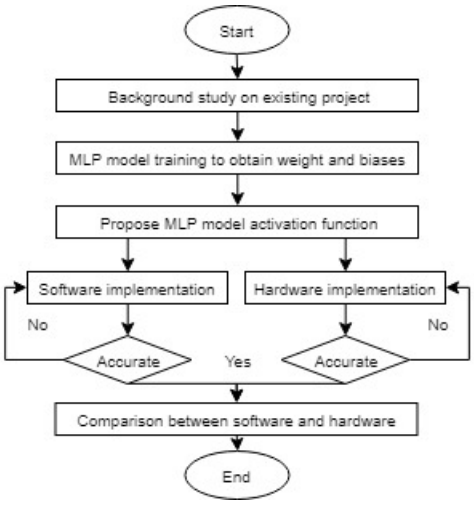

Figure 2: General flow chart of the research

3.2. Data acquisition

The color code (CC) will vary according to x and y axis. The CC has been placed at 30cm from ground level as it was the desired position for tracking camera of cart follower. CMUcam5 will illustrate the cart meanwhile the targeted illustrated by CC from 20cm to 69cm. The perpendicular distance is variate for each centimeter. In addition, angle of the CC has been chosen as manipulated variable to determine the movement of the CC to the right and left. Figure 3 shows the experimental set up of data collection. The step size for the angle is 5°. Table 3 shows the range of angles according to the distance. Each manipulation of distance and angle between the camera and color pattern obtained a different set of raw data. These raw data were used to train the model of the ANN in order to generate the weights and biases used to predict the output distance and angle.

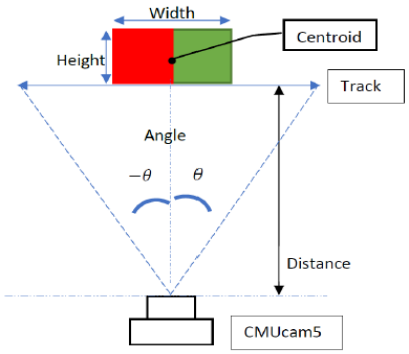

Figure 3: Experimental setup for data acquisition

3.3. Data training

The proposed model made up of three layers. They are input, hidden and output layer. Backpropagation MLP is used to update the overall system. Weights and biases are improved until ideal value has been reached. Cost function is used to figure out the expected output and pathway to enhance the weights and biases. The RMSE value is reduced throughout the training processes. The gradient function is decided from MLP which associated with reverse computation and plays an important role in balancing the weights and biases. The output for the MLP system can be shown by dot product Y=W.X where Y is the final output, W is weight and X is a vector. The system will efficiently worked if the weights are ideal and the training is well converged.

3.4. Simulation of MLP model

After the weights and biases have been obtained, the entire model was simulated to evaluate the model endurance. Raw data was directly fed into the input block as well as to the ANN function block and creating the desired output of distance and angle. An evaluation of the system reliability has been made from the output for error test analysis. Figure 4 shows the Simulink block diagram for the MLP model.

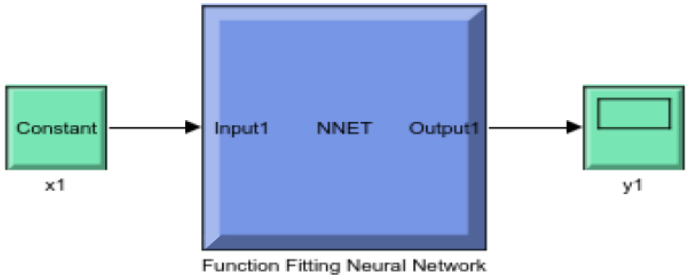

Figure 4: Simulink for the MLP model

3.5. Hardware implementation of ANN in FPGA

The hardware implementation was performed by using Verilog HDL language. Each implemented block represents as a CLB. The blocks are separated into branches due to multi-operation point of IP block. There are two output blocks due to two final output desired by the designed model. Figure 5 shows the MLP model block diagram.

The multi-cylce of IP block foating point can run in parallel. The sequential state operation relying on the start and done signal. Both start and done pins of the block indicate as the start and end of arithmetic computations respectively. If all of the IP block start signal simultaneously, it is considered parallel while programming to use done signal after to feed to other IP block can consider sequential. Single HDL code compilation can contain multiple start and done signal. Figure 6 shows the IP block for multi cycle floating point used for various float number computation in FPGA. 10 hidden layer networks were being fed into the output layer due to 10 hidden neurons (HN) used. Figure 7 illustrate the overall layer of the HN output block diagram.

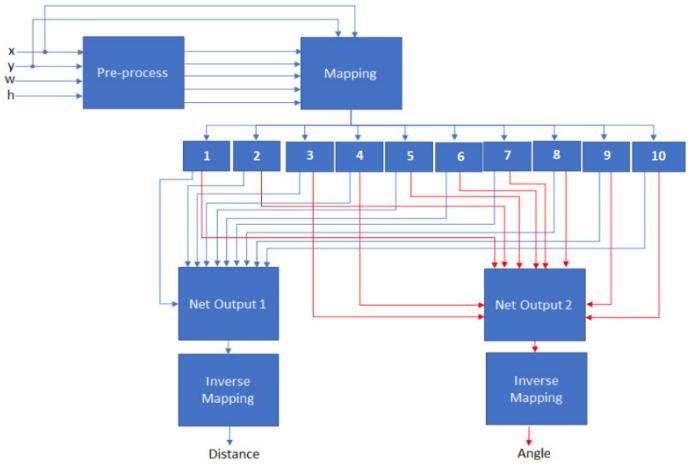

Figure 5: MLP model block diagram

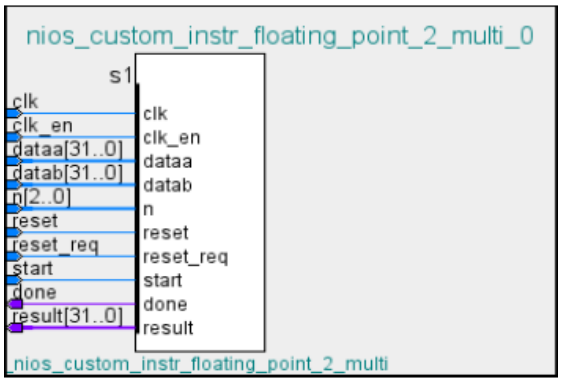

Figure 6: IP block for multi cycle floating point

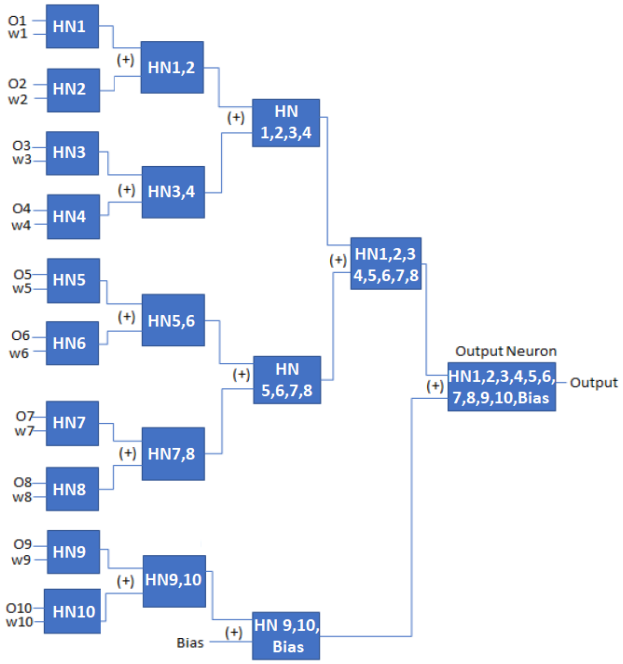

Figure 7: FPGA HN layer block diagram for one output neuron

3.6. Software implementation of ANN in FPGA

The system consist of a clock to sample data, a NIOS 2 processor was used to grab the C Code program, an on-chip memory was used to store the program and a JTAG interface was used as debugger. The C code was compiled and run in SOC RAM in FPGA. The SOC system shown in Figure 8 is modelled after the FPGA to execute the C code of the ANN program.

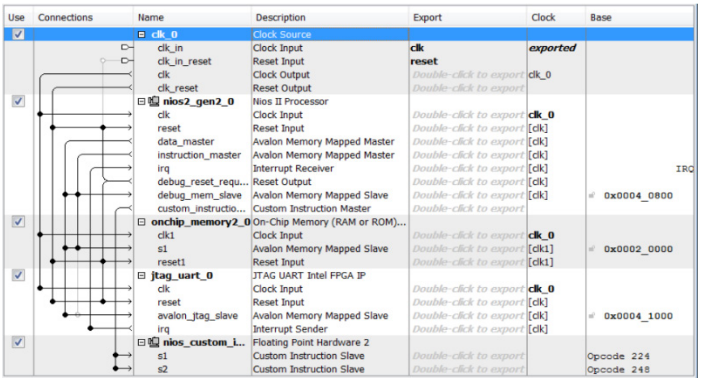

Figure 8: SOC system for software implementation

3.7. Comparison analysis of performance between hardware and software implementation MLP model

There are a few analysis done upon the completion of the FPGA model. The system reliability was relied on the output precision. The simulated output is compared with the real data to get the percentage error. Hence, the reliability of the proposed system can be evaluated. Equation (1) shows the calculation of percentage error:

$$\%error = \frac{|Actual\ data - Stimulated\ data|}{Actual\ data} x\ 100\% \quad (1)$$

The system efficiency for both of hardware and software implementation was computed in MATLAB. After that, the expected output from both of the implementations were compared to inspect the system precision.

An additional analysis for determination of the reliability of the model was carried out using RMSE calculated from output data of the simulation. The purpose of the RMSE analysis on the model is to compare the regression between output from model in software implementation and hardware implementation of the MLP. By using this method, more accurate evaluation for the reliability of the system can be established. The formula of the RMSE is as equation (2):

$$RMSE = \sqrt{\frac{\sum_{i=1}^{n}(Actual\ data - Stimulated\ data)^2}{n}} \quad (2)$$

The execution time for both types of implementation were evaluated in ModelSim testbench interface to compare the performance. The execution time for hardware model was evaluated from the beginning of input signal to the MLP network up to the output signal at output layer meanwhile the software model was evaluated from the signal function to end of execution line in the instruction coding.

Table 1: Part of acquisition data

Distance (cm)	Angle (°)	X (pixel)	Y (pixel)	Width (pixel)	Height (pixel)
20	-10	133	93	200	111
	0	163	93	208	112
	10	193	92	202	111
30	-10	126	94	144	81
	0	161	94	151	82
	10	197	92	147	81
40	-10	125	103	108	59
	0	162	102	113	60
	10	200	100	109	59
50	-10	123	103	88	47
	0	161	102	91	48
	10	200	100	88	47
60	-10	122	98	75	41
	0	162	96	78	41
	10	202	95	76	40

4. Results and discussions

4.1. Data acquisition

The sets of data taken from Pixy CMUcam5 camera are distance, angle x-coordinate, y-coordinate, width and height. The

area was internally calculated from width and height. Table 1 shows some parts of the acquisition data which are then used for further analysis in this research.

4.2. Weight and biases of MLP data training

Each neuron mapping produced single weight. As 10HNs present in the network, 10 weights generated and mapped to single output neuron. The total weights created were 20 since two output desired by the proposed design. Afterwards, two biases were created for each output neurons. Table 2 presents the generated weights and biases from the hidden to output layer of the network.

Table 2: Weights and biases generated from hidden to output layer

Output of HN	Distance weights	Angle weights
1st input	0.3574	0.6727
2nd input	1.1827	0.0759
3rd input	-0.3486	0.1218
4th input	-0.9544	-0.2467
5th input	-0.6976	-0.8491
6th input	-0.8869	0.3532
7th input	-0.5178	0.7513
8th input	0.5719	-0.3702
9th input	0.5328	-0.4183
10th input	0.8046	-0.0626
Bias	0.5993	0.2710

4.3. Simulation of MLP model

All output distance obtained from the MATLAB Simulink simulation showed no significant differences as the outputs resemble closely to each other with less than 3. By considering that the difference between the percentage error is low, practically it is absolutely normal and acceptable considering that the factors affecting the model in real world is taken into account in the simulation. Even though, an ideal case of equivalent percentage error for each data is impossible to be obtained as there will still be the linearity factor that affect the training process. Then, at three different angles of -10°, 0° and 10°, RMSE of 0.469, 0.479 and 0.267 respectively were successfully obtained. Similar to the case of non-equivalent percentage error produced, it is probably caused by linearity factor during raw data training where the training software is not linear and consistent. During initial training of raw data, random numbers are assigned as weight and bias to each neuron. Each cycle of repetitive training will constantly update these random numbers to predict the closest targeted output.

There are slight differences between calculated RMSE and percentage error for each output data due to short training time. The improvement could be made if the training is carried out rapidly on the data and will enhance the predicted output more accurately. Nevertheless, the percentage error and RMSE evaluation is only used as a reference to determine the reliability of the model developed. As stated in the scope, ANN and data training is only used as a tool to implementing the operating system of Cart Follower using the FPGA. As the training is done using MATLAB software, a Simulink simulation was performed to examine the reliability of the model before implementing it into the FPGA. Therefore, the percentage error from Table 3 as well as the RMSE calculated are used only as a reference where they have successfully proved that the model developed is fully functional and reliable. The actual distance was the directly measured distance meanwhile simulated distance was obtained by ANN computations.

Table 3: Data from MLP model for angle -10º, 0º, 10º

Angle (º)	Actual distance (cm)	Simulated distance (cm)	Percentage error (%)	RMSE
-10	20	19.48	2.65	0.469
	30	29.53	1.57	
	40	39.98	0.05	
	50	49.95	0.12	
	60	59.24	1.28	
0	20	19.76	1.20	0.479
	30	29.16	2.80	
	40	40.04	0.10	
	50	50.18	0.36	
	60	60.59	0.98	
10	20	19.86	0.75	0.267
	30	30.02	0.07	
	40	40.37	0.92	
	50	49.72	0.70	
	60	60.27	0.45	

4.4. Hardware implementation of ANN in FPGA

The execution time of hardware implemented model running at 1.91µs outperform the software implemented model. The reason behind was hardware implemented model is running in parallel meanwhile the software implemented model that is running in series. Figure 9 shows MLP hardware implemented model simulated in the ModelSim testbench.

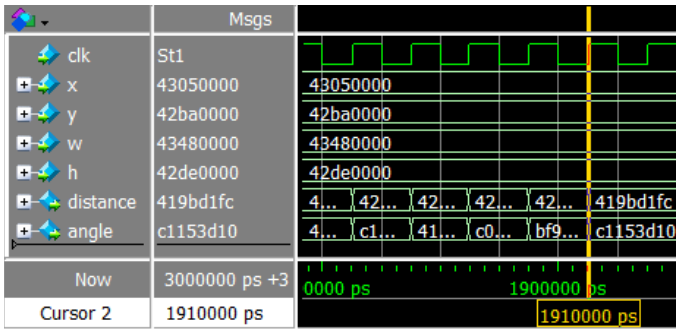

Figure 9: Hardware implemented model simulated using SOC system FPGA

4.5. Software implementation of ANN in FPGA

As the program code stops at address 20080h in the on-chip memory, the time is calculated from the start exert of reset bit to the address where the program code ends. Cursor 2 indicates the time reset start to exert while cursor 1 shows the time at address 20080h of the memory. Execution time is calculated from start of reset bit to the address 20080h where the code ends. The performance showed that it operated at 79.048532µs. Figure 10

shows the result of the software implemented model simulated using SOC system FPGA.

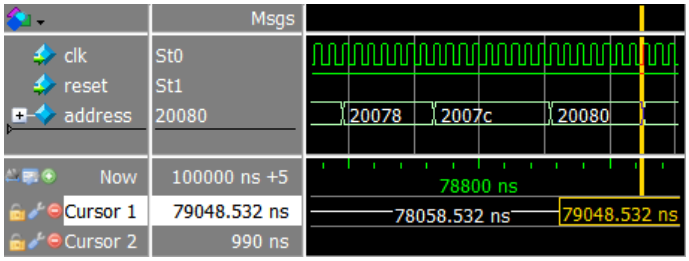

Figure 10: Software implemented model simulated using SOC system FPGA

4.6. Comparison analysis of performance between hardware and software implementation MLP model

The RMSE value for hardware and software implemented model are same at angle -10°, 0° and 10° as shown in Table 4. Past researchers presented with the deficiency of hardware implemented model precision since the floating point implementation was complex. A sign number is introduced to counter this problems. The usage of floating point can give an impact in increasing the efficiency of ANN MLP algorithm. As the hardware implemented model included the IP block floating point, the precision of the hardware can be said as same as software in terms of tracking performance of ANN with CC.

The execution time of hardware implemented model is at 1.91µs meanwhile software implemented model is at 78.06µs. This shows that performance of hardware is better than the software implemented. The reason behind was the software implemented model is running in sequential meanwhile hardware implemented model running in parallel. The software implemented model itself can only run in sequentially due to fetching of C code program that only has single lane to process data. It can be run in parallel but with aid of hardware implemented model. Table 4 presents the comparison between the hardware and software MLP model.

Table 4: Comparison between hardware and software MLP model

Implementation	Hardware	Software
RMSE at angle -10º	0.469	0.469
RMSE at angle 0º	0.479	0.479
RMSE at angle 10º	0.267	0.267
Execution time (µs)	1.91	79.05

5. Conclusions

In a nutshell, the objectives set for this research met the target. The hardware and software implementation in FPGA was performed with Verilog HDL. Floating point method was used in dealing with arithmetic calculation. The RMSE values for each angle of -10°, 0° and 10° show that the hardware implemented model was able to track the CC at high precision as software implemented model. The output distance produced from both of implementation appeared to possess an equal percentage error. Besides that, both the hardware and software implemented models at angles -10°, 0° and 10° also showed similar RMSE which are 0.469, 0.479 and 0.267 respectively. It has been proved that hardware implemented model is reliable as the software implemented model in term of target accuracy. This suited the first objective expectations.

The evaluation of execution time performance of both models show that hardware implementation model performed better than software implementation. The hardware and software implemented model operated at an execution time of 1.91µs and 79.05µs respectively. It is proven that model runs in parallel exhibited better performance than sequential. Therefore, the second objective is achieved.

The future development of this project can be enhanced by online training in FPGA. The application of this project can be applied to outdoor environment for various usage. The tracking system can be further developed with various AI systems like genetic algorithm, fuzzy or differential evolution for obtaining more comparison of FPGA controlled cart systems.

Conflict of Interest

The authors declare no conflict of interest.

Acknowledgement

The authors would like to thank Universiti Sains Malaysia (USM) for the support of the research under grant no 305/PELECT/6013112.

References

[1] G.A. Bekey, "Autonomous Robots: From Biological Inspiration to Implementation and Control", MIT Press, 2005.
[2] T. Lozano-Perez, "Autonomous Robot Vehicles", Springer Science & Business Media, pp. 462, 2012.
[3] T. Bräunl, 2008. "Embedded robotics: Mobile robot design and applications with embedded systems", Springer Science & Business Media, pp. 434, 2013.
[4] G. Taylor and L. Kleeman, "Visual Perception and Robotic Manipulation: 3D Object Recognition, Tracking and Hand-Eye Coordination", vol. Springer Tracts in Advanced Robotics, Springer, pp.218, 2008.
[5] J.M. Zurada, "Introduction to artificial Neural System", (Vol. 8). St. Paul: West publishing company, 1992.
[6] M. Frutos-Pascual and B. G. Zapirain, "Review of the Use of AI Techniques in Serious Games: Decision Making and Machine Learning," IEEE Transactions on Computational Intelligence and AI in Games, 2015.
[7] N. J. Nilsson, "Principles of Artificial Intelligence", Morgan Kaufmann, 2014.
[8] W. Burgard, A. Derr, D. Fox and A. Cremers, " Integrating global position estimation and position tracking for mobile robots: The Dynamic Markov Localization approach," In IEEE/RSJ International Conference, Victoria, BC, Canada, Vol. 2, pp. 730-735, 1998. https://doi.org/10.1109/IROS.1998.727279
[9] M. Ghandour, H. Liu, N. Stoll and K. Thurow, "Human Robot Interaction for Hybrid Collision Avoidance System for Indoor Mobile Robots" Advances in Science, Technology and Engineering Systems (ASTES) Journal Vol. 2, No. 3, 650-657, 2017.
[10] M.F. Ahmad, S.S.N. Alhady, S. Kaharuddin and W.A.F.W. Othman, "Visual based sensor cart follower for wheelchair by using microcontroller". In 5th International Conference on Control System, Computing and Engineering (ICCSCE), pp. 123-128. IEEE International Conference, Penang, Malaysia 2015. https://doi.org/10.1109/ICCSCE.2015.7482170
[11] M.F. Ahmad, H.J. Rong, S.S.N. Alhady, W. Rahiman and W.A.F.W. Othman, "Colour tracking technique by using Pixy CMUcam5 for wheelchair luggage follower". In 7th International Conference on Control System, Computing and Engineering (ICCSCE), pp. 187-192. IEEE International Conference, Penang 2017. https://doi.org/10.1109/ICCSCE.2017.8284402
[12] M.F. Ahmad, S.S.N. Alhady, W. Rahiman, W.A.F.W. Othman and A.A.M. Zahir, "Visual Based Distance Recognition Technique by Using Pixy CMUcam5". In Intelligent Manufacturing & Mechatronics: Proceedings of Symposium, Pekan, Pahang, Malaysia (pp. 479-485). Springer Singapore, 2018. https://doi.org/10.1007/978-981-10-8788-2_43
[13] M.F. Ahmad, S.S.N. Alhady, W. Rahiman, W.A.F.W. Othman and A.A.M. Zahir, "RGB Classification Determination with Different Light Intensity Using Pixy CMUcam5". In Intelligent Manufacturing & Mechatronics: Proceedings of Symposium, Pekan, Pahang, Malaysia (pp. 517-525). Springer Singapore, 2018. https://doi.org/10.1007/978-981-10-8788-2_46

[14] C.M. Soria, R. Carelli, R. Kelly and J.M.I. Zannatha, "Coordinated control of mobile robots based on artificial vision". International Journal of Computers Communications & Control, 1(2), pp.85-94, 2006. https://doi.org/10.15837/ijccc.2006.2.2288

[15] Z. Wang and M. Schwager, "Kinematic Multi-Robot Manipulation with no Communication Using force feedback," In IEEE International Conference on Robotics and Automation (ICRA), Stockholm, Sweden, pp. 427-432, 2016.

[16] E. Prassler, D. Bank and B. Kluge. "Motion coordination between a human and a mobile robot" In *IEEE/RSJ International Conference on Intelligent Robots and Systems* (Vol. 2, pp. 1228-1233). IEEE, 2002. https://doi.org/10.1109/IRDS.2002.1043910

[17] T. Yoshimi, M. Nishiyama, T. Sonoura, H. Nakamoto, S. Tokura, H. Sato, F. Ozaki, N. Matsuhira and H. Mizoguchi, "Development of a Person Following Robot with Vision Based Target Detection," In IEEE/RSJ International Conference on Intelligent Robots and Systems, Beijing, China, pp. 5286-5291, 2006. https://doi.org/10.1109/IROS.2006.282029

[18] M. Pakdaman and M.M. Sanaatiyan, "Design and Implementation of Line Follower Robot," In Second International Conference on Computer and Electrical Engineering, Dubai, United Arab Emirates, Vol.2, pp. 585-590, 2009. https://doi.org/10.1109/ICCEE.2009.43

[19] R.C. Luo, C.H. Huang, T.T. Lin, "Human tracking and following using sound source localization for multisensor based mobile assistive companion robot," In 36th Annual Conference on IEEE Industrial Electronics Society, Glendale, USA, pp. 1552-1557, 2010. https://doi.org/10.1109/IECON.2010.5675451

[20] S.O. Bamgbose, X. Li and L. Qian, "Trajectory Tracking Control Optimization with Neural Network for Autonomous Vehicles" Advances in Science, Technology and Engineering Systems (ASTES) Journal Vol. 4, No. 1, 217-224, 2019.

[21] M.L Chang, "Device architecture". In *Reconfigurable Computing*, Morgan Kaufmann, pp 3-27, 2008. https://doi.org/10.1016/B978-012370522-8.50005-4

[22] R.D. Abdu-Aljabar, "Design and Implementation of Neural Network in FPGA", In Journal of Engineering and Development, Vol. 16, No.3, pp. 73-90, 2012.

[23] P. Škoda, T. Lipić, Á. Srp, B.M. Rogina, K. Skala and F. Vajda, "Implementation framework for Artificial Neural Networks on FPGA," In Proceedings of the 34th International Convention MIPRO, Opatija, pp. 274-278, 2011.

[24] L.Y. Tat, S.S.N. Alhady, W.A.F.W. Othman and W. Rahiman, "Investigation on MLP Artificial Neural Network Using FPGA for Autonomous Cart Follower System", In 9th International Conference on Robotic, Vision, Signal Processing and Power Applications, Springer, Singapore, pp. 125-131, 2016. https://doi.org/10.1007/978-981-10-1721-6_14

[25] S. Agatonovic-Kustrin and R. Beresford,"Basic concepts of artificial neural network (ANN) modeling and its application in pharmaceutical research", Journal of Pharmaceutical and Biomedical Analysis, Volume 22, Issue 5, Pages 717-727, 2000. https://doi.org/10.1016/S0731-7085(99)00272-1

[26] I.N. Da-Silva, D.H. Spatti, R.A. Flauzino, L.H.B. Liboni, S.F. Dos Reis Alves, "Artificial Neural Network", Springer International Publishing, Edition 1, pp.21-24, 2017.

[27] R. Manickam, "Back Propagation Neural Network for Prediction of Some Shell Moulding Parameters", Periodica Polytechnica, Mechanical Engineering, 60(4), pp. 203-208, 2016. https://doi.org/10.3311/PPme.8684

[28] F.W. Wibowo, "An Analysis of FPGA Hardware Platform Based Artificial Neural Network", In Journal of Physics: Conference Series, Vol. 1201, No. 1, pp. 1-9. IOP Publishing, 2019. https://doi.org/10.1088/1742-6596/1201/1/012009

[29] N.B. Gaikwad, V. Tiwari, A. Keskar and N.C. Shivaprakash, "Efficient FPGA Implementation of Multilayer Perceptron for Real-time Human Activity Classification", In *IEEE Access*, 7, pp.26696-26706, 2019. https://doi.org/10.1109/ACCESS.2019.2900084

[30] X. Zeng, Z. Li, J. Wan, J. Zhang, M. Ren, W. Gao, Z. Li and B. Zhang, "Embedded Hardware Artificial Neural Network Control for Global and Real-time Imbalance Current Suppression of Parallel Connected IGBTs." In *IEEE Transactions on Industrial Electronics*, 2019. https://doi.org/10.1109/TIE.2019.2905825

[31] T. Jia, T. Guo, X. Wang, D. Zhao, C. Wang, Z. Zhang, S. Lei, W. Liu, H. Liu and X. Li, "Mixed Natural Gas Online Recognition Device Based on a Neural Network Algorithm Implemented by an FPGA", Sensors, 19(9), pp.2090. https://doi.org/10.3390/s19092090

[32] J. Renteria-Cedano, J. Rivera, F. Sandoval-Ibarra, S. Ortega-Cisneros and R. Loo-Yau, "SoC Design Based on a FPGA for a Configurable Neural Network Trained by Means of an EKF". Electronics, 8(7), pp.761. https://doi.org/10.3390/electronics8070761

ASTES

Advances in Science, Technology and Engineering Systems Journal Vol. 4, No. 4, 517-521 (2019)

www.astesj.com

Special Issue on Multidisciplinary Sciences and Engineering

ASTESJ

ISSN: 2415-6698

Mechanical Behaviors of Kaolin Powder Filler Polypropylene/Low Density Polyethylene Blends

Pham Thi Hong Nga*

Hochiminh City University of Technology and Education, Mechanical Engineering Faculty, Metal and Technology Department, 70000, Vietnam

ARTICLE INFO

Article history:
Received: 23 June, 2019
Accepted: 14 August, 2019
Online: 23 August, 2019

Keywords:
Kaolin
PP/LDPE blend
Tensile strength

ABSTRACT

In this work, kaolin powder was filled in PP/LDPE blend as the filler with the amount from 0 to 14 wt%. The ratio of PP/LDPE was fixed as 50/50 in all the experiments. The tensile strength, impact strength, and hardness were investigated in according with ASTM. The results showed that the tensile strength of PP/LDPE blend was slightly increased, the hardness was also increased while the impact strength was decreased in the presence of kaolin powder as the filler from 0 to 14 wt.%.

1. Introduction

Mixing of two or more different polymers is now considered as an economical way to the development of new polymers [1]. Low-density polyethylene (LDPE) has good mechanical properties, withstand high temperatures, easy to handle so they have wide applications in the industry [2]. PP also has some characteristics such as high stiffness, low plasticity, but these characteristics making the PP structure are easily destroyed, so the PP applications are also limited [3]. Therefore, to improve the mechanical properties of PP, and to create new materials with appropriate characteristics, LDPE has been studied and combined with PP to form PP/LDPE blend composition. Although, PP is similar to LDPE, they are different in some significant properties, PP/LDPE blends produce immiscible form.

The recent work of L.F. Kadhim et al [4], who investigated the mixures of PP and LDPE in the following percentages of LDPE by weight: 25, 50, 75. The results showing that the addition of LDPE to PP, have been declined the tensile strength, flexural strength, flexural modulus and hardness while the density improved LDPE as a result of the nature of LDPE is more flexible than PP. However, they are still only used for business purposes. One of the most important ways of polymer mixing is the incorporation of fillers to enhance mechanical toughness. As fillers, kaolin, $CaCO_3$, and talc are used along with engineering polymers to reduce both the production costs and to improve the properties. PP/LDPE/filler blends have been studied by different researchers from different aspects [5-7]. In types of filler, kaolin has certain advantages to improve the characteristics of PP/LDPE blend composition. It changes bonding between polymer blends to enhance bonding between blends and to create a chemical bond course between the blends of polymers and kaolin, therefore to improve the mechanical properties of PP/LDPE blends [8-11]. Many studies have so far been done on investigating PP/LDPE/Kaolin composites. According to S.N. Mustafa et al, the addition of kaolin powder to the PP/LDPE blend leads to increase the tensile strength, modulus of elasticity, shore-D hardness and impact strength and it decreases the elongation at break [12]. Water absorption of the PP/LDPE/kaolin composites behaves as function of time has also been investigated, and it increases by increasing immersion time for the same filler content, while the absorbed amount of water increases, by increasing the wt.% of kaolin at constant immersion time.

Table 1: Compositions of the samples (wt.%)

Material	Components (wt.%)				
	Samples				
	S1	S2	S3	S4	S5
50% PP and 50% PE	100	97	95	90	86
Kaolin	0	3	5	10	14

2. Experimental

2.1. Materials

PP (LyondellBasell - Moplen HP500N, origin Saudi Arabia) and LDPE (SABIC - LDPE 4024, origin Saudi Arabia) supplied

* Pham Thi Hong Nga, Email: hongnga@hcmute.edu.vn

by Thuan Thang Plastics Co., Ltd. Kaolin ($Al_2Si_2O_5(OH)_4$) were collected from Tran Tien Chemical Company. Kaolin has a particle size of 44 µm, specific gravity 2.58 - 2.63g/cm^3, and whiteness 89 - 93%.

Figure 1: The sample after pressing

In the preparation of the blends, samples including PP/LDPE and kaolin were put into the mixer according to the ratios (Table 1). These composites are called as S1, S2, S3, S4 and S5. All compounds were prepared by using system of mixing and extruding machine Polylab OS - Haake (Germany). Basic parameters of the system are 20 cm^3 sealed mixing chamber, the device extracts two screws L/D = 25, D = 16mm, one-screw extruder connected with sheet extrusion system (0.2 - 1.2 mm x 100mm). Samples were mixed for 6~7 minutes at a mixing temperature of 180ºC. After mixing, the sample are pressed to plates with the temperature of the tray at 180ºC. The pressing process was carried out for 5 minutes and then cooled for 20 minutes. All of these blends were prepared as samples keeping the PP/LDPE (50/50) ratio constant. The sample after pressing is 50 x145 mm and the thickness is 3.2 mm (Figure 1). The samples are then cut to the size of the tensile test specimen and the impact strength test specimen.

2.2. Experimental methods

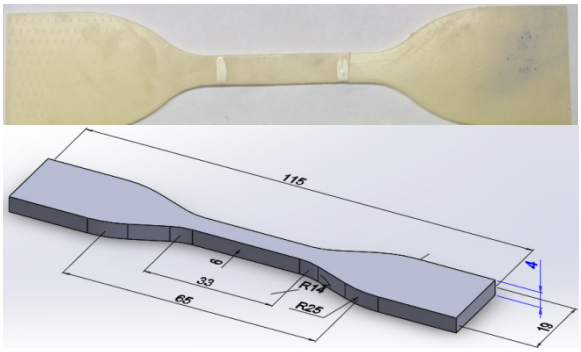

Figure 2: Tensile strength of test sample

The tensile properties were determined following the ASTM D638-02 procedure, using type IV test specimen dimensions (Figure 2) and using a Universal testing machine (Shimadzu Autograph AG-X Plus 20kN). This machine has the longitudinal stretch with high resolution camera (1.8 µm) and does not touch sample test. The crosshead speed was set at 50 mm/min at room temperature and four samples were tested for each composition.

The Izod impact strength was investigated according to ASTM D256. The composites were produced as 3.2x12.7x64 mm and a triangular with an angle of 45o, the radius of a glider at the bottom of the groove is r = 0.25 mm, shown in Figure 3. The experiment was performed with 5J collision energy and about 60 mm in length at room temperature. Five samples were tested for each composition.

Shore D scale was used to determine the hardness values of all samples. The tests were carried out the SHORE D Durometer DESIK. The durometer measures hardness by determining the depth of penetration into the material under test. The dial was graduated from 0-100 with a pointer sweep of 265º. Five samples of each formulation were tested and the average values were reported. The Fracture surface of each specimen in bending strength test was observed by Scanning Electron Microscope (HITACHI S - high resolution – 4800) with acceleration 5.0 kV. The surface of the samples used for SEM all was platinum-sputtered with a conductive layer before observation.

Figure 3: Sample measurement of impact resistance

3. Result

3.1. Tensile strength

Figure 4 shows the stress-strain curve when pulling of the samples. Table 2 shows the tensile strength results of each sample group. From the data in Table 2, a chart showing the average value of the tensile strength of each sample group was established (Figure 5). The results of elongation at break in Figure 4 indicating the sample S4 at 3.50532% has the lowest elongation at break and sample S5 has the highest elongation at break (4.50412%). These values are an indication of the ductility of PP/LDPE/Kaolin blends. The higher value of elongation is showing the blend more ductile.

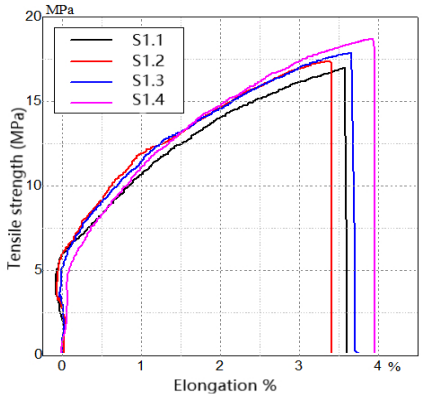

a) Sample S1 (0 wt.% kaolin content)

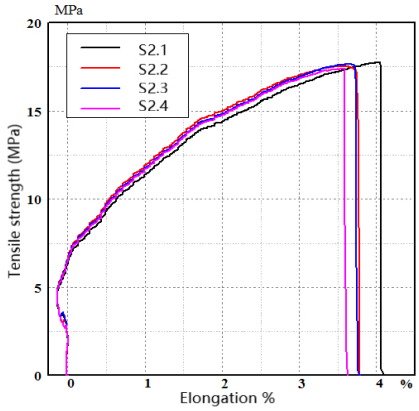

b) Sample S2 (3 wt.% kaolin content)

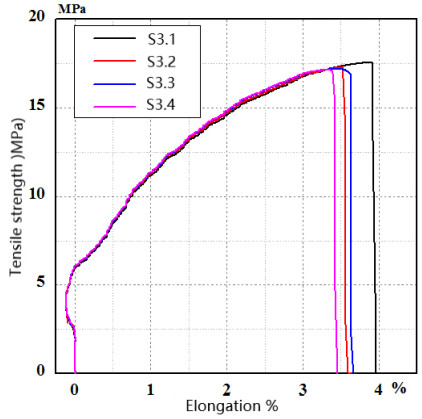

c) Sample S3 (5 wt.% kaolin content)

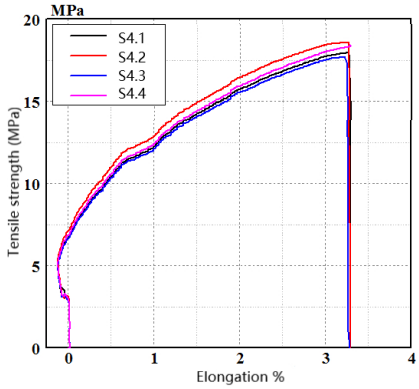

d) Sample S4 (10 wt.% kaolin content)

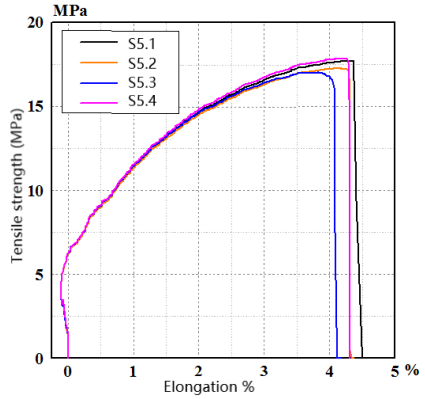

e) Sample S5 (14 wt.% kaolin content)

Figure 4: Stress-strain curve when pulling of the samples

Table 2: Results of tensile testing of samples

Sample	Average Tensile strength (MPa)	Average Strain (%)
S1	17.4904	3.69081
S2	17.5919	4.39359
S3	17.3139	3.68962
S4	18.1919	3.50532
S5	17.4757	4.50412

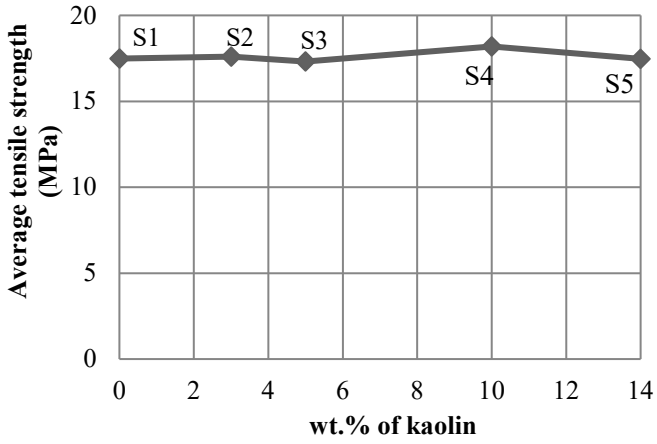

Figure 5: Average tensile strength of the samples

Figure 5 shows the average tensile results of the five samples. The tensile strength of PP/LDPE/Kaolin blends is increased with the addition of kaolin from 3% to 10 wt.%. 10% kaolin addition will have significant increase up to 18.1919 MPa comparing with the sample without kaolin (17.4904 MPa) while the higher amount of 14 % kaolin didn't seem to have better significant improvements. Tensile strength is an indication of the stiffness of a material. The adding of kaolin filler into the PP/LDPE matrix improves the stiffness of the blends. In the sample S4, the tensile strength is highest due to the distribution of filler on the PP/LDPE composite substrate surface that creates a hierarchical crystalline process between bridges. With sample S3, the tensile strength is lowest (17.3139 MPa) due to the large concentration of fillers in a given region which affects the crystallization. However, if there is more filler content in the polymer matrix will lead to the formation of the micro-filler and uneven kaolin particle size, and induces the difficulty of achieving a filling of filler in the PP/LDPE composite matrix forming holes [2]. This result influences the stress concentration at the boundary of the particle/ matrix and leads to a decreasing in particle/ matrix interactions. Therefore, it has a small effect on tensile strength [9].

3.2. Impact strength

The impact properties of PP/LDPE/Kaolin blends are summarized in Table 3 and Figure 6. As shown in the figure, the impact strength of PP/LDPE/Kaolin blends were decreased when increasing kaolin filler, 1.68806 kJ/m^2 for sample S1, 1.54280 kJ/m^2 for sample S2, 1.49422 kJ/m^2 for sample S3, 1.46986 kJ/m^2 for sample S4 and 1.30425 kJ/m^2 for sample S5. The reason is that PP/LDPE blends produce immiscible form because of the low interfacial adhesion. However, the immiscibility is good enough to preserve the good features of each polymer components of the blend. For example the impact strength of a polymer cannot be improved significantly by adding fillers with it [4]. In addition, in the mixture of PP/LDPE, kaolin acts as an evenly distribute effect in the PP/LDPE matrix and it will affect the chemical bonds between the kaolin and the PP/LDPE mixture [10]. For this reason, increasing kaolin filler content probably increased the level of stress concentration in the PP/LDPE composites with the resultant decrease in impact strength [9].

Table 3: Results of impact strength testing of samples

Sample	Average impact strength (kJ/m^2)
S1	1.68806
S2	1.54280
S3	1.49422
S4	1.46986
S5	1.30425

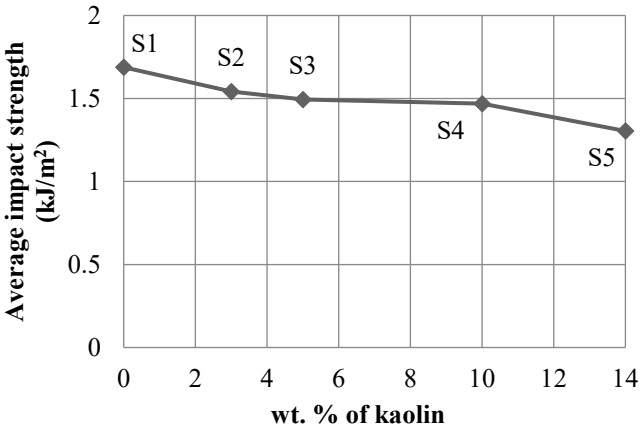

Figure 6: Impact strength of the samples

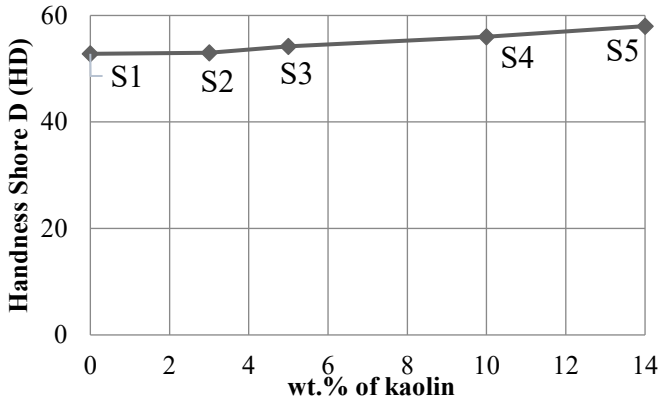

Figure 7: Hardness of the samples

3.3. Hardness

The hardness of PP/LDPE/Kaolin blends are showed in Figure 7. The hardness of PP/LDPE/Kaolin blends were all higher than the unfilled sample. The tests of hardness properties can evaluate the effects of adding kaolin fillers in PP/LDPE. It is evident from Figure 7 that a significant increase 52.8, 53, 54.2, 56 and 58 Shore D with adding 3, 5, 10, 14% kaolin, respectively. This is attributed to the fact that this filler acts as a reinforcing filler. Incorporation of the filler into the polymer matrix enhanced the stiffness of the material. The increase in hardness is due to the structure of the composite occurring in most reinforcement fillers. The higher the percentage of the filler incorporated, the harder the material, and the more rigid it becomes [10]. In composite PP/LDPE/kaolin, the mixture is characterized by the dispersion of vertical kaolin crystals in conjunction with the direction lines. When kaolin is combined with a thermoplastic mixture, it increases the hardness and produces concentrated stress, this also contributes to the reduction of the impact strength when added with kaolin filler [8].

3.4. Microstructure

To better analyze the mechanical properties of the PP/LDPE/Kaolin mixture. SEM micrographs for the PP/LDPE/Kaolin blends were conducted. The results were shown in Figure 8. The sample S1 can see the pictures of the spherulites of PP in LDPE. PP is presumed to be the dispersed phase due to its high viscosity and elasticity. The PP spherulites size is coarse and could be easily distinguished. The reason is that PP and PE are compatible but only partially miscible. The PP/LDPE pairs tend to separate into two liquid phases. During the process of PP crystallization, the growth of PP spherulites in a "homogeneous" melt of a mixture of PE and PP will involve the propagating PP spherulite front encountering domains of PE melt [11]. When adding kaolin, PP spherulites is finer. The increasing the content of kaolin, the finer of the PP spherulites also increases.

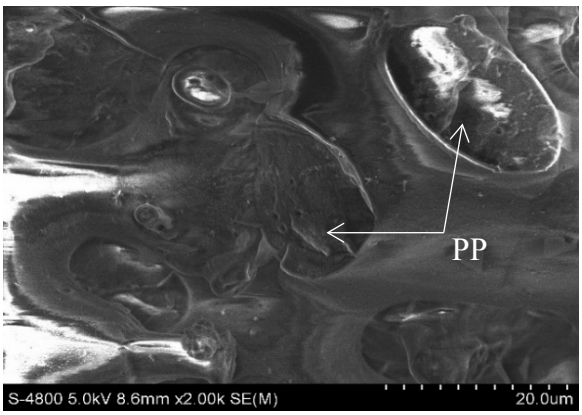

a) Sample S1 (0 wt.% kaolin content)

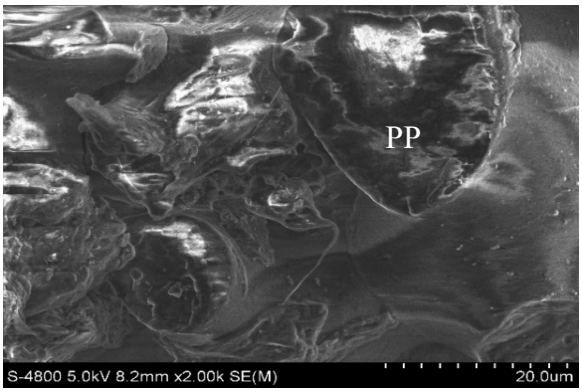

b) Sample S2 (3 wt.% kaolin content)

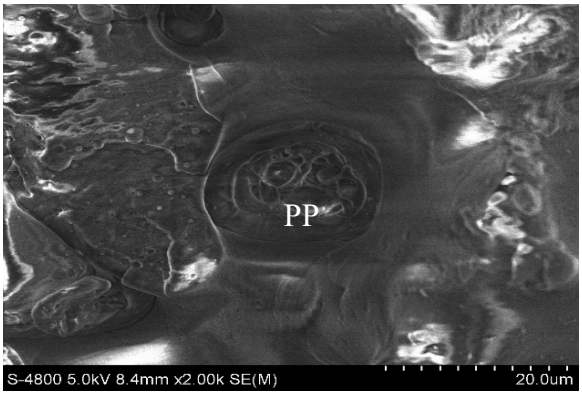

c) Sample S3 (5 wt.% kaolin content)

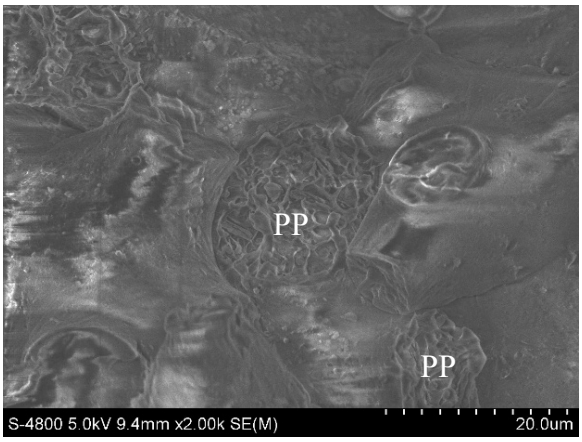

d) Sample S4 (10 wt.% kaolin content)

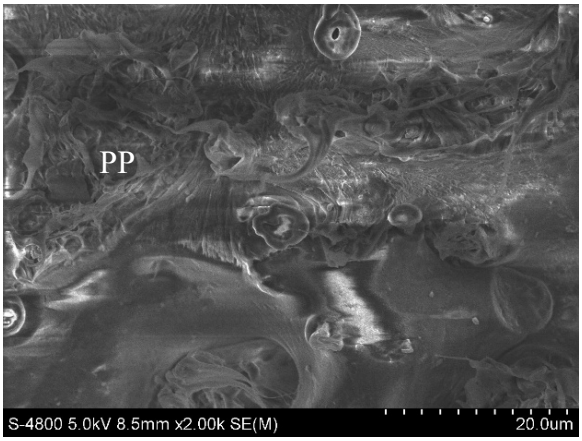

e) Sample S5 (14 wt.% kaolin content)

Figure 8: Surface collapse microstructure

4. Conclusion

From the above results, it was found that The tensile strength of PP/LDPE/Kaolin blends is increased with the addition of kaolin from 3% to 10 wt.%, but higher contents of kaolin 14% decreased the tensile strength.

When adding kaolin with PP/LDPE blend to increase the hardness but at the same time, it creates concentrated stress that reduces the impact strength. Adding kaolin to the PP/LDPE blend composition reduced the impact strength from 1.68806 kJ/m^2 to 1.30425 kJ/m^2 when increasing kaolin filler. On the contrary, the hardness of the PP/LDPE/Kaolin blends are increased by increasing the content of kaolin from 52.8 Shore D in samples without kaolin fillers to 58 Shore D in sample adding 14 wt.% kaolin filler.

Conflict of Interest

The authors declare no conflict of interest.

Acknowledgment

We are acknowledging HCMC University of Technology and Education, Dong Nhan Phat Co., Ltd and Material Testing Laboratory (HCMUTE). They gave me an opportunity to join in their team, accessed to the laboratory and research machines. Without their appreciated support it would not be possible to conduct this research.

References

[1] P. T. H. Nga; T. N. Thien, "Effect of Kaolin on the Mechanical Property of Polypropylene/Low Density Polyethylene Blend", 4th International Conference on Green Technology and Sustainable Development (GTSD), HCM City, Vietnam, 2018. DOI: 10.1109/GTSD.2018.8595576.

[2] M. Guessoum, S. Nekkaa, F. Fenouillot-Rimlinger, N. Haddaoui, "Effects of Kaolin Surface Treatments on the Thermomechanical Properties and on the egradation of Polypropylene", Hindawi Publishing Corporation International Journal of Polymer Science, 2012, 1-9, 2012. http://dx.doi.org/10.1155/2012/549154.

[3] H. Essabir, M. O. Bensalah, D. Rodrigue, D. Rodrigue, R. Bouhfid, A. e. k. Qaiss, "A comparison between bio- and mineral calcium carbonate on the properties of polypropylene composites", Construction and Building Materials, 134, 549-555, 2017. https://doi.org/10.1016/j.conbuildmat.2016.12.199.

[4] L. F. Kadhim, Z. F. Kadhim, "Studying The Properties of PP/LDPE polymer blend", Journal of Babylon University/ Engineering Sciences, 25(1), 193-201, 2017.

[5] M.S. Hassanien, A.I. Seedahmed, "Mechanical and rheological properties of polypropylene (PP)/ linear low density polyethylene (LLDPE) blend filled with talc and calcium carbonate compositions", Int J Eng Sci Res Technol, 4(1), 383-387, 2015.

[6] K. Şirin, M. Balcan, F. Doğan, The Influence of Filler Component on Mechanical Properties and Thermal Analysis of PP-LDPE and PP-LDPE/DAP Ternary Composites: Polypropylene, InTech China, 2012.

[7] M. Thomas, A. D. Kamble, N. John, "A Study on the Influence of Compatibilizer and Mica Filler on the Properties of Thermoplastic Polyurethane/Polyolefins Blends", Chem Sci Trans., 2(1), 181-191, 2013. DOI: 10.7598/cst2013.286.

[8] E.M. Khalaf, S.A. Awad, "Improvement of Mechanical and Water Absorbance Properties of Low-Density Polyethylene (LDPE) by using White Kaolin Powder (WK)", J. Adv. Chem. Sci., 3(1), 426-427, 2017.

[9] A. Mallika, A. K. Barik, B. Pal, "Comparative studies on physico-mechanical properties of compositematerials of low density polyethylene and raw/calcined kaolin", Journal of Asian Ceramic Societies, 3, 212-216, 2015. http://dx.doi.org/10.1016/j.jascer.2015.03.001.

[10] C. Onuoha, O.O. Onyemaobi, C.N. Anyakwo, G.C. Onuegbu, "Effect of filler loading and particle size on the mechanical properties of periwinkle shell filled recycled polypropylene composites", Am J Eng Res, 6(4), 72-79, 2017.

[11] R.A. Shanks, J. Li, L. Yu, "Polypropylene–polyethylene blend morphology controlled by time–temperature–miscibility", Polymer, 4(1), 2133-2139, 2000. https://doi.org/10.1016/S0032-3861(99)00399-7.

[12] S. N. Mustafa, "Effect of kaolin on the mechanical properties of polypropylene/ polyethylene composite material", Diyala Journal of Engineering Sciences, 5(2), 162-178, 2012.

ASTES

Advances in Science, Technology and Engineering Systems Journal Vol. 4, No. 4, 522-528 (2019)

www.astesj.com

Special Issue on Advancement in Engineering and Computer Science

ASTESJ

ISSN: 2415-6698

The Fusing Framework Between Lifting Carrier and Tractor-Trailer for Modern Transportation

Ha Quang Thinh Ngo[1], Thanh Phuong Nguyen[2,*], Hung Nguyen[2]

[1]*Department of Mechatronics Engineering, HCMC University of Technology, Vietnam National University-Ho Chi Minh City (VNU-HCM), Vietnam*

[2]*Institute of Engineering, HCMC University of Technology (HUTECH), Vietnam*

ARTICLE INFO

Article history:
Received: 12 June, 2019
Accepted: 06 August, 2019
Online: 25 August, 2019

Keywords:
Robotics
Motion Control
Industrial Automation

ABSTRACT

The integrating model becomes one of key trends in engineering design. The more the product has functional specifications, the more the industrial consumer apply in many fields. In this paper, a fusion design of architecture platform for autonomous system is demonstrated. It is greater due to combining the specifications of various types in commercial market such as driving structure, multi-functional model or autonomous level. Therefore, plentiful advantages of systems are converged into one platform. From customer's requirements, the system parameters and specifications are offered to consult during the process of design. To compare with previous works, the enhancement of tractor-trailer, lifting-carrier and auto-feeder using differential driving mechanism is merged successfully. The detailed design of prototype involves the development of hardware components and infrastructure. Later, the modeling of autonomous system is simulated on computer to meet the employed conditions. The force analyzing scheme helps to predict the working ability to complete their mission. To verify the proposed design, an experimental version of this system is tested in different cases. In mode of lifting carrier, the vehicle and cargo that become a rigid body, follow the reference trajectory in practical map. In another circumstance, vehicle plays a role as leader which take along with cargo, as follower. From these results, it can be seen that the proposed design is feasible, effective and capable in real world. In future works, a fleet of autonomous vehicles mixing multi-modes in the same map should be considered.

1. Introduction

In the worldwide era, a large-scale system becomes more popular due to its huge advantages. Especially, in online shopping business, it needs a thousand of employers who work in distribution center or warehouse every day. Reducing the labor cost means that enormous profits are earnt. Therefore, the producer would always discover the methods to lessen the operating payment. One of common ideas is to use autonomous vehicle that carry goods to human operators [1, 2]. Various challenges had to be overcome in order to make this viable system, from design of robust autonomous vehicles, real-time communication, the coordination of vehicle and various control algorithms which permit the system to adapt and reconfigure itself leaning on the environment and working conditions. Generally speaking, grounded automated vehicle (GAV) is digested into several sub-categories. Authors in [3, 4] posed the lifting type of vehicle to elevate cargo in production site. The veridical product has three wheels including one driven wheel and two driving wheels. Two driving wheels of GAV have independent brush motors while the other is passive wheel. This model is very widespread nowadays since its movement is free and high loading capability.

The second one is forklift type with steering mechanism [5, 6]. This kind of vehicle often appears in port transportation, harbor storehouse or container yard. The main benefits are to provide heavy loading ability and powerful lifting mechanism. In most of its applications, it requires human to sit on. The diesel engine version is cheaper than one using electric engine. However, because its dimension is large, it needs more space to operate than others. In the other style of GAV, i.e. tractor-trailer transporter [7, 8], the long combination vehicle is gradually becoming more public in certain circumstances because of vantages related to decrease costs for material transportation and diminish fuel

* Thanh Phuong Nguyen, Email: nt.phuong@hutech.edu.vn

consumption. This research implements active trailer steering control to improve the maneuverability of long truck-trailer combinations. The problem of swept path width during cornering could be solved by nonlinear control strategies. The effectiveness of proposed approach is evidenced on experimental platform.

In reality, there is a need to integrate these above vehicles into a compact unit. The emerging trend helps to overcome the existing limitations such as particular control problems of model type, enhancing carrier, reducing shared workspace, improving low speed maneuverability and so on. Besides, the saving cost on buying an integrated platform is rather than separated ones. In this paper, we present a fusion design of automated vehicle in multi-applications. After the problem statement is given in Section II, the novel idea based on combining between lifting carrier and truck-trailer model is to provide many expandable developments. The study of proposed pattern that is demonstrated in Section III enables the modern mechatronics system design. Section IV performs the actualizing works in each type whenever vehicle adapts to different scenarios. Later, the verification of proposed design is proved through experimental tests of Section V. Finally, some conclusions about this approach are commented for further development in Section VI.

2. Problem Statement

GAV or autonomous robot which is energized by electric power, play the role as a potential means of transportation in future. Due to great rewards in logistics, e-commerce, factory automation, social service and in some situations, public carriage, it has attracted the attention of industry and academic. There are numerous forms of classifications in GAV, such as wheeled structure, driving mechanism or their purposes. Referring to four wheels and driving by front-side, authors [11] investigated the control scheme to realize the yaw moment in presence of unknown mismatched disturbances. An integral sliding mode control was embedded into differential drive assistance steering (DDAS) to guarantee the transient control performance. In the case of complete failure of active front-wheel steering system, a robust composite nonlinear feedback strategy [12] to achieve path following was studied in detail. Besides, by utilizing fault-tolerant control with DDAS, an innovative multiple-disturbances observer-based method was applied in considering the tire force saturations. With a variable speed integral PID controller and a coordinated control system based on adaptive weighting dependent vehicle speed [13], both the ideal steering wheel torque and expected yaw rate could be obtained. However, they are hard to employ in commercial market owing to unreachable real-time performance, especially in emergency stop case. Via driving mechanism in rear-side, some car prototypes have been commercialized effectively. The control problem seems to be more difficult since the leading angle is adjusted lately. Furthermore, the head of car is light weight. It tends to be unstable when running at high velocity. To be more flexible, four wheels of electric vehicle have been driven. In [14], the wheel driving torque on each motor could be modulated precisely and continuously to attain not only maneuverability but also energy-saving mode simultaneously. The distribution strategy of torque control using multi-objective optimization was categorized into high layer and low layer. Although the developed method was simulated, the effectiveness of this approach has not verified in experimental platform yet.

In the other configuration, the three wheels framework becomes one of key topics to develop. In [15], to decline the error dynamic stabilization problem, a nonlinear sliding mode control law is employed to surpass. The control organization is uniformly asymptotically stable if unknown disturbances and modeling uncertainties are bounded. It utilized the nonholonomic constraints and transitional trajectory to acquire feasible state trajectories. Though, in practical context, the mass changes incessantly and it is hard to measure inertial moment of whole system (vehicle and load) precisely. The most concern of two-wheeled configuration is balancing control algorithm. The reporters [16] analyzed a passive inverted pendulum model as an investigational device. The sampling effect of the digital control is simulated as a zero-order hold. The stabilization of the upright position is possible by choosing proper control parameters as function of the sampling period of the controller. There are many limitations such that nonlinear characteristics (friction, behavior of electro-mechanical) are not mentioned while they still occur in model. Also, the system coefficients are not prearranged exactly. Sometimes, the omni-directional mobile robot including four mecanum wheels was installed in manufacturing fields. The authors [17] introduced the design and development of omni-based robot orienting to intelligent factory. The upper sections are named as control level and application level while the lower one is chassis frame. Each modularized wheel was located on a vertical suspension mechanism to ensure the moving stability and keep the distances of four wheels invariable. In the unknown semi-structured indoor environment, the data from a Kinect visual sensor and four-wheel encoders were fused to localize the mobile robot using an extended Kalman filter with specific processing. The existing difficulties in the model are to eliminate the slipping phenomenon on mecanum wheel and restrict loading competence.

The other types of GAV are forklift truck and tractor-trailer vehicle. The prototype forklift is regularly applied in container yard, pallet-based storehouse or cold storage. The structure of forklift [18-20] entails of a single active rear wheel and two non-driven front wheels balanced in electric stacker. Around the automatic forklift, several sensing modules, for instance, positioning encoder, laser scanner or GPS-indoor are often attached to collect environmental information. The drawbacks of forklift robot are too dangerous to actuate in medium or small-scale area, high maintenance cost and inflexible motion. In the coordinated control approach [21, 22], a tractor-trailer vehicle could be ensured to track trajectory and maintain vehicle kinematics restriction and dynamics maneuvers simultaneously. In the level of kinematics, linear quadratic regulator and model predictive control were used to assess the posture controller separately. For dynamics analysis, sliding mode control and global terminal sliding mode control were inspected to design the dynamic controller for the tracking of the desired velocities generated online. Nevertheless, the viability and application of this method are still questioned.

As a result, the incorporated requirements become an inevitable trend in our era. The contributions in this paper are, (a) analyzing the fusing hardware of models between tractor-trailer form and lifting carrier form, (b) build up an experimental platform of GAV based on the analysis design positively and enforce it safely on working map.

3. Analysis of Fusing Model

Based on the new trend of fusion, multi-function should be merged various roles into one platform. For instance, the autonomous vehicle is able to elevate cargo in vertical direction and pull freight horizontally. The vertical lifting vehicle modeling is illustrated as Fig. 1. It is assumed that vehicle and freight become a rigid body which has total weight m_{vl} .

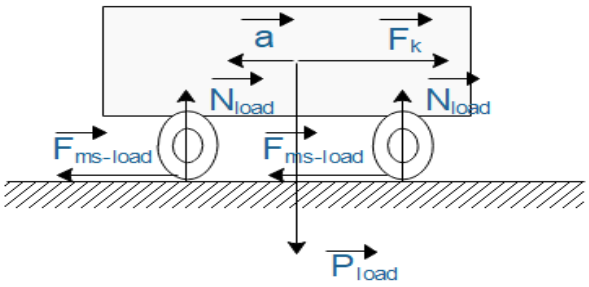

Figure 1: Forces act on lifting type model.

$\vec{a}$: acceleration of rigid body

$\vec{P}_{load}$: gravity force of rigid body

$\vec{N}_{load}$: reaction force on plane due to Newton's law

$\vec{F}_{ms-load}$: friction force between wheel and plane

$\vec{F}_k$: driving force from motors

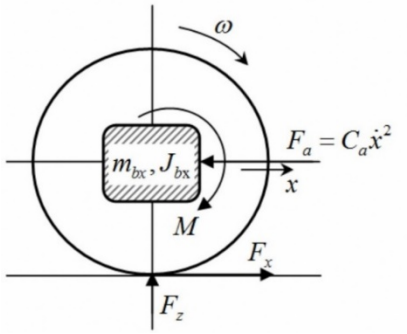

Figure 2: Analysis of driving wheel actuator.

According to second law of Newton, we have

$$\sum \vec{F} = m\vec{a} \Leftrightarrow m_{vl}\vec{a} = \vec{F}_k + \vec{F}_{ms-load} \quad (1)$$

$$F_k = m_{vl}a + F_{ms-load} \quad (2)$$

$$F_k = m_{vl}a + P_{load}\mu_{ms-load} \quad (3)$$

The force F_k is estimated as 17,405 N approximately. It is considered that vehicle moves on high stiffness plane as Fig. 2. If there is no slipping phenomenon, then, the constraints of design parameters to avoid this problem must be met below condition.

$$P_c \le P_k \le P_\varphi \quad (4)$$

where $P_c = F_k + P_f + P_i + P_\omega + P_j$

The force P_f helps maintaining driving wheel and plane in contact.

$$P_f = \mu' N = \mu' m_{vl} g \quad (5)$$

The inertial moment of driving wheel J_{wheel} is computed as.

$$J_{wheel} = \frac{1}{2} m_{wheel} 2r_{wheel}^2 \quad (6)$$

The symbol r_{wheel} is radius of driving wheel. Therefore,

$$P_j = \left(m_{vl} + \frac{J_{wheel}}{r_{wheel}^2} \right) a \quad (7)$$

Due to the movement on flat, the drag force P_i could be cancelled. The volume of vehicle is small, hence, the air resistance force P_ω is ignored.

By choosing adhesion coefficient $\varphi = 0.7$, the force P_φ is determined as.

$$P_\varphi = \varphi m_{vl} g \quad (8)$$

A relationship between driving force and moment of driving wheel is presented as.

$$P_k = \frac{M_1}{r_{wheel}} \quad (9)$$

As a result, the moment of driving motor M_1 , which is essential to control the system, should be complied with following constraint.

$$2,71 \le M_1 \le 24,89 \quad (10)$$

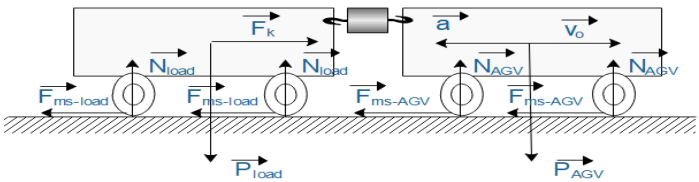

Figure 3: Forces act on tractor-trailer type model.

To certify the operation of truck-trailer type, an analysis of this modeling is shown as Fig. 3. The leader and follower are connected via a hook. The first vehicle is active drive while the other is passive one. In this case, we concern on interacting forces among them and angular driving wheels.

Theoretically speaking, the leader vehicle obligates to provide larger traction force to drive a chain of followers. This additional force is deliberated as $F_k^{'}$. Thus, the new force F_k^{new} that is necessary to drive whole system is denoted.

$$F_k^{new} = F_k + F_k^{'} \tag{11}$$

Consider that it pulls the followers not greater than its weight. Adding the safe ratio as our experiences, the new force F_k^{new} could be rewritten as.

$$F_k^{new} = 2,2F_k \tag{12}$$

Besides, the factors (material, structure or inside components) of driving wheel would affect on adhesion coefficient ϕ. The estimated moment of driving motor M_2 is renewed as.

$$4,32 \le M_2 \le 38,73 \tag{13}$$

4. Fusion Design in Proposed Hardware

In this section, the detailed design of proposed model is mentioned. Fig. 4 shows the inside frame of mechanical parts in vehicle. Generally speaking, the architecture of system is classified into three main layers (base, middle and lifting layer) and one intermediate layer. The base layer is the lowest one and stiff enough to bear the entire mass of whole system. The driving mechanism connoting DC motors with gears, drivers, soft couplings, battery, electric cylinder and so on, is located on base layer. Four rolling actuators that are hang on middle layer play a role as feeding actuator automatically. One electric cylinder is situated at center of the middle layer to upraise goods. Eventually, the lifting layer is at top. The electromagnetic lock, dwelling in this layer, is exploited to pull load horizontally. The intermediate one is a framework for holding and suspending among layers.

1-Driving wheels

2-Bearing

3-Soft coupling

4-Jig of motor

5-DC motor

6-Caster wheel

7-Loadcell

8-Shaft of intermediate layer

9-Battery tray

10-Electric piston

11-Inductive proximity sensor

12-Linear actuator

13- Electromagnetic lock

14- Lifting layer

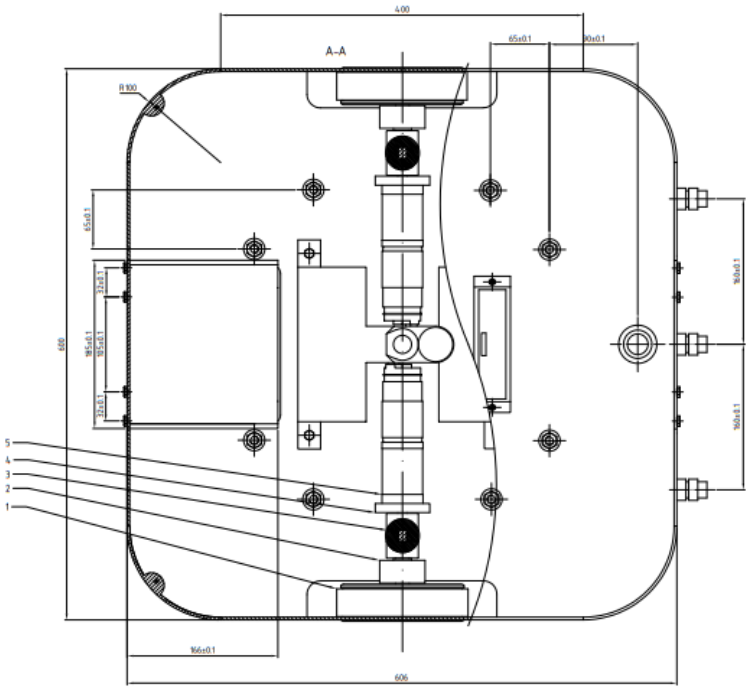

(a)

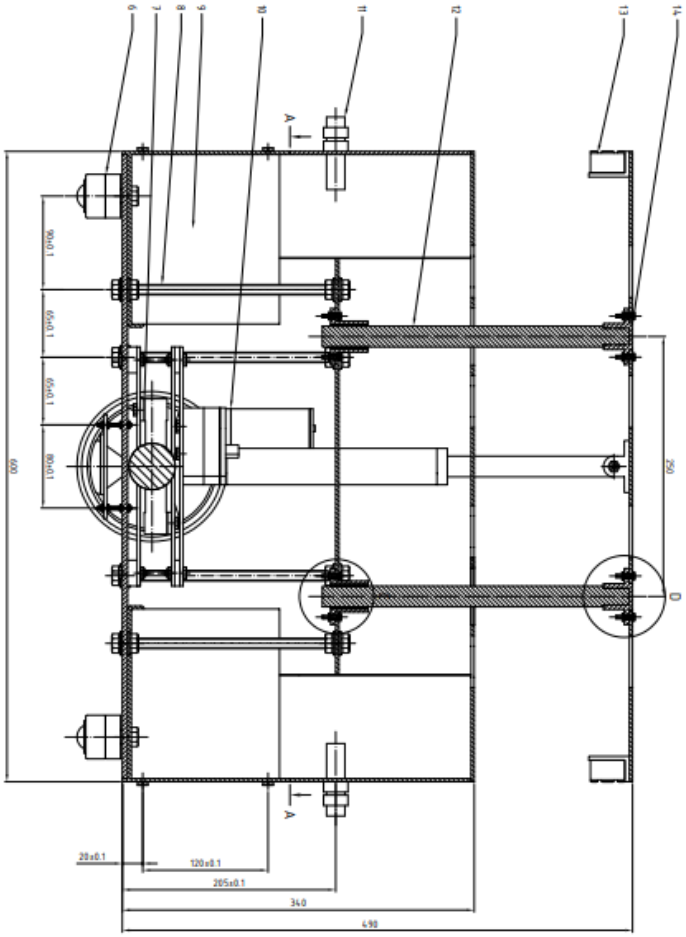

(b)

Figure 4: Vertical view (a) and horizontal view (b) of hardware structure design.

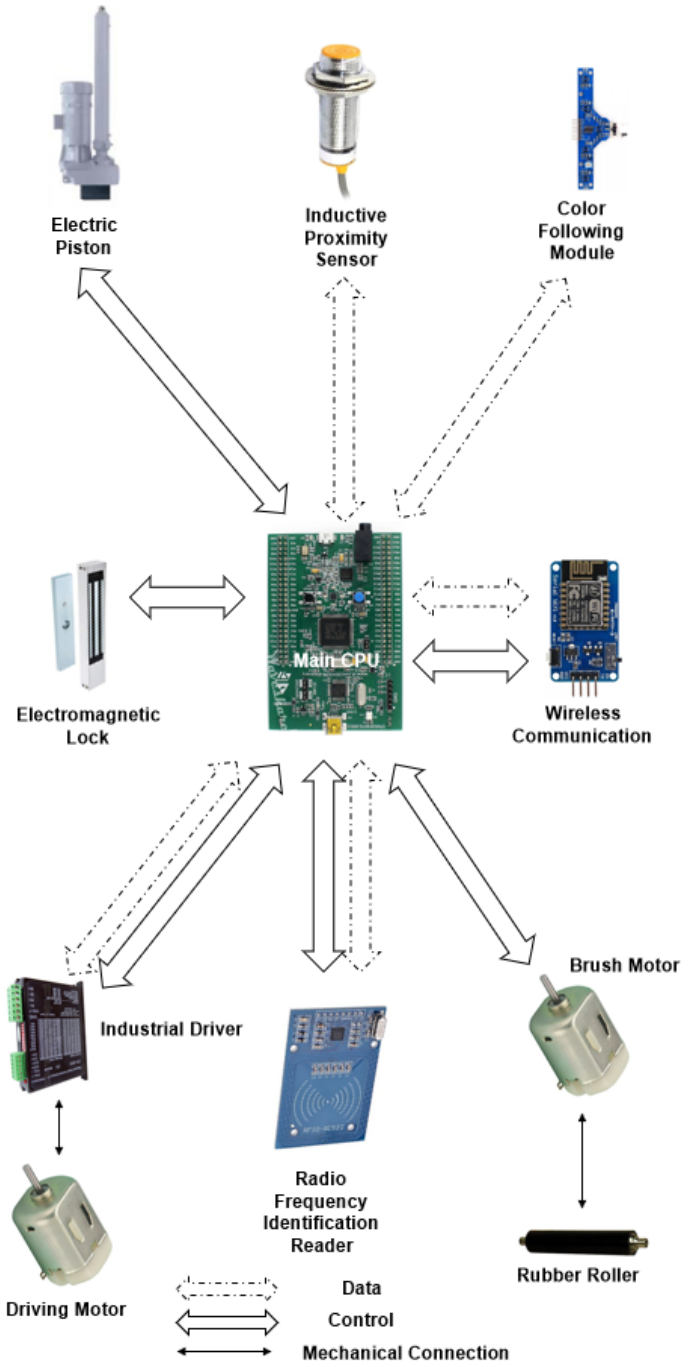

Figure 5: Diagram of data and control bus in proposed system.

Fig. 5 demonstrates the threads of data transmission and elements of control scheme in proposed system. It is powered by 32-bit MCU up to 168 MHz with floating point unit, 1 Mbyte flash memory, 192 Kbyte RAM, various I/Os, three channels of 12-bit ADC, two channels of DAC providing high performance and wide range of applications. For the internal signals, the data bus accommodates exchanging information (sensors or network protocol) whilst the control bus encompasses synchronizing interface (actuators, drivers). Due to centralized control method, the system is effective, reliable highly and simple to debug. However, to enlarge the real time performance, the coding needs to be optimized in firmware level.

The navigation problem of vehicle is also an attractive issue in control of system. The Radio Frequency Identification (RFID) technology is involved to lessen the burden data transmission. In each crossroad or corner, RFID card is occupied under the line guide. In the bottom side of vehicle, the card reader is stayed at central point to read and notify the unique code to host computer. The operator, who sits in center control room, could determine where the system locates in working map.

5. Research Results

It has been known that the combining approach must deal with various challenges and the gap between computational design and real world should be as small as possible. Henceforth, the system is validated experimentally in real scenario shown in Fig. 6. The architecture of control topology consists of local controllers and central one. The main microprocessor in local controller is powerful with high computing ability, fast processing and expandable peripherals. The host personal computer is with i7 core, high speed clock and visual monitoring capability. The supervisor would stay in control area to supervise the operation of system. The local controllers and central manager are contacted via wireless communication. The control messages are unceasingly transferred among them to prevent unfortunate incident.

Figure 6: Experimental model of proposed vehicle.

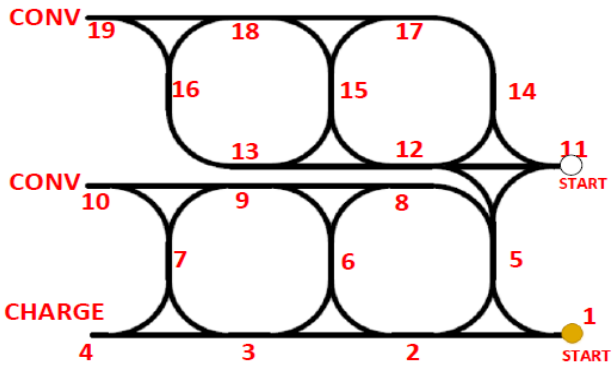

Figure 7: Overview of mapping area in workspace.

To imitate the practical situations in factory or distribution center, an overview of mapping working sector is drawn in Fig. 7. For multi-agent system, there are two reference regions are in parallel to enhance industrial productivity. The start points, charging section and conversing node are formed to offer various circumstances. At initial stage, vehicle moves to cargo's location

and bring to target position. In the case that the cargo must be out of storage, vehicle takes to conversing node. The battery management is gathered at charging station. Whenever level of energy is low, autonomous vehicle sends a notification to host server and move to charging node.

Figure 8: Experimental test scenario of tractor-trailer model.

Figure 9: Experimental test scenario of lifting model.

The shelf of cargo is made of steel and its height comply with industrial standard. There are only two floors, but its floors can be extendable. Four caster wheels are attached under the shelf to assist the free motion. The experimental validations include two-fold: first, vehicle begins at start point, it passes serial points to target position. Then, the lifting layer is gone up as height as the bottom floor of shelf. At that moment, the local controller activates electromagnetic lock to maintain force. It drives the shelf according to reference path as Fig. 8. The reverse process is actuated in target position: inactivate the electric lock, lift down and gradually move to next position.

Sequently, the lifting mode is experimented as Fig. 9. In this case, the autonomous vehicle is compelled to accomplish the mission: brings the rack of payload from initial position to final location. Launching at start point, it comes to site of shelf by tracking linear and circular path. Later, vehicle orders lifting part to move up elevating the shelf. At this time, vehicle and cargo become a rigid body. Both of them are conveyed to final place and released there. The grounded robot could come back start point and ready for next task.

Table 1: Comparative Tracking Error Results in Experimental Tests

Test case	RMS	Average
Lifting model	0.157	0.268
Truck-trailer model	0.082	0.194

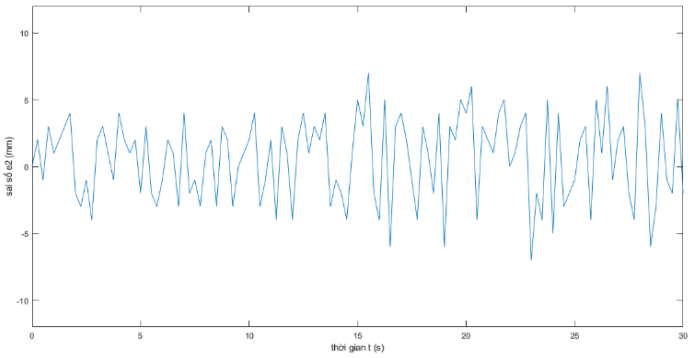

(a)

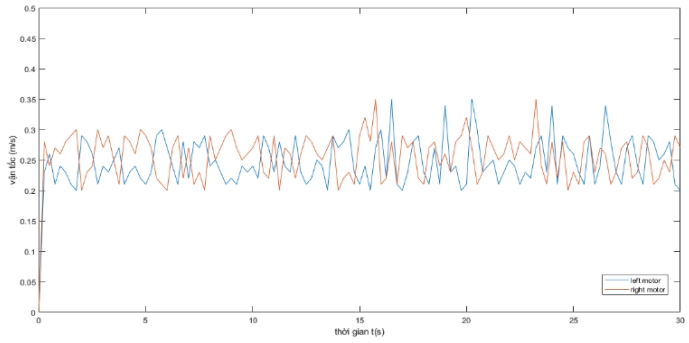

(b)

Figure 10: Experimental performance of truck-trailer model, (a) tracking error, (b) velocity of left wheel and right wheel.

The monitoring parameters in this study are tracking errors and control speeds. In differential drive, the variations in velocity of left and right wheels have an effect on directional movement. The tracking error governs the output performance in whole system. Fig. 10 and Fig. 11 show experimental results in two case studies respectively. In truck-trailer test, the leader must take a follower behind carefully. The motion of trailer affects on tracking error of front-runner. If leader moves so fast, it tends to deviate from reference path at corner. Otherwise, the force is too small to steer a follower or time-consuming motion costs too much.

In lifting test, the weight of whole system including total mass on shelf plus itself is heavier. Consequently, the motion seems to be more difficult. The value of tracking error, in this scene, is larger than others while the velocities of wheels are adjusted continuously. To visualize the differences in two cases, Table 1 reports the tracking error (Root-Mean-Square value and average value). From these results, it could be seen obviously that tracking error in lifting mode is larger than one in truck-trailer mode. The reason is that the control scheme drives harder when vehicle and cargo become a rigid body.

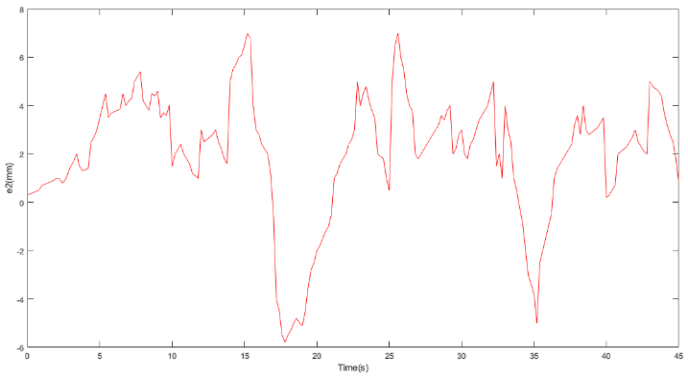

(a)

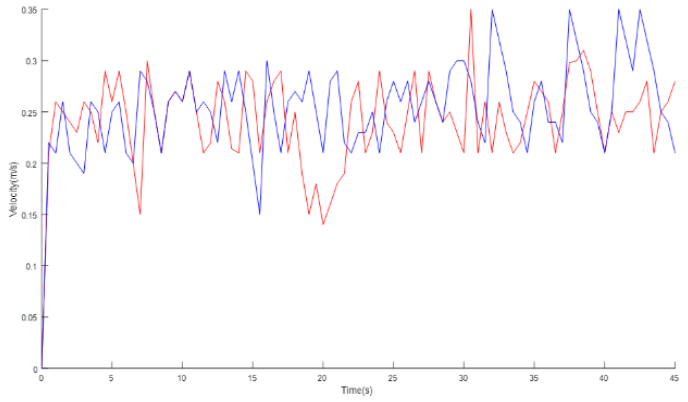

(b)

Figure 11: Experimental performance of lifting model, (a) tracking error, (b) velocity of left wheel and right wheel.

6. Conclusions

In this paper, a multi-purposes implementation for autonomous grounded vehicle is fused into an unique framework in practical factory. The proposed design is feasible, low cost and complies with industrial solicitations whilst it still conserves flexible motion. Furthermore, the integrating approach ensures that it is not only useful in various applications, but also it provides wide development trends, such as smaller, smarter or more convenient. From the successful results of research, it could be achievable in logistics, manufacturing industry, material transportation and training.

Conflict of Interest

The authors declare no conflict of interest.

References

[1] R. D'Andrea and P. Wurman, "Future challenges of coordinating hundreds of autonomous vehicles in distribution facilities" in IEEE International Conference on Technologies for Practical Robot Applications, 2008, https://doi.org/10.1109/TEPRA.2008.4686677.

[2] H. Q. T. Ngo, T. P. Nguyen and H. Nguyen, Research and develop of AGV platform for logistics warehouse environment; Vancouver: Springer-Verlag, 2018, https://doi.org/10.1007/978-3-030-02683-7_32.

[3] D. Chen, Z. Shi, P. Yuan and Z. Li, "Trajectory tracking control method and experiment of AGV" in IEEE Advanced Motion Control, 2016, . https://doi.org/10.1109/AMC.2016.7496323.

[4] V. Q. Nguyen, H. M. Eum, J. S. Lee and C. H. Huyn, "Vision Sensor-based Driving Algorithm for Indoor Automatic Guided Vehicles," International Journal of Fuzzy Logic and Intelligent Systems, **13**(2), pp. 140-146, 2013.

[5] T. A. Tamba, Q. T. T. Bui and K. S. Hong, "Trajectory generation of an unmanned forklift for autonomous operation in material handling system" in SICE Annual Conference, 2008, https://doi.org/10.1109/SICE.2008.4654955.

[6] J. X. Xiao and F. L. Lu, "An improvement of the shortest path algorithm based on Dijkstra algorithm" in International Conference on Computer and Automation Engineering, Singapore, 2010, https://doi.org/10.1109/ICCAE.2010.5451564.

[7] P. Ritzen, E. Roebroek, N. van de Wouw, Z. P. Jiang and H. Nijmeijer, "Trailer steering control of a tractor-trailer robot," IEEE Transactions on Control Systems Technology, **24**(4), 1240-1252, 2016, https://doi.org/10.1109/TCST.2015.2499699.

[8] M. A. Guney and I. A. Raptis, "A robotic experimental platform for testing and validating warehouse automation algorithms" in International Conference on Technologies for Practical Robot Applications, MA, USA, 2015, https://doi.org/10.1109/TePRA.2015.7219693.

[9] C. T. V. Kelen, P. M. G. Jorge, S. B. Thales, C. A. Roberto, M. S. Rafael, B. Marcelo and A. P. C. Glauco, "Robotic forklifts for intelligent warehouses: routing, path planning and auto-localization" in International Conference on Technologies for Practical Robot Applications, Vina del Mar, Chile, 2010, https://doi.org/10.1109/ICIT.2010.5472487.

[10] H. Q. T. Ngo, T. P. Nguyen, V. N. S. Huynh, T. S. Le, C. T. Nguyen, "Experimental comparison of complementatry filter and Kalman filter design for low-cost sensor in quadcopter," International Conference on System Science and Engineering, pp. 488-493, 2017, https://doi.org/ 10.1109/ICSSE.2017.8030922.

[11] C. Hu, R. Wang, F. Yan, Y. Huang, H. Wang and C. Wei,"Differential steering based yaw stabilization using ISMC for independently actuated electric vehicles," IEEE Transactions on Intelligent Transportation Systems, vol. 19, no. 2, pp. 627-638, 2018.

[12] C. Hu, R. Wang, F. Yan and H. R. Karimi,"Robust composite nonlinear feeback path following control for independently actuated autonomous vehicles with differential steering," IEEE Transactions on Transportation Electrification, vol. 2, no. 3, 2016.

[13] T. Chen, X. Xu, Y. Li, W. Wang and L. Chen, "Speed-dependent coordinated control of differential and assisted steering for in-wheel motor driven electric vehicles," Proc. of the Institution of Mechanical Engineers Part D: Journal of Automobile Engineering, vol. 232, no. 9, pp. 1206-1220, 2018.

[14] C. Lin, Z. Xu, "Wheel torque distribution of four-wheel-drive electric vehicles based on multi-objective optimization," Energies, vol. 8, no. 5, pp. 3815-3831, 2015.

[15] H. Ashrafiuon, S. Nersesov, G. Clayton, "Trajectory tracking control of planar underactuated vehicles," IEEE Transactions on Automatic Control, vol. 62, no. 4, 2016.

[16] B. A. Kovacs, G. Stepan, Z. Wang, T. Insperger, "On the stability of two-wheeled vehicle balancing passive human subjects," 12th IFAC Symposium on Robot Control, vol. 51, no. 22, pp. 337-342, 2018.

[17] J. Qian, B. Zi, D. Wang, Y. Ma, D. Zhang, "The design and development of an omni-directional mobile robot oriented to an intelligent manufacturing system," Sensors, vol. 17, pp. 1-15, 2017.

[18] D. Ilangasinghe, M. Parnichkun, "Navigation control of an automatic guided forklift," 2019 First International Symposium on Instrumentation, Control, Artificial Intelligence and Robotics, pp. 123-126, 2019.

[19] H. Q. T. Ngo, Q. C. Nguyen, T. P. Nguyen, "Design and implementation of high performance motion controller for 2-D delta robot," Seventh International Conference on Information Science and Technology, pp. 129-134, 2017, https://doi.org/10.1109/ICIST.2017.7926505.

[20] J. L. Syu, H. T. Li, J. S. Chiang, C. H. Hsia, P. H. Wu, C. F. Hsieh, S. A. Li, "A computer vision assissted system for autonomous forklift vehicles in real factory environment," Multimedia Tools Applications, vol. 76, no. 18, pp. 18387-18407, 2017.

[21] Ngo, Ha Q.T.; Phan, Mai-Ha. 2019. "Design of an Open Platform for Multi-Disciplinary Approach in Project-Based Learning of an EPICS Class." Electronics 8, no. 2: 200.

[22] M. Yue, X. Hou, R. Gao, J. Chen, "Trajectory tracking control for tractor-trailer vehicles: a coordinated control approach," Nonlinear Dynamics, vol. 91, no. 2, pp. 1061-1074, 2018.

ASTES

Advances in Science, Technology and Engineering Systems Journal Vol. 4, No. 4, 529-538 (2019)

www.astesj.com

ASTESJ

ISSN: 2415-6698

Preparation of Lead, Lead Alloy(S) and Other Salts from Exhausted Rechargeable Lead Batteries

Mahmoud Abdel-Hamed Rabah[1, *], Maie Ibrahim Abdul Aziz El-Gammal[2], Mahmoud Salem Ibrahim[2], Omar Mohamed Helmy Abdul Aziz[2]

[1]*Chemical and electrochemical metallurgy, Central metallurgical research and development Institute CMRDI, Helwan,11421, Cairo, Egypt.*

[2]*Environmental Science Department, Faculty of Science, Damietta Univ. Egypt*

ARTICLE INFO

Article history:
Received: 04 March, 2019
Accepted: 16 August, 2019
Online: 25 August, 2019

Keywords:
Rechargeable batteries
Pure lead
Secondary lead-aluminium
Magnesium alloy
Nickel and cobalt
Hydrometallurgy

ABSTRACT

Metals of lead and some lead alloys, lead oxide, nickel and cobalt were recovered from exhausted battery by combined hydrometallurgy and pyro metallurgical method. The spent batteries were dismantled and leached in hot 2M and 5M nitric acid. The unleached fraction was heated with sodium carbonate to produce lead oxide. Salts in the leached solution were analyzed by Inductively Coupled Plasma ICP. Lead was precipitated as hydroxide on cold with ammonia. Nickel and cobalt metals in solution were extracted by solvent extraction using LEWATIT MP 600 ion exchange resin. Metals loaded by the organic phase were stripped by HCl. Metals hydroxides were reduced with ascorbic acid or hydrazine hydrate to ultrafine free metals, Lead alloys were prepared by encapsulating the alloying metal oxide or organic salts in the host lead metal and heated at 800 °C. The end products were investigated with Energy-dispersive X-ray spectroscopy (EDX), X-ray diffraction (XRD), X-ray fluorescence (XRF), Inductively Coupled Plasma (ICP), and Scanning Electron Microscope (SEM). Results revealed that the spent grids contain 94.2 % lead, aluminium 0.12% nickel 0.05 % and cobalt 0.053 %. The particle size of the reduced metals was found in range of 15-60 um, LEWATIT MP 600 ion exchange resin is specific adsorbent for nickel and cobalt. Distribution constant Kd value of the stripping step decreased in the order Ni and Co. Lead-Al-Mg alloy was prepared by heat treatment of terminal taps at 500 °C. The obtained lead alloys were investigated with EDX and SEM. The extent of recovery of lead metal and lead calcium aluminum alloy amount to 94.3% and 96.4% with high purity. Lead -calcium alloy was homogeneous and contain calcium particles with 5 ums.

1. Introduction

Rechargeable batteries are usually used for temporary power supply in general and in houses in particular in case the main power shutoff accidentally The Bureau of Mines [1] has investigated an electrolytic recycling process to recover lead and improve secondary recovery of metals and minerals from scrap batteries Metallic fraction of the crushed batteries is directly melted and cast as anodes for electro refining The sludge is leached with ammonium carbonate [(NH4)2CO3] and ammonium bisulfite (NH4HSO3) to convert lead sulfate (PbSO4) and lead dioxide (PbO2) to lead carbonate (PbCO3), . . The lead metal grids and plates are separated from the sludge by ball milling, washing, and screening by the Betts process using waste fluosilicic acid as the electrolyte.

Battery is made of groups of plates connected together by external flag terminal made of lead alloy. Lead oxide(s), sulphate powders filling in the grids openings to form the electrically active material. In the charged state, the negative plate paste is lead-calcium grid loaded with lead sulphate; the positive electrode is lead dioxide. Both of these lead materials are in a spongy form to optimize surface area and thereby maximize the electrical capacity [1] The conductivity media is potassium hydroxide in low quantity just sufficient to moisten the electrode paste. In the discharging state, the negative lead plate loses electrons and got oxidized to a higher lead oxidation state. Lead-calcium alloy provides benefits of good grid density, conductivity, & tensile

*Mahmoud Abdel-Hamed Rabah, Email: mrabah010@gmail.com

strength. It reduces water consumption over life of battery, it also reduces electrolyte & hydrogen gas evolution. Better self-discharge characteristics- (typically .05% per day at 25°C) is attained with this alloy together with stable rate under float charge over the life of the battery and constant current draw [2] Chen et al [3] repor4ted recovery of lead from fly ash of waste lead-acid batteries. The lead salt is lead sulphate (PbSO4) and lead oxy sulphate (Pb2OSO4). Nitric acid and sodium hydroxide were used for leaching of the fly ash sample. With S/L of 60 gL-1, the leach extent of Pb was 43% and 67% in 2M acidic and basic solutions, respectively. Anglesite is soluble in NaOH whereas lanarkite is mildly soluble in HNO3. Lead metal was recovered by electrolysis from the leach solution with the help of an electrolytic cell fitted with graphite coated with titanium (Ti-DSA) anodes and stainless-steel cathode. Properties of anodes deposited with lead dioxides were analyzed by cyclic voltammetry... Junqing et al, 2012, [4] recovered method, in which high purity metallic Pb is directly produced by electrolyzing PbO obtained from waste lead acid batteries in alkaline solution A hydrometallurgical process has been proposed [5, 6] to recover valuable metals from spent lithium-ion batteries in citric acid media. A process was reported including the steps of calcinations of a spent paste treated with an alkali carbonate or hydroxide or any mixture thereof, and elemental sulphur at a temperature of up to 600° C., followed by washing with water. The heat treated and washed paste was dissolved in an alkali molten electrolyte, and lead was electro-won from the alkali molten electrolyte. The spent electrolyte was reused in the process [7]. Molten flux salts displayed good thermal stability and solvent properties; these characteristics helped their use in materials preparation [8], solar power plants [9], and the getting rid of paints or coating from metal surfaces [10]. An up to date technology, adapted a molten salt to the smelting processes of antimony and bismuth through the use of sodium hydroxide and a mixed molten salt in the NaOH–Na2CO3 2CaO system [11, 12]. Separation of minor elements using Lewisite exchange resin was reported by Badawy et al. [13]. Yoheeswaran1 et al [14], recovered lead metal from used lead acid batteries, by the hydrometallurgical method. The treatment of used batteries for recovering lead was claimed to be important from the point of view of lead production as well as pollution abatement as otherwise the battery scarp leads to serious disposal problems. The pyrometallurgical and other methods suggested in the past decades, were found to be impracticable, and a new method was investigated. Lead metal recovery from spent lead acid batteries applying an electrochemical method comprising two successive steps; lead leaching and electrode position. It was found that 95% of lead metal was leached by 2M of nitric acid and the electrode position step more than 90% of lead metal could be recovered with low current efficiency from the leaching solution. The method adopted was reported to be promising and had great potential for removal of lead from used lead acid batteries. E-waste generation was growing at about 15% and is expected to cross 800,000 tons per year in 2012 in some countries like India. The composition of spent batteries was very diverse and contained over 1000 different substances, which falls under organic and inorganic fractions [Viraja Bhat, 15]. Yunjian Ma and Kiqyiang Qui [16] investigated a compatible environmental process consisted of hydrometallurgical desulfurization and vacuum thermal reduction to recycle lead. Lead paste was desulfurized with sodium carbonate, by which, the content of sulfur declined from 7.87% to 0.26%. Charcoal was used to reduce the desulphurization lead paste under vacuum. Under the optimized reaction conditions, i.e., vacuum thermal reduction at temperature 850 °C under 20 Pa for 45 min,

The aim of this work is to extract metal lead. Lead aluminium-magnesium alloy and some salts from exhausted plates and grids of electrolyte-free rechargeable lead batteries... Recovery of lead metal was performed using hydrometallurgical and pyro metallurgy whereas the alloying elements of aluminium and Magnesium were extracted by solvent extraction technique, Parameters influencing these processes such as temperature, time, and pH value and mole ratio of the reagents were studied.

2. Materials and Methods

2.1. Experimental Details

A sample of about ten Kg of used rechargeable lead batteries was supplied by the waste collection stores, Cairo. The sample was washed with water and left to dry in normal ambient conditions. Figure 1 shows a photograph of the collected spent rechargeable acid lead batteries

Figure 1 Different models of the spent batteries used in this study

The chemicals used for leaching, precipitation, separation and salts preparation were chemically pure grade. Nitric, formic, acetic acids and calcium carbonate, oxide and hydroxide. Sodium, and potassium were of ADWIC supplier (Egypt) Table 1 summarizes the properties of chemicals used.

Table 1 Properties of the chemicals used in this study

Supplier	Purpose	Properties	Product
CH_3COOH	90 %		
Nitric acid	SP. Gr. 1.044 – 1.049 SP.Gr.1.18 (AR)		Riedel- de Hein ADWIC
H_2SO_4	Min. assay 36 % Fuming 69 %	Leaching Process	
HCl	H_2SO_4 95-97% Extra pure SP.Gr.1.18 (AR)		Riedel- de Hein ADWIC
Ca carbonate, EJSF2 Ca oxide	99.3, 1.6 um 3.34 g/cm^3, 1.57 um	Synthesis process	Green Egypt Sigma Aldrich

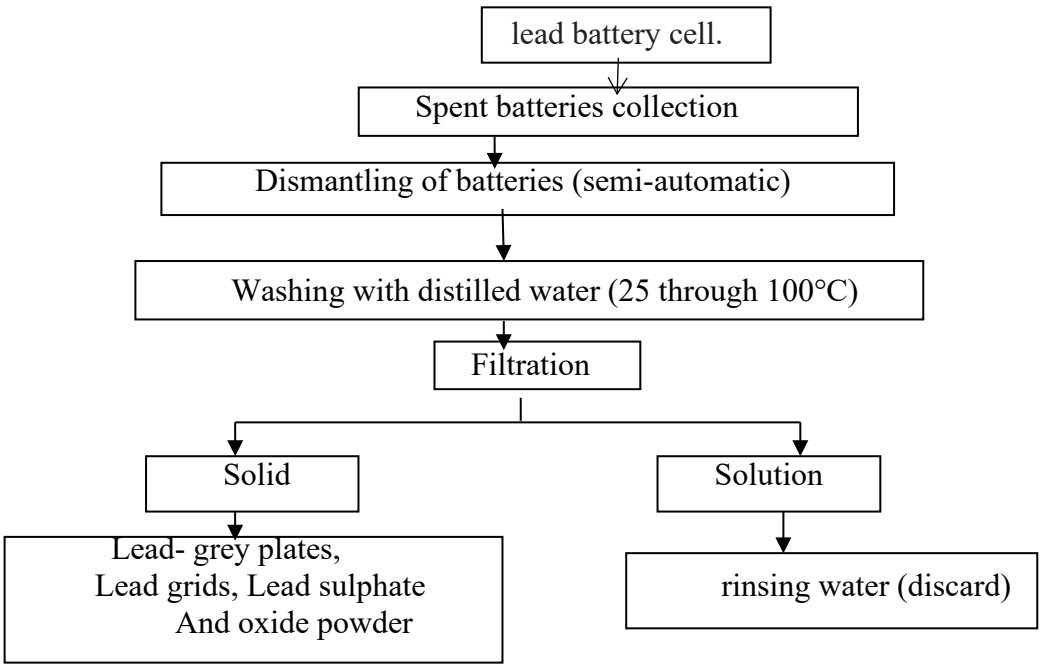

Fig. 2 A conceptual process flow sheet to method to recover lead and lead alloys from exhausted rechargeable acid.

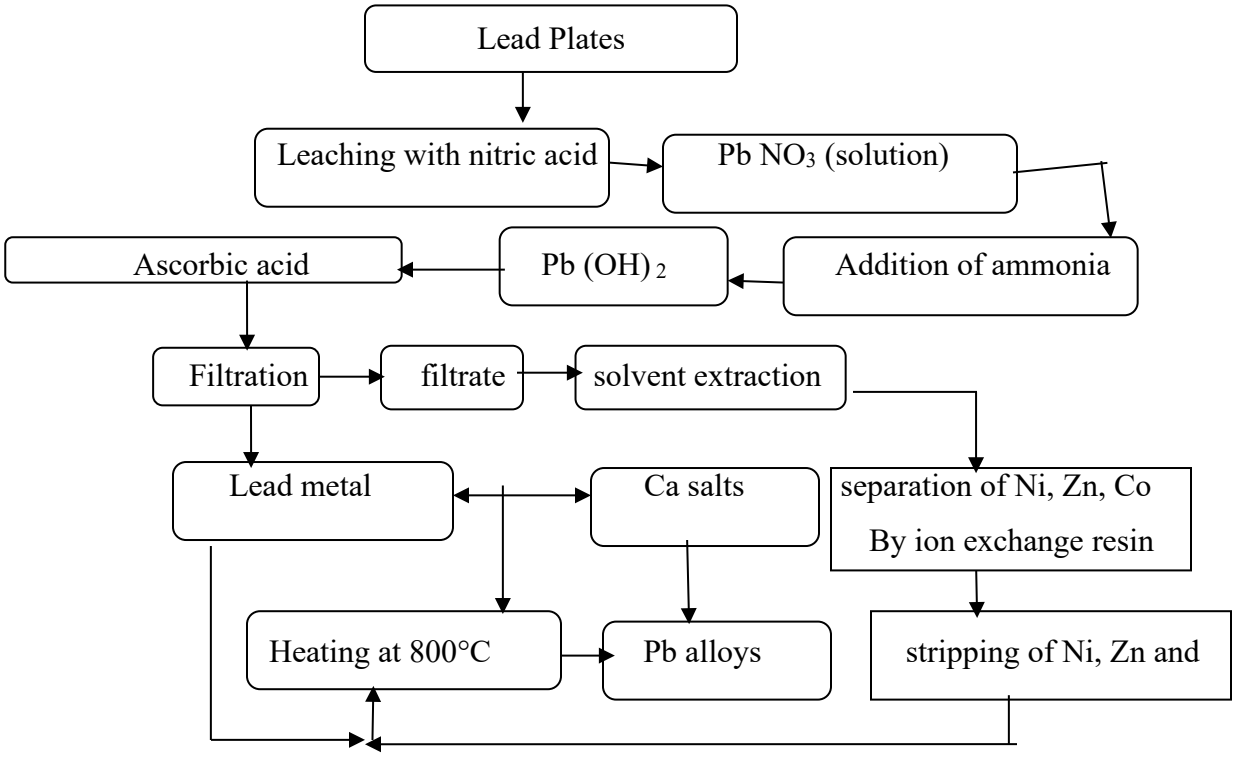

Fig. 3 Process flow sheet for the preparation of lead alloys from spent grids of the battery

Organic solvents were used to extract soluble ions of some metals that go into the filtered solution after the leaching process. Table 2 shows the type and properties of the solvents used.

An ion exchange resin Lewatite MP 600 (Merck) was used for ion exchange experiments. It was converted to chloride form before use by thoroughly washing with 0.1-2 M HCl acid in a column for 3 days. It was then washed with aqueous ethanol (70%). The treated resin was then dried under vacuum at 25°C.

A dyestuff of 4-(2-pyridylazo) resorcinol (product of Merck) was used weighing 10 g of molecular weight amounting to 215.21 was used. A 0.02 M stock solution was prepared by dissolving 0.538 g in 0.25-liter 80 % aqueous ethanol. Standard 0.2M bi-sodium hydrogen phosphate Na_2HPO_4 and 0.1 M citric acid $C_6H_8O_7.H_2O$ solutions were used as buffer solutions for pH control.

Table 2 Properties of the solvents used in this work

Solvent #	Property	Solvent #	Property
(1) Acetic acid	(0.1M – 1M)	(3) Acetone /water	25%-75%
(2) Ethanol/ water	10% - 75%	(4) Diethyl ether	50 %

2.2. Method of leaching and preparation of lead-calcium alloy from SLB.

Figures 2 and 3 show a process flow sheet of the applied method to recover lead and lead-alloys from exhausted rechargeable acid.

An ion exchange resin Lewatite MP 600 (Merck) was used for ion exchange experiments. It was converted to chloride form before use by thoroughly washing with 0.1-2 M HCl acid in a column for 3 days. It was then washed with aqueous ethanol (70%). The treated resin was then dried under vacuum at 25°C.

A dyestuff of 4-(2-pyridylazo) resorcinol (product of Merck) was used weighing 10 g of molecular weight amounting to 215.21 was used. A 0.02 M stock solution was prepared by dissolving 0.538 g in 0.25-liter 80 % aqueous ethanol. Standard 0.2M bi-sodium hydrogen phosphate Na_2HPO_4 and 0.1 M citric acid $C_6H_8O_7.H_2O$ solutions were used as buffer solutions for pH control.

2.3. Method of leaching and preparation of lead-calcium alloy from SLB.

Figures 2 and 3 show a process flow sheet of the applied method to recover lead and lead-alloys from exhausted rechargeable acid.

2.4. Determination of lead and other metals in the battery.

Lead. Calcium and other metals content in the exhausted grids were determined by XRF. Leaching was done by 3M nitric acid. The obtained leachate was analyzed by ICP. The unleached residue was also analyzed by XRD.

2.5. Description of the method used to extract minor metals in the leached solution

The method used was given by Badawy et al. [13]. The resin was de-mineralized by packing 1 g of the resin in a glass column through which HCl acid (2M – 0.01 M) was passed for nearly three days to assure that all the resin converts to the chloride form. It was leached with 1 L of 1% (NH_4) OH followed by 1 L of 4% sodium sulfate solution. The pH of the prepared metal salt solution(s) (≈ 100 mL) was adjusted to the required value by addition of the buffer solution before starting the adsorption experiments. The pH-adjusted solution was then run through the resin in the column. Ion exchange experiments were conducted by packing 0.2 g Lewisite MP 600 in the column. A solution containing the metal ions was then poured onto the top of the column and allowed to flow at a rate of 0.5 mL/min. The solution was recycled through the column for completely satisfying adsorption of the metal ions.

The effluent was collected in a separating flask. The chloride content in the aliquots from each leach was determined by titration against standard 0.05 N silver nitrate using potassium chromate as an indicator. Stripping of the loaded metals was conducted by eluting with 4 M HCl solution. The collected chloride solutions were separately concentrated by evaporation under vacuum. Chloride was either electrolyzed to prepare the respective metal or converted to insoluble carbonate that was reacted with the acid of concern (inorganic or organic) to prepare the required salt.

Determination of chromium, zinc, cadmium and nickel ions was carried out with the help of a UV-visible atomic absorption spectrophotometer Milton Roy model 20D for the resin and the metals ions determination.

The pH-adjusted solution was then run through the resin in the column. Ion exchange experiments were conducted by packing 0.2 g Lewisite MP 600 in the column. The solution containing the metal ions was then poured onto the top of the column and allowed to flow at a rate of 0.5 mL/min. The solution was recycled through the column for completely satisfying adsorption of the metal ions.

The effluent was collected in a separating flask. The chloride content in the aliquots from each leach was determined by titration against standard 0.05 N silver nitrate using potassium chromate as an indicator. Stripping of the loaded metals was conducted by eluting with 4 M HCl solution. The collected chloride solutions were separately concentrated by evaporation under vacuum. Chloride was either electrolyzed to prepare the respective metal or converted to insoluble carbonate that was reacted with the acid of concern (inorganic or organic) to prepare the required salt.

Determination of chromium, zinc, cadmium and nickel ions was carried out with the help of a UV-visible atomic absorption spectrophotometer Milton Roy model 20D for the resin and the metals ions determination.

The pH value was measured by a based bench pH meter (Hanna model 211) fitted with HFB electrode. Measurements were conducted at 25°C ± 0.2°C.

The exchange capacity of the resin ε_r was computed from the following relation, Kunin, [17].

$$E_r = \frac{V_{(AgnO3)}.\ N_{(AgNO3)}}{W_r} \times 100 \quad \ldots\ldots\ldots (1)$$

Where V is the volume, N is the normality, W is the weight of the resin sample.

The distribution coefficient K_d was determined from the relation given by John et al. [18]

$$K_{D} = \frac{\Delta C \times V_{\text{metal solution}}}{C_f.\ g} \ldots \quad (2)$$

Where ΔC is the change in concentration of the metal in solution before (C_i) and after the experiment (C_f), V is the volume and g are the weight of the resin. Sorption extent (%) was determined from the relation reported by Fethiye and Erol 2005 [19].

$$\text{Sorption \%} = \Delta C / C_i \times 100 \quad (3)$$

2.6. Method of preparation of the metals and their salts

The exhausted batteries under investigation were dissolved in 1.1 stoichiometric ratios of 3 M nitric acid at room temperature till complete dissolution (usually takes time). The volume of the solution as adjusted to 250 ml by distilled water**.** The nitrate solution was treated with an ammonia solution. The prepared nitrate or hydroxide salts were used to prepare free metals of lead or base metals by reduction with ascorbic acid or to prepare carbonate, chloride, sulphate, format, oxalate, citrate and acetate salts...

3. Results and Discussion

Fig. 4 shows the XRD of the lead paste. It is seen that the major content is lead sulphate, lead oxide while lead dioxide is minor. It is seen that major peaks appeared with intensity > 600 at 2θ 20-35 are assigned to the presence of lead sulphate, lead oxide PbO and lead dioxide PbO_2. These compounds were also detected with lower intensity (<200) at 2θ ?50 -< 80. Fig 5 shows the XRD pattern examined at low 2θ value of 18 and more. Fig. 5 confirms the presence of minor elements of nickel and cobalt. Table 3 confirms the presence of these minor elements. It is worth noting that lead alloy with this composition is recommended in the manufacture of batteries to help adequate mechanical and thermal stability of the battery during recharging and discharging operations.

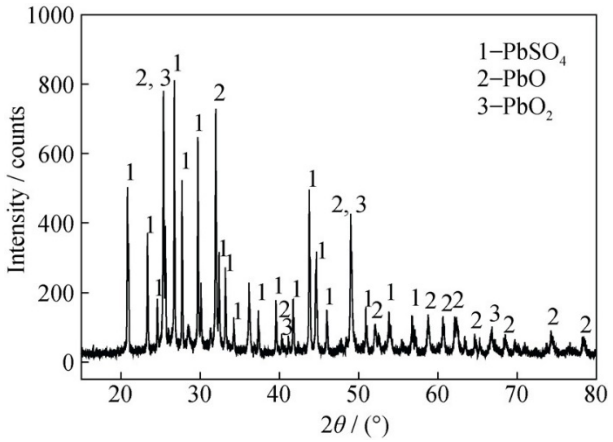

Figure 4 The XRD of the lead paste 46

It is seen that lead metal conistitutes the major element that amounjts to 94.2 % by weight. Other elements are in minor percentages. It is also seen that the weight percentage of these minor elements decreases in the order Si, Al, Ru, Zr, Co Ni, Cu and Zn. The common elements in commercial use aovered by solvent extraction technique.

This is very clear that lead compounds in grey plates were lead sulphate. The lead compounds in the brown plates were lead oxide and partly lead dioxide. Lead compounds decreased in the order sulphate, oxide and dioxide. Concerning the minor compounds, Ni and cobalt were present nearly in equal amounts (Fig. 3). Table 3 shows the elements present in the exhausted plates as detected by XRF analysis.

It is seen that lead metal is the major element that constitutes 94.2 % by weight. Other elements are in minor percentages. It is also seen that the weight percentage of these minor elements decreases in the order Si, Al, Ru, Zr, Co-Ni, Cu and Zn. The common elements in commercial use are Ni and Co and Zn. These were recovered by solvent extraction.

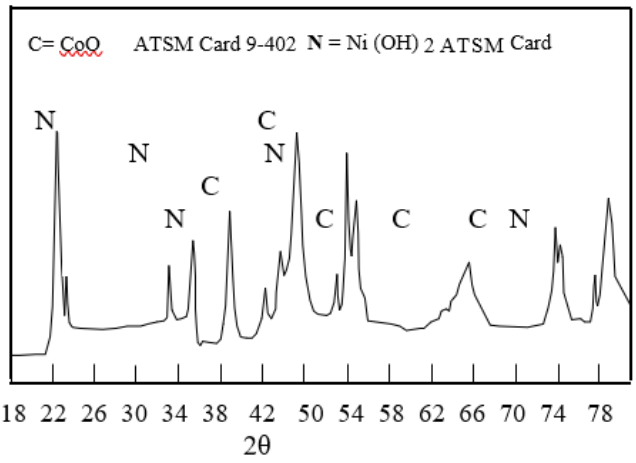

Figure 5 XRD pattern of the minor elements in the battery positive plates

Table 3 The XRF analysis of the elements present in the exhausted plate

Metal	% wt.
Lead	94.2
Nickel	0.05
zinc	0.0030
Cobalt	0.053
Copper	0.0272
Zirconium	0.0727
Rhobidium	0.0842
Aluminium	0.12
Silicon	0.24

technique. Fig. 6 shows the extent of leaching lead from the spent plates using 2M and 5M nitric acid at room temperature. The use of sulphuric acid instead of nitric acid was discarded because the reaction stopped rapidly because lead sulphate is immiscible in water. It can be seen that the leaching process takes time to react with lead compounds. The extent of leaching increases with time to give the maximum extent of 38.4 % after 7 days with 2N acid. More concentrated nitric acid (5M) gives less extent of leaching (32 %). using 2M and 5 M nitric acid at 80 °C shows that 5M nitric is more reactive as compared to 2M concentration. After 6 days the maximum extent of leaching amounts to 38$ and 14 $ with 5M and 2M respectively

Figure 7 shows the effect of time on the leaching extent of the brown paste of the battery using 3M and 5M nitric acid at 80 C. It can be seen that the extent of leaching increases linearly with increase in time attaining a value of about 40% after 6 days. The corresponding value taking place with 3M acid amounts to about 10%. Figure 8 shows the effect of nitric acid concentration on

leaching lead sulphate and lead oxide at room temperature for 6 days. It is seen that lead sulphate displays a higher extent of leaching compared to lead oxide up to 5 days. After 6 days lead oxide is readily more leached as compared to lead sulphate.

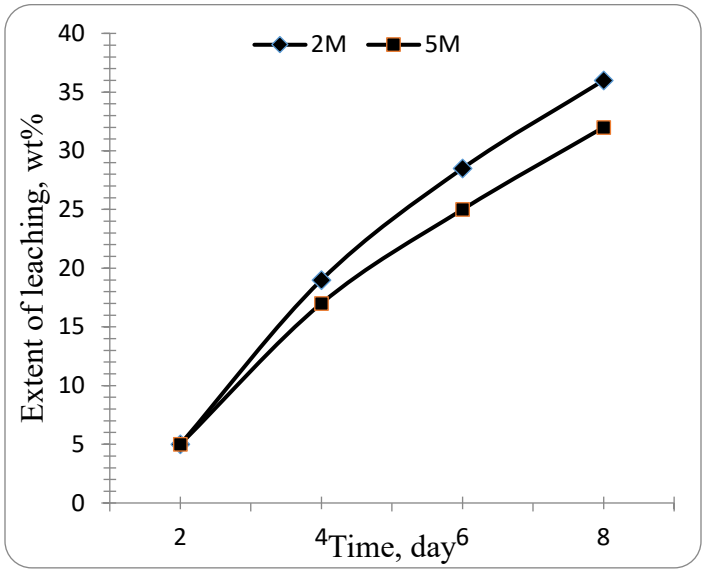

Figure. 6 Effect of time on the leaching extent of grey grids using 2 M and 5 M nitric acid at room temperature

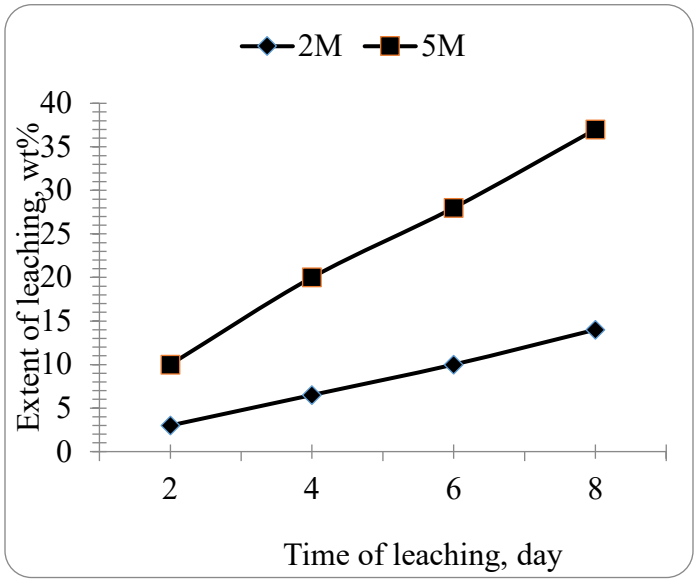

Figure 7. The effect of time on the extent of acid leaching of brown paste using 2M and 5M nitric acid at 80°C

Fig. 9 shows the effect of temperature on the leaching extent of lead oxide present in the battery. It can be seen that increasing the leaching temperature increases the leaching extent. The optimum acid concentration is 3.5 M.

Fig. 10 shows the coefficient of distribution Kd value of Zn ions extracted from the leaching solution using the exchange resin Lewatite. with different concentration of Zn as affected by the amount of the ion exchange resin added at room temperature. It can be seen that the coefficient extent decreases regularly with the corresponding increase in the amount of the used resin and the concentration of Zn ions in the solution.

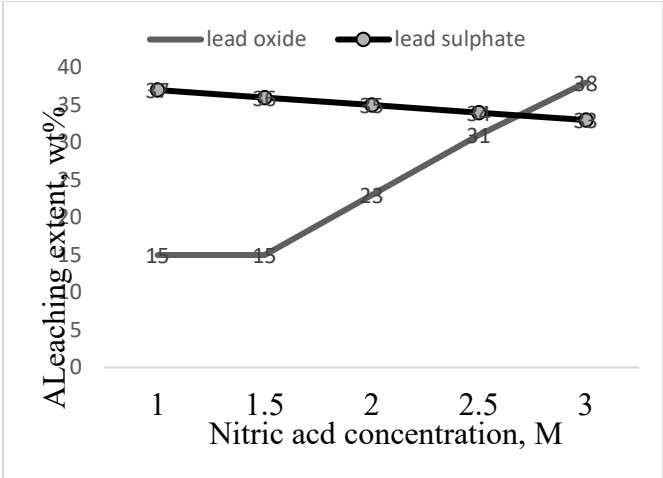

Figure 8 Effect of nitric acid concentration on leaching lead sulphate and lead oxide at room temperature for 6 days.

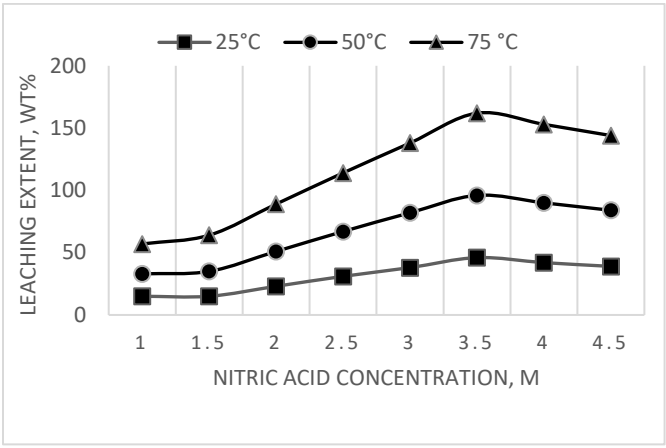

Figure 9 Effect of temperature on the leaching extent of lead oxide present in the battery.

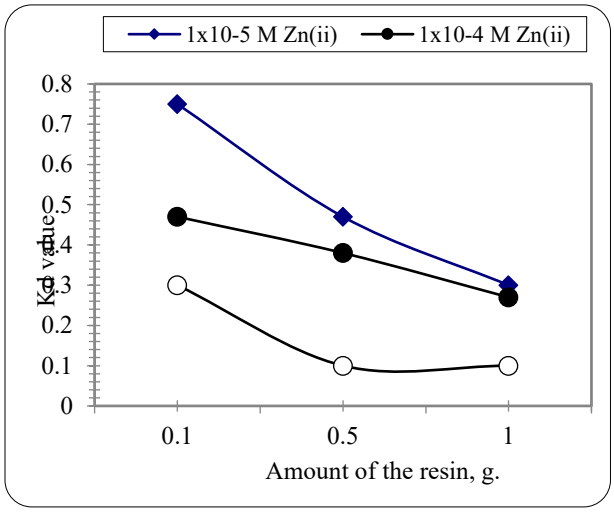

Figure 10 The Kd value for Zn from solution with different concentration of Zn as affected by the amount of the ion exchange resin

Fig. 11 shows The Kd value for Co from solution with different concentration of Co as affected by the amount of the ion exchange resin. It can be seen that with and the same metal ion concentration in the solution, the Kd value increases with the decrease in

concentration. This statement is logic as given in equation (2). The value of the denominator decreases that gives a corresponding increase in Kd value. The effect of change in g value is less significant as compared to the change in C value.

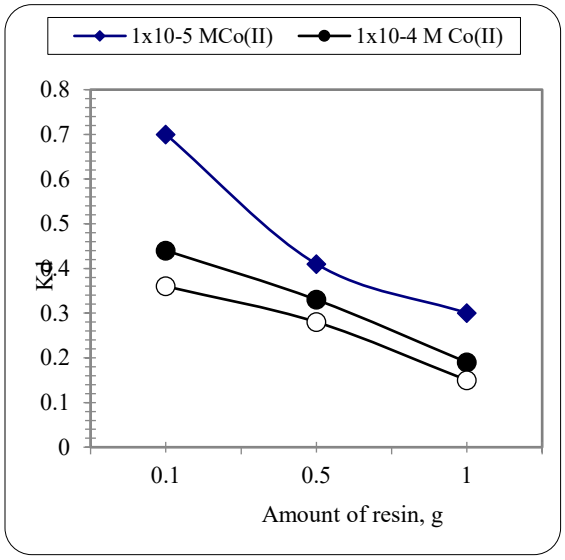

Figure 11 The Kd value for Co extraction from solution with different concentration of Co as affected by the amount of the ion exchange resin

Figure 12 shows the effect of pH value on the Kd value with nickel ions. It can be seen that the effect of pH becomes significant at values ≥ 8.5. At pH 9 the Kd value is highest. Fig. 12 confirms the same findings obtained with Zn ions given in Fig. 13.

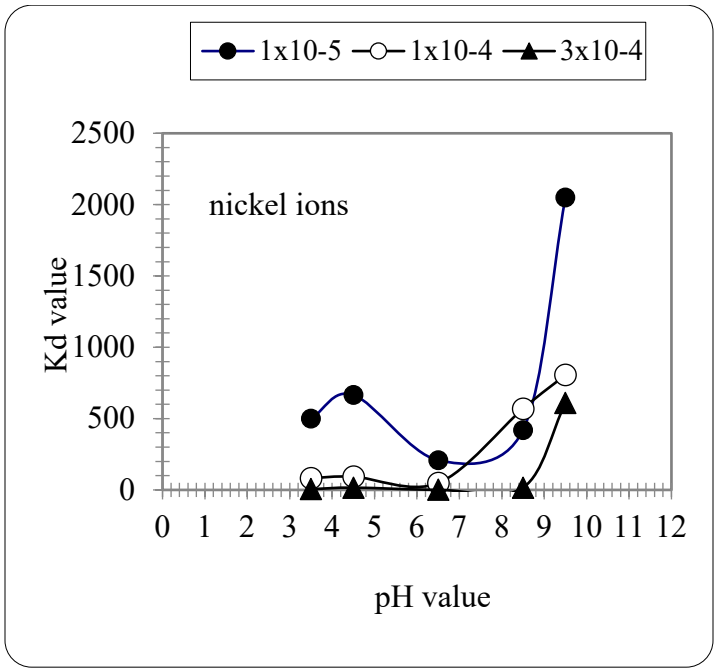

Figure 12 The Kd value for Ni extraction from solution with different concentration as affected by the pH value of the extraction medium

Fig. 14 shows the effect of type of solvent on the obtained metal powder after stripping. It iss seen that solvent 2 gives Ni and Al in nanosize. Solvent 1 gives the same effect with Aluminium. Other solvents give metals with larger size.

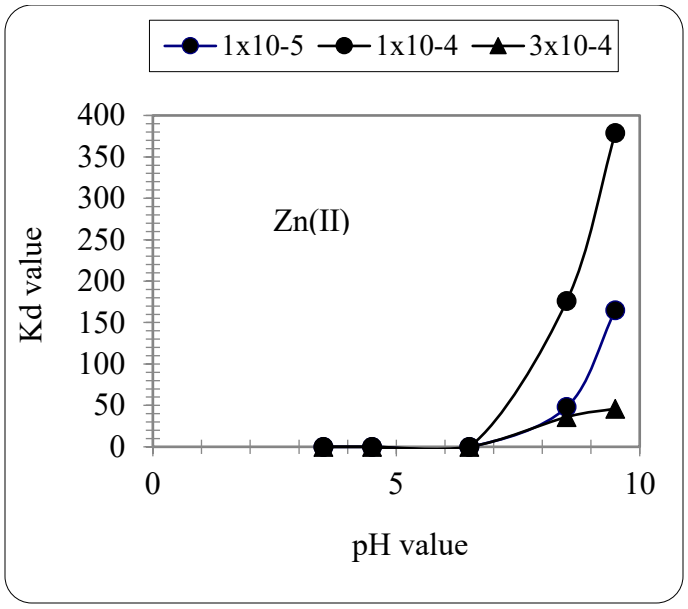

Figure. 13 Effect of pH value on the Kd value with Zn ions.

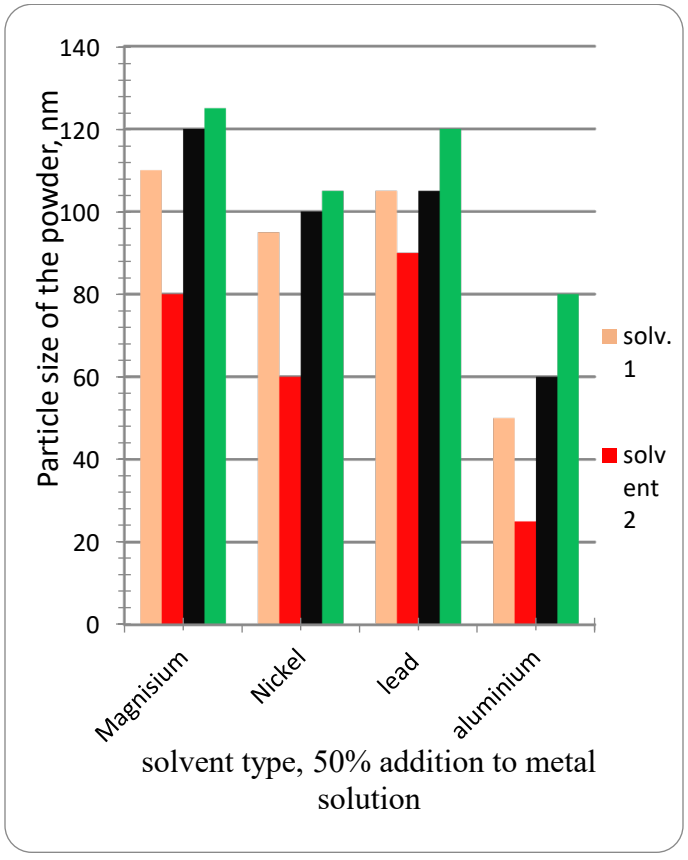

Figure. 14 The effect of type of solvent on the obtained metal powder after stripping

Table 3 shows that lead content in the battery amounts to 94.2 % by weight together with other 8 elements in a minor percentage. Leaching process in this study was carried out at room temperature to save energy although it takes time. The chemical reactions to leach the detected metals taking place according to

$$M+xHNO_3 \longrightarrow M(NO_3)x_{-1}NO_2 + H_2O\ldots\ldots \quad \{1\}$$

Table 4 shows the prepared salts from the spent battery and its purity extent. Table 5 shows the chemical composition of the residue

Table 4 the prepared salts of lead and its purity extent

Lead salt	Added reagent	Prepared salt	Purity of product
Lead nitrate	Sulphric acid	Lead sulphate	99.6
	HCl	Lead chloride	99.2
	Sod. carbonate	L:ead carbonate	100
lead hydroxide	Acetic acid	Lead acetate	pure
	Oxalic acid	Lead oxalate	pure
	Formic acid	Lead format	pure
	Citric acid	Lead citrate	pure

The unleached fraction remaining after nitric acid leaching was analyzed by XRF.

According to the law of mass action, increasing the nitric acid concentration in the reactants would enhance the leaching extent of lead oxide whereas lead sulphate was unleached. This finding finds support from the fact that sulphate radical is strong to be leached with nitric acid at room temperature. The leaching process is judged by the results given in Fig. 8. The nitrate salt was converted to hydroxide with the action of ammonia solution. This step was necessary to reduce the hydroxide gel to elemental nanoparticles of lead by ascorbic acid as follows:

Reduction of metals hydroxides

Ascorbic acid reduces hydroxide salts of lead and basic metals to free fine particles as follows

$Pb(OH)_2$ + 2 ascorbic acid ⟶ $2H_2O$ + Pb + 2 oxidized ascorbic acid.

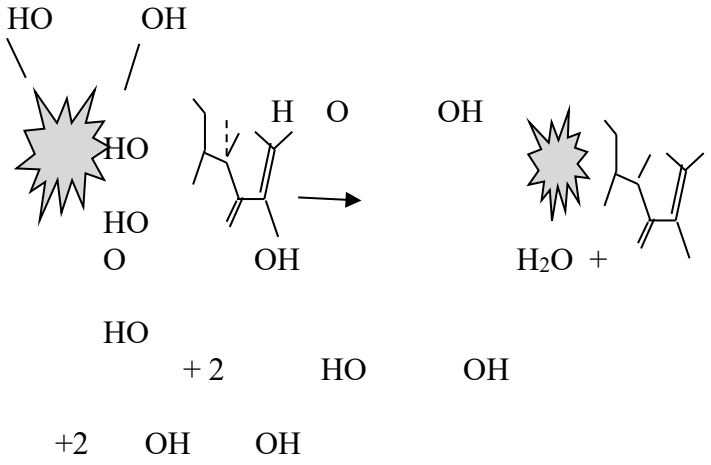

Lead hydroxide + 2 ascorbic acid water lead metal oxidized ascorbic acid

Table 5 the chemical composition of the residue

Plate	Composition
Grey	Lead sulphate 100%
Brown	Lead oxide PbO/PbO_2

Lead metal in battery plates is present in three forms; a grid made of lead alloy in the form of net-shaped structure loaded with lead sulphate or lead oxide-free metal. Heating the terminal tap of the battery gives lead alloy composed of lead-aluminium-magnesium as revealed from EDX pattern confirmed with SEM image given in Fig. 14. It is composed of 95.83 % wt Pb 1.25% Mg and 2.92 % Al. SEM/EDX is a combination tool, with two instruments working in partnership [20]. These two instruments operate simultaneously to complement each other's data acquisition, guided by the instrumental operator. Scanning electron microscopy (SEM) provides an image (i.e., morphological information or surface features) on a magnified scale—X 10 to X 100,000, although the usual range is perhaps X50 to X5000. Energy dispersive x-ray (EDX) determines the elemental composition of an area, with a sensitivity of perhaps 0.1 to 1 per cent composition and with a spatial resolution of 1 μm. EDX is commonly used for elements with atomic number ≥11 (sodium), but thin window EDX systems can also detect elements with atomic number ≥5 (boron). With these two instruments operating together, the instrumentalist can scan areas of potential interest, zoom in with higher magnification, and determine elemental compositions in selected areas of interest.

Lead is a soft and ductile metal and lead alloys are used on a large scale. The alloying elements may be antimony, tin, arsenic, and calcium are. Antimony is used to give greater hardness and strength, as in storage battery grids (0.5 to 25%), sheet, pipe, and castings. Antimony contents in the lead-antimony alloys are usually 2 to 5%.

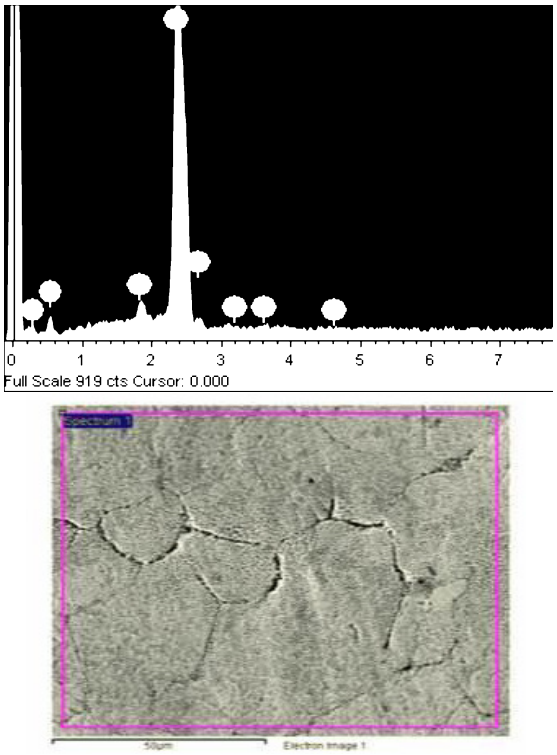

Figure 15 (a) The EDX of the melted terminal tap, (b) the SEM of Pb Al alloy.

Fig. 15 shows the EDX and SEM images of lead obtained by melting the terminal tap of the battery under an inert atmosphere. Fig 15 {a} is the EDX pattern of a lead alloy of the terminal tap. Fig. 15(b) is the SEM of the Pb Al. Alloy after annealing at 500 °C Results revealed that only 15-20 % of lead is obtained by simple heating of all the battery plates even in reducing conditions. It becomes legitimate to apply the modified method capable to produce the high extent of lead recovery. In this context, Yoheeswaran1 et al., [15], reported that the recovery of 95% of lead metal from lead-acid batteries by 2M of nitric acid It is found that 95% of lead metal was leached and more than 90% of lead metal can be recovered by electrochemical method with low current efficiency from Pan the leaching solution.

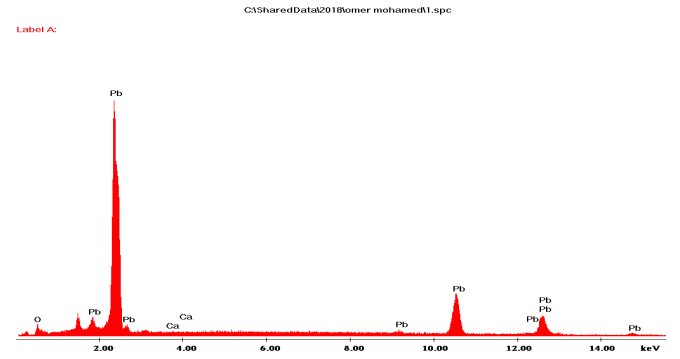

EDX pattern of lead Ca, 0.18 %, 3% Al, 94% Pb

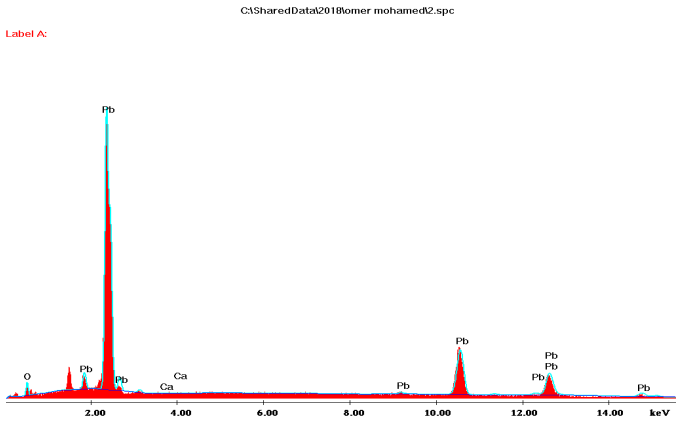

EDX pattern of lead Ca0.08 %

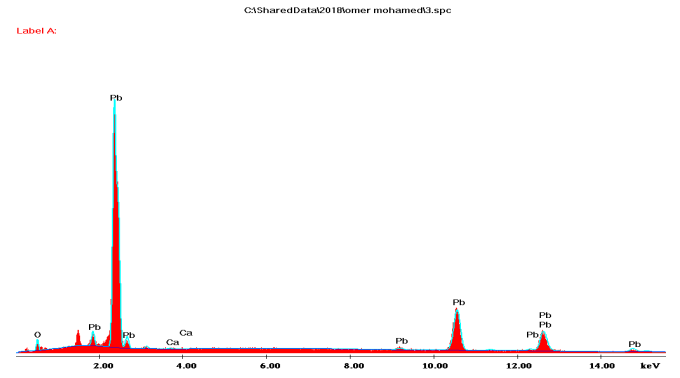

Pb 93.66% Ca 0.32 %, Ca 0.32 %,

Figure. 16 EDX pattern of lead alloys containing different alloying elements.

The method adopted seemed promising and had great potential for removal of lead from used lead-acid batteries. Fig. 16 shows the EDX pattern of lead alloys with calcium (0.018% and aluminium 0.03%, lead alloyed with 0.08% calcium and 0.32% calcium. In this pattern, the main electron beam appeared at 3.00 Kev is stable at a relative height of 66.2 % with all alloys is assigned to elemental lead. The spectra of the alloying elements appeared at 11 Kev with lower relative height pf 10 % and 7 % are for Al and Calcium respectively [22].

Unified Numbering System (UNS) designations for various pure lead grades and lead-base alloys is as follows [23].

- Pure leads L5xx00 - L5xx99
- Lead - calcium alloys L5x700 - L5x899
- Lead - strontium alloys L552xx - L55299

Lead-calcium alloys are used in several applications, particularly, storage battery grids and casting applications. Pb-Ca alloys contain 0.03 to 0.15% Ca. aluminum is now added to calcium-lead and calcium-tin-lead alloys to stabilize calcium. Alloying tin to lead increases hardness and strength. However, lead-tin alloys are usually used for their good melting, casting, and physical properties as in type metals and solders.

4. Conclusion

The output conclusion of this work is that exhausted rechargeable batteries are essential resource for recovery of nonferrous precious metals like lead and lead alloys. Other metals value (Ca. Al, Ni, Co) are present and were successfully recovered. The method used to achieve the goal of this study was simple and friendly environmentally. Preparation of lead metal was matched by a combined hydrometallurgy and pyrometallurgy. The battery was dismantled and the plates were separately leached in nitric acid whereby the nitrate salt was converted to hydroxide by ammonia solution. The hydroxide was reduced to metal lead nanoparticles by ascorbic acid, Alternatively, the lead sulphate and oxide packing the grids were thermally heated with carbon at about 900 ^{o}C to give free metal lead. Alloys of lead with calcium and aluminium has been matched applying the combined hydrometallurgy and pyro metallurgy methods. The extent of recovery amounts to 94.3 % with pure lead and 99.6% with lead alloys of aluminium and calcium. Valuable salts of lead including organic salts were also prepared in highly pure grade.

References

[1] E. R, Cole A. Y. Lee. D.L. Paulson,"Recovery of Lead from Battery Sludge by Electrowinning", JOM, August 1983, Volume 35, Issue 8, pp 42–46 , 1983

[2] A., Smaniotto, A. Antunes, I. doNascimento, L. Filho D. Luciana, D. Venquiaruto. D. Oliveira, M. , AltemirMossi H. Treichel and R. Dallago J. hazmat..07. pp 26. 2009.

[3] C. S Chen, Y.J[2,] Shih, Y.H. Huang "Recovery of lead from smelting fly ash of waste lead-acid battery by leaching and electrowinning. m Waste Management, 52:212-20, 2016

[4] Junqing Pan, ChaoZhang Yanzhi Sun Zihao Wang "A new process of lead recovery from waste lead-acid batteries by electrolysis of alkaline lead oxide solution", Electrochemistry Communications. V 19, June 2012, pp 70-72, 2012.

[5] X., Chen, "Hydrometallurgical process for the recovery of metal values from spent lithium-ion batteries in citric acid media", Waste management and research J. Vol 32, Issue 11, 2014. https://doi.org/10.1177/0734242X14557380

[6] D. Andrews, A, Raychaudhuri, and C. Frias. Environmentally sound technologies for recycling secondary lead, J. Power Source, 88. V1, p. 124., 2000.
[7] X. Chen, , Hydrometallurgical process for the recovery of metal values from spent lithium-ion batteries in citric acid media, WASTE MANAGEMENT AND RESEARCH J. Vol 32, Issue 11, 2014
[8] E. Margulis, (Hafia, IL), Process for the recovery of lead from spent batteries, USA Patent 4058396, 10/27/ 1998
[9] G.Z. Chen, D.J. Fray, and T.W. Farthing, Direct electrochemical reduction of titanium dioxide to titanium in molten calcium chloride, Nature, 407(6). 2000
[10] D. Zhou, C.Y. Zhao, and Y. Tian, Review on thermal energy storage with phase change materials (PCMs) in building applications, Appl. Energy, 92 p. 593. 2012
[11] Y.Y. Long, J.Z. Li, D.H. Timmer, R.E. Jones, and M.A. Gonzalez, Modeling and optimization of the molten salt cleaning process, J. Clean. Prod., 68, p. 243. 2013
[12] J.G. Yang, C.B. Tang, Y.M. Chen, and M.T. Tang, Separation of antimony from a stibnite concentrate through a low-temperature smelting process to eliminate SO emission, Metall. Mater. Trans. B, 42 No. 1, p. 30.2011
[13] N. Badawy, M. A. Rabah and R. Hasan 2013 Recovery of some heavy metals from electroplating rinsing wastewater by LEWATIT MP 600 ion exchange resin., Int. Journal of Environment and waste management, IJEWM, 12(1) 33-51. DOI: 10.1504/IJEWM. 054778. 2013
[14] Y.J.-Chu, and G. T. Townsend, "Leaching of Lead from Computer Printed Wire Boards and Cathode Ray Tubes by Municipal Solid Waste Landfill Leachates Department of Environmental Engineering Sciences, University of Florida, Gainesville, Florida 32611-6450 Environ. Sci. Technol., 2003, 37 (20), pp 4778–478 2003
[15] E. Yoheeswaran1, S. Govindaradjane, and T. Sundararajan, "Recovery of Lead Metal from Lead Acid Battery by Hydrometallurgical Method", International Journal of Engineering Science and Innovative Technology (IJESIT) Volume 2, Issue 1, January 2013
[16] Viraja Bhat et., al, "Development of an integrated model to recover precious metals from electronic scrap – A novel strategy for e-waste management, Procedia social and behavioral 37, 397-406, 2012.
[17] Y. Ma and K, Qui "Recovery of lead from lead paste in spent lead acid battery by hydrometallurgical desulfurization and vacuum thermal reduction", Waste Management 40. 03, 010,2 015
[18] R. Kunin, A., Rohn. and H. Company (Eds), Philadelphia Pennsylvania, New York, John Wiley and Sons, Second Edition, 1170.2016
[19] E,G, John, W., Gary and A., Georgiann Preconcentration of trace metal ions by combined complexation-anion exchange Part I. Cobalt, zinc and cadmium with 2-(3′-sulfobenzoyl)-pyridine-2-pyridylhydrazone. Anal. Chim. Acta , 81, 349. 1976.
[20] G. Fethiye and P. Erol Removal of Cr (VI) from aqueous solution by two Lewatit-anion exchange resins. Journal of Hazardous Materials. 119, (1-3), 175-182. 2005.
[21] E.R., Bagherian, F. Ongchang, M., Cooper, et al., "Effect of antimony addition relative to microstructure and mechanical properties of continuous cast lead alloy", Metal, May 25th - 27th 2016, Brno, Czech Republic. 2016.
[22] M. T. Riaz, Y. Fan, J. Ahmad, M. A. Khan, and E. M. Ahmed, "Research on the Protection of Hybrid HVDC System," in 2018 International Conference on Power Generation Systems and Renewable Energy Technologies (PGSRET), 2018, pp. 1–6.
[23] https://en.wikipedia.org/wiki/Unified numbering system.

ASTES

Advances in Science, Technology and Engineering Systems Journal Vol. 4, No. 4, 539-544 (2019)

www.astesj.com

ASTESJ

ISSN: 2415-6698

Communication Management of Digital Information Data in Human Resources as a Policy Making Strategic Program for University

Edi Suryadi*

Department of Office Management Education, and Communication Science Faculty of Business Economics Education, Universitas Pendidikan Indonesia, Bandung, 40154 West Java Indonesia.

ARTICLE INFO

Article history:
Received: 13 July, 2019
Accepted: 15 August, 2019
Online: 25 August, 2019

Keywords:
Communications
Human Resources
Policy Maker
Strategic University

ABSTRACT

Modern universities aim at carrying capacity human resources component in its tri dharma (Three Pillars of Higher Education). UPI with sufficient conditions in the management of several resources has undoubtedly tried to establish itself as a modern university. The superior human resource support in every competition and the university's tri dharma is the primary resource of UPI. The results of all HR roles have become inputs for the management of digital data and information. Therefore, communication management containing the university's strategic policies can be effectively and promptly translated as well as implemented by human resources. To conduct dissemination and sustainability both nationally and internationally, this research formulated three main components in managing policy communication on human resources in a modern university, which include: (a) architecture vision, (b) value change; (c) flow diagrams, all of which refer to the achievement of vision and mission.

1. Introduction

Universities comprise of many ranking systems such as webometrics, Q-Start, and many more. These systems can also be categorized according to specific parameters which constitute the institution's education system and wealth of knowledge required for students to compete with other educational schools across the globe. These mutual competitions create an impact on the policy of each institution respectively. The need for higher educational level has continuously evolved with the need for leaders to obtain data and information from all university resources, especially those with available human resources. A qualified human resource condition can be a source of honesty policy with target program performance and some functional institutional ranking parameters.

The above phenomenon cannot be separated from what has been conducted by Universitas Pendidikan Indonesia (UPI). With the new leadership, UPI has begun to launch Operational Standards and Work Procedures [1] and the establishment of new university tools capable of boosting and penetrating the parameter and certification systems of higher institutions in Indonesia, Southeast Asia, and even the World. UPI's strategy in maintaining and improving these ranking parameters is applicable at the national and international levels.

Some achievement supported by the human resources owned by UPI has been internationally recognized with a good number carried out by correlating MoU with some Western universities. UPI has been able to display some level of solidity in facilitating lecturers to conduct research. At the time of this study, about 3500 research titles had already been completed by UPI lecturers within the last three years [2]. A look at the statement indicates that during the university's communication management some managerial facets underwent transition. Therefore, a critical analysis is required for the administration, to produce strategic communication. This happens to be one of the main focuses and reason why the research is continuously conducted at all levels.

Lecturers and students achievement were appreciated and the policy strategy, a manifestation of the UPI vision with the slogan "Leading and Out Standing"[3]. The existing communication management skills are expected to realize Sustainability University in the future. In this study, UPI will be able to strengthen the wrong policies and the programs of achievement of sustainable human resource development. Based on the above explanation, the research focuses on analyzing the Digital Information Data Communication Management Study in the form of Architecture Vision, Value Chain, and Flow Diagram within the Directorate of Human Resources in using UPI in Modern University.

* Edi Suryadi, Email: edi_suryadi@upi.edu

2. Literature Review

2.1. Communication Management of Modern University

The study of communication management plays an essential role in education. It is the main character of a university intending to penetrate the modern reputation. [4] Explains the relationship between the world of education and communication science, as follows:

”Education and communication management influence the energy levels of change and improvement. Strong communications keep everyone focused on goals and priorities while providing feedback on progress and the required course corrections. Effective communication strategies, systems, and practices have a huge and direct effect on an organization's learning and innovation."

If viewed from the institutional systems owned by UPI in current time, especially with the new SOTK (an Organizational Structure and Work Procedure of UPI), some shifts concerning basic tasks and functions will be slightly different from those obtained between 2010-2015 [1]. The differences are seen from the UPI and Vice-Rectors for Academic and Student Affairs, Vice Rector for Finance and Resources, Vice Rector for Planning and Facilities, and Vice-Rector for Research and International Relations. When viewed from the leadership and UPI’s organizational structure from 2016-2020, it is clearly in transition, and requires a common understanding of the elements involved, especially in terms of the university’s internal environment management [3]. As the largest university in Indonesia, even Southeast Asia can be the best, especially if the track record of its management journey is quite dynamic. Some experts are very interested in UPI's ability to transform from its status as a regular PTN (government university) to PTN BHMN (a government university and a law bureau of government), PT BHMN and eventually became PTN BH (government university and a law bureau).

UPI as a university is the incarnation of ex-IKIP LPTK trained achievers. It utilizes a dual curriculum characteristic comprising of educated and non-educated people with qualified human resources. Results of the previous research indicate that the UPI eventually adopted a layered model for its educational purposes [5]. This means that it follows the educational and non-education strategy with the graduate having a certificate of teaching, while the non-educational graduates, must take some educational courses. The success is inseparable from the qualifications of human resources.

If viewed from the perspective of human resources, finances, assets, and educational services, UPI students will undergo a transition period or development from the "technical service" unit to "Directorate." Even in the current educational path, it has implemented a "Department" owned by each faculty. According to William Bridges [6], the transition management should indulge in managerial renewal and immediately regain and reintroduce the three-phase energy in its organizational life cycle, which includes (1) dreaming back dreams; (2) restoring the spirit of work; And (3) reorganizing the organization.

2.2. Strategy Formulate Performance Assessment System

Strategic management is an anticipated manageria technique which can be realized in organizational leadership. Many strategies have been played to implement the right UPI strategy in the practice of university leadership management. However, the results tend to vary with the numerous changing demands of society. [7], the strategic management process includes four essential elements: (1) environmental attenuation; (2) Strategy formulation; (3) implementation of the strategy; and (4) evaluation and control.

Communication Management deals with how leaders who become top managers analyze their needs and human resources. This effort is important because in managing an organization, leaders tend to adopt behavioral styles which grow and develop concerning a specific form and color management. Based on this phenomenon, [7] responded with a study called Policy Development, according to him, "Management now has to establish policies to determine the basic rules to be implemented in the University. These policies will guide the decision-making process in the organization. Of course, all must be supported by an accurate data information system, therefore, the existence of a management information systems owned by the University will be essential. As explained by [8], SIM is rationally integrated, i.e., a collection of semi-separated information systems integrated through activities relating to each other and primarily carried out by passing data between Systems.

Through the support of digital data and with the formulation of human resource management, a quality digitalized university will be achieved. In this case, [9] explains:

> “Virtual community is an aggregation of individuals who interact around a shared interest. While this definition strips the world of its usually understood meaning, it is in accordance with the business world.”

In the context of UPI which has some business field of education, the formation of virtual academic is very appropriate, thereby, making it a virtual or digital university.

2.3 Digital Resource Information Data of the University

A campus designed with the utilization of ICT facilities in the hope of all communities, considering the fact that future educational institutions should be able to be accessed quickly and easily by the wider community. No distance and space prevent people in need of academic services. All management policies on digital campuses are expected to build up for future generations. Starting from the present generation, UPI has begun to socialize its educational services digitally[10]. This comprises of the digital implementation of new enrollment techniques, student guidance services, learning monitoring and evaluation system[2]. In practice, all academic community has started to migrate its services. Starting from employing lecturers and management with the ability to utilize digital tools and facilities.

Some foreign universities such as those in the UK, Cambridge University, Texas University, California University, Ohio University, have been making use of digitalized campus system since 1997[11]. [11] Further explained that:

> “Digital generation is distinct from others in terms of its technological process as opposed to its old analog processing method."

From the above statement, it can be deduced that the digital generation born after the non-digital or analog period fades away, thereby, contributing to its success. People in the analog period

are trying to be more effective in carrying out their educational responsibilities duties by utilizing digital systems. In the context of research on UPI policy management, digital concepts can be applied to all UPI academic community which in 2 decades has been able to utilize these systems [12],[13] to support the implementation of its management functions.

In this study, several important studies on strategic communications management regarding human resources of a university are expected to be able to find new formulations to assist in the success of university quality achievement programs. The study of effective policy communication management [13] will undoubtedly be an important study of stakeholders in higher education environments. As explained by [4],:

Effective communication strategies, systems, and practices: (a) Deliver clear and consistent messages to all parts of an organization; (b) Are simple, direct, and fast with a minimal number of filters and interpreters; (c) Inspire and energize; (d) Are user-friendly, human, and personal; (e) provide information, experiences, learning ideas, direction, and feedback in all directions of an organization; (f) Provide multiple channels; (g) Are only possible in an atmosphere of trust.

From the above opinion, the main factor of the effective strategic management with regards to the Strategic Communication System [14] will be able to provide clarity as follows: (a) Deliver a clear and consistent message to all parts of the organization, (b) Deliver what is simple, direct, and fast with a minimal number of filters and interpreters, (c) Inspire and energize students, (d) Is user-friendly, human, and private, (e) Placement of information, experience, learning, ideas, direction, and feedback equally in all directions up, down, and throughout the organization, (f) Provide multiple channels, (g) Is it possible only in an atmosphere of trust and openness.

3. Methodology/Materials

This research will be conducted using the Qualitative approach in the form of Explanation Survey on work unit of Human Resources, Infrastructure, Finance, and Development Planning in UPI environment, concerning data, information management, and policy communication management model built in supporting the modern university[15]. Data collection is done by distributing questionnaires to members of the research with some leaders in the UPI environment. Study documentation and observation on all practice of policy communication strategy [14] conducted on UPI. Data analysis was done by descriptive qualitative data from[16].

4. Result and Findings

4.1. Design Flow Diagram Architecture Vision of HR Directorate

The need to develop a flow diagram as one of the guidelines in understanding the overall steps of work within the Directorate of Human Resources is an important step. During the analysis stage, several aspects of the needs program activities in previous years can be adequately detected [13]. The analysis results achieved during the Plan and Development process have obtained some participants utilized as a source of input team of the UPI human resources. Each flow diagram is intended to provide clarity on the primary task of each unit and sub-unit existing within the Directorate of Human Resources UPI.

The development forms associated with data processing and digital information has been in existence universities located in Indonesia, with several types of internal management website[17] built, such as the model information system Human Resources Information System (SISUDAMA, *Model of Information System HRD*). Digital data management system related to human resources in UPI environment, starting from: (a) Management of system to fulfill human resource requirement; (b) Management of the HR data placement system of each work unit; (c) management of empowerment systems; (d) Management of a career evaluation system.

1) Management of recruitment system or fulfillment of human resource needs.
   After placement is conducted, it is analyzed in the unit or sub-unit where shortages are incurred. Furthermore, the method of meeting the needs of human resources is in accordance with rough treatment, opportunity, or balance of energy in each unit. The fulfillment process in addition to system-based performance is also aimed at the ability for every candidate to continue assessing if the performance to be submitted is excellent following the standards. Usually, the place or unit where the candidate or employee works provides recommendations on the assessment of available prospective resources needed in supporting all tasks of the HR unit work.
2) Management of HR data unit placement system.
   The management of HR data placement system is performed on all resources with each system enforced. If associated with lecturers, then the submission is made starting from the process level, to the human resources directorate called and participated in the selection process. Similarly, the needs of employees may recommend employees or staff from specific fields to help other parties.
3) Management of Human Resource Development or Empowerment system.
   The Directorate of Human Resources manages systems Development career applicable to the university. Through this, the career system is applied in the form of a lecturer development information system for lecturers and education personnel. Mapping tasks at the university level also do it. There are some programs aimed at becoming a benchmark for the success of the educational career development of personnel within the UPI environment, using data stored on the university page, with the address http://kepakaran.upi.edu/index.php/
   Based on the results of the information system expertise, human resources, especially lecturers will obtain development services by utilizing digital data through the development information systems accessible on http://bangdos.upi.edu/. In this page, educators can undergo self-development using data information on self-development in several areas during a career at every level.
4) Management of HR career evaluation system.
   The evaluation system managed by the Directorate of Human Resources UPI is based on digital information, all the performance and career appraisal programs are aimed at processing Digital Lecturer Workload System. As for educational personnel processes through the Employment Assessment System, both systems are designed digitally

and used online. This supportive information system is available on its website http://www.upi.edu/.

5) Management of Digital Information Data of UPI. Human Resources in the framework of Embodiments of Quality of Human Resources

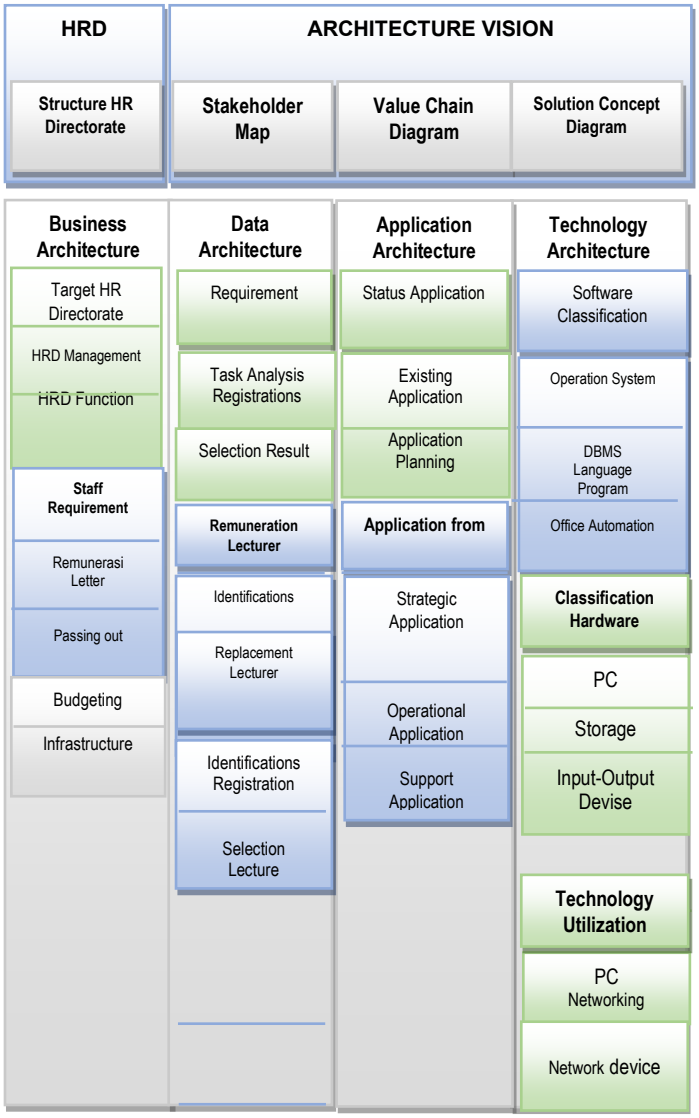

Figure 1: Architecture Vision of Communication management of Director Human Resource UPI

Management and resource quality improvement policies [18] are translated into programs in order to: (1) improve the quality of human resource management performance, finances, facilities and other activities that are efficient, transparent and accountable to support the enhancement of academic performance quality; (2) implementation of human resource management information system, finance, and facilities within the framework of an information management system of UPI integrated with ICT-based; (3) improves coordination effectiveness across management functions such as human resource management, finance, facilities, ICT, and other activities among work / academic units synergistically to support its performance quality; (4) improvement of quality standards for human resource management, finance and facilities oriented to international standards to meet management and / or stakeholder needs; (5) improvement of quality and / or capacity of human resources, finance, facilities and ICT; (6) development and implementation of lecturer career development system in accordance with the needs of universities and professions; (7) preparation and implementation of lecturer recruitment and / or assignment mechanism consistently; (8) improvement of effectiveness and follow-up of employee performance evaluation result (lecturer, librarian, laboratory, technician, and administration staff); (9) development and / or implementation of a fair and fair integrated compensation / remuneration system; (10) development and / or implementation of employee welfare system; (11) improvement of financial system and financial report quality improvement; (12) the implementation of performance-based budgeting policy as a form of budget adjusted to the achievements to be achieved; And (13) strengthening the function and role of the library as a teaching library [17].

Currently, human resources owned by UPI consists of lecturers and educational staff. Education personnel includes academic laboratory institutions, learning technology institutions, libraries, staffing analysts, archivists, and general functionalities. UPI lecturers amounted to 1,325 people, consisting of 1,251 government officers (PNS) and 74 non-PNS. From the findings on the management of research data relating to the Human Resources Directorate, there is a communication management model as described by the researchers in the following sections [19] [5].

From the result of analysis above, an Architecture Vision built to support the success of Human Resources Directorate of UPI, as shown in the picture below.

4.2. Value Chain of Digital Information Mobile Management HRD in UPI

From the design of communication management development above, the stages of Management Communications Policy within the Directorate of Human Resources UPI can be described as Business Modeling (Business Architecture) [20]. It is a part of the University of Education in Indonesia which aims to manage human resources by conducting tasks and functions of the main activities, such as the Recruitment CPNS, Remuneration Lecturer, Administration Letter, and Pensions CPNS. This main activity will require support from other sectors such as Administration, Finance, and Infrastructure[21]. Identification of main and supporting activities in the UPI Human Resources Directorate can be described by using the value chain of [12] shown in the following figure 2.

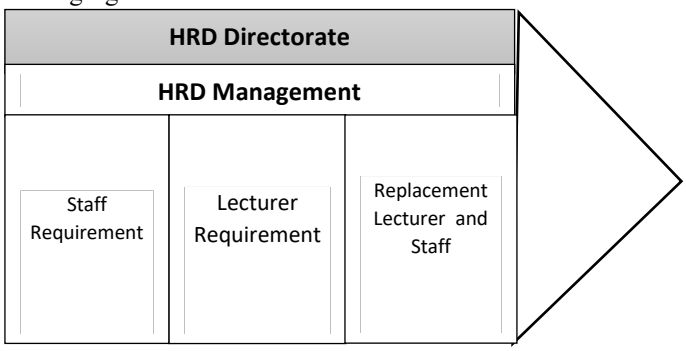

Figure 2: Value Chain of HR Directorate of UPI

Analyzing the thought on the review of work programs and policy communication strategies for the HR field is followed by strategic analysis [22]. From the results of this research, the needs of the HR on the assessment system for aspects of human resources as well as with Sarana is analyzed using reference sources and demands from ministry of research and higher education. Referral standard for inconsistencies relating to Educational Services, (Bureau of competence, Facilities) on human resource mapping is based on assessment center on human resources, facilities, infrastructure, and external reference documents for UPI have been developed by internal Directorate [10].

Example: Assessment System on human resources related to employment. Similarly, regarding facilities and infrastructure, with UKT as an example, basically, the database owned by UPI, can take ISO report data [23]. Mapping can be conducted with this database, for example, the submission of needs should be based on value assessment. To achieve this, the database system for facilities and infrastructure needs a support system developed to disseminate the lower level [14].

The policy is poorly understood at the user level, therefore,in the future the research findings will further clarify the targets of all policies relating to areas under the database jurisdiction (performance indicators) [24]. Data can be obtained from each faculty and can also be thought of as a Multisite campus [25] used to develop a modern campus. It is possible that other campuses imitate UPI. Regardless of this, Multisite campus [18] can be done by mapping the competence of excellence in each campus area, (source reference Data source international university). For example Base in Sonkla, regional needs site [5].

The Vice Rector for Human Resources explains that assessment centers should be kept in SPM, but its inputs and references can be from recommendation associated with this research with the report stored in the form of a database [13]. This is similar to the expertise folder that comprises of UPI, because this digital data will be the basis for making the reports in the field. From the above research findings, the communication management policy model of HR will then be implemented with regards to the Value Chain [21] model above. The important aspect of it is the number of duty that will be implemented by the human resources while carrying out their duties from:

1) Recruitment of CPNS, prospective civil servants and their establishment in UPI.
2) Lecturer Remuneration, activity from the beginning of the recruitment stage to its result determination stage.
3) Pension Lecturer, Activity of pension management process for lecturer in Directorate of Human Resources Universitas Pendidikan Indonesia.

In addition to the above main tasks, there are also supporting duties, which include:

1) Administration, Activity in administrative management within the organization that promotes main activities related to the administration as well as recording in the maintenance of infrastructure, facilities, and infrastructure of UPI Directorate of Human Resources.
2) Finance, Activities in financial management within the organization that supports the main activities related to cash inflow, cash outflow and investment and funding maintenance infrastructure, facilities and infrastructure Directorate of Human Resources UPI.
3) Facilities and infrastructure, activities to provide support in the form of services for all parts of the Directorate of Human Resources UPI and manage and improve infrastructure, facilities, and infrastructure.

4.3. Modeling Functions of Business Directorate of Human Resources in UPI

Modeling business functions with organizational units will be further illustrated using business models. This can be built in the form of component interaction with the organizational unit by describing each task, as displayed in the picture[26]. From the flow diagram developed above, a minimal main task is performed by the unit associated with measurable tasks [27],[28] as shown in the table below.

Table 1: Human Resources Recruitment

No	HR Management	Description
1.	Ministry of Education	Responsible for determining the allocation of candidates needs based on employees requirements
2.	Directorate of Hingher Education	Responsible for determining the allocation and specification of prospective employees needs as specified by the Ministry of National Education
3.	Faculty/ Department	Responsible for the implementation of prospective employee recruitment activities
4.	Admission Committee	Carry out operational activities in the acceptance of prospective employees in UPI environment
5.	Prospective applicants	Register and follow the perspective stages determined by the admissions committee

From the data and information digital results extracted, a communication management policy model is formed [27] which can be recommended from the results of research, as seen in the chart in figure 3.

5. Conclusion

From the field studies and the results obtained from analyzing the Communications "Digital Information Data" as a Policy Material Program, it can be concluded that there are some important aspects within the Directorate of Human Resources in UPI. The architectural digital-based model is developed through the instruction of new organizational structure frame work including needs fulfillment, placement, development, service, career support, remuneration, and preparation. The development of value chain pattern aimed at supporting the main tasks of Human Resources to extract data and information orientation stored in the form of physical and semi-digital data, expected to

sustain the quality of policy. The design of the flow diagram model for each task is still in the adjustment stage along with new policies that require further refinement. There are at least five groups of flow diagrams to be developed including those of acceptance, placement, career development, remuneration, and retirement.

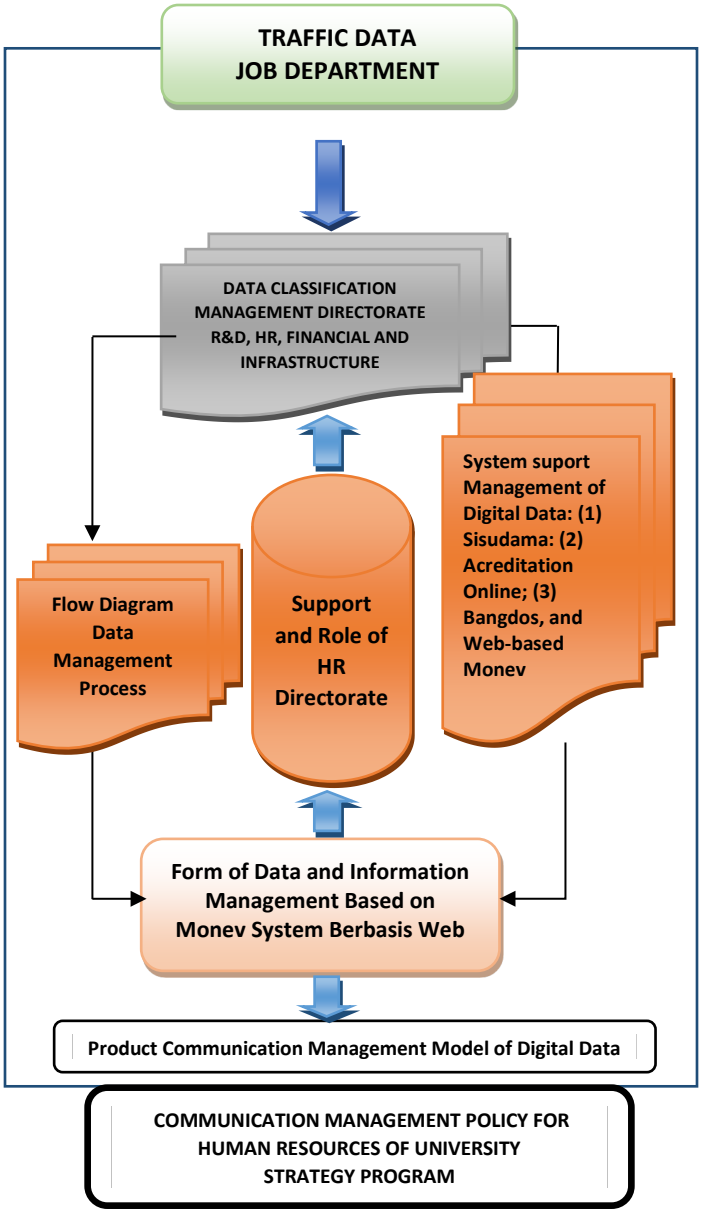

Figure 3: Communication Management Model of Policy Strategic Program Universitas Pendidikan Indonesia in Human Resources

Conflict of Interest

The authors declare no conflict of interest.

Acknowledgment

This work was conducted with research funding University Grant of Universitas Pendidikan Indonesia with grant on July, 2018.

References

[1] B. of Trustees,"Annual Budget Work Plan Guidelines for 2016 of Universitas Pendidikan Indonesia", Board of Trustees, 2016.

[2] D. Darmawan, H. Kartawinata, and W. Astorina, "Development of Web-Based Electronic Learning System (WELS) in Improving the Effectiveness of the Study at Vocational High School ' Dharma Nusantara", 14(4),pp.562-573, 2018, DOI : 10.3844/jcssp.2018.562.573

[3] B. of Trustees, "Strategic Plan 2016-2020 of Universitas Pendidikan Indonesia. Bandung: Board of Trustees", 2016.

[4] J. Clemmer "Communication Strategy in Education", 2012

[5] Suryadi, E and Darmawan, D, "Communication Management of Digital Information Data In The Field Of Human Resources As A Policy Making Resource of University Strategic Program," pp. 1–7, 2017.

[6] W. Bridges, "Managing Transitions: Managing Transitions: Overcoming the Tiring Transition of Organizations", PT. Bhuana Ilmu Populer, 2002.

[7] L. T. Hunger, D.J & Wheelen, "Strategic Management",2003.

[8] G. Scott, M, "Principles of Management Information Systems", 2011.

[9] C. Consalvo, M & Ess, The Handbook of Internet Studies," 2011.

[10] U. G. Mada and U. A. Dahlan, "Resource Management And Conversion Process In Multi-Format Distributed World Web3d Framework," 97(4), pp. 1129–1145, 2019.

[11] R. Buchingham, D & Willet, "Digital Generation : Child, Young People, and New Media", Lawrence Erlbaum, 2006.

[12] F. Michard, T. J. Gan, and H. Kehlet, "Digital innovations and emerging technologies for enhanced recovery programmes," Br. J. Anaesth., 119(1), 31–39, 2017.

[13] L. U. Khan, "Visible light communication : applications , architecture , standardization and, Digit. Communication. Networks", 3(2), pp.78–88, 2017.

[14] S. Illingworth, "Seminars in Cell & Developmental Biology Delivering effective science communication : advice from a professional science communicator," Semin. Cell Dev. Biol., 70 (3),pp.10–16, 2017.

[15] F. Beer, "Communication Strategy", Prentice Hall Company,2013.

[16] M. B. Miles, A. M. Huberman, and J. Saldaña, "Qualitative Data Analysis", 1993

[17] I. Indu, P. M. R. Anand, and V. Bhaskar, "Engineering Science and Technology, an International Journal Identity and access management in cloud environment : Mechanisms and challenges," Eng. Sci. Technol. an Int. J., 21(4),pp.574–588, 2018.

[18] E. E. H. Doyle, D. M. Johnston, R. Smith, and D. Paton, "International Journal of Disaster Risk Reduction Communicating model uncertainty for natural hazards : A qualitative systematic thematic review", Int. J. Disaster Risk Reduct., 33(10),pp. 449–476, 2019.

[19] M.W.A. of UPI, "Strategic Plan of Universitas Pendidikan Indonesia", UPI Press, 2015.

[20] U. Stikubank and N. Sciences, "Multi-Layer Framework For Security And Privacy Based Risk Evaluation On", 97(5), pp. 1423–1433, 2019.

[21] K. Hersey, P & Blancshard, "Management of Organizational Behavior: Utilization of Human Resources", Erlangga, 1982.

[22] D. M. Grunig, J.E., Grunig, L.A. & Dozier, "Excellent Public Relations and Effective Organisations, Mahwah", Lawrence Erlbaum, 2002.

[23] UNESCO, "Education Strategic in Higher Education for Dynamic Community in the World", UNESCO Officer Research, 2009.

[24] Directorate. of ICT, "Report of ICT Directorate of UPI in 2010: Information Communication Technology Directorate of Universitas Pendidikan Indonesia", 2010.

[25] G. Gaither, "Multicampus System: Perspectives on Practice and Prospects", Stylus Publishing, LLC , 1999.

[26] Sukarni, "Study of Communication Theory in Organizations", 2012.

[27] R. E. Jack and P. G. Schyns, "Review The Human Face as a Dynamic Tool for Social Communication, Curriculum Bio l"., 14(34), 2015.

[28] S. K. Das, "Mobility Management — A personal perspective", 131(1), pp.26–31, 2018.

Advances in Science, Technology and Engineering Systems Journal Vol. 4, No. 4, 545-560 (2019)

www.astesj.com

Special Issue on Advancement in Engineering and Computer Science

ASTESJ

ISSN: 2415-6698

Study and Implementation of Various Image De-Noising Methods for Traffic Sign Board Recognition

M. Monica Subashini[*,1], Abhinav Deshpande[1], Ramani Kannan[2]

[1]School of Electronics Engineering (SENSE), Vellore Institute of Technology (VIT), Vellore, 632014, India

[2]Department of Electrical and Electronics Engineering, Universiti Teknologi PETRONAS (UTP), 32610, Malaysia

ARTICLE INFO

Article history:
Received: 04 March, 2019
Accepted: 29 July, 2019
Online: 25 August, 2019

Keywords:
Color
Shape
Image De-noising
Gaussian Filter
Deep Neural Network (DNN)
Harmonic Filter
Arithmetic Mean Filter
Circular Averaging Filter (Pillbox)
Anisotropic Diffusion Filtering
Non-Local Means

ABSTRACT

The problem of recognizing traffic sign boards in a correct fashion is one of the major challenges since there is an alarming rate of increase in the number of road accidents happening because of incorrect interpretation of traffic sign boards in bad weather conditions. In this paper, a comparative analysis of various noise removal techniques based on calculating different parameters which decide the quality of input roadway symbol like Mean Squared Error (MSE), Peak Signal to Noise Ratio (PSNR) as well as Structural Similarity for measuring Image Quality (SSIM) is being performed and the best technique will be chosen among them which gives minimum Mean Squared Error (MSE) value and maximum Peak Signal to Noise Ratio (PSNR) and Structural Similarity for measuring the Image Quality (SSIM) values. This technique will be quite useful for de-noising a given image which is present in both the testing and the training image databases.

1. Introduction

There is a huge demand in the market as there is a rapid development in improving the existing system which ensures in giving security to the driver during the course of driving a vehicle. This leads to the development of a system that provides a helping hand thereby incorporating new techniques used for the purpose of detecting as well as recognizing the traffic signs. Nowadays, many automobile industries are extending in the market due to an increase in the demand for smart cars as a result of the rising competition among its fellow industries [1-5].

In the areas where there is a large amount of travelling, the regulation of the speed of the vehicles is done by the use of sign boards. They are used for limiting the current velocity of moving vehicles and are considered to be a part that comprises of some major categories of traffic signs [6-10].

A rise in the number of roadway accidents is observed because of ignoring the sign boards which try to limit the velocity of a moving vehicle for the persons who are driving a vehicle. Generally, it is observed that the persons who are not aware of the potential danger during the course of driving consequently meet a serious accident thereby even leading to their deaths [11-15]. There is an urgent need for development of a system which can be used to recognize the Speed Limit Signs (SLS) in an automatic fashion and may be used for alerting the driver [16-20]. There are two major steps which are involved in the processes of detecting and recognizing the Speed Limit Signs (SLS). The first step is to detect the potential candidates which are known as the Regions of Interest (ROI) usually comprising sign board images and the second step is to recognize the ROI in order to extract the correct category of sign board images [21-25].

During the course of driving a vehicle [26-35], the driver tends to ignore the speed limit sign boards that convey a message to restrict the velocity of a moving vehicle thereby suffering from a

[*]M.Monica Subashini, School of Electrical Engineering, VIT, Vellore.
monicasubashini.m@vit.ac.in

collision which may ultimately lead to the death of the driver consequently becoming a reason for increasing number of roadway accidents [36-45]. The development of a system that is capable of recognizing the Speed Limit Signs (SLS) in an automatic fashion as well as alerting the driver at the same time is the need of the hour [46-50].

It is generally observed that various automobile industries are increasing in the market because of the demand of smart cars. This is the result of the rising competition among its fellow industries thereby facilitating the growth of systems. It would provide a helping hand thereby incorporating some new techniques used for the purpose of detecting as well as recognizing the traffic signs. In recent years, since there is a large requirement in the market because of rapid growth in the improvement of the existing system, a secure driving environment is provided [1-5]. The maximum speed limit sign boards are generally employed to restrict the velocity of a moving vehicle and are used for regulating the velocity of a vehicle in the case of areas where there is a large amount of travelling thereby comprising of a major category of traffic signs [6-10]. During the course of driving a vehicle, the driver tends to ignore the speed limit sign boards that convey a message to restrict the velocity of a moving vehicle thereby suffering from a collision which may ultimately lead to the death of the driver consequently becoming a reason for increasing number of roadway accidents. The development of a system that is capable of recognizing the Speed Limit Signs (SLS) in an automatic fashion as well as alerting the driver at the same time is the need of the hour [11-15]. The process of detecting as well as recognizing the SLS normally comprises of two major steps namely, detecting the potential candidates known as the Regions of Interest (ROI's) consisting of the sign board images and recognizing the ROI so that the category of sign board images can be extracted in a correct fashion [16-20]. The main objective of detecting a sign board image can be accomplished with the help of extracting the primary visual features like the color and the shape which are present inside a given input image [21-25] such as the color feature is employed for detecting the red SLS while the shape feature is employed for detecting circular or rectangular sign board images [26-30]. If we study the research work which is done in the past, we will come to know that the rectangular speed limit signs [31-35] are usually detected with the help of shape-based methods [36-40], for example, if we study the research work which is carried out by [41-45] we will find that the rate of detecting the sign board images was increased in the rough conditions, especially, during the night time [46-50].

The circular sign board images are detected by making use of the color-based and/or the shape-based methods, for example, if we consider the research work which is carried out by [1-5]. Next step which is involved in the process of recognizing the SLS comprises of two important techniques, namely, the processes of recognizing sign boards that are available in a broad range as well as recognizing each and every character on a given sign board. If we take an example of strategy that incorporates recognizing a given sign board which is made available in a wide range, one may find a complete candidate sign to be considered for recognizing process [6-10]. If we take the example of digit-based methods, the process of extracting multiple characters for recognizing numerical portrait of velocity which is exhibited by a moving vehicle rather than classifying a complete sign board image treating it as a single entity is performed [11-15]. The process of recognizing sign board images is treated as one of the important factors for driver assistance system because it plays an important part in controlling the road traffic thereby issuing a warning signal and giving proper guidance to the drivers [16-20]. It is observed that ignoring the sign boards because of distraction or being in a psychological state by the drivers is the main cause of roadway accidents which are occurring in last few years [21-25]. There is an urgent need for incorporating an automatic system for the purpose of recognizing the sign boards and is considered to be a main factor for building an autonomous navigation system [26-30]. In order to detect and recognize the sign boards [31-35] with a faster speed and higher efficiency, particularly, in a real time scenario, the proposed system [36-40] should have a higher precision so that the process identification of sign board images can be performed in a correct manner [41-45]. The detection and the recognition efficiencies can be affected if the system is busy in managing certain complicated issues [46-50].

The various problems that are associated with these systems include the variations in the illumination such as light levels, twilight, fog, rain and shadow, motion blur and sign occlusion [1-10]. The effectiveness can be considered to be one among the major factors because the complete navigation system is damaged by the improper classification and lack of detection of sign board images. But, later it was revealed that the systems that are currently present in the literature part are unable to provide 100% accuracy. The research scholars were motivated by the results which are given in the section above and there was an improvement in the performance of system that is capable of detecting as well as recognizing the sign board images even in the complicated situations and thus highlights the importance of our research work in building this method that is being presented in this review paper. A novel technique which is used for the process of detecting, tracking and classifying the sign boards at a faster speed from a moving vehicle even in the difficult conditions was proposed by [11-20]. In order to extract the candidate regions of the sign boards, a color-based segmentation technique was being proposed in the course of detecting the sign board images. The HOG features are applied in order to encode the sign board images which are detected and the feature vectors are also computed. The process of detecting and recognizing the sign board images in an automatic manner remains as one of the daunting task that comprises of a variety of areas of application, for example, if we consider reinforcements resulting from a rapid growth in the arena of providing a safe driving environment to a driver who is driving a vehicle, taking a survey of existing road conditions that are prevalent in our surroundings so that potential dangers can be judged and proper steps can be implemented in order to prevent them from happening [21-30].

1.1. Traffic signs interpretation

When we compare the research work which is done on automatically detecting and recognizing symbol-based traffic sign board images and recognizing the textual information which is present inside the sign board images, we will find that a small amount of research work is done on recognizing the textual information which is present within a sign board image in comparison with the former [31-40]. One of the main difficulties that are associated with this procedure such as presence of variation in lighting conditions as well as shadowing effect that is caused due to improper lighting conditions, the effect of causing a blur, causing an occluding effect due to improper and less amount of light as well as deteriorating of sign board images can be considered responsible for causing this scenario to a smaller extent [41-50]. During the course of driving, we cannot distinguish in between sign board images as well as images that belong to some another class other than sign boards merely on grounds that provides the information which is provided by their primary visual features like the color and the shape but some extra temporal or contextual information should also be provided supplementing this information, since the information that is given by color and the shape of traffic signs as well as non-traffic signs proves to be inadequate [1-10]. Based on this hypothesis, it is observed that there are large numbers of images that does not fall in the class of sign boards which are classified from images falling in a particular class of sign boards although detected successfully from the original images which is found most frequently within a sign board image that tends to appear in somewhat cluttering fashion, as we normally observe in the case of a road scene [11-20]. It is generally observed that when there is lack of some supplementary information such as the structural and temporal information, there are large numbers of false positives (FPs) that are detected by the system especially when we observe the top scene, thus facilitating the process of detecting the traffic signs which is present in both the images in a rather successful manner [21-30]. The possible solution to this problem was provided by the use of primary visual features like the color and shape of traffic sign board images that are employed in the process of detection of a large number of text-based traffic sign board images. One should also take proper care that no True Positives (TPs) are ignored thus reflecting the importance of the process of over segmentation [31-40]. In order to eliminate unlikely candidates, an enormous amount of candidate regions which are detected with the help of structure of the scene and the temporal information that is conveyed by them were diminished to a greater extent [41-50]. One of the main objectives of an intelligent transportation system is to provide a safe and secure driving environment thereby ensuring the safety of the surrounding traffic. We can devise a new technique ensuring the safety of the surrounding traffic by implementing an on-board camera-based driver alert system which helps in recognizing sign board images such as stop signs and speed limit signs [1-10]. Traffic Sign board images convey important information regarding the present condition about the roadway as well as tend to provide other information for the purpose of navigation. They can be thought of as planar rigid objects which are having different colors and shapes. The primary visual characteristics of an image constitute the color, shape and pictogram which help us to provide relevant information which is embedded in it. The area of Intelligent Transportation Systems is gaining popularity nowadays and many car manufacturing companies are focusing their eyes on the area of Advanced Driver Assistance Systems since it contains a broad spectrum available for carrying out research and development especially in the domain of Traffic Sign Recognition [11-20]. In the year 2008, Mobil eye entered into a joint venture ship with Continental AG and three additional new updates were installed in the BMW 7 series that comprised of lane departure warning, speed limit information based on the method of detecting sign board images and intelligent headlight control. One of the major challenging tasks which is confronted by modern car manufacturing companies is to recognize the sign boards correctly particularly in an uncontrolled environment [21-30].

There are three steps in a typical traffic sign board image recognition system that mainly consists of detecting a particular traffic sign from other signs by using some detection method followed immediately by the process of elimination of noise from it with the help of some pre-processing techniques and finally recognizing that traffic sign by using some pattern recognition and machine learning approaches. We can augment the existing system with the help of tracking algorithm so that the speed of recognition can be increased, so that we can focus on a tiny region of the object which is detected for the purpose of recognition. In this research paper, more emphasis is laid on the process of recognizing traffic sign board images; we can leave the remaining three methods, viz., detection, rectification and tracking. One can find the research work done on the problem of recognizing traffic signs dating from the last century, and the proof of this work is found in an ancient survey which was lastly updated in May 1999, given in [31-40]. Since, there are plenty of techniques available in the field of recognizing traffic sign boards over a past few decades, we do not try to give a comprehensive literature survey, and instead concentrate on several background work most relevant to the present research. Due to the growth of different intelligent methods pertaining to driver assistance systems (DAS), it is trying to prove its superiority over the currently existing approaches which are present in Intelligent Transportation Systems. In the DAS, the task of detecting and recognizing traffic signs can be considered as one of the major approaches for acquiring information regarding a safe driving environment and we can also take precautionary measures in order to overcome the potential hazards faced by driver particularly while driving a vehicle along the road. The process of recognizing the sign board images, that too in a real environment, proves to be a herculean task if we want the technique to be done with greater accuracy and within a stipulated time, since the visibility of sign boards can be affected due to some undesirable factors to a larger extent. So far, many algorithms have been proposed for traffic sign recognition [41-50]. In [1-10], an entirely different approach of the currently prevailing AdaBoost algorithm is utilized in order to detect a

traffic sign by deployment of batteries of classifier algorithms that are given proper training to split the classes in an error correcting output code framework. A robust sign similarity measure which is built by using the SimBoost or a fuzzy regression tree framework, a technique which is used for recognizing traffic signs is proposed in [11-20]. We all are familiar with the Support Vector Machine (SVM) algorithm which happens to be a good classifier that is very popular in the domain of computer vision. In order to facilitate the process of detecting and recognizing road signs in an automatic fashion, an entirely different method is presented in [21-30] in which a SVM is used for traffic sign detection while a Gaussian kernel SVM is adopted for traffic sign recognition [31-40]. In order to classify an unknown traffic sign, an Eigen-based traffic sign recognition system was proposed in [41-50] taking the help of Principal Component Analysis (PCA algorithm) by selecting the most effective components of traffic sign board images. Boosted by the successful applications on handwritten digits recognition, convolutional neural network (CNN) has also been employed on traffic sign classification [1-10]. In [11-20], instead of various features, a CNN is trained directly with the raw pixel values of traffic sign images. Moreover, a better result is obtained by integrating the results obtained by a CNN and a multilayer perceptron (MLP). Gradient orientation is one kind of useful information in various object recognition methods, including the traffic signs. Traffic scene analysis is a very important topic in computer vision and intelligent systems [21-30]. The traffic signs are manufactured in such a fashion that they convey important information regarding the present condition and other information of the road. They are rigid and simple shapes with eye catching colors and the information they carry is easy to understand. However, accidents may still occur when drivers do not pay attention to a traffic sign in time [31-40]. So, in order to overcome these difficulties, there is an urgent need for implementing an automatic real time traffic sign recognition system which is capable of detecting and recognizing traffic sign board images. The above factors make the problem of detecting and recognizing traffic sign boards very complicated and still remains a daunting task for most of the research scholars [41-50].

1.2. Signs interpretation methods

There has been a lot of improvement in the field of detecting and recognizing the textual information which is present inside an image [1-10]. The different techniques which has led to an improvement in this area can be classified into two major types, one is the Region-Based Methods and another one is the Connected Component (CC) based methods [11-20]. The local features for example, texture are used by the region based methods for the purpose of locating the regions which contain the textual information in an image and the connected component-based methods are used for the purpose of segmentation of the characters that are present in the textual information within a particular traffic sign board image on an individual basis with the help of information like the intensity, color distribution and the edges of an image [21-30]. The Connected Component based methods normally comprises of three stages, the first stage is used for the purpose of detecting CCs which are present inside an image followed by a second stage in which the CCs that are not very similar are eliminated based on their features which is subsequently followed by a final stage in which grouping of the remaining CCs is performed into words or lines [31-40]. It was revealed that the amount of research work which targeted specifically on the task of detecting the textual information which is present inside a particular traffic sign board image is restricted to a narrow spectrum because of the difficulty in performing the given task. The methods that are currently available in the literature consist of two steps, the first step is the process of detecting a given sign board image and the second step is the process of recognizing a particular image [41-50]. The research work which is carried by founding the candidate regions by combining the characteristics that are obtained by combination of Shi characteristics as well as Tomasi characteristics, the prototypes that are obtained through the mixing of characteristics that are derived from Gaussian functions as well as that which are obtained by the process of analyzing a given image on the basis of its geometrical properties. It was postulated on the basis of the textual information which is present inside a given sign board image that is visible if we take some plane surface that is oriented in the upward direction thereby giving due regards towards the movement as well as the axis of the camera that exhibits the photonic characteristics and properties. If we consider the real world, it may be possible that the sign boards which contain the textual information within it may tend to appear if one looks it from its own perspective to be somewhat in synchronism with the original image of the sign board [1-10]. So, there is an urgent need for incorporating a perspective transform which gives the OCR a better possibility of performing the task of recognizing the textual information that is contained inside a sign board image. The process of matching of the candidate regions with the help of consecutive frames was done and the process of interpretation was then performed with the help of an OCR system when their size was considered to be adequate. The detection rate was found to be 88.9% and the false detection rate was found to be 9.2%, which was based on database containing 22 video sequences with video sequence having a length of 30 seconds duration. The work which was done by [11-20] comprised of segmentation of the areas that are present inside an image and the extraction of these regions seem to attract the research scholar for the purpose of carrying out his own research which is propounded on the grounds of the information that is conveyed by the primary visual characteristics of an image thereby taking help of some limiting criterion that is applied to channels that contain the chromaticity as well as the luminosity components if we consider the most popular technique which is deployed for the purpose of segmentation of sign board images [21-30]. If we compare the tracing of outer boundaries that are present inside every single blob with the help of Fourier transformation by adopting an approach that increases the speed

of computation of the process thereby reducing the duration that is required for every single computation with those obtained by adopting the same method from an arbitrary uniform plane lamina which can be considered as an example for the purpose of implementing our technique was being employed in order to find the rectangular regions [31-40]. The quadruple corners which can be thought of as an area that resembles a rectangle were being searched by deploying the process by taking peaks of the area that is traced from an entire image with the help of transformation of complete image using Fourier method thereby increasing the speed for carrying out the process of computation thus reducing the duration required for every single computation and by taking help of aforementioned corners, thereby carrying out the task of rotation of corresponding areas that are chosen for the purpose of extraction from complete image trying for the process of alignment of the textual information consisting of mainly the characters that is present inside a given sign board image particularly in upward direction. If we consider the point of view of a vehicle, it is revealed that the above method is not sufficient if we try to consider the process of recovering above area that is present on the chassis of the vehicle if the point of view of the observer is taken for the process of consideration which consists of textual information inside a sign board image and the perspective correction which is given in [41-50] tries to provide a more robust solution to this problem. There was a lack of output that represents the content which is illustrated in a more sophisticated fashion thereby giving the amount of content which is extracted from a given sign board image which is contributed through the research work that is illustrated in the existing literature. If we consider some existing techniques that are given by [1-10], we will come to know that they exhibit some peculiar characteristics that mainly focuses on taking help from MSERs that mainly exerts a thrust on detecting both the images that represent the significant information related to existing road conditions as well as if we consider some characters that are present in the textual information which is contained within a given sign board image. If we try to combine the processes of segregating the original image as well as the characters that are present in an image if we try to see the image particularly in sunlight thereby constituting a container, we come to know of the interesting fact that the areas which are present on the chassis of a vehicle having a whitish as well as bluish appearance are subjected to the process of detecting each of the components that are present inside a given video sequence [11-20]. By taking help from both the mechanical systems that tend to classify the basis functions thereby supporting the conventional technique which can be deployed for the process of classifying a given image as well as the classification method that is presented by some research scholars, these regions were then again subjected to the process of classification. More emphasis was placed on the geo-localization of sign board images with the help of information which is supplied by a Global Positioning System, and the technique was then applied to single images, without the use of temporal information [21-30]. If we try to make an approximation about size of our complete world, we will come to know that height of textual content which is present inside an image was used along with the spacing in between our camera and images that carry some message about the prevalent road conditions. The rates that are required for the processes of detecting, recognizing as well as classifying the words, numerical characters as well as symbolic information that is represented by the alphabets present on a particular sign board image that are taken from shorter, longer as well as medium distances in between the observer and the sign board images were being given by the existing authors. If we consider the ranges for the process of detecting and recognizing the traffic sign board images, it was found that the range for detecting the sign boards was lying in between 13.09% and 90.18%, while the range for the process of recognizing the sign boards was found lying in between 8.51% and 87.50%. Our proposed method overcomes the numerous limitations which are faced by the method that were proposed by [31-40] in which postulates were propounded for the method of detecting traffic sign board images that comprised of textual information within it and are sufficient for providing a high recall rate. The additional FPs was eliminated by making use of structural and temporal information that is conveyed by a particular image by our technique which is being propounded in the above section. One can find the output of system which we derived in the course of performing experiments that get highlighted from our research work are sufficient enough for giving a proof to the proposed method which is described in the section above. The research work which was done by [41-50] used a rough OCR technique in detecting and recognizing the textual information contained in the sign boards was superceded by our proposed method that uses the concept of recovering original information contained in sign board images comprising point of view from an observer as well as techniques that involve the usage of merging two portions of any kind of objects that is present along lateral portions of an object. One may find manuscripts from earlier and past research works which reflect our propounded system performing with better outcomes alone is sufficient enough for giving a proof to our proposed method which is given the section above. If we consider the research work which was done [1-10] takes the help of temporal information used for detecting symbol-based traffic sign board images which is further contributed by the research work that is described in this review paper by embedding the structural information that is present in the scene. We can find a huge amount of research work that focuses on the problem of detecting the textual information which is present in sign board images by taking help from a mobile sensor and mainly depends on the devices that can be worn by the driver, for example, the techniques that are mentioned in [11-20] and the methods which are mainly applicable to mobile robotics can be found in the research work that is presented by [21-30]. We can find a number

of databases which are used for the purpose of validation of systems used for detecting and recognizing the sign board images which includes the famous dataset which is included in the research work that is done by [31-40] as well as the database that is included in the research work which is done by [41-50]. The above databases find no use in order to validate our proposed method which is entirely based upon detecting and recognizing the sign boards containing textual information within them and are more concentrated upon the process of detecting the symbol-based sign boards. A camera with knowledge of all the parameters used in the process of calibration was used for extracting the data [1-10]. One may consider the process of recognizing a particular sign board image amongst all other members, a Herculean task when it comes to recognizing sign board image from a group of other sign boards. It is found that a variety of techniques are available in the arena of classifying known sign board images ranging from ordinary methods like the matching of templates to sophisticated machine learning techniques. One of the very significant and most important algorithms which are employed to perform the task of classifying multiple sign board images can be attributed to well-known Support Vector Machine (SVM) algorithm. If the transcripts authored by [11-20] are considered, one can find the significance attached to automatically detecting and recognizing sign board images taking help of Support Vector Machines (SVMs) in combination with Gaussian kernels. However, the system was required to classify candidate blobs into a shape class before recognition. As a sequence, only the pixels that were part of the sign were used to construct the feature vector. In [21-30] different methods other than those which are currently available in the context of detecting and recognizing sign boards in an automatic fashion were brought to the notice of people. It can be very well understood from this study that a comparatively greater emphasis was laid in enhancing the accuracy of existing methodologies prevalent in detecting and recognizing sign boards in an automatic fashion thereby resulting in the reduction of number of support vectors which are required in due course of the complete process leading to a sudden fall in the necessity of memory and time for testing new samples [31-40]. An SVM segmentation approach for traffic sign recognition was given in [41-50] while in [1-10], an effective strategy helping in the process of recognizing slanted speed limit signs by extracting the rotation invariant features with the help of Fourier based wavelet descriptor was introduced. The different categories of sign board images were classified with the help of Support Vector Machines (SVMs) consisting of binary tree architecture. In [11-20], a shape-based classification was developed using an SVM. In order to represent the features, two types of features including a binary image and Zernike moments were used. The main objective behind carrying out this research work was recognizing seven categories of traffic sign shapes as well as five categories of speed limit signs. In addition to SVMs, AdaBoost is also a popular classification approach. A color insensitive Haar wavelets feature combined with the AdaBoost algorithm was introduced in to develop a country-independent recognition module [21-30]. By using the concept of a class similarity measure that is learnt from image pairs, realization was achieved with the help of a new newer version of the existing AdaBoost algorithm which is known as SimBoost algorithm [31-40]. The solution to the problem of classification between multiple classes can be obtained if we compare the similarities between an unknown example and prototype from each class, subjected to the condition that an estimate of the similarities between any two images is made available. The stop and give way signs in different and complex surroundings were successfully classified by taking help from an array of weak classifiers in a reliable fashion. [41-50] took the help of classifiers which are trained to refine the type of traffic sign like neural networks and AdaBoost classifiers was also being taken. With the help of AdaBoost feature selection procedure, suitable features were chosen from a very large pool of features consisting of Haar, moment, symmetry, frequency and other features. The results which were obtained from the various classifier algorithms were combined over time and merging of the signs that are quite similar on both the sides of the roadway was accomplished taking help of fusion module that incorporated combining a Bayesian network and a decision tree [1-10]. An Error Correcting Output Codes (ECOC) which takes help from a forest of optimal tree structures that are embedded in the ECOC matrix were also being formulated along with the existing methods. An entirely different approach that is suitable for classifying sign boards belonging to different classes by using the ECOC technique was introduced [11-20]. The ensemble of binary classifiers that were given training on categories of sign board images, having two partitions was taken and the ECOC was being implemented with the help of above scheme [21-30]. The decomposition of the original problem into a set of complementary problem having two classes that are encoded in ECOC matrix which tend to share the classifiers across the original classes was performed. In [31-40], a comparison was performed considering the class specific sets of discriminative local regions in between a discrete color image of the viewed sign with other images. By using the principal of one versus all dissimilarity maximization, they were learnt in offline mode from the standard templates of sign board images [41-50]. The comparison in between the robust discrete color image was initiated by using a color distance transform which served as a basis for defining this dissimilarity. It becomes a challenging task when it comes to the method of comparison of the actual performance since there is no such kind of ideal database or procedure for performance evaluation of several machine learning approaches that try to find a solution to the problem of recognizing traffic signs, even though they are present in the literature part [1-10]. There has been a rapid growth in research and development sector especially in the area of detecting and recognizing traffic sign board images over the last few decades.

Several novel ideas and effective methods have been proposed [11-20]. Usually, the detection part hunts [21-30] potential regions of traffic signs whereas the category to which a traffic sign belongs is determined by the recognition part [31-40]. The traditional methods which are used for the purpose of detecting sign boards can be grouped into three main classes, viz., color-based methods, shape-based methods and the sliding window-based methods [41-50].

1.3. Definitions of various Performance Metrics used for Image Quality Evaluation

The various performance metrics such as the Mean Squared Error (MSE), Peak Signal to Noise Ratio (PSNR) as well as the Structural Similarity for measuring the Image Quality (SSIM) which are used for evaluating the quality of a given traffic sign board image are defined as follows:

1.3.1. Mean Squared Error (MSE)

The Mean Squared Error (MSE) or the Mean Squared Deviation (MSD) of an estimator or of a procedure for estimating an unobserved quantity is defined as the average of the squares of the errors that is the average squared difference in between the estimated values and what is estimated. The mathematical equation which governs the Mean Squared Error (MSE) is given as below:

$$\text{Mean Squared Error (MSE)} = \frac{1}{n}\sum \qquad I = n + 1^{n+q}\,(Y_i - Y_i') \quad (1)$$

where n is the total number of predictions generated from a sample of n data points on all the variables, Y is the vector of observed values of the variable being predicted.

where M × N represents the size of an image.

1.3.2. Peak Signal to Noise Ratio (PSNR):

The Peak Signal to Noise Ratio (PSNR) is defined as the ratio in between the maximum possible power of a given signal and the power of corrupting noise that affects the fidelity of its representation. The mathematical equation which governs the Peak Signal to Noise Ratio (PSNR) is given as below:

$$\text{Peak Signal to Noise Ratio (PSNR)} = 20\log_{10}(MAX_I) - 10\log_{10}(\text{MSE}) \quad (2)$$

where MAX_I is the maximum possible pixel value of the image and MSE is the Mean Squared Error, I is the m × n noise free monochrome image and its noisy approximation is denoted by K.

1.3.3. Structural Similarity for measuring the Image Quality (SSIM)

The Structural Similarity for measuring the Image Quality (SSIM) is defined as the technique which is used for measuring the similarity in between two images and it is also employed to predict the perceived quality of digital television and cinematic pictures as well as other kinds of digital images and videos. The mathematical equation which governs the Structural Similarity for measuring Image Quality (SSIM) is given as below:

$$\text{Structural Similarity for measuring Image Quality (SSIM)} = (2\mu_x\mu_y + c_1)(2\sigma xy + c_2)/(\mu_x^2 + \mu_y^2 + c_1)(\sigma_x^2 + \sigma_y^2 + c_2) \quad (3)$$

where

μ_x is the average of x
μ_y is the average of y
σ_x^2 is the variance of x
σ_y^2 is the variance of y
σ_{xy} is the covariance of x and y

c_1 and c_2 are the two variables to stabilize the division with weak denominator.

2. Software Tool used

The MATLAB R2019a software is utilized in the synthesis of various roadway symbols from input test dataset during the course of performing experimental procedure.

3. Experimental Results and Discussion

A set of various roadway symbol images belonging to numerous categories is taken into consideration which comprising a total number of 679 roadway symbols constituting training dataset belonging to 18 different classes of roadway symbols and there are a total number of 48 roadway symbols incorporating testing dataset.

The training dataset comprises of symbols containing some printed details embedded on their outer surface and symbols that do not have any kind of printed details embedded on their outer surface. This manuscript depicts the numerous roadway symbols incorporated in dataset used for implementing this research project.

Some examples of traffic sign board images comprising of various colors and shapes which are present in the training image database as well as testing image database are depicted in the section of this manuscript (Figure 1 and Figure 2) shown as below:

Figure 1 Examples of various roadway symbols from the Training image database

A short summary of numerous methods incorporated during the course of investigation is given in section 3.1.

Figure 2 Examples of various roadway symbols from the Testing image database

3.1. Anisotropic Diffusion Filtering Type 1

The technique of Anisotropic Diffusion Filtering which is also popular by another name Perona Malik Diffusion is primarily used to reduce the unwanted disturbance present in roadway symbols. The technique of Anisotropic Diffusion Filtering Type 1 can be represented with the help of a mathematical equation which is given as follows:

$$c\,(\|\otimes I\|) = 1/1 + (\|\otimes\ I\|/K)^2 \qquad (4)$$

where the constant K controls the sensitivity to edges and is usually chosen experimentally or as a function of the noise in the image, □ denotes the Laplacian operator and it also denotes the gradient and c (x, y, t) is the diffusion coefficient and it controls the rate of diffusion and is usually chosen as a function of the image gradient so as to preserve the edges in the image, I (:, t) : Ω → R be a family of gray scale images.

The results which are obtained after carrying out the process of Anisotropic Diffusion Filtering Type 1 of the roadway symbols comprising input testing image database (Figure 3) are depicted as below:

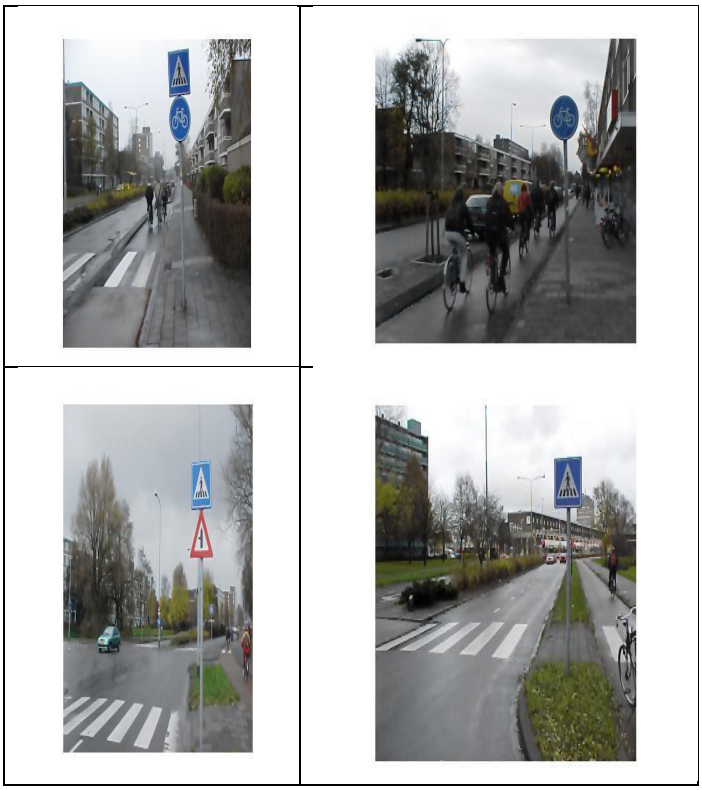

Figure 3 Testing image database Anisotropic Diffusion Filtering Type 1 Results

The results which are obtained after carrying out the process of Anisotropic Diffusion Filtering Type 1 of the roadway symbols comprising input training image database (Figure 4) are depicted as below:

Figure 4 Training image database Anisotropic Diffusion Filtering Type 1 Results

3.2. Non-Local Means Type 2

In this technique of Non-Local Means Filtering, a given color image is converted into the L*a*b color space thereby facilitating the Non-Local Means Filter to smooth the colors which are having similarity in visual perception. For the purpose of computing the numerical value of standard deviation and the Euclidean distance from the origin (e_{dist}), a homogenous L*a*b patch from the image is being extracted so that the standard deviation of e_{dist} is calculated in order to estimate the amount of noise contained in it. The mathematical equation which governs the process of Non-Local Means Type 2 is given as follows:

$$u(p) = 1/C(p) \int_{\Omega} v(q) f(p, q) dq \quad (5)$$

where u (p) is the filtered value of the image at the point p, v (q) is the unfiltered value of the image at the point q, f (p, q) is the weighting function and the integral is evaluated over $\forall q \in \Omega$ and the normalizing factor C (p) is given by the formula which is given as follows:

$$C(p) = \int_{\Omega} f(p, q) dq \quad (6)$$

The results which are obtained after carrying out the process of Non-Local Means Type 2 of the roadway symbols comprising input testing image database (Figure 5) are depicted as below:

Figure 5 Testing image database Non-Local Means Type 2 Results

The results which are obtained after carrying out the process of Non-Local Means Type 2 of the roadway symbols comprising input training image database (Figure 6) are depicted as below:

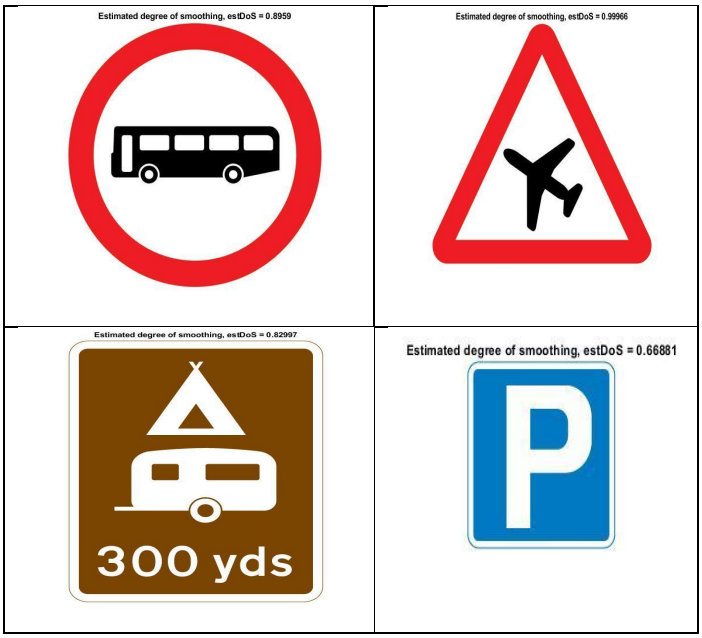

Figure 6 Training image database Non-Local Means Type 2 Results

3.3. Image Denoising using Deep Neural Network (DNN)

In this technique of denoising a given gray scale image by using a Deep Neural Network (DNN), the pretrained denoising convolutional neural network named as 'DnCNN' is being retrieved and the amount of noise which is present in the noisy version of the original gray scale image is subjected to the process of removal.

The results which are obtained after carrying out the process of Image Denoising using Deep Neural Network (DNN) of the roadway symbols comprising input testing image database (Figure 7) are depicted as below:

Figure 7 Testing image database Image Denoising using Deep Neural Network (DNN)

The results which are obtained after carrying out the process of Image Denoising using Deep Neural Network (DNN) of the roadway symbols comprising input training image database (Figure 8) are depicted as below:

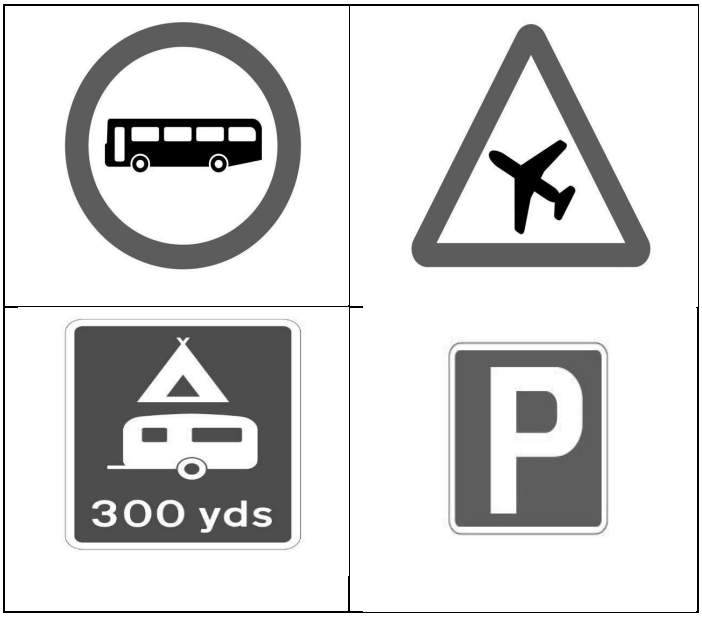

Figure 8 Training image database Image Denoising using Deep Neural Network (DNN) Results

The comparative analysis of various image denoising techniques based on various image quality metrics like Mean Squared Error (MSE), Peak Signal to Noise Ratio (PSNR) and the Structural Similarity for measuring the image quality (SSIM) from the past 2-3 years comprising input testing image database is given in the tabulated fashion which is shown (Table 1) as below:

Table 1: Comparative Analysis of Image Denoising Techniques based on various Image Quality Metrics like Mean Squared Error (MSE), Peak Signal to Noise Ratio (PSNR) and Structural Similarity for measuring the Image Quality (SSIM) for Testing image database from the past 2-3 years

S. No.	Year	Techniques used	Mean Squared Error (MSE) Values	Peak Signal to Noise Ratio (PSNR) Values	Structural Similarity for measuring image Quality (SSIM) Values
1.	2018	Anisotropic Diffusion Filtering Type 1	40.282	32.121	0.892
2.	2018	Non-Local Means Type 2	0.676	51.479	0.995
3.	2017	Image Denoising using Deep Neural Network (DNN)	1.640	47.1174	0.997

The comparative analysis of various image denoising techniques based on various image quality metrics like Mean Squared Error (MSE), Peak Signal to Noise Ratio (PSNR) and the Structural Similarity for measuring the image quality (SSIM) from the past 2-3 years comprising input training image database is given in the tabulated fashion which is shown (Table 2) as below:

Table 2: Comparative Analysis of various combinations of Image Denoising Techniques based on various Image Quality Metrics like Mean Squared Error (MSE), Peak Signal to Noise Ratio (PSNR) and Structural Similarity for measuring the Image Quality (SSIM) for Training image database from the past 2-3 years

S. No.	Year	Techniques used	Mean Squared Error (MSE) Values	Peak Signal to Noise Ratio (PSNR) Values	Structural Similarity for measuring image Quality (SSIM) Values
1.	2018	Anisotropic Diffusion Filtering Type 1	110.887	27.897	0.877
2.	2018	Non-Local Means Type 2	0.080	61.175	0.999
3.	2017	Image Denoising using Deep Neural Network (DNN)	0.970	51.267	0.998

3.4. Arithmetic Mean Filter

The Arithmetic Mean can be defined as being equal to the sum of the numerical values of each and every observation divided by the total number of observations. The arithmetic means of a given set of numbers each one is having a numerical value a_1, a_2, a_3, ……..., a_n can be calculated by using the formula which is given as below:

$$\text{Arithmetic Mean (A.M.)} = a_1 + a_2 + a_3 + \ldots\ldots\ldots + a_n/n \quad (7)$$

where a_1, a_2, a_3,……., a_n are n number of physical quantities, n is the total number of physical quantities and A.M. is the Arithmetic Mean of the n number of physical quantities which are taken into consideration.

The results which are obtained after carrying out experiments with the help of an Arithmetic Mean Filter (Figure 9) are presented as below:

Figure 9 Testing image database Arithmetic Mean Filtering Results

3.5. Circular Averaging Filter (Pillbox)

The technique of removing salt and pepper noise from an image can be accomplished with the help of smoothing filter which also helps in removing the sharp edges thereby refining the small contours as well as ridges from it. It is useful in removing minute information before the operation of extracting an object having greater size from the image resulting in the amalgamation of tiny regions in between the two portions that are present in lines or curves, thereby telling its significance about the reason for including in the pre-processing step. The results that are obtained after applying Averaging Filter to the roadway symbols that are present in our image dataset are presented in the below section of this manuscript (Figure 10) as follows:

Figure 10 Testing image database Circular Averaging Filter (Pillbox) Results

3.6. Harmonic Mean Filter

A Harmonic Mean Filter can be defined as the reciprocal of the arithmetic mean of the reciprocals of a given set of observations. The Harmonic Mean can be calculated by using the mathematical expression which is given as below:

$$\text{Harmonic Mean (H.M.)} = \frac{1}{x_1} + \frac{1}{x_2} + \frac{1}{x_3} + \ldots\ldots\ldots + \frac{1}{x_n} \quad (8)$$

The results which are obtained after carrying out experiments with the help of a Harmonic Mean Filter (Figure 11) are presented as below:

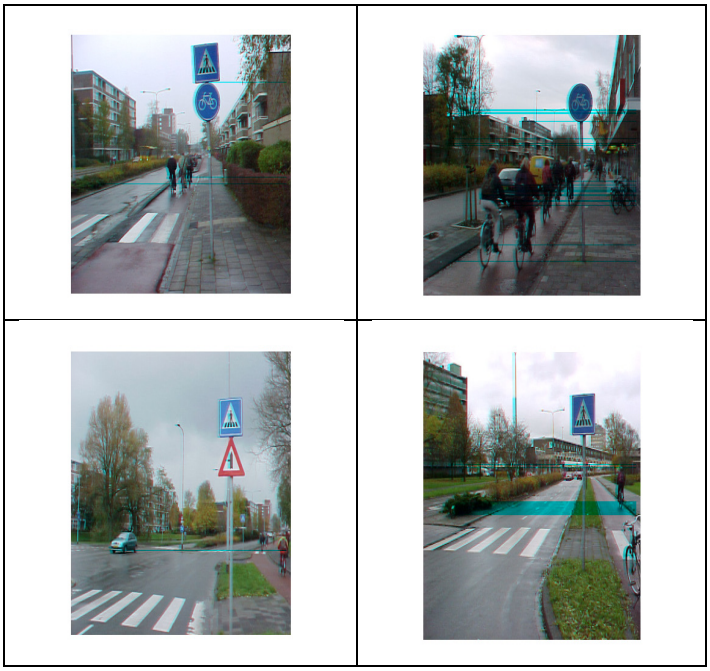

Figure 11 Testing image database Harmonic Filter Results

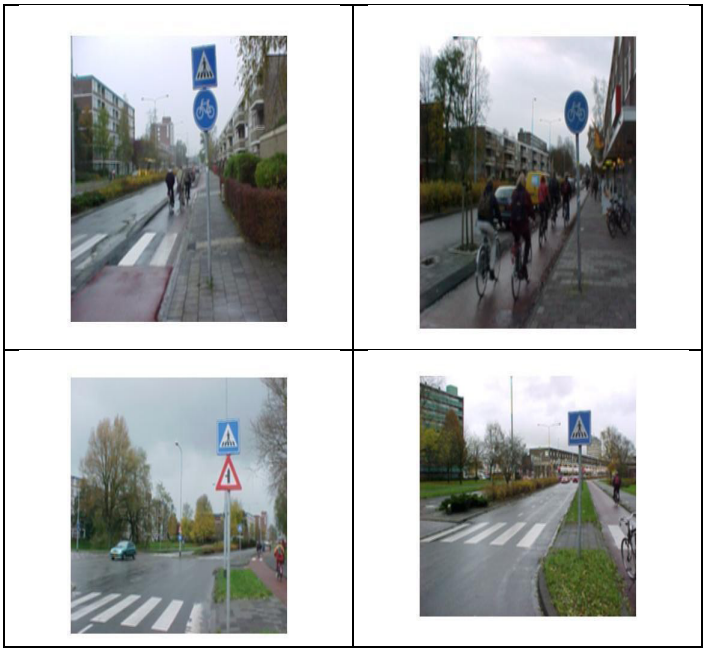

Figure 12 Testing image database Box Filter Results

3.7. Box Filter

The Box Blur or sometimes called as Box Linear filter can be defined as a spatial domain linear filter in which each pixel in the resulting image possess a value which is equal to the average value of its neighboring pixels present in the original input image. It is a type of low pass or a blurring filter.

The results obtained after carrying out experiments with the help of a Box Filter are presented in Figure 12.

3.8. Gaussian Filter

The Gaussian function is defined as follows:

$$g(x, y) = 1/2\pi\sigma^2 e^{-(x2 + y2)/2\sigma2} \quad (9)$$

where a, b and c are the arbitrary constants, x is the distance from the origin in the horizontal axis, y is the distance from the origin in the vertical axis and σ is the standard deviation of the Gaussian distribution. The Gaussian function is derived from the name of a well-known scientist named Carl Friedrich Gauss. The results which are obtained after carrying out experiments with the help of a Gaussian Filter (Figure 13) are presented as below:

Figure 13 Testing image database Gaussian Filter Results

The comparative analysis of various image denoising techniques based on various image quality metrics like Mean Squared Error (MSE), Peak Signal to Noise Ratio (PSNR) and the Structural Similarity for measuring the Image Quality (SSIM) comprising the input testing image database is given in a tabulated fashion which is shown (Table 3) as below:

Table 3 Comparative Analysis of various Image Denoising Techniques based on various Image Quality Metrics like Mean Squared Error (MSE), Peak Signal to Noise Ratio (PSNR) and Structural Similarity for measuring the Image Quality (SSIM) for Testing image database from the research paper presented in IEEE ESTCON-ICIAS-2018 International Conference held at UTP, Malaysia from 13th-15th August 2018

S. No.	Year	Techniques used	Mean Squared Error (MSE) Values	Peak Signal to Noise Ratio (PSNR) Values	Structural Similarity for measuring image Quality (SSIM) Values
1.	2006	Gaussian Filter	22.820	35.054	0.985
2.	2006	Box Filter	529.370	21.329	0.634
3.	-	Arithmetic Mean Filter	381.839	22.656	0.729
4.	2006	Circular Averaging Filter (Pillbox)	459.299	21.961	0.666
5.	-	Harmonic Mean Filter	321.160	24.146	0.862

4. Novelty of the Proposed Research Work

The main objective of our proposed research work is to identify the best technique which helps in removing the noise which is naturally present in an image among various noise removal techniques based on different image quality metrics like Mean Squared Error (MSE), Peak Signal to Noise Ratio (PSNR) and the Structural Similarity for measuring Image Quality (SSIM).

The best technique is identified from its counterparts by assuming that it is having the least numerical value of Mean Squared Error (MSE) as well as it is also having the greatest numerical value of Peak Signal to Noise Ratio (PSNR) and Structural Similarity for measuring Image Quality (SSIM).

The Non-Local Means Type 2 and the Image Denoising using Deep Neural Network (DNN) techniques were combined and applied to the input traffic sign board images which are present in the testing image database and the results so obtained are shown in (Figure 14) as below:

After the process of calculating the numerical values of Mean Squared Error (MSE), Peak Signal to Noise Ratio (PSNR) and the Structural Similarity for measuring the Image Quality (SSIM) was completed, it was observed that the Mean Squared Error (MSE) value was found out to be 113.83027446809 and the Peak Signal to Noise Ratio (PSNR) and the Structural Similarity for measuring the Image Quality (SSIM) values were found out to be 31.578017021277 and 0.90815744680851 respectively.

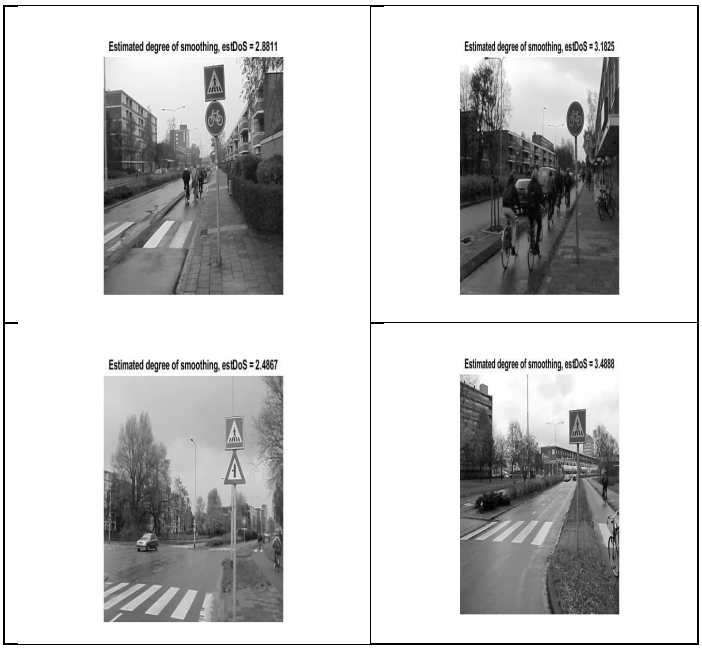

Figure 14 Testing image database Results obtained by combining the Non-Local Means Type 2 + Image Denoising using Deep Neural Network (DNN) Techniques

The technique of Anisotropic Diffusion Filtering Type 1 was combined with Non-Local Means Type 2 technique and applied to the input traffic sign board images which are present in the testing image database and the results so obtained are shown in (Figure 15) as below:

After the process of calculating the numerical values of Mean Squared Error (MSE), Peak Signal to Noise Ratio (PSNR) and the Structural Similarity for measuring the Image Quality (SSIM) was completed, it was observed that the Mean Squared Error (MSE) value was found out to be 1.5655462333826 and the Peak Signal to Noise Ratio (PSNR) and the Structural Similarity for measuring the Image Quality (SSIM) values were found out to be 47.416585376662 and 0.99865745937961 respectively.

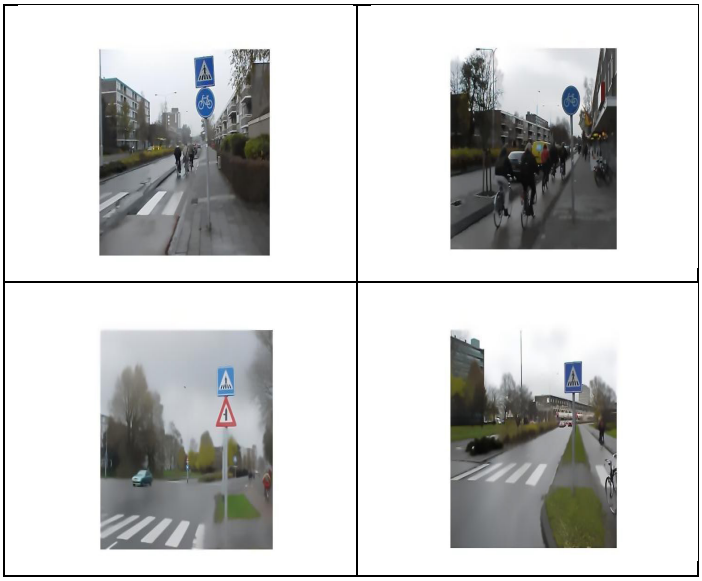

Figure 15 Testing image database Results obtained by combining the Anisotropic Diffusion Filtering Type 1 + Non-Local Means Type 2 Techniques

The techniques of Non-Local Means Type 2 and Anisotropic Diffusion Filtering Type 1 were combined and applied to the input traffic sign board images which are present in the training image database and the results were obtained after the execution of this experimental procedure which are shown in the figure that is given (Figure 16) as below and the numerical values of the Mean Squared Error (MSE), Peak Signal to Noise Ratio (PSNR) and the Structural Similarity for measuring the Image Quality (SSIM) were found out to be 255.94895760709, 24.440101624815 and 0.95028419497784 respectively.

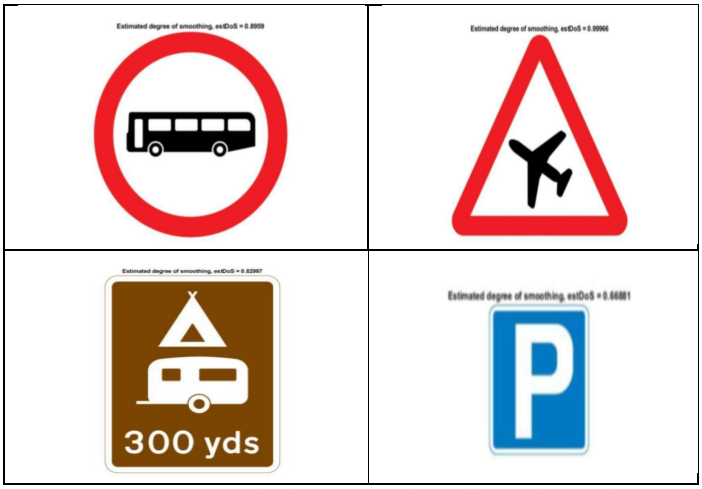

Figure 16 Training image database Results obtained by combining the Non-Local Means Type 2 + Anisotropic Diffusion Filtering Type 1 Techniques

The Non-Local Means Type 2, Anisotropic Diffusion Filtering Type 1 and Non-Local Means Type 2 techniques were combined and applied to the input traffic sign board images which are present in the training image database and the results which are obtained after the execution of the experimental procedure are shown in the figure which is given (Figure 17) as below and the numerical values of the Mean Squared Error (MSE), Peak Signal to Noise Ratio (PSNR) and Structural Similarity for measuring the Image Quality (SSIM) were found out to be 76.349860118168, 31.671063072378 and 0.97056218611521 respectively.

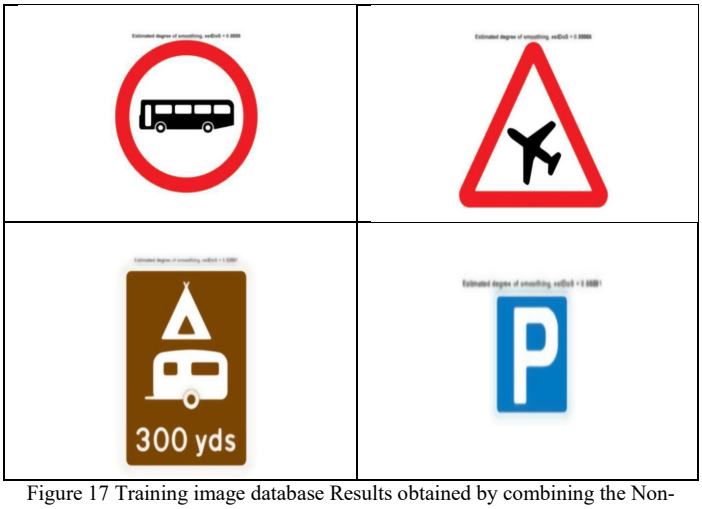

Figure 17 Training image database Results obtained by combining the Non-Local Means Type 2 + Anisotropic Diffusion Filtering Type 1 + Non-Local Means Type 2 Techniques

The techniques of Non-Local Means Type 2, Anisotropic Diffusion Filtering Type 1, Non-Local Means Type 2 and Image Denoising using Deep Neural Network (DNN) were combined and applied to the input traffic sign board images which are present in the training image database and the results which are obtained after carrying out the experimental procedure are shown in the figure which is given (Figure 18) as below and the numerical values of the Mean Squared Error (MSE), Peak Signal to Noise Ratio (PSNR) and Structural Similarity for measuring the Image Quality (SSIM) were found out to be 0.022547858197932, 66.103574150665 and 0.99989054652881 respectively.

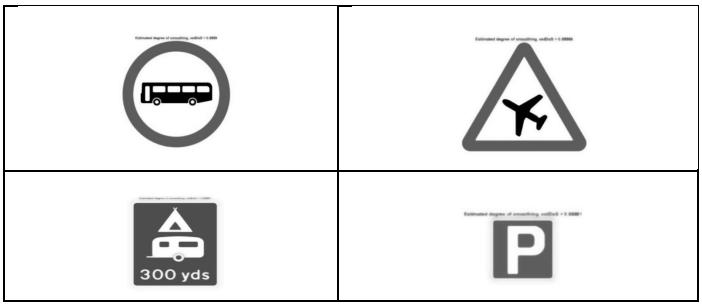

Figure 18 Training image database Results obtained by combining the Non-Local Means Type 2 + Anisotropic Diffusion Filtering Type 1 + Non-Local Means Type 2 + Image Denoising using Deep Neural Network (DNN) Techniques

The comparison of these image quality parameter numerical values for different combinations of Anisotropic Diffusion Filtering Type 1, Non-Local Means Type 2 and the Image Denoising using Deep Neural Network (DNN) techniques which are employed for removal of noise present in the testing image database is given in the tabulated fashion shown (Table 4) as below:

The comparison of these image quality parameter numerical values for different combinations of Anisotropic Diffusion Filtering Type 1, Non-Local Means Type 2 and the Image Denoising using Deep Neural Network (DNN) techniques which are employed for removal of noise present in the training image database is given in the tabulated fashion shown in Table 5:

Table 4 Comparative Analysis of various combinations of Image Denoising Techniques based on various Image Quality Metrics like Mean Squared Error (MSE), Peak Signal to Noise Ratio (PSNR) and Structural Similarity for measuring the Image Quality (SSIM) for Testing image database

S. No.	Year	Techniques used	Mean Squared Error (MSE) Values	Peak Signal to Noise Ratio (PSNR) Values	Structural Similarity for measuring Image Quality (SSIM) Values
1.	2018	Anisotropic Diffusion Filtering Type 1	40.282	32.121	0.892
2.	2018	Non-Local Means Type 2	0.676	51.479	0.995
3.	2017	Image Denoising using Deep Neural Network (DNN)	1.640	47.117	0.997
4.	2018 + 2018	Anisotropic Diffusion Filtering Type 1 + Non-Local Means Type 2	113.830	31.578	0.908
5.	**2018 + 2018 + 2017**	**Anisotropic Diffusion Filtering Type 1 + Non-Local Means Type 2 + Image Denoising using Deep Neural Network (DNN)**	**0.137**	**61.466**	**0.999**

Table 5 Comparative Analysis of various combinations of Image Denoising Techniques based on various Image Quality Metrics like Mean Squared Error (MSE), Peak Signal to Noise Ratio (PSNR) and Structural Similarity for measuring the Image Quality (SSIM) for Training image database

S. No.	Year	Techniques used	Mean Squared Error (MSE) Values	Peak Signal to Noise Ratio (PSNR) Values	Structural Similarity for measuring Image Quality (SSIM) Values
1.	2018	Anisotropic Diffusion Filtering Type 1	110.887	27.897	0.877
2.	2018	Non-Local Means Type 2	0.080	61.175	0.999
3.	2017	Image Denoising using Deep Neural Network (DNN)	0.970	51.267	0.998
4.	2018 + 2017	Non-Local Means Type 2 + Image Denoising using Deep Neural Network (DNN)	1.565	47.416	0.998
5.	2018 + 2018	Non-Local Means Type 2 + Anisotropic Diffusion Filtering Type 1	255.948	24.440	0.950
6.	2018 + 2018 + 2018	Non-Local Means Type 2 + Anisotropic Diffusion Filtering Type 1 + Non-Local Means Type 2	76.349	31.671	0.970
7.	**2018 + 2018 + 2018 + 2017**	**Non-Local Means Type 2 + Anisotropic Diffusion Filtering Type 1 + Non-Local Means Type 2 + Image Denoising using Deep Neural Network (DNN)**	**0.022**	**66.103**	**0.999**

If the testing image database is considered, it is observed that if the techniques of Anisotropic Diffusion Filtering Type 1, Non-Local Means Type 2 and Image Denoising using Deep Neural Network (DNN) are combined, the numerical values of different image quality metrics like the Mean Squared Error (MSE), Peak Signal to Noise Ratio (PSNR) and the Structural Similarity for measuring the Image Quality (SSIM) were found out to be 0.13772127659574, 61.466536170213 and 0.99981489361702 respectively. Therefore, it is clear that the above technique which is mentioned in this research paper proves to be the best technique which can be used for the purpose of noise removal from input traffic sign board images present in the testing image database since the numerical values of Mean Squared Error (MSE) is the least as compared with its other counterparts and the numerical values of the Peak Signal to Noise Ratio (PSNR) as well as the Structural Similarity for measuring the Image Quality (SSIM) are the greatest as compared with its other counterparts.

If the training image database is considered, it is observed that if the techniques of Non-Local Means Type 2, Anisotropic Diffusion Filtering Type 1, Non-Local Means Type 2 and Image Denoising using Deep Neural Network (DNN) are combined, the numerical values of different image quality metrics like the Mean Squared Error (MSE), Peak Signal to Noise Ratio (PSNR) and the Structural Similarity for measuring the Image Quality (SSIM) were found out to be 0.022547858197932, 66.103574150665 and 0.99989054652881 respectively. Therefore, it is clear that the above technique which is mentioned in this research paper proves to be the best technique which can be used for the purpose of noise removal from input traffic sign board images present in the training image database since the numerical values of different image quality metrics like the Mean Squared Error (MSE) is the least as compared with its other counterparts and the numerical values of the Peak Signal to Noise Ratio (PSNR) as well as the Structural Similarity for measuring the Image Quality (SSIM) are the greatest as compared with its other counterparts.

Conclusion and Future Scope

In this paper, a comparison of various image denoising techniques was done in order to choose the best technique among a set of three different techniques and their three different combinations which was being applied to the traffic sign board images present in the testing image database and four different techniques and their seven different combinations to the traffic sign board images present in the training image database based on calculating different parameters which decide the quality of input roadway symbols like Mean Squared Error (MSE), Peak Signal to Noise Ratio (PSNR) as well as Structural Similarity for measuring Image Quality (SSIM) and after a thorough comparison, it was concluded that the combination of Anisotropic Diffusion Filtering Type 1, Non-Local Means Type 2 and Image Denoising using Deep Neural Network (DNN) techniques which was being applied to the traffic sign board images present in the testing image database and the combination of Non-Local Means Type 2, Anisotropic Diffusion Filtering Type 1, Non-Local Means Type 2 and Image Denoising using Deep Neural Network (DNN) techniques which was being applied to the images which are present in the training image database has the maximum Peak Signal to Noise Ratio (PSNR) as well as Structural Similarity for measuring Image Quality (SSIM) values and a minimum Mean Squared Error (MSE) value as compared to other techniques. These techniques will be applied to the traffic sign board images which are present in both the testing as well as training image databases in future research work for the purpose of noise removal from input traffic sign board images.

Conflict of Interest

The authors mention and acknowledge the funding sources which were provided during the course of performing the research work and there are no significant conflicts of interest.

Acknowledgments

A sincere vote of thanksgiving must be extended to Vellore Institute of Technology, Vellore administration and every one among the stakeholders whose contribution towards the completion of this work in a successful fashion paved the way for implementing it on a broad level.

References

[1] Yu-Mei Huang, Hui-Yin Yan, You-Wei Wen, Xue Yang, “Rank minimization with applications to image noise removal”, Elsevier- Information Sciences, Volume 429, March 2018, pp. 147-163.

[2] Anissa Selmani, Hassene Seddik, “Anisotropic smart shape-adapted image smoothing without conductance function efficient for impulse noise removal”, Elsevier- Digital Signal Processing, Volume 75, April 2018, pp. 83-95.

[3] Tingting Yang, Xiang Long, Arun Kumar Sangaiah, Zhigao Zheng, Chao Tong, “Deep detection network for real-life traffic sign in vehicular networks”, Elsevier- Computer Networks, Volume 136, March 2018, pp. 95-104.

[4] Yong Chen, Ting-Zhu Huang, Liang-Jian Deng, Xi-Le Zhao, Min Wang, “Group sparsity-based regularization model for remote sensing image stripe noise removal”, Elsevier- Neurocomputing, Volume 267, 6 December 2017, pp. 95-106.

[5] Jing Dong, Zifa Han, Yuxin Zhao, Wenwu Wang, Ales Prochazka, Jonathon Chambers, “Sparse analysis model based multiplicative noise removal with enhanced regularization”, Elsevier- Signal Processing, Volume 137, August 2017, pp. 160-176.

[6] Lianghai Jin, Zhiliang Zhu, Xiangyang Xu, Xiang Li, “Two-stage quaternion switching vector filter for color impulse noise removal”, Elsevier- Signal Processing, Volume 128, November 2016, pp. 171-185.

[7] De-Yong Lu, “A hybrid optimization method for multiplicative noise and blur removal”, Elsevier- Journal of Computational and Applied Mathematics, Volume 302, 15 August 2016, pp. 224-233.

[8] Xianquan Zhang, Feng Ding, Zhenjun Tang, Chunqiang Yu, “Salt and pepper noise removal with image inpainting”, Elsevier- AEU - International Journal of Electronics and Communications, Volume 69, Issue 1, January 2015, pp. 307-313.

[9] Jielin Jiang, Jian Yang, Yan Cui, Lei Luo, “Mixed noise removal by weighted low rank model”, Elsevier- Neurocomputing, Volume 151, Part 2, 5 March 2015, pp. 817-826.

[10] Tudor Barbu, “Robust Anisotropic Diffusion Scheme for Image Noise Removal”, Elsevier- Procedia Computer Science, Volume 35, September 2014, pp. 522-530.

[11] Xia Chen, Chen Tang, Xiusheng Yan, “Switching degenerate diffusion PDE filter based on impulse like probability for universal impulse noise removal”, Elsevier- AEU - International Journal of Electronics and Communications, Volume 68, Issue 9, September 2014, pp. 851-857.

[12] Xiubao Sui, Qian Chen, Guohua Gu, "Adaptive grayscale adjustment-based stripe noise removal method of single image", Elsevier- Infrared Physics & Technology, Volume 60, September 2013, pp. 121-128.
[13] Floris Gisolf, Anwar Malgoezar, Teun Baar, Zeno Geradts, "Improving source camera identification using a simplified total variation-based noise removal algorithm", Elsevier- Digital Investigation, Volume 10, Issue 3, October 2013, pp. 207-214.
[14] Jourabloo, A. H. Feghahati, M. Jamzad, "New algorithms for recovering highly corrupted images with impulse noise", Elsevier- Scientia Iranica, Volume 19, Issue 6, December 2012, pp. 1738-1745.
[15] Lianghai Jin, Caiquan Xiong, Hong Liu, "Improved bilateral filter for suppressing mixed noise in color images", Elsevier- Digital Signal Processing, Volume 22, Issue 6, December 2012, pp. 903-912.
[16] Wei Ding, "A New Method for Image Noise Removal using Chaos-PSO and Nonlinear ICA", Elsevier- Procedia Engineering, Volume 24, December 2011, pp. 111-115.
[17] Tom Mélange, Mike Nachtegael, Stefan Schulte, Etienne E. Kerre, "A fuzzy filter for the removal of random impulse noise in image sequences", Elsevier- Image and Vision Computing, Volume 29, Issue 6, May 2011, pp. 407-419.
[18] Ovidiu Ghita, Paul F. Whelan, "A new GVF-based image enhancement formulation for use in the presence of mixed noise", Elsevier- Pattern Recognition, Volume 43, Issue 8, August 2010, pp. 2646-2658.
[19] K. Kannan, B. Rajesh Kanna, C. Aravindan, "Root Mean Square filter for noisy images based on hyper graph model", Elsevier- Image and Vision Computing, Volume 28, Issue 9, September 2010, pp. 1329-1338.
[20] Huaping Liu, Yulong Liu, Fuchun Sun, "Traffic sign recognition using group sparse coding", Elsevier- Information Sciences, Volume 266, January 2014, pp. 75-89.
[21] Zhan-Li Sun, Han Wang, Wai-Shing Lau, Gerald Seet, Danwei Wang, "Application of BW-ELM model on traffic sign recognition", Elsevier- Neurocomputing, Volume 128, October 2014, pp. 153-159.
[22] Fatin Zaklouta, Bogdan Stanciulescu, "Real-time traffic sign recognition in three stages", Elsevier- Robotics and Autonomous Systems, Volume 62, August 2012, pp. 16-24.
[23] Shuihua Wang, Hangrong Pan, Chenyang Zhang, Yingli Tian, "RGB-D image-based detection of stairs, pedestrian crosswalks and traffic Signs", Elsevier- Journal of Visual Communication and Image Retrieval, Volume 25, November 2014, pp. 263-272.
[24] Jonathan J. Kay, Peter T. Savolainen, Timothy J. Gates, Tapan K. Datta, "Driver behavior during bicycle passing maneuvers in response to aShare the Road sign treatment", Elsevier-Accident Analysis and Prevention, Volume 70, April 2014, pp. 92-99.
[25] Jesmin Khan, Sharif Bhuiyan, Reza Adhami, "Hierarchical clustering of EMD based interest points for road sign detection", Elsevier- Optics & Laser Technology, Volume 57, October 2014, pp. 271-283.
[26] Zong-Yao Chen, Wei-Chao Lin, Shih-Wen Ke, Chih-Fong Tsai, "Evolutionary feature and instance selection for traffic sign recognition", Elsevier- Computers in Industry, Volume 74, September 2015, pp. 201-211.
[27] Samuele Salti, Alioscia Petrelli, Federico Tombari, Nicola Fioraio, Luigi Di Stefano, "Traffic sign detection via interest region extraction", Elsevier- Pattern Recognition, Volume 48, June 2014, pp. 1039-1049.
[28] J.M. Lillo-Castellano, I. Mora-Jiménez, C. Figuera-Pozuelo, J.L.Rojo-Álvarez, "Traffic sign segmentation and classification using statistical learning methods", Elsevier- Neurocomputing, Volume 153, November 2015, pp. 286-299.
[29] Haojie Li, Fuming Sun, Lijuan Liu, Ling Wang, "A novel traffic sign detection method via color segmentation and robust shape matching", Elsevier- Neurocomputing, Volume 169, May 2015, pp. 77-88.
[30] Zhenyu An, Zhenwei Shi, Ying Wu, Changshui Zhang, "A novel unsupervised approach to discovering regions of interest in traffic images", Elsevier- Pattern Recognition, Volume 48, February 2015, pp. 2581-2591.
[31] Yingying Zhu, Chengquan Zhang, Duoyou Zhou, Xinggang Wang, Xiang Bai, Wenyu Liu, "Traffic sign detection and recognition using fully convolutional Network guided proposals", Elsevier- Neurocomputing, Volume 214, July 2016, pp. 758-766.
[32] Ayou Ellahyani, Mohamed El Ansari, Ilyas El Jaafari, "Traffic sign detection and recognition based on random forests", Elsevier- Applied Soft Computing, Volume 46, February 2016, pp. 805-815.
[33] Selcan Kaplan Berkaya, Huseyin Gunduz, Ozgur Ozsen, Cuneyt Akinlar, Serkan Gunal, "On circular traffic sign detection and recognition", Elsevier- Expert Systems with Applications, Volume 48, 2016, pp. 67-75.
[34] Yongtao Yu, Jonathan Li, Chenglu Wen, Haiyan Guan, Huan Luo, Cheng Wang, "Bag-of-visual-phrases and hierarchical deep models for traffic sign detection and recognition in mobile laser scanning data", Elsevier- ISPRS Journal of Photogrammetry and Remote Sensing, Volume 113, January 2016, pp. 106-123.
[35] Hamed Habibi Aghdam, Elnaz Jahani Heravi, Domenec Puig, "A practical approach for detection and classification of traffic signs using Convolutional Neural Networks", Elsevier- Robotics and Autonomous Systems, Volume 84, July 2016, pp. 97-112.
[36] Mario Soilan, Belen Riveiro, Joaquin Martinez-Sanchez, Pedro Arias, "Traffic sign detection in MLS acquired point clouds for geometric and image-based semantic inventory", Elsevier- ISPRS Journal of Photogrammetry and Remote Sensing, Volume 114, February 2016, pp. 92-101.
[37] Y.Ouerhani, A. Alfalou, M. Desthieux, C. Brosseau, "Advanced driver assistance system: Road sign identification using VIAPIX system and a correlation technique", Elsevier- Optics and Lasers in Engineering, Volume 89, May 2016, pp. 184-194.
[38] Jack Greenhalgh and Majid Mirmehdi, "Recognizing Text-Based Traffic Signs", IEEE Transactions on Intelligent Transportation Systems, Vol. 16, No. 3, June 2015, pp. 1360-1369.
[39] Nadra Ben Romdhane, Hazar Mliki, Mohamed Hammami, "An Improved Traffic Signs Recognition and Tracking Method for Driver Assistance System", in the Proceedings of IEEE International Conference on Information Security (ICIS'2016), June 26-29, 2016, Okayama, Japan.
[40] Ruben Laguna, Ruben Barrientos, L. Felipe Blazquez, Luis J. Miguel, "Traffic sign recognition application based on image processing techniques", in the Proceedings of the Elsevier- Proceedings of the 19th World Congress, The International Federation of Automatic Control, Cape Town, South Africa. August 24-29, 2014, pp. 104-109.
[41] Tingting Yang, Xiang Long, Arun Kumar Sangaiah, Zhigao Zheng, Chao Tong, "Deep detection network for real-life traffic sign in vehicular networks", Elsevier- Computer Networks, Volume 136, May 2018, pp. 95-104.
[42] S.M. Bascon, J.A. Rodriguez, S.L. Arroyo, A.F. Caballero, F. Lopez-Ferreras, "An optimization on pictogram identification for the road-sign recognition task using SVMs", Computer Vision Image Understanding, Volume 114, Issue 3, 2010, pp. 373-383.
[43] C.C. Chang, Y.P. Hsieh, "A fast VQ codebook search with initialization and search order", Information Sciences, Volume 183, Issue 1, 2012, pp. 132-139.
[44] Ciresan, U. Meier, J. Mascim, J. Schmidhuber, "A committee of neural networks for traffic signs classification", in Proceedings of International Joint Conference on Neural Networks (IJCNN), July 2011, pp. 1918-1921.
[45] S.Escalera, O. Pujol, P. Radeva, "Traffic sign recognition system with b-correction", Elsevier- Machine Vision Applications, Volume 21, Issue 2, 2010, pp. 99-111.
[46] H. Gomez-Moreno, S. Maldonado-Bascon, P. Gil-Jimenez, S. Lafuente-Arroyo, "Goal evaluation of segmentation algorithms for traffic sign recognition", IEEE Transactions on Intelligent Transportation Systems, Volume 11, Issue 4, 2010, pp. 917-930.
[47] Y. Gu, T. Yendo, M.P. Tehrani, T. Fujii, M. Tanimoto, "Traffic sign detection in dual-focal active camera system", in the Proceedings of IEEE Intelligent Vehicles Symposium (IV), 2011, pp. 1054-1059.
[48] Haojie Li, Fuming Sun, Lijuan Liu, Ling Wang, "A novel traffic sign detection method via color segmentation and robust shape matching", Elsevier- Neurocomputing, Volume 169, December 2015, pp. 77-88.
[49] Y. Huang, K. Huang, Y. Yu, T. Tan, "Salient coding for image classification", in the Proceedings of Computer Vision and Pattern Recognition (CVPR), 2011, pp. 1753-1760.
[50] Alexander Shustanov, Pavel Yakimov, "CNN Design for Real-Time Traffic Sign Recognition", Elsevier- September 2017, pp. 718-725.

Advances in Science, Technology and Engineering Systems Journal Vol. 4, No. 4, 561-573 (2019)

www.astesj.com

Special Issue on Advancement in Engineering and Computer Science

ASTESJ

ISSN: 2415-6698

A Lightweight, Hardware-Based Support for Isolation in Mixed-Criticality Network-on-Chip Architectures

Giacomo Valente, Paolo Giammatteo, Vittoriano Muttillo, Luigi Pomante*, Tania Di Mascio

Center of Excellence DEWS, Università degli Studi dell'Aquila, 67100 L'Aquila, Italy

ARTICLEINFO

Article history:
Received: 15 June, 2019
Accepted: 31 July, 2019
Online: 25 August, 2019

Keywords:
Network on Chip
Isolation
Mixed-Criticality
Hardware Support

ABSTRACT

Spatial and temporal isolation is a crucial issue in embedded systems executing multiple tasks with several levels of criticality. This is considerably significant in the context of multi-processor (or multi-core) embedded systems running multiple mixed-criticality applications in parallel. This work deals with the issue of isolation of different application classes on Network on Chip (NoC) architectures and proposes a lightweight hardware mechanism able to support mixed-criticality requirements and specifically designed to be introduced into existing network interfaces. This mechanism supports the execution of different and contemporary applications with several criticality levels by supervising the messages exchange among network nodes, with the introduction of limited hardware and software overhead on the monitored network. The proposed solution is described and evaluated by means of logical simulations and an implementation on reconfigurable logic, using a reference NoC architecture with mesh topology. Scalability of the proposed approach is also discussed and evaluated by means of network simulations. Results show an area occupation less than 1% in a 3x3 mesh NoC, and a good scalability of the proposed mechanism in an 8x8 mesh network, indicating it as a valid lightweight solution able to enforce isolation in NoCs.

1. Introduction

It is possible to define the criticality of the generic component of a system as the level of assurance needed for that element [1]. Embedded system is a clear example of mixed-criticality system if different software elements executing on the same hardware platform possess two or more levels of criticality. The fundamental problems in mixed-criticality system management are (i) the simultaneous satisfaction of discordant requirements regarding advantageous access to shared resources, in order to make the most of performance of the system, (ii) and a strict partitioning to avoid disorder between different elements.

Regarding single-processor embedded systems, it is essential to guarantee the isolation between tasks in terms of time, and several techniques able to ensure temporal determinism of running have been presented in scientific literature [2]. On the other hand, about multi-processor systems, different applications run in parallel on different processors. The applications must compete in accessing shared resources, taking advantage of the specific communication architectures of different hardware implementations. Recently, it was possible to observe a growing interest towards the usage of Network on Chip (NoC) architectures [3] as a platform for systems with high mixed criticality. Compared to traditional shared (hierarchical) bus solutions, NoCs can more efficiently support the implementation of multi and many core systems. Table 1 (inspired by the works presented in [4] and [5]) provides a qualitative comparison of the two approaches.

In this prospective, the present work shows a mechanism with lightweight hardware for the management of mixed criticality in a multi-processor embedded system conceived on a Network on Chip. In particular, the aim is to give a hardware-based support in order to control the flow of the messages through the NoC, with the goal of guaranteeing a reserved access to the NoC itself on the base of the criticality level of the different tasks running on the NoC nodes. In such a way, the proposed mechanism supports spatial and temporal isolation, since, in a given period, only a subset of the tasks can access the NoC and the connected resources. Indeed, temporal isolation ensures no interference in the time domain among tasks to access to a shared resource (i.e., mutual exclusive access), while spatial isolation protects a shared resource

*Luigi Pomante, Email: luigi.pomante@univaq.it

Table 1: Shared bus vs. NOC: a qualitative comparison

	Concurrent access to different resources	Throughput	Physical implementation Overhead	Scalability	Design complexity	Power dissipation	Area occupation	Max frequency
Shared Bus	-	-	=	-	+	-	-	-
NoC	+	+	=	+	-	+	+	+

so that tasks are able to freely perform access only to a part of it, or only a subset of existing tasks are able to access to that resource [6].

The main characteristics of the proposed mechanism are the following ones:

- limited effect on system performance, thanks to a hardware-based approach;
- no limit on the number of criticality levels in the system;
- supporting both spatial and temporal isolation.

In particularly, the innovation points of the proposed approach are the followings:

- independency from NoC topology, i.e., it can be adapted to each NoC scenario;
- portability among different networks.

It is worth noting that this paper extends the one presented in [7], by providing:

- detailed HW design, described in Hardware Description Language (HDL), together with logical simulation (sec. 4);
- extended scalability analysis by means of OMNET++ simulations (sec. 5 and 6).

The paper is outlined in this way. Section 2 describes the most important concepts related to the management of isolation in the context of mixed-criticality in multi-processor and NoC based systems; the section also briefly summarizes the current main existing strategies for the effective management of the different criticality levels. Section 3 shows the proposed mechanism and details its advantages. Section 4 illustrates the detailed HDL-based HW design and simulation issues. Section 5 and 6 show the analysis of a simulated platform that helps to test the effectiveness of the proposed mechanism for NoC with more nodes. Finally, Section 7 summarizes conclusions and discusses future works.

2. Isolation in Mixed-Criticality Systems

Spatial and temporal isolation is a fundamental issue for embedded systems. In particular, for those systems that perform multiple activities with different levels of criticality, or better to say, mixed critical embedded systems. The topic is particularly significant for areas such as aeronautics and automotive. Several standards have the specific purpose of finding a solution to this problem and two significant examples are the AUTOMOTIVE OPEN SYSTEM ARCHITECTURE (AUTOSAR, [8]), a software architecture in the automotive area, and the Aeronautical Radio INCorporated (ARINC, [9]), which gives the specifications for spatial and temporal sectioning in avionics applications critical for safety (ARINC 653).

In order to examine the issue of mixed criticality, different analytical models can be followed [1]. Usually, applications are modelled as a group of elements. Each one consists of a finite number of tasks. Each task is expected on a processing resource, that can be shared among different tasks. For the present analysis, each task executes a specific activity by performing a certain number of jobs and it is periodically scheduled on a shared processing resource.

Focusing on criticality, several schemes have been presented in literature defining of levels of criticality, from the easiest one, where only two levels are allowed (i.e., non-critical and critical), up to configurations where the number of allowed levels is potentially unlimited [10]. Focusing on isolation, the tasks belonging to components with a lower criticality level shall not be able to interfere with higher criticality ones.

In literature, different studies have analyzed the problem of the management of mixed criticality in single processor systems, from the isolation point of view [2]. A static allocation of memory during compilation phase is an appropriate strategy in order to reach spatial isolation. Contrarily, a Memory Management Unit and a Memory Protection Unit could support isolation for dynamic memory allocation. Another appropriate strategy in order to reach isolation between tasks with several criticality levels is virtualization. Anyway, full virtualization is generally not satisfactory for embedded systems (especially if exists real-time constraints), indeed the required overhead may be impactful on the temporal constraints of the application. The usage of Hypervisors [11] in these situations permits to run ate the same time several operating systems upon a platform in sharing with low overhead, but still maintaining the isolation of time and space [12].

It is fundamental in a multi-processor system with shared bus architecture, administer the access to shared communication elements. This could be done by partitioning the system in order to eliminate disturbances among applications executing on different cores, or on peripherals device with DMA. The issue of partitioning in multi-processor systems is already addressed by Pellizzoni et al. [13], with the definition of the Architectural Analysis and Design Language, which is a form of Architectural Description Language used for mixed-critical systems that supports by construction the monitoring and optimization of the communication and processing phase. The time-triggered model [14] is a different method of partitioning, where a high level of criticality is related to the time-triggered traffic, while traffic

Table 2: Routing arbitration policies for NoCs.

Arbitration Policy	Round Robin	Time Division Multiplexing	Fixed Priority
Description	Usually aimed at obtaining fairness on arbitration, but not used in real-time systems, given the problems in calculating the worst-case latencies for the various transactions.	The various data flows are statically allocated to separated time slots. This arbitration policy is largely adopted in real-time and mixed criticality implementations, but determining a reservation scheme for the various time slots is not trivial.	The various transactions are managed based on predefined priority levels.

triggered by events is generally the best effort. Time-Triggered Ethernet or TTP/C are kind of protocols that support this kind of communication mechanism called Time-Division Multiple Access (TDMA). If no isolation-oriented strategies are implemented, the management of shared resources is usually demanded to the specific bus arbitration.

Finally, in a multi-processor system based on NoC, router arbitration schemes are fundamental. Generally, NoCs are conceived on the arbitration policies shown in Table 2.

2.1. State of Art

Schoeberl [15] suggested a regular structured time-triggered NoC (TDMA-based) capable to support foreseeable communications both on-chip and off-chip. This architecture uses a pseudo-static communication schedule implemented in a Cyclone II EP2C35 *Field-Programmable Gate Array* (FPGA) on the Altera DE2 board. The underlying network topology is simple (e.g., ring structure) and optimized for easy routing (wire routing, not message routing). They implement a simple demo application (a voting triple modular redundancy sensor), but they evaluate the scheduling policy offline for each different scenario. An advanced tool to calculate and verify the schedule is important to render the proposed NoC useful.

Tobuschat [16] developed a NoC capable to support natively a mixed criticality. This system is conceived on a methodology (namely, back suction) capable to maximize the bandwidth allocated for low importance messages, guarantying that the most critical messages are delivered by satisfying the related deadlines. The authors said that sufficient independence is reached, and worst-case behavior can be predicted through the usage of virtualization, monitoring infrastructure, and control mechanisms. Programming of the monitors is only possible by the system controller, so its correct implementation becomes an essential point of this work, introducing additional load to the system. Furthermore, the knowledge of all possible interference enables timing predictable behavior of the whole system, but this assumption is not simple to verify with respect to real scenarios.

Burns [17] described the Wormhole Protocol for Mixed Criticality (WPMC). This protocol points out the dual-criticality, fixed priority NoCs. Furthermore, if an infraction in transaction deadlines is catched, it permits to limit the use of communication elements in favor of high criticality transactions. Successively, WPMC has been updated in order to advance the low criticality packets average latency and the latency of the worst-case of the high criticality ones [18]. The main limitations of this work are related to the maximum number of criticality levels considered (not more than two), the lack of a mode change protocol among several criticality levels, and the study of mixed-criticality end-to-end latency analysis (i.e., considering task execution as well as traffic-flows).

More in general, state of art solutions to provide isolation converge on two main areas: Time Division Multiplexing, that implies a conservative design with increased resource requirements [15], and Monitoring of the System, to react in case of unexpected situations.

The mechanism proposed in this paper falls in the second category, with the novelty that the monitoring mechanism is moved into the NoC itself, involving only NoC interconnection elements and not NoC nodes. This specific aspect will be analyzed, in more detail, in the following section. In this way, the introduced mechanism is independent from the NoC topology, as the control action can be applied independently from the specific NoC architecture. The mechanism is also easily portable, as it is simple to introduce custom communication control strategies into existing network interfaces. These are the two main advances respect to the state of art.

3. Proposed HW Support for Isolation

This paper proposes a mechanism able to consider the different criticality levels of tasks running on a NoC, and to regulate the network traffic basing on specific network parameters. The system model is firstly introduced, then the proposed mechanism is detailed and analyzed.

3.1. System Model

In the proposed approach, a NoC consists of, at least, two *Nodes* (N) and one or more *Routers* (R). Every node includes one or more processors/cores, memories, and other peripherals. Intra-node communications can entrust on several approaches (generally a hierarchical bus and shared-memory structure). These internal details are not a constraint for the proposed structure, so they will be considered abstracted from now on. Inter-node communications are conceived on message passing: this implies that every node possess a *Network Interface* (*NI*), exploited to send/receive messages, and linked to a single router port. Every single router can be linked, to other *NI* and/or to other routers, considering on the NoC topology. The routers transmit the messages to final nodes according to the used routing protocol.

In Figure 1, it is shown a schematic reference NoC, consisting of four nodes and routers connected in a mesh topology. Every node of the NoC run one or more tasks T_i. In our case a task could represent an OS process, thread or simply a generic abstraction of a piece of software that executes a specific function). Each task is characterized at least by a *task criticality level* (c_i), i.e., the level of insurance associated to the task itself. Each task has a default criticality statically assigned at design-time and can deliver a

message (M) over the NoC through the NI of the node on which it is running. Every message is then outlined by a *priority* equal to the sender task criticality.

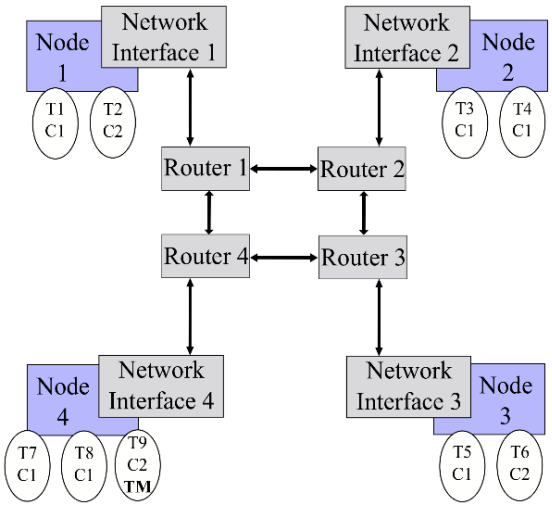

Figure 1: NoC with 4 nodes in a mesh topology.

3.2. Proposed HW mechanism

In order to define a mechanism supporting isolation, the network status is characterized by a global parameter named *Severity*. At certain time, the NoC will perform with a level of severity S in the range [1, Smax]. The isolation mechanism relies on the following two hypotheses:

- for a given temporal instant, only the messages sent by tasks with a criticality level $c \geq S$ can be transmitted by the NI and forwarded to the routers;
- the severity level can be modified, at run-time, by tasks that have specific privileges. These tasks (*Task Masters*, indicated as TM in Figure 1) are statically defined at design time.

At start-up, the system works in the least conservative mode, with a minimum severity level. If an anomaly condition is detected, and tasks with high criticality need to be executed, the system may switch to higher severity level, causing those tasks with higher criticality to access the network without competition with lower criticality ones. The following additional hypotheses are assumed:

- each NI can store the severity level of the network, to allow the transmission of new messages only if their criticality is greater or equal than S;
- the severity level of the network could be modified (raised or lowered) by a TM, by introducing inside the network a message which change the *severity*. This message is propagated to all network nodes and processed inside the NI. The reception of a message with a change in severity will activate an update of the severity level memorized inside the interface.

Being only the TM able to change the NoC Severity, the configuration of the system results to be protected: indeed, an untrustworthy entity is not able to change this configuration and possibly corrupt the system itself. The condition to prompt for a Severity change depends on the presence of anomalies: metrics able to indicate when an anomaly is verified can be defined, depending on the application executed on the NoC; then, by monitoring these metrics, it is possible to relate the TM transmission of a Severity change with the anomaly identification.

Observing Figure 1 and supposing that it is related to a scenario with two levels of criticality and two levels of severity, when the NoC possess a severity level equal to one, all the tasks can send and receive messages through the network. The routers could use a simple *First-in First-out* (FIFO) policy to manage the message forwarding toward the proper ports: when the FIFO is full, the message is rejected by the router, waiting for space in the queue. When a TM (T9 in the example of Figure 1) starts the procedure to change the level of severity of the NoC, all the NI shall be notified in order to update the corresponding value. When the severity level reaches the value of two, only T2, T6 and T9 are enabled to send messages while all the tasks will be able only to receive them. It is important noting that the designer owns the responsibility in order to eliminate, or to keep tolerable, conditions where a task cannot react to the message of a more critical one due to the NoC severity level possessed in that moment.

The reference HW design of the severity management mechanism, able to implement the isolation mechanism above described, is shown in Figure 2. It has an *Input Buffer* (called Message Buffer in the figure) to manage message traffic from the node: when a message from the node reaches the input of the buffer, the *Comparator* module checks if the criticality of the input message is greater or equal than the current network severity (stored in the *Severity Register*). If that is the case, the output of the comparator will be low, and the message will be stored into the *Message Buffer*. Otherwise, the output of the comparator will be high, and the message will be rejected: specifically, the loading of the message buffer will be inhibited, and a reject notification will be sent to the node. This functionality is described in the flowchart shown in Figure 3, where the methods *fillInputBuffer(), Analyze(), StoreMessageBuffer()* and *Reject()* implement, respectively, the reading from the node, the analysis of the received *Message*, the storage into the message buffer to transmit along the NoC and the rejection of the *Message*.

As above indicated, the aim of the proposed hardware mechanism is to assist the NoC design where, at a certain time, only the packets sent by a task with criticality greater or equal than the severity of the NoC are transmitted. The NI of nodes that executes the sending tasks blocks all other messages. It should be highlighted that this degradation is often tolerable in systems with mixed-criticality [17], as it eliminates any influence between lower and higher criticality flow. It can be noticed that the suggested solution does not reduce the number of criticality network levels. Also, it can be noticed that the proposed mechanism supports both spatial and temporal isolations: the former is ensured by the fact that only tasks with criticality greater than S can use the network resources to send messages. The latter is ensured by the fact that Severity can be changed over time, so giving the opportunity to all the tasks to access the network resource in specific temporal slots while still being able to assure that the most critical ones, when needed, can run without interferences due to less critical tasks.

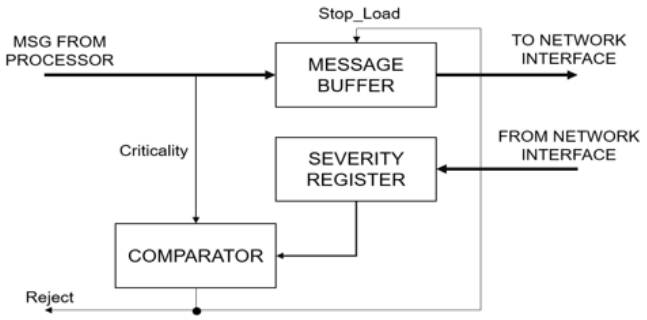

Figure 2: Implementation of the mechanism in a Network Interface (NI).

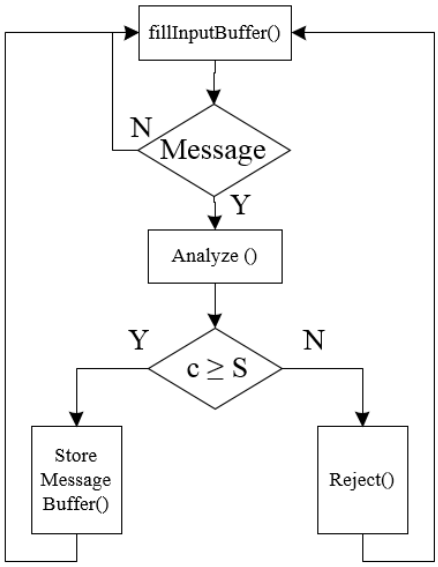

Figure 3: Functionality of the proposed HW mechanism.

4. HW Mechanism Design and Validation

This section presents the approach adopted to design and validate the proposed HW mechanism. The interests have been focused on three features: behavior validation, practicability check, and evaluation of the scalability. Regarding the first one, it allows to check if the developed mechanism behaves as expected. It is mainly based on HDL-based design and simulations. The second feature allows to check if this mechanism is possible to realize on real systems. It is based on a *Hardware-In-the-Loop (HIL)* approach applied to a simple NoC implementation on an FPGA platform. The final and third one (described in section 5) allows to check if it is possible to exploit the mechanism in real-size NoC. So, it is based on a *Network Simulation* approach to validate behavior and evaluate scalability, without the need to develop very complex NoCs. So, the following paragraphs, presents all the details needed to understand the performed HDL-based design and simulations activities.

4.1. Selected Reference NoC

A reference NoC has been considered for validation activities. It is an open-source NoC [19] described in HDL, that can be simulated and synthetized on FPGA. Such a NoC is of interest, since its design is very simple, allowing to reduce the number of required logic units for prototypal implementations. Moreover, it is provided with a MATLAB program to monitor the network traffic at run-time.

The reference NoC architecture consists of a network of nodes able to send and receive data, in order to complete their actions. Devices in nodes can be of different types, such as processors, memories and input/output devices. A network adapter is used to connect a device to a router, and a router connects the node to the rest of the network. Packet switching is used as a communication method across the network, with packets used as the communication medium.

Specifically, there are three types of packets in the network: *write*, *read_request* and *read_return*, as shown in Figure 4. All of them have a header, to indicate their type, and other fields depending on their goal.

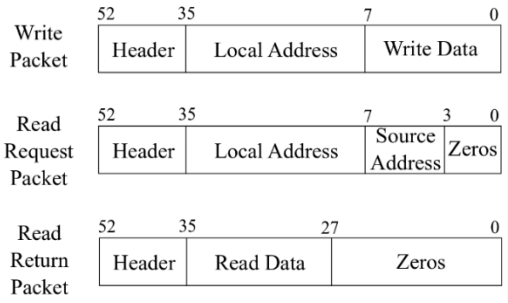

Figure 4: Packets of the reference NoC.

The *write* packet is sent by a master node to write data to a slave, while a *read_request* is sent by a master node to a slave one, and the latter replies with a *read_return* packet. *write* and *read_request* packets require a destination address: the reference NoC has a 32-bit address space, where the first 4 bits are used as the unique node IDs, while the remaining 28 bits are used for local addresses. The *read_request* packet also contains the source ID used by the receiver to send the *read_return*. *read_return* packets only contain the destination node ID of the source where they are replying to. A *write_packet* contains 8-bits of write data, while a *read_return* contains 8-bits of read data. The packets are sent over one clock cycle, rather than broken up over multiple clock cycles, to keep the hardware and logic simple.

Focusing on *network adapter* (NA), it represents interface between the node and the router, and its purpose is to convert signals from the local bus into a suitable packet format for the network, and back again. There are two types of network adapters and devices: *master* and *slave*. The *master network adapter* receives the following signals from the master device: *write_address*, *write_enable*, *write_data* and *read_request*. A master device can connect to the network adapter and the network should be totally transparent. The NA sends back *not_ready*, *read_return* and *read_*data. Any device wishing to connect to the network needs to handle a *not_ready* signal from the network adapter. Its output interface with a router is a *packet_data_out*. It can receive a busy signal from the router and a *read_return* packet.

Routers have five sets of channels connected to them, as shown in Figure 5. As the mesh organization is used in the network, four directions can be identified: *north*, *east*, *south*, *west*, and one additional channel going toward the *local* network adapter. The router is clocked with the global clock of the system. In order to

move the packets around the network from sources to destinations, routers look at a special field of the incoming packets, called *xy-counters* [19]: they give priority to *y-direction*, firstly check in what vertical direction they should forward the packet, and then checking for the horizontal one. If a router receives a packet in which both x and y counters are set to 0, then it indicates that the packet was destined for that router and that it has now reached its destination (and should be forwarded to the local network adapter).

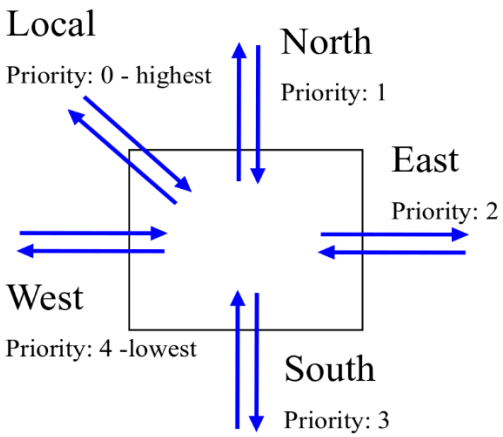

Figure 5: Router.

In order to support on debugging actions, a hardware monitoring system is offered together with the reference NoC [20] [21]. The monitoring system interfaces with an UART controller, allowing the communication with a host computer. A MATLAB program is also provided to be executed on host computer, providing a visual representation of the current traffic on the network, which is updated several times per second.

The proposed HW isolation mechanism has been integrated in an instance of the reference NoC discussed in the previous sub-section, composed of 16 nodes in a mesh topology, shown in Figure 6. Each device within a node is represented by a simple *finite state machine* that acts as a master or slave processor (in the following TP — *Test Processor*), executing some specific instructions.

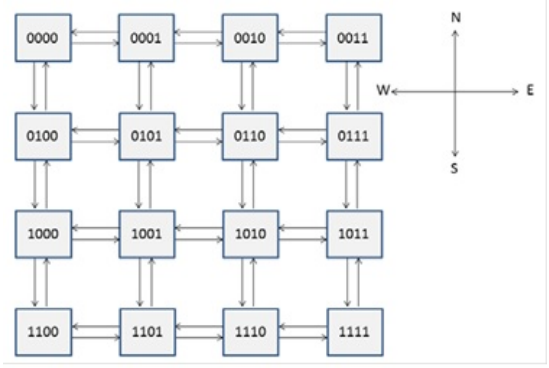

Figure 6: Reference 16 meshed nodes NoC.

In such a reference NoC, *Severity* and *Criticality* concepts have been introduced. If a TP tries to send a message with criticality less than current network severity, the message is blocked by NA. It is worth noting that messages are not blocked by routers, since, in this case, they are unaware of the isolation mechanisms. This improves portability but also means that, when a severity change occurs, all the packets already inside the networks are still able to freely circulate. In this case, they will be managed accordingly to their priority, as expected by the type of NoC. For validation purposes, *Criticality*, *Severity* and *Priority* have been set in the interval [0, 7]. In order to support the proposed approach, the NoC has been modified to introduce a fourth type of packet, called *severity_change,* shown in Figure 7. The goal of the packet is to allow a *master* task to trigger a severity change.

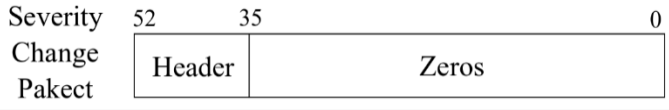

Figure 7: Packets managed by the reference NoC.

Together with the introduction of a new packet type, further assumptions have been done to reduce the management complexity of the network, focusing on the purpose of the tests:

- TM has been associated to the node in the upper-right corner of NoC shown in Figure 6. The corresponding TP is the only one able to change the severity of the network.
- Severity change requests are forwarded by following a snake-coil path, as shown in Figure 8. Routers forward such a packet only in one fixed direction

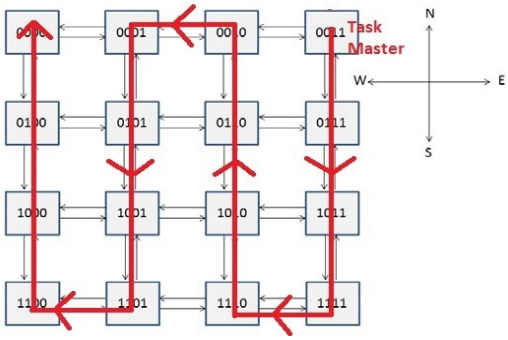

Figure 8: Snake-coil path.

Master and slave NA adopt a two-levels input buffer at both TP and Router side. By means of them and a proper busy signal, it is possible avoid losing input packets. If two packets are concurrently coming from TP and Router, they are managed at the same time, if possible, otherwise they are serialized giving priority to the one with greater criticality. As said before, the criticality/severity check is performed only in Master NA, specifically by checking the input buffer at TP side. This represents the major change with respect to the reference NoC. Another important one is that, if a message coming from TP is not accepted by NA, TP is notified by means of a proper *msg_rejected* signal. A detailed view on NA modifications is shown in Figure 9 and Figure 10.

The router is identical to the reference NoC one, apart from the need of improving the existing priority-based routing approach. In fact, in the case of concurrent packets forwarding, greater priority shall be given to criticality instead than to the port. It is worth noting that such a policy is simply priority-based, i.e., the router does not need to know about the criticality/severity mechanisms (in fact it is designed to work without knowing anything about the current severity level).

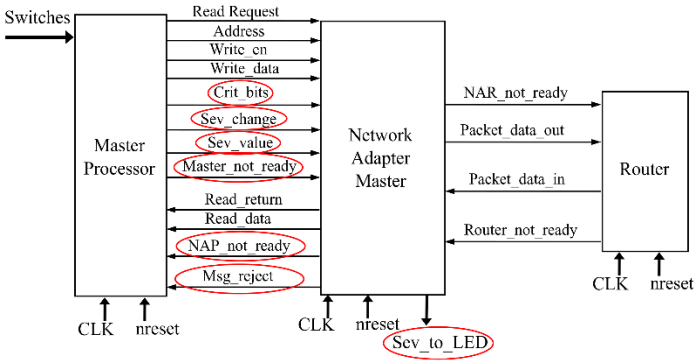

Figure 9: Modified master NA.

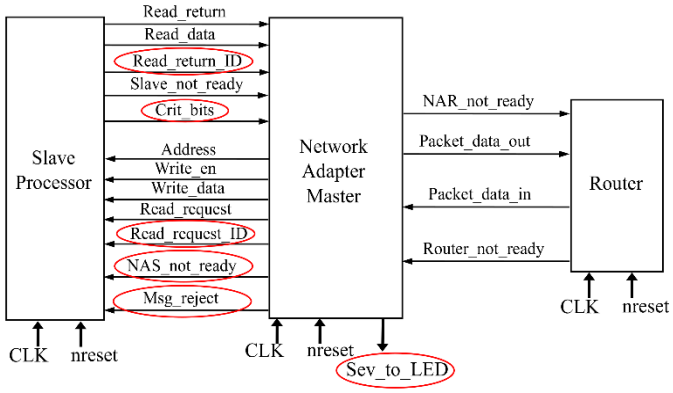

Figure 10: Modified slave NA.

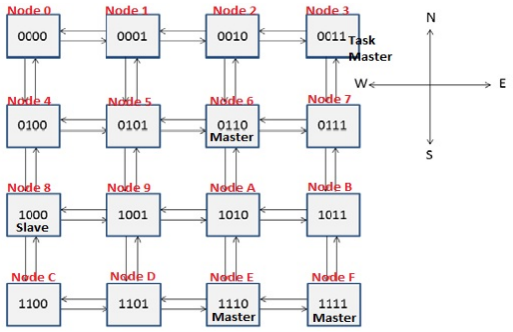

Figure 11: Simulated NoC.

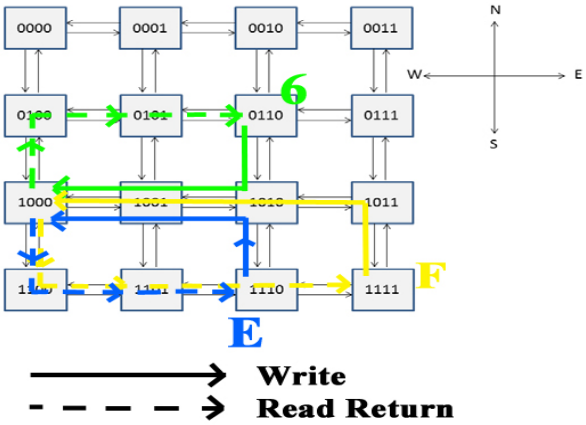

Figure 12: Write and read_return paths.

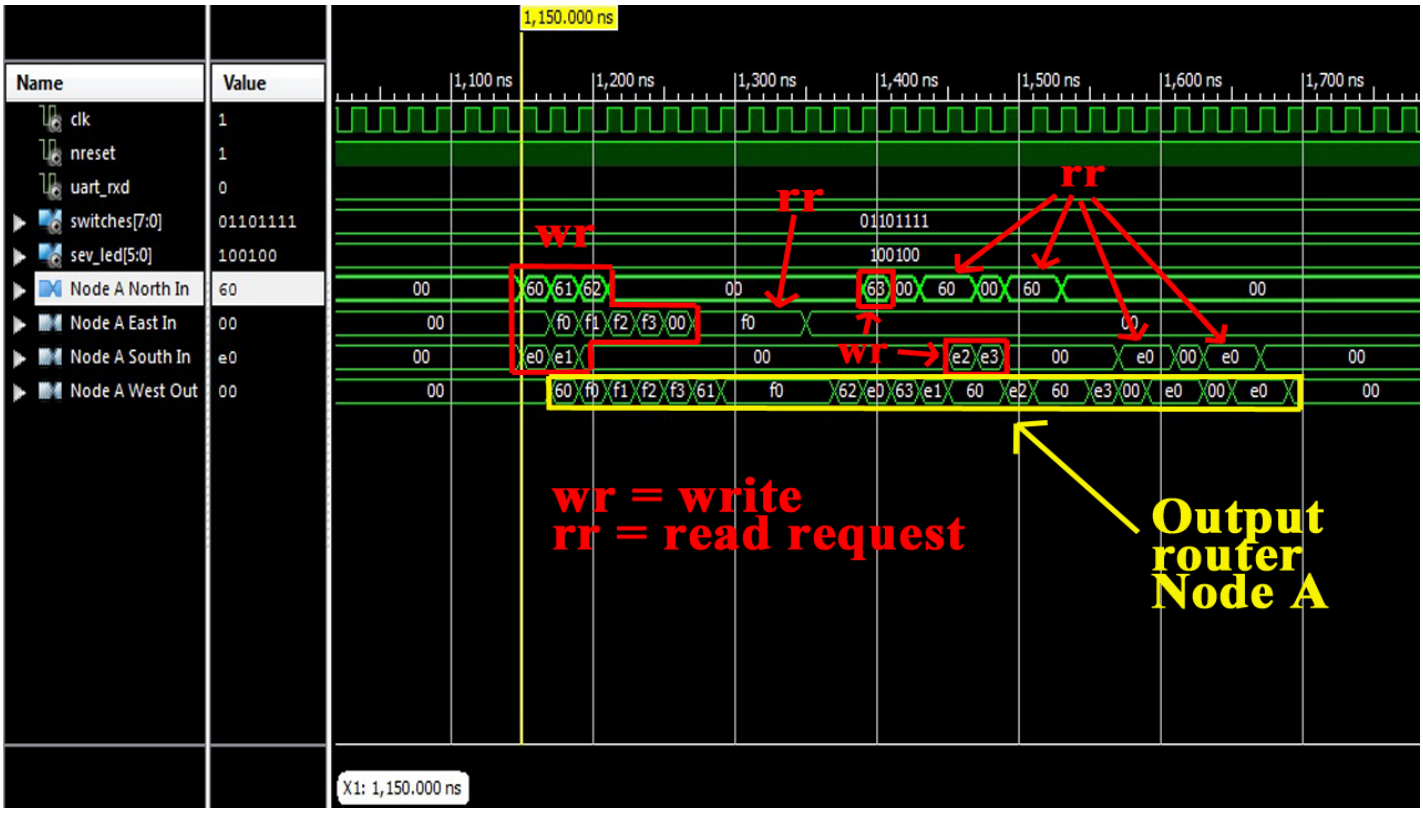

Figure 13: Packet forwarding in router close to node A

4.1. Validation by means of logical simulation

The above discussed NoC has been described in VHDL and simulated by means of Xilinx *ISim* [22]. In this way, it has been possible to verify the right forwarding of packets and the behavior of the proposed mechanism. In Figure 11, the simulated NoC is shown: it is composed of 16 nodes with different IDs (represented both in binary and hexadecimal base). Nodes 6, E and F are the master ones (i.e., they have a master NA and a master TP). In the considered test case, they perform some writings and readings by involving node 8 (*slave*). Written data (*write_data*) are composed of node ID and a progressive number (from 0 to 3, since, in the considered test case, each node performs 4 consecutive writing). In Figure 12, the main communication paths between the masters and slave node number 8 are shown.

Test 1 – Router packet forwarding

The first proposed test has the goal of verifying the correct packets forwarding done by routers. In Figure 13, it is shown the router close to master Node A managing input from ports N, E, and S, and forwarding them towards W (since all the write operations are related to node 8). The reported values represent the *write_data* field in hexadecimal base. In the presented test case, master NAs make use of their 3-bits ID LSB as criticality values for their sent messages; with this assumption, the following criticality values have been considered: criticality 6 for node 6 (110), criticality 6 for node E (110), criticality 7 for node F (111).

In Figure 13, it can be noticed that packets from nodes 6 and E reach the router with 1 clock cycle anticipation (since node F is far than the others). It is also possible to notice that the first two *write* packets (60 and e0), that requires the same output port, are correctly forwarded giving priority to the packet 60 (same criticality, but N port). Then, the newly arrived f0 is quickly forwarded, since it has greater criticality with respect to e0. The output is the sequence f0, f1, f2, f3. Since also the *read_request* packets form F have criticality 7, they are always forwarded in a single clock cycle (f0 is high for 4 clock cycles).

Test 2 – Isolation

In Figure 14, the isolation capability of the proposed mechanism is verified. Considering a severity level set to maximum value (i.e., 7) and stored by each NA, a TP tries to send a message with criticality less than the current severity. In particular, the TP tries to send 4 *write* and 4 *read_request* packets with criticality 6 (110); it receives the *msg_rejected* signal for 8 clock cycles. It is worth noting that, in this test, *msg_rejected* notifications are not managed in any way by the TP (e.g., no tentative resending).

Test 3 - Severity change

In Figure 15, a severity change in the NoC is shown. It is possible to notice the *severity_change* packet (highlighted in red) firstly sent by node 3 (the only allowed to do it, since it is supposed to be the only one to have a TM) to its NA. Then, such a command is forwarded to the whole NoC (following the path already shown in Figure 8), i.e., each NA updates its internal current severity value and setups a new message to forward the severity_change command to the next node.

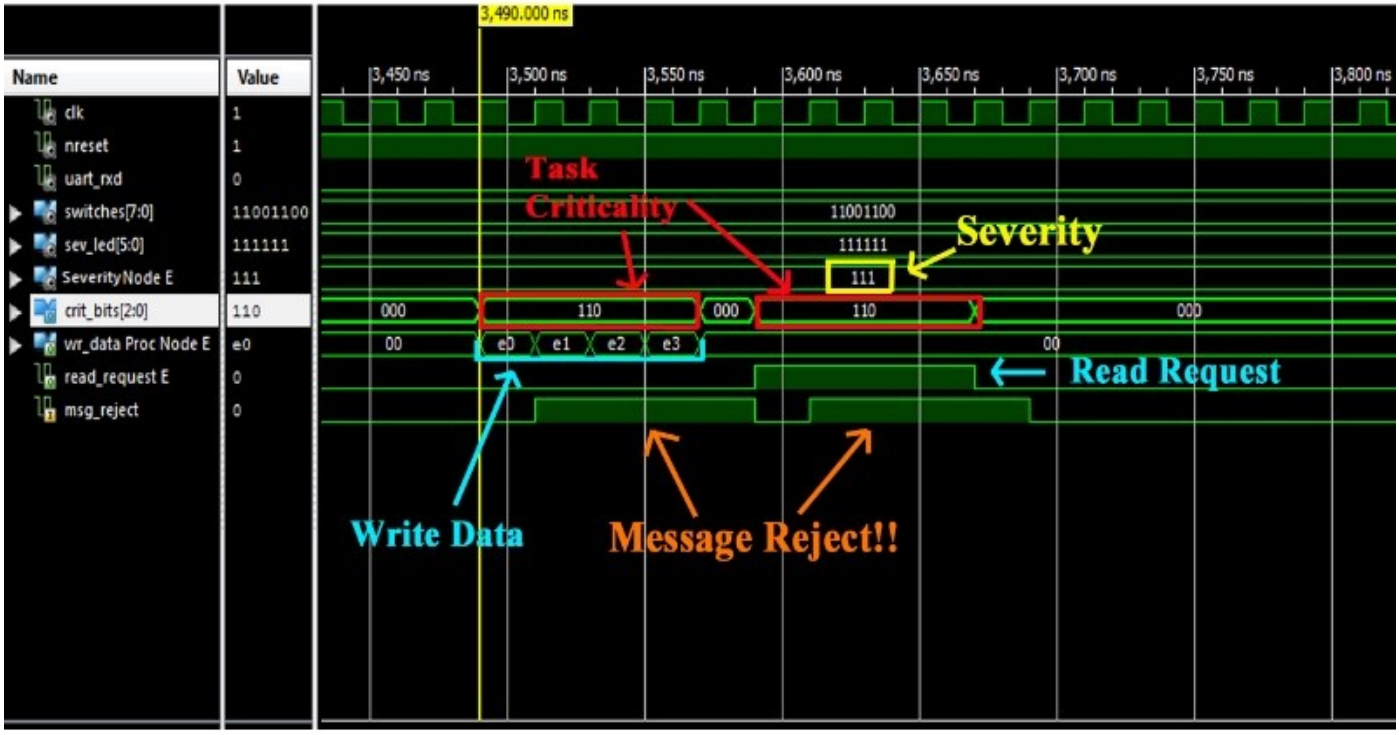

Figure 14: Criticality/Severity check.

4.2. HIL-based validation

In order to validate a prototypal implementation of the proposed mechanism, an instance of the reference NoC, enriched with that mechanism, has been implemented on a Xilinx Spartan-3 FPGA [23] using Xilinx *ISE Design Suite 14.7* [24]. The testbed is shown in Figure 16. The prototype consists in a NoC with a 3x3 mesh topology, where each node device is represented by a master or slave *Dummy Processor* (DP), namely a simple finite state machine that acts as a processor executing some specific instructions. Such a network implements an 8-level Severity and Criticality system. To keep low the complexity, while focusing on proposed mechanism features, the TM has been associated to the node in the upper-right corner so that the corresponding DP is the only one able to change the severity of the NoC (actually, the corresponding dummy processor has been designed so that the user can manually decide when to do severity changes and at what value, by using board switches). Aside from the node at the top right that holds the Task Master, all other nodes have been randomly distributed between the two master and slave types, and the associated Dummy Processors have been configured to create a decent amount of traffic packets at all criticality levels in the network. Severity change requests are forwarded to the other nodes by following a fixed snake-coil path, as shown in Figure 17.

All packets are forwarded by routers with a *Packet-Criticality* based priority policy [19]: the routers first check in which vertical direction they should forward the packet, and then check for the horizontal one. If a router receives a packet in which both x and y counters are set to 0, then it indicates that the packet was destined for that node and that it has now reached its destination. If, at a given time, two or more packets from the input ports are destined to the same output port, a conflict occurs, and priority is given to the packet with the highest criticality, whereas other packets are blocked before they can be sorted out later. In the case of equal criticality, priority is given according to the input port of the conflict packets, by following the descending order: Local, North, East, South and West. It is worth noting that such a policy is simply priority-based, i.e. the router does not need to know about the criticality/severity mechanism (indeed it is designed to work without knowing nothing about the current severity level).

Master and slave NA adopt a two-level input buffer at both DP and Router side. By means of them and a proper busy signal, it is possible avoiding losing input packets.

After the system implementation on Spartan 3 FPGA, the monitoring system and the MATLAB program have been used to check the NoC status. Red wires indicate connections that have a lot of traffic, yellow ones indicate a small amount of traffic while white ones indicate no traffic at all. Other than the traffic, it is also possible to check the amount of *busy* and *msg_rejected* events. In Figure 18, it is possible to notice that with a low severity level (000) traffic is quite high, since all the nodes are able to send messages

After the setting of a severity change to the highest severity level (111) (the changing of severity using the TM is shown in Figure 17), the traffic appears to be heavily reduced, as shown in Figure 19. The area occupations are reported in Table 3. The impact is very small, so the adjective “lightweight”.

Figure 15: Severity Change.

Table 3: Area occupation.

	FFs	LUTs	f_{MAX}
Complete NoC with the proposed mechanism	37 %	70 %	125 MHz
Proposed mechanism (area per each NI)	1 (<1%)	2 (<1%)	-
Proposed mechanism (area in 3x3 mesh)	9	18	-

5. Scalability evaluation

In this section, a model of the reference NoC has been developed using the Omnet++ simulator [25] with the aim to evaluate the scalability of the proposed mechanism. The model of the NoC supports *n*-levels Severity and Criticality. Multiple standard (unprivileged) tasks and Master tasks can be statically associated to each node of the network, and different traffic patterns can be associated with each task. The simulator includes a statistic unit able to investigate the traffic sequences, and the possibility to use a flexible time base module able to model synchronous and asynchronous NoC. In the case of synchronous NoC, the model of the network makes use of a module (named the Time-base synchronizer) able to generate clock messages, ensuring synchronous communication between the various nodes. Other model features are the following:

- in a fixed, predetermined device, a single TM executes on the platform
- each router uses the *xy* routing strategy shown previously and the broadcasting of the Severity Change Packet;
- the TM can determine the traffic status and eventually its congestion, by inserting a special broadcast packet called the Inquire Packet (IP);

The TM will modify the severity by sending a *Severity Change Packet* if the measured congestion status exceeds a predefined threshold, or if there is a timeout elapse. This severity administration policy needs an additional overhead for the development of the routers, as every router should be capable to follow the number of queued packets and deal with the IP. Furthermore, the suggested enquiry strategy needs the insertion of additional packets inside the network, possibly disturbing with device traffic.

In Figure 20, there is the result of a simulation of the modelled system in case of a synchronous 8x8 NoC. This figure shows the total number of packets inserted into the network over time, reported in generic time units (i.e., number of clock cycles) and two indices of the network status: the number of queued packets at a certain time and the current network severity. It should be observed that the value of the two network indices is multiplied by one hundred for a better clarity of the figure. It can be seen that the traffic regulation mechanism is adequately capable to limit the traffic of the network in case of congestion, allowing only the successful transactions of high criticality messages in a timely manner: this shows the feedback that the proposed mechanism can provide when unexpected behavior from the tasks are verified.

In Figure 21, it is reported the number of total sent messages (red line) and the number of dropped messages (blue line). The number of dropped messages is lower than the total messages that go through the network. In particular, the number of total messages in the tested time interval is $4.14 \cdot 10^6$, while the number of dropped messages is $3.00 \cdot 10^6$.

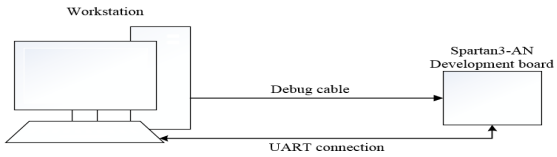

Figure 16: Testbed.

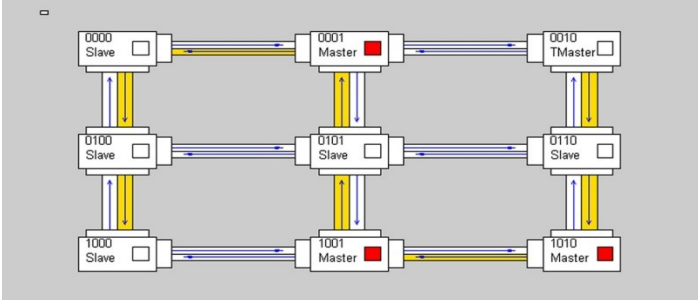

Figure 17: Snake-coil path.

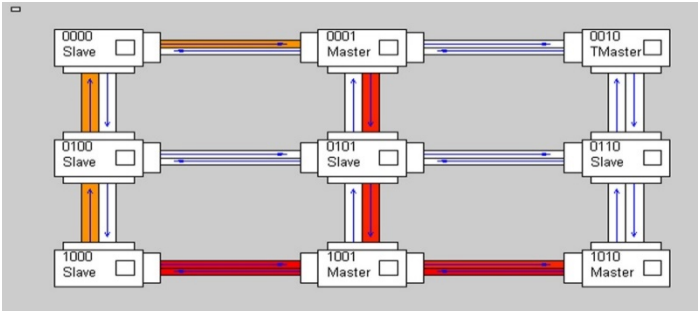

Figure 18: Network traffic with low severity (000).

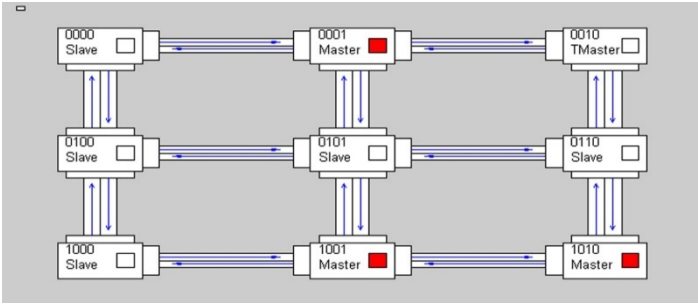

Figure 19: Network traffic with high severity (111).

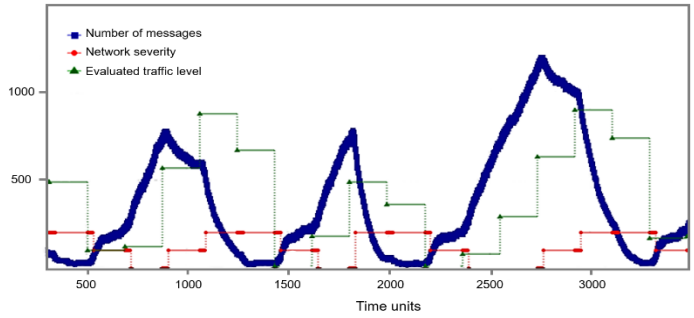

Figure 20: Simulation of a synchronous 8x8 mesh network.

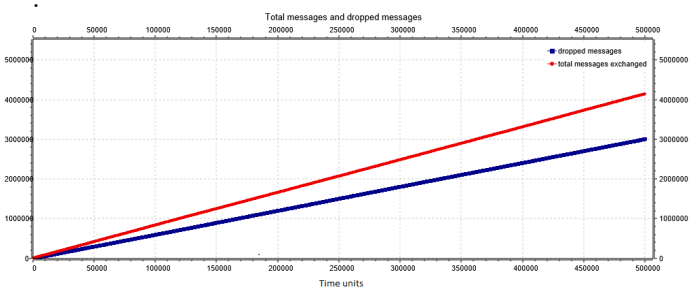

Figure 21: Number of total messages (red line) and number of dropped messages (blue line) for a synchronous 8x8 mesh network.

6. Further Analysis

Thanks to effort spent on creating a model, further analysis has been done by means of system simulations, introducing other aspects and evaluating a different broadcast strategy and a different management of the control traffic messages.

6.1. Different broadcast strategy

In this test, routers have the possibility of changing the broadcast of the Severity Change Packet. There are two possibilities:

- *snake-coil strategy*: the message, with TM in the node at the top right of the network, is broadcast one router at a time in a north-south direction, then moves one step to the left when the message reaches a router located at the northern or southern limit in the network itself and resume the journey in the north-south direction. The method is already described and used in the previous two sections.
- *star-broadcast strategy*: it takes its name from the design formed by the overall path travelled by the messages. The origin node of the messages can be in any position. The first router forwards the packet to all the connected ports in order to reach the maximum number of routers. Routers located along the north-south axis respect to the first router forward the message to the east, west and north, if they received the message from the south, or forward it to east, west and south, if they received it from the north. Finally, the routers that receive the packet from the east [or west] forward the broadcast packet along the west [or east] direction in order to make the broadcast packet continue along the east-west axis (see Figure 22).

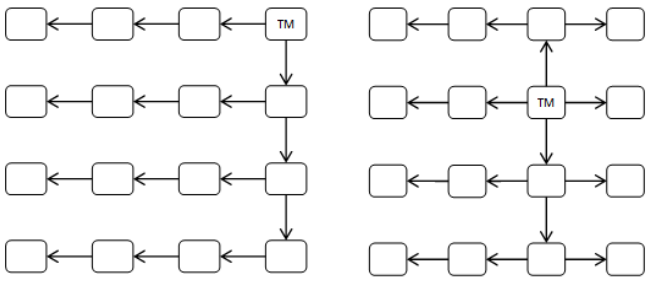

Figure 22: Star-broadcast strategy.

In Figure 23, it is shown the behavior of the system in case of a synchronous 8x8 NoC with the star-broadcast strategy instead of snake-coil one. As in previous section, the value of the two network indicators is scaled by a factor of one hundred for better clarity of the graph. Here, the TM periodically sends a control signal to which all routers respond by entering their own maximum queue value. In this period, the TM waits a maximum time equal to 10 clock cycles between one message and another before deciding to change the severity of the network. After this time, if the TM does not receive all the answers, then the network severity increases, trying to moderate the circulation of messages. Vice versa, when all the messages are received by the TM, the latter can decide to decrease the severity of the network. When all the messages are received, the TM in this test evaluates the average of the received answers.

The test shows that the proposed mechanism manages to control the flow of messages within the network, although the network itself is flooded with many control messages. The peak of messages reached within the network exceeds one thousand units, a situation in which the severity of the network is zero. In this case, there are several messages in the network and the TM fails to receive all the control messages, so the network severity is raised to one (one hundred in Figure 23).

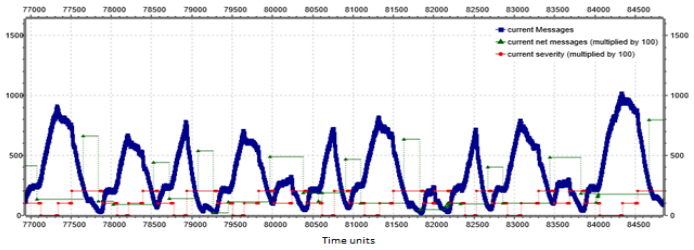

Figure 23: Simulation of a synchronous 8x8 mesh network without traffic control and with star-broadcast strategy

This leads to a decrease of messages in the network, but not enough so the TM causes another increase in severity. With severity two (two hundred in Figure 23), the severity does not decrease until the value answered by all nodes is less than a threshold value. The response received from all the nodes is averaged in order to obtain an indicative value of the network state. The value is considered only when the responses are received from all the routers. Subsequently, two tests are conducted on this type of broadcast strategy. The first one, shown in Figure 24, uses an exact average value obtained from all the responses received. In the second case, shown in Figure 25, the average is modified in correspondence of a minimum value in order to be higher.

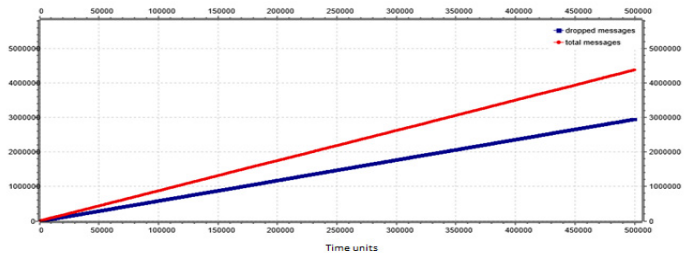

Figure 24: Number of total messages (red line) and number of dropped messages (blue line) for a synchronous 8x8 mesh network with star-broadcast strategy, exact average case.

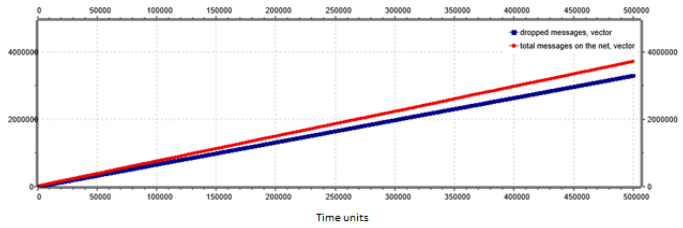

Figure 25: Number of total messages (red line) and number of dropped messages (blue line) for a synchronous 8x8 mesh network with star-broadcast strategy, modified average case.

Considering these two results, the network that performs best for message delivery time is the one that uses the modified average of traffic. However, this method results in a lower number of total messages sent over the network. Furthermore, with the use of the modified average, the maximum capacity of the routers results decreased in messages of a 20%.

6.2. Control traffic messages management

In this situation, devices and routers use two types of states to differentiate the type of messages processed, by extending the functionalities already present in the implemented NoC. Here, a single slot is dedicated to control traffic messages management. Two states have been identified:

- State zero indicates classic operation, i.e. read, write and reply messages are exchanged.
- State one only messages intended for traffic control are exchanged.

The traffic control messages in this type of network have a priority equal to that of the TM, in order to do not mix service messages with those of communication useful between the cores. Currently this functionality is supported only for a synchronous NoC. For a synchronous 8x8-node networks with control traffic messages management, the best behavior is obtained with the star-broadcast strategy (see Figure 26 and Figure 27). Here, there is a better delivery time for all messages.

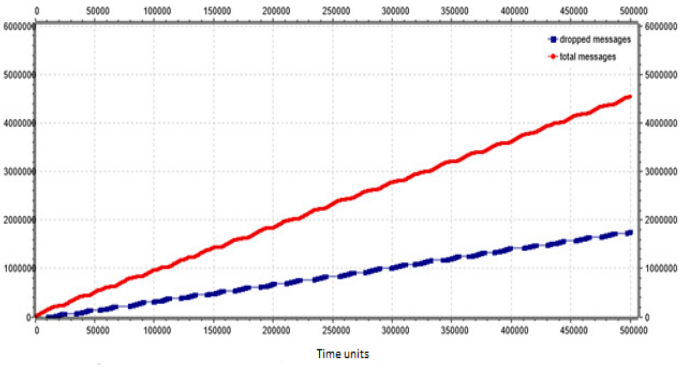

Figure 26: Number of total messages (red line) and number of dropped messages (blue line) for an 8x8 mesh network with control traffic messages management and snake coil strategy.

Analyzing all the experimental results for 64-node networks without control traffic messages management, the broadcast strategy that behaves best is the snake coil, unless the star-broadcast strategy modifies the average of the messages received. Therefore, if we consider the modified average, the star-broadcast improves and shortens the delivery time of the messages.

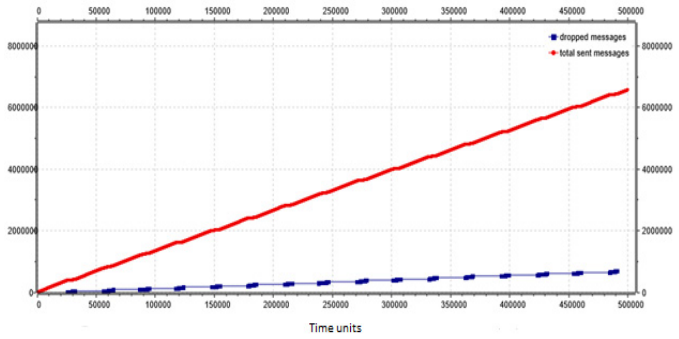

Figure 27: Number of total messages (red line) and number of dropped messages (blue line) for an 8x8 mesh network with control traffic messages management and star-broadcast strategy.

For the 64-node network with control traffic messages management, the best behavior is given by the star-broadcast. It must be remembered that, in the network with state, a fixed delay is introduced in the maximum time of delivery of the messages equal to the time of control necessary to probe the network. Despite this, the star-broadcast strategy keeps the average delivery time of messages low, even if it has a high delivery time.

7. Conclusions

Isolation is an important issue for embedded systems on which multiple tasks with different level of criticality are running. This paper has suggested a lightweight isolation mechanism to be introduced into existing Networks on Chip. This mechanism supports the execution of multiple applications with different criticality levels by supervising the packet exchange between network nodes. It does not reduce the criticality levels and it supports both spatial and temporal isolation. The system main innovation is its autonomy from the topology of the NoC and its easily flexibility among different NoCs. Small NoC implementations have been provided, showing the small impact in the area occupation, and motivating the adjective “lightweight”. Simulation on a network simulator has been proposed to evaluate the behavior of the mechanism on a NoC with more elements, and the feedback applied when there are unexpected situations is shown.

8. Future Works

Future works involve a further analysis to precisely characterize the overhead of proposed mechanism in a real existing NoC solution, and to investigate the best severity change policy. Moreover, given the outlined results, the possibility of adding a lightweight support for network status analysis will be explored as well.

Conflict of Interest

The authors declare no conflict of interest.

Acknowledgements

Authors would like to thank you Fabio Federici, Mattia Micozzi, Riccardo Cardinali and Biagio Iorio for the support on solving technical issues and precious feedbacks.

References

[1] A. Burns, R.I. Davis, "A survey of research into mixed criticality systems", ACM Computer Surveys, 50(6):1–37, 2017.
[2] S.K. Baruah, S. Vestal, "Schedulability analysis of sporadic tasks with multiple criticality specifications," in 2008 Proceedings of the 20th Euromicro Conference on Real-Time Systems (ECRTS), Prague, Czech.
[3] A. Agarwal, C. Iskander, R. Shankar, "Survey of Network on Chip (NoC) Architectures & Contributions," Journal of Engineering, Computing and Architecture, 3(1), 2009.
[4] R. Kamal, N. Yadav, "NoC and Bus Architecture: a comparison", International Journal of Engineering Science and Technology (IJEST), 4(4), April 2012.
[5] A. Achballah, S. Saoud "A Survey of Network-On-Chip Tools", International Journal of Advanced Computer Science and Applications (IJACSA), 4(9), 2013.
[6] A. Esper, G. Nelissen, V. Nelis, E. Tovar, "How realistic is the mixed-criticality real-time system model?", In Proceedings of the 23rd International Conference on Real Time and Networks Systems, RTNS '15, pages 139–148.
[7] F. Federici, M. Micozzi, V. Muttillo, L. Pomante and G. Valente, "Simulation-Based Analysis of a Hardware Mechanism to Support Isolation in Mixed-Criticality Network on Chip," 2017 European Modelling Symposium (EMS), Manchester, 2017, pp. 185-190.
[8] "AUTOSAR". [Online]. Available: https://www.autosar.org/ [Accessed: 13-June-2019].
[9] "ARINC". [Online]. Available: https://www.aviation-ia.com/ [Accessed: 13-June-2019].
[10] P. Ekberg, M. Stigge, N. Guan, W. Yi, "State-based mode switching with applications to mixed criticality systems," in 2013 Proceedings of the 1st International Workshop on Mixed Criticality Systems (WMC), Vancouver, Canada.
[11] Andrew S. Tanenbaum and Herbert Bos. 2014. Modern Operating Systems (4th ed.). Prentice Hall Press, Upper Saddle River, NJ, USA.
[12] V. Muttillo, G. Valente, L. Pomante. 2018, "Criticality-driven Design Space Exploration for Mixed-Criticality Heterogeneous Parallel Embedded Systems," In Proceedings of the 9th Workshop and 7th Workshop on Parallel Programming and RunTime Management Techniques for Manycore Architectures and Design Tools and Architectures for Multicore Embedded Computing Platforms (PARMA-DITAM '18).
[13] R. Pellizzoni, P. Meredith, M-Y. Nam, M. Sun, M. Caccamo, and L. Sha, "Handling mixed-criticality in SoC-based real-time embedded systems," in 2009 Proceedings Of the 7th ACM international conference on Embedded software (EMSOFT), Grenoble, France.
[14] H. Kopetz, A. Ademaj, P. Grillinger, and K. Steinhammer, "The time-triggered ethernet (TTE) design," in 2005 Proceedings of the Eighth IEEE International Symposium on Object-Oriented Real-Time Distributed Computing (ISORC 05), Seattle, WA, USA.
[15] M. Schoeberl, "A time-triggered network-on-chip," in 2007 Proceedings of the International Conference on Field-Programmable Logic and its Applications (FPL 2007), Amsterdam, The Netherlands.
[16] S. Tobuschat, P. Axer, R. Ernst, J. Diemer, "IDAMC: A NoC for mixed criticality systems," in 2013 Proceedings of the IEEE 19th International Conference on Embedded and RealTime Computing Systems and Applications (RTCSA), Hakodate, Japan.
[17] A. Burns, J. Harbin and L. S. Indrusiak, "A Wormhole NoC Protocol for Mixed Criticality Systems," in 2014 IEEE Real-Time Systems Symposium (RTSS), Rome, Italy.
[18] L. S. Indrusiak, J. Harbin and A. Burns, "Average and Worst-Case Latency Improvements in Mixed-Criticality Wormhole Networks-on-Chip," in 2015 27th Euromicro Conference on Real-Time Systems (ECRTS), Lund, Sweden.
[19] G. Best, M. Birman, O. Rahnama, W. Pawlak. "Design and implementation of a simple mesh Network-on-Chip". [Online]. Available: https://github.com/mattbirman/Network-on-Chip-in-VHDL [Accessed: 13-June-2019].
[20] G. Valente et al., "A Flexible Profiling Sub-System for Reconfigurable Logic Architectures," 2016 24th Euromicro International Conference on Parallel, Distributed, and Network-Based Processing (PDP), Heraklion, 2016, pp. 373-376.
[21] A. Moro, F. Federici, G. Valente, L. Pomante, M. Faccio and V. Muttillo, "Hardware performance sniffers for embedded systems profiling," 2015 12th International Workshop on Intelligent Solutions in Embedded Systems (WISES), Ancona, 2015, pp. 29-34.
[22] "ISIM". [Online]. Available: www.xilinx.com [Accessed: 13-June-2019].
[23] "Xilinx Spartan3AN" Data Sheet [Online]. Available: https://www.xilinx.com/support/documentation/data_sheets/ds557.pdf, [Accessed: 24-May-2019].
[24] "Xilinx ISE Design Suite 14.7" [Online]. Available: https://www.xilinx.com/products/design-tools/ise-design-suite.html, [Accessed: 28-July-2019].
[25] "Omnet++". [Online]. Available: https://omnetpp.org/, [Accessed: 13-June-2019].

ASTES

Advances in Science, Technology and Engineering Systems Journal Vol. 4, No. 4, 574-584 (2019)

www.astesj.com

Special Issue on Advancement in Engineering and Computer Science

ASTESJ

ISSN: 2415-6698

Multiple-Optimization based-design of RF Integrated Inductors

Houcine Marouani[*,1], Amin Sallem[1], MondherChaoui[1], Pedro Pereira[2], Nouri Masmoudi[1]

[1]*LETI-ENIS, University of Sfax, Tunisia*

[2]*CTS-UNINOVA, FCT NOVA, Portugal*

A R T I C L E I N F O

Article history:
Received: 22 May, 2019
Accepted: 11 August, 2019
Online: 25 August, 2019

Keywords:
Metaheuristics; Particle Swarm Optimization; Gravitational Search Algorithm; Differential Evolution;
Multi-objective MOPSO;
PESAII;
MOEA/D;
RF Integrated Inductors;

A B S T R A C T

In this paper, a *multiple-objective Metaheuristics study is discussed. Initially, three mono-objective metaheuristics will be explored in order to design and optimize Radio-Frequency integrated inductors. These metaheuristics are: An evolutionary algorithm called The Differential Evolution (DE), An algorithm supported on Newton's laws of gravity and motion called the Gravitational Search Algorithm (GSA) and, finally, A swarm intelligence algorithm called the Particle Swarm Optimization (PSO). The performances of these three mono-objective metaheuristics are evaluated and compared over three benchmark functions and one application to optimize the layout of a RF silicon-based planar spiral inductor, the double π-model is adopted. Secondly, three references multi-objective metaheuristics using Pareto front are used respectively the multi-objective PSO (MOPSO), the Pareto envelope-based selection algorithm-II (PESAII) and the multi-objective evolutionary algorithm based on decomposition (MOEA/D). The performances of these multi-objective optimization algorithms are evaluated and compared over two bi-objective benchmark functions and the same application used in the first section. Two conflicting performances were optimized, namely the quality factor 'Q' (to be maximized) and the device area 'dout' (to be minimized) for the RF inductor. It was concluded that the multiple-objective PSO are significantly more efficient and robust for difficult problems than the other metaheuristics.*

1. Introduction

Nowadays, the advances in the integration technology agree the conception and the realization of complex integrated electronic systems. Therefore, the decision-making must be broached in an optimal way. Decision making can be seen as a set of the following steps: "Formulation", "Modelling", "Optimization", and "Implementation" of the problem [1]. In order to increase the accuracy of the optimization model, or algorithm, up to an adequate solution is establish, the decision making process could be repeated. The block "Optimization of the problem" is a vital part of this process and can be found in many areas, like engineering among others, and particularly in the topic of Radio Frequency (RF) circuit design [2-4].

The mono-objective optimization algorithms are classified into two categories: the heuristics and the metaheuristics algorithms. In fact, the first category is developed to solve a specific problem [5]. The second category represent a group of optimization techniques where theses popularity are increased during the last two decades and being considered the most successful and promising optimization algorithms [6–8]. The most used ones in the literature are the Evolutionary Algorithms (EA) such as local search (LS), simulated annealing (SA), tabu search (TS), genetic algorithms (GA) [9-14] etc.

Recently, a new group of nature inspired metaheuristic algorithms were published in literature. These metaheuristics are part of Swarm Intelligence. These techniques are based on animal behaviour and insect conduct, aiming to mimic their skills solving daily problems. In the area of Radio Frequency (RF) circuit design, Swarm Intelligence (SI) techniques are broadly applied, and among such techniques the PSO "Particle Swarm Optimization" [15–17], and the ACO "Ant Colony Optimization" [18–21], are the most used.

In this paper a multiple-objective metaheuristics study is discussed. Firstly, we propose to evaluate and compare such references mono-objective metaheuristics optimizing such

[*]Corresponding Author: Houcine Marouani, LETI-ENIS, Université of Sfax, Road Soukra km 4 3038 Sfax, Tunisia, +21652930505
houcine.marouani@gmail.com

benchmark functions and one Radio-Frequency application in terms of convergence, robustness and time computing. Three mono-objective algorithms are considered: An evolutionary algorithm entitled the Differential Evolution (DE), an algorithm based on Newton's laws of gravity and motion entitled the Gravitational Search Algorithm (GSA) [22, 23], and a swarm intelligence algorithm entitled the Particle Swarm Optimization (PSO). The drive issue for this comparative study is to give some sort of substantiation for the choice of the "best" metaheuristic among others [24]. Secondly, multi-objective problems are discussed. A study was conducted to the maximization of the quality factor Q and the minimization of the device area d_{out} for the Radio-Frequency (RF) integrated inductor circuit [25-30]. Three algorithms for multi-objective Pareto optimization [31-39] are used. An evaluation concerning the performances of the three abovementioned multi-objective metaheuristics: the convergence and the robustness analyses are offered [40-41].

The structure of this work is the following. Section 2 presents a summary of the mono-objective metaheuristics used. Results and analysis regarding the convergence and the robustness study of the three algorithms over three benchmarks functions are offered in Section 3. Section 4 reports the application of these mono-objective optimization applied to the layout of a RF silicon-based planar spiral inductor. Section 5 presents the uses of multi-objective algorithm to optimize both the maximum quality factor and to minimize the device area of the RF inductor with three multi-objective algorithms: the multi-objective particle swarm optimization (MOPSO), the Pareto Envelope-based Selection Algorithm II (PESAII) and the Multi-Objective Evolutionary Algorithm based on Decomposition (MOEA/D). A comparison of its performance's meters is concluded. Finally, Section 6 wrap up the final remarks, conclusion and future works.

2. An overview on the mono-objective metaheuristics

2.1. Differential Evolution algorithm

In 1997, Storn and Price developed the differential evolution (DE), which belongs to evolutionary algorithm category. It is an effective, robust and simple global optimization algorithm [13].

Differential evolution algorithm is similar to the genetic algorithm [25], uses similar genetic operators like crossover, mutation and selection operators. Comparing both algorithms, the best solutions achieve are dependent of the process, the genetic algorithm relies on crossover operators while the differential evolution algorithm on the mutation operation (differential strategy) [26]. DE generates new candidates (trial vectors) of its population according to target vector manipulation and difference vector. Afterwards, it compares the performance of the resulting candidate against the original members, and if it shows to have a better solution, it changes it; else, keep the original candidate. The differential evolution algorithm technique uses three operators: mutation, crossover and selection.

2.1.1. Mutation Operator

The *mutation* operator is defined as follows:

$$V_i^{k+1} = X_{r1}^k + F\ (X_{r2}^k - X_{r3}^k) \tag{1}$$

Where V^{k+1} is the i^{th} trial vector produced by the mutation strategy; k represents the generation to which the population belongs; $r1$, $r2$, and $r3$ are mutually exclusive integers arbitrarily generated from 1 to N (N is the population size) and F is a scaling factor with optimal value in the range of *0.5 to 1.0*.

2.1.2. Crossover Operator

One the *mutation* operation is done, the crossover operator is applied to maintain the miscellany of the population. The crossover operator generates the offspring individual U_i at the k^{th} generation by selecting the solution component values from X_i or V_i, using the following equation (2):

$$U_{ij}^{k+1} = \begin{cases} V_{ij}^{k+1}\ if\ \ rand \le CR \\ X_{ij}^k\ otherwise, \end{cases} \tag{2}$$

where CR: the crossover probability $\in [0, 1]$.

2.1.3. Selection Operator

The selection operator is adopted to compare the trial vector U_i^k with the target vector X_i^k if the fitness of the trial vector is more suitable than the target vector. Such operation, which occurs every k^{th} generation, is presented in equation (3):

$$X_i^{k+1} = \begin{cases} U_i^k\ if\ f(U_i^k) \le f(X_i^k) \\ X_i^k\ otherwise, \end{cases} \tag{3}$$

where f: the fitness function.

The flowchart of DE algorithm is given in Figure 1.

2.2. Gravitational Search Algorithm

In [22, 23], the authors proposed the gravitational search algorithm as a new swarm intelligence metaheuristic. This metaheuristic is based on Newton's laws of gravity and motion. In GSA, a cluster of agents (solutions) named masses are used to solve and find the optimal solution (best agent). Based on the gravitational force, where all objects are attracted among each other, and this force causes a global movement of such objects towards objects with heavier masses [23]. The weightier masses, representing the best solutions, are known for moving slowly compared to those less heavy. The GSA is represented by N agents, where the position of the i^{th} object is defined with (4):

$$X_i = (x_i^1, ..., x_i^d, ..., x_i^N) \text{ for } i = 1, 2, ..., N \tag{4}$$

where x_i^d is the position of ith object in the d^{th} dimension and N is dimension of the problem to be optimized.

The mass values of every objects are defined by (5):

$$M_i(t) = \frac{fit_i(t) - worst(t)}{\sum_{j=1}^{N} (fit_j(t) - worst(t))} \tag{5}$$

where $fit_i(t)$, $M_i(t)$ represents the fitness value and the mass value of the object *i* at *t*, and $worst(t)$ is evaluated by (6):

$$worst(t) = \max_{j\in\{1,\ldots,N\}} fit_j(t) \tag{6}$$

To estimate the total forces and the acceleration of an agent, it should be evaluated over gravity law, equation (7), then equation (8). Resulting, the new velocity is calculated by equation (9) and the new position is computed by equation (10).

$$F_i^d(t) = \sum_{j\in kbest, j\neq i} rand_j G(t)\frac{M_j(t)M_i(t)}{R_{ij}(t)+\varepsilon}(x_j^d(t)-x_i^d(t)) \tag{7}$$

$$a_i^d(t) = \frac{F_i^d(t)}{M_i(t)} = \\ = \sum_{j\in kbest, j\neq i} rand_j G(t)\frac{M_j(t)}{R_{ij}(t)+\varepsilon}(x_j^d(t)-x_i^d(t)) \tag{8}$$

$$v_i^d(t+1) = rand_i \times v_i^d(t) + a_i^d(t) \tag{9}$$

$$x_i^d(t+1) = x_i^d(t) + v_i^d(t+1) \tag{10}$$

where $R_{ij}(t)$ is the Euclidian distance between two agents, *i* and *j* defined as $R_{ij}(t) = \| X_i(t), X_j(t) \|_2$. k_{best} is the set of first *K* agents with the best fitness value and biggest mass. k_{best} is a function of time, which is initialized to k_0 at the beginning and is decreased with time. k_0 is adjusted to *N* and reduced linearly to 1. Moreover, *G* is reduced in a exponentially way from G_0 toward zero by time.

The flowchart of GSA algorithm is given in Figure 2.

2.3. Particle swarm optimization

The particle swarm optimization algorithm is a swarm-intelligent metaheuristic proposed by Kennedy and Eberhart [15]. PSO is an optimization algorithm that describes the social behavior of animals like birds and fish in search of food.

In PSO, each particle (solution) flies through the design/search space and moves randomly in the following three simple rules:

- Cohesion: the particles are attracted to the average position of the group or best position 'p_{best}';
- Alignment: the optimal value attained until here via every particle in the social neighbourhood 'l_{best}',
- Separation: to avoid collisions, particles keep a certain distance between them, the optimal particle position found in all the swarm 'g_{best}'.

Therefore, the new velocity and the particle position on the next iteration are performed through equations (11) and (12):

$$\vec{v}_{k+1}^{i} = \omega_k \vec{v}_k^{i} + c_1 r_1(\vec{p}_k^{i} - \vec{x}_k^{i}) + c_2 r_2(\vec{p}_k^{g} - \vec{x}_k^{i}) \tag{11}$$

$$\vec{x}_{k+1}^{i} = \vec{x}_k^{i} + \vec{v}_{k+1}^{i} \tag{12}$$

ω_k is an inertia weight, defined via a decreased inertia function by equation (13) in the training progress for objective the reduction of the influence of the past velocities.

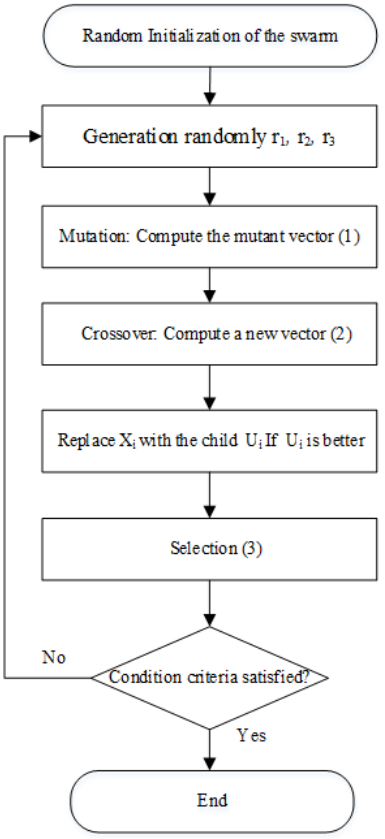

Figure 1: DE Flowchart

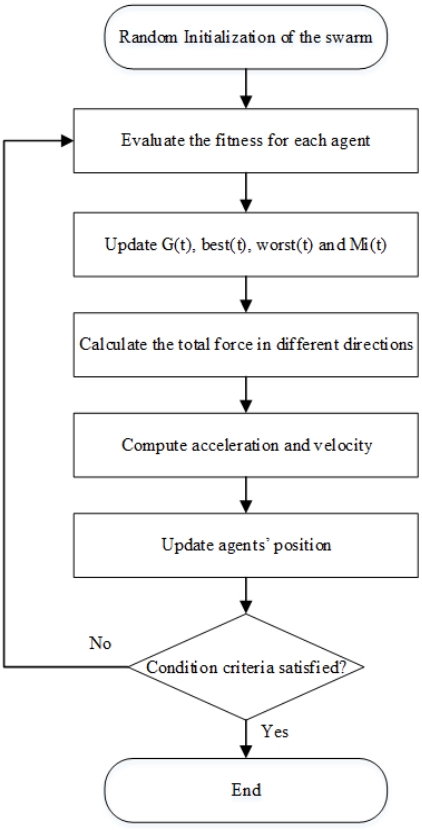

Figure 2: GSA Flowchart

Where

c_1 : the cognition learning rate,

c_2 : the social learning rate,

p_k^i : the best individual position,

p_k^g : the best global position,

$r_{1,2}$: two random parameters $\in [0,1]$.

$$\omega_k = \omega_k^{max} - \frac{\omega_k^{max} - \omega_k^{min}}{total\_iter} iter \quad (13)$$

where

ω_k^{max} : the initial weight,

ω_k^{min} : the final weight,

total_iter: the number of the total iteration,
iter: the number of the current iteration.

The flowchart of PSO algorithm is given in Figure 3.

3. Application examples: the mono-objective problems

A. Benchmark function

Three mono-objective metaheuristics are used respectively the DE, GSA and PSO over three benchmark functions. A robustness study regarding the aforementioned metaheuristics is presented. The parameters used to characterize the three algorithms are shown in Tables 1, 2 and 3. For simulation and study proposes, the three metaheuristics were tested 100 times for each one of the benchmark functions.

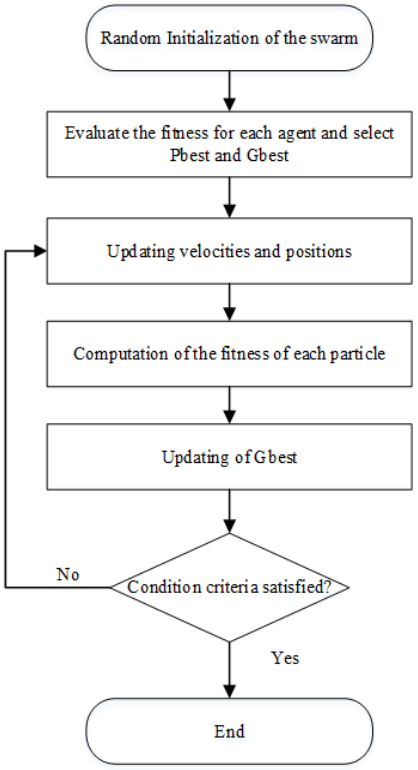

Figure 3: PSO Flowchart

Table 1: The DE parameters

Population size	*Number of Iterations.*	*beta_min*	*beta_max*	*CR*
100	1000	0.2	0.8	0.2

Table 2: The GSA parameters

Number of agents	*Number of Iterations.*	*Elitist Check*	*Rpower*	*min_flag*
100	1000	1.0	1.0	1.0

Table 3: The PSO parameters

Swarm size	*Number of Iterations.*	*w*	*c1*	*c2*
100	1000	1.0	1.5	2.0

3.1. Benchmark function application

In object to check performances of such mono-objective metaheuristics, a bunch of commonly used benchmark functions, considering this sort of problems/algorithms, were used [24]. These problems permit testing these mono-objective algorithms to confirm their convergence, concerning the approximation to the global solution [8, 18, 24]. The set of three benchmark functions are offered in Table 4.

Table 4: The benchmark functions

Item Function	*Objective functions to minimize*
Function #1	$F1 = \sum_{i=1}^{n} x_i^2$ Range: [-100; 100]; Dim n=2
Function #5	$F5 = \sum_{i=1}^{n-1} [100(x_{i+1} - x_i^2)^2 + (x_i - 1)^2]$ Range: [-30; 30]; Dim n=2
Function #7	$F7 = \sum_{i=1}^{n} [1:dim].*(x_i^4) + rand$ Range: [-1.28; 1.28]; Dim n=2

3.2. Optimization results

Function F1

The results of the benchmark function F1 are compared via the correspondent three optimization algorithms, as illustrated in Figure 4.

A Boxplots representation is used (due to probabilistic characteristic of these metaheuristics) to display the distribution of obtained measures [27]. In the following, 100 runs are considered for this function. The robustness analysis using the box-plot for the benchmark function F1 is presented in Figure 5.

Function F5

The results of the benchmark function F5, via the correspondent three optimization algorithms, are represented in Figure 6.

In the following, 100 runs are considered for function F5. The robustness analysis using the box-plot for the benchmark function is presented in Figure 7.

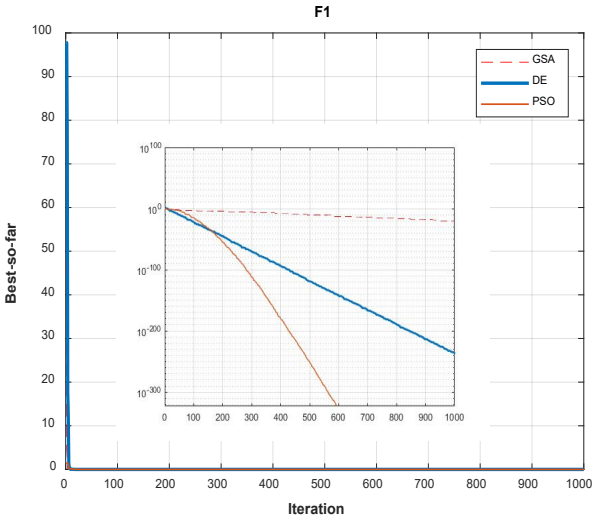

Figure 4: Convergence results of F1 with GSA, DE and PSO.

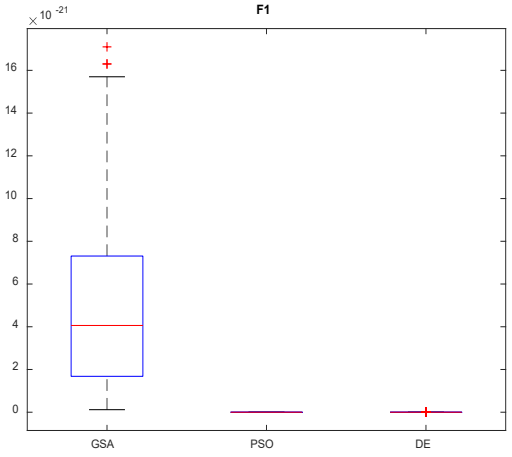

Figure 5: Robustness analysis of F1

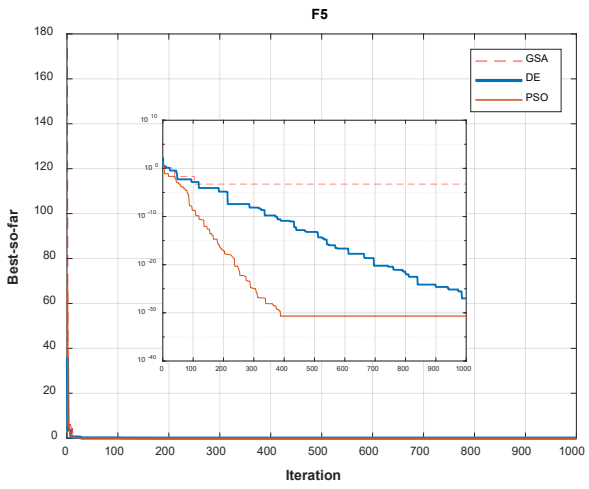

Figure 6: Convergence results of F5 with GSA, DE and PSO.

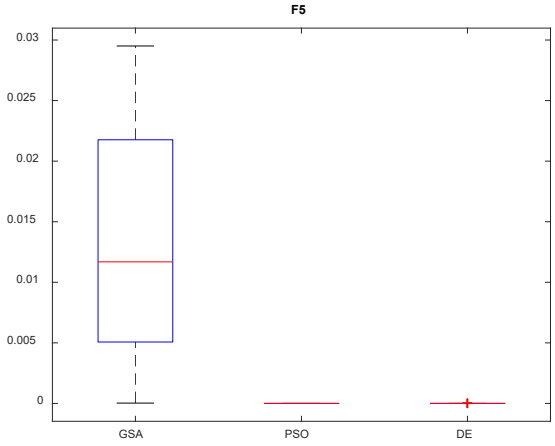

Figure 7: Robustness results of F5.

Function F7

The optimization results of the benchmark function F7, via the corresponding three algorithms, is illustrated in Figure 8. 100 runs are considered for function 7. The robustness analysis using the box-plot for the benchmark function F7 is presented in Figure 9.

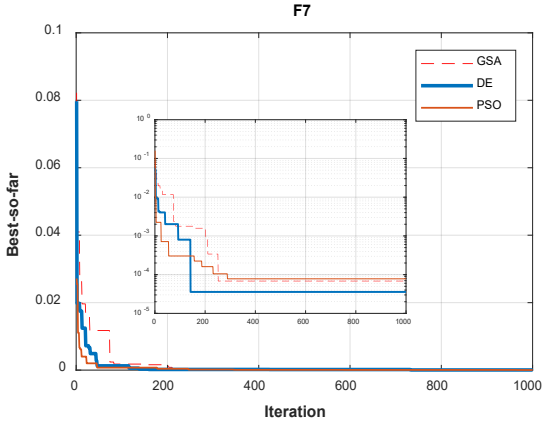

Figure 8: Convergence results of F7 with GSA, DE and PSO.

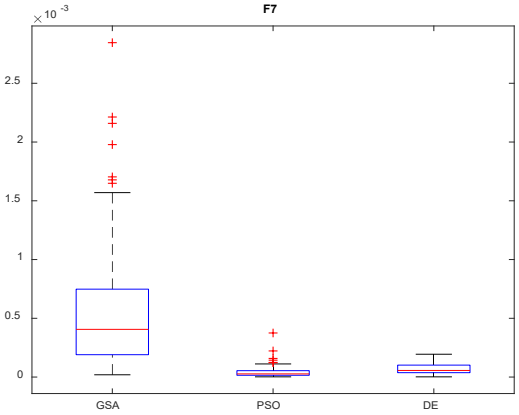

Figure 9: Robustness results of F7.

Figure 10 presents a Radio Chart representation of the average (AVG) execution times over 100 runs of three algorithm GSA, DE and PSO for the three benchmark functions.

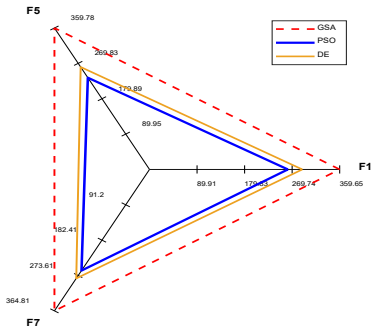

Figure 10: The average computing time of GSA, DE and PSO.

In accordance with the convergence of results regarding the three mono-objective metaheuristics according to the three benchmarks functions (Figures 4, 6 and 8) and the robustness results displayed in Figures 5, 7 and 9, we notice that DE and PSO have the better results compared to GSA.

The average executing time is illustrated in Figure 10. This figure shows that PSO is faster than DE and GSA.

Therefore, and according to the results achieved, the PSO algorithm is the most efficient algorithm, as it presents a best compromise among convergence, robustness and computational time.

B. Application example: RF spiral inductors

a. An overview on the integrated spiral inductors

CMOS technology is nowadays the only option able to fit the low-cost demand and to integrate digital, as well as analog radio-frequency (RF) modules on a single chip to realize the RF system on-chip (SoC). The efficiency and reliability of CMOS-RF blocks can be improved by means of on-chip passive devices (same substrate), such as voltage-controlled oscillators (VCO), low-noise amplifiers (LNA) and especially CMOS spiral inductor. Spiral inductor is broadly used and their applications in millimeter-wave circuit are investigated. High performance on-chip inductor has become increasingly important with their increasingly frequencies operation of the circuits.

Integrated spiral inductors models are based on the layout parameters, as displayed in Figure 11. These parameters are:

- w: the inductor width,
- s: the spacing between track,
- n: the number of turns,
- N_{side}: the inductor shape (square, hexagonal, octagonal),
- d_{in}: the internal diameter,
- d_{out}: the external diameter.

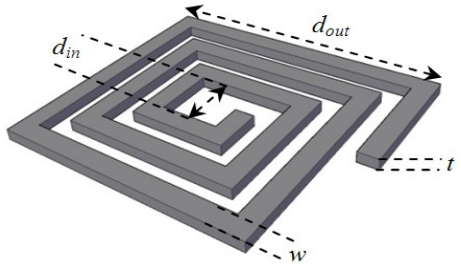

Figure 11: Layout characteristics for a square inductor.

For assessing the quality of the inductor design, different characteristics may be considered: the quality factor (Q), the operation frequency for the maximum Q, the self-resonant frequency f_{SR}, the inductance value L or the area. In this work, two parameters are selected: the quality factor Q and the device area d_{out}. Therefore, all the abovementioned characteristics are strongly dependent on the spiral inductor geometric parameters, technological constraints parameters and the application of this RF inductor.

At high frequencies, the simple but widely used single-π equivalent-circuit model can't accurately characterize the electrical performance of silicon-based planar spiral inductor. Many other equivalent-circuit inductor models have been reported in past decade [28]. In this paper, the double-π model is adopted and illustrated in Figure 12. This model lumped-element is evaluated with a wide range of equations and these values are specified in [29-30]. This model is represented by:

- DC parameters (Rs, Rp, Lo, Lp);
- Crossover capacitance, Cs: referred as the capacitance between the spiral and the underpass required to connect the outside to the inner turn of the planar inductor;
- Metal-to-metal capacitance, Cc: effect due to the proximity of inductor tracks;
- Metal-to-substrate capacitance, Cox;
- Rsub and Csub: the ohmic losses in the conductive silicon substrate;
- Rsc: the electric coupling between lines over the conductive substrate.

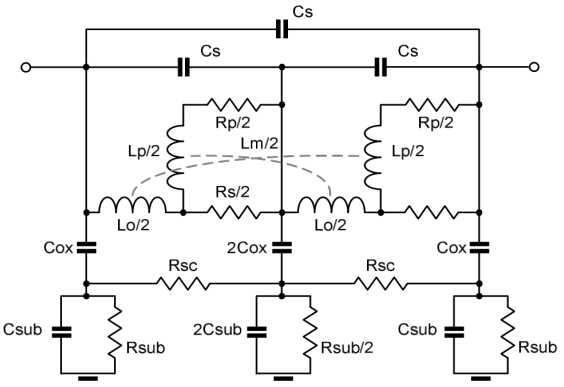

Figure 12: Inductor double π-model.

Table 5: Physical parameters

Parameters	Value
Metal Thickness (t)	2.8 µm
Space between turns (s)	2.5 µm
Sheet Resistance	10 mΩ/□
Oxide Thickness	5.42 µm
Oxide Thickness between spiral and underpass	0.26 µm
Oxide Permittivity (ε_r)	4
Substrate Thickness	700 µm
Substrate Permittivity (ε_r)	11.9
Substrate Resistivity	28 Ω cm

b. Optimization results

In this section, results highlight the ability of the PSO algorithm to perform the spiral inductor on Silicon technologies, the UMC130 technology is addressed. The conception for two inductors with 5.0 nH value, 6 nH value operating at 0.7 and 1 GHz, respectively, is considered. The technological and physical parameters are presented in Table 5, whereas the determination of the layout parameters is enabled with the uses of the constraint's parameters or technology constraints represented in Table 6. In addition, is considered a minimum space between tracks (s) of 2.5 µm and a maximum output diameter dout of 250 µm.

Table 6: Constraints parameters

Parameters	Min	Max
w (µm)	5.0	20.0
d_{in}(µm)	20.0	80.0
n	1.5	15.5

The inductor quality factor Q, desired to be higher as possible, is the objective function to be optimized.

Figures 13 displays the optimization results with PSO algorithm (13.a, 13.b) for two inductors: the first inductor of 5.0 nH value operating at 0.7 GHz and the second inductor of 6 nH value operating at 1 GHz. The maximization of the quality factor Q is addressed.

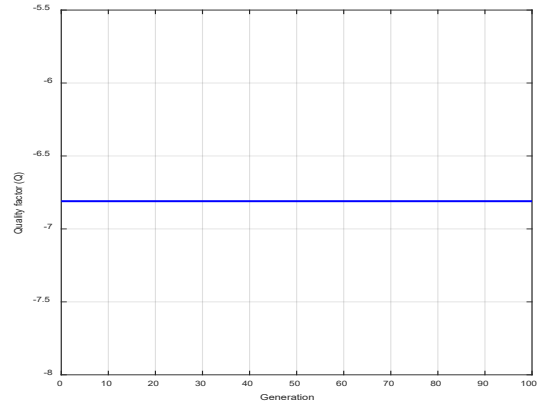

(a)

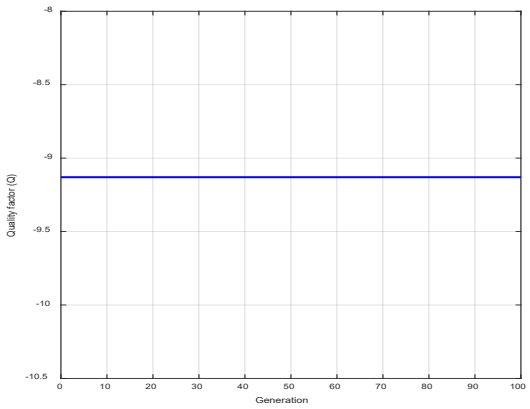

(b)

Figure 13: Optimization results with PSO (Quality factor Q vs. Generation): (a) 5 nH, frequency= 0.7 GHz, (b) 6 nH, frequency= 1 GHz.

Table 7 gives the optimization results values (inductor sizes) with PSO algorithm.

Table 7: Optimization and simulation results

L = 5nH, Frequency = 0.7 GHz					
Algorithm	w (µm)	d_{in} (µm)	n	$d_{out\text{-}Op}$ (µm)	Q_{Op}
PSO	10.88	60.40	5.67	206.91	6.81
L = 6nH, Frequency = 1.0 GHz					
Algorithm	w (µm)	d_{in} (µm)	n	$d_{out\text{-}Op}$ (µm)	Q_{Op}
PSO	9.00	61.90	6.08	196.90	9.13

4. Application examples: the multi-objective Optimization Algorithms

4.1. The multi-objective particle swarm optimization

Multi-Objective Particle Swarm Optimization (MOPSO) is proposed by Coello *et al*., [31]. The goal of the MOPSO and generally all the multi-objective algorithms is to provide a set of Pareto optimal solutions (with non-dominated solutions) of the aforementioned problem. All the non-dominated particles, this means all solutions, in the swarm are then collected into a sub-swarm named *repository*, and each particle selects its global best target. A group of MOPSO can be found in related literature, like:

- The non-dominated sorting PSO [32],
- The MOPSO using the Crowding Distance mechanism associated with a mutation operator which increasing the exploration ability of the particles and maintains the diversity of non-dominated solutions in the external archive by MOPSO-CD [33-35],
- The MOPSO using the Crowding Distance mechanism associated with a mutation operator and the Roulette Wheel selection technique to select social leader or global best to avoid an excessive number of non-dominated solutions in the external archive MOPSO-CDR [36].

The MOPSO version used in this paper use the Grid Making technique, instead of the crowing-distance computation which requires sorting the population consistent with each objective function value in ascending order of magnitude. This version uses the Grid Making technique with the mutation operator and the Roulette Wheel selection called MOPSO-GMR [37]. The flowchart of MOPSO algorithm is given in Figure 14.

4.2. Multi-Objective Evolutionary Algorithm based on Decomposition

The multi-Objective Evolutionary Algorithm supported on Decomposition (MOEA/D) is an evolutionary algorithm. The MOEA/D has adopted a technique that consists in decomposing the multi-objective optimization problems into several single-objective, called sub-problems. Each sub-problem has its own best solution ever found which is determined associating all of solutions found by algorithm. There are several methods to define the decomposed objective functions, for example: the weighted sum,

the distance or the norm of difference vector, the predefined ideal point in the objective space. The MOEA/D algorithm is developed by Zhang and Li [38]. The flowchart of MOEA/D algorithm is given in Figure 15.

4.3. Pareto Envelope-based Selection Algorithm II

The third multi-objective algorithm is an evolutionary algorithm: Pareto Envelope-based Selection Algorithm II (PESA-II). The PESA-II is based in the same genetic algorithm mechanism associated with the selection based on Pareto envelope. The PESA-II is configured with an external archive to save the approximate Pareto solutions. This means that the Parents and the mutants are selected based on the grids created as well as in the geographical distribution of archive members (external archive) [39].

The general process of the PESAII algorithm is as follows, with IP is the size of the internal population and EP is the size of the external populations(archive). The flowchart of PESAII algorithm is given in Figure 16.

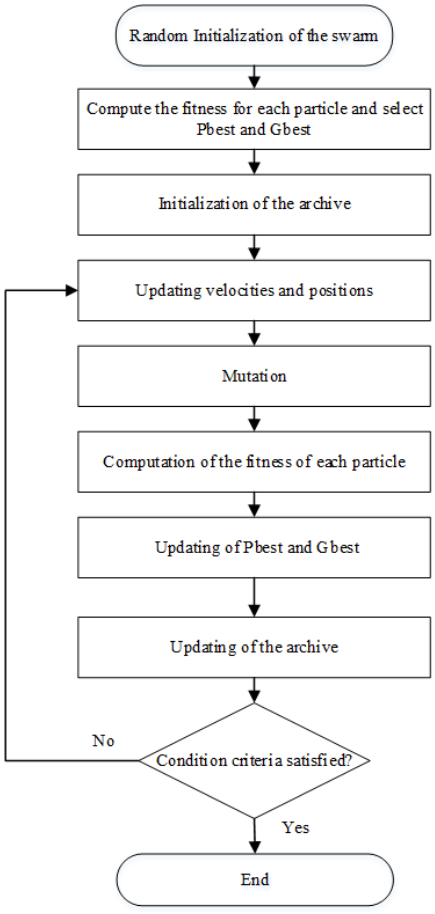

Figure 14: MOPSO Flowchart

4.4. Performances metrics: Hypervolume (HV)

The quality of the Pareto Fronts obtained by the multi-objectives algorithms can be evaluated through a few metrics. The most used performance metric was the *hypervolume* (HV) metric, also known as *S-metric* or *hyper-area*. The hypervolume indicator considers all three aspects: accuracy, diversity and cardinality.

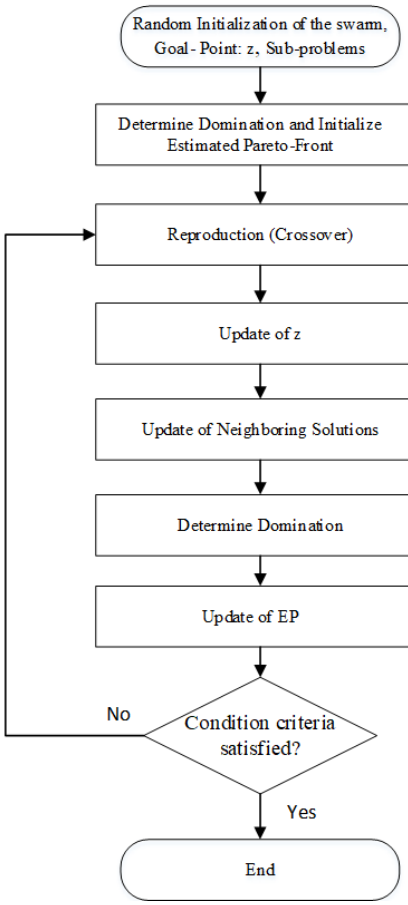

Figure 15: MOEA/D Flowchart

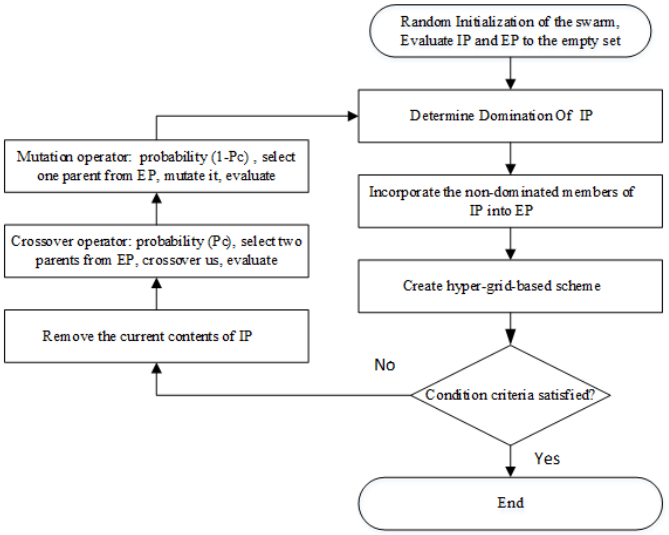

Figure 16: PESAII Flowchart

Thus, it is possible to measure the size of the objective space enclosed by an approximation set. To compute such enclosed space a reference point must be adopted. Figure 17 display a graphical representation of this performance indicator. Whenever one approximation set completely dominates another approximation set, the first HV will be superior than the second. Therefore, the HV is supposed to be *Pareto compliant* [40-41].

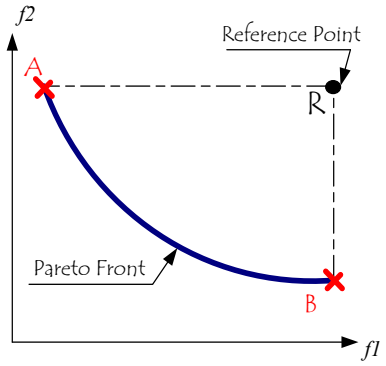

Figure 17: Example of the dominated Hypervolume in 2D.

4.5. Results of the test function and RF inductor applications

The aim consists of optimizing two conflicting performances: maximizing the Quality factor Q, and minimizing the device area, d_{out} by generating the trade-off surface (Pareto front). We give optimization results using the well-known PESAII and MOEA/D techniques for a RF inductor with value of 6 nH at 1 GHz. Also, two test function of ZDT family are used for benchmarking the performance of multi-objective Pareto optimization methods are illustrated in table 8.

Table 8: Multi-objective benchmark functions of Zitzler (ZDT)

Item Function	Objective functions to minimize
ZDT1 Objectives=2 Range: [0; 1]; Dim n=30	$f_1(x) = x_1$ $f_2(x) = g(x)\left[1-\sqrt{\frac{x_1}{g(x)}}\right]$ $with\ g(x) = 1+9\left[\frac{\sum_{i=2}^{n} x_i}{(n-1)}\right]$
ZDT6 Objectives=2 Range: [0; 1]; Dim n=10	$f_1(x) = 1-e^{(-4x_1)}\sin^6(6\pi x_1)$ $f_2(x) = g(x)\left[1-(\frac{f_1(x)}{g(x)})^2\right]$ $with\ g(x) = 1+9\left[\frac{\sum_{i=2}^{n} x_i}{(n-1)}\right]^{\frac{1}{4}}$

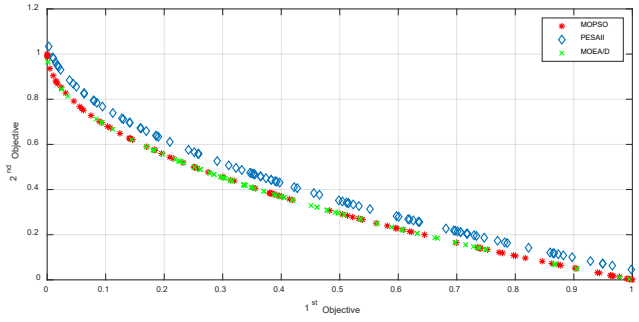

Figure 18: Pareto Front (MOPSO vs. PESAII vs MOEA/D) for ZDT1.

Figure 18, 19 and 20 represents the Pareto fronts obtained using MOPSO, PESAII and MOEA/D for ZDT1, ZDT6 and RF inductor application, respectively. Where it can be noticed that the better distribution given by MOPSO, when compared to PESAII and MOEA/D.

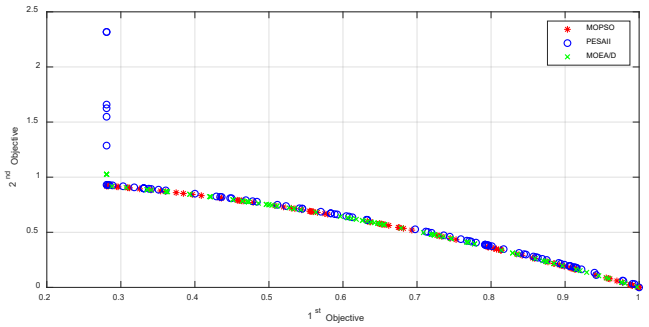

Figure 19: Pareto Front (MOPSO vs. PESAII vs MOEA/D) for ZDT6.

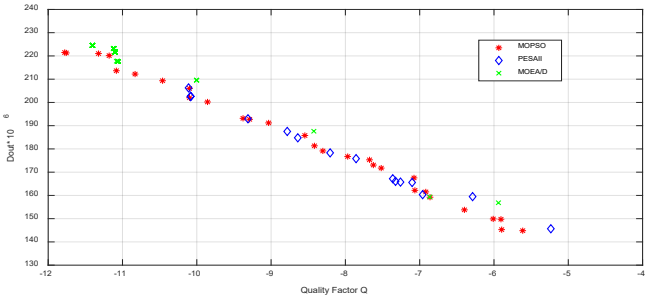

Figure 20: Pareto Front (MOPSO vs. PESAII vs MOEA/D) for RF inductor.

4.5.1. The hyper-volume indicator HV

Table 9 presents the average, maximum, minimum, and deviation values of the hypervolume indicator, over 20 runs of each algorithm, for two test function ZDT1, ZDT6 and the RF inductor application.

Table 9: Average, max, min, and standard deviations of the hypervolume indicator

		PESAII	MOEA/D	MOPSO
ZDT1	Avg	0.6918	0.7291	0.7587
	Max	0.7087	0.7563	0.7609
	Min	0.6643	0.6488	0.7558
	Std	0.0139	0.0346	0.0019
ZDT6	Avg	0.4782	0.4506	0.4869
	Max	0.4873	0.4843	0.4893
	Min	0.4675	0.3840	0.4849
	Std	0.0063	0.0577	0.0016
RF Inductor	Avg	0.5235	0.3272	0.5496
	Max	0.5260	0.4113	0.5508
	Min	0.5196	0.2663	0.5476
	Std	0.0025	0.0577	0.0017

Figure 21 represents the average value of the HV indicators for the 3 multi-objective problems. As a consequence, the MOPSO algorithm admits the highest average value of the HV indicator.

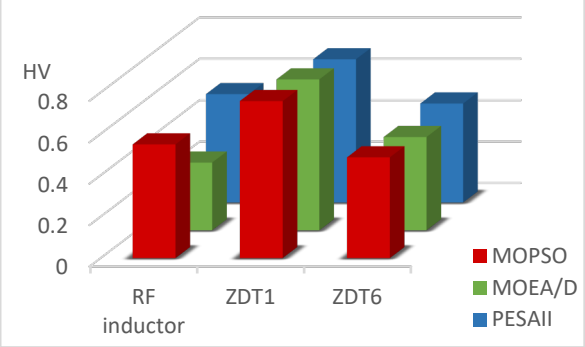

Figure 21: Average values of the HV indicators for the 3 multi-objective problems

4.5.2. *Computing time*

The maximum and the minimum execution times over 20 runs of each algorithm, is given in Table 10. Figure 16 displays the average value of the execution times.

Table 10: Average, Max and Min of the execution time

Time(S)		PESAII	MOEA/D	MOPSO
ZDT1	Avg	152.69	278.48	62.94
	Max	157.56	281.77	73.90
	Min	149.64	275.02	55.67
ZDT6	Avg	130.46	281.47	58.55
	Max	137.07	294.05	66.35
	Min	125.49	268.88	54.36
RF Inductor	Avg	105.91	166.25	54.71
	Max	106.53	221.28	58.07
	Min	105.28	141.38	51.58

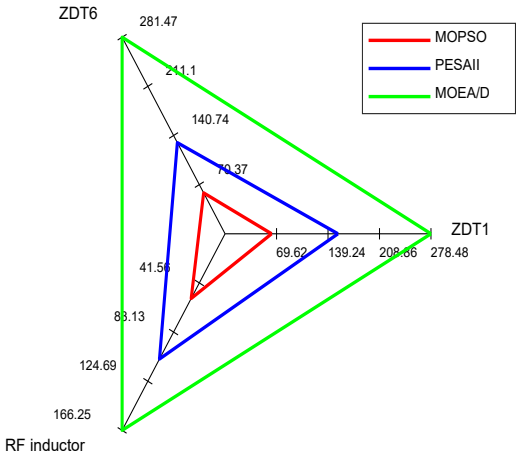

Figure 22: AVG execution time considering the three multi-objective problems

A comparison of the execution times is illustrated using the Radio Chart representation (figure 12) aiming to highlight the speediness of each algorithm. It can easily conclude that MOPSO is the faster when compared with other metaheuristics.

5. Conclusion

An objective comparison among the optimization results obtained via multiple-objective metaheuristics, dealing with performance optimization of RF circuits, is presented in this work. In first part, mono-objective metaheuristics are used. Among these metaheuristics the Swarm Intelligence metaheuristics like the Particle Swarm Optimization (PSO) and the Evolutionary Algorithms such us the Gravitational Search Algorithm (GSA) and the differential evolution algorithm (DE). These three algorithms were used to optimize three benchmark functions and the RF integrated inductors configured with the inductor double π-model. Results obtained shows that the use of swarm-based techniques in sizing and designing RF circuit offers a good argument, principally the PSO algorithm. In second part of this paper, we applied the multi-objective technique to solve two conflicting performances problem: the quality factor (Q) maximization as well as the minimization of the device area (dout) of the same RF application example using three multi-objective algorithms: firstly the multi-objective particle swarm optimization (MOPSO); secondly the multi-objective Evolutionary Algorithm based on decomposition (MOEA/D) and, a third one, the Pareto Envelope-based Selection Algorithm-II (PESA-II) by generating the trade-off surface (Pareto-front). The results obtained, which are supported by two performance metrics, a) the hypervolume indicator (HV) and b) the execution time, shows the following: MOPSO is better than other metaheuristics according to HV indicators, also MOPSO is the faster than other metaheuristics according to the CPU computing times.

References

[1] E.-G. Talbi, Metaheuristics: from design to implementation, Wiley, 2009.
[2] J. Dréo, A. Pétrowski, P. Siarry, E. Taillard, Metaheuristics for hard optimization: methods and case studies, Springer, 2006.
[3] M. Köppen, G. Schaefer, A. Abraham, Intelligent Computational Optimization in Engineering, Springer, 2011.
[4] F. Padilla, A. Torres, J. Ponce, M. D. Torres, S. Ratté, E. Ponce-de-Leon, "Evolvable metaheuristics on circuit design", in: Advances in analog circuits, E. Tlelo-Cuautle (Ed.), Intech, 2011. http://dx.doi.org/10.5772/14688
[5] G. Polya, How to Solve It, Princeton University Press, Princeton, NJ, 1945.
[6] A. Daniel, Evolutionary Computation for Modeling and Optimization, Springer, 2006.
[7] A. E. Eiben, J. E. Smith, Introduction to evolutionary computing, Natural Computing Series, Springer, 2007.
[8] P. Siarry, Z. Michalewicz, Advances in metaheuristics for hard optimization, Natural Computing Series, Springer, 2008.
[9] J. Holland, Adaptation in Natural and Artificial Systems: An Introductory Analysis with Applications to Biology, Control, and Artificial Intelligence, University of Michigan Press, 1975.
[10] D. E. Goldberg, Genetic Algorithms in Search, Optimization, and Machine Learning, Addison-Wesley Educational Publishers Inc, 1989.
[11] K. Y. Lee, M. A. El-Sharkawi, Modern Heuristic Optimization Techniques: Theory and Applications to Power Systems, IEEE Press Series on Power Engineering, 2008.
[12] S. Kirkpatrick, C.D. Gelatt, M.P. Vecchi, ''Optimization by Simulated Annealing'', Science, New Series, 220(4598), 671-680, 1983. https://doi.org/10.1126/science.220.4598.671
[13] K.V. Price, R. M. Storn, J. A. Lampinen, Differential Evolution: a practical approach to global optimization, Springer, 2006.
[14] M. Fakhfakh, Y. Cooren, A. Sallem, M. Loulou, P. Siarry, ''Analog circuit design optimization through the particle swarm optimization technique'',

Analog integrated circuits and signal processing, 63(1), 71--82, 2009. https://doi.org/10.1007/s10470-009-9361-3
[15] J. Kennedy, R. C. Eberhart, ‘‘Particle swarm optimization’’, Proceedings of the IEEE international conference on neural networks,1942-1948, 1995.
[16] R. A. Vural, T. Yildirim, ‘‘Analog circuit sizing via swarm intelligence’’, AEU - International journal of electronics and communications, 66(9), 732--740, 2012. https://doi.org/10.1016/j.aeue.2012.01.003
[17] B. Benhala, P. Pereira, A. Sallem, Focus on Swarm Intelligence Research and Applications, Nova Science Publishers, 2017.
[18] A. Sallem, B. Benhala, M. Kotti, M. Fakhfakh, A. Ahaitouf, M. Loulou, ‘‘Application of swarm intelligence techniques to the design of analog circuits: evaluation and comparison’’, Analog Integrated Circuits and Signal, Processing, 75(3), 499-516, Springer, 2013. https://doi.org/10.1007/s10470-013-0054-6
[19] M. Kotti, B, Benhala, M. Fakhfakh, A. Ahaitouf, B. Benlahbib, M. Loulou, A. Mecheqrane, ‘‘Comparison between PSO and ACO techniques for analog circuit performance optimization’’, The international conference on microelectronics, 2011. https://doi.org/10.1109/ICM.2011.6177367
[20] B. Benhala, A. Ahaitouf, M. Fakhfakh, A. Mechaqrane, B. Benlahbib, ‘‘Optimal analog circuit sizing via ant colony optimization technique’’, International journal of computer science and network security, 11(6), 223-231, 2011.
[21] B. Benhala, A. Ahaitouf, M. Kotti, M. Fakhfakh, B. Benlahbib, A. Mecheqrane, M. Loulou, F. Abdi, E. Abarkane, “Application of the ACO technique to the optimization of analog circuit performances”, In: Analog Circuits: Applications, Design and Performance, E. Tlelo Cuautle (Ed.), NOVA Science Publishers, Inc, 2011.
[22] E. Rashedi, H. Nezamabadi-pour, S. Saryazdi, ‘‘GSA: A Gravitational Search Algorithm’’, Information Sciences, 179, 2232--2248, 2009. https://doi.org/10.1016/j.ins.2009.03.004
[23] S. Jianga, Y. Wanga, Z. Jiaa, ‘‘Convergence analysis and performance of an improved gravitational search algorithm’’, Applied Soft Computing, 24, 363-384, 2014. https://doi.org/10.1016/j.asoc.2014.07.016
[24] https://www.sfu.ca/~ssurjano/optimization.html(Accessed 13May 2019).
[25] D. E. Goldberg, Genetic Algorithms in Search, Optimization, and Machine Learning, Addison-Wesley Educational Publishers Inc, 1989.
[26] M. Ali, A. Torn, ‘‘Population set based global optimization algorithms: some modifications and numerical studies’’, Computer Operation Research, 31(10), 1703-1725, 2004. https://doi.org/10.1016/S0305-0548(03)00116-3
[27] J. M. Chambers, W. S. Cleveland, B. Kleiner, P. A. Tukey, Graphical methods for data analysis, Duxbury Press, 1983.
[28] Yu Cao, R. A. Groves, N. D. Zamdmer, J.-O. Plouchart, R. A. Wachnik, Xuejue Huang, T. -J. King, Chenming Hu, ‘‘Frequency-independent equivalent-circuit model for on chip spiral inductors’’, IEEE Journal of Solid-State Circuits, 38(3), 419-426, 2003. https://doi.org/10.1109/JSSC.2002.808285
[29] P. Pereira, A. Sallem, M. Fakhfakh, M. H. Fino, F. Coito, A Technology Aware Optimization of RF Integrated Inductors, In: Tlelo-Cuautle E. (ed.) Analog Circuits: Applications, Design and Performance, Nova Science Publishers, Inc., 213-234, 2012.
[30] P. Pereira, M. H. Fino, F. Coito, M. Ventim-Neves, ‘‘RF Integrated Inductor Modeling and its Application to Optimization-Based Design’’, In: Analog Integrated Circuits and Signal Processing, 73(1), 4-55, Springer Netherlands, 2011. https://doi.org/10.1007/s10470-011-9682-x
[31] A. C. Coello and M. S. Lechuga, “MOPSO: A Proposal for Multiple Objective Particle Swarm (2002),” Proc. 2002 Congr. Evol. Comput. CEC’02 (Cat. No.02TH8600), 2, 1051–1056, 2002.
[32] X. Li, “A Non-dominated Sorting Particle Swarm Optimizer for Multiobjective Optimization,” 37–48, 2007,2003. https://doi.org/10.1007/3-540-45105-6_4
[33] M. R. Sierra and C. A. Coello, “Improving PSO-Based Multi-objective Optimization Using Crowding, Mutation and ∈-Dominance,” in EMO’2005, LNCS 3410. 505–519, 2010. https://doi.org/10.1.1.79.8066
[34] Deb, K., Pratap, A., Agarwal, S.; Meyarivan, T., “A fast and elitist multi-objective genetic algorithm: NSGA-II”, IEEE Transactions on Evolutionary Computation, 6(2): 182-197. https://doi.org/10.1.1.17.7771
[35] A. Sallem, B. Benhala, M. Kotti, M. Fakhfakh, A. Ahaitouf, and M. Loulou, “Application of swarm intelligence techniques to the design of analog circuits: Evaluation and comparison,” Analog Integr. Circuits Signal Process., 75(3), 499–516, 2013. https://doi.org/10.1007/s10470-013-0054-6
[36] R. A. Santana, M. R. Pontes, and C. J. A. Bastos-Filho, “A multiple objective particle swarm optimization approach using crowding distance and roulette wheel,” in ISDA 2009 - 9th International Conference on Intelligent Systems: Design and Applications, 1, 237–242, 2009. https://doi.org/10.1109/ISDA.2009.73
[37] http://yarpiz.com/category/multiobjective-optimization(Accessed 13 May 2019).
[38] Z. Qingfu and L. Hui, “MOEA/D: A Multiobjective Evolutionary Algorithm Based on Decomposition,” IEEE Trans. Evol. Comput., 11(6), 712–731, 2007. https://doi.org/10.1109/TEVC.2007.892759
[39] D. W. Corne, J. D. Knowles, and M. J. Oates, “The Pareto Envelope-Based Selection Algorithm for Multiobjective Optimization,” no. Mcdm, 839–848, 2000. https://doi.org/10.1007/3-540-45356-3_82
[40] L. Thiele and E. Zitzler, “Multiobjective Evolutionary Algorithms: A Comparative Case Study and the Strength Pareto Approach,” IEEE Trans. Evol. Comput., 3(4), 257–271, 1999.
[41] E. Zitzler, D. Brockhoff, and L. Thiele, “The hypervolume indicator revisited: On the design of pareto-compliant indicators via weighted integration,” Evolutionary Multi-Criterion Optimization. 862–876, Springer, 2007. https://doi.org/10.1007/978-3-540-70928-2_64